

Vijay Kumar Thakur · Michael R. Kessler
Editors

Liquid Crystalline Polymers

Volume 1—Structure and Chemistry

 Springer

Liquid Crystalline Polymers

Vijay Kumar Thakur • Michael R. Kessler
Editors

Liquid Crystalline Polymers

Volume 1—Structure and Chemistry

 Springer

Editors

Vijay Kumar Thakur
School of Mechanical and Materials
Engineering
Washington State University
Pullman, WA, USA

Michael R. Kessler
School of Mechanical and Materials
Engineering
Washington State University
Pullman, WA, USA

ISBN 978-3-319-22893-8

ISBN 978-3-319-22894-5 (eBook)

DOI 10.1007/978-3-319-22894-5

Library of Congress Control Number: 2015946615

Springer Cham Heidelberg New York Dordrecht London

© Springer International Publishing Switzerland 2016

This work is subject to copyright. All rights are reserved by the Publisher, whether the whole or part of the material is concerned, specifically the rights of translation, reprinting, reuse of illustrations, recitation, broadcasting, reproduction on microfilms or in any other physical way, and transmission or information storage and retrieval, electronic adaptation, computer software, or by similar or dissimilar methodology now known or hereafter developed.

The use of general descriptive names, registered names, trademarks, service marks, etc. in this publication does not imply, even in the absence of a specific statement, that such names are exempt from the relevant protective laws and regulations and therefore free for general use.

The publisher, the authors and the editors are safe to assume that the advice and information in this book are believed to be true and accurate at the date of publication. Neither the publisher nor the authors or the editors give a warranty, express or implied, with respect to the material contained herein or for any errors or omissions that may have been made.

Printed on acid-free paper

Springer International Publishing AG Switzerland is part of Springer Science+Business Media (www.springer.com)

Preface

Liquid crystalline polymers (LCPs) constitute an important class of materials that represents new advanced organic functional materials combining both anisotropic order of liquid crystals and excellent mechanical properties of polymers. These are one of the most important macromolecular systems having the capability of self-organization because of their unique molecular architectures with high anisotropy. The most distinguished feature of liquid crystalline polymers lies in that they exhibit intermediate morphological states between crystalline (or glassy) and liquid states, where macromolecular chains can be self-organized into a wide spectrum of ordered structures such as nematic, smectic, and cholesteric mesophases. Since the last few years, study on LCPs has been a flourishing research field due to their broad promising applications in various high-technology areas such as various organic optoelectronic applications, nonlinear optical materials, tunable diffraction gratings, thermal insulated materials, and the high-performance Kevlar fiber. Over the past decades, numerous endeavors have been made to rationally design and synthesize liquid crystalline polymers with controllable supramolecular structures. When mesogenic groups, such as calamitic, discotic, and bent-cored ones, are introduced into polymers, liquid crystalline (LC) phases may form, resulting in LC polymers (LCPs). LCPs can be classified into several general categories based on their architecture and position of mesogens in the polymer chain. Most frequently, LCPs are categorized into three types, namely, main-chain (MCLCPs), side-chain (SCLCPs), or main-chain/side-chain combined (MCSCCLCPs) LCP, depending on where mesogenic units are incorporated.

The advancement in the knowledge of structure and chemistry of liquid crystalline polymers, physical properties, and technical applications coincided with a period of rapid expansion in terms of the physical techniques available to the materials. This, together with great advances in the theoretical study and the rapid progress in computer simulation techniques, has made liquid crystals an exciting area for scientific research with many fundamental challenges. Indeed, the study of LCPs is an attractive research field that has engrossed significant curiosity, and their synthesis from different sources has awakened quite an

enormous deal of scientific awareness. The exploration of these innovative materials is still a challenge since the rapid development of different technologies demands new advanced materials, which possess as wide a range of properties as possible. Scientists in collaborations with industries are extensively developing new classes of “liquid crystalline polymers.” Different kinds of advanced materials can be obtained by the exploration of liquid crystalline polymers. This book is solely focused on the “liquid crystalline polymers” and deals with the “structural and chemistry” aspects of these materials. Several critical issues and suggestions for future work are comprehensively discussed in this book with the hope that the book will provide a deep insight into the state-of-art of “liquid crystalline polymers.” We would like to thank the publisher for the invaluable help in the organization of the editing process.

Pullman, WA, USA

Vijay Kumar Thakur
Michael R. Kessler

Contents

1	Liquid Crystalline Epoxy Resins	1
	Yuzhan Li and Michael R. Kessler	
2	Structure and Phase Transitions of Polymer Liquid Crystals, Revealed by Means of Differential Scanning Calorimetry, <i>Real-Time</i> Synchrotron WAXD, MAXS and SAXS and Microscopy	19
	Ginka Exner, Ernesto Pérez, and Manya Krasteva	
3	Block Copolymers Containing Mesogen-Jacketed Liquid Crystalline Polymers as Rod Blocks: Synthesis and Self-Assembly	53
	Zhihao Shen and Qi-Feng Zhou	
4	Computer Simulation of Side-Chain Liquid Crystal Polymer Melts and Elastomers	93
	Jaroslav M. Ilnytskyi, Marina Saphiannikova, Dieter Neher, and Michael P. Allen	
5	Side-Chain Liquid Crystalline Polymers: Controlled Synthesis and Hierarchical Structure Characterization	131
	Shi Pan, Bin Mu, Bin Wu, Zehua Shi, and Dongzhong Chen	
6	Effects of Hydrogen-Bonding on the Liquid Crystalline Properties of Dendritic Polymers	173
	Michael Arkas and Aggeliki Papavasiliou	
7	Polymer Dispersed Liquid Crystals	195
	Shri Singh, Jagdeesh Kumar Srivastava, and Rajendra Kumar Singh	
8	LCP Based Polymer Blend Nanocomposites	251
	Ganesh Chandra Nayak and Chapal Kumar Das	

9	Liquid Crystalline Polymers from Renewable Resources: Synthesis and Properties	273
	K.Y. Sandhya, A. Saritha, and Kuruvilla Joseph	
10	Light-Emitting Field-Effect Transistors with π-Conjugated Liquid Crystalline Polymer	307
	Hisao Yanagi, Yusuke Ohtsuka, Tatsuya Muneishi, and Atsushi Ishizumi	
11	Photoactive Liquid Crystalline Polymer	327
	Asit Baran Samui and Srinivasa Rao Venukonda	
12	Combined Main-Chain/Side-Chain Liquid Crystalline Polymers: Synthesis and Supramolecular Ordering	363
	Wenyi Huang	
13	Supramolecular (Hydrogen-Bonded and Halogen-Bonded) Liquid Crystalline Polymers	391
	Qun Ye, Jianwei Xu, and Chaobin He	
14	Models of Liquid Crystalline Polymer Fibers	411
	J.I. Ramos	
15	Relationship Between Composition, Structure and Dynamics of Main-Chain Liquid Crystalline Polymers with Biphenyl Mesogens	453
	Aránzazu Martínez-Gómez, Mario Encinar, Juan P. Fernández-Blázquez, Ramón G. Rubio, and Ernesto Pérez	
16	Introduction to Liquid Crystalline Polymers	477
	Dumitru Pavel	
17	Smectic Phases of Liquid Crystalline Rod-Like Helical Polymers	501
	Kento Okoshi	
18	Metal Containing Liquid Crystalline Polymers	517
	Sachin Kumar Singh and Bachcha Singh	
19	Integration of Liquid-Crystalline Elastomers in MEMS/MOEMS	531
	Antoni Sánchez-Ferrer, Núria Torras, and Jaume Esteve	
20	Discotic Liquid Crystalline Polymers: Structure and Chemistry	583
	Harpreet Singh, Sandeep Kumar, and Santanu Kumar Pal	
	Index	617

About the Editors

Vijay Kumar Thakur, Ph.D.

Staff Scientist

School of Mechanical and Materials Engineering,

Washington State University, USA

PO BOX 642920, Pullman, WA 99164-2920

Email: vijayisu@hotmail.com; drvijay.kumar@wsu.edu



Dr. Vijay Kumar Thakur has been working as a Research Faculty (Staff Scientist) in the School of Mechanical and Materials Engineering at Washington State University, United States, since September 2013. His former appointments include being a Research Scientist in Temasek Laboratories at Nanyang Technological University, Singapore, and a Visiting Research Fellow in the Department of Chemical and Materials Engineering at LHU, Taiwan. His research interests include the synthesis and processing of bio-based polymers, nanomaterials, polymer micro-/nanocomposites, nanoelectronic materials, novel high dielectric constant materials, electrochromic materials for energy storage, green synthesis of nanomaterials, and surface functionalization of polymers/nanomaterials. He did his postdoctorate in materials science at Iowa State University, United States, and his Ph.D. in polymer science (2009) at the National Institute of Technology. In his academic carrier, he has published more than 80 SCI journal research articles in the field of polymers/materials science and holds one US patent. He has also published 20 books and 35 five book chapters on the advanced state-of-the-art of polymers/materials science with numerous publishers. He is an editorial board member of several international journals and also is member of scientific bodies around the world. Some of his significant appointments include: Advisory Editor for

SpringerPlus (SCI); Associate Editor for Materials Express (SCI); Associate Editor for Current Smart Materials; Regional Editor for Recent Patents on Materials Science (Scopus) and Regional Editor for Current Biochemical Engineering (CAS). He also serves on the Editorial Advisory Board of Polymers for Advanced Technologies (SCI) and is on Editorial Board of Journal of Macromolecular Science, Part A Pure and Applied Chemistry (SCI); International Journal of Industrial Chemistry (SCI) and Energies (SCI).

Michael R. Kessler, Ph.D., P.E.

Professor and Berry Family Director
School of Mechanical and Materials Engineering,
Washington State University, USA
PO BOX 642920, Pullman, WA 99164-2920
Email: michaelr.kessler@wsu.edu



Professor Kessler is an expert in the mechanics, processing, and characterization of polymer matrix composites and nanocomposites. His research thrusts include the development of multifunctional materials (including the development of self-healing structural composites), polymer matrix composites for extreme environments, bio-renewable polymers and composites, and the evaluation of these materials using experimental mechanics and thermal analysis. These broad-based topics span the fields of organic chemistry, applied mechanics, and processing science. He has extensive experience in processing and characterizing thermosets including those created through ring-opening metathesis polymerization (ROMP), such as polydicyclopentadiene, and the cyclotrimerization of cyanate ester resins. In addition to his responsibilities as Professor of mechanical and materials engineering at Washington State University, he serves as the Director of the school. He has developed an active research group with external funding of over ten million dollars—including funding from the National Science Foundation, ACS Petroleum Research Fund, Strategic Environmental Research and Development Program (SERDP), Department of Defense, Department of Agriculture, and NASA. His honors include the Army Research Office Young Investigator Award, the Air Force Office of Scientific Research Young Investigator Award, the NSF CAREER Award, and the Elsevier Young Composites Researcher Award from the American Society for Composites. He has >110 journal papers and 3700 citations, holds six patents, edited a book on the characterization of composite materials, presented >200 talks at national and international meetings, and serves as a frequent reviewer and referee in his field.

Chapter 1

Liquid Crystalline Epoxy Resins

Yuzhan Li and Michael R. Kessler

1.1 Introduction

The idea of developing crosslinked liquid crystalline (LC) networks was proposed by Nobel laureate, Pierre-Gilles de Gennes in 1969 (Gennes and Prost 1995). Subsequent efforts in this area resulted in a group of materials known as liquid crystalline thermosets (LCTs), which combines the outstanding properties of both liquid crystals and crosslinked thermosets (Shiota and Ober 1997a; Douglas 2002; Barclay and Ober 1993). A great number of LCTs have been synthesized using a variety of monomers, including epoxy (Carfagna et al. 1997; Giamberini et al. 1995; Mallon and Adams 1993), acrylate (Hikmet and Broer 1991; Hikmet et al. 1992; Litt et al. 1993; Holter et al. 1996), maleimide (Hoyt and Benicewicz 1990a, b), and cyanate ester (Mormann and Zimmermann 1995, 1996; Barclay et al. 1992a; Mormann and Kuckertz 1998). These materials exhibit properties that transcend their amorphous counterparts because of a polydomain structure. Among all the LCTs synthesized, liquid crystalline epoxy resins (LCERs) have received the most attention because of their diverse applications, such as microelectronics packaging materials, optical wave guides, adhesives, color filters, and structural materials. LCERs are generally formed upon curing of low molecular weight, rigid rod epoxy monomers with amines or anhydrides, resulting in the retention of a LC phase by the three dimensional crosslinking networks. Early investigation of LCERs focused on molecular architecture of the epoxy monomers and the related LC phase transition. Subsequent work involves studies on cure kinetics, phase evolution, molecular orientation and thermomechanical characterization of the LCERs. More recently, there have been efforts on fabrication of composites and nanocomposites using LCERs.

Y. Li • M.R. Kessler (✉)

School of Mechanical and Materials Engineering, Washington State University,
Pullman, WA, USA

e-mail: MichaelR.Kessler@wsu.edu

1.2 Molecular Structures

1.2.1 Molecular Structure of Monomers

A typical structure of liquid crystalline epoxy (LCE) monomers is shown in Fig. 1.1, which contains a rigid core known as a mesogen or mesogenic group. The functional epoxy groups are connected to the mesogen through alkyl flexible spacers.

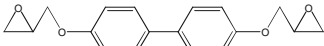
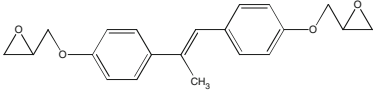
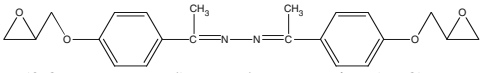
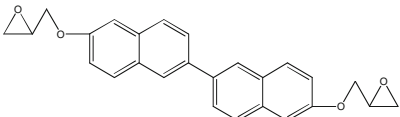
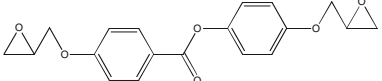
The thermal and LC behavior of LCE monomers are highly dependent on their molecular structures. A large number of monomers with different mesogen structures have been synthesized and are listed in Table 1.1, including biphenyl (Su et al. 2000; Mormann and Brocher 1996; Lee et al. 1998; Broer et al. 1993; Su 1993; Lu et al. 2001; Liu et al. 2006; Mititelu and Cascaval 2005; Ochi et al. 1995), methylstilbene (Cho et al. 2006a; Barclay et al. 1992b; Sue et al. 1997a, b), azomethine (Choi et al. 2000; Gao et al. 2007), naphthyl (Lee and Jang 1999), and phenyl benzoate (Shiota and Ober 1996; Lee and Jang 2006; Lee 2006a; Jahromi et al. 1994). Generally, LCE monomers fall into the category of thermotropic liquid crystals, and therefore exhibit temperature dependent phase behavior. They also follow basic rules for liquid crystals. Some typical LC phases observed in LCE monomers are shown in Fig. 1.2. The nematic phase is characterized by a long range orientational order but lack of positional order, while the smectic phase possesses orientational order as well as a layered ordering. The cholesteric phase is featured by a nematic ordering of molecules within layers that are arranged in a helical manner.

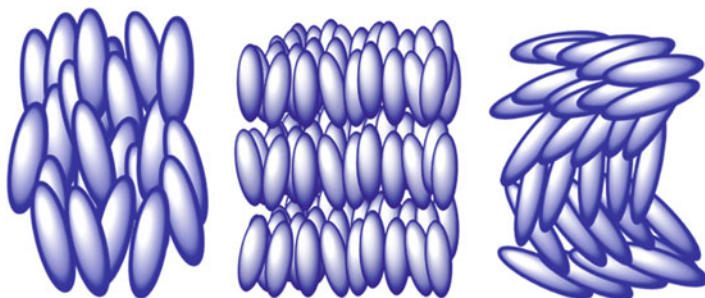
Lee and coworkers synthesized a series of phenyl benzoate based LC epoxy monomers with different mesogenic structures and investigated the effect of mesogenic length on LC phase transition of the monomers (Lee and Jang 2006). The mesogenic length was increased by connecting additional phenol benzoate groups to the mesogen, as shown in Fig. 1.3, resulting in monomers with different aspect ratio. The LC phase transition was examined using a polarized optical microscope equipped with a hot stage. Results showed that the mesogen structure had great influence on the phase behavior of the monomers. LCE 1 (see Fig. 1.3) did not show any LC behavior. LCE 2 exhibited a monotropic nematic phase on cooling from 93 to 79 °C. Both LCE 3 and LCE 4 showed a nematic phase on heating. However, in the case of LCE 3 the LC phase were stable between 181 to 229 °C, whereas LCE 4 showed an LC phase over a wider temperature range from 192 to 271 °C.



Fig. 1.1 Typical chemical structure of LC epoxy monomers, with a rigid mesogen core, alkyl flexible spacers, and epoxy functional groups on the ends

Table 1.1 Typical chemical structure of LCE monomers

Mesogenic groups	Chemical structure
Biphenyl	 4,4'-Diglycidyloxybiphenyl (BP)
Methylstilbene	 4,4'-Diglycidyloxy- α -methylstilbene (DOMS)
Azomethine	 p-(2,3-epoxypropyl)acetophenone azine (EF3)
Binaphthyl	 6,6'-Bis(2,3-epoxypropoxy)-2,2'-binaphthyl (EPBN)
Phenyl benzoate	 p'-(2,3-epoxypropoxy)-phenyl-p-(2,3-epoxypropoxy)benzoate (PHBHQ)

**Fig. 1.2** Typical LC phases observed in LCERs. From left to right: nematic phase, smectic phase, and cholesteric phase

Lee and coworkers also examined the effect of substituents on thermal and curing behavior of LCE 3 (Lee and Jang 1998). Chlorine and methyl groups were introduced as substituents to the central benzene ring. The nematic transition temperature and isotropization temperature showed a decrease of 23 °C and 7 °C, respectively for the chlorine substituted monomer, and a decrease of 50 °C and 13 °C, respectively for the methyl substituted monomer. This was ascribed to the change of polarity of the mesogen, which increases the interaction between neighboring chains.

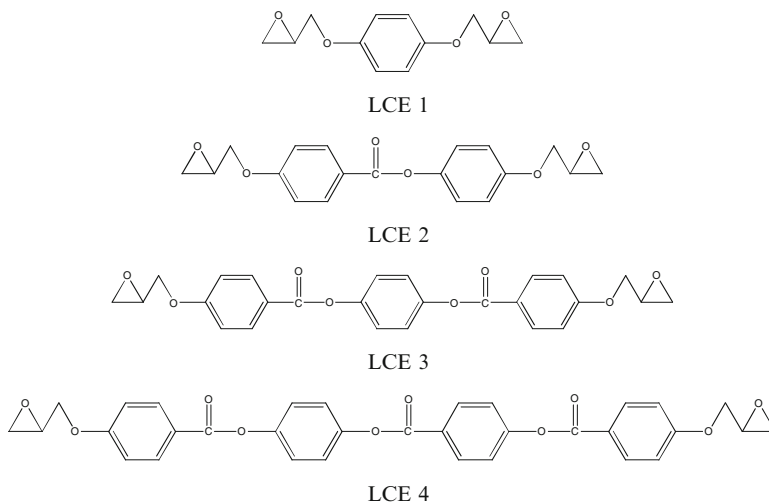


Fig. 1.3 LC epoxy monomers with different mesogenic length. Reprinted from Ref. 35, Copyright (2006), with permission from Elsevier

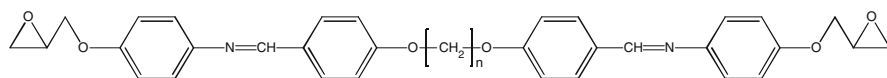


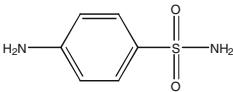
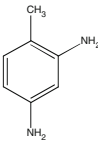
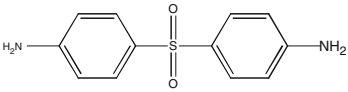
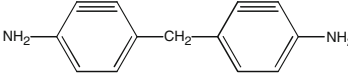
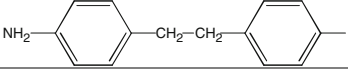
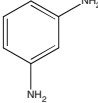
Fig. 1.4 LC twin epoxy monomers, $n = 6, 7, 8$ and 9

In addition to mesogens, the structure of flexible spacers also affect the thermal and LC properties of the monomers. For example, Choi and coworkers synthesized an azomethine-based twin epoxy monomer (Choi et al. 2000), in which two mesogens were connected directly through a flexible spacer, as shown in Fig. 1.4. The thermal and LC properties of the monomers with different spacer lengths were examined using differential scanning calorimetry (DSC) as well as polarized optical microscopy (POM). The LC transition temperature and isotropization temperature decreased in a zig-zag fashion with increasing spacer length, indicating an odd-even effect. Monomers with even numbers of methylene units showed higher degree of order and stronger chain interactions, and therefore had high melting and isotropization temperatures.

1.2.2 Molecular Structure of Curing Agents

Similar to conventional epoxy resins, LCE monomers need to react with curing agents to form three-dimensional crosslinked networks. It is worth mentioning that the LCER networks may not necessarily exhibit the same LC phase as the monomer does. In some cases, a LC phase can be developed during the curing reaction even if

Table 1.2 Commonly used curing agents for LCERs

Name	Chemical structure
Sulfanilamide (SAA)	
2,4-Diaminotoluene (DAT)	
4,4'-Diaminodiphenylsulfone (DDS)	
4,4'-Diaminodiphenylmethane (DDM)	
4,4'-Diaminodiphenylethane (DDE)	
m-Phenylenediamine (PDA)	

the monomer is not liquid crystalline. Some commonly used curing agents are listed in Table 1.2. The choice of curing agent affects the formation and development of an LC phase. For example, the use of sulfanilamide (SAA) tends to facilitate the formation of a smectic LC phase because of the unequal reactivity of the amine groups, which results in a layered stack of the LCE monomers.

1.3 Cure Behavior

Generally, the curing reaction of epoxy resin starts from the reaction of an epoxy group with a primary amine, which produces a secondary alcohol and a secondary amine which in turn reacts with other epoxy groups to form a tertiary amine and two secondary hydroxyl groups. The hydroxyl groups serve as catalysts to accelerate the curing reaction. Therefore, the curing reaction of epoxy usually can be described using autocatalytic models. However, the formation of the LC phase has a dramatic influence on the curing behavior of LCERs, and results in unusual curing phenomena that are not observed in amorphous epoxy systems.

1.3.1 Reaction Kinetics

As mentioned previously, the kinetics of conventional epoxy-amine reaction is usually characterized by an autocatalysis mechanism. In the case of LCER, however, the kinetic parameters are affected by the LC phase, especially when the monomer is not liquid crystalline and a LC phase is developed during the curing reaction. As a result, in addition to reactions associated with the epoxy-amine chemistry, the phase transition also needs to be considered and incorporated into reaction models. Several research groups have investigated the curing behavior of LCERs (Zhang and Vyazovkin 2006; Rosu et al. 2004; Carfagna et al. 1993; Micco et al. 1997; Lee et al. 2004; Cai et al. 2007; Vyazovkin et al. 2003). One of the early studies on cure kinetics of LCER was performed by Amendola and coworkers on the DOMS/DAT system (Amendola et al. 1995). A series of isothermal curing experiments were carried out in the temperature range between 130 and 190 °C as shown in Fig. 1.5.

It was found that for the resins cured at temperatures equal to or lower than 180 °C, an additional exothermic peak was observed, which was explained as a phase transition of the reacting system from an isotropic phase to an LC phase. This hypothesis was supported by the POM experiments. In contrast, if the reaction was carried out at a temperature higher than 190 °C, the LC phase cannot be observed under polarized light and only a single DSC exotherm is present, similar to the curing behavior of amorphous epoxy resins. The reaction kinetics was also examined by analyzing the primary and secondary amine reactions separately. The results showed that the addition of secondary amine was much faster than that of the primary one, which contradicts that was observed for conventional epoxies and was attributed to the formation of the LC phase. Mititelu and coworkers also reported a higher reactivity of secondary amine of another LCER system (Mititelu et al. 2000). They investigated the kinetic behavior of BP/DDS using size exclusion chromatography, where the disappearance of the monomers and the appearance of the oligomers were monitored through a differential refractometer. The curing reaction was carried out at several temperatures. Results showed that the reaction rate constant of secondary amines was four times higher than that of primary amines when the resin was cured at 145 °C. They also found that the ratio of reaction rates of secondary amine to primary amine decreased with increasing temperature as the LC phase formation was affected by the fast crosslinking reaction. A detailed kinetic study of LCER was performed by Liu et al for DOMS/SAA system (Liu et al. 1997), in which a big deviation from the autocatalytic model was observed, and a kinetic model considering both chemical reaction and LC phase formation was proposed to describe the isothermal curing behavior. The system also showed two exothermic peaks in isothermal curing experiments at certain temperatures. A parallel experiment was carried out on a microscope equipped with a hot stage to examine the LC texture. The data indicated that the change of reaction rate was related to the LC texture formation.

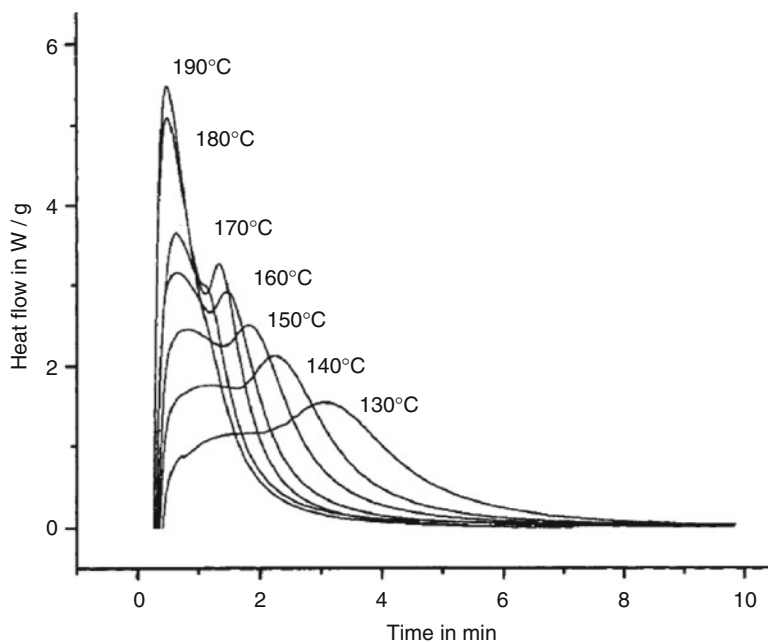


Fig. 1.5 Isothermal DSC curing curves of DOMS/DAT at different temperatures. Reprinted from Ref. 46, Copyright (2003), with permission from John Wiley and Sons

In related work, we investigated the curing behavior of BP/SAA system using dynamic DSC curing experiments with different heating rates (Li and Kessler 2014a).

As shown in Fig. 1.6, the resins cured at 1, 2, 3, and 4 °C/min developed an LC phase, confirmed by double exothermic DSC peaks and POM results, whereas for the resins cured at 10, 15, 20, 25 °C/min, only one exothermic peak was observed, indicating an amorphous structure of the resins. Temperature modulated DSC was also used to separate reversible and non-reversible thermal events involved in the curing process. In addition to the reversible melting peak, an additional reversible peak was detected and was thought to be caused by the LC phase formation. The variation in activation energy with the degree of cure was determined using the Friedman differential isoconversional kinetic analysis. The resins cured in amorphous phase showed a gradual increase in activation energy as observed for conventional epoxy resins. In the case of LCER, however, the activation energy showed a decrease in the early stage of curing, which was ascribed to a decrease in viscosity due to the phase transition of the reacting medium from an isotropic phase to an LC phase. In addition, a multi-step model was developed to describe the curing behavior of the LCER. The step of the LC phase formation was regarded as an independent reaction step and was modeled using a function of n -dimensional nucleation growth.

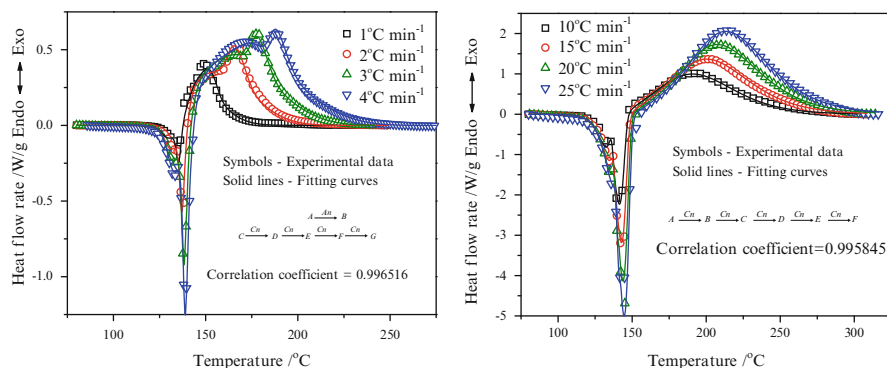


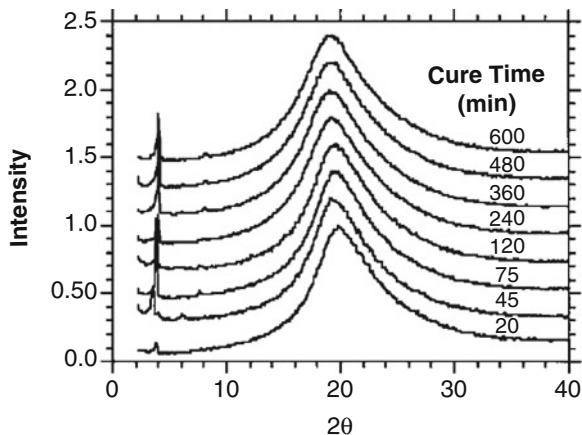
Fig. 1.6 Dynamic DSC curing curves and model fitting results of BP/SAA at different heating rates. Reprinted from Ref. (Li and Kessler 2014a), Copyright (2014), with permission from Springer

1.3.2 LC Phase Formation

Compared to the large number of reports on monomer synthesis and reaction kinetics, few studies have been published on the LC structure evolution upon curing (Shiota and Ober 1997b; Lin et al. 1994; Cho et al. 2006b; Cho and Douglas 2002). The formation of the LC phase is a complicated process and is affected by several factors, including chemical structure and phase behavior of the monomer, the reactivity of the amine curing agent, and curing conditions. A detailed study was performed by Lin and coworkers on the DOMS/SAA system (Lin et al. 1997). The LC phase formation was characterized using different techniques, including DSC, POM, X-ray diffraction (XRD), and parallel plate rheology. The authors first investigated the isotropic transition temperature of the LC phase as a function of reaction time. It was found that the LC phase stability increased with increasing reaction time. Although the DOMS monomer showed a monotropic nematic LC phase, a smectic LC phase was developed during the curing reaction as confirmed by the diffraction peak at lower Bragg angle shown in Fig. 1.7. This was thought to be caused by the use of SAA as a curing agent. As shown in Table 1.2, the two amine groups in SAA have unequal reactivity. The aromatic amine tends to react first due to an electron donating effect of the benzene ring, resulting in an extension of the polymer chain which favors the formation of a layered smectic structure.

Harada et al. also performed a detailed study on LC phase formation of a LCER based on azomethine mesogens (Harada et al. 2013). They monitored the phase transformation by simultaneous SAXS/WAXS measurements using synchrotron radiation. Three different curing agents were used, including DDE, DDM, and PDA. They found that a nematic phase was developed in the early stage of the curing process and was transformed into a smectic phase depending on the choice of curing agent. When a curing agent with a planar structure was used, in the case of DDE and PDA, the mesogens tend to form a densely stacked layers, leading to the

Fig. 1.7 XRD spectra of DOMS/SAA at different reaction times under 120 °C. Reprinted from Ref. (Lin et al. 1997), Copyright (1998), with permission from John Wiley and Sons



highly ordered smectic phase. The LC phase formation of another LCER system, BP/SAA, was examined by us using POM. Figure 1.8 shows the POM images taken at different reaction times (Li et al. 2013). The reacting system was initially isotropic, and a smectic LC birefringence was observed after 19 min of the curing reaction and was stable when the resin was cooled to room temperature.

1.4 Properties

LCERs are characterized by a polydomain structure, which is expected to have different mechanical behavior and properties from their amorphous counterparts. One of the most significant improvements of LCERs is their fracture toughness (Liu et al. 2011; Harada et al. 2006, 2009; Shiota and Ober 1998).

1.4.1 Mechanical Properties

A detailed deformation study on LCER was performed by Ortiz and coworkers on a DOMS/DDM system (Ortiz et al. 1998, 2000). The curing temperature was adjusted to produce resins with different micro-structure, including amorphous phase, smectic LC phase, and nematic LC phase. A commercially available, diglycidyl ether of bisphenol A (DGEBA) epoxy resin was also prepared and was compared to the fracture behavior of the LCER system. The fracture toughness measurements were conducted according to ASTM E399-83 standards using a chevron notched bending technique. The load-displacement curves for the resins cured in different micro-structures are shown in Fig. 1.9. The results showed that the fracture behavior of the resins is highly dependent on the structure of the material. The DGEBA resin

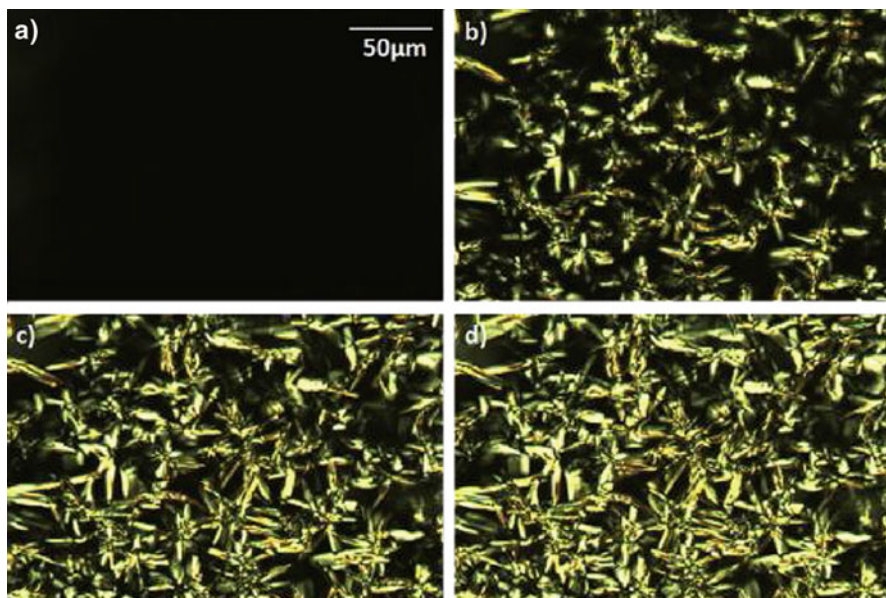


Fig. 1.8 POM images of isothermal curing of BP/SAA at 170 °C. (a) 18 min; (b) 20 min; (c) 22 min; (d) 24 min. Reprinted from Ref. (Harada et al. 2009), Copyright (2013), with permission from Elsevier

exhibited a brittle, catastrophic failure with a fracture toughness value, G_{Ic} , of 0.4 kJ/m². However, when the bisphenol A molecules were replaced with relatively rigid methylstyrene molecules, the resin showed a non-uniform crack propagation after the initial fast crack propagation, and the G_{Ic} value increased to 0.68 kJ/m². Further improvement on fracture toughness was observed when the resin was cured into a nematic LC phase with a G_{Ic} of 0.75 kJ/m². The smectic LCER exhibited a slow and stable crack propagation after the initial cracking and showed the highest fracture toughness with a G_{Ic} value of 1.62 kJ/m². A toughening mechanism was proposed by the authors. It was thought that the crack propagation was reduced by bulk, homogeneous plastic yielding of isolated smectic LC domains, which created microscopic defects and voids around the crack tip. Harada and coworkers investigated fracture behavior of an azomethine-based LCER resin using polarized infrared spectrometer and found that the resin cured into a smectic phase showed the highest fracture toughness (Harada et al. 2004a, 2010). The dichroic ratio maps of the network chain orientation were constructed to explain the change in microstructure of the resins. It was found that the high fracture toughness was resulted from the large-scale deformation with collapse of the smectic domain structure and reorientation of the network chains near crack.

In addition to fracture behavior, the presence of the LC phase also affects other mechanical properties of the resin. We recently investigated the viscoelastic properties of a biphenyl-based LCER using dynamic mechanical analysis (Li and

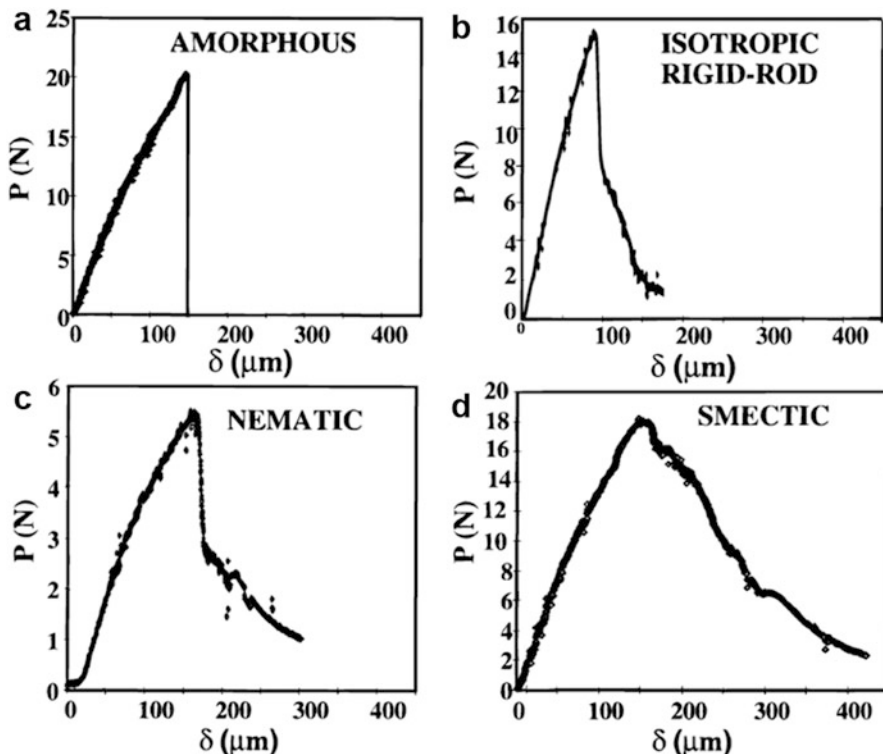


Fig. 1.9 Load-displacement curved for resins in the chevron-notched three-point bending fracture toughness tests. (a) DGEBA/DDM isotropic thermoset; (b) DOMS/DDM isotropic thermoset; (c) DOMS/DDM nematic thermoset; (d) DOMS/DDM smectic thermoset. Reprinted from Ref. (Ortiz et al. 1998), Copyright (1998), with permission from American Chemical Society

Kessler 2014b). The creep behavior of a BP/SAA system was studied and compared with that of a non-LCER prepared from the same epoxy monomer. The resins cured into the LC phase exhibited lower values of creep strain and creep strain rates. The data was then evaluated using Burgers' model to explain the reinforcing effect of the LC phase. It was found that the resistance to permanent creep deformation of the resin was significantly improved after introducing the LC phase, which act as crosslinks, tying amorphous regions together, thus greatly restricting the mobility of the networks.

1.4.2 Moisture Resistance

The moisture resistance of a DOMS/SAA system was investigated by Nie and coworkers using dynamic vapor sorption tests over a wide range of environmental temperatures, and was compared with that of a DGEBA/SAA system (Nie

et al. 2013). The results showed that the moisture permeation in LCER is slower than that in the amorphous epoxy resin. This was attributed to the ordered, closely-packed structure of the smectic phase formed upon curing, which creates a strong barrier toward the water permeation. In the case of the DGEBA/SAA system, the amorphous structure of the epoxy monomer poses less restriction to the passing water molecules.

1.5 Orientation

One of the most interesting properties of LCERs is their ability to be oriented under external fields, which can result in materials with anisotropic properties. Generally, the orientation of LCERs can be achieved by applying external forces in the early stage of the curing reaction when viscosity of the system is low. Subsequent crosslinking reaction will stabilize the LC phases as well as their orientation. Various techniques have been utilized to produce orientation LCERs, including mechanical field orientation (Hikmet and Broer 1991; Barclay et al. 1992b; Shiota and Ober 1998; Broer and Mol 1991; Lee and Jang 2007; Lee 2006b), electric field orientation (Korner et al. 1996; Koerner et al. 2011; Shiota and Ober 1997c), and magnetic field orientation (Pottie et al. 2008; Castell et al. 2003; Jahromi 1994; Jahromi et al. 1995; Tan et al. 2000; Li and Kessler 2013; Harada et al. 2003, 2004b; Lincoln and Douglas 1999; Benicewicz et al. 1998).

1.5.1 *Electric Field Orientation*

Because of the dielectric anisotropy, LC molecules show active response to an electric field. An early work performed by Korner and coworkers demonstrated the ability of orienting liquid crystalline dicyanate using electric field. Later the technique was applied on a phenyl benzoate based LCER system. The curing reaction was conducted under the influence of alternating electric fields. It was found that the LC domains can be aligned perpendicular to the electric field. After alignment the material showed anisotropic thermal expansion behavior. In the glassy region, a negative coefficient of thermal expansion (CTE) was observed in the direction of orientation, which was attributed to the highly ordered networks.

1.5.2 *Magnetic Field Orientation*

Compared to electric field orientation, the use of magnetic fields to align LCERs has been extensively investigated and has proven to be an effective way of tailoring the physical and mechanical properties of the resins. The driving force for the

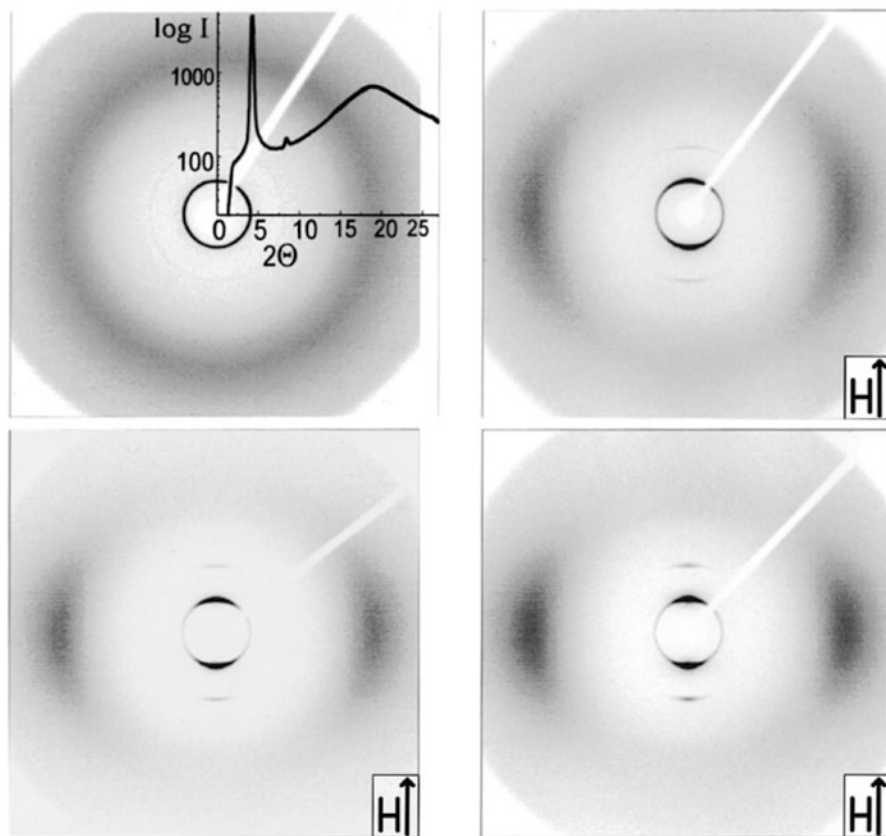


Fig. 1.10 Effect of magnetic field strength on X-ray diffraction patterns of the LCERs. *Top left:* 0 T; *top right:* 3 T; *bottom left:* 9 T; *bottom right:* 18 T. Reprinted from Ref. (Benicewicz et al. 1998), Copyright (1998), with permission from American Chemical Society

orientation of LC molecules under magnetic fields is their anisotropic diamagnetic susceptibility, which forces the molecules to align themselves along the field direction to reduce free energy. A detailed study was performed by Benicewicz et al. on DOMS/SAA system (Benicewicz et al. 1998). The orientation of the LCER was characterized using two-dimensional X-ray diffraction. The effect of magnetic field strength on degree of orientation and related mechanical properties was examined as shown in Fig. 1.10.

An order parameter of 0.8 was achieved for the resin cured under a 12 T magnetic field. The tensile modulus of the resulting resin was 8.1 GPa compared to 3.1 GPa of unoriented resins. A significant reduction of CTE was also observed in the direction of orientation. The effect of curing agent on the alignment of LCERs was investigated by Pottie and coworkers (Pottie et al. 2008). They found the LCERs obtained from aliphatic amine curing agents exhibited lower degree of orientation compared to those cured with aromatic amines. This was ascribed to the

higher reactivity of the aliphatic amines which prevented the alignment of the mesogens.

1.6 Conclusions and Perspectives

LCERs are a novel class of thermosetting materials combining the useful benefits of epoxy resins and liquid crystals. In spite of their outstanding properties, only a few studies have investigated the potential use of LCERs as matrices for high performance composites or nanocomposites. In addition, systematic studies on orientation of LCERs using external fields are necessary to fully understand and exploit the outstanding properties after alignment.

References

- Amendola E, Carfagna C, Giamberini M, Pisaniello G (1995) Curing reactions of a liquid crystalline epoxy resins based on the diglycidyl ether of 4,4'-dihydroxy- α -methylstilbene. *Macromol Chem Phys* 196(5):1577–1591
- Barclay GG, Ober CK (1993) Liquid-crystalline and rigid-rod networks. *Prog Polym Sci* 18 (5):899–945
- Barclay GG, Ober CK, Papathomas KI, Wang DW (1992a) Rigid-rod thermosets based on 1,3,5-triazine-linkd aromatic ester segments. *Macromolecules* 25(11):2947–2954
- Barclay GG, Ober CK, Papathomas KI, Wang DW (1992b) Liquid crystalline epoxy thermosets based on dihydroxymethylstilbene—synthesis and characterization. *J Polym Sci A Polym Chem* 30(9):1831–1843
- Benicewicz BC, Smith ME, Earls JD, Priester RD, Setz SM, Duran RS, Douglas EP (1998) Magnetic field orientation of liquid crystalline epoxy thermosets. *Macromolecules* 31 (15):4730–4738
- Broer DJ, Mol GN (1991) Anisotropic thermal expansion of densely cross-linked oriented polymer networks. *Polym Eng Sci* 31(9):625–631
- Broer DJ, Lub J, Mol GN (1993) Synthesis and photopolymerization of a liquid crystalline diepoxide. *Macromolecules* 26(6):1244–1247
- Cai ZQ, Sun JZ, Wang DD, Zhou QY (2007) Studies on curing kinetics of a novel combined liquid crystalline epoxy containing tetramethylbiphenyl and aromatic ester-type mesogenic group with diaminodiphenylsulfone. *J Polym Sci A Polym Chem* 45(17):3922–3928
- Carfagna C, Amendola E, Giamberini M, Filippov AG, Bauer RS (1993) Curing kinetics of liquid crystalline epoxy resins. *Liq Cryst* 13(4):571–584
- Carfagna C, Amendola E, Giamberini M (1997) Liquid crystalline epoxy based thermosetting polymers. *Prog Polym Sci* 22(8):1607–1647
- Castell P, Serra A, Galia M, Giamberini M, Carfagna C (2003) Anisotropic thermosets from liquid-crystalline azomethynic epoxy resins and primary aromatic diamines. *J Polym Sci A Polym Chem* 41(1):1–12
- Cho SH, Douglas EP (2002) Gelation and development of liquid crystalline order during cure of a rigid-rod epoxy. *Macromolecules* 35(11):4550–4552
- Cho SH, Lee JY, Douglas EP, Lee JY (2006a) Synthesis and thermal properties of liquid crystalline thermoset containing rigid-rod epoxy. *High Perform Polym* 18(1):83–99

- Cho S, Douglas EP, Lee JY (2006b) Transition diagrams for a liquid crystalline thermoset containing a rigid-rod epoxy. *Polym Eng Sci* 46(5):623–629
- Choi EJ, Ahn HK, Lee JK, Jin JI (2000) Liquid crystalline twin epoxy monomers based on azomethine mesogen: synthesis and curing with aromatic diamines. *Polymer* 41(21):7617–7625
- Douglas EP (2002) Liquid crystalline thermosets, *Encyclopedia of polymer science and technology*. Wiley, New York
- Gao ZY, Yu YF, Xu YZ, Li SJ (2007) Synthesis and characterization of a liquid crystalline epoxy containing azomethine mesogen for modification of epoxy resin. *J Appl Polym Sci* 105(4):1861–1868
- Gennes PGD, Prost J (1995) *The physics of liquid crystals*. Clarendon Press, Oxford
- Giamberini M, Amendola E, Carfagna C (1995) Liquid crystalline epoxy thermosets. *Mol Cryst Liq Cryst Sci Technol A Mol Cryst Liq Cryst* 266:9–22
- Harada M, Ochi M, Tobita M, Kimura T, Ishigaki T, Shimoyama N, Aoki H (2003) Thermal-conductivity properties of liquid-crystalline epoxy resin cured under a magnetic field. *J Polym Sci B Polym Phys* 41(14):1739–1743
- Harada M, Aoyama K, Ochi M (2004a) Fracture mechanism of liquid-crystalline epoxy resin system with different phase structures. *J Polym Sci B Polym Phys* 42(22):4044–4052
- Harada M, Ochi M, Tobita M, Kimura T, Ishigaki T, Shimoyama N, Aoki H (2004b) Thermomechanical properties of liquid-crystalline epoxy networks arranged by a magnetic field. *J Polym Sci B Polym Phys* 42(5):758–765
- Harada M, Watanabe Y, Tanaka Y, Ochi M (2006) Thermal properties and fracture toughness of a liquid-crystalline epoxy resin cured with an aromatic diamine crosslinker having a mesogenic group. *J Polym Sci B Polym Phys* 44(17):2486–2494
- Harada M, Sumitomo K, Nishimoto Y, Ochi M (2009) Relationship between fracture toughness and domain size of liquid-crystalline epoxy resins having polydomain structure. *J Polym Sci B Polym Phys* 47(2):156–165
- Harada M, Okamoto N, Ochi M (2010) Fracture toughness and fracture mechanism of liquid-crystalline epoxy resins with different polydomain structures. *J Polym Sci B Polym Phys* 48(22):2337–2345
- Harada M, Ando J, Hattori S, Sakurai S, Sakamoto N, Yamasaki T, Masunaga H, Ochi M (2013) In-situ analysis of the structural formation process of liquid-crystalline epoxy thermosets by simultaneous SAXS/WAXS measurements using synchrotron radiation. *Polymer Journal* 45(1):43–49
- Hikmet RAM, Broer DJ (1991) Dynamic mechanical properties of anisotropic networkers formed by liquid crystalline acrylates. *Polymer* 32(9):1627–1632
- Hikmet RAM, Lub J, Vanderbrink PM (1992) Structure and mobility within anisotropic networks obtained by photopolymerization of liquid crystal molecules. *Macromolecules* 25(16):4194–4199
- Holter D, Frey H, Mulhaupt R, Klee JE (1996) Liquid crystalline thermosets based on branched bismethacrylates. *Macromolecules* 29(22):7003–7011
- Hoyt AE, Benicewicz BC (1990a) Rigid rod molecules as liquid crystal thermosets. I. rigid rod amides. *J Polym Sci A Polym Chem* 28(12):3403–3415
- Hoyt AE, Benicewicz BC (1990b) Rigid rod molecules as liquid crystal thermosets. II. Rigid rod esters. *J Polym Sci A Polym Chem* 28(12):3417–3427
- Jahromi S (1994) Liquid crystalline epoxide thermosets—a deuterium nuclear-magnetic-resonance study. *Macromolecules* 27(10):2804–2813
- Jahromi S, Lub J, Mol GN (1994) Synthesis and photoinitiated polymerization of liquid crystalline diepoxide. *Polymer* 35(3):622–629
- Jahromi S, Kuipers WAG, Norder B, Mijs WJ (1995) Liquid crystalline epoxide thermosets—dynamic mechanical and thermal properties. *Macromolecules* 28(7):2201–2211
- Koerner H, Ober CK, Ku H (2011) Probing electric field response of LC thermosets via time-resolved X-ray and dielectric spectroscopy. *Polymer* 52(10):2206–2213

- Korner H, Shiota A, Bunning TJ, Ober CK (1996) Orientation-on-demand thin films: curing of liquid crystalline networks in ac electric fields. *Science* 272(5259):252–255
- Lee JY (2006a) The effect of substituent on the anisotropic orientation of liquid crystalline epoxy compounds. *Polym Bull* 57(6):983–988
- Lee JY (2006b) Transverse alignment of liquid crystalline epoxy resin on carbon fiber surface. *J Appl Polym Sci* 102(1):684–689
- Lee JY, Jang JS (1998) Effect of substituents on the curing of liquid crystalline epoxy resin. *J Polym Sci A Polym Chem* 36(6):911–917
- Lee JY, Jang JS (1999) Synthesis and curing of liquid crystalline epoxy resin based on naphthalene mesogen. *J Polym Sci A Polym Chem* 37(4):419–425
- Lee JY, Jang JS (2006) The effect of mesogenic length on the curing behavior and properties of liquid crystalline epoxy resins. *Polymer* 47(9):3036–3042
- Lee JY, Jang J (2007) Anisotropically ordered liquid crystalline epoxy network on carbon fiber surface. *Polym Bull* 59(2):261–267
- Lee JY, Jang JS, Hwang SS, Hong SM, Kim KU (1998) Synthesis and curing of liquid crystalline epoxy resins based on 4,4'-biphenol. *Polymer* 39(24):6121–6126
- Lee JY, Song YW, Shim MJ (2004) Reaction kinetics of liquid crystalline epoxy (LCE) with azomethine cured with diamine. *J Ind Eng Chem* 10(4):601–607
- Li YZ, Kessler MR (2013) Liquid crystalline epoxy resin based on biphenyl mesogen: Effect of magnetic field orientation during cure. *Polymer* 54(21):5741–5746
- Li Y, Kessler M (2014a) Cure kinetics of liquid crystalline epoxy resins based on biphenyl mesogen. *J Therm Anal Calorim* 117(1):481–488
- Li Y, Kessler MR (2014b) Creep-resistant behavior of self-reinforcing liquid crystalline epoxy resins. *Polymer* 55(8):2021–2027
- Li YZ, Badrinarayanan P, Kessler MR (2013) Liquid crystalline epoxy resin based on biphenyl mesogen: Thermal characterization. *Polymer* 54(12):3017–3025
- Lin QH, Yee AF, Earls JD, Hefner RE, Sue HJ (1994) Phase transformation of a liquid crystalline epoxy during curing. *Polymer* 35(12):2679–2682
- Lin QH, Yee AF, Sue HJ, Earls JD, Hefner RE (1997) Evolution of structure and properties of a liquid crystalline epoxy during curing. *J Polym Sci B Polym Phys* 35(14):2363–2378
- Lincoln DM, Douglas EP (1999) Control of orientation in liquid crystalline epoxies via magnetic field processing. *Polym Eng Sci* 39(10):1903–1912
- Litt MH, Whang WT, Yen KT, Qian XJ (1993) Cross-linked liquid crystal networks from liquid crystalline monomers—synthesis and mechanical properties. *J Polym Sci A Polym Chem* 31(1):183–191
- Liu JP, Wang CC, Campbell GA, Earls JD, Priester RD (1997) Effects of liquid crystalline structure formation on the curing kinetics of an epoxy resin. *J Polym Sci A Polym Chem* 35(6):1105–1124
- Liu GD, Gao JG, Song LL, Hou WJ, Zhang LC (2006) Synthesis and curing of liquid-crystalline epoxy resins containing a biphenyl mesogen. *Macromol Chem Phys* 207(23):2222–2231
- Liu YL, Cai ZQ, Wang WC, Wen XF, Pi PH, Zheng DF, Cheng JA, Yang ZR (2011) Mechanical properties and morphology studies of thermosets from a liquid-crystalline epoxy resin with biphenol and aromatic ester groups. *Macromol Mater Eng* 296(1):83–91
- Lu MG, Shim MJ, Kim SW (2001) Curing reaction and phase change in a liquid crystalline monomer. *Macromol Chem Phys* 202(2):223–230
- Mallon JJ, Adams PM (1993) Synthesis and characterization of novel epoxy monomers and liquid-crystal thermosets. *J Polym Sci A Polym Chem* 31(9):2249–2260
- Micco G, Giamberini M, Amendola E, Carfagna C, Astarita G (1997) Modeling of curing reaction kinetics in liquid-crystalline epoxy resins. *Ind Eng Chem Res* 36(8):2976–2983
- Mittelau A, Cascaval CN (2005) Liquid crystalline epoxy thermoset obtained from biphenyl mesogen. *Polym Plast Technol Eng* 44(1):151–162

- Mititelu A, Hamaide T, Novat C, Dupuy J, Cascaval CN, Simionescu BC, Navard P (2000) Curing kinetics of liquid-crystalline epoxy resins with inverse reactivity ratios. *Macromol Chem Phys* 201(12):1209–1213
- Mormann W, Brocher M (1996) “Liquid crystalline” thermosets from 4,4'-bis(2,3-epoxypropoxy) biphenyl and aromatic diamines. *Macromol Chem Phys* 197(6):1841–1851
- Mormann W, Kuckertz C (1998) Liquid crystalline cyanurate thermosets through cyclotrimerisation of novel triaromatic dicyanates. *Macromol Chem Phys* 199(5):845–851
- Mormann W, Zimmermann J (1995) Synthesis and mesogenic properties of diaromatic cyanate and isocyanate-monomers for liquid crystalline thermosets. *Liq Cryst* 19(2):227–233
- Mormann W, Zimmermann JG (1996) Liquid crystalline thermosets through cyclotrimerization of diaromatic dicyanates. *Macromolecules* 29(4):1105–1109
- Nie L, Burgess A, Ryan A (2013) Moisture permeation in liquid crystalline epoxy thermosets. *Macromol Chem Phys* 214(2):225–235
- Ochi M, Tsuyuno N, Sakaga K, Nakanishi Y, Murata Y (1995) Effect of network structure on thermal and mechanical properties of biphenyl type epoxy resins cured with phenols. *J Appl Polym Sci* 56(9):1161–1167
- Ortiz C, Kim R, Rodighiero E, Ober CK, Kramer EJ (1998) Deformation of a polydomain, liquid crystalline epoxy-based thermoset. *Macromolecules* 31(13):4074–4088
- Ortiz C, Belenky L, Ober CK, Kramer EJ (2000) Microdeformation of a polydomain, smectic liquid crystalline thermoset. *J Mater Sci* 35(8):2079–2086
- Pottier L, Costa-Torro F, Tessier M, Davidson P, Fradet A (2008) Investigation of anisotropic epoxy-amine thermosets synthesised in a magnetic field. *Liq Cryst* 35(8):913–924
- Rosu D, Mititelu A, Cascaval CN (2004) Cure kinetics of a liquid-crystalline epoxy resin studied by non-isothermal data. *Polym Test* 23(2):209–215
- Shiota A, Ober CK (1996) Synthesis and curing of novel LC twin epoxy monomers for liquid crystal thermosets. *J Polym Sci A Polym Chem* 34(7):1291–1303
- Shiota A, Ober CK (1997a) Rigid rod and liquid crystalline thermosets. *Prog Polym Sci* 22(5):975–1000
- Shiota A, Ober CK (1997b) Analysis of smectic structure formation in liquid crystalline thermosets. *Polymer* 38(23):5857–5867
- Shiota A, Ober CK (1997c) Orientation of liquid crystalline epoxides under ac electric fields. *Macromolecules* 30(15):4278–4287
- Shiota A, Ober CK (1998) Smectic networks obtained from twin LC epoxy monomers—mechanical deformation of the smectic networks. *J Polym Sci B Polym Phys* 36(1):31–38
- Su WFA (1993) Thermoplastic and thermoset main-chain liquid crystal polymers prepared from biphenyl mesogen. *J Polym Sci A Polym Chem* 31(13):3251–3256
- Su WFA, Chen KC, Tseng SY (2000) Effects of chemical structure changes on thermal, mechanical, and crystalline properties of rigid rod epoxy resins. *J Appl Polym Sci* 78(2):446–451
- Sue HJ, Earls JD, Hefner RE (1997a) Fracture behaviour of liquid crystal epoxy resin systems based on the diglycidyl ether of 4,4'-dihydroxy- α -methylstilbene and sulphanilamide.1. Effects of curing variations. *J Mater Sci* 32(15):4031–4037
- Sue HJ, Earls JD, Hefner RE (1997b) Fracture behaviour of liquid crystal epoxy resin systems based on diglycidyl ether of 4,4'-dihydroxy- α -methylstilbene.2. Effect due to blending with TACTIX* 556 epoxy resin and phenolic monomers. *J Mater Sci* 32(15):4039–4046
- Tan CB, Sun H, Fung BM, Grady BP (2000) Properties of liquid crystal epoxy thermosets cured in a magnetic field. *Macromolecules* 33(17):6249–6254
- Vyazovkin S, Mititelu A, Sbirrazzuoli N (2003) Kinetics of epoxy-amine curing accompanied by the formation of liquid crystalline structure. *Macromol Rapid Commun* 24(18):1060–1065
- Zhang YX, Vyazovkin S (2006) Comparative cure behavior of DGEBA and DGEBP with 4-nitro-1,2-phenylenediamine. *Polymer* 47(19):6659–6663

Chapter 2

Structure and Phase Transitions of Polymer Liquid Crystals, Revealed by Means of Differential Scanning Calorimetry, *Real-Time* Synchrotron WAXD, MAXS and SAXS and Microscopy

Ginka Exner, Ernesto Pérez, and Manya Krasteva

2.1 Introduction

Liquid-crystalline polymers (LCPs) or Polymer liquid-crystals (Barón 2001; Barón and Stepto 2002) constitute an important class of materials. In the last years they regain the scientific interest especially in relation with the synthesis of bio-inspired and smart materials (Liu et al. 2013; Moritsugu et al. 2011; Ahir et al. 2006; Li et al. 2012; Lee and White 2012). For instance, low surface energy LCPs possessing high hydrophobicity and lipophobicity (Martinelli et al. 2010) or hydrophobicity and oleophobicity (Caillier et al. 2008) are synthesized, mimicking the plant leaf and fruit surfaces. Another direction, which gives a push to new LCPs developments is the need for sustainable materials based on renewable raw materials such as cellulose and starch, which are abundant and biodegradable (Huang and Shi 2012; Hu et al. 2010; Waigh et al. 1998, 2000). LCPs are not far from the state of the art efforts to design nanomaterials, in which the self-assembling of LCPs might be utilized to improve the dispersion of the carbon based nanoparticles and to orient them inside the LCP bulk (Pisitsak et al. 2012; Ji et al. 2010; Okano et al. 2010; Kim 2009). They might also govern the properties of amphiphiles, polymers and proteins

G. Exner (✉)

Department of Experimental Physics, Faculty of Physics, Plovdiv University,
“Paisii Hilendarski”, 24 Tzar Asen Str., Plovdiv 4000, Bulgaria
e-mail: ginka.exner@gmail.com

E. Pérez

Instituto de Ciencia y Tecnología de Polímeros (CSIC), 3 Juan de la Cierva,
Madrid 28006, Spain
e-mail: ernestop@ictp.csic.es

M. Krasteva

Department of General Physics, Faculty of Physics, Sofia University “St. Kliment Ohridski”,
5 James Bourchier Blvd., Sofia 1164, Bulgaria
e-mail: manya.nikolaeva.krasteva@yahoo.com

at the interface with them (Lockwood et al. 2008). LCPs play also an important role in the development of high performance materials. To this aim composites, copolymers and blends with PLCs are fabricated (Álvarez et al. 2007; Ma et al. 2007; Georgiev et al. 2005; Du et al. 2005), already existing LCPs are chemically modified (Wei et al. 2014) or new LCPs are synthesized (Al-Muaiikel and Aly 2013; Fang et al. 2013; Petr and Hammond 2011; Mcculloch et al. 2006).

The broad spectrum of applications of LCPs, the complex demands for material properties depending on the particular application, and the well-known structure-properties relationship require reliable and detailed analysis of the structure and the phase transitions of LCPs to be made. Taking into account the vast number of existing liquid crystalline (LC) phases, their strong dependence on molecular weight, spacer length and its structure, polydispersity, tacticity and specific experimental conditions (temperature, pressure or cooling/heating rate) (Katerska et al. 2010; Takahashi et al. 2014; Rodríguez-Amor et al. 2008; Chiferii et al. 1982), the phase behavior of PLCs may be rather complex. Hence, only technique is insufficient to reliably meet such demands and various experimental methods, such as real-time X-ray scattering, differential scanning calorimetry (DSC) and microscopy (polarized (POM), scanning electron (SEM), transmission electron or atom force (AFM)) are needed for the correct interpretation of the nature and the behavior of the LCPs.

This chapter presents some of the possibilities to combine different techniques and explains in details the characteristics which can be derived from the raw data whose knowledge can be used to reveal the overall picture of the structure and the phase transitions of two thermotropic LCPs: Poly(hexane-1,7-diyil-4,4'-biphenyldicarboxylate) (P6MB), and Poly(heptane-1,7-diyil-4,4'-biphenyldicarboxylate) (P7MB).

2.2 Thermotropic Liquid Crystals

Liquid crystals are known to exhibit mesomorphic properties i.e., together with other two families of related substances (plastic crystals and condis crystals) their molecular order occupies position between real crystals and ordinary liquids (Wunderlich 2005; Barón and Stepto 2002; Barón 2001; Collier 1992). Liquid crystals can be classified: (a) according to their molar mass as low-molar-mass (or molecular liquid crystals) and polymer liquid crystals; (b) depending on the specific conditions, at which liquid crystallinity appears they may be lyotropic (LC phases are displayed when amphiphilic molecules are dissolved in solvents), thermotropic (LC behavior is caused by temperature variation), barotropic (LC behavior is exhibited at pressure variation), enantiotropic (when the LC is stable over definite temperature or pressure range), amphitropic (material which could exhibit both thermotropic and lyotropic mesophases) and monotropic (when the mesophase is metastable and is formed by undercooling an isotropic melt or an enantiotropic mesophase at given pressure); (c) depending on the degree of order

(see below); (d) depending on the architecture of their chemical structure, where one distinguishes more than 20 different classes.

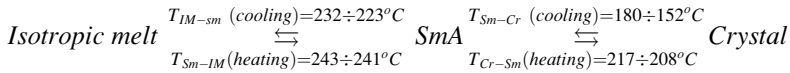
The real three dimensional crystallinity requires three types of order to be present: (a) orientational—the molecules are aligned along a well defined spatial direction (called director); (b) translational—when the system is invariant with respect to space translations by an integer number; (c) bond-orientational order—when the direction of the lines, connecting any two adjacent molecules is preserved over a long distances. LC phases are less ordered compared to the real crystals and they are divided into three main groups: (a) nematics, which possess only orientational order; (b) smectics, which display orientational and translational order in at least one direction; (c) cholesterics, which possess orientational order and translational order in one direction and in addition some persistent angle of inclination of the average molecular axis from layer to layer. This classification should be considered in a general sense, since for instance some highly ordered smectic phases with bond orientational order, such as SmF, SmE, SmB, SmI, also exist (Martinelli et al. 2010; Yoon et al. 1997).

Even after so many years of investigations, the nature of the liquid crystallinity is still not completely understood. It seems to be proven that liquid crystallinity appears when the molecules possess asymmetry in their shape but also electrical, steric, biphylic and flexibility molecular asymmetry (Petrov 1999). In low-molar-mass compounds LC phases appear as a consequence of such asymmetry only, whereas in polymers the LC behavior originates from the balance between the molecular segments possessing asymmetry, called mesogens or mesogenic groups (Barón and Stepto 2002), and the overall polymer conformation. Depending on the way the mesogens are attached to the polymer chain, LCPs are divided into several main groups: main-chain LCPs, where the mesogens are incorporated into the polymer backbone so that two consecutive mesogens are interconnected via flexible part, called spacer; side-chain, where the mesogens are attached to the polymer as pendants; combined main-chain/side-chain, where mesogens are in both positions (Yang et al. 2012); and newly developed class of mesogen-jacked, where the central rigid portion of the LC side groups are laterally attached to the backbone chain without or with only very short flexible spacers (Chen et al. 2010; Guan et al. 2009).

In order to illustrate the essential advantages of using complex of techniques in the investigation of the structure and phase transitions, examples with main-chain thermotropic liquid crystalline polyesters, with biphenyl mesogen, are given. Even though very extensive studies were carried out and recent considerable progress in establishing the structure-properties relationship has been achieved on such LCPs, depending on their chemical structure of the spacer (with varying flexibility and length), the molar mass, copolymerization, and cooling rate (Takahashi et al. 2014; Martínez-Gómez et al. 2010; Katerska et al. 2010; Ranganathan and Ramesh 2006; Watanabe et al. 1997; Rodríguez-Amor et al. 2008) to fulfil the purpose of this chapter two representatives, with very simple structure were chosen. These LCPs consist of biphenyl unit as a mesogen and flexible spacer with 6 (for P6MB) and 7 (for P7MB) methylene units. Details on polymer preparation can be found elsewhere (Bello et al. 1993). The synthesised in our laboratory LCPs were:

P7MB which intrinsic viscosity, measured in chloroform at 25 °C amounts to 1.03 dL/g and that of P6MB—0.9 dL/g.

Upon cooling from an isotropic melt (IM) state, P6MB forms Smectic A (SmA) LC phase. The smectic structure is stable only within a limited temperature interval and further cooling causes its partial crystallization. Upon subsequent heating, the crystalline (Cr) phase transforms back into Smectic, showing the enantiotropic behavior of the SmA phase, which melts at elevated temperature (Katerska et al. 2010):



Upon cooling, P7MB also exhibits Smectic type of order (at about 150 °C) but in this case Smectic CA phase is observed (SmCA) (Pérez et al. 2003). This peculiar phase is characterized by constant angle of inclination of the mesogens with respect to the normal to the mesogenic layers, but the inclination is in opposite direction in each neighboring layer (Watanabe et al. 1997). The smectic phase crystallizes upon further cooling (at about 140 °C). Subsequent heating causes the P7MB crystalline phase to melt directly at about 167 °C, showing the monotropic behavior of the SmCA phase in this LCP.

Thus, the difference in one methylene unit in the spacer between P6MB and P7MB leads to significant changes in their thermal behavior and type of LC phase.

2.3 Differential Scanning Calorimetry

According to the first law of thermodynamics which accounts for the conservation of energy:

$$\Delta U = \delta Q + \delta A, \quad (2.1)$$

where ΔU is the change in the internal energy of the system; δQ is the heat added to the system; δA is the work performed on the system and $\delta A = - p.dV$ (p denotes pressure, V —volume).

The definition of enthalpy is:

$$H = U + p.V, \quad (2.2)$$

where U is the internal energy of the system; p is the pressure; V is the volume.

The enthalpy change is then described by:

$$\Delta H = \Delta U + \Delta(p.V) \quad (2.3)$$

$$\Delta H = \Delta U + \Delta p.V + p.\Delta V \quad (2.4)$$

Using (2.1) one gets:

$$\Delta H = \delta Q - p.\Delta V + (\Delta p.V + p.\Delta V) \quad (2.5)$$

Finally, after cancelling some of the terms:

$$\Delta H = \delta Q + \Delta p.V \quad (2.6)$$

During DSC experiments the pressure is constant ($\Delta p = 0$), hence (2.6) transforms to:

$$\Delta H(p = const) = \delta Q \quad (2.7)$$

Equation (2.7) shows that by means of DSC one measures the heat necessary for the system to undergo a phase transition. It is well known that most of the LC transitions are first order phase transitions, i.e., generation or absorption of heat takes place, making the DSC method one of the very adequate means for investigation of their phase transitions. The main advantage of DSC is that it is rapid and requires a small amount of the substance (typically several milligrams). The basis equipment and the main principles of DSC can be found in some general readings (Wunderlich 2005; Bershtein and Egorov 1994; Hatakeyama and Quinn 1999).

The main parameters that can be derived from DSC, concerning the phase transitions of LCPs are (Wunderlich 2005; Bershtein and Egorov 1994; Hatakeyama and Quinn 1999):

- Onset temperature of the phase transition, T_0 . This is the temperature, at which the heat capacity (C_p) trace diverges from the base line, indicating the beginning of the phase transition;
- End-temperature of the phase transition, T_{end} . This is the temperature at the end of the DSC peak, where C_p trace still diverges from the base line;
- Temperature of the phase transition, T_x , usually measured at the maximum of the DSC endo- or exotherms. Index x denotes the type of the transition. For instance when the transition is from Isotropic melt to Smectic LC phase x is expressed as *IM-Sm*;
- Temperature interval of the phase transition, ΔT_x with x having the same meaning as above. This is the temperature span between the onset and the end temperatures of the DSC peak;
- Enthalpy of the phase transition, ΔH_x with x having the same meaning as above. The enthalpy is proportional to the integral area of the DSC peak.

DSC is also appropriate for investigations of phase transition kinetics both at isothermal and at non-isothermal conditions. At isothermal conditions the Avrami equation is usually applied, whereas at non-isothermal conditions one has the choice among several existing methods. Even though these methods were originally

developed for polymers, since LCP phase transitions still describe disorder-order transformation in polymers, they can be applied in describing the LCP phase transitions.

2.3.1 Phase Transition at Isothermal Conditions

Isothermal kinetics investigations are based on DSC traces, recorded at different constant temperatures. This is accomplished by fast jump from high temperature (or glassy state), at which the LCP is in isotropic melt (or glassy) state, to the desired iso-temperature (T_{iso}). Then DSC curves are recorded with time. Figure 2.1a shows such DSC curves for P7MB at iso-temperatures, at which IM-Sm phase transition from melt takes place (Todorova et al. 2004a). As explained by Mezghani and Phillips (Mark 1996), the Avrami equation was derived from prior work by Poisson devoted to waves created by raindrops on a pond leading to the following equation:

$$\alpha(t) = 1 - \exp(-K \cdot t^n), \quad (2.8)$$

where $\alpha(t)$ is the mass (or volume) fraction of the LCP which is already in the LC phase; K is Avrami rate constant, which describes the overall rate of transformation; n denotes the Avrami index. n is integer in the ideal case.

Both parameters K and n characterize the nucleation type and growth geometry, as summarized in Table 2.1. The model considers two distinct cases: (a) homogeneous nucleation (thermal nuclei) with constant nucleation rate ($\dot{N} = \text{const}$), where the nuclei evolve continuously in space with time; (b) heterogeneous nucleation (athermal nuclei) with constant nucleation density ($\dot{N} = \text{const}$), where the nuclei growth is instantaneous at the very beginning of the process and the nuclei size increases with time until the boundaries come into contact entirely filling the space. Avrami equation treats only the time span between nucleation and filled space, called primary crystallization. The subsequent processes, called secondary crystallization, cannot be described by Avrami's formalism.

Important parameters, in Avrami analysis for the phase transition kinetics, in addition to n and K , are the half-time ($t_{1/2}$), time at maximum (t_{max}), and linear growth rate (G). $t_{1/2}$ denotes the time at which half of the material has been already transformed into the new phase. t_{max} is determined by the maximum of the transformational rate. Both times could be deduced for instance directly by modeling the DSC peak with an appropriate function (typically Gaussian, when the degree of undercooling is small and the peak has symmetric shape or Asymmetric-double-sigmoidal otherwise) assigning them to the position of the gravity center and the maximum, respectively. The corresponding values for P7MB, denoted as $t_{1/2}^g$ and $t_{\text{max}}^{\text{DSC}}$, are listed in Table 2.2. Another possibility to derive these constants from theoretical predictions is based on Avrami parameters (Qui et al. 2000):

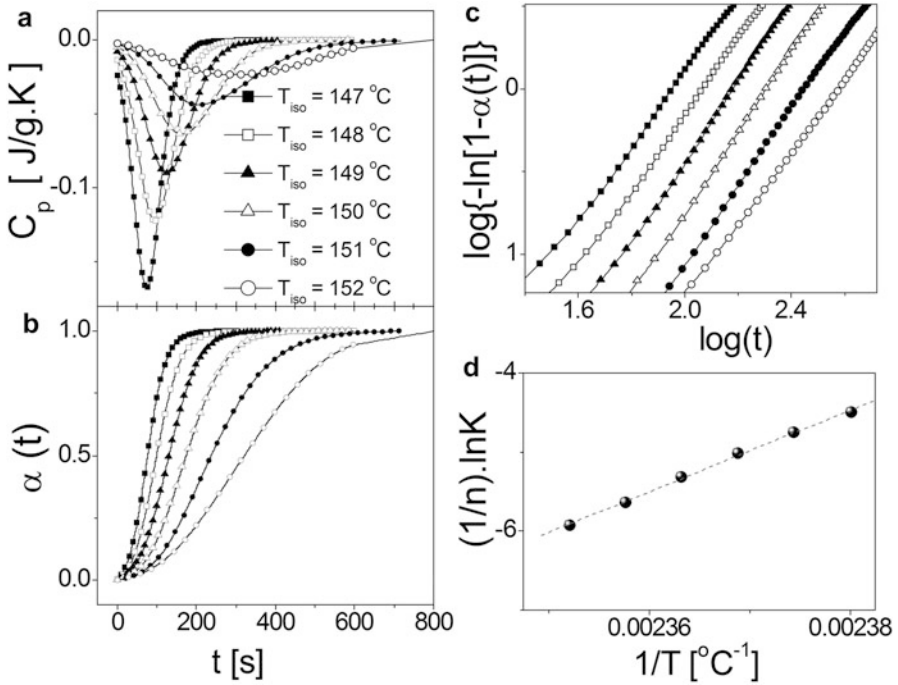


Fig. 2.1 Isothermal DSC experiments on P7MB at different temperatures 147 °C—*solid squares*, 148 °C—*open squares*, 149 °C—*solid triangles*, 150 °C—*open triangles*, 151 °C—*solid circles*, 152 °C—*open circles*: (a) DSC runs; (b) Normalized degree of transformation; and (c) Avrami plots (presenting the dependence from $\alpha(t)=0.1$ to $\alpha(t)=0.9$); (d) Plot for activation energy calculation

Table 2.1 Avrami index (n) and Avrami rate constant (K) values for the different types of growing geometries

Shape of the growing crystal	Nucleation mode	n	K
Rod	Heterogeneous	1	NGA
	Homogeneous	2	GA/\dot{N}^2
Disc	Heterogeneous	2	$\pi NG^2 D$
	Homogeneous	3	$(\pi/3)G^2 \dot{N} D$
Sphere	Heterogeneous	3	$(4\pi/3)NG^3$
	Homogeneous	4	$(\pi/3)\dot{N}G^3$
Sheaf	Heterogeneous	5	—
	Homogeneous	6	—

A constant area of the rod, D thickness of the disc, G linear growth rate, N nucleation density, \dot{N} nucleation rate (Mark 1996)

Table 2.2 Avrami kinetics parameters for IM-Sm phase transition in P7MB

Parameter	T _{iso} [°C]					
	147	148	149	150	151	152
n	2.29	2.35	2.49	2.49	2.35	2.22
K ^{1/n} [s ⁻¹]	1.1 × 10 ⁻³	8.7 × 10 ⁻³	6.4 × 10 ⁻³	4.9 × 10 ⁻³	3.6 × 10 ⁻³	2.6 × 10 ⁻³
t _{1/2} ^g [s]	76	101	132	178	249	324
t _{1/2} ^α [s]	77	100	131	174	236	308
t _{1/2} ^t = (ln2/K) ^{1/n} [s]	76	100	131	175	240	319
G ^g [s ⁻¹]	0.0131	0.0099	0.0076	0.0056	0.0040	0.0031
G ^α [s ⁻¹]	0.0130	0.0100	0.0076	0.0058	0.0042	0.0033
G ^t [s ⁻¹]	0.0131	0.0100	0.0076	0.0057	0.0042	0.0031
t _{max} ^{DSC} [s]	75	96	126	163	207	292
t _{max} ^t = ((n-1)/n.K) ^{1/n} [s]	70	92	123	163	219	283
G _{max} ^{DSC} [s ⁻¹]	0.0133	0.0104	0.0079	0.0061	0.0048	0.0034
G _{max} ^t [s ⁻¹]	0.0143	0.0109	0.0081	0.0061	0.0046	0.0035
ΔH _{IM-Sm} [kJ/mol]	5.1	4.8	4.5	4.2	4.1	3.3

Avrami index (n), Avrami rate constant (K), half-time (t_{1/2}), time at maximum (t_{max}), and linear growth rate (G), obtained by different methods (see text); the last two rows show the enthalpy values of the IM-Sm transition

Values in the table are rounded off based on significant figures

$$t_{1/2} = (\ln 2 / K)^{1/n} \quad (2.9)$$

$$t_{\max} = [(n - 1) / n \cdot K]^{1/n} \quad (2.10)$$

The linear growth rate G is inversely proportional to the time (t_{1/2}^g or t_{max}^{DSC}). It can be obtained either from the time constants, evaluated by direct DSC curve treatment (see Table 2.2 for the G^g and G_{max}^{DSC} values) or from the times calculated according to (2.9) and (2.10), the corresponding values are listed in Table 2.2 as G^t and G_{max}^t.

In practice, Avrami's analysis starts with calculation of the normalized degree of transformation, α(t) (Bershtein and Egorov 1994):

$$\alpha(t_i) = \frac{\int_{t_0}^{t_i} C_p(t) dt}{\int_{t_0}^{t_\infty} C_p(t) dt} = \frac{\int_{t_0}^{t_i} \frac{dH(t)}{dt} dt}{\Delta H}, \quad (2.11)$$

where $C_p(t)$ is heat capacity; $\alpha(t_i)$ denotes the degree of transformation at moment t_i ; ΔH is the full enthalpy of the transition; the integrals denote the enthalpy in the time interval from t_0 to t_i .

The obtained values are then plotted, as shown in Fig. 2.1b. It is possible to obtain $t_{1/2}$ value from such plots, simply by reading the time at $\alpha(t) = 0.5$. The extracted values are listed in Table 2.2 as $t_{1/2}^\alpha$. Further on, there are two possibilities for the analysis, either to fit the curves with (2.8) utilizing special software or to plot the Avrami equation in double logarithmic form:

$$\log\{-\ln[1 - (t)]\} = \log K + n \log t \quad (2.12)$$

As shown in Fig. 2.1c, the dependence $\log\{-\ln[1 - (t)]\}$ versus $\log t$ is linear, where the slope equals Avrami constant and the intercept at $\log t = 0$ gives the $\log K$ value.

As an example, the results for P7MB are summarized in Table 2.2. As it can be seen: (a) the values of n are non-integer. This could mean that the growing morphology has to be considered either as homogeneous growth of cylinders, or homogeneous/heterogeneous growth of discs which cannot be deduced solely on the basis of Avrami analysis; (b) the $t_{1/2}$ and t_{\max} values are the same within the error limits independent of the method used; (c) the $t_{1/2}$ dependence on T_{iso} is exponential; (d) t_{\max} increases with T_{iso} nonlinearly; (e) the process of IM-Sm transition at these temperatures takes place close to the equilibrium, manifested by the symmetrical DSC peaks and hence t_{\max} and $t_{1/2}$ values almost coincide.

Interestingly, the IM-Sm phase transition enthalpies (included also in Table 2.2) were lower in comparison to the Sm-Cr transition (varying with T_{iso} from 5.7 ± 0.2 J/mol.K to 6.5 ± 0.2 J/mol.K), in contrast to the general understanding that the existing partial order facilitates and accelerates the crystallization processes (Zhu and Yan 2001; Li et al. 2003). As will be seen later on, complementary results obtained by X-ray analysis were essential in finding an explanation for this phenomenon.

Another important characteristic of the phase transition is its activation energy, which is given, for thermally driven process by (Cui et al. 2005):

$$\frac{1}{n}(\ln K) = \ln k_0 - \frac{\Delta E}{RT}, \quad (2.13)$$

where n , K are the Avrami parameters; k_0 is a temperature independent pre-exponential factor; ΔE is the activation energy; R is the universal gas constant (8.314 J/(mol.K)); T is temperature (in K).

According to (2.11), the dependence $(1/n) \cdot \ln K$ on $1/T$ has to be linear with a slope of $\Delta E/R$. Fig. 2.1d shows that this equation holds for the IM-Sm phase transition. The activation energy in this case is $\Delta E_{\text{IM-Sm}} = 430$ kJ/mol.

2.3.2 Phase Transition at Non-isothermal Conditions

Isothermal conditions are rarely used in practice so the kinetics investigations under non-isothermal conditions are of practical importance. Several theoretical or semi-empirical models have been developed and thoroughly described in some review articles (Lorenzo and Silvestre 1999; Liu et al. 1997; Long et al. 1995) but very few investigations on PLCs have been undertaken until now (Kumar et al. 2002; Kozlovski 2001; Martins et al. 1998; Gopakumar et al. 1997; Liu and Lee 1995).

For this analysis, DSC traces recorded at different cooling rates are needed. For instance, DSC thermograms showing IM-Sm phase transition of P7MB (Todorova et al. 2004a) at different cooling rates (2, 4, 6, 10 and 20 °C/min) can be recorded, as shown in Fig. 2.2a. The DSC exotherms, after appropriate baseline subtraction, were approximated by Asymmetric-double-sigmoidal functions, which shape accounts for the non-equilibrium conditions of the IM-Sm transition. The peak onset and peak end temperatures define the temperature interval $\Delta T_{\text{IM-Sm}} = (T_{\text{end}} - T_0)$ of the transition, whereas the peak maximum (T_{max}) equals the transition temperature. As an example, the obtained values for P7MB are listed in Table 2.3. T_{max} , T_0 and T_{end} cooling rate dependences follow exponential law. The enthalpy (ΔH) of the process is calculated, based on the integral area of the peak. The IM-Sm transition enthalpy of P7MB amounts to $\Delta H_{\text{IM-Sm}} = 5.1 \pm 0.1$ kJ/mol, independent of the cooling rate. For P6MB, the IM-Sm phase transition takes place at about 85 °C higher temperature compared to P7MB (Katerska et al. 2010) and its enthalpy $\Delta H_{\text{IM-Sm}} = 9.5 \pm 0.2$ kJ/mol is also higher, emphasizing the crucial role of the chemical structure on the thermal properties of thermotropic LCPs. In this particular case, the so called even-odd effect is observed (Watanabe et al. 1997). As at isothermal conditions, for both LCPs the Sm-Cr transition enthalpies were about 1 kJ/mol.K higher compared to the IM-Sm transition.

The temperature interval for the IM-Sm transition in P7MB extends from about 11–14 °C with increasing cooling rate. The relative small broadening of the peak and its constant enthalpy indicate that the transition process is faster compared to the rate at which heat can be released by conduction (Cheng 1988).

The DSC curves for the IM-Sm phase transition from Fig. 2.2a can be further used for kinetics investigations. As a first step, the relative degree of transformation ($\alpha_c(T_i)$), depending on temperature, can be derived from the equation:

$$\alpha_c(T_i) = \frac{\int_{T_0}^{T_i} C_p(T) dT}{\int_{T_0}^{T_\infty} C_p(T) dT}, \quad (2.14)$$

where $C_p(T)$ is the heat capacity; T is the temperature; T_0 is the onset temperature;

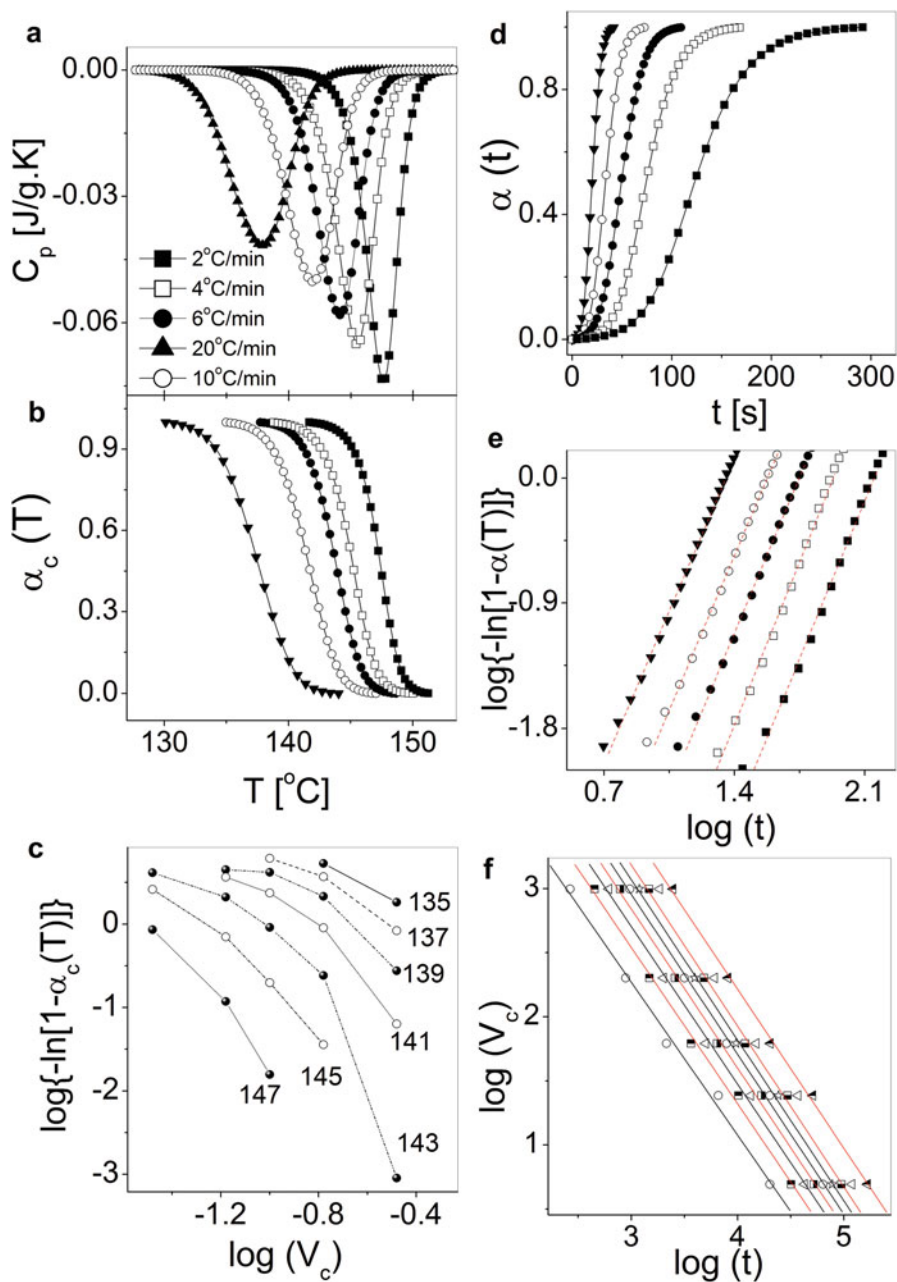


Fig. 2.2 (a) DSC exotherms, showing non-isothermal IM-Sm phase transition in P7MB at different cooling rates, shown in the figure; (b) DSC peaks transformed into degree of transformation, $\alpha_c(t)$, according to (2.14); (c) Ozawa plots at constant temperatures, given in °C in the figure; (d) $\alpha_c(t)$ time dependence of the DSC curves from (a); (e) Avrami plot; (f) Liu-Mo plot

Table 2.3 Kinetics parameters of non-isothermal IM-Sm transition of P7MB

v_c	[°C/min]	2	4	6	10	20
T_0 [°C]		151.5	150.2	148.8	147.2	144.2
T_{end} [°C]		141.8	138.6	137.6	134.8	130.0
ΔT [°C]		9.7	11.6	11.2	12.4	14.2
T_{max} [°C]		148.1	145.5	144.1	141.9	137.9
$t_{1/2}$ [s]		122	75	49	33	20
t_{max} [s]		124	76	50	33	20
m		3.54	3.72	3.36	3.26	3.27
$\log K_A$		-7.56	-7.12	-5.86	-5.13	-4.41
K_{max} [s ⁻¹]		0.0081	0.0132	0.0202	0.0299	0.0502
C_z		0.75	0.74	0.83	0.87	0.89

T_0 is the onset temperature, T_{end} is the temperature at the end of the transition, ΔT is the temperature span of the transition, T_{max} marks the maximum rate of transformation, $t_{1/2}$ is the half time, t_{max} is time at maximum, m is Avrami index, K_A is Avrami rate constant, K_{max} is the value of the rate constant at the DSC exotherm maximum, C_z is the kinetic crystallizability. Values in the table are rounded off based on significant figures.

T^∞ is the temperature at infinity and it is replaced by T_{end} ; T_i represents the temperature at which the degree of transformation is $\alpha_c(T_i)$.

The calculated temperature dependences of $\alpha_c(T)$ at different cooling rates are shown in Fig. 2.2b. The curves are almost parallel to each other and shift to lower temperatures with increasing cooling rate indicating that the transformation is control by nucleation (Cheng 1988). At low cooling rates, the experimental time is sufficient to activate the nuclei at higher temperatures, whereas at high cooling rates, the nuclei appear at lower temperatures.

Several methods for non-isothermal kinetics investigations exist. The most common one is that of Ozawa (Lorenzo and Silvestre 1999; Long et al. 1995) who modified the Avrami equation so that the amount of the transformed material $\alpha_c(T)$, after continuous cooling (or heating) with constant rate (v_c), to a temperature T , can be determined by the equation (Long et al. 1995):

$$\alpha_c(T) = 1 - \exp \left[- \frac{K_o(T)}{v_c^M} \right], \quad (2.15)$$

where $K_o(T)$ is the cooling transition function of the process (parameter introduced by Ozawa which takes into account the geometry and change in the nucleation and growth rates); M is Ozawa exponent (relates to but differs from Avrami index).

Formulating his equation, Ozawa assumed that the mathematical derivation of Avrami, describing the kinetics of isothermal transformation, is valid and that the effect of secondary crystallization is negligible. Application of this method is hence restricted to systems where M is constant independent of temperature.

In logarithmic scale Ozawa's equation takes the form:

$$\log\{-\ln[1 - \alpha_c(T)]\} = \log K_0(T) - M \cdot \log(v_c) \quad (2.16)$$

Hence the dependence $\log\{-\ln[1 - \alpha_c(T)]\}$ versus $\log(v_c)$ should yield a straight line. In order to obtain Ozawa plots one fixes the temperature and reads the $\alpha_c(T_{\text{fix}})$ from the different cooling rates curves (Fig. 2.2b). Then the values are plotted, as shown in Fig. 2.2c. Unfortunately, these plots do not represent straight lines, which mean that the Ozawa's equation fails to explain the non-isothermal IM-Sm transition behavior of P7MB. This is probably related to few factors such as dependence of smectic domain dimensions on phase transition temperature, and variation of Ozawa exponent with temperature, neglected in his theory. In some similar polymers the divergence from Ozawa's analysis has been attributed to the rigidity of the macromolecules (Long et al. 1995).

Another possibility to derive the kinetics parameters of the system is to apply the Avrami equation, where one should transform the temperature scale into time scale, according to the following equation:

$$t_i = \frac{T_0 - T_i}{v_c}, \quad (2.17)$$

where t_i is time; T_0 coincides with the onset of the DSC exotherm; T_i is the temperature at time t_i ; v_c is the cooling rate.

The transformed curves are plotted in Fig. 2.2d. In case of non-isothermal transitions, the Avrami law is supposed to be still valid:

$$1 - \alpha_c(t) = \exp(K_A \cdot t^m), \quad (2.18)$$

which in double logarithmic form reads:

$$\log\{-\ln[1 - \alpha_c(t)]\} = \log K_A + m \cdot \log t, \quad (2.19)$$

Plots of $\log\{-\ln[1 - \alpha_c(t)]\}$ dependence on $\log(t)$ are shown in Fig. 2.2e. As expected, the initial parts of the curves obey linear law, so the slopes and intercepts give the Avrami parameters m and K_A . Note that the physical meaning of the two parameters differs from the situation of isothermal crystallization and the values cannot be used for straight comparison with those obtained from isothermal kinetics since the temperature change influences the nucleation as well as the growth process. In addition, as in the isothermal case, t_{max} , $t_{1/2}$ times have to be derived. All parameters for the P7MB IM-Sm phase transition are listed in Table 2.3.

Jeziorny, considering the cooling rate dependence of Avrami rate constant in this case proposed a correction, which some authors tried to apply (Cui et al. 2005):

$$\ln K_z = (\ln K_A) / v_c, \quad (2.20)$$

where K_z is the kinetic crystallization rate, similar to Avrami rate constant at isothermal conditions.

Table 2.4 Kinetics parameters of the Liu-Mo model for P7MB IM-Sm phase transition

$\alpha_c(T)$	0.1	0.2	0.3	0.4	0.5	0.6	0.7	0.8	0.9
$\ln[F(T)]$	5.9	6.2	6.4	6.6	6.7	6.8	6.9	7.1	7.2
a	1.19	1.22	1.23	1.24	1.25	1.25	1.26	1.26	1.24

Values in the table are rounded off based on significant figures

Applying Jeziorni's correction, however, does not always lead to meaningful results. K_A and K_z have the same dimensions and for this reason the correction has to be dimensionless. Further improvements are also needed in respect to the physical sense of these quantities.

Finally a method, combining those of Avrami and Ozawa, has been introduced by Liu et al. (1997):

$$\log K_A + m.\log t = \log K_o(T) - M.\log v_c, \quad (2.21)$$

which can be rearranged as:

$$\log v_c = \log F(T) - a.\log t, \quad (2.22)$$

where $F(T) = [(K_0(T) / K_A)^{1/M}]$ refers to the value of cooling rate, which has to be chosen within unit crystallization time when the measured system amounts to a certain degree of transformation, $a = m/M$ is the ratio of Avrami index to Ozawa exponent. According to (2.22), at a given degree of transformation, the plot of $\log v_c$ versus $\log t$ yields linear relationship. From the obtained lines (Fig. 2.2f) the corresponding kinetics parameters $F(T)$ (the intercept) and a (the slope) were estimated, see Table 2.4. $F(T)$ increases with the cooling rate. Similar trend is observed for many other polymers, but profound understanding of the exact meaning of the obtained results is still missing.

Ziabicki treated the non-isothermal kinetics problem, assuming that the shape of the plots of rate coefficient versus temperature are represented by Gaussian function. These assumptions allow one to calculate C_z , a parameter known as kinetic crystallizability (see in Supaphol et al. 2003):

$$C_z = \int_{T_g}^{T_m} K(T)dT \approx 1.064K_{\max}D, \quad (2.23)$$

where K_{\max} is the value of K , corresponding to the maximum of the crystallization exotherm; D is the width of the crystallization exotherm at half height; T_m and T_g are the melting temperature and glass transition temperature, respectively.

The kinetic crystallizability characterizes the degree of transformation per unit cooling rate, over the temperature range ($T_g - T_m$). When C_z is higher the phase transition ability of the material grows and it undergoes transformation even at very

high cooling rates (for $C_z > 33$). If C_z is around 1 or less, the phase transition takes place only at slow cooling rates. According to our results for P7MB the kinetic crystallizabilities were $C_z^{IM-Sm} \approx 0,81$ and $C_z^{Sm-Cr} \approx 1,3$, i.e., the processes should be possible only at low cooling rates, just in contrast to the real situation (see also the X-ray results). Therefore, this model needs an improvement as well.

The activation energy, in case of non-isothermal crystallization with varying cooling rate, can be calculated based on the method proposed by Kissinger (see Lorenzo and Silvestre 1999; Yongjin et al. 2003):

$$\frac{d[\ln(v_c/T_{max}^2)]}{d(1/T_{max})} = -\frac{\Delta E}{R}, \quad (2.24)$$

where v_c is the cooling rate; T_{max} represent the temperature of phase transition; R is the universal gas constant; ΔE is the activation energy.

The derived values for P7MB are $\Delta E_{IM-Sm} = 330.9$ kJ/mol, $\Delta E_{Sm-Cr} = 338.4$ kJ/mol. As it is seen, the activation energy for crystallization is again higher than required for IM-Sm transition.

In summary, from DSC experiments one obtains the temperature at which the particular phase transition takes place, its activation energy and enthalpy, and its kinetics at iso- or non-isothermal conditions but in practice this method does not provide any information about the type of the transformation. Therefore, additional techniques need to be applied in order to investigate the type of the structural changes observed.

2.4 Real-Time X-Ray Experiments

2.4.1 Synchrotron Radiation

In the early sixties, Synchrotron radiation (SR) was regarded as an unwanted but inevitable by-product of elementary particle acceleration in the storage rings, whereas nowadays it presents a powerful tool, which was instrumental for R. J. Lefkowitz and B. K. Kobilka in performing their remarkable investigations, for which they were awarded the Nobel Prize in Chemistry in 2012 (<http://www.nobelprize.org>).

SR stands for the intensive electromagnetic waves generated when high energy particles, accelerated to nearly the speed of light, are deflected in a strong magnetic field (Baltá-Calleja and Vonk 1989). It covers broad range of the electromagnetic spectrum and has continuous spectral distribution. Relativistic effects provoke sharp forward peaking of the radiation and lead to substantial increase in the total radiated energy. SR has become an essential tool for X-ray structural investigations due to: continuous X-rays spectrum, which allows one to extend the wavelengths

range used; very high intensity of the radiation and brightness of the source as compared with conventional X-ray equipment; high collimation of the beam and well defined time structure which is a copy of the electron pulse structure of the beam. Owing to the synchrotron radiation features, the measuring times are quite short, enabling investigation of very fast processes (in the order of nano- or even picoseconds), such as LCP phase transitions. Thanks to the high brightness and the use of two-dimensional detectors, one can gather very accurate, space and time discriminate, experimental information.

In other words, synchrotron measurements are performed at the same conditions, as used e.g., in the DSC experiments, the X-ray patterns are recorded in real-time and precise comparison with appropriate coupling of the results with other techniques gives better insight into the investigated processes. The angular resolution, in the synchrotron X-ray experiments, is also much better than that of conventional instruments, the advantage of which will be shown here.

Soon after the discovery of the X-ray diffraction by Laue (more than 100 years ago) and the first diffraction experiments of the father and son Bragg this technique was recognized as a very powerful tool for investigation of the structure of the condensed matter. The basics of X-ray diffraction analysis of polymers can be found in few classical books (Baltá-Calleja and Vonk 1989; Roe 2000; Guinier 1994). A single X-ray pattern represents the dependence of the diffracted/scattered intensity (I) on the diffraction/scattering angle (θ) and depending on the θ range one distinguishes:

- Wide angle X-ray scattering (diffraction) (WAXS), at large θ values. This angular range contains information about inter- and intramolecular distances—for instance the real three-dimensional crystalline structures are presented by many discrete reflections (diffraction peaks), by which the crystal unit cell could be identified. In the case of LCPs, in this range one gets a broad reflection (called halo) in classical nematic and smectic phases and several peaks overlapping the halo in higher order mesophases are observed;
- Middle angle X-ray scattering (MAXS), at intermediate θ values. Typical for this range is the information related to the appearance of smectic layer spacings of several nanometers (Guan et al. 2009; Martinelli et al. 2010; Katerska et al. 2010, Gomes et al. 2009);
- Small-angle X-ray scattering (SAXS), at small θ values. Investigations in this region are important for the nanostructured materials. SAXS peaks or intensity variation appear because of the electron density difference between the phases (Baltá-Calleja and Vonk 1989; Chu and Hsiao 2001).

2.4.1.1 X-Ray Scattering Results at Isothermal Conditions

For the particular investigations on P7MB described here (performed at Daresbury Laboratory (station 8.2) and in A2 beam line at HASYLAB, Hamburg) X-ray patterns were recorded every 10 s. The temperature protocol was the same as that

for the DSC measurements: starting from isotropic melt (or glassy state) jumping to the desired iso-temperature and keeping recording patterns as long as they stopped changing their profile. Later on, after appropriate corrections were made (beam-line software is usually used), the deconvolution method was applied, where the peaks were either mathematically modeled with different types of functions or the raw data were treated according to appropriate theoretical models.

2.4.1.2 WAXS

An example of real-time WAXS results is given in (Fig. 2.3) for P7MB. At high iso-temperatures, and at the early times at the lower T_{iso} , only a liquid-like diffuse scattering was observed (Fig. 2.3a). Since such pattern is generated by averaged inter- or intramolecular distances and their distribution is expected to be completely random, Gaussian function was chosen to model it. The parameters of the peaks (maximum, area, FWHM) were further used to extract the needed structural parameters.

In a first step after the deconvolution, Bragg's law, giving the geometrical condition for having a diffraction maximum at given space point is applied:

$$2d_{hkl} \sin \theta = n\lambda, \quad (2.25)$$

where d_{hkl} is d-spacing of the planes with Miller indices (hkl); θ is the diffraction angle; n is the order of diffraction; λ is the X-ray wavelength.

The equation can be rewritten in term of scattering vector ($s = 2\sin\theta/\lambda$), in which form the X-ray plots are given in this section:

$$d = \frac{1}{n \cdot s}, \quad (2.26)$$

where, in practice, s equals the peak maximum value obtained from the deconvolution procedure.

From the FWHM of the peaks (Δs) the correlation length, ξ , can be calculated. This parameter describes in LC phases the intramolecular correlation (Scherrer's formula):

$$\xi = \frac{1}{\Delta s} \quad (2.27)$$

At later times and relatively low iso-temperatures, lower than 140 °C for P7MB, Fig. 2.3a, the Sm phase underwent partial crystallization, manifested by the appearance of sharp WAXS peaks, overlapping the liquid-like halo. Quantitative measure of this process is the degree of crystallinity, X_{cr} :

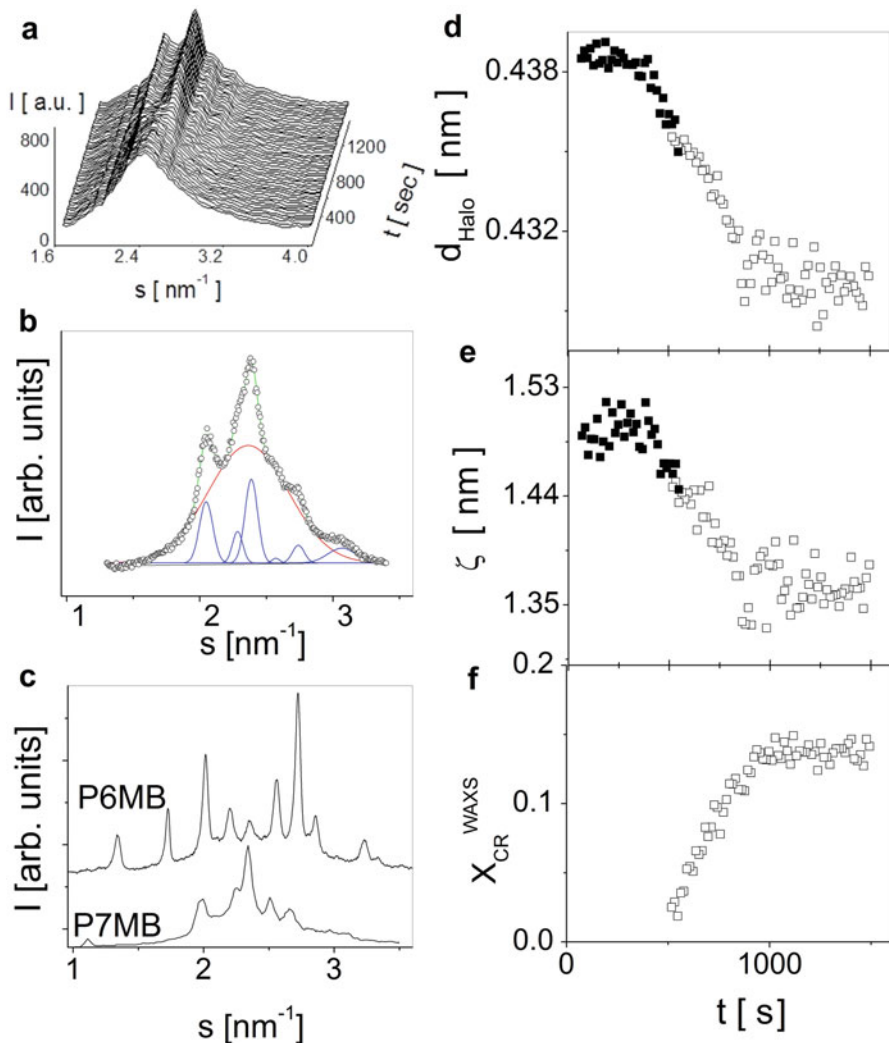


Fig. 2.3 (a) Time evolution of P7MB WAXS pattern at $T_{\text{iso}} = 135$ °C; (b) crystalline (blue lines) peaks, halo (red line) and overall profile (green line) obtained from the experimental data (open circles) by means of deconvolution; (c) WAXS of highly crystalline P6MB and P7MB; P7MB time dependences of: (d) halo d-spacing, d_{halo} ; (e) correlation length, ξ ; and (f) degree of crystallinity, $X_{\text{cr}}^{\text{WAXS}}$. The filled symbols represent the parameters of the halo in Sm phase and the open symbols show them during and after crystallization

$$X_{cr} = \frac{\sum I_{cr}}{I_{tot}} \quad (2.28)$$

where $\sum I_{cr}$ is the sum of the integral intensities of all crystalline reflections; I_{tot} is the total integral intensity.

The crystalline peaks parameters were obtained by means of deconvolution of the WAXS patterns with Gaussian functions, as shown in Fig. 2.3b. The area under the peaks is utilized in the calculations based on (2.28), because it is proportional to the quantity of the material undergoing phase transition.

According to our results (see Fig. 2.3d–f) the following conclusions can be drawn: (a) the halo distance of about 0.43 nm, considered as indication of the absence of long-range orientational order inside the SmCA layers, decreases during the crystallization process, i.e., the molecules become closely packed. Actually, before drawing such a conclusion, the continuity of the halo position before and after the appearance of the WAXS crystalline peaks has to be verified. This is satisfied in the given example, as shown in Fig. 2.3d with filled and unfilled symbols, respectively; (b) the correlation length decreases, which is a hint that the correlational motions of the neighboring molecules are further restricted during the Sm-Cr transition. This result concerns the mechanism of crystal phase formation i.e., the collective motions are not favored but just the opposite tendency occurred; (c) the degree of crystallinity is quite low for P7MB.

The capability of P7MB to crystallize was further investigated by isothermal crystallization experiments at 150 °C for two weeks and the crystallinity did not exceed 50 % (Fig. 2.3c), whereas P6MB crystallized easily, reaching more than 80 % crystallinity (Fig. 2.3c). Another noticeable difference between both LCPs is that P6MB displays three distinct polymorphic (α -, β -, and γ -) crystalline phases (Katerska et al. 2010), whereas P7MB displays only crystal phase.

2.4.1.3 MAXS

The MAXS scattering interval is relevant to the mesogenic layer d-spacing (d_{MAXS}). The calculation of d_{MAXS} is based also on (2.25). For P7MB, its time dependence at two different T_{iso} is shown in Fig. 2.4a, d. At high T_{iso} , a peak centered at about 1.745 nm appears and its d-spacing remains constant during the measurements (Fig. 2.4a). The integral intensity of the peak is proportional to the quantity of the material already transformed into the new phase, and as expected, it increases with time reaching constant value at the latest stage of the measurement (Fig. 2.4b).

Considering simultaneously the results from WAXS and MAXS, represented by diffuse halo and a peak, respectively, one concludes that the observed transition is IM-Sm phase transition. In this particular case the type of the Sm phase was a priori known to be SmCA (Watanabe et al. 1997; Gomez et al. 2009) but in cases when it has to be determined, oriented samples and 2D detector have to be employed.

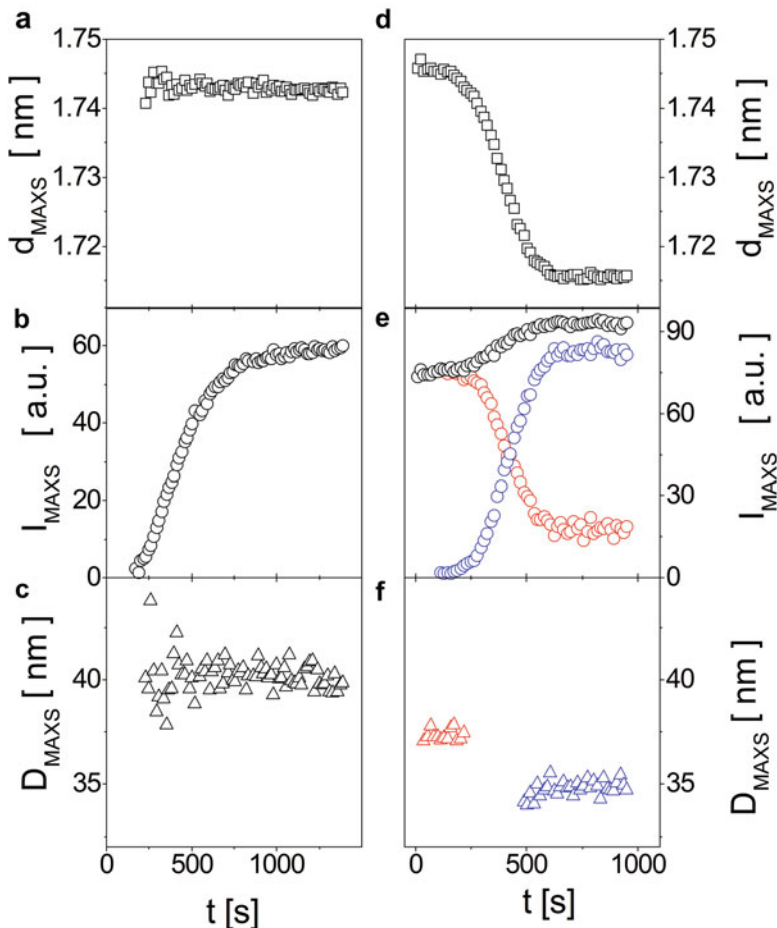


Fig. 2.4 MAXS peak parameters d -spacing, d_{MAXS} , integral intensity, I_{MAXS} , and domain dimension, D_{MAXS} at $T_{\text{iso}} = 153\text{ }^{\circ}\text{C}$ (a–c) and at $T_{\text{iso}} = 135\text{ }^{\circ}\text{C}$ (d–f), respectively. The intensities and the domain dimensions for the smectic (red symbols) and for the crystalline peak (blue symbol) are also presented

In the analysis, the correlation length, ξ (2.26) of the MAXS peak should be considered as a measure of the size of the domain dimensions in direction perpendicular to the mesogenic layers. ξ can be defined as $\xi = \frac{D}{k}$, where D is the domain dimension and the coefficient k incorporates all factors which affect the final values of ξ (such as experimental broadening of the peak, possible domain size polydispersity, macromolecular polydispersity, etc.). Under the assumption that the factors affecting k remain constant during the experiment, the correlation length remains proportional to the domain dimensions. Within the frames of a single experiment, as well as when using the same material in the same experimental set-up, this condition is fulfilled. Although, the actual values of the domain dimensions cannot

be derived without additional knowledge, one can still use the time dependences of ξ to estimate the relative variance of the Sm domain dimensions. Consequently, according to Fig. 2.4c, the smectic domains have the same constant size ($D \approx k.40$ nm) during the experiment, which means that the Sm phase is organized into domains formed at the very beginning of the transition, providing a clue about the hierarchical structuring of the material.

At lower temperature, the Sm peak was already grown when the measurements began i.e., the smectic phase formation had been very fast even at low undercoolings (in contrast to Ziabicki's model predictions—see Sect. 2.3.2), since the time for reaching T_{iso} in this experiments was less than a minute. An example of the time evolution of the MAXS peak parameters at lower temperatures ($T_{\text{iso}} = 135^\circ\text{C}$) is shown in Fig. 2.4d–f. The impression is that the Sm d-spacing decreases with time (Fig. 2.4d) but our analysis (Pérez et al. 2003) showed that actually the Sm peak disappeared gradually and a new Cr peak with very close d-spacing appeared. This result shows clearly the advantage of using high resolution real-time synchrotron experiments because this splitting could not be detected with common X-ray laboratory equipment.

A closer inspection of the combined WAXS and MAXS results revealed that when the MAXS peak d-spacing values started to decrease the crystalline peaks growth became evident. Consequently the Sm-Cr phase transition took place.

Keeping the d-spacings of the Sm and Cr phases fixed, deconvolution gives the intensity evolution of both peaks with time (shown with different colors in Fig. 2.4e). Based on the FWHMs (full width at the half maxima), the Sm and Cr domain dimensions were calculated. As seen in Fig. 2.4f, the Cr domains are smaller than that of the Sm phase but again constant in size.

Noteworthy, the Sm integral intensity was subjected to Avrami analysis and values here were very similar to those obtained from DSC (at $T_{\text{iso}} = 153^\circ\text{C}$ — $n = 2.21$, $K = 4.1 \times 10^{-3} [\text{s}^{-n}]$ and at $T_{\text{iso}} = 155^\circ\text{C}$ — $n = 1.98$, $K = 1.8 \times 10^{-3} [\text{s}^{-n}]$).

2.4.1.4 SAXS

Because of the inverse proportionality between θ and the estimated distances (see (2.23)) the largest distances are evaluated in the SAXS scattering interval. Here, the existence of hierarchical structuring in the material of order of nanometres could be verified. The main concept is that nanostructured materials have different electron densities of the different phases, usually being disordered (amorphous) and ordered (crystalline). The electron density of the minor phase (smaller volume fraction) could be presented as a function of the matrix electron density (major volume fraction). When the electron phase difference increases, the SAXS peak intensity increases, too.

As it is well known from the theory, the amplitude of the scattered radiation— $F(\mathbf{s})$ in wave-vector \mathbf{s} space is a Fourier transform of the electron density $\rho(\mathbf{r})$ in real (\mathbf{r}) space (Glatter and Kratki 1982):

$$\mathbf{F}(s) = \iiint dV \cdot \rho(\mathbf{r}) \cdot \mathbf{e}^{-is \cdot \mathbf{r}}, \quad (2.29)$$

where the integral is over the entire space volume, V .

Intensity of the scattered radiation is proportional to the square of the amplitude, hence:

$$I = |\mathbf{F}(s)|^2 = |\mathbf{F}(s) \cdot \mathbf{F}^*(s)|^2 = \iiint dV_1 \iiint dV_2 \cdot \rho(\mathbf{r}_1) \cdot \mathbf{e}^{-is \cdot \mathbf{r}_1} \rho(\mathbf{r}_2) \cdot \mathbf{e}^{-is \cdot \mathbf{r}_2} \quad (2.30)$$

Introducing $\mathbf{r} = \mathbf{r}_2 - \mathbf{r}_1$ and $\eta(\mathbf{r}) = \bar{\rho}^2(\mathbf{r}) = \int \int \int d\mathbf{V}_1 \cdot \rho(\mathbf{r}_1) \cdot \rho(\mathbf{r}_1)$ and transforming the equation to spherical coordinates (2.29) gives:

$$I(s) = \int 4\pi r^2 \rho^2(r) \cdot \mathbf{e}^{-i \cdot s \cdot r} dr \quad (2.31)$$

When a particle is located in a matrix, the density will exhibit a mean value $\tilde{\rho}$ in almost the entire volume, deviating from it (having value ρ) only in the space point where the particle is found. By introducing an autocorrelation function:

$$\gamma(\mathbf{r}) = \tilde{\eta}^2 = \tilde{\rho}^2 + \mathbf{V} \cdot \rho^2 \quad (2.32)$$

which depends on the mean density difference rather than on the absolute values of the densities. In this sense, such function has the meaning of average product of two fluctuations at a distance r from each other. In the one dimensional case the function takes the form:

$$\gamma_1(x) = \int 4\pi s^2 I_1(s) \mathbf{e}^{-is \cdot x} ds \quad (2.33)$$

The normalized real part of it reads:

$$\gamma_1(x) = \frac{\int 4\pi s^2 I_1(s) \cos(2\pi s x) ds}{\int 4\pi s^2 I_1(s) ds} \quad (2.34)$$

The denominator here is called Porod's invariant (Q):

$$Q = \int 4\pi s^2 I_1(s) ds \quad (2.35)$$

and it accounts for the constant number of the scatterers, i.e., depending on the number, the density and the spatial distribution of the phases, the SAXS profile may look different but the total integral intensity remains constant.

It shall be emphasized, that adequate parameters are achieved by one dimensional correlation function analysis only if an appropriate model of the system is developed in advance. In practice, very often a two-phase quasi-periodic model with alternating layers of amorphous and crystalline material is adopted (see (2.34)).

Prior to the data treatment, the smoothed and corrected for background scattering SAXS intensity profiles are subjected to Lorentz correction (Cser 2001), where the intensity is multiplied by s^2 . The structural parameter derived is called long period (L). Its values can be determined either from the position of the peak maximum in the Lorentz corrected SAXS patterns using (2.25), L_{Lor} , or from the second maximum of the normalized one-dimensional correlation function, $\gamma_1(x)$ (Baltá-Calleja and Vonk 1989).

At high T_{iso} , the SAXS patterns of P7MB did not present any specific features, whereas at lower T_{iso} , together with the crystallization, SAXS intensity increased and these patterns were subjected to $\gamma_1(x)$ analysis.

The two phase quasi-periodic model was validated for P7MB and representative results for one dimensional correlation function analysis at a chosen T_{iso} are shown in Fig. 2.5. The analysis of a single $K(x)$, which is the non-normalized $\gamma_1(x)$ function, yields (see Fig. 2.5a):

- Long period, L_γ , this is the place of the second maximum in the $K(x)$ dependence;
- the degree of crystallinity within the lamellar stacks X_c^{SAXS} by the help of the equation:

$$A = X_c^{SAXS}(1 - X_c^{SAXS}).L_\gamma, \quad (2.36)$$

where A is the intercept of the linear regression (LR) to the autocorrelation triangle (ACT) with the axis x (Todorova et al. 2004b; Goderis et al. 1999; Guinier 1994);

- The layer thickness of the minor fraction (in our case, because of the low crystallinity of P7MB this was supposed to be the crystalline phase), l_c :

$$l_c = L_\gamma.X_c^{SAXS} \quad (2.37)$$

- The layer thickness of the major fraction (the amorphous/smectic one in the case of P7MB), l_a :

$$l_a = L_\gamma - l_c \quad (2.38)$$

- Porod's invariant, Q_{id} , which can be graphically obtained from the intercept of the LRACT of the non-normalized correlation function with the $\gamma_1(x)$ axis. In this case it is given by:

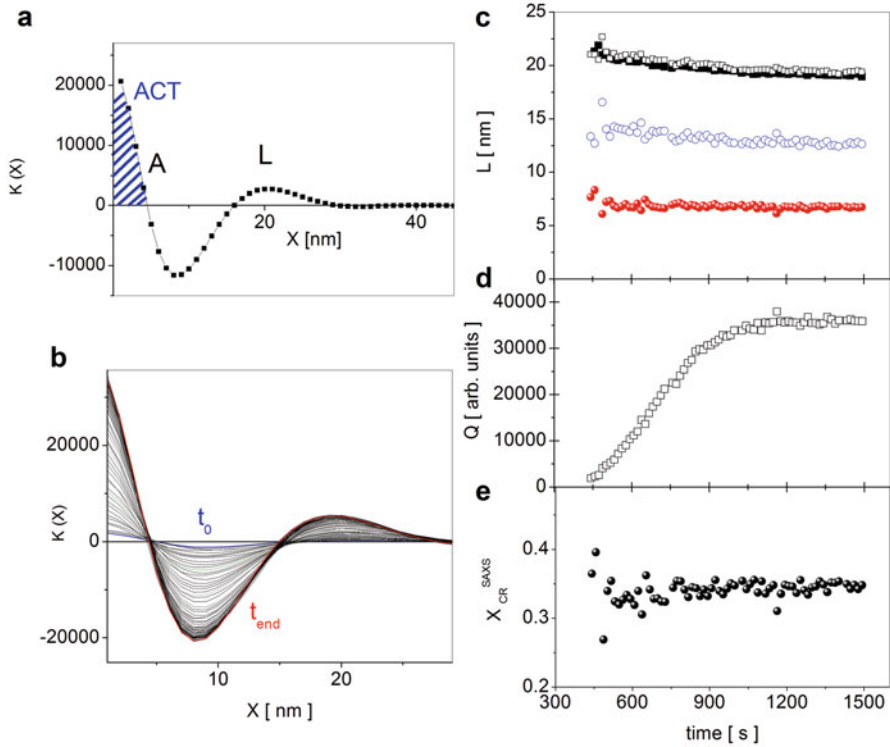


Fig. 2.5 (a) Single curve of the non-normalized one dimensional function, $K(x)$ —see text; (b) time evolution of $K(x)$ at $T_{\text{iso}} = 135 \text{ }^\circ\text{C}$: the initial time t_0 and the end time t_{end} are marked with different colors; (c) Long period, L (L_{Lor} —open squares, L_r —filled squares, see text), amorphous layer thicknesses, l_a (open circles in blue), and crystalline layer thickness, l_c (filled circles in red) dependencies on time, obtained from $K(x)$ analysis; (d) Time dependence of Porod's invariant, Q ; (e) Degree of crystallinity, $X_{\text{cr}}^{\text{SAXS}}$, dependence on time

$$Q_{id} = C\alpha_s X_s^{\text{SAXS}} (1 - X_c^{\text{SAXS}}) \Delta\rho^2, \quad (2.39)$$

where C is a constant, which accounts for the relative scale (the SAXS intensity is not in absolute units), and α_s is a filling factor, giving the fraction of the semi-crystalline stacks within the entire volume (Goderis et al. 1999).

In Fig. 2.5b the time evolution of the non-normalized one dimensional correlation function, $K(x)$ is presented. With time, the first maximum at $x = 0$ of the curves moves to higher $K(x)$ values, the minimum becomes more pronounced, and the second maximum slightly shifts towards smaller values. The long period (Fig. 2.5c) has a value of about 20 nm, slightly decreasing with time, as shown in the same figure. The smaller values are a result of the decreasing layer thickness of the amorphous phase. The crystal layer thickness remains constant. The Porod's invariant values increase with time stepwise (Fig. 2.5d), as a result of increasing electron

contrast between the two phases present. The degree of crystallinity is low and independent of time (Fig. 2.5e).

SAXS investigations on P7MB crystallized from glassy state were also performed (Todorova et al. 2003). The melt was inserted into ice-water. Interestingly, a long period of about 10 nm was observed for the quenched samples. Annealing at different T_{iso} showed increasing of the long period up to about 35 nm with temperature.

2.4.2 X-Ray Scattering Results at Non-isothermal Conditions

2.4.2.1 WAXS

Cooling of P7MB from IM showed WAXS range behavior was very similar to the one at low T_{iso} isothermal conditions. Interesting finding here was that the d-spacing of the halo became sharper at the temperature of IM-Sm phase transition and the correlation length increased. This finding is just in contrast with the observed ξ decrease during Sm-Cr transition. The observed degree of crystallinity was low—about 22 %.

2.4.2.2 MAXS

In Fig. 2.6, the temperature dependences of the structural parameters of MAXS peaks of P7MB and P6MB are plotted for a cooling rate 10 °C/min. The particular changes in these parameters are closely coupled with the observed exothermal peaks in the DSC (Fig. 2.6 d, h). Based on the results the following conclusions could be derived (Katerska et al. 2010; Todorova et al. 2004a, b; Pérez et al. 2003): (a) in the high temperature interval a smectic phase, manifested by the appearance of a MAXS peak is formed in both LCs; (b) d_{Sm} increases as temperature decreases, having a negative temperature coefficient $\beta_T = d(d_s)/dT$. This unusual β_T behavior ($\beta_T < 0$) was explained by gosh-trans conformational change in the spacers, giving rise to more elongated overall conformation of the molecules; (c) the values of d_{Sm} are higher for P6MB, as explained by even-odd effect; (d) during Sm-Cr transition the smectic peak disappears and a new peak with smaller d-spacing (close to but shifted from the first one) appears. This is more pronounced in P6MB but is valid for P7MB either; (e) the domains are formed during the IM-Sm phase transition and they decrease in size when the crystallization takes place. The domain size seems to be larger for P7MB; (f) the degree of crystallinity for P7MB is much lower (about 30 %) than for P6MB (up to 80 %); (g) P7MB Sm phase is monotropic whereas P6MB is enantiotropic; (h) P7MB possesses only one crystalline form, whereas P6MB exhibits three polymorphic forms.

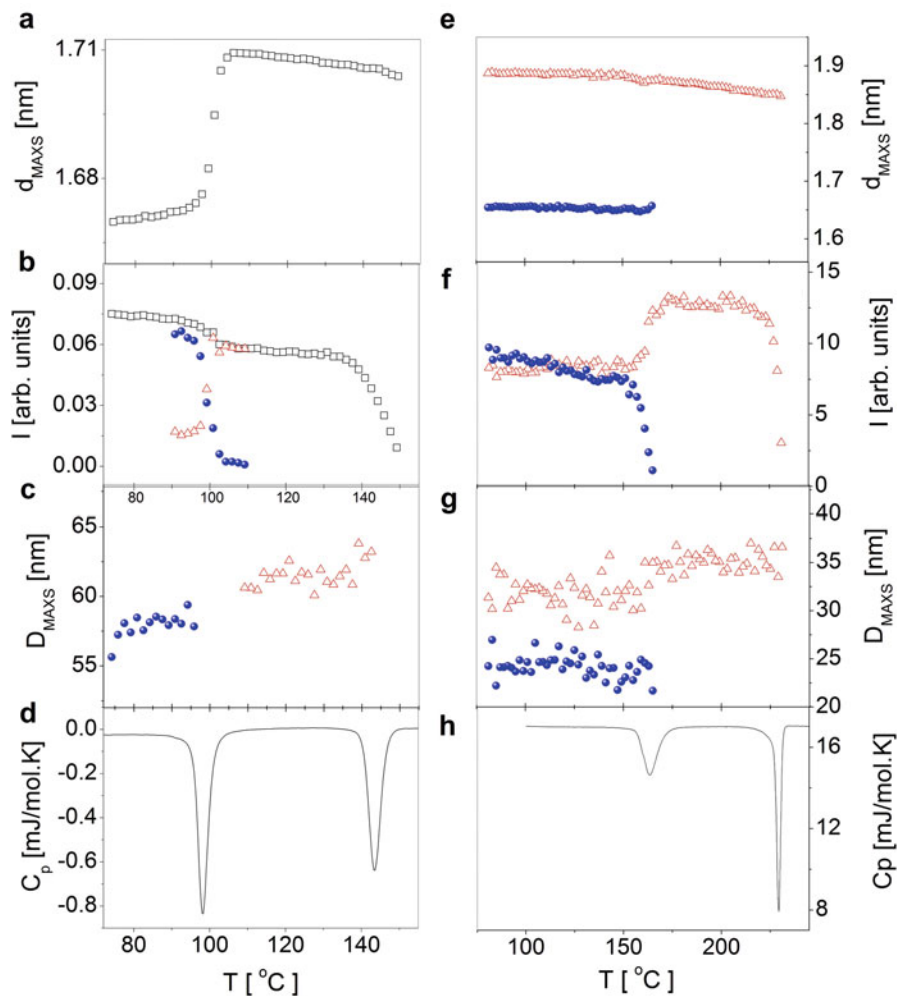


Fig. 2.6 d_{MAXS} , I_{MAXS} , D_{MAXS} temperature dependences of P7MB (a–c) and of P6MB (e–g) at cooling rate $v_c = 10^{\circ}\text{C}/\text{min}$, together with DSC traces for P7MB (d) and P6MB (h) cooled at the same rate

Noteworthy, from the real-time experiments it became clear that P6MB is very sensitive to the cooling rate (Katerska et al. 2010), building different polymorphs and/or presenting coexistence of more than one polymorph under the same conditions. This casts doubt on the assumption of existence of one more polymorph arising under high pressure based on common X-ray results.

Another important result is the perfect match between DSC and real-time X-ray results emphasizing the advantage of using more than one experimental technique. Such combination eliminates ambiguity originating from the DSC analysis if used alone. It can also be applied as a cross-check or to confirm some of the hypotheses.

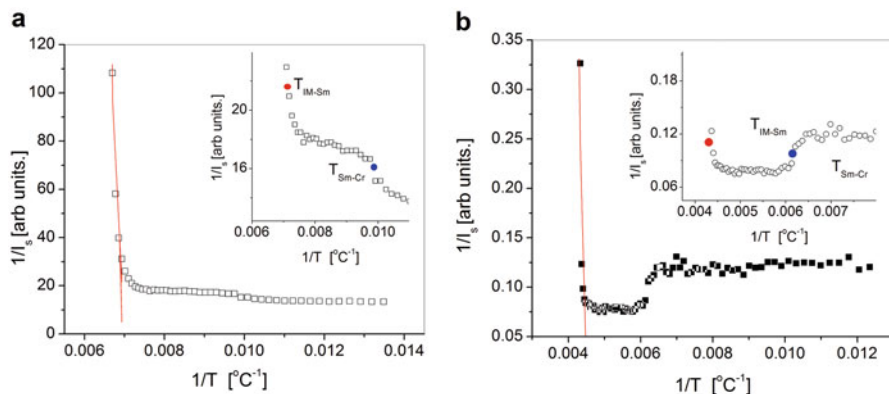


Fig. 2.7 Plot I^{-1} versus T^{-1} of the smectic peak intensity for: (a) P7MB and (b) P6MB at $10^{\circ}\text{C}/\text{min}$ cooling rate. The temperatures of IM-Sm and Sm-Cr phase transitions are marked with red and blue dots, respectively, in the inset

For instance, in order to explain the unexpectedly high activation energy of the Sm-Cr phase transition in comparison to the one for the IM-Sm transition, obtained from the DSC analysis, a new mechanism of smectic phase formation, the so called nanophase separation was proposed (Krasteva et al. 2003). This mechanism was useful to explain the early stages prior to the polymer crystallization (Olmsted et al. 1998; Kaji et al. 1998; Matsuba et al. 1999). According to these authors, the nanophase separation results from orientational fluctuations in the system. In the case of P6MB and P7MB, one could expect that at decreasing temperature random fluctuations occur in the regions with more extended segments (more rigid as well, having more trans- conformations). The fluctuation wavelength increases with time (temperature), according to the principle of minimum energy, separating the flexible from the rigid segments and arranging them similar to the Smectic order. When a critical value of the fluctuation wavelength is reached, then real nucleation and growth take place. One could assume that the wavelength of these fluctuations is of the order of d_{MAXS} (Krasteva et al. 2003) and then the plot of the MAXS peak I^{-1} versus T^{-1} has to display initial linear dependence (Strobl 1996). Figure 2.7 represents such dependences, where the linear parts are clearly visible, confirming the nanophase separation mechanism during the induction period prior to the real phase transition. Hence, since the mechanism of Sm phase formation is quite complex, one should apply Kissinger's equation for calculation of the activation energy with caution.

2.4.2.3 SAXS

The analysis at non-isothermal conditions (cooling from a melt state) showed that no SAXS peak appeared in the Smectic phase for both P7MB and P6MB. This result was interpreted as an excellent capability of these LCPs to be transformed

into smectic phase i.e., without amorphous regions present in the entire volume. An SAXS peak appeared simultaneously with the crystallization of both LCPs. A long period of about 24 nm for P7MB and 28 nm for P6MB was derived. These values increase by about 15 nm during the subsequent melting process.

SAXS curves can be used for another type of analysis as well. For instance Guinier (1994) proposed an equation from which the so called radius of inertia, R_g , can be derived:

$$I = I_0 \cdot \exp \left[-\frac{(R_g \cdot s)^2}{3} \right] \quad (2.40)$$

As suggested from the MAXS analysis, the Sm and Cr phases are organized into domains. If this is really the case, the plot $\log I$ versus s^2 yields a linear part with a slope equal to $R_g^2/3$. Surprisingly, the results were consistent with the domain dimensions, calculated above (see Fig. 2.6c, g). AFM results proved this organization once again (Hu et al. 2006).

The complex behavior as revealed here, with lamellar structure consisting of domains, clearly explains the non-integer values of Avrami constant and the deviations from the other standard kinetics models.

2.5 Microscopy

Microscopy methods are widely used since visualization techniques are simple for interpretation and very informative. This group of methods includes—polarized light, scanning electron, transmission electron, and recently newly developed atom force microscopies.

The most commonly used one for the investigation of LCPs is POM (Fang et al. 2013; Petr and Hammond 2011; Okano et al. 2010; Lockwood et al. 2008; Huang and Shi 2012; Hu et al. 2012; Caillier et al. 2008; Al-Muaiikel and Aly 2013; Wei et al. 2014; Wojtczak et al. 2014; Lee and White 2012). Characteristic POM textures, obtained under cross-polarizers and sometimes wave-plates, result from the well-known optical activity of the PLCs, possessing some degree of order (similar to the crystals) and owing to specific singularities in their order (Collier 1992; Gray and Winsor 1974). Here one can mention the nematic droplets, nematic marbled texture, Shlieren textures, “Moire” texture, pattern-like cracks in the holesteric LC, and focal conic texture which is representative for some smectic phases. Though very effective for an initial determination of optical activity this method has to be used with caution, since when mesogens are incorporated into polymer chains, effect such as chain entanglement, folded chains, chain ends, and specific chain conformation may greatly affect the observed texture. In addition, polymorphism and simultaneous existence of several phases can cause misleading

results. This technique can be however successfully used as real-time method for detecting phase transitions in the LCPs.

Important part of the LCPs investigation is defining their morphology, since it affects many of their physical properties—adhesive, elastic, optical, electrical and so on. It can be greatly affected by the specific experimental conditions. Scanning electron microscopy is very useful in such studies. Since most of the LCPs are dielectrics the samples are initially covered by nanolayer of gold. Morphology of interest is surface and volume. For volume investigation, fracturing in liquid nitrogen is usually employed. Figure 2.8 demonstrates the morphology of P7MB (Fig. 2.8a–d) and P6MB (Fig. 2.8e–h) for samples prepared under different conditions. The highly crystalline P7MB sample (Fig. 2.8a, b) consists of very fine lamellae, confirming the applicability of the two-phase model in the SAXS analysis for this polymer. In contrast, the morphology of the highly crystalline P6MB, as revealed in Fig. 2.8e, f comprises fen-like (at magnification 3500) and conic (at magnification 5000) structures. The quenched (in ice-water) sample of P7MB represents the morphology of the smectic phase mainly (according to our X-ray results) and as it was previously discussed the expected morphology is quite complex—small domains, organized into thick lamellae (Fig. 2.8c, d). In contrast, bended lamellae structure (at magnification 3500) and bended lamellae and fibrill structure (at magnification 5000) are the characteristics of quenched P6MB. The results presented here confirm once again the conclusions derived by the previously described methods.

The most recent progress, achieved in revealing the LCPs morphology is related to the application of AFM (Martinelli et al. 2010; McCulloch et al. 2006; Caillier et al. 2008). This method is very promising since the AMF resolution is in order of nanometers and the results are directly comparable with X-ray methods.

2.6 Concluding Remarks

The chapter has made it clear that there are a lot of advantages in applying various techniques in the investigations of the structure and phase transitions of LCPs. Such multiple technique approach helps one: (a) to reveal different aspects of the problems and to combine them; (b) to provide cross-check possibilities for verification of the hypotheses; (c) to gain deeper insight into the investigated problems. All these features serve to meet the high industrial demands and to enable optimization and fine tuning for specific and desired properties.

The future perspectives in the field are in real-time simultaneous realization of several different experiments (for instance real-time SAXS/MAXS/WAXS/DSC experiments at varying temperature and/or under pressure already possible at some synchrotrons). Such approach will provide fully consistent results and all uncertainties and ambiguities, when each of the methods is employed separately, even with exact reproduction of the experimental conditions, will be completely eliminated.

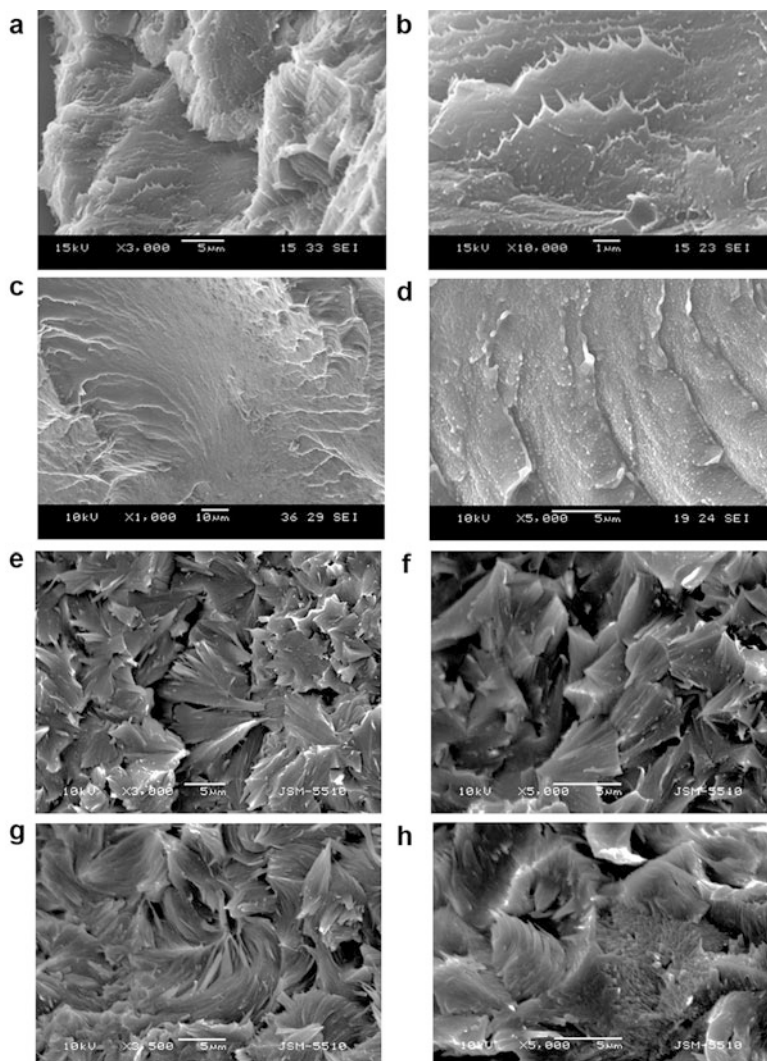


Fig. 2.8 SEM images at different magnifications: highly crystalline P7MB (a, b), quenched P7MB (c, d), highly crystalline P6MB (e, f) and quenched P6MB (g, h)

References

- Ahir SV, Tajbakhsh AR, Terentjev EM (2006) Self-assembled shape-memory fibers of triblock liquid-crystal polymers. *Adv Funct Mater* 16(4):556–560
- Al-Muaikel NS, Aly KI (2013) Liquid crystalline polymers xiii main chain thermotropic copoly (arylidene-ether)s containing 4-tertiary butyl-cyclohexanone moiety linked with polymethylene spacers. *Open J Org Polym Mater* 3:19–26

- Álvarez C, Martínez-Gómez A, Pérez E, de la Orden MU, Martínez Urreaga J (2007) Thermal and morphological characteristics of polypropylene/smectic polyester blends. *Polymer* 48 (11):3137–3147
- Baltá-Calleja FJ, Vonk CG (1989) X-ray scattering of synthetic polymers, vol 8, Polymer science library. Elsevier, Amsterdam
- Barón M (2001) Definitions of basic terms relating to low-molar-mass and polymer liquid crystals (IUPAC Recommendations 2001). *Pure Appl Chem* 73(5):845–895
- Barón M, Stepto RFT (2002) Definitions of basic terms relating to polymer liquid crystals. *Pure Appl Chem* 74(3):493–509
- Bello A, Riande E, Perez E, Marugan MM, Perena JM (1993) Influence of the spacer on the thermotropic and conformational properties of poly[oxybis(trimethylene) p, p'-bibenzoate] and poly(heptamethylene p, p'-bibenzoate). *Macromolecules* 26(5):1072–1077
- Bershtein VA, Egorov VM (1994) Differential scanning calorimetry of polymers—physics, chemistry, analysis, , technology. Ellis Horwood Technology, New York
- Caillier L, Taffin de Givenchy E, Gériibaldi S, Guittard E (2008) Liquid crystal polymers for non-reconstructing fluorinated surfaces. *J Mater Chem* 18:5382–5389
- Chen X-F, Shen Z, Wan X-H, Fan X-H, Chen E-Q, Ma Y, Zhou Q-F (2010) Mesogen-jacketed liquid crystalline polymers. *Chem Soc Rev* 39:3072–3101
- Cheng SZD (1988) Kinetics of mesophase transition in thermotropic copolyesters. 1. Calorimetric study. *Macromolecules* 21:2475–2484
- Chiferii A, Krigbaum WR, Meyer RB (eds) (1982) Polymer liquid crystals. Academic, New York
- Chu B, Hsiao B (2001) Small-angle X-ray scattering of polymers. *Chem Rev* 101:1727–1761
- Collier AA (ed) (1992) Liquid crystal polymers: from structure to applications. Elsevier Applied Science, London
- Cser F (2001) About the Lorentz correction used in interpretation of small-angle X-ray scattering data of semicrystalline polymers. *J Appl Polym Sci* 80:358–366
- Cui X, Shengbo Q, Yan D (2005) Isothermal and nonisothermal crystallization kinetics of novel odd-odd polyamide 9 11. *Eur Polym J* 41:3060–3068
- Du XH, Wang Y-Z, Chen X-T, Tang X-D (2005) Properties of phosphorus-containing thermotropic liquid crystal copolyester/poly(ethylene terephthalate) blends. *Polym Degrad Stabil* 88:52–56
- Fang L, Zhang H, Li Z, Zhang Y, Zhang Y, Zhang H (2013) Synthesis of reactive azobenzene main-chain liquid crystalline polymers via michael addition polymerization and photomechanical effects of their supramolecular hydrogen-bonded fibers. *Macromolecules* 46:7650–7660
- Georgiev G, Cebe P, Capel M (2005) Effects of nematic polymer liquid crystal on crystallization and structure of PET/Vectra blends. *J Mater Sci* 40(5):1141–1152
- Glatter O, Kratki O (eds) (1982) Small angle X-ray scattering. Academic Press, London
- Goderis B, Reynaers H, Kkoch MHJ, Mathot VBF (1999) Use of SAXS and linear correlation functions for the determination of the crystallinity and morphology of semicrystalline polymers. Application to linear polyethylene. *J Polym Sci B Polym Phys* 37:1715–1738
- Gomez M, Nogales A, Garcia-Gutierrez MC, Ezquerro TA (eds) (2009) Applications of synchrotron light to scattering and diffraction in materials and life sciences, vol 776, Lecture notes in physics. Springer, Berlin
- Gopakumar TG, Ghadage RS, Ponrathnam S, Rajan CR (1997) Poly(phenylene sulfide)/liquid crystalline polymer blends: 1. Non-isothermal crystallization kinetics. *Polymer* 38 (9):2209–2214
- Gray GW, Winsor PA (eds) (1974) Liquid crystals and plastic crystals, vol 2, Physico-chemical properties and methods of investigation. Ellis Horwood, Chichester
- Guan Y, Chen X, Shen Z, Wan X, Zhou Q (2009) Structure–property relationship of thermotropic liquid-crystalline vinyl polymers containing no traditional mesogen. *Polymer* 50:936–944
- Guinier A (1994) X-ray diffraction in crystals, imperfect crystals, and amorphous bodies. Courier Dover, Mineola

- Hatakeyama T, Quinn FX (1999) Thermal analysis fundamentals and applications to polymer science, 2nd edn. Wiley, New York
- Hu YS, Hiltner A, Baer E (2006) Solid state structure and oxygen transport properties of copolyesters based on smectic poly(hexamethylene 4,4'-biphenylate). *Polymer* 47:2423–2433
- Hu T, Yi J, Xiao J, Zhang H (2010) Effect of flexible spacer length on the mesophase structures of main-chain/side-chain liquid crystalline polymers based on ethyl cellulose. *Polym J* 42:752–758
- Hu J-S, Zhang X, Jia Y-G, Meng Q-B (2012) Synthesis and phase behaviour of chiral liquid crystalline monomers based on menthyl groups, smectic polymers and cholesteric elastomers. *Liq Cryst* 39(1):121–131
- Huang W, Shi E (2012) High-performance thermotropic starch-based liquid crystalline polymer. *Carbohydr Polym* 90:703–708
- Ji Y, Huang YY, Rungsawang R, Terentjev EM (2010) Dispersion and alignment of carbon nanotubes in liquid crystalline polymers and elastomers. *Adv Mater* 22:3436–3440
- Kaji K, Matsunaga S, Matsuba G, Kanaya T, Nishida IM (1998) A new discovery of microphase separation initiating in the induction period of polymer crystallization: characteristic wavelength at high temperatures. *ICR Annu Rep* 5:26–27
- Katerska B, Exner G, Pérez E, Krasteva MN (2010) Cooling rate effect on the phase transitions in a polymer liquid crystal: DSC and real-time MAXS and WAXS experiments. *Eur Polym J* 46:1623–1632
- Kim JY (2009) Carbon nanotube-reinforced thermotropic liquid crystal polymer nanocomposites. *Materials* 2:1955–1974
- Kozlovski MV (2001) Kinetically controlled phase transitions in side chain liquid crystalline polymers. *Cryst Res Technol* 36(8-10):1083–1093
- Krasteva MN, Todorova GK, Pérez E, Marugan MM, Pereña JM (2003) Phase transitions of liquid crystalline polyesters: poly(heptane-1,7-diyol-4,4'-biphenylidicarboxylate). *J Mater Sci Mater Electron* 14:821–822
- Kumar PA, Swathi P, Pisipati VGKM (2002) Orthogonal smectic layers favour nucleation through diffusion-controlled transformations: a systematic crystallization kinetics study. *Z Naturforsch* 57a:226–232
- Lee KM, White TJ (2012) Photochemical mechanism and photothermal considerations in the mechanical response of monodomain, azobenzene-functionalized liquid crystal polymer networks. *Macromolecules* 45(17):7163–7177
- Li Y, Zhang G, Zhu Z, Yan D (2003) Isothermal and nonisothermal crystallization kinetics of partially melted nylon 10 12. *J of Appl Polym Sci* 88:1311–1319
- Li C, Cheng F, J-a L, Zhao Y, Liu M, Iang L, Yu Y (2012) Light-controlled quick switch of adhesion on a micro-arrayed liquid crystal polymer superhydrophobic film. *Soft Matter* 8:3730
- Liu S-F, Lee Y-D (1995) Characterization and kinetics of mesophase transition for naphthalene-based thermotropic polyesters with polymethylene spacers. *Macromol Chem Phys* 196(2):629–643
- Liu T, Mo Z, Wang S, Zhang H (1997) Nonisothermal melt and cold crystallization kinetics of poly(aryl ether ether ketone ketone). *Polym Eng Sci* 37(3):568–575
- Liu K, Tian Y, Jiang L (2013) Bio-inspired superoleophobic and smart materials: design, fabrication, and application. *Prog Mater Sci* 58(4):503–564
- Lockwood NA, Gupta JK, Abbott NL (2008) Self-assembly of amphiphiles, polymers and proteins at interfaces between thermotropic liquid crystals and aqueous phases. *Surf Sci Rep* 63:255–293
- Long Y, Shanks RA, Stachurski ZH (1995) Kinetics of polymer crystallization. *Prog Pol Sci* 20:651–701
- Lorenzo MI, Silvestre C (1999) Non-isothermal crystallization of polymers. *Prog Pol Sci* 24:917–950
- Ma H, Collard DM, Schiraldi DA, Kumar S (2007) Structure and dynamic mechanical properties of poly(ethylene terephthalate-co-4,4'-biphenylate) fibers. *Polymer* 48:1651–1658

- Mark JE (ed) (1996) *Physical properties of polymers handbook*. Springer Science + Business Media, New York
- Martinelli E, Paoli F, Gallot B, Galli G (2010) Mesophase structure of low-wetting liquid crystalline polyacrylates with new perfluoroalkyl benzoate side groups. *J Polym Sci A Polym Chem* 48:4128–4139
- Martínez-Gómez A, Pérez E, Bello A (2010) Polymesomorphism and orientation in liquid crystalline poly(triethylene glycol p, p'-bibenzoate). *Colloid Pol Sci* 288(8):859–867
- Martins JCA, Novak KM, Gomes AS (1998) Non-isothermal crystallization kinetics of thermotropic polyesters with flexible spacers in the main chain. *Polymer* 39(26):6941–6944
- Matsuba G, Kaji K, Nishida K, Kanaya T, Imai M (1999) Conformational change and orientation fluctuations prior to crystallization of crystalline polystyrenes. *ICR Annual Reports* 6:26–27
- Mcculloch I, Heeney M, Bailey C, Genevicius K, Macdonald I, Shkunov M, Sparrowe D, Tierney S, Wagner R, Zhang W, Chabinye ML, Kline RJ, McGehee MD, Toney MF (2006) Liquid-crystalline semiconducting polymers with high charge-carrier mobility. *Nat Mater* 5:328–333
- Moritsugu M, Ishikawa T, Kawata T, Ogata T, Kuwahara Y, Kurihara S (2011) Thermal and photochemical control of molecular orientation of Azo-functionalized polymer liquid crystals and application for photo-rewritable paper. *Macromol Rapid Comm* 32(9):1546–1550
- Okano K, Noguchi I, Yamashita T (2010) Anisotropic carbon nanotube films fabricated from a lyotropic liquid-crystalline polymer. *Macromolecules* 43:5496–5499
- Olmsted PD, Poon WCK, McLeish TCB, Terrill NJ, Ryan AJ (1998) Spinodal-assisted crystallization in polymer melts. *Phys Rev Lett* 81:373–376
- Pérez E, Todorova G, Krasteva M, Pereña JM, Bello A, Marugan MM (2003) Structure and phase transitions of poly(heptamethylene p, p'-bibenzoate): time resolved synchrotron WAXS and DSC studies. *Macrom Chem Phys* 204:1791–1799
- Petr M, Hammond PT (2011) Room temperature rapid photoresponsive azobenzene side chain liquid crystal polymer. *Macromolecules* 44:8880–8885
- Petrov A (1999) *The lyotropic state of matter: molecular physics and living matter*. Gordon & Breach, New York
- Pisitsak P, Magaraphan R, Jana SC (2012) Electrically conductive compounds of polycarbonate, liquid crystalline polymer, and multiwalled carbon nanotubes. *J Nanomater* 2012:Article ID 642080
- Qui Z, Mo Z, Zhang H, Sheng S, Song C (2000) Isothermal melt and cold crystallization kinetics of poly(aryl ether ketone ether ketone ketone). *J Polym Sci B Polym Phys* 38:1992–1997
- Ranganathan C, Ramesh C (2006) Synthesis and characterization of main chain thermotropic liquid crystalline polyesters based on methyl 4-[40-(x-hydroxyalkoxy)biphenyl-4-yl]-4-oxobutyrate: Effects of keto group and connectivity on mesophasic characteristics of biphenyl based AB-type polyesters. *React Funct Polym* 66:1003–1013
- Rodríguez-Amor V, Fernández-Blázquez JP, Bello A, Pérez E, Cerrada ML (2008) Molecular weight effect on the obtainment of parallel and perpendicular orientation in thermotropic poly(diethylene glycol p, p'-bibenzoate). *Polymer Bulletin* 60:89–96
- Roe R-J (2000) *Methods of x-ray and neutron scattering in polymer science*. Oxford University Press, New York
- Strobl GR (1996) *The physics of polymers, concept for understanding their structure and behavior*. Springer, Berlin
- Supaphol P, Dangseeyun N, Sriramoan P, Nithitanakul M (2003) Nonisothermal melt-crystallization kinetics of three linear aromatic polyesters. *Thermochimic Acta* 406:207–220
- Takahashi C, Yoshihara S, Kang S, Sakajiri K, Watanabe J, Tokita M (2014) Decrease in the isotropization temperature and enthalpy of main-chain polymer smectic liquid crystals as a result of the inclusion of chain ends. *Polymer* 55:2609–2613
- Todorova GK, Krasteva MN, Iliev M, Pérez E, Bello A, Pereña JM (2003) Structure of crystallized from liquid-crystalline glass poly(heptane-1,7-diyil-4,4'-biphenyldicarboxylate). *Heron press science series, vol 4. Meeting in physics, Sofia University, Sofia, pp. 129–132*

- Todorova G, Pérez E, Marugan MM, Kresteva M (2004a) Phase transitions in poly(heptane-1,7-diyil biphenyl-4,4'-dicarboxylate). *Macromol Symp* 212:479–502
- Todorova GK, Krasteva MN, Pérez E, Pereña JM, Bello A (2004b) Structure and phase transitions of poly(heptamethylene p, p'-bibenzoate) as studied by DSC and real-time SAXS/MAXS employing synchrotron radiation. *Macromolecules* 37(1):118–125
- Waigh TA, Perry P, Riekel C, Gidley MJ, Donald AM (1998) Chiral side-chain liquid crystalline polymeric properties of starch. *Macromolecules* 31:7980–7984
- Waigh TA, Kato KL, Donald AM, Gidley MJ, Clarke CJ, Riekel C (2000) Side-chain liquid crystalline model for starch. *Starch/Starke* 52:450–460
- Watanabe J, Hayashi M, Nakata Y, Niori T, Tokita M (1997) Smectic liquid crystals in main-chain polymers. *Prog Pol Sci* 22(5):1053–1087
- Wei P, Cakmak M, Chen Y, Wang X, Wang Y, Wang Y (2014) The influence of bisphenol AF unit on thermal behavior of thermotropic liquid crystal copolyesters. *Thermochem Acta* 586:45–51
- Wojtczak M, Dutkiewicz S, Galeski A, Piorkowska E (2014) Structure and characterization of random aliphatic–aromatic copolyester. *Eur Polym J* 55:86–97
- Wunderlich B (2005) *Thermal analysis of polymeric materials*. Springer, Berlin
- Yang G, Tang P, Yang Y (2012) Uniaxial–biaxial nematic phase transition in combined main-chain/side-chain liquid crystal polymers using self-consistent field theory. *Macromolecules* 2012(45):3590–3603
- Yongjin L, Zhang G, Zhu X, Yan D (2003) Isothermal and nonisothermal crystallization kinetics of partially melting nylon 10 12. *J Appl Polym Sci* 88:1311–1319
- Yoon Y, Ho R-M, Li F, Leland ME, Park J-Y, Cheng SZD, Percec V, Chu P (1997) *Prog Pol Sci* 22:765–794
- Zhu X, Yan D (2001) Influence of the order of polymer melt on the crystallization behavior: II. Crystallization kinetics of isotactic polypropylene. *Colloid Polym Sci* 279(6):546–553

Chapter 3

Block Copolymers Containing Mesogen-Jacketed Liquid Crystalline Polymers as Rod Blocks: Synthesis and Self-Assembly

Zhihao Shen and Qi-Feng Zhou

3.1 Introduction

When mesogenic groups, such as calamitic, discotic, and bent-cored ones, are introduced into polymers, liquid crystalline (LC) phases may form, resulting in LC polymers (LCPs). In general, LCPs can be categorized into three types, namely, main-chain (MCLCPs), side-chain (SCLCPs), or main-chain/side-chain combined (MCSCCLCPs) LCPs, depending on where mesogenic units are incorporated (Wang and Zhou 2004). And the mesogens such as calamitic ones in SCLCPs can be attached to the polymer backbone either longitudinally (end-on) or laterally (side-on) (McArdle 1989).

For SCLCPs, because the flexible polymer backbone has the tendency to take the random-coil conformation, its motion will disrupt the parallel alignment of side-chain mesogens for the formation of LC phases. The decoupling concept, proposed by Finkelmann et al. (1978), is an important development for the molecular design of SCLCPs. Flexible spacers are introduced into end-on SCLCPs between the mesogenic side chain and the polymer main chain. With a long enough flexible spacer, the motion of side-chain mesogens with an ordered packing can be decoupled from the dynamics of the flexible main chain, leading to polymers with liquid crystallinity. This strategy has been proven very successful in designing end-on SCLCPs (Finkelmann and Rehage 1984). On the basis of this concept, they also reported the first side-on SCLCPs (Hessel and Finkelmann 1985, 1986). Percec and co-workers synthesized decoupled SCLCPs by utilizing immiscible polymer main chain and side groups, taking advantage of the microphase separation between these two components (Hsu and Percec 1987; Percec and Hahn 1989).

Z. Shen (✉) • Q.-F. Zhou

Beijing National Laboratory for Molecular Sciences, Department of Polymer Science and Engineering, and Key Laboratory of Polymer Chemistry and Physics of Ministry of Education, Center for Soft Matter Science and Engineering, College of Chemistry and Molecular Engineering, Peking University, Beijing 100871, China
e-mail: zshen@pku.edu.cn

In the late 1980s, Zhou et al. proposed and synthesized a special kind of side-on SCLCPs, namely, mesogen-jacketed liquid crystalline polymers (MJLCPs), which are also called rigid side-group type liquid crystalline polymers (Wan et al. 1995; Zhou et al. 1987, 1989). Chemically speaking, MJLCPs belong to side-chain polymers, in which side groups (often mesogenic ones) are connected to the polymer backbone with a short spacer or with a single covalent bond (Chen et al. 2010). Different from the decoupling concept, the design of the first MJLCPs was based on two considerations. First, the torque exerted by the backbone on the side chain should be minimal when the side chains are side-on attached. Second, there will be a “jacketing” effect owing to the steric requirements of the densely attached, bulky side groups. Such an effect forces the polymer backbone to take an extended-chain conformation, resulting in a rigid or semi-rigid macromolecular chain. As a result, the physical properties of MJLCPs are similar to those of rigid or semi-rigid MCLCPs. And the whole MJLCP chain can act like a supramolecular rod to form LC phases. The “jacketing” effect found in MJLCPs also plays an important role in the formation of LC phases for dendron-jacketed polymers developed by Percec and co-workers (Percec and Tomazos 1992; Rosen et al. 2009; Rudick and Percec 2008).

After Zhou et al. proposed the jacketed model for MJLCPs (Zhou et al. 1987, 1989), Hardouin et al. carried out small-angle neutron scattering (SANS) experiments on side-on SCLCPs (Hardouin et al. 1991, 1992) to study the conformation and rigidity of these polymers. The results confirmed that the jacketed model and the large prolate anisotropy of conformation for the nematic LC polymers. For some of the polymers, the backbone has an anisotropy as strong as that of MCLCPs, and the whole polymer is rod-like (Lecommandoux et al. 1997).

In addition, oriented rigid or semi-rigid polymers such as MCLCPs show banded textures under polarized light microscopy (PLM) (Wang and Zhou 2004). The MJLCPs synthesized by Zhou et al. (Zhou et al. 1989) are the first series of side-chain polymers exhibiting banded textures (Xu et al. 1993a, b). Banded textures have also been observed in many other MJLCPs (Tu et al. 2000a; Ye et al. 2004; Zhou et al. 1993), confirming the significant chain rigidity of these polymers.

Furthermore, an MJLCP forms a hexagonal columnar (Φ_H) phase (Tu et al. 2000a), as determined by two-dimensional (2D) wide-angle X-ray diffraction (WAXD). The formation of such supramolecular columnar LC phases with the whole MJLCP chains as the mesogens is another evidence of the rigid nature of these polymers. Other columnar phases have also been found in MJLCPs, including columnar nematic (Φ_N), hexatic columnar nematic (Φ_{HN}), and rectangular columnar (Φ_R) phases (Chen et al. 2010). In addition to columnar phases, smectic A (SmA) and smectic C (SmC) phases have also been observed in MJLCPs with more rigid side chains or with special side-chain interactions such as hydrogen-bonding and ionic interaction (Chen et al. 2010). Therefore, MJLCPs can be either rod-like to form columnar phases or sheet-like to form smectic phases (Fig. 3.1) (Chen et al. 2010).

Block copolymers (BCPs) are composed of two or more covalently linked homopolymer chains. Because of the chemical differences between the constituting

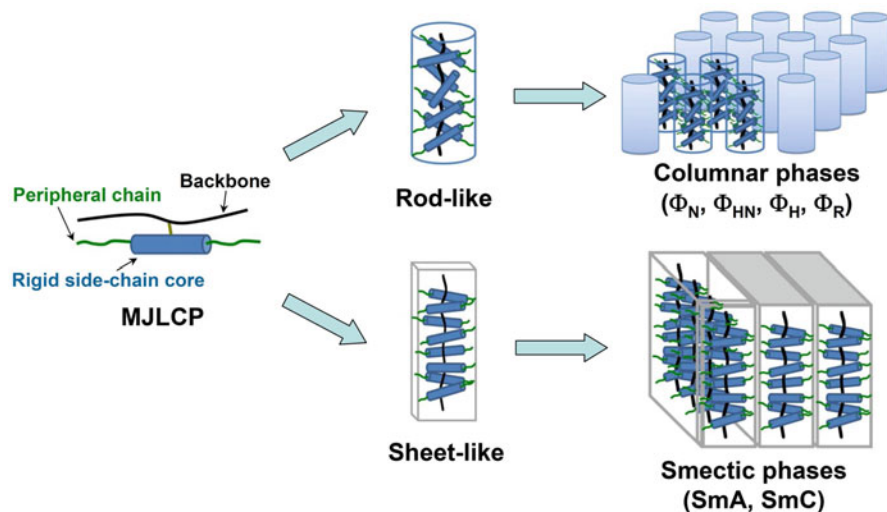


Fig. 3.1 Schematic representation of MJLCPs and the formation of different types of LC phases. Reprinted and adapted with permission of the Royal Society of Chemistry (Chen et al. 2010)

blocks, they phase separate. Owing to the chemical connection between the blocks, the phase separation is on the nano-scale, leading to various ordered structures with periodicities usually in the range of 10–100 nm (Bates 1991; Bates and Fredrickson 1990; Hamley 1998; Muthukumar et al. 1997). For coil–coil diblock copolymers (diBCPs), the final phase structures (or nano-sized morphologies) are determined by three crucial parameters, the volume fraction f of the individual block, the Flory-Huggins interaction parameter χ , and the total degree of polymerization (DP) of the BCP N (Khandpur et al. 1995). With increasing f , coil–coil diBCPs can self-assemble into equilibrium body centered cubic arrays of spheres (BCC), hexagonally packed cylinders (HEX), bicontinuous double gyroid (GYR), and lamellae (LAM), and then into inverse GYR, HEX, and BCC (Bates and Fredrickson 1990; Hajduk et al. 1994; Matsen and Bates 1996a, b). Some weakly segregated coil–coil diBCPs can also form other nanostructures, including the metastable hexagonally perforated lamellar (HPL) phase and the stable $Fddd$ phase (Khandpur et al. 1995; Kim et al. 2008, 2009; Matsen 2012).

Compared with coil–coil diBCPs, rod–coil BCPs containing LC rod-like polymers have two additional factors which impact their self-assembly, the parallel aligning tendency of the rod-like segments and the conformational or geometric asymmetry between the rod and coil blocks (Bates et al. 1994; Halperin 1990; Olsen and Segalman 2005, 2007; Olsen et al. 2008b; Williams and Fredrickson 1992). As a result, rod–coil BCPs have relatively strong tendency to microphase separate because of the abovementioned parallel alignment or LC interaction of the rod-like chains, and even rod–coil small molecules, oligomers, and low-molecular weight (MW) BCPs can self-assemble into ordered nanostructures (Lee et al. 1998; Ryu et al. 2004). In addition, the conformational or geometric asymmetry between the

different blocks results in asymmetric phase diagrams with respect to composition. And LAM exists in a wider range of composition in rod-coil diBCPs owing to the preference of long rods to a flat intermaterial dividing surface (IMDS) (Chen et al. 1996; Lee et al. 2001; Olsen and Segalman 2005; Williams and Fredrickson 1992). Wang reviewed the theoretical and simulation studies on self-assembly of melts and thin films of rod-coil BCPs, emphasizing the effects of conformational asymmetry between the two types of blocks and the orientational interaction between the rod chains (Wang 2011). He also compared the different chain models and different calculation or simulation methods used in literature. Finally, when the rod-like blocks are liquid crystalline, rod-coil diBCPs will form various hierarchical structures with LC phases on the length scale of 1–10 nm (Lee et al. 2001).

Although the lengths of commonly used rod blocks such as polypeptides (Gallot 1996; Klok et al. 2000), polyisocyanates (Chen et al. 1995, 1996), and conjugated polymers (Olsen et al. 2006, 2007, 2008a; Olsen and Segalman 2005; Tao et al. 2007) can be tuned by controlling their MWs, shape-persistent MJLCPs have some advantages owing to the structural tunability and relative ease of control during polymerization (Chen et al. 2010). For MJLCPs, the rod diameters can be readily controlled by the molecular design of the side chains. In addition, the surface properties of the MJLCP rods can be easily modulated by using different peripheral chains at the ends of the side chains. Furthermore, unlike MCLCPs and most conjugated polymers which are usually synthesized by condensation polymerization, many MJLCPs are obtained from controlled/living radical polymerizations of mostly vinyl monomers, leading to rod-like polymers with tunable rod lengths by controlling the DPs.

To date, many MJLCP-based BCPs, including rod-coil and rod-rod diBCPs, have been designed and successfully synthesized with various polymerization methods, such as nitroxide-mediated radical polymerization (NMRP) and atom transfer radical polymerization (ATRP) (Gopalan et al. 2003; Wan et al. 1998, 2000; Yi et al. 2004; Zhang et al. 2002b; Zhou et al. 2010). Different MJLCPs have been utilized, and the coil blocks include polystyrene (PS), poly(methyl methacrylate) (PMMA), poly(*n*-butyl acrylate) (PBA), polydimethylsiloxane (PDMS), polybutadiene (PB), poly(ethylene oxide) (PEO), and poly(ϵ -caprolactone) (PCL) (Chen et al. 2010). Even ABC-type linear (Shi et al. 2014; Zhang et al. 2005a) and star-shaped (Wang et al. 2005) BCPs have been prepared. The various aspects, such as hierarchical structures and competition between microphase separation and LC phase formation, of self-assembling behaviors of BCPs containing MJLCPs in bulk (Li et al. 2004; Tenneti et al. 2005), in dilute solutions (Tu et al. 2000b, 2003a), and in films (Huang et al. 2006; Shi et al. 2012b) have been investigated.

This chapter covers the synthesis and phase behaviors of MJLCPs, preparation of BCPs containing MJLCPs, and the self-assembly of such BCPs, with emphasis on the latter two.

3.2 Synthesis and Phase Behaviors of MJLCPs

3.2.1 Molecular Design and Synthesis of MJLCPs

3.2.1.1 Molecular Design of MJLCPs

The molecular design of MJLCPs involves considerations on the detailed structures of the constituting parts of the polymers. Therefore, the shape and rigidity of the side chain, the length and type of the linkage between the side chain and the backbone, and the structure of the polymer backbone need to be carefully selected. Figure 3.2 illustrates the chemical structures of some MJLCPs.

The first MJLCPs are based on polyacrylates with a short linkage between the mesogenic side chain and the backbone (Zhou et al. 1987). Then polystyrene-based MJLCPs were synthesized from 2-vinylhydroquinone-derived monomers, with the mesogenic side chain connected to the backbone with a carbon-carbon single bond (Zhou et al. 1989). Since then, several series of polystyrene-based MJLCPs have been designed and synthesized. The monomers are derivatives of 2-vinyl-1,4-phenylene-diamine (Zhang et al. 1997), 2-vinylterephthalic acid (Liu et al. 1998; Zhang et al. 1999a), and vinyl terphenyl (Yu et al. 2003a; Zhu et al. 2007). In most cases, the calamitic mesogens of these polymers contain three phenyl rings connected with various linkages such as ester and amide linkages at the *para* positions. And the mesogens usually have flexible aliphatic tails. All these MJLCPs show stable LC phases, usually with isotropization temperatures higher than decomposition temperatures. As expected, when the conjugation length or the rigidity of the mesogenic side group is increased, smectic LC polymers such as polymers **1** (Chen et al. 2007, 2009) and **2** (Chai et al. 2007) in Fig. 3.2 are obtained.

Side chains of MJLCPs synthesized earlier are mesogenic ones in order to ensure liquid crystallinity of the resulting side-on side-chain polymers. In addition to calamitic mesogens, bent-cored (Chen et al. 2006c; Xu et al. 2009) and discotic mesogens (Yu et al. 2013) have also been used in the side chains to obtain MJLCPs. On the other hand, because the rigidity and therefore the ability to form LC phases of MJLCPs originate from the “jacketing” effect, the use of mesogenic groups in the side chains may not be necessary. In fact, when the rigidity of the side chain is reduced by using semi-rigid cycloalkyl groups (Wan et al. 2003; Zhang et al. 1999b) and Y-shaped alkoxy chains (Guan et al. 2009; Tu et al. 2000a) to replace the alkoxyphenyl side group, the resultant polymers still form LC phases when they are heated above their respective glass transition temperatures (T_g 's). With the decrease in chain rigidity leading to the decreased isotropization temperature, the polymer with a cyclopentyl group in the side chain becomes the first MJLCP to have a high but detectable isotropization temperature before decomposition (Tu et al. 1999). And polymers with cyclic side groups of appropriate sizes are quite rigid and liquid crystalline (Mei et al. 2010, 2012). Furthermore, even when flexible linear aliphatic tails are directly attached at the two ends of the central

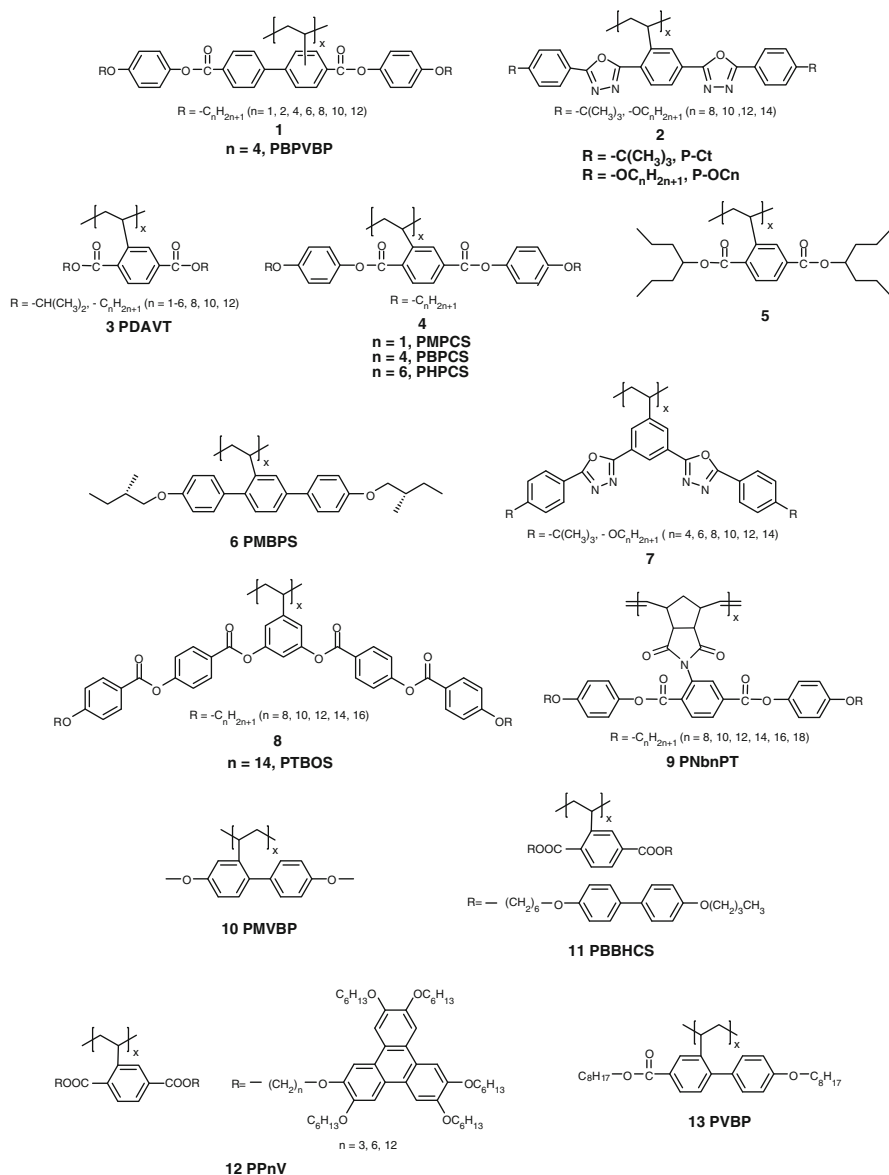


Fig. 3.2 Chemical structures of some typical MJLCs

phenyl ring, stable LC phases are still observed in polymer **3** (PDAVT, Fig. 3.2) that has a suitable tail length (Yin et al. 2003a, b).

When special interactions are introduced into side chains, the resulting jacketed polymers also form stable LC phases. Microphase separation between incompatible segments in side chains can stabilize LC phases. Pugh and co-workers designed and

synthesized LC polymers having *n*-alkoxy substituents terminated with incompatible fluorocarbon (Arehart and Pugh 1997; Small and Pugh 2002) or oligodimethylsiloxane (Pugh et al. 1998) segments. Ober et al. obtained MJLCPs with side-chain mesogens containing semifluorinated tails (Gopalan et al. 2002). Introduction of side-chain functional groups that have other non-covalent interactions, such as hydrogen-bonding (Cheng et al. 2011a) and ionic interaction (Cheng et al. 2011b), also leads to MJLCPs with stable LC phases.

While many MJLCPs are based on polyacrylate, polymethacrylate, and polystyrene main chains, MJLCPs with a polysiloxane backbone have been synthesized through hydrosilylation of polymethylhydrosiloxane with styrenic derivatives (Zhang et al. 2010). In addition to flexible backbones, relatively rigid polynorbornene has also been utilized to obtain jacketed polymers exhibiting LC phases. Pugh et al. prepared polynorbornene-based LCPs with a short flexible linkage between the side-chain mesogen and the backbone (Arehart and Pugh 1997; Pugh et al. 1998; Pugh and Schrock 1992). Recently two new series of MJLCPs with a polynorbornene backbone were synthesized (Yang et al. 2013; Zhu et al. 2014b). MJLCPs with other types of rigid main chains such as polyacetylenes (Chen et al. 2006b; Peng et al. 2010; Yu et al. 2013) and polythiophenes (Yang et al. 2009, 2010) have also been obtained.

3.2.1.2 Synthesis of MJLCPs

As side-chain polymers, most MJLCPs can be obtained by radical polymerizations under mild reaction conditions, with fewer purity requirements of solvents and reagents. Conventional free radical polymerization has been carried out to synthesize MJLCPs (Zhou et al. 1987, 1989, 1993). Some living polymerization methods such as anionic polymerization cannot be utilized due to the presence of functional groups in the mesogenic side chains of most MJLCPs. With the development of controlled/living radical polymerization techniques (Hawker et al. 2001; Matyjaszewski and Xia 2001; Wang and Matyjaszewski 1995), such polymerization methods as NMRP and ATRP can be applied to obtain MJLCPs with controlled MWs and MW distributions (MWDs) (Chen et al. 2010; Gao et al. 2009a). For example, both NMRP (Wan et al. 1999) and ATRP (Zhang et al. 2002a) can be used to synthesize the typical MJLCP, poly{2,5-bis[(4-methoxyphenyl)oxycarbonyl]styrene} (PMPCS) (polymer **4** with $n = 1$, Fig. 3.2). The monomer of PMPCS, MPCS, polymerizes much faster than styrene, possibly due to the “jacketing” effect and the presence of the LC phase of the resulting polymer as well as the electronic effect of the acetoxy groups (Gopalan and Ober 2001; Pragliola et al. 1999). Similarly, controlled/living radical polymerization, mostly ATRP, has also been applied to synthesize many other MJLCPs such as polymers **1** (PBPVBP) (Chen et al. 2007) and poly{2,5-bis[(4-butoxyphenyl)oxycarbonyl]styrene} (PBPCS, polymer **4** with $n = 4$) (Zhao et al. 2006) in Fig. 3.2.

In addition to free radical polymerization, other synthetic methods have been employed to obtain MJLCPs with different polymer backbones. Polymer reaction of the polymethylsiloxane precursor with styrenic compounds yields MJLCPs with a short spacer (Zhang et al. 2010). MJLCPs with a polynorbornene backbone can be synthesized by living ring-opening metathesis polymerization, resulting in controlled MWs and fairly narrow MWDs (Pugh and Schrock 1992; Yang et al. 2013; Zhu et al. 2014b). Polyacetylene-based MJLCPs have been synthesized by transition-metal catalyzed metathesis polymerization (Chen et al. 2006b; Peng et al. 2010; Yu et al. 2013). Supramolecular approaches can also be used to prepare MJLCPs. Hydrogen-bonding has been utilized to obtain supramolecular jacketed polymers exhibiting LC phases (Xu et al. 2012).

3.2.2 Phase Structures of MJLCPs

The phase structures of MJLCPs can be mainly determined by X-ray scattering and optical microscopic methods. As previously mentioned, banded textures from PLM observation of sheared polymer samples prove the rigid nature of MJLCPs. In addition, *Schlieren* texture with both 2-brush and 4-brush patterns proves a (columnar) nematic phase, while focal-conic fan textures indicate smectic phases. WAXD, especially 2D experiments on oriented samples such as fibers or sheared films, is the most important technique for the confirmation of the rigid nature of MJLCP chains, the conjecture of MJLCPs being supramolecular rod-like mesogens, and the determination of the LC phase structures (Chen et al. 2010; Tu et al. 2000a; Xu et al. 1994; Ye et al. 2004; Yin et al. 2003b). Previous research on a wide range of MJLCPs has demonstrated that many MJLCPs can form columnar phases. In addition, some MJLCPs exhibit smectic phases such as SmA (Chai et al. 2007; Chen et al. 2007) and SmC (Chen et al. 2009).

3.2.2.1 Columnar Phases of MJLCPs

The first MJLCPs were proposed to be nematic phases mainly based on PLM results (Zhou et al. 1987, 1989). However, on the basis of the jacketed model and the rigidity of MJLCPs, such nematic phases are actually Φ_N phases formed by the supramolecular MJLCP rods. Φ_N phases have been observed in many other MJLCPs (Jin et al. 2010; Ye et al. 2004). Other columnar phases including more ordered ones like 2D Φ_H (Chen et al. 2006c; Tu et al. 2000a; Xu et al. 2009) and Φ_R (Chen et al. 2006c) phases have also been identified.

Polymer **5** (Fig. 3.2) with a non-mesogenic bulky side group was the first MJLCP that was determined by WAXD to form a Φ_H phase (Tu et al. 2000a). Its 2D WAXD fiber pattern shows three low-angle equatorial diffractions with a scattering vector ratio of $1:3^{1/2}:4^{1/2}$, which are (100), (110), and (200) diffractions of a 2D hexagonal

packing. And the a parameter of the Φ_H phase is comparable to the side-chain length. In addition, polarized FTIR results suggest that the side group is perpendicular to the polymer main chain. The above results indicate a cylindrical polymer chain with its diameter similar to the length of the side chain. Other polymers, such as some PDAVT polymers (Yin et al. 2003b) and MJLCPs with cyclic side groups (Mei et al. 2010, 2012), can also form Φ_H phases.

The typical and frequently used MJLCP, PMPCS, with a high MW forms a Φ_{HN} phase (Ye et al. 2004). The 2D WAXD pattern with the X-ray beam along the shear direction demonstrates that the lateral packing of the PMPCS rods has a local sixfold symmetry. However, there are no higher-order diffractions, indicating the order is not long-range and it is between those of the Φ_N and Φ_H phases. Φ_{HN} phases are also formed by PBPCS (Zhao et al. 2006) and poly{(+)-2,5-bis[4'-(S)-2-methylbutoxy]phenyl]styrene} (PMBPS, polymer 6) (Liu et al. 2007) in Fig. 3.2.

The shape of the side chain greatly impacts the LC structures of MJLCPs. Those with bent-cored mesogenic side chains tend to form columnar phases, such as polymers 7 (Xu et al. 2009) and 8 (Chen et al. 2006c) in Fig. 3.2. Both series of polymers can exhibit Φ_H phases. In addition, the 8 polymers with relatively short terminal aliphatic chains develop into Φ_R phases, while those with relatively long aliphatic tails form Φ_H phases, confirming the influence of peripheral chains on the LC phase behaviors of MJLCPs. In addition, polymer 8 with $n = 12$ in Fig. 3.2 shows both Φ_H and Φ_R phases. And MJLCPs with dendronized side groups also show columnar phases (Jin et al. 2010). Depending on the generation of the dendron unit and the polymer MW, the polymer shows a Φ_{HN} or Φ_N phase.

3.2.2.2 Smectic Phases of MJLCPs

Pugh et al. first successfully induced layered structures in polynorbornene-based side-on SCLCPs with a short spacer by incorporating fluorocarbon segment-terminated n -alkoxy substituents in the side group (Arehart and Pugh 1997; Small and Pugh 2002). The immiscibility between the fluorocarbon and hydrocarbon segments helps stabilize the smectic (SmA and SmC) phases in the polymers. Similarly, the introduction of immiscible hydrocarbon and oligodimethylsiloxane components in the side chain also induces SmC phases (Pugh et al. 1998). In addition, they also observed SmA and SmC phases in a polynorbornene-based side-on SCLCP containing a short spacer and fluorine-substituted benzene rings in the side chain (Kim et al. 2000, 2001; Pugh et al. 1997). And there is a second-order phase transition between the SmC and the SmA phases (Kim et al. 2000). A smectic (SmC) phase was observed by Ober and co-workers in an MJLCP with semifluorinated tails in the side groups (Gopalan et al. 2002). The polymer is proposed to be packed in a “herring bone” arrangement.

MJLCPs with more rigid side-chain cores leading to increased side-chain rigidity and interactions can also display smectic phases. Polymers 1, which have a

biphenyl group instead of a phenyl one in the center of the rigid side-chain core compared with polymer **4**, exhibit SmA phases (Chen et al. 2007). In the 1D WAXD patterns of polymers **1**, the strong low-angle diffractions have a scattering vector ratio of 1:2:3 or 1:2, indicating a smectic ordering. And in the 2D WAXD patterns that were obtained as the X-ray beam was perpendicular to the shear (meridian) direction, the strong diffractions attributed to the layered structures are located on the equator, with the amorphous scattering concentrated on the meridian, indicating SmA phases. And those polymers with longer tails develop into SmC phases (Chen et al. 2009). MJLCPs in smectic phases possess a sheet-like conformation with the parallel alignment of main chains (Fig. 3.1). MJLCP **2** (Fig. 3.2) with a more rigid side-chain core having 1,3,4-oxadiazole units changes from a Φ_{HN} phase for P-Ct to a SmA phase for P-OCn (Chai et al. 2007), indicating that the microphase separation between the flexible aliphatic tails and the rigid aromatic core plays an important role in the formation of layered structures. As mentioned above, the shape (or architecture) of the side chain influences the phase structures of MJLCPs. When the linear rigid side-chain core in polymer **2** is replaced with a bent-type core, all the resulting polymers **7** form Φ_{H} phases instead of SmA structures (Xu et al. 2009).

With the introduction of H-bonding, MJLCPs having amide linkages in the side chain can form SmA phases (Cheng et al. 2011a). In this series of polymers, the increased immiscibility between the longer aliphatic tails and the aromatic core also favors the formation of layered structures. Similar phenomena were observed in the two new series of MJLCPs with a polynorbornene backbone synthesized by Yang et al. (Yang et al. 2013) and our research group (Zhu et al. 2014b). The chemical structure of the latter one, polymer **9**, is shown in Fig. 3.2. For both series of polymers, the terminal alkoxy chains in the side group have to be long enough for the polymers to exhibit LC phases. In addition, the introduction of ionic interaction into side chains also leads to MJLCPs showing smectic phases (Cheng et al. 2011b). Furthermore, MJLCPs with a rigid polyacetylene backbone also form smectic phases (Chen et al. 2006b).

3.2.3 *Molecular Weight Dependence of Phase Behaviors of MJLCPs*

The phase structures of MJLCPs are influenced by many factors, such as backbone flexibility, molecular architecture, the structure and size of the side chain, molecular weight, and so on (Chen et al. 2010). Because of the extended-chain conformation of MJLCPs, their LC behaviors are dependent on MWs. The length of a rod-like MJLCP is almost linearly proportional to its MW, which thus influences the aspect ratio of such a supramolecular rod as well as the LC phase behaviour of the polymer. For example, PMPCS with an MW (measured by GPC) lower than 1.0×10^4 g/mol is always amorphous (Ye et al. 2004). It enters into a stable Φ_{N}

phase after annealing at high temperatures when the MW is in between 1.0×10^4 and 1.6×10^4 g/mol. And samples with MWs higher than 1.6×10^4 g/mol display a Φ_{HN} phase after annealing at high temperatures.

Such MW-dependent phase behaviors have also been observed in other MJLCP systems (Liu et al. 2007; Zhao et al. 2006). Recently a new MJLCP, poly(4'-(methoxy)-2-vinylbiphenyl-4-methyl ether) (PMVBP) (polymer **10** in Fig. 3.2), containing a biphenyl core in the side chain was synthesized by our group (Zhang et al. 2014). It has a relatively high T_g (as high as ca. 210 °C). The LC phase behavior is also strongly dependent upon its MW. Because of the relatively small MW of the repeat unit, it has a low threshold MW of ca. 0.53×10^4 g/mol for LC formation. Samples with high enough MWs form a Φ_{H} phase after being heated to high temperatures.

3.2.4 Re-entrant Phase Behaviors of Some MJLCPs

For MJLCPs, the as-prepared samples are usually amorphous, and the LC phases are formed upon heating above T_g . And the LC phases generally remain after the samples are cooled to ambient temperature. However, some MJLCPs exhibit the unusual, re-entrant phase behavior, which was first observed in PHPCS (polymer **4** with $n=6$, Fig. 3.2) (Yu et al. 2003b). PHPCS re-enters into isotropic liquid during cooling with the disappearance of the LC phase. PBPCS also shows a similar behavior, as demonstrated by differential scanning calorimetry (DSC), PLM, WAXD, and rheological results (Chen et al. 2010; Zhao et al. 2006). This unusual phase behaviour is similar to the re-entrant isotropic phase caused by the rod-coil conformational transformation in polypeptides (Lin 1997). Polydialkoxyporphazenes also have a similar columnar-isotropic transition (Papkov et al. 1992). For MJLCPs, the polymer conformation changes from a worm-like chain to an extended one with the formation of the LC phase, which is stabilized by the higher entropy gain due to the increased freedom of the bulky side chains compared to the entropy loss of the main chains (Zhao et al. 2006).

3.2.5 Main-Chain/Side-Chain Combined LCPs Based on MJLCPs

Rod-like MJLCPs can serve as main chains of MCSCLCPs. The MCSCLCP with a PDAVT backbone and two biphenyl mesogens at the two ends of the side chain, poly{2,5-bis[6-(4-butoxy-4'-oxybiphenyl)hexyloxycarbonyl]styrene} (PBBHCS, polymer **11** in Fig. 3.2) was synthesized by ATRP (Xie et al. 2008). Because each repeat unit has two biphenyl units, the high grafting density of mesogens makes this and similar polymers (Xie et al. 2011) also structurally different from

other MCSCLCPs. In fact, 2D WAXD patterns with the X-ray incident beam in three orthogonal directions demonstrate that PBBHCS with a sufficiently high MW is hierarchically ordered at low temperatures (Xie et al. 2010). The MJLCP main chains form a 2D Φ_R phase on the nanometer scale and serve as the scaffold, while the biphenyl mesogens develop into a smectic E (SmE)-like structure on the subnanometer scale within the space between the main-chain scaffold. And the structure possesses a biaxial orientation with the axes of the backbone and the side chain perpendicular to each other, possibly leading to better mechanical properties. Upon heating, the biphenyl units lose the SmE-like order. In the meanwhile, the columnar phase formed by the MJLCP main chains remains. Further increasing temperature transforms the main-chain Φ_R structure into a SmA phase before the polymer reaches the isotropic state. When the calamitic side-chain mesogen is changed to azobenzene, the resulting MCSCLCP exhibits a somewhat similar phase behaviour except that at low temperatures the azobenzene mesogens possess a smectic B-like packing (Xie et al. 2011). The main-chain scaffold is stable even with the conformational change of the azobenzene moieties by UV irradiation.

MCSCLCPs with triphenylene (Tp) discotic mesogens in the side chains have also been synthesized and investigated (Zhu et al. 2012, 2014a). The phase behaviors of the polymers, poly{2,5-bis[(3,6,7,10,11-pentakis(hexyloxy)triphenylen)-2-oxyalkyloxy]styrene} (PPnV, polymer **12** in Fig. 3.2, $n = 3, 6, 12$, which is the number of carbons in the flexible spacer between the rigid core and Tp units in the side chains), are strongly dependent on the spacer length. PP3V and PP6V self-assemble into Φ_R phases developed by the MJLCP rod-like supramolecular mesogens at relatively high temperatures (Zhu et al. 2012). At low temperatures, they form hierarchical structures that include the discotic nematic (N_D) phase of the Tp units. In addition, PP6V displays the more symmetric Φ_H structure at temperatures higher than 225 °C. In these polymers, the different ordered structures self-organized by the two LC building blocks are both competitive and promotive to each other. For PP12V, the low-temperature Φ_H phase formed by the discotic mesogens destroys the ordered packing of the main chains (Zhu et al. 2014a). At high temperatures, the Tp units disorders, leaving with a larger-scale Φ_N phase formed by the polymer as a whole. Furthermore, PP12V exhibits a re-entrant isotropic phase at medium temperatures.

3.3 Synthesis of Block Copolymers Based on MJLCPs

Various types of MJLCP-containing BCPs have been designed and synthesized. They span from linear (including linear AB diBCPs and ABA/ABC triblock copolymers, triBCPs) to star ones. For AB diBCPs, there are rod-coil, rod-rod, SCLCP-rod, brush-rod, and dendritic-rod diBCPs depending on the type of the second component.

3.3.1 AB Diblock Copolymers

3.3.1.1 Rod-Coil Diblock Copolymers

Although anionic polymerization is an excellent strategy for synthesizing rod-coil BCPs because of its control over MW, MWD, and polymer architecture, the limitations on the choice of monomers and reaction conditions make it generally unsuitable to prepare MJLCPs owing to significant side reactions. Fortunately, controlled/living radical polymerization techniques (Georges et al. 1993; Malmstrom and Hawker 1998; Matyjaszewski and Xia 2001; Wang and Matyjaszewski 1995) can be used to synthesize a variety of rod-coil BCPs with functional groups, including rod-coil BCPs containing MJLCPs.

NMRP

The control over the length of the rod-like MJLCP (PMPCS) was first accomplished by using TEMPO-mediated radical polymerization (Wan et al. 1998, 2000). Rod-coil diBCP PS-*b*-PMPCS was obtained by sequential NMRP (Fig. 3.3). On the basis of solubility considerations, PS-TEMPO was synthesized by the living free radical polymerization in bulk, while the chain extension by PMPCS was carried out in solution. The same approach was employed to obtain PS-*b*-PMPCS samples with different compositions and MWs (Li et al. 2004; Tu et al. 2000b).

Ober and co-workers also synthesized rod-coil diBCPs using such a stable free radical polymerization (SFRP) method with a monofunctionalized PS-TEMPO macroinitiator (Gopalan et al. 2002, 2003). One of the MJLCP blocks contains semifluorinated peripheral chains (Gopalan et al. 2002). In both cases, rod-coil diBCPs with controlled MWs and relatively narrow polydispersities were obtained.

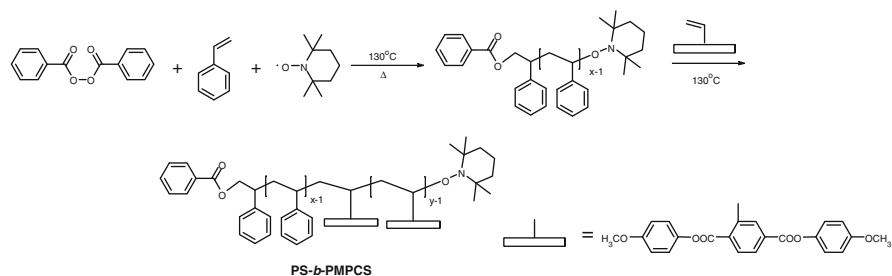


Fig. 3.3 Synthetic route of PS-*b*-PMPCS by sequential NMRP

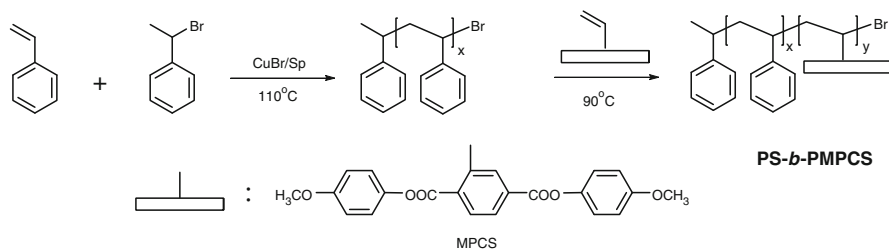


Fig. 3.4 Synthetic route of PS-*b*-PMPCS by sequential ATRP

ATRP

In addition to NMRP, MJLCPs can also be synthesized by ATRP (Chen et al. 2010; Gao et al. 2009a; Zhang et al. 2002a). Therefore, rod-coil diBCPs with MJLCPs as the rod blocks can be prepared by ATRP. When the coil block can also be synthesized by ATRP, the sequential ATRP strategy can be used (Gao et al. 2005; Zhang et al. 2002b, 2003). Additionally, readily available coil blocks can be converted and then used as ATRP macroinitiators to polymerize MJLCP monomers (Huang et al. 2005; Shi et al. 2011; Yi et al. 2003). Some coil blocks such as PCL can be synthesized by ring-opening polymerization (ROP) and then used to initiate ATRP of MJLCP monomers (Shi et al. 2005; Zhao et al. 2005).

Sequential ATRP

The first successful application of sequential ATRP to the synthesis of rod-coil diBCPs with MJLCP blocks is the preparation of PS-*b*-PMPCS (Zhang et al. 2002b). As shown in Fig. 3.4, the PS macroinitiator was first prepared by Cu-catalyzed ATRP. Then diBCPs with different MWs and relatively low polydispersity indexes (PDIs) were synthesized by further ATRP of MPCs.

Many other rod-coil diBCPs were later synthesized by using this approach (Gao et al. 2005; Guan et al. 2010; Tenneti et al. 2008; Wen et al. 2013; Zhang et al. 2003). In the synthetic procedure, the sequence of the two ATRP processes is mainly determined by the initiation efficiencies of the two monomers. Although either of the monomers can be polymerized first to obtain the diBCP, as in the block copolymerization of PBA and PMPCS (Gao et al. 2005), the results may be quite different. Only when the PBA-Br macroinitiator was used to initiate the polymerization of MPCs, was a symmetrically monomodal and relatively narrow peak corresponding to the diBCP observed in the gel permeation chromatographic (GPC) curve, indicating a highly efficient, well-controlled block copolymerization process. The PBA-*b*-PMPCS diBCPs obtained had PDIs lower than 1.20.

ATRP Initiated by Macroinitiators Synthesized from Commercial Coil Polymers

For commercially available coil polymers, such as PDMS and PEO, if the functional end groups are not suitable for ATRP, they can be functionalized and then

used as ATRP macroinitiators. Typically, 2-bromo-2-methylprorionyl bromide is used to react with the hydroxyl end groups. Such a reaction has been applied to obtain PDMS (Shi et al. 2011, 2012a, 2013; Yi et al. 2003) and PEO (Huang et al. 2005; Zhang et al. 2005c) macroinitiators. From PDMS macroinitiators, PDMS-*b*-PMPCS (Shi et al. 2011, 2013; Yi et al. 2003) and PDMS-*b*-PBPCS (Shi et al. 2012a) have been synthesized. PEO-*b*-PMPCS (Huang et al. 2005) and PEO-*b*-PMBPS (Zhang et al. 2005c) have been prepared from PEO macroinitiators. With careful control in the preparation of the macroinitiators and the subsequent ATRP, MJLCP-based BCPs with narrow MWDs ($PDI < 1.10$) can be obtained (Shi et al. 2011, 2012a, 2013).

ATRP Following ROP

Cyclic monomers like ϵ -caprolactone can be polymerized by ROP. Similar to the methodology described in the previous section, the resulting polymers with hydroxyl end groups can react with 2-bromo-2-methylprorionyl bromide to give ATRP macroinitiators. Subsequent ATRP of MJLCP monomers yields rod-coil diBCPs. PCL-*b*-PMPCS was synthesized by using this strategy (Shi et al. 2005; Zhao et al. 2005). Kinetic studies prove the controlled nature of the ATRP process employed even at relatively high conversions. PCL-*b*-PMPCS diBCPs with relatively narrow MWDs ($PDI \leq 1.11$) were obtained (Zhao et al. 2005).

3.3.1.2 Rod-Rod Diblock Copolymers

When two rod-like MJLCP chains are covalently connected, a rod-rod type diBCP containing two MJLCPs are obtained. Wan et al. synthesized such rod-rod diBCPs having PMBPS and poly[2,5-bis(4'-hexyloxyphenyl)styrene] (PBHPS) by sequential ATRP (Cui et al. 2010). Because of the similarity in the chemical structures of the two monomers, either one can be polymerized first by ATRP. Consequently, both PMBPS-*b*-PBHPS and PBHPS-*b*-PMBPS with similar MWDs were synthesized.

On the other hand, to covalently connect an MJLCP rod with a dissimilar type of rod block, such as a polypeptide, different synthetic strategies other than sequential controlled radical polymerization are required owing to varied methods for the preparation of the two rod blocks. One of the approaches is to synthesize the two rods separately and then connect them using an efficient coupling reaction. This method was carried out to obtain a rod-rod diBCP containing an MJLCP block, PMPCS, and a polypeptide block, poly(γ -benzyl-L-glutamate) (PBLG), by taking advantage of the highly efficient click chemistry (Zhou et al. 2010). A bromine-containing α -alkyne difunctional initiator was used for the copper-mediated ATRP of MPCS to obtain the α -alkyne PMPCS homopolymers. And ring-opening polymerization of γ -benzyl-L-glutamate *N*-carboxyanhydride (NCA) initiated by an amino-containing α -azide initiator was employed to synthesize the α -azido PBLG homopolymers. Subsequently, copper-catalyzed Huisgen's 1,3-dipolar cycloaddition (click chemistry) was utilized to connect the two rigid-rod blocks. The PDI

values of the resultant PMPCS-*b*-PBLG diBCPs were approximately 1.30. Similarly, a rod-rod diBCP containing the PBLG block and a different MJLCP block, poly[octyl-4'-(octyloxy)-2-vinylbiphenyl-4-carboxylate] (PVBP, polymer **13** Fig. 3.2), has also been synthesized in a recent study (Zhou et al. 2013).

3.3.1.3 SCLCP-Rod Diblock Copolymers

Zhang, Chen, and co-workers synthesized an SCLCP-rod diBCP containing an SCLCP poly[ω -(4'-methoxybiphenyl-4-yloxy)hexyl methacrylate] (PMBHMA), PMBHMA-*b*-PMPCS (Xie et al. 2009). Another living radical polymerization method, reversible addition-fragmentation chain transfer (RAFT) polymerization, was utilized to obtain the diBCP. The chain transfer agent (CTA), 2-(2-cyanopropyl)dithiobenzoate (CPDB), based on dithiobenzoate works for both monomers of PMHBMA and PMPCS. Therefore, RAFT was carried out sequentially to synthesize the diBCP with PDI < 1.30.

3.3.1.4 Brush-Rod Diblock Copolymers

A brush-rod type diBCP containing an MJLCP, PMBPS, and a polymethacrylate with poly(ethylene glycol) (PEG) side chains (PPEGMA) was synthesized by sequential ATRP (Cao et al. 2007). The PPEGMA brush was prepared with the grafting-through technique by ATRP of the PEGMA macromonomer, and then it was used as the macroinitiator to initiate ATRP of the monomer of PMBPS, MBPS. The two resulting brush-rod diBCP samples had PDIs of ca. 1.40.

3.3.1.5 Dendritic-Rod Diblock Copolymers

Recently, dendritic-rod type diBCPs containing rod-like PMPCS and a semi-rigid Percec-type dendron with hydrophilic PEG tails, PEG(G_m) (where m is the number of dendron generation, and $m = 1, 2, 3$), were synthesized (Cai et al. 2014). The diBCPs were prepared by NMRP of MPCPS in solution using the dendritic macroinitiators with different dendron generations. After the acetylene-terminated dendrons were prepared with the divergent strategy, the TEMPO group was incorporated at the focal point by esterification reaction, and the PEG tails were introduced by a typical click reaction, the Huisgen's 1,3-dipolar cycloaddition reaction, leading to the dendritic macroinitiators (Cai et al. 2012). The dendritic-rod diBCPs obtained had PDI values in the range of 1.2–1.4.

3.3.2 ABA Triblock Copolymers

ABA-type linear triBCPs containing MJLCP rod blocks are usually prepared by polymerizing the A monomer initiated by the difunctional macroinitiator of the middle B block. Similar controlled/living radical polymerization methods to those employed in synthesizing AB diBCPs can be utilized. For example, the sequential NMRP technique has been used to synthesize ABA triBCPs containing an MJLCP, poly{2,5-(4-butylbenzoyl)oxystyrene} (PBBOS) (Gopalan et al. 2003) or PMPCS (Gao et al. 2007), as the end A block, with PS or polyisoprene (PI) as the middle B block, respectively.

Sequential ATRP has also been successfully applied to synthesize MJLCP-containing ABA triBCPs. Difunctional PBA macroinitiators were obtained by ATRP and then used for chain extension by MPCS (Yi et al. 2004). PMPCS-*b*-PBA-*b*-PMPCS triBCPs obtained had high MWs over 7×10^4 g/mol and PDIs close to 1.10. Recently, ABA triBCPs with an MJLCP, poly[2,5-di(*n*-hexogycarbonyl)styrene] (PDHCS), as the middle block were prepared, also by sequential ATRP (Liu et al. 2014). The end A block is poly(4-vinylpyridine) (P4VP). The resulting P4VP-*b*-PDHCS-*b*-P4VP triBCPs had controlled MWs, with PDI values of approximately 1.40.

ABA triBCP PMBPS-*b*-PEO-*b*-PMBPS was synthesized with ATRP by using a difunctional PEO macroinitiator prepared from commercially available PEO with hydroxyl groups at both ends (Zhang et al. 2005b). The triBCP obtained had a relatively narrow polydispersity. For the synthesis of ABA triBCPs containing PCL as the middle B block, ROP of ϵ -caprolactone followed by ATRP of MPCS was applied (Shi et al. 2005). ROP of ϵ -caprolactone initiated by ethylene glycol led to PCL end-capped with two hydroxyl groups, which was modified by 2-bromoisobutryl bromide to become the difunctional ATRP macroinitiator Br-PCL-Br. The resulting PMPCS-*b*-PCL-*b*-PMPCS triBCPs had controlled MWs and PDI values of approximately 1.30.

In addition, ABA triBCPs with polyisobutylene (PIB) as the middle coil block and PMPCS as the end A rod block were synthesized by the combination of living cationic polymerization of isobutylene and subsequent ATRP of MPCS (Gao et al. 2008). PIB synthesized by living cationic polymerization initiated by 1,4-bis(2-chloro-2-propyl)benzene was introduced with short PS segments at the chain ends to form the difunctional Cl-PIB-Cl macroinitiator. Further ATRP of MPCS resulted in triBCPs with varying MWs and compositions. The PDIs of the triBCPs were below 1.40.

3.3.3 ABC Triblock Copolymers

ABC-type linear triBCPs containing rod-like MJLCP blocks can also be synthesized using the strategies mentioned above. TriBCP PEO-*b*-PMMA-*b*-PMPCS was

prepared by ATRP from a PEO macroinitiator (Zhang et al. 2005a). The PEO-Br macroinitiator was prepared from the monofunctionalized PEO (PEO-OH) by the reaction with 2-bromoisobutyryl bromide. It was then used to initiate the ATRP of methyl methacrylate (MMA) first to synthesize the diBCP macroinitiator, which subsequently initiated the ATRP of MPCPS, leading to the PEO-*b*-PMMA-*b*-PMPCPS triBCPs with PDI values in the range of 1.10–1.20. With the replacement of the PEO macroinitiator by a PDMS one and PMMA by PS, a triBCP, PDMS-*b*-PS-*b*-PMPCPS, was obtained by using the same synthetic approach (Shi et al. 2014). The triBCP had a PDI of 1.13.

3.3.4 Star Block Copolymers

When star-shaped, multifunctional macroinitiators are used to synthesize BCPs, star BCPs can be obtained. Ober et al. prepared the first three-armed star BCP containing an MJLCP block, PBBOS, by the sequential NMRP strategy (Gopalan et al. 2003). A TEMPO-based trifunctional initiator initiated the polymerization of styrene, leading to the star PS macroinitiator. Then this macroinitiator was used to polymerize [2,5-(4-butylbenzoyl)oxystyrene] (BBOS) to obtain the well-defined tri-armed star BCP with the MJLCP PBBOS as the rod block.

Zhang and co-workers synthesized several star BCPs with MJLCP rod blocks (Chen et al. 2006a; Shi et al. 2004; Wang et al. 2005). With a four-armed star initiator, they obtained four-armed rod-coil star BCPs by using sequential ATRP of MMA and MPCPS (Wang et al. 2005). The resultant star-shaped (PMMA-*b*-PMPCPS)₄ BCPs had narrow MWDs. In a different approach, a PS macroinitiator prepared by ATRP was converted to a difunctional macroinitiator, which then initiated the ATRP of MPCPS (Chen et al. 2006a). The tri-armed star polymer obtained is a miktoarm star BCP with one PS arm and two PMPCPS arms. A star-shaped rod-coil BCP (PCL-*b*-PMPCPS)₃ was synthesized by ATRP (Shi et al. 2004). The PCL macroinitiator was prepared from a tri-armed star (PCL-OH)₃ synthesized by ROP. The resultant tri-armed star BCPs had controlled MWs and PDI values of less than 1.35.

3.4 Self-Assembly of Block Copolymers Based on MJLCPs

3.4.1 Self-Assembly in Bulk

Because of chemical differences or distinctive physical properties between the composing blocks, most MJLCP-based BCPs studied microphase separate in bulk. Same as other microphase-separated BCPs, they can self-assemble into ordered nanostructures. Furthermore, the jacketed polymers exhibit LC properties

when their MWs are sufficiently high, resulting in hierarchical structures. Finally, the self-assembled structures can undergo phase transitions under certain conditions, making structural control possible.

3.4.1.1 Microphase Separation and Properties

In the early studies on BCPs containing MJLCP rod blocks, microphase separation of the BCPs was confirmed by the observation of individual glass transitions of the constituting blocks and liquid crystallinity of the MJLCP blocks. For example, DSC results of the first MJLCP-based BCPs, PS-*b*-PMPCS, demonstrate two distinct glass transitions of the PS and PMPCS blocks, clearly indicating microphase separation of the BCPs (Wan et al. 2000). PDMS-*b*-PMPCS also exhibits two distinctive glass transitions with a temperature difference of about 250 °C owing to the low T_g (ca. -120 °C) of PDMS and the relatively high T_g (ca. 130 °C) of PMPCS (Yi et al. 2003). Recently, a rod-coil-rod ABA-type triBCP, PMVBP-*b*-PDMS-*b*-PMVBP, was synthesized (Li et al. 2014). Similarly, it had a significantly large difference in T_g 's, due to the relatively high T_g of PMVBP. PBA-*b*-PMPCS also have two different T_g 's, one at ca. -45 °C for PBA and the other at ca. 115 °C for PMPCS (Gao et al. 2005).

The liquid crystallinity of the MJLCPs is an important aspect in the research of MJLCP-based BCPs. The BCPs show a similar MW effect on liquid crystallinity to that for MJLCP homopolymers. Only MJLCP blocks with high enough MWs in the BCPs exhibit LC behaviors, as expected and also demonstrated by several examples such as PS-*b*-PMPCS (Zhang et al. 2002b), PDMS-*b*-PMPCS (Yi et al. 2003), PMMA-*b*-PMPCS (Zhang et al. 2003), and the miktoarm star block copolymer with one PS arm and two PMPCS arms (Chen et al. 2006a).

In addition, the coil block in rod-coil BCPs usually has a negligible effect on the LC properties of the MJLCP blocks (Yi et al. 2003). However, it is a different case for rod-rod BCPs, especially when the two rods have different diameters. Taking PVBP-*b*-PBLG as an example, the Φ_N phase of PVBP and the Φ_H phase of PBLG disrupt each other possibly owing to the packing frustration caused by the size disparity (Zhou et al. 2013).

Other properties of BCPs containing MJLCPs with special properties have also been studied. For BCPs with semifluorinated MJLCP blocks, the surfaces are covered with fairly hydrophobic CF₂ groups, leading to relatively high water contact angle values (Gopalan et al. 2002). And the maximum optical rotation value of the BCP almost doubles from that of the helical macroinitiator used to initiate ATRP of an achiral MJLCP monomer, owing to the chiral induction ability of helical MJLCPs on achiral ones (Cui et al. 2010).

3.4.1.2 Self-Assembled Nanostructures

Rod-coil BCPs having MJLCP rod blocks can self-assemble into various ordered nanostructures, including BCC, HEX, and LAM structures observed in PDMS-*b*-PMPCS (Shi et al. 2011, 2013) and PDMS-*b*-PBPCS (Shi et al. 2012a). PDMS-*b*-PMPCS BCPs having PMPCS blocks with relatively low MWs also form GYR and *Fddd* phases (Shi et al. 2013). The *Fddd* morphology is not commonly observed for rod-coil BCPs. As rod-coil BCPs, the phase diagrams of these MJLCP-containing BCPs are also asymmetric, with a larger area of the LAM morphology compared to the phase diagrams of coil-coil BCPs. The highly ordered nanostructures exhibited by the PDMS-*b*-PMPCS BCPs containing low-MW PMPCS blocks indicate a strong phase separation tendency for PDMS and PMPCS. Some of the nanostructures possess relatively small periodicities of less than 20 nm.

Perforated layer structures, including a tetragonally perforated lamellar (TPL) morphology with a fourfold symmetry which was confirmed by small-angle X-ray scattering (SAXS) and transmission electron microscopic (TEM) results, were observed in a series of PS-*b*-PMPCS diBCPs (Tenneti et al. 2005). The degree of perforation increases with increasing volume fraction of the PS block. The TPL structure was found for the first time to be formed by the sample having a PMPCS volume fraction (f_{PMPCS}) of 0.37 and a relatively low MW. The structure was also observed in a blend of a higher-MW BCP and PS homopolymer with an f_{PMPCS} of 0.48 for the blend. Such a significant phase boundary shift is owing to the rod-coil nature of the BCP. Recently, a rectangular cylinder morphology was reported for a rod-coil BCP having a main-chain/side-chain combined LCP, PS-*b*-PBBHCS (Wen et al. 2013). A HEX morphology with coil cylinders in the rod matrix is formed in rod-coil-rod PMPCS-*b*-PIB-*b*-PMPCS triBCPs with high rod fractions (Gao et al. 2008). Such a nanostructure, rarely observed for rod-coil BCPs, had a curved IMDS with the rod block at the convex side. Polystyrene-*block*-poly{3,5-bis[(4'-(4''-tetradecanoylbenzoyl)oxy)benzoyl]oxy}styrene} (PS-*b*-PTBOS) forms coil spheres in the rod matrix (Tenneti et al. 2008). The morphology is stabilized by reduced interaction among the PTBOS (polymer **8** with $n = 14$ in Fig. 3.2) rod blocks owing to the covering of the rod surface by the soft shell.

3.4.1.3 Hierarchical Structures

The first example of hierarchical structures of BCPs containing MJLCP rod blocks was found in PS-*b*-PMPCS rod-coil diBCPs (Li et al. 2004). A lamellar structure was identified in a symmetric PS-*b*-PMPCS sample with a relatively low MW, as verified by both SAXS and TEM results. PMPCS forms a Φ_N phase in its sublayer, with the columns aligned parallel to the lamellar normal. In addition, the PMPCS columns are packed in a bilayer manner (Fig. 3.5). Therefore, the hierarchical structure is similar to a “bilayer SmA” phase found in LC small molecules and rod-coil oligomers. The TPL morphology formed by asymmetric PS-*b*-PMPCS is

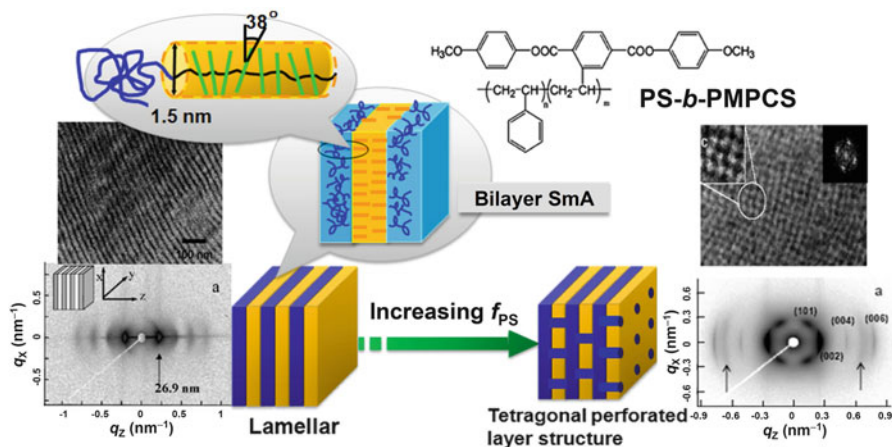


Fig. 3.5 Hierarchical self-assembled supramolecular structures of PS-*b*-PMPCS. For the symmetric BCP with a relatively low MW, a lamellar nanostructure is formed, as shown in the TEM micrograph and the 2D SAXS pattern. The PMPCS columns are aligned parallel to the lamellar normal. The packing of the rod-coil BCP resembles a “bilayer SmA” structure. When the volume fraction of PS (f_{PS}) is increased to obtain an asymmetric BCP, a TPL structure is formed, in which coils (PS) punctuate the LC layers, and the PS chains in the LC layer are packed in a tetragonal instead of hexagonal lattice shown by the TEM and 2D SAXS results. Reprinted and adapted with permissions of the American Chemical Society and the Royal Society of Chemistry (Chen et al. 2010; Li et al. 2004; Tenneti et al. 2005)

also a hierarchical structure, with PMPCS being liquid crystalline (Fig. 3.5) (Tenneti et al. 2005). In addition, the MCSCLCP-containing rod-coil BCP PS-*b*-PBBHCS forms a hierarchical structure with three length scales (Wen et al. 2013). Such a complex structure combines the microphase separation of the BCP and the hierarchically ordered LC structure with two length scales of the MCSCLCP.

The rod-coil-rod ABA-type MJLCP-based triBCP, PMPCS-*b*-PI-*b*-PMPCS, forms lamellar structures, and the PMPCS rods form a Φ_N phase (Gao et al. 2007). Similarly, PMPCS-*b*-PIB-*b*-PMPCS also self-assembles into hierarchical structures, depending on the volume fraction of the PMPCS rod block (Gao et al. 2008). TriBCPs with relatively symmetric compositions form lamellar structures, while those having high f_{PMPCS} values exhibit HEX morphologies with coil cylinders in the rod matrix. PMPCS blocks in all the triBCPs studied are liquid crystalline owing to their high MWs.

Within the microphase-separated lamellar structure of the PCL-*b*-PMPCS diBCP, the PCL block crystallizes in the one-dimensional (1D) confinement, while the PMPCS block can be liquid crystalline (Liu et al. 2008). Detailed structural studies demonstrate that both the crystalline PCL and the LC PMPCS chains are aligned parallel to the lamellar normal.

In the rod-rod diBCP PMPCS-*b*-PBLG, a hexagon-in-lamella hierarchical structure is formed (Zhou et al. 2010) when the volume fraction of PBLG (f_{PBLG}) is ca. 0.50. PMPCS is in a Φ_{HN} phase, and PBLG has a Φ_H structure. Both rods are

stacked in a bilayer manner and aligned parallel to the lamellar normal. PMPCS-*b*-PBLG with an f_{PBLG} of 0.69 forms a hexagon-in-cylinder morphology, with PMPCS cylinders in the PBLG matrix. And both rods have interdigitated packing and parallel orientation. When the PMPCS rod is replaced with PVBP which has a larger diameter than PBLG, the microphase-separated structures are all lamellar (Zhou et al. 2013). The phases of the two rods vary with the composition of the BCP, and the two rods are not aligned parallel any more.

In the SCLCP-rod diBCP containing the MJLCP PMPCS, PMBHMA-*b*-PMPCS, with a PMPCS volume fraction of ca. 0.49, a lamellar self-assembled morphology was observed (Xie et al. 2009). The PMPCS rods in the columnar LC phase are aligned parallel to the lamellar normal. Its LC phase does not change or greatly affect the LC behavior of the PMBHMA block. The SmA phase existing for the PMBHMA homopolymer disappears for the BCP, while its nematic phase is stabilized in a wider temperature range, indicating the confinement effect in this BCP system. In addition, the PMBHMA block forms a SmE phase in small domains with homogeneous orientation at low temperatures, owing to the nano-confinement imposed by the rigid PMPCS sublayers.

3.4.1.4 Interplay Between Microphase Separation and LC Phase Formation

In the self-assembly of rod-coil BCPs containing LCPs, microphase separation of the BCP and LC phase formation of the LCP block influence and compete with each other (Lee et al. 2001; Thomas et al. 1997). Such phenomena have also been observed in BCPs with MJLCP rod blocks. A good example is the rod-coil diBCP PS-*b*-PTBOS (Tenneti et al. 2008). The PTBOS homopolymer forms a Φ_{H} phase when the MW is high enough. However, in the self-assembled coil spheres of the BCP, the LC order of PTBOS is reduced to Φ_{N} mainly due to the curved IMDS. The competition between microphase separation and LC phase formation is also observed in the coil-rich PS-*b*-PTBOS sample. The PTBOS block is again only in the Φ_{N} phase within a perforated lamellar morphology. The reduction in the order of the LC phase can be attributed to the bending of the rods under the influence of a splaying stress field owing to the lateral repulsion of the coil chains. The PTBOS block changes back to the Φ_{H} phase in the LAM structure of the PS-*b*-PTBOS/oligo-PS blend having a relatively symmetric composition, with the release of the abovementioned repulsion.

On the other hand, for the rod-coil BCP with a main-chain/side-chain combined LCP, PS-*b*-PBBHCS, the microphase separation of the BCP can stabilize the hierarchical LC structure of PBBHCS (Wen et al. 2013). Same as the homopolymers, the PBBHCS block forms a hierarchical LC structure with a Φ_{R} phase of the main chain on the nanometer scale and the packing of the biphenyl mesogen in the side chains on the subnanometer scale. Compared to the case of the homopolymers with comparable MWs, the LC structure of the PBBHCS block in the BCP on two length scales is more stable.

For the rod–rod diBCP PVBP-*b*-PBLG with different rod diameters, the microphase-separated structure becomes more ordered with decreasing content of the PBLG block for BCPs with a similar length of the PVBP rod, as demonstrated by more high-order reflections in SAXS profiles (Zhou et al. 2013). With increasing volume fraction of PVBP (f_{PVBP}), the self-assembled structure changes from a poorly ordered one to interdigitated lamellae then to a bilayer lamellar morphology.

3.4.1.5 Interplay Between Microphase Separation and Crystallization

For rod–coil BCPs with a crystalline coil block, the crystallization of the coil further complicates the self-assembling behavior. For the PCL-*b*-PMPCS diBCPs and the PMPCS-*b*-PCL-*b*-PMPCS triBCPs with PCL blocks of fixed lengths, the melting process of the PCL block becomes weaker in DSC thermograms with increasing length of the PMPCS rod block (Shi et al. 2005). At the same time, the melting temperature (T_m) also shows a slight decrease.

Similar behaviors were observed in other PCL-*b*-PMPCS diBCP samples (Zhao et al. 2005). The crystallization rate of PCL in the 1D confinement is different depending on the phase structure of PMPCS which forms the rigid confinement (Liu et al. 2008). The PCL chains confined by the LC PMPCS blocks are more stretched compared with those in the amorphous confinement, leading to faster crystallization and an increased fold length.

3.4.1.6 Morphological Control and Transitions

As from the phase diagrams, the morphologies of BCPs can be readily controlled by varying composition, MW, or temperature. With increasing temperature, the ordered structures will eventually disorder, going through an order-disorder transition (ODT). And many order-order transitions (OOTs) can occur between different ordered structures of BCPs by changing the temperature owing to the change in the Flory-Huggins interaction parameter χ (Kimishima et al. 2000). Applying an external field (Schmidt et al. 2010), adding a selective solvent (Li et al. 2007), or blending a homopolymer (Lodge et al. 2002) can also induce OOTs. For liquid crystalline BCPs, OOTs can be triggered by the phase transformation of the LC block (Sänger et al. 1997).

Morphological Control

While it is a common practice to obtain different self-assembled structures by synthesizing BCPs with different compositions, blending the BCPs with homopolymers of low MWs is a facile and effective method to adjust the composition and therefore the morphology, which can also be applied to BCPs containing MJLCPs. With this approach, a highly ordered TPL structure is formed by a

high-MW PS-*b*-PMPCS sample when it is blended with a PS homopolymer (Tenneti et al. 2005). Similarly, a hierarchical LAM structure with the MJLCP, PTBOS, block in the Φ_H phase is obtained by blending a PS oligomer with the PS-*b*-PTBOS diBCP (Tenneti et al. 2008).

Besides the structural change when homopolymers are blended, the size of the self-assembled structure will certainly increase if the structure remains the same, simply due to the increased overall MW. By blending PMPCS-*b*-PIB-*b*-PMPCS with either the coil PIB or the rod PMPCS homopolymer with a relatively low MW, morphological transformation or size increase is realized (Gao et al. 2009b). Adding either the coil PIB or the rod PMPCS homopolymer into the lamellar triBCP leads to a new lamellar structure with a larger layer spacing. In particular, addition of the coil homopolymer into a HEX-structured triBCP sample results in a phase transition to a lamellar morphology.

ODTs

While many MJLCP-based BCPs have ODTs with transition temperatures that are too high to be experimentally observed, the ODT of PS-*b*-PBBOS occurs between 120 and 150 °C, as determined by variable-temperature SAXS experiments (Gopalan et al. 2003). The intensity of the reflection peak attributed to the microstructure begins to decrease on heating to 120 °C, and the peak disappears at 150 °C. The morphology can be formed again after slow cooling due to very slow ordering kinetics.

Irreversible OOTs

Many MJLCPs such as PMPCS undergo irreversible phase transitions from the amorphous state, which is the unstable state at low temperatures, to the LC phases at temperatures above their respective T_g 's. Consequently, BCPs containing such MJLCP rod blocks can have irreversible OOTs during the amorphous-LC phase transformations. A LAM-LAM OOT was observed in triBCP PMPCS-*b*-PIB-*b*-PMPCS (Gao et al. 2008). The lamellar spacing has a jump during heating when the PMPCS block enters into the LC phase, while its change is gradual during cooling, indicating the irreversible nature of the OOT on heating. DiBCP PCL-*b*-PMPCS exhibits a similar LAM-LAM OOT with a significant increase in the lamellar spacing during heating (Liu et al. 2008).

Another type of irreversible OOTs was observed in a PDMS-*b*-PMPCS diBCP sample (Shi et al. 2013). It is a HEX-LAM transition for a PDMS-*b*-PMPCS sample with a high-MW PMPCS block which forms the LC phase when the diBCP is annealed at high temperatures, as demonstrated by SAXS, wide-angle X-ray scattering (WAXS), and TEM results (Fig. 3.6). The linear ABC triBCP PDMS-*b*-PS-*b*-PMPCS also shows an irreversible OOT accompanied with the amorphous-LC phase transition of PMPCS during heating (Shi et al. 2014). The self-assembled

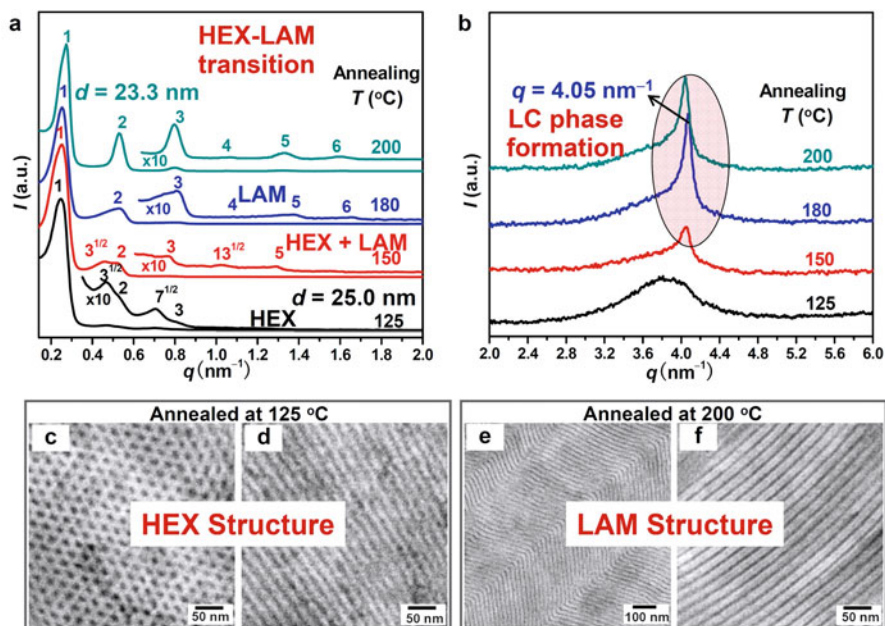


Fig. 3.6 HEX-LAM OOT in PDMS₅₈-*b*-PMPCS₄₄ induced by the amorphous-LC phase transition of PMPCS. The sample self-assembles into a cylinder structure when it is annealed at relatively low temperatures, while the morphology becomes lamellae at high annealing temperatures, as shown by the SAXS results (a). The OOT is associated with the LC formation of PMPCS on the basis of WAXS results (b). TEM results confirm the HEX (c, d) and LAM (e, f) structures when the sample is annealed at different temperatures. Reprinted and adapted with permission of the American Chemical Society (Shi et al. 2013)

nanostructure of the triBCP changes from core-shell hexagonally packed cylinders (CSH) to a three-phase four-layer lamellar (LAM-3P4L) structure after annealing above 140 °C.

BCPs with other MJLCPs that have similar LC phase behaviors to PMPCS can also undergo irreversible OOTs. For the diBCP poly(isobutyl methacrylate)-*block*-poly[2,5-di(isopropylxycarbonyl)styrene] PiBMA-*b*-PiPCS, the MJLCP block PiPCS forms a Φ_H LC phase at high temperatures when its DP is over 168 (Guan et al. 2010). PiBMA-*b*-PiPCS changes from an undetermined microstructure to a lamellar morphology when PiPCS transforms from the isotropic state into the Φ_H phase.

Reversible OOTs

Because the LC phase behaviors of MJLCPs are MW-dependent, MJLCPs with low enough MWs are always amorphous in the whole temperature range. Thus, BCPs containing low-MW, and thus amorphous, MJLCPs can undergo reversible OOTs

by changing the temperature. For example, PDMS-*b*-PMPCS diBCPs with low-MW PMPCS blocks exhibit GYR-*Fddd* and HEX-BCC OOTs with the increase in annealing temperature (Shi et al. 2013).

On the other hand, for BCPs having MJLCP blocks with reversible LC phase transitions, the OOTs induced by the LC transformations with changing temperature should be reversible. A reversible BCC-HEX OOT was observed in PDMS-*b*-PBPCS because the MJLCP block PBPCS has a reversible isotropic-LC phase transition (Shi et al. 2012a). In addition, because of the re-entrant LC phase behavior of PBPCS (Zhao et al. 2006), the sequence of the BCC-HEX transition is reversed compared with that in other BCPs containing regular LCs.

Furthermore, for PDMS-*b*-PMPCS, because supercritical CO₂ (scCO₂) can be regarded as a selective solvent for the PDMS block, it has been used to induce a HEX-LAM OOT (Shi et al. 2011). The OOT is caused by increases in the apparent volume fraction of the coil PDMS block and the effective Flory-Huggins interaction parameter. The transformed LAM structure is retained when CO₂ is released, owing to the high T_g of PMPCS. And the HEX structure is recovered after the sample is annealed at high temperatures in vacuum. Such a HEX-LAM OOT is critically dependent on the location of the BCP sample in the phase diagram. The other HEX-structured PDMS-*b*-PMPCS sample only shows an increase in the periodic size. And no OOT is observed for the LAM-structured BCP sample also due to its location in the phase diagram.

3.4.2 Self-Assembly in Films

There are only a few examples of self-assembled structures in films for BCPs with MJLCP blocks. Hierarchical structures were observed (Fig. 3.7) in thin films of asymmetric AB/AC blends of rod-coil diBCP PDMS-*b*-PMPCS (DMPCS, AB) and coil-coil diBCP PDMS-*b*-PMMA (DMMA, AC) (Shi et al. 2012b). The common block PDMS is the minor component in both diBCPs. For the DMPCS/DMMA BCP blends, SAXS results show that macrophase separation and microphase separation both occur in bulk, resulting in hierarchical structures that were directly observed by TEM. The samples used are a HEX-structured DMPCS (DMPCS_{HEX}), a HEX-structured DMMA (DMMA_{HEX}) with vertical cylinders, and a vertical lamellar DMPCS (DMPCS_{LAM}). For the thin film of the DMPCS_{HEX}/DMMA_{HEX} blends with 75 wt% of one diBCP, subordered macrophase-separated structures along with ordered nanostructures in the macrodomains were observed. The blend having 75 wt% of DMMA_{HEX} has a more ordered macrophase-separated submicrometer structure, with more smooth interfaces of the macrodomains. The thin film of the DMPCS_{LAM}/DMMA_{HEX} blend with 75 wt% of DMPCS_{LAM} exhibits hamburger-like structures in the DMPCS_{LAM} matrix as a result of the solubilized DMMA in DMPCS_{LAM} on the segmental length scale. Short DMPCS lamellae of a few layers are uniformly distributed in the DMMA_{HEX} matrix when there is 25 wt% of DMPCS_{LAM} in the blend.

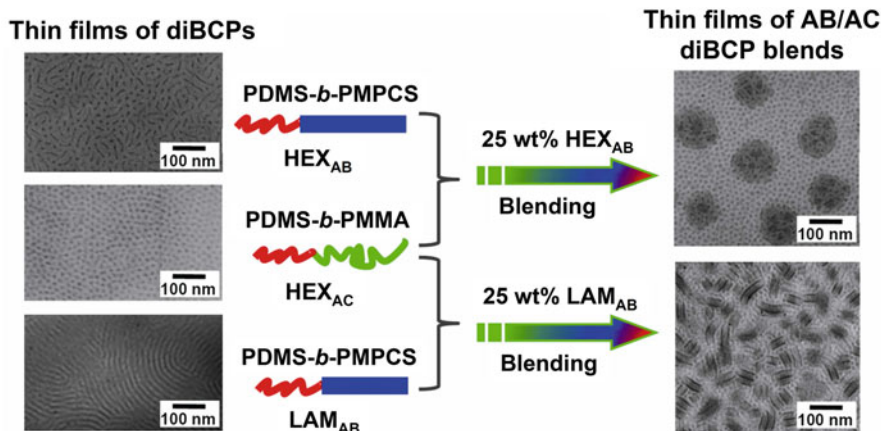


Fig. 3.7 Hierarchical structures in thin films of asymmetric blends of rod-coil PDMS-*b*-PMPCS and coil-coil PDMS-*b*-PMMA. TEM results demonstrate that the thin film of the blend containing 75 wt% of vertical DMMA_{HEX} and 25 wt% of DMPCS_{HEX} displays a subordered macrophase-separated structure and ordered nanostructures in the macrodomains. The thin film of the blend containing 75 wt% of vertical DMMA_{HEX} and 25 wt% of vertical DMPCS_{LAM} exhibits hamburger-like structures which are short DMPCS lamellae of a few layers uniformly distributed in the DMMA_{HEX} matrix. Reprinted and adapted with permission of the American Chemical Society (Shi et al. 2012b)

Monolayer films are formed by hexagonally packed core-shell spherical micelles of the PS-*b*-PMPCS diBCP after evaporation of a selective solvent (Tu et al. 2009). By varying the length of PMPCS while fixing the length of PS, the micelle size can be readily controlled, with the sphere diameters ranging from several tens of nanometers to over 100 nm. Solutions of larger spherical micelles form more ordered films than those from smaller micelles. The monolayer film self-assembled from the largest spherical micelles exhibits a broad adsorption peak with the maximum at 545 nm in the UV-vis spectrum, and it appears red in the optical microscope operated in the reflection mode. Monolayer films formed by cylindrical worm-like micelles were also obtained.

Ordered monolayers are formed by the amphiphilic rod-coil diBCP PEO-*b*-PMBPS with a majority of hydrophobic component at the air-water interface (Zhang et al. 2006). The monolayers can be transferred to a mica substrate by using the Langmuir-Blodgett (LB) technique. Initially, spherical aggregates at the surface form in the LB monolayers. With increasing surface pressure, the morphology changes to long cylindrical aggregates following the pancake-brush conformational transformation of the BCP. The similar morphological transition occurs for the series of PEO-*b*-PMBPS BCPs when the rod content is increased. The structural reorganization behavior of PEO-*b*-PMBPS is distinctly different from that of the PEO-*b*-PS BCP, possibly owing to the orientation of the PMBPS rod block.

3.4.3 Self-Assembly in Solutions

3.4.3.1 Rod–Coil Diblock Copolymers

The self-assembling behavior of the rod–coil diBCP PS-*b*-PMPCS has been investigated systematically. The BCP forms a core-shell nanostructure with a PMPCS core and a PS shell when its dilute solution is cooled (Tu et al. 2000b). Static and dynamic laser light scattering (LLS) results give the core radius (R_c) and the shell thickness (ΔR). When more chains are aggregated into the core-shell nanostructure with increasing concentration, R_c , which is associated with the contour length of the PMPCS block, remains constant, while the shell becomes thicker. The above results indicate the insertion of the PMPCS rod blocks into the core due to the attraction between the insoluble PMPCS rods and the stretch of PS chains in the shell caused by the repulsion between the soluble PS coils.

Further study on PS-*b*-PMPCS diBCPs with the same PS length and different PMPCS lengths shows that the morphology varies with the rod length, with the size controlled by the rod length (Tu et al. 2003b). In addition, the critical association concentration (CAC) decreases with increasing MW of the PMPCS rod (Tu et al. 2003a). The BCPs form core-shell nanostructures, confirmed by LLS and TEM results. Core-shell micelles are also formed by the rod–coil diBCP PBA-*b*-PMPCS (Gao et al. 2005).

The self-assembly of the amphiphilic rod–coil diBCP PEO-*b*-PMBPS in solutions has also been studied systematically. The BCP forms different supramolecular structures such as spherical micelles, vesicles, and large compound vesicles (LCVs) in aqueous solutions with varying block lengths and initial concentrations (Zhang et al. 2005c). The solvent effect on the water-induced aggregation behavior of the BCP has also been investigated (Zhang et al. 2008). In dioxane, narrowly distributed spheres form with the addition of water, while the aggregates formed in tetrahydrofuran (THF) have a bimodal distribution. The solvent-induced association and micellization of PEO-*b*-PMBPS diBCPs with a fixed PEO length and varying PMBPS lengths have been investigated in situ by LLS (Lin et al. 2009). PEO-*b*-PMBPS remains the single-chain state in dioxane which is a selective solvent for the PMBPS block. When the selective solvent for the PEO block, water, is added, PEO-*b*-PMBPS goes through the association governed by PEO and the micellization governed by PMBPS. With increasing water content, formation of associate, formation of micelles, and breakdown of associate occur in sequence. Mixed structures of associate and micelles are obtained under certain conditions, with the structure of the associate “frozen” by the rod chains.

3.4.3.2 Brush–Rod Diblock Copolymers

The self-assembly of the amphiphilic PPEGMA-*b*-PMBPS brush–rod diBCP varies by using different methods (Cao et al. 2007). For the PPEGMA₃₇-*b*-PMBPS₈₇

sample, spherical morphologies dominate independent of the initial concentration and the water addition rate. For PPEGMA₃₇-*b*-PMBPS₁₄₁ with increased hydrophobicity, primary spheres and large compound spherical or rod-like micelles form at the same time with a slow addition of water, while the sample self-assembles into spherical aggregates only when the water addition rate is high or when its THF solution is poured into a large amount of water.

Kinetic study on PPEGMA₃₇-*b*-PMBPS₁₄₁ by time-resolved LLS and TEM demonstrates that the BCP undergoes a sphere-rod transition (Lin et al. 2010). Spherical large compound micelles (LCMs) are formed in the THF/water mixed solvent. The LCMs transform to large compound rods (LCRs) within hours. A higher polymer concentration and an intermediate water content favor such a sphere-rod transition, which is also contributed by the depletion effect of free polymer chains in addition to the instability or defects of the LCMs.

3.4.3.3 Dendritic-Rod Diblock Copolymers

The self-assembly of the dendritic-rod diBCP PEG(*G_m*)-*b*-PMPCS changes from vesicles to LCVs then to short cylindrical micelles with the increase in dendron generation, as shown in Fig. 3.8 (Cai et al. 2014). Stable LCVs with surfaces having narrowly distributed pores are formed by PEG(*G₂*)-*b*-PMPCS in a THF/water

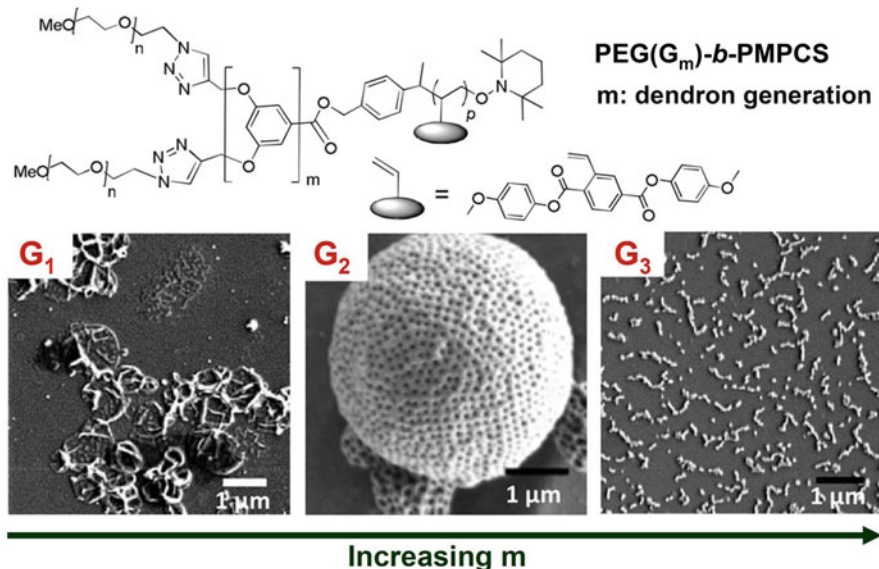


Fig. 3.8 Self-assembled structures of a dendritic-rod diBCP PEG(*G_m*)-*b*-PMPCS. With increasing dendron generation, the morphology undergoes transitions from vesicles to LCVs then to short cylindrical micelles, as illustrated by TEM results. Reprinted and adapted with permission of the American Chemical Society (Cai et al. 2014)

mixed solvent. There are two steps in the formation of such a supramolecular structure on nano- and micro-length scales. The first one is the morphological transformation, while the second one is the fusion or differentiation of vesicles. Vesicles are always the precursors of LCVs regardless of the initial morphology. On the other hand, the structures of the final LCVs are dependent upon the rate of water addition, with spherical LCVs for slow water addition and irregular (or deformed spherical) LCVs for fast water addition.

3.4.3.4 ABA Triblock Copolymers

The ABA-type amphiphilic triBCP PMBPS-*b*-PEO-*b*-PMBPS with the helical PMBPS forms vesicular aggregates in a mixed solvent of dioxane and water (Zhang et al. 2005b). The vesicles have a wide distribution of sizes. However, their thicknesses are quite uniform, at 27 ± 3 nm. In addition, the sizes of the vesicles are not dependent on the initial polymer concentration, and the PMBPS chains are packed in an interdigitated manner in the vesicles.

3.5 Conclusion and Future Perspective

3.5.1 Conclusion

In conclusion, as shape persistent polymer chains, MJLCPs have tunable dimensions which can be controlled by using controlled/living radical polymerization methods. They form columnar or smectic LC phases, which can be adjusted by suitable molecular design of MJLCPs. Rod-like MJLCPs have been widely used as rod building blocks in constructing BCPs, including linear and star BCPs. Such MJLCP-containing BCPs can be synthesized by various strategies, such as sequential NMRP, sequential ATRP, combination of ROP, ATRP, and click chemistry, and ATRP initiated by macroinitiators converted from commercial coil polymers. With the use of controlled polymerization techniques, these BCPs are well-defined, having controlled MWs and compositions.

BCPs with MJLCPs can self-assemble into various ordered nanostructures in bulk, including commonly observed BCC, HEX, LAM, and GYR morphologies as well as *Fddd* and TPL structures. For rod-coil BCPs, the introduction of liquid crystalline blocks enhances the phase separation abilities so that BCPs with relatively low MWs can still form ordered nanostructures, leading to morphologies with relatively small periodicities. In addition to the microphase-separated nanostructures, the LC phases formed by MJLCPs render hierarchical structures in these BCPs. Such structures can be controlled by using different methods, such as varying composition, changing temperature, using selective solvents, and tuning the phase structures of the MJLCP blocks. The different morphologies of the BCPs

can also be converted with these methods. And the OOTs can be either irreversible or reversible, depending on the properties of the MJLCP blocks and the methods applied to induce the phase transitions. Furthermore, BCPs having MJLCPs with re-entrant LC phase behaviors may exhibit unusual phase transitions compared to other BCP systems.

MJLCP-containing BCPs can also form ordered structures in thin films. And thin films of BCP blends display morphologies with two length scales. Finally, BCPs with MJLCP blocks can form various morphologies in solutions. Sometimes complex or hierarchical structures can be observed. These aggregated morphologies are dependent on the chemical structures of the BCPs, the type of the solvent, and even the rate of solvent addition.

3.5.2 Future Perspective

The synthesis and self-assembly of MJLCP-containing rod-coil BCPs have been systematically investigated. However, linear ABC triBCPs or BCPs with other more complex architectures have been less frequently studied. The morphologies of these BCPs may be different from BCPs with all coil blocks. The studies in these systems may be intriguing in both theoretical and experimental aspects. The advantage of using MJLCP rod blocks still lies in their relative ease in synthesis and superb controllability. In addition, MJLCP-containing BCPs that can form ordered nanostructures can serve as precursors to generate nanoporous materials, which can be used as nanocarriers and separation membranes. And the nanostructures formed by BCPs with relatively low MWs may be utilized as templates having periodicities under 20 nm.

ABA-type triBCPs containing a hard A block may be used as thermoplastic elastomers (TPEs). For example, the ABA-type triBCP PMPCS-*b*-PBA-*b*-PMPCS with a PMPCS hard A block and a PBA soft B block is elastomeric, with a potential as LC TPEs (Yi et al. 2004). The results from dynamic mechanical analysis (DMA) and tensile tests show that there is a well-defined rubbery plateau between two relaxation processes in the curve of temperature dependence of the dynamic shear storage modulus (G'). The sample does not flow above the T_g of the PMPCS block. The LC PMPCS domains serve as the physical network which persists at temperatures of at least 200 °C. Recently a new thermoplastic elastomer based on an ABA-type triBCP P4VP-*b*-PDHCS-*b*-P4VP was reported by Yang, Chen, and co-workers (Liu et al. 2014). In this system, the MJLCP PDHCS is the soft block, while P4VP serves as the hard block. The addition of zinc perchlorate extends the rubbery plateau of the resulting hybrid. Research in this area may result in potentially useful TPEs based on MJLCP-containing BCPs.

References

- Arehart SV, Pugh C (1997) Induction of smectic layering in nematic liquid crystals using immiscible components.1. Laterally attached side-chain liquid crystalline poly(norbornene)s and their low molar mass analogs with hydrocarbon/fluorocarbon substituents. *J Am Chem Soc* 119:3027–3037
- Bates FS (1991) Polymer-polymer phase behavior. *Science* 251:898–905
- Bates FS, Fredrickson GH (1990) Block copolymer thermodynamics: theory and experiment. *Annu Rev Phys Chem* 41:525–557
- Bates FS, Schulz MF, Khandpur AK, Forster S, Rosedale JH, Almdal K, Mortensen K (1994) Fluctuations, conformational asymmetry and block copolymer phase behaviour. *Faraday Discuss* 98:7–18
- Cai HH, Jiang GL, Shen ZH, Fan XH (2012) Effects of dendron generation and salt concentration on phase structures of dendritic-linear block copolymers with a semirigid dendron containing PEG tails. *Macromolecules* 45:6176–6184
- Cai HH, Jiang GL, Chen CY, Li ZB, Shen ZH, Fan XH (2014) New morphologies and phase transitions of Rod-coil dendritic-linear block copolymers depending on dendron generation and preparation procedure. *Macromolecules* 47:146–151
- Cao H, Lin W, Liu A, Zhang J, Wan X, Zhou Q (2007) Synthesis and self-assembly of brush-rod diblock copolymers in the mixed solvent of TBT/H₂O. *Macromol Rapid Commun* 28:1883–1888
- Chai CP, Zhu XQ, Wang P, Ren MQ, Chen XF, Xu YD, Fan XH, Ye C, Chen EQ, Zhou QF (2007) Synthesis and phase structures of mesogen-jacketed liquid crystalline polymers containing 1,3,4-oxadiazole based side chains. *Macromolecules* 40:9361–9370
- Chen JT, Thomas EL, Ober CK, Hwang SS (1995) Zigzag morphology of a poly(styrene-*b*-hexyl isocyanate) rod-coil block-copolymer. *Macromolecules* 28:1688–1697
- Chen JT, Thomas EL, Ober CK, Mao GP (1996) Self-assembled smectic phases in rod-coil block copolymers. *Science* 273:343–346
- Chen JF, Wang XZ, Liao XJ, Zhang HL, Wang XY, Zhou QF (2006a) Synthesis and characterization of novel mesogen-jacketed liquid crystalline miktoarm star rod-coil block copolymer. *Macromol Rapid Commun* 27:51–56
- Chen L, Chen YW, Zha DJ, Yang Y (2006b) Synthesis and properties of polyacetylenes with directly attached bis(4-alkoxyphenyl)terephthalate mesogens as pendants. *J Polym Sci A Polym Chem* 44:2499–2509
- Chen XF, Tenneti KK, Li CY, Bai YW, Zhou R, Wan XH, Fan XH, Zhou QF (2006c) Design, synthesis, and characterization of bent-core mesogen-jacketed liquid crystalline polymers. *Macromolecules* 39:517–527
- Chen S, Gao LC, Zhao XD, Chen XF, Fan XH, Xie PY, Zhou QF (2007) Synthesis and properties of mesogen-jacketed liquid crystalline polymers with asymmetry mesogenic core. *Macromolecules* 40:5718–5725
- Chen S, Zhang L-Y, Gao L-C, Chen X-F, Fan X-H, Shen Z, Zhou Q-F (2009) Influence of alkoxy tail length and unbalanced mesogenic core on phase behavior of mesogen-jacketed liquid crystalline polymers. *J Polym Sci A Polym Chem* 47:505–514
- Chen X-F, Shen Z, Wan X-H, Fan X-H, Chen E-Q, Ma Y, Zhou Q-F (2010) Mesogen-jacketed liquid crystalline polymers. *Chem Soc Rev* 39:3072–3101
- Cheng YH, Chen WP, Shen Z, Fan XH, Zhu MF, Zhou QF (2011a) Influences of hydrogen bonding and peripheral chain length on mesophase structures of mesogen-jacketed liquid crystalline polymers with amide side-chain linkages. *Macromolecules* 44:1429–1437
- Cheng YH, Chen WP, Zheng C, Qu W, Wu HL, Shen ZH, Liang DH, Fan XH, Zhu MF, Zhou QF (2011b) Synthesis and phase structures of mesogen-jacketed liquid crystalline polyelectrolytes and their ionic complexes. *Macromolecules* 44:3973–3980

- Cui JX, Liu AH, Cao HQ, Wan XH, Zhou QF (2010) Unusual chiral transfer in radical copolymerization of vinyl monomers bearing side-on p-terphenyl pendants. *Chem Asian J* 5:1139–1145
- Finkelmann H, Rehage G (1984) Liquid-crystal side-chain polymers. *Adv Polym Sci* 60:97–172
- Finkelmann H, Ringsdorf H, Wendorff JH (1978) Model considerations and examples of enantiotropic liquid-crystalline polymers—polyreactions in ordered systems. *Macromol Chem Phys* 179:273–276; 14. *Makromol. Chem*
- Gallot B (1996) Comb-like and block liquid crystalline polymers for biological applications. *Prog Polym Sci* 21:1035–1088
- Gao LC, Pan QW, Yi Y, Fan XH, Chen XF, Zhou QF (2005) Copolymers of 2,5-bis[(4-methoxyphenyl) oxycarbonyl]styrene with n-butyl acrylate: Design, synthesis, and characterization. *J Polym Sci A Polym Chem* 43:5935–5943
- Gao LC, Pan QW, Wang C, Yi Y, Chen XF, Fan XH, Zhou QF (2007) ABA-type liquid crystalline triblock copolymers via nitroxide-mediated radical polymerization: design, synthesis, and morphologies. *J Polym Sci A Polym Chem* 45:5949–5956
- Gao LC, Zhang CL, Liu X, Fan XH, Wu YX, Chen XF, Shen ZH, Zhou QF (2008) ABA type liquid crystalline triblock copolymers by combination of living cationic polymerization and ATRP: synthesis and self-assembly. *Soft Matter* 4:1230–1236
- Gao L-C, Fan X-H, Shen Z-H, Chen X, Zhou Q-F (2009a) Jacketed polymers: Controlled synthesis of mesogen-jacketed polymers and block copolymers. *J Polym Sci A Polym Chem* 47:319–330
- Gao LC, Yao J, Shen Z, Wu YX, Chen XF, Fan XH, Zhou QF (2009b) Self-assembly of rod-coil-rod triblock copolymer and homopolymer blends. *Macromolecules* 42:1047–1050
- Georges MK, Veregin RPN, Kazmaier PM, Hamer GK (1993) Narrow molecular-weight resins by a free-radical polymerization process. *Macromolecules* 26:2987–2988
- Gopalan P, Ober CK (2001) Highly reactive 2,5-disubstituted styrene-based monomer polymerized via stable free radical polymerization: effect of substitution and liquid crystallinity on polymerization. *Macromolecules* 34:5120–5124
- Gopalan P, Andruzzi L, Li XF, Ober CK (2002) Fluorinated mesogen-jacketed liquid-crystalline polymers as surface-modifying agents: design, synthesis and characterization. *Macromol Chem Phys* 203:1573–1583
- Gopalan P, Zhang YM, Li XF, Wiesner U, Ober CK (2003) Liquid crystalline rod-coil block copolymers by stable free radical polymerization: synthesis, morphology, and rheology. *Macromolecules* 36:3357–3364
- Guan Y, Chen XF, Shen ZH, Wan XH, Zhou QF (2009) Structure-property relationship of thermotropic liquid-crystalline vinyl polymers containing no traditional mesogen. *Polymer* 50:936–944
- Guan Y, Chen XF, Ma HY, Shen ZH, Wan XH (2010) Order-order transition induced by mesophase formation in a novel type of diblock copolymers based on poly(isobutyl methacrylate) and poly[2,5-di(isopropoxyoxycarbonyl)styrene]. *Soft Matter* 6:922–927
- Hajduk DA, Harper PE, Gruner SM, Honeker CC, Kim G, Thomas EL, Fetters LJ (1994) The gyroid: a new equilibrium morphology in weakly segregated diblock copolymers. *Macromolecules* 27:4063–4075
- Halperin A (1990) Rod-coil copolymers: their aggregation behavior. *Macromolecules* 23:2724–2731
- Hamley IW (1998) *The physics of block copolymers*. Oxford University Press, Oxford
- Hardouin F, Mery S, Achard MF, Noirez L, Keller P (1991) Evidence for a jacketed nematic polymer. *J Phys II* 1:511–520
- Hardouin F, Leroux N, Mery S, Noirez L (1992) Small-angle neutron-scattering experiments on side-on fixed liquid-crystal polysiloxanes. *J Phys II* 2:271–278
- Hawker CJ, Bosman AW, Harth E (2001) New polymer synthesis by nitroxide mediated living radical polymerizations. *Chem Rev* 101:3661–3688
- Hessel F, Finkelmann H (1985) A new class of liquid-crystal side-chain polymers—mesogenic groups laterally attached to the polymer backbone. *Polym Bull* 14:375–378

- Hessel F, Finkelmann H (1986) Optical biaxiality of nematic LC-side chain polymers with laterally attached mesogenic groups. *Polym Bull* 15:349–352
- Hsu CS, Percec V (1987) Liquid-crystalline polymers containing heterocycloalkane mesogens. 4. Biphasic side-chain liquid-crystalline polysiloxanes containing trans 5-(n-decanyl)-2-(4-methoxyphenyl)-1,3-dioxane and trans 2-(n-decanyl)-5-(4-methoxyphenyl)-1,3-dioxane mesogens. *Polym Bull* 17:49–54
- Huang Y, Wang J, Liu XB, Zhang HL, Chen XF, Zhuang WC, Chen X, Ye C, Wan XH, Chen EQ, Zhou QF (2005) Crystallization, melting, and morphology of a poly(ethylene oxide) diblock copolymer containing a tablet-like block of poly {2,5-bis[(4-methoxyphenyl)oxycarbonyl]styrene}. *Polymer* 46:10148–10157
- Huang Y, Liu XB, Zhang HL, Zhu DS, Sun YJ, Yan SK, Wang J, Chen XF, Wan XH, Chen EQ, Zhou QF (2006) AFM study of crystallization and melting of a poly(ethylene oxide) diblock copolymer containing a tablet-like block of poly {2,5-bis[(4-methoxyphenyl)oxycarbonyl]styrene} in ultrathin films. *Polymer* 47:1217–1225
- Jin H, Xu YD, Shen ZH, Zou DC, Wang D, Zhang N, Fan XH, Zhou QF (2010) Jacketed polymers with dendritic carbazole side groups and their applications in blue light-emitting diodes. *Macromolecules* 43:8468–8478
- Khandpur AK, Foerster S, Bates FS, Hamley IW, Ryan AJ, Bras W, Almdal K, Mortensen K (1995) Polyisoprene-polystyrene diblock copolymer phase diagram near the order-disorder transition. *Macromolecules* 28:8796–8806
- Kim GH, Pugh C, Cheng SZD (2000) A new route to stabilize the smectic C phase in a series of laterally attached side-chain liquid crystalline polynorbornenes with a one-carbon spacer. *Macromolecules* 33:8983–8991
- Kim GH, Jin S, Pugh C, Cheng SZD (2001) Effect of the length of the substituents on the phase structure and transition behavior of a series of laterally attached side-chain liquid-crystal line polynorbornenes. *J Polym Sci B Polym Phys* 39:3029–3037
- Kim MI, Wakada T, Akasaka S, Nishitsuji S, Saijo K, Hasegawa H, Ito K, Takenaka M (2008) Stability of the Fddd phase in diblock copolymer melts. *Macromolecules* 41:7667–7670
- Kim MI, Wakada T, Akasaka S, Nishitsuji S, Saijo K, Hasegawa H, Ito K, Takenaka M (2009) Determination of the Fddd phase boundary in polystyrene-block-polyisoprene diblock copolymer melts. *Macromolecules* 42:5266–5271
- Kimishima K, Koga T, Hashimoto T (2000) Order-order phase transition between spherical and cylindrical microdomain structures of block copolymer. I. Mechanism of the transition. *Macromolecules* 33:968–977
- Klok HA, Langenwalter JF, Lecommandoux S (2000) Self-assembly of peptide-based diblock oligomers. *Macromolecules* 33:7819–7826
- Lecommandoux S, Achard MF, Hardouin F, Brulet A, Cotton JP (1997) Are nematic side-on polymers totally extended? A SANS study. *Liq Cryst* 22:549–555
- Lee M, Cho B-K, Kim H, Yoon J-Y, Zin W-C (1998) Self-organization of Rod-coil molecules with layered crystalline states into thermotropic liquid crystalline assemblies. *J Am Chem Soc* 120:9168–9179
- Lee M, Cho B-K, Zin W-C (2001) Supramolecular structures from rod-coil block copolymers. *Chem Rev* 101:3869–3892
- Li CY, Tenneti KK, Zhang D, Zhang HL, Wan XH, Chen EQ, Zhou QF, Carlos AO, Igos S, Hsiao BS (2004) Hierarchical assembly of a series of rod-coil block copolymers: supramolecular LC phase in nanoenvironment. *Macromolecules* 37:2854–2860
- Li M, Liu Y, Nie H, Bansil R, Steinhart M (2007) Kinetics of hexagonal-body-centered cubic transition in a triblock copolymer in a selective solvent: Time-resolved small-angle X-ray scattering measurements and model calculations. *Macromolecules* 40:9491–9502
- Li CF, Zhang QK, Tian HJ, Chai CP, Gao LC, Shen ZH, Fan XH, Luo YJ (2014) Hierarchically ordered ABA triblock copolymer with large difference in glass transition temperatures of the two blocks. *J Polym Sci A: Polym Chem* 52:1737–1744
- Lin JP (1997) Re-entrant isotropic transition of polypeptide liquid crystal. *Polymer* 38:4837–4841

- Lin WR, Zhang J, Wan XH, Liang DH, Zhou QF (2009) Solvent-induced association and micellization of rod-coil diblock copolymer. *Macromolecules* 42:4090–4098
- Lin WR, Zheng C, Wan XH, Liang DH, Zhou QF (2010) Transition of large compound micelles into cylinders in dilute solution: kinetic study. *Macromolecules* 43:5405–5410
- Liu YX, Zhang D, Wan XH, Zhou QF (1998) Synthesis of a novel “mesogen-jacketed liquid crystal polymer” based on vinylterephthalic acid. *Chinese J Polym Sci* 16:283–288
- Liu AH, Zhi J, Cui JX, Wan XH, Zhou QF (2007) Thermotropic and chiroptical properties of poly {(+)-2,5-bis[4-((S)-2-methylbutoxy)phenyl] styrene} and its random copolymer with polystyrene. *Macromolecules* 40:8233–8243
- Liu XB, Zhao YF, Chen EQ, Ye C, Shen ZH, Fan XH, Cheng SZD, Zhou QF (2008) Lamella-to-lamella transition and effect of coil-stretching on crystallization in a rod-coil diblock copolymer containing poly (epsilon-caprolactone). *Macromolecules* 41:5223–5229
- Liu X, Zhao RY, Zhao TP, Liu CY, Yang S, Chen EQ (2014) An ABA triblock containing a central soft block of poly[2,5-di(n-hexogycarbonyl) styrene] and outer hard block of poly (4-vinylpyridine): synthesis, phase behavior and mechanical enhancement. *RSC Adv* 4:18431–18441
- Lodge TP, Pudil B, Hanley KJ (2002) The full phase behavior for block copolymers in solvents of varying selectivity. *Macromolecules* 35:4707–4717
- Malmstrom EE, Hawker CJ (1998) Macromolecular engineering via ‘living’ free radical polymerizations. *Macromol Chem Phys* 199:923–935
- Matsen MW (2012) Self-consistent field theory for melts of Low-molecular-weight diblock copolymer. *Macromolecules* 45:8502–8509
- Matsen MW, Bates FS (1996a) Origins of complex self-assembly in block copolymers. *Macromolecules* 29:7641–7644
- Matsen MW, Bates FS (1996b) Unifying weak- and strong-segregation block copolymer theories. *Macromolecules* 29:1091–1098
- Matyjaszewski K, Xia JH (2001) Atom transfer radical polymerization. *Chem Rev* 101:2921–2990
- McArdle CB (1989) Side chain liquid crystal polymers. Blackie and Son Ltd, Glasgow
- Mei X, Chu Y, Cui JX, Shen ZH, Wan XH (2010) Steric interaction between flexible main chain and nonmesogenic cyclic pendants leading to thermotropic liquid crystalline property. *Macromolecules* 43:8942–8949
- Mei X, Zhang J, Shen ZH, Wan XH (2012) Synthesis, liquid crystalline properties, and lithium complexes of vinyl polymers with cyclic pendants containing ethylene oxide units. *Polym Chem* 3:2857–2866
- Muthukumar M, Ober CK, Thomas EL (1997) Competing interactions and levels of ordering in self-organizing polymeric materials. *Science* 277:1225–1232
- Olsen BD, Segalman RA (2005) Structure and thermodynamics of weakly segregated rod-coil block copolymers. *Macromolecules* 38:10127–10137
- Olsen BD, Segalman RA (2007) Nonlamellar phases in asymmetric rod-coil block copolymers at increased segregation strengths. *Macromolecules* 40:6922–6929
- Olsen BD, Jang SY, Luning JM, Segalman RA (2006) Higher order liquid crystalline structure in low-polydispersity DEH-PPV. *Macromolecules* 39:4469–4479
- Olsen BD, Li XF, Wang J, Segalman RA (2007) Thin film structure of symmetric rod-coil block copolymers. *Macromolecules* 40:3287–3295
- Olsen BD, Alcazar D, Krikorian V, Toney MF, Thomas EL, Segalman RA (2008a) Crystalline structure in thin films of DEH-PPV homopolymer and PPV-b-PI rod-coil block copolymers. *Macromolecules* 41:58–66
- Olsen BD, Shah M, Ganesan V, Segalman RA (2008b) Universalization of the phase diagram for a model rod-coil diblock copolymer. *Macromolecules* 41:6809–6817
- Papkov VS, Ilina MN, Zhukov VP, Tsvankin DJ, Tur DR (1992) Unusual phase-behavior of some poly(dialkoxyposphazenes). *Macromolecules* 25:2033–2040
- Peng H, Chen Y, Chen L, He X, Li F (2010) Luminescent mesogen jacketed poly(1-alkyne) bearing lateral terphenyl with hexyloxy tail. *J Polym Sci A Polym Chem* 48:5679–5692

- Percec V, Hahn B (1989) Liquid-crystalline polymers containing heterocycloalkanedyl groups as mesogens.7. Molecular-weight and composition effects on the phase-transitions of poly(methylsiloxane)s and poly(methylsiloxane-co-dimethylsiloxane)s containing 2-[4-(2(S)-methyl-1-butoxyphenyl]-5-(11-undecanyl)-1,3,2-dioxaborinane side groups. *Macromolecules* 22:1588–1599
- Percec V, Tomazos D (1992) Molecular engineering of side-chain liquid-crystalline polymers by living cationic polymerization. *Adv Mater* 4:548–561
- Pragliola S, Ober CK, Mather PT, Jeon HG (1999) Mesogen-jacketed liquid crystalline polymers via stable free radical polymerization. *Macromol Chem Phys* 200:2338–2344
- Pugh C, Schrock RR (1992) Synthesis of side-chain liquid-crystal polymers by living ring-opening metathesis polymerization.3. Influence of molecular-weight, interconnecting unit, and substituent on the mesomorphic behavior of polymers with laterally attached mesogens. *Macromolecules* 25:6593–6604
- Pugh C, Dharia J, Arehart SV (1997) Correlation of model compounds and laterally attached side-chain liquid crystalline polynorbornenes with a 1-carbon spacer. *Macromolecules* 30:4520–4532
- Pugh C, Bae JY, Dharia J, Ge JJ, Cheng SZD (1998) Induction of smectic layering in nematic liquid crystals using immiscible components. 2. Laterally attached side-chain liquid-crystalline poly(norbornene)s and their low-molar-mass analogues with hydrocarbon/oligodimethylsiloxane substituents. *Macromolecules* 31:5188–5200
- Rosen BM, Wilson CJ, Wilson DA, Peterca M, Imam MR, Percec V (2009) Dendron-mediated self-assembly, disassembly, and self-organization of complex systems. *Chem Rev* 109:6275–6540
- Rudick JG, Percec V (2008) Induced helical backbone conformations of self-organizable dendronized polymers. *Acc Chem Res* 41:1641–1652
- Ryu J-H, Oh N-K, Zin W-C, Lee M (2004) Self-assembly of rod-coil molecules into molecular length-dependent organization. *J Am Chem Soc* 126:3551–3558
- Sänger J, Gronski W, Maas S, Stühn B, Heck B (1997) Structural transition in a nematic LC block copolymer induced by the transition to the LC phase. *Macromolecules* 30:6783–6787
- Schmidt K, Pester CW, Schoberth HG, Zettl H, Schindler KA, Boeker A (2010) Electric field induced gyroid-to-cylinder transitions in concentrated diblock copolymer solutions. *Macromolecules* 43:4268–4274
- Shi M, Zhang HL, Chen J, Wan XY, Zhou QF (2004) Synthesis and characterization of a novel star shaped rod-coil block copolymer. *Polym Bull* 52:401–408
- Shi M, Zhang HL, Chen JF, Wang XZ, Wang XY (2005) Synthesis and characterization of novel AB and ABA rod-coil block copolymers. *J Polym Res* 12:413–420
- Shi LY, Shen ZH, Fan XH (2011) Order-order transition in a rod-coil diblock copolymer induced by supercritical CO₂. *Macromolecules* 44:2900–2907
- Shi LY, Hsieh IF, Zhou Y, Yu XF, Tian HJ, Pan Y, Fan XH, Shen ZH (2012a) Thermoreversible order-order transition of a diblock copolymer induced by the unusual coil-rod conformational change of one block. *Macromolecules* 45:9719–9726
- Shi LY, Zhou Y, Shen ZH, Fan XH (2012b) Hierarchical structures in thin films of macrophase- and microphase-separated AB/AC diblock copolymer blends. *Macromolecules* 45:5530–5537
- Shi LY, Zhou Y, Fan XH, Shen ZH (2013) Remarkably rich variety of nanostructures and order-order transitions in a Rod-coil diblock copolymer. *Macromolecules* 46:5308–5316
- Shi L-Y, Pan Y, Zhang Q-K, Zhou Y, Fan X-H, Shen Z (2014) Synthesis and self-assembly of a linear coil-coil-rod ABC triblock copolymer. *Chin. J. Polym. Sci.* 32:accepted
- Small AC, Pugh C (2002) Induction of smectic layering in nematic liquid crystals using immiscible components. 5. Laterally attached side-chain liquid crystalline poly(norbornene)s and their low molar mass model compounds with short fluorocarbon segments. *Macromolecules* 35:2105–2115
- Tao YF, Zohar H, Olsen BD, Segalman RA (2007) Hierarchical nanostructure control in rod-coil block copolymers with magnetic fields. *Nano Lett* 7:2742–2746

- Tenneti KK, Chen XF, Li CY, Tu YF, Wan XH, Zhou QF, Sics I, Hsiao BS (2005) Perforated layer structures in liquid crystalline rod-coil block copolymers. *J Am Chem Soc* 127:15481–15490
- Tenneti KK, Chen XF, Li CY, Wan XH, Fan XH, Zhou QF, Rong LX, Hsiao BS (2008) Competition between liquid crystallinity and block copolymer self-assembly in core-shell rod-coil block copolymers. *Soft Matter* 4:458–461
- Thomas EL, Chen JT, O'Rourke MJE, Ober CK, Mao G (1997) Influence of a liquid crystalline block on the microdomain structure of block copolymers. *Macromol Symp* 117:241–256
- Tu HL, Zhang D, Wan XH, Chen XF, Liu YX, Zhang HL, Zhou QF (1999) Mesogen-jacketed liquid crystalline polymer with flexible dicyclopentyl terephthalate as side group. *Macromol Rapid Commun* 20:549–551
- Tu HL, Wan XH, Liu YX, Chen XF, Zhang D, Zhou QF, Shen ZH, Ge JJ, Jin S, Cheng SZD (2000a) Self-assembly-induced supramolecular hexagonal columnar liquid crystalline phase using laterally attached nonmesogenic templates. *Macromolecules* 33:6315–6320
- Tu YF, Wan XH, Zhang D, Zhou QF, Wu C (2000b) Self-assembled nanostructure of a novel coil-rod diblock copolymer in dilute solution. *J Am Chem Soc* 122:10201–10205
- Tu YF, Wan XH, Zhang HL, Fan XH, Chen XF, Zhou QF, Chau KC (2003a) Self-assembled nanostructures of rod-coil diblock copolymers with different rod lengths. *Macromolecules* 36:6565–6569
- Tu YF, Wan XH, Zhang HL, Fan XH, Lu DN, Chen XF, Zhou QF (2003b) Self-assembly of rod-coil diblock copolymers—influence of the rod length. *Chinese J Polym Sci* 21:569–573
- Tu YF, Graham MJ, Van Horn RM, Chen EQ, Fan XH, Chen XF, Zhou QF, Wan XH, Harris FW, Cheng SZD (2009) Controlled organization of self-assembled rod-coil block copolymer micelles. *Polymer* 50:5170–5174
- Wan X, Zhang F, Wu P, Zhang D, Feng X, Zhou Q-F (1995) Characterization of the chain stiffness for a mesogen-jacketed liquid crystal polymer: poly{2,5-BIS [(4-Methoxybenzoyl)Oxy] Styrene}. *Macromol Symp* 96:207–218
- Wan XH, Tu YF, Zhang D, Zhou QF (1998) “Living” free radical synthesis of novel rodcoil diblock copolymers with polystyrene and mesogen-jacketed liquid crystal polymer segments. *Chinese J Polym Sci* 16:377–380
- Wan XH, Tu HL, Tu YF, Zhang D, Sun L, Zhou QF, Dong YP, Tang M (1999) Nitroxide-mediated free radical synthesis of mesogen-jacketed liquid crystal polymers. *Chinese J Polym Sci* 17:189–192
- Wan XH, Tu YF, Zhang D, Zhou QF (2000) Nitroxide-mediated ‘living’ free radical synthesis of novel rod-coil diblock copolymers with polystyrene and mesogen-jacketed liquid-crystal polymer segments. *Polym Int* 49:243–247
- Wan XH, Tu HL, Liu YX, Zhang D, Chen XF, Zhang HL, Zhou QF (2003) A new strategy for the design of liquid crystalline polymers with flexible and apolar building blocks. *Chinese J Polym Sci* 21:21–27
- Wang QA (2011) Theory and simulation of the self-assembly of rod-coil block copolymer melts: recent progress. *Soft Matter* 7:3711–3716
- Wang JS, Matyjaszewski K (1995) Controlled living radical polymerization—atom-transfer radical polymerization in the presence of transition-metal complexes. *J Am Chem Soc* 117:5614–5615
- Wang X-J, Zhou Q-F (2004) *Liquid crystalline polymers*. World Scientific, Singapore
- Wang XZ, Zhang HL, Mao S, Wang XY, Zhou QF (2005) Synthesis of a novel liquid crystal rod-coil star block copolymer consisting of poly(methyl methacrylate) and poly{2,5-bis [(4-methoxy-phenyl)oxycarbonyl] styrene} via atom transfer radical polymerization. *J Polym Sci A Polym Chem* 43:733–741
- Wen GH, Zhang B, Xie HL, Liu X, Zhong GQ, Zhang HL, Chen EQ (2013) Microphase separation facilitating and stabilizing hierarchical segment self-assembly of combined main-chain/side-chain liquid crystalline polymer in diblock copolymer. *Macromolecules* 46:5249–5259
- Williams DRM, Fredrickson GH (1992) Cylindrical micelles in rigid-flexible diblock copolymers. *Macromolecules* 25:3561–3568

- Xie HL, Hu TH, Zhang XF, Zhang HL, Chen EQ, Zhou QF (2008) Design, synthesis, and characterization of a combined main-chain/side-chain liquid crystalline polymer based on mesogen-jacketed liquid crystal polymer via atom transfer radical polymerization. *J Polym Sci A Polym Chem* 46:7310–7320
- Xie HL, Liu YX, Zhong GQ, Zhang HL, Chen EQ, Zhou QF (2009) Design, synthesis, and multiple hierarchical ordering of a novel side-chain liquid crystalline-rod diblock copolymer. *Macromolecules* 42:8774–8780
- Xie H-L, Jie C-K, Yu Z-Q, Liu X-B, Zhang H-L, Shen Z, Chen E-Q, Zhou Q-F (2010) Hierarchical supramolecular ordering with biaxial orientation of a combined main-chain/side-chain liquid-crystalline polymer obtained from radical polymerization of 2-vinylterephthalate. *J Am Chem Soc* 132:8071–8080
- Xie H-L, Wang S-J, Zhong G-Q, Liu Y-X, Zhang H-L, Chen E-Q (2011) Combined main-chain/side-chain liquid crystalline polymer with main-chain on the basis of “jacketing” effect and side-chain containing azobenzene groups. *Macromolecules* 44:7600–7609
- Xu GZ, Wu W, Shen DY, Hou JN, Zhang SF, Xu M, Zhou QF (1993a) Morphological-study of oriented films obtained from side-chain liquid-crystalline polymers. *Polymer* 34:1818–1822
- Xu GZ, Wu W, Xu M, Zhou QF (1993b) Banded texture in oriented films of a side-chain liquid-crystalline polymer. *J Polym Sci B Polym Phys* 31:229–230
- Xu GZ, Hou JN, Zhu SN, Yang XZ, Xu M, Zhou QF (1994) The peculiarity of side-chain liquid-crystalline polymers with mesogenic units attached directly in a side-on mode. *Polymer* 35:5441–5446
- Xu YD, Yang Q, Shen ZH, Chen XF, Fan XH, Zhou QF (2009) Effects of mesogenic shape and flexibility on the phase structures of mesogen-jacketed liquid crystalline polymers with bent side groups containing 1,3,4-oxadiazole. *Macromolecules* 42:2542–2550
- Xu YD, Qu W, Yang Q, Zheng JK, Shen ZH, Fan XH, Zhou QF (2012) Synthesis and characterization of mesogen-jacketed liquid crystalline polymers through hydrogen-bonding. *Macromolecules* 45:2682–2689
- Yang Q, Jin H, Xu YD, Wang P, Liang XC, Shen ZH, Chen XF, Zou DC, Fan XH, Zhou QF (2009) Synthesis, photophysics, and electroluminescence of mesogen-jacketed 2D conjugated copolymers based on fluorene-thiophene-oxadiazole derivative. *Macromolecules* 42:1037–1046
- Yang Q, Xu YD, Jin H, Shen ZH, Chen XF, Zou DC, Fan XH, Zhou QF (2010) A novel mesogen-jacketed liquid crystalline electroluminescent polymer with both thiophene and oxadiazole in conjugated side chain. *J Polym Sci A Polym Chem* 48:1502–1515
- Yang H, Zhang F, Lin B-P, Keller P, Zhang X-Q, Sun Y, Guo L-X (2013) Mesogen-jacketed liquid crystalline polymers and elastomers bearing polynorbornene backbone. *J Mater Chem C* 1:1482–1490
- Ye C, Zhang HL, Huang Y, Chen EQ, Lu YL, Shen DY, Wan XH, Shen ZH, Cheng SZD, Zhou QF (2004) Molecular weight dependence of phase structures and transitions of mesogen-jacketed liquid crystalline polymers based on 2-vinylterephthalic acids. *Macromolecules* 37:7188–7196
- Yi Y, Wan XH, Fan XH, Dong R, Zhou QF (2003) Synthesis of a novel hybrid liquid-crystalline rod-coil diblock copolymer. *J Polym Sci A Polym Chem* 41:1799–1806
- Yi Y, Fan XH, Wan XH, Li L, Zhao N, Chen XF, Xu J, Zhou QF (2004) ABA type triblock copolymer based on mesogen-jacketed liquid crystalline polymer: design, synthesis, and potential as thermoplastic elastomer. *Macromolecules* 37:7610–7618
- Yin XY, Chen EQ, Wan XH, Zhou QF (2003a) Synthesis and characterization of newly designed poly[di(alkyl) vinylterephthalate]s. *Chinese J Polym Sci* 21:9–14
- Yin XY, Ye C, Ma X, Chen EQ, Qi XY, Duan XF, Wan XH, Cheng SZD, Zhou QF (2003b) Manipulating supramolecular self-assembly via tailoring pendant group size of linear vinyl polymers. *J Am Chem Soc* 125:6854–6855
- Yu ZN, Tu HL, Wan XH, Chen XF, Zhou QF (2003a) Synthesis and characterization of mesogen-jacketed liquid-crystal polymers based on 2,5-bis(4'-alkoxyphenyl)styrene. *J Polym Sci A Polym Chem* 41:1454–1464

- Yu ZN, Wan XH, Tu HL, Chen XF, Zhou QF (2003b) A novel thermotropic behavior of a mesogen-jacketed liquid crystal polymer. *Acta Polym. Sin.*:430-433
- Yu ZQ, Lam JWY, Zhao KQ, Zhu CZ, Yang S, Lin JS, Li BS, Liu JH, Chen EQ, Tang BZ (2013) Mesogen jacketed liquid crystalline polyacetylene containing triphenylene discogen: synthesis and phase structure. *Polym Chem* 4:996-1005
- Zhang D, Zhou QF, Ma YG, Wan XH, Feng XD (1997) Mesogen-jacketed liquid crystal polymers with mesogens of aromatic amide structure. *Polym Adv Technol* 8:227-233
- Zhang D, Liu YX, Wan XH, Zhou QF (1999a) Synthesis and characterization of a new series of "mesogen-jacketed liquid crystal polymers" based on the newly synthesized vinylterephthalic acid. *Macromolecules* 32:5183-5185
- Zhang D, Liu YX, Wan XH, Zhou QF (1999b) Synthesis of a new side-chain type liquid crystal polymer poly[dicyclohexyl vinylterephthalate]. *Macromolecules* 32:4494-4496
- Zhang H, Yu Z, Wan X, Zhou QF, Woo EM (2002a) Effects of molecular weight on liquid-crystalline behavior of a mesogen-jacketed liquid crystal polymer synthesized by atom transfer radical polymerization. *Polymer* 43:2357-2361
- Zhang HL, Tu YF, Wan XH, Zhou QF, Woo EM (2002b) Atom-transfer radical polymerization to synthesize novel liquid crystalline diblock copolymers with polystyrene and mesogen-jacketed liquid crystal polymer segments. *J Polym Res* 9:11-15
- Zhang HL, Chen XF, Wan XH, Zhou QF, Woo EM (2003) Synthesis and characterization of novel rod-coil diblock copolymers of poly(methyl methacrylate) and liquid crystalline segments of poly(2,5-bis[4-methoxyphenyl]oxycarbonyl] styrene). *Polym Int* 52:92-97
- Zhang HL, Sun XY, Wang XY, Zhou QF (2005a) Synthesis of a novel ABC triblock copolymer with a rigid-rod block via atom transfer radical polymerization. *Macromol Rapid Commun* 26:407-411
- Zhang J, Yu Y, Wan XH, Chen XF, Zhou QF (2005b) Synthesis of an optically active triblock copolymer and its self-assembly behavior in dioxane/water. *Acta Polym. Sin.*:305-308
- Zhang J, Yu ZN, Wan XH, Chen XF, Zhou QF (2005c) Synthesis and characterization of helix-coil diblock copolymers with controlled supramolecular architectures in aqueous solution. *Macromol Rapid Commun* 26:1241-1245
- Zhang J, Cao HQ, Wan XH, Zhou QF (2006) Molecular reorganization of rod-coil diblock copolymers at the air-water interface. *Langmuir* 22:6587-6592
- Zhang J, Lin WR, Liu AH, Yu ZN, Wan XH, Liang DH, Zhou QF (2008) Solvent effect on the aggregation behavior of rod-coil diblock copolymers. *Langmuir* 24:3780-3786
- Zhang LY, Chen S, Zhao H, Shen ZH, Chen XF, Fan XH, Zhou QF (2010) Synthesis and properties of a series of mesogen-jacketed liquid crystalline polymers with polysiloxane backbones. *Macromolecules* 43:6024-6032
- Zhang Q-K, Tian H-J, Li C-F, Zhu Y-F, Liang Y, Shen Z, Fan X-H (2014) Synthesis and phase behavior of a new 2-vinylbiphenyl-based mesogen-jacketed liquid crystalline polymer with high glass transition temperature and low threshold molecular weight. *Polym Chem* 5:4526-4533
- Zhao YF, Fan XH, Chen XF, Wan XH, Zhou QF (2005) Synthesis and characterization of diblock copolymers based on crystallizable poly(epsilon-caprolactone) and mesogen-jacketed liquid crystalline polymer block. *Polymer* 46:5396-5405
- Zhao Y-F, Fan X-H, Wan X-H, Chen X-F, Yi WL-S, Dong X, Zhou Q-F (2006) Unusual phase behavior of a mesogen-jacketed liquid crystalline polymer synthesized by atom transfer radical polymerization. *Macromolecules* 39:948-956
- Zhou QF, Li HM, Feng XD (1987) Synthesis of liquid-crystalline polyacrylates with laterally substituted mesogens. *Macromolecules* 20:233-234
- Zhou QF, Zhu XL, Wen ZQ (1989) Liquid-crystalline side-chain polymers without flexible spacer. *Macromolecules* 22:491-493
- Zhou QF, Wan XH, Zhu XL, Zhang F, Feng XD (1993) Restudy of the old poly-2,5-di(benzoyloxy)styrene as a new liquid-crystal polymer. *Mol Cryst Liq Cryst* 231:107-117

- Zhou QH, Zheng JK, Shen ZH, Fan XH, Chen XF, Zhou QF (2010) Synthesis and hierarchical self-assembly of rod rod block copolymers via click chemistry between mesogen-jacketed liquid crystalline polymers and helical polypeptides. *Macromolecules* 43:5637–5646
- Zhou F, Ye TY, Shi LY, Xie C, Chang SK, Fan XH, Shen ZH (2013) Synthesis and self-assembly of rod-rod block copolymers with different rod diameters. *Macromolecules* 46:8253–8263
- Zhu ZG, Zhi JG, Liu AH, Cui JX, Tang H, Qiao WQ, Wan XH, Zhou QF (2007) Synthesis and characterization of a thermotropic liquid-crystalline poly[2,5-bis(4'-alkoxycarbonylphenyl)styrene]. *J Polym Sci A Polym Chem* 45:830–847
- Zhu YF, Guan XL, Shen ZH, Fan XH, Zhou QF (2012) Competition and promotion between Two different liquid-crystalline building blocks: mesogen-jacketed liquid-crystalline polymers and triphenylene discotic liquid crystals. *Macromolecules* 45:3346–3355
- Zhu YF, Tian HJ, Wu HW, Hao DZ, Zhou Y, Shen ZH, Zou DC, Sun PC, Fan XH, Zhou QF (2014a) Ordered nanostructures at Two different length scales mediated by temperature: a triphenylene-containing mesogen-jacketed liquid crystalline polymer with a long spacer. *J Polym Sci A Polym Chem* 52:295–304
- Zhu YF, Zhang ZY, Zhang QK, Hou PP, Hao DZ, Qiao YY, Shen ZH, Fan XH, Zhou QF (2014b) Mesogen-jacketed liquid crystalline polymers with a polynorborene main chain: green synthesis and phase behaviors. *Macromolecules* 47:2803–2810

Chapter 4

Computer Simulation of Side-Chain Liquid Crystal Polymer Melts and Elastomers

Jaroslav M. Ilnytskyi, Marina Saphiannikova, Dieter Neher,
and Michael P. Allen

The combination of liquid-crystalline (LC) groups and a polymeric matrix is particularly appealing to the materials scientist, in view of the large number of applications which exist for both parent subsystems (Chung 2008). Moreover, composite systems of this type, LC polymers, exhibit a synergy, i.e. the presence of properties not observed in their constituent parts.

This is particularly true for side-chain liquid crystal polymers (SCLCPs) containing photo-active chromophore groups. Such photoactive SCLCPs find their application in modern photonics, electronics and opto-mechanics. In particular, these are successfully used to produce alignment layers for LC fluorescent polymers in display and semiconductor technology (Sainova et al. 2002; Zen et al. 2002), to build waveguides and waveguide couplers (Viswanathan et al. 1999; Natansohn and Rochon 1999), as data storage media (Berg et al. 1996; Rasmussen et al. 1999; Zilker et al. 1998; Stracke et al. 2000), as labels in quality product protection (Stiller et al. 2005), and in a number of other applications.

J.M. Ilnytskyi (✉)

Institute for Condensed Matter Physics of National Academy of Sciences of Ukraine,
1, Svientsitskii Str., 79011 Lviv, Ukraine
e-mail: iln@icmp.lviv.ua

M. Saphiannikova

Leibniz-Institut für Polymerforschung Dresden e.V., Hohe Strasse 6, 01069 Dresden, Germany
e-mail: grenzer@ipfdd.de

D. Neher

Institute for Physics and Astronomy, University of Potsdam, Karl-Liebknecht-Strasse 24-25,
14476 Potsdam-Golm, Germany
e-mail: neher@uni-potsdam.de

M.P. Allen

Department of Physics, University of Warwick, Coventry CV4 7AL, UK

H.H. Wills Physics Laboratory, Royal Fort, Tyndall Avenue, Bristol BS8 1TL, UK
e-mail: m.p.allen@warwick.ac.uk; m.p.allen@bristol.ac.uk

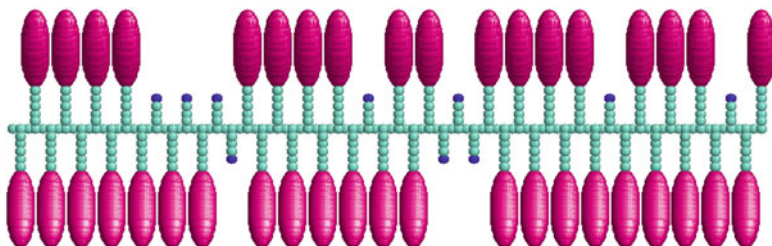


Fig. 4.1 Schematic representation of a single SCLCP molecule. *Green-gray spheres*: hydrocarbon groups. *Magenta ellipsoids*: mesogen groups (including the case of chromophores). *Blue spheres*: chemically reactive groups intended to crosslink into a polymer network (elastomer). Reproduced from Ilnytskyi et al. (2012) with permission from The Royal Society of Chemistry

Schematically, a single SCLCP molecule is shown in Fig. 4.1. It contains a backbone and pendant spacer chains, some of which are terminated by a mesogen (including the case of chromophore mesogens). The length of the backbone is L_b monomers, whereas that of each spacer is L_c . The branching functionalization of the SCLCP is constant and equal to k_f ; therefore, the number of attached side-chains is equal to $N_c = L_b/k_f$. The bulk phase behavior of such systems free of mechanical or optical perturbations is well studied experimentally (Collings and Hird 2001; Rutloh et al. 2000; Freiberg et al. 2003). An important factor in their phase diagram is the amount of coupling between the chromophores and the backbone, which is determined by the spacer length, L_c . For large values of L_c , both subsystems are decoupled, and microphase separation drives the system into lamellar smectic phase(s). For instance, one or several smectic phases are observed for the siloxane SCLCP at $L_c \geq 6$. With the decrease of L_c the coupling between the two subsystems increases and either nematic ($L_c = 3 - 5$) or even no LC phases ($L_c \leq 2$) are found (Collings and Hird 2001). In the latter case, the SCLCP is characterized by a high glass transition temperature, T_g , and is in an amorphous state at room temperature. Other factors defining the phase diagram of real SCLCPs are the transient dipole moment of LC groups, steric effects, etc. (Collings and Hird 2001).

External stimuli applied to the SCLCP melt, in the form of mechanical deformation, illumination (for photo-sensitive SCLCPs), or by other means, generate internal stress in the material. Due to the viscoelasticity of the material, it is relaxed via deformation (at short time scales) and via flow (at large time scales), unless the diffusion of the system is suppressed by jamming it in between substrate plates. The exact scenario for the stress relaxation is highly dependent on details of the molecular architecture.

Another way to suppress the diffusivity of the system on large time scales is to perform crosslinking of the melt. As a result, side-chain liquid crystal elastomers (SCLCEs) can be formed, the systems fabricated experimentally since the 1980s (Finkelmann et al. 1981, 1984). Their mechanical properties are similar to the case of non-LC polymer networks in terms of high elasticity, whereas the response to external electromagnetic stimuli is driven by the LC groups. Due to coupling

between these two constituent subsystems, a number of opto- and thermo-mechanical effects are observed in SCLCEs, bringing them into the wider class of shape-memory polymers (Behl and Lendlein 2007; Ahn et al. 2011). For instance, reversible shape changes at the LC order-disorder transition provide a basis for applications of SCLCE as low-frequency actuators and sensors (i.e. artificial muscles) (Shenoy et al. 2002; Spillmann et al. 2007). A separate class of technologically interesting materials are SCLCEs containing chromophore groups (Ikeda et al. 2007).

4.1 Side-Chain Liquid Crystal Polymers: Modelling of Equilibrium Properties

4.1.1 *Semi-atomistic Molecular Dynamics Modelling*

Practically reasonable system sizes for atomic-resolution simulations of LC melts and networks lie within the 10–100 nm range, well below the typical dimensions of real physical samples that demonstrate elasticity. In this context, the issue arises of how phenomena occurring at smaller length scales in such a material influence its macroscopic behavior. As discussed in Hill (1984, 1985) and Matouš and Geubelle (2005), at the micro-level the material response is heterogeneous, whereas at the macro-level it appears homogeneous. One could explain this by averaging the material properties over a large number of inhomogeneous fragments [in the same way that “self-averaging” applies to the description of disordered critical systems (Aharony and Harris 1996; Binder 1986; Wiseman and Domany 1998)]. Therefore, when performing mapping of the properties of a small system onto those of a larger one, several issues should be considered. First of all, for the case of SCLCEs, we assume the affine deformation of a small volume element. Secondly, a reduction of both the number and the length-scale of the structural inhomogeneities is performed. For instance, better homogeneity of the polymer network can be achieved by performing spatially-controlled crosslinking. One can also imitate self-averaging within a larger system by averaging the properties of interest obtained for a number of different replicas of the small-size system. All this brings the properties obtained for the small-size system closer to those for their larger counterpart. More discussion of computational approaches addressing the relation between micro- and macro-scales in composite systems can be found elsewhere (Matouš and Geubelle 2005; Michel et al. 1999).

The model used in this study belongs to the class of semi-atomistic models, in which a group of atoms is treated as a single particle. It is a classical mechanical description, which focuses on the most relevant features of the LC polymers, namely the (variable) flexibility of polymer chains and the ability of mesogens to form LC phases. For the case of the SCLCP molecule shown in Fig. 4.1, two types of particle would suffice. These are spherically-symmetrical particles representing

hydrocarbon CH_n groups, and anisometric ones representing elongated mesogens. Such models have proven to be successful in a number of studies (Stimson and Wilson 2005; Wilson 1997; McBride and Wilson 1999; Wilson et al. 2003, 2005). The set of potentials that govern interaction within the polymer scaffold are united-atom force fields, developed for branched alkanes by various groups, e.g. by Vlught et al. (1999). These are normally split into bonded and non-bonded interactions. The bonded interactions include bond stretching V_b , bond angle bending V_a , pseudo bond angle bending V_z (see below) and torsional V_t energy terms given by the following expressions

$$V_b = \sum_{i=1}^{N_b} \frac{k_b}{2} (\ell_i - \ell_0)^2, \quad (4.1a)$$

$$V_a = \sum_{i=1}^{N_a} \frac{k_a}{2} (\vartheta_i - \vartheta_0)^2, \quad (4.1b)$$

$$V_z = \sum_{i=1}^{N_z} \frac{k_z}{2} (\zeta_i - \zeta_0)^2, \quad (4.1c)$$

$$V_t = \sum_{i=1}^{N_t} \sum_{n=1}^3 C_n \cos^n \phi_i, \quad (4.1d)$$

where ℓ_i , ϑ_i , ζ_i and ϕ_i denote the i -th bond length, bond angle, pseudo bond angle and torsion angle, respectively. Their respective totals are N_b , N_a , N_z and N_t . We consider different parameters for the hydrocarbon groups: CH, CH_2 and CH_3 . Then, ℓ_0 , ϑ_0 and ζ_0 are the reference bond length, valence angle and pseudo bond angle, respectively. The energy term V_z was introduced by Wilson (1997), where ζ_i is measured between the long axis of the i -th mesogen and the direction of the bond that connects it to the last pseudo-atom of a spacer (here the value for the reference angle $\zeta_0 = \pi$ is used). This interaction prevents the mesogen from unphysical free rotations with respect to the last atom of the spacer. The torsional energy V_t has a Ryckaert–Bellemans form (Ryckaert and Bellemans 1975) with the chain stiffness defined via the set of constants, C_n . In our simulations we consider two cases: flexible chains and stiff chains with different sets of constants C_n . The force-field constants used in this study are given below.

The non-bonded interactions include the hydrocarbon–hydrocarbon, mesogen–mesogen and mixed hydrocarbon–mesogen terms. The hydrocarbon–hydrocarbon interaction is of the Lennard-Jones form:

$$V_{aa} = \sum_{\langle ij \rangle} \left[\frac{a_i a_j}{r_{ij}^{12}} - \frac{c_i c_j}{r_{ij}^6} \right], \quad (4.2)$$

where r_{ij} is the distance between the i -th and the j -th particles, and a_i, c_i are factorized Lennard-Jones energy parameters. The mesogens are considered to be

rigid anisometric objects that interact via the Gay–Berne potential (Gay and Berne 1981):

$$V_{\text{mm}} = \sum_{\langle ij \rangle} 4\varepsilon_{ij} \left[(\rho_{ij})^{-12} - (\rho_{ij})^{-6} \right], \quad (4.3)$$

where ε_{ij} and ρ_{ij} are effective energy and reduced distance parameters, respectively, and both are functions of the mesogen orientations \mathbf{e}_i , \mathbf{e}_j and their interconnecting vector \mathbf{r}_{ij} . Complete expressions can be found elsewhere (Gay and Berne 1981). Similar expressions can be derived for the mixed interactions between the i -th hydrocarbon and j -th mesogen, using the extended Gay–Berne potential (Cleaver et al. 1996):

$$V_{\text{am}} = \sum_{\langle ij \rangle} 4\varepsilon'_{ij} \left[(\rho'_{ij})^{-12} - (\rho'_{ij})^{-6} \right]. \quad (4.4)$$

The meaning of ε'_{ij} and ρ'_{ij} is similar to that for ε_{ij} and ρ_{ij} ; more details can be found elsewhere (Wilson 1997; Ilnytskyi and Wilson 2001). The Lennard-Jones interactions are cut at $r_c = 9.8 \text{ \AA}$ and the long-range correction to the potential energy and the virial are evaluated (Allen and Tildesley 1989), while the Gay–Berne and mixed interactions are cut at $r_c = 18.9 \text{ \AA}$ and $r_c = 16.5 \text{ \AA}$, respectively, and shifted in such a way that $V_{\text{mm}} = 0$ and $V_{\text{am}} = 0$ when $r = r_c$.

Here we will list a complete set of force-field parameters used in the simulations. Masses are $0.232 \times 10^{-25} \text{ kg}$ for the spherical particles and $0.375 \times 10^{-24} \text{ kg}$ for the mesogens; the moment of inertia for the latter is $0.469 \times 10^{-23} \text{ kg \AA}^2$. The pairs of $\{a, c\}$ energy parameters for the Lennard-Jones potential V_{aa} are: $\{2112.19, 39.4193\}$, $\{1877.05, 30.9202\}$ and $\{1222.83, 17.7425\}$ for CH_3 , CH_2 and CH particles, respectively, all in units of $(10^{-20} \text{ J})^{1/2}$ and length units of \AA . The parameters of the Gay-Berne potential are as follows: $\sigma_0 = 5 \text{ \AA}$, $\varepsilon_0 = 0.561 \times 10^{-20} \text{ J}$, $\kappa = 3$, $\kappa' = 5$, $\mu = 1$, $\nu = 2$, where we follow the designations of Gay and Berne (1981). The bond length ℓ_0 in the expression for V_b is 1.540 \AA and 7.075 \AA for sphere-sphere and sphere-mesogen bonds, respectively; the bond energy constant is $k_b = 361.291 \times 10^{-20} \text{ J/\AA}^2$ in both cases. The bond angle ϑ_0 in the expression for V_a is 1.9897 rad and 1.9548 rad for linear and branched chain fragments, respectively; the bend energy constant is $k_a = 86.291 \times 10^{-20} \text{ J/rad}^2$ in both cases. The parameters of the pseudo bond angle interaction V_z are chosen as $\zeta_0 = \pi$ and $k_z = k_a$. Finally, the set of constants C_n for the torsional potential V_t are used to tune the flexibility of chains. For the case of flexible chains we use the following sets (all in units of 10^{-20} J): $\{1.3941, 2.7868, 0.18824, -4.3691\}$ and $\{0.51505, 1.2689, 0.37022, -2.3984\}$ for linear and branched fragments, respectively. For stiff chains the following set is used: $\{1.79, 5.57, 1.38, -8.74\}$ in the same energy units.

The MD simulations are performed with the aid of the parallel program GBMOLDD (Ilnytskyi and Wilson 2001, 2002). A simulation box of dimensions L_x , L_y and L_z , with periodic boundary conditions, that mimicks the behavior of a volume element

in the bulk, is used. We employed the $NP_{xx}P_{yy}P_{zz}T$ ensemble, that is a simplified version of the Parrinello-Rahman scheme (Parrinello and Rahman 1981), where only the principal stresses, σ_{xx} , σ_{yy} , σ_{zz} are constrained (the equations of motion can be found in Ilnytskyi and Neher (2007)). Two types of simulation are undertaken in this study: under atmospheric pressure, P_{atm} , and under external uniaxial load. In the first case, all three principal stresses are constrained at the same value of P_{atm} . In the second case, a load P_L is introduced along one of the axes, $\alpha = \{x, y, z\}$, by constraining $\sigma_{\alpha\alpha}$ to $P_{\text{atm}} - P_L$, whereas both other stresses, $\sigma_{\beta\beta}$ and $\sigma_{\gamma\gamma}$ are constrained at $P_{\text{atm}} + P_L/2$. In this way the trace of the stress tensor is always equal to $3P_{\text{atm}}$. For the integration of the equations of motion we used the leap-frog algorithm; the RATTLE constraint has been applied for the integration of the mesogen rotation (Ilnytskyi and Wilson 2002). A time step $\Delta t = 2$ fs was found to be acceptable for all production runs.

The anisotropic deformation of the simulation box at each time instant t is monitored via the three principal strains, $\varepsilon_\alpha = L_\alpha(t)/L_\alpha(0)$, where $L_\alpha(t)$ is the dimension of the box along the corresponding spatial axis α at time t . We define the strain along the symmetry axis (e.g. nematic director, axis of applied load, etc.), as $\varepsilon_{\parallel} = L_{\parallel}(t)/L_{\parallel}(0)$.

To characterize the LC order of the mesogens, we evaluate the nematic order parameter with respect to the director, S_2 , and also the order parameters S_α evaluated with respect to each spatial axis α :

$$S_2 = \langle P_2(\cos \theta_i) \rangle_i, \quad S_\alpha = \langle P_2(e_{\alpha,i}) \rangle_i. \quad (4.5)$$

Here, $P_2(x) = \frac{1}{2}(3x^2 - 1)$ is the second Legendre polynomial, and θ_i is the angle between i -th mesogen orientation \mathbf{e}_i and the nematic director. The components of \mathbf{e}_i are denoted $e_{\alpha,i}$ and the averaging is performed over all the mesogens within the system.

The distribution of the particles of the k -th polymer chain in space is characterized by the components of the gyration tensor:

$$G_{\alpha\beta}^{[k]} = \frac{1}{N} \sum_{i=1}^N (r_{i,\alpha}^{[k]} - R_\alpha^{[k]})(r_{i,\beta}^{[k]} - R_\beta^{[k]}). \quad (4.6)$$

Here i indexes the particle with position $r_{i,\alpha}^{[k]}$ which belongs to k -th chain, and $\mathbf{R}^{[k]}$ is the position of the center of mass of the k -th chain. The gyration tensor can be rotated into a particular frame (e.g. one related to the nematic director). Let us denote the components of the rotated tensor as $Q_{\alpha\beta}^{[k]}$ and their averages over similar chains and over time as $Q_{\alpha\beta} = \langle Q_{\alpha\beta}^{[k]} \rangle_{k,t}$. These components provide an average distribution of particles with respect to the axes of the required frame. Other properties are also used, namely the average radius of gyration R_g , defined via:

$$R_g^2 = \sum_{\alpha=1}^3 Q_{\alpha\alpha}, \quad (4.7)$$

as well as the anisotropy of the gyration tensor with respect to a prescribed axis α (e.g. the director, axis of applied load, etc.):

$$\frac{R_{\parallel}}{R_{\perp}} = \frac{\sqrt{Q_{\alpha\alpha}}}{\left(\sqrt{Q_{\beta\beta}} + \sqrt{Q_{\gamma\gamma}}\right)/2}, \quad (4.8)$$

where β, γ stand for the other two axes perpendicular to α . The shape anisotropy of backbones and side-chains is also characterized by the relations between the average semi-axes of their equivalent ellipsoids. In this case the components of $G_{\alpha\beta}^{[k]}$ are not averaged, but the tensor is diagonalized for each chain k and the squared semiaxes $(\sigma_{\alpha}^{[k]})^2$ are found as its eigenvalues. These are then averaged over k and over time to yield the average values $\sigma_{\alpha}^2 = \langle (\sigma_{\alpha}^{[k]})^2 \rangle_{k,t}$, $\sigma_1^2 > \sigma_2^2 > \sigma_3^2$. Finally, the average end-to-end distance R_{1N} for particular types of chain (backbones, side-chains, etc.) can also be evaluated from its square as

$$R_{1N}^2 = \left\langle \sum_{\alpha=1}^3 [r_{1,\alpha}^{[k]} - r_{N,\alpha}^{[k]}]^2 \right\rangle_{k,t}. \quad (4.9)$$

4.1.2 Properties of SCLCP in a Weak Coupling Limit

We will study the phase behavior of the SCLCP model shown schematically in Fig. 4.1 in two limiting cases. Let us proceed to the first one, the “weakly-coupled” model, which describes the SCLCP where the two subsystems, backbone and mesogens, are essentially decoupled. The backbone is assumed to be flexible (mimicking a methacrylate or similar chain), while the spacer length is relatively long. The parameters chosen for our analysis are: $L_b = 39$, $L_c = 10$, functionalization $k_f = 4$, the number of attached side-chains $N_c = 10$.

The initial configuration was built of 64 SCLCP molecules with a regular double-layered lamellar arrangement. The melting runs were undertaken for up to 16 ns. The simulations were performed in the $NP_{xx}P_{yy}P_{zz}T$ ensemble at atmospheric pressure, and at a set of temperatures ranging from 450 to 600 K. The melt of SCLCPs preserves a stable smectic order at $T = 485\text{K}$ and below, and melts quickly into the isotropic phase when annealed to $T > 520\text{K}$. At intermediate temperatures, $T = 490\text{--}495\text{ K}$, the smectic phase melts slowly. Therefore, we estimated the smectic to isotropic (SI) transition temperature to be $T_{\text{SI}} \sim 490\text{K}$. No evidence for the nematic phase was found, in agreement with the phase diagrams of real SCLCPs with a long (6–10 hydrocarbons) spacer and syndiotactic structure (Collings and Hird 2001).

After these preliminary estimates for the order–disorder transition temperature, a smectic phase was grown out of the isotropic phase. Due to the small system size and the possibility for the system to be locked in a metastable state (typical for the molecular dynamics simulation of viscous systems), the growth of the smectic

phase was assisted by applying an external uniaxial field. This affects the orientations of the mesogens and is introduced via the rotational energy

$$U_i^{\text{Field}} = -F \cdot P_2(\cos \theta_i), \quad (4.10)$$

where $F > 0$ is the field strength, θ_i is the angle between the long axis of the i -th mesogen and the direction of the field. Throughout this study we will use the reduced field strength, f , where $F = f \cdot 10^{-20}$ J. The field-assisted growth of the smectic phase was performed close to the transition, at $T = 490$ K.

The value of the field strength f determines the reorientation rate of the mesogens and it has a profound effect on the formation of the smectic phase. If the mesogen reorientation rate is of the same order as the equilibrium relaxation times for backbones and side-chains, then concerted rearrangement of the molecules as a whole takes place. This is indicated in Fig. 4.2, where the evolution of the orientational order parameters S_2 is shown at $f = 0.2$ for the mesogens and for the long axes of equivalent ellipsoids for backbones and side chains (solid symbols). After the field is switched off and the temperature is reduced to 485 K, the smectic order remains stable in all subsystems (see open symbols). Therefore, one may conclude that the system is steered successfully into a global minimum state. However, when a stronger field is applied, $f > 0.5$, the reorientation rate of the mesogens does not conform with those for the polymer chains. As a result, when the field is switched off and the temperature is reduced, the system evolves into a metastable polydomain, globally isotropic state (Ilnytskyi and Neher 2007).

The smectic phase, a snapshot of which is depicted in Fig. 4.3, has a structure typical of a microphase-separated lamellar phase. It is of a “sandwich” type made of alternating layers of mesogens, side-chains and backbones. The real LCSCP system microphase separates due to poor miscibility between alkyl chains and mesogens containing aromatic groups. In our model, this effect is mapped onto poor miscibility between spherical and elongated particles. However, the shape characteristics of the polymer chains display only minor changes when undergoing the isotropic–smectic

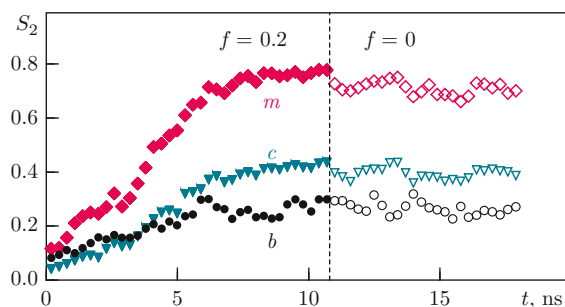


Fig. 4.2 Evolution of the orientational order parameters for the mesogens (m), side chains (c) and backbones (b) during the field-induced growth of the smectic phase: $f = 0.2$, $T = 490$ K (*filled symbols*) and during the relaxation with no field: $f = 0.0$, $T = 485$ K (*open symbols*). Reprinted with permission from Ilnytskyi and Neher (2007). Copyright 2007, AIP Publishing LLC

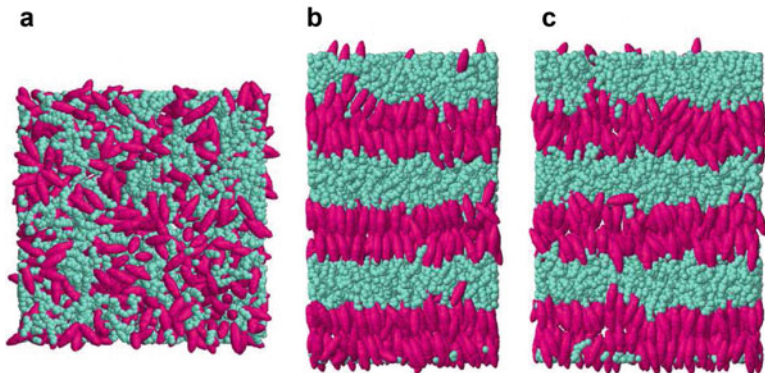


Fig. 4.3 Snapshots showing different stages of the monodomain smectic phase growth. (a) Initial isotropic state at $T = 490\text{K}$; (b) smectic structure formed at $T = 490\text{K}$ with the aid of the field $f = 0.2$; (c) the same structure relaxed at $T = 485\text{K}$ with the field switched off. (a), (b), (c) represent system states at $t = 0$, $t = 11\text{ns}$ and $t = 18\text{ns}$, as shown in Fig. 4.2

Table 4.1 Average shape parameters for the backbones and side-chains in the isotropic and smectic phases, see text for the notations; R_{1N}^4 is defined as the fourth moment of the end-to-end distance, analogous to Eq. (4.9) for R_{1N}^2 .

Chains	Backbones		Side-chains		Gaussian
	Isotropic	Smectic	Isotropic	Smectic	
$R_g^2, \text{\AA}^2$	62(4)	66(3)	10.4(1)	10.9(1)	
$R_{1N}^2, \text{\AA}^2$	410(30)	460(30)	86(2)	94(1)	
R_{1N}^2/R_g^2	6.7(3)	6.9(3)	8.27(7)	8.58(4)	6
$R_{1N}^4/(R_{1N}^2)^2$	1.4(1)	1.5(1)	1.06(1)	1.04(1)	5/3
σ_2^2/σ_3^2	3.5(3)	3.7(3)	4.3(1)	4.1(1)	2.5
σ_1^2/σ_3^2	18(2)	20(2)	48(2)	57(2)	11.8

Numbers in parentheses are estimated errors in the last quoted digit. Exact values (where appropriate) for the Gaussian chain are also provided

transition. These are shown in Table 4.1 for the backbones and side-chains. As one can see from the relevant columns, backbones demonstrate no changes in their shape, whereas the side-chains become more anisotropic in the smectic phase, as evidenced by the increase of the σ_1^2/σ_3^2 ratio by 19%. Backbones and, to a much greater extent, the side chains, adopt conformations that deviate from that of the ideal Gaussian chain. This effect can be explained by specific topological constraints in the SCLCP structure. Specifically, the side chains are grafted to the backbone at one end and have a large mesogen unit attached at another end. Clearly, this restricts their conformational freedom.

Given the minor influence of the phases on the shape properties of the backbones and side-chains, the difference, as also evidenced in Fig. 4.3, should be reflected in their spatial arrangement. The averaged mass distribution of chains in space is given by the components of the gyration tensor rotated into the director frame, Q_{aa} , introduced above. The values for Q_{aa} in the isotropic and smectic phases are

Table 4.2 Averaged diagonal components of the mass distribution tensor in the director frame for backbones and side-chains in the isotropic and smectic phases

Chains	Backbones		Side-chains	
Phase	Isotropic	Smectic	Isotropic	Smectic
Q_{xx}	20(2)	28(2)	3.5(2)	2.3(1)
Q_{yy}	21(2)	31(3)	3.4(1)	2.3(1)
Q_{zz}	21(2)	7(1)	3.5(1)	6.2(1)

Numbers in parentheses are estimated errors in the last quoted digit

compared in Table 4.2 for both the backbones and the side-chains. As one can see, the mass distribution of the backbones and side chains in the smectic phases is markedly different from that in the isotropic phase. For the side-chains, $Q_{zz} > \frac{1}{2}(Q_{xx} + Q_{yy})$ in the smectic phase, indicating that the mass distribution of these follows the orientation of the mesogens. In this way the fragment of a mesogen plus a side-chain behaves similarly to low-molecular-weight LC molecules like the *n*-CB cyanobiphenyls. For the backbones, $Q_{zz} < \frac{1}{2}(Q_{xx} + Q_{yy})$ in the same phase, corresponding to their confinement in the relatively thin layers perpendicular to the nematic director. This quantifies the visual appearance of the smectic phase, provided in Fig. 4.3. Such a microphase-separated lamellar structure of the smectic phase mimics that of the experimental systems (Dimitrova 2000; Stimson and Wilson 2005).

The lamellar structure of the smectic phase manifests itself also through an essential anisotropy of the internal dynamics of its constituent fragments. This dynamics can be monitored by following the behavior of the mean-square displacement of each fragment k (e.g. backbone), defined as

$$g(t) = \left\langle \left[\mathbf{R}^{[k]}(t) - \mathbf{R}^{[k]}(0) \right]^2 \right\rangle, \quad (4.11)$$

where $\mathbf{R}^{[k]}(t) = \{X^{[k]}(t), Y^{[k]}(t), Z^{[k]}(t)\}$ is the center-of-mass position (COM) of the k -th fragment at time t . In the smectic phase we are interested in the parallel and perpendicular contributions (relative to the mesogen director):

$$g^\perp(t) = \left\langle [X^{[k]}(t) - X^{[k]}(0)]^2 + [Y^{[k]}(t) - Y^{[k]}(0)]^2 \right\rangle, \quad (4.12a)$$

$$g^\parallel(t) = \left\langle [Z^{[k]}(t) - Z^{[k]}(0)]^2 \right\rangle. \quad (4.12b)$$

On a long time scale the macromolecules behave diffusively (Doi and Edwards 1994):

$$\lim_{t \rightarrow \infty} g(t) = 6Dt, \quad \lim_{t \rightarrow \infty} g^\perp(t) = 4D^\perp t, \quad \lim_{t \rightarrow \infty} g^\parallel(t) = 2D^\parallel t, \quad (4.13)$$

where D , D^\perp and D^\parallel are the corresponding diffusion coefficients. It is obvious that if the macromolecule reaches the diffusive regime, then this will also hold for its

Table 4.3 Diffusion coefficients D_m, D_b, D_c for the mesogen, backbone and side chain centers-of-mass, respectively, in isotropic and smectic phases. The parallel and perpendicular contributions are presented in the latter case

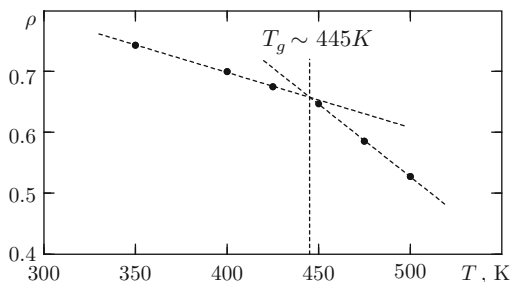
Phase	Isotropic				Smectic	
T	600 K	520 K	495 K	485 K	485 K	
					D^\perp	D^\parallel
D_m	194(6)	159(7)	48(2)	36(2)	40(8)	5.76(6)
D_b	195(8)	157(8)	46(4)	26(3)	38(0)	0.06(3)
D_c	194(7)	158(7)	47(4)	30(2)	40(8)	0.95(7)

constituents. We estimated the diffusion coefficient D separately for the backbones, side-chains and mesogens. Runs of about 10 ns in duration were used, with mean-square displacements computed up to two-thirds of this time with reasonable statistics. Diffusion coefficients were estimated from linear fits to $g(t)$ at long times, according to Eq. (4.13). The results are collected in Table 4.3. In the smectic phase the diffusion is found to be severely hampered along the mesogen director. D^\parallel is one to three orders of magnitude smaller than D^\perp (see last two columns of Table 4.3). D^\perp is found to be almost the same as in the overcooled isotropic phase, prepared by cooling the isotropic phase at $T = 495\text{K}$ down to $T = 485\text{K}$ with no aligning field. This means that all the constituents of the polymer subsystem are still very mobile in the planes perpendicular to the nematic director. These properties of the isotropic and smectic phases are relevant to our studies of the behavior of SCLCPs and SCLCEs under external perturbations, considered in the subsequent sections.

4.1.3 Properties of SCLCP in a Strong Coupling Limit

The strongly-coupled model is characterised by the following parameters: $L_b = 39$, $L_c = 2$, functionalization $k_f = 4$, the number of attached side-chains $N_c = 10$. Both backbone and spacers are modelled as stiff chains with appropriate parameters $\{C_i\}$ for the torsional potential V_t , discussed in detail at the beginning of Sect. 4.1. In our simulations, 96 side-chain molecules are packed into the simulation box in a regular geometric way (5664 polymer beads and 960 azobenzenes in total). This configuration is first heated up to $T = 700\text{K}$ to erase the memory of the initial packing. After that the melt was cooled down to $T = 500\text{K}$ and equilibrated for 10 ns. To be able to relate the simulation temperatures to that of the glass transition, T_g , we performed a rather brief simulation. This was done via step-by-step cooling of the melt within the temperature interval $T \in [350\text{K}, 500\text{K}]$. The temperature was reduced in steps of 10–25 K by resetting it to a lower value and then allowing the system 4–8 ns to equilibrate. The glass transition temperature T_g is then estimated from the change of the slope in the density–temperature plot, see Fig. 4.4, and found to lie between 440 and 450K.

Fig. 4.4 Estimate of the glass transition temperature $T_g \sim 445\text{K}$ from the change of slope in a density–temperature plot, in the strongly coupled model. Reprinted with permission from Ilnytskyi et al. (2011). Copyright 2011, AIP Publishing LLC



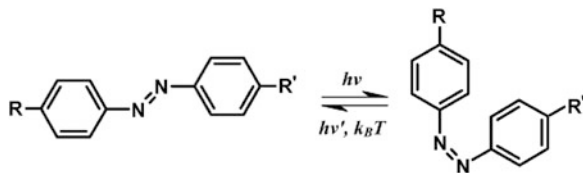
We should remark here that a thorough study of the system behavior at and below T_g , as well as a more precise estimate for T_g itself depending on cooling rate, is beyond the scope of this chapter. Otherwise, extremely long special purpose simulations, and application of special techniques, would be required (Han et al. 1994; Lyulin et al. 2003). Besides that, the glass transition in a polymer LC can be associated not only with a freezing of the torsion angles (as in an ordinary polymer) but also with a strengthening of the LC interaction.

To look for the possibility for forming a monodomain nematic or smectic phase, we applied an external uniaxial aligning field, similarly to the case of the weakly-coupled model, Eq.(4.10). These attempts were unsuccessful and no stable monodomain ordered phases were found, in accordance with the typical phase diagrams of side-chain LC polymers with short spacers (Collings and Hird 2001; Rutloh et al. 2000; Freiberg et al. 2003). Instead, the polymer was found to adopt a polydomain LC phase, with strong intradomain LC interactions, which act as physical crosslinks (Gallani et al. 1994).

4.2 Photo-Induced Deformations in SCLCP

The isomerization state of photo-active mesogens (chromophores) can be manipulated by suitable illumination. The most well-known example is azobenzene, which undergoes a photoisomerization from the prolate *trans* to bent *cis* isomer and *vice versa*, see Fig.4.5. In the case of an azobenzene-containing SCLCP, the photoisomerization induces changes in the LC subsystem and, via coupling to the polymer component, generates internal stress in the material. The exact microscopic mechanism of the stress relaxation depends on the details of the polymer molecular architecture. This was clearly demonstrated in the experimental work of Bublitz et al. (2000) via illumination of free-floating azo-polymer droplets with a uniform linearly polarized beam. In the case of the polymer P6a12 (a molecular architecture with weak coupling) the droplet was found to contract along the polarization vector. On the contrary, in the case of the polymer E1aP (a molecular architecture with stiff backbone and strong coupling) the droplet was found to extend along the polarization vector (Bublitz et al. 2000). These

Fig. 4.5 The photoisomerization of azobenzene chromophores. Reprinted with permission from Ilnytskyi et al. (2011). Copyright 2011, AIP Publishing LLC



findings are closely related to the bending of azobenzene-containing elastomers when illuminated (Camacho-Lopez et al. 2004; Ikeda et al. 2007). In yet another experiment, a linearly polarized beam was applied through an optical mask with light stripes. In this case, either hills or trenches were observed in illuminated areas, again depending on the details of the polymer (Holme et al. 1999). Under spatially modulated illumination (a holographic-like setup) the even more striking effect of surface relief grating (SRG) formation was discovered in 1995 (Rochon et al. 1995; Kim et al. 1995), which has received considerable attention since then (Viswanathan et al. 1999; Oliveira et al. 2002; Hvilsted and Ramanujam 2001; Barrett et al. 2007).

SRGs can be inscribed in both weakly- and strongly-coupled azo-polymers (for reviews, see Viswanathan et al. 1999; Oliveira et al. 2002; Barrett et al. 2007). The effect is puzzling in the way that SRG formation takes place in amorphous azo-polymers well below the glass transition temperature T_g . Several models (Barrett et al. 1998; Kumar et al. 1998; Lefin et al. 1998; Pedersen et al. 1998; Baldus and Zilker 2001; Bublitz et al. 2001; Gaididei et al. 2002; Oliveira et al. 2002) have been suggested towards the explanation of the origin of the inscribing force, but none of them describes satisfactorily the light-induced motion of the azobenzene polymers at a molecular level (Saphiannikova et al. 2004; Saphiannikova and Neher 2005). Some of them assume a considerable degree of photoinduced plasticization, at least comparable with that at the glass transition. However, only very weak plasticization has been found in mechanical experiments (Mechau et al. 2002, 2005), leading to the conclusion that illumination of an azobenzene polymer layer with actinic light cannot induce a transition into a macroscopic low-viscosity melt. A thermodynamic theory, valid for amorphous azo-polymers with weak interactions between azobenzenes, was developed in Saphiannikova and Neher (2005) and Toshchevnikov et al. (2009). A number of optical setups can be used to produce the SRG, in particular, ones utilizing linearly and circularly polarized light [for more details, see review papers (Viswanathan et al. 1999; Oliveira et al. 2002)]. Nunzi and coworkers demonstrated that the use of an incoherent light source is also efficient for the deformation of azopolymer nanospheres (Barillé et al. 2010), and for printing a well organized pattern at the surface of an azopolymer thin film (Kandjani et al. 2005). In our study we focus our attention on the case of linearly polarized light.

The photoisomerization of azobenzene is a complex quantum mechanical phenomenon which involves excitation of the electrons of the N=N double bond, and takes place on the time-scale of tens of picoseconds (Michl and Thulstrup 1995).

However, given the scale of the force-field modeling employed here, one can reduce it to the same classical mechanical level. It is assumed here that the material contains azobenzene chromophores with such chemical substituents (e.g. NO_2) that continuous *trans-cis-trans* isomerization cycles occur at a certain wavelength of the illumination. Given that the rate of the *trans-cis* photoisomerization is proportional to $\cos^2\theta_i$ (θ_i is the angle between the long axis of the i -th *trans*-isomer and the light polarization), the *trans*-isomers are to be found predominantly perpendicular to the light polarization (orientational hole-burning effect). On the classical mechanical level this effect can be modeled by introducing a reorienting field which acts on each *trans*-isomer. The corresponding energy reads:

$$U_i^{\text{azofield}}(\theta_i) = F \cdot P_2(\cos\theta_i). \quad (4.14)$$

Here the field strength is $F > 0$ (again we will use the reduced field strength, f , where $F = f \cdot 10^{-20}$ J), θ_i is the angle between the long axis of the i -th *trans*-azobenzene and the direction of the field, and $P_2(x)$ is the second Legendre polynomial. The derivative of $U_i^{\text{azofield}}(\theta_i)$ with respect to θ_i is related to the torque acting on the i -th azobenzene. One should note that, while both electric and magnetic fields align the azobenzenes uniaxially [this corresponds to Eq. (4.10) with $f > 0$], the model field defined via Eq. (4.14) with $f > 0$ forces azobenzenes to stay preferentially in the plane perpendicular to the field direction. The latter can be associated with the polarization of the beam.

The aim of this study is to find the most relevant mechanisms for the photo-induced deformations and, therefore, some aspects of the photoisomerization are not considered. These are, in particular, the presence of *cis*-isomers and the kinetics of the photostationary state. The only effect being taken into account is the reorientation of the *trans*-isomers of the azobenzenes when the material approaches the photostationary state. Throughout this study, however, we discuss the possible relevance of the *cis*-isomers in each particular case.

4.2.1 Modelling of Photo-Induced Deformations in Weakly Coupled SCLCP

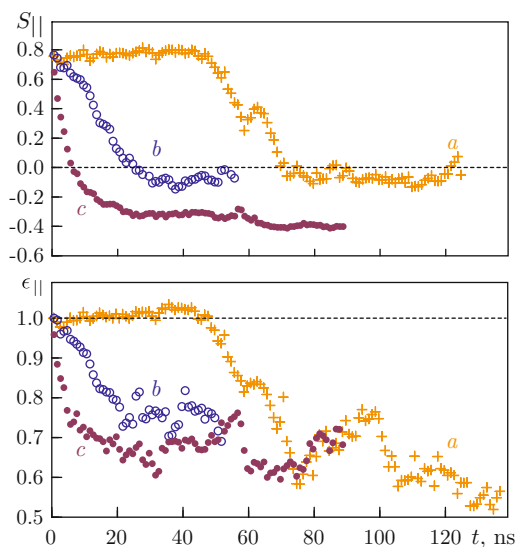
We consider the SCLCP in a weak coupling limit represented by exactly the same model as in Sect. 4.1. A monodomain smectic volume element, obtained with the aid of aligning field (4.10) is well equilibrated at $T = 485\text{K}$, which is just below $T_{\text{SI}} \sim 490\text{K}$ (Ilnytskyi and Neher 2007). The azobenzene director is collinear with the Z axis, and initial values for both order parameters are equal: $S_{\parallel} = S_2 \approx 0.75$. In the absence of an external field the phase is stable for at least 120 ns with minimal fluctuations of the order parameters and of the box dimensions. With application of the field along the nematic director, this arrangement becomes energetically unfavorable and a torque applied to each chromophore attempts to reorient it

perpendicularly to the field. The rate of the reorientation depends on the field strength f , but is also affected by coupling of the chromophores to the polymer matrix.

What kind of response of the polymer matrix can be expected? If the field is strong enough (large f), then the time scale of chromophore reorientation may become much shorter than typical relaxation times of the polymer matrix. In this case one, generally, expects development of the internal stress and deformation of the volume element. At small values of field strength f , the time scales of both processes may become of the same order. Then, one may expect several scenarios: (a) reorientation of azobenzenes with no deformation of the polymer (due to stress relaxation); (b) monotonical deformation of the polymer over an extended time interval, “in phase” with reorientation of chromophores; or (c) deformation of the polymer on a similar time scale as for the moderately strong field case (phase-transition-like changes).

We found only two scenarios. At field strengths of $f = 0.015\text{--}0.020$, the typical “weak field scenario” with the SI transition was observed [see results averaged over this interval marked (b) in Fig. 4.6]. Unfortunately, these particular simulation runs cannot be prolonged due to the effect of “monolayering” of the simulation box, in which case the simulations are terminated. The reason behind this shortcoming is that the $NP_{xx}P_{yy}P_{zz}T$ ensemble is not well suited for the simulation of isotropic phases, where random fluctuations of the simulation box dimensions take place (Allen and Tildesley 1989). The run with a very weak field, $f = 0.005$, turned out to be unaffected by this problem for more than 120 ns [curves (a) in Fig. 4.6]. The SI phase transition takes place during the time interval $t \sim 45\text{--}65$ ns, after which no apparent changes are observed for about 45 ns in the smectic phase, but the duration of the transition (approximately 20 ns) is the same as for the

Fig. 4.6 Field-induced changes in the order parameters of azobenzenes, S_{\parallel} (top frame), and in the strain along the field, ϵ_{\parallel} (bottom frame), for the monodomain smectic phase at $T = 485\text{K}$. (a) $f = 0.005$; (b) average over $f = 0.015$, $f = 0.017$ and $f = 0.020$ runs; (c) average over $f = 0.1$ and $f = 0.16$ runs. Reprinted with permission from Ilnytskiy et al. (2011). Copyright 2011, AIP Publishing LLC



case of higher field strengths $f = 0.015\text{--}0.020$. Therefore, fourfold reduction of the field strength has the effect of merely time shifting the transition, but not changing its typical time scale.

The SI transition is accompanied by an essential contraction of the simulation box along the direction of the field (see the curves for the strain ε_{\parallel} in Fig. 4.6, curve a). We can conclude that, at least within a time window of 120 ns, we hit some interval of field strengths f for which the SI transition can be achieved solely due to the reorientation of *trans*-azobenzenes [with no formation of *cis*-isomers, as in the case of the real photo-chemical transition (Ikeda et al. 1990, 2002; Ikeda 2003; Barrett et al. 2007)]. Deformation of the box can be explained by the following considerations. The duration of the SI transition is about 20 ns (the time interval $t \sim 45\text{--}65$ ns in Fig. 4.6), and it is shorter than the estimated relaxation times for the chromophore reorientations in the equilibrium state, $\tau \approx 43$ ns (Ilnytskyi and Neher 2007). As a result, the polymer is not given enough time to relax during the transition, and deformation of the polymer matrix takes place. The synchronicity in changes of S_{\parallel} and ε_{\parallel} , clearly seen in Fig. 4.6, indicates a strong coupling between the amount of the orientational order of the mesogens and the shape of the simulation box.

With the increase of f beyond $f \sim 0.020$ one observes the “strong field” scenario, in which two processes take place (see curves c in Fig. 4.6). The first process is the SI transition which occurs for $t < t^* \approx 5$ ns. It is followed by the second process, for $t > t^*$, during which the smectic phase is regrown with its director now being perpendicular to the field [relevant snapshots can be found elsewhere (Ilnytskyi et al. 2006)]. Typical time scales of these transitions depend on the strength of the field; the data averaged over $f = 0.1$ and $f = 0.16$ runs are shown in Fig. 4.6 (curve c). One can conclude that in the first process the field acts as a “melter” of the smectic phase and in the second as an aid for the self-assembly of the isotropic melt into the smectic phase. In this way, the “strong field” scenario combines both effects of the photo-induced order–disorder transition and of the photo-alignment in azo-polymers (Ichimura 2000; Ikeda et al. 2002; Ikeda 2003). Generally speaking, during the field-aided self-assembly the possibility of the planar phase exists, in which chromophore orientations are confined within the planes (perpendicular to the direction of the field) but with no orientational order within the planes. However, this phase is observed in none of the simulations being performed. The in-plane $2D$ symmetry is always broken in favour of the smectic layers. This is in agreement with predictions of the thermodynamic theory developed recently for LC azobenzene elastomers (Toshchevnikov et al. 2012; Toshchevnikov and Saphiannikova 2014).

One should stress that, for the “strong field” scenario, the anisotropic deformation of a volume element occurs only during the first process ($t < t^*$, SI transition), where ε_{\parallel} decreases significantly. The second process, for ($t > t^*$, isotropic–smectic transition), takes place with no apparent systematic changes in the box dimensions. Therefore, the contraction of the volume element is reported for our model for both “weak field” and “strong field” scenarios. We can deduce that contraction of the smectic monodomain sample along the field is achieved primarily due to the destruction of the initial smectic order.

One may conclude that the defining factor in contraction of the volume element along the field is the “randomization” of the azobenzene orientations. The spacers are also known to align partially along the nematic director in the smectic phase (Illytskyi and Neher 2007); therefore these also add to the net effect. The contribution from the rearrangements of the backbones is also present in the deformation of the volume element observed as the result of the simulations. However, due to their flexibility, their effect is minor (Illytskyi et al. 2011).

4.2.2 *Modelling of Photo-Induced Deformations in Strongly Coupled SCLCP*

The strongly-coupled model is used to simulate photo-induced deformations in amorphous azo-polymers. The properties of this model, and the estimate for the glass transition temperature, have been discussed in the relevant part of Sect. 4.1.

Most SRG inscriptions in amorphous systems are performed at $T < T_g$, aimed at fabrication of technologically desirable long-term stable gratings. However, even the changes in the inscription process when one approaches T_g may shed much light on the tendencies of the relevant mechanisms at still lower temperatures. It was shown in recent experiments (Veer et al. 2008, 2009) that under continuous exposure the grating height decays exponentially with the temperature increase, and no permanent SRG can be recorded if $T > T_g - 20^\circ\text{C}$. However, under pulse-like exposure, the grating still exists as long as the actinic light is on. It follows that at $T \sim T_g$ the SRG can be stable over a short time interval, whereas subsequent stress relaxation prevents formation of a permanent grating.

We perform MD simulations both above T_g and at $T \sim T_g$. All results presented in this section are obtained on macroscopically isotropic volume elements. Three simulations were undertaken at each field strength f (the field in each case was directed along the X , Y and Z axes, respectively) and the results were averaged over these three runs. In this way, we attempt to exclude the possibility that the effects being observed are related to the fluctuations. This also mimics some minimal sample averaging, combined with the averaging over the runs with close values of f .

Let us first discuss the results obtained at $T = 500\text{K} > T_g$, where the melt has viscoelastic properties. Photo-induced deformations take place within a certain interval of field strengths: $f = 1\text{--}1.7$. Here we will restrict our discussion to the single case of $f = 1.6$. The field is switched on at $t = 0$ and switched off at $t = 24\text{ns}$. The evolution of the order parameter along the field S_{\parallel} (shown separately for the backbones and mesogens), and the photo-induced strain ε_{\parallel} , are presented in the two left frames of Fig. 4.7.

Similarly to the case of the weakly-coupled model, considered in the previous section, the effect of photo-induced reorientation of chromophores is observed clearly. The changes in the order parameter of the backbones are found to take place on the same time scale; this indicates the reorientation of the molecule as a

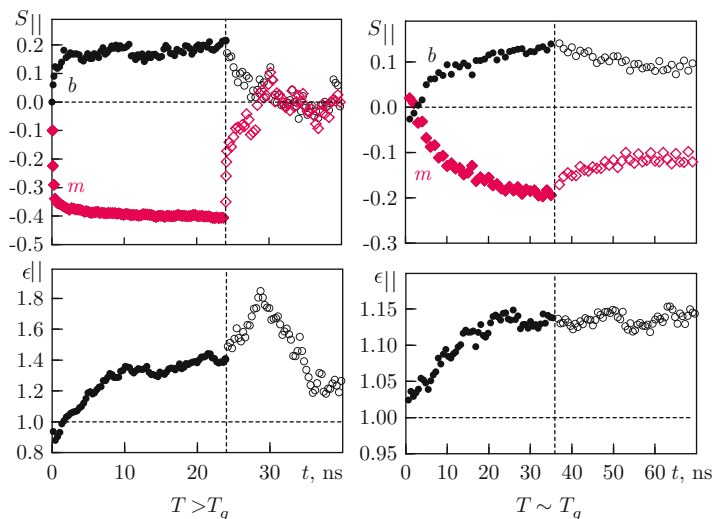


Fig. 4.7 Evolution of the order parameter S_{\parallel} , and the photo-induced strain ϵ_{\parallel} , along the external field (shown in *solid symbols*) and after the field is switched off (*open symbols*). The values of S_{\parallel} for both the backbones (*b*) and the mesogens (*m*) are indicated. *Left frames* show the case $T = 500$ K $> T_g$ at field strength $f = 1.6$. *Right frames* show the case $T = 450$ K $\sim T_g$, for which the data is averaged over the results for $f = 0.15, 0.20$ and 0.50 . Reprinted with permission from Ilnytskyi et al. (2011). Copyright 2011, AIP Publishing LLC

whole (due to the strong coupling nature of this molecular architecture). The effect of backbone stretch is also present, but it is relatively weak (Ilnytskyi et al. 2011).

It is very important to note that the same principal structural changes (reorientation of the chromophores and backbones perpendicularly and parallel to the field, respectively) are observed as in the case of the weakly-coupled SCLCP azo-polymer. However, the mechanical response of the strongly-coupled system is the opposite: the volume element extends about 140% along the field (Fig. 4.7, bottom frame). As far as the backbone reorientation contributes to the volume element expansion, one can conclude that this effect is more essential than the reorientation of chromophores. The result can be attributed to backbone stiffness and to a short spacer, which helps to transfer any torque imposed on the chromophores straight to the backbones.

The changes are, however, reversible. After the field is switched off at time $t = 24$ ns, within 10–15 ns the field-induced state of the polymer reverts back to almost the initial state. In particular, the order parameter of backbones along the field S_{\parallel} decreases, and the strain of the volume element in the same direction ϵ_{\parallel} changes back towards the initial value. This mimics the experimental findings on impermanent SRGs if performed in amorphous materials that are not deep enough in a glassy state (Veer et al. 2008, 2009). The analysis of the model structure formed under the field, which corresponds to the time interval $t = 20$ – 24 ns, reveals that it is a polydomain one with strong local liquid crystallinity (Ilnytskyi et al. 2011).

The field effectively drives the system to a state with similar structure as is observed at and below its glass transition temperature T_g . After the field is switched off, the system recovers the structure it had at $T > T_g$.

Most SRGs are recorded deep below T_g ; typical recording times for amorphous systems range from seconds to days. Such time scales are inaccessible for semi-atomistic simulations. Therefore, we limit our analysis to the tendencies undergone by the process of photo-induced deformations when one approaches the glass transition temperature. These could be extrapolated further to the $T < T_g$ region. Therefore, the simulations are performed at $T = 450\text{K} \sim T_g$, where the estimate for $T_g \approx 445\text{K}$ is based on Fig. 4.4. A well equilibrated configuration was prepared by cooling the melt from $T = 500\text{K}$ down to $T = 450\text{K}$ and by subsequent equilibration for a relatively long time of 65 ns. Similarly to the case of $T = 500\text{K}$, an external field was applied in turn along each spatial axis and the results were averaged over the three runs. The effect of photo-induced deformation was observed in the range of $f \sim 0.1\text{--}0.7$, and these values are essentially lower than $f \sim 1$ required in the case of $T = 500\text{K}$.

All properties of interest are found to behave quite similarly for field strengths $f = 0.15, 0.20$ and 0.50 (here one can ignore small differences in reorientation dynamics in this interval of values of f), and, therefore, the results are averaged over these runs to improve statistics. The data is shown in the right frames of Fig. 4.7. The changes in orientational order parameters for chromophores and backbones, acquired due to application of the field, are found to be stable after the field is switched off (at $t = 37\text{ns}$) for at least another 30ns. This is in a sharp contrast to the case of $T = 500\text{K}$, when the order vanishes in about 5 ns after the field is switched off. The same holds true also for the strain of the volume element along the field, ε_{\parallel} , which is found to behave smoothly with no “kick” after the field is switched off. The expansion of the box acquired along the applied field is preserved for at least another 30 ns after the field is switched off. More precise determination of the stability of field-induced deformation requires much longer simulation runs which, in turn, needs a simulation box of a larger size. The reason for this is that the film can turn into a monolayer in one of the dimensions perpendicular to the field, due to spontaneous shape fluctuations.

Let us consider again the possible role of the *cis*-isomers, which have not been taken into account explicitly here. Their presence will dilute, and, therefore, lessen the local LC ordering and decrease the role of physical crosslinks, the effect that prevents mechanical changes at higher values of field f . Otherwise, the *cis*-isomers will decrease the net torque applied on each molecule, which may result in a need for stronger fields to be applied or longer time to achieve the deformation. In any case, the same basic mechanism is expected to hold.

The results obtained at both $T > T_g$ and $T \sim T_g$ provide evidence for the following microscopic mechanism for photo-induced deformations in a strongly-coupled model SCLCP. First of all, due to the strong coupling between chromophores and backbones, the molecules behave similarly to rigid bodies (the time scale of the order parameter evolution for both chromophores and backbones is the same). Given suitable conditions, these massive molecular reorientations lead to the

build-up of anisotropic internal stress, which causes temporary or permanent deformation of the volume element. In the case of $T > T_g$ the deformation is observed at moderately large field strengths, $f = 1-2$, in which case the system is driven first to the state with higher density (typical for the temperature range $T < T_g$). The deformations are temporal, inasmuch as, upon switching the field off, the system reverts back to almost the initial (pre-field) state. In the case of temperatures $T \sim T_g$, the initial density of the melt is essentially higher and the internal stress (and, consequently, anisotropic deformation) is developed at much weaker fields, $f = 0.1-0.7$, and stays permanent during at least the simulation time of 30 ns performed in this study. The sign of the deformation (extension of the volume element along the field direction) highlights the role of backbone rigidity, in that the effect of backbone reorientation wins over the effect of chromophore reorientation perpendicularly to the field.

4.3 Elasticity and Memory Effects in SCLCE

4.3.1 Preparation of the Elastomer and Shift of the Smectic-Isotropic Transition

As already discussed above, the elastomer matrix acquires some new properties as compared to the case of the melt. Specifically, the viscosity of the polymer subsystem is suppressed in favor of elasticity. The latter provides the reversibility of the system response when it is perturbed via some external stimulus. Modeling of these effects is the subject of the current section.

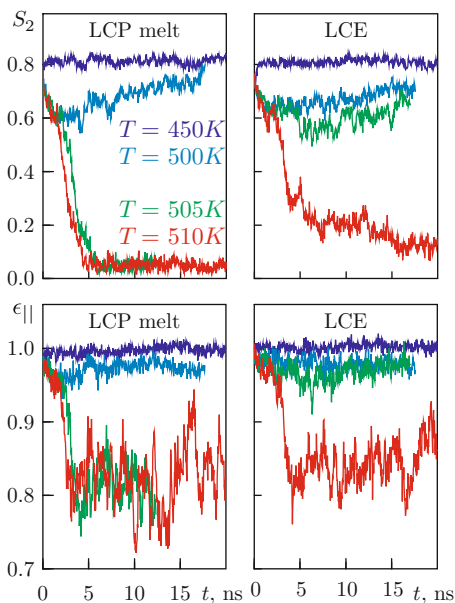
The SCLCE is prepared by crosslinking the SCLCP melt, which is equilibrated in the smectic phase. For this purpose we used the model depicted in Fig. 4.1 and described in detail in Sect. 4.1. The following parameters are used: $L_b = 100$, $L_c = 6$ and $k_f = 2$. Out of $N_c = 50$ pendant side chains, 40 are terminated by a mesogen, whereas the remaining 10 are terminated by chemically active particles, which can form crosslinks. Both backbone and side chains are chosen to be flexible, with appropriate parameters $\{C_i\}$ for the torsional potential V_t , discussed in detail in Sect. 4.1. The smectic phase was prepared with the aid of the aligning field of Eq. (4.10), as described above for the case of the weakly-coupled limit.

To avoid disruption of the initial smectic structure of the melt, we opted to use “rubber band” crosslinks of about 4Å in length that are longer than true “chemical” bond lengths (e.g. $\sim 1.54\text{\AA}$ for hydrocarbons) instead of forcing reactive sites into closer contact. $N_{cl} = N_{mol} = 28$ crosslinks are made using an algorithm which attempts to crosslink homogeneously through the simulation box; more details are given elsewhere (Ilnytskyi et al. 2012).

One can classify the effects observed in LCEs under external stimuli on the basis of the physical nature of the latter. Let us start from the effects connected with temperature change. For weakly crosslinked networks, the LC groups retain the

ability to form LC phases, and the LC transitions are the only principal changes undergone by LCEs on varying the temperature (presuming the temperatures to lie above the glass transition temperature). Crosslinking stabilizes the LC phase in which the network is originally formed, due to memorizing the backbone conformations (Symons et al. 1993, 1999; Davis and Mitchell 1996; Warner et al. 1988). This is indicated by a rise of the order–disorder transition temperature, if crosslinking was performed in an ordered phase. The exact amount of the shift of the transition temperature depends on crosslink density, the level of nematic order, and other factors (Symons et al. 1999) but is, typically, a few degrees for weakly crosslinked LCEs. One, however, needs to take into account that, in contrast to low-molecular-weight LC materials, the order–disorder phase transition in LCEs is more smeared. The isotropic–nematic coexistence over a broad temperature range suggests that the heterogeneity in the samples introduces a distribution of transition temperatures (Zhang et al. 2006). Therefore, one might refer rather to a certain “transition region”, which defines an approximate interval for the SI transition temperature, T_{SI} . This interval is estimated from a series of heating runs performed at a range of temperatures, each run started from the same smectic sample being equilibrated at 450 K for at least 10 ns. The evolution of the order parameter S_2 is shown in Fig. 4.8 for both cases of LCP melt and LCE. The transition region is found to be 500–505 K for the melt and 505–510 K for the elastomer, respectively. Therefore, the estimated increase of the transition temperature due to crosslinking of the melt is $\sim 5^\circ\text{C}$, in agreement with typical experimental findings (Symons et al. 1993, 1999; Davis and Mitchell 1996; Warner et al. 1988).

Fig. 4.8 *Top row:* evolution of the nematic order parameter for the LC groups in the LCP melt (*left frame*) and in the LCE (*right frame*) upon heating the initial smectic sample equilibrated at $T = 450\text{K}$ up to higher temperatures indicated in the *left frame* of the plot. *Bottom row:* the same for the uniaxial strain of the sample ϵ_{\parallel} along the initial nematic director. Adapted from Ilnytskyi et al. (2012) with permission from The Royal Society of Chemistry



It is well known from the experiments that the change of LC order is accompanied by deformation of the material along the director axis (Schätzle et al. 1989; Assfalg and Finkelmann 1989; Tajbakhsh and Terentjev 2001; Hirschmann et al. 2001; Cladis 2001; Warner and Terentjev 2003). A wide range of strain values have been observed, from 0.29 (Tajbakhsh and Terentjev 2001) to 0.95 (Mitchell et al. 1993; Hirschmann et al. 2001). The amount of strain depends on the coupling between the average anisotropy of polymer chains and the nematic order parameter, and it has some specific features outlined below. Small-angle neutron scattering experiments on deuterium labeled mixtures have revealed that both types of backbone anisotropy, parallel and perpendicular to the director, are possible (Mitchell et al. 1991; Kirste and Ohm 1985; Keller et al. 1985), as well as switching between the two (reminiscent of the odd-even effect in nematics) (Mitchell et al. 1992). In this respect, positive and negative coupling coefficients are often used indicating that backbones are extended parallel or normal to the liquid crystal director, respectively. As remarked in Küpfer and Finkelmann (1991), for nematic polymers, typical ratios between radii of gyration of backbones parallel and perpendicular to the director, R_{\parallel}/R_{\perp} , are found close to 0.7 or 1.3. For smectic polymers, backbones are confined inside layers and R_{\parallel}/R_{\perp} is much smaller than one (Ilnytskyi and Neher 2007).

This effect is also reproduced in our simulation, evidenced by the behavior of a uniaxial strain ε_{\parallel} along the axis of the initial director; see relevant frames of Fig. 4.8. In the case of our model, the backbone is flexible and the coupling between the nematic director and backbones is negative; thus both compete in influencing the shape of the sample. However, as in the case of the similar weakly-coupled model with different values for L_b , L_c and k_f , discussed in Sect. 4.2, the sample contracts when driven through the SI transition. This, presumably, can be attributed to the flexibility of the model backbone in both cases. It is important to note that the transition-induced strain is weakly dependent on whether the crosslinking is performed or not. In both cases of melt and network, it is of the order of 0.8, see Fig. 4.8. However, despite much similarity between the cases of LCP melt and LCE in terms of deformation upon entering the isotropic phase, both systems demonstrate quite different attitudes towards the shape memory effects. This is considered in detail in the following section.

4.3.2 Memory Effects

Due to coupling between the LC and polymer subsystems, LCEs display a number of reversible opto- and thermo-mechanical effects, which brings them into the wider class of shape-memory polymers (Behl and Lendlein 2007; Ahn et al. 2011). In particular, the sample may be held at temperatures well above the nematic–isotropic transition for extended periods (2 weeks), but on cooling into the LC phase region, the original monodomain order is recovered with the same director alignment (Legge et al. 1991). This is in contrast to the case of an uncrosslinked sample of the same copolymer, in which case no retention of the global orientation was

shown after holding the sample for 60 s in the isotropic state (Legge et al. 1991). These thermo-mechanical memory effects, observed experimentally (Legge et al. 1991; Mitchell et al. 1993), form a basis for possible technological applications of LCEs as artificial muscles (Shenoy et al. 2002; Spillmann et al. 2007).

We aim to reproduce, by simulation, the reversibility of the orientational order, and of the sample shape, when the LCE is driven on a temperature scale back and forth through the order–disorder transition. To this end, we performed a set of runs started from the initial smectic phase that is equilibrated at 450 K. This phase is subjected to annealing at 510 K. During the process, we picked samples annealed for 4, 12, 20 and 28 ns and performed their quench at $T = 450\text{K}$ for at least 20 ns. The main question is whether or not this quenching will revert the structure to the initial smectic phase. The answer is *no* for the case of the LCP melt [the plots are given elsewhere (Ilnytskyi et al. 2012) and are not repeated here]. However, for the case of the LCE, complete reversibility of the structure is observed at least within a time window 40 ns of our simulations. In particular, the behavior of the mesogen order parameter S_2 , as evidenced in Fig. 4.9, indicates that the LC subsystem self-assembles back into the smectic phase as the result of quenching. The evolution of the uniaxial strain ϵ_{\parallel} along the axis of the initial nematic director is also shown in Fig. 4.9. The initial strain fully recovers for all quenching runs performed. The evolution of the order parameter, and that of the strain upon quenching, are found to

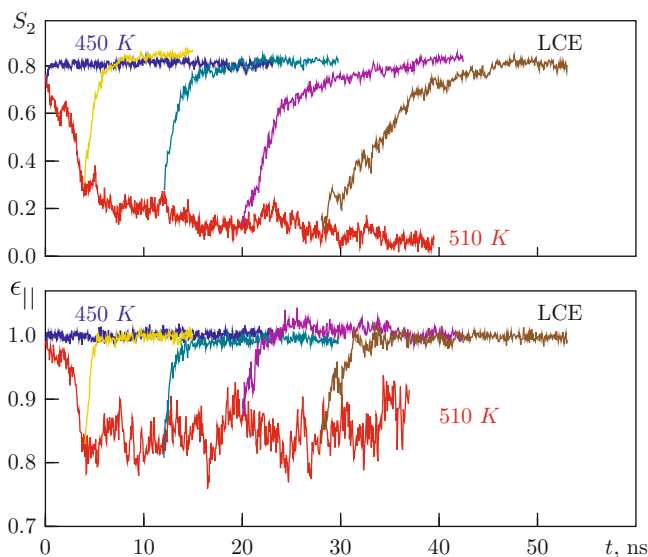


Fig. 4.9 *Top frame:* nematic order parameter S_2 , *bottom frame:* uniaxial strain ϵ_{\parallel} along the axis of the initial nematic director during annealing-quenching runs of LCE. The initial structure is well equilibrated at 450 K in the smectic phase (*blue curve*). An annealing run is performed at $T = 510$ K (*red curve*) and quenching runs are performed back to $T = 450\text{K}$ (*other colors*) for the structures partly annealed for 4, 12, 20 and 28 ns. Adapted from Ilnytskyi et al. (2012) with permission from The Royal Society of Chemistry

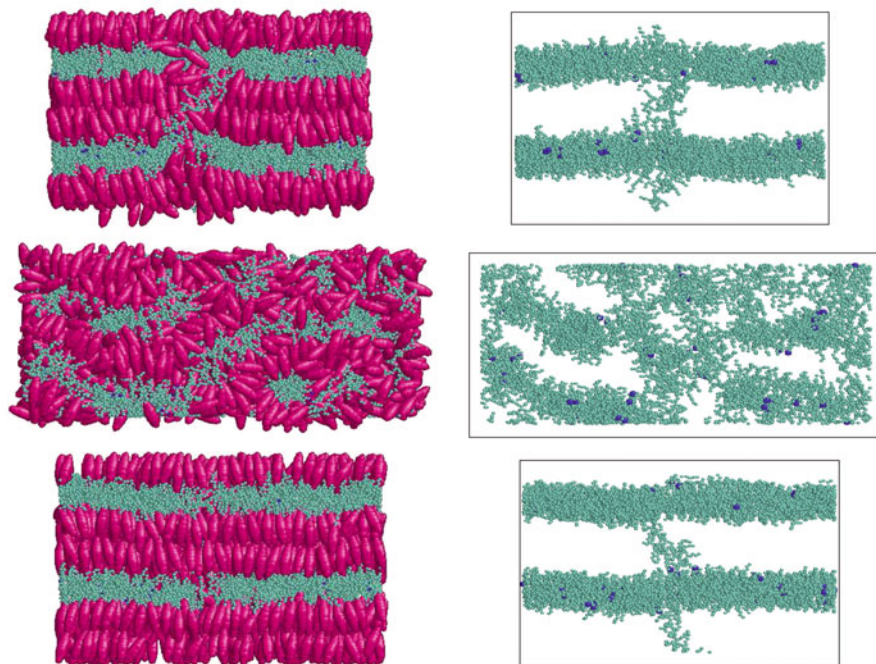


Fig. 4.10 *Top row*: snapshots for the initial smectic phase at $t=0$. *Middle row*: structure partly annealed at 510 K for 20 ns. *Bottom row*: recovered smectic structure as the result of quenching back to 450 K. Snapshots showing both polymer and mesogens are on the *left*, snapshots showing backbones only are on the *right*. Reproduced from Ilnytskyi et al. (2012) with permission from The Royal Society of Chemistry

be fully synchronized. Visual representation of this memory effect is provided in Fig. 4.10, where snapshots are given for the initial structure, partly annealed structure after 20 ns, and recovered structure.

The reversibility of the smectic structure upon annealing/quenching runs in the LCE case can be interpreted by hampering the diffusion via crosslinking. As one can see from Fig. 4.10, the partly annealed structure preserves the essentials of the layered structure of the initial phase, despite the layers being bent and distorted. This memory effect of the polymer matrix plays the principal role in a quick rebuild of an exact replica of the initial smectic structure.

4.3.3 *Stress-Driven Effects in the Isotropic and Smectic Phases*

Let us switch now to the opposite type of effect, in which a mechanical load is used as a driving stimulus. It has been known since the early studies that in this way one can manipulate the LC order of the LCE (Finkelmann et al. 1981, 1984; Mitchell

et al. 1987; Degert et al. 1992). A fundamental mechanism here is that an applied stress induces an anisotropy in the polymer backbone, which results in a macroscopic alignment of the director by virtue of coupling (Hirschmann et al. 2001). Due to this, the load induces remarkable changes in the structure of the LCE, if its axis is not collinear with the axis of initial anisotropy of backbones.

When applied to a globally isotropic sample, a uniaxial load is able to induce homogeneous LC order. This effect is used for fabrication of liquid single crystal elastomers via a two-stage crosslinking technique (Küpfer and Finkelmann 1991). On the other hand, when applied to an initially ordered monodomain nematic LCE, the load may change the already-existing LC order (Finkelmann et al. 1981; Küpfer and Finkelmann 1991; Mitchell et al. 1993). In the case of positive LC-backbone coupling, the changes occur when the load axis is not collinear with the initial director, due to the arguments above. When the load is applied normally to the director, then the sample first turns opaque (accompanied by softening of the material) and then a monodomain sample is formed in which the director is parallel to the load (Küpfer and Finkelmann 1991). The opaque state turns out to have a periodic V-shaped pattern. When the strain is applied nearly normal to the initial director, molecular rearrangement is accompanied by a decrease in nematic order parameter during the rotation (Roberts et al. 1997). Wide-angle X-ray scattering and optical microscopy studies have revealed a single director orientation throughout the switching process; broad optical-texture variations are observed after the director flip has occurred, although the sample remains optically clear throughout the process (Roberts et al. 1997). Director reorientation in nematic LCEs is also extensively discussed theoretically (Verwey et al. 1996; Warner and Terentjev 1996; Bladon et al. 1993, 1994; Weilepp and Brand 1996).

Much less work has been done on smectic-A elastomers. It was found (Nishikawa et al. 1997) that macroscopically uniformly aligned smectic-A LCEs are characterized by a highly anisotropic solid-like response, with an elastic constant along the layer normal about two orders of magnitude larger than that in the layer plane. When the sample is deformed parallel to the layers, it responds as a two-dimensional elastic network: the sample stays clear up to high strains of 200 %, and maintains its full width in the direction parallel to the layer normal (Nishikawa et al. 1997). However, when the sample is stretched along the layer normal (parallel to the director), stress-driven changes in the LC order are observed, due to negative backbone-LC coupling. If the load is applied in this way, and it exceeds a threshold value, then a breakdown of the monodomain structure is observed, resulting in a completely turbid sample (Nishikawa et al. 1997) suggesting layer undulation (see Fig. 14 in Nishikawa and Finkelmann 1999). This turbidity is the result of textured deformations that are formed as a response on a macroscopically homogenous strain (Biggins 2009; Kundler and Finkelmann 1995, 1998).

This behavior can be explained as follows. When the LCE is stretched and the nematic director rotates, the energy of the deformation is much reduced if the elastomer also shears. The sample is split into stripes that alternate between equal and opposite director rotation and shear (Verwey et al. 1996; Finkelmann et al. 1997; Biggins 2009). This scenario is especially true for smectic LCEs, that

are layered, and there is a large energy penalty associated with causing the director to deviate from the smectic layer normal, or changing the inter-layer spacing (Adams and Warner 2005). The uniform director rotation *vs* patterned stripes scenario, when the LCE is stretched perpendicularly to the director, may also depend on the details of sample preparation (Zhang et al. 2006).

To model these experimental effects, we simulated a creep experiment, and compared the output depending on the sample phase and whether or not it is crosslinked. The results for the mechanical properties in terms of the evolution of the strain parallel (ϵ_{\parallel}) and perpendicular (ϵ_{\perp}) to the load axis during a creep are collected in Fig. 4.11. In the case of the isotropic phase, the LCP melt behaves in a purely viscous manner: ϵ_{\parallel} increases sharply until the sample fractures (indicated by “ \times ” symbols), see curves marked as “LCP melt” in Fig. 4.11a. On the contrary, the isotropic phase of the LCE (prepared by heating up and equilibrating the smectic at $T = 510\text{K}$) demonstrates a viscoelastic behavior. In particular, the sample has a viscous regime for $t < t^* \sim 20\text{ns}$, whereas for $t > t^*$ it displays elasticity, in which case ϵ_{\parallel} saturates. In the latter regime, the sample withstands a load of at least 37atm, see the same plot, curves marked as “LCE”. The changes in the structure of the sample under load will be considered below.

The creep of the smectic LCP melt leads to very similar results when the load is applied along or perpendicular to the nematic director. The former case is shown in Fig. 4.11b. Contrary to the case of the isotropic LCP melt, a plateau in ϵ_{\parallel} exists at the start of the creep, where the sample keeps its shape, but accumulates small structural changes. The latter then lead to the disintegration of the sample, very similar to the case of the isotropic LCP melt (Fig. 4.11a, curves marked as “LCP melt”). The smectic LCP melt, therefore, behaves as a “soft solid”.

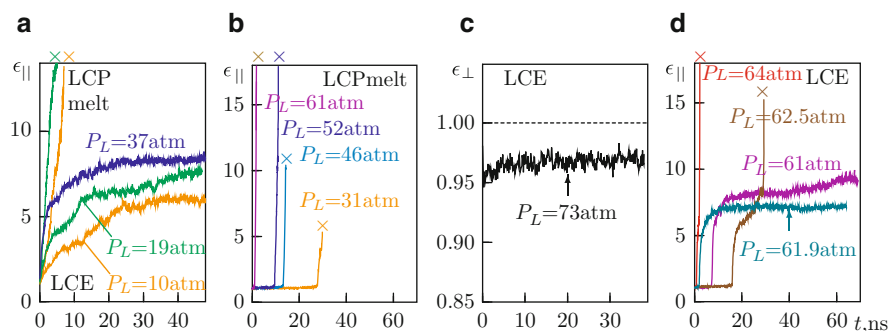


Fig. 4.11 Evolution of a uniaxial strain parallel (ϵ_{\parallel}) or perpendicular (ϵ_{\perp}) to the load axis during the simulation of a creep experiment of LCP and LCE in different phases. Amount of applied load P_L is shown in each case; *cross-symbols* indicate fracturing of the sample. (a) Isotropic phase, both cases of LCP melt and LCE are combined and marked in one plot. (b) Smectic phase, LCP melt, load axis is collinear with nematic director. (c) Smectic phase, LCE, load axis is perpendicular to nematic director; ϵ_{\perp} (which is collinear with the director) is shown. (d) Smectic phase, LCE, load axis is collinear with nematic director. Adapted from Ilynyskiy et al. (2012) with permission from The Royal Society of Chemistry

The behavior of the smectic LCE under creep is essentially anisotropic and closely follows that of real systems, discussed above. First we simulated a creep experiment with a load $P_L = 73\text{atm}$ applied perpendicular to the nematic director (e.g. along the Y axis). The load axis in this case is located within the 2D layers of the crosslinked polymer, as seen in Fig. 4.10. The network is found to stretch along the axis of load by 230 %, but displays remarkably little deformation along the axis of the nematic director, as monitored by the behavior of ε_{\perp} in that direction, see Fig. 4.11c. The case when the load is applied parallel to the director is shown in Fig. 4.11d. Here we have observed several regimes exhibited in the previous cases. Namely, at moderate load $P_L \leq 62\text{atm}$ there are: (i) an initial “solid-like” regime with constant strain, where the smectic phase withstands the load; (ii) a transition-like shape transformation, when the deformation along the load, ε_{\parallel} , rapidly increases; and (iii) a plateau-like region, where the sample is kept by elastic forces. At higher load, $P_L > 62\text{atm}$, the sample behavior is dominated by the fourth regime, (iv) disintegration.

To clarify the origin of the transition-like shape transformation denoted as (ii) above, we focus on properties that characterize the microscopic state of the backbones and mesogens. The level of backbone stretch along the axis of the load is characterized by the ratio R_{\parallel}/R_{\perp} between the two components of the radius of gyration, respectively along and perpendicular to the load. The anisotropy of orientational order of mesogens with respect to the load axis is characterized by the respective order parameters S_{\parallel} and S_{\perp} . Due to rapid disintegration of both isotropic and smectic LCP melts, we limit our study to the LCE case only.

The results for the isotropic LCE are shown in Fig. 4.12a. One can observe that in the viscous regime $t < t^*$ the backbone anisotropy increases sharply. At the end

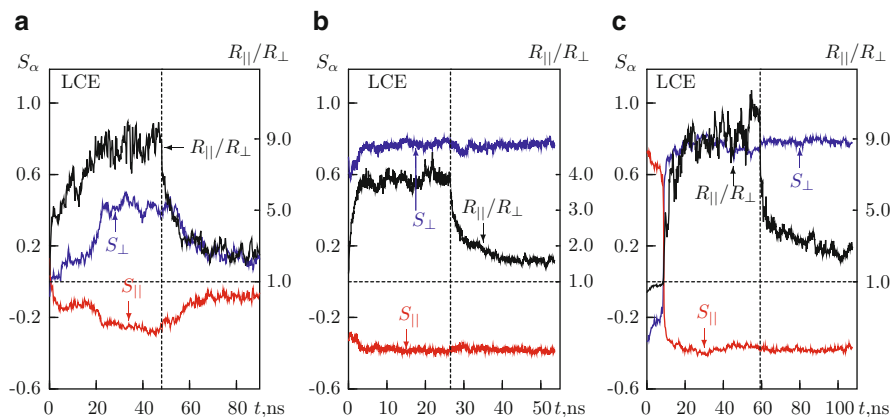


Fig. 4.12 Gyration radius anisotropy R_{\parallel}/R_{\perp} for the backbones, and orientational order parameters S_{\parallel} and S_{\perp} for the mesogens, with respect to the direction of uniaxial load. (a) Isotropic phase. (b) Smectic phase, load axis is perpendicular to the nematic director. (c) Smectic phase, load axis is parallel to the nematic director. Adapted from Ilynyskiy et al. (2012) with permission from The Royal Society of Chemistry

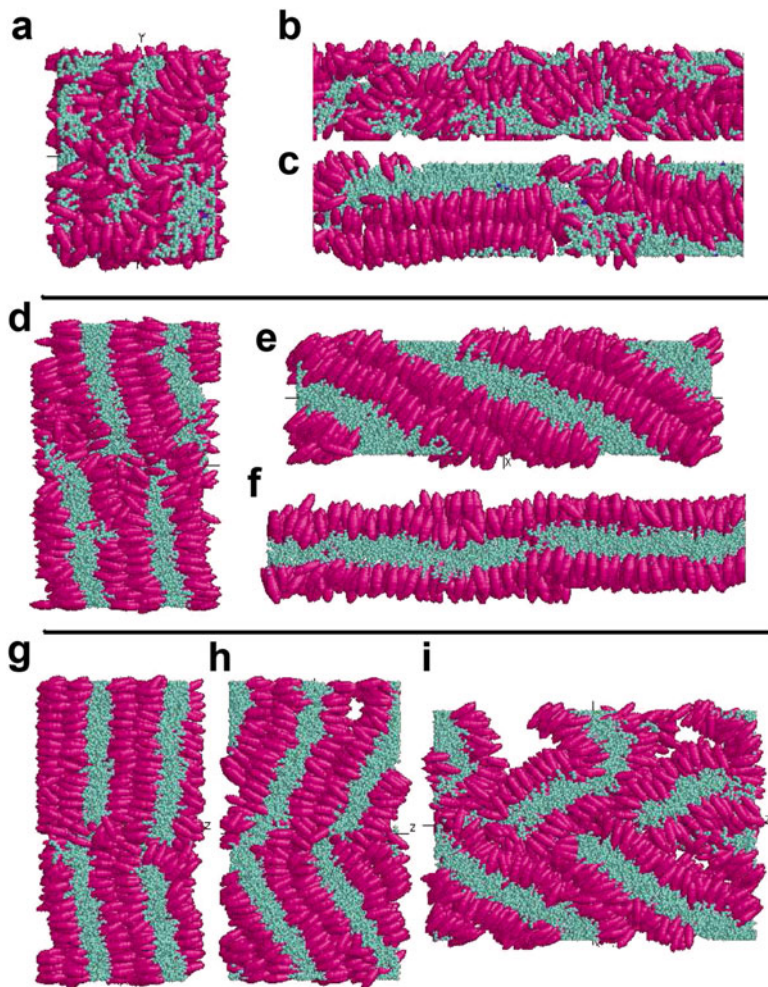


Fig. 4.13 Snapshots illustrating the structural changes of the LCE upon application of an external uniaxial load. (a, b, c) Isotropic phase at $T = 510\text{K}$ being under load of $P_L = 37\text{atm}$ for 0, 16 ns and 48 ns, respectively. (d, e, f) Sample 1 of smectic phase at $T = 480\text{K}$ being under load of $P_L = 73\text{ atm}$ for 0, 8.8 ns and 31.8 ns, respectively. (g, h, i) Sample 2 of smectic phase at the same temperature and load as the previous one, being under load for 0, 1.6 ns and 1.88 ns, respectively. Adapted from Ilnytskyi et al. (2012) with permission from The Royal Society of Chemistry

of this regime the mesogens follow the spatial redistribution of the backbones indicated by the increase of their order parameter S_{\perp} . The formation of this stress-induced ordered phase is displayed in Fig. 4.13, frames a–c. One can deduce that, for the negative coupling between the two subsystems to work, and for the ordered phase to form, considerable backbone anisotropy of at least 5–6 is required. On release of the stress, the backbones ordering moves back towards the pre-deformational initial state, but a residual backbone anisotropy of about 2.5–3,

and residual order of $S_y = 0.15$, are still preserved 40 ns after the load was released, see Fig. 4.12a.

For the case of the smectic LCE, as follows from the discussion of the experimental results above, the existing LC order can be changed or remain intact when a uniaxial load is applied. The result depends on the choice of the load axis. On a par with the experimental findings, we found that when the load is applied perpendicular to the director in our model SCLCE, it has no effect on the mesogen order. This is clearly seen in Fig. 4.12b. While the R_{\parallel}/R_{\perp} ratio changes, essentially following the load, only negligible changes are observed for the order parameters S_{\parallel} and S_{\perp} . The polymer and mesogen subsystems appear to be completely decoupled. The survival of smectic layers is evidenced also by virtually no change of ε_{\perp} in Fig. 4.11c; this reproduces experimental findings on the unchanged transparency of a smectic film under load, in similar conditions (Nishikawa et al. 1997).

However, the situation is the opposite when the load is applied parallel to the nematic director. We will focus on the effect the load has for two characteristic smectic LCE samples that differ in their preparation history. Namely, in the case of *sample I*, a freshly made network is crosslinked at 450 K, then equilibrated at this temperature for 27.2 ns, and finally heated up to 480 K for another 23.3 ns. In the case of *sample II*, the same fresh network was first heated to 500 K for 17.6 ns and then cooled down to 480 K for another 22.9 ns. The evolution of the backbone radius of gyration ratio R_{\parallel}/R_{\perp} , as well as the mesogen order parameters S_{\parallel} and S_{\perp} along and perpendicular to the load, respectively, are shown in Fig. 4.12c. The case of *sample I* under a load of $P_{\perp} = 73\text{atm}$ is shown. All three properties, R_{\parallel}/R_{\perp} , S_{\parallel} , and S_{\perp} undergo considerable changes. During the initial stage (1–10 ns), R_{\parallel}/R_{\perp} changes gradually from an initial value of 0.4 to approximately 1, whereas S_{\parallel} decreases from 0.75 to about 0.55 and S_{\perp} increases from -0.34 to -0.1 . At $t = 10\text{ns}$, the system undergoes a sharp transformation characterized by a jump of R_{\parallel}/R_{\perp} up to 5, and a rapid exchange of values between S_{\parallel} and S_{\perp} , which indicates director reorientation. The threshold value of R_{\parallel}/R_{\perp} , at which this transformation starts, is about 1.2–1.25. In the new state, with a reoriented nematic director, R_{\parallel}/R_{\perp} increases further up to about 9–10, but with only minimal changes to S_{\parallel} and S_{\perp} . The behavior of the sample in this latter state is very similar to the one observed in Fig. 4.12b, when the load is applied perpendicular to the nematic director. This comes as no surprise, since after the director reorientation takes place at time $t \approx 10$ ns in Fig. 4.12c, the new director is perpendicular to the load axis. The director reorientation is illustrated by snapshots presented in Fig. 4.13, frames d–f. The snapshots also confirm the integrity of the sample at all stages. One can also note that at an early stage of director reorientation ($t < 8.6\text{ns}$) the load somewhat reduces the defects found in the layered structure. After releasing the load, at time $t = 60\text{ns}$ (see Fig. 4.12c), the mesogen order parameters do not change, whereas the backbone anisotropy decreases down to $R_{\parallel}/R_{\perp} \approx 2.5$. This value is exactly the reciprocal of the initial value $R_{\parallel}/R_{\perp} = 0.4$ at time $t = 0$, indicating that the reoriented smectic phase of *sample I* at the end of the simulation has the same properties as the initial one at $t = 0$ (taking into account the swap between the axes denoted as \parallel and \perp).

Let us switch now to *sample II*, which differs from *sample I* by its thermal history, as already discussed above. A load of the same strength, $P_L = 73\text{atm}$, is applied at the same temperature, $T = 480\text{K}$, with the load axis parallel to the director. As a result of the load, *sample II* develops a stripe-like director pattern (with only two stripes within a single periodic box) during the first 1.5–2 ns, but in 4 ns time the sample fractures, as shown in Fig. 4.13, frames g–i. It is interesting to note, that both *sample I* and *sample II* have a similar defect in their lamellar structure before the load is applied (see Fig. 4.13 frames d and g, respectively). However, radically different director responses are found in these samples upon application of the load in the same direction and of the same amount. *Sample I* demonstrates a gradual reorientation of the director, whereas *sample II* develops a stripe-like pattern under load. As follows from the snapshots presented in Fig. 4.13, the layer normal for *sample I* at $t = 0$ is not exactly parallel to the Z axis. Therefore, the results obtained in our simulations can be related to the experiments performed on nematic LCEs when the direction of the applied load is not exactly perpendicular to the director. In this case, gradual director reorientation is found (Kundler and Finkelmann 1995; Roberts et al. 1997). *Sample II* at $t = 0$ demonstrates two smectic regions with slightly different angles between their respective layer normals and the Z axis. The formation of a stripe-like pattern can be explained in two possible ways. The first explanation is that the layer normal averaged over the sample volume is parallel to the Z axis. Then, this case is similar to the experiments on nematic LCEs when the load is applied perpendicular to the director, and stripe formation is also observed (Küpfer and Finkelmann 1991). The second explanation could be the presence of the defect which separates the two smectic regions in the initial configuration. Upon application of the load, the directors in each region rotate independently, which results in a V-shaped or chevron-like structure. Indeed, the wedge of this pattern is developed exactly at the defect position. As follows from these simulations, both the thermal history and, possibly, the existing defects in structure, play an important role in the kind of response developed under load. Similar remarks on the role of the preparation history of the sample on its behavior under stress were made earlier, in the experimental work of Zhang et al. (2006). These results lead us to believe that the simulations are correctly embodying the essential physics, but our model system is rather small to be able to study periodic stripe formation as found experimentally (Küpfer and Finkelmann 1991; Kundler and Finkelmann 1995, 1998; Nishikawa et al. 1997; Nishikawa and Finkelmann 1999; Verwey et al. 1996; Finkelmann et al. 1997; Biggins 2009), and discussed theoretically (Adams and Warner 2005; Fried and Sellers 2006).

4.4 Conclusions

In this chapter we consider equilibrium properties and stimuli response of liquid crystal polymers with side-chain molecular architecture. The semi-atomistic molecular dynamics simulation technique is employed, where groups of atoms are

represented as spherical and non-spherical bodies. Following the experimental data, we focus on several aspects of such systems that govern their properties and the response to external perturbations. These are: (a) the level of rigidity of the polymer backbone; (b) the amount of coupling between the polymer and liquid crystal subsystems; and (c) the existence of crosslinks.

Two characteristic models are considered, termed the weakly- and strongly-coupled models, where the naming reflects the amount of coupling between the polymer backbone and pendant mesogens. The former has a flexible backbone and long spacer of six to ten monomers, and is found to exhibit isotropic and smectic-A phases, in accordance with the experimental phase diagrams for real systems of this architecture. The smectic-A phase has a lamellar, sandwich-like internal structure, with backbones jammed in planes perpendicular to the nematic director. The diffusion of all its constituents, estimated in the course of our simulations, is severely hampered along the nematic director. On the contrary, the strongly-coupled model exhibits no ordered liquid crystal phases, and we concentrated mainly on an estimate for its glass transition temperature.

When the mesogens act as chromophores (the best known example being an azobenzene group), a number of related photo-mechanical effects are observed, e.g. surface relief grating formation. To model these effects we reduce the quantum photo-isomerization of azobenzene to the level of a classical field that reorients their *trans* isomers perpendicular to the light polarization. Then, we use the experimental evidence that free-floating droplets of the polymer P6a12 (flexible backbone, long spacer) contract along the polarization vector, whereas droplets of E1aP (backbone containing aromatic rings, short spacer) extend in this direction. Similar results are obtained in the experiments with an optical mask. The molecular details of P6a12 and E1aP map well onto the weakly- and strongly-coupled models, respectively. We found that for both models the photo-induced reorientation of chromophores is followed by repacking of the polymer backbones. However, in the case of the weakly-coupled model, the dominant effect is the photo-induced smectic–isotropic phase transition, which leads to the contraction of the volume element along the light polarization. For the case of the strongly-coupled model, the reorientation of stiff backbones is a dominant effect leading to the expansion of the volume element along the light polarization. The latter is irreversible only when the polymer is at or below the glass transition temperature, correlating well with the experimental results on recording of the surface gratings.

With crosslinking of the melt, a new set of memory effects emerge, related to the elasticity of the polymer network. To improve mapping of the properties of our relatively small model system onto those of a macro-sample, we use a controllable crosslinking algorithm applied in the smectic-A phase. The weakly crosslinked smectic elastomer is characterized by an increase of its smectic–isotropic transition temperature of about 5° , as compared to its non-crosslinked counterpart; the shift is of the order of typical experimental values. The sample reproduces memory effects in its liquid-crystalline order and shape, when driven through the smectic–isotropic transition; the effect does not exist for a non-crosslinked system. When the elastomer is heated above the smectic–isotropic transition temperature and stretched, a

stress-induced smectic phase is observed. We also reproduce the experimentally observed anisotropy in the response of the smectic elastomer to a uniaxial load. In particular, smectic order is preserved when the system is stretched perpendicularly to the nematic director, even for a strain of about 200 %. On the contrary, when the load is applied parallel to the nematic director, one observes director reorientation or V-shaped stripes. To clarify the role of molecular architecture in the response of the smectic elastomer more precisely, significantly larger system sizes are required.

The results presented in this Chapter make some progress on the way of a more general agenda: simulation-based prediction of the macro-properties of polymer liquid crystals depending on the details of their molecular architecture. So far, the main achievement is in reproducing the existing experimental results and suggesting and verifying underlying microscopic mechanisms. More precise material–model bridging is required to be able to predict some new features or reproduce the existing effects on a more exact quantitative level. This program requires the use of precisely-tuned parametrized interaction potentials, as well as the use of large-scale system sizes.

Acknowledgements The authors acknowledge financial support under DFG Grant GR 3725/2-2. J.I. and M.S. thank V. Toshchevikov for stimulating discussions.

References

- Adams J, Warner M (2005) Elasticity of smectic-A elastomers. *Phys Rev E* 71(2):021708
- Aharony A, Harris A (1996) Absence of self-averaging and universal fluctuations in random systems near critical points. *Phys Rev Lett* 77(18):3700–3703
- Ahn S, Deshmukh P, Gopinadhan M, Osuji CO, Kasi RM (2011) Side-chain liquid crystalline polymer networks: exploiting nanoscale smectic polymorphism to design shape-memory polymers. *ACS Nano* 5(4):3085–3095
- Allen MP, Tildesley DJ (1989) *Computer simulation of liquids*. Oxford University Press, Oxford
- Assfalg N, Finkelmann H (1989) A composite of a nematic and an isotropic elastomer \pm a rubber analogous to a “bimetal”. *Kaut Gummi Kunstst* 52(10):677–678
- Baldus O, Zilker S (2001) Surface relief gratings in photoaddressable polymers generated by cw holography. *Appl Phys B Lasers Opt* 72(4):425–427
- Barillé R, Tajalli P, Kucharski S, Ortyl E, Nunzi JM (2010) Photoinduced deformation of azopolymer nanometric spheres. *Appl Phys Lett* 96(16):163104
- Barrett CJ, Rochon PL, Natansohn AL (1998) Model of laser-driven mass transport in thin films of dye-functionalized polymers. *J Chem Phys* 109(4):1505
- Barrett CJ, Mamiya J, Yager KG, Ikeda T (2007) Photo-mechanical effects in azobenzene-containing soft materials. *Soft Matter* 3(10):1249
- Behl M, Lendlein A (2007) Shape-memory polymers. *Mater Today* 10(4):20–28
- Berg RH, Hvilsted S, Ramanujam PS (1996) Peptide oligomers for holographic data storage. *Nature* 383(6600):505–508
- Biggins JS (2009) Textured deformations in liquid crystal elastomers. *Liq Cryst* 36(10–11):1139–1156
- Binder K (1986) Spin glasses: experimental facts, theoretical concepts, and open questions. *Rev Mod Phys* 58(4):801–976

- Bladon P, Terentjev E, Warner M (1993) Transitions and instabilities in liquid crystal elastomers. *Phys Rev E* 47(6):R3838–R3840
- Bladon P, Warner M, Terentjev EM (1994) Orientational order in strained nematic networks. *Macromolecules* 27(24):7067–7075
- Bublitz D, Helgert M, Fleck B, Wenke L, Hvilsted S, Ramanujam P (2000) Photoinduced deformation of azobenzene polyester films. *Appl Phys B Lasers Opt* 70(6):863–865
- Bublitz D, Fleck B, Wenke L (2001) A model for surface-relief formation in azobenzene polymers. *Appl Phys B Lasers Opt* 72(8):931–936
- Camacho-Lopez M, Finkelmann H, Palfy-Muhoray P, Shelley M (2004) Fast liquid-crystal elastomer swims into the dark. *Nat Mater* 3(5):307–310
- Chung TS (ed) (2008) Thermotropic liquid crystalline polymers. Technomic, Lancaster
- Cladis PE (2001) Phase transitions in liquid crystalline elastomers. A fundamental aspect of lces as artificial muscles. In: Ehrhard P, Riley D (eds) *Proceedings of Euromech colloquium 408*. Kluwer Academic, Dordrecht, pp 429–483
- Cleaver D, Care C, Allen M, Neal M (1996) Extension and generalization of the Gay-Berne potential. *Phys Rev E* 54(1):559–567
- Collings PJ, Hird M (2001) *Introduction to liquid crystals*. Taylor and Francis, London
- Davis FJ, Mitchell GR (1996) Liquid crystal elastomers: controlled crosslinking in the liquid crystal phase. *Polymer* 37(8):1345–1351
- Degert C, Davidson P, Megtert S, Petermann D, Mauzac M (1992) X-ray diffraction by liquid-crystalline elastomers. *Liq Cryst* 12(5):779–798
- Dimitrova A (2000) Investigation of the main chain orientation in side-chain liquid crystalline polymers by natural abundance ^{13}C NMR. Ph.D. thesis, University of Halle
- Doi M, Edwards SF (1994) *The theory of polymer dynamics*. Clarendon Press, Oxford
- Finkelmann H, Kock HJ, Rehage G (1981) Investigations on liquid crystalline polysiloxanes 3. Liquid crystalline elastomers – a new type of liquid crystalline material. *Makromol Chem Rapid Commun* 2(4):317–322
- Finkelmann H, Kock HJ, Gleim W, Rehage G (1984) Investigations on liquid crystalline polysiloxanes, 5. Orientation of LC-elastomers by mechanical forces. *Makromol Chem Rapid Commun* 5(5):287–293
- Finkelmann H, Kundler I, Terentjev EM, Warner M (1997) Critical stripe-domain instability of nematic elastomers. *J Phys II* 7(8):1059–1069
- Freiberg S, Lagagné-Labarhet F, Rochon P, Natansohn A (2003) Synthesis and characterization of a series of azobenzene-containing side-chain liquid crystalline polymers. *Macromolecules* 36(8):2680–2688
- Fried E, Sellers S (2006) Soft elasticity is not necessary for striping in nematic elastomers. *J Appl Phys* 100(4):043521
- Gaididei Y, Christiansen P, Ramanujam P (2002) Theory of photoinduced deformation of molecular films. *Appl Phys B Lasers Opt* 74(2):139–146
- Gallani J, Hilliou L, Martinoty P, Keller P (1994) Abnormal viscoelastic behavior of side-chain liquid-crystal polymers. *Phys Rev Lett* 72(13):2109–2112
- Gay JG, Berne BJ (1981) Modification of the overlap potential to mimic a linear site-site potential. *J Chem Phys* 74(6):3316
- Han J, Gee RH, Boyd RH (1994) Glass transition temperatures of polymers from molecular dynamics simulations. *Macromolecules* 27(26):7781–7784
- Hill R (1984) On macroscopic effects of heterogeneity in elastoplastic media at finite strain. *Math Proc Camb* 95(03):481
- Hill R (1985) On the micro-to-macro transition in constitutive analyses of elastoplastic response at finite strain. *Math Proc Camb* 98(03):579
- Hirschmann H, Roberts P, Davis F, Guo W, Hasson C, Mitchell G (2001) Liquid crystalline elastomers: the relationship between macroscopic behaviour and the level of backbone anisotropy. *Polymer* 42(16):7063–7071

- Holme NCR, Nikolova L, Hvilsted S, Rasmussen PH, Berg RH, Ramanujam PS (1999) Optically induced surface relief phenomena in azobenzene polymers. *Appl Phys Lett* 74(4):519
- Hvilsted S, Ramanujam PS (2001) The azobenzene optical storage puzzle – demands on the polymer scaffold? *Monatsh Chem* 132(1):43–51
- Ichimura K (2000) Photoalignment of liquid-crystal systems. *Chem Rev* 100(5):1847–1874
- Ikeda T (2003) Photomodulation of liquid crystal orientations for photonic applications. *J Mater Chem* 13(9):2037–2057
- Ikeda T, Horiuchi S, Karanjit DB, Kurihara S, Tazuke S (1990) Photochemically induced isothermal phase transition in polymer liquid crystals with mesogenic phenyl benzoate side chains. 2. Photochemically induced isothermal phase transition behaviors. *Macromolecules* 23(1):42–48
- Ikeda T, Yoneyama S, Yamamoto T, Hasegawa M (2002) Refractive-index modulation by means of photosensitive liquid crystals. *Mol Cryst Liq Cryst* 375:45–60
- Ikeda T, Mamiya J, Yu Y (2007) Photomechanics of liquid-crystalline elastomers and other polymers. *Angew Chem Int Ed* 46(4):506–528
- Ilnytskyi J, Wilson MR (2001) A domain decomposition molecular dynamics program for the simulation of flexible molecules with an arbitrary topology of Lennard-Jones and/or Gay-Berne sites. *Comput Phys Commun* 134(1):23–32
- Ilnytskyi J, Saphiannikova M, Neher D (2006) Photo-induced deformations in azobenzene-containing side-chain polymers: molecular dynamics study. *Condens Matter Phys* 9(1):87–94
- Ilnytskyi JM, Neher D (2007) Structure and internal dynamics of a side chain liquid crystalline polymer in various phases by molecular dynamics simulations: a step towards coarse graining. *J Chem Phys* 126(17):174905
- Ilnytskyi JM, Wilson MR (2002) A domain decomposition molecular dynamics program for the simulation of flexible molecules of spherically-symmetrical and nonspherical sites. II. Extension to NVT and NPT ensembles. *Comput Phys Commun* 148(1):43–58
- Ilnytskyi JM, Neher D, Saphiannikova M (2011) Opposite photo-induced deformations in azobenzene-containing polymers with different molecular architecture: molecular dynamics study. *J Chem Phys* 135(4):044901
- Ilnytskyi JM, Saphiannikova M, Neher D, Allen MP (2012) Modelling elasticity and memory effects in liquid crystalline elastomers by molecular dynamics simulations. *Soft Matter* 8(43):11123–11134
- Kandjani SA, Barille R, Dabos-Seignon S, Nunzi JM, Ortyl E, Kucharski S (2005) Incoherent light-induced self-organization of molecules. *Opt Lett* 30(23):3177
- Keller P, Carvalho B, Cotton JP, Lambert M, Moussa F, Pépy G (1985) Side chain mesomorphic polymers: studies of labelled backbones by neutron scattering. *J Phys Lett (Paris)* 46(22):1065–1071
- Kim DY, Tripathy SK, Li L, Kumar J (1995) Laser-induced holographic surface relief gratings on nonlinear optical polymer films. *Appl Phys Lett* 66(10):1166
- Kirste RG, Ohm HG (1985) The conformation of liquid-crystalline polymers as revealed by neutron scattering. *Makromol Chem Rapid Commun* 6(3):179–185
- Kumar J, Li L, Jiang XL, Kim D, Lee TS, Tripathy S (1998) Gradient force: The mechanism for surface relief grating formation in azobenzene functionalized polymers. *Appl Phys Lett* 72(17):2096
- Kundler I, Finkelmann H (1995) Strain-induced director reorientation in nematic liquid single crystal elastomers. *Makromol Rapid Commun* 16(9):679–686
- Kundler I, Finkelmann H (1998) Director reorientation via stripe-domains in nematic elastomers: influence of cross-link density, anisotropy of the network and smectic clusters. *Makromol Chem Phys* 199(4):677–686
- Küpfer J, Finkelmann H (1991) Nematic liquid single crystal elastomers. *Makromol Chem Rapid Commun* 12(12):717–726
- Lefin P, Fiorini C, Nunzi JM (1998) Anisotropy of the photo-induced translation diffusion of azobenzene dyes in polymer matrices. *Pure Appl Opt* 7(1):71–82

- Legge CH, Davis FJ, Mitchell GR (1991) Memory effects in liquid crystal elastomers. *J Phys II* 1 (10):1253–1261
- Lyulin AV, Balabaev NK, Michels MAJ (2003) Molecular-weight and cooling-rate dependence of simulated T_g for amorphous polystyrene. *Macromolecules* 36(22):8574–8575
- Matouš K, Geubelle PH (2005) Multiscale modelling of particle debonding in reinforced elastomers subjected to finite deformations. *Int J Numer Meth Eng* 65(2):190–223
- McBride C, Wilson MR (1999) Molecular dynamics simulations of a flexible liquid crystal. *Mol Phys* 97(4):511–522
- Mechau N, Neher D, Börger V, Menzel H, Urayama K (2002) Optically driven diffusion and mechanical softening in azobenzene polymer layers. *Appl Phys Lett* 81(25):4715
- Mechau N, Saphiannikova M, Neher D (2005) Dielectric and mechanical properties of azobenzene polymer layers under visible and ultraviolet irradiation. *Macromolecules* 38(9):3894–3902
- Michel JC, Moulinec H, Suquet P (1999) Effective properties of composite materials with periodic microstructure: a computational approach. *Comput Method Appl Mech Eng* 172 (1–4):109–143
- Michl J, Thulstrup EW (1995) Spectroscopy with polarized light: solute alignment by photoselection, liquid crystal, polymers, and membranes. Corrected Software Edition. VCH Publishers, New York
- Mitchell G, Davis F, Guo W, Cywinski R (1991) Coupling between mesogenic units and polymer backbone in side-chain liquid crystal polymers and elastomers. *Polymer* 32(8):1347–1353
- Mitchell G, Davis F, Guo W (1993) Strain-induced transitions in liquid-crystal elastomers. *Phys Rev Lett* 71(18):2947–2950
- Mitchell GR, Davis FJ, Ashman A (1987) Structural studies of side-chain liquid crystal polymers and elastomers. *Polymer* 28(4):639–647
- Mitchell GR, Coulter M, Davis FJ, Guo W (1992) The effect of the spacer length on the nature of coupling in side chain liquid crystals polymers and elastomers. *J Phys II* 2(5):1121–1132
- Natansohn A, Rochon P (1999) Photoinduced motions in azobenzene-based amorphous polymers: possible photonic devices. *Adv Mater* 11(16):1387–1391
- Nishikawa E, Finkelmann H (1999) Smectic-A liquid single crystal elastomers - strain induced break-down of smectic layers. *Macromol Chem Phys* 200(2):312–322
- Nishikawa E, Finkelmann H, Brand HR (1997) Smectic A liquid single crystal elastomers showing macroscopic in-plane fluidity. *Macromol Rapid Commun* 18(2):65–71
- Oliveira ON, Kumar LL, Tripathy SK (2002) Surface-relief gratings on azobenzene-containing films. In: Sekkat Z, Knoll W (eds) Photoreactive organic thin films. Academic, California, pp 429–483
- Parrinello M, Rahman A (1981) Polymorphic transitions in single crystals: A new molecular dynamics method. *J Appl Phys* 52(12):7182
- Pedersen T, Johansen P, Holme N, Ramanujam P, Hvilsted S (1998) Mean-field theory of photoinduced formation of surface reliefs in side-chain azobenzene polymers. *Phys Rev Lett* 80(1):89–92
- Rasmussen PH, Ramanujam PS, Hvilsted S, Berg RH (1999) A remarkably efficient azobenzene peptide for holographic information storage. *J Am Chem Soc* 121(20):4738–4743
- Roberts PMS, Mitchell GR, Davis FJ, Pople JA (1997) Mechanical switching and soft elasticity in liquid crystal elastomers. *Mol Cryst Liq Cryst* 299(1):181–186
- Rochon P, Batalla E, Natansohn A (1995) Optically induced surface gratings on azoaromatic polymer films. *Appl Phys Lett* 66(2):136
- Rutloh M, Stumpe J, Stachanov L, Kostromin S, Shibaev V (2000) Influence of liquid crystallinity and aggregation on photo-orientation. *Mol Cryst Liq Cryst* 352(1):149–157
- Ryckaert JP, Bellemans A (1975) Molecular dynamics of liquid n-butane near its boiling point. *Chem Phys Lett* 30(1):123–125
- Sainova D, Zen A, Nothofer HG, Asawapirom U, Scherf U, Hagen R, Bieringer T, Kostromine S, Neher D (2002) Photoaddressable alignment layers for fluorescent polymers in polarized electroluminescence devices. *Adv Funct Mater* 12(1):49

- Saphiannikova M, Neher D (2005) Thermodynamic theory of light-induced material transport in amorphous azobenzene polymer films. *J Phys Chem B* 109(41):19428–19436
- Saphiannikova M, Geue TM, Henneberg O, Morawetz K, Pietsch U (2004) Linear viscoelastic analysis of formation and relaxation of azobenzene polymer gratings. *J Chem Phys* 120(8):4039
- Schätzle J, Kaufhold W, Finkelmann H (1989) Nematic elastomers: the influence of external mechanical stress on the liquid-crystalline phase behavior. *Makromolekul Chem* 190(12):3269–3284
- Shenoy DK, Thomse III DL, Srinivasan A, Keller P, Ratna BR (2002) Carbon coated liquid crystal elastomer film for artificial muscle applications. *Sensors Actuators A Phys* 96(2–3):184–188
- Spillmann CM, Naciri J, Martin BD, Farahat W, Herr H, Ratna BR (2007) Stacking nematic elastomers for artificial muscle applications. *Sensors Actuators A Phys* 133(2):500–505
- Stiller B, Geue T, Morawetz K, Saphiannikova M (2005) Optical patterning in azobenzene polymer films. *J Microsc* 219(3):109–114
- Stimson LM, Wilson MR (2005) Molecular dynamics simulations of side chain liquid crystal polymer molecules in isotropic and liquid-crystalline melts. *J Chem Phys* 123(3):034908
- Stracke A, Wendorff JH, Goldmann D, Janietz D, Stiller B (2000) Gain effects in optical storage: thermal induction of a surface relief grating in a smectic liquid crystal. *Adv Mater* 12(4):282–285
- Symons AJ, Davis FJ, Mitchell GR (1993) Liquid crystal elastomers interaction between the network and smectic ordering. *Liq Cryst* 14(3):853–860
- Symons AJ, Davis FJ, Mitchell GR (1999) Side-chain liquid crystalline elastomers: the relationship between the orientational ordering of the polymer backbone and the length of the coupling chain. *Polymer* 40(19):5365–5370
- Tajbakhsh A, Terentjev E (2001) Spontaneous thermal expansion of nematic elastomers. *Eur Phys J E* 6(2):181–188
- Toshchevikov V, Saphiannikova M (2014) Theory of light-induced deformation of azobenzene elastomers: effects of the liquid-crystalline interactions and biaxiality. *J Phys Chem B* 118(42):12297–12309. doi10.1021/jp5063226. <http://dx.doi.org/10.1021/jp5063226>
- Toshchevikov V, Saphiannikova M, Heinrich G (2009) Microscopic theory of light-induced deformation in amorphous side-chain azobenzene polymers. *J Phys Chem B* 113(15):5032–5045
- Toshchevikov VP, Grenzer MS, Heinrich G (2012) Effects of the liquid-crystalline order on the light-induced deformation of azobenzene elastomers. In: Zamboni R, Kajzar F, Szep AA (eds) *Optical materials and biomaterials in security and defence systems technology IX, SPIE*
- Veer PU, Pietsch U, Rochon PL, Saphiannikova M (2008) Temperature dependent analysis of grating formation on azobenzene polymer films. *Mol Cryst Liq Cryst* 486(1):66/[1108]–78/[1120]
- Veer PU, Pietsch U, Saphiannikova M (2009) Time and temperature dependence of surface relief grating formation in polymers containing azobenzene groups with different dipole moment. *J Appl Phys* 106(1):014909
- Verwey GC, Warner M, Terentjev EM (1996) Elastic instability and stripe domains in liquid crystalline elastomers. *J Phys II* 6(9):1273–1290
- Viswanathan NK, Kim DY, Bian S, Williams J, Liu W, Li L, Samuelson L, Kumar J, Tripathy SK (1999) Surface relief structures on azo polymer films. *J Mater Chem* 9(9):1941–1955
- Vlugt TJH, Krishna R, Smit B (1999) Molecular simulations of adsorption isotherms for linear and branched alkanes and their mixtures in silicalite. *J Phys Chem B* 103(7):1102–1118
- Warner M, Terentjev E (1996) Nematic elastomers – a new state of matter? *Prog Polym Sci* 21(5):853–891
- Warner M, Terentjev E (2003) Thermal and photo-actuation in nematic elastomers. *Macromol Symp* 200(1):81–92
- Warner M, Gelling KP, Vilgis TA (1988) Theory of nematic networks. *J Chem Phys* 88(6):4008–4013

- Weilepp J, Brand HR (1996) Director reorientation in nematic-liquid-single-crystal elastomers by external mechanical stress. *Europhys Lett* 34(7):495–500
- Wilson MR (1997) Molecular dynamics simulations of flexible liquid crystal molecules using a Gay-Berne/Lennard-Jones model. *J Chem Phys* 107(20):8654
- Wilson MR, Ilnytskyi JM, Stimson LM (2003) Computer simulations of a liquid crystalline dendrimer in liquid crystalline solvents. *J Chem Phys* 119(6):3509
- Wilson MR, Stimson LM, Ilnytskyi JM, Hughes ZE (2005) Computer simulations of liquid crystal polymers and dendrimers. In: Pasini P, Zannoni C, Žumer S (eds) *NATO science series II: mathematics, physics and chemistry*. Springer, New York, pp 57–81
- Wiseman S, Domany E (1998) Self-averaging, distribution of pseudocritical temperatures, and finite size scaling in critical disordered systems. *Phys Rev E* 58(3):2938–2951
- Zen A, Neher D, Bauer C, Asawapirom U, Scherf U, Hagen R, Kostromine S, Mahr RF (2002) Polarization-sensitive photoconductivity in aligned polyfluorene layers. *Appl Phys Lett* 80(25):4699
- Zhang F, Heiney P, Srinivasan A, Naciri J, Ratna B (2006) Structure of nematic liquid crystalline elastomers under uniaxial deformation. *Phys Rev E* 73(2)
- Zilker SJ, Bieringer T, Haarer D, Stein RS, van Egmond JW, Kostromine SG (1998) Holographic data storage in amorphous polymers. *Adv Mater* 10(11):855–859

Chapter 5

Side-Chain Liquid Crystalline Polymers: Controlled Synthesis and Hierarchical Structure Characterization

Shi Pan, Bin Mu, Bin Wu, Zehua Shi, and Dongzhong Chen

5.1 General Introduction

Liquid crystalline polymers (LCPs) represent a kind of advanced organic functional materials combining both anisotropic order of liquid crystal and excellent mechanical properties of polymer. Study on LCPs has been a flourishing research field due to their broad promising applications in various high-technology areas such as various organic optoelectronic applications, non-linear optical materials, tunable diffraction gratings, thermal insulated materials, and the high performance Kevlar fiber. It's convenient to divide LCPs into several general categories based on their architecture and position of mesogens in the polymer chain. Generally speaking, mesogens can be introduced as building blocks in main chain, as side groups or acting as cross linkers, to form main-chain LCPs, side-chain LCPs or LCP networks/elastomers respectively, as shown in Fig. 5.1. Side-chain LCPs have developed steadily ever since the innovative “spacer decoupling principle” suggested by Finkelmann et al. (1978a, b).

Certainly, some further detailed classification can be subdivided. For side-chain LCPs, end-on and side-on types are called according to their linking site of mesogenic units to the polymer backbone, longitudinally at the end or laterally in the middle of mesogens. Moreover, if very short spacers were adopted or no spacers for side-on type attachment, a dense “jacket” would surround the partially extended polymer backbone (Wang and Zhou 2004). Such type of LCPs was pioneered by Zhou et al. and given the name of “mesogen-jacketed liquid crystalline polymer (MJLCP)” (Chen et al. 2010; Zhou et al. 1987). Note that the subdivision of end-on and side-on types is based on calamitic or bent-core mesogen units, while as for

S. Pan • B. Mu • B. Wu • Z. Shi • D. Chen (✉)

Department of Polymer Science and Engineering, School of Chemistry and Chemical Engineering, Key Laboratory of High Performance Polymer Materials and Technology of Ministry of Education, Nanjing University, 22 Hankou Road, Nanjing 210093, China
e-mail: cdz@nju.edu.cn

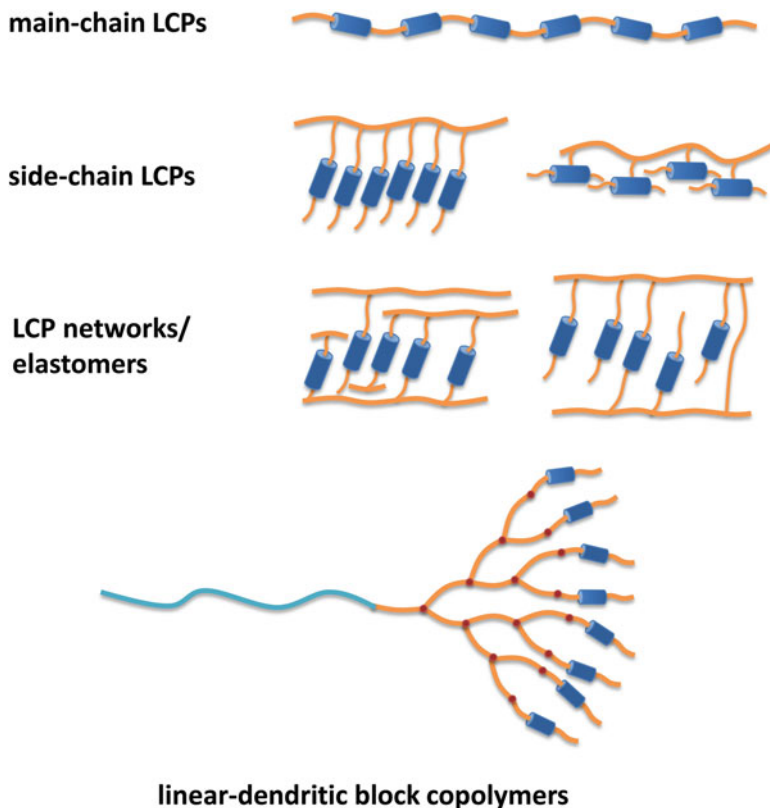


Fig. 5.1 Some liquid crystalline polymer (LCP) categories based on calamitic mesogens: main-chain LCPs, side-chain LCPs, LCP networks/elastomers and linear-dendritic block copolymers (LDBC) with side-chain type dendritic segments

discotic LCPs, usually there is no such classification considering the geometry of disc-like mesogenic units, except for some extremely special occasions (Zhu et al. 2012, 2014).

These categories may also overlap on some occasions. For instance, liquid crystal elastomers (LCEs) combine anisotropic characteristics of LC phases and elasticity of polymer networks (Ikeda et al. 2007). The key character of chemistry structure for LCEs is their lightly cross-linked network system, which implies that they also possess some common features of LCPs. Also, the combined main-chain/side-chain liquid crystalline polymers have been studied in depth (Demus et al. 1998; Ge et al. 1997; Zhou and Han 2005), showing some interesting LC properties for their comprehensive nature comprising main-chain and side-chain LCPs.

On the other hand, LCPs can also be classified by their mesogenic orders. Nematic, smectic and cholesteric LCPs can be categorized in this way, according to specific orientation and positional order. In this Chapter, we shall mainly employ

the classification based on type and location of mesogens rather than mesogenic orders.

Main-chain LCPs are usually obtained via stepwise polymerization. The mesogenic units in polymer backbone exhibit a strong tendency of orientation along the chain axis. Nowadays, many industrialized main-chain LCPs have been developed for high-performance materials with wide applications. The wholly aromatic polyamides, prepared by elaborate linear condensation polymerization, are representative main-chain LCPs showing lyotropic liquid crystalline order. Among them, poly-paraphenylene diamine terephthalamide is probably the most famous synthetic fiber, commonly known as “Kevlar”. The wholly aromatic polyesters are another kind of typical thermotropic main-chain LCPs widely used as high performance polymer materials. Considering the general theme of this Chapter, main-chain LCPs will not be covered in the following content.

The controlled synthesis and hierarchical structure investigations of side-chain LCPs constitute the primary topics in this Chapter. The introduction of dendritic segments is a fantastic idea in molecular designing of LCPs, for their ordered supramolecular assembly capabilities can considerably enhance the functionality of LCPs and provide particular scaffolds for creation of novel LC materials (Donnio et al. 2007). Dendritic polymers fall into three categories: dendrimers/dendrons, hyperbranched polymers, dendronized polymers. Dendrimers and dendrons can be regarded as ideal branched polymers, wherein each repeat unit introduces a new AB_n multifunctional moiety (Rosen et al. 2009). So in this chapter, besides “ordinary” side-chain LCPs, side-chain liquid crystalline dendrimers especially linear–dendritic block copolymers (LDBC) will also be briefly reviewed.

Liquid crystalline (LC) dendrimers can also be classified according to the locations of mesogen units. Thus, main-chain and side-chain LC dendrimers are proposed analogously. Side-chain LC dendrimers possess an overall structure generally consists of mesogenic or pro-mesogenic units attached on the branch terminals of the flexible dendritic network (Donnio et al. 2007; Donnio and Guillon 2006), which can be further divided into end-on and side-on types based on the linking site of mesogenic units. Main-chain LC dendrimers, on the other hand, have their mesogenic units located at every level of the dendritic hierarchy (Donnio et al. 2007). Restricted by the Chapter space, systematic introduction of liquid crystalline dendrimers is not allowed here. Interested readers are suggested to read the thorough review by Rosen et al. (2009). In this Chapter, liquid crystalline LDBC (as shown in Fig. 5.1) composed of a linear polymer chain and a LC dendritic block will be concisely reviewed.

We shall not try to cover every corner of side-chain LCPs in this Chapter, and the main theme of this Chapter will be a combination of controlled synthesis, rational molecular design and hierarchical organization behaviors, mainly based on two kinds of widely used mesogenic units of calamitic azobenzene (AZO) and discotic triphenylene (TP) derivatives. Some recent progress on liquid crystalline block copolymers based on side-chain LCPs, including linear–dendritic block copolymers, will be briefly summarized. We hope that the summary and some comments put forward here will help to stimulate and promote the sustained and extensive research in side-chain LCPs and related fields.

5.2 Side-Chain LCPs Based on Calamitic and Discotic Mesogens

Side-chain LCPs usually comprise several structural motifs: the polymer backbone, the spacer (the connecting moiety) and the mesogen units (Wang and Zhou 2004). The linking or anchoring group and the number of mesogens per repeat unit (“mesogen density”) are some additional factors for the design and synthesis of side-chain LCPs (Trimmel et al. 2005).

The strong tendency to form random coil conformations of the flexible main chain (backbone) conflicts with the anisotropic ordering organization of the attached side-chain mesogenic units. Therefore in order to achieve LC phases, it seems the key point is to reconcile the contradiction between the polymer backbone and side-chain mesogens. In 1978, Finkelmann et al. (1978a, b) proposed the deeply influential “spacer decoupling principle”—flexible spacers between main chain and rigid mesogens to decouple the interference for allowing the mesogenic units to take preferable orientations and realize well organization. Since then, syntheses of side-chain LCPs have been mostly complying with this classical principle, and variant length spacers have been employed for the formation and retaining of liquid crystalline phases in side-chain LCPs (Demus et al. 1998; Wang and Zhou 2004). In some cases, the influence of spacer type and length on LC phases is complicated. For example, Gemmell et al. (1985) reported large differences in the thermal stability of smectic phases in side-chain LCPs with an even or odd number of methylene groups. Recently, Wang and Wang (2010) carried out a detailed theoretical study on the spacer conformation of side-chain LCPs. Generally, as the flexibility of polymer backbone increases, the glass transition temperature usually decreases, while the corresponding isotropization temperature increases (Demus et al. 1998). However, Shibaev et al (1982) reported that in some specific cases with polyacrylate and polymethacrylate main chain, when flexible spacers were introduced between the main chain and the mesogens, their mesophases and transition temperatures were almost unchanged.

Different shape mesogens as shown in Fig. 5.2 are employed in side-chain LCPs. Among them, the most commonly used types in the construction of side-chain LCPs are the calamitic and discotic mesogens, which are also the types of mesogens primarily employed in our laboratory such as azobenzene and triphenylene derivatives. Therefore in this Chapter, we shall concentrate on side-chain LCPs bearing these two types of mesogens. For LCPs built with other kinds of side-chain mesogens such as sanidic (boardlike) and bent-core (banana-shaped), interested readers can refer to some critical review publications such as by Reddy and Tschierske (2006) and Voigt-Martin et al. (1995).

Calamitic mesogens hold the overwhelming dominance in side-chain LCPs, accordingly various molecular structures have been developed so far. Because of the simplicity, appropriate rigidity and dimensions, biphenyl derivatives are one of the most commonly used calamitic mesogens. One can expect that composition and structure of mesogens will largely determine the LC properties of side-chain LCPs,

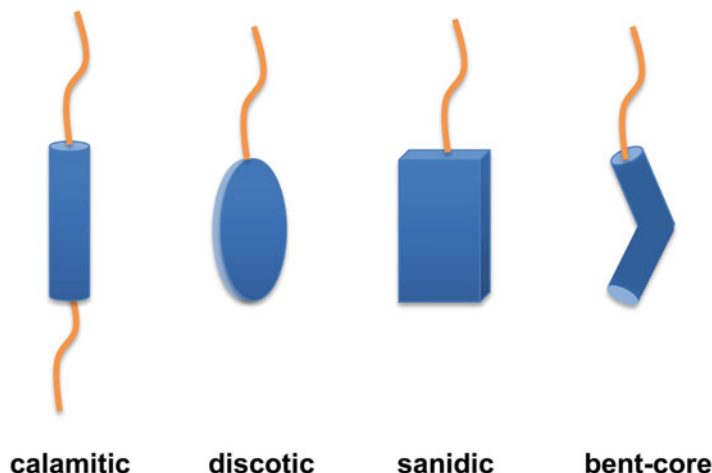


Fig. 5.2 Sketching of different shape mesogenic units used in side-chain LCs

so variant modifications have been applied to the biphenyl core such as introducing electronwithdrawing groups (Akiyama et al. 1999), prolonged mesogen skeleton (Kumar et al. 2007), chiral centers (Hsiue et al. 2001) and cholesterol groups (Scheerder et al. 2000) (Fig. 5.3a–d). Relatively simple calamitic mesogen units like (a) in Fig. 5.3 usually rendered smectic or nematic phases, and substitution on the end with longer linear alkyl or alkoxy groups favored the formation of smectic phases (Wang and Zhou 2004). The mesogens shown in Fig. 5.3b not only extended the rigid core length, but also introduced photo-crosslinkable vinyl junctions. Mesogen units modified with halogen-containing chiral centres offered side-chain LCs ferroelectric properties (c in Fig. 5.3), which usually showed a typical smectic C* phase (Beyer et al. 2007; Ikeda et al. 1993).

Research on side-chain LCs with calamitic mesogens of azobenzene derivatives has been one of the most active research fields in liquid crystals and functional polymer materials. The rigid structure with a large aspect ratio makes azobenzene a classical calamitic mesogen, which is even more attractive than above mentioned biphenyl derivatives. More importantly, the reversible photo-isomerization and light-induced orientation ability of azobenzene derivatives endow their liquid crystalline polymers with fascinating applications, such as functioning as photo-mechanical materials (Beyer et al. 2007; Ikeda et al. 1993), holographic optical storage and surface patterning (Matharu et al. 2007; Natansohn and Rochon 2002), light-controllable micelles/vesicles (Wang and Wang 2013; Zhao and Ikeda 2009), light-controllable LB films (Zou et al. 2010). In fact, azobenzenes have long been used as organic chromophores for optical switching applications as a T-type photochromic system: the photogenerated isomer thermally reverts to its initial form. These photo reactions may affect some other physicochemical properties, such as redox potential, fluorescent intensity, acid/base strength, dielectric constant, dipolar moment, and molecular shape (García-Amorós and Velasco 2012).

main chain



R=

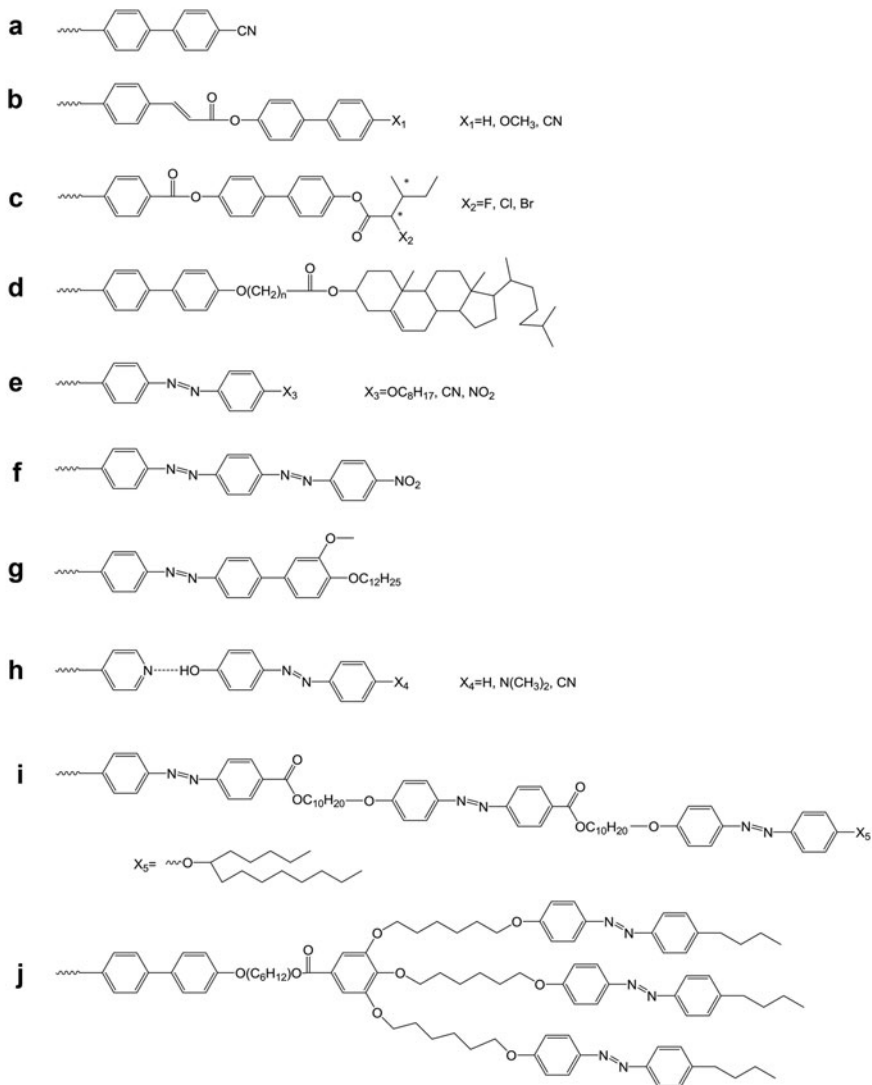


Fig. 5.3 Several typical calamitic mesogens derived from biphenyl or azobenzene rigid cores for side-chain LCs, and the details of the polymer backbone and spacers are omitted for clarity

Moreover, hardly any side reactions occurred in the photo-isomerization process of azobenzene chromophores and the timescale ranges from microseconds down to sub-nanoseconds, with 10^5 – 10^6 times reversible cycles before fatigue (Goulet Hanssens and Barrett 2013).

Generally, azobenzene derivatives fall into three basic categories: azobenzene-type molecules, aminoazobenzene-type molecules, and pseudo-stilbenes (“push-pull”). From the first type to the last one, they are characterized by the decreasing of thermal relaxation time in *cis* \rightarrow *trans* isomerization, and the absorption wavelength red shift for inducing the *trans* \rightarrow *cis* isomerization. This variation in properties offers azobenzene based LCPs significant advantages over other side-chain LCPs. For instance, π – π^* absorption of pseudo-stilbene chromophores shifts to lower energy toward the red even over the *n*– π^* absorption (Zhao and Ikeda 2009). Therefore, pseudo-stilbene-containing LCPs are more sensitive to local environment, enabling better photoinduced anisotropy, surface-relief-grating (SRG) formation, and nonlinear optical (NLO) properties (Wang et al. 2009). Yu et al. (2006a) reported a new liquid crystalline block copolymer based on pseudo-stilbene type azobenzene with a cyano group, showing much enhanced photo-orientation ability. It is fairly convenient to obtain a wide variety of azobenzene chromophore based molecular architectures with facile anchoring and modifications (Mahimwalla et al. 2012) as briefly gathered in Fig. 5.3e–j (García et al. 2012; Hosono et al. 2010; Li et al. 2010; Shi et al. 2012a, b; Sun et al. 2007; Vapaavuori et al. 2011; Yu et al. 2006a; Zhu and Wang 2013). As pioneered and recently summarized by Zhao and Ikeda (2009), azobenzene based LCPs bridged the interdisciplinary fields between polymer, liquid crystals and photochemistry.

Side-chain LCPs based on calamitic mesogens have been so far extensively studied, and various synthetic methods like free radical polymerization, ring-opening metathesis polymerization (ROMP), condensation polymerization and polymer analogous reactions were widely used in the preparation of calamitic type LCPs with variant architectures. However, side-chain LCPs based on discotic mesogen units were much less explored, due to the relatively short history of discovery and certain degree of synthetic difficulties (Kumar 2010). Nevertheless, since the first discotic side-chain LCP reported by Kreuder and Ringsdorf (1983), this field has attracted great attention owing to their capability of self-assembling into well-ordered supramolecular structures, together with various mesophases and unique optoelectronic properties. Up to now, discotic LCs have been demonstrated as promising materials in various applications such as one-dimensional conductors, photovoltaic solar cells, anisotropic photoconductors and especially as optical compensation films in practical liquid crystal display (LCD) (Kumar 2006; Laschat et al. 2007; Sergeyev et al. 2007). The most famous industrially successful case was the negative birefringence optical compensation film made from discotic nematic liquid crystals widely used for enlarging view angles in LCD invented by Fuji photo film lab (Kawata 2002).

Figure 5.4 shows several typical discotic mesogens used in discotic side-chain LCPs. Discotic liquid crystals were first discovered by Chandrasekhar et al. in 1977 (Chandrasekhar et al. 1977). They usually contain two motifs: rigid aromatic core

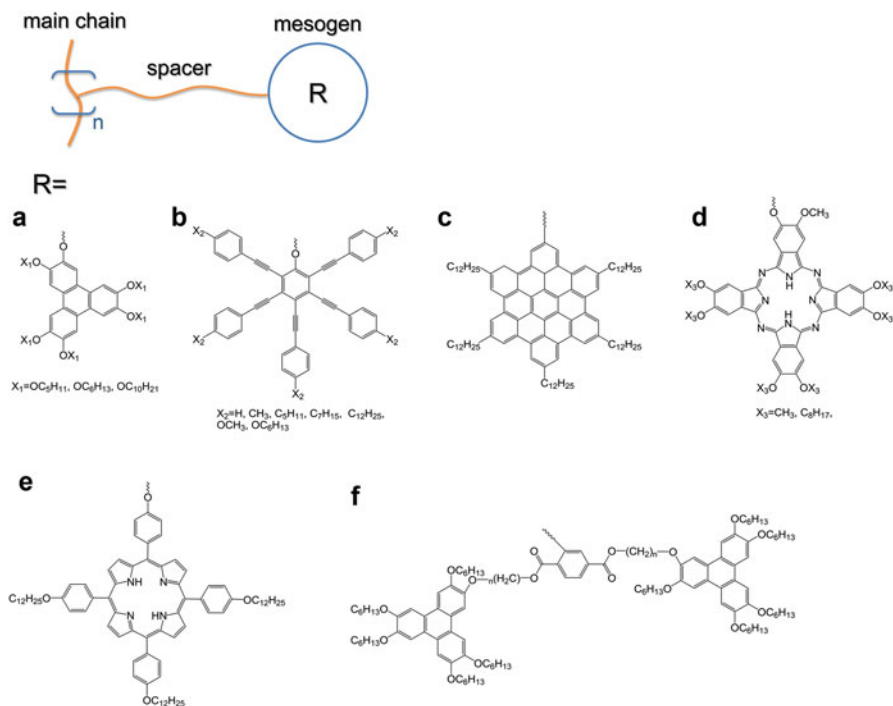


Fig. 5.4 Some typical discotic mesogen units used for side-chain LCs, and the details of the polymer backbone and spacers are omitted for clarity

with flat or nearly flat structure and several flexible peripheral side chains. Discotic mesogens generally tend to self-organize into columns via π - π stacking, van der Waals' force, and in some cases hydrogen bonding or dipole-dipole interactions (Fletcher and Luckhurst 1995). Other than columnar phases, nematic (Bisoyi and Kumar 2010) and smectic phases (Kouwer and Mehl 2009) can also be formed. Discotic cylinders will further self-assemble into variant 2D columnar mesophases (Fig. 5.5), such as hexagonal columnar phase (Col_h), rectangular columnar phase (Col_r), columnar oblique phase (Col_{ob}), columnar plastic phase (Col_p), columnar helical phase (H) and columnar lamellar phase (Col_l) (Kumar 2006). Taking triphenylene derivatives for example, in ordered columnar phases, the intercolumnar spacing usually ranges from 20 to 40 Å, and the intracolumnar distance (face to face between discs) ranges within 3.5–4.2 Å. The intracolumnar electron conductivity is much larger than intercolumnar conductivity (over 1000 times) (Boden et al. 1993). Such kind of unique columnar assembly feature makes discotic LC materials promising one-dimensional (1D) conductive organic semiconductors.

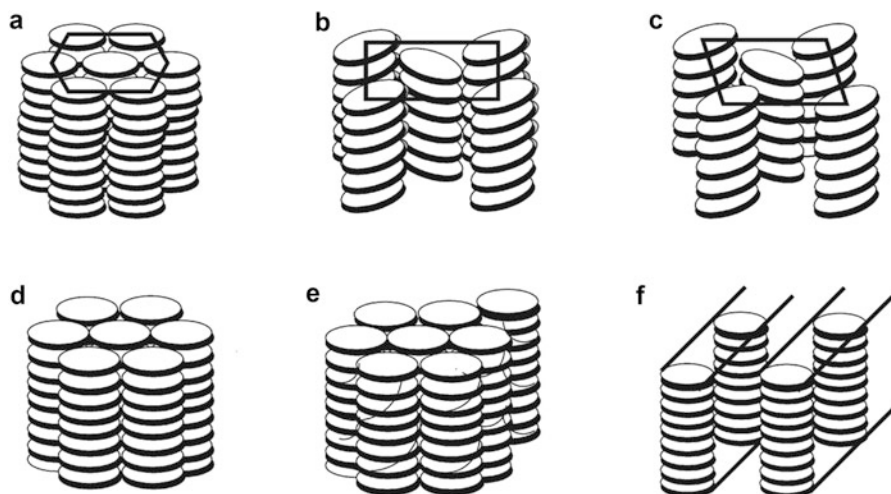


Fig. 5.5 Structures of various columnar phase of discotic mesogens. (a) Hexagonal columnar phase (Col_h); (b) rectangular columnar phase (Col_r); (c) columnar oblique phase (Col_{ob}); (d) columnar plastic phase (Col_p); (e) columnar helical phase (H); (f) columnar lamellar phase (Col_L). Reproduced from {Kumar 2006} with permission of The Royal Society of Chemistry

Many discotic mesogens have been introduced in side-chain LCPs, such as triphenylene (Kreuder and Ringsdorf 1983; Wu et al. 2013) (Fig. 5.4a), alkynylbenzene (Kouwer et al. 2002a, b, 2001, 2003) (Fig. 5.4b), hexabenzocoronene (Thünemann et al. 1999, 2003) (Fig. 5.4c), phthalocyanine (Ganicz et al. 2012; Van der Pol et al. 1989) (Fig. 5.4d) and porphyrin derivatives (de Witte et al. 2003) (Fig. 5.4e). Overall, triphenylene (TP) derivatives are the most widely used discotic mesogens for their relatively easy availability, quite strong self-assembly ability and high performance (Pal et al. 2013). TP core is a kind of rigid planar structure with an 18π aromatic delocalizing electrons, and TP was first proposed as a discotic mesogen by Billard et al. (1978). Most research efforts in TP-based discotic LC materials aim at higher carrier mobility for optoelectronic applications. For instance, hexakis(pentyloxy)triphenylene and hexabutoxytriphenylene render relative high carrier mobility for their highly ordered columnar plastic phases (Adam et al. 1996). Despite that at present the optoelectronic performance of TP-based LCPs is significantly weaker compared with their low molecular weight counterparts, but their suitability for low cost solution process is very attractive and promising for organic electronic material applications such as cheap disposable devices. However, although many polymerization methods have been attempted, so far the road toward preparation of well-controlled TP-based LCPs and optoelectronic high performance is still full of challenges until very recently some essential progress is achieved on their controlled synthesis and hierarchical structure understanding in our lab.

5.3 Synthesis of Side-Chain LCPs: Controlled Radical Polymerization (CRP) and Rational Macromolecular Design

Side-chain LCPs can be readily prepared by direct radical polymerization, ring opening metathesis polymerization (ROMP), ionic polymerization, and step condensation polymerization, etc. Upon considering the polymer backbone and mesogens separately, some specific approaches have also been adopted for side-chain LCP preparation such as polymer analogous reaction and supramolecular assembly.

Condensation polymerization is widely used in construction of main-chain polymers, while its applications in building side-chain LCPs are rare. Some earlier related examples of condensation polymerization were mostly concentrated on combined main-chain and side-chain LCPs (Reck and Ringsdorf 1985). Interested readers are recommended to refer to the Chapter by Zentel in *Handbook of Liquid Crystals* (Demus et al. 1998).

Ring opening metathesis polymerization (ROMP) is a relatively new strategy in polymer synthetic chemistry (Schrock 1990; Bielawski and Grubbs 2007; Trimmel et al. 2005). The key concept of ROMP is based on olefin metathesis which originates from research efforts around mid-1950s. Nowadays, the identification of key intermediates of the olefin metathesis promotes the continuously development of catalysts with definite structure and high efficiency, which in turn significantly boosts broad applications of ROMP, including syntheses of side-chain LCPs with various mesogen units (Weck et al. 1997; Li et al. 2003; Xia et al. 2008; Haque et al. 2013). Due to its living polymerization character, well-defined polymers with predetermined degree of polymerization (DP) and narrow polydispersity index (PDI) can be realized by choosing a suitable catalyst system. Monomers with specific olefin ring structure and complex initiators (or catalysts) system are the main characteristics of ROMP compared with radical polymerization, and moreover, the unsaturated bonds and other functional groups of the monomers will be preserved in the resulting polymers obviously differentiated from products obtained by other methods (Bielawski and Grubbs 2007). These features endow polymers by ROMP with some unique advantages such as special Z/E isomerization and tacticity of the polymer chain. For instance, compared with other living polymerization approaches, ROMP could proceed in air thanks to its wieldy nature and result in much more ordered mesophase structures for SCLCPs (Haque et al. 2013).

Before the broad adoption of controlled radical polymerization methods, controlled cationic polymerization was considered as one of the most successful tools for controlled synthesis of side-chain LCPs for its living polymerization characteristic and suitability for many vinyl ether monomers. An early comprehensive review on this topic was presented by Percec and Tomazos (1992).

Up to now, the overwhelming majority of side-chain LCPs were prepared by conventional radical polymerization, which suffered from high PDI and lack of effective control over molecular weights of the resulting polymers. Although living

anionic polymerization is a possible solution, the extremely stringent reaction conditions and limited suitable monomers eventually restrict its broad application in side-chain LCPs. Therefore, nowadays controlled/living radical polymerization (CRP) is becoming more and more widely used in construction of side-chain LCPs with well-controlled molecular weights and narrow PDI, well-defined chain structure and topology under relatively mild reaction conditions. The “living polymerization” concept was first revolutionarily proposed by Szwarc in 1956 based on anionic polymerization (Szwarc et al. 1956). The general principle of controlled/living radical polymerization is to introduce a fast and adjustable equilibrium between active and dormant species, extending the life of propagating chains from milliseconds to minutes or hours thus providing a route to controlled polymerization (Braunecker and Matyjaszewski 2007). So far, several influential CRP techniques have been developed, such as initiator-transfer-termination system (Iniferter), nitroxide mediated polymerization (NMP), atom transfer radical polymerization (ATRP) and reversible addition-fragmentation chain transfer polymerization (RAFT). Regarding the construction of side-chain LCPs, ATRP and RAFT are the most commonly adopted techniques, and we shall therefore mainly focus on these two methods. Interested readers for other two CRP methods can refer to some representative review articles on Iniferter (Otsu and Matsumoto 1998) and NMP (Brinks and Studer 2009).

5.3.1 *Side-Chain LCPs Prepared by ATRP Approach*

ATRP was discovered almost simultaneously by Matyjaszewski group (Wang and Matyjaszewski 1995) and Sawamoto group (Kato et al. 1995) in 1995. After nearly 20 year’s development, the ATRP method becomes simple and easy to operate as well as possessing good reproducibility, especially compatible with various functional groups. A profound review on ATRP was presented by Matyjaszewski and Xia (2001). The functionality of initiators and monomers can be well compatible by ATRP, leading to side-chain LCPs with various functional groups, compositions and topology structures, especially convenient for block copolymers preparation. ATRP initiators with specific functional groups can render the resulting polymers various terminal functionalities. Furthermore, the halogen group capped polymer chain can act as a macroinitiator and continue to initiate other monomers to polymerize thus extending the chain and construct block copolymer or easily realize transformation into other functional groups. These CRP methods are sometimes coupled simultaneously with some high-efficiency postpolymerization reactions such as Click chemistry (Binder and Sachsenhofer 2007; Kolb et al. 2001) and “Post Azo Coupling Reaction” (PACR) (Wang et al. 1997a, b) for the construction of various architectural block copolymers, for instance, star-shaped polymers, grafted polymers and brush-shaped polymers.

Star-shaped side-chain LCPs are usually derived from multi-functional initiators showing particular bulk and solution properties. Zhang et al. (2008) utilized a

trifunctional initiator 1,3,5-(2-bromo-2-methylpropionato) benzene for the preparation of three-armed side-chain LCPs via ATRP: a star-shaped MMAZO (methacrylate monomer with azobenzene as side-chain mesogen) based side-chain LC homopolymer PMMAZO or block copolymer PMMAZO-*b*-PMMA. The latter copolymer was obtained using three-arm star PMMA (poly(methyl methacrylate)) as the macroinitiator. Barberá et al. (2008) adopted the same trifunctional initiator for the construction of a similar star-shaped side-chain LCP using an azobenzene mesogen with a chiral center, endowing the polymer with photo-induced chiral arrangements. Recently, He et al. (2009) prepared a star-shaped LCP by ATRP polymerization of MMAZO using a new cyclodextrin (CD) derivative bearing bromide functional groups as the macroinitiator showing potential information memory characteristics.

Liquid crystalline block copolymers (LCBCPs) are usually prepared by adopting macroinitiators as the initial or middle (for ABA or star-shaped copolymers) blocks. End-functionalized PEG/PEO (polyethylene glycol/polyethylene oxide) segments are probably the most widely used macroinitiator, partly because of its good solubility in both water and most organic solvents. As a coil linear polar block, PEG bears high incompatibility with other blocks, offering the driving force for microphase separation. Some well organized review and books by Zhao and Ikeda (2009), Zhao and He (2009) and Wang group (2013) have been published including azobenzene based LCBCPs containing PEG blocks. Very recently, our group (Wu et al. 2013) have just carried out a rational design, controlled synthesis of a series of triphenylene-based discotic LCBCPs via PEG macroinitiators of different lengths, where an intriguing microphase-separated superstructure evolution and columnar order change as a function of temperature and discotic block content have been demonstrated. He et al. (2008) prepared several side-chain ABC triblock LC copolymers by ATRP with different DPs using PEG as the macroinitiator. Wang L et al. (2010) reported a series of side-chain LCPs made of laterally attached photoluminescent *p*-quinquephenyl repeat units using monofunctional PS and PEG as macroinitiators. Some specific macroinitiators for ATRP with more complex structures have been prepared by other polymerization methods such as living cationic polymerization (Gao et al. 2008) and stepwise condensation polymerization (Ishige et al. 2011).

As mentioned above, aside from the macroinitiator pathway, LCBCPs can also be prepared by combining several recently developed high-efficiency reactions like Click chemistry together with ATRP. Click chemistry refers to a highly efficient synthetic strategy that can bind small building blocks together quickly and reliably, usually featuring carbon-hetero atom connections in a mild environment friendly way, which was first proposed by Sharpless (Kolb et al. 2001). The most popular example of Click chemistry is Huisgen's 1,3-dipolar reaction through the Cu^I-catalyzed azide-alkyne cycloaddition (CuAAC). The end halogen groups of the obtained polymers through ATRP provide convenience for transforming into specific groups for subsequent Click procedure, and the functional groups introduced through the initiator well reserved in the resulting polymers can also be used for Click reactions. By means of Click chemistry, various LCBCPs can be prepared

conveniently by coupling distinct blocks constructed and characterized separately, which was extremely helpful as a viable route for introducing some specific blocks not available by usual macroinitiator synthetic pathway (Wurm and Frey 2011). It is worthy mentioning that acidic groups are not tolerated by ATRP system, so functional groups like alkynyl hydrogen for Click chemistry should be protected before ATRP process. Recently, Berges et al. (2012) prepared bi-azide-terminated polyesters N_3 -PE $_x$ - N_3 by polycondensation and alkyne-functionalized PMMAs via ATRP, then a triblock copolymer was obtained through linking them together via Click reaction. Blasco et al. (2012) “clicked” a LC aliphatic polyester dendron functionalized with sixteen 4-cyanoazobenzene mesogens to a linear block of poly(methyl methacrylate), poly(ethyl methacrylate) or poly(styrene) for the construction of liquid crystalline linear–dendritic block copolymers (LDBC). Other than Click chemistry, macromolecular azo-coupling reaction was also developed to synthesize LC amphiphilic copolymers together with ATRP. He et al. (2012) carried out such macromolecular azo-coupling reaction between the diazonium salt functionalized PEG and the ATRP-prepared polymer blocks with terminal groups suitable for azo-coupling, leading to a “Y”-shaped LCBCP with an azobenzene group in the middle as a linkage ending with photoresponsive potential.

Some other applications of ATRP for construction of specific side-chain LCPs such as graft copolymers (Börner et al. 2002; Ferji et al. 2013), cyclic polymers (Laurent and Grayson 2006) and surface initiated polymer (SIP) brushes with LC functionality (Camorani et al. 2009) have also been widely reported.

5.3.2 Side-Chain LCPs Prepared via RAFT Approach

According to Braunecker and Matyjaszewski (2007), there exist two approaches to establish the equilibrium between dormant and active species: persistent radical effect (PRE) as functioning in ATRP method, and degenerative transfer (DT) as operating in RAFT process. RAFT synthesis technique was invented by CSIRO group in Australia (Chiefari et al. 1998), and a French group Charlot at Rhodia Chimie applied a patent with the same mechanism at about the same time (Corpart et al. 1998). Since then, the group of CSIRO continued to work in this fascinating field and presented consecutive reviews on RAFT (Moad et al. 2008, 2009, 2012). Recently, Keddie (2014) reviewed the latest progress of RAFT focusing on the preparation of variant block copolymers. The RAFT polymerization mechanism involves a sequence of addition fragmentation equilibria, and the adoption of a suitable highly efficient chain-transfer agent (CTA) is of crucial importance for a successful RAFT process. CTAs are in principle organic compounds with a thiocarbonylthio moiety that can be briefly described as $ZC(=S)SR$, wherein double bond $C=S$ is reactive to radical addition and Z substituent endues CTA appropriate reactivity and R substituent serves as a good leaving group capable of efficiently re-initiating polymerization at its radical form $R\cdot$ (Moad et al. 2008; Semsarilar and Sébastien 2010). The reversible chain transfer from a propagating

chain to the CTA enables rapid equilibrium between the active propagating radicals and the corresponding dormant species, endowing the polymerization procedure “living” and “controllable” characteristics. RAFT process is generally more similar to traditional radical polymerization, and possesses many advantages compared with other CRP methods like ATRP. A significantly larger range of monomers can be used in RAFT systems. Some monomers like acrylic acid and sodium *p*-styrene sulfonate are not suitable for ATRP method unless with protection of sensitive groups, but they are well tolerated by RAFT systems. Furthermore, from our experience, for side-chain discotic LCPs preparation, ATRP method did not work or could only achieve limited DP while RAFT process operated smoothly in a well controlled way. RAFT approach is also technically metal-free, and easy to process. However, as the key component of RAFT system, the CTAs are not always easy to prepare and the commercial CTAs are usually quite expensive. Although RAFT is a metal-free process, the CTA fragment (thiocarbonylthio group) attached in the resulting polymer will sharpen the final product’s toxicity and thus restrict its application in biomedical fields, therefore, on some occasions removal or transformation of the thiocarbonylthio groups become a required procedure (Moad et al. 2008).

RAFT method has been widely and successfully applied in macromolecular engineering of block copolymers (Chong et al. 1999; Convertine et al. 2006; Favier et al. 2004), star-shaped polymers (Huang et al. 2006; Mayadunne et al. 2003; Stenzel and Davis 2002), dendritic polymers (Patton et al. 2008) and surface-initiated polymer brushes (Yu et al. 2004), etc. Applications in building side-chain LCPs have also been widely reported. Hao et al. (2003) prepared a series of side-chain LCPs bearing biphenyl as the mesogen using 2-(2-cyanopropyl) dithiobenzoate (CPDB) as the RAFT agent. The thermal behavior of polymer with different chain lengths was studied, and it turned out that the stable LC mesophase range increased with increasing polymer chain length. Zhao et al. (2008) adopted the same RAFT agent CPDB in preparing the first diblock copolymer with low PDIs composed of two different side-chain liquid crystalline blocks containing azobenzene mesogens. CPDB was also used by Xie et al. (2009) for preparing a novel side-chain LC diblock copolymer PMBHMA-*b*-PMPCS, wherein the PMBHMA (poly[ω -(4'-methoxybiphenyl-4-yloxy)hexyl methacrylate]) block was a conventional side-chain LC block, and the PMPCS (poly{2,5-bis[(4-methoxyphenyl)oxycarbonyl] styrene}) block was a typical mesogen-jacketed LC block that was capable of assembling into a rigid rod.

The RAFT method offers a convenient pathway to introduce specific blocks into side-chain LCP systems, which renders the polymer functional properties such as amphiphathy. Boisse et al. (2009) and Zhang et al. (2012) prepared a series of amphiphilic diblock copolymers via RAFT, wherein the hydrophobic block was a cholesteryl-based smectic LC polymer, while the hydrophilic block was either a neutral polymer with a lower critical solution temperature or a random copolymer with acrylic acid and poly(ethylene oxide) side chains. Zhou et al. (2011) adopted a PEG block as a bifunctional macromolecular RAFT agent (CTA-PEG-CTA) for the construction of novel “LC-semicrystalline-LC” triblock copolymers. Of course,

similar to ATRP approach, LC block copolymers can be built by combining specific reactions together with RAFT, such as macromolecular azo-coupling reaction. For example, He et al. (2013) demonstrated an amphiphilic diblock copolymer by a combination of macromolecular azo-coupling reaction and RAFT. Moreover, the organo-catalytic coupling via the thiol-ene Click reaction was adopted for RAFT-prepared precursors in construction of more complex polymer systems such as star-shaped polymers (Chan et al. 2008).

Functionalized CTA itself renders more application possibilities. For instance, Meuer et al. (2008) used α -pyrene containing CTA for preparing α -pyrene functionalized PMMA via RAFT. The polymer itself is not liquid crystalline, but the α -pyrene is an efficient anchoring unit for solubilizing and disentangling multi-walled carbon nanotubes (MWCNTs), which will then self-organize as liquid crystalline phases in PMMA and PEG matrices. However, as mentioned above that the thiocarbonylthio group is detrimental to some applications, so removal or transformation steps are sometimes necessary. In the side-chain LCP films through RAFT method reported by Kawatsuki et al. (2010), the residual dithiobenzoate end groups were thermally decomposed to get colorless polymers. Nevertheless, some modification could be made to utilize the thiocarbonylthio groups as well. Gao et al. (2007) presented a new approach to prepare Ag nanoparticles protected by side-chain LCPs. A homopolymer bearing side-chain azobenzene mesogens was prepared by RAFT, and then the thiocarbonylthio end groups of the obtained polymer were reduced using NaBH_4 into thiol groups. The interactions between Ag and thiol groups eventually coated the Ag nanoparticle with side-chain LCPs. Likewise, aside from the thiol group from CTA fragment, another thiol group was introduced at the other end of the polymer chain, and a cyclic polymer with a disulfide linkage was then obtained after a simple oxidation process (Stamenović et al. 2013).

5.3.3 Other Synthetic Methods for Side-Chain LCPs

Although most of side-chain LCPs nowadays are obtained by direct radical polymerization, polymer analogous reactions still play an important role in preparing some specific side-chain LCPs. As a matter of fact, the very first discotic side-chain LCP was prepared by attaching discotic mesogens to the polysiloxane main-chain through hydrosilylation reaction (Kreuder and Ringsdorf 1983), which was a typical polymer analogous reaction. Hydrosilylation is a very classical approach in preparing side-chain LCPs that is adopted widely even today. The Si–O bond is highly flexible thus the calamitic side-chain LCPs based on polysiloxane backbone exhibit a strong tendency to form smectic LC phases. Zental group (Beyer et al. 2007; Öge and Zentel 1996) prepared various ferroelectric LC polymers with calamitic mesogens bearing chiral centers attached to polysiloxane backbone via hydrosilylation. Recently, polymer analogous reactions are often combined with CRP methods like ATRP and RAFT. For instance, in a recent work by

Royes et al. (2012), well-defined azobenzene containing side-chain LCPs were achieved through postpolymerization click reactions of azide terminated mesogens with poly(propargyl methacrylate), which was obtained via ATRP with the active alkyne hydrogen of propargyl protected during the ATRP process.

Polymer analogous reaction approach is even more important when the target LCP can not be obtained by direct polymerization from the corresponding mesogenic monomer. For instance, the controlled synthesis of discotic LCBCPs still remains a challenge, and although there were attempts to prepare TP-based homopolymers and block copolymers via ATRP, only limited DP around 8 of the LC block was realized (Otmakhova et al. 2003). Recently, based on block copolymers PEG-*b*-PHEMA via ATRP using PEG macroinitiator, a series of well-defined discotic LC diblock copolymers have been prepared in our laboratory by attaching side-chain triphenylene mesogens to PHEA (poly(2-hydroxyethyl acrylate)) block through polymer analogous esterification (Wu et al. 2013). In general, aminoazobenzene-containing monomers demonstrate significant inhibition effects to free radicals, so the preparation of LCBCPs via CRP with aminoazobenzene or similar push-pull structure mesogens is rather difficult. Wang et al. (2007) prepared a diblock copolymer PEG-*b*-PEMA via ATRP. The PEG block was used as the macroinitiator, and the PEMA block contained side chains with aniline groups. Then the azo-coupling reaction was carried out between the side-chain aniline groups and newly added diazonium salt in a polymer analogous reaction manner, thus a well-defined aminoazobenzene-containing LCBCP was prepared. However, it is worth to note that there always exist difficulties in carrying polymer analogous reaction to 100 % completion, and even high-efficiency reaction and prolonged reaction time can not essentially solve the problem (Wang and Zhou 2004).

Side-chain LCPs obtained via supramolecular self-assembly, on the other hand, demonstrate some interesting specific characteristics compared with the aforementioned approaches. This Chapter will not present detailed comments on such side-chain LCPs and interested readers can refer to critical reviews by Kato et al. (2001, 2006).

5.3.4 Synthetic Approaches for Liquid Crystalline Linear–Dendritic Block Copolymers (LDBC)s

Liquid crystalline block copolymers (LCBCPs) combine the molecular level order of liquid crystals and the nano- or submicrometer scale microphase separation morphology of block copolymers, making them one of the most important research directions in soft matter. Linear–dendritic block copolymers (LDBC)s, on the other hand, take a step further from block copolymers by introducing regularly branched and multi-functional dendritic blocks, leading to a promising field for advanced organic nanomaterials. The possible synergistic interactions make LDBC)s a promising and inspiring macromolecular platform rather than simple addition of two

distinct blocks. Therefore, when mesogenic units are introduced in the dendritic segments of LDBC systems, one can expect even more exciting properties for the liquid crystalline LDBCs such as curvature effect on mesophases and hierarchical superstructure organization.

The idea of LDBCs was first pioneered by Gitsov et al. (1992), and poly(benzyl ether) dendrons of variant generations (called Fréchet-type dendrons) were adopted (Gillies and Fréchet 2002; Gitsov et al. 1993; Gitsov and Frechet 1993; Yu et al. 1999). Based on the pioneering works by Fréchet et al., Percec group carried out systematic and groundbreaking works in developing a family of Percec-type dendrons and their complex self-assembly behavior investigation (Rosen et al. 2009). Critical reviews regarding LDBCs have been presented by Gitsov (2008) and Frey group (Wurm and Frey 2011). Recently, Blasco et al. (2014) reviewed LDBCs bearing stimuli-responsive functional groups, and Dong and Liu (2013) gave a brief review on the applications of LDBCs in bionanotechnology.

As for the synthesis of LDBCs, we would like to give a brief introduction to the preparation methods of dendrimers before going on about LDBCs, considering the importance of dendritic block construction. The synthesis of dendrimers characterizes repeated interactive reactions by multi-branched monomer units, which renders dendrimers precisely controlled structure and large amount of functional terminals. Depending on growing directions, the synthetic routes of dendrimers fall into two basic types: divergent and convergent approaches. The divergent approach was first proposed by Tomalia et al. (1985) and Newkome et al. (1985). In divergent approach, the dendrimer grows from a “core”, followed by the iterative repetition of a two-step synthetic process leading to higher generations. However, the number of active terminals increases dramatically with increasing generation, which may introduce defects due to incomplete reactions. For this reason, products of each procedure have to go through tedious careful purifications. Even so, the divergent approach still remains the most suitable approach for large-scale preparations of many high-generation dendrimers (Wurm and Frey 2011). On the other hand, convergent approach was first adopted by Fréchet (1994), wherein dendrimers were prepared via convergent coupling of prefabricated branched units. Nearly all poly(benzyl ether) dendrons were prepared through this route (Wurm and Frey 2011). Limited active sites are involved in each step of convergent approach, which technically reduces the difficulties in reaction completion and for further purification. But for higher generations, the high steric hindrance still evidently depresses the reaction efficiency. Some other less classical synthetic approaches, such as “solid-surface convergent method” (Bharathi et al. 1995) have also been developed.

As for construction of LDBCs, three different strategies are widely used according to the sequence of building linear chain and dendron blocks: the chain-first approach, the dendron-first approach and the coupling approach as schematically presented in Fig. 5.6.

The chain-first approach is in general the most frequently used approach for the preparation of LDBCs, which usually starts from a terminally functionalized linear polymer chain obtained via controlled/living polymerization with the terminal group as the initial point for construction of dendritic part in a divergent manner.

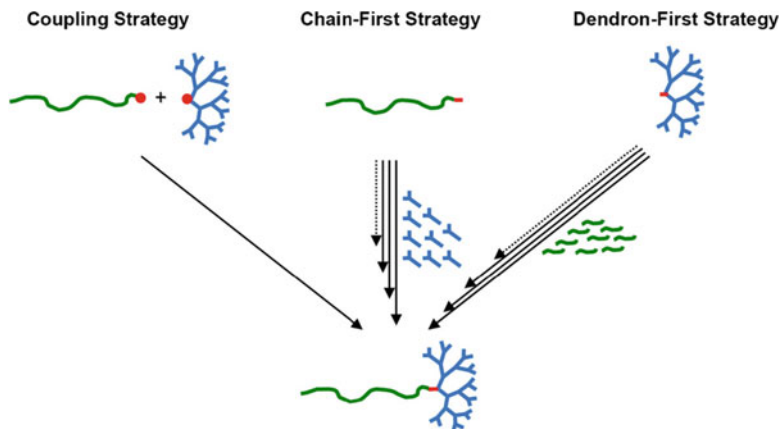


Fig. 5.6 Three strategies for preparing LDBC. Reprinted from Progress in Polymer Science, 36, Frederik Wurm and Holger Frey, Linear-dendritic block copolymers: The state of the art and exciting perspectives, 1–52, Copyright (2011), with permission from Elsevier

The first example dated back to 1994 by Chapman et al. (1994). The divergent manner of chain-first approach requires 100 % completeness of reactions at each step and entire elimination of the excessive reagents, which is never easy. Still the possibility of some undesired side reactions such as back-folding could introduce defects in LDBC. The dendron-first approach, on the other hand, requires a dendritic macromolecular initiator, which is mostly prepared through convergent method for preserving an active focal point of the dendron segment. Then, anionic ring-opening polymerization (ROP) and controlled radical polymerizations (CRP) like ATRP, RAFT and NMP were adopted for construction of the linear segment. However, because of the frequently adoption of convergent method in preparing dendrons in dendron-first approach, there still remain some drawbacks as mentioned above from convergent method itself.

The coupling approach achieves the construction of LDBC through conjugation of the terminal functional group of the linear chain and the active reaction site at focal point of the dendron segment. Actually the coupling approach was exactly the technology adopted in preparing the first LDBC by Gitsov et al. (1992). It turns out that the traditional linear block copolymers are difficult to synthesize in this way due to the strong shielding effects with both coil chains. However, the dendrons usually come with moderate molecular weights and may have some peculiar effects on the coupling efficiency of the focal functionality (Wurm and Frey 2011), which in turn significantly benefit the coupling process. In the first attempt by Gitsov et al. (1992), detailed kinetics study demonstrated that Williamson reaction rate even increased when longer PEG chains and higher generations of the dendron segment were used. Recently, thanks to the intensive development of highly efficient new coupling methods such as Click chemistry, various LDBC through the coupling approach have been constructed.

5.4 Research Progress of Side-Chain LCPs with Calamitic Azobenzene or Discotic Triphenylene Mesogens: Hierarchical Bulk Structure Evolution, Assembly Behaviors in Solution and Stimuli-Responsive Properties

In this section, we shall present a brief review of side-chain LCPs regarding the structures and properties. Herein, liquid crystalline LDBC s are also included as a specific kind of side-chain LCPs with dendritic side chain LC segments as stated in the previous section. As mentioned in section 2, azobenzene and triphenylene mesogens are typical and the most widely used calamitic and discotic mesogens. Therefore, we shall still focus on LCPs bearing these two types of side-chain mesogens.

5.4.1 *Side-Chain LCPs Containing Azobenzene Based Calamitic Mesogens*

When talking about macromolecular engineering of azobenzene (AZO) containing side-chain LCPs in the classical way, one may give much consideration on the flexibility/plasticity of the main chain backbone, the length/pliability of the corresponding spacer, the synthesis of mesogen units and the architecture of the whole polymer. Actually, azobenzene containing polymers have gone much further than that, as the photo-isomerization and light-induced motion ability of azobenzene derivatives endue azobenzene based LCPs with fascinating applications.

According to the comprehensive review by Natansohn and Rochon (2002), the motion of azobenzene chromophores within polymers can be classified into three levels: the molecular level, the nanometer scale behavior, and the micrometer (macroscopic) performance. Various optical applications originate from these motion levels, such as photo-induced anisotropy or dichroism (Natansohn and Rochon 2002), photo-induced phase transitions (Zhao and Ikeda 2009), surface relief gratings (SRGs) (Oliveira et al. 2005; Viswanathan et al. 1999), photo-induced chirality (Choi et al. 2007), nonlinear optical (NLO) materials (Yesodha et al. 2004), photomechanics (Ikeda et al. 2007) and command surface (Ichimura 2000). From the critical reviews by Kumar and Neckers (1989), Natansohn and Rochon (1999, 2002), Barrett et al. (2007), Ikeda et al. (2007) and Ichimura (2000), one can cognize the vigorously developed research field.

Other than UV or visible light triggered isomerization, recently, several phenomena of photo-induced motions are becoming the hot topics in the field of side-chain LCPs containing azobenzene. When the polymer film is irradiated with a linear polarized light (LPL), the long axis of AZO mesogens of the polymer will

take an orientation almost perpendicular to the polarizing direction, which is widely known as Weigert effect (Yu 2014). Since the *trans*-AZO possesses rigid rod-like geometry while the *cis*-AZO is bent usually resulting in disorder, photo-irradiated phase transition can occur in some cases. Even more, molecular cooperative motion (MCM) (Yu 2014; Zhao and Ikeda 2009), namely the cooperative motions of AZO and photo inert mesogens, endows such kind of LCPs with amplified light responsive properties. Therefore, tailoring of the architecture and content of azobenzene units together with variant backbone topology and spacers renders azobenzene containing side-chain LCPs powerful self-assembling capability and fascinating functions.

There is a close relationship between the photochromic group architecture, phase behavior, thermal properties of bulk polymer, and kinetics of chromophore photo-orientation. The constitution characteristics of AZO containing side-chain LCPs make up of the basis for future applications. For instance, the polymer backbone of AZO containing side-chain LCPs may have strong impact on thermal properties, thus significantly influence their mesophases and light-response behavior. Recently, Petr and Hammond (2011) reported a photoresponsive side-chain LCP showing nematic phase at room temperature by attaching AZO mesogens to a polysiloxane backbone. Upon irradiation by UV, the resulting *cis*-form AZO interrupted the nematic order and the bulk film quickly began to undergo isotropization. This phase transition is surprisingly fast, which could be readily observed under POM with black isotropic domains emanating from the nematic Schlieren texture domain boundaries. Similarly, many studies have lately been reported about the effect of several constitution characteristics on the corresponding phase behaviors and light-induced orientations, such as spacers and terminal groups. Recently, several reports performed a series of intensive studies on the effects of alkyl tail length (Chen S et al. 2013), mesogen attaching positions (Yang et al. 2010) and mesogen density (Wang Q et al. 2010) of side-chain AZO containing polymethacrylates. The phase behaviors of polymers were investigated by a combination of multiple characterization techniques such as DSC, POM and SAXS. A series of polymers PMAzoCOOR_m (m = 1–18) were prepared with variant alkyl tail length. For m = 1–6, the polymers exhibited a SmA phase, while polymers with m = 2, 3, 4, and 5 showed an additional SmC phase. For m = 8, 10, 14, 18, the polymers exhibited a bilayer SmA phase. Furthermore, polymethacrylates containing *para*-, *meta*- and *ortho*-monosubstituted azobenzene moieties in the side chain were investigated in comparison. The polymers with *para*- and *meta*-monosubstituted azobenzene derivatives exhibited a SmA phase, while those with *ortho*-substituted ones of the most different geometry from traditional “end-on” side-chain LCPs, did not show any LC mesophase at all. LCPs attached by side-chain groups with variant branched single, double, and triple AZO arms were employed for the investigation of mesogen density. Single-armed LCP only exhibited a smetic phase, while double, and triple-armed showed nematic and smetic phases with even broader temperature range. In addition, the clearing temperatures increased with the increasing mesogen densities. Zhu and Wang (2013) prepared similar side-chain LCPs bearing branched AZO side-chain groups

with two and three AZO arms, wherein the three-armed AZO polymer showed a well organized SmA mesophase in the lower temperature range. Aside from adding branched arms in a parallel connection style, mesogen density could also be increased in tandem by simply attaching AZOs head to tail. Hosono et al. (2010) prepared a polymer brush carrying three AZO units in series for each side chain. Through a simple one-step hot-pressing process on the oriented Teflon sheet, the polymer achieved large-area 3D order and the resulting polymer film could even behave photomechanical bending without any crosslinking process.

5.4.1.1 Phase Behavior and Superstructure Evolution of Azobenzene Containing Block Copolymers in the Bulk

Block copolymers, which usually demonstrate amphiphilic property by a combination of immiscible blocks, are capable of constructing a variety of ordered nanostructures such as lamellar, cylindrical, double gyroid, and spherical phases through microphase segregation or self-assembly. Liquid crystalline block copolymers (LCBCPs), combining the molecular level order of liquid crystals and the nanometer or sub-micrometer microphase separation structure of block copolymers, constitute a kind of intriguing soft matter materials. A step further, introducing of AZO moieties renders LCBCPs with light-responsive capabilities. The interplay of photo-activity and microphase-separated structure generates exciting possibilities. Abundant reviews have been published in this field (Gohy and Zhao 2013; Yu 2014; Zhao and He 2009). In this section and the next, we shall go over the latest research progress on AZO containing block copolymers in the bulk and in solution.

Considering AZO containing LCBCPs at the bulk solid state, various self-assembled nano-scale domain morphologies can be realized, which can be further readily adjusted by the AZO block LC order and its photoinduced motion. The orientational order of AZO block can be easily tuned by various external stimulations, such as thermal annealing, photo-induced alignment, mechanical orientation and electric/magnetic field (Zhao and Ikeda 2009). Thus the photo-active AZO blocks can trigger optical responsiveness of these block copolymer materials owing to their bringing about motions from molecular level to nanometer scale. On the other hand, the non-LC blocks can also deliver special properties, such as easy solubility, optical transparency (Yu et al. 2007), and photoresponse enhancement (Haque et al. 2012). Komura and Iyoda (2007), Tian et al. (2002), Yu et al. (2006a, b) presented serial impressive works on side-chain AZO containing diblock copolymers. The series of PEG-*b*-PMMAZOs were prepared by ATRP using PEG macroinitiators, wherein PEG blocks of various lengths were adopted as the minority hydrophilic segments and the well-defined AZO containing polymethacrylate PMMAZO blocks were introduced as the hydrophobic, liquid crystalline and photo-responsive majority segments. Periodic nanostructures on the bulk films were developed through the interplay between the microphase separation morphology and the regular periodicity of LC order, as designated as

“supramolecular cooperative motions” (SMCMs) (Yu et al. 2006b). Through long-time annealing of the films on the substrate, highly ordered microphase separation with hexagonally arranged PEG cylinders was achieved (Tian et al. 2002). During annealing, the AZO moieties took a perpendicular orientation against the substrate surface, and those PEG cylinders also took a highly ordered perpendicularly orientation through SMCMs. This array-type arrangement and its cross sectional image could be clearly observed using atom force microscopy (AFM) by cleavage preparation (Komura and Iyoda 2007). Different orientation directions of the PEG cylinders could also be readily realized through rubbing (Yu et al. 2006b) or photo-induced alignment (Yu et al. 2006a). Morikawa et al. (2007) prepared a similar diblock copolymer using PS as the non-LC segment instead of PEG. Microphase separated nanocylinder domains of PS were introduced by a combination of LPL irradiation and annealing followed by slow cooling process. For real-time monitoring of the corresponding microphase separation and photo-orientation procedure by LPL, a poly(butyl methacrylate) (PBMA) block was introduced in replacement of PS block by the same group (Fukuhara et al. 2013; Nagano et al. 2012). The resulted PBMA-*b*-PMMAZO copolymers were then examined with time-resolved SAXS/WAXS and GI-SAXS.

A family of “ABA-type” triblock copolymers were prepared by He et al. (2003), Tang et al. (2007a, b) and Kadota et al. (2005), wherein a central PEG block (macroinitiator) were sandwiched by two terminal PMMA blocks containing side-chain AZO units. Crystalline, smectic and/or nematic phases were observed for triblock copolymers of different compositions. The DSC study indicated that PEG crystallization only occurred above weight fraction 42 %, otherwise due to interfaces enhancement between the PEG and LC blocks with increasing AZO block content, crystallization of PEG block was eventually completely suppressed (He et al. 2003; Tang et al. 2007a). The tail substituent effects of AZO mesogens were also investigated (Tang et al. 2007b). Through Langmuir-Blodgett technology from water surface, clear AFM images of this ABA triblock copolymer monolayer on mica were observed (Kadota et al. 2005). The monolayer with their AZO units in *cis*-form gave characteristic elongated branched flat stripe patterns with about 30 nm widths in topological AFM images. After thermal reversion to the *trans*-form, the stripe-shaped domains turned into dot structures. The difference in compatibility with water between *cis*-AZO and *trans*-AZO contributed to this organized morphology difference of AFM images.

Recently, Menghetti et al. (2012) carried out a comparative study regarding optical writing properties between block copolymer and random copolymer based on azobenzene methacrylate (MAZO) LC monomer and methyl methacrylate (MMA) co-monomer. It turned out that stable and intense pulses as short as 100 ms could develop a significant local birefringence increase for the block copolymers thanks to their microphase separation, whereas not for the corresponding random copolymer. Chen et al. (2011) reported a detailed study on the phase diagram of polystyrene-*b*-poly(*n*-butyl methacrylate) (PS-*b*-PnBMA) block copolymers, wherein AZO units were attached to the PnBMA block through postfunctionalization replacing the butyl side group at different degree, thus the

content of AZO units could be adjusted. LCBCPs with similar structure feature were prepared by Del Barrio et al. (2013) attaching the AZO units to the poly(4-vinylpyridine) block via supramolecular self-assembly approach. Han et al. (2010) synthesized the first example of diblock copolymer containing both poly(3-hexylthiophene) (P3HT) and side-chain AZO block. The AZO block was designed with a higher clearing temperature than P3HT block, in which way the AZO block showed liquid crystalline property while keeping the P3HT block in its isotropic phase. Then the alignment of the P3HT nanodomains could be well adjusted along with the photo-induced orientation of AZO units.

Besides linear LCBCPs, the bulk and solution behaviors of linear-dendritic block copolymers (LDBC) have also been extensively studied. However, so far very few studies appeared on LDBC with mesogens showing liquid crystalline mesophases, despite this kind of novel LCBCPs has been predicted more than a decade ago (Demus et al. 1998). Recently, a series of azobenzene containing LDBC were synthesized, and systematic investigations were carried out on their bulk (Blasco et al. 2012; Del Barrio et al. 2009), solution (Blasco et al. 2013a, b; Del Barrio et al. 2010) and LB film (Giner et al. 2011) behaviors. Theoretical simulation studies on these AZO containing LDBC were also reported by Lin et al. (2012) lately. Most of the reported AZO containing LDBC were composed of a linear PEG segment and an AZO containing dendritic aliphatic ester block PDMPA of different generations from 2,2-bis(hydroxymethyl)propionic acid (bis-MPA). The self-organization behaviors of these LDBC in solution, which will be discussed in the next section, were extraordinary rich, while the bulk morphology was quite monotonous with largely lamellar structures as revealed by XRD and TEM investigations, even when the linear PEG segment was replaced by other different blocks such as PMMA, poly(ethyl methacrylate) (PEMA) or PS (Blasco et al. 2012).

Nevertheless, multiple mesophases and hierarchical superstructures in the bulk solid-state can be achieved by rational design of the AZO containing dendritic segments. Recently, our group (Shi et al. 2012a, b) synthesized a series of LDBC consisting of a linear PEG block ($DP = 49$) and dendritic polyamidoamine (PAMAM) segments of generation G0–G3, wherein AZO units bearing an octyloxy tail and a flexible ten-methylene spacer were attached at the periphery of the PAMAM dendron (Fig. 5.7). Their thermal behaviors, liquid crystalline mesophases and hierarchical superstructures were intensively studied by a combination of TGA, DSC, POM, SAXS/WAXS and TEM. Along with increasing generations, a hierarchical structure evolution exhibited. LDBC composing dendrons of G0–G2 demonstrated well-defined lamellar structures, where distinct microphase separation between the hydrophilic PEG blocks and hydrophobic PAMAM dendrons occurred, with only a slight change in layer spacing between 12.2 and 13.0 nm. Among them, mPEG-G0-(AZO)₂ displayed a simple lamellar structure (Fig. 5.7b), while owing to further microphase separation between PAMAM dendrons and AZO units within the dendritic blocks, mPEG-G1-(AZO)₄ and mPEG-G2-(AZO)₈ developed into hierarchical structures of “tetragonal-within-lamellar” (Fig. 5.7c) and “lamellar-within-lamellar” (Fig. 5.7d),

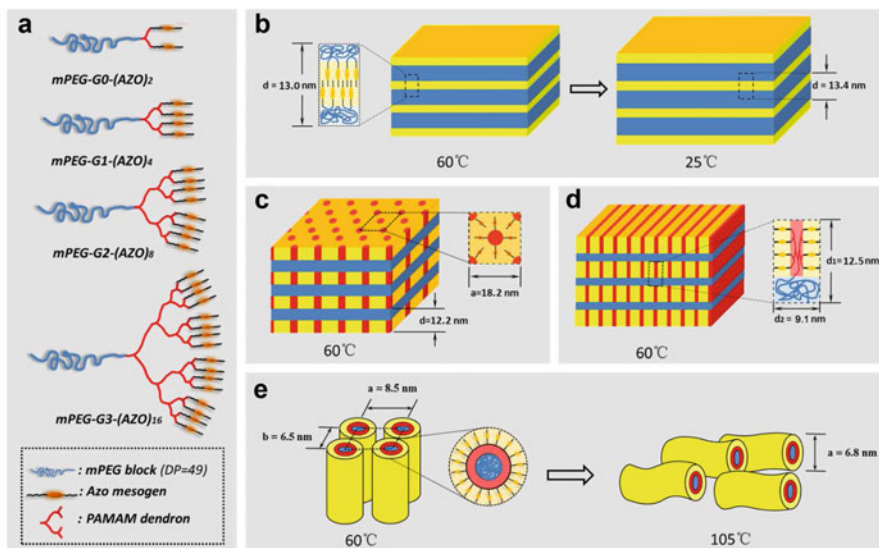
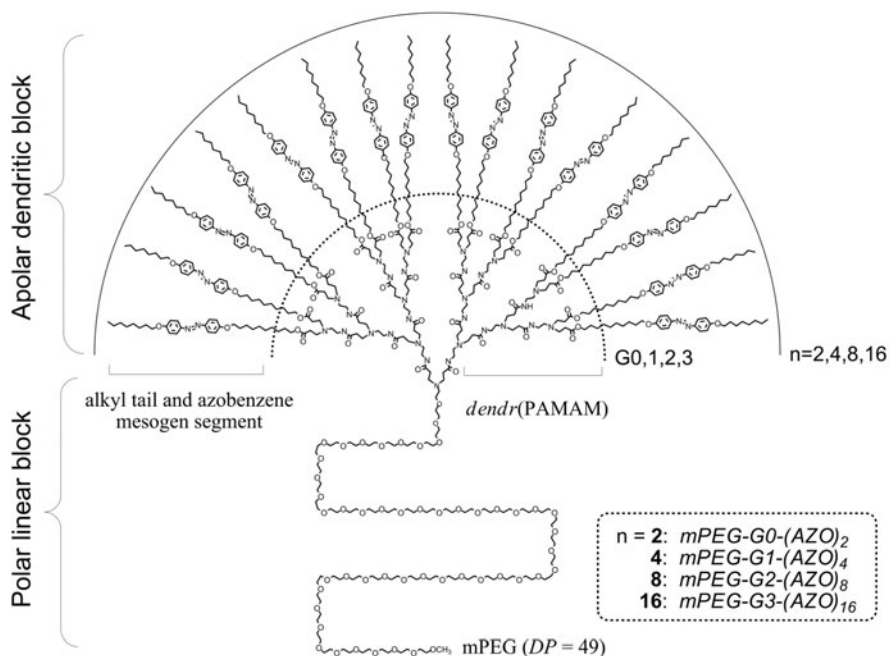


Fig. 5.7 Molecular structures of a series of AZO containing LDBC with a PEG linear block and PAMAM dendritic segments and proposed model for self-assembled superstructures of various generation LDBC and their liquid crystalline mesophases. Reproduced from (Shi et al. 2012b) with permission of The Royal Society of Chemistry

respectively. Different from aforementioned generally lamellar structure with some intralamellar structure suborganization, a striking real columnar structure was formed for LDBC with the investigated highest generation mPEG-G3-(AZO)₁₆. These columns organized in 2D rectangular structure at low-temperature with the PEG core and the peripheral AZO mesogens, while disaggregated into a disordered columnar mesophase upon heating to higher temperature. In this study, the adoption of alkyloxy tails for the AZO units is crucial for the construction of hierarchical superstructures and mesophases, for similar LDBC systems with nitroazobenzene groups attached through six-methylene spacer examined in our laboratory even did not show a distinct phase separation structure. Moreover, it turned out that the complex lamellar mesophases of G1 and G2 LDBCs transformed into micellar or network cubic structures upon cooling to ambient solidification temperature with PEG crystallization, which demonstrated a complete inverse phase change tendency due to the curvature effect of the specific linear–dendritic architecture. Furthermore, such kind of azobenzene-containing liquid crystalline LDBCs films displayed generation dependent or morphology determined photophysical characteristics, therefore, novel optical storage materials might be designed and fine-tuned just by simply changing the dendritic segment generation.

5.4.1.2 Assembled Structures of Azobenzene Containing Block Copolymers in Solution

Amphiphilic property can be easily introduced into LCBCPs by specific macromolecular engineering. By rational macromolecular design and proper solvent combination choice, various self-assembled aggregates such as vesicles and micelles or more complicated structures, can be realized in solution of LCBCPs, leading to many specific properties and applications (Discher and Eisenberg 2002; Li and Keller 2009; Rosler et al. 2001). Adoption of AZO units in amphiphilic LCBCPs assembly renders the system photo-responsive characteristics. For instance, LPL-induced orientation (Weigert effect) of AZO units brings about photo-induced assembly deformations, and the AZO *trans*–*cis* isomerization can result in micelle disaggregation or vesicle fusion. Wang group (Li et al. 2005, 2006; Liu et al. 2008, 2009, 2010) performed systematical investigation on photo-induced deformation of colloidal spheres based on amphiphilic AZO polymers. The LCP colloidal spheres elongated along the polarization direction of the incident Ar⁺ laser, and the effects of several structural factors on the deformation were detailedly discussed. Su et al. (2007) reported the real-time fusion process of the giant micro-vesicles under the irradiation of 365 nm light based on amphiphilic AZO containing LCBCPs.

Spherical micelles are the most commonly obtained assemblage in solution from AZO containing LCBCPs. The AZO blocks usually show hydrophobic character and form the micelle core, while the other hydrophilic segments like PEG shape the corona. Thus, through the response of AZO units, photo-induced morphological change of micelles can be realized. Recently, Jochum and Theato (2010) reported a

temperature and light controlled micelle formation and disruption. Solution of the block copolymer poly(ethyleneoxide)-*b*-poly(*N*-isopropylacrylamide) (PEO-*b*-PNIPAM), wherein azobenzene units was adopted as side groups in PNIPAM blocks, demonstrated micelle formation when heated from 20 to 50 °C and the process was fully reversible, which was confirmed by turbidimetry, fluorescence, NMR and dynamic light scattering (DLS) measurements. Also, micellar disruption was observed by UV irradiation and the micelle reformed after a thermal relaxation process. Besides micellar disruption by *trans*-*cis* isomerization, it was demonstrated that in another research of AZO containing LCBCPs, where non-radiative *trans*-*cis* isomerization relaxation of azobenzene moiety was hindered, UV irradiation could also influence the intensity of fluorescence emission through the formation and size change of aggregates (Xiang et al. 2010). Recent years, the reversible host-guest inclusion complexation between AZO and cyclodextrin (CD) has been widely investigated in polymer systems (Tomatsu et al. 2005; Yan Q et al. 2011). Through hydrophobic and van der Waals interactions, *trans*-AZO matches well with CD thus forming inclusion complex, while *cis*-AZO does not. Thus, AZO containing block copolymers can self-assemble into micelles through host-guest complexation between β -CD and *trans*-AZO side groups, whereas transformation into *cis*-AZO will result in disassembly. In a recent example presented by Wang et al. (2013), micelles formed in aqueous solution from PAZO-*b*-PS diblock copolymer and β -CD demonstrated reversible disassembly and re-assembly with alternating UV and visible light irradiation.

Preparation of vesicles from AZO containing LCBCPs was also extensively studied. Similarly, features of the resulting vesicles such as size, regularity, fluorescence emission and morphology can also be tuned via AZO units through light irradiation. Recently, Dong et al. (2013) reported a reversible fluorescence decrease and recovery phenomenon during the *trans*-*cis* isomerization process of the vesicle formed from poly(ethylene glycol)-*b*-poly(dimethylamino azobenzene) (PEG-*b*-PDMA-AZO) in solution. Yan B et al. (2011) reported a photo-softening effect on the proton transfer across the vesicle membrane. Other photo-induced effects such as UV/visible light induced vesicle fission (Chen K et al. 2013) and LPL induced vesicle deformation (Wu et al. 2011) were also reported from AZO containing LCBCPs. Besides, sizes and morphologies of vesicles can usually be adjusted via rational molecular design of AZO containing amphiphilic LCBCPs. Structural factors such as content of AZO units (Jin et al. 2010) and the corresponding spacer lengths (Shen et al. 2013) have demonstrated significant effects on the shape and morphologies of vesicles.

For AZO containing linear-dendritic block copolymers (LDBC), even more abundant self-assembly structures have been observed from solutions. As mentioned in Sect. 5.4.1.1, Blasco et al. (2013a, b), Del Barrio et al. (2010) presented systematic investigations on the solution behaviors of such kind of LDBC. Solution behavior (Shi et al. 2012a) of a series of liquid crystalline LDBC was also carried out in our lab with azobenzene mesogens as mentioned in the previous section: mPEG-*dendr*(PAMAM)-(AZO)_{*n*} (*n* = 2, 4, 8, 16), wherein the effect of water content in the dioxane/H₂O mixed solution and initial copolymer

concentration were investigated especially for the lower generation dendritic segment copolymers. G0 copolymer mPEG-*dendr*(PAMAM)-(AZO)₂ assembled into nanofibers in a solution with 28 wt% water, and nanospheres were formed when water content increased. G1 copolymer mPEG-*dendr*(PAMAM)-(AZO)₄ formed nanospheres in a solution with 17 wt% water, and oval sheets were obtained with nanorods attached to both ends when water content reaching 28 wt%. Such peculiar oval sheet assemblies, which might represent the intermediate state between one-dimensional nanofibers and two-dimensional nanosheets, were reminiscent of the formation of membranes in biosystems, and could possibly open a new pathway for construction of biomimetic structures. Moreover, polymeric vesicles and large compound micelles (LCMs) were generated from G2 and G3 copolymers in solution respectively.

5.4.2 Phase Behavior and Hierarchical Structures of Polymers Containing Triphenylene Based Discotic Mesogen Side Groups

The first reported discotic LC polymer was a polysiloxane bearing triphenylene (TP) based discotic mesogens as the side chains via hydrosilylation reaction (Kreuder and Ringsdorf 1983). Several critical reviews and books on polymers containing TP mesogenic units have been presented (Bisoyi and Kumar 2010; Kumar 2004, 2005). The spacer effect was preliminarily investigated by Werth and Spiess (1993) mainly based on TP-based polysiloxane backbone side-chain LCPs. It was found that in contrast with the calamitic LC polymer system where the decoupling of the mesogen from the polymer main chain was of crucial importance and became more effective with increasing spacer length, for discotic LC polymers, the longer spacers did not lead to higher ordered phases, presumably due to the decoupling aspect of the spacer was overruled by the diluting perturbation on the columnar packing, and the columnar phases reacted by a change in symmetry or by a distortion of the resulting mesophases even resulted in the breakdown of the columnar phase.

Polysiloxane is a kind of very flexible polymer backbone, thus the adoption of more universal backbones like polymethacrylate or polyacrylate is quite desirable for side-chain discotic LCPs. However, only nematic columnar (N_{col}) phases complexed with trinitrofluorenone (TNF) through charge-transfer (CT) interactions were observed from the early attempts by Ringsdorf et al. (1989). Generally, the rigid polymethacrylate backbone suppressed the formation of LC mesophases, unless properly modified with flexible diethylenoxy spacer (Boden et al. 1998). Talroze et al. (2000) prepared random copolymers based on the monomers of TP-containing methacrylate and hydroxyethyl acrylate, which showed wide range columnar mesophases.

More diverse backbones were introduced with some specific polymerization techniques, such as step condensation polymerization (Catry et al. 1993; Imrie et al. 2004; Karthaus et al. 1992; Ringsdorf et al. 1989) and ROMP (Weck et al. 1997). For instance, Karthaus et al. (1992) reported a combined main-chain and side-chain LC polymers via condensation polymerization, wherein both AZO and TP units were introduced, while the resulting polymers did not show any LC mesophases. Weck et al. (1997) synthesized discotic LCPs bearing alkoxy-substituted TP moieties in the side-chain by ROMP using ruthenium catalysts. The original backbones were poly(norbornene) or poly(butadiene), and hydrogenation of the poly(butadiene) using Crabtree's catalyst gave saturated poly(butane)-backbone polymers. It turned out that discotic hexagonal columnar mesophases were realized only for decyloxy-substituted TP-based polymers while not for the pentoxy-substituted TP systems.

Xing et al. (2008) synthesized rigid poly(1-alkyne) carrying side-chain TP units with different peripheral alkyloxy chain lengths. The polymers with shorter and longer peripheral alkyloxy chains adopted a hexagonal columnar structure, while those intermediate ones formed mixed mesophases. Recently, the same group reported a new type of liquid crystalline polyacetylene containing side-chain TP units with very short spacers (Yu et al. 2013), which exhibited mesogen jacketed liquid crystalline polymer (MJLCP) properties. Side-chain TP-containing MJLCPs with different spacer lengths (n) between the central paraphthalate and TP units were also reported (Zhu et al. 2012, 2014). In this case, the T_g of resulting polymers decreased with longer spacers. Polymers with relatively short ($n = 3$) or medium spacers ($n = 6$) demonstrated rectangular or hexagonal columnar mesophases at higher temperature and merely rectangular columnar mesophase at lower temperature, wherein the TP units formed discotic nematic (N_D) phase within the columns. As for the longest spacer ($n = 12$), the low-temperature phase was a hexagonal columnar structure, and the high-temperature phase was an N_{col} phase formed by the MJLCP chain as a whole. Specially, a re-entrant isotropic phase was found in the medium temperature range.

Side-chain TP units were also introduced in some specific polymer systems. Pal and Kumar (2008) prepared a novel ionic discotic liquid crystalline polymer from TP-substituted 1-vinylimidazole monomer for combining ionic liquids and discotic liquid crystals. A transition from glassy state to rectangular columnar phase of the polymer took place at 224 °C and the columnar LC phase sustained till 244 °C. Recently, Tahar-Djebbar et al. (2011) and Zeng et al. (2014) reported a series of π -conjugated polythiophene bearing TP units in the side chains. Novel hierarchical "lamello-columnar" phases were developed, wherein the TP units constituted a 2D columnar lattice and the main-chain formed the general lamellar structure.

Although new advances keep emerging from various very closely related fields since the introduction of TP into polymeric systems, whereas the precise synthesis of homopolymers and block copolymers containing side-chain TP units with well-defined structures and compositions remains a challenge. In an early attempt by Boden et al. (1999), TP-containing LCBCP was obtained by attaching TP units to poly(*p*-methoxystyrene)-*b*-poly(*p*-hydroxystyrene) backbone via polymer

analogous reaction, while the resulting block copolymer did not show any LC mesophases. Likewise, through polymer analogous reactions, Stillings et al. (2010) prepared TP-based side-chain homopolymer and block copolymer by attaching TP units to poly(but-3-en-1-ol) and poly(but-3-en-1-ol)-*b*-polystyrene backbones. It is interesting to find that in the bulk films of the block copolymer, microphase separation took place between the TP-containing poly(but-3-en-1-ol) block and the PS block leading to an ordered smectic phase, wherein the TP units assembled into cylinders lying perpendicularly to the microphase separated layers, which demonstrated a uniform perpendicular TP columnar orientation induced by “slit-like” nanospace confinement.

Despite polymer analogous reactions have been widely employed with some relatively successful examples, their intrinsic shortage of incomplete reaction makes them unsuitable for the preparation of strictly well-defined polymers. Thus many efforts have been making to synthesize TP-containing LC polymers through direct synthesis such as radical polymerization. Otmakhova et al. (2003) reported TP-based side-chain block copolymers of 2,6,7,10,11-pentapentyloxy-3-(3-acryloylpropyloxy) triphenylene (PPAT) and *tert*-butyl acrylate (*t*-BA) through ATRP. This approach eventually obtained the homopolymer with a limited DP around 8, which might originate from the special assembly of monomers in solution. Nevertheless, the resulting homopolymer could be used as the macroinitiator for variant molecular weight block copolymer preparation through polymerization of *t*-BA by ATRP. All the resulted LCBCPs with different poly(*t*-BA) block contents displayed microphase separation, and XRD measurements confirmed that both the homopolymer and block copolymers showed columnar mesophases.

Very recently, our group (Wu et al. 2013) synthesized a well-defined block copolymer poly(ethylene glycol)-*b*-poly(2-hydroxyethyl acrylate) (PEG-*b*-PHEA) with PEG macroinitiators of various molecular weights via ATRP, then a series of side-chain discotic LCPs were prepared by attaching side-chain triphenylene mesogens to the PHEA block through polymer analogous esterification (Fig. 5.8). The resulting block copolymers, with various discotic LC block weight fraction ($f_{w, \text{DLC}}$), showed a narrow PDI value no larger than 1.11. Thermal behaviors and corresponding mesophase structures as a function of $f_{w, \text{DLC}}$ and temperature were studied by a combination of POM, DSC and SAXS/WAXS. At relatively low temperatures, block copolymers with lower DLC contents ($f_{w, \text{DLC}} = 37$ and 43 %) formed lamellar structures and underwent order-order transitions (OOT) upon PEG region crystallization at 45 °C, meanwhile a phase transition from N_D to N_{col} took place at about 25 °C within the microdomain of TP units. In case of intermediate $f_{w, \text{DLC}}$ value (62 %), hexagonal packed cylinders (HPCs) of amorphous PEG segments were formed above 35 °C within the matrix of TP moieties, which eventually turned into a mixed lamellar structure upon cooling below 35 °C together with PEG crystallization. HPC structures were also generated in copolymers with higher $f_{w, \text{DLC}}$ (67 and 80 %), in which case the TP matrix showed N_D or N_{col} mesophases. In the case of the highest $f_{w, \text{DLC}}$ (around 90 %), an overall N_D phase was developed. The compared homopolymer prepared from small molecular

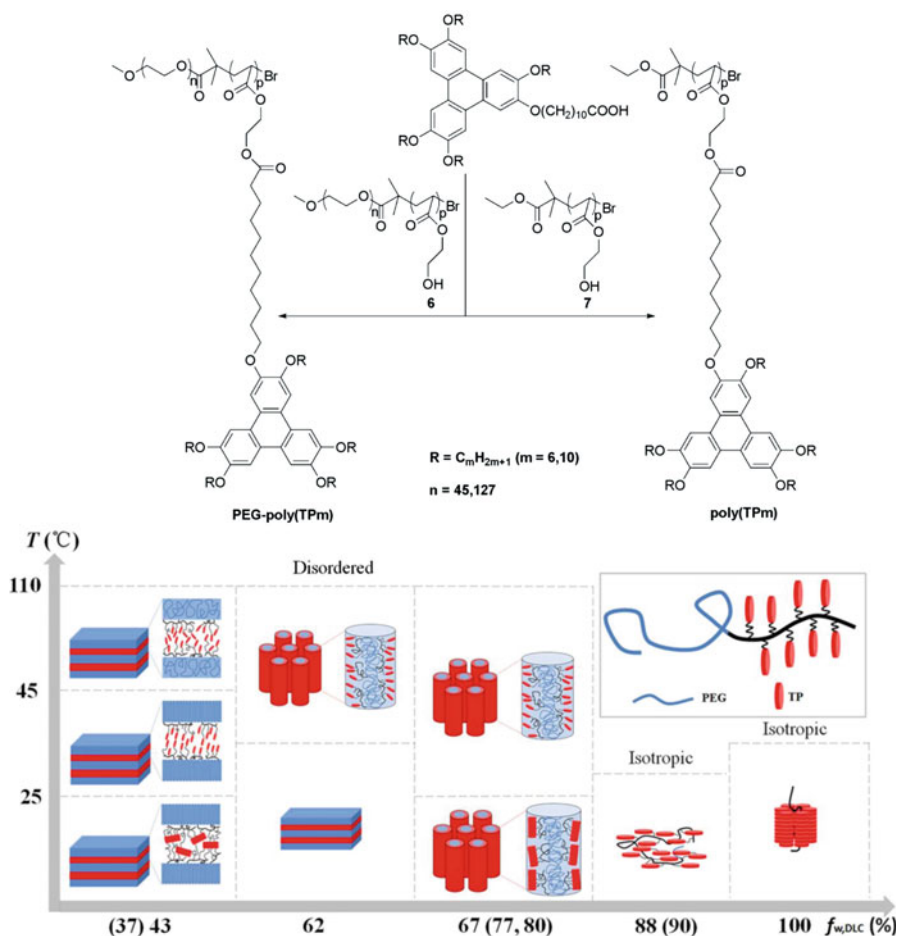


Fig. 5.8 Chemical structure of the block copolymers and schematic presentation of the hierarchical superstructure evolution. Reprinted with permission from (Wu B, Mu B, Wang S, Duan J, Fang J, Cheng R, Chen D (2013) Triphenylene-based side chain liquid crystalline block copolymers containing a PEG block: controlled synthesis, microphase structures evolution and their interplay with discotic mesogenic orders. *Macromolecules* 46: 2916–2929). Copyright (2013) American Chemical Society

initiator, on the other hand, demonstrated an ordered columnar phase. The presence of an overall N_D phase in the high discotic LC content copolymer is quite inspiring, for it may open a new way for achieving such important discotic LC mesophase applying in widening view angle for liquid crystal display (LCD) just by introducing an appropriate short block. This study enhanced the understanding of the interplay between microphase separation and discotic LC order, which would inspire further explorations for side-chain discotic LCPs leading to various applications.

5.5 Conclusions and Future Perspective

In this Chapter, we have reviewed the recent research progress in the side-chain liquid crystalline polymers (LCPs) mainly based on typical rod-like (calamitic) mesogen azobenzene derivatives and disc-like (discotic) mesogen triphenylene (TP) derivatives. Three main aspects have been focused on: controlled synthesis, rational macromolecular design and LC mesophase behaviors pertaining to their hierarchical structures. Controlled syntheses via CRP methods especially ATRP and RAFT endue the resulted polymers many attributes such as well-controlled DP and narrow PDI, well-defined architecture and terminal groups under relatively mild reaction conditions. With such advantages ATRP and RAFT synthesis techniques have made tremendous contributions to macromolecular design of side-chain LCPs. Rational consideration should be given to the backbone, the spacer, the mesogen units and many other factors regarding the construction of side-chain LCPs. Among mesogenic units, calamitic azobenzene derivatives possess rigid skeletons as well as fascinating photo-responsive properties, and discotic triphenylene derivatives are widely used for their easy availability, powerful self-assembly ability and high performance. In complex side-chain LCP systems, the coexistence and interplay of hierarchical superstructures and LC mesophases may lead to various novel intriguing applications.

Particularly, liquid crystalline block copolymers (LCBCPs) give a chance for investigating the LC phase behavior within constrained nanodomains as a consequence of microphase separation of distinct blocks. On the other hand, the morphological nanodomains of block copolymers will be modified and adjusted by mesogenic ordering and orientation. As a hot research field in soft matter materials, LCBCPs combining molecular level LC order and nano- or submicrometer scale microphase separation morphology may serve as intriguing advanced organic optoelectronic materials. They can also be employed as fascinating templates for controlled preparation of inorganic semiconductors or hybrid functional materials.

References

- Adam D, Roemhildt W, Haarer D (1996) Charge-carrier transport in liquid-crystal based organic photoconductors. *Jpn J Appl Phys* 1(35):1826–1831
- Akiyama E, Nagase Y, Koide N, Araki K (1999) New side chain liquid crystalline polymers: synthesis and thermal properties of side chain polyacrylates having segmented spacers. *Liq Cryst* 26:1029–1037
- Barberá J, Giorgini L, Paris F, Salatelli E, Tejedor RM, Angiolini L (2008) Supramolecular chirality and reversible chiroptical switching in new chiral liquid-crystal azopolymers. *Chemistry* 14:11209–11221
- Barrett CJ, Mamiya J, Yager KG, Ikeda T (2007) Photomechanical effects in azobenzene-containing soft materials. *Soft Matter* 3:1249–1261

- Berges C, Javakhishvili I, Hvilsted S, Sánchez C, Alcalá R (2012) Photoresponsive azopolyester-PMMA block copolymers obtained by combination of ATRP, polycondensation, and “click” chemistry. *Macromol Chem Phys* 213:2299–2310
- Beyer P, Krueger M, Giesselmann F, Zentel R (2007) Photoresponsive ferroelectric liquid-crystalline polymers. *Adv Funct Mater* 17:109–114
- Bharathi P, Patel U, Kawaguchi T, Pesak DJ, Moore JS (1995) Improvements in the synthesis of phenylacetylene monodendrons including a solid-phase convergent method. *Macromolecules* 28:5955–5963
- Bielawski CW, Grubbs RH (2007) Living ring-opening metathesis polymerization. *Prog Polym Sci* 32:1–29
- Billard J, Dubois JC, Huutinh N, Zann A (1978) Mesophase of disc-like molecules. *Nouv J Chim* 2:535–540
- Binder WH, Sachsenhofer R (2007) ‘click’ chemistry in polymer and materials science. *Macromol Rapid Commun* 28:15–54
- Bisoyi HK, Kumar S (2010) Discotic nematic liquid crystals: science and technology. *Chem Soc Rev* 39:264–285
- Blasco E, Barrio JD, Piñol M, Oriol L, Berges C, Sánchez C, Alcalá R (2012) Azobenzene-containing linear-dendritic block copolymers prepared by sequential ATRP and click chemistry. *Polymer* 53:4604–4613
- Blasco E, Serrano JL, Piñol M, Oriol L (2013a) Light responsive vesicles based on linear-dendritic block copolymers using azobenzene-aliphatic codendrons. *Macromolecules* 46:5951–5960
- Blasco E, Del Barrio J, Sánchez-Somolinos C, Piñol M, Oriol L (2013b) Light induced molecular release from vesicles based on amphiphilic linear-dendritic block copolymers. *Polym Chem* 4:2246–2254
- Blasco E, Piñol M, Oriol L (2014) Responsive linear-dendritic block copolymers. *Macromol Rapid Commun* 35:1090–1115
- Boden N, Bushby RJ, Clements J (1993) Mechanism of quasi-one-dimensional electronic conductivity in discotic liquid crystals. *J Chem Phys* 98:5920–5931
- Boden N, Bushby RJ, Lu ZB (1998) A rational synthesis of polyacrylates with discogenic side groups. *Liq Cryst* 25:47–58
- Boden N, Bushby RJ, Lu Z, Eichhorn H (1999) Discotic liquid crystalline block copolymers 1: side-chain discotic liquid crystalline diblock copolymers. *Mol Cryst Liq Cryst Sci Technol A* 332:2791–2801
- Boisse S, Rieger J, Di-Cicco A, Albouy P, Bui C, Li M, Charleux B (2009) Synthesis via RAFT of amphiphilic block copolymers with liquid-crystalline hydrophobic block and their self-assembly in water. *Macromolecules* 42:8688–8696
- Börner HG, Duran D, Matyjaszewski K, Da Silva M, Sheiko SS (2002) Synthesis of molecular brushes with gradient in grafting density by atom transfer polymerization. *Macromolecules* 35:3387–3394
- Braunecker WA, Matyjaszewski K (2007) Controlled/living radical polymerization: features, developments, and perspectives. *Prog Polym Sci* 32:93–146
- Brinks MK, Studer A (2009) Polymer brushes by nitroxide-mediated polymerization. *Macromol Rapid Commun* 30:1043–1057
- Camorani P, Cristofolini L, Fontana MP, Angiolini L, Giorgini L, Paris F (2009) Azo-containing polymer brushes: photoalignment and application as command surfaces. *Mol Cryst Liq Cryst* 502:56–64
- Catry C, Van der Auweraer M, De Schryver FC, Bengs H, Häussling L, Karthaus O, Ringsdorf H (1993) Conductivity and photoconductivity of undoped and doped Langmuir-blodgett films of a polymer with hexaalkoxytriphenylene side-groups. *Die Makromol Chem* 194:2985–2999
- Chan JW, Yu B, Hoyle CE, Lowe AB (2008) Convergent synthesis of 3-arm star polymers from RAFT-prepared poly (n, n-diethylacrylamide) via a thiol-ene click reaction. *Chem Commun* 40:4959–4961

- Chandrasekhar S, Sadashiva BK, Suresh KA (1977) Liquid crystals of disc-like molecules. *Pramana* 9:471–480
- Chapman TM, Hillyer GL, Mahan EJ, Shaffer KA (1994) Hydraamphiphiles: novel linear dendritic block copolymer surfactants. *J Am Chem Soc* 116:11195–11196
- Chen X, Shen Z, Wan X, Fan X, Chen E, Ma Y, Zhou Q (2010) Mesogen-jacketed liquid crystalline polymers. *Chem Soc Rev* 39:3072–3101
- Chen W, Wei X, Balazs AC, Matyjaszewski K, Russell TP (2011) Phase behavior and photoresponse of azobenzene-containing polystyrene-block-poly (n-butyl methacrylate) block copolymers. *Macromolecules* 44:1125–1131
- Chen K, Xue G, Shen G, Cai J, Zou G, Li Y, Zhang Q (2013) UV and visible light induced fission of azobenzene-containing polymer vesicles. *RSC Adv* 3:8208–8210
- Chen S, Ling A, Zhang HL (2013) Synthesis and phase behaviors of side-chain liquid-crystalline polymers containing azobenzene mesogen with the different length alkyl tail. *J Polym Sci A Polym Chem* 51:2759–2768
- Chiefari J, Chong YK, Ercole F, Krstina J, Jeffery J, Le TP, Mayadunne RT, Meijs GF, Moad CL, Moad G, Rizzardo E, Thang SH (1998) Living free-radical polymerization by reversible addition-fragmentation chain transfer: the RAFT process. *Macromolecules* 31:5559–5562
- Choi S, Kawauchi S, Ha NY, Takezoe H (2007) Photoinduced chirality in azobenzene-containing polymer systems. *Phys Chem Chem Phys* 9:3671–3682
- Chong YK, Le TP, Moad G, Rizzardo E, Thang SH (1999) A more versatile route to block copolymers and other polymers of complex architecture by living radical polymerization: the RAFT process. *Macromolecules* 32:2071–2074
- Convertine AJ, Lokitz BS, Vasileva Y, Myrick LJ, Scales CW, Lowe AB, McCormick CL (2006) Direct synthesis of thermally responsive DMA/NIPAM diblock and DMA/NIPAM/DMA triblock copolymers via aqueous, room temperature RAFT polymerization. *Macromolecules* 39:1724–1730
- Corpart P, Charmot D, Biadatti T, Zard S, Michelet D (1998) Block polymer synthesis by controlled radical polymerization. WO9858974
- de Witte PAJ, Castriciano M, Cornelissen JJLM, Scolaro LM, Nolte RJM, Rowan AE (2003) Helical polymer-anchored porphyrin nanorods. *Chem-Eur J* 9:1775–1781
- Del Barrio J, Oriol L, Alcalá R, Sánchez C (2009) Azobenzene-containing linear-dendritic diblock copolymers by click chemistry: synthesis, characterization, morphological study, and photoinduction of optical anisotropy. *Macromolecules* 42:5752–5760
- Del Barrio J, Oriol L, Sánchez C, Serrano JL, Di Cicco A, Keller P, Li M (2010) Self-assembly of linear-dendritic diblock copolymers: from nanofibers to polymersomes. *J Am Chem Soc* 132:3762–3769
- Del Barrio J, Blasco E, Oriol L, Alcalá R, Sánchez Somolinos C (2013) Diblock copolymer-azobenzene complexes through hydrogen bonding: self-assembly and stable photoinduced optical anisotropy. *J Polym Sci A Polym Chem* 51:1716–1725
- Demus D, Goodby J, Gray GW, Spiess HW, Vill V (1998) Handbook of liquid crystals, vol 3. Wiley-VCH, Weinheim
- Discher DE, Eisenberg A (2002) Materials science: soft surfaces: polymer vesicles. *Science* 297:967–973
- Dong C, Liu G (2013) Linear-dendritic biodegradable block copolymers: from synthesis to application in bionanotechnology. *Polym Chem* 4:46–52
- Dong R, Zhu B, Zhou Y, Yan D, Zhu X (2013) Reversible photoisomerization of azobenzene-containing polymeric systems driven by visible light. *Polym Chem* 4:912–915
- Donnio B, Guillon D (2006) Liquid crystalline dendrimers and polypedes. *Adv Polym Sci* 201:45–155
- Donnio B, Buathong S, Bury I, Guillon D (2007) Liquid crystalline dendrimers. *Chem Soc Rev* 36:1495–1513

- Favier A, D'Agosto F, Charreyre M, Pichot C (2004) Synthesis of n-acryloxysuccinimide copolymers by RAFT polymerization, as reactive building blocks with full control of composition and molecular weights. *Polymer* 45:7821–7830
- Ferji K, Nouvel C, Babin J, Albouy PA, Li MH, Six JL (2013) Controlled synthesis of new amphiphilic glycopolymers with liquid crystal grafts. *J Polym Sci A Polym Chem* 51:3829–3839
- Finkelmann H, Ringsdorf H, Wendorff JH (1978a) Polyreactions in ordered systems, 14. Model considerations and examples of enantiotropic liquid crystalline polymers. *Makromol Chem* 179:273–276
- Finkelmann H, Ringsdorf H, Siol W, Wendorff JH (1978b) Polyreactions in ordered systems, 15. Synthesis of cholesteric liquid crystalline polymers. *Makromol Chem* 179:829–832
- Fletcher ID, Luckhurst GR (1995) The synthesis and characterization of novel non-symmetric dimers with rod-like and disc-like mesogenic units. *Liq Cryst* 18:175–183
- Frechet JMJ (1994) Functional polymers and dendrimers: reactivity, molecular architecture, and interfacial energy. *Science* 263:1710–1715
- Fukuhara K, Fujii Y, Nagashima Y, Hara M, Nagano S, Seki T (2013) Liquid-crystalline polymer and block copolymer domain alignment controlled by free-surface segregation. *Angew Chem Int Ed* 52:5988–5991
- Ganicz T, Makowski T, Stanczyk WA, Tracz A (2012) Side chain polysiloxanes with phthalocyanine moieties. *Express Polym Lett* 6:373–382
- Gao J, Sun Y, Zhou J, Zheng Z, Chen H, Su W, Zhang Q (2007) Preparation of Ag nanoparticles terminally-protected side-chain liquid crystalline azobenzene polymers by RAFT polymerization. *J Polym Sci A Polym Chem* 45:380–5386
- Gao L, Zhang C, Liu X, Fan X, Wu Y, Chen X, Shen Z, Zhou Q (2008) ABA type liquid crystalline triblock copolymers by combination of living cationic polymerization and ATRP: synthesis and self-assembly. *Soft Matter* 4:1230–1236
- García T, Larios-López L, Rodríguez-González RJ, Martínez-Ponce G, Solano C, Navarro-Rodríguez D (2012) Liquid-crystalline polymers bearing phenylene (azobenzene) moieties substituted with an electron-donor or electron-acceptor lateral group. Synthesis, mesomorphic behavior and photo-induced isomerization. *Polymer* 53:2049–2061
- García-Amorós J, Velasco D (2012) Recent advances towards azobenzene-based light-driven real-time information-transmitting materials. *Beilstein J Org Chem* 8:1003–1017
- Ge JJ, Zhang A, McCreight KW, Ho R, Wang S, Jin X, Harris FW, Cheng SZ (1997) Phase structures, transition behaviors, and surface alignment in polymers containing rigid-rodlike backbones with flexible side chains. 1. Monotropic phase behavior in a main-chain/side-chain liquid crystalline polyester. *Macromolecules* 30:6498–6506
- Gemmell PA, Gray GW, Lacey D, Alimoglu AK, Ledwith A (1985) Polymers with rigid anisotropic side groups: 2. Synthesis and properties of some side chain acrylate and methacrylate liquid crystal polymers containing the 4'-alkylbiphenyl-4-yl moiety. *Polymer* 26:615–621
- Gillies ER, Fréchet JM (2002) Designing macromolecules for therapeutic applications: polyester dendrimer poly (ethylene oxide)“bow-tie” hybrids with tunable molecular weight and architecture. *J Am Chem Soc* 124:14137–14146
- Giner I, Haro M, Gascón I, Barrio JD, Carmen López M (2011) Air–water interfacial behavior of linear-dendritic block copolymers containing peg and azobenzene chromophores. *J Colloid Interf Sci* 359:389–398
- Gitsov I (2008) Hybrid linear dendritic macromolecules: from synthesis to applications. *J Polym Sci A Polym Chem* 46:5295–5314
- Gitsov I, Fréchet JM (1993) Solution and solid-state properties of hybrid linear-dendritic block copolymers. *Macromolecules* 26:6536–6546
- Gitsov I, Wooley KL, Fréchet JM (1992) Novel polyether copolymers consisting of linear and dendritic blocks. *Angew Chem Int Ed* 31:1200–1202

- Gitsov I, Wooley KL, Hawker CJ, Ivanova PT, Frechet JM (1993) Reactivity of dendritic macromolecules toward linear polymers. *Macromolecules* 26:5621–5627
- Gohy J, Zhao Y (2013) Photo-responsive block copolymer micelles: design and behavior. *Chem Soc Rev* 42:7117–7129
- Goulet Hanssens A, Barrett CJ (2013) Photo-control of biological systems with azobenzene polymers. *J Polym Sci A Polym Chem* 51:3058–3070
- Han D, Tong X, Zhao Y, Zhao Y (2010) Block copolymers comprising π -conjugated and liquid crystalline subunits: induction of macroscopic nanodomain orientation. *Angew Chem Int Ed* 49:9162–9165
- Hao X, Heuts J, Barner Kowollik C, Davis TP, Evans E (2003) Living free-radical polymerization (reversible addition-fragmentation chain transfer) of 6-[4-(4'-methoxyphenyl) phenoxy] hexyl methacrylate: a route to architectural control of side-chain liquid-crystalline polymers. *J Polym Sci A Polym Chem* 41:2949–2963
- Haque HA, Nagano S, Seki T (2012) Lubricant effect of flexible chain in the photoinduced motions of surface-grafted liquid crystalline azobenzene polymer brush. *Macromolecules* 45:6095–6103
- Haque HA, Kekehi S, Hara M, Nagano S, Seki T (2013) High-density liquid-crystalline azobenzene polymer brush attained by surface-initiated ring-opening metathesis polymerization. *Langmuir* 29:7571–7575
- He X, Zhang H, Yan D, Wang X (2003) Synthesis of side-chain liquid-crystalline homopolymers and triblock copolymers with p-methoxyazobenzene moieties and poly (ethylene glycol) as coil segments by atom transfer radical polymerization and their thermotropic phase behavior. *J Polym Sci A Polym Chem* 41:2854–2864
- He X, Sun W, Yan D, Xie M, Zhang Y (2008) Synthesis and characterization of side-chain liquid crystalline abc triblock copolymers with p-methoxyazobenzene moieties by atom transfer radical polymerization. *J Polym Sci A Polym Chem* 46:4442–4450
- He T, Hu T, Zhang X, Zhong G, Zhang H (2009) Synthesis and characterization of a novel liquid crystalline star-shaped polymer based on α -CD core via ATRP. *J Appl Polym Sci* 112:2120–2126
- He Y, He W, Wei R, Chen Z, Wang X (2012) Synthesizing amphiphilic block copolymers through macromolecular azo-coupling reaction. *Chem Commun* 48:1036–1038
- He Y, He W, Liu D, Gu T, Wei R, Wang X (2013) Synthesis of block copolymers via the combination of RAFT and a macromolecular azo coupling reaction. *Polym Chem* 4:402–406
- Hosono N, Kajitani T, Fukushima T, Ito K, Sasaki S, Takata M, Aida T (2010) Large-area three-dimensional molecular ordering of a polymer brush by one-step processing. *Science* 330:808–811
- Hsiue G, Sha Y, Hsieh S, Jeng R, Kuo W (2001) Synthesis and characterization of halogen-containing ferroelectric liquid crystals and side chain liquid crystalline polymers. *Liq Cryst* 28:365–374
- Huang J, Wan D, Huang J (2006) Polymerization of ethyl acrylate using hyperbranched polyglycerol with multi-RAFT groups as chain transfer agent. *J Appl Polym Sci* 100:2203–2209
- Ichimura K (2010) Photoalignment of liquid-crystal systems. *Chem Rev* 100:1847–1874
- Ikeda T, Sasaki T, Ichimura K (1993) Photochemical switching of polarization in ferroelectric liquid-crystal films. *Nature* 361:428–430
- Ikeda T, Mamiya J, Yu Y (2007) Photomechanics of liquid-crystalline elastomers and other polymers. *Angew Chem Int Ed* 46:506–528
- Imrie CT, Inkster RT, Lu Z, Ingram MD (2004) Discotic side group liquid crystal polymer electrolytes. *Mol Cryst Liq Cryst* 408:33–43
- Ishige R, Ishii T, Tokita M, Koga M, Kang S, Watanabe J (2011) Well-ordered lamellar microphase-separated morphology of an ABA triblock copolymer containing a main-chain liquid crystalline polyester as the middle segment. *Macromolecules* 44:4586–4588

- Jin Q, Liu G, Liu X, Ji J (2010) Photo-responsive supramolecular self-assembly and disassembly of an azobenzene-containing block copolymer. *Soft Matter* 6:5589–5595
- Jochum FD, Theato P (2010) Thermo- and light responsive micellation of azobenzene containing block copolymers. *Chem Commun* 46:6717–6719
- Kadota S, Aoki K, Nagano S, Seki T (2005) Photocontrolled microphase separation of block copolymers in two dimensions. *J Am Chem Soc* 127:8266–8267
- Karthauss O, Ringsdorf H, Ebert M, Wendorff JH (1992) Polyesters containing both rodlike and disklike mesogens. *Makromol Chem* 193:507–513
- Kato M, Kamigaito M, Sawamoto M, Higashimura T (1995) Polymerization of methyl methacrylate with the carbon tetrachloride/dichlorotris-(triphenylphosphine) ruthenium (ii)/methylaluminum bis (2, 6-di-tert-butylphenoxide) initiating system: possibility of living radical polymerization. *Macromolecules* 28:1721–1723
- Kato T, Mizoshita N, Kanie K (2001) Hydrogen-bonded liquid crystalline materials: supramolecular polymeric assembly and the induction of dynamic function. *Macromol Rapid Commun* 22:797–814
- Kato T, Mizoshita N, Kishimoto K (2006) Functional liquid-crystalline assemblies: self-organized soft materials. *Angew Chem Int Ed* 45:38–68
- Kawata K (2002) Orientation control and fixation of discotic liquid crystal. *Chem Rec* 2:59–80
- Kawatsuki N, Matsuda T, Kondo M (2010) Photoinduced orientation of liquid crystalline copolymer films with cinnamic acid side groups synthesized by RAFT polymerization. *Mol Cryst Liq Cryst* 529:10–19
- Keddie DJ (2014) A guide to the synthesis of block copolymers using reversible-addition fragmentation chain transfer (RAFT) polymerization. *Chem Soc Rev* 43:496–505
- Kolb HC, Finn MG, Sharpless KB (2001) Click chemistry: diverse chemical function from a few good reactions. *Angew Chem Int Ed* 40:2004–2021
- Komura M, Iyoda T (2007) AFM cross-sectional imaging of perpendicularly oriented nanocylinder structures of microphase-separated block copolymer films by crystal-like cleavage. *Macromolecules* 40:4106–4108
- Kouwer PHJ, Mehl GH (2009) Hierarchical organisation in shape-amphiphilic liquid crystals. *J Mater Chem* 19:1564–1575
- Kouwer PHJ, Gast J, Jager WF, Mijs WJ, Picken SJ (2001) A series of novel liquid crystalline polymers showing a nematic discotic and/or a nematic columnar phase. *Mol Cryst Liq Cryst Sci Technol A* 364:225–234
- Kouwer PHJ, van den Berg O, Jager WF, Mijs WJ, Picken SJ (2002a) Induced liquid crystalline diversity in molecular and polymeric charge-transfer complexes of discotic mesogens. *Macromolecules* 35:2576–2582
- Kouwer PHJ, Jager WF, Mijs WJ, Picken SJ (2002b) Charge transfer complexes of discotic liquid crystals: a flexible route to a wide variety of mesophases. *Macromolecules* 35:4322–4329
- Kouwer PHJ, Jager WF, Mijs WJ, Picken SJ (2003) Specific interactions in discotic liquid crystals. *J Mater Chem* 13:458–469
- Kreuder W, Ringsdorf H (1983) Liquid crystalline polymers with disk-like mesogens. *Makromol Chem Rapid Commun* 4:807–815
- Kumar S (2004) Recent developments in the chemistry of triphenylene-based discotic liquid crystals. *Liq Cryst* 31:1037–1059
- Kumar S (2005) Triphenylene-based discotic liquid crystal dimers, oligomers and polymers. *Liq Cryst* 32:1089–1113
- Kumar S (2006) Self-organization of disc-like molecules: chemical aspects. *Chem Soc Rev* 35:83–109
- Kumar S (2010) Chemistry of discotic liquid crystals: from monomers to polymers. CRC, Boca Raton
- Kumar GS, Neckers DC (1989) Photochemistry of azobenzene-containing polymers. *Chem Rev* 89:1915–1925

- Kumar RM, Saravanan C, Senthil S, Kannan P (2007) Synthesis, characterization and photolysis studies on liquid crystalline poly[4-(4'-x-biphenyl)yl-4''-(m-methacryloyloxyalkoxy) cinnamate]'s. *Eur Polym J* 43:2648–2659
- Laschat S, Baro A, Steinke N, Giesselmann F, Haegele C, Scalia G, Judele R, Kapatsina E, Sauer S, Schreivogel A, Tosoni M (2007) Discotic liquid crystals: from tailor-made synthesis to plastic electronics. *Angew Chem Int Ed* 46:4832–4887
- Laurent BA, Grayson SM (2006) An efficient route to well-defined macrocyclic polymers via “click” cyclization. *J Am Chem Soc* 128:4238–4239
- Li M, Keller P (2009) Stimuli-responsive polymer vesicles. *Soft Matter* 5:927–937
- Li MH, Keller P, Albouy PA (2003) Novel liquid crystalline block copolymers by ATRP and ROMP. *Macromolecules* 36:2284–2292
- Li Y, He Y, Tong X, Wang X (2005) Photoinduced deformation of amphiphilic azo polymer colloidal spheres. *J Am Chem Soc* 127:2402–2403
- Li Y, He Y, Tong X, Wang X (2006) Stretching effect of linearly polarized Ar⁺ laser single-beam on azo polymer colloidal spheres. *Langmuir* 22:2288–2291
- Li Z, Zhang Y, Zhu L, Shen T, Zhang H (2010) Efficient synthesis of photoresponsive azobenzene-containing side-chain liquid crystalline polymers with high molecular weights by click chemistry. *Polym Chem* 1:1501–1511
- Lin Y, Chang H, Sheng Y, Tsao H (2012) Photoresponsive polymersomes formed by amphiphilic linear–dendritic block copolymers: generation-dependent aggregation behavior. *Macromolecules* 45:7143–7156
- Liu J, He Y, Wang X (2008) Azo polymer colloidal spheres containing different amounts of functional groups and their photoinduced deformation behavior. *Langmuir* 24:678–682
- Liu J, He Y, Wang X (2009) Size-dependent light-driven effect observed for azo polymer colloidal spheres with different average diameters. *Langmuir* 25:5974–5979
- Liu J, He Y, Wang X (2010) Influence of chromophoric electron-withdrawing groups on photo-induced deformation of azo polymer colloids. *Polymer* 51:2879–2886
- Mahimwalla Z, Yager KG, Mamiya J, Shishido A, Priimagi A, Barrett CJ (2012) Azobenzene photomechanics: prospects and potential applications. *Polym Bull* 69:967–1006
- Matharu AS, Jeeva S, Ramanujam PS (2007) Liquid crystals for holographic optical data storage. *Chem Soc Rev* 36:1868–1880
- Matyjaszewski K, Xia J (2001) Atom transfer radical polymerization. *Chem Rev* 101:2921–2990
- Mayadunne RTA, Jeffery J, Moad G, Rizzardo E (2003) Living free radical polymerization with reversible addition-fragmentation chain transfer (RAFT polymerization): approaches to star polymers. *Macromolecules* 36:1505–1513
- Menghetti S, Alderighi M, Galli G, Tantussi F, Morandini M, Fuso F, Allegrini M (2012) All-optical pulsed writing in azobenzene copolymer films in the sub-millisecond regime. *J Mater Chem* 22:14510–14517
- Meuer S, Braun L, Zentel R (2008) Solubilisation of multi walled carbon nanotubes by α -pyrene functionalised PMMA and their liquid crystalline self-organisation. *Chem Commun* 27:3166–3168
- Moad G, Rizzardo E, Thang SH (2008) Toward living radical polymerization. *Acc Chem Res* 41:1133–1142
- Moad G, Rizzardo E, Thang SH (2009) Living radical polymerization by the RAFT process—a second update. *Aust J Chem* 62:1402–1472
- Moad G, Rizzardo E, Thang SH (2012) Living radical polymerization by the RAFT process—a third update. *Aust J Chem* 65:985–1076
- Morikawa Y, Kondo T, Nagano S, Seki T (2007) Photoinduced 3D ordering and patterning of microphase-separated nanostructure in polystyrene-based block copolymer. *Chem Mater* 19:1540–1542
- Nagano S, Koizuka Y, Murase T, Sano M, Shinohara Y, Amemiya Y, Seki T (2012) Synergy effect on morphology switching: real-time observation of photo-orientation of microphase separation in a block copolymer. *Angew Chem Int Ed* 51:5884–5888

- Natansohn A, Rochon P (1999) Photoinduced motions in azobenzene-based amorphous polymers. Possible photonic devices. *Adv Mater* 11:1387–1391
- Natansohn A, Rochon P (2002) Photoinduced motions in azo-containing polymers. *Chem Rev* 102:4139–4176
- Newkome GR, Yao Z, Baker GR, Gupta VK (1985) Micelles. Part 1. Cascade molecules: a new approach to micelles. A [27]-arborol. *J Org Chem* 50:2003–2004
- Öge T, Zentel R (1996) Manipulation of the ferroelectricity in LC polymers via photomechanical isomerization of azobenzene moieties. *Macromol Chem Phys* 197:1805–1813
- Oliveira ON, Dos Santos DS, Balogh DT, Zucolotto V, Mendonca CR (2005) Optical storage and surface-relief gratings in azobenzene-containing nanostructured films. *Adv Colloid Interface Sci* 116:179–192
- Otmakhova OA, Kuptsov SA, Talroze RV, Patten TE (2003) Preparation of discotic liquid crystal/amorphous block copolymers and evidence for microphase separated amorphous/LC structure. *Macromolecules* 36:3432–3435
- Otsu T, Matsumoto A (1998) Controlled synthesis of polymers using the iniferter technique: developments in living radical polymerization. *Adv Polym Sci* 136:75–137
- Pal SK, Kumar S (2008) Novel triphenylene-based ionic discotic liquid crystalline polymers. *Liq Cryst* 35:381–384
- Pal SK, Setia S, Avinash BS, Kumar S (2013) Triphenylene-based discotic liquid crystals: recent advances. *Liq Cryst* 40:1769–1816
- Patton DL, Taranekar P, Fulghum T, Advincula R (2008) Electrochemically active dendritic-linear block copolymers via RAFT polymerization: synthesis, characterization, and electrodeposition properties. *Macromolecules* 41:6703–6713
- Percec V, Tomazos D (1992) Molecular engineering of side-chain liquid-crystalline polymers by living cationic polymerization. *Adv Mater* 4:548–561
- Petr M, Hammond PT (2011) Room temperature rapid photoresponsive azobenzene side chain liquid crystal polymer. *Macromolecules* 44:8880–8885
- Reck B, Ringsdorf H (1985) Combined liquid crystalline polymers: mesogens in the main chain and as side groups. *Makromol Chem Rapid Commun* 6:291–299
- Reddy RA, Tschierske C (2006) Bent-core liquid crystals: polar order, superstructural chirality and spontaneous desymmetrisation in soft matter systems. *J Mater Chem* 16:907–961
- Ringsdorf H, Wüstefeld R, Zerta E, Ebert M, Wendorff JH (1989) Induction of liquid crystalline phases: formation of discotic systems by doping amorphous polymers with electron acceptors. *Angew Chem Int Ed* 28:914–918
- Rosen BM, Wilson CJ, Wilson DA, Peterca M, Imam MR, Percec V (2009) Dendron-mediated self-assembly, disassembly, and self-organization of complex systems. *Chem Rev* 109:6275–6540
- Rosler A, Vandermeulen GWM, Klok H (2001) Advanced drug delivery devices via self-assembly of amphiphilic block copolymers. *Adv Drug Deliv Rev* 53:95–108
- Royes J, Rebolé J, Custardoy L, Gimeno N, Oriol L, Tejedor RM, Piñol M (2012) Preparation of side-chain liquid crystalline azopolymers by CuAAC postfunctionalization using bifunctional azides: induction of chirality using circularly polarized light. *J Polym Sci A Polym Chem* 50:1579–1590
- Scheerder J, Marcelis A, Achten R, Sudhölter EJ (2000) Synthesis and thermotropic properties of novel side-chain dimer liquid crystalline polymers. *Macromol Chem Phys* 201:1303–1310
- Schrock RR (1990) Living ring-opening metathesis polymerization catalyzed by well-characterized transition-metal alkylidene complexes. *Acc Chem Res* 23:158–165
- Semsarilar M, Sébastien P (2010) ‘Green’ reversible addition-fragmentation chain-transfer (RAFT) polymerization. *Nat Chem* 2:811–820
- Sergeyev S, Pisula W, Geerts YH (2007) Discotic liquid crystals: a new generation of organic semiconductors. *Chem Soc Rev* 36:1902–1929
- Shen G, Xue G, Cai J, Zou G, Li Y, Zhang Q (2013) Photo-induced reversible uniform to Janus shape change of vesicles composed of PNIPAM-b-PazPy2. *Soft Matter* 9:2512–2517

- Shi Z, Lu H, Chen Z, Cheng R, Chen D (2012a) Rational design, syntheses, characterization and solution behavior of amphiphilic azobenzene-containing linear-dendritic block copolymers. *Polymer* 53:359–369
- Shi Z, Chen D, Lu H, Wu B, Ma J, Cheng R, Fang J, Chen X (2012b) Self-assembled hierarchical structure evolution of azobenzene-containing linear-dendritic liquid crystalline block copolymers. *Soft Matter* 8:6174–6184
- Shibaev VP, Kostromin SG, Plate NA (1982) Thermotropic liquid-crystalline polymers—VI: comb-like liquid-crystalline polymers of the smectic and nematic types with cyanobiphenyl groups in the side-chains. *Eur Polym J* 18:651–659
- Stamenović MM, Espeel P, Baba E, Yamamoto T, Tezuka Y, Du Prez FE (2013) Straightforward synthesis of functionalized cyclic polymers in high yield via RAFT and thiolactone–disulfide chemistry. *Polym Chem* 4:184–193
- Stenzel MH, Davis TP (2002) Star polymer synthesis using trithiocarbonate functional β -cyclodextrin cores (reversible addition-fragmentation chain-transfer polymerization). *J Polym Sci A Polym Chem* 40:4498–4512
- Stillings C, Pettau R, Wendorff JH, Schmidt HW, Kreger K (2010) Lamellar nanoconfinement effects in discotic liquid crystalline block copolymers. *Macromol Chem Phys* 211:250–258
- Su W, Luo Y, Yan Q, Wu S, Han K, Zhang Q, Gu Y, Li Y (2007) Photoinduced fusion of microvesicles self-assembled from azobenzene-containing amphiphilic diblock copolymers. *Macromol Rapid Commun* 28:1251–1256
- Sun B, Zhu X, Zhu J, Cheng Z, Zhang Z (2007) A novel synthetic method for well-defined polymers containing benzotriazole and diazobenzene chromophores. *Macromol Chem Phys* 208:1101–1109
- Szwarc M, Levy M, Milkovich R (1956) Polymerization initiated by electron transfer to monomer. A new method of formation of block polymers I. *J Am Chem Soc* 78:2656–2657
- Tahar-Djebbar I, Nekelson F, Heinrich B, Donnio B, Guillon D, Kreher D, Mathevet F, Attias A (2011) Lamello-columnar mesophase formation in a side-chain liquid crystal π -conjugated polymer architecture. *Chem Mater* 23:4653–4656
- Talroze RV, Otmakhova OA, Koval MA, Kuptsov SA, Platé NA, Finkelmann H (2000) Acrylate based polymers and networks containing triphenylene groups: synthesis and structures. *Macromol Chem Phys* 201:877–881
- Tang X, Gao L, Fan X, Zhou Q (2007a) ABA-type amphiphilic triblock copolymers containing p-ethoxy azobenzene via atom transfer radical polymerization: synthesis, characterization, and properties. *J Polym Sci A Polym Chem* 45:2225–2234
- Tang X, Gao L, Fan X, Zhou Q (2007b) Effect of the terminal substituent of azobenzene on the properties of ABA triblock copolymers via atom transfer radical polymerization. *J Polym Sci A Polym Chem* 45:5190–5198
- Thünemann AF, Ruppelt D, Ito S, Mullen K (1999) Supramolecular architecture of a functionalized hexabenzocoronene and its complex with polyethyleneimine. *J Mater Chem* 9:1055–1057
- Thünemann AF, Kubowicz S, Burger C, Watson MD, Tchebotareva N, Muellen K (2003) A-helical-within-discotic columnar structures of a complex between poly(ethylene oxide)-block-poly(L-lysine) and a hexa-peri-hexabenzocoronene. *J Am Chem Soc* 125:352–356
- Tian Y, Watanabe K, Kong X, Abe J, Iyoda T (2002) Synthesis, nanostructures, and functionality of amphiphilic liquid crystalline block copolymers with azobenzene moieties. *Macromolecules* 35:3739–3747
- Tomalia DA, Baker H, Dewald J, Hall M, Kallos G, Martin S, Roeck J, Ryder J, Smith P (1985) A new class of polymers: starburst-dendritic macromolecules. *Polym J* 17:117–132
- Tomatsu I, Hashidzume A, Harada A (2005) Photoresponsive hydrogel system using molecular recognition of α -cyclodextrin. *Macromolecules* 38:5223–5227
- Trimmel G, Riegler S, Fuchs G, Slugovc C, Stelzer F (2005) Liquid crystalline polymers by metathesis polymerization. *Adv Polym Sci* 176:43–87

- Van der Pol JF, Neeleman E, Nolte RJ, Zwikker JW, Drenth W (1989) Asymmetrically substituted liquid-crystalline phthalocyanines and side-chain polymers derived from them. *Die Makromol Chem* 190:2727–2745
- Vapaavuori J, Valtavirta V, Alasaarela T, Mamiya J, Priimagi A, Shishido A, Kaivola M (2011) Efficient surface structuring and photoalignment of supramolecular polymer–azobenzene complexes through rational chromophore design. *J Mater Chem* 21:15437–15441
- Viswanathan NK, Kim DY, Bian S, Williams J, Liu W, Li L, Samuelson L, Kumar J, Tripathy SK (1999) Surface relief structures on azo polymer films. *J Mater Chem* 9:1941–1955
- Voigt-Martin IG, Simon P, Bauer S, Ringsdorf H (1995) Structure and defects in sanidic liquid crystalline polymers. 1. *Macromolecules* 28:236–242
- Wang J, Matyjaszewski K (1995) Controlled/"living" radical polymerization. Atom transfer radical polymerization in the presence of transition-metal complexes. *J Am Chem Soc* 117:5614–5615
- Wang R, Wang Z (2010) Theory of side-chain liquid crystal polymers: bulk behavior and chain conformation. *Macromolecules* 43:10096–10106
- Wang D, Wang X (2013) Amphiphilic azo polymers: molecular engineering, self-assembly and photoresponsive properties. *Prog Polym Sci* 38(2):271–301
- Wang X, Zhou Q (2004) *Liquid crystalline polymers*. World Scientific, Singapore
- Wang X, Kumar J, Tripathy SK, Li L, Chen J, Marturunkakul S (1997a) Epoxy-based nonlinear optical polymers from post azo coupling reaction. *Macromolecules* 30:219–225
- Wang X, Chen J, Marturunkakul S, Li L, Kumar J, Tripathy SK (1997b) Epoxy-based nonlinear optical polymers functionalized with tricyanovinyl chromophores. *Chem Mater* 9:45–50
- Wang D, Ye G, Wang X (2007) Synthesis of aminoazobenzene-containing diblock copolymer and photoinduced deformation behavior of its micelle-like aggregates. *Macromol Rapid Commun* 28:2237–2243
- Wang D, Liu J, Ye G, Wang X (2009) Amphiphilic block copolymers bearing strong push–pull azo chromophores: synthesis, micelle formation and photoinduced shape deformation. *Polymer* 50:418–427
- Wang L, Li K, Lin H (2010) Synthesis and characterization of side-chain liquid-crystalline block-copolymers containing laterally attached photoluminescent quinquenphenyl units via ATRP. *Polymer* 51:75–83
- Wang Q, Yang C, Xie H, Wang X, Zhang H (2010) Effect of mesogenic density on liquid-crystalline behaviours of polymethacrylates bearing azobenzene mesogen. *Liq Cryst* 37:435–443
- Wang S, Shen Q, Nawaz MH, Zhang W (2013) Photocontrolled reversible supramolecular assemblies of a diblock azo-copolymer based on β -cyclodextrin–azo host–guest inclusion complexation. *Polym Chem* 4:2151–2157
- Weck M, Mohr B, Maughon BR, Grubbs RH (1997) Synthesis of discotic columnar side-chain liquid crystalline polymers by ring-opening metathesis polymerization (POMP). *Macromolecules* 30:6430–6437
- Werth M, Spiess HW (1993) The role of the spacer in discotic polymers. *Makromol Chem Rapid Commun* 14:329–338
- Wu S, Wang L, Kroeger A, Wu Y, Zhang Q, Bubeck C (2011) Block copolymers of PS-b-PEO co-assembled with azobenzene-containing homopolymers and their photoresponsive properties. *Soft Matter* 7:11535–11545
- Wu B, Mu B, Wang S, Duan J, Fang J, Cheng R, Chen D (2013) Triphenylene-based side chain liquid crystalline block copolymers containing a PEG block: controlled synthesis, microphase structures evolution and their interplay with discotic mesogenic orders. *Macromolecules* 46:2916–2929
- Wurm F, Frey H (2011) Linear–dendritic block copolymers: the state of the art and exciting perspectives. *Prog Polym Sci* 36:1–52
- Xia Y, Verduzco R, Grubbs RH, Kornfield JA (2008) Well-defined liquid crystal gels from telechelic polymers. *J Am Chem Soc* 130:1735–1740

- Xiang Y, Xue X, Zhu J, Zhang Z, Zhang W, Zhou N, Zhu X (2010) Fluorescence behavior of an azobenzene-containing amphiphilic diblock copolymer. *Polym Chem* 1:1453–1458
- Xie H, Liu Y, Zhong G, Zhang H, Chen E, Zhou Q (2009) Design, synthesis, and multiple hierarchical ordering of a novel side-chain liquid crystalline-rod diblock copolymer. *Macromolecules* 42:8774–8780
- Xing C, Lam JW, Zhao K, Tang BZ (2008) Synthesis and liquid crystalline properties of poly (1-alkyne)s carrying triphenylene discogens. *J Polym Sci A Polym Chem* 46:2960–2974
- Yan B, Tong X, Ayotte P, Zhao Y (2011) Light-responsive block copolymer vesicles based on a photo-softening effect. *Soft Matter* 7:10001–10009
- Yan Q, Xin Y, Zhou R, Yin Y, Yuan J (2011) Light-controlled smart nanotubes based on the orthogonal assembly of two homopolymers. *Chem Commun* 47:9594–9596
- Yang C, Wang Q, Xie H, Zhong G, Zhang H (2010) Synthesis and characterisation of polymethacrylates containing para-, meta- and ortho-monosubstituted azobenzene moieties in the side chain. *Liq Cryst* 37:1339–1346
- Yesodha SK, Sadasivan Pillai CK, Tsutsumi N (2004) Stable polymeric materials for nonlinear optics: a review based on azobenzene systems. *Prog Polym Sci* 29:45–74
- Yu H (2014) Recent advances in photoresponsive liquid-crystalline polymers containing azobenzene chromophores. *J Mater Chem C* 2:3047–3054
- Yu D, Vladimirov N, Fréchet JM (1999) MALDI-TOF in the characterizations of dendritic-linear block copolymers and stars. *Macromolecules* 32:5186–5192
- Yu WH, Kang ET, Neoh KG (2004) Functionalization of hydrogen-terminated Si(100) substrate by surface-initiated RAFT polymerization of 4-vinylbenzyl chloride and subsequent derivatization for photoinduced metallization. *Ind Eng Chem Res* 43:5194–5202
- Yu H, Iyoda T, Ikeda T (2006a) Photoinduced alignment of nanocylinders by supramolecular cooperative motions. *J Am Chem Soc* 128:11010–11011
- Yu H, Li J, Ikeda T, Iyoda T (2006b) Macroscopic parallel nanocylinder array fabrication using a simple rubbing technique. *Adv Mater* 18:2213–2215
- Yu H, Asaoka S, Shishido A, Iyoda T, Ikeda T (2007) Photoinduced nanoscale cooperative motion in a well-defined triblock copolymer. *Small* 3:768–771
- Yu Z, Lam JW, Zhao K, Zhu C, Yang S, Lin J, Li BS, Liu J, Chen E, Tang BZ (2013) Mesogen jacketed liquid crystalline polyacetylene containing triphenylene discogen: synthesis and phase structure. *Polym Chem* 4:996–1005
- Zeng D, Tahar-Djebbar I, Xiao Y, Kameche F, Kayunkid N, Brinkmann M, Guillon D, Heinrich B, Donnio B, Ivanov DA (2014) Intertwined lamello-columnar coassemblies in liquid-crystalline side-chain π -conjugated polymers: toward a new class of nanostructured supramolecular organic semiconductors. *Macromolecules* 47:1715–1731
- Zhang Y, Zhang W, Chen X, Cheng Z, Wu J, Zhu J, Zhu X (2008) Synthesis of novel three-arm star azo side-chain liquid crystalline polymer via ATRP and photoinduced surface relief gratings. *J Polym Sci A Polym Chem* 46:777–789
- Zhang X, Boissé S, Bui C, Albouy P, Brûlet A, Li M, Rieger J, Charleux B (2012) Amphiphilic liquid-crystal block copolymer nanofibers via RAFT-mediated dispersion polymerization. *Soft Matter* 8:1130–1141
- Zhao Y, He J (2009) Azobenzene-containing block copolymers: the interplay of light and morphology enables new functions. *Soft Matter* 5:2686–2693
- Zhao Y, Ikeda T (2009) Smart light-responsive materials: azobenzene-containing polymers and liquid crystals. John Wiley & Sons, New Jersey
- Zhao Y, Qi B, Tong X, Zhao Y (2008) Synthesis of double side-chain liquid crystalline block copolymers using RAFT polymerization and the orientational cooperative effect. *Macromolecules* 41:3823–3831
- Zhou M, Han CD (2005) Synthesis and characterization of a combined main-chain/side-chain liquid-crystalline polymer exhibiting both thermotropic and lyotropic characteristics and its lyotropic phase behavior. *Macromolecules* 38:9602–9609

- Zhou QF, Li HM, Feng XD (1987) Synthesis of liquid-crystalline polyacrylates with laterally substituted mesogens. *Macromolecules* 20:233–234
- Zhou Y, Ahn S, Lakhman RK, Gopinadhan M, Osuji CO, Kasi RM (2011) Tailoring crystallization behavior of PEO-based liquid crystalline block copolymers through variation in liquid crystalline content. *Macromolecules* 44:3924–3934
- Zhu Y, Wang X (2013) Synthesis and photoresponsive properties of two liquid crystalline polymers bearing branched azobenzene-containing side chains. *Polym Chem* 4:5108–5118
- Zhu Y, Guan X, Shen Z, Fan X, Zhou Q (2012) Competition and promotion between two different liquid-crystalline building blocks: mesogen-jacketed liquid-crystalline polymers and triphenylene discotic liquid crystals. *Macromolecules* 45:3346–3355
- Zhu YF, Tian HJ, Wu HW, Hao DZ, Zhou Y, Shen Z, Zou DC, Sun PC, Fan XH, Zhou QF (2014) Ordered nanostructures at two different length scales mediated by temperature: a triphenylene-containing mesogen-jacketed liquid crystalline polymer with a long spacer. *J Polym Sci A Polym Chem* 52:295–304
- Zou G, Jiang H, Zhang Q, Kohn H, Manaka T, Iwamoto M (2010) Chiroptical switch based on azobenzene-substituted polydiacetylene 1D films under thermal and photic stimuli. *J Mater Chem* 20:285–291

Chapter 6

Effects of Hydrogen-Bonding on the Liquid Crystalline Properties of Dendritic Polymers

Michael Arkas and Aggeliki Papavasiliou

Dendritic polymers have shape reminiscent of the braches of a tree. They may be symmetrical dendrimers, symmetrical fragments thereof called dendrons or their non symmetrical analogues, the hyperbranched polymers. All classes possess a nucleus or core, the inner branches which often form cavities and the external branches which are functionalized with characteristic groups. It is evident that in most cases the chemical environment of the core, the branches and the external groups is completely different. This anisotropy is among the most interesting properties of the dendritic polymers and makes them ideal candidates for formation of liquid crystalline phases. Dendritic mesogens or dendromesogens consist an interesting separate class of liquid crystalline polymers having different properties and behaviour from both main-chain and side chain liquid crystalline polymers (Matheus et al. 1998; Emrick and Fréchet 1999; Fischer and Vögtle 1999; Moore 1999; Schlenk and Frey 1999; Adronov and Frechet 2000; Smith and Diederich 2000; Grayson and Fréchet 2001; Ponomarenco et al. 2001; Tschierske 2001, 2002; Diele 2002; Guillon and Deschenaux 2002; Caminade et al. 2003; Lee et al. 2005).

An investigation of the mesomorphic properties of a very large number of dendritic polymers and a detailed characterization of their multiple liquid crystalline phases deriving from their diversified molecular architecture is developing as a consequence of the overall increasing scientific research for the prospected applications of these macromolecules during the previous two decades (Inoue 2000; Sun et al. 2001; Bergenudd et al. 2002; Burkinshaw et al. 2002; Arkas et al. 2003, 2005a, b, 2006, 2010; Kolhe et al. 2003; Seiler et al. 2003; Allabashi et al. 2007; Tsetsekou et al. 2008; Arkas and Tsiourvas 2009; Tsiourvas et al. 2011, 2013a, b; Arkas 2013). In order to build dendritic polymers exhibiting liquid crystal phases, a

M. Arkas • A. Papavasiliou (✉)
Institute of Advanced Materials, Physicochemical Processes, Nanotechnology & Microsystems, NCSR Demokritos, Patriarchou Gregoriou Str., Aghia Paraskevi, Attiki 15310, Greece
e-mail: m.arkas@inn.demokritos.gr

variety of strategies have been employed. The most typical method for the induction of mesophases is the functionalization of dendritic polymers in order to self assemble preferably into cylindrical (Percec et al. 1992, 1993a, b, c, 1994, 1995, 1996a, b, 1998a, c; Johansson et al. 1994, 1996; Percec and Schlueter 1997; Pesak and Moore 1997; Brewis and Clarkson 1998; Meier and Lehmann 1998; Prokhorova et al. 1998a, b; Suárez et al. 1998; Prokhorova et al. 1999) or spherical (Balagurusamy et al. 1997; Hudson et al. 1997; Percec et al. 1998b, c, 2008, 2009; Yin et al. 1998) shapes. The intrinsic property of dendritic macromolecules to form inner part (core) and an outer external surface with different properties mainly in terms of polarity and flexibility leads to microphase separation which is regarded as the main factor inducing the formation of these assemblies and governing their organization.

Inter and intra molecular hydrogen bonds may alter drastically the shape of dendritic molecules and/or the functionalization of the external groups. In addition they are reported to contribute to the rigidity of a particular part of the mesogenic molecules, most often its central core, resulting in more ordered and more thermally stable liquid crystalline properties with wider temperature range and higher transition temperatures (Donnio et al. 2002; Gehringer et al. 2005). By being weaker and by having different nature from the traditional conventional covalent bonding, hydrogen bonding is directional more versatile, reversible and allows very important biological processes such as molecular recognition. In addition by being dynamic in nature, hydrogen bonding presents a feasible way to prepare functional materials reacting to small changes of the external environment. In this context, the role of hydrogen bonding on microphase separation and mesophase formation of dendritic polymers became a very interesting field of research.

6.1 Dendromesogens Based on Hydrogen Bonds of the External Groups

The simplest method of generating liquid crystalline character via hydrogen bonding in dendritic polymers is the modification of the properties of the external surface. This can be achieved by various methods. The basic strategy consists of two stages (a) chemical modification of the external groups in order to render them capable of forming hydrogen bonds by certain complementary molecules having specific shape (rigid rod, disk) or properties (solubility) capable of inducing liquid crystalline character called mesogens and (b) interact the modified groups with the mesogens bearing the complementary moieties in the melt or in specific solvents in order to form supramolecular complexes.

6.1.1 Hydrogen Bonding with Rigid Rod Shaped Molecules

Felekis et al. (2005) functionalized diaminobutane poly(propyleneimine) dendrimers (DAB) of second to fifth generations with pyridyl moieties (Fig. 6.1a). Subsequent interaction of these modified dendrimers with 3-cholesteryloxycarbonylpropanoic acid through slow evaporation of DMF solutions formed supramolecular hydrogen-bonded complexes via intermolecular hydrogen bonding between the nitrogen of the pyridine ring and the hydroxyl group of the carboxylic acid exhibiting smectic A phases over a relatively broad temperature range.

In the same context Xu et al. (2008) starting from a series of cyclotriphosphazenes that were modified by stilbazolyl, Schiff bases and azopyridyl-type mesogenic groups, as central dendrimeric cores, functionalized them with mono, bis, and tris(alkyloxy)benzoic acids via hydrogen bonds by mixing them in chloroform (Fig. 6.1b). While the rigid core precursors did not exhibit liquid crystalline character most of them, when interacted with six monoalkyloxybenzoic acid molecules via intermolecular hydrogen bonding formed smectic or nematic mesophases. Weak single hydrogen bonds were proven strong enough to direct the star-shaped supramolecular assembly and induce liquid crystallinity.

Based on the same principle Didehban et al. (2009) obtained nematic and smectic liquid crystals from three generations of dendritic 5-hydroxyisophthalic acids when they reacted in the melt with an alkoxy-stilbazole bearing a pyridyl group due to the hydrogen bond interactions between the carboxylic acid of the dendron and the nitrogen of the pyridyl group (Fig. 6.2a).

6.1.2 Hydrogen Bonding of the Core with Dendrons

The basic strategy described in the previous chapter can be reversed. A dendritic core can be used as proton acceptor. For example trans-4-hexyloxy-4'-stilbazole a molecule with two pyridyl moieties by formation of hydrogen bonds with the carboxyl groups of two 3,5-dihydroxybenzoic acid dendrons which acted as proton donors exhibited nematic and smectic mesophases (Fig. 6.2b, Didehban et al. 2010). Using the same method and choosing tricarboxylic triphenylene bearing short pentyloxy chains as core and monopyridyl dendrons bearing long dodecyloxy chains as branches connected via complementary hydrogen-bonds Ishihara et al. (2007) obtained supramolecular complexes exhibiting columnar hexagonal mesophase only when all the carboxyl groups could form hydrogen bonds i.e., at 1:3 molar stoichiometry. Another attempt with a functionalized triphenylene derivative i.e., fluoroalkyl side chain-substituted 2,6,10-tris-carboxymethoxy-3,7,11-tris(4,4,5,5,6,6,7,7,7-nonafluoroheptyloxy)triphenylene provided again columnar hexagonal liquid crystal when this core compound formed a 1:3 complex with the second generation dendron 3,5-bis(3,4-bis-dodecyloxybenzyloxy)-N-pyridin-4-yl-benzamide through complementary hydrogen bonding (Ishihara et al 2014).

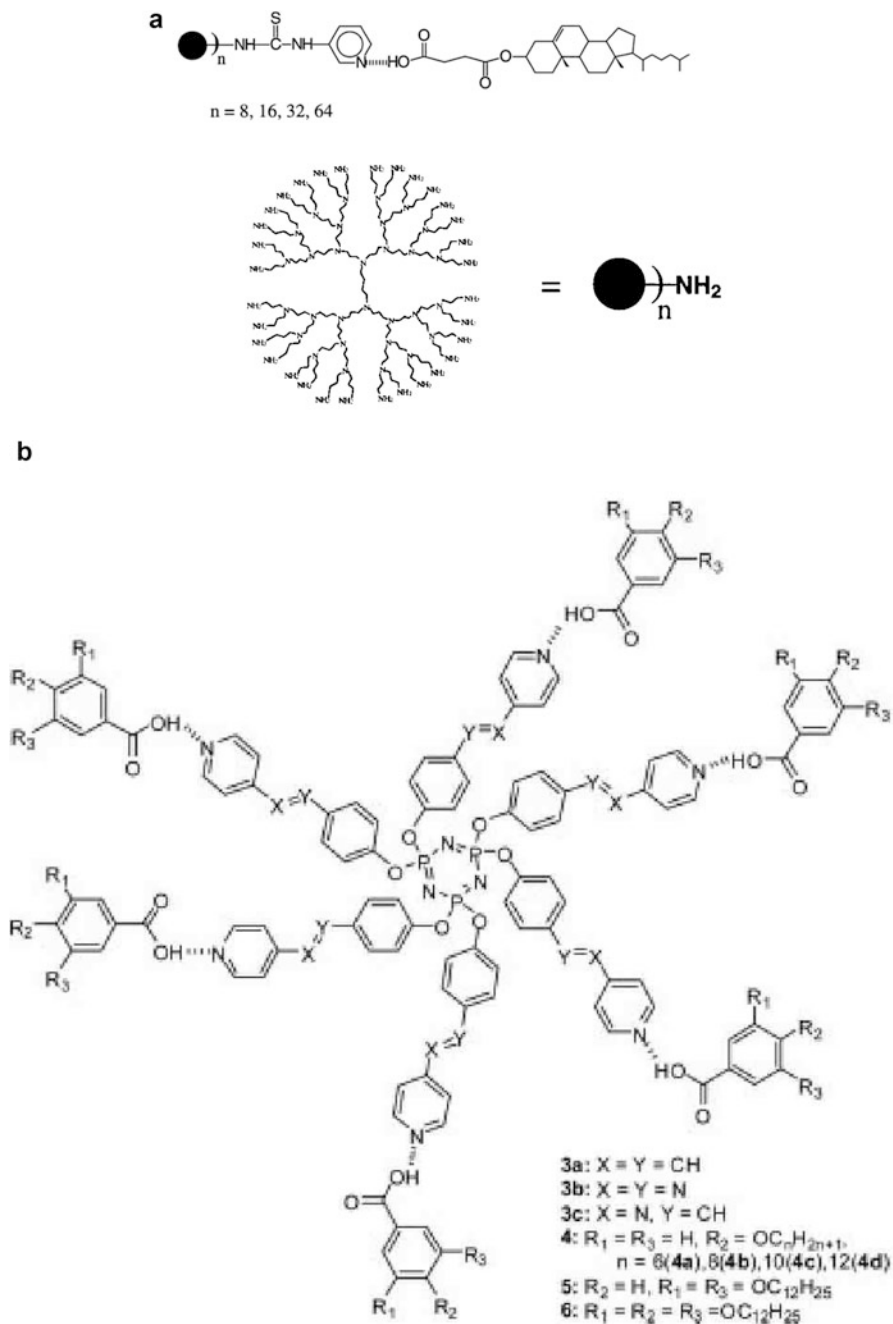


Fig. 6.1 (a) Diaminobutane poly(propyleneimine) dendrimers (DAB) of second to fifth generations functionalized with pyridyl moieties and their interaction with 3-cholesteryloxycarbonylpropanoic acid. (b) Cyclotriphosphazenes modified by stilbazolyl, Schiff bases and azopyridyl-type mesogenic groups, as central dendrimeric cores functionalized with mono, bis, and tris(alkyloxy)benzoic acids via hydrogen bonds

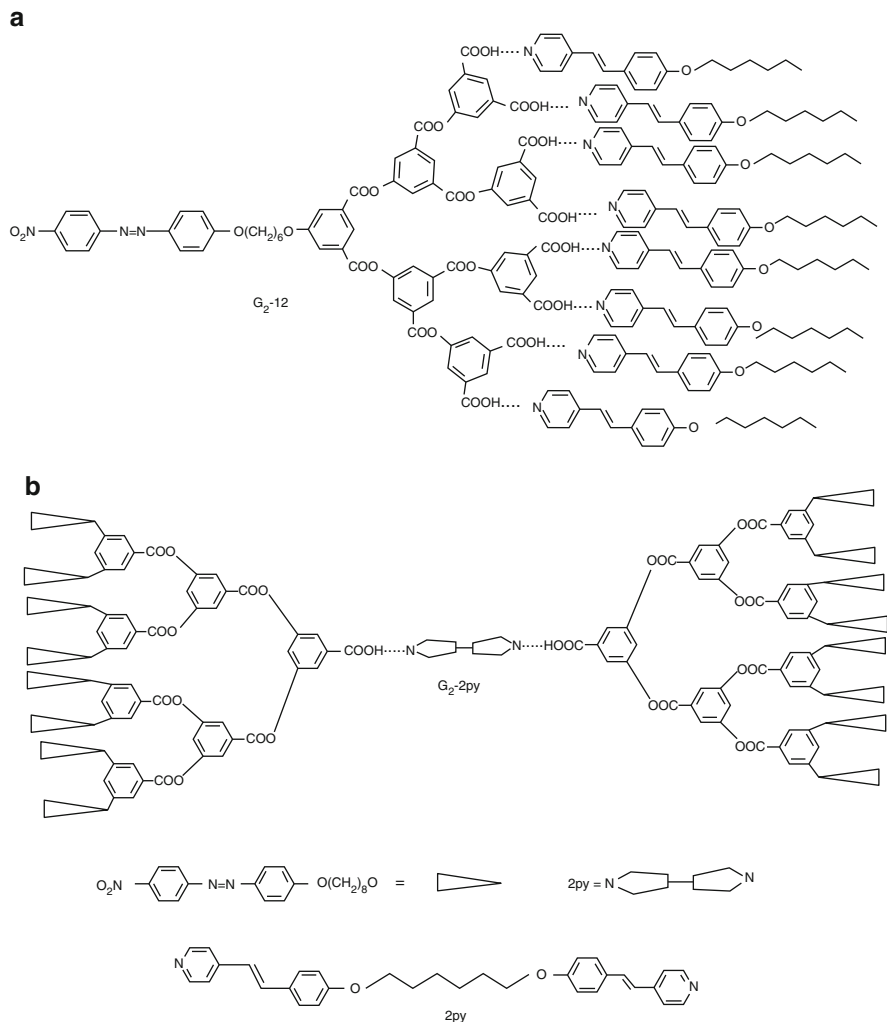


Fig. 6.2 (a) Hydrogen bonding between (a) dendritic 5-hydroxyisophthalic acids and alkoxy-stilbazoles bearing a pyridyl group. (b) trans-4-hexyloxy-4'-stilbazole bearing two pyridyl moieties with two 3,5-dihydroxybenzoic acid dendrons

Castelar et al. (2013) synthesized two families of supramolecular dendritic complexes. Using a triazine moiety as an electron-transporting central core they attached three peripheral dendrons of generations 1 and 2 derived from bis(hydroxymethyl)propionic acid by double hydrogen bonding of carboxylic acid groups with the amino groups and the aromatic nitrogens. The dendrons which were designed as hole-transporting moieties contained 5-[4-(4-butoxybenzoyloxy)phenoxy]pentanoic acid (family A) or cholesteryl hemisuccinate (family B) as promesogenic units. The supramolecular complexes exhibited nematic and smectic A phases.

6.1.3 Multiple Hydrogen Bonding and Molecular Recognition

Though one hydrogen bond between complementary moieties seems enough to induce supramolecular complexes exhibiting mesophases the development of liquid crystalline aggregates through multiple hydrogen bonding and molecular recognition presents particular interest since it refers to the complex biological structures encountered in nature rendering these superstructures useful models for understanding the rules governing the organization through hydrogen bonding in nature. One such example is the columnar hexagonal phase resulting by hydrogen-bonding interactions between a 3-pentyl benzotri(imidazole) core and benzoic acids bearing acryloxy substituted dodecyloxy chains (Lee et al. 2001). Analogous results have been obtained by Kraft et al. (2000) for alkoxy-substituted benzoic acids forming supramolecular hydrogen bonded complexes around a tribasic core

6.1.4 Hydrogen Bonding with Disk Shaped Molecules

Poly(propylene-imine) dendrimer is also reported to exhibit columnar mesophases when the external amino groups form hydrogen bonds with acid functionalized discotic molecules. Fitié et al. (2008) synthesized supramolecular complexes from Poly(propylene-imine) and (((3,5-bis((decylamino)carbonyl)benzoyl)amino)undecanoic acid) at various ratios. All the complexes self-assembled into well-ordered oblique columnar liquid crystalline superlattices. These mesomorphic structures derive from the combination of an orthogonal pattern of hydrogen bonds with ionic interactions in a perpendicular plane which confine the dendrimers in columns.

6.2 Induction and/or Stabilization of Mesomorphism Based on Intra and Intermolecular Bonds

In series of systematic comparative studies (Barberá et al. 1999, 2005; Marcos et al. 2001; Donnio et al. 2002, 2007) liquid crystalline polypropylene imine (DAB) and polyamidoamine (PAMAM) dendrimers functionalized by terminal calamitic promesogenic units that carried alkoxy chains (Fig. 6.3a), the mesophases observed by functionalized PAMAM dendritic polymers were thermodynamically more stable than those exhibited by analogous PPI dendrimers. This was attributed to the presence of intra and inter molecular hydrogen bonds between the amide groups present only in PAMAM and the consequent rigidification of the inner dendritic structures. Moreover it was reported that the alteration of some geometrical parameters such as the surface of the calamitic mesogens caused by the addition of a second or a third alkoxy chain which leads them to radial disposition, in synergy with the presence of intra- and intermolecular hydrogen bonds which results in the

stable aggregation of the central dendritic structure play a crucial role in the organization of the functionalized polymers into columnar hexagonal liquid crystalline phases instead of lamellar smectic A or C.

The same effect was observed in dendrimers with cyclotriphosphazene core and branches formed by polycatenar benzamide groups functionalized by dodecyloxy aliphatic chains (Barberá et al. 2006). IR measurements proved that the columnar mesophases observed over a range of temperatures derive from the stabilization of the stacking of the discotic structures by the intermolecular H-bonding of the benzamide groups.

Another example of liquid crystalline phase induction due the enhanced rigidity of the dendritic molecules attributed to hydrogen bonding is hyperbranched polyethylene imine functionalized with long aliphatic chains. These functionalized hyperbranched poly(ethylene imine) polymers exhibit columnar rectangular and lamellar (SmA and SmB) mesophases in contrast to their symmetric analogs i.e., propylene imine dendrimers. (Tsiourvas and Arkas 2013) This profound difference is attributed to the fact that the former due to their asymmetry possess secondary amino groups which reside not only close to the periphery but even near the core of the molecule. Since both secondary and primary amino groups are functionalized (alkylated) the subsequent creation of urea groups results in hydrogen bonding formation throughout the interior of the hyperbranched polymer. These hydrogen bonds enhance the rigidity of the inner part of the molecules and in synergy with the difference in polarity due to the polar character of the same urea groups lead to segregation between the rigid polar segments of the core and the flexible non polar segments of the aliphatic chains and thus to the induction of liquid crystalline properties. Analogous results have been obtained by Stebani and Lattermann (1995) (Fig. 6.3b) with smaller polyethylene imine symmetrical dendrimers where external amino groups of the first generation are functionalized by benzoyl groups substituted by two decyloxy chains. In this case microphase separation from the flexible non polar alkyl chains is achieved by the enhancement of the dendrimer polarity by amide groups and its rigidity by the formation of hydrogen bonds between the same. For this compound a spherulitic texture was recognized and was attributed to a columnar mesophase structure. Intramolecular H-bonding between the urea groups has also been reported to stabilize thermotropic mesophases with homeotropic orientation observed for poly(propylene imine) dendrimers modified peripherally with urea oligo(p-phenylene vinylene)s bearing a 3,4,5-tri(dodecyloxy)phenyl mesogenic units (Precup-Blaga et al. 2003) The increased temperature range of the liquid crystalline phases of the higher generation dendrimers was attributed to stronger hydrogen-bonding interactions due to the more dense-shell packing and the closer proximity of the urea groups.

H-bonding interactions deriving from a combination of different groups such as ureas and amides can also enhance the stability of the mesophases. Zhou et al. (2008) (Fig. 6.3c) confirmed that symmetrical dendritic trisureas such as cyanophenylazo tributyl and tridecyl-1,3,5-(benzene-1,3,5-triyl)tris-3-phenylureas mixed with symmetrical trisamide gelators such as N^1, N^3, N^5 -trioctadecylbenzene-1,3,5-tricarboxamide (G1) display liquid crystalline properties in the form of thermotropic liquid crystals and liquid crystalline gels. Both trisureas have lamellar

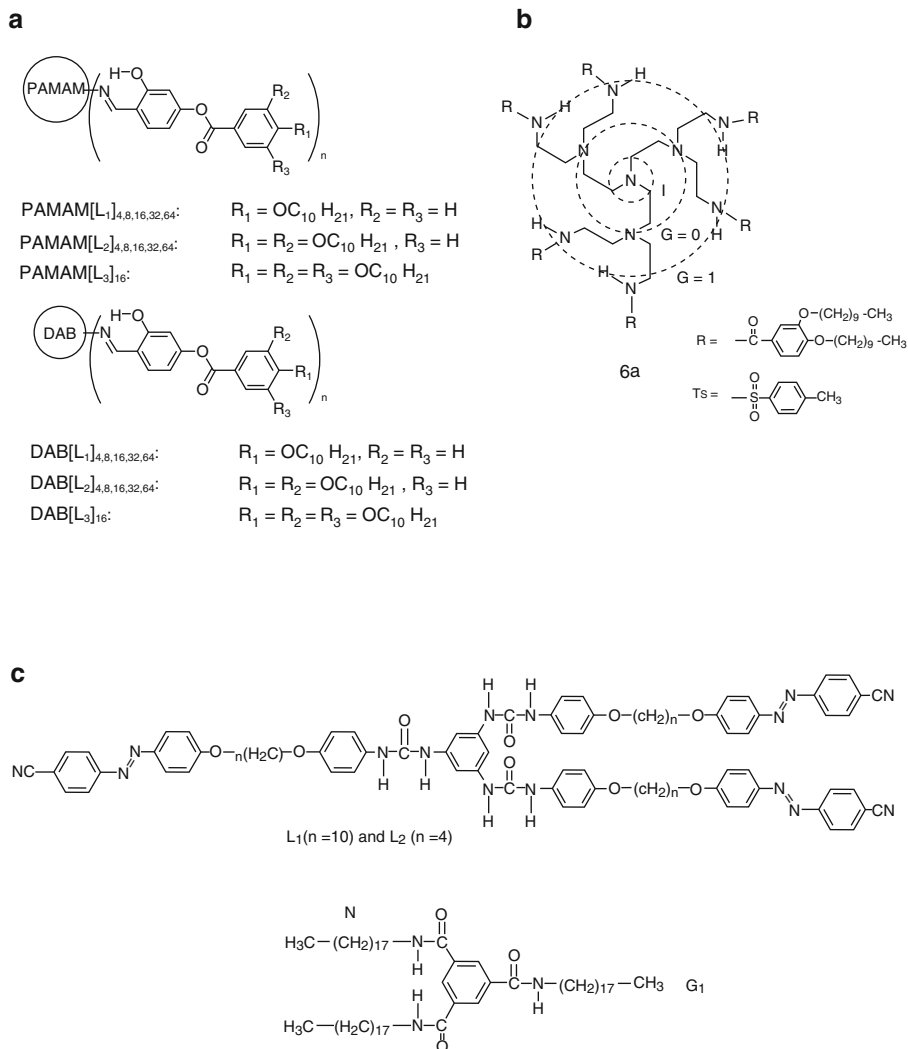


Fig. 6.3 (a) Polypropylene imine (DAB) and polyamidoamine (PAMAM) dendrimers functionalized by terminal calamitic promesogenic bearing chains. (b) Polyethylene imine symmetrical dendrimers where external amino groups of the first generation are functionalized by benzoyl groups substituted by two decyloxy chains. (c) Symmetrical dendritic trisureas cyanophenylazo tributyl and tridecyl-1,3,5-(benzene-1,3,5-triyl)tris-3-phenylureas (L₁ or L₂) and symmetrical trisamide gelator N¹,N³,N⁵-trioctadecylbenzene-1,3,5-tricarboxamide (G₁)

structures in high temperatures whereas their mixtures with the gelator exhibited columnar rectangular and hexagonal mesophases with thermal stability up to 240 °C. The role of the hydrogen bonds was ascertained by temperature dependent FTIR spectroscopy which revealed that the hydrogen bonding network between ureas and amides was much more organized than the respective urea and amide analogues.

Rigidification of the cores of dendritic molecules leading to the formation of non-tilted discotic columnar hexagonal mesophases has also been reported by Shu et al. (2013). Hydrazone molecules functionalized with flexible dendritic groups containing linear hexyloxy, octyloxy, and decyloxy chains, formed mesophases where the hydrazone discs were rigidified by intramolecular hydrogen bonds. In another example monodendrons consisting of *L*-alanine at their core and long alkyl chains at the periphery exhibited thermotropic columnar hexagonal and columnar rectangular liquid-crystalline phases stabilized by hydrogen-bonded clusters (Anokhin et al. 2012).

6.3 Intermolecular Hydrogen Bonds Defining the Shape of Mesomorphic Dendritic Molecules and the Organization of the Liquid Crystalline Phases

One of the most important works in this particular field has been performed by Takashi Kato and his group. Through a series of studies in dendritic polymers they managed to prove direct correlation between the hydrogen bonding patterns, the shapes of the molecules and the nature of liquid crystalline phases. Firstly they focused on the derivatives of folic acid, an important biologically active molecule. By increasing the length of the alkyl chains of the 2-(3,4-dialkoxyphenyl)ethyl derivatives and by inducing ion–dipolar interaction between the pterin ring and metal cations they managed to direct hydrogen-bonding network into forming dendritic disk-like aggregations of tetramers of pterin ring of folic acid resulting in hexagonal columnar and nematic columnar instead of lamellar mesophases (Kanie et al. 2001a, Fig. 6.4a). The same derivatives produced identical effect when they formed lyotropic mesophases in organic solvents. A change of the liquid crystalline phases from lamellar to columnar nematic has been observed in more hydrophobic solvents attributed to the change of the hydrogen bonding patterns from ribbon to disk (Kanie et al. 2001b). Furthermore when 2-(3,4-dialkoxyphenyl) ethyl moieties were replaced by respective dialkoxyoligo(glutamic acid) moieties (Fig. 6.4b) hexagonal columnar and *Pm3n* cubic LC phases were formed (Kato et al. 2004).

Moreover since the dialkoxyoligo(glutamic acid) derivatives possess three chiral centers they examined the possibility of chiral mesomorphic behavior. Indeed formation of chiral hexagonal columnar and *Pm3n* cubic liquid crystalline phases were observed in the presence of sodium triflate ($\text{NaOSO}_2\text{CF}_3$) in all three γ -Bis(*L*-glutamoyl) *N*-[N^{10} -(trifluoroacetyl)pteroyl] *L*-glutamic acid tetra{2-[3,4-di(alcyloxy)phenyl]ethyl} esters.

The tetra{2-[3,4-di(hexyloxy)phenyl]ethyl} compound together with its *D*-glutamoyl *D*-glutamic acid enantiomer and the *L*-glutamoyl *D*-glutamic acid diastereomer also exhibited respective thermotropic chiral *Pm3n* cubic and chiral hexagonal columnar mesophases (Kamikawa et al. 2005) and also lyotropic chiral

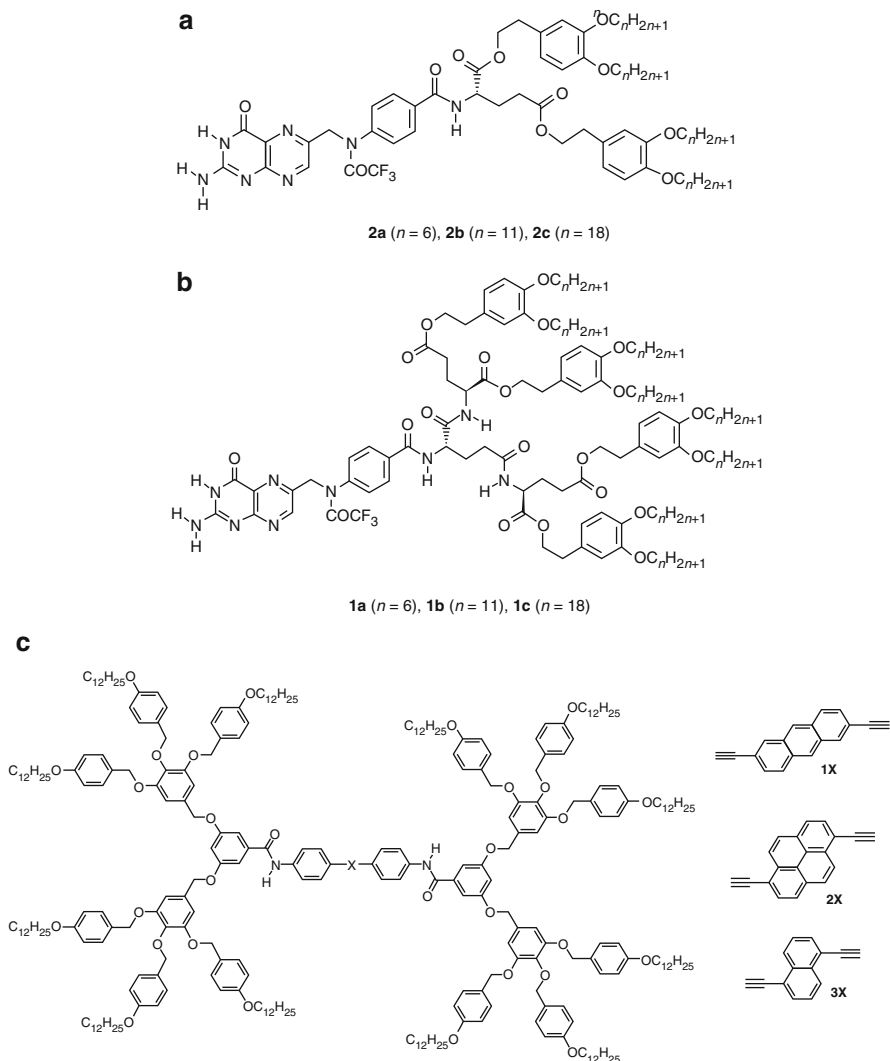


Fig. 6.4 (a) 2-(3,4-dialkoxyphenyl)ethyl and (b) dialkoxyoligo(glutamic acid) derivatives of folic acid. (c) Dendrimers from benzyloxy derivatives of pyrene anthracene and naphthalene functionalized by dodecyloxy chains

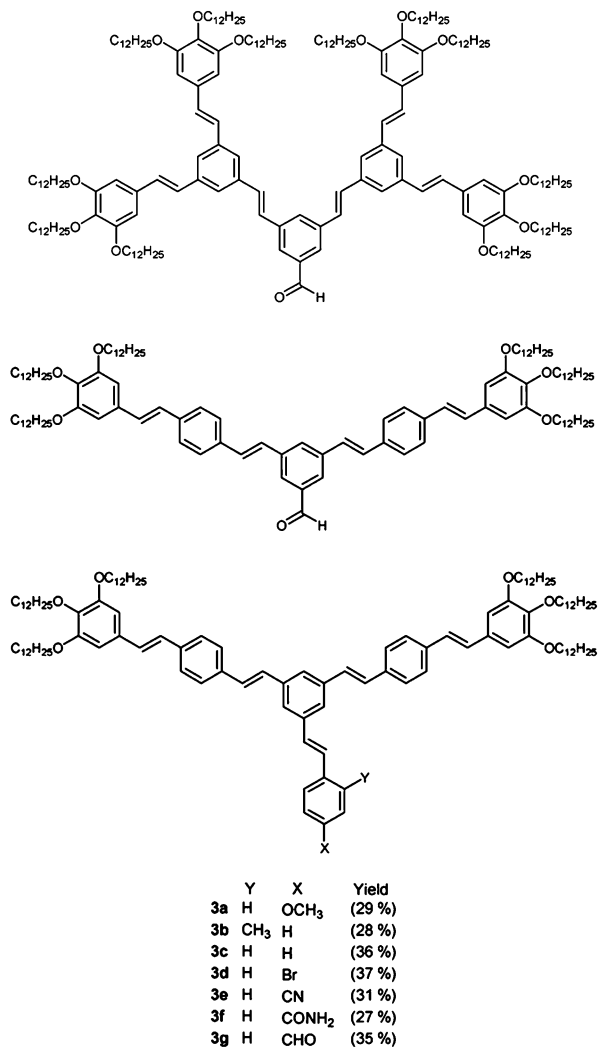
hexagonal columnar liquid crystalline phases (Kamikawa et al. 2004). More specifically the two enantiomers in polar chloroform in the presence of sodium triflate self-organize into the same chiral columnar assemblies but with reversed helicity. In this case the transfer of the chirality from the molecular level of the oligo (glutamate) parts to the supramolecular chirality was attributed to the cooperative ion–dipolar interactions and hydrogen bonds. Most impressively all three diastereomers in a lipophilic environment such as dodecane produced chiral assemblies

even in the absence of sodium triflate. In this case the chiral aggregates were formed solely through lipophilic interactions of the alkyl chains of the solvent with the smaller aliphatic chains of the dendritic tetramers resulting to the increase of the lipophilic fraction. This in turn, in cooperation with the hydrogen bonds, enhances microphase segregation resulting in the induction of chirality at the supramolecular aggregates without the presence of a metal ion.

In another example where materials with photoluminescent properties are concerned, the role of the intermolecular hydrogen bonds is not limited to the stabilization or even the formation of liquid crystalline phase but also induces a change in the self-assembled structures at a molecular level when shearing is applied (Yamane et al. 2012). Dendrimers from benzyloxy derivatives of pyrene (Fig. 6.4c) functionalized by dodecyloxy chains undergo a transition from a micellar $Pm3n$ cubic to a $P2/a$ columnar rectangular phase with subsequent change of the photoluminescence color from yellow to blue-green upon mechanical shearing (Sagara and Kato 2008). IR measurements indicated that in the cubic phase hydrogen bonds of the amide groups were weaker whereas in the columnar phase a downshift of the C=O groups revealed a stronger H-bonds network in a completely different pattern. Respective derivatives of anthracene (Fig. 6.4c) apart from piezochromic exhibit thermochromic properties too. On rapid cooling from the isotropic phase by putting the isotropic sample onto a metal substrate at room temperature exhibited a metastable $Pm3n$ cubic phase and yellow photoluminescence (Sagara et al. 2009). Conventional slow cooling i.e., up to 10 °C/min produced columnar rectangular phase with emission of blue light. The metastable cubic phase in turn can undergo transition to the stable columnar phase through heating or mechanical shearing. This behaviour was attributed to the differences in the hydrogen bond patterns. Longer intermolecular hydrogen bonds between the amide groups of adjacent molecules in combination with π - π stacking of the anthracene cores lead to segmented columnar structures and a cubic phase whereas stronger shorter, up to 5 Å, hydrogen bonds in a linear pattern result in the more ordered longer columns of the columnar rectangular phase. Analogous results are obtained when anthracene is replaced by naphthalene (Sagara and Kato 2011a, Fig. 6.4c) whereas mixtures 1:1 of two 9,10-bis(phenylethynyl)anthracene derivatives, each bearing different benzyloxy dendron functionalized by trimethyldodecyloxy aliphatic chains exhibit three mesophases with three different hydrogen patterns and a three-colored luminescence (Sagara and Kato 2011b). When the benzyloxy derivatives of pyrene were replaced by oligopeptides supramolecular chiral columnar liquid crystals are produced. The synergy intermolecular hydrogen bonding of the peptide bonds and electron donor-acceptor interactions is controlling supramolecular chirality (Kamikawa and Kato 2006).

Alteration between columnar hexagonal and cubic mesophases due to hydrogen bond interactions is also described by Lehmann and his co-workers (2005) for stilbenoid dendrons (Fig. 6.5) bearing long dodecyloxy chains at their periphery. Stable ordered cubic mesophase was observed only when the dendron possessed amide groups and thus was capable of intermolecular hydrogen bonding. Replacement of the amide functionality even with groups capable of other type of

Fig. 6.5 Stilbenoid dendrons bearing long dodecyloxy chains at their periphery



interactions such as dipole–dipole led to monotropic disordered columnar hexagonal phases.

In another example of mixtures of two similar dendritic polymers Percec et al. (2003) studied the self assembly of two benzamide derivatives i.e., N-[3,4,5-Tris(4'-dodecyloxybenzyloxy)phenyl]-3,4,5-tris(4'-dodecyloxybenzyloxy) benzamide which forms a columnar hexagonal mesophase and its polymethacrylate (Fig. 6.6a) which presents a columnar nematic phase with short-range hexagonal order, in different ratios. Again intermolecular hydrogen bonds form between amide groups which reside in the core of both dendritic compounds. In this way supramolecular columns deriving from the coassembly of these two dendritic building blocks

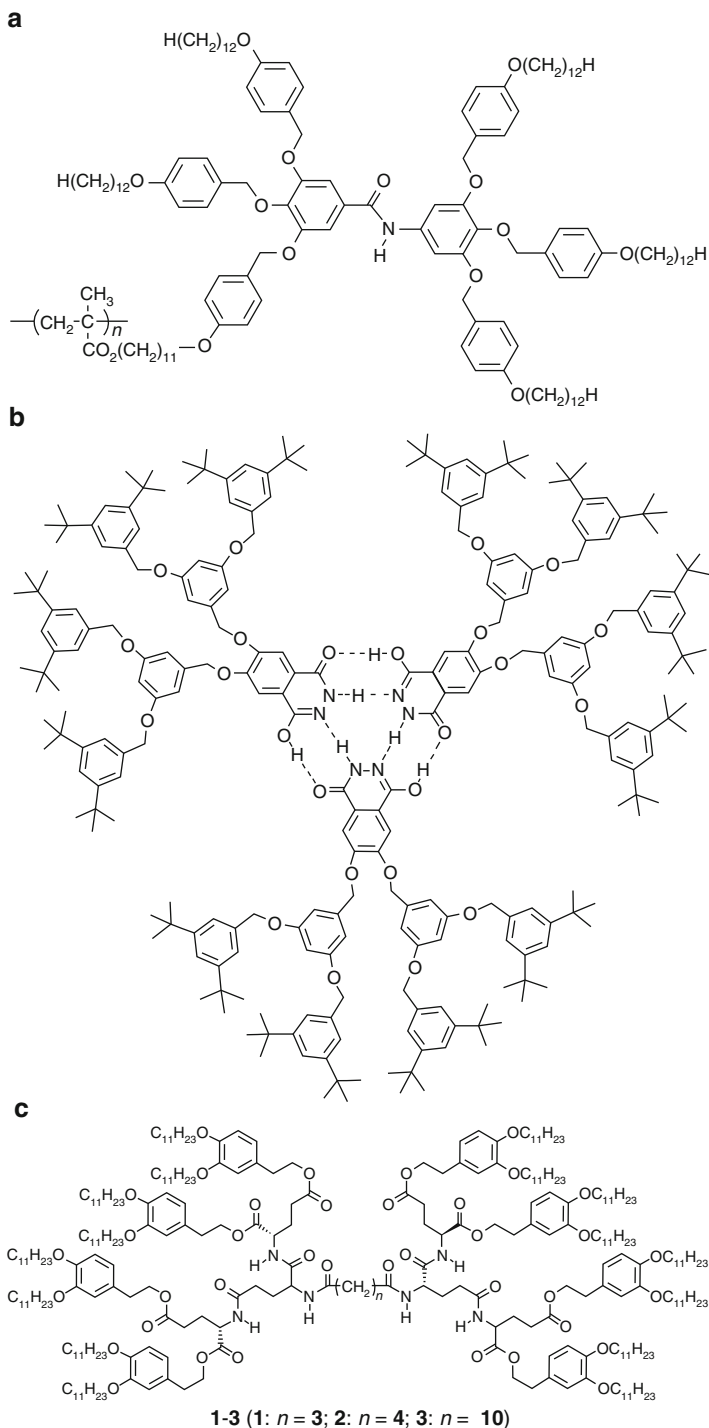


Fig. 6.6 (a) N-[3,4,5-Tris(4'-dodecyloxybenzyloxy)phenyl]-3,4,5-tris(4'-dodecyloxybenzyloxy)benzamide polymethacrylate. (b) self-assembly of phthalhydrazides into trimeric disks through hydrogen bonding. (c) Dendritic peptides from glutamic acid monomers functionalized by undecyl benzalo lipophilic segments

are bonded along their center with the polymethacrylic analog acting as a matrix (host) and the monomer as a guest to create novel liquid crystalline “superlattices”. Apart from the liquid crystalline phases observed for the pure compounds when polymethacrylate is present at high molar ratios a columnar hexagonal superlattice is formed which is replaced by simple-rectangular columnar superlattice, and a centered-rectangular columnar superlattice, at mixtures with about equimolar quantities. Replacement of N-[3,4,5-Tris(4'-dodecyloxybenzyloxy)phenyl]-3,4,5-tris(4'-dodecyloxybenzyloxy)benzamide by benzamide dendrons with alkyl chains of different lengths affords bisdendritic benzamides (Percec et al. 1999). Dodecyloxy benzamides coupled with benzamides with dissimilar but long alkyl tails with at least 6 up to 18 carbon atoms self-assemble in hexagonal columnar lattices. The respective N-methylated benzamides did not exhibit liquid crystalline phases demonstrating thus the crucial role of hydrogen bonding in the organization of these molecules at high temperatures.

Apart from the formation of column axes hydrogen bonds can also be employed for the achievement oligomeric disk like conformations. Taking advantage of the capability of phthalhydrazide to self-assemble through hydrogen bonding into trimeric disks in their lactim-lactam tautomerization Suárez et al. (1998, Fig. 6.6b) obtained columnar hexagonal and rectangular liquid crystalline phases from 6,7-Bis(alkyloxy)-2,3-dihydrophthalazine-1,4-diones with 8, 12 and 16 carbon atoms.

In a biomimetic approach Kamikawa et al. 2010 (Fig. 6.6c), prepared a series of dendritic peptides from glutamic acid monomers functionalized by undecyl benzalo lipophilic segments Thermally stable columnar rectangular (p2gg, c2mm) and hexagonal phases (p6mm) were obtained when all the peptide groups contributed to the formation of intra and intermolecular hydrogen bonds. In contrast when half of the glutamate moieties were in the dissociated state a dynamic equilibrium of hydrogen bonds was observed by IR spectroscopy and a less thermally stable columnar hexagonal phase was produced. Apart from the stabilization of the hexagonal and rectangular columnar structures the hydrogen bonds also play an important role to the transfer of the molecular chirality to the supramolecular structures via intermolecular interactions. Another similar example establishing the importance of hydrogen bonds in the formation of chiral supramolecular aggregates from chiral dendritic monomers based on peptides is the work of (Gao et al. 2011). Starting by perylene bisimides at the core they introduced peptides on its two ends functionalized by dodecyloxy branches. The resulting dendrimers presented ordered columnar mesophases even at room temperature. Optical activity was observed and was attributed to helical conformation of the columns due to the hydrogen bonds of the peptide groups at the periphery of the bisimides.

An exotic class of Janus-like (from the roman god of beginnings and transitions who was depicted as having two faces looking at the future and the past) diblock codendritic polymers which are formed by combination of two independent

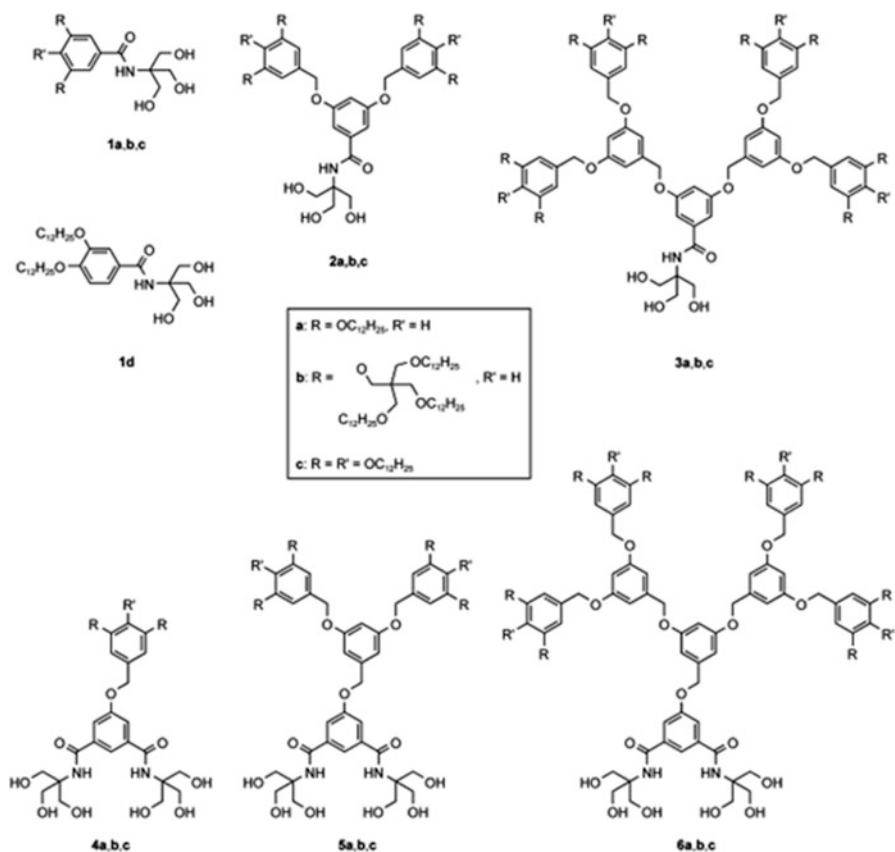


Fig. 6.7 Janus-like diblock codendritic polymers that present mesomorphism through hydrogen bonding interactions

dendrons of different chemical nature can also present mesomorphism through hydrogen bonding interactions. Guillon and his group synthesized three series of amphiphilic compounds containing two discrete segments one hydrophilic containing hydroxyl groups and the other hydrophobic, containing poly(benzyl ether) branches bearing linear or branched dodecyloxy chains by combining different generations of these two dendrons (Bury et al. 2006). The nature of the resulting liquid-crystalline phases was governed by the ability to form strong intermolecular hydrogen bonding network and the hydrophilic/hydrophobic balance. When a dense and interlocked hydrogen-bonding pattern of the hydroxyl groups is stereochemically favored dendritic copolymers self-assemble into Colh-p6mm phases with stable hydrogen bonded cores comprising the polar segments whereas when this is not possible *Cub-Imm* and *Cub-Pmn* emerge (Fig. 6.7).

6.4 Conclusion and Future Perspective

It is evident from all the examples presented that a wide variety of chiral or non-chiral liquid crystalline structures, such as lamellar smectic A, B and C, columnar hexagonal and rectangular and cubic can derive from dendritic polymers with functional groups capable of hydrogen bonding. These examples cover almost the entire range of mesophases observed for liquid crystalline monomers. Hydrogen bonding can induce or influence liquid crystallinity of dendrimers in three major ways.

1. By molecular assembly. A variety of structural units such as dendritic polymers, dendritic cores, dendrons and mesogens of specific shape and properties can be interconnected to form supramolecular complexes exhibiting liquid crystalline phases. As a general rule dendritic polymers of higher generations forming hydrogen bonds with calamitic mesogens and dendrons with calamitic branches hydrogen bonded with dendritic central cores present nematic and lamellar i.e., smectic phases whereas multiple hydrogen bonding, small rigid dendrons connected with a dendritic polyaromatic core and disk shaped mesogens favor columnar hexagonal mesophases.
2. By stabilizing the shape of the supramolecular complex by rigidifying certain parts, most frequently the central core. The development of hydrogen bonding network between functional groups such as ureas and amides allows to dendritic polymers that do not possess rigid calamitic or disk structural units to exhibit mesomorphism. This kind of hydrogen bonding interactions result mainly in the thermodynamic stabilization of the mesophase rendering for example monotropic mesophases (i.e., mesophases emerging only on cooling compounds from the melt) to enantiotropic or enhancing the thermal stability and the temperature range of the mesophases. Furthermore in the cases where, often in synergy with other factors, the extent of rigidification of the dendritic structures leads to the formation of disk shaped molecules interconnected through rigid axes, the organization of supramolecular assemblies is enhanced and nematic or lamellar mesophases are converted to columnar hexagonal or rectangular.
3. By defining or modifying the shape of dendritic monomers and supramolecular aggregates. Alterations of the hydrogen bonding network that take place either by supramolecular interactions, such as electrostatic interactions with dipoles or ions, interactions with appropriate polymeric matrices, and lipophilic π - π interactions of aromatic rings or long aliphatic chains either by external stimuli such as thermal treatment, pH, light, electric and magnetic field or mechanical. Usually this kind of interactions enhances the organization and the stability of the hydrogen bonding pattern which in turn leads to more organized mesophases. As a general result lamellar and cubic mesophases are transformed to columnar hexagonal. In addition though the same interactions the chirality of the dendritic monomers can be transferred to supramolecular aggregation by the formation of helicoid columns.

Self-assembled amphiphilic dendritic polymers are considered to be model compounds for biological systems like liposomes vesicles or micelles. Hydrogen bonding, is a non-covalent and thus weaker selective, reversible and more flexible intermolecular interaction and it is considered as the most important driving force to the formation of these versatile supramolecular architectures. In addition, functional groups capable of multiple hydrogen bonding formation from complementary components such as DNA bases, or amino acids can be used for programmed generation of nanoscale architectures through molecular recognition. Understanding thus and control of the self assembly of such dendritic polymers via hydrogen bonding is of crucial importance not only for the research in the field of liquid crystals but also in many areas where supramolecular organizes are involved such as cell membranes and organic–inorganic nanohybrids. Functional materials for biological applications based on specifically designed dendritic molecules with tailor made hydrogen bonding patterns can be developed.

In another connection the weak and flexible nature of the hydrogen bonds renders the liquid crystalline dendritic polymers very interesting candidates for applications in materials science. Dynamic and complex properties are deriving since the dendrimers undergo structural changes as a result of external stimuli or in synergy with secondary supramolecular interactions. These compounds have possible applications in the areas of sensors, and displays.

References

- Adronov A, Fréchet JMJ (2000) Light-harvesting dendrimers. *Chem Commun* 18:1701–1710
- Allabashi R, Arkas M, Hörmann G, Tsiourvas D (2007) Removal of some organic pollutants in water employing ceramic membranes impregnated with cross-linked silylated dendritic and cyclodextrin polymers. *Water Res* 41(2):476–486
- Anokhin DV, Lejnieks J, Mourran A, Zhu X, Keul H, Möller M, Konovalov O, Erina N, Ivanov DA (2012) Interplay between H-bonding and alkyl-chain ordering in self-assembly of monodendritic L-alanine derivatives. *Chemphyschem* 13:1470–1478
- Arkas M (2013) Hybrid organoceramics deriving from dendritic polymers, methods of preparation, optimization techniques and prospected applications. *Recent advances in ceramic materials research*. New York, Nova Science, pp 1–30
- Arkas M, Tsiourvas D (2009) Organic/inorganic hybrid nanospheres based on hyperbranched poly(ethylene imine) encapsulated into silica for the sorption of toxic metal ions and polycyclic aromatic hydrocarbons from water. *J Hazard Mater* 170(1):35–42
- Arkas M, Tsiourvas D, Paleos CM (2003) Functional dendrimeric “nanosponges” for the removal of polycyclic aromatic hydrocarbons from water. *Chem Mater* 15:2844–2847
- Arkas M, Eleades L, Paleos CM, Tsiourvas D (2005a) Alkylated hyperbranched polymers as molecular nanosponges for the purification of water from polycyclic aromatic hydrocarbons. *J Appl Polym Sci* 97(6):2299–2305
- Arkas M, Tsiourvas D, Paleos CM (2005b) Organosilicon dendritic networks in porous ceramics for water purification. *Chem Mater* 17(13):3439–3444
- Arkas M, Allabashi R, Tsiourvas D, Mattausch E-M, Perfler R (2006) Organic/inorganic hybrid filters based on dendritic and cyclodextrin “nanosponges” for the removal of organic pollutants from water. *Environ Sci Technol* 40(8):2771–2777

- Arkas M, Tsiourvas D, Paleos CM (2010) Functional dendritic polymers for the development of hybrid materials for water purification macromol. *Macromol Mater Eng* 295(10):883–898
- Balagurusamy VSK, Ungar G, Percec V, Johansson G (1997) Rational design of the first spherical supramolecular dendrimers self-organized in a novel thermotropic cubic liquid-crystalline phase and the determination of their shape by X-ray analysis. *J Am Chem Soc* 119:1539–1555
- Barberá J, Marcos M, Serrano JL (1999) Dendromesogens: liquid crystal organizations versus starburst structures. *Chem Eur J* 5:1834–1840
- Barberá J, Donnio B, Gehringer L, Guillon D, Marcos M, Omenat A, Serrano JL (2005) Self-organization of nanostructured functional dendrimers. *J Mater Chem* 15:4093–4105
- Barberá J, Jiménez J, Laguna A, Oriol L, Pérez S, Serrano JL (2006) Cyclotriphosphazene as a dendritic core for the preparation of columnar supermolecular liquid crystals. *Chem Mater* 18:5437–5445
- Bergenudd H, Eriksson P, De Armit C, Stenberg B, Malmström Jonsson E (2002) Synthesis and evaluation of hyperbranched phenolic antioxidants of three different generations. *Polym Degrad Stab* 76:503–508
- Brewis M, Clarkson GJ (1998) Phthalocyanines substituted with dendritic wedges: glass-forming columnar mesogens. *Chem Commun* 9:969–970
- Burkinshaw SM, Froehling PE, Mignanelli M (2002) The effect of hyperbranched polymers on the dyeing of polypropylene fibres. *Dyes Pigm* 53:229–235
- Bury I, Heinrich B, Bourgogne C, Guillon D, Donnio B (2006) Supramolecular self-organization of “Janus-like” diblock codendrimers: synthesis, thermal behavior, and phase structure modeling. *Chem Eur J* 12:8396–8413
- Caminade AM, Turrin CO, Sutra P, Majoral JP (2003) Fluorinated dendrimers. *Curr Opin Colloid Interface Sci* 8:282–295
- Castelar S, Barberá J, Marcos M, Romero P, Serrano JL, Golemme A, Termine R (2013) Supramolecular dendrimers based on the self-assembly of carbazole-derived dendrons and triazine rings: liquid crystal, photophysical and electrochemical properties. *J Mater Chem C* 1:7321–7332
- Didehban K, Namazi H, Entezami AA (2009) Dendrimer-based hydrogen-bonded liquid crystalline complexes: synthesis and characterization. *Eur Polym J* 45:1836–1844
- Didehban K, Namazi H, Entezami AA (2010) Non-covalent dendrimer-based liquid crystalline complexes: synthesis and characterization. *Eur Polym J* 46:1923–1931
- Diele S (2002) *Curr Opin Colloid Interface Sci* 7:333–342
- Donnio B, Barberá J, Giménez R, Guillon D, Marcos M, Serrano JL (2002) Controlled molecular conformation and morphology in poly(amidoamine) (PAMAM) and poly(propyleneimine) (DAB) dendrimers. *Macromolecules* 35:370–381
- Donnio B, Buathong S, Bury I, Guillon D (2007) Liquid crystalline dendrimers. *Chem Soc Rev* 36:1495–1513
- Emrick T, Fréchet JMJ (1999) Erratum to ‘self-assembly of dendritic structures’. *Curr Opin Colloid Interface Sci* 4:15–23
- Felekis T, Tsiourvas D, Tziveleka L, Paleos CM (2005) Hydrogen-bonded liquid crystals derived from supramolecular complexes of pyridylated poly(propyleneimine) dendrimers and a cholesterol-based carboxylic acid. *Liq Cryst* 32:39–43
- Fischer M, Vögtle F (1999) Dendrimers: from design to application—a progress report. *Angew Chem Int Ed* 38:884–905
- Fitié CFC, Tomatsu I, Byelov D, de Jeu WH, Sijbesma RP (2008) Nanostructured materials through orthogonal self-assembly in a columnar liquid crystal. *Chem Mater* 20:2394–2404
- Gao B, Xia D, Zhang L, Bai Q, Bai L, Yang T, Ba X (2011) Helical columnar liquid crystals based on dendritic peptides substituted perylene bisimides. *J Mater Chem* 21:15975–15980
- Gehringer L, Bourgogne C, Guillon D, Donnio B (2005) Main-chain liquid-crystalline dendrimers based on amido-core moieties—effect of the core structure. *J Mater Chem* 15:1696–1703
- Grayson SM, Fréchet JMJ (2001) Convergent dendrons and dendrimers: from synthesis to applications. *Chem Rev* 101:3819–3868

- Guillon D, Deschenaux R (2002) Liquid-crystalline dendrimers. *Curr Opin Solid State Mater Sci* 6:515–525
- Hudson SD, Jung HT, Percec V, Cho WD, Johansson G, Ungar G, Balagurusamy VSK (1997) Direct visualization of individual cylindrical and spherical supramolecular dendrimers. *Science* 278:449–452
- Inoue K (2000) Functional dendrimers, hyperbranched and star polymers. *Prog Polym Sci* 25:453–571
- Ishihara S, Furuki Y, Takeoka S (2007) A hydrogen-bonded supramolecular hexagonal columnar liquid crystal composed of a tricarboxylic triphenylene and monopyridyl dendrons. *Chem Lett* 16(5):441–451
- Ishihara S, Furuki Y, Hill JP, Ariga K, Takeoka S (2014) Homeotropic alignment of dendritic columnar liquid crystal induced by hydrogen-bonded triphenylene core bearing fluoroalkyl chains. *J Nanosci Nanotechnol* 14(7):5130–5137
- Johansson G, Percec V, Ungar G, Abramic DJ (1994) Molecular recognition directed self-assembly of tubular liquid crystalline and crystalline supramolecular architectures from taper shaped (15-crown-5)methyl 3,4,5-tris(p-alkyloxybenzyloxy)benzoates and (15-crown-5) methyl 3,4,5-tris(p-dodecyloxy)benzoate. *J Chem Soc Perkin Trans 1*:447–459
- Johansson G, Percec V, Ungar G, Zhou JP (1996) Fluorophobic effect in the self-assembly of polymers and model compounds containing tapered groups into supramolecular columns. *Macromolecules* 29:646–656
- Kamikawa Y, Kato T (2006) One-dimensional chiral self-assembly of pyrene derivatives based on dendritic oligopeptides. *Org Lett* 8:2463–2466
- Kamikawa Y, Nishii M, Kato T (2004) Self-assembly of folic acid derivatives: induction of supramolecular chirality by hierarchical chiral structures. *Chem Eur J* 10:5942–5951
- Kamikawa Y, Nishii M, Kato T (2005) Supramolecular chiral cubic phases formed by folic acid derivatives. *Mol Cryst Liq Cryst* 435:755–765
- Kamikawa Y, Fujimoto N, Donnio B, Guillon D, Kato T (2010) Self-assembled structures of liquid-crystalline oligopeptide dimmers. *Mol Cryst Liq Cryst* 516:132–143
- Kanie K, Nishii M, Yasuda T, Taki T, Ujiie S, Kato T (2001a) Self-assembly of thermotropic liquid-crystalline folic acid derivatives: hydrogen-bonded complexes forming layers and columns. *J Mater Chem* 11:2875–2886
- Kanie K, Yasuda T, Nishii M, Ujiie S, Kato T (2001b) Hydrogen-bonded lyotropic liquid crystals of folic acids: responses to environment by exhibiting different complex patterns. *Chem Lett* 30:480–481
- Kato T, Matsuoka T, Nishii M, Kamikawa Y, Kanie K, Nishimura T, Yashima E, Ujiie S (2004) Supramolecular chirality of thermotropic liquid-crystalline folic acid derivatives. *Angew Chem Int Ed* 43:1969–1972
- Kolhe P, Misra E, Kannan RM, Kannan S, Lieh-Lai M (2003) Drug complexation, in vitro release and cellular entry of dendrimers and hyperbranched polymers. *Int J Pharm* 259:143–160
- Kraft A, Reichert A, Kleppinger R (2000) Supramolecular liquid crystals with columnar mesophases through self-assembly of carboxylic acids around a tribasic core. *Chem Commun* 12:1015–1016
- Lee H-K, Lee H, Ko YH, Chang YJ, Oh N-K, Zin W-C, Kim K (2001) Synthesis of a nanoporous polymer with hexagonal channels from supramolecular discotic liquid crystals. *Angew Chem Int Ed* 40:2669–2671
- Lee CC, MacKay JA, Fréchet JMJ, Szoka FC (2005) Designing dendrimers for biological applications. *Nat Biotechnol* 23:1517–26
- Lehmann M, Köhn C, Meier H, Renker S, Oehlhofb A (2005) Supramolecular order of stilbenoid dendrons: importance of weak interactions. *J Mater Chem* 16:441–451
- Marcos M, Giménez R, Serrano JL, Donnio B, Heinrich B, Guillon D (2001) Dendromesogens: liquid crystal organisations versus starburst structures. *Chem Eur J* 7:1006–1013
- Matheus OA, Shipway AN, Stoddart JF (1998) Dendrimers—branching out from curiosities into new technologies. *Prog Polym Sci* 23:1–56

- Meier H, Lehmann M (1998) Stilbenoid dendrimers. *Angew Chem Int Ed Engl* 37:643–645
- Moore JS (1999) Supramolecular polymers. *Curr Opin Colloid Interface Sci* 4:108–116
- Percec V, Schlueter D (1997) Mechanistic investigations on the formation of supramolecular cylindrical shaped oligomers and polymers by living ring opening metathesis polymerization of a 7-oxanorbornene monomer substituted with two tapered monodendrons. *Macromolecules* 30:5783–5790
- Percec V, Heck J, Lee M, Ungar G, Alvarez-Castillo A (1992) Poly{2-vinyloxyethyl 3,4,5-tris [4-(n-dodecanyloxy)benzyloxy]benzoate}: a self-assembled supramolecular polymer similar to tobacco mosaic virus. *Mater Chem* 2:1033–1039
- Percec V, Heck J, Tomazos D, Falkenberg F, Blackwell H, Ungar G (1993a) Self-assembly of taper-shaped monoesters of oligo(ethylene oxide) with 3,4,5-tris(p-dodecyloxybenzyloxy) benzoic acid and of their polymethacrylates into tubular supramolecular architectures displaying a columnar mesophase. *J Chem Soc Perkin Trans 1*:2799–2811
- Percec V, Heck JA, Tomazos D, Ungar G (1993b) The influence of the complexation of sodium and lithium triflate on the self-assembly of tubular-supramolecular architectures displaying a columnar mesophase based on taper-shaped monoesters of oligoethylene oxide with 3,4,5-tris [p-(n-dodecan-1-yloxy)benzyloxy]benzoic acid and of their polymethacrylates. *J Chem Soc Perkin Trans 2*:2381–2388
- Percec V, Johansson G, Heck J, Ungar G, Batty SV (1993c) Molecular recognition directed self-assembly of supramolecular cylindrical channel-like architectures from 6,7,9,10,12,13,15,16-octahydro-1,4,7,10,13-pentaoxabenzocyclopentadecen-2-ylmethyl 3,4,5-tris(p-dodecyloxybenzyloxy)benzoate. *J Chem Soc Perkin Trans 1*:1411–1420
- Percec V, Tomazos D, Heck J, Blackwell H, Ungar G (1994) Self-assembly of taper-shaped monoesters of oligo(ethylene oxide) with 3,4,5-tris(n-dodecan-1-yloxy)benzoic acid and of their polymethacrylates into tubular supramolecular architectures displaying a columnar hexagonal mesophase. *J Chem Soc Perkin Trans 2*:31–44
- Percec V, Schlueter D, Kwon YK, Blackwell J, Moller M, Slangen PJ (1995) Dramatic stabilization of a hexagonal columnar mesophase generated from supramolecular and macromolecular columns by the semifluorination of the alkyl groups of their tapered building blocks. *Macromolecules* 28:8807–8818
- Percec V, Johansson G, Ungar G, Zhou J (1996a) Fluorophobic effect induces the self-assembly of semifluorinated tapered monodendrons containing crown ethers into supramolecular columnar dendrimers which exhibit a homeotropic hexagonal columnar liquid crystalline phase. *J Am Chem Soc* 118:9855–9866
- Percec V, Schlueter D, Ronda JC, Johansson G, Ungar G, Zhou JP (1996b) Tubular architectures from polymers with tapered side groups. assembly of side groups via a rigid helical chain conformation and flexible helical chain conformation induced via assembly of side groups. *Macromolecules* 29:1464–1472
- Percec V, Ahn CH, Cho WD, Jamieson AM, Kim J, Leman T, Schmidt M, Gerle M, Möller M, Percec V, Ahn CH, Ungar G, Yearley DJP, Moller M, Sheiko SS (1998a) Controlling polymer shape through the self-assembly of dendritic side-groups. *Nature* 391:161–164
- Percec V, Cho WD, Mosier PE, Ungar G, Yearley DJP (1998b) Structural analysis of cylindrical and spherical supramolecular dendrimers quantifies the concept of monodendron shape control by generation number. *J Am Chem Soc* 120:11061–11070
- Percec V, Schlueter D, Ungar G, Cheng SZD, Zhang A (1998c) Hierarchical control of internal superstructure, diameter, and stability of supramolecular and macromolecular columns generated from tapered monodendritic building blocks. *Macromolecules* 31:1745–1762
- Percec V, Ahn CH, Bera TK, Ungar G, Yearley DJP (1999) Coassembly of a hexagonal columnar liquid crystalline superlattice from polymer(s) coated with a three-cylindrical bundle supramolecular dendrimer. *Chem Eur J* 5:1070–1083
- Percec V, Bera TK, Glodde M, Fu Q, Balagurusamy VSK, Heiney PA (2003) Hierarchical self-assembly, coassembly, and self-organization of novel liquid crystalline lattices and

- superlattices from a twin-tapered dendritic benzamide and its four-cylinder-bundle supramolecular polymer. *Chem Eur J* 9:921–935
- Percec V, Peterca M, Dulcey AE, Imam MR, Hudson SD, Nummelin ASP, Heiney PA (2008) Hollow spherical supramolecular dendrimers. *J Am Chem Soc* 130:13079–13094
- Percec V, Peterca M, Tsuda Y, Rosen BM, Uchida S, Imam MR, Ungar G, Heiney PA (2009) Elucidating the structure of the Pm3n cubic phase of supramolecular dendrimers through the modification of their aliphatic to aromatic volume ratio. *Chem. Eur J* 15:8994–9004
- Pesak D, Moore JS (1997) Columnar liquid crystals from shape-persistent dendritic molecules. *Angew Chem Int Ed Engl* 36:1636–1639
- Ponomarenko SA, Boiko NI, Shibaev VP (2001) Liquid-crystalline dendrimers. *Polym Sci Ser C* 43:1–45
- Precup-Blaga FS, Schenning APHJ, Meijer EW (2003) Liquid crystalline oligo(p-phenylene vinylene)-terminated poly(propylene imine) dendrimers. Synthesis and characterization. *Macromolecules* 36:565–572
- Prokhorova SA, Sheiko SS, Cheng SZD, Zhang A, Ungar G, Yeardeley DJP (1998a) Visualizable cylindrical macromolecules with controlled stiffness from backbones containing libraries of self-assembling dendritic side groups. *J Am Chem Soc* 120:8619–8631
- Prokhorova SA, Sheiko SS, Moller M, Ahn CH, Percec V (1998b) Molecular imaging of monodendron jacketed linear polymers by scanning force microscopy. *Macromol Rapid Commun* 19:359–366
- Prokhorova SA, Sheiko SS, Ahn CH, Percec V, Moller M (1999) Molecular conformations of monodendron-jacketed polymers by scanning force microscopy. *Macromolecules* 32:2653–2660
- Sagara Y, Kato T (2008) Stimuli-responsive luminescent liquid crystals: change of photoluminescent colors triggered by a shear-induced phase transition. *Angew Chem Int Ed* 47:5175–5178
- Sagara Y, Kato T (2011a) A mechanical and thermal responsive luminescent liquid crystal forming a colourless film under room light. *Supramol Chem* 23:310–314
- Sagara Y, Kato T (2011b) Brightly tricolored mechanochromic luminescence from a single-luminophore liquid crystal: Reversible writing and erasing of images. *Angew Chem Int Ed* 50:9128–9132
- Sagara BY, Yamane S, Mutai T, Araki K, Kato T (2009) A stimuli-responsive, photoluminescent, anthracene-based liquid crystal: emission color determined by thermal and mechanical processes. *Adv Funct Mater* 19:1869–1875
- Schlenk C, Frey H (1999) Carbosilane dendrimers—synthesis, functionalization, application. *Monatsh Chem* 130:3–14
- Seiler M, Köhler D, Arlt W (2003) Hyperbranched polymers: new selective solvents for extractive distillation and solvent extraction. *Sep Purif Technol* 30:179–197
- Shu J, Dudenko D, Esmaeili M, Park JH, Puniredd SR, Chang JY, Breiby DW, Pisula W, Hansen MR (2013) Coexistence of helical morphologies in columnar stacks of star-shaped discotic hydrazones. *J Am Chem Soc* 135:11075–11086
- Smith DK, Diederich F (2000) Supramolecular dendrimer chemistry: a journey through the branched architecture. *Top Curr Chem* 210:183–227
- Stebani U, Lattermann G (1995) Unconventional mesogens of hyperbranched amides and corresponding ammonium derivatives. *Adv Mater* 7:578–581
- Suárez M, Lehn JM, Zimmerman SC, Skoulios A, Heinrich B (1998) Supramolecular liquid crystals. self-assembly of a trimeric supramolecular disk and its self-organization into a columnar discotic mesophase. *J Am Chem Soc* 120:9526–9532
- Sun Q, Xu K, Jacky W, Lam Y, Cha JAK, Zhang X et al (2001) Nanostructured magnetoceramics from hyperbranched polymer precursors. *Mater Sci Eng C* 16:107–112
- Tschierske C (2001) Micro-segregation, molecular shape and molecular topology—partners for the design of liquid crystalline materials with complex mesophase morphologies. *J Mater Chem* 11:2647–2671

- Tschierske C (2002) Liquid crystalline materials with complex mesophase morphologies. *Curr Opin Colloid Interface Sci* 7:69–80
- Tsetsekou A, Arkas M, Kritikaki A, Simonetis S, Tsiourvas D (2008) Optimization of hybrid hyperbranched polymer/ceramic filters for the efficient absorption of polyaromatic hydrocarbons from water. *J Membrane Sci* 311(1-2):128–135
- Tsiourvas D, Arkas M (2013) Columnar and smectic self-assembly deriving from non ionic amphiphilic hyperbranched polyethylene imine polymers and induced by hydrogen bonding and segregation into polar and non polar parts. *Polymer* 54:1114–1122
- Tsiourvas D, Tsetsekou A, Arkas M, Diplas S, Mastrogianni E (2011) Covalent attachment of a bioactive hyperbranched polymeric layer to titanium surface for the biomimetic growth of calcium phosphates. *J Mater Sci Mater Med* 22(1):85–96
- Tsiourvas D, Arkas M, Paleos CM (2013a) Organic/inorganic hybrid materials based on functional dendrimers and hyperbranched polymers for water purification. *Water treatment processes*. Nova Science, New York, pp 334–355
- Tsiourvas D, Tsetsekou A, Papavasiliou A, Arkas M, Boukos N (2013b) A novel hybrid sol-gel method for the synthesis of highly porous silica employing hyperbranched poly(ethyleneimine) as a reactive template. *Micropor Mesopor* 175:59–66
- Xu J, Ling TC, He C (2008) Hydrogen bond-directed self-assembly of peripherally modified cyclotriphosphazenes with a homeotropic liquid crystalline phase. *J Polym Sci A Polym Chem* 46:4691–4703
- Yamane S, Tanabe K, Sagara Y, Kato T (2012) Stimuli-responsive photoluminescent liquid crystals. *Top Curr Chem* 318:395–406
- Yin R, Zhu Y, Tomalia DA, Ibuki H (1998) Architectural copolymers: rod-shaped, cylindrical dendrimers. *J Am Chem Soc* 120:2678–2679
- Zhou Y, Xu M, Li T, Guo Y, Ya T, Xiao S, Li F, Huang C (2008) Stabilization of the mesomorphic phase in a self-assembled two-component system. *J Colloid Interface Sci* 321:205–211

Chapter 7

Polymer Dispersed Liquid Crystals

Shri Singh, Jagdeesh Kumar Srivastava, and Rajendra Kumar Singh

7.1 Introduction: An Overview

During the past three decades, intense studies have been carried out to understand the behaviour of dispersed liquid crystals in various media. One of the most common outcomes related with these dispersion studies on liquid crystals is the polymer dispersed liquid crystals (PDLCs) (Drzaic 1995; Crawford and Zumer 1996; Simoni 1997; Higgins 2000; Dierking 2000, 2003; Vicari 2003; Crawford 2005; Yang and Wu 2006; Dunmur and Sluckin 2010). These systems are interesting from both technical applications and understanding of the behaviour of liquid crystals in a confined environment. Various binary and multi component mixtures of both liquid crystals and polymers with other additives (like dyes, nano particles, etc.) have been used to improve its technological applications. In general, PDLCs are the micrometer-sized birefringent liquid crystalline droplets, dispersed in an optically transparent and uniform polymer matrix having spatially varying refractive index and efficient light-scattering properties. It is useful in the study of problems related with phase separation, miscibility, droplet configuration, surface anchoring, etc. It is also useful in various device development applications like smart windows, light shutters, modulators, sensors, optical switches, holographic films and most interestingly the display devices.

Recently, important results on the dispersion studies of liquid crystals in photo-aligned materials (Yaroshchuk and Reznikov 2012), adhesives (Zou and Fang 2011), smart windows (Cupelli et al. 2009) and conducting polymers (Buyuktanir et al. 2006; Kim et al. 2008), etc., have been reported. Self-assembling of liquid crystalline materials in pyroelectric substrates (Sheraw et al. 2002; Merola et al. 2012), phosphonium type zwitterions (Ueda et al. 2011) and phase

S. Singh, Ph.D. (✉) • J.K. Srivastava, Ph.D. • R.K. Singh, Ph.D.
Department of Physics, Faculty of Science, Banaras Hindu University,
Varanasi, Uttar Pradesh 221005, India
e-mail: srsingh23@gmail.com; jagdish.bhu@gmail.com; rajendrasingh.bhu@gmail.com

segregated liquid crystal gels (Hikmet 1992; Guymon et al. 1997; Kato 2002) are also of much interest.

Dispersion of particles in a host medium is the part of our everyday life and an important area for fundamental research. In wider sense, dispersion may be in the form of emulsion, colloidal suspension, aerosols, etc. In emulsion, surfactant-coated liquid droplets are dispersed in a fluid environment. Colloidal suspensions are observed for the dispersion of solid particles in the fluid medium and aerosol with fluid or solid particles floating in a gaseous phase. The physics of colloidal dispersions in nematic liquid crystals has been discussed in detail by Stark (Stark 2001). Dispersion studies on liquid crystals give rise to an important area of scientific and technological developments. A great deal of interesting physics is associated with the liquid crystalline materials confined into small cavities. It leads to the observed changes in the mesoscopic properties of liquid crystalline materials in confined geometry as compared to their bulk counter parts (Golemme et al. 1988a). Consequently, the liquid crystal dispersion has been the subject of continuous attention in the recent past (Wu 1986; Simoni et al. 1993; Sutherland et al. 1994; Drzaic 1995; Crawford and Zumer 1996; Hourri et al. 2001; Yamamoto 2001; Iannacchione et al. 2003; Leheny et al. 2003; Vicari 2003; Stannarius and Kremer 2004; Pasini et al. 2003; Spicer 2005; Cristaldi et al. 2009).

Dispersion study of liquid crystals in polymers constitutes an important area because of its wide applicability in various scientific (Drzaic 1995; Crawford and Zumer 1996; Mucha 2003; Pasini et al. 2003) and device development applications (Klosowicz and Zmija 1995; Simoni 1997; Vicari 2003; Crawford 2005; Lowe and Kriss 2006; Yang and Wu 2006). In a polymer matrix, liquid crystals may exist as a discrete droplet (Chien et al. 1992; Roussel et al. 2002; Hoppe et al. 2003), an interpenetrating network with the polymer (Ciferri 1991; Collyer 1993; Carfagna 1994; Zumer et al. 1995; Collings and Hird 1997; Dierking 2000; Wang and Zohu 2004), or something in-between (Demus and Richter 1978; Demus et al. 1999; Serbutoviez et al. 1996; Benmouna et al. 1999, 2000; Boussoualem et al. 2004; Xie et al. 2005). Confinement of liquid crystals in micrometer size polymer cavities of complex shapes is generally termed as polymer dispersed liquid crystals (PDLCs). Depending upon the nature and compositions of both liquid crystals and polymers some other sub classified terms like polymer network liquid crystal (PNLC), polymer dispersed ferroelectric liquid crystal (PDFLC), polymer stabilized ferroelectric liquid crystal (PSFLC), holographic PDLC (HPDLC), etc., are also common to PDLCs. Starting with the earlier work on PDLCs by Fergason (1984, 1985), Drzaic (1986) and Doane et al. (1986, 1987), presently, a large number of groups are working in the field of PDLCs. Different properties of PDLCs like droplet morphology, birefringence, light scattering, flexibility, self-supportability and electro-optical properties make them interesting for various display applications. As a result much of the works on PDLCs aim to optimize its suitability for display applications by incorporating new modes for displays.

In spite of its strong device development applicability, PDLCs are also interesting from scientific point of view. Several fundamental studies related with mixing and phase separation of liquid crystals with polymers (Smith and Vaz 1988; Smith

1990, 1993a, b), their thermal characterizations (Smith et al. 1992; Russell et al. 1995), phase behavior (Chiu and Kyu 1995, 1998; Riccardi et al. 1998a, b; Benmouna et al. 1998), phase stability (Dorgan 1991, 1995; Shen and Kyu 1995; Riccardi et al. 1998a, b), phase diagrams and morphology (Amundson et al. 1997; Roussel et al. 2000), anchoring and droplet deformation using NMR techniques (Crawford et al. 1991b; Iannacchione et al. 1997; Ambrozic et al. 1997; Vilfan et al. 1999a, b), different computer simulations to investigate droplet configurations (Erdmann et al. 1990; Berggren et al. 1994; Priezjev and Pelcivits 2000; Springer and Higgins 2000), electro-optical properties of PDLCs (LeGrange et al. 1997; Jadzyn et al. 1999; Nicoletta et al. 2000; Smith et al. 2000), and many more other investigations have been carried out.

Thrust remains continued in the current millennium as well, which results in a large number of articles covering both the experimental and theoretical aspects of PDLCs. Matsuyama (2010) has discussed the theory of phase separation in the binary mixtures of low molecular weight liquid crystal and a rod like polymer using mean field theory. Both the experimental and simulation studies have been carried out to investigate phase equilibrium and growth morphology for the mixture of polystyrene and cyanobiphenyl (Soule et al. 2009). PDLCs with micrometer size droplets useful for diffractive optics have been investigated by Hadjichristov et al. (2009). Phase separation kinetics of polymer dispersed liquid crystals confined between two parallel walls using time dependent Ginzburg–Landau Model has been discussed by Xia et al. (2006). Expression for topological point defects in nematic liquid crystals (Kleman and Lavrentovich 2006) and optical phase shift of light propagating through LC droplets in PDLCs (Dick and Loiko 2004) have also been highlighted.

Monte Carlo and molecular dynamics simulations have been carried out to investigate the different properties of PDLCs. Phase behavior of nematogen (Almarza et al. 2010), surface induced ordering and influence of director fluctuation in PDLCs, using simulated NMR spectra (Amimori et al. 2005; Preeti et al. 2009), nematic cells with defect patterns (Backer et al. 2008), computer simulations of nematic liquid crystal tactoids (Bates 2003), director configuration in confined nematics (Priezjev and Pelcivits 2000), opto-mechanical and other light scattering properties of stretched PDLC films (Zumer and Doane 1986; Kiselev et al. 2004; Amimori et al. 2003) and molecular dynamic simulation studies on LCs and PDLCs (Care and Cleaver 2005; Jeon et al. 2007; Wilson 2007; Zheng et al. 2008) are of much interest.

Performance of PDLC based devices has been improved by using different mixtures of liquid crystals, polymers and other additives. Many studies reveal the importance of electro-optical properties of PDLCs using gold nano particles (Hinjosa and Sharma 2010), reverse mode operation in PDLCs (Cupelli et al. 2011), reconfigurable LC droplets (Ren et al. 2009), electrowetting (Fan et al. 2009), electro-optical switching of HPDLC diffraction gratings using SiO₂ and clay as nanocomponent (Busbee et al. 2009; Pavani et al. 2009). For flexible display devices, PDLCs with conducting polymers (Sheraw et al. 2002; Roussel et al. 2003; Ebru et al. 2006; Kim et al. 2008) and PEO-based liquid crystalline

block copolymer (Zhou et al. 2011) have been investigated. In past few years the thermal, morphological, phase behavior and electro-optical properties of PDLCs using different polymer matrices have been studied by many research groups (Malik et al. 2003, 2008; Malik and Raina 2004; Chen and Shanks 2007; Kumar and Raina 2007; Deshmukh and Malik 2008; Ganesan et al. 2009; Meng et al. 2010; Perju et al. 2011; Dzhons et al. 2011; Shanks and Staszczuk 2012; Srivastava et al. 2011, 2012; Song et al. 2012a, b).

Purpose of the present chapter is to provide self-contained overview of the polymer dispersed liquid crystals for attracting the interest of novice readers. An attempt is also made to generate curiosity among the established workers by making them familiar with some of the very recent development in the area of PDLCs. The present chapter provides a comprehensive view on different aspects of PDLCs viz., methods for preparation; basic techniques for characterization; their morphological, electro-optical and temporal behavior; various applications, and, the basic theoretical understanding of miscibility and phase related phenomenon. Some non-conventional methods for the preparation of PDLC films, different director configuration and their *inter-se* transformations within the LC droplets and future perspectives have also been discussed.

7.2 Polymer Dispersed Liquid Crystal (PDLC) Films

In their most common form, a PDLC consists of micron-sized birefringent liquid crystalline droplets, dispersed uniformly in an optically active and transparent polymer matrix, having spatially varying refractive index and efficient light-scattering properties. The light scattering may be switched on by applying an electric field across the film which reorients the molecular directors in nematic droplets to match their ordinary refractive index (η_o) with the refractive index of the polymer (η_p), thereby, making the film transparent. PDLC films are prepared with the aim to couple the peculiar mechanical properties of a polymeric film (flexibility and high mechanical resistance) and the peculiar electro-optical properties of LCs (electrically controllable high optical anisotropy). In PDLCs, confinement of liquid crystals into small cavities dominates over the bulk properties of liquid crystals (Parmar and Singh 1992; Parmar and Holmes 1993; Shen and Kyu 1995).

The microscopic structural arrangement of PDLCs itself is very complex, but in simplest form it can be sketched as an optically non-absorbing inhomogeneous material composed of an isotropic solid phase (i.e., the polymer), containing almost spherical droplets filled with an anisotropic liquid (i.e., a nematic liquid crystal). In PDLCs, both polymer and liquid crystal have slightly different refractive index values. When no field is applied to the film, director of the nematic droplets has no preferred orientation with respect to the plane of the film. In this case, the difference between refractive indices of polymer and liquid crystal results in the scattering of incident light. Therefore, film becomes opaque. On the other hand, when electric field is applied to the film it tends to reorient nematic liquid crystal droplets in such a

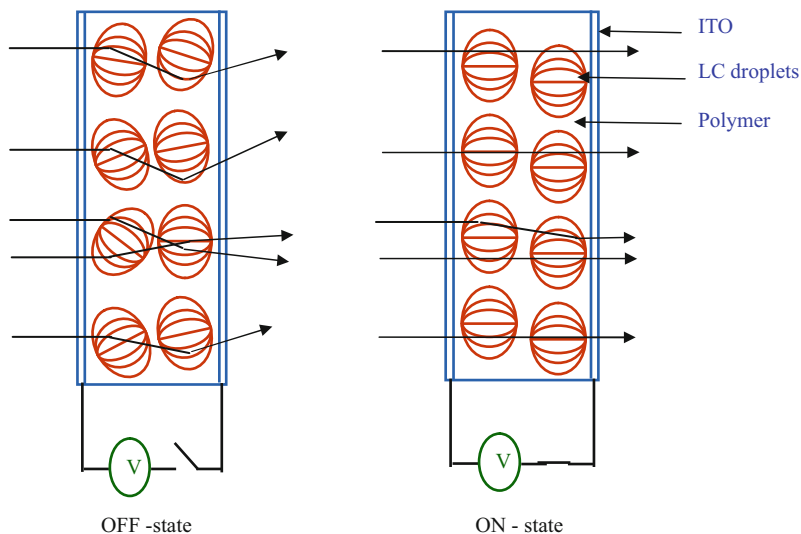


Fig. 7.1 Operating principle of a common PDLC device. (a) OFF-state, (b) ON-state

manner that the director becomes parallel to the field (or otherwise, perpendicular to the plane of the film). In this case, ordinary refractive index (η_o) component of liquid crystal matches with refractive index of the polymer (η_p). Thus, light incident on normal to the film, passes through it without being scattered and film becomes transparent. The operating principal of a common PDLC device is shown in Fig. 7.1.

There are certain aspects common to all PDLC films which need to be explored properly for optimized utility of a particular PDLC film in typical applications. These include film thickness; liquid crystal droplet size and shape; refractive indices, solubility/miscibility behavior, etc. of the constituting liquid crystals and polymers.

Both the operating voltage and light scattering properties of PDLCs depend strongly on the PDLC *film thickness* (Drzaic 1995). Usually it is controlled by using spacers of known dimension. Spacer may be a thin polymer film, Mylar sheet, glass and plastic rods (or spheres), etc. PDLC film thickness is measured conveniently by interferometry. In interference pattern, fringes of different series are observed due to phase shift of the light reflected from the front and rear surfaces of the film. Light reflected from rear surface, suffers a phase shift in proportion to the distance travelled inside the film (i.e., twice the film thickness). Once these fringes are identified, PDLC film thickness can also be obtained.

The *droplets shape, size and distribution* influence strongly the scattering, reorientation and electro-optical properties of the PDLC films. It is usually determined by scanning electron microscopy after removing liquid crystals from polymer network using suitable solvents (Havens et al. 1990; Vaz et al. 1991). In some cases it can also be determined by the image analysis of the morphologies obtained from optical microscopy (Golovataya et al. 1990). One direct method to obtain the

average droplet size involves counting droplets of different sizes in POM images (Hadjichristov et al. 2009). In indirect methods, light scattering and electro-optical properties can also be used to estimate the average droplet size (Lackner et al. 1989; Vaz et al. 1991).

Issues related with *refractive indices and solubility/miscibility* behavior of liquid crystal and polymer complicate the analysis and optimization of PDLC devices. In many of the applications it is mandatory to minimize the haziness of the PDLC films. Haziness effect is minimized by a suitable choice of liquid crystal and polymer constituents with closely matched values of refractive index components (Drzaic 1995). Further, due to *solubility/miscibility* of liquid crystal in polymer, various properties of the PDLC films like transparency, dielectric constant, conductivity and mechanical stability get changed (Ferguson 1985; Drzaic 1986; Doane et al. 1986; Golemme et al. 1988a, b; Simoni et al. 1992b; Crawford and Zumer 1996; Mei and Higgins 1998; Mertelj and Copic 1998). Studies on the solubility limit of liquid crystals in different polymer matrices can also be useful in developing an idea about the droplet morphology and their dispersion in polymer matrices (Smith and Vaz 1988; Smith 1990, 1993a, b; Smith et al. 1992; Srivastava et al. 2011).

The solubility parameters or rather the difference in solubility parameter components are significant in determining the solubility of a system. The term solubility parameter was first used by Hildebrand and Scott (Hildebrand and Scott 1950, 1962) and is defined as the square root of the cohesive energy density,

$$\delta = \left(\frac{E_{coh}}{V} \right)^{\frac{1}{2}} \quad (7.1)$$

and

$$E_{coh} = \Delta U = \Delta H - P\Delta V \quad (7.2)$$

where, E_{coh} is the cohesive energy and V the molar volume of the substance.

Regular improvements in the studies related with solubility parameter components have been made by several groups (Burrell 1957, 1962, 1972; Blanks and Prausnitz 1964; Hansen 1967a, b, c; Hansen and Skaarup 1967; Hansen and Beerbower 1971; Gardon and Teas 1976; Hoftyzer and Krevelen 1976; Hoy 1970, 1985, 1989; Barton 1985, 1991). Presently, the solubility parameter approach proposed by Hansen (2007) with the help of computer programme data is widely in use. In this approach three distinct solubility parameter components representing dispersion (D), polar (P) and hydrogen bond (H) interactions are used (Hansen 2007) and the total cohesive energy (E_{coh}) is written as the sum of the individual energy terms,

$$E_{coh} = E_D + E_P + E_H \quad (7.3)$$

Its division by the molar volume (V) gives the square of the total (or Hildebrand) solubility parameter as the sum of the squares of the Hansen solubility parameter components related with dispersion (D), polar (P), and hydrogen bond interaction (H).

$$\frac{E}{V} = \frac{E_D}{V} + \frac{E_P}{V} + \frac{E_H}{V} \quad (7.4)$$

$$\delta^2 = \delta_D^2 + \delta_P^2 + \delta_H^2 \quad (7.5)$$

Analytically, solubility parameter components are determined by using the methods developed by (i) Hoftzyer and Krevelen (1976) and Hoy (1985, 1989) and then taking the average of the two for a fair estimation. Specific group contribution to the molar volume has been reported by Fedors (1974). Detailed studies related with solubility parameter and group contribution are reported in literature (Krevelen and Nijenhuis 2009). Here we provide only a brief description of the methods.

- **Method of Hoftzyer and Van Krevelen:** It predicts solubility parameter components from group contributions using relations (Hoftzyer and Krevelen 1976),

$$\delta_D = \frac{\sum F_{Di}}{V}; \quad \delta_P = \frac{\sqrt{\sum F_{Pi}^2}}{V}; \quad \delta_H = \sqrt{\frac{\sum E_{Hi}}{V}} \quad (7.6)$$

where, F_{Di} and F_{Pi} are, respectively, the group contributions due to dispersion and polar components of the molar attraction function and E_{Hi} is the contribution due to hydrogen bonding forces to the cohesive energy of each structural group and V is the molar volume of the substance.

- **Method of Hoy:** In many respects this method is different from that of Hoftzyer and Krevelen (1976) and makes use of a number of equations as given in (7.7). It contains four additive molar functions, a number of auxiliary equations and the final expressions for the solubility parameter δ_i and its components, total group contributions F_t , group contribution due to polar components F_p and the molecular volume V of the substance.

Additive molar functions	Auxiliary equations	δ_i and its components
$F_t = \sum N_i F_{t,i}$	$\alpha(P) = \frac{777 \Delta_{\tau}^{(P)}}{V}$	$\delta_i = \frac{(F_i + B)}{V}$, $B = 277$
$F_p = \sum N_i F_{p,i}$	$n = \frac{0.5}{\Delta_{\tau}^{(P)}}$	$\delta_p = \delta_i \left(\frac{1}{\alpha} \frac{F_p}{F_t + B} \right)^{\frac{1}{2}}$
$V = \sum N_i V_i$	---	$\delta_H = \delta_i \left[(\alpha - 1) / \alpha \right]^{\frac{1}{2}}$
$\Delta_{\tau}^{(P)} = \sum N_i \Delta_{\tau,i}^{(P)}$	---	$\delta_D = (\delta_i^2 - \delta_P^2 - \delta_H^2)^{\frac{1}{2}}$

$\Delta_{\tau}^{(P)}$ is the Lydersen correction for non-ideality, derived by Hoy (1985, 1989) and is to be multiplied by 2/3 for bi, tri and tetra-valent groups in the saturated ring.

7.3 Methods for Preparation of PDLC Films

Formation of PDLC films starts with coating of a fluid system as a thin film (which contains both the polymer and the liquid crystals) and then causes it to solidify. Over the years, a number of ways have been developed for the formation of PDLCs films. However, all these fall into two general categories (i) the microencapsulation and (ii) the phase separation methods. Recipes for the preparation of PDLCs are documented well in the literature (Drzaic 1995; Higgins 2000; Mucha 2003; Vicari 2003). We mention here, briefly, these two methods and a few nonconventional methods developed recently in the following sub sections. Depending upon the specific requirements of PDLC properties, various combinations of these methods are adopted in practice.

7.3.1 *Microencapsulation Method*

It is the simplest method for preparing PDLC films (Ferguson 1984, 1985). In it, first, an emulsion of water-soluble polymer and water insoluble liquid crystal is prepared by rapid stirring. The PDLC films are formed using spin-coating or simple deposition of an appropriate amount on a glass substrate (preferably coated with indium tin oxide, i.e., ITO) and letting the water to evaporate normally. In most of the general cases, water soluble polymer polyvinylalcohol (PVA) is used with different mesogenic materials. Because of the insolubility of liquid crystals in aqueous media, in microencapsulation, phase separation is achieved automatically. As a result, films produced in this way are reproducible and problem related with the plasticisation of polymer is not observed. However, hygroscopic nature of polymers sensibly reduces its abilities.

7.3.2 *Phase Separation Methods*

In this technique, as developed by Doane and co-workers (1986, 1987), the PDLC films are formed by a homogeneous solution of liquid crystal and polymer. During the solidification of homogenous solution most of the liquid crystal molecules are expelled from the polymer via various phase separation mechanism and liquid crystal molecules aggregate in droplets which remain embedded in the polymer film. There are various ways to implement this method as described below.

7.3.2.1 Polymerisation Induced Phase Separation (PIPS) Method

In PIPS method, the polymerisation is induced by an exposure of a homogeneous solution of liquid crystal and low molecular weight monomer or oligomer to heat, light or radiation. During the polymerisation, solubility of polymer and liquid crystal decreases and phase separation occurs. Due to phase separation, polymer chain forms a matrix surrounding discrete liquid crystalline domains. The PDLC films formed by PIPS method are quite durable, leading to good stability of PDLC based devices. One concern in the PIPS process is that it is sensitive to temperature, light intensity of the photo curing system, presence of impurity, solubility characteristic and molecular weight of the starting materials. Small variation in these parameters leads to different morphologies of the films with different electro-optical responses.

7.3.2.2 Solvent Induced Phase Separation (SIPS) Method

The SIPS is a process in which mutually soluble polymers and liquid crystals are mixed with an organic solvent to form a single-phase mixture. Evaporation of the solvent from the mixture causes phase separation of the polymer and liquid crystalline phases. Due to mutual solubility of liquid crystal and polymer, significant plasticization of polymers is observed. Although the plasticization may cause problems in some applications, it can also be useful in increasing the mouldability and flexibility of the film.

7.3.2.3 Thermal Induced Phase Separation (TIPS) Method

It refers to the mixing of liquid crystals in a thermoplastic melt at high temperature. On cooling the mixture, solidification of polymer induces phase separation of liquid crystals. This method is useful where a prefabricated cell is to be filled with the PDLC material. Further moderate solubility of liquid crystals in polymers leads to the plasticization of the polymers. As a result, a comparative reduction in both the number and size of droplets is observed.

7.3.3 Some Other Non-conventional Methods

Apart from the afore-mentioned conventional approaches, recently, several non conventional approaches have also been developed for the preparation of PDLCs films.

Kumano et al. (2011) have studied the multicolor PDLCs formed by *impregnation* of two liquid crystals 4-cyano-4'-pentylbiphenyl (5CB) and 4-(trans-4-pentyl-cyclohexyl)

benzointrile (PCH5) in the porous networks composed of N-methyl methacrylamide (MMAA) and N,N'-methylene-bis-acrylamide(BIS) as the monomer and cross-linker, respectively. This material changes its structural color covering the whole *visible region* in response to temperature by means of changes in both the diffraction properties and the wavelength dispersions of its refractive indices. At lower temperature, the randomly arranged LC in porous polymer network gives a translucent or milky appearance due to the scattering of the applied white light. However, at higher temperatures when LC reaches at isotropic state, a particular wavelength of light can predominantly be transmitted through the composite material at which the two wavelength dependent dispersion curves for the porous polymer network and LC intersect. Moreover, the point of intersection of the two wavelength dependent dispersion curves varies with temperature. As a result, the composite material exhibits bright coloration and also reveals a change in color in response to temperature. In addition, the structural color of this system may also be tuned by the application of electric field.

In another approach, Zou and Fang (2011) have used PlatSil Gel-10 (a platinum cure silicone kit) and 5CB to develop a free standing *adhesive PDLC film* and studied the change in its LC director configuration on different substrates. The unique feature of the adhesive PDLC film is that its structural and orientational patterns can be printed directly on different substrates by combining soft lithography with cohesive mechanical failure. In the printed PDLC films, director configuration of the dispersed 5CB droplets gets changed by change in the nature of the substrate surfaces. On the glass substrate, phase separation of 5CB from PlatSil Gel-10 shows radial configuration with maltese type crosses. A freestanding PDLC film is formed by peeling it from the glass substrate. When this freestanding film is placed on a rubbed polyimide coated glass substrate it generates parallel alignment of liquid crystal along the rubbing direction and again switches back to radial configuration after peeling out from the polyimide surface. When the film is placed on the adhesive side of 3M tape, the initial radial configuration of 5CB droplet gradually becomes parallel. This radial to vertical configuration is reversible for peeling off the films from 3M tape. Further, the LC droplets remain in the radial configuration when the film is placed on the non-adhesive side of 3M tape. Switching between radial and parallel configurations is due to strong adhesion of the PDLC film which makes an interfacial contact between polymer surface and PDLC film (De Gennes and Prost 1993).

Reversible fragmentation and self-assembling of liquid crystal droplets on *functionalized pyroelectric substrate* have also been reported by Merola et al. (2012). They have used 6CHBT and lithium niobate (LN) as liquid crystalline material and pyroelectric substrates, respectively. Initially, LN is functionalized in various ferroelectric domains by micro-engineering and then its surface is covered by a film of hydrophobic polymer i.e., polydimethylsiloxane (PDMS). Due to hydrophobic (i.e., non-wetting) nature of PDMS when a nematic liquid crystal (6CHBT) comes in contact with PDMS substrate it is difficult to obtain a homogeneous thin layer of 6CHBT. Instead, due to thermodynamic instability, 6CHBT arranges itself in drops with a relatively large contact angle. In this case various

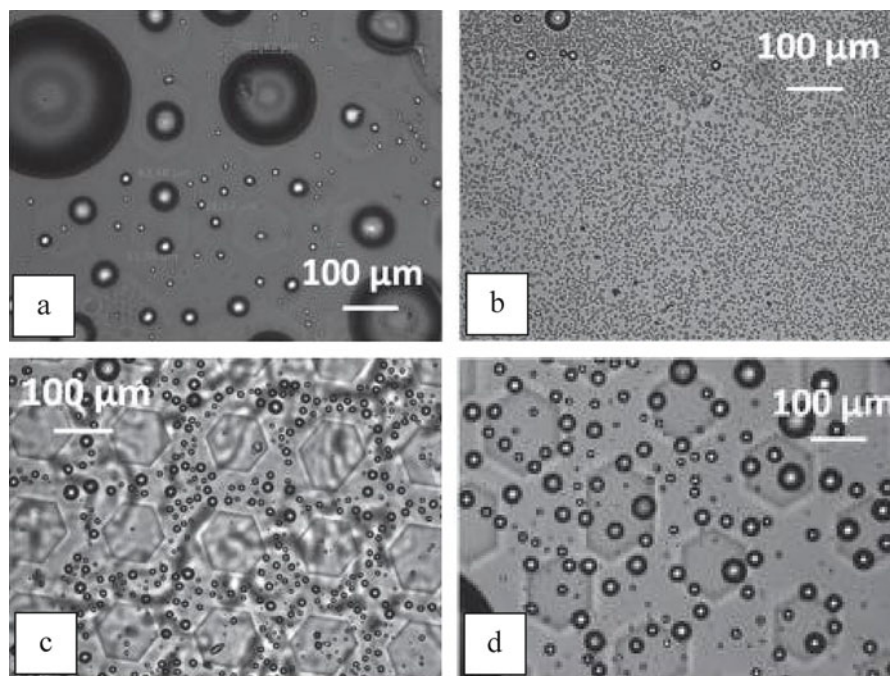


Fig. 7.2 Temporal evolution of nematic liquid crystal (6CHBT) in contact with fabricated PDMS substrate (a) scattered LC drops on the substrate before heating, (b) fragmented LC droplets after heating at 90°C , (c) with LN hexagonal domains after 2 h from the beginning of cooling, (d) coalesced LC drops on the substrate after some days at room temperature (Reprinted with permission from *Adv. Funct. Mater.*, 2012, **22**, 3267–3272. ©2012, John Wiley and Sons, Merola et al. 2012. Figure 3a, b, d and g)

geometrical structures of LN wafer, being present below the PDMS layers are capable to drive these small droplets. Due to change in the geometry of the LN substrate (i.e., the change in pyro-electrophoretic effect), fragmentation of LC droplets into smaller ones, their migration to the different regions of the sample, coalescence in bigger drops with the possibility of new fragmentation, matrix arrangement and lens effects, etc., have been observed. This study provides completely a new approach to manipulate liquid crystal by pyroelectric effect where the strong electric field generated brought a thermal stimulus which allows to manipulate liquid crystals in 2D on a substrate (Fig. 7.2).

The *holographic gratings* POLICRYPS and POLIPHEN have been proposed to realize a channel structure in which the polymer and LC molecules are almost completely phase separated. Consequently, very high diffraction efficiencies and time response in microseconds were achieved (Caputo et al. 2004). Pavani et al. (2009) have developed a PDLC material to record holographic diffraction gratings. They have used a PDLC layer consisting of monomers (N,N'-methylenebisacrylamide and n-vinyl-2-pyrrolidinone), photo initiator

(erythrosine B, triethanolamine (TEA)) and LCs (E7) and exposed it to an optical interference pattern. Solidification of polymer through PIPS process under modulated refractive index pattern leads to the development of holographic PDLC gratings with spatially periodic and alternating polymer-LC rich planes.

Through a careful selection of LC, polymer, initiator and other organic additives, switching speed and other optical properties of HPDLCs can be optimized for a given application. Busbee et al. (2009) have demonstrated the incorporation of high volume fractions of chemically *functionalized silica nanoparticle* into electrically switchable HPDLCs with sub-micrometer lattice constants. They have used pentyltriethoxysilane (PTES) and methacryloxypropyl-trimethoxysilane (MPTMS) to get functionalized nanoparticles. Due to chemical functionalization, silica nanoparticles are not sequestered into the liquid crystal but it covalently copolymerizes with the acrylate monomer and do not aggregate. Relatively large change in the electro-optical properties of PDLCs films as an effect of *gold nanoparticles* have been studied by Hinjosa and Sharma (2010). Due to inclusion of small concentration of nanoparticles local electric field is buildup in PDLC. It lowers the threshold voltage needed to switch on the electric field, increases optical transmission at certain voltage and influence the frequency response of PDLCs.

Use of *conducting polymer* poly(3,4-ethylenedioxy thiophene): p-toluene sulfonate (PEDOT:PTS) as electrodes in PDLCs have demonstrated a better electrical performance and light transmittance in similar devices using indium tin oxide as electrodes (Kim et al. 2008). Moreover, use of conductive polymers as electrode layer provides additional flexibility for PDLC device fabrication. Vapor-phase deposited polymerization technique was used for preparing ultrathin layer of PEDOT:PTS conducting layer on polyethylene terephthalate (PET) substrate in the presence of 'iron (III) p-toluene sulfonate (PTS)' solution. Iron (III) salt works as an oxidant for polymerization of PEDOT:PTS on the PET substrate and also provides dopant ions for the conductivity of the polymers. Fabrication of organic thin-film transistor (OTFT) driven PDLC on flexible polymer substrate polyethylene naphthalate film have also been reported (Sheraw et al. 2002). Uses of other conducting polymers such as polyacetylene, polyaniline, polypyrrole, polythiophene, etc., in flexible displays have also been reported (Groenendaal and Gevaert 2005).

7.4 Techniques for Characterization of PDLC Films

With the development of PDLCs, during the past three decades, several experimental techniques have been used to characterize its thermal, morphological and electro-optical behavior. Efforts have also been made to investigate various physical problems related with the phase separation, miscibility behavior, droplet configuration, surface anchoring, etc. Although the description of various characterization techniques used for PDLCs is well documented, for the awareness of novice readers a brief description about some of them is given in the following subsections.

7.4.1 *Differential Scanning Calorimetric (DSC) and Thermogravimetric (TGA) Analyses*

The DSC is one of the most powerful tools to study the phase transitions occurring in the material. In PDLCS, it is used to investigate the thermal behavior and different mesophase crystallization, melting and glass transition temperature (Hatakeyama and Liu 1998; Cheng 2002; Hohne et al. 2003; Reading and Hourston 2006). Whenever, phase transition occurs, heat is either evolved (exothermic) or absorbed (endothermic) by the material. DSC measures this heat difference through a controlled temperature programme by comparing the energy inputs between the sample and the reference pans as a function of temperature or time. The exact phase transition temperature of the material is determined as the peak of transition which results due to change in the heat of the sample pan as compared with the reference pan. Depending upon the method of measurement, two types of DSC instruments, i.e., heat-flux DSC (Gmelin 1997) and power-compensation DSC (Menczel and Leslie 1990; Menczel and Prime 2009; Schick and Hohne 1991) are in common use.

Thermogravimetric analysis (TGA) is used effectively for quantitative analysis of thermal reactions which are accompanied by mass change. For example, evaporation, decomposition, gas absorption, desorption, dehydration, etc. It is also used to determine the thermal stability of the materials. For TGA investigations, material is subjected either to a constant heating rate (dynamic measurement) or a constant temperature (isothermal measurement) or a non-linear temperature measurement under inert atmosphere. TGA measurements are usually displayed by a curve in which the mass of the material is plotted against temperature and/or time. The first derivative of the TGA curve with respect to temperature or time shows the rate at which the mass changes and is known as the differential thermo gravimetric analysis (DTGA) curve. The basic instrumental requirement for thermogravimetry is a precision balance with a furnace programmed for a linear rise of temperature with time.

7.4.2 *Polarization Optical Microscopy (POM)*

Polarization optical microscopy is one of the most popular and familiar tools to investigate the morphological changes observed in these materials (Fayolle et al. 1979; Crawford et al. 1991c; Jain and Rout 1991; Kitzerow and Crooker 1993; Lovinger et al. 1994; Amundson 1996; Mirau and Srinivasarao 1997; Yamaguchi et al. 1998; Natarajan et al. 1997; Drzaic and Muller 1989; Magagnini et al. 1999; Coleman et al. 2003; Formentin et al. 2008; Galyametdinov et al. 2008). It provides information not only about the various mesophases present in the material but also about the changes observed in their textures when confined to certain geometry. Morphological changes in the films are observed as a function of temperature, voltage and other physical parameters. When the films are kept in the

path of the light beam crossed with polarizers, birefringent LC droplets alter the polarization state of light passing through them. This alteration results as an increase in the optical power transmitted through the microscope. The distinctive microscopic patterns provide proper information about the local liquid crystal orientation, their overall configuration and mode of anchoring (i.e., homogeneous or homeotropic) at the polymer interface. Depending upon the specific requirement of the material POM can be operated in transmitted or incident light modes.

7.4.3 X-ray Diffraction (XRD)

The X-ray diffraction technique (XRD) is commonly used for the characterization of materials, particularly the crystal structure and lattice parameter evaluations. It includes single-crystal and powder XRDs. The X-rays diffraction pattern essentially results from the combination of two different phenomenon (i) scattering of X-rays by each individual atoms lying in a plane and (ii) subsequent interference between the waves scattered by these atoms. This leads to the well known Bragg's diffraction. Well defined sharp peaks are obtained for crystalline lattice but the amorphous systems give broad hallows at low angles. It is well known that a crystalline lattice gives diffraction maxima at well defined ' θ ' values (characteristics of the material) corresponding to different ' d ' values for specified planes governed by Bragg's law

$$2d_{hkl} \sin\theta_B = n\lambda,$$

where, n is an integer, λ is the radiation wavelength, θ_B is the Bragg's diffraction angle and d_{hkl} is the distance between the reflecting parallel planes. The peak position (i.e. 2θ) is characteristic of the diffraction from a particular (hkl) plane (Azaroff 1968).

7.4.4 Fourier Transformed Infrared (FTIR) Spectroscopy

The FTIR spectroscopy is the technique used for the determination of molecular vibrational modes involving various structural bonds and groups in liquids, gases, powders, films, etc. In FTIR, determination of specific vibrational frequencies at which sample absorbs the IR radiation gives information about the functional groups or molecules present in the material, and hence information about the chemical specificity of the material. Any shift in these vibrational frequencies gives information about the possible interaction or changes occurring in the materials.

The FTIR spectrometer basically consists of a source of radiation in mid-infra-red region (viz., usually a silicon carbide rod known as globars), an interferometer

and a detector. The most commonly used detectors are made of pyroelectric deuterated triglycine sulphate (DTGS) and photo conducting mercury cadmium telluride (MCT). Interferometer allows simultaneous measurement of all the wavelengths in the MIR range and consists of a beam splitter, a fixed mirror, a movable mirror, and a drive and positioning mechanism. The intensity of the radiation at the detector is a function of the optical path difference of the beams in both the arms of the interferometer. Interferogram is obtained as a plot of intensity vs. wavenumber (cm^{-1}) using mathematical Fourier transformation (Kellner et al. 2004; Griffiths and Haseth 2007; Harris 2007).

7.4.5 Nuclear Magnetic Resonance (NMR) Spectroscopy

NMR is a powerful technique used frequently to investigate the director structures within the microscopic cavities (Drzaic 1995; Pasini et al. 2003). It is equally applicable to submicron size droplets where optical methods fail to generate useful information due to higher wavelength of light as compared with the droplet diameter. Chemical specificity (Golemme et al. 1988b) and other aspects of nematic dispersion, including molecular orientation, rotation, diffusion, dynamic processes, interfacial effects in proximity to polymer surfaces, etc., have been explored using this technique. Both ^{13}C NMR and ^2H NMR have been used to investigate the PDLC films but usually the solid-state ^2H NMR is preferred over the ^{13}C NMR. In ^2H NMR, advantage is taken of the fact that deuteron possesses nuclear spin = 1 and a nonzero quadrupolar moment. There is an additional perturbative contribution in the energy level of deuteron coming from quadrupolar interaction between deuteron and the electric field gradient of the C–D bonds of the molecules. In the isotropic states, the perturbative contributions are completely averaged out in a single narrow line of width below 100 Hz by the molecular motion, but the same is not true for nematic (or other anisotropic) phase. In later case, single narrow line splits into a doublet with splitting being typically of the order of ~ 100 kHz. Since NMR spectrum reflects the response of all the molecules in a sample, its use for PDLCs system provides specific information about the contributions made by individual droplets (by their director configurations) in the spectra.

In PDLC films, both experimental and theoretical NMR spectra have been studied frequently to determine the director fields, orientations and diffusion within (or in between) the cavities (Crawford et al. 1991b; Buchert et al. 1993a, b). These studies include the detailed models of organizational and diffusional effects on the line shapes and splitting. Radial and bipolar orientations have been distinguished by diffusion properties of the nematic within the droplets (Golemme et al. 1988a). For radial droplets, molecular orientation is a sensitive function of position so diffusion changes the orientation of the molecule. In this case, NMR spectra observed earlier in the absence of (or slow) diffusion limit collapses into a single line centered at zero quadrupolar splitting in the presence of (or fast) fast diffusion limits. However, in bipolar droplet, nematic is oriented more-or-less in the same direction and

molecular diffusion makes only a partial averaging of the two lines of quadrupolar splitting in spectrum (Pasini et al. 2003). Further studies include, director alignment in the LC/polymer network system (Stannarius et al. 1991), electric field driven reorientation of submicron droplets (Aloe et al. 1991), weakly oriented ordered surface layer in the isotropic phase of a liquid crystalline material (Dolinsek et al. 1991; Crawford et al. 1991a, 1992).

Solid-state ^{13}C NMR technique has been used to understand the importance of the molecular motion of the liquid crystalline materials in switching phenomenon for PDLCs. A proper understanding of the switching behavior of LC molecules within the PDLC films will enhance its use by minimizing both the LC concentration and switching voltage while maintaining the good scattering properties of the PDLC films. Vilfan et al. (2003) have used low frequency proton NMR relaxometry in the kilohertz frequency range to study the spin–lattice relaxation of 5CB above nematic to isotropic transition in microdroplets of a PDLC film. Change in the mobility of the molecular segments of 5CB molecules in epoxy based polymer results due to increased interaction between LC and polymer. Molecular motion of LC within the droplet gets restricted due to decreased droplet size in PDLC films as a result of increased contact between the polymer matrix and the liquid crystal (Vilfan et al. 2003).

Apart from the afore-mentioned techniques some other approaches have also been used to determine the liquid crystal organizations in PDLCs. Angle-dependent light scattering studies (Zumer and Doane 1986; Zumer 1988; Whitehead et al. 1993) have been used to deduce the predominant liquid crystal configuration in PDLCs. Fourier transformed Raman spectroscopy has been used to provide chemically specific orientational information of the PDLC materials (Andreev et al. 1997). The order and dynamics of the LC material inside the nanosized droplets of a holographic PDLC film is recently investigated using ESR spin probe (Bacchiocchi et al. 2009). It determines the LC local director configuration inside the alternatively arranged LC nanodroplet and polymer layers.

7.4.6 Dielectric Relaxation Spectroscopy (DRS)

Dielectric relaxation spectroscopy is a well established technique to study the dynamics and motional behavior of liquid crystals in bulk as well as in confined geometries (Kramer and Schoenhals 2003; Kao 2004; Rzoska and Zhelezny 2004; Barsoukov and Macdonald 2005; Raikher and Shliomis 1994). When a dielectric material is placed in an external electric field E , dipole moment is induced in the material and it gets polarized under the influence of the field. One or more than one contributions, i.e., electronic, ionic, orientational and translational polarization may cause polarization in a dielectric material. Macroscopic polarization ' P ' i.e., the average value of induced dipole moment per unit volume of the material is defined as the sum of the microscopic dipole moment \mathbf{p}_i of individual molecules within the volume V ,

$$\mathbf{P} = \frac{1}{V} \sum_i \mathbf{p}_i \quad (7.9)$$

In linear approximation, macroscopic polarization of a dielectric material is proportional to the strength of the applied external electric field \mathbf{E} :

$$\mathbf{P} = \varepsilon_0 \chi \mathbf{E} \quad (7.10)$$

where, χ is the dielectric susceptibility of the material and $\varepsilon_0 (=8.854 \times 10^{-12} \text{ F m}^{-1})$ is the dielectric permittivity of the free space.

According to Maxwell, matter can be treated as a continuum and the field inside the matter is the direct result of the electric displacement (electric induction) vector \mathbf{D} , which is electric field correction for the polarization:

$$\mathbf{D} = \varepsilon_0 \mathbf{E} + \mathbf{P} \quad (7.11)$$

From (7.10) and (7.11), we get,

$$\mathbf{D} = \varepsilon_0 \mathbf{E} + \varepsilon_0 \chi \mathbf{E} = \varepsilon_0 \mathbf{E} (1 + \chi) = \varepsilon_0 \varepsilon^* \mathbf{E} \quad (7.12)$$

where $\varepsilon^* = (1 + \chi)$ is called the relative permittivity or complex dielectric constant of the material. Normally ε^* is a complex quantity and is given by

$$\varepsilon^* = \varepsilon' - j\varepsilon'' \quad (7.13)$$

where, $j = \sqrt{-1}$, and, ε' and ε'' are the real and imaginary parts of complex dielectric constant (ε^*), respectively. In general, the real part of dielectric constant (ε') provides information about the charge storage capacity of the material, whereas imaginary part (ε'' , also termed as dielectric loss) provides information about the loss from the material. Further, the ratio $\varepsilon''/\varepsilon'$ is used to obtain information about the dielectric relaxation processes occurring in the material and is described as loss tangent (i.e., $\tan \delta$)

$$\tan \delta = \frac{\varepsilon''}{\varepsilon'} \quad (7.14)$$

The relaxation processes occurring in the material are investigated by studying $\tan \delta$ as a function of frequency of the applied signal and temperature. Either of the plots, i.e., $\tan \delta$ or dielectric loss (ε'') vs. frequency of the applied signal gives a peak value, described by the relation $\omega\tau = 1$, where τ is the relaxation time and ω is the angular frequency of the applied signal (Kramer and Schoenhals 2003).

In PDLCs, dielectric relaxation spectroscopy has been used frequently to study the various interesting results related with anchoring effect and motion of the LC molecules in microscopic cavities (Jadzyn et al. 1999; Ganesan et al. 2009),

alignment and director order parameter of LC molecules (Williams et al. 2001), interfacial polarization process due to accumulation of charges at LC/polymer interface (Boussoualem et al. 2004), electro-wetting and reconfiguration effects (Fan et al. 2009; Ren et al. 2009), etc.

7.5 Droplet Morphologies and Director Configurations in PDLC Films

The confinement of LCs in microscopic droplets, their shape, size and alignment play a significant role in governing the ordering, dynamics, scattering and other electro-optical properties of PDLCs. These properties depend strongly upon the nature and composition of LC and polymer constituents, their refractive indices, solubility parameter, miscibility behavior, etc. Several groups are engaged actively in studying and characterizing the properties of PDLCs by using various binary and multi-component mixtures with other additives (Busbee et al. 2009; Pavani et al. 2009; Hinjosa and Sharma 2010; Cupelli et al. 2011; Zhou et al. 2011). In the following subsection, we provide a brief glimpse of some significant contributions made in this direction.

7.5.1 Droplet Morphologies

Polarizing optical microscopy has been used widely to perform morphological investigations on PDLCs. It shows the significant changes in the phase behavior of LCs confined in microscopic sized cavities as compared with their bulk counter parts. Various types of liquid crystal organizations such as axial, radial, bipolar, toroidal, etc. have been observed in PDLC films when observed through POM.

One of the earlier most studied PDLC film was prepared by using an LC mixture (E7) and side-chain liquid crystal epoxy polymers (LCEP) with cyanobiphenyl pendants (Chien et al. 1992). After the thermal induced phase separation (TIPS) process the POM images show radial nematic configurations which were quite different from the characteristic nematic textures observed earlier in pure LCEPs (Fig. 7.3a, b). Progress continues with the use of different LC and polymer materials to investigate the morphological changes observed in PDLCs when LC gets confined in microscopic cavities of polymers. For unpolymerized and UV-polymerized 2-ethyl hexyl acrylate (EHA) mixtures with E7, nematic droplets with a twisted radial structure inside the droplet have been observed (Roussel et al. 2000). It indicates the homeotropic anchoring at the polymer LC interface. As an effect of coalescence/diffusion phenomena significant changes in the size, shape, spatial distribution, number density, etc., of nematic droplets have been observed with the lapse of time (Fig. 7.3c, d). In the blends of polystyrene and EBBA (at different

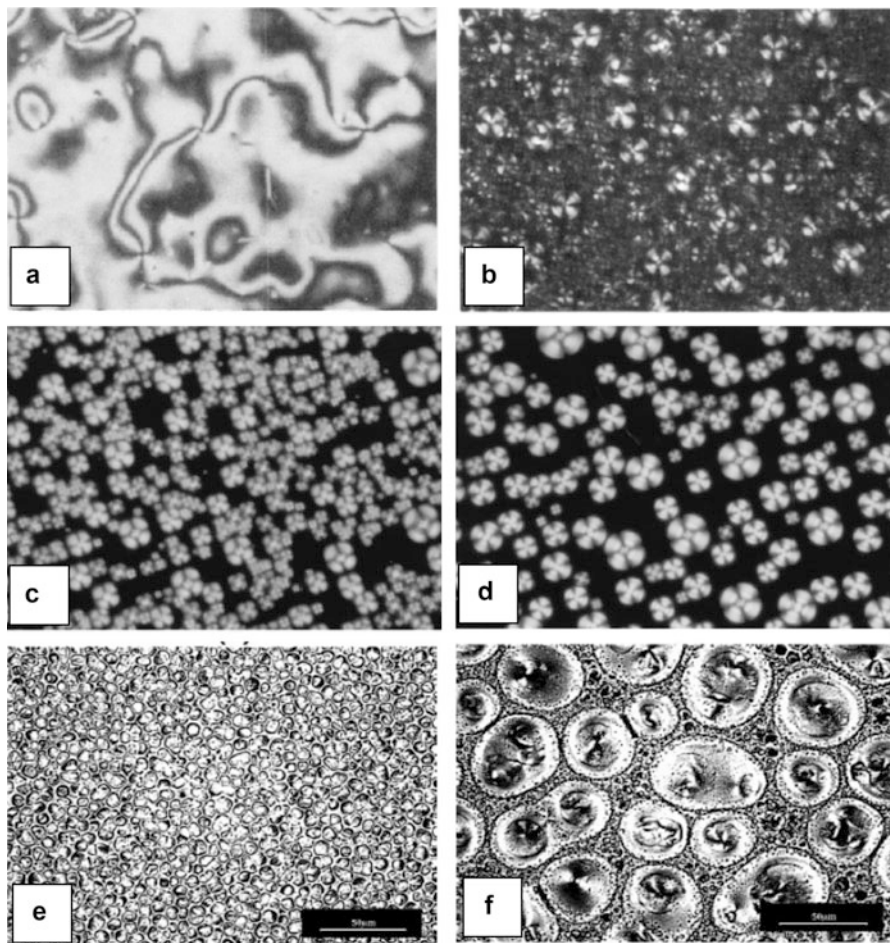


Fig. 7.3 POM images of (a) anisotropic LCEP-3 and (b) LCEP-3 dispersed liquid crystals (E7) (50/50) (Reprinted with permission from *Macromolecules*, 1992, **25**, 133–137. ©1992, American Chemical Society, Chien et al. 1992, Figure 2 and 3), PEHA/E7 (50:50) film as a function of time elapsed after UV exposure for (c) 30 min and (d) 15 h (Reprinted with permission from *Phys. Rev. E.*, 2000, **62**, 2310–2316. ©2000, American Physical Society, Roussel et al. 2000, Figure 8), EBBA/PS (80:20) arising by (e) fast and (f) slow cooling from 130 °C (Reprinted with permission from *Macromol. Chem. Phys.*, 2003, **204**, 928–935. ©2003, WILEY-VCH Verlag GmbH & Co KGaA, Weinheim, Hoppe et al. 2003, Figure 3d and 4d)

compositions), cooling at faster and slower rates results in the LC droplets of smaller and larger sizes, respectively (Fig. 7.3e, f). Changes in the phase diagram and different morphologies generated in these blends were studied by Hoppe et al. (2003).

Several other studies reveal that with changes in the surface anchoring conditions at LC/polymer interface, alignment of LC droplets gets changed. Polystyrene macro-iniferter (MI) has been used to control the alignment of LC molecules at the

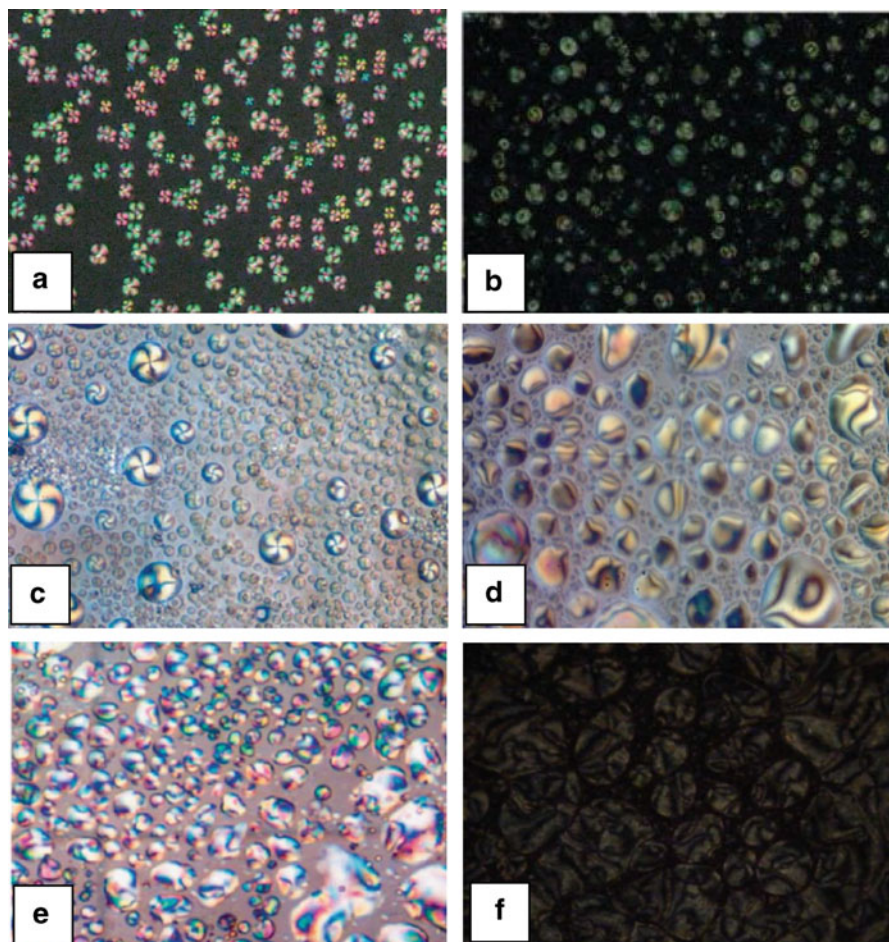


Fig. 7.4 POM images of PDLC films for MI:BA:E7 = 5:35:50 (by weight) using MI concentrations (a) 0.1 % and (b) 1 % (Reprinted with permission from *Liq. Cryst.*, 2009, **36**, 933–938. ©2009, Taylor & Francis, Yan et al. 2009, Figure 4b and d), for 30 wt% and 75 wt% of UDDBA in PMMA showing (c) radial and (d) bipolar configurations, for 75 wt% of DDBA in PMMA showing (e) randomly oriented nematic droplets (Reprinted with permission from *Liq. Cryst.*, 2011, **38**, 849–859. ©2011, Taylor & Francis, Srivastava et al. 2011, Figure 4d and Figure 7c, d) and (f) for 60 wt% of UDDBA in P(VdF–HFP) showing nematic droplets with schlieren textures (Reprinted with permission from *Liq. Cryst.*, 2012, **39**, 1402–1413. ©2012, Taylor & Francis, Srivastava et al. 2012, Figure 4e)

droplet walls in PDLC films of butyl acrylate and E7 (Yan et al. 2009). Initially, at lower composition of MI, relatively small surface interaction favors the radial configuration which changes to bipolar one with increase in the composition of MI (Fig. 7.4a, b). Morphological changes observed in LC material consisting of decyloxy benzoic acid with different alkyl chains in PMMA matrix show that the randomly oriented nematic droplets and schlieren textures which were observed in

the pure mesogens get changed into radial (with maltese type crosses) and bipolar configurations. Change in the droplet morphologies due to the change in the polymer constituents and rate of cooling from an isotropic state have also been reported (Fig. 7.4c–f) (Srivastava et al. 2011, 2012).

Different types of morphological and electro-optical studies in PDLCs have been carried out as an effect of polymer viscosity, dye concentration, etc. Change in the droplet morphology and optical properties of PDLC films of a commercially available UV curable polymer NOA-65 and low molar mass nematic liquid crystal E-8 (BDH, UK) as an effect of temperature and applied voltage are shown in Fig. 7.5a, b. The POM images show LC droplets which have initially the bipolar configurations with random distribution of molecular axes get arranged into maltese type crosses with molecular axes oriented along the direction of applied electric field with increase in the applied voltage. Moreover, with increase in the temperature, effective voltage drops across the LC droplets. Consequently, the optical transmission and threshold voltage V_{th} decrease (Malik and Raina 2004). Effect of the polymer viscosity on the morphology of the PDLC films using ferroelectric liquid crystal ZLI-3654 and commercially available UV curable Norland polymers (NOA series of different viscosities) show that for unaligned films, LC droplet size increases with increase in the polymer viscosity whereas in aligned films, LC droplets get elongated along the rubbing direction of the alignment (Fig. 7.5c, d).

Also, dispersed films show that as compared with pure FLC, spontaneous polarization of the films decreases up to 50 % with increase in the polymer viscosity (Malik et al. 2003). Further, low viscosity based PDFLC film shows fast switching behavior than higher viscosity based PDFLC films (Malik et al. 2010). Optical contrast and electro optical response of the PDLC films may be tuned by using different concentrations of dyes as dopants in LC materials. Use of dye influences LC droplet size, and samples with low concentration of dye, provide an improved contrast ratio and reduced threshold voltage. The morphological changes observed as an effect of different concentration anthraquinone dye and applied voltages in PDLC films of NOA65 and E7 are shown in Fig. 7.5e–h (Kumar and Raina 2007).

7.5.2 Director Configurations

Morphological investigations of various PDLC films show a number of LC configurations and their *inter-se* transformation within/in-between the droplets of a PDLC film. Usually, four common types of LC configurations which are *bipolar*, *radial*, *toroidal* and *axial* have been observed in these droplets (Fig. 7.6).

These configurations depend strongly on the size, shape and strength of interfacial interaction at LC/polymer interface and can be manipulated by external parameters, like temperature, electric field, magnetic field, etc. With variation in these parameters droplets in one configuration may become unstable and transformed into a more stable configuration. Basically two approaches are

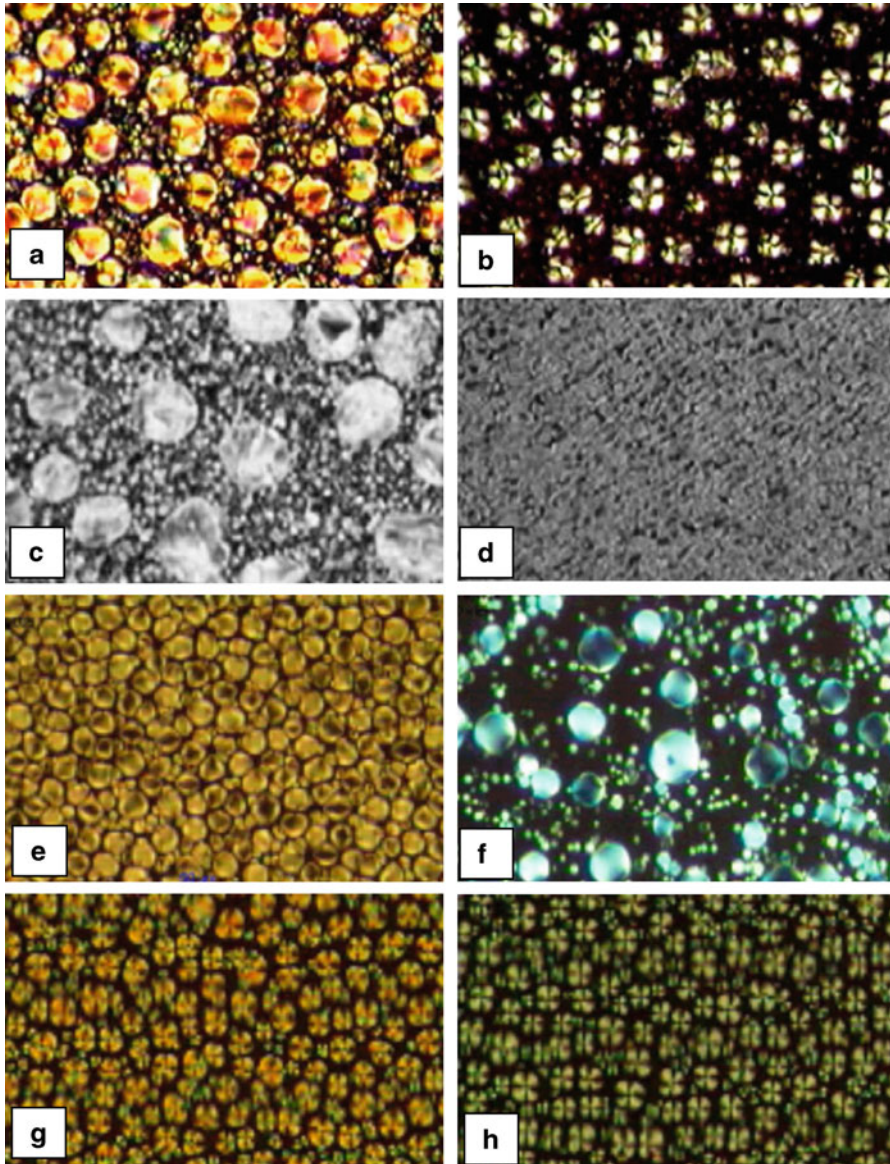


Fig. 7.5 Morphologies for PDNLC film at 55 °C in external field ($f = 1$ kHz) of (a) 5 V and (b) 25 V (Reprinted with permission from *Optical Materials*, 2004, **27**, 613–617. ©2004, Elsevier B. V., Malik and Raina 2004, Figure 1b, d), for PDFLC films using multi-component FLC mixture ZLI-3654 and UV curable polymer NOA-65 under (c) unaligned and (d) aligned conditions (Reprinted with permission from *Current Applied Physics*, 2003, **3**, 325–329. ©2003, Elsevier B. V., Malik et al. 2003, Figure 1c and Figure 3b), for DPDLC films with dye concentrations (e) 0.25 % and (f) 0.5 %, and, with applied voltages (g) 10 V and (h) 20 V on films with dye concentration of 0.25 % (Reprinted with permission from *Curr. App. Phys.*, 2007, **7**, 636–642. ©2003, Elsevier Science B. V., Kumar and Raina 2007, Figure 3b, c and Figure 5c, d)

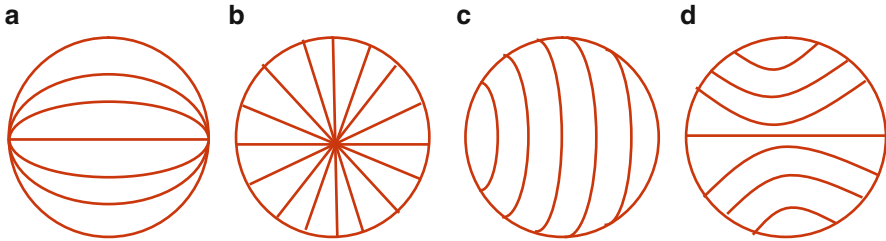


Fig. 7.6 Nematic director configurations: (a) bipolar, (b) radial, (c) toroidal, (d) axial

employed to analyze these droplet configurations. First one is based on analytical/numerical approach and other one is on the computer simulation approaches. In specific situations, computer simulation gives a better result but approximations lead to a better understanding of the related phenomenon. In both the cases, numerical computation must also be performed. In analytical/numerical approach, droplet configurations have been discussed using certain basic assumptions (Zumer and Doane 1986; Bloisi and Vicari 2003):

1. Droplets are ellipsoidal (or more preferably spherical) in shape with a well defined droplet direction along the major axis under zero (or no external) field. These droplet directions get changed with the application of external field in such a manner that the droplet director (\hat{n}) be defined as the average direction of the nematic director inside the droplet.
2. Another assumption is the elastic constants approximations according to which

$$K_{11} = K_{22} = K_{33} = K$$

$$K_T = K_{22}/K_{11}; K_B = K_{33}/K_{11}; K_T = K_B = K$$

Bipolar and radial configurations result at zero fields with strong planar and homeotropic surface anchoring, whereas, toroidal and axial configurations are found for the conditions, $K_{33} \ll K_{11}$ and planar surface anchoring, and, $K_{33} \ll K_{11}$ and homeotropic surface anchoring, respectively. Some times more complex configurations like twisted configuration may also occur for larger values of splay elastic constant i.e., $K_{11} \gg K_{22} + 0.431 K_{33}$ (Drzaic 1995).

7.5.3 Transformation Between the Droplet Structures

Within the LC droplets, transformations between different configurations provide information about the various physical parameters useful to describe the liquid crystalline states and also to explore their properties in device applications. Nematic droplets and their transformation between different configurations have been nicely discussed in literature (Drzaic 1995; Páram and Nieves 2009; Kleman and Lavrentovich 2006; Leon et al. 2011a, b). Here we summarize, in brief, some basic transformation between these configurations.

Radial-axial configuration can be induced in a number of ways such as with the change in electric or magnetic field (Candau et al. 1973), surface anchoring energy, elastic constants, etc. Strong polar anchoring favors the radial structure whereas a strong external field induces axial structure. Axial structure can also be generated in the absence of external field if anchoring strength is sufficiently weak (Erdmann et al. 1990). A more detailed theoretical discussion for these transformations has been given by Zumer and Kralj (1992). Their results predict that the stability of radial-axial configuration depends on the relative value of the surface elastic constant i.e., K_{24} as compared with other nematic elastic constant. Calculations predict that K_{24} has only a minor effect on the director configuration within the radial or axial droplet but a more significant effect on the relative stability between these configurations. For sufficiently large droplets (1–50 μm) linear dependence on electric field and droplet size was observed for radial-axial transformation (Kovalchuk et al. 1988) but for very small droplets weak anchoring becomes more pronounced and favors the axial configuration.

The transformation between the *bipolar-radial* and *radial-bipolar* structure arises due to change in the surface alignment from parallel to perpendicular (Volvoik and Lavrentovich 1983). Starting with a bipolar droplet, transformation begins with a disclination (in the form of annular ring) on the droplet equator. With increase in the tilt angle as a change in the alignment, ring disclination moves towards the pole while point defect (boojums) at the pole becomes larger and dissipates. Once the ring defect contracts to a point defect it forms a point defect (hedgehog) which detaches from the surface and moves into the centre of the droplet forming a radial structure. Radial-bipolar transformation begins with the boojums at the pole and hedgehog moving towards the pole when alignment changes from perpendicular to parallel. Further, the intermediate states of the bipolar-radial and radial-bipolar structures are similar but not identical. Therefore, these transitions are not symmetric in the sense of possessing identical intermediate droplet configurations.

Besides the afore-mentioned droplet configurations within the droplets some other transitions have also been reported. These transitions are bipolar-twisted bipolar and bipolar-concentric (Drzaic 1988a), bipolar with twist wall (Reamey et al. 1992), radial-escaped radial (Xu et al. 1992) transition, etc. Additionally, cholesteric droplets also show several transitions such as, radial line (spherulite)—planer transitions (Yang and Crooker 1991; Kitzerow and Crooker 1992), helical unwinding of spherulite (Kitzerow and Crooker 1993), twisted helical transitions (Kurik and Lavrentovich 1982), etc. Defects play an important role in studying the various configurations within the droplet. They arise due to manipulation of the external parameters. Various configurations occur as a result of contraction between the line and point defects, associated escaped defects structures, and difference in the direction of rotation of nematic director on opposite sides of the droplet.

7.5.4 Interfacial Effects

In PDLCs films, different LC configurations occur due to change in interfacial properties at the LC/polymer interfaces. A number of constraints like, LC/polymer composition, their constituent, curing or exposure time to radiation, nature and concentration of the dopant, heating and cooling rates, etc., affect the interfacial properties in a typical PDLC film. Interfacial forces play an important role in determining liquid crystal anchoring (i.e., homogeneous or homeotropic) at the LC/polymer interface and also the droplet configuration (Erdmann et al. 1990; Mcfarland et al. 1993; Mirau and Srinivasarao 1997). Any small alteration in these forces may cause significant changes in LC droplet configuration. For large droplets of few microns size these changes can easily be observed using POM technique, but for very fine microscopic droplet other probes like NMR, IR imaging, AFM are used. Usually, solid-state ^1H and ^{13}C NMR are used to study the static and dynamic properties of interfacial regions in inhomogeneous materials (Crawford et al. 1991b, 1992; Allender et al. 1991; Cross and Fung 1992, 1993; Mirau and Srinivasarao 1997).

^2H NMR spectroscopy and relaxometry is a very sensitive technique to study the surface-induced order and molecular dynamics in isotropic phase of LCs in confined geometries. Due to the absence of the long-range orientational order in isotropic phase it is very useful in studying the surface interactions. It is also suitable for measuring the degree of orientational order in the isotropic phase for cylindrical, spherical and other irregular cavities. Vilfan et al. (1999a, b) have studied the two representative systems of confined LC (i) 8CB in cylindrical cavities of anopore membranes and (ii) 5CB with an embedded polymer network. They found substantial increase in the spin–lattice relaxation (T_1^{-1}) and transverse relaxation (T_2^{-1}) rates being stimulated by the surface induced orders. Measurement of T_1^{-1} provides insight into the molecular dynamics in confined LCs. In bulk isotropic phase, T_1^{-1} is increased due to local molecular reorientations which have at least one correlation time in nanosecond range. But in nematic phase, abrupt decrease in T_1^{-1} is observed, as the orientational ordering takes place and imposes limitation on the molecular rotational mobility. At temperatures much above the nematic-isotropic transition due to random motion of molecules both T_1^{-1} and T_2^{-1} are equal. But, for decreasing temperature near nematic-isotropic transition, T_2^{-1} attains a greater value due to short range anisotropy within the isotropic phase. Increase in T_2^{-1} provides information about the effect of spatial constraints on molecular mobility and on the surface orientational order parameter.

^{13}C -NMR provides a convenient method for the determination of order parameters of bulk LC by measuring the anisotropic chemical shift (Guo and Fung 1991, 1992). But it is also useful in investigating the orientational order of LC droplets confined in a polymer matrix. Roussel et al. (2002) have determined the orientational ordering of 5CB droplets confined in a polyethylhexylacrylate (PEHA) matrix using NMR and other probes. Aliphatic region of the spectra shows that the 2-ethyl hexyl fragment of the polymer chain is partially ordered due to

interdigitation with 5CB molecules at the polymer/LC interface. Moreover, due to higher chemical shift in anisotropic state, aromatic NMR signals were used for the calculation of the order parameter. Further, as suggested in the literature (Buchert et al. 1993a, b; Vilfan et al. 1995, 1999a, b), in smaller droplets enhanced LC/polymer contact limits the mobility of LC in the droplets as compared to LC in bulk. Its morphological study shows homeotropic anchoring of nematic director in droplets. It suggests that the polymer surface influences the surface orientational order and may lead to an increase of the nematic order in smaller cavities. It suggests that the interfacial effects at LC/polymer interface significantly affect the director orientational order of the nematic LCs in smaller cavities. Application of electric and magnetic fields might also increase the order parameter for confined LCs and also induce a transformation of the director configuration leading to radial or axial configuration (Crawford and Doane 1992; Erdmann et al. 1990). The aliphatic chains of the polymers are also known to provoke a surface induced order (Proust et al. 1972; Crawford et al. 1996; Amundson and Srinivasarao 1998; Roussel et al. 2000).

In other methods, AFM technique has been used for characterizing and understanding the interfacial effect in various PDLC films (Herod and Duran 1998a, b). Optical contrast mechanism (using IR imaging) has also been explored for getting specific information about interfacial effects as a change in refractive index near LC/polymer interface (Bhargava et al. 1998).

7.6 Electro-Optical Properties

There are a number of parameters which influence the properties of a PDLC film in device development applications. These are concerned with its film thickness, droplet size and shape, morphology, polymer plasticisation, composition, refractive indices, etc. Optimum voltage required to activate a PDLC device depends strongly on the thickness of the film. Both the average droplet size and its distribution play an important role in defining the microstructures for device applications. Scattering and reorientation properties of the film depend strongly upon the droplet size. A number of features of PDLC make it useful in various device development applications: (i) It does not require any rigid boundary and can be used to develop large and flexible films, (ii) It does not require any polarizer or other optical element except transparent electrode to provide optical contrast, thus useful in the development of compact devices and (iii) It requires much smaller amount of liquid crystal as compared with LC based devices, thus has an economic incentive also.

In generalized terms, basic principal of PDLC films operation includes field-dependent light scattering from the 'standard' nematic droplets. In these materials, scattering phenomenon depends on the refractive indices of LC and polymer constituents and also on the applied electric field, being 'typical' for most of the PDLCs. The other optical properties which have been explored in PDLCs are dichoric absorbance, reflection of polarized light, nonlinear optical effects, etc.

Depending upon the applied electric field (or voltage) other useful electro-optical properties include operating voltages and voltage holding ratio, optical contrast, PDLCs response time and switching speeds, memory effects, conductivity, polarization and depolarization effect, etc., in PDLC films (Vaz and Montgomery 1989; Zhang et al. 1992; Jain et al. 1993; Im et al. 1995; Drzaic 1995; Bouteiller and Barny 1996). The field-dependent properties of PDLC films are determined by both reactive and resistive effects (Drzaic 1995). Reactive effects are those which are out of phase with the applied voltage and stores energy within the film, while resistive effects are in phase and dissipate energy through the creation of heat. Depolarization charges and director reorientation in PDLC films appear as reactive elements, while movement of ions through the polymer and liquid crystal and other electro-chemical processes at the electrodes are all examples of dissipative resistive elements. PDLC films are often discussed by an equivalent electric circuit model, in which film components are treated as a network of resistor and capacitor. In the simplest case, PDLC film consists of three elements, a parallel resistor and capacitor for liquid crystal/polymer composite and a series resistor for the conducting substance.

A brief description about some of the important electro-optical properties of PDLC films are given in the following subsections.

7.6.1 Light Scattering Properties

In PDLC due to mismatching between the ordinary and extraordinary components of the refractive indices of the LC materials and with the refractive index of the polymer matrix, light passing through the film gets scattered significantly. However, if there is no mismatch between the refractive index, light scattering vanishes. The amount of scattering depends upon a number of parameters concerning the state of polarization, angle of incidence, wavelength etc. of the incident light beam, various operating conditions like temperature, nature (waveform) and amplitude of the applied electric or magnetic fields, constituents, composition, dielectric, elastic and refractive index properties of LC and polymers, shape, size and distribution of LC droplets in PDLC films, etc. (Bloisi and Vicari 2003).

Initially, application of a suitable electric field aligns the LC molecules in a direction parallel to the field. As a consequence light incident normal to the field gets transmitted perfectly. But when the field is removed, due to change in LC orientation, incident light gets scattered randomly resulting a decrease in the overall transmittance value. The fundamental question in the light scattering problem is to determine the electromagnetic field at an arbitrary point in the surrounding medium of the scattering object (an LC molecule with certain dipole distribution in the case of PDLCs). Generally, superposition of electromagnetic fields coming from the incident light and the scattered one is taken into consideration for studying the scattering problems. Rigorous solution to the scattering problems are little tedious and beyond the scope of the present chapter. It involves certain assumption/

approximation related to anomalous diffraction, optical resonance, Raman scattering, Rayleigh scattering, Rayleigh–Jeans approximation, etc. and is described properly in literature (Van De Hulst 1957; Zumer 1988; Basile et al. 1993; Bloisi et al. 1995; Bloisi and Vicari 2003; Dick and Loiko 2001).

7.6.2 Response Time of PDLCs

PDLC films are often characterized by their ability to respond quickly to the changes occurring in the applied field, i.e., the rise and decay times. The time needed for transmitted intensity to reach (or fall) at 90 % of the saturation value, after application (or removal) of driving voltages are defined as ‘rise’ and ‘decay’ times, respectively. The typical orders of magnitudes of response time ranges from 1 to 10 ms for rise and 10 to 100 ms for decay times (Vaz and Montgomery 1989; Zhang et al. 1992; Jain et al. 1993). Dual frequency LCs mixtures have been used to speed up decay time. For applied field of low frequencies, it behaves as a positive LC and for high frequencies it behaves as a negative LC. PDLC film can be switch on by a low-frequency electric field, while a high frequency electric field is used to rotate LC molecules away from aligned direction. Some times cholesteric dopants are also used to reduce the decay time (Lu and Yang 1994).

7.6.3 Conductivity and Dielectric Properties of PDLCs

The inhomogeneous nature of the PDLC films along with intrinsic anisotropy of liquid crystals makes it interesting for various electric applications (Cupelli et al. 2009, 2011; Drzaic 1995). Since, both the conductivity and dielectric properties of the liquid crystals are anisotropic, depolarization fields across the droplets depend upon its (droplet) orientation. The movement of ions and the creation of depolarization field affect both the reorientation and dynamics of LC droplets inside the PDLC films. Therefore, change in the LC droplet size and director orientations can be explained by making use of polarization and depolarization fields. Polarization charge opposes the local field so it can either reduce or enhance the local field in different portions of the film. With application of an external field, movement of ions establishes a depolarization field in the direction opposite to the applied field. As a result, effective field across the LC droplets reduces (a Maxwell–Wagner effect) in the whole PDLC film (Rout and Jain 1992a, b; Zhong et al. 1992; Kuriakose et al. 2014). If the polymer is more conductive than the LC material, polarization field will enhance the field across the LC droplets. A reduced (or enhanced) field across the droplet requires a higher (or lower) external voltage applied to the films for droplet reorientation.

Ionic motions in the film can be frozen out if the frequency of the applied signal is high enough. It also becomes insignificant if the ionic concentration within the

film is very low. It can be explained by considering that in PDLC films, polymer matrix serves the role of a trapping medium for the motion of ions, so there would not be sufficient number of ions to create significant depolarization field. Another possibility is associated with orientation of droplets that exerts an alignment effect on the neighboring droplets (Drzaic 1995; Cupelli et al. 2009, 2011). The dipolar fields, i.e., the mean dielectric constant of the medium, surrounding these droplets depend on the extent of orientation of neighboring droplets. As long as the dielectric constant of the polymer and liquid crystal differ, bound depolarization charges will enhance the field across one medium at the expense of the field across the other. As a result, even in the limit of zero-conductivity field across the droplet will not be equal to the applied field. Since, PDLC film represents a mixed dielectric, change in its free energy density with applied field results due to contributions both from the liquid crystal and polymer components. Initially, the free energy density of the liquid crystal portion in PDLC film changes due to reorientation of LC molecules with the application of the field. This reorientation of LC molecules also alters the depolarization field across the polymer and causes a change in the free energy density of the polymer portion of the film. As LC gets more and more aligned, it increases its dielectric constant and depolarization field across the polymer portions of the film. Consequently, the total field and the free energy density across the polymer portion of the film decreases.

The conductivity of the polymer and LC components influence the operation of PDLC in various ways, i.e., fringing field effect, shielding effects, electrode effects, image stacking (Lowe and Kriss 2006), etc. Mobile ions within the film move under the influence of external field, setting up a depolarization field which tends to cancel the applied field. The nature of the depolarization field depends on the relative conductivity of the polymer and liquid crystals. If the LC is more conductive than the polymer, charge will be build up at the LC/polymer interface which tends to cancel the field across the droplet. Increasing the conductivity of the polymer allows the charge to leak into the polymer, thereby reducing this depolarization effect. However, if the film becomes too conductive, charges accumulate at the electrode interfaces and cancel the field across the entire film except near the electrodes. Moreover, conductivity is relative and depends on the frequency of the applied field (or voltage). If the time scale of interest is slow enough to allow the ionic moments to influence the field across the film, it becomes more conductive, but for sufficiently high frequencies film conductivity invariably gets suppressed.

7.6.4 Reverse Mode Operation in PDLCs

Contrary to the normal PDLCs, reverse mode PDLCs have high OFF state transmittance which turn opaque in ON state. Actually, the anchoring characteristics of LCs at the polymer/LC boundaries play the key role in determining the ON and OFF states transmittance. For reverse mode PDLCs, in OFF state, the built-in DC electric field aligns uniformly the LC director orientation and leads to a high

OFF state transmittance. However, in ON state due to depolarization of built-in DC electric field (either from bound or mobile charges) the LC director orientation gets distributed randomly and an opaque ON state is observed. Built-in DC electric field is developed due to separation of ionic impurities at LC droplet/polymer interface when a high intensity electric field (i.e., a charge process) is applied to the PDLC film for some time. Such phenomenon is also known as Maxwell-Wagner effect (Rout and Jain 1992a, b; Zhong et al. 1992). It depends strongly on the charging temperature, charging field and charging time. Higher values of these parameters result in the higher value of built-in DC electric field. To avoid the ion remix, field is usually stored during the cooling process. Modulation in the built-in DC electric field allows transmittance tuning in PDLC films with change in its morphological, dielectric and surface anchoring properties (Rout and Jain 1992a, b; Zhong et al. 1992). It also converts the conventional quadratic electro-optical response of PDLC into a quasi-linear one (Blinov et al. 1998; Nicoletta et al. 2000)

Reverse mode PDLCs are preferred in various building and automotive applications (Hikmet 1990, 1992). Reverse mode PDLC films with positive dielectric anisotropic liquid crystal E49, polymer polymethylmethacrylate (PMMA) and lipophilic ionic liquid (1-butyl-3-methylimidazolium hexafluorophosphate) as dopant have been prepared and studied by Cupelli et al. (2011). They found that the use of ionic liquid as dopant setups a large built-in DC electric field in PDLCs and give OFF state transmittances up to 75 % with uniform alignment to LC director configuration. In another work, they have studied self-adjusting smart windows based on reverse mode operation PDLC (Cupelli et al. 2009). Photoconductive material (zinc phthalocyanine) and ionic liquid (1-hexyl-3-methylimidazolium bis(trifluoromethylsulfonyl)imide) were used as dopant. This self-adjusting chromogenic material is suitable for external glazing and is also able to self-increase its scattering as a function of the impinging light intensity.

7.6.5 Non-linear Effects in PDLCs

Nonlinearity has an important role in the development of PDLCs and some very interesting non linear effects have been observed in PDLCs. These include studies related with second harmonic generation (SHG), laser irradiation, Bragg diffraction, Kerr effect, quasi linear response, etc.

In PDLCs, LC/polymer interface acts as a non centro-symmetric object and produce *SHG* when irradiated with light beam of sufficient intensity. Initially, when there is no phase separation, i.e., in isotropic polymer/nematic state, SHG signals were not observed. But, with increase in anisotropy, surface structures are defined more clearly and SHG signal occurs significantly. SHG signals are also affected with the application of field due to typical index matching of the dielectric constant of the LC and polymer when nematic gets oriented properly (Huang and Chen 1991; Yuan et al. 1991).

Several nonlinear optical effects based on the *laser heating* of PDLC films have been investigated (Simoni et al. 1989, 1990, 1991, 1992b; Cipparrone et al. 1990). Using a four-wave mixing process self-transparency effect in PDLC films have been studied. Initially, spatially varying refractive index grating was formed due to local heating of the material. Local heating occurs in the high intensity areas of the interference pattern when two lasers of the same frequency cross at small angle. Further, grating diffracts the two incident waves to create two new waves, and thereby completing four-wave mixing process. Until the laser intensity has reached a threshold value no diffraction pattern was observed but above the threshold, additional diffracted beams were observed (Simoni et al. 1992a). The response time of these effects was of the order of tens of milliseconds, consisted with thermal effects as the source of the behavior. For increasing the absorbance of the laser beam sometimes dyes have also been used (Simoni et al. 1989; Cipparrone et al. 1990). In another work laser beam of lower intensities and AC field below threshold have also been used (Simoni et al. 1992b).

Interfering laser beams have been used to set up a permanent *diffraction grating* profile in photopolymerized PDLC films (Lackner et al. 1989; Sutherland 1989; Sutherland et al. 1993, 1994; Tanaka et al. 1993, 1994). Sutherland has differentiated between Raman–Nath and Bragg-type gratings developed in these films (Lackner et al. 1989; Sutherland 1989; Muhoray and West 1989). Macroscopically, Raman–Nath gratings show multiple diffraction orders while microscopically it shows a gradual variation in droplet size or density. For Bragg gratings, a single diffraction order is observed macroscopically while microscopically the film shows sharp boundaries between areas containing a high droplet density and the areas with virtually no droplets.

Sansone et al. (1990, 1994) have observed *Kerr effects* in PLDC films using submicron droplet sizes. In Kerr effect, fluid exhibits the properties of uniaxial crystal due to induced birefringence when electric field is applied. At molecular level, Kerr effect for an isotropic state arises due to contributions from molecular hyper polarizability, anisotropic polarizability and permanent dipole moments of the constituent molecules. However, for liquid crystals it depends on the collective molecular rotation of the constituent molecules. In the liquid crystals, reorientation of the molecular director also changes the refractive index which leads to larger value Kerr constants as compared with isotropic fluids. This effect has been used to minimize the scattering from PDLC films of submicron sized droplets, thereby increasing the transparency of the films (Sansone et al. 1990, 1994).

7.7 Time Dependent Phenomenon in PDLCs

Several studies reveal that the phase, morphology, reorientation dynamics, LC/polymer composition, etc., in PDLCs are influenced significantly with the evolution of time (Drzaic 1988b; Challa et al. 1995). Various interesting results

occur when PDLC films are monitored at different time scales during the process of curing and electrical treatments. Change in the morphology, and electro-optical properties of PDLC films have been reported with change in the curing time (i.e., time of exposure to UV or other radiations). Field induced reorientation processes are found to be quite complex for different time scales in microsecond to millisecond range (Drzaic 1988b).

7.7.1 Time Evolution of PDLC Films

The phase separation processes in PDLCs have been studied extensively by a number of groups (Mcfarland et al. 1993; Challa et al. 1997a, b; Wall and Koenig 1998; Bhargava et al. 1999). They have investigated the evolution of the droplets using visual and IR spectroscopic methods. In one of the works, Mcfarland et al. (1993) have found that with evolution of time, the IR bands associated with the polymer gets broadened while the bands associated with the LC became narrower. They attributed that with phase separation polymer becomes less fluid (and leads to broadening of associated IR bands) while LC becomes more fluid (and leads to narrowing of associated IR bands). It suggests that in the typical PDLC there is a continuous occurring of phase separation process with evolution of time. In their later works, they reported studies related with diffusion liquid crystal in polymer regions by IR micro spectroscopic imaging (Challa et al. 1997a, b; Wall and Koenig 1998). For better understanding of the phase separation process light scattering (Golemme et al. 1998), IR methods (Wall and Koenig 1997; Bhargava et al. 1999) have been used along with other techniques (Roussel et al. 1998).

7.7.2 Dynamics of PDLC Films

Dynamic light scattering (Mertelj et al. 1997; Mertelj and Copic 1998) and theoretical (Kelly and Muhoray 1997) studies on PDLC droplets show significant difference in the properties of the droplets as compared with bulk LC materials. These differences lead to a change in reorientation dynamics of PDLCs and result mainly due to confinement of LC into microscopic polymer cavities, interfacial interactions at the LC/polymer interface and contributions from elastic constant terms to the free energy (Zumer and Doane 1986; Kitzerow 1994) in a PDLC film, with change in the shape, size, interfacial interaction, LC configuration, etc.; dynamics varies for both between the droplets and with the droplets (Drzaic 1988b; Wu et al. 1989; Lin et al. 1995; Brazeau et al. 1998).

7.8 Theoretical Developments in PDLCs

Dispersions of liquid crystal molecules in flexible polymer matrices are interesting as the multi-component systems that furnish valuable information on the coupling between the two species (Drzaic 1995; Klosowicz and Zmija 1995; Serbutoviez et al. 1996; Simoni 1997). They combine the common properties of polymers and liquid crystals. Most of these PDLCs exhibit liquid–liquid immiscibility which leads to the formation of mesogenic phases during cooling cycle. Interesting changes in the isotropic–nematic phase transitions have been observed with variations in the compositions of the constituents. Mesogenic changes observed in PDLCs can be studied by their thermal and morphological investigations and construction of the equilibrium phase diagram. Flory–Huggins (FH) theory (Flory 1953) for the isotropic phase of mixing, Maier–Saupe (MS) theory (Maier and Saupe 1959, 1960) of nematic orders and its generalization by McMillan to include smectic ordering (McMillan 1971) have been used widely to understand the effect of polymers and LC constituents on the equilibrium phase diagram (Shen and Kyu 1995; Chiu and Kyu 1995; Riccardi et al. 1998a, b; Benmouna et al. 1998, 2000; Roussel et al. 2000; Soule et al. 2009).

The properties of PDLCs are quite sensitive to both the polymer and LC constituents in the mixture. Large differences have been observed due to change in one of these two constituents (Riccardi et al. 1998a, b; Benmouna et al. 1999; Hoppe et al. 2003; Mucha 2003). Polystyrene (PS) with commercially available nematics like 8CB, E7 and EBBA has been widely used to investigate the phase diagram and concept of miscibility in PDLCs (Riccardi et al. 1998a, b; Benmouna et al. 1999, 2000; Roussel et al. 2000; Hoppe et al. 2003; Soule et al. 2009). Miscibility of polymers has attracted much attention because it provides a route to improve compatibility between different polymers and other immiscible counterparts (Lejardi et al. 2011).

Poly(ethylene oxide) (PEO) is one of these miscible polymers, utilized in the formation of a triblock copolymer having some LC content (Zhou et al. 2011). It is a semi-crystalline material with spherulite structure having lower melting point and two glass transition temperatures T_G (Jin et al. 2002; Zhou et al. 2011). With the addition of some kind of diluents, appreciable changes in the microstructures and phase diagram of PEO have been observed (Talibuddin et al. 1996; Srivastava et al. 2012). Poly(methyl methacrylate) (PMMA) is also a useful polymer in studies related with PDLCs (Chen and Shanks 2007; Deshmukh and Malik 2008; Ganesan et al. 2009; Zhou et al. 2011). It exhibits useful electro-optical and mechanical properties and offers higher thermal stability to the PDLC films. Another important class of polymers consists of vinylidene fluoride (VdF). Because of its fluorine constituent, it is easily cross-linkable to form a homopolymer of VdF itself, i.e., PVdF or other copolymers, having different fluoroolefins like tetrafluoroethylene, hexafluoropropylene, etc. (Tatemoto et al. 1981; Ameduri 2009). The PVdF based polymers support partial crystallinity with microporous geometry having high thermal and mechanical stability. These polymers have shown their importance in

various studies related with the polymer gel electrolytes as well (Abbrent et al. 2001; Huang and Wunder 2001; Cheng et al. 2004, 2005; Xi et al. 2005; Kim et al. 2009; Vijaykumar et al. 2009; Shirey and Maranas 2009; Wu et al. 2010; Zalewska et al. 2010). Dielectric relaxation spectroscopic investigations have been carried out to study the hindered motion of LC in PVdF based polymer cavities (Ganesan et al. 2009).

Some other common polymers used in the PDLC applications are: epoxy based polymers (Smith and Vaz 1988), ethyl hexyl acrylate (EHA) (Im et al. 1995; Roussel et al. 2000; 2002), ethoxy benzylidene butylaniline (EBBA) (Hoppe et al. 2003), NOA series polymers (Zhou et al. 2004; Kumar and Raina 2007), PN314 (Williams et al. 2001), PlatSil Gel (Zou and Fang 2011), PolyBed (Russell et al. 1995), Polybutyl methacrylate (PBMA) (Manohar et al. 2006), Polysilixane (Bedjaoui et al. 2004), etc.

The general equation:

In PDLCs, the thermodynamic phase behavior of polymers and LC materials are usually described by combining the theoretical methods developed separately for LCs and polymers (McMillan 1971; Shen and Kyu 1995; Chiu and Kyu 1995, 1998; Riccardi et al. 1998a, b; Mucha 2003). The analysis of the experimental data provides useful information about the effects of the polymer size, transition temperature and interaction mechanism on the isotropic to nematic (and/or smectic) transition (Benmouna et al. 1998, 1999, 2000; Roussel et al. 2000, 2002; Hoppe et al. 2003; Boussoualem et al. 2004; Soule et al. 2009). The total free energy of a system is written as a sum of two contributions (i) the free energy, $f^{(i)}$ for isotropic state of mixing described by Flory–Huggins lattice model and (ii) the anisotropic contribution to the free energy, $f^{(a)}$ due to the occurrence of mesoscopic transitions.

$$f = f^{(i)} + f^{(a)}. \quad (7.14)$$

The choice of the two contributions depends on the nature of transitions for the phases in equilibrium. The equilibrium may exist either between two isotropic phases or one isotropic and one anisotropic (nematic/smectic) phase or one isotropic and two anisotropic (both nematic and smectic) phases. The free energies for these phases have been explained by a combination of FH theory of isotropic mixing, the MS theory of nematic order and McMillan model to include smectic order. A brief description of these theories follows:

7.8.1 Flory–Huggins Theory

In this model (Flory 1953; Orwoll and Arnold 1996; Schuld and Wolf 1999; Krevelen and Nijenhuis 2009) the free energy density of a binary mixture under mean field approximation is expressed as

$$\frac{f^{(i)}}{k_B T} = \frac{\varphi_1}{N_1} \ln \varphi_1 + \frac{\varphi_2}{N_2} \ln \varphi_2 + \chi \varphi_1 \varphi_2 \quad (7.15)$$

where φ_1 , φ_2 and χ represent, respectively, the volume fraction of liquid crystal, polymer material and FH interaction parameter. N_1 and N_2 are the number of molecules of liquid crystal and polymer, respectively. Parameter χ is often used to obtain the best fit with the experimental data in the portion of the phase diagram where the isotropic interactions are most significant. It is defined by the relation

$$\chi = A + \frac{B}{T} \quad (7.16)$$

Here, A and B are constants independent of temperature.

7.8.2 Mair–Saupe–Macmillan Theory

In the Maier–Saupe theory, it is assumed that the polymer chains are flexible having no mesogenic part and the anisotropic contribution to the free energy is only due to the nematic ordering (Maier and Saupe 1959, 1960; De Gennes 1974; De Gennes and Prost 1993, 1995; Chandrasekhar 1977; Singh 2000, 2002). McMillan (1971) generalized this theory to account smectic ordering as well (Chandrasekhar 1977; Singh 2000, 2002). Thus in PDLCs the relative contribution of anisotropic free energy to the total free energy is strongly dependent on the order parameters. The nematic and smectic order parameters S and σ are described, respectively, by the relations,

$$S = \langle P_2(\cos \theta_{12}) \rangle \quad (7.17)$$

and

$$\sigma = \frac{1}{2} \left\langle (3 \cos^2 \theta - 1) \cos \frac{2\pi z}{d} \right\rangle \quad (7.18)$$

where, P_2 is the second rank Legendre polynomial, θ_{12} is the angle between two molecular axes, θ is the angle between the director of LC molecules and reference axis and d is the inter layer spacing between consecutive smectic layers. The angular bracket denotes the ensemble averaging.

Using McMillan's idea for smectic ordering, the partition function for generalized Maier–Saupe–McMillan theory includes terms for both the nematic and smectic ordering and is given by the relation

$$Z = \iint d \cos \theta dz \exp \left[\frac{m_n}{2} (3 \cos^2 \theta - 1) \right] \exp \left[\frac{m_s}{2} (3 \cos^2 \theta - 1) \cos \frac{2\pi z}{d} \right] \quad (7.19)$$

where, m_n and m_s are the mean-field parameters which are described in terms of order parameters S and σ ,

$$m_n = \nu S \varphi_1; \quad m_s = \zeta \nu \sigma \varphi_1 \quad (7.20)$$

Here $\nu = 4.54 \frac{T_{NI}}{T}$ represents the Maier–Saupe quadrupole interaction parameter and ζ is the strength of smectic interaction to incorporate the McMillan's idea in the MS theory. It depends on the ratio of T_{SN}/T_{NI} . With this generalization, the overall anisotropic contribution to the free energy is given by the relation,

$$\frac{f^{(a)}}{k_B T} = \frac{\varphi_1}{N_1} \left[-\ln Z + \frac{1}{2} \nu \varphi_1 (S^2 + \zeta \sigma^2) \right] \quad (7.21)$$

Using the afore-mentioned theories, miscibility and phase behavior of LC/polymer constituents in PDLC films have been well studied and reported in the literature (Shen and Kyu 1995; Chiu and Kyu 1995; Riccardi et al. 1998a, b; Benmouna et al. 1999, 2000; Roussel et al. 2000; Hoppe et al. 2003; Soule et al. 2009; Lejardi et al. 2011; Srivastava et al. 2012).

7.9 Applications of PDLCs

Due to their peculiar electro-optical and mechanical properties PDLCs have been used in various device development applications and are beneficial over LCs based devices. For example, some of the important PDLCs applications are—eye protection viewer (Land and Schmitt 1995), flexible displays (Sheraw et al. 2002), holographic PDLCs (Sutherland 1991; Sutherland et al. 1994, 1998), heat-resistant PDLC light modulator (Takizawa et al. 1999; Fujikake et al. 2000), spatial light modulator (Vicari 2003), projection displays (Shikama et al. 1995; Kikuchi et al. 2000), dichoric dye based displays (Bahadur 1991; Drzaic et al. 1990, 1992; Drzaic 1991), direct view scattering mode and cholesteric displays (Nolan et al. 1993; Fujikake et al. 1993), scattering polarizers (Aphonin 1995, 1996; Bloisi et al. 1996, 1997), sensors (Parmar and Singh 1992; Tabib et al. 2000; Jain and Thakur 1992; Jain et al. 1993), smart windows (Lampert 1998; Sanchez et al. 2002; Drzaic and Muller 1989), second harmonic generators (Li et al. 1991; Macdonald et al. 1998), etc. These applications have been nicely described in literatures (Bloisi and Vicari 2003; Drzaic 1995).

7.10 Recent Advances in PDLCs

In spite of a large number of meticulous reports on polymer dispersed liquid crystals (PDLCs) during the last three decades, it is still a promising field of research and has the potential to divert the attention of workers for contributing in this area. Present section provides a brief account of the streamlined works

carried out in last few years in the area of PDLCs, liquid crystal droplets confined in other microscopic cavities, and interpenetrating liquid crystals and polymer networks.

Electro-optical investigations of PDLC films have been a part of considerable research for several research groups. Alteration in any of the polymer, LC and other constituents or operating conditions effect significantly the electro-optical properties of the PDLC films (Kashima et al. 2010; Dzhons et al. 2011; Song et al. 2012a, b; Liu et al. 2012a, 2013; Shao et al. 2012, 2014; Lu et al. 2013; Yang et al. 2014). Doping has a significant contribution in modifying the electro-optical and other intrinsic anisotropic properties of PDLCs. Multidirectional light-controlled reflective PDLC film with doping of dye has been reported with enhanced contrast ratio and image brightness of the films (Jeon et al. 2012). PDLCs with reverse mode operations have been studied in polymerized mixtures of liquid crystalline monomer (1,4-bis{4-(6-(acryloyloxy)hexyloxy)benzoyloxy} benzene and the eutectic nematic liquid crystal (ZLI 4788, Merck chemicals) doping with single walled carbon nanotubes (Filpo et al. 2012). Reverse mode PDLCs using cetyltrimethylammonium bromide (CTAB) coated on ITO glass have also been prepared by the vertical alignment of LCs (Lee et al. 2014). In both the studies significant changes in the electro-optical properties of the PDLC films have been reported due to presence of doped materials.

In some other works, NMR relaxometry studies in low frequency regions (of few MHz) show significant increase in the proton spin–lattice relaxation rates in the nematic and smectic phases of 8OCB LC molecules embedded in nano-porous airoxil matrix (Rajeswari et al. 2012). In this work authors have also reported that the individual dynamic processes like translational diffusion and reorientation of the molecules within the voids remain unaffected due to confinement. Liu et al. (2012b) have characterized the optically switchable photonic crystals based on SiO₂ inverse opals infiltrated with photoresponsive liquid crystal, viz., a mixture of nematic LC (E7) and photochromic LC, 4-butyl-4-methoxyazobenzene (BMAB). They reported that nematic-isotropic phase transition of E7 inside the opals is triggered by the trans-cis isomerization of BMAB upon UV photoirradiation and leads to a change in refractive index contrast between E7 and SiO₂ inverse opal (Liu et al. 2012b). Drastic changes in the electro-optical properties of the PDLC films consisting of photosensitive monomer (NOA65) and nematic liquid crystals (E7) have been reported by using montmorillonite (MMT) clay as dopant after being modified by conducting pentamerous oligoaniline (POA) (Tsai et al. 2012). The transmission contrast ratio of the films was found to increase by five times whereas the driving voltage is lowered by almost 70 %. Significant decrease in the PDLC response time has also been obtained.

Another tool which has been explored widely in the field of PDLCs is related with its holographic techniques. It has been studied so intensively that a separate abbreviation HPDLCs is given to these types of PDLCs. Dramatic changes in the electro-optical properties of PDLCs and various device fabrications have been reported using HPDLC. Interest is still a burgeoning area to work (Zheng et al. 2012; Diao et al. 2014; Jang and Kim 2011; Liu et al. 2012c). Some of the

recently developed applications of HPDLC includes rewritable holograms based on azobenzene containing liquid crystalline polymers (Shishido 2010), liquid crystal lasers as a ultrathin and highly versatile laser sources having wideband tunability, large coherence and multidirectional emission capability (Coles and Morris 2010), dual wavelength distributed feedback laser empowered by dye-doped HPDLC (Diao et al. 2012), linear variable optical filters using a single beam one-step holographic interferometry method (Moein et al. 2014), monochromatic visible light photoinitiator for storage of colored 3D images (Peng et al. 2014), HPDLC based photonic quasicrystals for linearly polarized low threshold lasing (Luo et al. 2012), etc.

Confinement of liquid crystal in microscopic cavities results in a number of complicated director fields which depends on the size and shape of the drop, presence of external field, elastic properties of LC, anchoring and other topological constraints on the LC director at the boundaries of the drop, i.e. the confining volume (Leon and Nieves 2011). Recently, very interesting studies on the morphogenesis of the defects and disclination in liquid crystals confined in different geometries during phase transitions (Leon et al. 2011a, b; Kim et al. 2013), controlled generation of the defect lines by imposing topological constraints on nematic microdrops in hand-drawn silica structures (Campbell et al. 2014), effect of colloidal dispersion on the topology of liquid crystals for self-assembling of composite material with pre-engineered properties and structures in different non-trivial configurations like, a superstructure of knot-shaped particles linked by nematic field (Martinez et al. 2014), control over the number and orientation of defects by functionalizing the unavoidable defects with the help of spherical colloid particles, coated on the thin layered nematic liquid crystal shell of varying thickness (Leon et al. 2011b), design of functional soft materials based on the confinement induced LC ordering, triggered by interaction with bio-molecular species and self assembling of amphiphiles (Miller et al. 2014), generation of double armed helical patterns by using paramagnetic polystyrene particles actuated by weak magnetic field and its control by an out-of-plane electric field (Navarro et al. 2011), etc. have been reported. Laser directed self assembled and facile erasable defect clusters and control of optical phase singularities in liquid crystals with probable applications in data storage, singular optics and other electro-optic devices have also been reported (Ackerman et al. 2012).

Self-assembled liquid crystals and LC polymer gels with interesting microstructures and electro-optical properties have been reported, recently, using photoinduced and some other techniques. Self-assembled randomly dispersed polymerized network of lysine based gelator and nematic LC molecules have been obtained by the formation of hydrogen bonds in the isotropic phase of the nematic LC molecule (Eimura et al. 2012). After the isotropic–nematic transition light-scattering nematic LC gels are formed which exhibits electro-optical switching between light scattering and transparent states with comparatively lower driving voltage than the non-polymerized LC gels. Philippe et al. (2011), have reported a 2D photoinduced self-organized periodic structure of commercial NLC mixture and photocurable reactive mesogens which gets stabilized in terms of morphology and electro-optic

response with application of strong electric field. Discontinuous volume change in a nematic liquid crystal cross-linked polymer gel containing small amount of azobenzene molecules and swollen by another nematic solvent (i.e., 5CB) has also been reported by Hayata et al. (2012). Volume change occurs near nematic-isotropic phase transition temperature of the LC polymer gel, due to loss of nematic order within the gel by trans-cis photoisomerization of azobenzene when exposed to UV irradiation. Magnetic-field directed self-assembly of a liquid crystalline block copolymer with brush-type architecture has been reported as a platform for creating functional materials (Deshmukh et al. 2014). Nematic LC-polymer network composite formed by photo-polymerization of the monomer under externally applied electric fields shows that the polymer network stabilizes both the director and electric polarization of the LC (Hicks et al. 2013).

Graphene oxide (GO) is a novel class of material exhibiting uniform electro-optical properties over an ultra-large GO sheet. Flow and field induced birefringence in the phase sequence of GO has shown the occurrence of phase transitions from isotropic to biphasic and biphasic to nematic phases (Shen et al. 2014). These GO-LC response is very sensitive to external stimulus. Shen et al. (2014) have reported an extremely large Kerr coefficient that is about three orders of magnitudes greater than the commonly known values for molecular liquid crystals. Due to extremely large Kerr coefficient it finds application in fabricating electro-optic devices with macroscopic electrodes, as well as well-aligned, defect-free GO sheets over wide areas. For further processing and fabrication of more complex architectures using GO dispersion its rheological behaviour for isotropic to LC and LC gel phases have been studied using ultra-large GO sheets (Naficy et al. 2014). It has been demonstrated that GO dispersions exhibit unique viscoelastic behavior, whereas the rheological behavior varies considerably with dispersion concentration.

7.11 Future Perspective and Challenges

Liquid crystals are partially ordered systems without a rigid, long-range structure. They are intermediate in symmetry and structure between the solid crystalline state and amorphous isotropic liquid state. The advancement in the knowledge of its chemical structure, physical properties and technical applications coincided with a period of rapid expansion in terms of the physical techniques available to the materials. This, together with great advances in the theory of condensed matter and the rapid progress in computer simulation techniques made liquid crystals an exciting area for scientific research with many fundamental challenges. On the other hand, polymer is a large molecule composed of identical structural unit (monomers), typically bonded by a covalent chemical. The polymerisation reaction leading to formation of polymer from the monomer, often requires a short initiator that might be the addition of a chemical initiator or the exposition to high energy UV photons. Due to the existence of both resistance and flexibility, they show

interesting mechanical properties. A very important step in the historical development of mesogenic materials took place in 1984, when Fergason prepared a polymeric film embedded with very small droplets (0.1–100 μm) of mesogenic materials. These kinds of materials are called polymer dispersed liquid crystals (PDLCs). These composite materials are simply a mixture of polymer and liquid crystal. PDLCs, consisting of micron sized LC droplets dispersed in a polymer matrix, are promising electro-optic material for displays, storage devices, light switches, tunable focus lenses, privacy windows, reverse mode PDLCs, photoinhibitor and so forth. Depending on the nature, properties and concentration of the polymers and the liquid crystals, a large variety of structures are possible in PDLCs. The study of PDLCs has attracted considerable attention, in recent decades, from the points of view of basic understanding as well as industrial and technological applications. A multi-disciplinary approach has emerged to be the essential necessity of studies in PDLCs, and, those working in the area are expected to have familiarity with the chemical constitution of the materials and their properties, together with the knowledge of the physics of the phenomenon which they exhibit. In our understanding a better knowledge of the structure and properties of polymer dispersed liquid crystals is of fundamental significance because of the exotic nature of their properties and continued requirement of technological applications. In view of these, the subject matter discussed in this chapter is full of challenge and curiosity.

In brief, from the studies on PDLCs we can conclude that there are large number of variables like solubility parameter, solubility limit, fraction of liquid crystal in LC rich domains inside the polymer matrix, composition of mesogens, polymer constituent, etc., which influence the PDLC film formation. Various other parameters like temperature, rate of cooling, applied field strength, exposure time to radiation, constrained on the surface anchoring, etc., have also significant effect on the droplet morphologies and electro-optical properties of PDLC films. Tuning among these variables would be useful in getting the PDLC films with uniform dispersion over a larger area for specific applications.

This chapter concerns with various techniques which have been used frequently in the preparation and characterization of PDLC films. Several other factors are also important to determine how these materials would be useful in commercial and scientific developments. Some of the problems which need to be encountered in future are given below.

Effect of surface anchoring on droplet configurations, order parameters and morphologies of the mesogens due to their confinement in homogeneous materials needs to be explored using NMR, AFM, IR imaging and other techniques. A more elaborate work to study the scattering phenomenon in PDLCs is also desired. Proper theoretical explanation for the observed changes in LC director configuration in microscopic droplets and other complex geometries is still lacking. Computer simulations are to be the best hope to provide answers not only to these interesting and important questions but also to resolve many issues regarding the structure and properties of PDLC films. The future directions of work in this area are likely to be the computer simulation and more neat-clean experimental data.

References

- Abbrent S, Plestil J, Hlavata D, Lindgren J, Tegenfeldt J, Wendsjo A (2001) Crystallinity and morphology of PVdF–HFP-based gel electrolytes. *Polymer* 42:1407–1416
- Ackerman PJ, Qi Z, Lin Y, Twombly CW, Laviada MJ, Lansac Y, Smalyukh II (2012) Laser-directed hierarchical assembly of liquid crystal defects and control of optical phase singularities. *Sci Rep* 2(414):1–8
- Allender DW, Crawford GP, Doane JW (1991) Determination of the liquid-crystal surface elastic constant K₂₄. *Phys Rev Lett* 67:1442
- Almarza NG, Martin C, Lomba E (2010) Phase behaviour of the confined lebowohl-lasher model. *Phys Rev E* 82:011140
- Aloe R, Chidichimo G, Golemme A (1991) Molecular reorientation in PDLC films monitored by ²H NMR: electric field induced reorientation mechanism and optical properties. *Mol Cryst Liq Cryst* 203:9–24
- Ambrozic M, Formoso P, Golemme A, Zumer S (1997) Anchoring and droplet deformation in polymer dispersed liquid crystals: NMR study in an electric field. *Phys Rev E* 56:1825–1832
- Ameduri B (2009) From vinylidene fluoride (VDF) to the applications of VDF-containing polymers and copolymers: recent developments and future trends. *Chem Rev* 109:6632–6686
- Amimori I, Priezjev NV, Pelcovits RA, Crawford GP (2003) Optomechanical properties of stretched polymer dispersed liquid crystal films for scattering polarizer applications. *J Appl Phys* 93:3248–3252
- Amimori I, Eakin JN, Qi J, Skacej G, Zumer S, Crawford GP (2005) Surface-induced orientational order in stretched nanoscale-sized polymer dispersed liquid-crystal droplets. *Phys Rev E* 71:031702
- Amundson K (1996) Electrooptic properties of a polymer-dispersed liquid-crystal: temperature dependence and phase behavior. *Phys Rev E* 53:2412
- Amundson KR, Srinivasarao M (1998) Surface anchoring and electro-optics of polymer dispersed liquid crystal films. *Phys Rev E* 58:R1211
- Amundson K, Blaaderen AV, Wiltzius P (1997) Morphology and electro-optic properties of polymer-dispersed liquid-crystal films. *Phys Rev E* 55:1646–1654
- Andreev GN, Jordanov B, Korte EH, Schrader B (1997) FT-Raman polarization spectroscopy of nonmesogenic guest molecules oriented in nematic liquid crystal solvents. *Appl Spectrosc* 51(11):1753–1756
- Aphonin OA (1995) Optical properties of stretched polymer dispersed liquid crystal films: angle-dependent polarized light scattering. *Liq Cryst* 19:469–480
- Aphonin OA (1996) Orientational ordering of bipolar nematic droplets in a stretched PVA matrix. *Mol Cryst Liq Cryst* 281:105–122
- Azaroff LV (1968) *Elements of X-ray crystallography*. McGraw Hill, New York
- Bacchicocchi C, Miglioli I, Arcioni A, Vecchi I, Rai K, Fontecchio A, Zannoni C (2009) Order and dynamics inside H-PDLC Nanodroplets: an ESR spin probe study. *J Phys Chem B* 113:5391–5402
- Backer AS, Jons ACC, Pelcovits RA (2008) Nematic cells with defect-patterned alignment layers. *Phys Rev E* 77:021701
- Bahadur B (ed) (1991) *Liquid crystals application and uses*. World Scientific, Singapore
- Barsoukov E, Macdonald JR (eds) (2005) *Impedance spectroscopy: theory, experiment and applications*, 2nd edn. Wiley, Hoboken
- Barton AFM (1985) Applications of solubility parameters and other cohesion energy parameters. *Polym Sci Technol Pure Appl Chem* 57:905–912
- Barton AFM (1991) *Handbook of solubility parameters and other cohesion parameters*, 2nd edn. CRC Press, Boca Raton
- Basile F, Bloisi F, Vicari L, Simoni F (1993) Optical phase shift of polymer-dispersed liquid crystals. *Phys Rev E* 48(1):432–438

- Bates MA (2003) Computer simulation studies of nematic liquid crystal tactoids. *Chem Phys Lett* 368:87–93
- Bedjaoui L, Gogibus N, Ewen B, Pakula T, Coqueret X, Benmouna M, Maschke U (2004) Preferential solvation of the eutectic mixture of liquid crystals E7 in a polysiloxane. *Polymer* 45:6555–6560
- Benmouna F, Bedjaoui L, Maschke U, Coquere X, Benmouna M (1998) On the phase behavior of blends of polymers and nematic liquid crystals. *Macromol Theory Simul* 7:599–611
- Benmouna F, Daoudi A, Roussel F, Buisine JM, Coqueret X, Maschke U (1999) Equilibrium phase diagram of polystyrene and 8CB. *J Polymer Sci B Polym Phys* 37:1841–1848
- Benmouna F, Daoudi A, Roussel F, Leclercq L, Buisine JM, Coqueret X, Benmouna M, Ewen B, Maschke U (2000) Effect of molecular weight on the phase diagram and thermal properties of poly(styrene)/8CB mixtures. *Macromolecules* 33:960–967
- Berggren E, Zannoni C, Chiccoli C, Pasini P, Semeria F (1994) Monte Carlo study of the effect of an applied field on the molecular organization of polymer dispersed liquid crystal droplets. *Phy Rev E* 49:614–622
- Bhargava R, Wang SQ, Koenig JL (1998) FTIR imaging of the interface in multi-component systems using optical effects induced by differences in refractive index. *Appl Spectrosc* 52:323
- Bhargava R, Wang SQ, Koenig JL (1999) FTIR imaging studies of a new two-step process to produce polymer dispersed liquid crystals. *Macromolecules* 32:2748
- Blanks RF, Prausnitz JM (1964) Thermodynamics of polymer solubility in polar and non-polar systems. *Ind Eng Chem Fundam* 3:1–8
- Blinov LM, Palto SP, Yakovlev SV, Sikharulidze DG (1998) Asymmetric electro-optical switching of a nematic cell controlled by a corona poled ferroelectric polymer layer. *Appl Phys Lett* 72:3377
- Bloisi F, Vicari L (2003) Laser beam manipulation by composite material electro-optic devices. *Opt Lasers Eng* 39:389–408
- Bloisi F, Terrecuso P, Vicari L, Simoni F (1995) Voltage controlled light transmittance in polymer dispersed liquid crystals. *Mol Cryst Liq Cryst* 266(1):229–239
- Bloisi F, Ruocchio C, Terrecuso P, Vicari L (1996) Optoelectronic polarizer by PDLC. *Liq Cryst* 20:377–379
- Bloisi F, Terrecuso L, Vicari L (1997) Polarized light scattering in a novel polymer dispersed liquid-crystal geometry. *J Opt Soc Am A* 14:662–668
- Boussoualem M, Roussel F, Ismaili M (2004) Thermophysical, dielectric, and electro-optic properties of nematic liquid crystal droplets confined to a thermoplastic polymer matrix. *Phys Rev E* 69:031702
- Bouteiller L, Barny PL (1996) Polymer-dispersed liquid crystals: preparation, operation and application. *Liq Cryst* 21:157–174
- Brazeau J, Chenard Y, Zhao Y (1998) Orientation in stretched polymer-dispersed liquid crystals. *Can J Chem* 76(11):1642–1647
- Buchert KL, Koenig JL, Wang SQ, West JL (1993a) Molecular-motion analysis of E7 in PDLCS as a function of droplet size using solid-state ^{13}C NMR relaxation spectroscopy. *Appl Spectrosc* 47(7):942–951
- Buchert KL, Koenig JL, Wang SQ, West JL (1993b) Molecular motion analysis of 5CB in PDLCS using solid-state ^{13}C NMR relaxation spectrometry. *Appl Spectrosc* 47(7):933–941
- Burrell H (1957) A solvent formulating chart. *Off Dig Fed Soc Paint Technol* 29:1159–1173
- Burrell H (1962) The use of the solubility parameter concept. In the United States, VI Federation d'Associations de Techniciens des Industries des Peintures, Vernis, Emaux et Encres d'Imprimerie de l'Europe Continentale Congress Book, pp 21–30
- Burrell H (1972) Solubility parameters for film formers. *Off Dig Fed Soc Paint Technol* 27:726–758
- Busbee JD, Yuhl AT, Natarajan LV, Tongdilia VP, Bunning TJ, Vaia RA, Barun PV (2009) SiO₂ nanoparticle sequestration via reactive functionalization in holographic polymer dispersed liquid crystals. *Adv Mater* 21:1–4

- Buyuktanir EA, Mitrokhin M, Holter B, Glushchenko A, West JL (2006) Flexible bistable smectic-A polymer dispersed liquid crystal display. *Jap J of App Phys* 45:4146–4151
- Campbell MG, Tasinkevych M, Smalyukh II (2014) Topological polymer dispersed liquid crystals with bulk nematic defect lines pinned to handlebody surfaces. *Phys Rev Lett* 112:197801
- Candau S, Roy PL, Debeauvais F (1973) Magnetic field effects in nematic and cholesteric droplets suspended in an isotropic liquid. *Mol Cryst Liq Cryst* 23:283–297
- Caputo R, Sio LD, Sukhov AV, Veltri A, Umeton C (2004) Development of a new kind of switchable holographic grating made of liquid-crystal films separated by slices of polymeric material. *Opt Lett* 29:1261–1263
- Care CM, Cleaver DJ (2005) Computer simulation of liquid crystals. *Rep Prog Phys* 68:2665–2700
- Carfagna C (ed) (1994) *Liquid crystalline polymer*. Pergamon, Oxford
- Challa SR, Wang SQ, Koenig JL (1995) Characterization of polymer-dispersed liquid-crystal systems by FTIR microspectroscopy. *Appl Spectrosc* 49(3):267–272
- Challa SR, Wang SQ, Koenig JL (1997a) Determination of solubility limits of photocured PDLC systems using infrared microspectroscopy. *Appl Spectrosc* 51(1):10–16
- Challa SR, Wang SQ, Koenig JL (1997b) In-situ diffusion and miscibility studies of thermoplastic PDLC systems by FTIR microspectroscopy. *Appl Spectrosc* 51(3):297–303
- Chandrasekhar S (1977) *Liquid crystals*. Cambridge University Press, Cambridge
- Chen LG, Shanks R (2007) Thermoplastic polymer-dispersed liquid crystals prepared from solvent-induced phase separation with predictions using solubility parameters. *Liq Cryst* 34:1349–1356
- Cheng SZD (ed) (2002) *Handbook of thermal analysis and calorimetry: applications to polymers and plastics*, vol 3. Elsevier, Amsterdam
- Cheng CL, Wan CC, Wang YY (2004) Preparation of porous, chemically cross-linked, PVdF-based gel polymer electrolytes for rechargeable lithium batteries. *J Power Sources* 134:202–210
- Cheng CL, Wan CC, Wang YY, Wu MS (2005) Thermal shutdown behavior of PVdF-HFP based polymer electrolytes comprising heat sensitive cross-linkable oligomers. *J Power Sources* 144:238–243
- Chien LC, Lin C, Fredley DS, McCragar JW (1992) Side-chain liquid-crystal epoxy polymer binders for polymer dispersed liquid crystals. *Macromolecules* 25:133–137
- Chiu HW, Kyu T (1995) Equilibrium phase behavior of nematic mixtures. *J Chem Phys* 103:7471–7748
- Chiu HW, Kyu T (1998) Phase equilibria of a nematic and smectic-A mixture. *J Chem Phys* 108:3249–3255
- Ciferri A (ed) (1991) *Liquid crystallinity in polymers: principles and fundamental properties*. VCH, New York
- Cipparrone G, Umeton C, Arabia G, Chidichimo G, Simoni F (1990) Nonlinear optical effects in polymer dispersed liquid crystals. *Mol Cryst Liq Cryst* 179:269–275
- Coleman DA, Fernsler J, Chattham N, Nakata M, Takanishi Y, Link DR, Shao RF, Jang WG, MacLenan JE, Korblova E, Mondain O, Weissflog W, Pelzl G, Chien LC, Walba DM, Zadadzinski J, Watanabe J, Takezoe H, Clark NA (2003) Polarization-modulated smectic liquid crystal phases. *Science* 301:1204–1211
- Coles H, Morris S (2010) Liquid-crystal lasers. *Nature Photonics* 4:676–685, www.nature.com/naturephotonics
- Collings PJ, Hird M (1997) *Introduction to liquid crystals: chemistry and physics*. Taylor & Francis, London
- Collyer AA (ed) (1993) *Liquid crystal polymers: from structure to applications*. Elsevier, Oxford
- Crawford GP (ed) (2005) *Flexible flat panel displays*. Wiley, Chichester
- Crawford GP, Doane JW (1992) Polymer dispersed liquid crystals. *Condens Matter News* 1:5–11
- Crawford GP, Zumer S (eds) (1996) *Liquid crystals in complex geometries*. Taylor & Francis, London

- Crawford GP, Stannarius R, Doane JW (1991a) Surface induced orientational order in the isotropic phase of a liquid crystal material. *Phys Rev A* 44:2558–2569
- Crawford GP, Yang DK, Zumer S, Finotello D, Doane JW (1991b) Ordering and self-diffusion in the first molecular layer at a liquid-crystal-polymer interface. *Phys Rev Lett* 66:723–726
- Crawford RO, Boyko EP, Wagner BG, Erdmann JH, Zumer S, Doane JW (1991c) Microscope textures of nematic droplets in polymer dispersed liquid crystals. *J Appl Phys* 69:6380–6386
- Crawford GP, Allender DW, Doane JW (1992) Surface elastic and molecular anchoring properties of nematic liquid crystals confined to cylindrical cavities. *Phys Rev A* 45:8693–8709
- Crawford GP, Crawford RJO, Doane JW, Zumer S (1996) Systematic study of orientational wetting and anchoring at a liquid-crystal-surfactant interface. *Phys Rev E* 53:3647
- Cristaldi DJR, Pennisi S, Pulvirenti F (2009) *Liquid crystal display drivers, techniques and circuits*. Springer, Dordrecht
- Cross CW, Fung BM (1992) Cross relaxation of polymer dispersed liquid crystal droplets. *J Chem Phys* 96:7086
- Cross CW, Fung BM (1993) Measurement of the cross relaxation rate for a polymer dispersed liquid crystal system. *J Chem Phys* 99:1425–1428
- Cupelli D, Nicolletta FP, Manfredi S, Vivacqua M, Formoso P, Filpo GD, Chidichimo G (2009) Self-adjusting smart windows based on polymer dispersed liquid crystals. *Sol Energy Mater Sol Cells* 93:2008–2012
- Cupelli D, Nicoletta FP, Filpo GD, Formoso P, Chidichimo G (2011) Reverse mode operation polymer dispersed liquid crystal with a positive dielectric anisotropy liquid crystal. *J Polym Sci B Polym Phys* 49:257–262
- De Gennes PG (1974) *The physics of liquid crystals*. Clarendon, Oxford
- De Gennes PG, Prost J (1993) *The physics of liquid crystals*, 2nd edn. Clarendon, Oxford
- De Gennes PG, Prost J (1995) *The physics of liquid crystals*. Oxford Science, New York
- Demus D, Richter L (1978) *Textures of liquid crystals*. Chemie, New York
- Demus D, Goodby J, Gray GW, Spiess HW, Vill V (eds) (1999) *Physical properties of liquid crystals*. Wiley-VCH, Weinheim
- Deshmukh RR, Malik PK (2008) Thermo-electro-optical studies on E7 and E8 nematic type liquid crystals dispersed in PMMA polymer matrix. *J Appl Poly Sci* 109:627–637
- Deshmukh P, Gopinadhan M, Choo Y, Ahn SK, Majewski PW, Yoon SY, Bakajin O, Elimelech M, Osuji CO, Kashi RM (2014) Molecular design of liquid crystalline brush-like block copolymer for magnetic field directed self assembly: a platform for functional materials. *ACS Macro Lett* 3:462–466
- Diao Z, Deng S, Huang W, Xuan Li HL, Liu Y, Ma J (2012) Organic dual-wavelength distributed feedback laser empowered by dye-doped holography. *J Mater Chem* 22:23331–23334
- Diao Z, Huang W, Peng Z, Mu Q, Liu Y, Ma J, Xuan L (2014) Anisotropic waveguide theory for electrically tunable distributed feedback laser from dye-doped holographic polymer dispersed liquid crystal. *Liq Cryst* 41(2):239–246
- Dick VP, Loiko V (2001) A model for coherent transmittance calculation for polymer dispersed liquid crystal films. *Liq Cryst* 28:1193–1198
- Dick VP, Loiko VA (2004) Optical phase shift by polymer dispersed liquid crystal films with fine droplets. *J Phys D Appl Phys* 37:1834–1840
- Dierking I (2000) Polymer network stabilized liquid crystals. *Adv Mater* 12:167–181
- Dierking I (2003) *Textures of liquid crystals*. Wiley-VCH, Weinheim
- Doane JW, Vaz NA, Wu BG, Zumer S (1986) Field controlled light scattering from nematic microdroplets. *Appl Phys Lett* 48:269–271
- Doane JW, Chidichimo G, Vaz NA (1987) Light modulating material comprising a liquid crystal dispersion in a plastic matrix. US Patent 4,688,900, pp 1–19
- Dolinsek J, Jarh O, Vilfan M, Zumer S, Blinc R, Doane JW, Crawford GP (1991) Two-dimensional deuteron nuclear magnetic resonance of a polymer dispersed nematic liquid crystal. *J Chem Phys* 95:2154–2161

- Dorgan JR (1991) Spinodal decomposition in mixtures containing nematogens. *Liq Cryst* 10:347–355
- Dorgan JR (1995) On the meaning of the spinodal in liquid-crystalline solutions. *Fluid Phase Equilib* 109:157–169
- Dzraic PS (1986) Polymer dispersed nematic liquid-crystal for large area displays and light valves. *J Appl Phys* 60:2142–2148
- Dzraic PS (1988a) A new director alignment for droplets of nematic liquid crystal with low bend to splay ratio. *Mol Cryst Liq Cryst* 154:289–306
- Dzraic PS (1988b) Reorientation dynamics of polymer dispersed nematic liquid crystal films. *Liq Cryst* 11(3):1543
- Dzraic PS (1991) Nematic droplet/polymer films for high-contrast colored reflective displays. *Displays* 12:2–13
- Dzraic PS (1995) *Liquid crystal dispersions*. World Scientific, Singapore
- Dzraic PS, Muller A (1989) Droplet shape and reorientation fields in nematic droplet/polymer films. *Liq Cryst* 5:1467–1475
- Dzraic PS, Wiley R, McCoy J, Guillaume A (1990) High brightness reflective displays using nematic droplet/polymer films. In *SID digest*, pp 210–213
- Dzraic PS, Gonzales AM, Jones P, Montoya W (1992) Diochoric based displays form nematic dispersion. In: *SID digest*, pp 571–574
- Dunmur D, Sluckin T (2010) *Soap, science and flat-screen TVs: a history of liquid crystals*. Oxford University Press, New York
- Dzhons MM, Bulgakova SA, Pantyukhina IA, Kazantzeva IA (2011) Effects of chemical structure and composition of the polymer matrix on the morphology and electro-optical performance of polymer-dispersed liquid crystal films. *Liq Cryst* 38:1263–1268
- Ebru A, Ktanir B, Mitrokhin M, Holter B, Glushchenko A, West JL (2006) Flexible bistable smectic-A polymer dispersed liquid crystal display. *Jap J Appl Phys* 45:4146–4151
- Eimura H, Yoshio M, Shoji Y, Hanabusa K, Kato T (2012) Liquid-crystalline gels exhibiting electrooptical light scattering properties: fibrous polymerized network of a lysine-based gelator having acrylate moieties. *Polym J* 44:594–599
- Erdmann JH, Zumer S, Doane JW (1990) Configuration transition in a nematic liquid crystal confined to a small spherical cavity. *Phys Rev Lett* 64:1907–1910
- Fan SK, Chiu CP, Lin JW (2009) Electrowetting on polymer dispersed liquid crystal. *Appl Phys Lett* 94:164109
- Fayolle B, Noel C, Billard J (1979) Investigation of polymer mesophases by optical microscopy. *J Phys* 3(Colloq):485–489
- Fedors RF (1974) A method for estimating both solubility parameters and molar volumes of liquids. *Polym Eng Sci* 14:147–154, 472
- Ferguson JL (1984) Encapsulated liquid crystal and method. US Patent 4,435,047
- Ferguson JL (1985) Polymer encapsulated liquid crystals for display and light control applications. *Tech Digest SID Int Symp* 16:68–70
- Filipo GD, Siprova S, Chidichimoa G, Mashin AI, Nicolettac FP, Cupellic D (2012) Alignment of single-walled carbon nanotubes in polymer dispersed liquid crystals. *Liq Cryst* 39(3):359–364
- Flory PJ (1953) *Principles of polymer chemistry*. Cornell University Press, Ithaca
- Formentin P, Palacios R, Borrull JF, Pallares J, Marsal LF (2008) Polymer-dispersed liquid crystal based on E7: morphology and characterization. *Synth Met* 158:1004–1008
- Fujikake H, Takizawa K, Kikuchi H, Fujii T (1993) Polymer dispersed LCLVs with gray scale memory. In *SID Digest*, pp 873–876
- Fujikake H, Tanaka Y, Kimura S, Asakawa H, Tamura T, Kita H, Takeuchi K, Ogawa H, Nagashima A, Utsumi Y, Takizawa K (2000) Heat-resistant liquid crystal light modulator containing polymer network for high-power luminaires. *Jpn J Appl Phys* 39:5870–5874
- Galyametdinov YG, Knyazev AA, Dzhabarov VI, Cardineals T, Driesen K, Walrand CG, Binnemans K (2008) Polarized luminescence from aligned samples of nematogenic lanthanide complexes. *Adv Mater* 20:252–257

- Ganesan LM, Frubing P, Mellinger A, Gerhard R (2009) Dielectric relaxation behaviour of nematic liquid crystals dispersed in poly(vinylidene fluoride-trifluoroethylene). *J Phys D Appl Phys* 42:092006
- Gardon JL, Teas JP (1976) Solubility parameters, in treatise on coatings. In: Myers RR, Long JS (eds) Characterization of coatings: physical techniques: part II, vol 2. Marcel Dekker, New York
- Gmelin E (1997) Classical temperature-modulated calorimetry: a review. *Thermochim Acta* 304–305:1–26
- Golemme A, Zumer S, Allender DW, Doane JW (1988a) Continuous nematic isotropic transition in submicron size liquid crystal droplets. *Phys Rev Lett* 61:2937–2940
- Golemme A, Zumer S, Doane JW, Neubert ME (1988b) Deuterium NMR of polymer dispersed liquid crystal. *Phys Rev A* 37:559–569
- Golemme A, Urso A, Simone BCD, Mashin A, Chidichimo G (1998) Phase separation kinetics in mixtures of polymers and liquid crystals. *Liq Cryst* 24:563
- Golovatyaya NM, Kurik MV, Lavrentovich OD (1990) Self-organization of polymer dispersed nematic droplets. *Liq Cryst* 7:287–291
- Griffiths PR, Haseth JAD (2007) Fourier transform infrared spectroscopy. Wiley, New York
- Groenendaal LB, Gevaert ANV (2005) Conductive polymer. In: Crawford GP (ed) Flexible flat panel display, Wiley-SID series in display technology. Wiley, Chichester
- Guo W, Fung BM (1991) Determination of the order parameters of liquid crystals from carbon-13 chemical shifts. *J Chem Phys* 95:3917–3923
- Guo W, Fung BM (1992) Optical and Raman spectroscopy of mass-selected tungsten dimers in argon matrices. *J Chem Phys* 97:8819
- Guymon CA, Hoggan EN, Clark NA, Rieker TP, Walba DM, Bowman CN (1997) Effects of monomer structure on their organization and polymerization in a smectic liquid crystal. *Science* 275:57–59
- Hadjichristov GB, Marinov YG, Petrov AG (2009) Linear size gradient single layers of polymer-dispersed liquid crystal micrometer-sized droplets for diffractive optics. *Opt Mater* 31:1578–1585
- Hansen CM (1967a) The three dimensional solubility parameter—key to paint component affinities I. *J Paint Technol* 39:104–117
- Hansen CM (1967b) The three dimensional solubility parameter—key to paint component affinities II. *J Paint Technol* 39:505–510
- Hansen CM (1967c) The three dimensional solubility parameter and solvent diffusion coefficient. Doctoral dissertation, Danish Technical Press, Copenhagen
- Hansen CM (2007) Hansen solubility parameter. CRC Press/Taylor & Francis, Boca Raton
- Hansen CM, Beerbower A (1971) Solubility parameters. In: Standen A (ed) Kirk–Othmer encyclopedia of chemical technology, vol Suppl, 2nd edn. Interscience, New York, pp 889–910
- Hansen CM, Skaarup K (1967) The three dimensional solubility parameter—key to paint component affinities III. *J Paint Technol* 39:511–514
- Harris DC (2007) Quantitative chemical analysis. Freeman W. H. & Company, New York
- Hatakeyama T, Liu Z (eds) (1998) Handbook of thermal analysis. Wiley, Chichester
- Havens JR, Leong DB, Reimer KB (1990) Quantitative SEM characterization of polymer dispersed liquid crystal films. *Mol Cryst Liq Cryst* 178:89–101
- Hayata Y, Nagano S, Takeoka Y, Seki T (2012) Photoinduced volume transition in liquid crystalline polymer gels swollen by a nematic solvent. *ACS Macro Lett* 1:1357–1361
- Herod TE, Duran RS (1998a) Polymer-dispersed liquid crystal monolayers. *Langmuir* 14:6956
- Herod TE, Duran RS (1998b) Two- and three-dimensional nanoparticles of liquid crystals prepared at the air/liquid interface. *Langmuir* 14:6606
- Hicks SE, Hurley SP, Yang YC, Yang DK (2013) Electric polarization frozen by a polymer network in nematic liquid crystals. *Soft Matter* 2013(9):3834–3839
- Higgins DA (2000) Probing the mesoscopic chemical and physical properties of polymer-dispersed liquid crystals. *Adv Mater* 12:251–264

- Hikmet RAM (1990) Electrically induced light scattering from anisotropic gels. *J Appl Phys* 68:4406–4412
- Hikmet RAM (1992) Anisotropic gels in liquid crystal devices. *Adv Mater* 10:679–683
- Hildebrand J, Scott RL (1950) The solubility of nonelectrolytes, 3rd edn. Reinhold, New York
- Hildebrand J, Scott RL (1962) Regular solutions. Prentice Hall, Englewood Cliffs
- Hinjosa A, Sharma SC (2010) Effect of gold nanoparticles on electro-optical properties of a polymer dispersed liquid crystal. *Appl Phys Lett* 97:081114
- Hoflyzer PJ, Krevelen DWV (1976). In Krevelen DWV, te Nijenhuis K (eds) (2009) Properties of polymers, 4th edn. Elsevier, Amsterdam, pp 213–216
- Hohne G, Hemminger WF, Flammersheim HJ (2003) Differential scanning calorimetry, 2nd edn. Springer, Berlin
- Hoppe CE, Galante MJ, Oyanguren PA, Williams RJJ (2003) Polymer-dispersed liquid crystals based on polystyrene and EBBA: analysis of phase diagram and morphologies generated. *Macromol Chem Phys* 204:928–935
- Hourri A, Bose TK, Thoen J (2001) Effect of silica aerosil dispersions on the dielectric properties of a nematic liquid crystal. *Phys Rev E* 63:051702
- Hoy KL (1970) New values of the solubility parameters from vapour pressure data. *J Paint Technol* 42:76
- Hoy KL (1985) Tables of solubility parameters, solvent and coatings materials research and development department, Union Carbide Corporation. In Krevelen DWV, te Nijenhuis K (eds) (2009) Properties of polymers, 4th edn, Elsevier, Amsterdam, pp 216–219
- Hoy KL (1989) Solubility parameter as a design parameter for water borne polymer and coatings. *J Coat Fab* 19:53
- Huang CT, Chen HF (1991) Second harmonic generation by thermoplastic polymer dispersed liquid crystal films. In: Huang CT, Chen HF (eds) Frontier of polymer research. Plenum, New York, pp 167–172
- Huang H, Wunder SL (2001) Preparation of microporous PVdF based polymer electrolytes. *J Power Sources* 97:649–653
- Iannacchione GS, Qian S, Finotello D, Aliev FM (1997) Liquid crystalline behavior of octylcyanobiphenyl confined to submicron-size randomly connected porous glasses. *Phys Rev E* 56:554–561
- Iannacchione GS, Park S, Garland CW, Birgeneau RJ, Leheny RL (2003) Smectic ordering in liquid-crystal-aerosil dispersions. II. Scaling analysis. *Phys Rev E* 67:011709
- Im SJ, Sung JH, Park WY, Sakong DS (1995) A study of electro-optical property and VHR of PDLC depending on the molecular structure of monomer and preparation process. *Synth Met* 71:2203–2204
- Jadzyn J, Zechowski C, Mucha M, Nastal E (1999) Dielectric relaxation in polymer dispersed nematic liquid crystal films. *Liq Cryst* 26:453–456
- Jain SC, Rout DK (1991) Electro-optic response of polymer dispersed liquid-crystal films. *J Appl Phys* 70:6988
- Jain SC, Thakur RS (1992) Thermo-electro-optic switch based on polymer dispersed liquid crystal composite. *Appl Phys Lett* 61:1641–1642
- Jain SC, Thakur RS, Lakshmikummar ST (1993) Switching response of a polymer dispersed liquid-crystal composite. *J Appl Phys* 73:3744–3748
- Jang MW, Kim BK (2011) Low driving voltage holographic polymer dispersed liquid crystals with chemically incorporated graphene oxide. *J Mater Chem* 21:19226–19232
- Jeon YJ, Bingzhu Y, Rhee JT, Cheung DL, Jamil M (2007) Application and new developments in polymer-dispersed liquid crystal simulation studies. *Macromol Theory Simul* 16:643–659
- Jeon YJ, Lee GH, Jang JE, Hwang KY, Ahmad F, Jamil M, Leec JW, Jung JE (2012) Applications of multidirectional reflective light-control films on reflective polymer-dispersed liquid crystal displays for enhancement in image quality at lower viewing angles. *Liq Cryst* 39 (11):1314–1319

- Jin X, Zhang S, Runt J (2002) Observation of fast dielectric relaxation in semi-crystalline poly (ethylene oxide). *Polymer* 43:6247–6254
- Kao KC (2004) Dielectric phenomena in solids. Elsevier Academic, London
- Kashima M, Cao H, Liu H, Meng Q, Wang D, Li F, Yang H (2010) Effects of the chain length of crosslinking agents on the electro-optical properties of polymer-dispersed liquid crystal films. *Liq Cryst* 37(3):339–343
- Kato T (2002) Self-assembly of phase-segregated liquid crystal structures. *Science* 295:2414–2418
- Kellner R, Mermet JM, Otto M, Valcarcel H, Widmer HM (2004) Analytical chemistry: a modern approach to analytical science, 2nd edn. Wiley–VCH, Weinheim
- Kelly JR, Muhoray PP (1997) Normal modes of director fluctuations in a nematic droplet. *Phys Rev E* 55(4):4378–4381
- Kikuchi H, Fujii T, Kawakita M, Fujikake H, Taktzawa K (2000) Design and fabrication of a projection display using optically addressed polymer-dispersed liquid crystal light valves. *Opt Eng* 39:656–669
- Kim JY, Woo HY, Baek JW, Kim TW, Song EA, Park SC, Ihm DW (2008) Polymer dispersed liquid crystal devices using highly conducting polymers as electrodes. *Appl Phys Lett* 92:183301
- Kim KS, Lee SB, Lee H, Kim HS, Lee Y, Kwack K (2009) Poly(vinylidene fluoride)-hexafluoropropylene–methyl N-methylpyrrolidinium-N-acetate trifluoromethane sulfonylimide-lithium trifluoromethanesulfonylimide gel electrolytes. *J Ind Engg Chem* 15:657–660
- Kim YK, Shiyanovskii SV, Lavrentovich OD (2013) Morphogenesis of defects and tactoids during isotropic-nematic phase transition in self-assembled lyotropic chromonic liquid crystals. *J Phys Condens Matter* 25:404202
- Kiselev AD, Yaroshchuk OV, Dolgov L (2004) Ordering of droplets and light scattering in polymer dispersed liquid crystal films. *J Phys Condens Matter* 16:7183–7197
- Kitzerow HS (1994) Polymer-dispersed liquid crystals—from the nematic curvilinear aligned phase to ferroelectric-films. *Liq Cryst* 16:1–31
- Kitzerow HS, Crooker PP (1992) Behaviour of polymer dispersed cholesteric droplets with negative dielectric anisotropy in electric fields. *Liq Cryst* 11:561–568
- Kitzerow HS, Crooker PP (1993) Electric field effects on the droplet structure in polymer dispersed cholesteric liquid crystals. *Liq Cryst* 13:31
- Kleman M, Lavrentovich OD (2006) Topological point defects in nematic liquid crystals. *Philos Mag* 86:4117–4137
- Klosowicz SJ, Zmija J (1995) Optics and electro-optics of polymer-dispersed liquid crystals: physics, technology and applications. *Opt Eng* 34(12):3440–3450, SPIE eBooks
- Kovalchuk AV, Kurik MV, Lavrentovich OD, Sergan VV (1988) Structural transformations in nematic droplets located in an external electric field. *Sov Phys JETP* 67:1065–1073
- Kramer F, Schoenhals A (eds) (2003) Broadband dielectric spectroscopy. Springer, Berlin
- Krevelen DWV, Nijenhuis KT (2009) Properties of polymers, 4th edn. Elsevier, Oxford
- Kumano N, Seki T, Ishii M, Nalamura H, Umemura T, Takeoka Y (2011) Multicolor polymer dispersed liquid crystals. *Adv Mater* 23:848–888
- Kumar P, Raina KK (2007) Morphological and electro-optical responses of dichoric polymer dispersed liquid crystal films. *Curr Appl Phys* 7:636–642
- Kuriakose M, Longuemart S, Depriester M, Delenclos S, Sahraoui AH (2014) Maxwell-Wagner-Sillars effects on the thermal-transport properties of polymer-dispersed liquid Crystals. *Phys Rev E* 89:022511
- Kurik MV, Lavrentovich OD (1982) Negative–positive monopole transitions in cholesteric liquid crystals. *Sov Phys JETP Lett* 35:445–447
- Lackner AM, Margerum JD, Ramos E, Lim KC (1989) Droplet size control in polymer dispersed liquid crystal films. In *Proc. SPIE* 1080, pp 53–61

- Lampert CM (1998) Smart switchable glazing for solar energy and daylight control. *Sol Energy Mater Sol Cells* 52:207–221
- Land PL, Schmitt MG (1995) Nonlinear optical scattering screen viewer. US Patent 5,448,382, 5 Sept
- Lee JW, Baek SD, Kim JK, Choi SJ, Ahmad F, Jamil M, Jeon YJ (2014) Effect of cetyltrimethylammonium bromide coatings on indium tin oxide surfaces in reverse mode polymer dispersed liquid crystal films. *Liq Cryst* 41(5):621–625
- LeGrange JD, Carter SA, Fuentes M, Boo J, Freeny AE, Cleveland W, Millerd TM (1997) Dependence of the electro-optical properties of polymer dispersed liquid crystals on the photopolymerization process. *J Appl Phys* 81:5984–5991
- Leheny RL, Park S, Birgeneau RJ, Gallani JL, Garland CW, Iannacchione GS (2003) Smectic ordering in liquid-crystal-aerosil dispersions. I. X-ray scattering. *Phys Rev E* 67:011708–011721
- Lejardi A, Meaurio E, Fernandez J, Sarasua JR (2011) Miscibility of poly(vinyl alcohol)-graft-hydroxy ester/poly(vinylpyrrolidone) blends. *Macromolecules* 44:7351–7363
- Leon TL, Nieves AF (2011) Drops and shells of liquid crystals. *Colloid Polym Sci* 289:345–359
- Leon TL, Koning V, Devaiah KBS, Vitelli V, Nieves AF (2011a) Frustrated nematic order in spherical geometries. *Nat Phys* 7:391–394
- Leon TL, Nieves AF, Nobili M, Blanc C (2011b) Nematic-smectic transition in spherical shells. *Phys Rev Lett* 106(247802):1–4
- Li L, Yuan HY, Palffy MP (1991) Second harmonic generation by polymer dispersed liquid crystal films. *Mol Cryst Liq Cryst* 198:239–246
- Lin H, Ding H, Kelly JR (1995) The mechanism of switching a PDLC film. *Mol Cryst Liq Cryst* 1:262–299
- Liu F, Cao H, Mao Q, Song P, Yang H (2012a) Effects of monomer structure on the morphology of polymer networks and the electro-optical properties of polymer-dispersed liquid crystal films. *Liq Cryst* 39(4):419–424
- Liu YJ, Cai Z, Leong ESP, Zhao XS, Teng JH (2012b) Optically switchable photonic crystals based on inverse opals partially infiltrated by photoresponsive liquid crystals. *J Mater Chem* 22:7609–7613
- Liu YJ, Su YC, Hsu YJ, Hsiao VKS (2012c) Light-induced spectral shifting generated from azo-dye doped holographic 2D gratings. *J Mater Chem* 22:14191–14195
- Liu Y, Li Y, Xiong H (2013) Dielectric chain dynamics of side-chain liquid crystalline polymer. *ACS Macro Lett* 2:45–48
- Lovinger AJ, Amundson KR, Davis DD (1994) Morphological investigation of UV curable polymer-dispersed liquid-crystal (PDLC) materials. *Chem Mater* 6:1726–1736
- Lowe AC, Kriss MA (eds) (2006) Introduction to microdisplays, Wiley–SID series in display technology. Wiley, West Sussex
- Lu ZJ, Yang DK (1994) Effects of chiral adopant on the performance of PDLC. *Appl Phys Lett* 65:505–507
- Lu Y, Wei J, Shi Y, Jin O, Guo J (2013) Effects of fabrication condition on the network morphology and electro-optical characteristics of polymer-dispersed bistable smectic A liquid crystal device. *Liq Cryst* 40(5):581–588
- Luo D, Du QG, Dai HT, Demir HV, Yang HZ, Ji W, Sun XW (2012) Strongly linearly polarized low threshold lasing of all organic photonic quasicrystals. *Sci Rep* 2:627. doi:[10.1038/srep00627](https://doi.org/10.1038/srep00627)
- Macdonald R, Kentischer F, Warnick P, Heppke G (1998) Antiferroelectricity and chiral order in new liquid crystals on nonchiral molecules studied by optical second harmonic generation. *Phys Rev Lett* 81:4408–4411
- Magagnini P, Paci M, Poli G, Tonti MS, Narducci P (1999) Polymer-dispersed liquid-crystal polymers (PDLCs): morphology of the LCP droplets. *Polym Eng Sci* 39:1891–1902
- Maier W, Saupe A (1959) Eine einfache molekularstatistische theorie der nematischen kristallin-flüssigen phase. Teil I, *Z Naturforsch Teil A* 14:882

- Maier W, Saupe A (1960) Eine einfache molekularstatistische theorie der nematischen kristallinflüssigen phase. Teil II, Z Naturforsch Teil A 15:287
- Malik P, Raina KK (2004) Droplet orientation and optical properties of polymer dispersed liquid crystal composite film. *Opt Mater* 27:613–617
- Malik P, Ahuja JK, Raina KK (2003) Effect of polymer viscosity on morphological and electro-optic properties of aligned polymer dispersed ferroelectric liquid crystal composite films. *Curr Appl Phys* 3:325–329
- Malik P, Bubnov AM, Raina KK (2008) Electro-optic and thermo-optic properties of phase separated polymer dispersed liquid crystal films. *Mol Cryst Liq Cryst* 494:242–251
- Malik P, Raina KK, Gathania AK (2010) Effects of polymer viscosity on the polymerization switching and electro-optical properties of unaligned liquid crystal/UV curable polymer composites. *Thin Solid Films* 519:1047–1051
- Manohar R, Tripathi G, Singh AK, Srivastava AK, Shukla JP, Prajapati AK (2006) Dielectric and optical properties of polymer–liquid crystal composite. *J Phys Chem Solid* 67:2300–2304
- Martinez A, Ravnik M, Brice L, Visvanathan R, Žumer S, Smalyukh II (2014) Mutually tangled colloidal knots and induced defect loops in nematic fields. *Nat Mater* 13(3):258–263, www.nature.com/naturematerials
- Matsuyama A (2010) Theory of binary mixtures of a rodlike polymer and a liquid crystal. *J Chem Phys* 132:214902–214912
- McFarland CA, Koenig JL, West JL (1993) Analysis of polymer-dispersed liquid crystals by infrared spectroscopy. *Appl Spectrosc* 47(3):598
- McMillan WL (1971) Simple molecular model for the smectic A phase of liquid crystals. *Phys Rev A* 4:1238–1246
- Mei E, Higgins DA (1998) Polymer-dispersed liquid crystal films studied by near-field scanning optical microscopy. *Langmuir* 14:1945–1950
- Menczel JD, Leslie TM (1990) Temperature calibration of a power compensation DSC on cooling. *Thermochim Acta* 166:309–317
- Menczel JD, Prime RB (eds) (2009) *Thermal analysis of polymers: fundamentals and applications*. Wiley, Hoboken
- Meng Q, Cao H, Kashima M, Liu H, Yang H (2010) Effects of the structures of epoxy monomers on the electro-optical properties of heat-cured polymer-dispersed liquid crystal films. *Liq Cryst* 37:189–193
- Merola F, Grilli S, Coppola S, Vespini V, De Nicola S, Maddalena P, Carfagna C, Ferraro P (2012) Reversible fragmentation and self-assembling of nematic liquid crystal droplets on functionalized pyro electric substrates. *Adv Funct Mater* 22:3267–3272
- Mertelj A, Copic M (1998) Dynamic light scattering in nematic liquid crystals in confined geometries. *Mol Cryst Liq Cryst Sci Technol A* 320:287–299
- Mertelj A, Spindler L, Copic M (1997) Dynamic light scattering in polymer-dispersed liquid crystals. *Phys Rev E* 56:549–553
- Miller DS, Wang X, Abbott NL (2014) Design of functional materials based on liquid crystalline droplets. *Chem Mater* 26:496–506
- Mirau PA, Srinivasarao M (1997) NMR characterization of liquid crystal polymer interactions in polymer-dispersed liquid crystals. *Appl Spectrosc* 51(11):1639–1643
- Moein T, Ji D, Zeng X, Ke L, Gan Q, Cartwright AN (2014) Holographic photopolymer linear variable filter with enhanced blue reflection. *ACS Appl Mater Interfaces* 6:3081–3087
- Mucha M (2003) Polymer as an important component of blends and composites with liquid crystals. *Prog Polym Sci* 28:837–873
- Muhoray PP, West JL (1989) Nonlinear optics of liquid crystals: collective reorientation effects. In *Proc. SPIE* 1080, pp 91–100
- Naficy S, Jalili R, Aboutalebi SH, Grokin RA, Konstantinov K, Innis PC, Spinks GM, Poulin P, Wallace GG (2014) Graphene oxide dispersions: tuning rheology to enable fabrication. *Mater Horiz* 1:326–331

- Natarajan LV, Sutherland RL, Bunning TJ, Tondiglia VP, Division of Polymer Chemistry, American Chemical Society (1997) Liquid crystal dispersions in polymers: novel nanostructures. *Polym Prepr* 38(214):634–663
- Navarro SH, Tierno P, Mullol JI, Sagues F (2011) Breaking the degeneracy of nematic liquid crystals by means of actuated anisometric paramagnetic colloids. *Soft Matter* 7:5109–5112
- Nicoletta FP, Cupelli D, De Flipo G, Macchione M, Chidichimo G (2000) Quasilinear electro-optical response in a polymer-dispersed nematic liquid crystal. *Appl Phys Lett* 77:3689–3691
- Nolan P, Tillin D, Coates D, Ginter E, Lueder E, Kallfass T (1993) Reflective mode PDLC displays—paper white display. In *Eurodisplay'93*. SID, Strasbourg, pp 397–400
- Orwoll RA, Arnold PA (1996) Polymer–solvent interaction parameter w . In: Mark JE (ed) *Physical properties of polymers handbook*. AIP Press, Woodbury, Chapter 14
- Pairam E, Nieves AF (2009) Generation and stability of toroidal droplets in a viscous liquid. *Phys Rev Lett* 102:234501
- Parmar DS, Holmes HK (1993) Skin friction measurement with partially exposed polymer dispersed liquid crystals. *Rev Sci Instrum* 64:538–541
- Parmar DS, Singh JJ (1992) Partially exposed polymer dispersed liquid crystals for boundary layer investigations. *Appl Phys Lett* 61:2039–2041
- Pasini P, Zannoni C, Zumer S (eds) (2003) *Computer simulations of liquid crystals and polymers*, Nato science series. Kluwer, Dordrecht
- Pavani K, Naydenova I, Raghavendra J, Martin S, Toal V (2009) Electro-optical switching of the holographic polymer dispersed liquid crystal diffraction gratings. *J Opt A Pure Appl Opt* 11:024023–024028
- Peng H, Bi S, Ni M, Xie X, Liao Y, Zhou X, Xue Z, Zhu J, Wei Y, Bowman CN, Mai YM (2014) Monochromatic visible light “photoinitiator”: janus-faced initiation and inhibition for storage of colored 3D images. *J Am Chem Soc* 136:8855–8858
- Perju E, Marin L, Grigoras VC, Bruma M (2011) Thermotropic and optical behaviour of new PDLC systems based on a polysulfone matrix and a cyanoazomethine liquid crystal. *Liq Cryst* 38:893–905
- Philippe J, Arcand B, Galstian T (2011) Self-organization of liquid-crystal and reactive-mesogen into 2D surface-stabilized structures. *Macromolecules* 44:344–348
- Preeti GS, Satyavathi N, Murthy KPN, Sastry VSS (2009) Anchoring transition and influence of director fluctuations in liquid crystal droplets. *Liq Cryst* 36:1379–1388
- Priezjev N, Pelcivits RA (2000) Surface extrapolation length and director structures in confined nematics. *Phys Rev E* 62:6734–6738
- Proust JE, Saraga LTM, Guyon E (1972) Orientation of a nematic liquid crystal by suitable boundary surfaces. *Solid State Commun* 11:1227–1230
- Raikher YL, Shliomis MI (1994) The effective field method in the orientational kinetics of magnetic fluids and liquid crystals. In: Coffey W (ed) *Advances in chemical physics: relaxation phenomena in condensed matter*, vol 2. Wiley, New York, pp 595–791
- Rajeswari M, Dhara S, Venu K, Sastry VSS, Dabrowski R (2012) Effect of confinement on molecular processes in the liquid crystal 8OCB: application of NMR relaxometry. *Soft Matter* 8:10008–10016
- Reading M, Hourston DJ (eds) (2006) *Modulated temperature differential scanning calorimetry: theoretical and practical applications in polymer characterisation*. Springer, Dordrecht
- Reamey RH, Montoya W, Wong A (1992) Video-microscopy of NCAP films: the observations of LC droplets in real time. In *Proc. SPIE* 1665, pp 2–7
- Ren H, Lee SH, Wu ST (2009) Reconfigurable liquid crystal droplets using a dielectric force. *Appl Phys Lett* 95:241108
- Riccardi CC, Borrajo J, Williams RJJ (1998a) Instability of a nematic phase described by the Maier–Saupe model. *J Chem Phys* 108:2571–2575
- Riccardi CC, Borrajo J, Williams RJJ, Siddiqi HM, Dumon M, Pascault JP (1998b) Multiple phase equilibria in polydisperse polymer/liquid crystal blends. *Macromolecules* 31:1124–1132

- Roussel F, Buisine JM, Maschke U, Coqueret X (1998) Photopolymerization kinetics and phase behaviour of acrylate based polymer dispersed liquid crystals. *Liq Cryst* 24:555
- Roussel F, Buisine JM, Maschke U, Coqueret X, Benmouna F (2000) Phase diagrams and morphology of polymer dispersed liquid crystals based on nematic-liquid-crystal-monofunctional-acrylate mixture. *Phys Rev E* 62:2310–2316
- Roussel F, Canlet C, Fung BM (2002) Morphology and orientational order of nematic liquid crystal droplets confined in a polymer matrix. *Phys Rev E* 65:021701
- Roussel F, King CY, Buisine JM (2003) Conducting polymers as driving electrodes for polymer-dispersed liquid-crystals display devices: on the electro-optical efficiency. *Eur Phys J E Soft Matter* 11:293–300
- Rout DK, Jain SC (1992a) Dielectric properties of a polymer dispersed liquid crystal film. *Mol Cryst Liq Cryst* 210:75–81
- Rout DK, Jain SC (1992b) Dielectric properties of polymer-liquid crystal composites. *Jpn J Appl Phys* 31:1396–1398
- Russell GM, Paterson BJA, Imrie CT, Heeks SK (1995) Thermal characterization of polymer-dispersed liquid crystals by differential scanning calorimetry. *Chem Mater* 7:2185–2189
- Rzoska SJ, Zhelezny VP (eds) (2004) Nonlinear dielectric phenomena in complex liquids. Kluwer Academic/Springer, Dordrecht
- Sanchez PJM, Vazquez C, Perez I, Rodriguez I, Oton JM (2002) Electro-optic system for online light transmission control of polymer-dispersed liquid crystal windows. *Opt Eng* 41:1608–1611
- Sansone MJ, Khanarian G, Leslie TM, Stiller M, Altman J, Elizondo P (1990) Large Kerr effects in transparent encapsulated liquid crystal. *J Appl Phys* 67:4253–4259
- Sansone MJ, Khanarian G, Kwiatek MS (1994) Large Kerr effects in transparent encapsulated liquid crystals. II. Frequency response. *J Appl Phys* 75:1715–1721
- Schick C, Hohne GWH (1991) On temperature calibration of power compensation DSC in cooling mode. *Thermochim Acta* 187:351–356
- Schuld N, Wolf BA (1999) Polymer–solvent interaction parameters. In: Brandrup J, Immergut EH, Grulke EA (eds) *Polymer handbook: part VII*, 4th edn. Wiley, New York, p 247
- Serbutoviez C, Kloosterboer JG, Boots HMJ, Ouwslages FJ (1996) Polymerization-induced phase separation. 2. Morphology of polymer-dispersed liquid crystal thin films. *Macromolecules* 29:7690–7698
- Shanks RA, Staszczuk D (2012) Thermal and optical characterization of polymer-dispersed liquid crystals. *Int J Poly Sci* 2012, 767581
- Shao L, Zhang Y, Liu C, Li J, Qin A, Wang Y (2012) Effect of graft polymer prepared by living radical polymerisation on electro-optical properties of polymer dispersed liquid crystal. *Liq Cryst* 39(12):1458–1464
- Shao L, Li J, Zhang Y, Gong S, Wang Y (2014) Effect of macro-RAFT agent on the morphology of polymer dispersed liquid crystals. *Liq Cryst* 41(5):652–661
- Shen C, Kyu T (1995) Spinodals in a polymer dispersed liquid crystal. *J Chem Phys* 102:556–562
- Shen TZ, Hong SH, Song JK (2014) Electro-optical switching of graphene oxide liquid crystals with an extremely large Kerr coefficient. *Nat Mater* 13:394–399
- Sheraw CD, Zhou L, Huang JR, Gundlach DJ, Jackson TN, Kane MG, Hill IG, Hammond MS, Campi J, Greening BK, Francl J, West J (2002) Organic thin film transistor driven polymer dispersed liquid crystal displays on flexible polymeric substrate. *Appl Phys Lett* 80:1088–1090
- Shikama S, Kida H, Daijogo A, Okamori S, Ishitani H, Maemura Y, Kondo M, Murai H, Yuki M (1995) High-luminance LCD projector using a Si TFT–PDLC light valves. *Digest SID* 95:231–234
- Shirey SKF, Maranas JK (2009) Effect of LiClO₄ on the structure and mobility of PEO-based solid polymer electrolytes. *Macromolecules* 42:2142–2156
- Shishido A (2010) Rewritable holograms based on azobenzene-containing liquid-crystalline polymers. *Polym J* 42:525–533

- Simoni F (1997) Nonlinear optical properties of liquid crystals and polymer dispersed liquid crystals. World Scientific, Singapore
- Simoni F, Cipparrone G, Umeton C, Arabia G, Chidichimo G (1989) Optical nonlinearities induced by thermal effects in polymer dispersed liquid crystals. *Appl Phys Lett* 54:896–897
- Simoni F, Cipparrone G, Umeton C (1990) Mirror less all optical bistability in polymer dispersed liquid crystals. *Appl Phys Lett* 57:1949–1951
- Simoni F, Cipparrone G, Duca D, Khoo IC (1991) Threshold degenerate wave mixing in dye doped polymer dispersed liquid crystals. *Opt Lett* 16:360–362
- Simoni F, Bloisi F, Vicari L (1992a) Transient amplitude grating in polymer dispersed liquid crystals. *Mol Cryst Liq Cryst* 223:169–179
- Simoni F, Duca BFD, Vicari L (1992b) Nonlinear diffraction driven by low frequency electric field in polymer dispersed liquid crystals. *Mol Cryst Liq Cryst* 212:279–287
- Simoni F, Bloisi F, Vicari L (1993) Optical switching and controlled self diffraction with polymer dispersed liquid crystals. *J Nonlinear Opt Phys Mat* 2:353–365
- Singh S (2000) Phase transition in liquid crystals. *Phys Rep* 324:107–269
- Singh S (2002) Liquid crystals: fundamentals. World Scientific, Singapore
- Smith GW (1990) Study of formation, phase behaviour, and microdroplet size of a polyurethane-based polymer dispersed liquid crystal. *Mol Cryst Liq Cryst* 180B:201–222
- Smith GW (1993a) Mixing and phase separation in liquid crystal/matrix systems. *Int J Mod Phys B* 7(25):4187–4213
- Smith GW (1993b) Mixing and phase separation of liquid crystal/matrix system: determination of the excess specific heat of mixing. *Phy Rev Lett* 70:198–201
- Smith GW, Vaz NA (1988) The relationship between formation kinetics and microdroplet size of epoxy-based polymer dispersed liquid crystals. *Liq Cryst* 3:543–571
- Smith GW, Ventouris GM, West JL (1992) A calorimetric determination of fundamental properties of polymer-dispersed liquid crystals. *Mol Cryst Liq Cryst* 213:11–30
- Smith RT, Popovich MM, Sagan SF (2000) Application-specific integrated lenses and filters for microdisplays using electrically switchable Bragg grating technology. *Proc SPIE* 4207:31–38
- Song P, Cao H, Wang F, Ellahi M, Yang H (2012a) Study of polymer-dispersed liquid crystal systems using epoxies/acrylates as hybrid polymer matrix components. *Liq Cryst* 39:903–909
- Song P, Cao H, Wang F, Liu F, Jingjing W, Ellahi M, Li F, Yang H (2012b) The UV polymerisation temperature dependence of polymer-dispersed liquid crystals based on epoxies/acrylates hybrid polymer matrix components. *Liq Cryst* 39:1131–1140
- Soule ER, Abukhdeir NM, Rey AD (2009) Thermodynamics, transition dynamics, and texturing in polymer-dispersed liquid crystals with mesogens exhibiting a direct isotropic/smectic A transition. *Macromolecules* 42:9486–9497
- Spicer PT (2005) Progress in liquid crystalline dispersions: cubosomes. *Curr Opin Colloid Interface Sci* 10:274–279
- Springer GH, Higgins DA (2000) Toroidal droplet formation in polymer dispersed liquid crystal films. *J Am Chem Soc* 122:6801–6802
- Srivastava JK, Singh RK, Dhar R, Singh S (2011) Thermal and morphological studies of liquid crystalline materials dispersed in a polymer matrix. *Liq Cryst* 38:849–859
- Srivastava JK, Singh RK, Dhar R, Singh S (2012) Phase diagrams and morphology of polymer-dispersed liquid crystals: an analysis. *Liq Cryst* 39:1402–1413
- Stannarius R, Kremer F (2004) Liquid crystals in confining geometries, vol 634, Lecture notes in physics. Springer, Heidelberg, pp 301–336
- Stannarius R, Crawford GP, Chien LC, Doane JW (1991) Nematic director orientation in a liquid crystal dispersed polymer: a deuterium nuclear magnetic resonance approach. *J Appl Phys* 70:135–143
- Stark H (2001) Physics of colloidal dispersions in nematic liquid crystals. *Phys Rep* 351:387–474
- Sutherland RL (1989) Optical limiters, switches and filters based on polymer dispersed liquid crystals. *Proc SPIE* 1080:83–90

- Sutherland RL (1991) Bragg scattering in permanent nonlinear-particle composite gratings. *J Opt Soc Am B* 8:1516–1525
- Sutherland RL, Tondiglia VP, Natarajan LV, Bunning TJ, Adams WW (1993) Bragg gratings in an acrylate polymer consisting of periodic polymer dispersed liquid crystal planes. *Chem Mater* 5:1533–1538
- Sutherland RL, Tondiglia VP, Natarajan LV, Bunning TJ, Adams WW (1994) Electrically switchable volume gratings in polymer dispersed liquid crystals. *Appl Phys Lett* 64:1074–1076
- Sutherland RL, Natarajan LV, Tondiglia VP, Bunning TJ (1998) Switchable holograms for displays and other applications. *Proc SPIE* 3421:8–18
- Tabib AM, Sutapun B, Srihirin T, Lando J, Adamovsky G (2000) Fiber optic electric field sensors using polymer-dispersed liquid crystal coatings and evanescent field interactions. *Sensors Actuators A Phys* 84:134–139
- Takizawa K, Fujii T, Fujikake H, Hirabayashi T, Tanaka Y, Hara K, Takano S, Asakawa H, Kita H (1999) Liquid-crystal luminaire consisting of an optical shutter and a metal halide lamp. *Appl Opt* 38:2570–2578
- Talibuddin S, Wu L, Runt J, Lin JS (1996) Microstructure of melt-miscible, semicrystalline polymer blends. *Macromolecules* 29:7527–7535
- Tanaka K, Kato K, Tsuru S, Sakai S (1993) A liquid crystal/polymer optical device formed by holography for reflective color display applications. In: *Euro display'93, SID, Strasbourg*, pp 109–111
- Tanaka K, Kato K, Tsuru S, Sakai S (1994) Holographically formed liquid crystal/polymer device for reflective color display. *J Soc Inf Disp* 2:37–40
- Tatemoto M, Suzuki T, Tomoda M, Furukawa Y, Ueta Y (1981) Cross linkable fluorine containing polymer and its production. *US Patent* 4,243,770, 6 Jan
- Tsai TY, Lee CY, Lee CJ, Lin MY, Wei L (2012) Polymer-dispersed liquid crystal nanocomposites comprising montmorillonite clay modified by conducting pentamers oligoaniline. *J Mater Chem* 22:13050–13056
- Ueda S, Kagimoto J, Ichikawa T, Kato T, Ohno H (2011) Anisotropic proton-conductive materials formed by the self-organization of phosphonium-type zwitterions. *Adv Mater* 23:3071–3074
- Van De Hulst HC (1957) *Light scattering by small particles*. Wiley, New York
- Vaz NA, Montgomery GP Jr (1989) Dual frequency addressing of polymer-dispersed liquid-crystal films. *J Appl Phys* 65:5043–5050
- Vaz N, Smith GW, Montgomery GP Jr (1991) Polymer dispersed liquid crystal films formed by electron beam cure. *Mol Cryst Liq Cryst* 197:83–101
- Vicari L (ed) (2003) *Optical applications of liquid crystals*. IOP, Bristol
- Vijaykumar G, Lee JM, Song M, Jin SH, Lee JW, Lee CW, Gal YS, Shim HJ, Kang Y, Lee GW, Kim K, Park NG, Kim S (2009) New liquid crystal-embedded PVdF-co-HFP-based polymer electrolytes for dye-sensitized solar cell applications. *Macromol Res* 17:963–968
- Vilfan M, Lahajnar G, Zupančič I, Žumer S, Blinc R, Crawford GP, Doane JW (1995) Dynamics of a nematic liquid crystal constrained by a polymer network: a proton NMR study. *J Chem Phys* 103:8726
- Vilfan M, Kopac NV, Zihel P, Crawford GP (1999a) Deuteron NMR relaxometry applied to confined liquid crystals. *Appl Magn Reson* 17:329–344
- Vilfan M, Vrbancic KN, Zala B, Zumer S, Crawford GP (1999b) Measurement of the surface-induced order in polymer dispersed liquid crystals: an approach by NMR relaxometry. *Phys Rev E* 59:R4754–R4757
- Vilfan M, Lahajnar G, Zupancic I, Zalar B (2003) Low-frequency proton NMR relaxometry of a polymer dispersed liquid crystal above T_{NI} . *Magn Reson Imaging* 21:169–175
- Volvoik GE, Lavrentovich OD (1983) Topological dynamics of defects: boojums in nematic drops. *Sov Phys JETP* 58:1159–1166
- Wall BG, Koenig JL (1997) Studying the curing kinetics of a diacrylate by using infrared spectroscopy. *Appl Spectrosc* 51(10):1453–1459

- Wall BG, Koenig JL (1998) Infrared microspectroscopic investigation of the diffusion of E7 intopoly(butyl methacrylate). *Appl Spectrosc* 52(11):1377–1382
- Wang XJ, Zohu QF (2004) Liquid crystalline polymers. World Scientific, Singapore
- Whitehead JB, Zumer S, Doane JW (1993) Light scattering from a dispersion of aligned nematic droplets. *J Appl Phys* 73:1057
- Williams G, Shinton SE, Aldridge GE (2001) Dielectric relaxation spectroscopy and alignment behaviour of a polymer dispersed liquid crystal and its component materials. *J Polym Sci B Polym Phys* 39:1173–1194
- Wilson MR (2007) Molecular simulation of liquid crystals: towards a better understanding of bulk structure and the prediction of material properties. *Chem Soc Rev* 36:1881–1888
- Wu ST (1986) Birefringence dispersions of liquid crystals. *Phys Rev A* 33:1270–1274
- Wu BG, Erdmann JH, Doane JW (1989) Response times and voltages for PDLC light shutters. *Liq Cryst* 5:1453–1465
- Wu F, Feng T, Wu C, Bai Y, Ye L, Chen J (2010) Thermally stable hyperbranched polyether-based polymer electrolyte for lithium-ion batteries. *J Phys D Appl Phys* 43:035501
- Xi J, Qiu X, Zheng S, Tang X (2005) Nanocomposite polymer electrolyte comprising PEO/LiClO₄ and solid super acid: effect of sulphated-zirconia on the crystallization kinetics of PEO. *Polymer* 46:5702–5706
- Xia J, Wang J, Lin Z, Qiu F, Yang Y (2006) Phase separation kinetics of polymer dispersed liquid crystal confined between two parallel walls. *Macromolecules* 39:2247–2253
- Xie XL, Mai YW, Zhou XP (2005) Dispersion and alignment of carbon nanotubes in polymer matrix. *Mater Sci Eng R* 49:89–112
- Xu F, Kitzerow HS, Crooker PP (1992) Electric-field effects on nematic droplets with negative dielectric anisotropy. *Phys Rev A* 46:6535–6540
- Yamaguchi T, Kawata Y, Mori Y (1998) Boundary condition effects on field induced diffusion modes in polymer dispersed liquid crystals. *Appl Phys Lett* 72:1170
- Yamamoto R (2001) Simulating particle dispersions in nematic liquid-crystal solvents. *Phys Rev Lett* 87:075502
- Yan B, He J, Xin D, Zhang K, Wang S, Pan C, Wang Y (2009) Control of liquid crystal droplet configuration in polymer dispersed liquid crystal with macro-iniferter polystyrene. *Liq Cryst* 36:933–938
- Yang DK, Crooker PP (1991) Field-induced textures of polymer dispersed chiral liquid crystal microdroplets. *Liq Cryst* 9:245–251
- Yang DK, Wu ST (2006) Fundamentals of liquid crystal devices. Wiley, Chichester
- Yang W, Lan T, Xia S, Ma L, Wang Y (2014) Influence of macroinitiator's glass transition temperature on the response times of polymer dispersed liquid crystals. *Liq Cryst* 41(2):202–206
- Yaroshchuk O, Reznikov Y (2012) Photoalignment of liquid crystals: basics and current trends. *J Mater Chem* 22:286–300
- Yuan HJ, Li L, West JL (1991) Nonlinear birefringence of liquid crystals. *Mol Cryst Liq Cryst* 199:223–232
- Zalewska A, Walkowiak M, Niedzicki L, Jesionowski T, Langwald N (2010) Study of the interfacial stability of PVdF/HFP gel electrolytes with sub-micro- and nano-sized surface-modified silica. *Electrochem Acta* 55:1308–1313
- Zhang GM, Hong Z, Changxing Z, Wu BG, Lin JW (1992) New rapid response polymer dispersed liquid crystal material. *Proc SPIE* 1815:233–237
- Zheng Z, Ma J, Liu Y, Xuan L (2008) Molecular dynamics of the interfacial properties of partially fluorinated polymer dispersed liquid crystal gratings. *J Phys D Appl Phys* 41:235302
- Zheng Z, Zhou L, Shen D, Xuan L (2012) Holographic polymer-dispersed liquid crystal grating with low scattering losses. *Liq Cryst* 39(3):387–391
- Zhong ZZ, Schuele DE, Gordon WL, Adamic KJ, Akins RB (1992) Dielectric properties of a PMMA/E7 polymer dispersed liquid crystal. *J Polym Sci B Polym Phys* 30:1443–1449

- Zhou J, Petti L, Mormile P, Roviello A (2004) Comparison of the thermo- and electro-optical properties of doped and un-doped MOM based PDLCs. *Opt Commun* 231:263–271
- Zhou Y, Ahn SK, Lakhman RK, Gopinadhan M, Osuji CO, Kasi RM (2011) Tailoring crystallization behavior of PEO-based liquid crystalline block copolymers through variation in liquid crystalline content. *Macromolecules* 44:3924–3934
- Zou J, Fang J (2011) Adhesive polymer dispersed liquid crystal films. *J Mater Chem* 21:9149–9153
- Zumer S (1988) Light scattering from nematic droplets: anomalous-diffraction approach. *Phys Rev A* 37:4006–4015
- Zumer S, Doane JW (1986) Light scattering from a small nematic droplet. *Phys Rev A* 34:3373–3386
- Zumer S, Kralj S (1992) Influence of K_{24} of the structure of nematic liquid crystal droplets. *Liq Cryst* 12:613–624
- Zumer S, Crawford GP, Doane JW (1995) Surface phenomena in microconfined liquid crystals: from cylindrical cavities to polymer networks. *Mol Cryst Liq Cryst* 261:577–592

Chapter 8

LCP Based Polymer Blend Nanocomposites

Ganesh Chandra Nayak and Chapal Kumar Das

8.1 Polymer Blends

Polymer blends are macroscopically homogeneous mixture of two or more different species of polymers. The advantages of polymer blends includes (1) production of materials with full set of desired properties at the lowest price, (2) improvement of engineering resins' performance, (3) enhancement of specific properties, (4) improved processibility, product uniformity, and scrap reduction, (5) quick formulation (6) high productivity, (7) reduction of the number of grades that needs to be manufactured and stored and (8) Inherent recyclability, etc. (Utracki 2002a). Polymer blends can be formed at various states of miscibility between the blend partners like completely miscible, phase separated and partially miscible and the properties of these blends can vary in line with the percentage of miscibility. Polymer blends properties, like mechanical, optical, rheological, dielectric, and barrier properties, depends on two major parameters: the control of the interface and the control of the morphology. Due to this, study and control of morphology of polymer blends has emerged as an area of continuous interest to polymer material scientists in the last few decades (Cahn and Hilliard 1958; Siggia 1979; Kessler et al. 1986). Miscible polymer blend is a polymer blend which is homogeneous down to the molecular level and associated with the negative value of the free energy of mixing and domain size is comparable to the dimensions of macromolecular statistical segment. The most important factor leading to miscibility in low molecular weight materials is the combinatorial entropy contribution which is very large compared to high molecular weight polymers. A miscible blend of two

G.C. Nayak (✉)

Department of Applied Chemistry, Indian School of Mines, Dhanbad, Jharkhand 826004, India
e-mail: gcnayak_bls@yahoo.co.in; nayak.g.ac@ismdanbad.ac.in

C.K. Das

Materials Science Centre, IIT Kharagpur, Kharagpur, West Bengal 721302, India
e-mail: ckd@matsc.iitkgp.ernet.in

polymers is going to have properties somewhere between those of the two unblended polymers. In partially miscible blends both the interacting phases are homogeneous. An example is the PC/ABS blends. In these blends, PC and the SAN phase of ABS partially dissolve in one another. In this case, the interphase is wide and the interfacial adhesion is reasonable. In immiscible blends the constituent polymers do not mix, but remain in separate phases, leading to the formation of a dispersion of one of the polymers in a continuous matrix of the other resulting which leads to the phase separation between the interacting polymers resulting in poor bonding but the immiscible materials upon blending are turned out to be nifty and useful.

8.2 Thermodynamics of Polymer Blends

If two polymers are mixed, the most expected result is a system that exhibits a complete phase separation due to the repulsive interaction between the polymeric components i.e. the chemical incompatibility between the polymers. The phase separation generally takes place when a single-phase system suffers a change of composition, temperature or pressure that forces it to enter either the metastable or the spinodal region. When the system enters from single-phase region into the metastable region, the phase separation occurs by the mechanism resembling crystallization—slow nucleation followed by growth of the phase separated domains. By contrast, when the system is forced to jump from a single-phase into the spinodal region of immiscibility the phases separate spontaneously by a mechanism called spinodal decomposition. The situation can be better explained by considering Fig. 1.1.

As shown in the Fig. 1.1a, the miscibility increases with temperature, and at the Upper Critical Solution Temperature (UCST), the blend forms a single phase. Similarly in Fig. 1.1b the polymers form a single phase at low temperatures, and phase separate as the temperature is increased above the LCST. This can occur if there are specific interactions between the polymers (such as hydrogen bonds), or if mixing results in a decrease in volume. As the temperature is increased, these attractive interactions eventually become disrupted, and the blend begins to phase-separate.

8.3 Factors Controlling the Miscibility of Polymer Blends

Generally mixing of two polymers lead to a two-phase system because polymers are thermodynamically immiscible and incompatible, this leads to high interfacial tension and poor interface adhesion. Consider a system of two polymers, A and B. If a small amount of B is added to pure A, the blend will be miscible and form a single phase. As more B is added, the blend becomes unstable and separates into

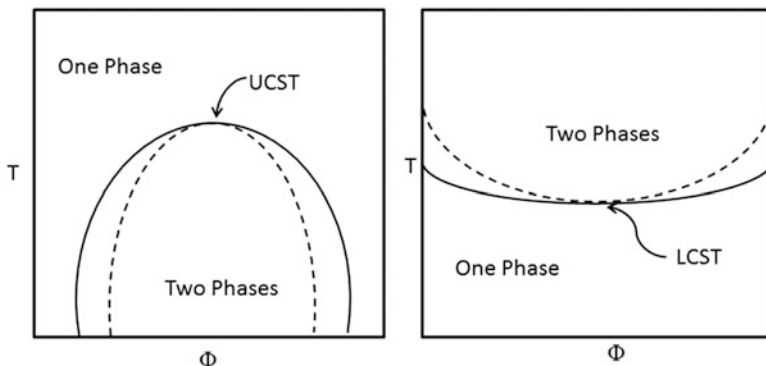


Fig. 1.1 (a) UCST type phase diagram, (b) LCST type phase diagram. *Solid lines* show the binodal curve, *broken lines* show the spinodal curve (Utracki 2002a, b; Siggia 1979)

two phases, one rich in polymer A, and the other rich in B. The miscibility of the system is also affected by temperature. Some blends phase separate on heating, while others phase-separate as the temperature decreases. This can occur if there are specific interactions between the polymers (such as hydrogen bonds), or if mixing results in a decrease in volume. As the temperature is increased, these attractive interactions eventually become disrupted, and the blend begins to phase-separate. A numbers of other factors also play role in the miscibility and immiscibility of polymer blends and alloys. Similar structured polymers or with similar polarity are likely to form miscible blends whereas different polarities produce immiscibility. Polymers of low molecular weight permits greater randomization on mixing and therefore greater gain of entropy, results in miscibility, while polymers of different molecular weight result in immiscibility. Polymers that are attached to each other by hydrogen bonds, ion-dipole, donor-acceptor adduct, transition metal complexes, etc. are likely to impart miscibility in blends and alloys. Separate phase is developed when a polymer is crystallized. When polymer in blend crystallize they will form two separate crystalline phases, it is rare for the two polymers to co-crystallize in a single crystalline phase. In immiscible or incompatible polymer blends, the phase rule explains quantitatively the extent to which they separate and the extent to which each phase are actually not pure polymer I and II, but rather solution of I in II and solution of II in I. The major phase will form the continuous matrix and control the properties, while the minor phase will form dispersed domain and it contributes certain specialized properties to the blend. The simplest shape of dispersed domain with minimum surface energy is spherical, as the attraction between the immiscible phases increases the size of sphere decreases and compatibility increases. When two polymers repel each other then they separate into different phases (incompatible) and the interface could be very weak and can fail under any kind of mechanical or thermal stress. Thus compatible blends must therefore have a strong interface which allows the stress to transfer. This shows that the compatible blends must have a broad transition region, which has the

ability to resist stress. This transition phase is referred as interphase. Difference between compatibility and incompatibility can be explained by broad strong interphase and sharp weak interface.

8.4 Compatibilization of Immiscible Polymer Blends

The compatibilization of immiscible polymers is one of the most important, widespread and difficult problems in contemporary applied polymer science. The compatibilization of immiscible blends can be accomplished by the optimization of the interfacial tension (to achieve the desired degree of dispersion), stabilization of the morphology against high stresses during blending (to get optimum structure) and enhancement of adhesion between the blend partners in the solid state (facilitating the stress transfer from one phase to other and hence improves the performance). There are several approaches adopted for making the incompatible polymer blends compatible, which includes:

1. Incorporation of specific interactive groups
2. In-situ polymerization
3. Addition of graft copolymer
4. Reactive compatibilization
5. Addition of Block copolymer
6. Nanoparticle compatibilization

Among these approaches co-polymer compatibilizer is widely adopted. Addition of a small amount of copolymer (block-, graft-, random-copolymer) mainly affects the interfacial tension coefficient and hence the size of dispersed phase. However, it has little effect on either the shear sensitivity of the blends morphology or their solid-state behavior. While the addition of di-block copolymer efficiently reduced the interfacial tension, the tri-block copolymer leads to better mechanical properties (Utracki 2002b). The morphology of immiscible blend depends on many factors, among which the flow history and the interfacial properties are the most important. Thus, the interfacial and rheological properties are the keys to morphology. Polymer blends with low interfacial tension tend to form co-continuous morphologies over a wider composition range than those with high interfacial tension. Several studies have investigated the effect of block copolymer on the boundaries of the region of co-continuity (Bourry and Favis 1998; Jorgensen 1999; Li et al. 2002; Chuai et al. 2003; Dedecker and Groeninckx 1998). In contrast to the expansion of co-continuity region, addition of block copolymer actually narrowed it. This result is surprising because the addition of block copolymer is expected to reduce the effective interfacial tension and thereby promote the formation of elongated domains, making co-continuous morphologies easier to generate. The possible cause for this observation could be the effect of block copolymer on the coalescence of domains i.e. the block copolymer stabilizes the droplet morphology of the polymer blends by reducing the coalescence tendency of the dispersed phase and hence cause the region of co-continuity to narrow down.

8.5 Liquid Crystalline Polymer

A liquid crystal, or mesophase, is a state of matter between the liquid and crystal states. Liquid crystals are ordered like crystals but flow like liquids. Liquid crystalline polymers (LCP) are usually classified into two groups: lyotropic LCPs and thermotropic LCPs, based on the conditions for the formation of their liquid crystalline state. Lyotropic LCPs are processed to high-strength, high-modulus fibers by a solution spinning technique whereas thermotropic LCPs can be processed and molded to structural parts of different shapes by means of conventional processing techniques for thermoplastics, such as extrusion and injection molding. The temperature at which phase transition from liquid crystal to melt state occurs is called the isotropization (T_i) or clearing temperature (T_c). Liquid crystals are classified according to the shape of the mesogens and the structure and appearance of the mesophases. Mesogens are either rod-like or disk-like and they are divided into three main classes: nematic, smectic, and cholesteric. The mesogenic units in a liquid crystalline polymer may be in the main chain or the side chain of the polymer. Polymeric liquid crystals are also classified according to their chemical structure and the conditions under which the LC state is formed. Main-chain LCPs may be either fully aromatic or built up of rigid mesogens and flexible spacers. In side-chain LCPs, the rigid mesogenic units usually are present in pendant side chains (Percec 1997). The potential applications of LCP includes: production of high-strength and high-modulus fibers, precision molded small components, films exhibiting excellent barrier properties, novel composites, processing aids in the melt, reversible information storage, electro-optical displays, and non-linear optical devices. Their applications arise directly from a number of interesting properties they exhibit, which typically include: low melt viscosity, fast cycle time in molding, very low mold shrinkage, excellent mechanical properties, good solvent resistance, low thermal expansion coefficient, low water absorption, excellent barrier properties, ferroelectric properties, and high continuous use temperatures (Han and Bhowmik 1997).

8.6 Polymer Blends Based on Liquid Crystalline Polymer

Polymer blends, containing liquid crystalline polymer, is a special class of composite, known as in-situ composites, where the reinforcement have been provided by the in-situ generated LCP fibers. These types of polymer blends were studied intensively by different research groups mainly due to two advantages; (1) in-situ fibrillation and reinforcement and (2) improved processibility. Both LCP and thermoplastics show shear-thinning behavior which promotes the fibrillation of the LCP to form rigid and highly oriented LCP fibers. Thermotropic LCPs can also function as a processing aid and a reinforcing agent to improve both the processibility and performance of thermoplastics. Because of its high cost, LCP is

used as the minor component in these types of blend systems. From a scientific viewpoint, several aspects of basic understanding are involved in order to develop marketable technology: the rheological behavior of LCP blends, orientation and crystallization of blend systems, interfacial interaction and compatibilization in LCP blends, microstructure development, and the processing-structure-property relationship in these LCP blends. There are several factors to be fine-tuned to achieve the in-situ fibrillation but the major road block is the incompatibility between the blend partners, containing LCP, which decreases the interfacial adhesion, enhances the interlayer slippage and hence restricts the fibrillation. To overcome this obstacle compatibilizers are being used which can restricts the interlayer slippage and enhance the fibrillation.

The research on LCP containing in-situ composite was started in the early 1980s. Siegmann et al. reported reduced melt viscosity of the polyamide/LCP blend, with only 5 % of LCP, and superior mechanical properties as compared to the individual components (Siegmann et al. 1985). They also analyzed the phase morphology of the polymer blends with various LCP contents and found that the domain structure changed from spherical to fibrillar with increasing LCP content. This was the first paper reporting in detail the LCP blends that were named later as “in-situ composites”. The fibrillation of LCPs in thermoplastic melts is influenced by several parameters, including the thermal characteristics of the component polymers and their compatibility, and processing parameters such as viscosity ratio, melt temperature, flow mode, and shear rate.

8.7 Major Factors Controlling the LCP Fibrillation

The morphological development of LCP containing polymer blends, during processing, depend on several factors like processing device, flow field, viscosity and viscosity ratio, processing temperature, interfacial tension, domain deformation, coalescence, breakup, and relaxation of the dispersed phase.

8.7.1 Viscosity Ratio

Viscosity ratio of the blend partners plays a crucial role in the LCP domain deformation and coalescence, under the shear flow. La Mantia and Valenza (1992) proposed that if the viscosity of TLCP was higher than matrix, large droplets of TLCP were formed, whereas fibrillation could only occur when the viscosity of the matrix was higher than that of the TLCP. Hence the viscosity ratio of TLCP to polymer matrix should be less than one in order to facilitate the deformation of LCP droplets to fibrillar form. In an extruder, the shear flow, before the die, could result in the domain deformation and fibrillation of LCP, if the viscosity ratio is 0.01 or smaller. Similarly at die entrance the coalescence and further deformation of the

LCP domains lead to the increase in volume and aspect ratio of the fibrils. In general, viscosity ratio, less than unity, is a necessary condition for the fibrillation of LCPs. Deformation of the droplet is dependent on the interaction between the viscous force and interfacial force. When the disruptive stress due to viscous drag of the medium is capable of overcoming the cohesive effect of surface tension, the suspended phase would be deformed and elongated into cylindrical shape (Lee et al. 2003a). Even though the viscosity ratio effect is a necessary condition for the fibrillation of LCP, it is not always sufficient condition. There are many LCP containing blends studied by several groups for the exploration of suitable conditions for the fibrillation of LCP.

Table 1.1 summarizes the effect of viscosity ratio on the LCP droplet morphology, in various polymer matrices along with their viscosity ratios. It can be seen that, viscosity ratio lower than unity, although necessary but not always a sufficient condition for the fibrillation of LCP.

8.7.2 Capillary Number

According to Taylor, droplets were deformed as spheroids under shearing, and the deformation of these droplets depended on dimensionless parameters such as the capillary number and the viscosity ratio (Taylor 1932, 1934; Heino and Seppala 1993). The Capillary number (Ca) is a dimensionless number that predicts fibrillation originated from the hydrodynamic theorem. The capillary number can be defined as the ratio of the shear stress acting on the LCP droplet by an external flow field to the interfacial tension which resists the deformation of the spherical droplet: The Ca can be measured by following the (1.1), which is represented as:

$$Ca = \eta_m \left[1 - (4\phi_d\phi_m)^{0.8} \right] \frac{d\gamma(16\lambda + 16)}{2\sigma(16\lambda + 16)} \quad (1.1)$$

where γ is the shear rate; d is the diameter of the dispersed phase droplet, σ is the interfacial tension, ϕ_d is the volume fraction of dispersed phase (LCP), ϕ_m is the volume fraction of the matrix phase, η_m is the viscosity of the matrix and $\lambda = \eta_{\text{LCP}}/\eta_m$ is the viscosity ratio. So the magnitude of Ca was affected by many factors such as shear rate (affects the size and shape of LCP fibers), interfacial tension (affects the drag force of viscous media upon LCP), LCP content (affects the coalescence and particle breakup), material properties, viscosity ratio and processing conditions which in turn influence the droplet-fibril transition. Generally the droplet-fiber transformation favored if the Ca exceed the critical limit by many fold. Heino et al. investigated various types of LCP/PP blends and noticed that, while fibrillar LCP was formed at viscosity ratios ranging from 0.5 to 1, spherical or cluster like morphology was exhibited for ratios above unity (Heino et al. 1994).

Table 1.1 Morphology of LCP containing polymer blends reported in the literature

System	Extrusion Temp (°C)	η_{LCP}/η_{matrix}	Morphology (with LCP concentrations indicated)	Ref.
LCP (PHB/HNA)/PC	310	<1	2.5 %, 5 %, 10 % fibrils; 25 %, 50 % droplets	Isayev and Modic (1987)
LCP (PHB/PET)/PC	240	<1	5 %, 10 % droplets	Nobile et al. (1989)
	260	<1	50 % thick fibers	
LCP (PHB/HNA)/PET	280–288	<1	20 %, 40 %, 60 % no fibril; 80 % fibrils; at high shear rates, 30 % fibrils	Ko and Wilkes (1989)
LCP (PHB/HNA)/PEEK	350	<1	2.5 %, 5 % no fibril; >10 % fibrils	Mehta and Isayev (1991)
LCP (PHB/PET)/PET	280	<1	Large L/D of die, no fibril; small L/D, lightly fibril	(Sukhadia, et al. 1990)
LCP (PHB/HNA)/PPO	310	<1	Most fibrils in skin, >50 % fibrils in core	Limtasiri and Isayev (1991)
Polyester/PC	270	<1	Fibrils at very high shear rates and small L/D	Kohli et al. (1989)
LCP (PHB/PET)/PA66	275	<1	No fibril in stable shear	Blizard and Baird (1987)
LCP (PHB/PET)/PC	260	<1	Extruding, 10 % droplets, 30 % fibrils, >50 % continuous	Blizard and Baird (1987)
LCP (PHB/HNA)/PC	260	Cross	Fibrils at high shear rates	Beery et al. (1991)
LCP (PHB/HNA)/PBT	260	>1	Droplets	Beery et al. (1991)
LCP (PHB/HNA)/PA66	260	>1	Droplets	Beery et al. (1991)
LCP (PHB/HNA)/PPS	285	>1	Droplets	Subramanian, and Isayev (1991)
LCP (PHB/HNA)/PS	295	>1	Spherical form	Choi et al. (1996)
LCP (PHB/PET)/PS	295	<1	Fibrils	Choi et al. (1996)

8.7.3 *Critical LCP Content*

The LCP content has critical effect on the geometry of LCP, in the polymer blend system. In the uncompatibilized blend system low concentration of LCP, below 5 wt%, results in geometry like spheroids or ellipsoids of LCP, regardless of the shear rate during mixing or extrusion (Song and Isayev 2010). However, higher LCP concentration, in excess of 20 wt%, gives rise to long LCP fibers. This is related to the magnitude of force exerted by the matrix phase on to the dispersed phase during blending. According to Taylor's theory (Taylor 1934), higher force is needed to deform a small particle as compared to a large particle. At lower concentration of LCP, the droplet size will be obviously smaller than that with the higher concentration, which makes it difficult to deform the smaller droplets into fibrillar form. Moreover, at low volume fraction of the LCP, the size of dispersed LCP phase may be too low such that the small and sparsely distributed LCP particles could not coalesce to any significant extent to form larger particles that were required for deformation to occur. This demonstrates that a lower limit of LCP concentration is essential for the development of in-situ fibrillation.

8.7.4 *Processing Equipment*

Extrusion has been the preferred method for the processing of LCP containing polymer blends over the conventional internal mixture. The extensional flows, such as melt drawing, are most effective to produce LCP micro-fibrils and the effectiveness increases with draw ratio. Drawing promotes fibrillation especially with high LCP content because it facilitates the deformation of the large LCP domains into fibrils under the applied extensional flow. It was determined that as draw ratio increased, the tensile modulus increased due to the improvement in the molecular orientation and the higher aspect ratio of the LCP fibrils. Kyotani et al. (1992) showed that addition of LCP to a polymer like PET, produced excellent molecular orientation, at a draw ratio of 80, which was not possible for the draw ratio of 120 in pure PET. This molecular alignment was reflected in the stiffness of the blend where the tensile modulus almost tripled. A schematic diagram of the post extrusion process adopted by Lee et al. (2003b) is shown in Fig. 1.2. In this mixing process, a post draw force has been exerted by few rollers which draw the fibers coming out of the extruder. The fibers are being passed through the water trough to cool them. They showed that the aspect ratio of the in situ LCP fibers can be controlled by the draw ratio.

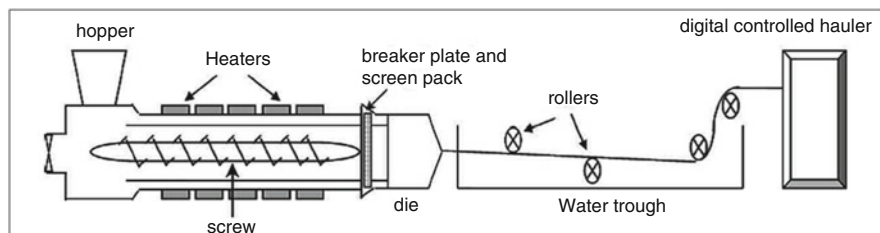


Fig. 1.2 Schematic setup for extrusion process (Lee et al. 2003b)

8.7.5 Interfacial Adhesion

Interfacial adhesion at the matrix-LCP interface has a significant role to play in the formation of in situ fibrillation of LCP. Generally, LCP/thermoplastics blends consist of two separate phases, which in most cases are immiscible. The poor adhesion between the components of the blends gives rise to polyblends having lower tensile modulus and strength than expected from the law of mixtures. In addition to that absence of interfacial adhesion promotes the interlayer slippage at the LCP matrix interface and restricts the LCP domain deformation and hence the fibrillation. Such situation can be resolved by the addition of suitable compatibilizer into the polymer blend system which can promote the interfacial adhesion. Better interfacial adhesion also helps in the stress transfer from matrix to dispersed LCP phase. The mechanical and thermal properties of the polymer blends can be enhanced by the addition of compatibilizer.

8.8 Carbon Nanotube

The CNT has gained tremendous momentum from the scientific community in the present decade because of their wide range of potential applications in several areas since its invention by Iijima in the year of 1991. MWCNT is considered to be the most promising nanomaterial due to its high flexibility, low mass density, high aspect ratio (typically $>10^3$), and exceptional mechanical, thermal, and electrical properties. The CNT is an allotropic modification of carbon and the extraordinary properties of the CNT are attributed to the unique tubular structure of the graphitic sheets, which is in the order of nanometers in diameter and microns in length. The carbon-carbon (C-C) chemical bond present in CNTs is completely formed by sp^2 hybridized bonding orbitals, which is comparatively stronger than the sp^3 types bonding structure located in diamond as a result it exhibits extremely high mechanical properties. The CNTs are mainly divided into two types depending on the reaction conditions of fabrication techniques; such as single-walled CNT (SWCNT) and multi-walled CNT (MWCNT). The SWCNT is made up of a single sheet of graphene layer, which is perfectly folded to form a hollow cylinder with a diameter

in order of 1 nm and up to few centimeters in length. The MWCNT consists of more than single concentric nested cylindrical graphene layers with an interlayer spacing of 0.35 nm (equal to the basal plane separation in turbostratic graphite), which are coaxially assembled around the central main hollow core by the van der Waals force of attraction between the adjacent graphene layers. MWCNT has diameters ranging from 2 to 10^2 nm and lengths in tens of microns. The whole families of CNTs are classified into three types of tubes of different diameters based on the rolling up of the graphene sheets along one of the symmetry axis (armchair and zigzag tubes) or in a direction that differs from a symmetry axis (chiral tubes). The functionalization of carbon nanotubes are carried out by different conventional (covalent, non-covalent exohedral, and endohedral functionalization) (Hirsch and Vostrowsky 2005) and non-conventional radiation induced graft polymerization (RIGP) (Jung et al. 2009), plasma treatment (Felten et al. 2005), and γ -irradiation (Skakalova et al. 2004) methods to improve its solubility, wetting, dispersion, processibility and properties. The covalent modification of CNTs is generally a successful and adopted technique to introduce some defects on the CNT surface where polar chemical functional groups like carboxyl, derivative of carboxyl, hydroxyl, amine, halogens etc. can be placed. The pristine CNTs has enormous prospect for extensive application in conducting plastics, energy storage, sensors, electronic devices, electron microscope tips, electron emission devices, structural materials, catalyst supports, biological applications, air and water filtration, ceramics and so on (Thostenson et al. 2001). The MWCNT is an ideal reinforcing nanofiller for the development of new generation high strength, lightweight, and multi-functional polymer nanocomposites for electromagnetic shielding, antistatic coatings, high strength low density corrosion resistant components, and lightweight energy storage applications (Coleman et al. 2006).

Carbon nanotubes are widely used as nanofillers for the fabrication of advanced polymeric nanocomposites due to its superior properties like high mechanical strength, excellent electrical and thermal conductivity. However, uniform dispersion of CNTs in the polymer matrix is the major obstacle for development of high performance nanocomposites. To improve the dispersion of CNTs in the polymer matrix, functionalization of CNTs has been done by several research groups. However chemical modification of CNTs introduces defective sites in CNTs and breaking of CNTs and thus property improvement of the nanocomposites falls below expectation. Non-covalent modification of CNTs, like ceramics coated CNTs, overcomes the above limitations of breaking and defective sites in CNTs which are developed by covalently bonded functional groups.

8.9 Effect of Compatibilizers on the Properties of LCP Containing Blends

Polymer blends, having LCP as minor components, are being studied extensively for the production of high performance materials with superior properties. However, as we know, most polymer blends are immiscible, i.e. simply mixing these polymer pairs cannot produce practically useful materials. With regard to this, improving the compatibility and controlling the phase separation and morphologies of polymer blends turn out to be most important parameters in polymer blending. In addition to this, the condition of blending must be optimized for the in-situ generation of LCP fibers, which not only improve the processibility of the polymer blends but also reinforce the base matrix. Many researchers have analyzed the effect of Compatibilizer on LCP based polymer blends with respect to different compatibilizers.

Seo et al. (1999a) demonstrated that addition of functionalized polypropylene (maleic-anhydride-grafted polypropylene, MA-PP) in TLCP (poly (ester amide))/nylon 6,6 blend facilitate the structural development of the TLCP by acting as a compatibilizer at the interface. Addition of MA-PP improved the mechanical properties of the resulted blend. From morphological observations it was evident that the interfacial adhesion was superior and the reduced particle size enables finely dispersed liquid crystalline polymer to be deformed by shear flow without strong elongation, even when the viscosity of the matrix is much lower than that of the liquid crystalline polymer. Krishnaswamy et al. (1999) investigated the influence of reactive terpolymer on the properties of in situ composites based on polyamides and thermotropic liquid crystalline polyesters. Small amounts of a reactive terpolymer added to a binary blend of polyamides and thermotropic liquid crystalline polyesters prior to injection molding yielded in situ composites with significantly higher modulus and strength along the reinforcement direction and substantially higher strength and toughness along the transverse direction of injection molded parts. Miller et al. (1995) observed that acrylic acid-functionalized polypropylene (PP-AA) was assessed as compatibilizers for polypropylene/liquid-crystal polymer (PP/LCP) blends. Incorporation of PP-AA increased the fiber crystallinity and fibers were oriented in the direction of flow field. This was attributed to the promotion of specific polar interactions between the blend components. Seo et al. (1999b) established the relationships between the properties of ternary blends of nylon 6, a thermotropic liquid crystalline polymer and a compatibilizer (maleic-anhydride-grafted polypropylene) under various processing conditions. The compatibilizer provides extrudate surface stability, thus enabling high drawing. The fibrillation of dispersed TLCP phase was evident.

The rheological, mechanical properties and micro-structural development during capillary flow of maleic anhydride compatibilized PA6 (MAP)/liquid crystalline polymers (LCPs) blends were studied by Meng and Tjong (1998). From SEM observations long and fine fibrils formation was evident. The rheological measurements showed that the viscosity ratio between the Vectra A950 and (PA6 (MAP))

matrix was much larger than unity. Chiou et al. (1996) used ethylene-glycidyl methacrylate copolymer (EGMA) as a reactive compatibilizer for the immiscible and incompatible blends of polypropylene (PP) and a liquid crystalline polymer (LCP). The epoxy functional groups of the EGMA copolymer reacted with the carboxylic acid and/or hydroxyl end-groups of LCP. The in situ-formed EGMA-g-LCP copolymer tends to reside along the interface of the PP/LCP and reduces the interfacial tension during melt processing. The lowering of crystallinity of the compatibilized blends was reflected in a substantial reduction in stiffness (in terms of the tensile modulus). However, the improved adhesion of the compatibilized blends resulting in an improvement in the toughness. As mentioned by Li et al. (2002), random styrene–maleic anhydride copolymer (RSMA) could be used as an effective compatibilizer in polyamide-6/liquid crystalline copolyester blend. The mechanical measurements illustrated that the stiffness, tensile strength, and toughness of the in situ composites were generally improved with increasing RSMA content. The results also showed that the maximum impact force (F_{\max}) and crack-initiation energy (E_{init}) tend to increase with increasing RSMA contents. From these results, it appeared that RSMA prolongs the crack-initiation time and increases the energies for crack initiation and impact fracture, thereby leading to toughening of LCP/PA6 in situ composites. Vallejo et al. (2000) reported the effect of an ionomer as a compatibilizer in PP/LCP blend system. The ionomer used as compatibilizer was an ethylene–methacrylic acid copolymer where methacrylic acid was partially neutralized with Zinc. The fibers of uncompatibilized blend were pulled out from the matrix, but those of compatibilized blends were mostly fractured. The improved morphology, gave rise to increase in modulus by 20 % and tensile strength by 32 %. Chin et al. (1996) investigated that solid epoxy had been demonstrated to be an effective compatibilizer for the incompatible PET/LCP blends. The LCP fibril formation was also enhanced after compatibilization and resulted in substantial improvement on both stiffness and toughness. Huang et al. (2001) reported the usefulness of styrene–acrylonitrile–glycidyl methacrylate (SAG) copolymers with various contents of glycidyl methacrylate (GMA) as compatibilizer for incompatible blends of styrene–acrylonitrile (SAN) and a liquid crystalline polymer (LCP). These SAG copolymers contain reactive glycidyl groups that are able to react with the carboxylic acid and/or hydroxyl end groups of the LCP to form the SAG-g-LCP copolymers during melt processing. Compatibilized SAN/LCP blends were observed with finer fibrils than those of the corresponding uncompatibilized blends.

The morphology, compatibility and mechanical properties of the blends of a co-polyester type LCP and ABS were studied by Xie et al. (2003). LCP fibrils were formed and distinct skin/core morphology was observed in the injection molded samples. At higher LCP concentration (50 wt%), phase inversion took place, where the dispersed LCP phase became a co-continuous phase. The blend modulus was lower than the values predicted by the rule of mixtures, suggesting a poor interface between the LCP droplets and ABS matrix. However, copolymer of styrene and maleic anhydride (SMA) used as compatibilizer, resulted in improvement in mechanical properties as well as interfacial adhesion.

8.10 Effect of Fillers on the Properties of LCP Containing Ternary Blends

From the above discussion it is clear that compatibilizer can significantly affect the ultimate properties of the LCP containing polymer blends. However, selection of compatibilizers for polymer blends consisting of engineering thermoplastics, having very high melting temperature, and LCP has been an area of concern because the compatibilizers must have sufficient thermal stability to sustain the processing temperature. In addition to this the dispersion of nanofillers, uniformly, in the blend matrix also presents separate problem. In order to overcome these problems, different research groups studied the effect of nanofillers as compatibilizers for these types of polymer blends, where the nanofillers act both as reinforcing agent and compatibilizer and also enhance the LCP fibrillation. This process produced a dual reinforcement effect on the polymer matrix where the LCP (in micro phase) and nanofillers (in nano phase) enhanced the mechanical properties of polymer blends. Some of the important works are cited in the following section. Jun et al. (2006) described the hydrodynamic effects arising from the presence of fillers in in-situ PSF/LCP hybrid composites. They showed that in presence of fillers the flow field changed from shear flow to elongational flow. So, in in-situ hybrid composites, containing LCP droplets and filler particles, extra hydrodynamic effects arise from the presence of filler particle and act on the morphological evolution of the LCP droplets. The study confirmed that the presence of rigid CaCO_3 whiskers altered the flow field and enhanced the vortex in the converging flow area at the entry of the capillary. It is this vortex enhancement that resulted in the increase of the elongational stress and promoted the fibrillation of the LCP droplet in PSF/LCP/whisker systems. They found that mainly spherical domains of LCP formed along with some ellipsoids in PSF/LCP binary blends. However, after the whisker was added into the binary blends, LCP fibrils with large aspect ratios were generated in all the hybrid composites; and with the incorporation of more whiskers, the larger aspect ratio of LCP was obtained. Incorporation of 2.1 vol% of whisker to the binary PSF/LCP blend increased the aspect ratio of LCP to three times, suggesting an enhanced fibrillation of LCP. At the maximum content 11.5 vol% of whiskers studied, the LCP average aspect ratio increases to 12.4. Similarly they found that addition of a small amount of whiskers to the PSF/LCP blend increased the volume-average diameter of LCP particles. Tjong and Meng (1999a, b) explored the effect of potassium titanate whiskers ($\text{K}_2\text{Ti}_6\text{O}_{13}$) on the properties of PA6/LCP blend system. The whisker was surface treated with tetrabutyl orthotitanate in order to improve the compatibility. They observed that the tensile modulus and tensile strength increased with the whisker content but impact strength varied up to 10 wt% of whisker after which it starts to decrease. LCP fibers were formed in the skin section of composite up to 10 wt% of whisker content but spherical domains of LCP were identified beyond the whisker content of 15 wt%. They also reported an enhancement of thermal stability with the addition of whisker. In another study they showed that incorporation of potassium titanate

whiskers in the maleic anhydride compatibilized PP/LCP blend system improved the fibrillation of LCP (Tjong and Meng 1999a, b). Due to the dual reinforcement of LCP fiber and whisker, the mechanical properties of the hybrid composites were found to be superior to the binary blend system. They ascribed this enhancement, in the mechanical properties, to the compatibilizing effect of maleic anhydride, which step up the interfacial adhesion to promote the LCP fibrillation and incorporation of whisker.

Lee et al. (2003c) studied the effect of nanosilica on the PP/LCP blend systems and found that the mixing sequence, the filler size, and the filler surface nature affected the rheology of the composites and the morphology of the LCP phase in the ternary composite. They have demonstrated that the droplet-fibril transition of LCP depends strongly on the compatibility between the filler and the PP matrix. According to this study, hydrophobic silica facilitated the fibrillation of LCP, because of preferential residence of the hydrophobic silica in the PP phase. They found that the hydrophilic-silica-filled ternary composite was more viscous than the hydrophobic-silica-filled one and they ascribed this phenomenon to the orientation of the LCP domains in the ternary composite; which was better in hydrophobic silica blend than that in the hydrophilic blend. It was also found that when LCP fibrils were developed, the fibrous LCP phase could readily lower the viscosity and could couple with the fillers to improve the shear-thinning response of the ternary composite. Silica was used as a viscosity thickening agent to improve the fibrillation of the LCP phase in PP/LCP blend system (Lee et al. 2002). It was shown that with the incorporation of 5–15 wt% of fillers, fibers of LCP were formed which improved the flow properties of the LCP/PP/SiO₂ composites. Addition of hydrophobic silica led to an increase of the aspect ratio of the LCP fibrils, which, in turn, improved their effectiveness as reinforcements and/or toughening agents. Zhang et al. (2003) also reported similar phenomenon for the PP/LCP/SiO₂ ternary blends. Zhang et al. (2005) studied the influence of nano-clay on the morphology of TLCP in nylon-6 matrix. They showed that clay platelets had dramatic influences on the dispersion and deformation of TLCP phase. With the addition of 3 wt% of nanoclay TLCP droplets got smaller as compared to the binary blend and deformed into fibrils at the clay loading up to 5 and 7 wt%. This enhanced fibrillation of TLCP droplets was attributed to the compatibilizing ability of the nanoclay particles which improve the interfacial adhesion and suppress the interfacial slip between TLCP and nylon phases in the melt, so that the shear stress was effectively transferred to the dispersed TLCP phase. Tang et al. (2010) reported the influences of blending sequence on viscosity reduction of high molecular mass polyethylene (HMMPE)/TLCP blend system filled with organoclay. They found that large amounts of organoclay formed partially intercalated structures in TLCP, when the organoclay was first blended with TLCP and then with HMMPE, with phase separation occurring at the temperature when TLCP was in the nematic phase, corresponding an antagonistic effect which weakens viscosity reduction ability of TLCP for HMMPE. However, with first blending of TLCP with HMMPE and then adding organoclay into the blend, most of the organoclay enriched on TLCP surfaces in the blend which prevents TLCP droplets from coalescing at high shear

stresses and enlarging the processing window. When the clay was added to the binary blend system, due to the polar nature of TLCP, the clay platelets showed preference for the TLCP phase. However, due to the high viscosity of HMMPE and short resident time all the clay platelets were not able to interact with TLCP as a result of which they were trapped in the PE matrix. Tan et al. (2006) demonstrated a phase diagram with PC/LCP blend system, for predicting the type and extent of fibrillation of the LCP phase in LCP-based polymer blends taking three factors into consideration namely, the shear rate, the LCP content in the blend, and interfacial adhesion between the LCP phase and the matrix polymer; which can be extended for other types of LCP containing blend systems. The effect of interfacial adhesion between the LCP and the PC matrix on fibrillation was considered by using a compatibilizer for the PC/LCP blend. They proposed a phase diagram with three regions (1) a lower region where no fibrillation occurred and the morphology of the LCP phase in the blend either existed in the form of spheroids or ellipsoids, (2) an intermediate region where the LCP existed predominately as short fibers with aspect ratios between 5 and 10, and (3) the upper region where the LCP phase developed into long continuous fibers. They have shown that the LCP content, in LCP containing blends, also plays a significant role for the development of fibers because below a critical domain size of LCP, the spheroid could not be deformed to form fibers. It was demonstrated that the fiber coalescence and fiber attrition processes occurred simultaneously during processing. Hence, the final morphology of the LCP in the blend depended on whether the fiber coalescence or attrition process was predominant at the specific combination of LCP content and processing shear rate. The use of a compatibilizer steps up the interfacial adhesion and also promotes more extensive fibrillation of the LCP phase. Wu et al. (2006) showed that in PC/TLCP blend system better compatibility and finer TLCP dispersion were reached in the unfilled blend, which made the fibrillation of TLCP difficult in capillary flow even at high shear rate. In contrast to this, well-developed TLCP fibrils were formed by capillary flow in nano-SiO₂ filled TLCP/PC blends. By increasing the nano-SiO₂ concentration and shear rate, the fibrillation of TLCP was significantly enhanced. They have ascribed this phenomenon to the selective distribution of nano-SiO₂ in PC and TLCP phases, driven by the interfacial tension thermodynamically and the viscosity discrepancy of components dynamically. During melt blending, the transesterification was reduced by the localization of nano-SiO₂ at the interface of TLCP/PC and subsequent increase in shear rate enlarged the viscosity disparity between TLCP and PC, thus made nano-SiO₂ particles migrate from the TLCP/PC interface to PC matrix. This migration of nano-SiO₂ and reduced transesterification enhanced the mobility of TLCP phase, promoted the coalescence and hence the fibrillation of TLCP droplets in capillary flow. Lee et al. (2003d) studied the effect of shear flow, extensional flow and addition of nanofillers on the fibrillar morphology of LCP in PP matrix. They showed that shear flow which predominates in injection molding is insufficient for the fibrillation of LCP, whereas under the extensional flow, the fibrillation could be improved but require an additional drawing process. However, incorporation of nanosilica promoted the LCP fibrillation under the shear flow due to the increased

viscous force of the matrix upon the LCP phase. In addition to that, presence of both nanosilica and LCP improved the properties of the ternary blend systems due to the dual reinforcement effect. Ding et al. (2004) studied the effect of glass beads (GB) on the properties of nylon/TLCP blend system. They showed that under strong extensional action of the micro-rollers of the GB, TLCP microfibrils with an average diameter of 30 nm are formed due to the thermodynamic and dynamic driving forces. In PA6/TLCP/GB ternary blends, a thermodynamically unsteady system is formed because of different interfacial tensions between PA6 and GB, and between TLCP and GB, respectively which drives the glass beads to migrate to the vicinity of the TLCP melt droplets resulting in the dispersion of TLCP coils during the melt flow. The extensional flow field formed by these micro-rollers of glass beads exerts strong extensional action on TLCP coils and formed the TLCP microfibrils with an average diameter of 30 nm. Elias et al. (2008) demonstrated the hydrophilic silica migrate from the PP matrix to the dispersed EVA domains in immiscible polypropylene/poly(ethylene-co-vinyl acetate) (PP/EVA) blend. It was also shown than silica can also able to migrate from a dispersed PP phase to an EVA matrix. However this migration was found to be slower than the migration from PP to the EVA phase. In case of hydrophobic silica, the nanofillers were found to be accumulated at the blend interface and in PP. The mechanism behind this migration was assigned to the shear induced movements and collisions with dispersed drops. Pisharath and Wong (2003) studied the effect of variation of LCP content in the rubber toughened nylon 6,6/LCP/short glass fiber blend system. They showed that maximum miscibility was achieved at 5 wt% of LCP, and decreased with increasing LCP content. They observed that LCP hybridization increased the interplanar spacing of hydrogen-bonded sheets of nylon crystals rather than the spacing between hydrogen-bonded chains. Garcia et al. (2004) studied the effect of glass fiber reinforced LCP content on the properties of PES/LCP blend system. They reported that despite of higher viscosity of glass fiber reinforced LCP, the viscosity of PSF/LCP blend decreases with the LCP content. The Young's modulus and notched impact strength of the composites increased while break properties decreased linearly with glass fiber reinforced LCP content. The composite with 10 % LCP showed an increase in stiffness of 18 %, 6.5-fold impact strength, and a tensile strength similar to that of PES. Tjong and Xu (2004) studied the PP/LCP blend system in presence of maleic anhydride (MA) grafted styrene ethylene butylene styrene (SEBS-g-MA) elastomers, with and without glass fibers. Addition of both LCP and glass fibers improved the tensile strength and stiffness of hybrid composites prepared at 265 and 285 °C due to the formation of long LCP fibrils at these temperatures, in presence of MA compatibilizer, which was not achieved at 220 °C leading to the poorer mechanical performance of the hybrid composites. The LCP fibrils act synergistically with short glass fibers as the load bearing agents and thereby improved the mechanical strength. However, composites prepared at higher temperatures of 310 °C exhibit poorer mechanical performance owing to the degradation of polymer matrices. He et al. (1997) studied the dual reinforcement of PES with TLCP and carbon fiber. They showed that in presence of TLCP the processibility of the ternary blends improved and the breakage of carbon fibers also

minimized during the blending process. The LCP fibers act as the reinforcing media although the major part of the reinforcement comes from the carbon fiber.

8.11 Effect of MWCNT and Modified MWCNT on LCP Based Polymer Blend Nanocomposites

We have studied the effect of MWCNT and its modification on various LCP based polymer blends to access its role in morphological growth of LCP during blending. Since dispersion of MWCNT in polymer matrix is a major challenge due to Van der Waals force between the nanotubes, the MWCNT surface was modified with SiC coating. This coating reduced the interaction between the nanotubes (which resulted in better dispersion in blend matrix) and also made the nanotube surface rough for physical anchoring of polymeric chains. Better dispersion of modified MWCNT exposed significant surface area of these nanotubes for interaction with the polymer matrix and rough surface increased the physical anchoring. Apart from dispersion of these nanofillers in the blend matrix, migration and localization of these nanofillers in the polymer blends can significantly alter the properties of the polymer blends (Nayak et al. 2012a, b). Dispersion of the nanofillers, in the polymer blends during mixing, has been controlled by two factors, kinetic and thermodynamic. During the initial stage of mixing the fillers distribution is controlled by the kinetic factor and fillers will be accommodated in the lower viscous phase. During mixing the thermodynamic effect comes into play and the migration of fillers occurs from the low viscous to the high viscous medium, if the affinity of the fillers towards the viscous polymer is higher than that with the low viscous medium. If the blending time is shorter than the complete migration time, nanotubes will be trapped at the interface and hence act as a bridge between the blend partners. On similar line, analysis of PEEK/LCP/MWCNTs and PEEK/LCP/SiC coated MWCNTs nanocomposites showed that incorporation of MWCNT to PEEK/LCP blend can enhance the droplet deformation and this effect was prominent in case of SiC coated MWCNT (Nayak et al. 2009). Dispersion of SiC coated MWCNTs was also found to be better than unmodified MWCNTs, in the blend matrix. Similar result was also observed in case of PEI/LCP, (Nayak et al. 2010) PPO/LCP (Nayak et al. 2011a) and PPS/LCP (Nayak et al. 2011b) blend systems. For all the systems, fibrillation of LCP increased with the incorporation of MWCNTs and the effect is more prominent for the SiC coated MWCNTs filled blend system. Nanocomposites with S-MWCNTs showed superior mechanical properties than the pure MWCNTs filled blend system. The better fibrillation of LCP, in presence of MWCNTs, was due to the bridging effect of nanotubes at the interface of blend partners which generated the drag force by the matrix phase upon the LCP domains as a result, the LCP domains were elongated in the flow direction. Owing to this fibrillation the base matrix was reinforced with both LCP fibers and MWCNTs. This synergetic reinforcement enhanced both thermal and mechanical properties of the LCP blend

nanocomposites. Due to high aspect ratio of MWCNTs, during mixing the nanotubes were trapped at the interface and hence bridged the two blend partners which prevented the phase separation. In addition to this the rough surface developed on MWCNT surface by SiC coating also triggered the physical anchoring of polymer chains which not only increased the drag force during blending, which facilitate LCP fibrillation but also decreased the LCP fiber pull out during tensile testing. Rheology of such systems, with MWCNT, greatly influenced by the nanotubes. Since most of the high performance polymers like PEI, PEEK, PPO and PPS are very difficult to process due to their high viscosity, LCP can enhance the processibility by acting as a lubricating agent. Once fibrillated, LCP can facilitate the flow during blending and due to its low viscosity can ease up mold filling. On comparison of compatibilizing ability of SiC coated MWCNT with organic compatibilizer polyphosphazene for the compatibilization of PEI/LCP blend, it was found that in presence of Polyphosphazene average particle size of LCP was reduced as compared to PEI/LCP binary blend. But fibrillation of LCP was observed for the PEI/LCP/SiC coated MWCNT system. This suggests that compared to organic compatibilizer; modified MWCNT can facilitate fibrillation of LCP to a greater extent.

8.12 Conclusion and Future Perspective

LCP based polymer blends can have a significant role for fabrication of high performance polymer blends. The incompatibility among the blend partners, which is a major road block for fibrillation LCP and hence the controlling factor for mechanical and thermal properties can be addressed with a suitable compatibilizer. However, for high performance polymers whose processing temperature exceeds 300 °C it is difficult to find a compatibilizer of such thermal stability. In this scenario, high aspect ratio carbon nanotube can be used as a compatibiliser for these systems which can enhance LCP fibrillation by acting as a bridging agent between the blend partners.

References

- Beery D, Keing S, Siegmann A (1991) Structure development during flow of polyblends containing liquid crystalline polymers. *Polym Eng Sci* 31:451
- Blizard KG, Baird DG (1987) The morphology and rheology of polymer blends containing a liquid crystalline copolyester. *Polym Eng Sci* 27:653
- Bourry D, Favis BD (1998) Cocontinuity and phase inversion in HDPE/PS blends: influence of interfacial modification and elasticity. *J Polym Sci B: Polym Phys* 36:1889
- Cahn JW, Hilliard JE (1958) Free energy of uniform system. I. Interfacial energy. *J Chem Phys* 31:688

- Chin HC, Chiou KC, Chang FC (1996) Reactive compatibilization of the poly(ethylene terephthalate)/liquid crystalline polymer blends by solid epoxy resin as a coupling agent. *J Appl Polym Sci* 60:2503
- Chiou YP, Chiou KC, Chang FC (1996) In situ compatibilized polypropylene/liquid crystalline polymer blends. *Polymer* 37:4099
- Choi GD, Kim SH, Jo WH (1996) Interrelationships between rheological, morphological and mechanical properties of polystyrene/liquid crystalline polymer blends. *Polym J* 28:527
- Chuai CZ, Almdal K, Jorgensen JL (2003) Phase continuity and inversion in polystyrene/poly(methyl methacrylate) blends. *Polymer* 44:481
- Coleman JN, Khan U, Gunko YK (2006) Mechanical reinforcement of polymers using carbon nanotubes. *Adv Mater* 18:689
- Dedecker K, Groeninckx G (1998) Reactive compatibilisation of A/(B/C) polymer blends. Part 2. Analysis of the phase inversion region and the co-continuous phase morphology. *Polymer* 39:4993
- Ding Y, Zhang J, Chen P, Zhang B, Yi Z, He J (2004) Hierarchical structure of thermotropic liquid crystalline polymer formed in blends jointly by dynamic and thermodynamic driving forces. *Polymer* 45:8051
- Elias L, Fenouillot F, Majeste JC, Martin J, Cassagnau P (2008) Migration of nanosilica particles in polymer blends. *J Polym Sci B* 46:1976
- Felten A, Bittencourt C, Pireaux JJ, Van Lier G, Charlier JC (2005) Radio frequency plasma functionalization of carbon nanotubes surface O₂, NH₃, and CF₄ treatments. *J Appl Phys* 98:074308
- Garcia M, Eguiazabal JI, Nazabal J (2004) Processability and mechanical performance of hybrid composites based on poly(ether sulfone) modified with a glass fiber-reinforced liquid crystalline polymer. *J Appl Polym Sci* 91:854
- Han H, Bhowmik PK (1997) Wholly aromatic liquid-crystalline polyesters. *Prog Polym Sci* 22:1431
- He J, Zhang H, Wang Y (1997) In-situ hybrid composites containing reinforcements at two orders of magnitude. *Polymer* 38:4279
- Heino MT, Seppla JV (1993) Studies on compatibilization of blends of polypropylene and a thermotropic liquid crystalline polymer. *J Appl Polym Sci* 48:1677
- Heino MT, Hietaoja PT, Vainio TP, Seppla JV (1994) Effect of viscosity ratio and processing conditions on the morphology of blends of liquid crystalline polymer and polypropylene. *J Appl Polym Sci* 51:259
- Hirsch A, Vostrowsky O (2005) Functionalization of carbon nanotubes. *Top Curr Chem* 245:193
- Huang JM, You MF, Chang FC (2001) In situ compatibilized SAN/LCP blends through reactive copolymers. *J Appl Polym Sci* 82:3321
- Isayev AI, Modic M (1987) Self-reinforced melt processable polymer composites: extrusion, compression, and injection molding. *Polym Compos* 8:158
- Jorgensen JL (1999) Structuring of interface-modified polymer blends. *J Int Polym Process* 3:213
- Jun C, Peng C, Lichuan W, Jun Z, Jiasong H (2006) Enhanced fibrillation of LCP by CaCO₃ whisker in polysulfone matrix through increasing elongational stress. *Polymer* 47:5402
- Jung CH, Kim DK, Choi JH, Shin K, Nho YC, Suh DH (2009) Functionalization of carbon nanotubes by radiation-induced graft polymerization. *J Nanosci Nanotechnol* 9:7126
- Kessler J, Kammer HW, Klostermann K (1986) Phase behavior of poly(methyl methacrylate) and poly(styrene-co-acrylonitrile) blends. *Polym Bull* 15:113
- Ko CU, Wilkes GL (1989) Morphological studies of blends containing liquid crystalline polymers with poly(ethylene terephthalate). *J Appl Polym Sci* 37:3063
- Kohli A, Chung N, Weiss RA (1989) The effect of deformation history on the morphology and properties of blends of polycarbonate and a thermotropic liquid crystalline polymer. *Polym Eng Sci* 29:573

- Krishnaswamy RK, Wadud SEB, Baird DG (1999) Influence of a reactive terpolymer on the properties of in situ composites based on polyamides and thermotropic liquid crystalline polyesters. *Polymer* 40:701
- Kyotani M, Kaito A, Nakayama K (1992) Mechanical and structural properties of extruded strands of blends containing a liquid crystalline polyester with poly(ethylene terephthalate). *Polymer* 33:4756
- La Mantia FP, Valenza A (1992) Shear flow characterization of blends containing liquid crystal polymers. *Macromol Chem Macromol Symp* 56:151
- Lee MW, Hu X, Yue CY, Li L, Tam KC, Nakayama K (2002) Novel approach to fibrillation of LCP in an LCP/PP blend. *J Appl Polym Sci* 86:2070
- Lee MW, Hu X, Li L, Yue CJ, Tam KC, Cheong LY (2003a) PP/LCP composites: effects of shear flow, extensional flow and nanofillers. *Compos Sci Technol* 63:1921
- Lee MW, Hu X, Li L, Chee YY, Tam KC (2003b) Flow behavior and microstructure evolution in novel SiO₂/PP/LCP ternary composites: effects of filler properties and mixing sequence. *Polym Int* 52:276
- Lee MW, Hu X, Yue CY, Li L, Tam KC (2003c) Effect of fillers on the structure and mechanical properties of LCP/PP/SiO₂ in-situ hybrid nanocomposites. *Compos Sci Technol* 63:339
- Li J, Ma PL, Favis BD (2002) The role of the blend interface type on morphology in co-continuous polymer blends. *Macromolecules* 35:2005
- Limtasiri T, Isayev AI (1991) Blends of thermotropic polyester with poly(phenylene oxide). *J Appl Polym Sci* 42:2923
- Mehta A, Isayev AI (1991) Rheology, morphology, and mechanical characteristics of poly(ether ether ketone) liquid crystal polymer blends. *Polym Eng Sci* 31:971
- Meng YZ, Tjong SC (1998) Rheology and morphology of compatibilized polyamide 6 blends containing liquid crystalline copolyesters. *Polymer* 39:99
- Miller MM, Cowie JMG, Tait JG, Brydon DL, Mather RR (1995) Fibers from polypropylene and liquid-crystal polymer blends using compatibilizing agents: 1. Assessment of functional and nonfunctional polypropylene-acrylic acid compatibilizers. *Polymer* 36:3107
- Nayak GC, Rajasekar R, Bose S, Das CK (2009) Effect of MWNTs and SiC coated MWNTs on properties of PEEK/LCP blend. *J Nanotechnol* 2009:6. doi:10.1155/2009/759374
- Nayak GC, Rajasekar R, Das CK (2010) Effect of SiC coated MWCNTs on the thermal and mechanical properties of PEI/LCP blend. *Compos Part A: Appl Sci Manuf* 41:1662–1667
- Nayak GC, Rajasekar R, Bose S, Das CK (2011a) Effect of modified MWCNT on the properties of PPO/LCP blend. *J Mater Sci* 46:2050–2057
- Nayak GC, Rajasekar R, Sahoo S, Das CK (2011b) Effect of polyphosphazene and modified carbon nanotubes on the morphological and thermo-mechanical properties of polyphenylene sulfide and liquid crystalline polymer blend system. *J Mater Sci* 46(24):7672–7680
- Nayak GC, Rajasekar R, Sahoo S, Das CK (2012a) Novel approach for the selective dispersion of MWCNT in the Nylon/SAN blend system. *Compos Part A: Appl Sci Manuf* 43(8):1242–1251
- Nayak GC, Sahoo S, Das S, Kartikeyan G, Das CK (2012b) Compatibilization of PEI/LCP blend using modified multi-walled carbon nanotubes and polyphosphazene as compatibilizers. *J Appl Polym Sci* 124:629–637
- Nobile MR, Amendola A, Nicolais L, Acierio D, Carfagna C (1989) Physical properties of blends of polycarbonate and a liquid crystalline copolyester. *Polym Eng Sci* 29:244
- Percec V (1997) *Handbook of liquid crystal research*. Oxford University Press, New York, p 259
- Pisharath S, Wong SC (2003) Development of the morphology and crystalline state due to hybridization of reinforced toughened nylon containing a liquid-crystalline polymer. *J Polym Sci B* 41:549
- Seo Y, Kim B, Kim KU (1999a) Structure development during flow of ternary blends of a polyamide (nylon 66), a thermotropic liquid crystalline polymer (poly(ester amide)) and a functionalized polypropylene. *Polymer* 40:4483

- Seo Y, Kim B, Kwak S, Kim KU, Kim J (1999b) Morphology and properties of compatibilized ternary blends (nylon 6/a thermotropic liquid crystalline polymer/a functionalized polypropylene) processed under different conditions. *Polymer* 40:4441
- Siegmann A, Dagan A, Kenig S (1985) Polyblends containing a liquid crystalline polymer. *Polymer* 26:1325
- Siggia ED (1979) Late stages of spinodal decomposition in binary mixtures. *Phys Rev A* 20:595
- Skakalova V, Dettlaff-Weglikowska U, Roth S (2004) Gamma-irradiated and functionalized single wall nanotubes. *Diamond Relat Mater* 13:296
- Song CH, Isayev AI (2010) Nanocomposites of liquid crystalline polymers dispersed in polyester matrices. In: Gupta RK, Elliot K, Kwang-Jea K (eds) *Polymer nanocomposites handbook*. Taylor & Francis, Boca Raton, p 253, Chapter 11
- Subramanian PR, Isayev AI (1991) Blends of a thermotropic liquid crystal polyester with poly(phenylene sulphide). *Polymer* 32:1961
- Sukhadia AM, Done D, Baird DG (1990) Characterization and processing of blends of polyethylene terephthalate with several liquid crystalline polymers. *Polym Eng Sci* 30:519
- Tan LP, Yue CY, Hu X, Nakayama K (2006) Phase diagram for predicting in situ fibrillation of LCP during molding. *Mater Manuf Process* 21:127
- Tang Y, Gao P, Ye L, Zhao C (2010) A comparative study of thermotropic LCP and organoclay as fillers in high molecular mass polyethylene with different blending sequences. *Polym Eng Sci* 50:1679
- Taylor GI (1932) The viscosity of a fluid containing small drops of another fluid. *Proc R Soc Lond Ser A* 138:41
- Taylor GI (1934) The formation of emulsions in definable fields of flow. *Proc R Soc Lond Ser A* 146:501
- Thostenson ET, Ren ZF, Chou TW (2001) Advances in the science and technology of CNTs and their composites: a review. *Compos Sci Technol* 61:1899
- Tjong SC, Meng YZ (1999a) Microstructural and mechanical characteristics of compatibilized polypropylene hybrid composites containing potassium titanate whisker and liquid crystalline copolyester. *Polymer* 40:7275
- Tjong SC, Meng YZ (1999b) Properties and morphology of polyamide 6 hybrid composites containing potassium titanate whisker and liquid crystalline copolyester. *Polymer* 40:1109
- Tjong SC, Xu SA (2004) Mechanical properties of glass fiber and liquid crystalline polymer reinforced polypropylene hybrid composites toughened with elastomers. *J Appl Polym Sci* 94:1539
- Utracki LA (2002a) *Polymer blends handbook*. Kluwer, Dordrecht, p 2
- Utracki LA (2002b) Compatibilization of polymer blends. *Can J Chem Eng* 80:1008
- Vallejo FJ, Eguiazabal JI, Nazabal J (2000) Compatibilization of PP/Vectra B "in situ" composites by means of an ionomer. *Polymer* 41:6311
- Wu L, Chen P, Zhang J, He J (2006) Inhibited transesterification and enhanced fibrillation of TLCP by nano-SiO₂ in polycarbonate matrix. *Polymer* 47:448
- Xie WB, Tam KC, Yue CY, Lam YC, Li L, Hu X (2003) Mechanical properties and morphology of LCP/ABS blends compatibilized with a styrene-maleic anhydride copolymer. *Polym Int* 52:733
- Zhang L, Tam KC, Gan LH, Yue CY, Lam YC, Hu X (2003) Effect of nano-silica filler on the rheological and morphological properties of polypropylene/liquid crystalline polymer blend. *J Appl Polym Sci* 87:1484
- Zhang B, Ding Y, Chen P, Liu C, Zhang J, He J, Hu G (2005) Fibrillation of thermotropic liquid crystalline polymer enhanced by nano-clay in nylon-6 matrix. *Polymer* 46:5385

Chapter 9

Liquid Crystalline Polymers from Renewable Resources: Synthesis and Properties

K.Y. Sandhya, A. Saritha, and Kuruvilla Joseph

9.1 Introduction

Synthesis of soft matter from renewable resources has gained a great deal of attention in the current research scenario. Effective utilization of bio mass as well as biodegradable industrial by-products towards the synthesis of soft materials like liquid crystals (LCs), which have a direct impact on the life and development of humanity is indeed a challenge to the growing research community. It is believed by the scientific community that only natural resources would be a viable solution to all the technological developments in the long run and hence it would be better to replace the non renewable resources with the easily available bio resources. The fact that natural products are stereo- and regiochemically pure makes them in essence special and reduces the dependence on expensive chiral catalysts and complex synthesis that are currently mandatory for selective functionalization in chemical industry.

LC is a unique state of matter which is between the solid and the liquid state. Within solids, particles (atoms, ions, molecules) are often localized in a regular crystal lattice and crystalline solids exhibit short as well as long-range order with regard to both position and orientation of the particles. The liquid crystalline phases—also known as mesophases—represent intermediate states between the ordered structure of solids and amorphous properties of liquids. In LC, the molecules may flow like a liquid and at the same time will maintain an ordered

K.Y. Sandhya • K. Joseph (✉)
Department of Chemistry, Indian Institute of Space Science and Technology, Valiamala,
Thiruvananthapuram, Kerala 695547, India
e-mail: sandhya@iist.ac.in; kjoseph.iist@gmail.com

A. Saritha
Department of Chemistry, Amrita Viswa Vidyapeetham University, Amritapuri, Kollam,
Kerala 690525, India
e-mail: sarithatvla@gmail.com

arrangement like a crystal, hence given the name “LC”. LC states show at least one orientational long range order and in some cases may show short range order as well, whereas positional long-range order of crystals disappears. Many different mesophases are known for LCs and the simplest mesophase among them is the nematic phase (Fig. 9.1) where positional order is totally lost but an orientational order remains. Smectic phase has a higher positional order with a layered arrangement (Fig. 9.1) and in each layer molecules have a nematic like arrangement. When molecules are arranged perpendicular to the layers, the phase is called smectic A and when it is tilted it is a smectic C. Many other phases are exhibited by LCs such as cholesteric phase (chiral nematic phase), columnar phase, etc. and the mesophases formed mainly dependent on the structure and shape of the mesogens. Materials that are capable of transforming into the liquid crystalline phase often consist of molecules with an anisometric shape called mesogens. Other than that the parameters that govern the formation of liquid crystalline phases are the aspect ratio of the mesogen, micro segregation effect, chirality etc. In addition to this, the very well known parameter, in the case of lyotropic LCs is the solvent concentration of the material and in thermotropic LCs is the temperature that affects the formation of the LC phase (Stegemeyer 1999).

The two methods by which a crystalline solid with its ordered structure can turn into a partially disordered LC are the melting and the dissolution depending on which the LCs are classified as thermotropic and lyotropic LCs, respectively. In thermotropic LCs, as mentioned earlier, the formation of mesophases occurs via a variation in temperature whereas in lyotropic LCs, the formation of mesophases requires the presence of a solvent and they are formed by mesogens; not the molecules themselves, their solvates as well as associates of the solvated molecules (Davidson and Gabriel 2005).

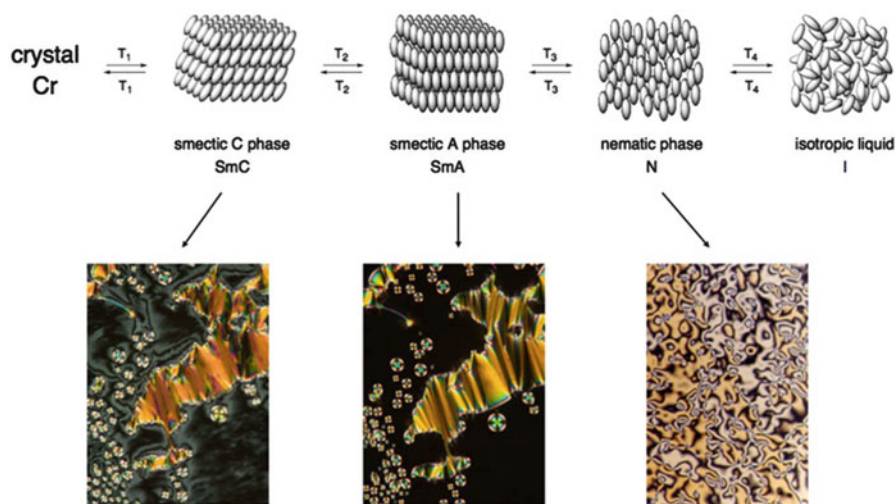


Fig. 9.1 Schematic of the molecular arrangements in various mesophases of a thermotropic LC and the corresponding representative textures

Liquid crystalline polymers (LCPs) form an important class of compounds with molecular self-orientation ability which finds application in high performance materials. LCPs have been synthesized from a large range of bio-based materials like cardanol, coconut oil, castor oil, lipids, cellulose etc. and been extracted from various natural sources. LCPs of biological origin like DNA, spider silk, polypeptides etc. are liquid crystalline in nature and the LC order is thought to play a critical role in the exceptional properties and functions of the biological structures.

Presence of molecular interactions in the system and the occurrence of semi rigid backbone contribute to the force pertaining to the formation of LCs from cellulose and its derivatives (Huang et al. 1995). Vegetable oils like coconut oil, olive oil can be used as an alternative to expensive fatty acids for the preparation of LCs because of their easy availability and low price. Aromatic polyamides derived from oils are not usually used for this purpose due to the difficulties associated with the fabrication. However to overcome this problem flexible groups are introduced in the rigid backbone of the aromatic polyamide so as to make them suitable for the preparation of liqLCPs (Abid et al. 2004). In this chapter we have tried to give a general idea about bio-based LCPs starting from the humble cardanol to the complicated biologically inspired LCPs.

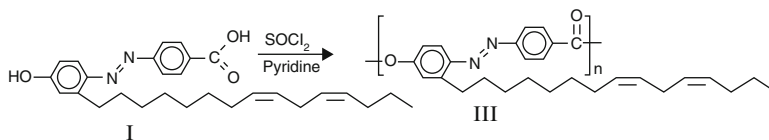
9.2 Synthesis of Liquid Crystalline Polymers

9.2.1 Natural Oil Based LCPs

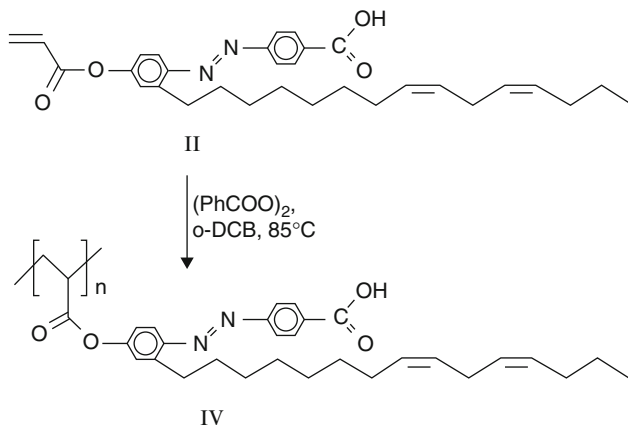
Cashew nut is grown extensively in the tropical regions and its shell is rich in natural long chain phenols; cardanol and cardol, which together are technically known as cashew nut shell liquid (CNSL). Cardanol the distilled product of CNSL, is a phenolic lipid which finds abundant applications in chemical industry. Cardanol has several specialties in its structure which enable it to get transformed into a number of high performance polymers and consists of four meta-alkyl phenols, with alkyl chains having different degree of unsaturation.

LCPs with cross-linked network structures containing azobenzene mesogens were synthesized from cardanol (Saminathan and Pillai 2000). They introduced the azobenzene group by the diazo coupling reaction between cardanol and 4-aminobenzoic acid. The resulting monomer, 4-[(4-cardanyl) azo] benzoic acid was polymerised by self-polycondensation using thionyl chloride and pyridine to get poly[4-[(4-cardanyl)azo]benzoic acid]. The monomer could also be converted to poly[4-[(4-acryloyloxycardanyl)azo]benzoic acid] through acryloylation, followed by free radical polymerization. Cationic polymerization of the monomer gave poly[4-[(4-cardanyl)azo]benzoic acid]. The schemes 9.1, 9.2 and 9.3 shows the preparation of the polymers from cardanol.

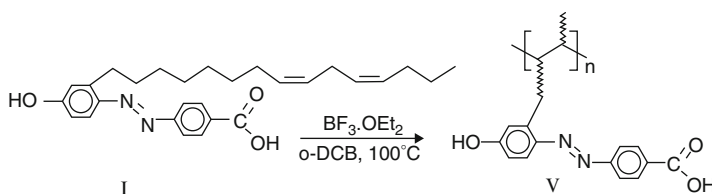
The phase behavior of these polymers was studied using hot stage polarized light microscope (PLM) and it was found that the poly[4-[(4-cardanyl)azo]benzoic acid] did not exhibit melting to form mesophase but started decomposing above 200 °C.



Scheme 9.1 Synthesis of poly[4-[(4-cardanyl)azo]benzoic acid]. Reproduced with permission from Saminathan and Pillai (2000). Copyright Elsevier



Scheme 9.2 Synthesis of poly[4-[(4-acryloyloxycardanyl)azo]benzoic acid]. Reproduced with permission from Saminathan and Pillai (2000). Copyright Elsevier



Scheme 9.3 Cationic polymerisation of 4-[(4-cardanyl)azo]benzoic acid. Reproduced with permission from Saminathan and Pillai (2000). Copyright Elsevier

On the other hand, the sample prepared by rapid melting below the decomposition temperature and quenching to room temperature showed threaded nematic texture. The polymer poly[4-[(4-acryloyloxycardanyl)azo]benzoic acid] melted at 153 °C exhibiting a clear schlieren texture (Fig. 9.2b) characteristic of nematic phase under PLM. The unsaturated C15 hydrocarbon side chain in cardanol is utilized for cross-linking reactions.

Castor oil contains a dicarboxylic acid of 36 carbon atoms, called dimer acid, which functions as an excellent precursor for LCPs in conjunction with aliphatic as

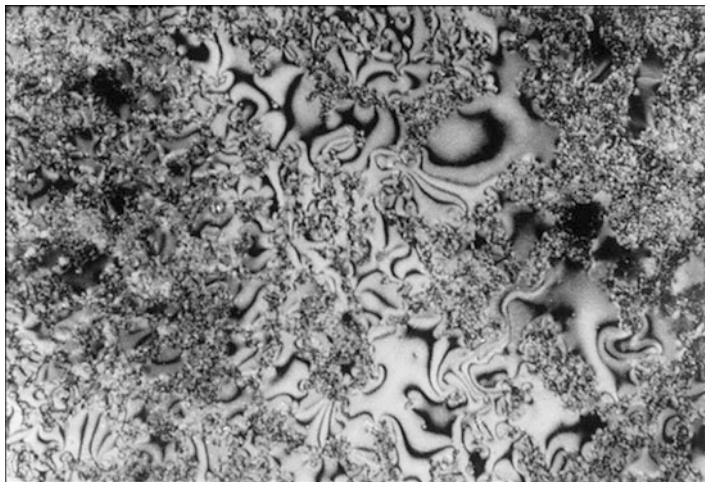


Fig. 9.2 The schlieren texture of poly[4-[(4-acryloyloxycardanyl)azo]benzoic acid]. Reproduced with permission from Saminathan and Pillai (2000). Copyright Elsevier

well as aromatic amines (Bajpai and Nivedita 1996). An aromatic aliphatic polyamide poly (p-phenylene dimeramide) [PPD] was prepared from the dimer acid and para phenylene. Lamellar LCs derived from natural sources like shea butter and jojoba oil are effective in replenishing the texture of the skin and hence widely used in the preparation of cosmetics and creams.

9.2.2 Lipid Based LCP

Amphiphilic lipids are a unique class of compounds that do not exhibit abrupt transitions from the solid to the liquid state, but do undergo ‘intermediate’ states, where properties of solid crystals and of liquids can be observed (Lee 1997). This so-called mesomorphic behavior can be attributed either to temperature changes, heating causes ‘chain melting’ which means transformation of the alkyl chains into a less ordered state owing to increased occurrence of thermodynamically unfavorable chain kinks and consequently increased chain space requirement (‘thermotropic phase transition’), or changes in hydration state, leading to polar head groups bind to water and become hydrated, which increases their respective space requirements and eventually results in changes in molecular packing (‘lyotropic phase change’). Egg lecithin and soya lecithin are excellent examples of this type of amphiphilic lipids that are capable of transformation into LCs and find application in parenteral drug administration. Liposomes are vesicles formed by amphiphilic phospholipid bilayers dispersed in aqueous media (Fig. 9.3). The vesicles are in fact dispersed lamellar LCs (Almgren 1980). Polymer stabilized liposomes (PSLO)

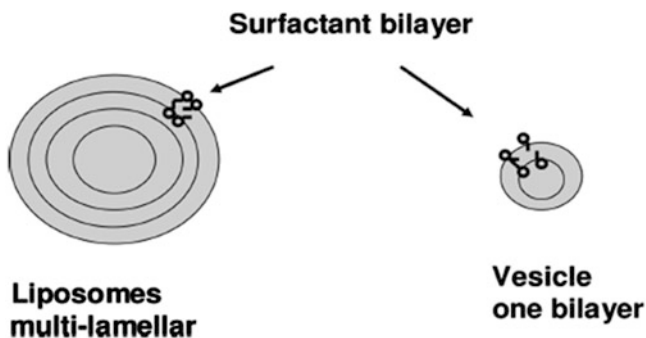
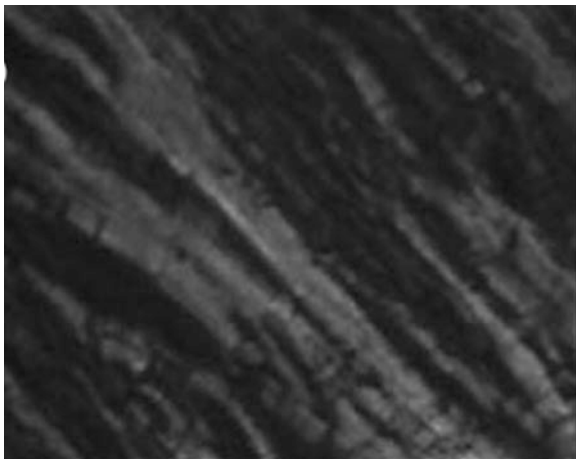


Fig. 9.3 Schematic representation of liposomes and vesicles. Reproduced with permission from *Colloids and Interface Science Series, Vol. 4 Colloids in Cosmetics and Personal Care*, Edited by Tharwat F. Tadros. Copyright 2008 Wiley

composed of phospholipids with polyethylene glycol chains attached to the polar head groups were prepared (Al-Bawab et al. 2005) by dissolving a blend of 1,2 dipalmitoyl-sn-glycero-3-phosphate monosodium (DPPA), 1,2 dipalmitoyl-sn-glycero-3-phosphocholine (DPPC), and 1,2 dipalmitoyl-sn-glycero-3-phosphoethanolamine N-[methoxy polyethyleneglycol] (DPPE-MPEG 5000) in polyethylene glycol followed by sonication and addition of glycerin and aqueous NaCl (Unger et al. 1992). This was followed by the addition of different amounts of orange oil to the liposome system and sonication by carefully controlling temperature within the range of 22–25 °C.

Liposomes and vesicles depicted in Fig. 9.3 are ideal systems for cosmetic applications. They offer a convenient method for solubilizing nonpolar active substances in the hydrocarbon core of the bilayer. Polar substances when intercalated in the aqueous layer of the bilayer, are capable of forming lamellar liquid crystalline phases without disrupting the stratum corneum. No facilitated transdermal transport is possible, thus eliminating skin irritation (Kim et al. 2009). Phospholipid liposomes can be used as *in vitro* indicators for studying skin irritation by surfactants. Glycolipids were developed by attaching a sugar group on the phenol as a hydrophilic head group and the effect of unsaturation on the gelation ability was thoroughly studied by conducting experiments with glycolipids substituted with different unsaturated chains in pure form as well as mixed form. The liquid crystalline properties of the glycolipids were studied by optical polarizing microscopy, differential scanning calorimetry (DSC) and X-ray diffraction (XRD) and the phases were identified as lamellar structure, the representative texture is shown in Fig. 9.4 (John and Vemula 2006).

Fig. 9.4 Optical micrograph of lamellar phase of the LC derived from the glycolipid. Reproduced with permission from John and Vemula (2006). Copyright RSC



9.2.3 Cellulose Based LCPs

9.2.3.1 Nanocellulose Based LCPs

It has been known a decade back that cellulose itself is liquid crystalline in nature (Klemm et al. 2005). Due to the high aspect ratio of cellulose nano crystals (CNC), there is possibility for the formation of liquid crystalline phases. The glass transition makes it difficult to study equilibrium phases at high particle concentrations and hence the LC behavior of CNC dispersions at concentrations above 10–15 wt% is largely unexplored. It is to be believed that the glassy state is a key component in explaining the absence of observed high-order LC phases and the great variety of structural features found in films formed by drying CNC suspensions. Suppressing the glass transition or at least shifting it to a higher concentration could possibly expect a transition into a columnar LC phase in CNC suspensions. The Onsager model predicts that the required volume fraction for LC formation is inversely proportional to the rod aspect ratio and the onset concentration of liquid crystallinity is expected to decrease if the rod-like CNC is longer and thinner. Indeed, dispersions of bacterial CNCs, with lengths on the order of 1–2 μm and an aspect ratio in the range of 50–100, show nematic ordering well below 1 wt% CNC, the texture obtained under polarized microscope is given in Fig. 9.5.

Detailed investigations on the influence of the CNC counter ions on the formation of the LC phase was done by researchers and this marked an era in the chemistry of CNCs (Dong et al. 1996a, b). By adding HCl at varying concentrations to a series of CNC suspensions within the biphasic regime, such that each suspension had a constant pH of 1.61, they effectively canceled out the effect of the counter ions introduced by the cellulose nanorods. The anisotropic volume fraction curve followed a linear dependence on the CNC concentration, as expected from Onsager theory.

Fig. 9.5 Dispersions of bacterial CNCs showing nematic ordering well below 1 wt% CNC (Reproduced with permission from Lagerwall et al. (2014). Copyright Nature Publishing Group)

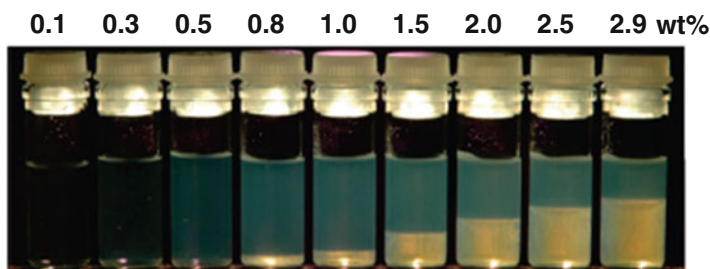
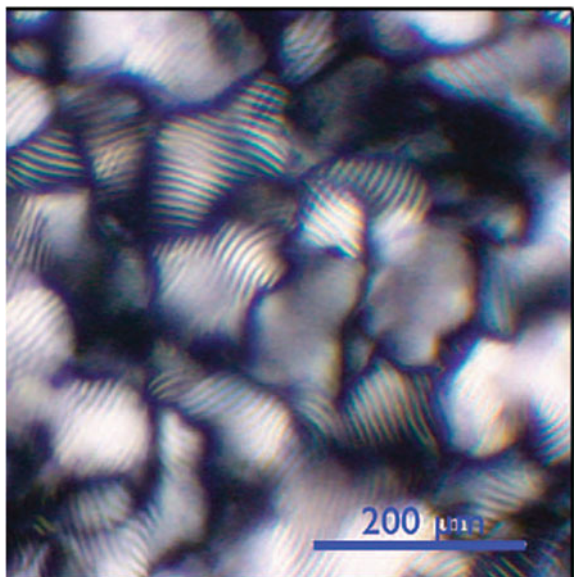


Fig. 9.6 Photograph of bacterial CNC dispersed in water at different concentrations. As the concentration increases the volume fraction of the cholesteric phase increases. Reproduced with permission from Hirai et al. 2009. Copyright ACS

Phase separation phenomena of aqueous suspensions of CNC have been studied for bacterial cellulose (BC) prepared by sulfuric acid hydrolysis (Hirai et al. 2009) and they observed an interesting and rather peculiar reversal in phase behavior in their study of bacterial CNC with added NaCl as indicated in Fig. 9.6. The shape and size distribution of BC nanocrystals in both the phases were determined by transmission electron microscopy (TEM) and atomic force microscopy (AFM). The surface charge density was determined by conductometric titration. Although the volume fraction of the cholesteric phase initially decreased with added salt, as expected, it started increasing again at concentrations greater than 0.75 mM NaCl. The entire CNC suspension was anisotropic at 2 mM NaCl, and because no stripes

indicative of a helical structure could be observed, the phase appears to have been chiral nematic with an infinite pitch (P) (Hirai et al. 2009).

The ability of CNC suspensions to form self-assembled helical structures suggests the potential of CNCs to be utilized as novel materials with attractive photonic and mechanical properties. While the CNC helix is always left-handed, reflecting the intrinsic chirality of crystalline cellulose, the value of the P can vary greatly, from less than 1 to 50 μm and beyond. The P depends on the quality of the CNC, on the concentration, on the ionic strength of the solution and may even on the temperature (Beck et al. 2013). Many aspects of helix formation are yet to be known. It is important to distinguish between the helical director modulation in liquid crystalline suspensions and helical structures found in dried films. While the former reflects equilibrium situation (provided there is sufficient equilibration time), the internal structure of a dried film is representative of the conditions prevailing within a domain when it entered the gel-like glassy state. The glass formation is a non equilibrium process that is difficult to control and there are strong variations from time to time and between different regions. Characteristic regularly spaced helix lines in an aqueous suspension with 5 wt% CNC derived by sulfuric acid hydrolysis of wood pulp is indicated in Fig. 9.7a. The distance between two lines is half the pitch ($P/2$), as illustrated in the schematic; hence, the equilibrated helix of this sample has a P of 13 μm . Figure 9.7b–d indicates the typical dried film of CNC (same source as above, starting concentration 4.8 wt%) with non uniform helix orientations and a strong spread in P , observed in reflection. In Fig. 9.7b, the film is illuminated with linear polarized light and observed through a crossed polarizer (analyzer). In Fig. 9.7c, d, it is illuminated with unpolarized light and observed through a $1/4$ phase plate followed by the analyzer, together constituting

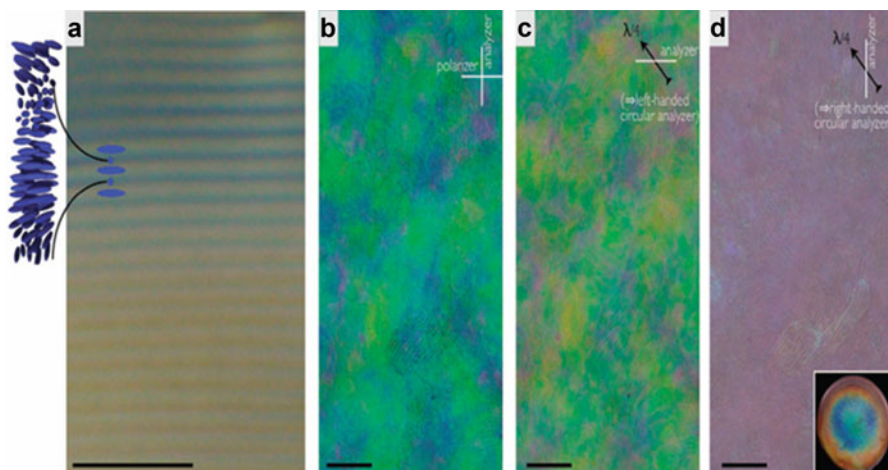


Fig. 9.7 Polarizing microscopy textural traces of CNC helix formation in the liquid crystalline (wet) state (a) and in solid CNC samples obtained by drying (b–d). Scale bars correspond to 50 μm (Reproduced with permission from Lagerwall et al. (2014). Copyright Nature Publishing group)

an analyzer for left- Fig. 9.7c and right-handed Fig. 9.7d circular polarization, respectively. The inset in Fig. 9.7d shows the iridescence from a macroscopic, dried CNC film on a circular glass substrate (25 mm in diameter) against a black background, viewed at a slight angle (Lagerwall et al. 2014).

Sulphuric acid when used as a hydrolyzing agent chemically reacts with the surface hydroxyl groups of CNCs to yield negatively charged (surface) sulfate groups that promote a perfectly uniform dispersion of the whiskers in water via electrostatic repulsions (Revol et al. 1992). The removal of the water phase leads to a situation in which the CNCs adopt configurations that minimize the existing electrostatic interactions. It is noteworthy that (homogeneous) concentrated suspensions self-organize into brilliant liquid crystalline arrangements, exactly similar to what occurs in non-flocculating suspensions of other rod-like particles, such as poly(tetrafluoroethylene) whiskers (Folda et al. 1998), tobacco mosaic viruses (TMV) (Oster 1950), DNA fragments etc.

The chiral nematic structure can be preserved after complete water evaporation to provide iridescent films of CNCs. These solid films, in addition to allowing fundamental studies of their striking behavior, have numerous potential applications such as coating materials for decorative materials and security papers (because the optical properties cannot be reproduced by printing or photocopying) (Revol et al. 1995). An investigation into these systems reveals that CNCs are randomly oriented in the dilute regime (isotropic phase). A nematic liquid crystalline alignment is adopted when the CNC concentration increases because these tactoids coalesce to form an anisotropic phase, which is characterized by a unidirectional self-orientation of the Cellulose nano rods. When the suspension of CNCs reaches a critical concentration, it forms a chiral nematic ordered phase displaying lines that are the signature of cholesteric LCs. Various factors such as size, shape, dispersity, charge, ionic strength of the solution (electrolyte) (Fleming et al. 2001), and external stimuli can affect the liquid crystallinity, p , domain size, ordering, and other properties (Moon et al. 2011). Films with uniform nanorod alignment achieved by shearing were studied in detail. The nature and density of the charges on the surface of CNCs have also been reported to affect the formation of the chiral nematic phase. By using post-sulfated HCl-hydrolyzed CNCs, which have sulfur content approximately one-third less than directly H_2SO_4 -hydrolyzed CNCs, it has given distinctly different behaviors. Indeed, post-sulfonated suspensions formed a birefringent glassy phase having a crosshatch pattern (Fig. 9.8) rather than a fingerprint pattern indicative of chiral nematic phases and are typical of directly sulfated CNCs (Araki et al. 2000).

The study of alignment of a liquid crystalline CNC suspension under shear flow with varying shear rates using X-rays was conducted by Ebeling et al. (1999) and found that the suspensions exhibited quite complex behavior, with results that are very much dependent on the shear rate. When the films prepared using different starting concentrations were dried under continuous shear flow, dried films gave interesting internal structures.

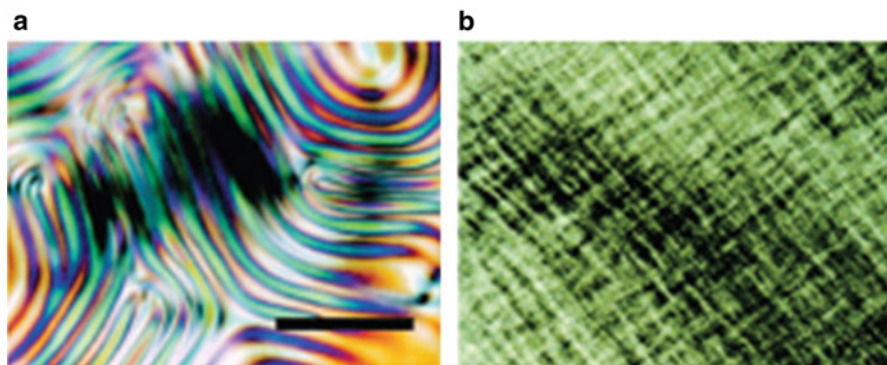


Fig. 9.8 Polarized-light micrographs of CNC suspensions: (a) fingerprint pattern in the chiral nematic phase of the directly H_2SO_4 -hydrolyzed suspension (initial solid content, 5.4 %); (b) crosshatch pattern of post sulfated suspension (solid content, 7.1 %). Reprinted with permission from Araki et al. (2000). Copyright 2000 American Chemical Society

9.2.3.2 Cellulose Derived LCPs

Cellulose constitutes the most abundant renewable polymer as it is derived from plants. As mentioned earlier, cellulose as such and a large number of its derivatives form liquid crystalline phases either lyotropic or thermotropic. Here we discuss the mesogenic properties of cellulose and its derivatives. Rogers et al. suggested an environmentally benign method for preparing cellulose solutions containing up to 25 wt% cellulose using ionic liquids. Compositions between 5 and 10 wt% cellulose were prepared using 1-butyl-3-methylimidazolium chloride ([C4mim]Cl) as the solvent. Viscous solutions of cellulose with concentrations above 10 wt% in [C4mim]Cl, yielded liquid crystalline materials and exhibited optical anisotropic and birefringence when viewed under polarized microscope. High-strength materials that conserve anisotropy in the solid phase are especially desirable, because of the enhanced mechanical properties they may possess (Swatloski et al. 2002).

It is noteworthy that, most of the cellulose derivatives exhibit cholesteric LC phases in solutions within certain concentration regions (lyotropic) or in the bulk within certain temperature regions (thermotropic). The physical packing (chiral arrangement) schemes of stiff cellulose chains are considered to be playing important roles in inducing the formation of cholesteric LC phases. In particular, when the flexible side chains are connected onto the cellulose backbones, the resulting hairy-rod cellulose polymers start forming these cholesteric LC phases. It is considered that the attachment of flexible side chains onto the rigid cellulose molecules facilitate the orientational order of the semi-rigid hairy-rod backbones (Tseng et al. 1982; Hou et al. 2000) is considered as one of the important approaches towards obtaining cellulose derivatives with cholesteric LC phase transitions. Among the cellulose derivatives, hydroxyl propyl cellulose (HPC) derivatives are

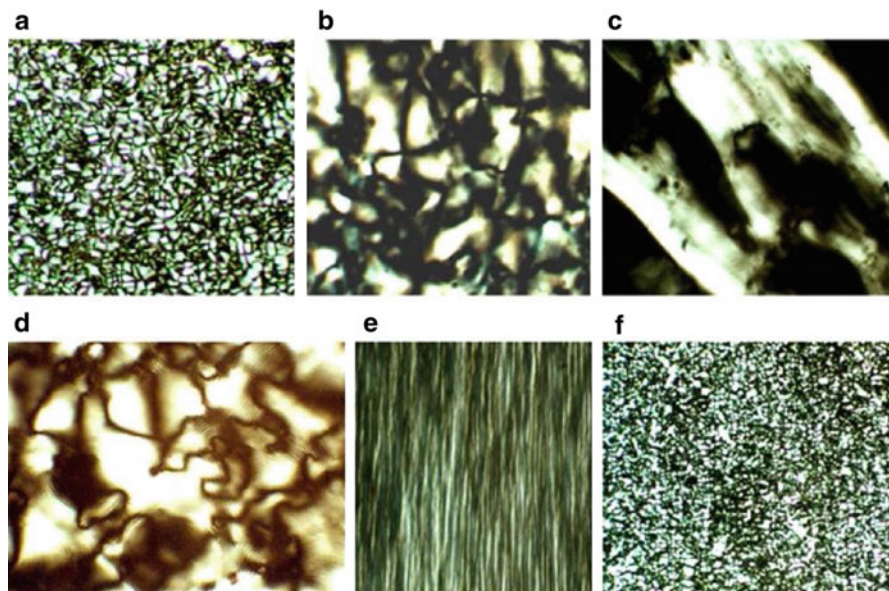


Fig. 9.9 Polarized light microscopic graphs of CnPC texture (at 25 °C): (a) C3PC 150°; (b) C6PC 750°; (c) C7PC 750°; (d) C10PC 375°; (e) C6PC 375°, *arrow* directs shear force direction; (f) C2PC annealed at 150 °C for 20 min, 150°. Reproduced with permission from Huang (2007) Copyright Elsevier

of specific interest because they can form either cholesteric lyotropic or thermotropic LC phases (Hou et al. 2000). LC behaviour of derivatives of HPC (CnPC) with different side chain lengths are studied (Huang 2007) as an attempt towards the systematic understanding of the side chain effect on the formation of thermotropic cholesteric LC phases and phase transitions as well as their unique selectivity for color reflections and the pitch distance in the cholesteric LC phases. The representative schlieren textures obtained for polymers C3PC, C4PC, C5PC, and C6PC at room temperature (Figs. 9.9a, b) represents the formation of the low-ordered LC phases. Under a mechanical shear force at elevated temperature, all of the CnPCs present typical banded textures of low-ordered LC phases (Fig. 9.9e for C6PC). At 150 °C, a Schlieren texture of C2PC retains before the isotropic melt (Fig. 9.9f). In this study it was found that the increase in the number of methylene units of side chain narrowed the thermotropic phase transition window and the layer spacing increases of the cholesteric LCs increases linearly with increase in the methylene units in the side chains, and the corresponding pitch distance of the cholesteric LC phases are strongly dependent on the number of methylene units in the side chains, and the twisting angle and the layer number in the helical structure are also depended on the length of methylene units in the side chains in this polymer series.

A particularly interesting property of the cellulose derivatives is that, based on different chemical structures, the materials can reflect light at a specific light

wavelength in a specific temperature region. Cellulose derivative with such property was prepared from HPC as follows. 5.0 g of HPC (corresponding to 41.71 mM of hydroxyl groups) was added to 30 mL acetone under a dry nitrogen atmosphere and was dissolved by heating the solution. Then 15.1 mL (125.13 mM) valeric acid chloride was swiftly added to the solution of HPC by using a syringe. After 2 h of reflux, the reaction mixture was poured into 200 mL of distilled water. After removing the liquid phase, a cream-colored, sticky material was obtained and then dissolved in 80 mL acetone and precipitated by adding 5 mL of water to the solution. The pasty product was liberated from the acetone/water by decantation. The second solution precipitation was repeatedly done and the product was obtained by drying at 60 °C for 48 h.

9.2.4 LCPs of Biological Origin

It is interesting to note that many of the biological structures exhibit liquid-crystal behavior, for instance glycolipids, polypeptides, DNA etc. exhibit various LC phases. The concentrated protein solution extruded by a spider to form silk is known to be in LC phase and the precise ordering of molecules in LC phases is thought to be critical to its renowned strength. The *in vivo* DNA concentrations are also thought to be in the LC phase. Likewise many such biological structures are proposed to be in LC phase and the LC phase may have a crucial role in their exceptional properties. It can be seen that all the systems mentioned are capable of forming self assembled structures.

9.2.4.1 Protein Based LCPs

Spider silk is made of β -crystallites enriched with polyalanine repeats of the protein within a matrix of the less ordered glycine-rich segments (Rathore and Sogah 2001). The polyalanine segments form transverse lamellae within oriented nanofibrils, when extruded from the duct and exhibit nematic ordering (Knight and Vollrath 2002). However, mechanically drawn fibres do not show the same texture, instead show a banded texture, indicating a periodic variation in director orientation, in contrast to fibres extruded from silk glands (Kerkam et al. 1991). Spider dragline silk is considered as a LC elastomer due to its structural and elastomeric properties. The nematic phase of spider and silkworm fibroin observed in aqueous solutions is thought to serve as an intermediate state in the *in vivo* processing route of fibril orientation. Similarly, fibrillation of the silk-moth chorion protein (found in the eggshell) is also considered to precede from LC phase nuclei, in particular amyloid spherulites. Silkworm (*Bombyx mori*) silk is rich in GAGAGS repeats. LC phases have been observed for block copolymers comprising PEG (polymer) conjugated to the *Bombyx mori*-silk inspired GAGA domain and for PEG/peptide multiblocks containing poly(alanine) repeats, based on the *Nephila clavipes* spider

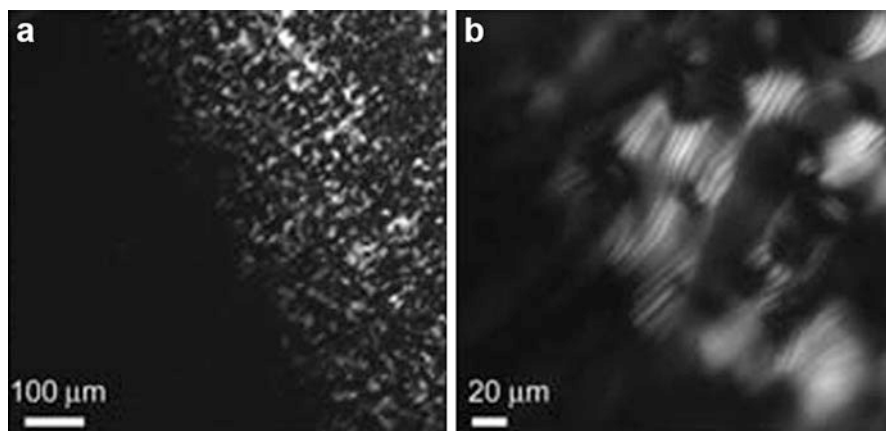


Fig. 9.10 Polarized optical microscopy images of (a) I/N interface in a type II collagen solution at 5 mg mL^{-1} in 0.5 M acetic acid, after drying, (b) same region at higher magnification showing typical fingerprint texture. Reproduced with permission from Belamie et al. (2006) Copyright IOP science

silk structure. Poly γ -benzyl-L-glutamate (PBLG), adopts an α -helical conformation in organic solvents and in the melt when the chain is sufficiently long (Elliott and Ambrose 1950) and forms chiral nematic and columnar phases in organic solvents such as *m*-cresol or pyridine (Luzzati et al. 1961; Robinson 1966).

The most significant helical bio macromolecule which forms LC phase, other than the DNA, is the collagen. Collagen, the most abundant protein in higher animals gives the supporting frame in which organs and tissues are shaped, and is also responsible for the firmness, elasticity and integrity of structures and hydration of the body. Type I collagen plays vital role in tissues such as tendon, skin, bone and cornea and the Type I collagen monomers can form nematic, precholesteric and cholesteric phases in dilute acid solution (Giraud-Guille 1992) (Fig. 9.10). Collagen possesses high tensile strength and good elasticity, and hence is considered as a biological LC elastomer. Liquid crystallinity of collagen is observed under conditions close to that of found in tissues ($50\text{--}200 \text{ mg mL}^{-1}$) (Giraud-Guille et al. 2008) Therefore, it can be thought that self-assembly of mesophases play a role in the mechanism of ordering of collagen in bones, fish scales and cornea as well as of chitin fibres from arthropods (Belamie et al. 2006).

Another protein structure which exhibit self assembly and LC phase is the neuronal proteins. The three filamentous proteins: filamentous actin (Safinya 2006; Hirst et al 2005), microtubules, (Choi et al. 2009; Safinya et al. 2011) and neurofilaments (Jones and Safinya 2008; Beck et al. 2010a, b; Deek et al. 2013) constitute the major protein fraction in the cytoskeleton of neurons. The lengths of rigid microtubules are in the order of millimeters, of semi-flexible filamentous actin is about one micron and of flexible neurofilaments is around 100–150 nm. The large difference in their rigidity leads to quite different hierarchical self-assembled structures for these different filamentous systems. The 3D bundles of MTs

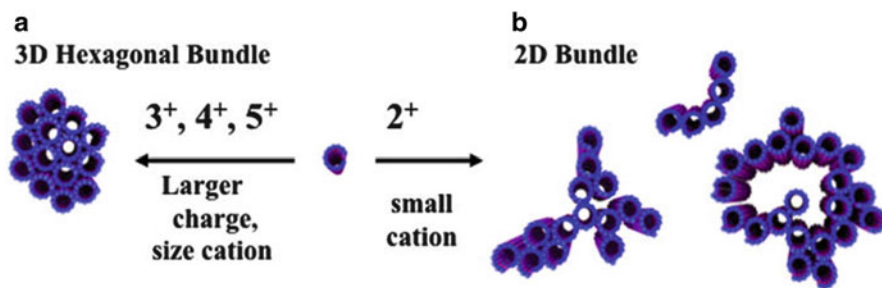


Fig. 9.11 Schematic of higher-order-assembly of microtubules in the presence of multivalent counterions. (a) Trivalent (spermidine [$\text{H}_3\text{N}^+(\text{CH}_2)_3\text{-NH}_2^+(\text{CH}_2)_4\text{-NH}_3^+$] and lysine3), tetravalent (spermine [$\text{H}_3\text{N}^+(\text{CH}_2)_3\text{-NH}_2^+(\text{CH}_2)_4\text{-NH}_2^+(\text{CH}_2)_3\text{-NH}_3^+$] and lysine4), and pentavalent (lysine5) cations lead to the formation of 3D bundles with hexagonal in-plane symmetry. (b) Divalent cations [Ba^{2+} , Ca^{2+} , Sr^{2+}] lead to the sheet-like 2D bundles with linear, branched, and loop morphologies. Reprinted with permission from Needleman et al. (2004). Copyright 2004, National Academy of Sciences, U.S.A

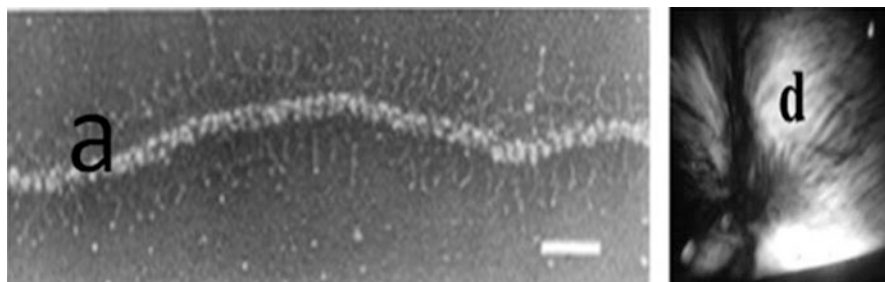


Fig. 9.12 (a) Electron micrograph of a mature neurofilament (glycerol sprayed/low-angle rotary metal shadowed on freshly cleaved mica). The side arms are clearly visible. The bar is 100 nm. (b) A reconstituted NF mixture forming a strongly birefringent hydrogel viewed between crossed polarizers shows the presence of nematic-like liquid crystalline texture. (a) is reproduced with permission from Herrmann, H.; Kreplak, L.; Aebi, U. *Methods in Cell Biology*. Omary, MB.; Pierre, AC., editors. Vol. 78. Academic Press; Waltham, MA: 2004. p. 3–24, (b) is reproduced with permission from Needleman DJ, Jones JB, Raviv U, Ojeda-Lopez MA, Miller HP, Li Y, Wilson L, Safinya CR. Supramolecular assembly of biological molecules purified from bovine nerve cells: from microtubule bundles and necklaces to neurofilament networks. *J Phys: Condens Matter*. 2005; 17:S3225–S3230

(Fig. 9.11), with in-plane hexagonal symmetry observed by small-angle-X-ray-scattering (SAXS) studies, are similar to that of freely suspended columnar phases of discotic LCs (Van Winkle and Clark 1982; Safinya et al. 1984).

Neurofilaments consist of three different molecular weight polypeptide subunits (Fig. 9.12a, labeled NF-L (L = Low, 60 kDa); NF-M (M = Medium, 100 kDa); and NF-H (H = High, 115 kDa)). Among the fractions only NF-L assemble in the absence of the other subunits and form stable filaments and both the NF-M or NF-H subunits require the presence of NF-L to form filaments. In buffer mimicking

physiological conditions, purified and re-assembled NFs may form an Onsager-like nematic LC gel phase, and tend to spontaneously assemble to form a 10 nm thick filamentous protein with highly charged C-terminal sidearms, which extend away from the filament (Fig. 9.12a) (Ching and Liem 1993; Fuchs and Cleveland 1998). PPLM observations revealed images of a nematic hydrogel (Fig. 9.12d), with long-range orientational order associated with the filamentous network (Beck et al. 2010a, b; Needleman et al. 2005; Jones and Safinya 2008; Hesse et al. 2008). The neurofilament nematic gel phase, made *in vitro* was found to be a thermodynamically stable phase and was found that the stability is dependent on the salt concentration. As a function of decreasing salt concentrations, the nematic gel phase undergoes reversible transitions to an isotropic gel followed by a new re-entrant LC gel phase (Deek et al. 2013).

Similarly, NF from the principal cytoskeletal constituent of myelinated axons vertebrates have an assembled filament structure with protruding flexible C-terminus side arms and exhibit LC phase (Fig. 9.13). The LC gel networks of the neurofilament assemblies assumed to play a key role in the mechanical stability of neuronal processes and in long myelinated neuronal axons, the neurofilaments form an aligned nematic liquid-crystal gel with an open-network structure and acts as a structural scaffold. The side arms play a critical role in modulating the forces

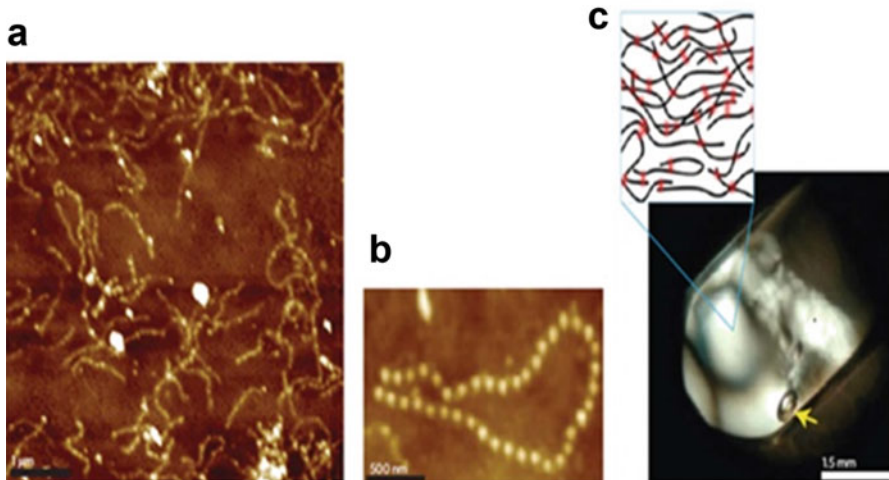


Fig. 9.13 Hierarchical neurofilament self-assembly. (a, b) AFM images that show a necklace structure and a preferred parallel configuration even at a low protein concentration. (c) Cross-polarized microscopy image of a neurofilament network in a quartz capillary. The nematic domain boundaries are a clear indication of the extended length scale of the ordered phase. The non-spherical bubble (yellow arrow) reveals the yield stress resisting surface tension, as expected for a gel. The inset illustrates the possible configurations and microscopic interactions, such as physical entanglement or intrafilament and interfilament interactions, leading to the nematic order. Reproduced with permission from Roy Beck et al. (2009). Copyright Nature Publishing group

between neurofilaments in their isotropic and liquid-crystal gel phases (Beck et al. 2009). The alignment of the neurofilament hydrogel is established clearly with the help of cross-polarized microscopy as shown in the Fig. 9.13.

DNA, a biopolymer, with its structure and functions based on self assembly, exhibiting liquid crystalline properties is not surprising. Michael W. Davidson and coworkers in 1998 showed that DNA exists in LC phases at certain DNA concentrations, thus exhibiting lyotropic LC behaviour. DNA has found to form at least three distinct liquid crystalline phases at concentrations comparable to those in vivo: a weakly birefringent, dynamic ‘precholesteric’ mesophase with microscopic textures intermediate between those of a nematic and a true cholesteric phase, a second mesophase which is a strongly birefringent, well-ordered cholesteric phase and at highest concentrations, a third phase which resembles that of smectic phases of thermotropic LCs (Davidson et al. 1998). Crystalline solutions of DNA at concentrations of 130–170 mg DNA mL⁻¹ at room temperature, become fully liquid crystalline at higher concentrations. Phase transition boundaries were in good agreement with predicted rigid rod behaviour when DNA was treated as a scaled rod with an effective radius of 21.5 Å at this ionic strength (Fig. 9.14).

It is well known that multivalent cations can condense DNA to LC phases, for instance, polyamines condense DNA to LC phases, cationic liposomes form a lamellar structure with DNA. Synchrotron X-ray scattering studies of cationic liposome (CL-DNA) complexes have led to the discovery of distinct structures such as a multilamellar phase with DNA layers sandwiched between cationic bilayer membranes (L_{α}^C), (Rädler et al. 1997) and an inverted hexagonal structure with DNA encapsulated within cationic lipid monolayer tubes (Koltover et al. 1998). The lamellar CL-DNA complex is a “hybrid” phase of matter with DNA chains layered between lipid bilayers (Fig. 9.15), forming a 3D smectic phase (Ewert et al. 2006; Zidovska et al. 2009).

9.2.4.2 Chitin and Chitosan Based LCP

Chitin, a long-chain polymer, found in the exoskeleton of arthropods such as crustacean and insects can be processed by acid hydrolysis to produce rod-like nanoparticles which can form a chiral nematic phase at sufficiently high volume fraction, depending on pH and ionic strength. Hydrolysis of α -chitin, obtained from crab shells generates rod-like crystallites, with a width and length of 6–8 and 100–200 nm, respectively, Figs. 9.16a, b show the representative textures. It has been proposed that the chiral nematic phase act as a template for the helicoidal arrangement of chitin microfilaments. Iridescent colouring of certain beetle wings (Fig. 9.18) is proposed to be due to the helicoidal stacking of fibrous chitin layers, and it is possible that LC phases may be acting as precursors to the stacking structure.

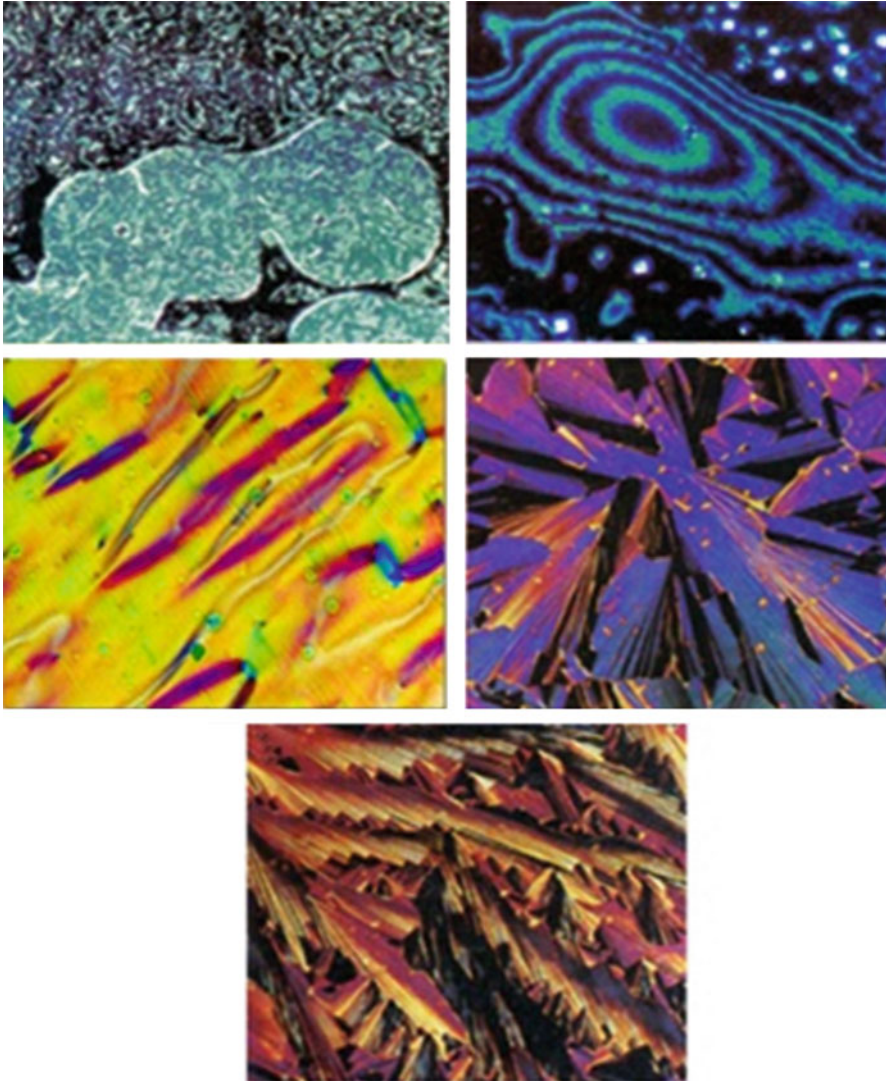


Fig. 9.14 (Top to bottom, anti clockwise): Low magnification views illustrating sharp transition zones between precholesteric and cholesteric domains, Weakly birefringent, diffuse ring texture of 'precholesteric' phase, Highly birefringent, fringe or chevron texture of magnetically aligned cholesteric phase of DNA, Focal-conic-fan texture of smectic-like phase, Pleated ribbon' texture of most concentrated smectic-like phase near open end of coverslip (Reproduced with permission from Teresa et al. (1998) Copyright Nature Publishing group)

Chitosan is yet another biologically derived polymer which can be converted to liquid crystalline material and several works have reported the preparation of LCs from chitosan and its derivatives. Similarly Sakurai and coworkers reported the preparation of thin films and fibres from 38 % chitosan/formic acid solution.

Fig. 9.15 The structure of three distinct cationic liposome CL-DNA complexes determined by synchrotron small-angle X-ray scattering. Reproduced with permission from Safinya et al. (2013). Copyright Taylor and Francis

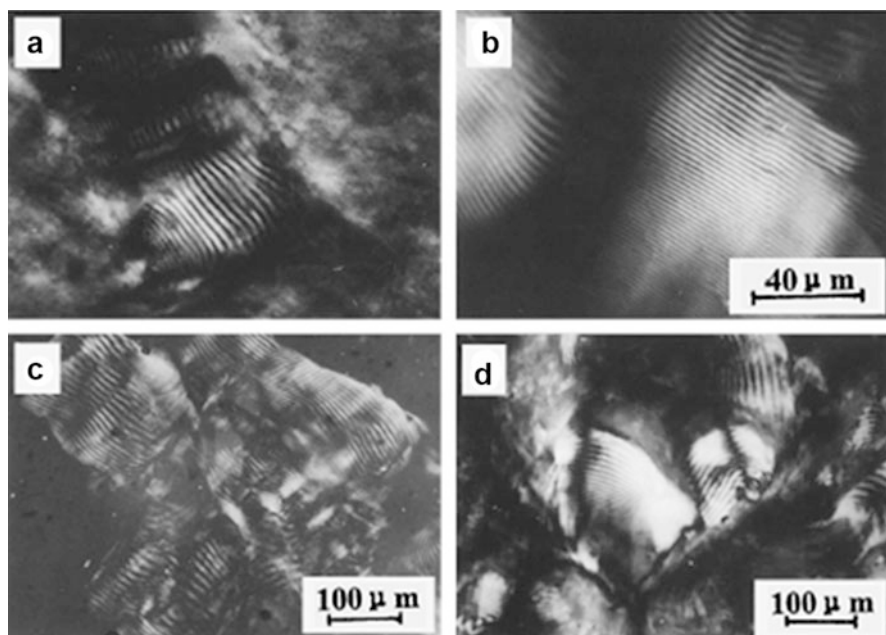
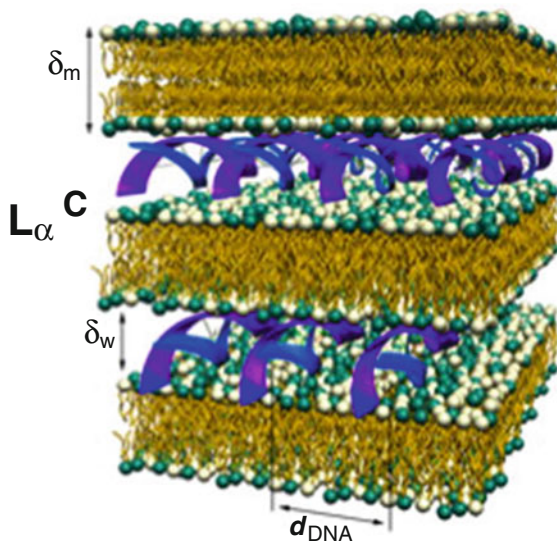


Fig. 9.16 (a) Photomicrographs of cholesteric LC texture of HPCS solutions (b) 15 wt% HPCS1/DCA solution; (c) 18 wt% HPCS6 aqueous solution; (d) HPCS7 wet product. Reproduced with permission from Yanming Dong et al. 2001. Copyright Elsevier

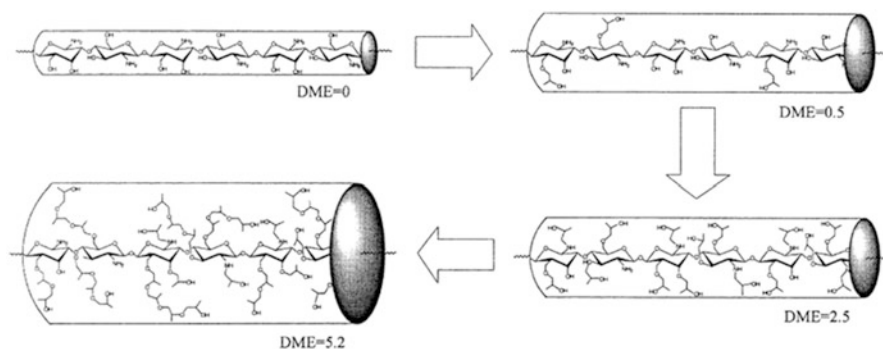


Fig. 9.17 Schematic illustration of the increase of HPCS molecular diameter with enhancement of DME. Reproduced with permission from Yanming Dong et al. (2001). Copyright Elsevier

Hydroxypropyl chitosan with different degree of molar etherification were prepared and studied by Yanming Dong and his coworkers (Dong et al. 2001). It was found that the critical concentration for formation of the lyotropic LC is very high in the case of chitosan due to the breaking of hydrogen bonds in chitosan. As a result a small substitution in chitosan thus results in a large increase in critical concentration. It can be shown that the diameter of the macromolecules increases with the increase of DME as shown in the Fig. 9.17. The chitosan derivatives were prepared as follows: an alkaline chitosan solution is prepared by dissolving chitosan in NaOH solution and stored at -18°C overnight before use. An excess of poly ethylene oxide is added to the defrozen alkali chitosan and stirred, refluxed and cooled and subsequently neutralized using HCl and washed with water and acetone alternately and dried in vacuum. The as prepared chitosan derivatives analysed in different solvents like water, formic acid and dichloroacetic acid were found to exhibit cholesteric liquid crystalline phase.

9.3 Characterization of Liquid Crystals

Several methods are used for the characterization of the liquid crystalline phase, some of the common techniques are DSC, PLM, XRD etc. Some of the characterization techniques of LCs are explained using examples.

9.3.1 Differential Scanning Calorimetry

DSC is an important tool to determine transition temperatures and to distinguish the different phases. The lamellar liquid crystalline structure of para phenylene dimeramide (PPD) synthesized using castor oil as precursor was confirmed using

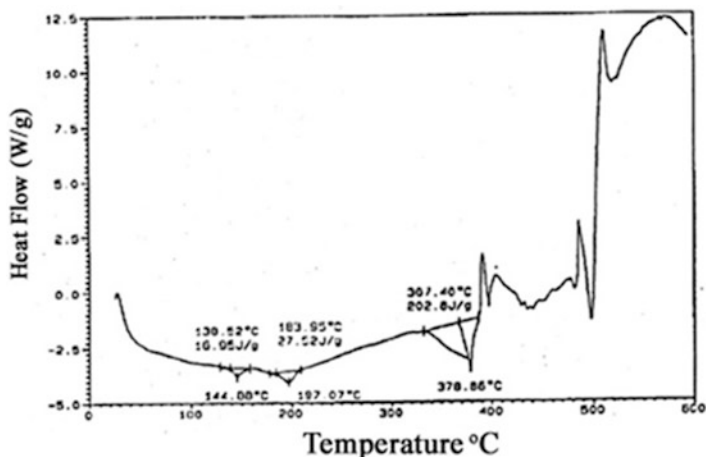


Fig. 9.18 DSC analysis of PPD (Reproduced with permission from Khare et al. 2013. Copyright KROS publisher)

this technique. The three endothermic curves in the DSC analysis (Fig. 9.18) indicate the presence of intermediate transitions/phases in the substance. From the PLM studies the peaks are assigned to the following phases: the first endotherm corresponds to the crystal to smectic phase transition, the second endotherm, smectic to nematic phase transition, and the third endotherm highlights the phase transition from nematic to isotropization.

DSC can also be used to study the dependence of the phase transitions on the structure of the compound. Figure 9.19 shows a set of DSC cooling diagrams for a series of aliphatic esters of 2-hydroxy propyl cellulose (CnPCs). It is evident that by increasing the length of the side chains, both the LC phase to the isotropic melt, ΔH_i and the LC phase to the isotropic melt transition temperatures T_i decreases. This shows that not only the backbones but also the side chains are involved in these transitions; the transitions are dependent on the length of the side chains significantly. When cooled further, it leads to a vitrification of the materials (as shown in Fig. 9.19). The glass transition temperature (T_g) of CnPC also decreases as the number of methylene units in the side chains increases. It is clear that the methylene units in the side chains not only serve as “diluent” but also involve in these phase transitions by providing contributions to the enthalpy of the isotropic melt to LC phase transitions. Moreover the methylene units of CnPC affect the T_g while the T_g drops with the increase in the length of the methylene units. Thus from the DSC it is evident that not only the backbones but also the side chains influence the formation of the LC phases and phase transitions.

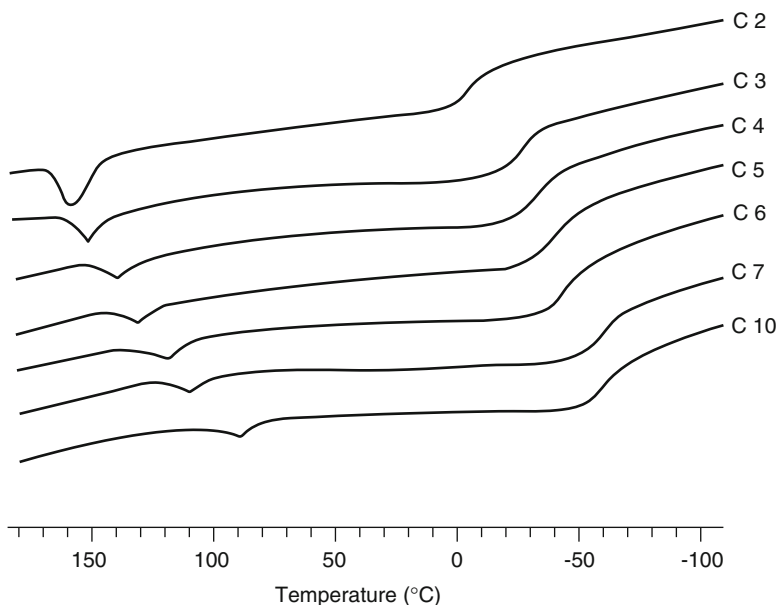


Fig. 9.19 DSC cooling curves of CnPC recorded at 15 K/min and normalized per gram of material. Reproduced with permission from Huang Polymer (2007). Copyright Elsevier

9.3.2 Polarized Light Microscopy

PLM is a widely used technique to study and identify the phases exhibited by LCs. A thin layer of a LC is placed in between two cover glass plates and viewed through a PLM under temperature or proper conditions depending on the type of LC phase, various textures can be observed. Beautiful kaleidoscopic images called textures are seen due to the interference between light waves passing through the specimen, which is already heavily given throughout the chapter.

The formation and growth of LCs in nanocellulose was observed by means of laser diffraction. The laser beam produces a diffraction pattern and the central spot of the ring grows into a steady circular ring showing the growth of LCs and their organization into larger assemblies which is confirmed by the appearance of concentric rings after some time. Optical microscopy is an important tool for the study of the structure of lamellar LCs. Many microscopic techniques like SEM, TEM and AFM are commonly used. Chiral nematic phases have been observed for concentrated solutions and melts of many cellulose derivatives (Gray 1995). Both left and right-handed solutions, melts and films have been observed for cellulose derivatives, but to date only left-handed helicoids have been observed for CNC suspensions and films. The assignment of handedness was based on TEM images of oblique microtomed sections of films cast from aqueous suspensions of CNCs, following the interpretation of the arcing observed in

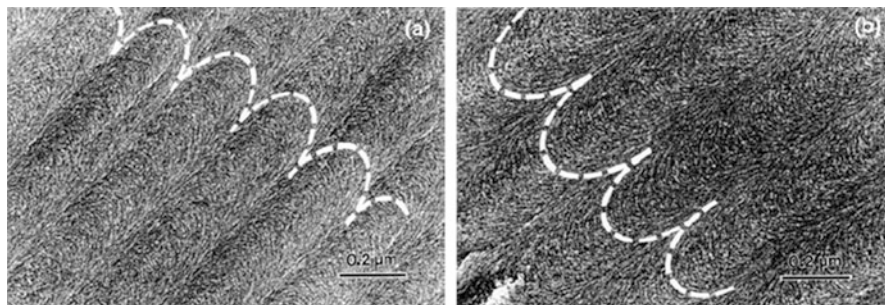


Fig. 9.20 Arcing observed in TEM images of thin oblique cross-sections through a planar chiral nematic film of wood CNCs cast from aqueous suspension on a Teflon substrate. The sections were cut at angles such that the top left-hand corner of the image was tilted (a) towards and (b) away from the observer (Giasson 1995) (Reproduced with permission from Dissertation, McGill University, Chap. 5, p 167)

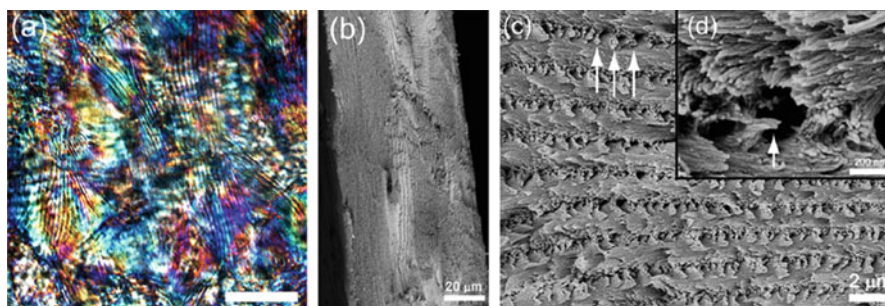


Fig. 9.21 (a) Optical microscope image (*crossed polars*) of the bulk CNC film (scale bar 40 μm), (b–d) SEM images of a fracture surface across the film (Majoinen et al. 2012) (Reproduced with permission from Springer)

natural composites by Bouligand (2008). Arcing observed in TEM images of thin oblique cross-sections through a planar chiral nematic film of wood CNCs cast from aqueous suspension on a Teflon substrate is shown in Fig. 9.20 (Giasson 1995).

When the cast CNC film is viewed in transmission between crossed polars in an optical microscope (Fig. 9.21a) the film shows the usual multi domain structure, where the direction of the chiral nematic axis changes with the location in the film. The shortest distance between the lines is $P/2$. The fan-like appearance found in the SEM in Fig. 9.10d corresponds to the cross-section of a left-handed helicoidal arrangement of CNC, with the axis of the helicoid from top to bottom of the image.

The LC properties exhibited by spherical nano cellulose suspensions were reported for the first time by Neng et al. and the liquid crystalline textures were carefully observed using PLM (Wang et al. 2008). The formation of nano crystals from spherical nanoparticles is thermodynamically unfavorable as per

Fig. 9.22 Schematic representation of chiral nematic ordering present in nanocrystalline phase (Reproduced with permission from Shopsowitz et al. (2010a, b). Copyright ACS 2010)

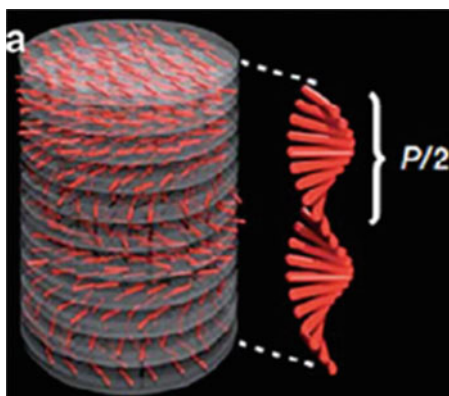
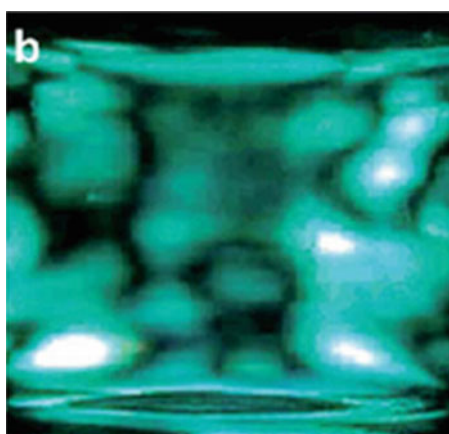


Fig. 9.23 Photograph of an aqueous suspension of tunicin whiskers as observed through cross nicols. Reproduced with permission from Azizi Samir et al. (2005). Copyright ACS 2005



Onsager's theory (Onsager 1949) whereas the LCs of rod like particles are more thermodynamically stable because of the gaining of translational entropy that overrides the loss of orientation entropy due to particle alignment (Jana 2004). The importance of cellulose lies in the fact that cellulose crystallites have a helical twist along the main axis, which can induce crystal suspensions to attain a helical twist normal to the main axis of the rod, and thus organize into a chiral nematic phase or cholesteric phase of stacked planes aligned along a perpendicular axis as shown in Fig. 9.22 (Shopsowitz et al. 2010a, b; Dong et al. 1996a, b).

This type of alignment can result in optical band gaps leading to the macroscopic birefringence of individual domains, which can be seen through crossed polarizers as the Schlieren texture as shown in Fig. 9.23 which depicts the photograph of aqueous suspension of tunicin whiskers as observed between cross nicols.

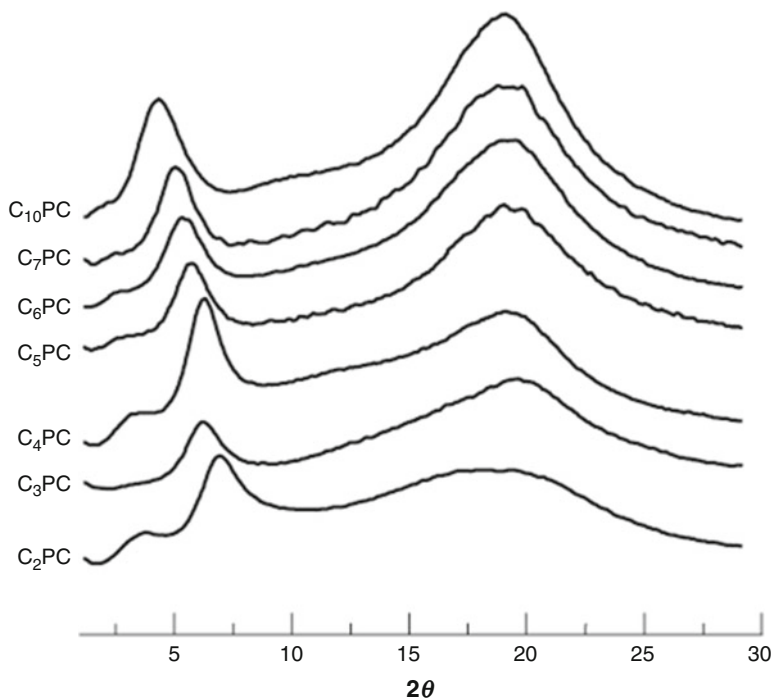


Fig. 9.24 1D WAXD powder diagram: CnPC bulk at room temperature on a glass slide in a reflection mode. Reproduced with permission from Huang (2007). Reproduced with permission from Elsevier

9.3.3 X-ray Diffraction Technique

The chain packing scheme of the thermotropic LC phase in CnPCs deduced based on wide angle XRD structural characterization technique (Fig. 9.24) displayed an intense diffraction peak in the low 2θ angle region between 3° and 8° . Furthermore, with increasing the number of methylene units, the d-spacing of the diffraction peak increases from 1.20 nm in C2PC to 1.37 nm in C5PC to 1.86 nm. These diffraction peaks represent the existence of short range or quasi-long-range positional order.

9.4 Applications of Liquid Crystals

LCs are well known for their display applications due to its light modulating properties and is been widely applied world over as display materials in computer monitors, flat panel displays, electronic display materials such as television, video etc. because of their energy efficiency and clarity compared to the conventional displays. These optical display films have uniform optical properties across the

surface area. For applications such as patterned polarization rotators for stereoscopic displays, polarization sensitive gratings, reflective colour filters and patterned polarizers, it is useful to locally tailor the optical properties of displays, adding chiral molecules to LCs, to control the twisting sense and the rotation angle, provides a method to prepare such films. Recently, new technologies have become available for the realization of such structured films. For instance, cholesteric liquid crystalline phases, the chiral nematic phases are well-known for their ability to rotate and reflect light. The wavelength of maximum reflection (λ) and the width of the band depend on the P of the cholesteric LC phase and the refractive indices (n_e and n_o) of the LCs [(1) and (2)]. The distance over which the molecules rotate 360° is called P .

$$\lambda = P \times n \quad (1)$$

$$\Delta\lambda = P \times \Delta n \quad (2)$$

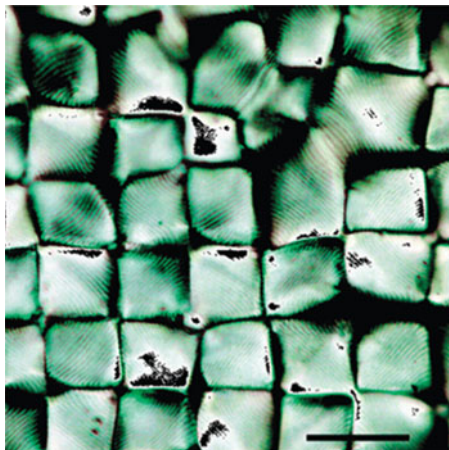
Here: n is the average refractive index of the film and Δn is the birefringence ($n_e - n_o$).

CNC which can form chiral nematic phases have been investigated by Wang et al. for optical display applications (Wang et al. 2008). They observed that liquid crystallinity of CNC suspensions coupled to the birefringent nature of the particles, leads to interesting optical phenomena. As the lyotropic LC onset concentration is reached, the particles align creating a macroscopic birefringence. Though it is extremely difficult to align and preserve the chiral nematic structure in films of LCs, if suitably stabilized, CNCs can preserve this structure upon drying to a thick film resulting in parabolic focal conic defect structures that are reminiscent of smectic and lamellar LCs of polymers and lipids (Saito et al. 2007) In this case, the chiral structure pitch determines size scales and results in dazzling optical displays as seen in Fig. 9.25. When the reflection wavelength of cholesteric LC is in the range of visible light, well oriented layers of the cholesteric LCs give rise to vivid iridescent colors and the color is angular dependent. For these reasons cholesteric LCs are being investigated for application as special pigments in paints. Because the reflected light is circularly polarized, the materials are also suitable for the preparation of polarization-sensitive optical components.

Chiral nematic LCs are gaining popularity in electrically switchable devices because of the improved colour, brightness and other enhanced properties it can offer. The devices are known as surface stabilized cholesteric texture devices and are of particular interest in applications that require good viewing angles and high brightness.

Another remarkable potential application of transparent CNC-templated material is its utilization in cholesteric-based mirrorless lasing (Finkelmann et al. 2001; Palfy-Muhoray et al. 2006). Recent work has confirmed that the combination of solidified cholesteric LC films with different pitch values with an intermediate film of non-chiral low molar mass nematic can produce broadband (essentially white light) cavity mode lasing with tunability offered by the switchable nematic layer

Fig. 9.25 Parabolic focal conics in CNCs viewed between crossed polarizers. Reprinted with permission from Roman and Gray (2005). Copyright American Chemical Society



(Takezoe 2010). Takanishi et al. proved that the combination of multiple solidified cholesteric layers can reduce the lasing threshold spectacularly (Takanishi et al. 2010).

It is remarkable that the phenomenon of transient electric birefringence effect is observed in CNC dispersions in both water as well as organic solvents. The outstanding properties which resulted offer the prospective to extend the aforementioned phenomenon to a variety of devices which are of tremendous efficacy in the present scenario such as: display technology superior to current TFT-LCD displays; variable density optical filters; light valves etc. The dielectric anisotropy of CNCs is positive, and an electric field thus acts to unwind the helix. It was reported that uniform CNC alignment in films obtained by drying CNC suspensions in the presence of electric fields with frequencies in the kHz–MHz range and an amplitude of $B2 \text{ kV cm}^{-1}$ (Habibi et al. 2008).

Inorganic materials are preferred in lasing applications when exposed to high intensity lights, due to their superior stability and life time compared to that of the organic counterparts. Cholesteric CNC suspensions have recently been used as templates to produce inorganic films with an internal left-handed helical structure (Shopsowitz et al. 2011, 2012). CNC templated films were produced by adding inorganic sol–gel precursors such as tetra methyl orthosilicate or 1, 2-bis (trimethoxysilyl) ethane and simply allowing a certain amount of the suspension to dry under ambient conditions in a Petri dish. The CNC self-assembles into a cholesteric phase as the concentration increases in the precursor solution, and the resulting film after solidification and calcination or acid treatment obtains an internal structure that is a replica of the CNC helix. CNC template method produces inorganic materials with helical structure same that of the CNC material, the templating method is schematically given in Fig. 9.26.

Generally, the helical P of the CNC-inorganic composite before calcination is larger than visible light wavelengths, and the initial composite film therefore shows

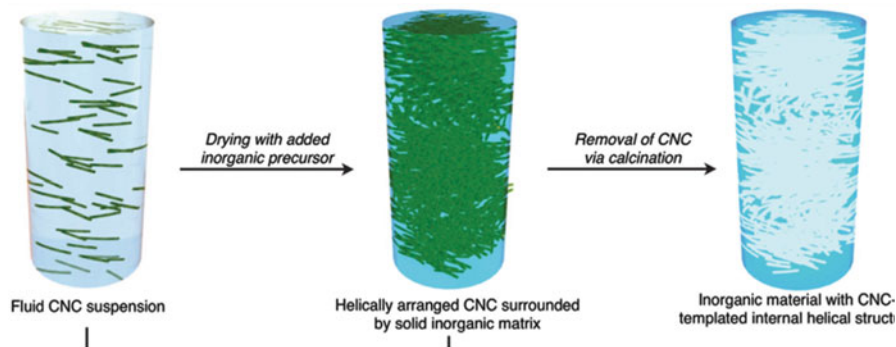


Fig. 9.26 Schematic illustration of the CNC-templating of inorganic materials. Fluid CNC suspension (*left*), which may be liquid crystalline or isotropic added with an inorganic precursor is dried to form CNC helix contained in an inorganic solid matrix (*middle*). By calcinating the sample, the CNCs are removed, leaving the inorganic material with a CNC-templated internal helical structure (*right*). Reproduced with permission from Shopsowitz et al. (2012). Copyright ACS 2013

no color. However, after the cellulose has been removed, the remaining inorganic film frequently shows visible Bragg reflection and the resulting characteristic iridescent colors. SEM investigations in these cases revealed that the removal of the CNCs leads to a compression of the helical structure such that the periodicity is small enough that the photonic band gap falls within the visible range. Films templated from CNCs are attractive because they combine the high surface area of mesoporous materials with the long-range ordering of LCs, specifically with the helical arrangement of the chiral nematic phase. Following this approach one can thus endow any inorganic material that can be templated from a CNC suspension with photonic crystal properties, with visible Bragg reflection if the pitch is in the range of a few hundred nm.

Another important work associated with the field of LC is the synthesis of polymer composites with chiral nematic photonic structures through the self-assembly of CNC dispersions in organic solvents (Clement et al. 2013). Upon neutralization of CNC-H with various strong bases and freeze-drying, Clement and coworkers were able to easily prepare dispersions of CNC-X ($X = \text{Li}^+, \text{Na}^+, \text{K}^+, \text{NH}_4^+, \text{NMe}^+, \text{NBu}_4^+$) in polar organic solvents including DMSO, formamide, N-methylformamide, or DMF using stirring and mild sonication. Commodity polymers, such as polystyrene (PS), poly(methyl methacrylate) (PMMA), polycarbonate (PC), and poly(9-vinylcarbazole) (PVK), are soluble in DMF and hence composite materials can be readily prepared using these polymers as matrix. Mixing these polymers with CNC-Na dispersions (3.5 wt%) in DMF followed by slow evaporation of the solvent is a facile way to prepare iridescent composite films with chiral nematic structure. The self-assembly of the organic CNC dispersions can be exploited to prepare iridescent polymeric composites simply by casting the CNC dispersion with a suitable polymer soluble in the organic solvent. This depicts a versatile method to generate new iridescent polymer composites with chiral

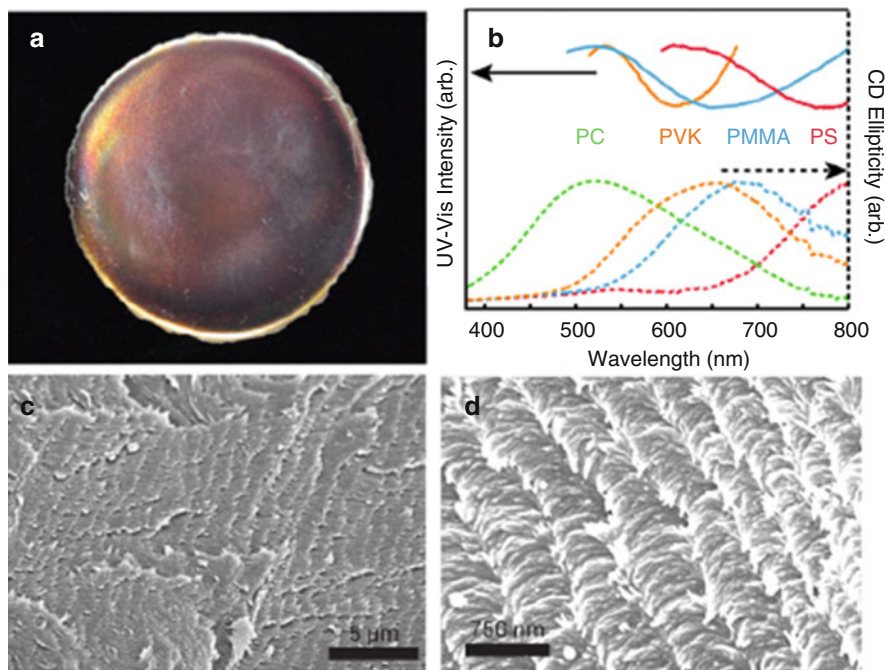


Fig. 9.27 (a) Photograph of an iridescent CNC-Na/PMMA composite film with chiral nematic ordering. (b) UV-vis and CD spectra of composites with 46 wt% polymer prepared with PS, PMMA, PC, and PVK (UV-vis spectrum of CNC-Na/PC is omitted because of strong absorption of the polymer around the reflected wavelength). (c) Representative SEM image of a CNC-Na/PC composite demonstrating the periodic layered structure. (d) At higher magnification, SEM shows the left-handed helical morphology of the spindle-shaped CNCs (Reproduced with permission from Clement et al. (2013). Copyright ACS 2013)

nematic structures by successfully dispersing neutralized CNC in polar organic solvents such as DMF. This approach is easily scalable to obtain large area thin films and coatings that could be used for applications such as reflective filters. It is anticipated that the general method of using organic dispersions of CNC as a chiral nematic template will pave the way to an expansive array of new photonic composites or mesoporous materials (Fig. 9.27).

9.5 Conclusions and Future Prospects

The study of LCs is an attractive research field that has engrossed significant curiosity and their synthesis from natural sources has awakened quite an enormous deal of scientific awareness. This is largely because of the vast prospective combined with the capacity for self-assembly of renewable materials like CNCs, natural oils etc. Interdisciplinary research in engineering, biology, physics, medicine, and

chemistry will be crucial for taking LC research to further heights and new applications and to provide a consistent understanding of these fascinating particles. The exploration of these molecular materials is still a challenge since the rapid development of display technology demands new LC materials, which possess as wide a range of properties as possible. Nanostructured films with a photonic band gap arising from the spontaneous helix formation in the cholesteric LC phase of CNC suspensions have been the emphasis of several studies in the current scenario and it is anticipated that this field will be the focus of serious research which will undeniably lead to diverse applications in the days to come. The exploitation of a CNC suspension as a self-assembled template for the synthesis of inorganic materials that adopt the CNC-derived periodic internal structure undoubtedly offers a promising and versatile platform for fabricating multifunctional mesoporous materials with photonic crystal properties and very large surface areas. The utilization of other inorganic materials with higher refractive indices may be predominantly remarkable for photonic devices such as tunable mirrorless lasers, and CNC-templated materials with specific surface functionalities may pave the way for the development of enantioselective sensors (Lagerwall et al. 2014). Furthermore, an analogous templating route could be utilized to fabricate sturdy and fracture resistant composite materials with a helical internal structure derived from CNC, that mimic many industrially useful and potential high-performance biomaterials such as lobster cuticle (Nikolov et al. 2010). Vital issues dealing with the sensitive balance between LC formation and gelation/glass formation have yet to be fully understood. It is seen that are both promoted by the high aspect ratio of CNC rods. In particular, when cholesteric structures with a short and highly specified pitch are desired, primarily for photonic devices, one must develop a means of handling the transition into a non equilibrium glassy state, as this becomes increasingly likely at the high CNC concentrations required for a short-pitch helix. To this end, controlled drying and alternative solvent removal strategies are of interest. Another possible approach to improving the control of the helical self-assembly could be to vary the atmospheric humidity during evaporation or to add a nonvolatile co-solvent (Zhang et al. 2008). Probably the most compelling direction of research into these systems seeks to understand the possibility of controlling the alignment of CNCs, in helical or non-helical states. Large-scale uniform alignment with control of the director and/or helix axis orientation has been made possible by using appropriately designed nano patterned substrates and/or subjecting the drying CNC suspension to appropriately selected mechanical, electrical or magnetic fields. Such control also deserves additional awareness and is indeed an essential prerequisite for quite a lot of significant applications such as lasers, security papers and certain sensors. Attempts to decrease the length distribution of CNCs sounds promising, as this could lead not only to the manifestation of smectic and/or columnar phases of CNCs, which are of primary concern, but also to other applications in nanostructured and ordered composite materials. The attractive optical properties of this self-assembled bio-derived photonic crystal have inspired several attempts to utilize CNC films in novel applications such as optical encryption 15 or as chiral templates.

Investigations of biologically inspired liquid crystalline structures will improve the understanding of the relation between the structure, functions and LC phases and may possibly lead to the recipes of creating super strength materials and may throw some light into the mechanisms of biological functions. As a conclusion we would like to comment that bio-inspired LCs/LCPs are a better way to future materials as it combines self-assembly, enhanced properties and functions and importantly eco-friendliness in the same package.

References

- Abid S, Gharbi RE, Gandini A (2004) Polyamides incorporating furan moieties. Synthesis and characterization of furan-aromatic homologues. *Polymer* 45:5793–5801
- Al-Bawab A, Heldt N, Li Y (2005) Emulsified orange oil in an aqueous vesicle solution. *J Dispers Sci Technol* 26:251–256
- Almgren M (1980) Migration of Pyrene between lipid vesicles in aqueous solution. A stopped-flow study. *Chem Phys Lett* 71(3):539–543
- Araki J, Wada M, Kuga S, Okano T (2000) Birefringent glassy phase of a cellulose microcrystal suspension. *Langmuir* 16:2413–2415
- Azizi Samir MAS, Alloin F, Dufresne A (2005) Review of recent research into cellulosic whiskers, their properties and their application in nanocomposite field. *Biomacromolecules* 6:612–626
- Bajpai UDN, Nivedita NP (1996) *Cheremisinoff multiphase reactor and polymerization system hydro-dynamics; advances in engineering fluid mechanics series*. Gulf Publishing Company, Houston, p 583
- Beck R, Deek J, Jones JB, Safinya CR (2009) Gel-expanded to gel-condensed transition in neurofilament networks revealed by direct force measurements. *Nat Mater* 9:40–46
- Beck R, Deek J, Choi MC, Ikawa T, Watanabe O, Frey E, Pincus PA, Safinya CR (2010a) Unconventional salt-switch from soft to stiff in single neurofilament biopolymers. *Langmuir* 26:18595–18599
- Beck R, Deek J, Jones JB, Safinya CR (2010b) Gel expanded–gel condensed transition in neurofilament networks revealed by direct force measurements. *Nat Mater* 9:40–46
- Beck S, Bouchard J, Chauve G, Berry R (2013) Controlled production of patterns in iridescent solid films of cellulose nanocrystals. *Cellulose* 20:1401–1411
- Belamie E, Mosser G, Gobeaux F, Giraud-Guille MM (2006) Possible transient liquid crystal phase during the laying out of connective tissues: α -chitin and collagen as models. *J Phys Condens Matter* 18:S115
- Bouligand Y (2008) Liquid crystals and biological morphogenesis: ancient and new questions. *C R Chim* 11:281–296
- Ching G, Liem RJ (1993) Assembly of type IV neuronal intermediate filaments in nonneuronal cells in the absence of preexisting cytoplasmic intermediate filaments. *J Cell Biol* 122:1323–1335
- Choi MC, Raviv U, Miller HP, Gaylord MR, Kiris E, Ventimiglia D, Needleman DJ, Kim MW, Wilson L, Feinstein SC, Safinya CR (2009) Human microtubule-associated-protein tau regulates the number of protofilaments in microtubules: a synchrotron X-ray scattering study. *Biophys J* 97:519–527
- Clement CY, Cheung MG, Kelly JA, Hamad WY, MacLachlan MJ (2013) Iridescent chiral nematic cellulose nanocrystal/polymer composites assembled in organic solvents. *ACS Macro Lett* 2(11):1016–1020
- Davidson P, Gabriel J-CP (2005) Mineral liquid crystals. *Curr Opin Colloid Interface Sci* 9 (2005):377–383

- Davidson MW, Strzelecka TE, Rill RL (1998) Multiple liquid crystal phases of DNA at high concentrations. *Lett Nat* 331:457–460
- Deek J, Chung PJ, Kayser J, Bausch AR, Safinya C (2013) Neurofilament sidearms modulate parallel and crossed-filament orientations inducing nematic to isotropic and re-entrant birefringent hydrogels. *Nat Commun* 4:2224
- Dong XM, Kimura T, Revol JF, Gray DG (1996a) Effects of ionic strength on the isotropic-chiral nematic phase transition of suspensions of cellulose crystallites. *Langmuir* 12:2076–2082
- Dong XM, Kimura T, Revol JF, Gray DG (1996b) Effects of ionic strength on the phase separation of suspensions of cellulose crystallites. *Langmuir* 12:2076–2082
- Dong Y, Wu Y, Wang J, Wang M (2001) Influence of degree of etherification of critical liquid crystal behavior of hydroxyl propyl chitosan. *Eur Polym J* 37:1713–1720, Elsevier
- Ebeling T, Paillet M, Borsali R, Diat O, Dufresne A, Cavaille JY, Chanzy H (1991) Shear-induced orientation phenomena in suspensions of cellulose microcrystals, revealed by small angle X-ray scattering. *Langmuir* 15:6123–6126
- Elliott A, Ambrose EJ (1950) *Discuss Faraday Soc* 9:246
- Ewert KK, Evans HM, Zidovska A, Bouxsein NF, Ahmad A, Safinya CR (2006) A columnar phase of dendritic lipid-based cationic liposome-DNA complexes for gene delivery: hexagonally ordered cylindrical micelles embedded in a DNA honeycomb lattice. *J Am Chem Soc* 128:3998–4006
- Finkelmann H, Kim ST, Munoz A, Palffy-Muhoray P, Taheri B (2001) Tunable mirrorless lasing in cholesteric liquid crystalline elastomers. *Adv Mater* 13:1069–1072
- Fleming K, Gray DG, Matthews S (2001) Cellulose crystallites. *Chemistry* 7:1831–1835
- Folda T, Hoffman H, Chanzy H, Smith P (1998) Liquid-crystalline suspensions of poly(tetrafluoroethylene) whiskers. *Nat Nanotechnol* 333:55–56
- Fuchs E, Cleveland DW (1998) A structural scaffolding of intermediate filaments in health and disease. *Science* 279:514–519
- Giasson J (1995) *Études microscopiques d'hélicoïdes de système mesocellulosiques in vitro* (Chapter 5). Dissertation, McGill University, p 167
- Giraud-Guille MM (1992) Liquid crystallinity in condensed type I collagen solutions. A clue to the packing of collagen in extracellular matrices. *J Mol Biol* 1992(224):861–873
- Giraud-Guille MM, Mosser G, Belamie E (2008) Liquid crystallinity in collagen systems in vitro and in vivo. *Curr Opin Colloid Interface Sci* 13:303–313
- Gray DG (1995) Chiral nematic ordering of polysaccharides. *Carbohydr Polym* 25(4):277–284
- Habibi Y, Heim T, Douillard R (2008) AC electric field-assisted assembly and alignment of cellulose nanocrystals. *J Polym Sci B Polym Phys* 46:1430–1436
- Hesse HC, Beck R, Ding C, Jones JB, Deek J, MacDonald NC, Li Y, Safinya CR (2008) Direct imaging of aligned neurofilament networks assembled using in situ dialysis in microchannels. *Langmuir* 24:8397–8401
- Hirai A, Inui O, Horii F, Tsuji M (2009) Phase separation behavior in aqueous suspensions of bacterial cellulose nanocrystals prepared by sulfuric acid treatment. *Langmuir* 25:497–502
- Hirst LS, Pynn R, Bruinsma RF, Safinya CR (2005) Hierarchical self-assembly of actin bundle networks: gels with surface protein skin layers. *J Chem Phys* 123:104902
- Hou HQ, Reuning A, Wendorff JH, Greiner A (2000) Tuning of pitch height in thermotropic cellulose esters. *Macromol Chem Phys* 201:2050–2054
- Huang Y, Liang W, Shen JR (1995) Molecular interactions and formation of lyotropic liquid crystals of hydroxyethyl cellulose acetate. *Polymer Bulletin* 35:357–364
- Huang B (2007) Aliphatic acid esters of (2-hydroxypropyl) cellulose—effect of side chain length on properties of cholesteric liquid crystals. *Polymer* 48(2007):264–269
- Jana NR (2004) Shape effect in nanoparticle self-assembly. *Angew Chem Int Ed Engl* 43:1536–1540
- John G, Vemula PK (2006) Design and development of soft nanomaterials from biobased amphiphiles. *Soft Matter* 2:909–914

- Jones JB, Safinya CR (2008) Interplay between liquid crystalline and isotropic gels in self-assembled neurofilament networks. *Biophys J* 95:823–825
- Kerkam K, Viney C, Kaplan DL, Lombardi S (1991) Liquid crystalline characteristics of *natural* silk secretions. *Nature* 349:596–598
- Khare K, Tiwari S, Reddy KV, Bajpai A, Nagaraju V (2013) Study of liquid-crystalline behaviour of aliphatic-aromatic polyamides derived from castor oil based dimer acid by DSC. *Indian J Adv Chem Sci* 2(1):89–94
- Kim I et al (2009) Liquid crystal O/W emulsions to mimic lipids and strengthen skin barrier function. *Cosm Toil*
- Klemm D, Heublein B, Fink HP, Bohn A (2005) Cellulose: fascinating biopolymer and sustainable raw material. *Angew Chem Int Ed Engl* 44:3358–3393
- Knight DP, Vollrath F (2002) Spinning an elastic ribbon of spider silk. *Philos Trans R Soc Lond B Biol Sci* 357(1418):219–227
- Koltover I, Salditt T, Rädler JO, Safinya CR (1998) An inverted hexagonal phase of cationic liposome-DNA complexes related to DNA release and delivery. *Science* 281:78–81
- Lagerwall JPF, Schütz C, Salajkova M, Noh JH, Park JH, Scalia G, Bergström L (2014) Cellulose nanocrystal-based materials: from liquid crystal self-assembly and glass formation to multifunctional thin films. *NPG Asia Mater* 6:e80
- Lee AG (1997) Lipid phase transitions and phase diagrams. I. Lipid phase transitions. *Biochim Biophys Acta* 472:237–281
- Luzzati V, Cesari M, Spach G, Masson F, Vincent B (1961) The structure of L-poly-gamma-benzyl glutamate in solution. Configuration of a helix different from helix alpha and transitions between helical forms. *J Mol Biol* 3:566–584
- Majoinen J, Kontturi E, Ikkala O, Gray DG (2012) SEM imaging of chiral nematic films cast from cellulose nanocrystal suspensions. *Cellulose* 19:1599–1605
- Moon RJ, Martini A, Nairn J, Simonsen J, Youngblood J (2011) Cellulose nanomaterials review: structure, properties and nanocomposites. *Chem Soc Rev* 40:3941–3994
- Needleman DJ, Ojeda-Lopez MA, Raviv U, Miller HP, Wilson L, Safinya CR (2004) Higher-order assembly of microtubules by counterions: from hexagonal bundles to living necklaces. *Proc Natl Acad Sci U S A* 101:16099–16103
- Needleman DJ, Jones JB, Raviv U, Ojeda-Lopez MA, Miller HP, Li Y, Wilson L, Safinya CR (2005) Supramolecular assembly of biological molecules purified from bovine nerve cells: from microtubule bundles and necklaces to neurofilament networks. *J Phys Condens Matter* 17:3225
- Nikolov S, Petrov M, Lympirakis L, Friak M, Sachs C, Fabritius H, Raabe D, Neugebauer J (2010) Revealing the design principles of high-performance biological composites using ab initio and multiscale simulations: the example of lobster cuticle. *Adv Mater* 22:19–526
- Onsager L (1949) Effects of shape on the interaction of colloidal particles. *Ann N Y Acad Sci* 51:627–659
- Oster G (1950) Two phase formation in solutions of tobacco mosaic virus and the problem of long range forces. *J Gen Physiol* 33:445–473
- Palfy-Muhoray P, Cao W, Moreira M, Taheri B, Munoz A (2006) Photonics and lasing in liquid crystal materials. *Philos Transact A Math Phys Eng Sci* 364:2747–2761
- Rädler JO, Koltover I, Salditt T, Safinya CR (1997) Structure of DNA-cationic liposome complexes: DNA intercalation in multilamellar membranes in distinct interhelical packing regimes. *Science* 275:810–814
- Rathore O, Sogah DY (2001) Self-assembly of beta-sheets into nanostructures by poly(alanine) segments incorporated in multiblock copolymers inspired by spider silk. *J Am Chem Soc* 123:5231–5239
- Revol JF, Bradford H, Giasson J, Marchessault RH, Gray DG (1992) Helicoidal self-ordering of cellulose microfibrils in aqueous suspension. *Int J Biol Macromol* 1992(14):170–172
- Revol J-F, Godbout JDL, Gray DG (1995) International Patent WO 95/21901

- Robinson C (1966) The cholesteric phase in polypeptide solutions and biological structures. *Mol Cryst* 1:467–494
- Roman M, Gray DG (2005) Parabolic focal conics in self-assembled solid films of cellulose nanocrystals. *Langmuir* 21:5555–5561
- Safinya CR (2006) Biophysics and biomaterials. In: Fraser G (ed) *The new physics for the twenty-first century*. Cambridge University Press, Cambridge
- Safinya CR, Liang KS, Varady WA, Clark NA, Andersson G (1984) Synchrotron X-ray study of the orientational ordering D2-D1 structural phase transition of freely suspended discotic strands in triphenylene-hexa-dodecanoate. *Phys Rev Lett* 53:1172–1175
- Safinya CR, Raviv U, Needleman DJ, Zidovska A, Choi MC, Ojeda-Lopez MA, Ewert KK, Li Y, Miller HP, Quispe J, Carragher B, Potter CS, Kim MW, Feinstein SC, Wilson L (2011) Nanoscale assembly in biological systems: from neuronal cytoskeletal proteins to curvature stabilizing lipids. *Adv Mater* 23:2260–2270
- Saito T, Kimura S, Nishiyama Y, Isogai A (2007) Cellulose nanofibers prepared by TEMPO mediated oxidation of native cellulose. *Biomacromolecules* 8:2485–2491
- Saminathan M, Pillai CKS (2000) Synthesis of novel liquid crystalline polymers with cross-linked network structures. *Polymer* 41:3103–3108
- Shopsowitz KE, Qi H, Hamad WY, MacLachlan MJ (2010a) Free-standing mesoporous silica films with tunable chiral nematic structures. *Nature* 2010(468):422–426
- Shopsowitz KE, Qi H, Hamad WY, MacLachlan MJ (2010b) Free-standing mesoporous silica with tunable chiral nematic structures. *Nature* 468:422–426
- Shopsowitz KE, Hamad WY, MacLachlan MJ (2011) Chiral nematic mesoporous carbon derived from nanocrystalline cellulose. *Angew Chem Int Ed* 50:10991–10995
- Shopsowitz KE, Stahl A, Hamad WY, MacLachlan MJ (2012) Hard templating of nanocrystalline titanium dioxide with chiral nematic ordering. *Angew Chem Int Ed Engl* 51:6886–6890
- Stegemeyer H (1999) *Lyotrope flüssigkristalle: Grundlagen, Entwicklung, Anwendung*. Steinkopff/Springer-Verlag, Darmstadt/Berlin
- Swatloski RP, Spear SK, Holbrey JD, Rogers RD (2002) Dissolution of cellulose with ionic liquids. *J Am Chem Soc* 124:4974–4975
- Takanishi Y, Ohtsuka Y, Suzuki G, Nishimura S, Takezoe H (2010) Low threshold lasing from dye-doped cholesteric liquid crystal multi-layered structures. *Opt Express* 18:12909–12914
- Takezoe H (2010) Broadband cavity-mode lasing from dye-doped nematic liquid crystals sandwiched by broadband cholesteric liquid crystal Bragg reflectors. *Adv Mater* 22:2680–2684
- Tseng SL, Laivins GV, Gray DG (1982) Esterification of 2-hydroxypropyl cellulose (HPC). *Macromolecules* 15:1262–1264
- Unger EC, Lund PJ, Shen DK, Fritz TA, Yellowhair D, New TE (1992) Nitrogen-filled liposomes as a vascular US contrast agent: preliminary evaluation. *Radiology* 185(2):453–456
- Van Winkle DH, Clark NA (1982) Freely suspended strands of tilted columnar liquid crystal phases: one dimensional nematics with orientational jumps. *Phys Rev Lett* 48:1407–1410
- Wang N, Ding E, Cheng RS (2008) Preparation and liquid crystalline properties of spherical cellulose nanocrystals. *Langmuir* 24(1):5–8
- Zhang Y, Yang S, Chen L, Evans JRG (2008) Shape changes during the drying of droplets of suspensions. *Langmuir* 24:3752–3758
- Zidovska A, Evans HM, Ewert KK, Quispe J, Carragher B, Potter CS, Safinya CR (2009) Liquid crystalline phases of dendritic lipid–DNA self-assemblies: lamellar, hexagonal and DNA bundles. *J Phys Chem B* 113:3694–3703

Chapter 10

Light-Emitting Field-Effect Transistors with π -Conjugated Liquid Crystalline Polymer

Hisao Yanagi, Yusuke Ohtsuka, Tatsuya Muneishi, and Atsushi Ishizumi

10.1 Introduction

10.1.1 Organic Light-Emitting Field-Effect Transistor

Along with commercialization of organic light-emitting diodes (OLEDs) (Tang and VanSlyke 1987; Sheats et al. 1996), much attention has now been paid on practical applications of organic optoelectronic devices such as organic field-effect transistors (OFETs) (Kudo et al. 1984) and organic photovoltaic (OPV) cells (Tang 1986). In OLEDs, the active layers are mostly composed of amorphous films of vapor-deposited small molecular species. In order to make more use of organic materials advantages, such as low cost, low temperature processing, and flexibility, further efforts have been made to develop polymeric thin film devices which are accessible by wet and printable processes (Broughes et al. 1990; Tsumura et al. 1986). On the other hand, OFET researches have been extensively performed with polycrystalline films of pentacene molecules (Kelly et al. 2003) and higher carrier mobility performances was reported for single crystals of small molecular materials such as rubrene (Takeya et al. 2007). In recent years, high-mobility OFETs comparable to single-crystal devices have also been reported for solution-processed polymeric films one after another.

In conjunction with the research progresses of OLEDs and OFETs, novel organic thin film devices, organic light-emitting field-effect transistors (OLEFETs), have been developed. This device combines charge carrier transport and light-emitting functions in a single device by using fluorescent molecular films as the active layer of OFET. The first successful OLEFET has been reported for vacuum-deposited tetracene films (Hepp et al. 2003). Then, polymeric OLEFETs have also

H. Yanagi (✉) • Y. Ohtsuka • T. Muneishi • A. Ishizumi
Graduate School of Materials Science, Nara Institute of Science and Technology, 8916-5
Takayama, Ikoma, Nara 630-0192, Japan
e-mail: yanagi@ms.naist.jp

been achieved by solution-casting methods (Ahles et al. 2004; Sakanoue et al. 2004). Under ambipolar carrier injection regime, a virtual p/n junction is formed in the channel between the source and drain electrodes by applying appropriate gate voltages. Transported electrons and holes from the opposite electrodes are recombined inside the channel and light emission occurs in a narrow line (Swensen et al. 2005; Zaumseil et al. 2006; Yamane et al. 2007). The line-shaped emission zone can be controlled to be apart from the electrodes, therefore, a quenching loss of emitted light at the electrode interface is reduced. Since the ambipolar channel is formed in a few-nm-thick layer of the active layer in contact with the dielectric surface, high density carriers flow within such a thin channel region. Single-crystal tetracene and rubrene OLEFETs demonstrated current density of several kA cm^{-2} by assuming one monolayer of accumulation thickness (Takenobu et al. 2008). Moreover, the maximum current density of 33 kA cm^{-2} was attained for a single-crystal OLEFET of a thiophene/phenylene co-oligomer (TPCO) (Sawabe et al. 2012).

10.1.2 Towards Organic Semiconductor Laser

Such an achievement of high current density in OLEFETs envisages us to realize organic semiconductor lasers (OSLs) by using molecular single crystals. Moreover, lateral propagation and linear confinement of the high-density carriers seem to be favorable to construct OSLs (Baldo et al. 2002). In fact, organic lasing has already been achieved under optical excitation for a number of small-molecular single crystals (Fichou et al. 1997; Horowitz et al. 1998; Ichikawa et al. 2005) as well as polymeric amorphous films (Tessler et al. 1996; Hide et al. 1996). However, organic lasing under electrical pumping is still challenging and no research has been succeeded yet by using OLEFETs. With an increase of current density beyond $\sim 1 \text{ kA cm}^{-2}$, the luminance of emitted light is rolled off. This is considered to be caused by annihilation processes among singlet, triplet excitons and polarons (Baldo et al. 2002) if high-density excited species are generated in such a low-dimensionally confined region of a few-nm scale. By contrast, the thickness of single-crystal cavity composed of those small molecules is typically a few μm , therefore, a sufficient number of excitons required for optical gain is not generated throughout the whole single-crystal medium under the ambipolar carrier injection regime. Consequently, the principle criteria of lasing with light amplification above a certain threshold of current density has not yet been observed.

In order to overcome such insufficient exciton accumulation within the active layer for OSL, alternate current (AC) gate operation of OLEFETs has been proposed (Yamao et al. 2008). Under the usual DC-gate operation, the ambipolar carrier injection occurs in a specific range of gate biases near the threshold voltages where the source-drain current by simultaneously injected electrons and holes is decreased as compared to that in unipolar transport regime. In the AC-gate operation, on the other hand, electrons and holes are alternately injected from oppositely

biased source and drain electrodes, respectively, and are diffused in the channel of crystal cavity. Electrons (holes) recombine with holes (electrons) which are accumulated in the previous half cycle of the AC gate voltage. The first AC-gate operation proposed by Yamao et al. (2008) was performed for a single-crystal OLEFET with TPCO. Under sinusoidal wave gate bias, the device exhibited an evolution of electroluminescence (EL) when the gate amplitude and frequency were increased. After this first demonstration of AC-gate operation, light-emitting performance has been improved by applying square-wave gate voltages to the single-crystal TPCO device (Yamao et al. 2010). The quick switch of the gate polarity in the square wave enabled efficient carrier recombination so that intense electroluminescence peaks were observed at each instance when the gate polarity changed. This light-emitting recombination under the AC-gate operation which may occur in thicker region of the single-crystal channel is favorable for efficient light emission towards OSL. Actually, Yamao et al. (2010) observed a narrowed emission peak in its electroluminescence spectrum under the square-wave AC-gate operation at 20 kHz. Although it needs to further confirm that this emission is really gain-narrowed with a certain threshold, this result noteworthy envisages us to realize organic lasers by this method.

10.1.3 *Light-Emitting Liquid-Crystalline Polymer*

Those single-crystalline media of small molecules like TPCOs are promising candidates for OSL owing to their high carrier mobility and light confinement structure with an excellent cavity quality. However, those molecular single crystals are very fragile and difficult to be directly grown on the substrate of OLEFET in particular with controlled dimensions for practical device fabrication. Therefore, the AC-gate operation should be also applied to polymeric materials for future flexible light-emitting devices. In view of these research backgrounds, we have started investigating the AC-gate operation of polymeric OLEFETs. Among a variety of light-emitting polymeric semiconductors, we have employed a liquid crystalline co-polymer consisting of π -conjugation with thiophene/fluorene units. Resembling TPCO which is a co-oligomer species of π -conjugating thiophene/phenylene, the thiophene/fluorene co-polymer exhibits ambipolar characteristics (Zheng et al. 2007). In particular, the π -conjugating backbone modified with side alkyl chains crystallize in a nematic phase. This liquid crystallization causes parallel orientation of the thiophene/fluorene planes which promotes carrier transport along the stacking direction of those π -electronic planes. On this basis, ambipolar carrier transports and electroluminescence were demonstrated for those copolymer thin films under conventional DC-operation of OLEFETs (Kajii et al. 2010). According to the reported energy levels of the highest occupied molecular orbital (HOMO) and lowest unoccupied molecular orbital (LUMO) of the thiophene/fluorene copolymer, the energy barrier for electron injection is higher than that for hole injection. Therefore, the light-emitting recombination is typically

obtained in the hole enhancement mode where the accumulated holes recombine with electrons at the drain electrode edges. For further progress of this liquid-crystalline co-polymer OLEFETs, we have investigated ambipolar characteristics and light-emitting behaviors under a variety of conditions of AC-gate operations for spin-coating thin films which are thermally annealed to different crystalline phases (Ohtsuka et al. 2012; Muneishi et al. 2014).

10.2 Preparation and Characterization of Liquid-Crystalline Polymer

10.2.1 Thin Film Preparation

As a liquid-crystalline thiophene/fluorene co-polymer, we chose poly [(9,9-dioctylfluorenyl-2,7-diyl)-co-bithiophene] (F8T2, Fig. 10.1a). A commercially available grade of F8T2 (Aldrich, $M_n > 20,000$) was used without further purification. Prior to thin film preparation, thermal properties of the F8T2 sample was examined by differential scanning calorimetry (DSC). The F8T2 powder exhibited a glass transition at $T_g = 125.5$ °C, and thermotropic transitions to the nematic phase at $T_m = 259.3$ °C and to the isotropic one at $T_i = 311.6$ °C. These phase transitions are almost identical to those reported in the literature (Kinder et al. 2004). For thin film preparation, 5.0 mg of F8T2 powder was dissolved in 1 mL chloroform. The solution was spin-coated on a substrate at 3000 rpm for 60 s. A glass slide ($10 \times 10 \times 1.1$ mm³) coated with indium-tin-oxide (ITO) was used as substrate. The ITO coating was served as a conductive electrode in the following OLEFET fabrication (Fig. 10.1b). According to the DSC result, the F8T2 films was annealed at specific temperatures in a range of 80–350 °C. After keeping for 30 min at the respective temperature, the film was cooled to room temperature at a rate of -60 °C/min in nitrogen.

10.2.2 Optical Characterization

During those thermal annealing processes, we observed morphological changes of the F8T2 films by in situ polarized transmission optical microscopy using an Olympus BX-51 microscope with a heating stage under nitrogen gas flow. The films at 80 and 150 °C showed completely dark images under the cross-Nicole polarization suggesting that those films were amorphous without containing any crystalline domains. When the annealing temperature was increased to 250 °C, ordering of polymer chains started to occur in the film so that the image showed partially transmitted regions. Further increase to 290 °C changed the image exhibiting bright grain structure with the nematic liquid-crystalline phase. With

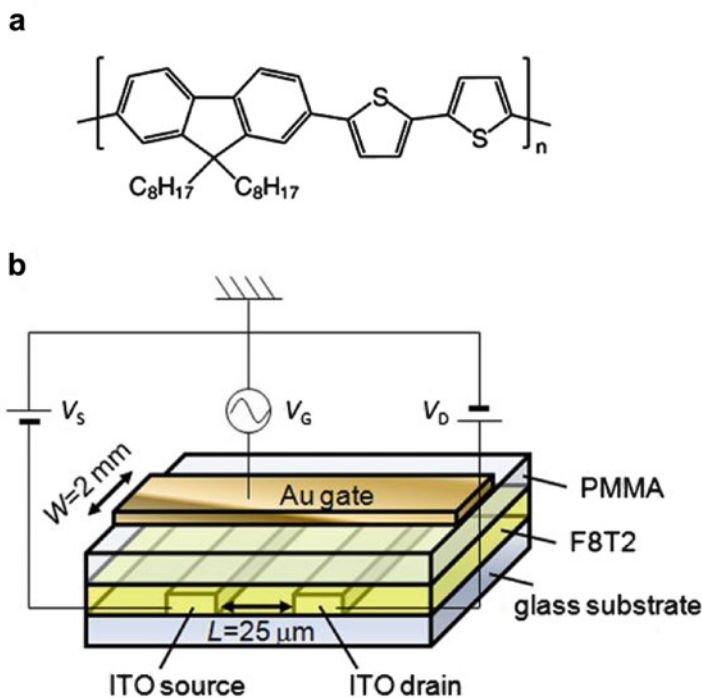


Fig. 10.1 Molecular structure of F8T2 (a) and schematic diagram of bottom-contact/top-gate OLEFET structure (b). Reproduced from Muneishi T, Ishizumi A, Yanagi H (2014) Annealing effect on light-emitting FET characteristics of π -conjugated liquid crystalline polymer. *Jpn. J. Appl. Phys.* 53: 01AB17 with permission from The Japan Society of Applied Physics

elevating annealing temperature up to 350 °C, the image turned dark again indicating that the film melted to an isotropic phase. After cooling to room temperature, the thickness of thus heat-treated F8T2 films was measured to be about 50 nm by a thickness profiler (Tenchor Alpha-Step). Temperature-dependent film structures of those cooled samples were also examined by optical microscopy. Figure 10.2 shows transmission micrographs under the cross-Nicole polarization for the F8T2 films annealed at 250, 290, and 350 °C, and then cooled to room temperature. The dark image in Fig. 10.2a indicates that the film annealed at 250 °C is almost amorphous although some portion of the film was crystallized. By contrast, the films annealed at 290 °C shows bright transmission as shown in Figs. 10.2b. The film consists of microcrystalline grains with a size of $\sim 10 \mu\text{m}$ suggesting that the quenching from this temperature gives rise to formation of the nematic phase. As compared to the dark image under in situ observation during annealing at 350 °C, the film cooled from 350 °C shows homogeneous transmission as shown in Fig. 10.2c. It indicates that the film crystallizes in homogeneous structure with finer grains when the film is quenched from the isotropic phase at 350 °C.

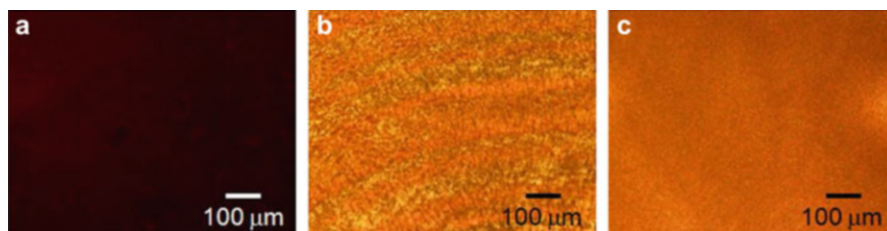


Fig. 10.2 Transmission optical micrographs of the F8T2 films annealed at 250 (a), 290 (b), and 350 °C (c) taken with cross-Nicole polarization. Reproduced from Muneishi T, Ishizumi A, Yanagi H (2014) Annealing effect on light-emitting FET characteristics of π -conjugated liquid crystalline polymer. *Jpn. J. Appl. Phys.* 53: 01AB17 with permission from The Japan Society of Applied Physics

10.2.3 Crystalline Structure

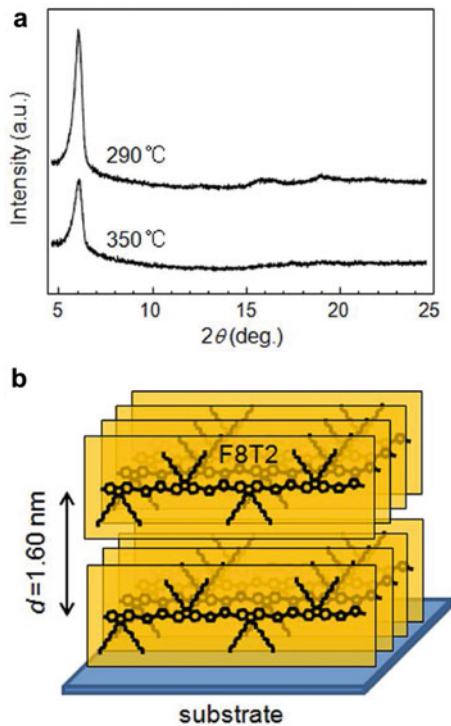
Crystalline structures of those F8T2 films were examined by X-ray diffraction (XRD) using an X-ray diffractometer (Rigaku, RINT-TTRIII/NM). Figure 10.3a shows $2\theta/\theta$ patterns of the films quenched from the annealing temperatures of 290 and 350 °C. Both patterns exhibit a single peak at 5.5° which corresponds to $d = 1.6$ nm. This spacing arises from the interchain distance between the stacked F8T2 lamellae in which the F8T2 chains are lying parallel on the substrate plane. According to these crystallographic observations by polarized optical microscopy and XRD, the film structure is estimated as is schematically shown in Fig. 10.3b. In the film quenched from 290 °C (Fig. 10.2b), the nematic domains are crystallized with this lamellae structure. Due to formation of these microcrystalline grains, this film contains a number of grain boundaries which affect the OLEFET characteristics as mentioned in the following section. On the other hand, there is no remarkable grains in the film annealed at 350 °C (Fig. 10.2c) suggesting that the quenching from the isotropic temperature formed less ordered fine crystallites in homogeneous morphology.

10.3 Light-Emitting Field-Effect Transistor with Liquid-Crystalline Polymer

10.3.1 Device Fabrication and Measurement Methods

Bottom-contact/top-gate OLEFET devices were fabricated as schematically shown in Fig. 10.1b. Onto a glass substrate ($1.0 \times 1.0 \times 1.1$ cm²), ITO coating with a resistivity of 9–15 Ω/sq is patterned in stripes of 200 μm width and 200 nm thickness. The gap between the ITO stripes is 25 μm . A pair of stripe-patterned ITO is served as the source/drain electrodes. After ultrasonic cleaning with

Fig. 10.3 (a) XRD patterns of the F8T2 films annealed at 290 and 350 °C. (b) Schematic diagram of presumed molecular alignment in the F8T2 film. Reproduced from Muneishi T, Ishizumi A, Yanagi H (2014) Annealing effect on light-emitting FET characteristics of π -conjugated liquid crystalline polymer. *Jpn. J. Appl. Phys.* 53: 01AB17 with permission from The Japan Society of Applied Physics



detergent, deionized water, acetone and ethanol, the ITO/glass surface was treated by UV/ozone exposure. As mentioned in the previous section, the F8T2 solution was spin-coated on the ITO/glass surface at 3000 rpm for 60 s. The casted film was annealed at 80, 150, 250, 290, and 350 °C in nitrogen gas flow for 30 min. After cooling to room temperature, the thickness of the deposited film was measured to be about 50 nm by a thickness profiler (Tenchor Alpha-Step). To construct the top-gate device, the F8T2 film was covered with a dielectric layer of polymethyl methacrylate (PMMA). A 900 mg/10 mL propylene glycol monomethyl ether acetate (PGMEA) solution of PMMA was spin-coated at 3000 rpm for 60 s. After drying at 80 °C for 30 min in nitrogen, the thickness of the PMMA film was 700–850 nm. On top of the PMMA dielectric layer, a gold (Au) film (2 mm wide and ~30 nm thick) was vacuum-deposited as a gate electrode. Consequently, the fabricated OLEFET has bottom-contact ITO source/drain electrodes with channel length $L = 25 \mu\text{m}$ and a Au top-gate channel with channel width $W = 2 \text{ mm}$ as schematically shown in Fig. 10.1b.

Field effect transistor and light-emitting characteristics were measured at room temperature in vacuum. The fabricated device was loaded in a chamber equipped with three tungsten needle probes and evacuated in a vacuum of 10^{-5} mbar. DC current–voltage output and transfer characteristics were measured using a semiconductor characterization system (KEITHLEY 4200). For AC-gate operations, a

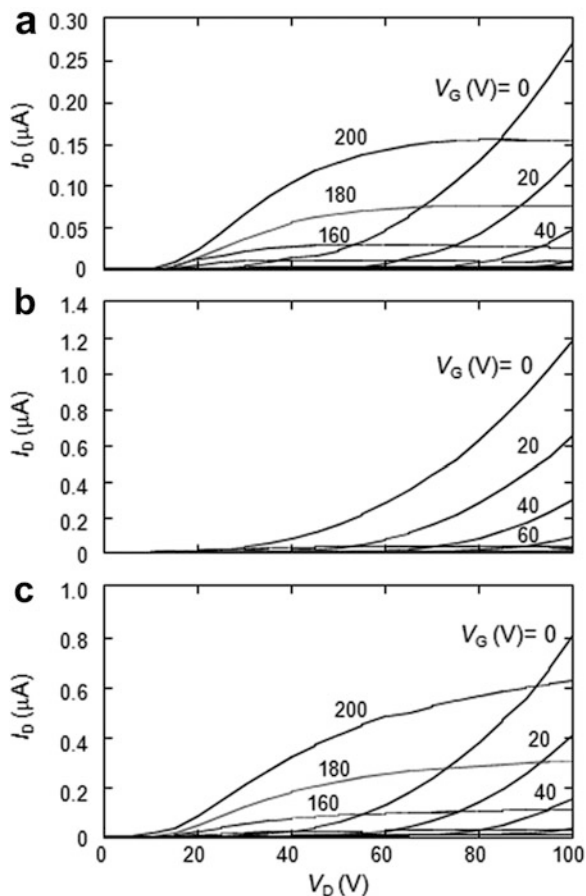
bi-polar power supply (Matsusada POPF120-2.5) and two DC power supplies (Takasago EX-375 L2) were connected as is shown with a circuit diagram in Fig. 10.1b. Electroluminescence (EL) was observed through a top window of the chamber using a stereo microscope (Olympus SZX-12) with a long WD objective lens (Mitsutoyo M Plan Apo 10x). The light intensity was measured with a photomultiplier (Hamamatsu Photonics R1477-561). Time responses of the light intensity was recorded as a function of the AC-gate voltage waves using a digital multimeter (Advantest R6551) and a digital oscilloscope (Tektronics TDS 3052B).

10.3.2 Transistor Characteristics Under DC Operation

The field-effect transistor characteristics of the OLEFET devices fabricated with different F8T2 films were first characterized under DC-gate operations. Figure 10.4 shows output characteristics of the F8T2 films quenched from annealing temperatures of 250, 290 and 350 °C. Drain current (I_D) was plotted as a function of drain voltage (V_D) under positive gate voltage (V_G) varying from 0 to 200 V. When the V_D was positively swept at constant V_G lower than 100 V, the positive I_D increased with an elevation of V_D for all three films. This I_D - V_D behavior is attributed to hole transport from the drain to the source electrode. When V_G is increased beyond 100 V, this hole current is extinct and the I_D - V_D curves change to the saturation regime at higher V_D due to electron injection from the source electrode. With increasing V_D , the drain current is saturated since the electron channel is pinched off when the V_D increases close to V_G . For the films annealed at 250 and 350 °C (Fig. 10.4a, c, respectively), this electron transport is clearly seen with saturated currents which are comparable to the hole currents observed at lower V_G . It demonstrates that these F8T2 films have well-balanced ambipolar characteristics. By contrast, the electron current is very low for the film annealed at 290 °C (Fig. 10.4b) indicating that unipolar hole transport is dominant in this film.

The hole and electron mobility (μ_h and μ_e) are estimated from the saturated regime of I_D for the F8T2 films annealed at different temperatures and summarized in Fig. 10.5a. The hole transport was obtained for all films and μ_h was estimated from the hole saturation regime of $V_D < 0$ and $V_G < 0$: $\mu_h = 2.5 \times 10^{-4}$, 6.4×10^{-5} , 2.5×10^{-4} , 9.7×10^{-4} and 9.8×10^{-4} cm² V⁻¹ s⁻¹ for the films annealed at 80, 150, 250, 290 and 350 °C, respectively. Electron transport was not obtained for the films annealed at 80 and 150 °C probably because their random chain conformation formed by annealing at lower temperature does not enable intermolecular electron hopping. The electron transport was observed when the film is annealed above 250 °C: $\mu_e = 7.8 \times 10^{-5}$, 4.4×10^{-5} and 3.7×10^{-4} cm² V⁻¹ s⁻¹ for the films annealed at 250, 290 and 350 °C, respectively. The μ_h of the film annealed at 350 °C is as same as that at 290 °C while its μ_e remarkably increased as compared to that at 250 °C. The μ_e of the film annealed at 290 °C slightly decreased in comparison with the film annealed at 250 °C while its μ_h increased four times as high as that at 250 °C.

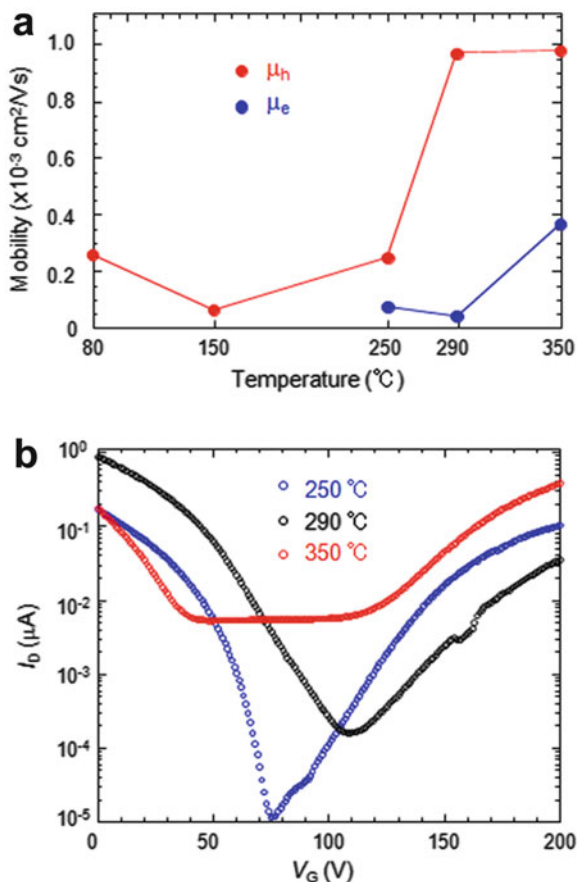
Fig. 10.4 Output characteristics of OLEFETs with the F8T2 films annealed at 250 (a), 290 (b), and 350 °C (c). Reproduced from Muneishi T, Ishizumi A, Yanagi H (2014) Annealing effect on light-emitting FET characteristics of π -conjugated liquid crystalline polymer. *Jpn. J. Appl. Phys.* 53: 01AB17 with permission from The Japan Society of Applied Physics



The observed ambipolarity for the present bottom-contact/top-gate device is owing to the PMMA dielectric layer which prevents electron trapping. However, it is noted that the threshold voltage for electron injection is considerably higher than that for hole injection estimated in the electron and hole enhancement mode, respectively. This difference is attributed to the HOMO and LUMO energies of F8T2 with respect to the electronic energy of the source/drain ITO electrodes. From the reported values of $E_{\text{HOMO}}/E_{\text{LUMO}} = -5.6/-3.2$ and $E_{\text{ITO}} = -4.8$ eV (Hamasaki et al. 2009), there is a higher injection barrier to electrons than to holes.

In Fig. 10.5b transfer characteristics are compared at $V_D = 100$ V for the F8T2 films annealed at 250, 290 and 350 °C. The I_D of the film annealed at 290 °C is remarkably lower in the electron transport regime at $V_G > 100$ V while the highest hole current is obtained at the low V_G region for this film. It is reported that the electron transport is blocked at grain boundaries (Koiwai et al. 2011). As seen in Fig. 10.2b, the F8T2 film quenched from the nematic phase at 290 °C formed a large number of boundaries among the microcrystalline grains. On the other hand,

Fig. 10.5 (a) Dependence of carrier mobilities in the F8T2 films on annealing temperatures from 80 to 350 °C. (b) Transfer characteristics of OLEFETs with the F8T2 films annealed at 250, 290, and 350 °C. Reproduced from Muneishi T, Ishizumi A, Yanagi H (2014) Annealing effect on light-emitting FET characteristics of π -conjugated liquid crystalline polymer. Jpn. J. Appl. Phys. 53: 01AB17 with permission from The Japan Society of Applied Physics



the hole currents decreased for the film annealed at 250 °C while its electron current increased as compared to that of the film annealed at 290 °C, resulting in a balanced ambipolar transport. This ambipolar behavior is also obtained for the film annealed at 350 °C with further increase of electron currents. It suggests that the entangled polymer chains in the polycrystalline film quenched from the isotropic phase at 350 °C promote in particular electron hopping. The microcrystalline structure in the film annealed at 250 °C has also ambipolar characteristics with well-balanced electron and hole currents when the gate voltages are appropriately applied for each carrier injection. However, its I_D value remarkably falls in the order of $10^{-5} \mu\text{A}$ at the voltage where the transfer characteristics change from hole transport regime to electron one. It suggests that the microcrystalline boundaries are also obstacle for carrier transport in particular at insufficient bias voltages.

The dependences of obtained carrier mobilities and transfer characteristics on annealing temperature suggest that the crystalline structure in the annealed films differently affect the transport of holes and electrons. Basically both carrier transports are improved by crystallization within the grains. In particular, the μ_h is

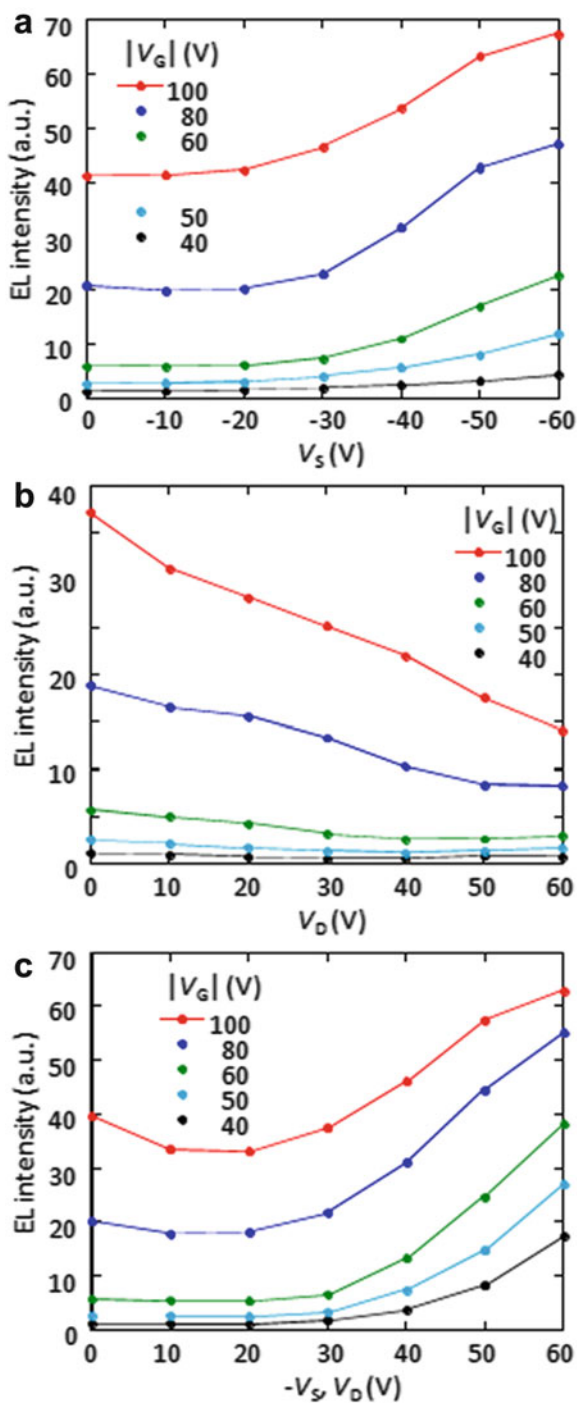
increased by interchain ordering and not sensitive to grain boundaries formed at higher annealing temperature. By contrast, the μ_e is considerably lowered by electron trapping at the grain boundaries in the microcrystalline film quenched from the liquid-crystalline phase annealed at 290 °C. As a consequence, the crystalline film with the nematic structure shows deteriorated ambipolar characteristics as compared to the less crystalline films annealed at 250 and 350 °C.

10.3.3 Light-Emitting Characteristics Under AC-Gate Operation

As mentioned in the previous section, transfer characteristics of the OLEFETs (Fig. 10.5b) indicate that the amipolar currents when electrons and holes are simultaneously injected are quite low in the wide region of V_G . Therefore, the light intensity was very weak under those conditions of DC-gate operations. Brighter light emission was obtained in the hole enhancement mode where the accumulated holes recombine with electrons injected at the drain electrode edge. On the other hand, under AC-gate operation a large number of holes and electrons can be alternately injected from appropriately biased source and/or drain electrodes resulting in light emission by recombination of accumulated geminate carriers. Hereafter, the fabricated OLEFETs were investigated under AC-gate operations.

Since it is expected that light-emitting performances depend on ambipolar characteristics, the AC-gate operation was carried out under different conditions of source/drain voltages, gate amplitude, gate waveform, and gate frequency using F8T2 films annealed at 350 °C. It is reported that electroluminescence is enhanced when a square wave AC voltage is applied to the gate electrode instead of a sinusoidal wave (Yamao et al. 2008, 2010). In the present study, therefore, light emission properties of the OLEFETs were measured under square-wave gate operations. Figure 10.6 shows dependences of light intensity on V_S and V_D under the square-wave gate frequency at $f=20$ kHz and amplitudes at $|V_G|=40, 50, 60, 80$ and 100 V. As shown in Fig. 10.6a, the V_S is first negatively biased from 0 to -60 V at $V_D=0$ V. Unexpectedly, light emission was obtained when the source and drain electrodes were not biased, i.e. $V_S=V_D=0$ V. The light intensity does not increase with decreasing V_S up to -20 V. Further negative biasing of $V_S < -20$ V increases the light intensity since the electron injection from both edges of the source electrode increases. On the other hand, the light intensity decreases as the V_D is positively biased at $V_S=0$ V in particular at higher $|V_G|$ as shown in Fig. 10.6b. The positive V_D bias remarkably decreases the electron injection from the drain electrode. When the negative V_S and positive V_D are applied with the same amplitude, the light intensity is first kept constant then increases with an elevation of $|V_S|$ and $|V_D|$ at $|V_G|=40, 50$ and 60 V as seen in Fig. 10.6c. When the $|V_G|$ is increased to 80 and 100 V the light intensity first decreases at $|V_S|=|V_D|=0-10$ V, and then increases at $|V_S|=|V_D| > 20$ V. These

Fig. 10.6 Dependences of light intensity on V_S at $V_D = 0$ V (a), on V_D at $V_S = 0$ V (b) and on $-V_S = V_D$ (c) obtained from OLEFET with F8T2 film annealed at 350 °C at different $|V_G|$. Reproduced from Ohtsuka Y, Ishizumi A, Yanagi H (2012) Light-emitting field-effect transistors with π -conjugated liquid-crystalline polymer driven by AC-gate voltages. *Org. Electron* 13: 1710–1715 with permission from Elsevier B.V.

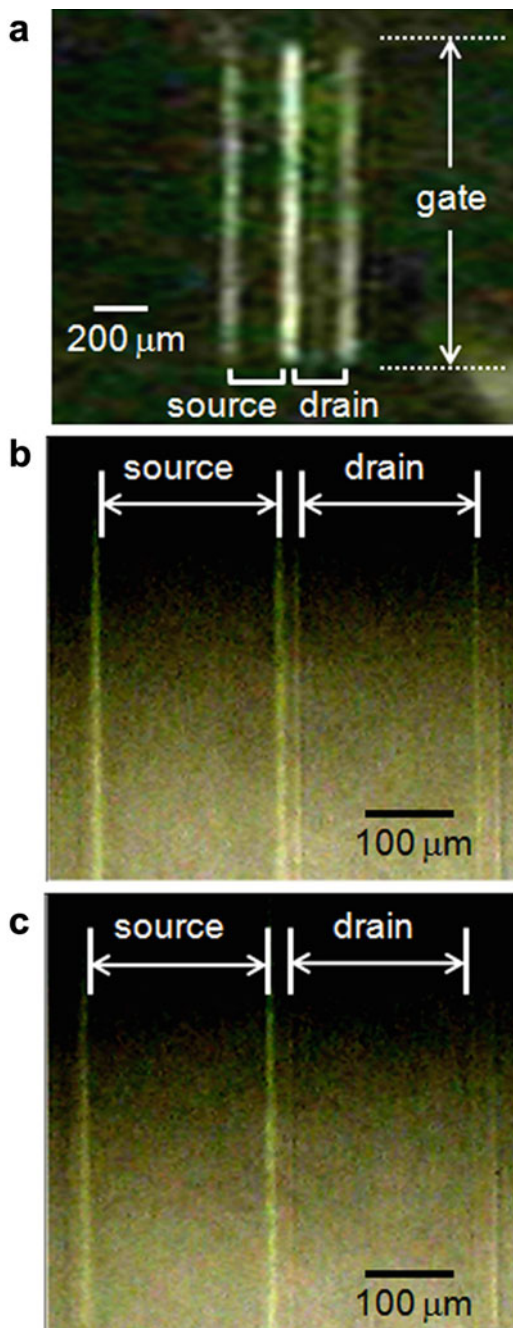


voltage-dependences in Fig. 10.6c are qualitatively explained by combining the results in Fig. 10.6a, b. However, it is noted that the light intensities at higher $|V_S|$ and $|V_D|$ in Fig. 10.6c are enhanced as compared to those estimated from the increase in Fig. 10.6a and the decrease in Fig. 10.6b.

We discuss first why the light emission is obtained at $V_S = V_D = 0$ V under AC-gate operation. As shown in Fig. 10.6a, the light intensity increases with an elevation of $|V_G|$ at $V_S = V_D = 0$ V. When the frequency f of square-wave gate biases is increased in a range of 1 Hz–20 kHz, the light intensity is also increased. Figure 10.7a shows a top-view image of the device driven at $V_S = V_D = 0$, $|V_G| = 120$ V and $f = 20$ kHz. The light emission is visible through the top-gate layer of Au crossing with a pair of the source/drain electrodes. The light emission appears not only at the center channel region but also at the left edge of the source electrode and the right edge of the drain electrode. The light intensity is higher at the center channel than at the outer edges. It suggests that the light emission occurs at the both side edges of the source and drain electrodes although the emission at the center channel is not well-resolved in this stereomicroscopic image. To clarify the appearance of light emission, the probe contact to the drain electrode was retracted so that the AC gate operates only against the source electrode. As a result, the light emission was observed only at the both side edges of the source electrode with same intensity. Similarly, the light emission occurred at the both edges of the drain electrode when the probe contact to the source electrode was retracted. These behaviors can be explained by the emission process reported for oligothiophene derivatives (Liu et al. 2010). The electron and hole carriers are alternately injected at each electrode under the AC-wave bias to the gate. In the positive half cycle of V_G , electrons are injected from the source and drain electrodes since both electrodes are grounded. When the V_G is switched to the negative half, holes are injected from both electrodes. These injected electrons (holes) recombine with the holes (electrons) accumulated in the previous half cycle of V_G . With increasing $|V_G|$ and f , the amount of accumulated carriers and the recombination cycles increase resulting in higher emission intensity. In Fig. 10.7a, the light emission is not observed in the stripe area of the source and drain electrodes of ITO. It is probably because the electric field is enhanced at the ITO step edge since the thickness of the F8T2 layer (50 nm) is considerably thin as compared to that of the ITO coating (200 nm). As a result, the carrier injection is enhanced at the step edges of ITO electrodes where a high electric field is concentrated.

In order to elucidate carrier injection and recombination dynamics, we observed time responses of light intensity with respect to the AC-gate wave. Figure 10.8a shows a time profile taken at $V_S = V_D = 0$ V with respect to the square-wave AC gate bias of $|V_G| = 120$ V and $f = 1$ kHz as is shown in Fig. 10.8e. It indicates that the light intensity rises steeply when the gate is switched to positive V_G and then gradually decays in the positive half period of V_G . On the other hand, the emission intensity appears in a sharp peak and immediately extinct when the V_G is switched to negative. It suggests that the amount of electrons accumulated in the half cycle of positive V_G is considerably smaller than that of holes accumulated in the half cycle of negative V_G . As mentioned in the Sect. 10.3.2., it is attributed to the higher

Fig. 10.7 Top-view micrographs of light emission from OLEFET with F8T2 film annealed at 350 °C under operations at $V_S = V_D = 0$ V, $|V_G| = 120$ V and $f = 20$ kHz (a), $V_S = -60$ V, $V_D = 0$ V, $|V_G| = 100$ V, $f = 20$ kHz (b) and $V_S = -60$ V, $V_D = 60$ V, $|V_G| = 100$ V, $f = 20$ kHz (c). Reproduced from Ohtsuka Y, Ishizumi A, Yanagi H (2012) Light-emitting field-effect transistors with π -conjugated liquid-crystalline polymer driven by AC-gate voltages. *Org. Electron* 13: 1710–1715 with permission from Elsevier B.V



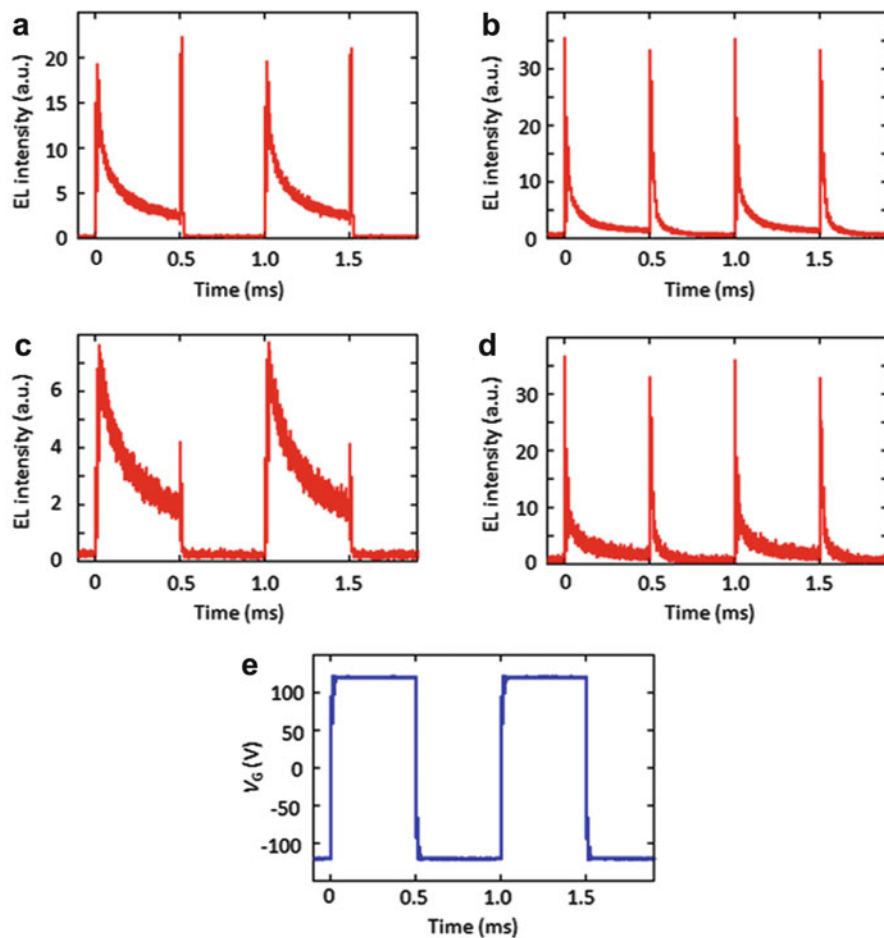


Fig. 10.8 Time responses of light intensity taken from OLEFET with F8T2 film annealed at 350 °C under operations at $V_S = V_D = 0$ V (a), $V_S = -50$ V, $V_D = 0$ V (b), $V_S = 0$ V, $V_D = 50$ V (c), $V_S = -50$ V, $V_D = 50$ V (d) with respect to square-wave form of $V_G = |120|$ V and $f = 1$ kHz (e). Reproduced from Ohtsuka Y, Ishizumi A, Yanagi H (2012) Light-emitting field-effect transistors with π -conjugated liquid-crystalline polymer driven by AC-gate voltages. *Org. Electron* 13: 1710–1715 with permission from Elsevier B.V

injection barrier for electrons than for holes owing to the HOMO/LUMO energies of F8T2 with respect to the work function of ITO source/drain electrodes. Therefore, the duration of the light intensity in the negative half cycles of V_G is very short as compared to in the positive half cycle. Figure 10.8b shows time response of light intensity when the V_S is biased to -50 V. The duration of light emission in the positive half cycles of V_G is shortened while that in the negative half cycles is elongated. The negative bias of V_S increases the electron injection from the source electrode in the positive V_G period while decreases the hole injection from the

source electrode in the negative V_G period. On the other hand, the durations of light emission in the positive and negative V_G cycles are elongated and shortened, respectively, when the V_D is biased to 50 V, as shown in Fig. 10.8c. The positive bias of V_D remarkably decreases the peak intensities when the V_G polarity is switched since the amount of electrons injected from the drain electrode is decreased. Figure 10.8d shows the time response of light intensity when the V_S and V_D are biased to -50 and 50 V, respectively. The peak intensity and duration of light emission are similar to that taken at $V_S = -50$ and $V_D = 0$ V (Fig. 10.8b) suggesting that the electron injection from the negatively biased source electrode is crucial for the light-emitting recombination.

Such dependences of EL characteristics on magnitude and polarity of V_S and V_D under AC-gate operations are further discussed by observing high magnification images of light emission. Figure 10.7b shows an optical micrograph of the device taken at $V_S = -60$ V, $V_D = 0$ V, $|V_G| = 100$ V, $f = 20$ kHz. It shows that the light emission is observed at both side edges of the source and drain electrodes. The light intensity at both edges of the source electrode is higher than that of the drain electrode edges since the negative V_S enhances the electron injection from the source electrode edges. Figure 10.7c shows an image taken at $V_S = -60$ V, $V_D = 60$ V, $|V_G| = 100$ V, $f = 20$ kHz. The light emission is not observed at both edges of the drain electrode while the light intensity at the right-side edge of the source electrode is slightly higher than that at the left-side edge emission. This enhanced emission is ascribed to recombination between electrons injected at the right-side edge of the source and holes which are injected from the drain electrode and transported along the channel. At $V_D = 60$ V, there are few electrons at the drain electrode edge, therefore, the holes are driven to move toward the source electrode biased at $V_S = -60$ V. These findings suggest that the present AC-gate polymer OLEFET can be effectively operated by making the best use of this channel recombination. If interdigitated source/drain electrodes are constructed, enhanced light emission will be obtained at both edges of all source electrodes.

As is expected from above-mentioned time responses and microscopic observations, the light-emitting behavior under AC-gate operations is modified when a sinusoidal AC wave is used as the gate bias. The light intensity in both positive and negative half cycles was decreased than in the case of the square-wave application. The gradual switching of the V_G decreases light-emitting recombination since the accumulation and injection of opposite carries are reduced when the V_G is continuously switched. Time-dependent EL intensity and current flow have been reported for the TPCO-crystal OLEFET operated with sinusoidal AC-gate voltages (Yamao et al. 2008). The time response of the present device operated with a sinusoidal wave ($V_G = |120|$ V and $f = 10$ kHz) at $V_S = V_D = 0$ V resembled this literature results at high f . The light intensity increases in the positive half cycles of V_G while the currents flow only in the negative half cycles of V_G . It suggests that the current is dominated by the holes transported in the channel while the light emission is governed by the injected electrons.

Finally, we compared light-emitting performances of the OLEFETs with F8T2 films annealed at different temperatures in order to examine the effect of crystalline

states as described in Sects. 10.2.3. and 10.3.2. The AC-gate operation was carried out with a square-wave bias of $|V_G| = 100$ V and $f = 20$ kHz for the F8T2 films annealed at 250, 290, and 350 °C. The V_D was set at 0 V while the V_S was at -60 V to enhance the electron transport. The EL intensity increased in the order of annealing temperature of $290 < 250 < 350$ °C. This order coincides with the order of μ_e as shown in Fig. 10.5a. It suggests again that the electron carrier generation is crucial for ambipolar OLEFET performances. Time responses of the EL intensity were also compared for the F8T2 films annealed at 250, 290, and 350 °C. The AC-gate operation was carried out at $-V_S = V_D = 50$ V with a square-wave gate of $|V_G| = 100$ V and $f = 1$ kHz. The time profiles of all films indicate that the light intensity rises steeply when the V_G is switched to positive and then quickly decays in the half period of positive V_G . It indicates again that the electrons injected from the source electrode recombine with the holes accumulated in the previous half cycle of negative V_G for all three devices. When the V_G is switched to negative, the sharp EL peak similarly appears but it immediately quenched in the negative period of V_G since the accumulated electrons in the previous cycle of positive V_G is less persistent. The EL intensity peak in the positive V_G is much higher than that in the negative V_G for the films annealed at 250 and 350 °C. However, this relative difference between the EL peak intensities in the positive and negative V_G cycles is less remarkable for the film annealed at 290 °C although its absolute EL intensity is much lower. It is probably because the electrons trapped at the grain boundaries in the channel contribute to the recombination with holes injected when the V_G is switched to negative. Consequently, the homogeneous F8T2 film obtained by annealing at isotropic temperature of 350 °C is most suitable for light-emitting layer of the present liquid-crystalline OLEFET under AC-gate operation.

10.4 Conclusions

Bottom-contact/top-gate OLEFETs were fabricated with a light-emitting π -conjugated liquid-crystalline thiophene/fluorene co-polymer, F8T2. Thin film structure and transistor characteristics of F8T2 were comparably characterized for spin-coating films which were annealed at different temperatures and quenched to room temperature. The amorphous films annealed far below the thermotropic transition temperature exhibited fully hole-transporting unipolar characteristics owing to random conformation of the F8T2 chains. By annealing at 250 °C close to the transition temperature, the film started to have ambipolar characteristics due to electron transport among partially aligned molecular chains. With increasing annealing temperature at 290 °C, the microcrystalline structure quenched from the nematic phase remarkably reduced the ambipolar transport probably due to electron trapping at the grain boundaries. On the other hand, when the F8T2 film was quenched from the isotropic melt at 350 °C, the device with less-crystallized homogeneous structure showed the highest ambipolar performance.

The fabricated OLEFETs exhibited light emission under AC-gate operations at different conditions of V_S , V_D , $|V_G|$ and f . Light emission was observed at both edges of the source and drain electrodes even at $V_S = V_D = 0$ V by applying square-wave voltages to the gate. According to the polarity switch of AC-gate voltages, electrons and holes are alternately injected from both source and drain electrodes, and recombine with the opposite carriers injected in the previous half cycle of V_G . The light emission is dominated by electron injection due to a higher barrier for electrons from the ITO electrode to the F8T2 film even if the electron and hole mobilities are in the same order of magnitude. As a result, the light intensity increased by applying negative V_S while V_D was kept at 0 V. On the other hand, the light emission is suppressed by applying positive V_D at $V_S = 0$ V. When the V_S and V_D were simultaneously biased negative and positive, respectively, the light intensity was enhanced in the center channel region by recombination between the holes transported from the drain and the electrons injected at the source electrode edge. Further progress of ambipolar liquid-crystalline polymer OLEFETs will be developed with well-designed electronic energy of materials and controlled crystalline morphology. The AC-gate operation with optimized device structures may lead to a new class of flexible light-emitting devices.

This chapter was written by reproducing and rearranging the texts and figures published in Refs. by Ohtsuka et al. (2012) and Muneishi et al. (2014).

This work was supported by Grant-in-Aid for Scientific Research (C) No.22550163 from the Japan Society for the Promotion of Science (JSPS). This work was also supported by the Green Photonics Project of Nara Institute of Science and Technology. The authors thank Mr. Fujiwara, Nara Institute of Science and Technology for his experimental support.

References

- Ahles M, Hepp A, Schmechel R, Segern H (2004) Light emission from a polymer transistors. *Appl Phys Lett* 84:428–430
- Baldo MA, Holmes RJ, Forrest SR (2002) Prospects for electrically pumped organic lasers. *Phys Rev B* 66:035321
- Broughes JH, Bradley DD, Brown AR, Marks RN, Mackay K, Friend RH, Burn PL, Holmes AB (1990) Light-emitting diodes based on conjugated polymers. *Nature* 347:539–541
- Fichou D, Delysse S, Nunzi JM (1997) First evidence of stimulated emission from a monolithic organic single crystal: α -octithiophene. *Adv Mater* 9:1178–1181
- Hamasaki T, Morimune T, Kajji H, Minakata S, Tsuruoka R, Nagamachi T, Ohmori Y (2009) Fabrication and characteristics of polyfluorene based organic photodetectors using fullerene derivatives. *Thin Solid Films* 518:548–550
- Hepp A, Heil H, Weise W, Ahles M, Schmechel R, von Seggern H (2003) Light-emitting field-effect transistor based on a tetracene thin film. *Phys Rev Lett* 91:91157406
- Hide F, Díaz-García MA, Schwartz BJ, Andersson MR, Pei Q, Heeger AJ (1996) Semiconducting polymers: a new class of solid-state laser materials. *Science* 273:1833–1836
- Horowitz Q, Valat P, Garnier F, Kouki F, Wintgens V (1998) Photoinduced spontaneous and stimulated emission in sexithiophene single crystals. *Opt Meter* 9:46–52

- Ichikawa M, Hibino R, Inoue M, Haritani T, Hotta S, Araki K, Koyama T, Taniguchi Y (2005) Laser oscillation in monolithic molecular single crystals. *Adv Mater* 17:2073–2077
- Kajii H, Koiwai K, Hirose Y, Ohmori Y (2010) Top-gate-type ambipolar organic field-effect transistors with indium-tin-oxide drain/source electrodes using polyfluorene derivatives. *Org Electr* 11:509–513
- Kelly TW, Boardman LD, Dunbar TD, Muyres DV, Pellerite MJ, Smith TP (2003) High-performance OFETs using surface-modified alumina dielectrics. *J Phys Chem B* 107:5877–5881
- Kinder L, Kanicki J, Swensen J, Petroff P (2004) *Synth Met* 146:181–185
- Koiwai K, Kajii H, Ohmori Y (2011) Effects of film morphology on ambipolar transport in top-gate-type organic field-effect transistors using poly(9,9-dioctylfluorene-co-bithiophene). *Synth Met* 161:2107–2112
- Kudo K, Yamashina M, Moriizumi T (1984) Field effect measurement organic Dye films. *Jpn J Appl Phys* 23:130
- Liu X, Wallmann I, Boudinov H, Hansen JK, Schiek M, Lutzen A, Rubahn HG (2010) AC-biased organic light-emitting field-effect transistors from naphthyl end-capped oligothiophenes. *Org Electr* 11:1096–1102
- Muneishi T, Ishizumi A, Yanagi H (2014) Annealing effect on light-emitting FET characteristics of π -conjugated liquid crystalline polymer. *Jpn J Appl Phys* 53:01AB17
- Ohtsuka Y, Ishizumi A, Yanagi H (2012) Light-emitting field-effect transistors with π -conjugated liquid-crystalline polymer driven by AC-gate voltages. *Org Electr* 13:1710–1715
- Sakanoue T, Fujiwara E, Yamada R, Tada H (2004) Visible light emission from polymer-based field-effect transistors. *Appl Phys Lett* 84:3037–3039
- Sawabe K, Imakawa M, Nakano M, Yamao T, Hotta S, Iwasa Y, Takenobu T (2012) Current-confinement structure and extremely high current density in organic light-emitting transistors. *Adv Mater* 24:6141–6146
- Sheats JR, Antoniadis H, Hueschen M, Leonard W, Miller J, Moon R, Roitman D, Stocking A (1996) Organic electroluminescent devices. *Science* 273:884–888
- Swensen J, Soci C, Heeger AJ (2005) Light emission from an ambipolar semiconducting polymer field-effect transistor. *Appl Phys Lett* 87:253511
- Takenobu T, Bisri SZ, Takahashi T, Yahiro M, Adachi C, Iwasa Y (2008) High current density in light-emitting transistors of organic single crystals. *Phys Rev Lett* 100:066601
- Takeya J, Yamagishi M, Tominari Y, Hirahara R, Nakazawa Y, Nishikawa T, Kawase T, Shimoda T, Ogawa S (2007) Very high-mobility organic single-crystal transistors with in-crystal conduction channels. *Appl Phys Lett* 80:102120
- Tang CW (1986) Two-layer organic photovoltaic cells. *Appl Phys Lett* 48:183–185
- Tang CW, VanSlyke SA (1987) Organic electroluminescent diodes. *Appl Phys Lett* 51:913–915
- Tessler N, Denton GJ, Friend RH (1996) Lasing from conjugated-polymer microcavities. *Nature* 382:695–697
- Tsumura A, Koezuka H, Ando T (1986) Macromolecular electronic device: field-effect transistor with a polythiophene thin film. *Appl Phys Lett* 49:1210–1212
- Yamane K, Yanagi H, Sawamoto A, Hotta S (2007) Ambipolar organic light emitting organic field effect transistor with modified asymmetric electrodes. *Appl Phys Lett* 90:162108
- Yamao T, Shimizu Y, Terasaki K, Hotta S (2008) Organic light-emitting field-effect transistors operated by alternating current gate voltages. *Adv Mater* 20:4109–4112
- Yamao T, Terasaki K, Shimizu Y, Hotta S (2010) Organic-crystal light-emitting field-effect transistors driven by square-wave gate voltages. *J Nanosci Nanotechnol* 10:1017–1020
- Zaumseil R, Friend RH, Sirringhaus H (2006) Spatial control of the recombination zone in an ambipolar light-emitting organic transistor. *Nat Mater* 5:69–74
- Zheng Z, Yim KH, Saifullah MSM, Welland ME, Friend RH, Kim JS, Huck WTS (2007) Uniaxial alignment of liquid-crystalline conjugated polymers by nanoconfinement. *Nano Lett* 7:987–992

Chapter 11

Photoactive Liquid Crystalline Polymer

Asit Baran Samui and Srinivasa Rao Venukonda

11.1 Introduction

The phenomenon of photoactivity is well-known over the centuries. Very first example is the discovery in 1867 by Fritzsche, when he observed the bleaching of an orange colored tetracene solution in daylight which regained the color at night (Bouas-Laurent and Dürr 2001). Since then, there were scanty reports of similar behaviour. During 1950s, comprehensive studies on the mechanisms and synthesis of relevant compounds were carried out, particularly by Hirshberg and Fisher 1954.

In this chapter the details of liquid crystalline polymer possessing photoactive character or having induced photoactivity will be discussed. The liquid crystals have several special characteristics such as rod like molecular structure, rigidity along the axis, strong dipole etc. These characteristics always provide scope for a range of unique manoeuvres of structure. The liquid crystals can be combined with polymers to form attractive materials having optical properties and responsiveness of liquid crystals along with mechanical properties and processing similar to that of polymers. These materials are finding important applications in displays (Hikmet 1990) along with application in smart devices such as artificial muscles which can respond to electric fields (Urayama et al. 2006), heat (Yusuf et al. 2004) and light (Yu et al. 2003a, b). The light is considered as most interesting and convenient among various stimulating sources, as it is a clean energy and can be manipulated conveniently and controlled precisely as required (Fig. 11.1). The sample can be changed isothermally from the ordered nematic to the disordered isotropic phase.

The particular applications, as mentioned above, are directly linked to the phase transition behaviour in liquid crystalline polymers (LCP). The extent of resultant

A.B. Samui (✉) • S.R. Venukonda
Department of Applied Chemistry, Defence Institute of Advanced Technology
(Deemed University), Girinagar, Pune, Maharashtra 411025, India
e-mail: absamui@gmail.com; asit_samui@yahoo.com

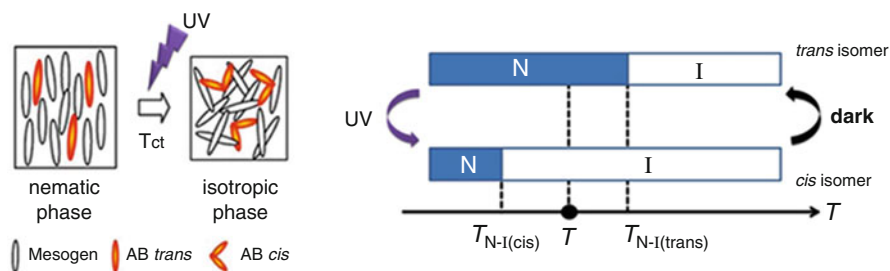


Fig. 11.1 Photo-induced nematic-to-isotropic phase transition in azobenzene-doped nematic Liquid crystals (Under permission as per © 2012 Garcia-Amorós and Velasco, licensee InTech.; Author: Garcia-Amorós, J., Velasco, D. (2012) Polysiloxane Side-Chain Azobenzene-Containing Liquid Single Crystal Elastomers for Photo-Active Artificial Muscle-Like Actuators. In: Boczkowska, A. (ed) Advanced Elastomers—Technology, Properties and Applications, Publisher: InTech, Chapter under CC BY 3.0 licence, pp. 61-88.; Original figure in: Legge, C. H., Mitchell, G. R. (1992) *J. Phys. D: Appl. Phys.*, 1992, 25, 492)

actuation depends mostly on manipulating the parameters. The liquid crystal phase stability depends on the anisotropic shape of the molecules. Thus, the change of molecular conformation by irradiation with light can be considered as the most direct way of controlling the properties of the liquid crystal.

For realizing photo-responsive smart polymers, the LCPs have to be either blended or functionalized with photosensitive molecules such as azobenzenes, cinnamic acid (CA), cinnamylidene, bisbenzylidene etc. Out of these moieties, azobenzene is the most popular and conveniently used photosensitive molecule because of its fast response on exposure to appropriate wavelength of light (Weigert F 1921). In fact, considerable research on utilizing trans–cis isomerization as the photo-active trigger was done by using azobenzene compounds (Rau 1990).

In an effort to design photoactive LC polymer systems, the early attempt was concentrated on dye molecules dispersed in LC polymer matrix after initial study of Weigert group (Weigert and Nakashima 1929). Shibaev et al., in his comprehensive review, discussed various approaches for designing photoactive LC polymer (Shibaev et al. 2003). The polarized light was used for inducing optical anisotropy in solid mixture. The use of polymer-dye blends and composites as materials with controllable optical properties have experienced certain problems originating from poor solubility, limitation in dye concentration (phase separation at increasing dye concentration), susceptibility to temperature (phase separation may occur) etc. Radical copolymerization of LC and photoactive monomers provides a convenient method for synthesis of photoactive LC polymers. The strategy of polycondensation of photoactive fragments with other blocks bearing the functional groups is also chosen, although rarely.

Photo-cross-linkable main-chain liquid crystalline polymers, containing photoactive bisbenzylidene cycloalkanone groups, make one very interesting class of LCP (Rao and Samui 2009). The bisbenzylidene containing side-chain and main chain polymers with structural variations include polyesters and polyester

epoxies (Ikeda et al. 1988; Samui et al. 2008), poly (phosphate esters) (Sakthivel and Kannan 2005), poly(azomethine ethers) (Iwan et al. 2010), polyphosphoramides (Kaniappan and Murugavel 2009), poly (siloxane ethers) (Racles et al. 2003), side chain methacrylate polymers (Gangadhara and Kishore 1995; Arun and Reddy 2004; Bobrovsky et al. 2001; Kumar et al. 2013) respectively. This class of mesogenic group possesses plenty of scopes for structural modification. Bisbenzylidene polymers are usually thermally stable and the photo crosslinking ability makes them more stable. Thus, having large electro-optic coefficient, these polymers make entry into the area of non-linear optics. The conjugated architecture has added another attribute as electrically conducting polymer.

Liquid crystal elastomers (LCEs) are soft materials which can be described as: (1) Rigid anisotropic LC moieties are incorporated into flexible polymer chains and (2) Randomly cross-linked forming initially isotropic or anisotropic rubbery structure depending on presence of external strain. These materials exhibit a unique interconversion of anisotropic liquid crystalline and the isotropic polymeric network. Photoactivity adds interesting behaviour making it photoactive liquid crystalline elastomer. Polymer network can be aligned or randomized at will by changing the irradiation and similarly the phase during polymerization. The schematics of the process are summarized in Fig. 11.2.

Their complex structure coupled with variable nature make them important for both investigations of basic scientific phenomena and technological applications, such as, artificial muscles (Buguin et al. 2006; Li and Keller 2006), shape memory

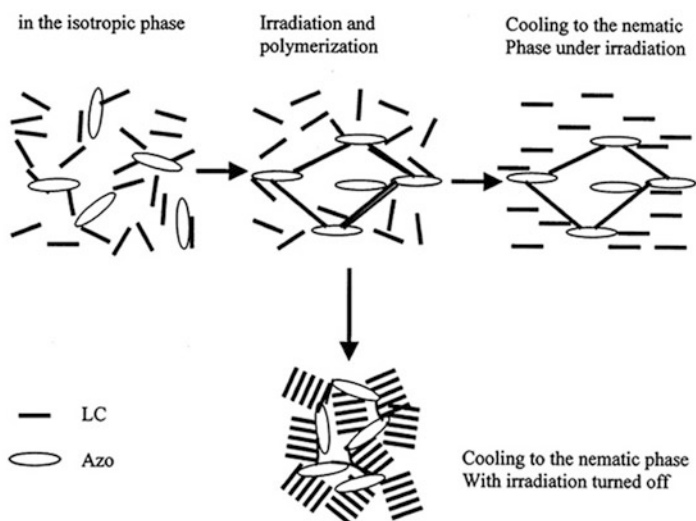


Fig. 11.2 Sketch for the formation of anisotropic azobenzene network in the isotropic phase and its effects on the induction of long-range liquid crystal orientation in the nematic phase (Reprinted with permission from ref 287. Copyright 2000 American Chemical Society: (287) Zhao, Y.; Chenard, Y. *Macromolecules* 2000, 33, 5891-5896)

polymers (Davis et al. 2011; Liu et al. 2007), sensors (Ohm et al. 2010), and other applications (Ohm et al. 2012; Sanchez-Ferrer et al. 2011).

The photoactive LCE maintains strong coupling between the orientational order and mechanical strain (Zhu et al. 2011). In such type of elastomer containing photosensitive molecules a local disorder is induced that produces a global change. The local disorder can change the orientational order which gives rise to internal stresses leading to strains and change of shape of the sample.

Polymer dispersed liquid crystal (PDLC) films comprise micron size liquid crystal (LC) droplets dispersed within polymer matrix. This combination maintains dual nature such as, electro-optical performance of liquid crystals and structural and mechanical advantages inherent to polymers. The PDLC devices can be switched between scattered opaque to transparent state by application of very small external electric field without using any polarizer. The material is of immense interest to researchers for basic studies as well as for industrial applications. Their possible application range from switchable displays, light windows (Simoni and Francescangeli 2000) to holographic gratings (Su et al. 2011) has been predicted.

Holographic polymer dispersed liquid crystals (H-PDLC) are usually formed by illumination of interference patterns on a mixture of photoactive monomers and liquid crystals (Kubyskyi et al. 2006). Local differences in photopolymerization rates and reduced miscibility, induces the LC domains to be periodically formed with the period of the interference pattern, in low light intensity areas. An electric field may be used to manipulate the orientation of the LC making the hologram to remain "hidden".

The photomechanical properties are the latest addition to polymeric systems which has tremendous industrial potential as photoactuator. The photoresponse of Poly (ethyl methacrylate) (PEMMA) doped with a spiroopyran (SP) derivative was studied by incorporating latter in a strip of former (Athanasios et al. 2005). The UV-induced conversion of the nonpolar SP to its polar merocyanine (MC) form can be done by exposure to 532 nm light. The possible aggregation of these MC isomers can lead to volume changes in the polymer. However, the effect is not significant to be useful. More effective approach was made by using photoisomerizable azo groups to get measurable work and generate significant forces (Lee et al. 2012). While amorphous polymers show promise as photomechanical materials, the search for better system continued. Currently highly ordered polymer systems are the material of choice for the purpose. In ordered materials, photoactive molecules' alignment maximizes the photomechanical displacements in the same direction. The Liquid crystal elastomers (LCEs) comprise a large family of ordered polymer solids which is considered as having potential material for applications as sensors and actuators (Ohm et al. 2010).

For aligning liquid crystal (LC) molecules, the rubbing technique on polymer-coated glass substrate surface has mostly been used (Seo et al. 1992; Arafune et al. 1998). Polyimide (PI) is preferred choice as an alignment layer which has required properties such as uniform alignment and thermal stability. However, rubbing technique has disadvantages, like generation of electrostatic charge and contaminating particles. Further, there exists difficulty in applying the technique for

large and flexible substrates. This prompted the development of newer technologies. There are some alternatives to rubbing technologies, such as; laser writing, microrubbing, ion beam irradiation and photoalignment (Chrzanowski et al. 2011). The non-contact nature of photoalignment eliminates the difficulties associated with rubbing technology. It is typical of all photoalignment technologies such that the polarized UV irradiation generates anisotropy in the photoactive material. There are variations of photoalignment mechanisms: (1) topochemical crosslinking in polymer structure, (2) photodegradation in polyimides, (3) cis-trans isomerization in azo-structure: pure-dye films, polymers containing azo-groups and monolayers of azo dyes and (4) pure reorientation of photo-chemically stable azo-dye molecules.

Photoinitiator introduction in to methacrylate-functionalized adhesives imparts light induced smartness to it. Almost complete loss of adhesion occurs on irradiation under a halogen lamp, the reason being photo-initiated crosslinking, which raises the elastic modulus (Corbett and Adams 2013). The switching is only one-way as the adhesive property cannot be recovered. Further, the two-way switching is also realized by using coumarin-functionalized acrylate adhesives, whereby UV-A radiation can be used to switch off adhesion and UV-C radiation is used to partially switch it on (Trenor et al. 2005).

11.2 Commonly Used Chromophore in Photoactive LCP

A photochromic compound is characterized by its ability to alternate between two different chemical forms having different absorption spectra, in response to irradiation by light of appropriate wave lengths. During the photoisomerization, not only the absorption spectra but also various physicochemical properties change, such as the refractive index, dielectric constant, oxidation/reduction potential and geometrical structure respectively. These molecular property changes can be applied to various photonic devices, such as erasable optical memory media and photo-optical switch components.

Liquid crystals (LCs) form supramolecular assemblies with unidirectional orientations of the molecular axis to develop optical anisotropy. There are several types of LCs which differ in the details of molecular order, molecular shape, and molecular weight. Consequently, the significance of the combination of LC systems with photochromes arises from the photo triggered amplification derived from the molecular order. This results in the remarkable transformation of optical properties, displaying the photo optic effect. The photo optic effect comes from photo induced changes in the level and direction of alignment of LC molecules.

The common photoactive moieties used for making photoactive LCP are fulgenic acid and fulgides, cinnamic acid, spiropyrans, bisbenzylidenes and azo benzenes respectively. After photochromism of arylfulgides was discovered by Stobbe at the end of the nineteenth century, Ulrich reported on Photochromic

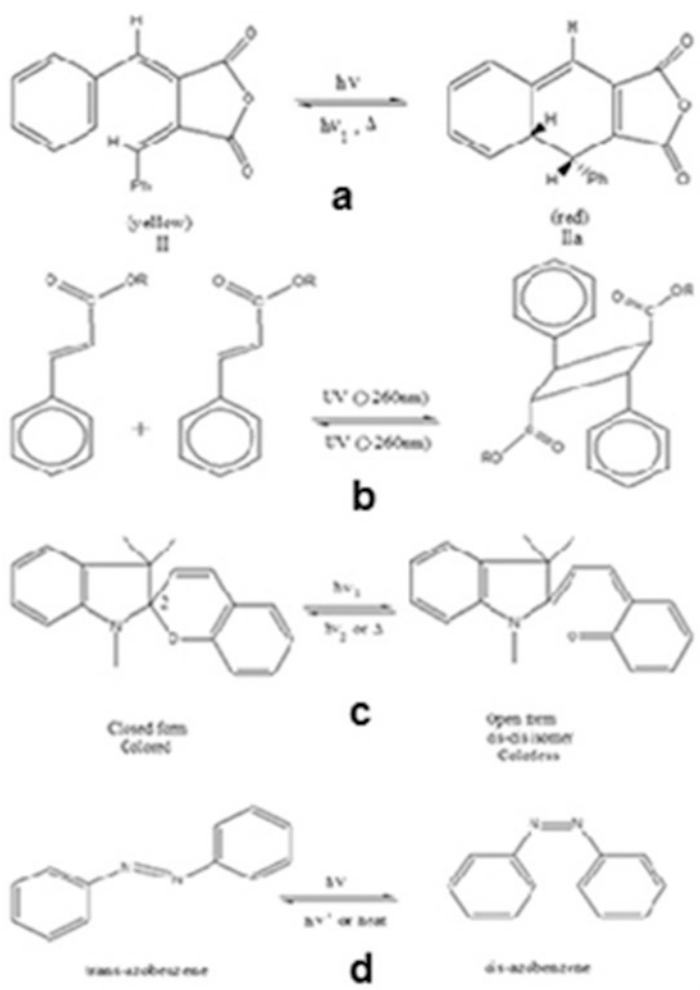


Fig. 11.3 Common chromophores and their photoactivity: (a) photoisomerization of fulgides via ring closure and back; (b) photodimerization of cinnamic acid derivative via cyclobutane ring formation; (c) photoactivity of spiropyrans via ring opening and back; (d) photoisomerization of azobenzene from trans to cis and back

thiophenefulgides (Ulrich et al. 1991). The derivatives of 1,3-butadien-2,3-dicarboxylic acid and its acid anhydride are named as ‘fulgenic acid’ and ‘fulgide’, respectively. Figure 11.3 incorporates few common examples of chromophores and their photochromic transformations.

Photochromic lenses, fluid flow visualization, and security inks and dyes are few examples which utilize the color changes of the two Fulgide species (Fan et al. 1999). Fulgide doped photopolymers can be used to form holographic recording medium (Tork et al. 2001).

Cinnamic acid derivatives constitute a series of photochemically reactive molecules which are able to form photoreversible covalent cross-links in polymers (Yu and Ikeda 2005). Polymers having cinnamic groups can be deformed and fixed into pre-determined shapes by ultraviolet light illumination, which generates photoreversible crosslinking. The original structure can be recovered at ambient temperatures when exposed to ultraviolet light of a different wavelength, which regenerates the double bonds by breaking cyclobutane ring (Lendlein et al. 2005).

The family of photochromic compound extends to Spiropyran, which is extensively studied as photochromic compound because of its potential applications in optical memory devices, optical switches and sensors (Lukyanov and Lukyanova 2005). The photochromism of spiropyrans is observed by transforming the ring from close to open by irradiation and back to close by using either thermal and or irradiation (at other wave length) method. Spiropyran units can be linked to polymer chain for imparting reversible response ability to external photonic stimuli (Florea et al. 2012).

Bisbenzylidene group is another versatile photo-active material series having liquid crystalline nature Murali and Samui, 2010. Many authors reported series of bisbenzylidene containing side-chain and main chain polymers with structural variations. Their photoactivity characteristics are dual in nature, exhibiting conversion from one to other chromophore isomeric form as well as reversible $2\pi + 2\pi$ photocrosslinking.

The most important photochromic compound is azobenzene which is an organic molecules having two aromatic rings linked by an azo group (N=N). Having many important properties, they are already being used for number of applications, mainly for chemical industry. Azobenzene dyes constitute about 60 % of the world production of industrial dyes (Hunger 2003). Similar to C=C double bond, the azobenzenes have two geometric isomers (*Z/E*) around the N=N double bond: the *trans* isomer (*E*) being more stable than the *cis* isomer (*Z*) (Merino and Ribagorda 2012). The energy barrier of the photoexcited state is $\sim 23 \text{ kcal mol}^{-1}$, which suggests that the *trans* isomer is prevalent in the dark at room temperature (Mahimwala et al. 2013).

The *trans*-azobenzene easily isomerizes to the *cis* isomer by irradiation in the wavelength region of 320–350 nm. The isomerization is easily reversible as the *trans* isomer is recovered when the *cis* isomer is irradiated in the wavelength range of 400–450 nm, or heated or left in dark. For many azobenzenes, the two photochemical conversions occur in picoseconds. The photoinduced isomerization of the azobenzenes makes considerable change in their physical properties, such as molecular geometry, dipole moment or absorption spectrum (Morgenstern 2009). The distance between the two carbon atoms in position 4 of the aromatic rings of azobenzene decreases from 9.0 Å in the *trans* form to 5.5 Å in the *cis* form (Koshima et al. 2009). The dipole moment also increases from 0 to 3 D from *trans* to *cis* form. Moreover, *cis* isomer is less stable than the *trans* one as because of its bent shape which increases the steric hindrance and at the same time adversely affects the conjugation of the *trans* linear form. Consequently, the metastable *cis*

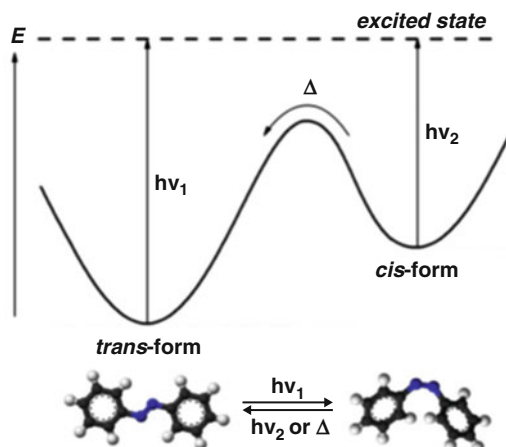


Fig. 11.4 Photochromism of azobenzene and energetic profile for its trans-to-cis and cis-to-trans isomerization processes (Under permission as per © 2012 Garcia-Amorós and Velasco, licensee InTech.; Author: Garcia-Amorós, J., Velasco, D. (2012) Polysiloxane Side-Chain Azobenzene-Containing Liquid Single Crystal Elastomers for Photo-Active Artificial Muscle-Like Actuators. In: Boczkowska, A. (ed) *Advanced Elastomers—Technology, Properties and Applications*, Publisher: InTech, Chapter under CC BY 3.0 licence, pp. 61-88.; Original figure in: Rau, H. in *Photochemistry and photophysics*; CRC Press Boca Raton FL, 1990)

isomer relaxes back quickly to the thermodynamically stable trans form isothermally in dark (Fig. 11.4) (Bronner and Tegeder 2014).

The most important requirement of a molecule to behave as a switch is the existence of two distinct and stable isomeric forms when an external stimulus is used. To summarize important requirements following may be mentioned: (Willner and Rubin 1996; Gust et al. 2012).

1. Two interconvertible structures forming the molecular switch must be easily and selectively produced by irradiation at suitable wavelength.
 2. The two isomers should not be interconverted over wide temperature range.
 3. The isomers should be able to interconvert without appreciable degradation.
 4. The two structural forms should be conveniently differentiated.
- etc.

After finding the unique behaviour of photochromes, scientists have realized that these have more potential than making color sunglasses. The optical switches and memories appear in the smart product arena. Further, the incorporation of such photoswitches allows fabrication of photoresponsive polymers and other materials which can be externally manipulated by light (Russev and Hecht 2010).

A range of photosensitive systems, such as smart polymers (Yu et al. 2003a, b; Yager and Barrett 2008) can be realized by using the isomerization abilities of azobenzene.

Chiral photoactive molecules form an exciting class of chromophore. As an example, arylidene menthanone derivatives combine photochromic and chiral properties (Vinogradov et al. 1990; Matharu et al. 2007; Shibaev et al. 2003).

They are very effective chiral dopants used for induction of chiral nematic phase by introduction into the nematic phase. Most of the arylidene-*p*-menthanone-3-one derivatives have high helical twisting power in the range from 20 to 50 μm^{-1} . The 1,2-arylidene-*p*-menthan-3-ones have an exo-cyclic double bond at *s*-cis position having ability to undergo E-Z isomerization. The E-Z-isomerization with respect to the double bond has been as evidenced by various experimental techniques.

The copolymers containing nematogenic and (–)-arylidene-*p*-menthan-3-one chiral photochromic moieties in one monomer unit were synthesized. By irradiation of films of the copolymers with UV radiation, the selective light reflection peak can be shifted to a longer wavelength region. Such behaviour suggests their consideration as promising materials for colour data recording and as storage media (Bobrosky et al. 1999).

11.3 Photoactive Liquid Crystalline Polymer (PLCP)

Among various inorganic and organic photoresponsive materials the most important role, obviously, being played by polymers because of the ability of combining various functional groups and fragments, as well as the ability of polymers to form stable films, fibres, and coatings that can be readily applied onto various substrates (metals, plastics, ceramics) by simple methods such as spin coating, dipping, lamination, etc. Generally, the optical and electrical properties strongly depend on orientation and morphology of the polymers (Bobrovsky et al. 2010). Thus, the optimization of the device performance is directly related to the way the supramolecular organisation of the material occurs (Cipparrone et al. 2010).

The reversible trans-cis photoisomerization of the N=N double bond of side chain liquid crystalline polymer (SCLCP) results in an angular reorientation of the azo chromophore perpendicular to the direction of polarization of the incident light.

The main feature that makes liquid crystalline polymers suitable for reversible optical storage is that the photoinduced anisotropy can be successfully erased and rewritten over thousands of cycles before significant fatigue of the material is observed (Holme et al. 1996).

However, these properties are dependent on the change of aggregation under polarized light, supramolecular order, and, more generally, the liquid crystallinity, which again depend on several parameters, such as, main chain properties, the spacer length, and the chromophore mobility (Wu et al. 1998a, b). Further, the spacer length can cause periodic changes in the transition properties based on whether there are an even or odd number of units in the LC polymer (Ruan et al. 2002).

Photosensitive LC polymers are generally obtained by three principal methods. The first approach involves simple physical mixing of photochromic dopant with

liquid crystal polymer. In this case, the polymer serves as matrix, or 'host' and the additive (photochromic dopant) as 'guest'. Such mixtures allow us to control the properties of the guest component by light irradiation without any changes in the matrix itself. In the second method PDLC and PDLC/chromophore blends and composites are included. Under third method, photochromic dopants are covalently attached to the polymer and liquid crystals are added in the matrix. In the fourth and most important method, incorporation of both mesogenic and photoactive moieties are done by covalently attaching to the polymer.

11.3.1 LCP/Chromophore Blend

There exists considerable interest in the synthesis and characterization of azobenzene containing polymers for several reasons as these materials possess unique optical properties. In the guest-host system, azobenzene guest molecules exist in trans form, with random orientation throughout the matrix. If the polymer film is then subjected to a linearly polarized light of suitable wavelength, the azobenzene moieties can be photoisomerized to the *cis* form. Liquid crystal display (LCD) are based on the guest-host effect which utilizes the convenient alignment of LC on application of electric voltage and the close reorientation of the dye guest (Grabcheva et al. 2003). This is responsible for selective absorption by the dyes. Due to the presence of dye, the LCDs function with only one polarizer and show a wide viewing angle and fairly good image contrast (Wolarz, et al. 1992). By using fluorescent dyes, the displays can function in both active and passive modes.

Double GH (DGH) displays concept is that the operation principle remains same but a second independent switchable layer is employed behind the first. The cells configuration is such that it acts as efficient polarizer at a selected wavelength only. The neutral polarizers used in conventional GH displays, having high absorption problem across the spectrum, can be dispensed with and the result is a brighter display (Uchida and Wada 1981). The Tri layer displays have also been attempted. It uses different colour dye in each layer which can be selectively switched to yield a range of colours (Castellano 1992).

11.3.2 Photoactive Liquid Crystalline Polymer Blends and Composites

The polymer-dispersed liquid crystals (PDLCs) is well known blend having excellent commercial application. PDLCs can be described as a dispersion of liquid crystal droplets in a solid polymer matrix. These tiny droplets (a few microns) make material to behave in a unique way. The orientation of director in dispersed liquid

crystal (LC) varies in random fashion from droplet to droplet in absence of the external electric field. In the presence of sufficient external electric field, the LC directors get aligned in the direction of electric field making the PDLC film appearing transparent. PDLC can be used for a variety of electro-optic applications ranging from switchable windows to projection displays

PDLCs can be formed from emulsions of liquid crystal and polymer. This combination maintains dual nature: electro-optical performance of liquid crystals and structural and mechanical advantages associated with polymers. New and unique optical properties can be harnessed by controlling the mixing ratios and fabrication methods respectively.

11.3.2.1 PDLC with Dye

Colored PDLC can be made by incorporating dyes in the PDLC material. The dye has dual role as it is distributed between LC droplets and matrix polymer. The latter is first UV cured with the help of dye. On the other hand, the orientation of the elongated dye molecule is controlled by the nematic director configuration inside the droplet. The absorbance by the dye is modulated by the nematic director alignment with an external electric field. The guest-host PDLC (nematic) sample, containing about 1 % dye concentration, shows higher transmission (~50 %) and faster switching responses (Malik et al. 2006)

The dichroic dye doped PDLC (DD-PDLC) has the potential to perform much better than conventional reflective-type twisted nematic LC display in some applications. This allows the doped PDLC to perform without polarizers, which results in increased reflectivity. Further, the viewing angle maintains higher contrast than isotropic dye (Wu and Fuh 2005) and the threshold voltage is reduced.

Holographic polymer dispersed liquid crystals (H-PDLC) are usually formed by the illumination of interference patterns on a mixture of photoactive monomers and liquid crystals (Kubytskyi et al. 2006). Local differences in photopolymerization rates and reduced miscibility of LC domains are formed in periodic fashion with the period of the interference pattern, in the area having low light intensity. An electric field manipulates the orientation of the LC so that the hologram will appear “hidden”, making the hologram electrically switchable. The field of possible applications of H-PDLC in a range of areas including switchable focus lenses, telecommunication, optical filters, flat-panel displays, etc.

The similar material using almost similar synthetic methodology is called nano-PDLC. The mixture of prepolymer and bulk LC is irradiated using strong UV to induce photo-polymerization. This allowed quick phase separation and produce fine LC droplets. The droplet size is usually less than 100 nm Sugiyama et. al, 1999. The high concentration of fine droplets generates large electro-optic effect with low propagation loss. The random characteristics of LC alignment suggest that nano-PDLC devices are insensitive to polarization. They switch at very fast speeds in the order of microsecond, making them ideal for wave front correction devices in

adaptive optics. However, the nano-PDLCs need significantly increased driving voltages and reduced stroke. Due to nano size of droplets this type of PDLC is non-scattering in nature. Instead, this transparent non-scattering material's response curve is quite sensitive to the amplitude of voltage. The variation increases with the applied voltage till constant value is reached. Nano-PDLCs are often termed as "Holographic PDLCS" (H-PDLCs). This is because of one particular application in which phase modulation properties are utilized as a method of producing reconfigurable holograms.

It is well known that an alignment change of LC materials in a periodic fashion can be easily induced by irradiation with interference patterns created by overlapping two coherent beams. This results in a large refractive-index modulation and the recorded grating exhibits high diffraction efficiency. In Azo-containing LC polymer film, both surface-relief and refractive-index gratings can be recorded (Mysliwiec et al. 2007). Further, this refractive index modulation fixed in LCP films (Yu 2014), called as photocontrollable nanostructures on the macroscopic scale, can be used with excellent reproducibility and mass production. It can form nano template for nanoengineering and nanofabrication.

The azo can be used as small molecule, as pendant group in copolymer, as segments in block copolymers and in other possible architectures. When siloxane group is used as spacer in LC polymers the glass transition temperature of the synthesized materials decreases due to flexibility of the siloxane unit. By using this architecture photoinduced nematic-to-isotropic phase transition at room temperature can be realized and real-time holographic gratings can be formed (Hasegawa et al. 1999).

The alignment of lyotropic liquid crystalline molecules can be controlled by using photoactive surfaces (command surface). This observation paved the way for optical control of nanochannels consisting of mesoporous materials (Ichimura et al. 2002).

New bent-core monomethacrylates and their side-chain polymers with 3,4'-biphenylene moiety as a central core and both *all*-ester and azo-ester lateral structures can be prepared (Gimeno et al. 2014)

As expected, significant stabilization of the lamellar SmCP mesophase ranges occurs after polymerization and the vitrification of these supramolecular organizations is observed at ambient temperature.

11.3.3 Photoactive Polymer Dye/LC Blend

The idea behind making azobenzene polymer network is not only to stabilize liquid crystal but also alter its orientation through irradiation of suitable wave length. When the azo monomer is polymerized and simultaneously irradiated, each photo-induced trans-cis isomerization is followed by thermally activated cis-trans isomerization, causing a small reorientation of the transition moment. After a large number of trans-cis-trans cycles, a preferential orientation of azobenzene groups

normal to the polarization plane occurs. The liquid crystals, present in the polymerization medium, are stabilized by a polymer network carrying azobenzene groups. The azobenzene orientation resulting from irradiation alters the director fields of surrounding liquid crystal molecules, leading to their orientation (Natansohn et al. 1994). This makes such methodology interesting for controlling the average liquid crystal orientation over macroscopic length scales. The method is able to promote and manipulate liquid crystal orientation in PSLC. Unlike surface alignment, the polymer network offers “volume” or “bulk” effects which can align liquid crystals in relatively thick films. As azobenzene groups are aligned only in areas exposed to irradiation, the orientation of liquid crystal molecules should occur only in those areas. Along with surface alignment, the irradiation regulated orientation could give PSLC materials more possibilities for designing electrooptical properties (Corvazier and Zhao 1999).

At low concentration ($\leq 10\%$) of azo monomer it is polymerized in presence of LC molecules to make polymer stabilized liquid crystals (PSLC) (Zhao 2003). The azo group undergoes photoisomerization during irradiation with linearly polarized light and the LC gets aligned perpendicularly to polarization direction. This alignment does not vanish like in other case due to presence of polymer network. The orientation of LC, being a rubbing free approach and having better control, make better application possibilities.

11.3.4 Photoactive LC Polymers

A polymer containing chromophore and mesogen can be called as photoactive LC polymer. Compared with low molecular weight liquid crystals, the polymers have the advantage that the structure remains unchanged during the transition from the liquid crystalline phase to the solid phase, permitting freezing of a liquid crystalline structure in the glassy state.

Principles of molecular design of photoactive LC polymers: The LCPs are well known for their importance in basic research as well as in commercial utilization. So far, several thousand LCPs have been synthesized and studied. The macromolecules of several thousand LCPs, reported so far, show one specific feature: they contain rigid (mesogenic) fragments which are shaped as rods and disks and also flexible fragments. These fragments can be connected to each other in various ways, such as main chain, side chain, combination of main and side chain and hyperbranched polymers. The PLCP has the benefit of the structure remaining unchanged during the transition from the liquid crystalline phase to the solid phase, permitting freezing of a liquid crystalline structure in the glassy state, which are distinct advantages over low molecular weight liquid crystals, which show phase separation, degradation etc.

11.3.4.1 Design of Main Chain Photoactive LC Polymer

Main chain photoactive polymers can have multiple of architecture; the most common is both chromophore and LC are present in the main chain. Mostly spacers are placed between LC and chromophore for facile alignment. Both the mesogen (Non-azo) and azo can be arranged in main chain by chemically attaching normally or as block polymer (Sanchez-Ferrer and Finkelmann 2013). However, this architecture is not so popular because of rigidity, and less facile orientation.

11.3.4.2 Side Chain Photoactive LC Polymer

The side chain LC/azo copolymer architecture is the arrangement of both LC and mesogen as pendant groups in a polymer chain. This enables the mobility of LC and chromophore to be different from the main chain. The decoupling of pendant groups is further facilitated by using appropriate spacer. This allows more effective photo alignment. The most popular method is the preparation of acrylate monomers containing chromophore and LC groups respectively. The radical polymerization is followed as the monomers are copolymerized at various mole ratios, preferably, the azo monomer concentration remaining much less than 50 % mole ratio.

A series of side-chain LCPs of 6-[4-(4-ethylphenyl)diazenylphenoxy]hexyl methacrylate and 4'-[6-(methacryloyloxy)hexyloxy]-4-cyanobiphenyl shows high alignment efficiency by using the method of irradiation: first with 366 nm unpolarized light and then with 436 nm linearly polarized light (Wu et al. 1999). It is one of the developments towards all-optic switching.

11.3.4.3 Photoactive Hyperbranched LC Polymer

Branched polymers are known by the presence of branch points or the presence of multiple numbers of end groups and make a special class of polymers lying between linear polymers and polymer networks. The branched polymers can have hyperbranched architecture which is amorphous, although there are examples of crystalline hyperbranched polymers. These polymers, having many unreacted chain ends, have properties highly dependent on the nature of the end groups. Obviously, the modification of the end groups provides an excellent route for controlling/modifying the properties of these polymers. New multifunctional polymers with selective end groups can be designed. These polymers have additional processing attributes, such as low viscosity and high functionality. The synthesis methodologies are plenty which include free radical, condensation, ring opening etc. Despite the high risk of gelation, the $A_2 + B_3$ polymerization (Jikei et al. 1999), used for many industrial applications, encouraged researchers to carry out extensive research to determine reaction parameters required to avoid gelation.

11.4 Photoactive Liquid Crystalline Elastomers

An isotropic rubber is obtained by cross-linking a soft polymer melt at random points, which suppress the large-scale Brownian motion of the polymer chains and also freeze the macroscopic configuration. The polymer segments between two cross-linked points remain in their equilibrium conformation possessing maximum disorder (Treloar 2005). On application of external stress, their equilibrium conformation is disturbed and the distance between the cross-linked points change. The free energy of the system increases as the configurational entropy is reduced. When the external stress is removed, the elastomer tries to go back to its original equilibrium conformation. Due to such type of behavior of the crosslinked network, elastomers are considered as “entropic-springs”.

The first liquid crystalline elastomer (LCE) was synthesized in 1981 by Finkelmann, et al. It was a polydomain nematic elastomer (Finkelmann et al. 1981) having polysiloxane backbone. The polysiloxane provided flexibility to the polymer network and allowed the modification for synthesis of new LCEs via reactive groups. The chemistry of LCEs has since developed which was followed by development of many materials with fascinating physical properties (Finkelmann et al. 1989).

Liquid-crystalline elastomers (LCEs) possess combination of two properties: liquid crystalline order and flexibility inherent in elastomeric structure. These materials find application in microengineering, where they can be integrated to effect movement of a reduced volume engine. There is a range of driving forces, such as, temperature, (Tajbakhsh and Terentjeva 2001) voltage, (Chambers et al. 2006) or light (Finkelmann et al. 2001; Camacho-Lopez et al. 2004). Specially, the light can change the liquid crystalline order, which in turn, produces such movements. The large, reversible shape changes in solids, to the tune of 10–400 %, can be induced optically by photoisomerizing monodomain nematic elastomer.

Among the LC phases, the nematic one, having approximately parallel orientation of mesogens along their longest axis, is the least ordered and less viscous state. This factor is responsible for easy manipulation of mesogen alignment than others. Hence, nematic liquid-crystalline materials are the most commonly used in elastomer structure.

After observing a p(NIPAM) hydrogel with spironaphthoxazine switching units, to have increased water up-take after UV-irradiation, (Kulawardana et al. 2009) it was felt that although hydrogels having photoresponsive units undergoing deformation when irradiated, they lack the stiffness required for converting the photonic energy into mechanical work or motion. This problem can be addressed by using photoactive liquid crystalline elastomers (LCEs). The key advantages of liquid crystals (LCs) originate from: (a) the anisotropy of optical and dielectric properties as well as birefringence; (b) the cooperative effects operating in the alignment

process, and (c) the alignment can be changed cooperatively by external fields at surfaces and interfaces. Therefore, LCEs offer great opportunity for a “tiny” light stimulus trigger a “big” macroscopic event. Further, the synthesis of azobenzene and its incorporation being simple, the fast response times, mesogens like structure, photochemistry being a clean process, their integration as photoswitches in to LCEs have become very natural. Conventional LCEs respond to thermal energy and undergo transition from nematic to the isotropic phase while contracting along the alignment direction and expanding while cooling. However, for some applications it is beneficial to avoid heating and therefore photo-induced phase transitions make an attractive alternative. Azobenzene elastomers are somewhat different from other azobenzene polymers in that these can be mechanically deformed to a large extent, which adds one additional degree of freedom.

Photoactive liquid-crystalline elastomers (LCEs) can be both main chain as well as side chain type where the mesogenic moieties can be incorporated in the polymer main chain (main-chain LCEs), or attached as pendant groups to the main polymer backbone (side-chain LCEs), generally via flexible spacers. The flexible spacer allows the polymer main chain to accommodate the anisotropic orientation of mesogenic side groups.

Main chain liquid crystal elastomers usually exhibit interesting properties such as three different regimes of elastic response; unconventional stress-strain relationship is one of them and the other is shape memory effect. The important parameters are their macroscopic behavior and the nature of domain structure, microscopic mesogenic phase structure, relaxation mechanism, and sample history respectively. Additionally, they are also interrelated. Side chain LCP has the great advantage that the orientation is decoupled from the main chain polymer. This allows innumerable manoeuvrability in respect of properties and orientation. Further, spacers will also have various options in determining the properties. As the side on addition is done to the main chain, photochromic groups can as well be connected with ease to make it photoactive. Further, the spacer and ligand to mesogen can be varied as per demand. Crosslinking can be done by using either normal crosslinker or an azo containing crosslinker (Fig. 11.5)

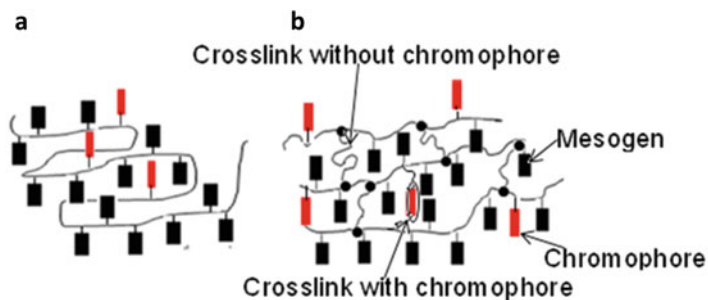


Fig. 11.5 Representative photoactive liquid crystalline elastomer: (a): side chain liquid crystalline elastomers; (b) crosslinked liquid crystalline elastomers

11.4.1 *Light-Induced Artificial Muscle-Like Actuation by LCEs*

Photo-active artificial muscle-like actuators convert light energy into mechanical energy whose output is in the form of displacement, strain, velocity and stress. Further, muscle like movements can be produced by soft material so that the deformation remains easy during irradiation. Polymers are very appropriate material for this purpose because of their many attractive properties and characteristics; such as lightweight, inexpensive, easy tailor-making, fracture tolerant, pliable and biocompatible (Ikeda et al. 2007). In a simple case of actuation in photoactive LCE, the array of nematic mesogen and chromophore in a matrix undergoes bending on irradiation along the nematic director. In one typical opto-mechanical experiment stress vs. time plot for a photo-active liquid single crystal elastomer, it can be observed that on irradiation, the internal stress created in the elastomer grows until the photo-stationary state is reached, i.e., a plateau is arrived. This corresponds to the maximum opto-mechanical response generated by the artificial muscle-like actuator. When the irradiation is stopped, the thermal back cis-to-trans isomerisation of the azo-dye occurs and the stress starts to decrease and continue until the initial stress value is recovered.

Generally, photo-active liquid-crystalline polymers and elastomers are multidomain in nature making the director changing abruptly from one domain to another. Hence, both LCPs and LCEs undergo deformation in isotropic way when non-polarized light falls, resulting in a low degree of deformation of the material (Barrett et al. 2007). However, these materials exhibit three-dimensional contraction and expansion movements when exposed to polarized light of appropriate wavelength (Yu and Ikeda 2011). Further, the bending direction of the LCE film can be controlled by the location of azo moiety within the elastomeric network; whether as crosslinker or as pendent group (Priimagi et al. 2012). There are many possibilities of incorporation of azo in LCE, either in main chain as comonomer or as side chain or even as crosslinker; each type acting differently. The photomechanical response can be correlated with the type of linking of azo group. Figure 11.6 shows the photomechanical response vs. thermomechanical response of nematic LCE having azo side group (Sanchez-Ferrer et al. 2011).

It can be observed from the figure that mechanical stress generated during irradiation-stage (first part; trans-cis) is the equilibrium stress due to photo and thermal isomerization (as during photoisomerization there is slight rise in temperature). The second part is purely thermal due to cis-trans isomerization. Further, it is apparent that photomechanical effect of azo-crosslinked LCE is much higher than azo pendent LCE. Higher photomechanical stress is due to more restricted movement in crosslinked system.

Further, in the nematic photoactive side chain LCEs (SCLCEs) (both for azo-crosslinked and azo pendant type) the two-ring azobenzene molecules exhibit higher response than the corresponding four-ring molecules, mainly for their higher

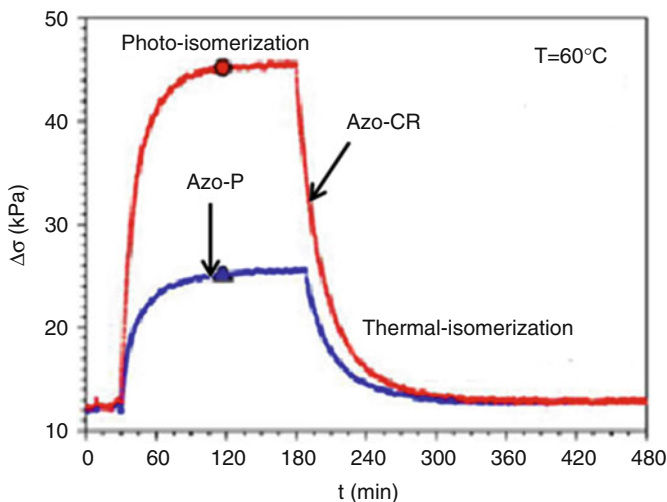


Fig. 11.6 Opto-mechanical experiment on the photoactive nematic side-chain liquid-crystalline elastomers at 60 °C for azo containing crosslinked elastomer: Azo as Pendant: Azo-P: Azo in crosslink: Azo-CR at $\lambda = 380$ nm (Reproduced with permission from SPIE; taken from article ‘Light-induced disorder in liquid-crystalline elastomers for actuation’ by Sánchez-Ferrer, A. (2011) Proc. of SPIE Vol. 8107. In (ed): Jaume Esteve, Eugene M. Terentjev, Eva M. Campo (2011) Nano-Opto-Mechanical Systems (NOMS), Proc. of SPIE Vol. 8107, 810702 © 2011 SPIE)

rigidity. The nematic photoactive SCLCEs with asymmetric azobenzene crosslinker shows the reverse effect as compared to the symmetric azo dyes; a decrease in the opto-mechanical effect during irradiation (trans to cis) and an increase during thermal relaxation process (cis-trans). The smectic photoactive LCE shows higher young modulus as compared to corresponding nematic LCEs; the presence of the smectic layers is responsible for enhancement of mechanical properties.

The first prototype of light-controlled plastic rotating motors was fabricated using laminated films of photo-sensitive LCEs (Yamada et al. 2008).

11.4.2 Light-Sensitive Liquid Crystal Elastomers for Hologram

In presence of photosensitive groups coupling between the LC orientational order of the mesogenic units and the conformational state of the former is observed (Corbett and Warner 2009; Xie and Zhang 2005). This coupling is responsible for cooperative response, due to which even a low degree of photo induced perturbations in trans- and cis-isomers ratio causes large change in LC order parameter and refractive index of the medium (Li et al. 2011; Tasic et al. 2013). This change

provides an opportunity to record high efficiency volume phase holograms. The rubber elasticity of the elastomer enables the recorded holographic structures to be reversibly expanded and contracted. Thus, the applicability of this material in mechanically tunable diffractive optical devices is very promising (Davis et al. 2010). At the surface layer strong absorption of the UV light occurs by trans isomer. This causes the decrease of intensity of recording radiation with increasing sample depth making the recording process progressively less effective. The numerical simulations revealed that in the beginning of the UV illumination the grating structure can be recorded in surface region up to a thickness of 2 μm (Gregorc et al. 2011; 2012). However, at longer illumination times a reduced concentration of the absorptive trans-azo mesogens occurs in the surface layer due to its isomerization to cis-isomer. The molar absorption coefficient of cis-isomer being much lower allows an increase of the penetration depth of the UV light and the effective thickness of the grating structure increases up to 20 μm at very long illumination time. Thus, although the kinetics of the trans-cis isomerization process is quite simple, its dependence on spatial variations of the UV light intensity and its non-local coupling to the LC orientational order results in a complicated time dependence of the refractive index modifications during holographic recording. However, the relaxation (spontaneous erasure) of the grating structure is regulated only by the thermally-induced cis-to-trans back-isomerization and therefore simple.

If the director points to unique direction in the field, the non-polarized light can be effectively used for changing mechanical properties, i.e., a monodomain sample is required. Further, the sample can exhibit maximum photo-mechanical stress.

11.4.3 *Liquid Single Crystal Elastomers (LSCEs)*

These make a subclass of liquid-crystalline polymers (Kupfer and Finkelmann 1991). LSCEs consist of weakly cross-linked polymer networks having macroscopic orientation of the director, \mathbf{n} .

During the last decades, the synthesis and study of azobenzene-containing LSCEs as light-driven artificial muscle-like actuators are very active. A typical synthesis method involves three stages, e.g., a stable elastomeric system is made which can be handled properly. This can be achieved by partial cross-linking. In the second stage the orientation of all different directors of the entire sample is executed by applying uniaxial force to the sample along its longest axis. After suitable time, a monodomain LCE is obtained, which is called as a LSCE and is perfectly transparent. In the third stage, the created anisotropic state is fixed by a second crosslinking reaction without removing the applied force. The process can be represented in a scheme (Fig. 11.7).

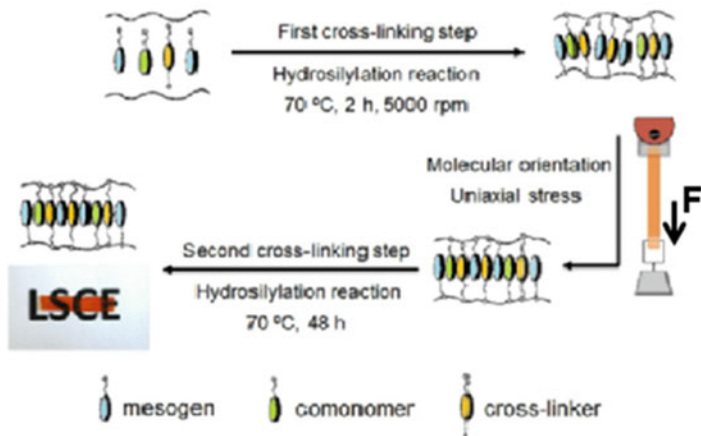
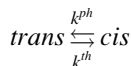


Fig. 11.7 Synthetic methodology in three steps used for preparing photo-active side-chain polysiloxane-based nematic LSCEs (Under permission as per © 2012 Garcia-Amorós and Velasco, licensee InTech.; Author: Garcia-Amorós, J., Velasco, D. (2012) Polysiloxane Side-Chain Azobenzene-Containing Liquid Single Crystal Elastomers for Photo-Active Artificial Muscle-Like Actuators. In: Boczkowska, A. (ed) *Advanced Elastomers—Technology, Properties and Applications*, Publisher: InTech, Chapter under CC BY 3.0 licence, pp. 61-88.; Original figure in: Kupfer, J., Finkelmann, H. (1991) Nematic liquid single crystal elastomers, *Makromol. Chem. Rapid Commun.*, 12(12): 717-726)

11.4.3.1 Opto-mechanical Effect in Liquid Single Crystal Elastomers

The optomechanical effect has already been described. When UV light falls on LSCEs, besides maximum stress that the system is able to generate, the time required by the network to produce its maximum mechanical response and that necessary to recover the initial state thermally are determined. Above three parameters are vital for complete performance evaluation of LSCEs for artificial muscle-like photo-actuation.

The UV-irradiation process of an LSCE is a bidirectional step, since the *trans*-to-*cis* photoisomerisation reaction competes with the thermal *cis*-to-*trans* isomerisation simultaneously.



Both individual isomerization processes follow a first order profile for low-molecular weight azo derivatives in isotropic and nematic solution as well as in dense polymer matrixes (Eisenbach 1978; Mahimwalla et al. 2012).

In 2008, Ikeda and co-workers exhibited application of photoactive LCE by utilizing the stretching and contraction of a main chain azobenzene. The LCE was used to design a light-driven motor system (Yamada et al. 2008). The LCE layer was laminated on a low density polyethylene film, which provided both mechanical

strength and flexibility. The ends of this laminated film were connected to form a belt. The resulting belt was placed over a homemade pulley system with LCE on the upper side. The film was simultaneously irradiated with UV-light in one area and with visible light in another area, which lead to rotational movement of the belt. It is implied that contracting and expanding motions in opposing regions of the film completes the process.

11.4.4 Nanoparticle-Liquid Crystalline Elastomer Composites

Photoactive LCE/nanoparticle composite of LCE needs discussion as this system also provides a new stimulant for actuation. The combination of suitable nanoparticles with LCEs makes multi-controlled actuation system responding to stimuli, such as, electric, magnetic fields, and broad-spectrum light. Moreover, there is strengthening effect due to nanoparticle dispersion in LCE, which may inversely affect the actuation properties. This prompted the study at very low level of nanoparticle modification which was found to be very successful.

As an example, both MWNTs and SWNTs are known to absorb light efficiently and convert the absorbed energy into heat (Ajayan et al. 2002; de la Zerda et al. 2011). In the visible as well as near-IR range, SWNTs show strong and specific absorptions (Hamon et al. 2001). Both act as nanoscale heating sources, changing photo-energy into heat. If the heat produced can be transferred efficiently throughout the matrix, the LCE nematic–isotropic phase transition can be triggered easily, leading to a shape change in the nanocomposite film. The dispersion of SWNTs (0.01 wt%) in LCE is found to be higher than the percolation threshold (Yang et al. 2008). Such a network can, effectively, serve as a thermal conduction pathway due to the high thermal conductivity of the SWNTs. Heat can be delivered throughout the LCE matrix uniformly and rapidly when irradiated with IR light source. At IR intensity of 45 mW/mm² ($\lambda = 808$ nm) the nanocomposite LCE contracted to 80 % of its maximum length. The temperature raised much above the Nematic-Isotropic transition temperature in 10 s. In similar time scale the reverse process occurs after switching off the source. White light also shows similar response.

In addition to visible and IR light, CNTs also show absorption in microwave, terahertz and megahertz frequency ranges (Mizuno et al. 2009). At high loading (>1 wt%) and corresponding alignment of CNTs can also make the LCE composites anisotropic at these frequencies. Using Terahertz frequency range of 0.2–3.5 THz, the absorption coefficient, parallel to the CNT alignment axis, is much larger than that in the perpendicular direction.

The noble metal nanoparticle (NP) incorporation in PDLC microstructure has another interesting feature. It is possible to create surface plasmon excitations (Hinojosa and Sharma 2010) at the NP-polymer interface which influences the electro-optical properties of PDLCs. Among few advantages, faster response in Ag

NPs doped PDLCs is observed (Zhu et al. 2009). Incorporation of inorganic NPs improves angular characteristics of light transmission through PDLCs (Yaroshchuk and Dolgov 2007). Incorporating ferroelectric nanoparticles like BaTiO₃ enhancement of electro-optical properties of liquid crystal cells is realized, which is the result of building up of local electric fields (Darla et al. 2014).

11.5 Dual Nature of Chromophore

11.5.1 Azobenzene

Azobenzene is a special molecule which undergoes rapid isomerization under light. Additionally, one of the isomer (trans-) possesses rigid rod structure akin to mesogen. This mesogen like structure can fit in conventional LC texture influencing photo response characteristics. On the other hand the molecule alone can function as mesogen while maintaining photoactive nature; thus exhibiting its dual nature.

Azobenzene can be designed by placing it in main chain, side chain, together both in main and side chain respectively. The main-chain azobenzene polymers are developed in the initial stages. However, those do not have appreciable orientational and deformational effects, as the mobility of azobenzenes is mostly restricted by their inclusion into the polymer backbone (Viswanathan et al. 1999). This result prompted developing the other two types.

Similar to other side-chain LC polymers, azobenzene containing side-chain LC polymers mainly form low-ordered LC phases, namely, nematic (N), smectic A (SmA) and C (SmC) phases (Eich et al. 1987; Rosenhauer et al. 2003; Abraham et al. 2005; Bublitz et al. 2000). Their phase structure and transition depend on various factors such as the chemical structure of azobenzene moieties, the spacer length, the tail of azo etc. These factors also influence their photoresponsive behavior. It has also been established that the branched and even dendritic polymer structures (Hvilsted and Ramanujam 2001) exhibit photoresponsive effects which are considerably smaller than those in linear azobenzene polymers.

Triblock copolymer having middle block with both LC and azo in combined pendant group shows typical self-assembly characteristics in to lamellar phase (Deng et al. 2008). The azobenzene-containing triblock copolymer exhibit surface alignment of the lamellas perpendicular to the substrate, whereas, the non-photoresponsive block copolymer organize the lamellas parallel to the substrate.

11.5.1.1 Macroscopic Motion

It is important to study the nanometer-scale azobenzene molecular conformational changes that give rise to macroscopic phenomena. The floating monolayers at a liquid surface, when irradiated, the generated bent cis-isomer leads to

reduction of limiting area per molecule of the polypeptide-azo monolayer (Higuchi et al. 1995). This can modify other bulk properties. For instance, some of the developments can be named as, photo-modulation of a monolayer's water contact angle (Luo et al. 2012), good photo-control over photo-patterning (Feng et al. 2001) and gradient in surface energy to move a macroscopic oil droplet (Ichimura et al. 2000). The running of molecular-level devices using light is definitely attractive in many applications, as the inherent limitations using other modes of energy are mostly avoided. It can be visualized that fast response and lack of waste products in azo isomerization are added advantage. The resulting molecular level motions have the potential to upscale to actual human-scale useful work. The progress is a continuous process. For example, an azo moiety linking two porphyrin rings is responsible for photo-control of electron transfer (Tsuchiya 1999), and different hydrogen-bonding networks (intermolecular and intramolecular) can be maintained by manipulating the isomeric state of the azo group linking two cyclic peptides (Vollmer et al. 1999). Another recent development includes osmotic pressure pumps (Masiero et al. 2008), created by the photo-controlled solubility of azobenzene, analytical columns, containing azo tethered silica columns, have increased effluent rate (Fujiwara et al. 2008), reversible light-controlled conductance switching (Pakula et al. 2010) etc.

Homogeneously aligned crosslinked LC polymer, containing low amount of azobenzene, bend towards actinic light source (Shimamura et al. 2011). Photomechanical response under pulsed irradiation can occur within sub-millisecond time scale. Further, a single laser pulse can be sufficient to bend the film.

Azotolane containing crosslinked LCP film, after upconversion nanophosphors incorporation, exhibits fast bending when exposed to continuous wave near-IR light ($\lambda = 980$ nm) (Wu et al. 2011). The trans-cis photoisomerization is the reason for bending. The noticeable point is that in off state the film becomes completely flat due to fast cis-trans back isomerization. Azobenzene containing thermoplastic elastomer can be made by grafting azobenzene derivative of polyacrylate onto a styrene-butadiene-styrene (SBS) triblock copolymer (Bai and Zhao 2001). In fact it remained first report of azobenzene containing elastomer.

Stretching a solution-cast film at room temperature easily leads to a long-range orientation of trans-azobenzene mesogens along the strain direction due to mechanical effect. When the stretched film is exposed to UV light (360 nm), the trans-cis photoisomerization takes place resulting in cis-isomer while getting disordered. On subsequent irradiation with visible light (440 nm), the cis-trans back-isomerization occurs while the trans-isomer recovers the earlier orientation. Such photoactive elastomers are employed as elastic holographic materials; the reason being that easy deformation can be used to enhance the diffraction efficiency (Zhao et al. 2003). The large and reversible elastic deformation also provides tunability to the grating in such a way that all the concerned parameters such as, period of grating, diffraction angle, and efficiency can be varied reversibly by simple mechanical deformation. Controlled azo side chain photoactive LCE, having rubbery

mid-block and azo methacrylate end blocks, can be designed by using ATRP method (Cui et al. 2004).

Photoisomerization under strain vs. order parameter study indicates that the order parameter, S , is around 0.38, indicating very good orientation of azobenzene mesogens in the trans form along the strain direction. After 10 min unpolarized UV light irradiation at 365 nm (100 mW/cm^2), the order parameter diminishes significantly (up to 0.17) due to isomerization to cis form with partial loss of orientation. The orientation recovery does not occur after isomerization back to trans form using unpolarized visible light (400 nm). However, in case of linearly polarized light, the greater strain recovery is observed ($S = 0.27$). Application can be visualized as medium for recording diffraction gratings whose attributes can be changed reversibly on elastic deformation of the film. For thin films of crosslinked azobenzene liquid-crystalline polymers (LCPs), fast, light-controlled bending and unbending can be observed (Chen et al. 2011), which prompts their application as a light-controlled actuator for micro device.

Another molecular design is based on siloxane-main chain photoactive liquid crystalline polymers with attachment of azo side groups through click chemistry route (Pandey et al. 2012a). Both trans and cis molar absorption coefficient ($\pi-\pi'$) and ($n-\pi'$) are very high and similar ($22,000\text{--}33,000 \text{ L mol}^{-1} \text{ cm}^{-1}$). The photoisomerization in chloroform solution shows two-stage kinetics. The polymer, in bilayer configuration, has shown photomechanical effect under unpolarized UV light. The fabrication of bilayer is done by casting polyvinyl chloride (PVA), which is later rubbed with silk cloth in one direction. The azo-polysiloxane film is cast on rubbed PVA film and the resulting oriented bilayer exhibits photomechanical effect. The contraction and consequent bending of the film can be observed along the director (Fig. 11.8).

Siloxane based, azo containing hyperbranched elastomers can exhibit optical activity (Pandey et al. 2012b). The photoisomerization in solution is more rapid than linear elastomer. The glass transition being very low the polymer is blended with poly (methyl methacrylate). Even then contraction along director is observed under non polarized UV light.

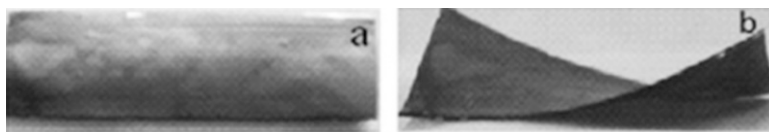


Fig. 11.8 Photomechanical bending of Azo-siloxane polymer under irradiation with UV light (a) before irradiation (b) after irradiation (Reference: Pandey, S., Kolli, B., Mishra, S. P., Samui, A.B. (2012) Siloxane Polymers Containing Azo Moieties Synthesized by Click Chemistry for Photo Responsive and Liquid Crystalline Applications, *J Polym Sci Part A: Polym Chem* 50: 1205–1215)

11.5.2 *Bis(benzylidene)*

A new class of polymer having dual functionality, such as photoresponsive and mesogenic nature is derived from bis(benzylidene) as building block (Gangadhara and Kishore 1993). Under photoresponsive nature it undergoes crosslinking via 2 + 2 cycloaddition. Photo-reactive main chain liquid crystalline polyesters, containing oxadiazole and bisbenzylidene cycloalkanone units exhibit fluorescence in addition to photoresponsive nature (Balamurugan and Kannan 2008). Band gap energies, as calculated from the absorption spectra, are in the range of 3.17–3.41 eV. During excitation around 360–389 nm, the PL spectra of polymers in solution exhibits blue-emission having maxima in the range of 411–438 nm.

Faster photo-induced behavior in hyperbranched architecture than the linear structure is usually observed. Acyclic units, associated with bis (benzylidene), facilitate photo-cycloaddition; five-membered rings showing better photoactivity as compared to six-membered rings (Murali and Samui 2010). Reasonably high photoactivity qualifies it for potential application as photo-responsive functional materials.

11.6 Miscellaneous

A photoactive liquid crystalline polymer with electrical conductivity can be designed by attaching photoactive moiety like azobenzene to electrically conductive LCP. Polyindole acts as LC polymer and electrical conductivity is inherent due to its conjugated nature. Along with azobenzene pendant group, a triple activity can be realized (Hosseini and Ashjari 2013).

Spatial organization and ordering of ionic liquid (IL) in nano- and mesoscale, originated from the research activities engaged with the development of anisotropic, ion-conductive thin films, not only represents interesting basic research, but also broadens the scopes of application of PILs, mainly in the areas of nanolithography, optoelectronics, nanophotonics, etc.

Prepolymerization ordering of bulk IL can be done by using the phenomenon of molecular self-assembly of mesogenic monomer. Subsequent photopolymerization is used to lock in situ ordering (Hoshino et al. 2003). The photopolymerized free-standing PIL film exhibits enhanced electrolytic conductivity parallel to the direction of the smectic A layers. One dimensional ion-conductive channels can be realized which can be oriented both perpendicular and parallel to the polymer film surface

11.7 Applications

Switchable gas permeation membranes can be fabricated by using photo-switchable low-molecular-weight liquid crystalline (LC) material as the active element. Different LC eutectic mixtures based on cyanobiphenyls and phenyl benzoates, doped

with mesogenic azo dyes, are introduced into commercially available track-etched porous polycarbonate membranes with cylindrical pores (0.40–10.0 μm). The photo-switchable cyanobiphenyl LC material exhibits low permeability in the nematic state, while the photogenerated isotropic state demonstrates higher sorption coefficient. Permeability switching times of the membranes can be maintained around 5 s using alternating UV and $>420\text{-nm}$ radiation at an intensity of 2 mW/cm^2 (Glowacki et al. 2009). A dye-doped LCE sample (5 mm \times 5 mm \times 0.32) mm, supported at one end, on irradiation by green light for 60 ms (at $\lambda = 514\text{ nm}$ from a continuous-wave Ar⁺ ion laser) undergoes large and rapid bending ($>45^\circ$ bend angle) after illumination at 600 mW. The axis of the cylindrical bend is parallel to the sample surface while remaining perpendicular to the nematic director. The sample exhibits fast response times at 600 mW, with a rise time of 20 ms and a relaxation time of 75 ms respectively (Camacho-Lopez et al. 2004). Further, the rapid material contraction along the nematic director at the irradiated surface is apparently volume-conserving as it is accompanied by expansion in the orthogonal direction. The contraction is the result of decreased orientational order at the surface only. The interaction with environment can be studied by illuminating LCE samples floating on water. The sample swims away from the light. The direction of the observed motion is perpendicular to the nematic director. The system, thus, is akin to a motor, where motion is caused by the transfer of energy, but not momentum, to the system. The illumination causes the flat sample to adopt a more compact, bent, configuration. In the off state, the sample unbends to resume its original flat shape; it is capable of doing work in this process. When the sample bends, it sinks lower in the water and the shape change increases the potential energy of the water. Energy for the swimming is, therefore, stored both in the LCE and in the water.

The orientation of phase separated structures can give nanochannels, which is always difficult to achieve. The development of liquid crystalline block copolymers make it simpler as LC orientation control techniques can be applied (Tomikawa et al. 2005). Shear flow at nematic temperatures orients the nonmesogenic microcylinders, along with the nematic mesogens of the LCP in the velocity direction (Tokita et al. 2006). This amounts to a possibility of controlling the orientation of a cylinder by using photo-orientation of liquid crystals. The orientation of PEO cylinder structure can be controlled by the supramolecular cooperative motions between the ordered azobenzene liquid crystals and PEO cylinder of azobenzene/polyethylene oxide (PEO) block copolymer via the polarization of the irradiating light (Fig. 11.9) (Yu et al. 2006).

Polymeric microactuators manufacturing is complicated due to the requirement of including electrodes for actuation or using lithographic techniques for patterning. As a solution, inkjet printing technology along with self-organizing liquid-crystal network actuators can be used to fabricate all-polymer microdevices (van Oosten et al. 2009). Multiple inks are used to fabricate microactuators with different subunits which can be selectively addressed by varying the wavelength of the light. The process can be used for large scale production of miniaturized active polymer systems at low cost.

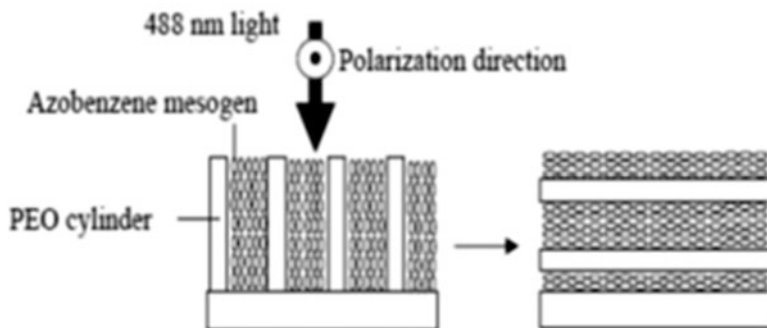


Fig. 11.9 Schematics of liquid crystal alignment and microphase-separated structures [Reprinted with permission from (Yu, H., Iyoda, T., Ikeda, T. (2006) Photoinduced alignment of nanocylinders by supramolecular cooperative motions. *J. Am. Chem. Soc.*, 128: 11010-11011). Copyright (2006) American Chemical Society

Devices based on liquid-crystal materials are being developed for spectroscopy, imaging and microscopy purposes, which are considered as newer techniques for optically probing biological systems. Biosensors fabricated with liquid-crystal materials can allow label-free observations of biological phenomena. Liquid-crystal polymers are also finding use in biomimicking colour-producing structures, lenses and muscle-like actuators (Woltman et al. 2007)

An optimized azobenzene precursor and polydimethylsiloxane-soft-template-based secondary replication can be utilized to prepare micro-arrayed liquid crystal polymer film cross-linked in the nematic phase (Li et al. 2012) If the micro-arrayed film is irradiated alternatively by using UV and visible light (365 nm/530 nm), it switches reversibly between superhydrophobic and hydrophilic state in quick time (<1 min).

A plastic robotic arm can be designed which can be powered solely by visible light (Yu and Ikeda 2011). Double-layered strips of two different polymeric materials, comprising a special cross-linked liquid crystalline polymer (CLCP) and an inactive polyethylene in a bilayer fashion are used for the purpose. By irradiating with blue light, the CLCP material can be induced to contract whereas polyethylene does not show any contraction. This causes a bending motion of the strip. The bend is found to be fully reversible. It allows the arm to flex in the middle like an elbow while gripping at end mimicking a hand. The force-per-unit-area was generated to the extent of 300 kPa as compared to muscles in the human body at 320 kPa. The product may find application in micromachining.

Crosslinked azobenzene liquid-crystalline polymer composite films have successfully demonstrated new sophisticated movements such as an inchworm walk and flexible robotic arm motion (Yamada et al. 2009). The polymer layer and laminated sections are alternated which make the film to behave like a hinge joint and move flexibly. The intensity of the light and the position on the film can be judiciously controlled to make the film move as planned. The polymers function

with a minimum of moving parts which has the ability to minimize the friction and surface contact problems. The designed light driven system can be employed for direct light-to-mechanical energy conversion, storage systems and in microfluidic devices.

11.8 Conclusion and Future Prospects

Photoactivity of liquid crystalline polymer and few common photoisomerizable moieties have been presented at the beginning of the chapter. Later, various forms of physical blends and chemical attachment possible have been presented and discussed in respect of their requirement, special feature, photoisomerization and effect on their behaviour and finally application possibilities have been discussed. A special group, in which chromophore showing photoisomerization can act like a mesogen. This has been presented to understand their interrelated properties. A special group, called as liquid crystalline elastomer, having maximum application possibilities, have been discussed in detail, particularly their photomechanical properties. The underlined principle for using liquid single crystal elastomer is presented and a typical synthesis and processing followed by discussion are presented. Finally, application possibilities are also presented. The intelligent materials are known to be very useful in many areas and the interdisciplinary fields such as the medicine, pharmacy, bioengineering, polymer, metallurgy, semiconductor, ceramics, electronics, and machinery. The application of such materials in human engineering, safety engineering, environmental research, and the study of the resources will always make a subject of future. With the maturation of the information display field, liquid-crystal materials research is undergoing a modern-day renaissance. New areas of application in the realms of biology and medicine are stimulating innovation in basic and applied research into these materials. The design of smart polymer in micro and nano level can make huge change in the state of understanding and their performance.

References

- Abraham S, Paul S, Narayan G, Prasad SK, Rao DSS, Jayaraman N, Das S (2005) Observation of a chiral smectic phase in azobenzene-linked bolaamphiphiles containing free sugars. *Adv Funct Mater* 15:1579–1584
- Ajayan PM, Terrones M, de la Guardia A, Huc V, Grobert N, Wei BQ, Lezec H, Ramanath G, Ebbesen TW (2002) Nanotubes in a flash—ignition and reconstruction. *Science* 296:705
- Arafune R, Sakamoto K, Ushioda S, Tanioka S, Murata S (1998) Importance of rubbing-induced inclination of polyimide backbone structures for determination of the pretilt angle of liquid crystals. *Phys Rev E* 58:5914
- Arun A, Reddy BSR (2004) The influence of comonomer (2-hydroxyethyl acrylate) and keto group on photocrosslinking property of arylidene polymers. *J Polym Sci Polym Chem* 42:3433–3444

- Athanassiou A, Kalyva M, Lakiotaki K, Georgiou S, Fotakis C (2005) All-optical reversible actuation of photochromic-polymer microsystems. *Adv Mater* 17:988–992
- Bai S, Zhao Y (2001) Azobenzene-containing thermoplastic elastomers: coupling mechanical and optical effects. *Macromolecules* 34:9032–9038
- Balamurugan R, Kannan P (2008) Photoreactive main chain liquid crystalline polyesters containing oxadiazole and bis(benzylidene) cycloalkanone units. *J Polym Sci Polym Chem* 46:5760–5775
- Barrett CJ, Mamiya J-I, Yager KG, Ikeda T (2007) Photo-mechanical effects in azobenzene containing soft materials. *Soft Matter* 3:1249–1261
- Bobrovsky AY, Boiko NI, Shibaev VP (1999) New chiral photochromic menthone-containing homopolymers and copolymers—synthesis, phase behaviour and photo-optical properties. *Liq Cryst* 26(2):1749–1765
- Bobrovsky AY, Boiko NI, Shibaev VP (2001) Chiral nematic copolymers with photoreversible and irreversible changing of helical supramolecular structure pitch. *Chem Mater* 13:1998–2001
- Bobrovsky A, Shibaev V, Elyashevich G, Rosova E, Shimkin A, Shirinyan V, Cheng K-L (2010) Photochromic composites based on porous stretched polyethylene filled by nematic liquid crystal mixtures. *Polym Adv Technol* 21:100–112
- Buguin, A.; Li, M-H.; Silberzan, P.; Ladoux, B.; Keller, P. (2006). Micro-Actuators: When Artificial Muscles Made of Nematic Liquid Crystal Elastomers Meet Soft Lithography. *J. Am. Chem. Soc.*, 128 (4), 1088–1089
- Bouas-Laurent H, Dürr H (2001) Organic photochromism (IUPAC Technical Report). *Pure Appl Chem* 73(4):639–665
- Bronner C, Tegeder P (2014) Photo-induced and thermal reactions in thin films of an azobenzene derivative on Bi(111). *New J Phys* 16:053004, 16 pp
- Blublitz D, Helgert M, Fleck B, Wenke L, Hvilsted S, Ramanujam PS (2000) Photoinduced deformation of azobenzene polyester films. *Appl Phys B* 70:863–865
- Camacho-Lopez M, Finkelmann H, Palfy-Muhoray P, Shelley M (2004) Fast liquid-crystal elastomer swims into the dark. *Nat Mater* 3:307–310
- Castellano JA (1992) Liquid crystal display. In: Castellano JA (ed) *Handbook of display technology*. Academic, San Diego, pp 181–250
- Chambers M, Zalar B, Remškar M, Žumer S, Finkelmann H (2006) Actuation of liquid crystal elastomers reprocessed with carbon nanoparticles. *Appl Phys Lett* 89:243116
- Chen M, Xiaozhen W, Xing X, Zhu Y, Liu Z, Cheng F, Yu Y (2011) Light-driven mobile robot based on light-induced bending polymer film. *J Mech Eng Res* 3(4):114–119
- Cheng F, Yin R, Zhang Y, Yen C-C, Yu Y (2010) Fully plastic microrobots which manipulate objects using only visible light. *Soft Matter* 6:3447–3449
- Chrzanowski MM, Zieliński J, Olifierczuk M, Kędzierski J, Nowinowski-ruszelnicki E (2011) Photoalignment - an alternative aligning technique for. *Liquid Crystal Displays* 48(1):7–13
- Cipparrone G, Pagliusi P, Provenzano C, Shibaev VP (2010) Polarization holographic recording in amorphous polymer with photoinduced linear and circular birefringence. *J Phys Chem B* 114 (27):8900–8904
- Corbett DR, Adams JM (2013) Tack energy and switchable adhesion of liquid crystal elastomers. *Soft Matter* 9:1151–1163
- Corbett D, Warner M (2009) Changing liquid crystal elastomer ordering with light—a route to opto-mechanically responsive materials. *Liquid Crystals* 36:1263–1280
- Corvazier L, Zhao Y (1999) Induction of liquid crystal orientation through azobenzene-containing polymer networks. *Macromolecules* 32:3195–3200
- Cui L, Tong X, Yan X, Liu G, Zhao Y (2004) Photoactive thermoplastic elastomers of azobenzene-containing triblock copolymers prepared through atom transfer radical polymerization. *Macromolecules* 37:7097–7104
- Darla MR, Hegde S, Varghese S (2014) Effect of BaTiO₃ nanoparticle on electro-optical properties of polymer dispersed liquid crystal displays. *J Crystal Process Technol* 4:60–63

- Davis SR, Farca G, Rommel SD, Johnson S, Anderson MH (2010) Liquid crystal waveguides: new devices enabled by >1000 waves of optical phase control. In: Chien L-C (ed) *Emerging liquid crystal technologies V*, Proc. of SPIE, vol 7618, 76180E(1–14) © 2010 SPIE
- Davis KA, Burke KA, Mather PT, Henderson JH (2011) Dynamic cell behavior on shape memory polymer substrates. *Biomaterials* 32:2285–2293
- de la Zerda A, Kim J-W, Galanzha EI, Gambhir SS, Zharov VP (2011) Advanced contrast nanoagents for photoacoustic molecular imaging, cytometry, blood test and photothermal theranostics. *Contrast Media Mol Imaging* 6:346–369
- Deng W, Albouy P-A, Lacaze E, Keller P, Wang X, Li MH (2008) Azobenzene-containing liquid crystal triblock copolymers: synthesis, characterization, and self-assembly behavior. *Macromolecules* 41:2459–2466
- Eich M, Wendorff JH, Reck B, Ringsdorf H (1987) Reversible digital and holographic optical storage in polymeric liquid-crystals. *Makromol Chem Rapid Commun* 8:59–63
- Eisenbach CD (1978) Effect of polymer matrix on the cis-trans isomerization of azobenzene residues in bulk polymers. *Makromol Chem* 179(10):2489–2506
- Fan M-G, Yu L, Zhao W (1999) Fulgide family compounds: synthesis, photochromism, and applications. In: Crano JC, Guglielmetti RJ (eds) *Organic photochromic and thermochromic compounds, vol 1: main photochromic families*. Plenum, New York, pp 141–206
- Feng CL, Zhang YJ, Jin J, Song YL, Xie LY, Qu GR, Jiang L, Zhu DB (2001) Reversible wettability of photoresponsive fluorine-containing azobenzene polymer in langmuir-blodgett films. *Langmuir* 17(15):4593–4597
- Finkelmann H, Kock HJ, Rehage G (1981) Investigations on liquid-crystalline polysiloxanes. 3. Liquid-crystalline elastomers—a new type of liquid-crystalline material. *Makromol Chem Rapid Commun* 2:317–322
- Finkelmann H, Gleim W, Hammerschmidt K, Schatzle J (1989) Liquid-crystal elastomers. *Makromol Chem Macromol Symp* 26(1):67
- Finkelmann H, Nishikawa E, Pereira GG, Warner M (2001) A new opto-mechanical effect in solids. *Phys Rev Lett* 87:015501:1–015501:4
- Florea L, Diamond D, Benito-Lopez F (2012) Photo-responsive polymeric structures based on spiro pyran. *Macromol Mater Eng* 297:1148–1159
- Fujiwara M, Akiyama M, Hata M, Shikawa K, Nomura R (2008) Photoinduced acceleration of the effluent rate of developing solvents in azobenzene-tethered silica gel. *ACS Nano* 2(8):1671–1681
- Gangadhara K, Kishore K (1993) Novel photocrosslinkable liquid-crystalline polymers: poly[bis(benzylidene)] esters. *Macromolecules* 26(12):2995–3003
- Gangadhara K, Kishore K (1995) A new class of photo-cross-linkable side chain liquid crystalline polymers containing bis(benzylidene)cyclohexanone units. *Macromolecules* 28(4):806–881
- Gimeno N, Pintre I, Martinez-Abadia M, Serrano JL, Ros MB (2014) Bent-core liquid crystal phases promoted by azo-containing molecules: from monomers to side-chain polymers. *RSC Adv* 2014(4):19694–19702
- Glowacki E, Marshall KL, Tang CW (2009) Photoswitchable gas permeation membranes based on azobenzene-doped liquid crystals. In: Khoo IC (ed) *Proc. SPIE 7414, Liquid Crystals XIII*, 74140H, San Diego, 2 August
- Grabcheva I, Moneva I, Wolarzb E, Bauman D (2003) Fluorescent 3-oxy benzantrone dyes in liquid crystalline media. *Dyes Pigments* 58:1–6
- Gregorc M, Zalar B, Domenici V, Ambrozic G, Drevensek-Olenik I, Fally M, Copic M (2011) Depth profile of optically recorded patterns in light-sensitive liquid-crystal elastomers. *Phys Rev E* 84:031707:1–031707:19
- Gregorc M, Li H, Domenici V, Ambrozic G, Copic M, Drevensek-Olenik I (2012) Kinetics of holographic recording and spontaneous erasure processes in light-sensitive liquid crystal elastomers. *Materials* 5:741–753
- Gust D, Andréasson J, Pischel U, Moore TA, Moore AL (2012) Data and signal processing using photochromic molecules. *Chem Commun* 48:1947–1957

- Hamon MA, Itkis ME, Niyogi S, Alvaraez T, Kuper C, Menon M, Haddon RC (2001) Effect of rehybridization on the electronic structure of single-walled carbon nanotubes. *J Am Chem Soc* 123:11292–11293
- Hasegawa M, Yamamoto T, Kanazawa A, Shiono T, Ikeda T, Nagase Y, Akiyama E, Takamura Y (1999) Real-time holographic grating by means of photoresponsive polymer liquid crystals with flexible siloxane spacer in the side chain. *J Mater Chem* 9:2765–2772
- Higuchi M, Minoura N, Kinoshita T (1995) Photo-responsive behavior of a monolayer composed of an azobenzene containing polypeptide in the main-chain. *Colloid Polymer Sci* 273 (11):1022–1027
- Hikmet RAM (1990) Electrically induced light-scattering from anisotropic gels. *J Appl Phys* 68 (9):4406–4412
- Hinojosa A, Sharma SC (2010) Effects of gold nanoparticles on electro-optical properties of a polymer-dispersed liquid crystal. *Appl Phys Lett* 97(8):081114
- Hirshberg Y, Fischer, E (1954) Photochromism and reversible multiple internal transitions in somespiropyrans at low temperatures. Part I. *J Chem Soc*, 0, 297–303
- Holme NCR, Ramanujam PS, Hvilsted S (1996) Photoinduced anisotropy measurements in liquid-crystalline azobenzene side-chain polyesters. *Appl Opt* 35:4622–4627
- Hoshino K, Yoshio M, Mukai T, Kishimoto K, Ohno H, Kato T (2003) *J Polym Sci Part A Polym Chem* 41:3486–3492
- Hosseini SH, Ashjari M (2013) Synthesis and characterization of polyindole with liquid crystalline azobenzene as side chains. *Int J Phys Sci* 8(32):1611–1622
- Hunger K (2003) *Industrial dyes: chemistry, properties and applications*. Wiley-VCH, Weinheim, pp 14–35
- Hvilsted S, Ramanujam PS (2001) The azobenzene optical storage puzzle—demands on the polymer scaffold? *Monatshefte für Chemie* 132:43–51
- Ichimura K, Oh S-K, Nakagawa M (2000) Light-driven motion of liquids on a photoresponsive surface. *Science* 288(5471):1624–1626
- Ichimura K, Fujiwara T, Momose M, Matsunaga D (2002) Surface-assisted photoalignment control of lyotropic liquid crystals. Part 1. Characterisation and photoalignment of aqueous solutions of a water-soluble dye as lyotropic liquid crystals. *J Mater Chem* 12:3380–3386
- Ikeda T, Itakura H, Lee C, Winnik FM, Tazuke S (1988) Topochemical photodimerization in polymer liquid crystals. *Macromolecules* 21(12):3536–3537
- Ikeda T, Mamiya J-I, Yu Y (2007) Photomechanics of liquid-crystalline elastomers and other polymers. *Angew Chem Int Ed* 46:506–528
- Iwan A, Palewicz M, Sikora A, Chmielowiec J, Hreniak A, Pasciak G, Bilski G (2010) Aliphatic–aromatic poly(azomethine)s with ester groups as thermotropic materials for opto(electronic) applications. *Synth Met* 160(17–18):1856–1867
- Jikei M, Chon SH, Kakimoto MA, Kawachi S, Imase T, Watanebe J (1999) Synthesis of hyperbranched aromatic polyamide from aromatic diamines and trimesic acid. *Macromolecules* 32(6):2061–2064
- Kaniappan K, Murugavel SC (2009) Photocrosslinkable phosphorus containing homo- and copolyesters: synthesis, characterization, and photosensitive properties. *J Appl Polym Sci* 111:1606–1614
- Koshima H, Ojima N, Uchimoto H (2009) Mechanical motion of azobenzene crystals upon photoirradiation. *J Am Chem Soc* 131:6890–6891
- Kubytzkyi V, Reshetnyak V (2006) Electrically controllable diffraction efficiency of H-PDLC film composed of ellipsoidal liquid crystal droplets. *Mol Cryst Liq Cryst* 453:321–332
- Kulawardana EU, Kuruwita-Mudiyanselage T, Neckers DC (2009) Dual responsive poly(*N*-isopropylacrylamide) hydrogels having spironaphthoxazines as pendant groups. *J Polym Sci Polym Chem* 47(13):3318–3325
- Kumar G, Subramanian K, Ganesan S (2013) Synthesis and characterisation of photo-cross-linkable liquid crystalline poly(*n*-[*n'*-fluorobenzoylstyryloxy] alkylmethacrylate)s and their fluorescence lifetime properties. *J Spectrosc* 181485, 13 pp

- Kupfer J, Finkelmann H (1991) Nematic liquid single crystal elastomers. *Makromol Chem Rapid Commun* 12(12):717–726
- Lee KM, Wang DH, Koerner H, Vaia RA, Tan L-S, White TJ (2012) *Angew Chem* 124:4193–4197
- Legge CH, Mitchell GR (1992) *J Phys D Appl Phys* 25:492
- Lendlein A, Jiang H, Junger O, Langer R (2005) Light induced shape-memory polymers. *Nature* 434:879–882
- Li MH, Keller P (2006) Artificial muscles based on liquid crystal elastomers. *Philos Trans R Soc Lond Ser A* 364:2763–2777
- Li MS, Fuh AY-G, Wu S-T (2011) Optical switch of diffractive light from a BCT photonic crystal based on HPDLC doped with azo component. *Opt Lett* 36(19):3864–3866
- Li C, Cheng F, Lv J-A, Zhao Y, Liu M, Jiang L, Yu Y (2012) Light-controlled quick switch of adhesion on a micro-arrayed liquid crystal polymer superhydrophobic film. *Soft Matter* 8:3730–3733
- Liu C, Qin H, Mather PT (2007) Review of progress in shape-memory polymers. *J Mater Chem* 17:1543–1558
- Lukyanov BS, Lukyanova MB (2005) Spiropyrans: synthesis, properties, and application. *Chem Heterocycl Comp* 41:281–311
- Luo M, Gupta R, Frechette J (2012) Modulating contact angle hysteresis to direct fluid droplets along a homogenous surface. *ACS Appl Mater Interfaces* 4(2):890–896
- Mahimwala Z, Yager KG, Mamiya J, Shishido A, Barrett CG (2013) Photo-mechanical azo polymers for light-powered actuation. In: Knopf GK, Otani Y (eds) *Photomechanical azo polymers*. CRC, Boca Raton, pp 107–152
- Mahimwalla Z, Yager KG, Mamiya J-I, Shishido A, Priimagi A, Barrett CJ (2012) Azobenzene photomechanics: prospects and potential applications. *Polym Bull* 69:967–1006
- Malik P, Kumar P, Raina KK (2006) Guest-host polymer dispersed liquid crystal display device: role of dichroic dye. In: *The 9th Asian symposium on information display*, October 8–12, New Delhi, India
- Masiero S, Lena S, Pieraccini S, Spada GP (2008) The direct conversion of light into continuous mechanical energy by photoreversible self-assembly: a prototype of a light-powered engine. *Angew Chem Int Ed* 47(17):3184–3187
- Matharu AS, Jeeva S, Ramanujam PS (2007) Liquid crystals for holographic optical data storage. *Chem Soc Rev* 36:1868–1880
- Merino E, Ribagorda M (2012) Control over molecular motion using the cis–trans photoisomerization of the azo group. *Beilstein J Org Chem* 2012(8):1071–1090
- Mizuno K, Ishii J, Kishida H, Hayamizu Y, Yasuda S, Futaba DN, Yunura M, Hata K (2009) A black body absorber from vertically aligned single-walled carbon nanotubes. *Proc Natl Acad Sci U S A* 106:6044–6047
- Morgenstern K (2009) [Isomerization reactions on single adsorbed molecules](#). *Acc Chem Res* 42:213–223
- Murali M, Samui AB (2010) Bis benzylidene cycloalkanones: a versatile molecule as polymer building block. *J Mater Chem* 20:2714–2737
- Mysliwiec J, Miniewicz A, Nespurek S, Studenovskiy M, Sedlakova Z (2007) Efficient holographic recording in novel azo-containing polymer. *Opt Mater* 29:1756–1762
- Natansohn A, Rochon P, Pezolet M, Audet P, Brown D, To S (1994) *Macromolecules* 27:2580–2585
- Ohm C, Brehmer M, Zentel R (2010) Liquid crystalline elastomers as actuators and sensors. *Adv Mater* 22:3366–3387
- Ohm C, Brehmer M, Zentel R (2012) Liquid crystal elastomers: materials and applications. In: de Jeu WH (ed) *Springer: Berlin and Heidelberg*
- Pakula C, Zaporotchenko V, Strunskus T, Zargarani D, Herges R, Faupel F (2010) Reversible light-controlled conductance switching of azobenzene-based metal/polymer nanocomposites. *Nanotechnology* 21(46):485201

- Pandey S, Kolli B, Mishra SP, Samui AB (2012a) Siloxane polymers containing azo moieties synthesized by click chemistry for photo responsive and liquid crystalline applications. *J Polym Sci Polym Chem* 50:1205–1215
- Pandey S, Mishra SP, Kolli B, Kanai T, Samui AB (2012b) Hyperbranched photo responsive and liquid crystalline azo-siloxane polymers synthesized by click chemistry. *J Polym Sci Polym Chem* 50:2659–2668
- Priimagi A, Shimamura A, Kondo M, Hiraoka T, Kubo S, Mamiya J-I, Kinoshita M, Ikeda T, Shishido A (2012) Location of the azobenzene moieties within the cross-linked liquid-crystalline polymers can dictate the direction of photoinduced bending. *ACS Macro Lett* 1(1):96–99
- Raclę C, Airinei A, Cozan V, Cazacu M, Sajo IE (2003) New arylidene–siloxane polyethers: liquid-crystalline and photosensitive properties. *J Appl Polym Sci* 90:3093–3099
- Rao VS, Samui AB (2008) Molecular engineering of photoactive liquid crystalline polyester epoxies containing benzylidene moiety. *J Polym Sci Polym Chem* 46:7637–7655
- Rao VS, Samui AB (2009) Structure–property relationship of photoactive liquid crystalline polyethers containing benzylidene moiety. *J Polym Sci Polym Chem* 47:2143–2155
- Rau H (1990) In: Rabek JF (ed) *Photochemistry and photophysics*, vol. II. CRC, Boca Raton
- Rosenhauer R, Kozlovsky MV, Stumpe J (2003) Photoinduced anisotropy in spin-coated films of chiral smectic copolymermethacrylates containing azobenzene side groups. *J Phys Chem A* 107(9):1441–1446
- Ruan J, Ge JJ, Zhang A, Jin S, Wang S-Y, Harris FW, Cheng SZD (2002) Polymorphous structures and their phase relationships in a main-chain/side-chain liquid crystalline polyester. *Macromolecules* 35(3):736–745
- Russev M-M, Hecht S (2010) Photoswitches: from molecules to materials. *Adv Mater* 22:3348–3360
- Sakthivel P, Kannan P (2005) Investigation on thermotropic liquid crystalline and photocrosslinkable polyarylidene arylphosphate esters containing cyclohexanone units. *Polymer* 46(23):9821–9830
- Sanchez-Ferrer A (2011) Light-induced disorder in liquid-crystalline elastomers for actuation. In: Esteve J, Terentjev EM, Campo EM (eds) *Nano-opto-mechanical systems (NOMS)*. Proc. of SPIE vol 8107, 810702, pp 1–8
- Sanchez-Ferrer A, Finkelmann H (2013) Opto-mechanical effect in photoactive nematic main-chain liquid-crystalline elastomers. *Soft Matter* 9:4621–4627
- Sanchez-Ferrer A, Fischl T, Stubenrauch M, Albrecht A, Wurmus H, Hoffmann M, Finkelmann H (2011) Liquid-crystalline elastomer microvalve for microfluidics. *Adv Mater* 23:4526–4530
- Seo D-S, Muroi K, Kobayashi S (1992) Generation of pretilt angles in nematic liquid crystal, 5CB, media aligned on polyimide films prepared by spin-coating and LB techniques: effect of rubbing. *Mol Cryst Liq Cryst* 213:223–228
- Shibaev V, Bobrovsky A, Boiko N (2003) Photoactive liquid crystalline polymer systems with light-controllable structure and optical properties. *Prog Polym Sci* 28:729–836
- Shimamura A, Priimagi A, Mamiya J-I, Kinoshita M, Ikeda T, Shishido A (2011) Photoinduced bending upon pulsed irradiation in azobenzene-containing crosslinked liquid-crystalline polymers. *J Nonlinear Optic Phys Mat* 20:405–413
- Simoni F, Francescangeli O (2000) Optical properties of polymer-dispersed liquid crystals. *Int J Polym Mater* 45(3–4):381–449
- Su Y-C, Chu C-C, Chang W-T, Hsiao V-K-S (2011) Characterization of optically switchable holographic polymer-dispersed liquid crystal transmission gratings. *Opt Mater* 34(1):251–255
- Sugiyama S, Sakata Y, Sakata S, Hayashi T (1999) Light processing and optical devices using nano-sized droplets of liquid crystal dispersed in polymer. *J Intell Mater Syst Struct* 10:489–492
- Tajbakhsh AR, Terentjeva EM (2001) Spontaneous thermal expansion of nematic elastomers. *Eur Phys J E6*:181–188

- Tasic B, Li W, Sánchez-Ferrer A, Copic M, Drevensek-Olenik I (2013) Light-induced refractive index modulation in photoactive liquid-crystalline elastomers. *Macromol Chem Phys* 214:2744–2751
- Tokita M, Adachi M, Takazawa F, Watanabe J (2006) Shear flow orientation of cylindrical microdomain in liquid crystalline diblock copolymer and its potentiality as anchoring substrate for nematic mesogens. *Jpn J Appl Phys* 45:9152–9156
- Tomikawa N, Lu Z, Itoh T, Imrie CT, Adachi M, Tokita M, Watanabe J (2005) Orientation of microphase-segregated cylinders in liquid crystalline diblock copolymer by magnetic field. *Jpn J Appl Phys* 44:L711–L714
- Tork A, Galstian TV, Lessard RA (2001) Fulgide-doped photopolymers as reversible storage media. In: Proc. SPIE 4342, Optical Data Storage, 593
- Treloar LRG (2005) The physics of rubber elasticity, 3rd edn. Oxford University Press, New York
- Trenor SR, Long TE, Love BJ (2005) Development of light-deactivatable PSA via photodimerization. *J Adhes* 81(2):213–229
- Tsuchiya S (1999) Intramolecular electron transfer of diporphyrins comprised of electron-deficient porphyrin and electron-rich porphyrin with photocontrolled isomerization. *J Am Chem Soc* 121(1):48–53
- Uchida T, Wada M (1981) Guest-host type liquid crystal displays. *Mol Cryst Liquid Cryst* 63(1):19–43
- Ulrich K, Port H, Wolf HC, Wormer J, Effenberger F, Ilge H-D (1991) Photochromic thiophene-fulgides. Photokinetics of two isopropyl derivatives. *Chem Phys* 154:311–322
- Urayama K, Honda S, Takigawa T (2006) Deformation coupled to director rotation in swollen nematic elastomers under electric fields. *Macromolecules* 39(5):1943–1949
- van Oosten CL, Bastiaansen CWM, Broe DJ (2009) Printed artificial cilia from liquid-crystal network actuators modularly driven by light. *Nat Mater* 8:677–682
- Vinogradov V, Khizhnyak A, Kutulya L, Yu R, Reshtnyak A (1990) Photoinduced charge of cholesteric Lc-pitch. *Mol Cryst Liq Cryst* 192:273–278
- Viswanathan NK, Kim DY, Bian S, Williams J, Liu W, Li L, Samuelson L, Kumar J, Tripathy SK (1999) Surface relief structures on azo polymer films. *J Mater Chem* 9:1941–1955
- Vollmer MS, Clark TD, Steinem C, Ghadiri MR (1999) Photoswitchable hydrogen-bonding in self-organized cylindrical peptide systems. *Angew Chem Int Ed* 38(11):1598–1601
- Weigert F (1921) About a new effect of radiation. *Nat Sci* 9(30):583–588
- Willner I, Rubin S (1996) Control of the structure and functions of biomaterials by light. *Angew Chem Int Ed Engl* 35(4):367–385
- Wolarz E, Moryson H, Bauman D (1992) Dichroic fluorescent dyes for ‘guest-host’ liquid crystal displays. *Displays* 13(4):171–178
- Woltman SJ, Jay GD, Crawford GP (2007) Liquid-crystal materials find a new order in biomedical applications. *Nat Mater* 6:929–938
- Wu S-T, Fuh AY-G (2005) Lasing in photonic crystals based on dye-doped holographic polymer-dispersed liquid crystal diffraction gratings. *Jpn J Appl Phys* 44:977
- Wu YDY, Tsutsumi O, Kanazawa A, Shiono T, Ikeda T (1998) Photoinduced alignment of polymer liquid crystals containing azobenzene moieties in the side chain. 1. Effect of light intensity on alignment behavior. *Macromolecules* 31:349–354
- Wu Y, Zhang Q, Kanazawa A, Shiono T, Ikeda T, Nagase Y (1999) Photoinduced alignment of polymer liquid crystals containing azobenzene moieties in the side chain. 5. Effect of the azo contents on alignment behavior and enhanced response. *Macromolecules* 32(12):3951–3956
- Wu W, Yao L, Yang T, Yin R, Li F, Yu Y (2011) NIR-light-induced deformation of cross-linked liquid-crystal polymers using upconversion nanophosphors. *J Am Chem Soc* 133(40):15810–15813
- Xie P, Zhang R (2005) Liquid crystal elastomers, networks and gels: advanced smart materials. *J Mater Chem* 15:2529–2550

- Yager KG, Barrett CJ (2008) Azobenzene polymers as photomechanical and multifunctional smart materials. In: Shahinpoor M, Schneider H-J (eds) *Intelligent materials*. RSC Publishing, Cambridge, UK, pp 424–446
- Yamada M, Kondo M, Mamiya J-I, Yu Y, Kinoshita M, Barrett CJ, Ikeda T (2008) Photomobile polymer materials: towards light-driven plastic motors. *Angew Chem Int Ed* 47:4986–4988
- Yamada M, Kondo M, Miyasato R, Naka Y, Mamiya J-I, Kinoshita M, Shishido A, Yu Y, Barrett CJ, Ikeda T (2009) Photomobile polymer materials-various three-dimensional movements. *J Mater Chem* 19:60–62
- Yang L, Setyowati K, Li A, Gong S, Chen J (2008) Reversible infrared actuation of carbon nanotube–liquid crystalline elastomer nanocomposites. *Adv Mater* 20:2271–2275
- Yaroshchuk V, Dolgov LO (2007) Electro-optics and structure of polymer dispersed liquid crystals doped with nanoparticles of inorganic materials. *Opt Mater* 29(8):1097–1102
- Yu H (2014) Recent advances in photoresponsive liquid-crystalline polymers containing azobenzene chromophores. *J Mater Chem C* 2:3047–3054
- Yu Y, Ikeda T (2005) Photodeformable polymers: a new kind of promising smart material for micro- and nano-applications. *Macromol Chem Phys* 206:1705–1708
- Yu H, Ikeda T (2011) Photocontrollable liquid-crystalline actuators. *Adv Mater* 23(19):2149–2180
- Yu YL, Nakano M, Ikeda T (2003a) Directed bending of polymer film by light— miniaturizing a simple photomechanical system could expand its range of applications. *Nature* 425(6954):145
- Yu Y, Nakano M, Ikeda T (2003b) Photomechanics: directed bending of a polymer film by light. *Nature* 425:145–146
- Yu H, Iyoda T, Ikeda T (2006) Photoinduced alignment of nanocylinders by supramolecular cooperative motions. *J Am Chem Soc* 128:11010–11011
- Yusuf Y, Ono Y, Sumisaki Y, Cladis PE, Brand HR, Finkelmann H, Kai S (2004) Swelling dynamics of liquid crystal elastomers swollen with low molecular liquid crystals. *Phys Rev E* 69(2):021710
- Zhao Y (2003) Design and study of new liquid crystal/polymer materials. *Chin J Polym Sci* 21(6):621–629
- Zhao Y, Chenard Y (2000) *Macromolecules* 33:5891–5896
- Zhao Y, Bai S, Asatryan K, Galstian T (2003) Holographic recording in a photoactive elastomer. *Adv Func Mater* 13(10):781–788
- Zhu T, Tan B, Pan X, Tao W, Xu J (2009) Electro-optical characteristic of frequency modulation in nano Ag doped PDLC. In: *IEEE proceedings of the symposium on photonics and optoelectronics*, Wuhan, 14–16 August, pp 1–4
- Zhu W, Shelley M, Palfy-Muhoray P (2011) Modeling and simulation of liquid-crystal elastomers. *Phys Rev E* 83:051703–051711

Chapter 12

Combined Main-Chain/Side-Chain Liquid Crystalline Polymers: Synthesis and Supramolecular Ordering

Wenyi Huang

12.1 Introduction

The self-reproduction of complex molecules and supramolecular structures in living systems are realized by self-organization and genetic code transfer (Champe and Harvey 1994). Liquid crystalline polymers represent one of the most important macromolecular systems that have the capability of self-organization because of their unique molecular architectures with high anisotropy (Collings and Hird 1997). Although liquid crystalline order exists in many natural biomacromolecules, modern chemistry allows scientists to synthesize a new family of liquid crystalline polymers that mimic biological systems to construct synthetic functional systems with ordered structures. The most distinguished feature of liquid crystalline polymers lies in that they exhibit intermediate morphological states between crystalline (or glassy) and liquid states, where macromolecular chains can be self-organized into a wide spectrum of ordered structures such as nematic, smectic, and cholesteric mesophases (Donald and Windle 1992). Over the past decades, numerous endeavors have been made to rationally design and synthesize liquid crystalline polymers with controllable supramolecular structures.

Liquid crystalline polymers are basically built up from rigid molecular units, the so-called mesogens, which are linked by covalent bonds to construct macromolecular chains, while small molecules containing mesogens afford liquid crystals. Figure 12.1 gives the schematic representation of integrating liquid crystal molecules (or mesogens) into macromolecules to form main-chain liquid crystalline polymers (MCLCPs) in which mesogens are incorporated into the macromolecular backbone, side-chain liquid crystalline polymers (SCLCPs) in which mesogens are attached onto flexible polymer chains, and combined main-chain/side-chain liquid

W. Huang (✉)

Materials Science & Engineering Core R&D, The Dow Chemical Company,
Midland, MI 48667, USA

e-mail: polymerhuang@yahoo.com

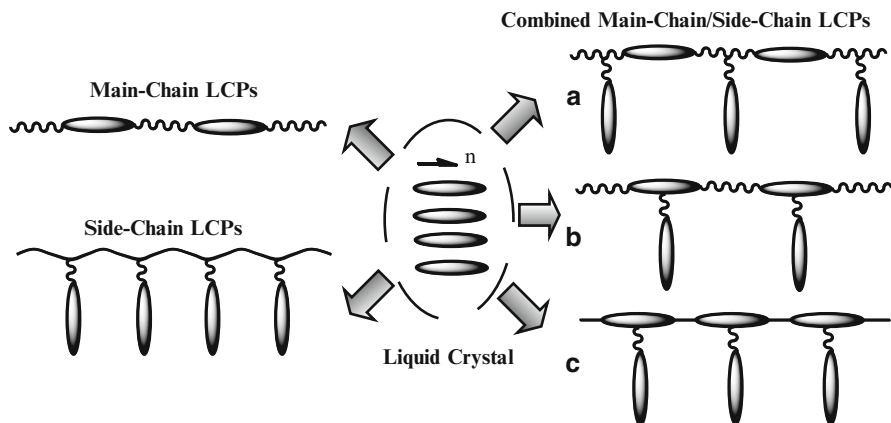


Fig. 12.1 Schematic representation of formation of main-chain liquid crystalline polymers (LCPs), side chain LCPs, and combined main-chain/side-chain LCPs with side-chain mesogens attached onto (a) main-chain flexible spacers, (b) main-chain mesogens having flexible spacers, and (c) rigid-rod main-chain LCP

crystalline polymers (MCSCCLCPs) consisted of a main-chain liquid crystalline backbone and side-chain mesogenic groups. The main-chain backbone of MCSCCLCPs may be either semi-rigid (Fig. 12.1a, b) or rigid (Fig. 12.1c) (Zentel and Brehmer 1996). As far as MCSCCLCPs are concerned, side-chain mesogens may be attached via flexible spacers onto main-chain flexible spacers or onto main-chain mesogens with or without flexible spacers. There are various terminal groups like $-\text{CN}$ and $-\text{OCH}_3$ that terminal groups of side-chain mesogenic moieties. If liquid crystalline polymers (LCPs) show ordered mesophases when they are heated to a certain temperature, they are called thermotropic LCPs, while lyotropic LCPs primarily depends on the concentration in a specific solvent to form mesophases.

Over 30 years ago the pioneering work of Reck and Ringsdorf (1985) gave great momentum to the synthesis of MCSCCLCPs, which opened the door to a whole variety of MCSCCLCP materials with a wide range of structural designs and synthetic methods. Ever since, intensive research efforts have been made to gain fundamental understanding of versatile supramolecular structures of MCSCCLCPs and their relationship with various properties of these polymers. Thus far, through molecular design, a couple of strategies have been applied to synthesize MCSCCLCPs. A number of research groups synthesized MCSCCLCPs by condensation polymerization (Zentel and Brehmer 1996) and free radical polymerization (Xie et al. 2010), while some research groups synthesized MCSCCLCPs by functionalization of biomolecules (Wu et al. 2003). Specific interactions were also demonstrated to be an effective approach for synthesizing MCSCCLCPs (Huang and Han 2006).

In particular, MCSCCLCPs have attracted much attention from academic interests in the study of the interplay between chemical structure and supramolecular

ordering. Emphasis has been placed on the investigation of influencing factors and their mutual effects on phase transition behaviors, which encompass the rigidity of main-chain backbone, attachment position onto either main-chain flexible spacer or mesogenic units, length of flexible spacer, molecular weight, and mesogen-grafting density (Xie et al. 2010, 2011; Huang and Shi 2012; Yang et al. 2012; Zhu et al. 2012; Wen et al. 2013). In turn, a variety of mesophases were observed because of the overall orientational order originating from interactions between main-chain and side-chain mesogens. The aim of this chapter is to give an overview of the chemistry of novel MCSCLCPs with an emphasis on current trends in synthetic methods, molecular design, supramolecular arrangements, properties, and applications.

12.2 Synthesis of Combined Main-Chain/Side-Chain Liquid Crystalline Polymers

To date, many synthetic strategies have been developed to synthesize MCSCLCPs due to the advancement of modern organic and polymer chemistry. Among these, synthetic methodologies such as condensation polymerization, free radical polymerization, atomic transfer radical polymerization, metathesis polymerization, polyaddition polymerization, grafting reactions, and self-assembly are extensively involved. The core mesogenic units in the main chain and side chain may be either identical or totally different, and representative mesogenic units include biphenylene, azobenzene, azoxybenzene, and *p*-phenylene benzoate. There are two ways to incorporate side-chain mesogens onto main-chain mesogens by either attaching side-chain mesogenic groups onto flexible spacers of a semi-flexible main-chain polymer or attaching side-chain mesogenic groups as lateral substituents onto mesogenic moieties of a semi-flexible or rigid-rod main-chain polymer.

12.2.1 Synthesis of Combined Main-Chain/Side-Chain Liquid Crystalline Polymers by Condensation Polymerization

12.2.1.1 Synthesis of MCSCLCPs with Side-Chain Mesogenic Units Attached onto Flexible Spacer Units of a Main-Chain Backbone

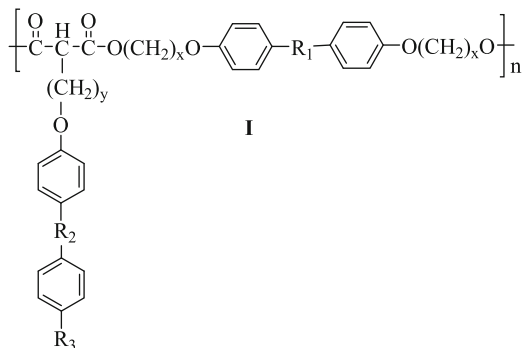
Condensation polymerization has been extensively used for achieving MCSCLCPs. The first example of combined MCSCLCPs (**I**) was synthesized by attaching side-chain mesogenic groups onto the flexible spacer of the main-chain backbone (Reck

Table 12.1 Phase transition temperatures of MCSCCLCPs with a chemical structure **I** (Reck and Ringsdorf 1985)

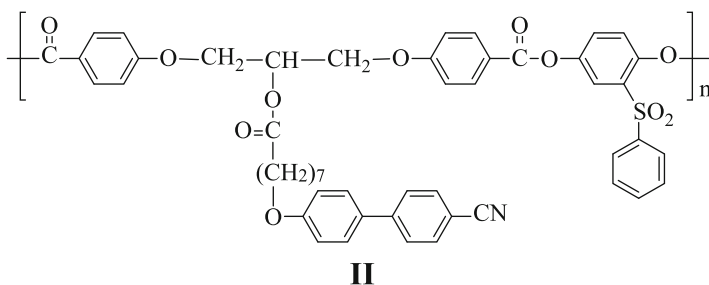
Sample No.	R ₁	R ₂	R ₃	x	y	Phase transition temperature (°C)
I-1	–	–N=N–	–OCH ₃	2	2	k 148s ₂ 176 i
I-2	–	–N=N–	–OCH ₃	2	6	k ₁ 124k ₂ 129 s _C 153 s _A 162 n 181 i
I-3	–	–N=N–	–OCH ₃	2	10	g 112k 162 (n 159) i
I-4	–	–N=N–	–CN	2	6	k ₁ 115k ₂ 140s ₂ 177 n 183 i
I-5	–	–N=N–	–OCH ₃	6	2	k ₁ 109k ₂ 120 n 153 i
I-6	–	–N=N–	–OCH ₃	6	6	k ₁ 108k ₂ 112 s _C 131 s _A 136 n 155 i
I-7	–	–N=N–	–OCH ₃	6	10	g 72s ₁ 120 s _C 139 s _A 154 i
I-8	–	–N=N–	–CN	6	6	g 61s ₁ 112s ₂ 184 i
I-9	–N=N–	–	–OCH ₃	2	6	k 112s ₂ 151 n 171 i
I-10	–N=N–	–	–OCH ₃	6	6	k 95 (s _C 90) n 152 i
I-11	–N=N–	–N=N–	–CN	2	6	g 53s ₂ 202 i
I-12	–N=N–	–N=N–	–CN	6	6	g 35s ₂ 189 i

Note: *g* glass transition temperature, *k* melting or solid-to-solid transition temperature, *s_A* smectic A, *s_C* smectic C, *s₁* unidentified ordered smectic mesophase, *s₂* unidentified disordered smectic mesophase, *n* nematic, *i* isotropic state

and Ringsdorf 1985). Specifically, these MCSCCLCPs were synthesized by melt polymerization at 200 °C between malonate monomers having side-chain mesogens and diols having main-chain mesogens using a catalyst system of diglyme and tetraisopropyl orthotitanate. As illustrated in Table 12.1, both nematic and smectic (*s_A* and *s_C*) mesophases were observed under optical microscope for these samples, and side-chain mesogens had broadened phase transition temperatures of their parental main-chain polymers. Furthermore, side-chain mesogens enhanced the stability of MCSCCLCPs, presumably due to interactions between main-chain mesogens and side-chain mesogens. This led the authors to hypothesize that side-chain mesogens were aligned parallel to main-chain mesogens.



Zhou and Han (2005) reported the synthesis of a MCSCLCP having a chemical structure **II**, which consisted of poly[(phenylsulfonyl)-*p*-phenylene-1,4-tetramethylenebis(4-oxybenzoate)] and a side-chain mesogen, 8-[(4-cyano-4'-phenyl)oxy]octanoic acid (7CNCOOH). This polymer was synthesized by condensation reaction between acid chloride monomer containing a side chain mesogen and a 1,4-biphenol monomer having phenylsulfonyl pendent group. This MCSCLCP exhibited a glass transition at 85 °C, and a nematic-to-isotropic (N-I) transition at 172 °C, which was 90 °C lower than that of the corresponding main-chain LCP. Thus, it was a glassy nematic LCP, arising from the bulky side-chain mesogen and pendent phenylsulfonyl group. As a result, lyotropic solutions with a concentration of 25–70 wt% in *o*-dichlorobenzene, *m*-dibromobenzene, or tetrachloroethane were successfully prepared from this particular LCP which allowed them to investigate rheological behaviors of lyotropic MCSCLCP and clarify one of the unresolved issues in LCP rheology, that is, the sign of first normal stress difference (N_1) in steady-state shear flow (Zhou and Han 2006). They demonstrated strong evidences of negative values of N_1 at intermediate shear rates for lyotropic solutions with concentrations up to ca. 27 wt%, which greatly supported theoretical predictions made by Marrucci and Maffettone (1989) and Larson (1990). In contrast, only positive values of first normal stress difference (N_1) in steady-state shear flow were observed in thermotropic states over the entire range of shear rates and temperatures investigated.



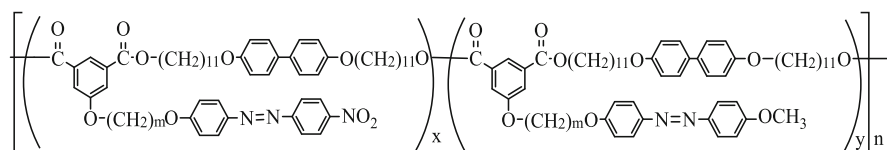
Another thermotropic MCSCLCPs (**III**) were synthesized by melt polymerization of isophthalate monomer and 11,11'-(4,4'-biphenylenedioxy)diundecanol using zinc acetate as a catalyst (Sato and Mizoi 2004; Sato et al. 2004). Isophthalate monomers contain nitro and methoxyazobenzene mesogenic units and three different aliphatic spacers (hexamethylene, octamethylene and decamethylene) in the side chain. As displayed in Table 12.2, homopolyisophthalates with the nitroazobenzene unit formed highly ordered smectic E mesophase, and those with methoxyazobenzene and their copolymers showed less ordered smectic B or smectic C mesophase. It should be pointed out that temperature ranges of smectic mesophases in copolymers showed a decreasing trend with increasing content of methoxyazobenzene. UV-vis spectra of the azobenzene-containing polymers exhibited absorption peak maxima both in solutions and in films. However, no

Table 12.2 Phase transition temperatures of MCSCLCPs with a chemical structure **III** (Sato and Mizoi 2004; Sato et al. 2004)

Sample no.	m	x/y ratio	Phase transition temperatures (°C)
III-1	6	1.0/0	k 68 s _E 143 i
III-2	6	0.8/0.2	g 40k 69 s _B 143 i
III-3	6	0.6/0.4	g 40k 72 s _B 141 i
III-4	6	0.5/0.5	g 43k 70 s _B 140 i
III-5	6	0.4/0.6	g 43k 73 s _B 140 i
III-6	6	0.2/0.8	g 40k 98 s _B 131 i
III-7	6	0/1	k ₁ 61k ₂ 108 s _C 133 i
III-8	8	1.0/0	k 77 s _E 141 i
III-9	8	0.8/0.2	k ₁ 68k ₂ 81 s _B 140 i
III-10	8	0.6/0.4	g 41k 84 s _B 140 i
III-11	8	0.5/0.5	g 43k 85 s _B 140 i
III-12	8	0.4/0.6	g 50k 86 s _B 139 i
III-13	8	0.2/0.8	g 51k ₁ 107k ₂ 123 s _B 137 i
III-14	8	0/1	g 60k 128 s _C 134 i
III-15	10	1.0/0	k 74 s _E 141 i
III-16	10	0.8/0.2	g 47k 87 s _B 140 i
III-17	10	0.6/0.4	g 47k 92 s _B 140 i
III-18	10	0.5/0.5	g 49k 91 s _B 140 i
III-19	10	0.4/0.6	g 54k 93 s _B 139 i
III-20	10	0.2/0.8	g 54k 91 s _B 135 i
III-21	10	0/1	g 53k ₁ 91k ₂ 101 s _B 133 i

Note: *g* glass transition temperature, *k* melting or solid-to-solid transition temperature, *s_B* and *s_E* are smectic B and smectic E, respectively, *i* isotropic state

fluorescent properties were observed, which might be attributed to the intra- and intermolecular quenching effects between electron-accepting nitro group and electron-donating methoxy group.

**III**

Because of unique features of chiral liquid crystalline polymers such as selective light reflection for cholesteric phase and ferroelectricity and fast switching times in electrical fields for chiral smectic C* phase (Zentel and Brehmer 1996), chiral mesogens have been introduced into MCSCLCPs (**IV**). These MCSCLCPs were prepared by melt polymerization of mesogenic malonates and mesogenic diols using tetraisopropyl orthotitanate as the catalyst at 140–150 °C (Kapitza and

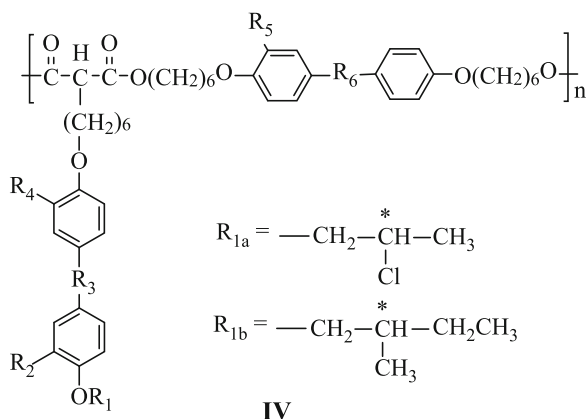
Table 12.3 Phase transition temperatures of MCSCLCPs with a chemical structure **IV** (Zentel and Brehmer 1996)

Sample no.	R ₁	R ₂	R ₃	R ₄	R ₅	R ₆	Phase transition temperature (°C)
IV-1	R_{1a}	H	H	Br	–	–	k 45 n* 111 i
IV-2	R_{1a}	H	H	H	–	–N=N–	k 109 s _C * 149 i
IV-3	R_{1a}	H	H	H	–	–N(O)= N–	k 57 s _C * 140 s _A 149 i
IV-4	R_{1b}	H	Br	Br	–	–	g 16s 37 i
IV-5	R_{1b}	H	Br	H	–	–N=N–	k 57 n* 88 i
IV-6	R_{1b}	H	Br	H	–	–N(O)= N–	g 12s 53 n* 91 i
IV-7	R_{1b}	H	Br	H	–	–	k 84 i
IV-8	R_{1b}	Br	H	Br	–N=N–	–	g 40 i
IV-9	R_{1b}	Br	H	H	–N=N–	–N=N–	g 38 i
IV-10	R_{1b}	Br	H	H	–N=N–	–N(O)= N–	g 41 i
IV-11	R_{1b}	Br	H	H	–N=N–	–	k 69 i
IV-12	R_{1b}	H	H	Br	–N(O)= N–	–	g 17 s 90 n* 96 i
IV-13	R_{1b}	H	H	H	–N(O)= N–	–N=N–	k 54 s _A 109 n* 141 i
IV-14	R_{1b}	H	H	H	–N(O)= N–	–N(O)= N–	g 20 s _A 108 n* 144 i
IV-15	R_{1b}	H	H	H	–N(O)= N–	–	k 77 s _C * 126 s _A 131 i
IV-16	R_{1b}	H	H	Br	–	–	k 59 s _C * 105 i
IV-17	R_{1b}	H	H	H	–	–N=N–	k 112 s _C * 129 n* 132 i
IV-18	R_{1b}	H	H	H	–	–N(O)= N–	k 63 s _C * 124 n* 133 i
IV-19	R_{1b}	H	H	H	–	–	k ₁ 151k ₂ 154 i
IV-20	R_{1b}	H	H	Br	–N=N–	–	k 56 s _C * 91 i
IV-21	R_{1b}	H	H	H	–N=N–	–N=N–	k 107 s _C * 111 n* 137 i
IV-22	R_{1b}	H	H	H	–N=N–	–N(O)= N–	k 53 s _C * 107 n* 138 i
IV-23	R_{1b}	H	H	H	–N=N–	–	k 130 s _C * 136 i

Note: *g* glass transition temperature, *k* melting or solid-to-solid transition temperature, *s_A* smectic A, *s_C** smectic C*, *n** cholesteric, *i* isotropic state

Zentel 1988). As indicated in Table 12.3, the dipole moment of –N(O)=N– was induced perpendicular to mesogenic groups, while other dipole moments were introduced by lateral substituents (e.g. R₁). As such, these polymers formed crystalline or highly ordered smectic phases at room temperature and showed cholesteric or chiral smectic mesophases at elevated temperatures. Lateral substituents not only decreased the melting temperature but also broadened mesophase transition temperatures. Dipole moments perpendicular to mesogenic groups or at the

chiral center facilitated high spontaneous polarisation in the chiral smectic C* phase (ferroelectricity).



Because of high temperature conditions required for the melt polymerization of chiral MCSCLCPs described above, judicious selection of chiral groups was necessary for preventing a racemization during the reaction. Later, a new synthetic route at room temperature was developed to address this issue (Kapitza and Zentel 1991). Specifically, precursor polymers with phenolic groups were first synthesized by the same melt polymerization process. Then, these precursor polymers with phenolic groups were reacted with chiral acid by esterification mechanism using a catalyst system of dicyclohexylcarbodiimide (DCC) and 4-dimethylaminopyridine (DMAP). The esterification yield was 90–100 %, affording 33 different chiral MCSCLCPs with cholesteric and chiral smectic C* mesophases.

12.2.1.2 Synthesis of MCSCLCPs with Side-Chain Mesogenic Units Attached onto Main-Chain Mesogenic Units

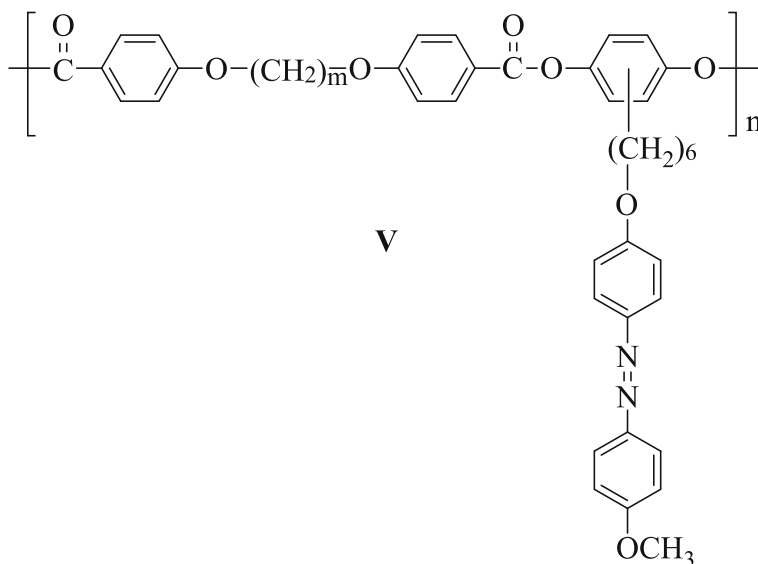
The other important family of MCSCLCP is referred to as those with side-chain mesogenic units as lateral substituents to a rigid rod polymer or to mesogenic units in semi-flexible main-chain LCPs. A series of combined MCSCLCPs (V) with side-chain mesogens attached onto main-chain mesogens were first reported by Reck and Ringdorf (1986). The design concept originated from lateral substituents in main-chain LCPs. The polymerization was accomplished by solution polymerization of hydroquinone monomers carrying a lateral mesogenic group and 4,4'-alkylenedioxydibenzoyl chlorides using tetrachloroethane as a solvent and pyridine as a catalyst. It can be seen from Table 12.4 that all polymers exhibited a glass transition temperature and a nematic-to-isotropic (N–I) transition temperature (>220 °C), while no crystallinity was observed for these polymers. The N–I

Table 12.4 Phase transition temperatures of MCSCLCPs with a chemical structure **V** (Reck and Ringsdorf 1986)

Sample no.	m	Phase transition temperature (°C)
V-1	2	g 90 n 310 i (decomposed)
V-2	6	g 56 n 268 i
V-3	9	g 45 n 221 i

Note: *g* glass transition temperature, *n* nematic phase, *i* isotropic state

transition temperature decreased with increasing length of flexible spacer in the main chain.



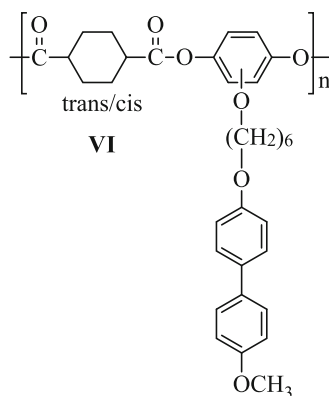
Rigid-rod main-chain LCPs have excellent mechanical properties but they are difficult to process because their clearing temperatures tend to be greater than their degradation temperatures. The lateral substitution of side-chain mesogens via a flexible spacer onto rigid rod main-chain LCPs is an effective way to reduce their clearing temperatures for practical applications. A series of MCSCLCPs were synthesized by melt polycondensation via transesterification reaction from trans-1,4-cyclohexanedicarboxylic acid, chloro-1,4-phenylene diacetate, and 6-(4-methoxy-4'-biphenyloxy)hexyl-1,4-phenylene diacetate (Reck et al. 1989). These MCSCLCPs combined both features of rigid-rod main-chain LCPs and of side-chain LCPs. The main-chain LCP, poly(chloro-1,4-phenylene-1,4-cyclohexanedicarboxylate), had a melting temperature of 309 °C. The introduction of small fraction (e.g. 10 mol%) of side-chain mesogenic groups significantly reduced the melting temperature to 240 °C, but the clearing temperature was still higher than 400 °C. When 100 mol% side-chain mesogenic monomers were used to polymerize with 1,4-cyclohexanedicarboxylate monomer, solution polymerization of acyl

Table 12.5 Phase transition temperatures of MCSCLCPs with a chemical structure **VI** (Reck et al. 1989)

Sample no.	Trans content (%)	Phase transition temperature (°C)
VI-1	97 ± 3	g 65k 183 n 337 i
VI-2	23 ± 3	g 60 i
VI-3	77 ± 3	g 64 n 212 i
VI-4	55 ± 3	g 57 n 130 i

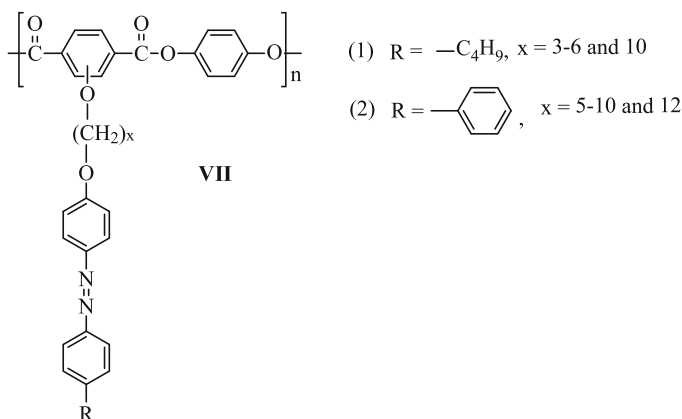
Note: *g* glass transition temperature, *k* melting temperature, *n* nematic phase, *i* isotropic state

chlorides and hydroquinone monomer containing side-chain mesogen was carried out using tetrachloroethane and pyridine as solvents. The thermal *trans-cis* isomerization occurred at temperatures above 250 °C, and thus the *cis*-contents could be achieved by thermal isomerization. The formed *cis*-units became a kink for disrupting the rigid rod main-chain structure, resulting in the reduction of clearing temperatures, as indicated in Table 12.5. However, in the case of excessive *cis*-contents (e.g. 77 %), the polymer became non-mesogenic as a result of only very few rod-like segments in the polymer backbone. This suggested that interactions between main-chain mesogens and side-chain mesogens in MCSCLCPs were a prerequisite for the formation of mesophase.

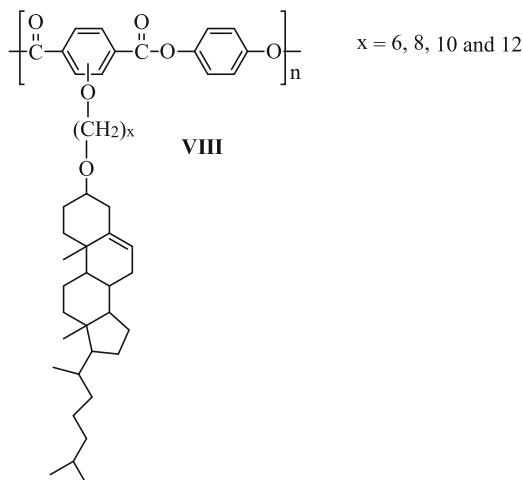


To understand the effect of flexible spacers on liquid crystalline properties of MCSCLCPs, Piao et al. (Piao et al. 1997) synthesized a series of MCSCLCPs (**VII**) carrying various lengths of oxypolymethyleneoxy spacers between a rigid-rod main-chain aromatic polyester and side-chain azobenzene mesogens by solution polymerization. It was borne out that shorter spacers ($x = 3-6$) favored the formation of nematic phases, whereas longer spacers ($x = 10$) favored the formation of biaxially oriented layered mesophases. The tentative hypothesis for this observation was that shorter spacers tended to prefer parallel orientation between a main-chain mesogenic backbone and pendent mesogenic groups through intramolecular interactions between them, leading to a nematic ordering in the melt. On the other hand,

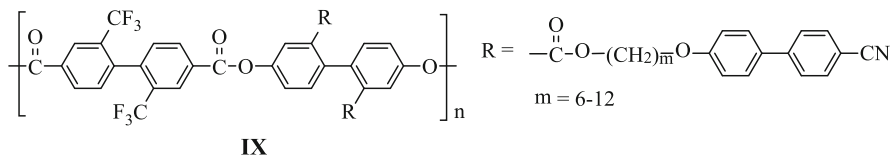
longer spacers would decouple interactions between main-chain and side-chain mesogens, resulting in the formation of a layered morphology in the melt. The other paper from the same group reported the substitution of n-butyl tail with phenyl group in order to increase the aromaticity or polarizability of side-chain mesogenic groups (Lee et al. 1999). It was anticipated to improve attractive interactions between main-chain and side-chain mesogens. As a result, all polymers formed nematic mesophases but not layered morphologies in melt, due to the parallel alignment of side-chain mesogens to main-chain mesogens. It should be mentioned that not only all these MCSCLCPs were semicrystalline, but also their clearing temperatures were higher than degradation temperatures.



Furthermore, Cha et al. (2001) reported the synthesis of MCSCLCPs (**VIII**) bearing pendant cholesterol moieties attached to the main-chain mesogenic backbone through oxyalkyleneoxy groups (hexamethylene, octamethylene, decamethylene, and dodecamethylene) of varying lengths. All these polymers were found to be amorphous due to the presence of irregularly placed bulky pendant cholesterol groups, but thermotropic. These polymers exhibited two thermal transitions before isotropization. The lower temperature transition occurred between 34 and 56 °C while the high-temperature one happened between 94 and 156 °C, both of which decreased with increasing spacer length. Noticeably, layered morphologies were formed in the mesophase especially for longer flexible spacers. The above observations demonstrated that the relative orientation of side-chain mesogenic units in MCSCLCPs with respect to their main-chain mesogens depended strongly on mutual interactions between the two structural elements. Consequently, the layered morphology was favorable if there was a great disparity in polarity between main-chain and side-chain mesogens, because side-chain mesogens would orient vertically to main-chain mesogens. The unique feature of biaxial orientation of MCSCLCPs has a great prospect in addressing the challenging issue existing in nematic LCPs, that is, the anisotropy in physical properties originating from the easy molecular orientation of nematic mesophase during processing.

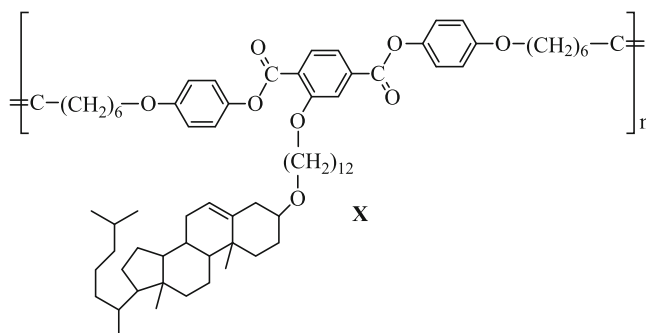


Because MCSCLCPs had potentials in the technological applications such as alignment layers in liquid crystal displays to achieve high pre-tilt angles, Ge et al. (1997) synthesized MCSCLCPs (**IX**) comprised of aromatic main chain mesogens and flexible aliphatic side chains with 4-cyanobiphenyl mesogenic groups. The polymerization of 2,2'-bis(trifluoromethyl)-4,4'-biphenyldiyl dicarbonyl chloride with 2,2'-bis[ω -[4-(4-cyanophenyl)phenoxy-*n*-alkoxy]carbonyl]]-4,4'-biphenyldiol was completed in a solution. These MCSCLCPs exhibited a complicated phase transition behavior, arising from the existence of monotropic phases. Specifically, thermal transitions for MCSCLCP (**IX**) with $m = 11$ were shown as follows during the decreasing temperature sequence: the I (the isotropic melt), the N (the nematic liquid crystal phase), the KT2 (the high temperature triclinic crystalline phase), the KT1 (the low temperature triclinic crystalline phase), and the KO (the highly ordered smectic crystal or relatively poor crystal having an orthorhombic lattice) phases.



12.2.2 *Synthesis of Combined Main-Chain/Side-Chain Liquid Crystalline Polymers by Acyclic Diene Metathesis Polymerization*

Acyclic diene metathesis polymerization (ADMET) proceeds in a step-growth manner with liberation of a gaseous ethylene side product. Joo et al. (2000) reported the use of ADMET for synthesizing main-chain, side-chain, and combined main-chain/side-chain liquid crystalline polyesters. The Grubbs' catalyst, bis(tricyclohexylphosphine)benzylideneruthenium dichloride, was employed and the reaction was conducted at 25–50 °C either in solution or bulk. The MCSCCLCP (**X**) was obtained from a diene monomer containing a built-in aromatic ester type mesogen bearing a cholesterol pendant via an oxydodecyloxy spacer. The advantage of this particular method lied in the fact that reasonably high molecular weight polymers could be prepared at a low temperature under very mild conditions. MCSCCLCP (**X**) had an average number molecular weight (M_n) of 53,200 with a polydispersity index of 2.9. Therefore, it was concluded that it was feasible to synthesize MCSCCLCPs containing functional side-chain groups without affecting the catalyst activity. MCSCCLCP (**X**) showed a glass transition temperature of 36 °C, a melting temperature of 68 °C, and a clearing temperature of 132 °C, and exhibited only polished marble textures for the nematic mesophase.



12.2.3 *Synthesis of Combined Main-Chain/Side-Chain Liquid Crystalline Polymers Based on Mesogen-Jacketed Liquid Crystalline Polymers*

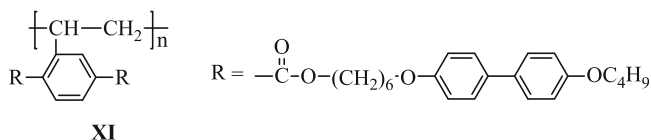
Mesogen-jacketed liquid crystalline polymers are a type of main-chain liquid crystalline polymers, which are not constructed by genuine mesogenic units in the main chain of polymers. As a matter of fact, bulky side groups that are crowded

around a flexible backbone force the flexible backbone to be rather extended and stiff by “jacketing” effect arising from the steric hindrance of pendent bulky groups (Zhou et al. 1987, 1989). As a consequence, these mesogen-jacketed liquid crystalline polymers exhibit liquid crystalline behaviors similar to the genuine main-chain LCs. As such, bulky pendent groups may pack parallel to one another to form columnar phase with two-dimensional long-range positional order, which may be considered as a molecular cylinder. It is worthy of noting that mesogen-jacketed liquid crystalline polymers are distinguished from conventional side-chain liquid crystalline polymers in that the absence of a flexible spacer between the flexible main-chain backbone and pendent side groups cause non-mesogenic side groups to fuse together to become a single conformational unit like a rigid rod. The question arises as to whether it is possible to synthesize mesogen-jacketed MCSCLCPs. When designing the polymer, the central rigid portion of the side chain should be attached to every second carbon atom along the backbone without a spacer might impose a great steric interaction on polyethylene backbone, resulting in a semi-rigid main chain; on the other hand, flexible spacers introduced in the side chain could facilitate mesophase formation of biphenyl moieties. Here, the function of vinyl monomer is twofold by providing strong “jacketing” effect to the backbone and forming liquid crystalline phases.

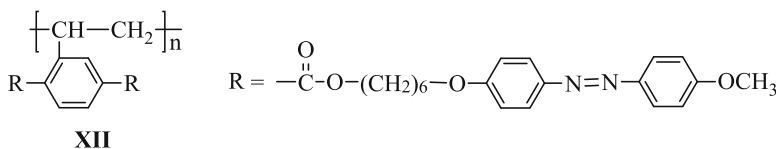
Xie et al. reported the first MCSCLCP (**XI**) with mesogen-jacketed liquid crystalline polymer rigid-rod main-chain and biphenyl as side-chain pendent groups by using atom transfer radical polymerization (ATRP) (Xie et al. 2008). Although the monomer containing side-chain mesogenic groups was rather bulky, ATRP method could be very effective in polymerization, affording polymers with well-controlled molecular weight and narrow molecular weight distribution. Differential scanning calorimetry (DSC) and optical microscope results revealed that phase behaviors of these polymers were rather complex with three different mesophases, which may be associated with the interplay between side-chain mesogens and main-chain jacketed mesogens of the polymer. Moreover, phase transition temperatures were also highly dependent on the molecular weight of the polymer, that is, higher molecular weight of the polymer led to higher phase transition temperatures.

Later, radical polymerization was used to prepare an MCSCLCP using the same monomer (Xie et al. 2010). Thermal transitions and hierarchical supramolecular ordering with biaxial orientation of this MCSCLCP were studied using differential scanning calorimetry, one- and two-dimensional wide-angle X-ray diffraction, and polarized light microscopy. Very recently, Wen et al. (2013) have synthesized a series of diblock copolymers composed of polystyrene and MCSCLCP (**XI**). Lamellar and rectangular cylinder morphologies were observed for these copolymers by small-angle X-ray scattering. As evidenced by differential scanning calorimetry and X-ray scattering results, MCSCLCP (**XI**) in the confined space of microphase separation was still able to exhibit its liquid crystalline structures with a rectangular main-chain scaffold on the nanometer scale and side-chain ordering on the subnanometer scale. Therefore, a three-length scale ordered

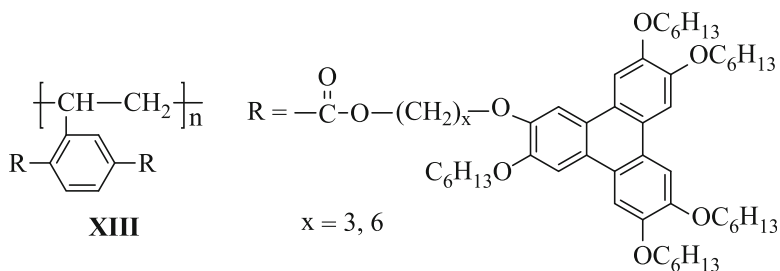
hierarchical structure could be observed in the same system, namely, microphase separation and double-length scale mesophase structure of the MCSCLCP.



Based on the same principle of molecular design, Xie et al. (2011) synthesized another MCSCLCP (XII) based on radical polymerization. Here, the side-chain mesogenic unit was azobenzene group. They confirmed that this MCSCLCP could form a hierarchically ordered structure with double orderings on both the nanometer and subnanometer length scales. The “jacketing” effect of pendent terephthalate side-chain to the polyethylene backbone constructed a two-dimensional centered rectangular scaffold. The packing of side-chain azobenzene mesogens inside the main-chain scaffold underwent the thermal transition from smectic B to smectic A, and then to isotropic. The confinement arising from the scaffold included the SmB-like packing and enhanced the stability of SmA-like structure. The hierarchically ordered structure rendered a biaxial orientation with side-chain mesogens perpendicular to main-chain mesogens. Upon UV irradiation, this MCSCLCP retained its liquid crystallinity even though azobenzene groups had been transformed into *cis*-conformation.



Interestingly, Zhu et al. (2012) introduced triphenylene units as side-chain mesogens for mesogen-jacketed MCSCLCPs. The polymer was synthesized through conventional free radical polymerization, and phase behaviors of these new MCSCLCPs were investigated. These MCSCLCPs exhibited excellent thermal stability. The attachment of discotic liquid crystals onto mesogen-jacketed liquid crystalline polymers had a significant effect on the liquid crystalline behavior of the polymer. These polymers formed rectangular columnar phases at relatively high temperatures. At low temperatures, triphenylene moieties in side chains formed a discotic nematic phase in conjunction with the columnar phase developed by rod-like supramolecular mesogens. For a longer flexible spacer, a higher symmetrical hexagonal columnar phase formed when the temperature exceeded 225 °C.

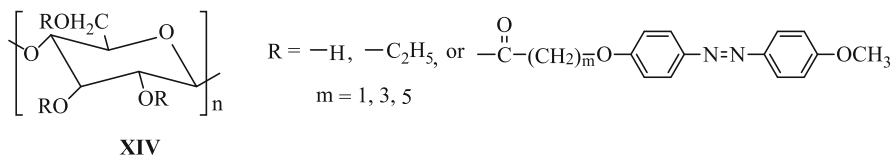


12.2.4 Synthesis of Combined Main-Chain/Side-Chain Liquid Crystalline Polymers Based on Biomacromolecules

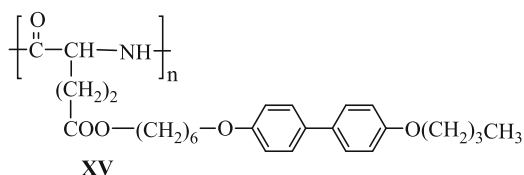
Cellulose is one of the most important biomacromolecules that can form cholesteric mesophases, and thus it can be regarded as a rigid rod main-chain LCP (Werbowyj and Gray 1976). The attachment of side-chain mesogens onto cellulose backbone via chemical bonds represents an alternative way to synthesize combined main-chain/side-chain liquid crystalline polymers. MCSCLCPs (XIV) were synthesized by coupling azobenzene-containing monomers having carboxylic acid end groups with ethyl cellulose. The esterification coupling reaction was enabled by using *N*, *N'*-dicyclohexylcarbodiimide (DCC) and 4-dimethylaminopyridine (DMAP) as a catalyst in tetrahydrofuran (THF) solvent homogeneously (Hu et al. 2010). For MCSCLCP (XIV) with $m = 3$, thermal transition temperatures and phase structures depended on the degree of substitution (DS). At a low DS, the liquid crystallinity of the polymer was dominated by the ethyl cellulose backbone. When the DS increased, thermal transition temperatures and phase structures changed dramatically, arising from structural irregularities due to the asymmetrical substitution of mesogens.

In order to explore the relationship between spacer length and mesophase structure, a series of MCSCLCPs (XIV) with various spacer lengths were synthesized (Hu et al. 2010). The spacer length had also played an important role in the formation of liquid crystalline phases of these polymers. Glass transition temperatures, phase transition temperatures and the corresponding enthalpy of transitions decreased with increasing flexible spacer length. The mesophase structures of the polymer consisted of a large-scale ordered lamellar structure composed of ethyl cellulose main-chain mesogens and a relatively small-scale ordered structure formed by azobenzene side chains. All polymers formed a similar lamellar structure on a large scale. The small-scale ordered structure became relatively disordered, that is, from crystal ($m = 1$) to smectic B ($m = 3$) to smectic A ($m = 5$) at low temperatures. This was ascribed to interactions between the rod-like ethyl cellulose

main-chain and side groups, as well as the π - π stacking of azobenzene mesogens of these MCSCLCPs.

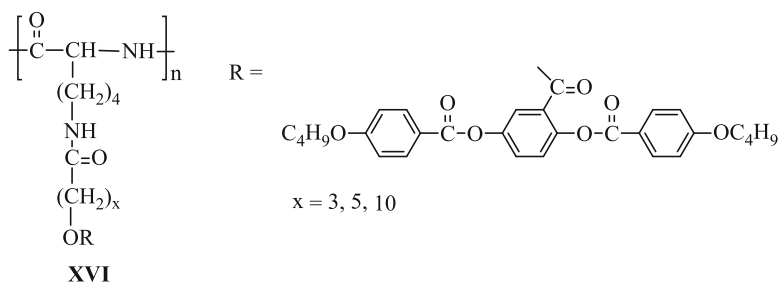


α -Helical polypeptides represent an important class of polymers that can form mesophase because of their rigid-rod shape. Watanabe and Tominaga (1993) synthesized a thermotropic MCSCLCP (XV) by linking a mesogenic biphenyl moiety to a mesogenic α -helical polypeptide with a flexible spacer. This MCSCLCP was prepared by an ester exchange reaction between poly(γ -methyl-L-glutamate) with 4-butoxy-4'-((ω -hydroxyhexyl)oxy)biphenyl in 1,2-dichloroethane using *p*-toluenesulfonic acid as a catalyst at 60 °C. This MCSCLCP had two thermal transition temperatures at 143 and 222 °C and correspondingly three distinct phases including crystalline, smectic A, and cholesteric phases. In the case of crystalline or smectic A phases, macromolecular chains constructed the characteristic layered structure in which α -helical main chains formed the layer while side-chain mesogenic groups were placed in the central part of layers with their long axes perpendicular to the layer. The cholesteric phase formed by main-chain α -helices occurred upon the collapse of the layered structure. These samples formed cholesteric liquid crystalline phases above the melting transition but formed layered structures at low temperatures driven by crystallization of side chains. The thermotropic transition behavior and mesophase structures were interpreted by the coupling effect of main-chain and side-chain mesogenic units.

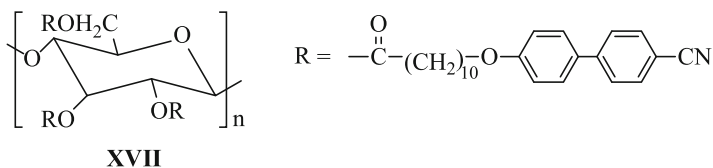


To obtain the coexistence of liquid crystalline ordering in both side-chain mesogens and main-chain rigid-rod polypeptide backbones, Schaefer et al. (2006) paved a new way to modify polypeptide by “side-on” approach, which facilitated the parallel orientation of side-chain mesogens with main-chain peptide backbones. Amino acid monomers with spacers of 3, 5, and 10 methylene units between lysine side chains and mesogens were first synthesized. Then, terminal acid groups of these mesogens were converted to *N*-hydroxylsuccinimide active esters that were subsequently coupled to ϵ -amino groups of $N\alpha$ -Z-L-lysine, yielding mesogen-derivatized lysines where the mesogen was coupled to the amino acid using a

robust amide linkage. The target MCSCLCPs were prepared by ring-opening polymerization using $(\text{PMe}_3)_4\text{Co}$ as an initiator in tetrahydrofuran solvent. The melting transition temperature and the degree of ordering of rodlike polypeptides in the liquid crystalline nematic state was finely tuned by varying the length of aliphatic linker between the polypeptide backbone and the mesogen. These MCSCLCPs displayed an unusual mesophase where both side-chain mesogenic group and polypeptide backbones formed ordered phases and coexisted in a nematic hexagonal structure. It was easy to draw fibers from the mesophase of these MCSCLCPs, indicative of good melt processability of this type of novel polypeptides.

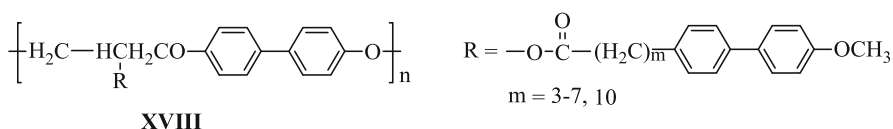


Although starch itself cannot form mesophase in thermotropic or lyotropic state, Huang et al. (Huang and Shi 2012) synthesized a thermotropic starch liquid crystalline polymer (**XVII**) by high-degree substitution (esterification) of hydroxyl groups on starch molecules with a mesogenic monomer, 11-(4'-cyano-biphenyl-4-yloxy)-undecanoic chloride, in the presence of pyridine. This unique starch-based liquid crystalline polymer might be also considered as a MCSCLCP. The long flexible spacer was judiciously selected for linking side-chain mesogens to the main-chain backbone, ensuring that the clearing temperature of this polymer would be less than its thermal degradation temperature. The elemental analysis showed that it had a degree of substitution of 2.68. This starch-based MCSCLCP exhibited a glass transition temperature of 29.6 °C and a nematic-to-isotropic transition temperature of 148.2 °C. Most interestingly, it showed a tensile strength of 37.9 ± 7 MPa and Young's modulus of 1.42 ± 0.14 GPa. This successful example may provoke the interest of engineering applications of starch.



12.2.5 Synthesis of Combined Main-Chain/Side-Chain Liquid Crystalline Polymers by Polyaddition

The polyaddition reaction between bis(epoxide) and “activated” diester was exploited by Chen et al. to synthesize MCSCLCPs (Chen et al. 1999). The first step of reaction was to synthesize six trimers with biphenyl mesogenic groups and polymethylene spacers. The second step of reaction was to polymerize these trimers and biphenol diglycidyl ether based on the addition reaction between epoxide and phenol ester functions. This polymerization was catalyzed by quaternary phosphonium chloride. It can be seen from Table 12.6 that there was a significant odd-even effect of the side-chain spacer not only on the thermal transition temperature but also on the crystallinity of MCSCLCPs. MCSCLCPs with even numbers of methylene units in the side-chain flexible spacer showed higher values of thermal transition temperatures and isotropization entropy. Specifically, all the MCSCLCPs were thermotropically nematic, although polymers with 3, 5 and 10 methylene units (m) in side-chain spacers were semicrystalline at room temperature, while other polymers were glassy.



12.2.6 Synthesis of Combined Main-Chain/Side-Chain Liquid Crystalline Polymers by Self-Assembly

Self assembly via specific interactions has been recognized as a powerful tool to construct a variety of supramolecular structures and has been turned out to be an intriguing pathway toward the synthesis of liquid crystals or liquid crystalline polymers (Kato and Frechet 1989a, b; Kato et al. 1999). Here, specific interactions

Table 12.6 Phase transition temperatures of MCSCLCPs with a chemical structure XVIII (Chen et al. 1999)

Sample no.	m	Phase transition temperature (°C)
XVIII-1	3	k 132.8 n 146.2 i
XVIII-2	4	g 73.1 n 156.1 i
XVIII-3	5	g 73.3k 99.5 n 127.3 i
XVIII-4	6	g 62.7 n 135.5 i
XVIII-5	7	g 55.1 n 118 i
XVIII-6	10	k 104.2 n 123.3 i

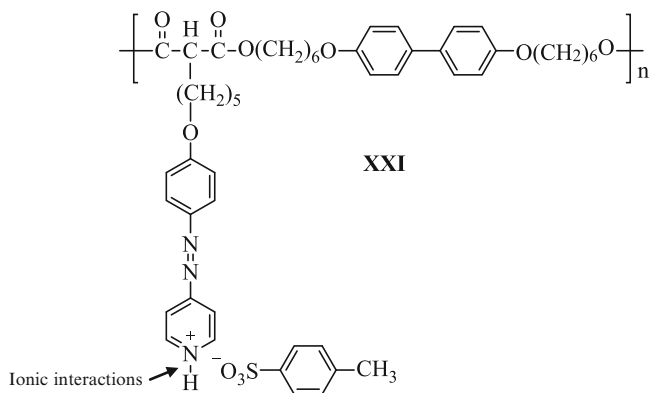
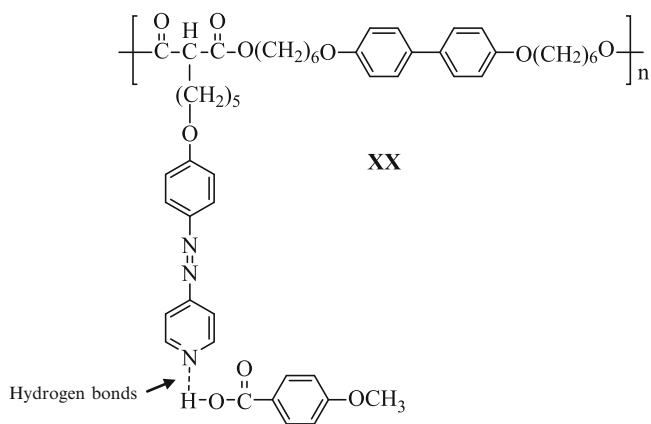
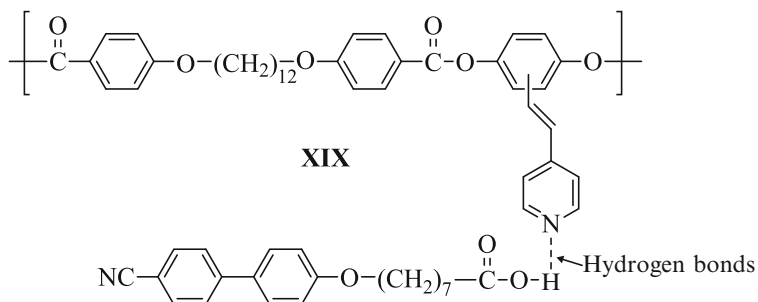
Note: g glass transition temperature, k melting temperature, n nematic phase, i isotropic state

are referred to as non-covalent interactions like hydrogen bonding, ionic interactions, electrostatic interactions, dipole-dipole interactions, π - π interactions, and metal-ion coordination, and the strength of these interactions ranges from 20 to 250 kJ/mol (Lehn 1988). Liquid crystalline anisotropies are a consequence of inter- and intramolecular-specific electronic and steric interactions. These interactions lead to the liquid crystalline long range order, which distinguishes mesophases from ordinary isotropic state (Kato and Mizoshita 2002). On one hand, the increased aspect ratio of supramolecular structure relative to constituent molecules stabilizes the mesophase of self-assembled systems. On the other hand, the anisotropy in the liquid crystal strongly enhances the strength of specific interactions (e.g. hydrogen bonding). Therefore, there is a strong cooperativity between association and induction of the liquid crystalline phase.

Huang and Han (2006) developed self-assembly strategy for building up the architecture of MCSCLCPs by specific interactions. In the first place, two different methods were used to obtain self-assembled MCSCLCPs by hydrogen bonding. The first method was to synthesize a main-chain liquid crystalline polymer with pendent pyridyl groups and then to combine, via hydrogen bonding, with a small mesogenic molecule having carboxylic acid group in a solvent, giving rise to a self-assembled MCSCLCP (**XIX**). In other words, the formation of MCSCLCP (**XIX**) was realized by hydrogen bonding between two mesogenic compounds. MCSCLCP (**XIX**) had a significant degree of hydrogen bonding at temperatures even above its clearing temperature as determined by temperature-dependent FTIR spectroscopy and underwent a glass transition at ca. 54 °C and a nematic-to-isotropic transition at ca. 154 °C. The second method employed was to first synthesize a main-chain liquid crystalline polymer having nonmesogenic side chain with azopyridyl group and then to combine, via hydrogen bonding, with a small nonmesogenic molecule (*p*-anisic acid) having carboxylic acid group in a solvent, giving rise to a self-assembled MCSCLCP (**XX**). In other words, the formation of MCSCLCP (**XX**) was realized by hydrogen bonding between the nonmesogenic azopyridyl group in the side chain of a MCLCP and a small nonmesogenic molecule having carboxylic acid group. MCSCLCP (**XX**) had a moderate degree of hydrogen bonding at temperatures even above its clearing temperature as determined by in situ FTIR spectroscopy and had a melting temperature of ca. 120 °C and a smectic-to-isotropic transition temperature of ca. 161 °C. The role of hydrogen bonding in the formation of self-assembled MCSCLCPs was investigated using in situ Fourier Transform Infrared (FTIR) spectroscopy.

Ionic interactions belong to the catalog of specific interactions that have higher strength than hydrogen bonding. A self-assembled MCSCLCP (**XXI**) was synthesized via ionic interactions between the nonmesogenic azopyridyl group in the side chain of an MCLCP and the sulfonic acid group in a small nonmesogenic molecule (*p*-toluenesulfonic acid) (Huang and Han 2006). MCSCLCP (**XXI**) had a glass transition temperature of ca. 58 °C, a melting temperature of ca. 110 °C, and a smectic-to-isotropic transition temperature of ca. 155 °C. Also, it showed strong ionic interactions persisting at temperatures well above the clearing temperature, as

determined by in situ FTIR spectroscopy. This observation explained why mesophase structure reappeared very quickly upon cooling from the isotropic state.



12.3 Supramolecular Ordering and Properties of Combined Main-Chain/Side-Chain Liquid Crystalline Polymers

The liquid crystallinity and supramolecular ordering of MCSCLCPs have immense impact on their performance, and thus numerous endeavors have been paid to gain in-depth insights into phase structures of these polymers. From the perspective of chemistry, a lot of strategies can be developed to tailor liquid crystalline properties of MCSCLCPs through the selection of mesogenic groups for both main-chain and side-chain of the polymer, altering the location of mesogens, and varying the length and types of flexible spacers. Indeed, the interplay between main chain and side chain of MCSCLCPs gives rise to the flexibility and versatility of liquid crystalline properties and supramolecular structures of these polymers. As aforementioned, a variety of MCSCLCPs have been accomplished in the past three decades, and accordingly, the correlation between liquid crystalline behavior and supramolecular structures have been elaborated on.

The thermal transition temperatures are generally measured by differential scanning calorimetry, and it has been demonstrated that the mesophase temperature range is surprisingly broadened in MCSCLCPs in comparison to the corresponding main-chain or side-chain LCPs. This can be ascribed to a synergistic stabilization of the mesophase between main-chain and side-chain mesogenic units in MCSCLCPs. Based on thermodynamic theory, Endres et al. (1990) investigated the structure-property relationship of MCSCLCPs. It was found that thermodynamic properties were governed by both enthalpy and entropy contributions from main-chain and side-chain mesogens in MCSCLCPs. Not only was the transition entropy strongly decreased with a decrease in spacer length, but also the transition enthalpy was a function of the length of flexible spacer. Thus, the side-chain arrangement and their interactions among themselves and with main-chain mesogens were crucial in controlling phase transition temperatures.

Polarized optical microscope has been widely used for detecting textures of mesophases of MCSCLCPs. In most cases, thin films are prepared by solution casting and placed between two glass slides. The temperature is controlled by a hot stage and real-time images can be taken for recording the variation of mesophase during heating and/or cooling cycles. Each type of mesophase has its characteristic pattern due to the macroscopic orientational order present in the sample. Furthermore, light scattering methods can be also employed for studying orientation correlations on a macroscopic scale for mesophases of MCSCLCPs. Moreover, electron microscopy was also employed to analyze structures of MCSCLCPs. Based on the observation of dark-field electron microscopy and electron diffraction, Voigt-Martin et al. (1988) concluded that the smectic layer spacing in MCSCLCPs, which did not correspond to spacings of the pure main-chain system, indicated that while molecular chains were fully extended in the oriented crystalline main-chain system, they were also forced to bend in MCSCLCPs. Nematic phases could occur only in those cases where there was a large difference between the length of the

main-chain and side-chain spacers. Combined MCSCLCPs with mesogenic side-chain groups grafted onto the main-chain mesogen units normally exhibited exclusively nematic mesophases.

However, the orientational order of MCSCLCPs on a supramolecular scale has to be examined by powder wide angle X-ray diffraction (WAXD) techniques (Donald and Windle 1992). MCSCLCPs have rich mesophases including nematic, smectic A, smectic C and higher ordered smectics quite in analogy to low molecular-weight liquid crystals. For a nematic mesophase, there exhibits a weak diffuse inner ring in WAXD patterns, which is associated with the length of molecules, and a strong diffuse ring at larger angles, indicative of the distance between neighboring molecules. The cholesteric mesophase shows a diffraction pattern similar to nematic mesophase. The diffraction pattern of the cholesteric mesophase is very similar to that of the nematic mesophase, and the existence of cybotactic groups can be also identified. The WAXD pattern of smectic A mesophase is characterized by one or more sharp inner reflections, which is related to smectic layers, as well as one diffuse outer ring, which is attributed to the short range order within layers. The WAXD pattern of smectic C is very similar to that of smectic A mesophase, but long axes of molecules are tilted with respect to the layer normal. The X-ray diffraction patterns of melt-drawn fibers of MCSCLCPs also throw light on the orientation of side-chain mesogens with main-chain mesogens.

Effects of chemical structures of achiral main-chain and chiral side-chain mesogens on the smectic layer spacing and on the formation of the superstructure were investigated by Mensinger et al. using small-angle X-ray scattering (SAXS) technique (Mensingher et al. 1992). Novel supramolecular structures for these chiral MCSCLCPs were revealed, which corresponded to bilayered and trilayered structures in smectic phases. Antiferroelectric ordering and ferroelectric ordering were assigned for the bilayered and trilayered structures, respectively, based on temperature-dependent SAXS data and the structure-property relationships for low molecular weight liquid crystals with similar chemical structures. Small angle neutron scattering (SANS) was also used for understanding synergistic interactions between main-chain mesogens and side-chain mesogens (Noirez et al. 1995). SANS results indicated that main-chain mesogens oriented parallel to the director, and thus MCSCLCPs was an intermediate state between main-chain LCPs and side-chain LCPs.

Furthermore, dielectric spectroscopy has also been examined to understand the supramolecular structure of MCSCLCPs. By doing this, Kremer et al. (1989) observed three relaxational processes related to the position and movement of side-chain mesogens in MCSCLCPs. These included an α -relaxation due to the glass process of the polymeric main chain coupled with side chain movements through spacers, a β_S -relaxation arising from the rotation of the mesogenic side chain around its long axis, and a β_m -relaxation, which was assigned to the rotation of the mesogenic group in the main chain around its long axis. By using broad-band dielectric spectroscopy, Endres et al. (1987) discovered that the rotation of side-chain mesogens relative to main-chain mesogens was not as strongly restricted as in side-chain liquid crystalline polymers. Thus, they attributed this to the fact that

side-chain mesogens were attached onto the flexible spacer within the main-chain backbone and that the concentration of side chains was comparatively small.

Yang et al. (2012) utilized semi-flexible chain self-consistent field theory (SCFT) coupled with the pseudospectral method to study isotropic-anisotropic phase transitions and conformation variations for MCSCLCPs. They considered two major interactions in their model, that is, the global coupling between backbone segments, between main-chain and side-chain mesogens, and between side-chain mesogens themselves, as well as the local coupling between main-chain mesogens and side-chain mesogens. The simulation results showed that when hinges were flexible, both global and local effects preferred parallel alignments of main-chain and side-chain mesogens, forming prolate uniaxial nematic phase. If the hinges were relatively stiff, the competition between global interaction preferring parallel orientations of the system and the perpendicular tendency of two components due to the comb architecture resulted in rich phases with various orientation modes.

12.4 Conclusions and Outlook

The combined main-chain/side-chain liquid crystalline polymers (MCSCLCPs) possess a unique hybrid structures, which combine chemical features of both main-chain and side-chain liquid crystalline polymers (LCPs). Because of the synergistic effect, the temperature range of thermal transition of mesophases for MCSCLCPs is largely broadened relative to the corresponding main-chain or side-chain LCPs. Such a synergistic effect may also lead to the breakthrough in properties of LCPs. For instance, the combination of high-modulus main-chain LCPs with flexible side-chain mesogens may afford excellent melt processability while maintaining high modulus and strength of main-chain LCPs. On the other hand, MCSCLCPs open new pathways to introduce a variety of functional groups into main-chain and/or side-chain mesogens, and thus lead to the formulation of advanced materials with tailored properties and desired supramolecular structures.

Judicious molecular design is required for achieving MCSCLCPs with biaxial orientation, which may endow resultant products with uniform bulk properties. This may overcome the deficiency of uniaxial orientation of conventional LCPs during processing, which results in good properties in one direction but poor properties in the other direction. Although sophisticated design principles are still not available, basic rules of thumb include dissimilar mesogens for pushing away side-chain mesogens from main-chain mesogens and controllable flexible spacers. Therefore, it is of utmost importance to gain better understanding of interactions between main-chain and side-chain mesogens. Among others, the rigidity of main-chain backbone, density of main-chain and side-chain mesogens and stereoregularity also play a crucial role in regulating the orientation of side-chain mesogens. Owing to their outstanding properties with proper structural designs, MCSCLCPs can be applied in many areas such as engineering plastics and optical and electro-optical devices.

The other possibility is to incorporate side-chain mesogens with high dipole-moment such that the main-chain mesogen would align along with the polymer flow while a magnetic field may be applied to induce the side-chain mesogens to orient perpendicular to the main-chain backbone. Due to the advancement of synthetic technology (e.g. living or controlled polymerization), MCSCCLCPs can be integrated into other polymers, thus forming block copolymers. This will lead to hierarchical structures with various topologies and open new opportunities for exploiting new functional materials with fine-tuning ordered structures. The attachment of side-chain mesogens onto a rigid-rod backbone, especially for biomacromolecules, broadens the scope of MCSCCLCPs and enables the synthesis of high-performance materials from renewable sources. The MCSCCLCPs can be further exploited for creating networks by crosslinking reactions (Zentel and Reckert 1986; Zentel et al. 1989; Pakula and Zentel 1991), thus forming combined main-chain/side-chain liquid crystalline elastomers for unusual mechanical properties.

Self-assembly by specific interactions offers an easier and more efficient methodology to create a new spectrum of MCSCCLCPs. Self-assembly driven by hydrogen bonding and ionic interactions have been extensively investigated, and other specific interactions like metal ion interactions and Coulombic interactions will be of particular interests to explore. The supramolecular structures observed in self-assembled MCSCCLCPs have thrown new light on the effect of side-chain mesogens induced by specific interactions on structure-property relationships. Future endeavor may direct toward the introduction of chiral nematic or ferroelectric systems via self-assembly for various opto-electronic and nanotechnology applications.

References

- Cha SW, Jin J-I, Kim D-C, Zin W-C (2001) Combined type liquid crystalline poly(oxy-1,4-phenyleneoxyterephthaloyl)s bearing cholesterol pendants attached through polymethylene spacers. *Macromolecules* 34:5342–5348
- Champe PC, Harvey RA (1994) Lippincott's illustrated reviews: biochemistry. J. B. Lippincott, Philadelphia
- Chen B-Q, Kameyama A, Nishikubo T (1999) New combined liquid crystalline polymers from polyaddition of biphenol diglycidyl ether and trimeric esters. *Macromolecules* 32:6485–6492
- Collings PJ, Hird M (1997) Introduction to liquid crystals chemistry and physics. Taylor and Francis, London
- Donald AM, Windle AH (1992) In: Donald AM, Windle AH (eds) Liquid crystalline polymers. Cambridge, Cambridge University Press
- Endres BW, Ebert M, Wendorff JH, Reck B, Ringsdorf H (1990) Combined main chain/side chain polymers. A new class of liquid crystalline polymers with unusual structural, thermodynamic and dynamic properties. *Liq Cryst* 7:217–239
- Endres BW, Wendorff JH, Reck B, Ringsdorf H (1987) Dielectric properties of a combined main-chain/side-chain liquid-crystalline polymer. *Makromol Chem* 188(6):1501–1509
- Ge JJ, Zhang A, McCreight KW, Ho R-M, Wang S-Y, Jin X, Harris FW, Cheng SZD (1997) Phase structures, transition behaviors, and surface alignment in polymers containing rigid-rodlike backbones with flexible side chains. 1. Monotropic phase behavior in a main-chain/side-chain liquid crystalline polyester. *Macromolecules* 30:6498–6506

- Hu T, Xie H, Xiao J, Zhang H, Chen E (2010) Design, synthesis, and characterization of a combined main-chain/side-chain liquid-crystalline polymer based on ethyl cellulose. *Cellulose* 17:547–558
- Huang W, Han CD (2006) Synthesis of combined main-chain/side-chain liquid-crystalline polymers via self-assembly. *Macromolecules* 39(14):4735–4745
- Huang W, Shi E (2012) High-performance thermotropic starch-based liquid crystalline polymer. *Carbohydr Polym* 90:703–708
- Joo S-H, Yun Y-K, Jin J-I, Kim D-C, Zin W-C (2000) Synthesis of liquid crystalline polyesters of various types by acyclic diene metathesis polymerization. *Macromolecules* 33:6704–6712
- Kapitza H, Zentel R (1988) Combined liquid-crystalline polymers with chiral phases, 2. Lateral substituents. *Macromol Chem Phys* 189:1793–1807
- Kapitza H, Zentel R (1991) Chiral liquid-crystalline polymers by polymer-analogous reactions. *Macromol Chem Phys* 192:1859–1872
- Kato T, Frechet JMJ (1989a) A new approach to mesophase stabilization through hydrogen bonding molecular interactions in binary mixtures. *J Am Chem Soc* 111:8533
- Kato T, Frechet JMJ (1989b) Stabilization of a liquid-crystalline phase through noncovalent interaction with a polymer side chain. *Macromolecules* 22:3818
- Kato T, Ihata O, Ujiie S, Tokita M, Watanabe J (1999) Self-assembly of liquid-crystalline polyamide complexes through the formation of double hydrogen bonds between a 2,6-bis(amino)pyridine moiety and benzoic acids. *Macromolecules* 31:3551
- Kato T, Mizoshita N (2002) Self-assembly and phase segregation in functional liquid crystals. *Curr Opin Solid State Mater Sci* 6:579–587
- Kremer F, Vallerien SU, Zentel R, Kapitza H (1989) Broad-band dielectric spectroscopy on a set of combined main-chain side-group liquid-crystalline polymers. *Macromolecules* 22(10):4040–4045
- Larson RG (1990) Arrested tumbling in shearing flows of liquid-crystal polymers. *Macromolecules* 23:3983–3992
- Lee J-W, Jin J-I, Jo B-W, Kim J-S, Zin W-C, Kang Y-S (1999) Synthesis and properties of combined type liquid crystalline polymers-aromatic polyesters bearing biphenylazophenyl mesogenic pendants connected to the backbone through polymethylene spacers. *Acta Polym* 50:399–407
- Lehn JM (1988) Supramolecular chemistry—scope and perspectives molecules, supermolecules, and molecular devices. *Angew Chem Int Ed Engl* 27:89–112
- Marrucci G, Maffettone PL (1989) Description of the liquid crystalline phase of rodlike polymers at high shear rates. *Macromolecules* 22:4076–4082
- Mensing H, Biswas A, Poths H (1992) Small-angle x-ray scattering investigations of novel superstructures in combined chiral liquid-crystalline polymers. *Macromolecules* 25(12):3156–3163
- Noirez L, Poths H, Zentel R, Strazielle C (1995) Direct observation of the main-chain conformation of a combined liquid-crystal polymer. *Liq Cryst* 18:123–127
- Pakula T, Zentel R (1991) Mechanical behavior of liquid-crystalline polymers and their networks. *Makromol Chem* 192:2401–2410
- Piao XL, Kim J-S, Yun Y-K, Jin J-I, Hong S-K (1997) Combined type liquid crystalline polymers composed of poly(p-phenylene terephthalate) main chain and azobenzene mesogenic side groups attached through polymethylene spacers. *Macromolecules* 30(8):2294–2299
- Reck B, Ringsdorf H (1985) Combined liquid crystalline polymers: mesogens in the main chain and as side groups. *Macromol Rapid Commun* 6:291–299
- Reck B, Ringsdorf H (1986) Combined liquid-crystalline polymers: rigid rod and semi-flexible main chain polyesters with lateral mesogenic groups. *Macromol Rapid Commun* 7:389–396
- Reck B, Ringsdorf H, Gardner K, Howard SJ (1989) Combined liquid-crystalline polymers: rigid-rod type main-chain polyester with lateral mesogenic groups. *Macromol Chem Phys* 190:2511–2526

- Sato M, Mizoi M (2004) Relationships between structures and liquid crystalline and optical properties in combined-type copolyisophthalates having nitro- and methoxyazobenzene units and aliphatic spacers in the side chain. *Polym J* (Tokyo, Japan) 36(8):607–616
- Sato M, Mizoi M, Yano H (2004) Liquid crystalline homopolyesters having main chain calamitic mesogens and one or two side chain azobenzene moieties in the repeat units. *Liq Cryst* 31(9):1219–1226
- Schaefer KE, Keller P, Deming TJ (2006) Thermotropic polypeptides bearing side-on mesogens. *Macromolecules* 39:19–22
- Voigt-Martin IG, Durst H, Reck B, Ringsdorf H (1988) Structure analysis of a combined main-chain/side-chain liquid crystalline polymer by electron microscopy. *Macromolecules* 21:1620–1626
- Watanabe J, Tominaga T (1993) Thermotropic liquid crystals in polypeptides with mesogenic side chains. *Macromolecules* 26:4032–4036
- Wen G-H, Zhang B, Xie H-L, Liu X, Zhong G-Q, Zhang H-L, Chen E-Q (2013) Microphase separation facilitating and stabilizing hierarchical segment self-assembly of combined main-chain/side-chain liquid crystalline polymer in diblock copolymer. *Macromolecules* 46(13):5249–5259
- Werbowj RS, Gray DG (1976) Liquid crystalline structure in aqueous hydroxypropyl cellulose solutions. *Mol Cryst Liq Cryst* 34:97–103
- Wu C, Gu Q, Huang Y, Chen S (2003) The synthesis and thermotropic behaviour of an ethyl cellulose derivative containing azobenzene-based mesogenic moieties. *Liq Cryst* 30:733–737
- Xie H-L, Jie C-K, Yu Z-Q, Liu X-B, Zhang H-L, Shen Z, Chen EQ, Zhou Q-F (2010) Hierarchical supramolecular ordering with biaxial orientation of a combined main-chain/side-chain liquid-crystalline polymer obtained from radical polymerization of 2-vinylterephthalate. *J Am Chem Soc* 132:8071–8080
- Xie H-L, Wang S-J, Zhong G-Q, Liu Y-X, Zhang H-L, Chen E-Q (2011) Combined main-chain/side-chain liquid crystalline polymer with main-chain on the basis of “jacketing” effect and side-chain containing azobenzene groups. *Macromolecules* 44(19):7600–7609
- Xie H, Hu T, Zhang H, Chen E, Zhou Q (2008) Design, synthesis, and characterization of a combined main-chain/side-chain liquid crystalline polymer based on mesogen-jacketed liquid crystal polymer via atom transfer radical polymerization. *J Polym Sci Polym Chem* 46:7310–7320
- Yang G, Tang P, Yang Y (2012) Uniaxial-biaxial nematic phase transition in combined main-chain/side-chain liquid crystal polymers using self-consistent field theory. *Macromolecules* 45(8):3590–3603
- Zentel R, Brehmer M (1996) Combined LC main chain/side chain polymers. *Acta Polym* 47:141–149
- Zentel R, Reckert G (1986) Liquid crystalline elastomers based on liquid crystalline side group, main chain and combined polymers. *Makromol Chem* 187:1915–1926
- Zentel R, Reckert G, Bualek S, Kapitza H (1989) Liquid-crystalline elastomers with cholesteric and chiral c^* phases. *Makromol Chem* 190:2869–2884
- Zhou M, Han CD (2005) Synthesis and characterization of a combined main-chain/side-chain liquid-crystalline polymer exhibiting both thermotropic and lyotropic characteristics and its lyotropic phase behavior. *Macromolecules* 38(23):9602–9609
- Zhou M, Han CD (2006) Rheology of a combined main-chain/side-chain liquid-crystalline polymer in the thermotropic and lyotropic states. *Macromolecules* 39(1):232–242
- Zhou Q, Zhu X, Wen Z (1989) Liquid-crystalline side-chain polymers without flexible spacer. *Macromolecules* 22:491–493
- Zhou QF, Li HM, Feng XD (1987) Synthesis of liquid-crystalline polyacrylates with laterally substituted mesogens. *Macromolecules* 20:233–234
- Zhu Y-F, Guan X-L, Shen Z, Fan X-H, Zhou Q-F (2012) Competition and promotion between two different liquid-crystalline building blocks: mesogen-jacketed liquid-crystalline polymers and triphenylene discotic liquid crystals. *Macromolecules* 45(8):3346–3355

Chapter 13

Supramolecular (Hydrogen-Bonded and Halogen-Bonded) Liquid Crystalline Polymers

Qun Ye, Jianwei Xu, and Chaobin He

13.1 Introduction

Liquid crystal (LC) materials represent an intriguing class of soft materials which have been intensively investigated as functional materials. The intrinsic self-assembly nature of LC materials at mesophases brings in advantages when the alignment or self-organization of the material becomes a requirement for a certain function. Ever since the development of liquid crystal display technology from the 1960s, tremendous efforts have been focused on the preparation of various types of liquid crystals, characterization and applications of their liquid crystalline properties. Conventional thermotropic LC materials are typically small molecules or polymers linked by covalent bonds. To further expand the functional capacity of liquid crystals, the concept of supramolecular chemistry has been implemented into the design and construction of novel LC materials.

Supramolecular chemistry involves construction of chemical architectures by reversible non-covalent interactions such as π - π interaction, van der Waals forces, ionic interaction, charge transfer (donor-acceptor) interaction, metal ion coordination, hydrogen bonding and halogen bonding (Lehn 1995). These non-covalent interactions have been utilized as versatile tools for the synthesis of supramolecular liquid crystalline small molecules and polymeric mesogens. This approach is rather

Q. Ye • J. Xu (✉) • C. He

A*STAR (Agency for Science, Technology and Research), Institute of Materials Research and Engineering, 3 Research Link, Singapore 117602, Singapore
e-mail: yeq@imre.a-star.edu.sg; jw-xu@imre.a-star.edu.sg

attractive mainly owing to the dynamic nature of the non-covalent interaction, which renders potential thermomechanical property and stimuli-responsive property to these dynamic systems. Among various non-covalent approaches used, hydrogen bonding (HB) and halogen bonding (XB) interactions are of particular interest and importance.

Hydrogen bonding has been long known as a weak electrostatic interaction force in nature. It is a directional interaction between a positively polarized hydrogen atom that is covalently linked to an electronegative atom (O, N, etc.) of a HB donor moiety, and a negatively polarized atom of a HB acceptor moiety. The bonding energy of HB varies from 1 to 40 kcal mol⁻¹, thus allowing feasible tuning of the strength of the associated supramolecular interactions. The concept of hydrogen bonding has become an essential part of supramolecular chemistry and the fundamentals about HB have been well summarized (Grabowski 2006). The development of hydrogen bonded LC materials starts from the late 1980s mainly pioneered by Kato and Fréchet, Lehn and Griffin. Over the past decades a large library of such HB induced LC materials has been prepared and investigated (Kato et al. 2006; Paleos and Tsiourvas 1995, 2001; Kato 2000; Brinke et al. 2007; Binder and Zirbs 2007; Rowan and Mather 2008). Among all HBs, the interaction between carboxylic acid and pyridine based moieties has been routinely used for the construction of supramolecular liquid crystalline mesogens.

Analogous to hydrogen bonding, halogen bonding (XB) involves the interactions between a halogen atom (Cl, Br, I) with an electron donating species. The basic concept of XB has been well summarized by Metrangolo and Resnati (Metrangolo and Resnati 2001; Metrangolo et al. 2005, 2008). Similar to hydrogen bonding, halogen bonding is also directional and dynamic. The bonding energy of XB varies in the range of 1–40 kcal mol⁻¹, very similarly to hydrogen bonding. Due to the relatively weak nature of HB and XB, moieties formed by HB and XB rapidly associate and dissociate at melt temperature and hence the formed mesomorphic materials possess a dynamic nature (Bladon and Griffin 1993). Compared with hydrogen bonding, the interest on halogen bonding and its application as a supramolecular tool to construct valuable functional materials for practical applications is still in its infancy. Nonetheless, application of the halogen bond as a versatile tool for the preparation of supramolecular dynamic LC materials has been demonstrated and quite a number of such materials are reported.

Supramolecular LC materials that can be constructed by hydrogen bonding and halogen bonding are summarized in Fig. 13.1. Small molecules such as calamitic (rod-like) and discotic (disk-like) and polymeric mesogens (side-chain, main-chain and network) can be prepared from complementary components through the dynamic hydrogen bonding and halogen bonding linkage. For the side chain LC polymers, they are typically prepared by linking mesogens to the polymer backbone through HB and XB. Main chain LC polymers are self-assembled using bifunctional donor/acceptor moieties. While for network type supramolecular LC polymers, the building blocks generally possess more than two functional sites. All these types of dynamic LCs will be illustrated with examples in the following section.

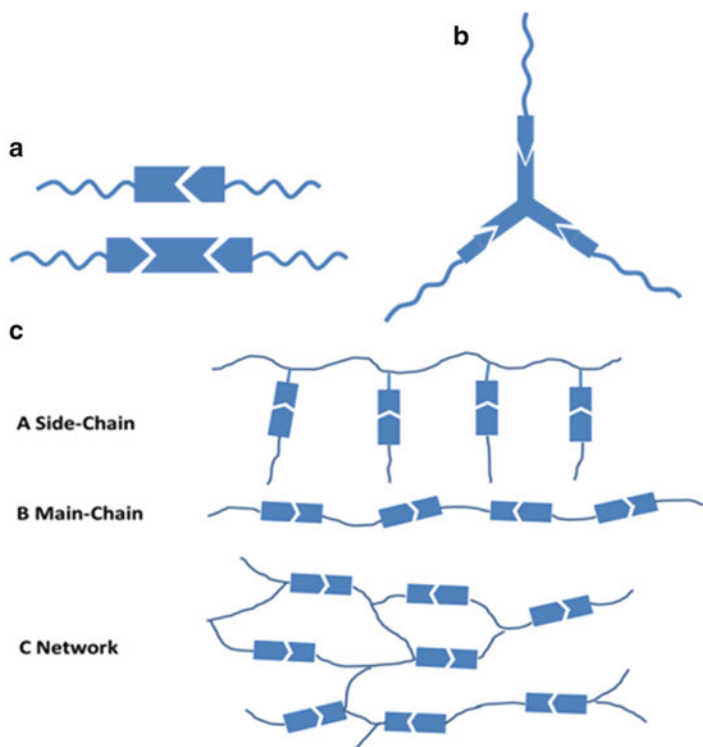


Fig. 13.1 Supramolecular liquid crystalline materials by hydrogen bonding and halogen bonding: (a) calamitic small molecules; (b) discotic small molecules; (c) polymeric materials including side-chain type, main-chain type and network type

Commonly used characterization methods for these dynamic LC systems include solid state NMR (Reddy et al. 2013), single crystal X-ray crystallography, X-ray photoelectron spectroscopy (XPS), Fourier-transform-infrared (FT-IR) spectroscopy, differential scanning calorimetry (DSC), X-ray diffraction (XRD) and polarized optical microscopy (POM). Especially, single crystal crystallography gives a direct evidence of HB and XB in the crystal state while FT-IR spectroscopy and XPS provide a direct evidence for the formation of HB and XB in the mesomorphic mixture. The vibrational band shift in FT-IR and the binding energy shift in XPS are generally considered as evidence for such dynamic interactions. Meanwhile, DSC, POM and XRD studies give more insights to the newly formed mesogens.

In this chapter, we aim to provide a summary of supramolecular polymeric LC materials with hydrogen bonding and halogen bonding adopted as the linking strategy. The dynamic nature as well as the mesogenic properties of both small molecule LCs and polymeric LCs will be discussed. The applications of these dynamic LC systems will be illustrated with examples.

13.2 Hydrogen-Bonded Liquid Crystalline Materials

13.2.1 Small Molecule LC Materials Based on Hydrogen Bonding

Calamitic (rod-like) small molecule mesogens are the first type of supramolecular LC materials prepared via hydrogen bonding. The most routinely used moieties are carboxylic acid and pyridines. Carboxylic acids serve as hydrogen donor while pyridines serve as hydrogen acceptor. Kato and Fréchet firstly prepared a HB complex between 4-butoxybenzoic acid and *trans*-4-[(4-ethoxybenzoyl)oxy]-4'-stilbazole (**C1** in Fig. 13.2) (Kato and Fréchet 1989a, b). Both monomer components are nematic in nature with nematic mesophase from 147 to 160 °C and 165 to 213 °C, respectively. After complexation, the 1:1 mixture features a smectic phase from 136 to 160 °C and a nematic phase from 160 to 238 °C. The strong stabilization of the mesophase compared with the monomers is attributed to the formation of a hydrogen bonded complex as shown in Fig. 13.2. The existing hydrogen bonding in the blend is confirmed by FT-IR spectroscopy. For the neat 4-butoxybenzoic acid, a stretching band at 1681 cm⁻¹ is observed originating from the carbonyl groups of the carboxylic acid dimer while for the 1:1 mixture, a new band at 1704 cm⁻¹ is observed which is assigned to the carbonyl group of the carboxylic acids complexed with pyridine. Similar design strategy is applied by the same group to synthesize liquid crystalline complexes with room-temperature mesophases and electrooptic effects (Fukumasa et al. 1993; Kato et al. 1995).

This series of supramolecular LC materials can be further extended by using bipyridine based moieties as the bifunctional hydrogen acceptors to prepare trimeric mesogens (**C2** in Fig. 13.2) (Kato et al. 1993). Moieties such as 4,4'-bipyridine or *trans*-1,2-bis(4-phridyl)ethylene can form hydrogen bonding with two 4-alkoxybenzoic acids on two sides to form extended mesogens. Nematic phases are observed for $n = 1-4$ whereas smectic phases are observed for $n = 5-10$. FT-IR spectrum of the 1:2 complex reveals O-H bands at 2500 and 1920 cm⁻¹ corresponding to strong hydrogen bonding in the blend. Carbonyl band at 1696 cm⁻¹ is assigned to the carbonyl in the carboxylic acid complexed with pyridine. The vibrational frequency of the carbonyl group is proposed to correlate to the state of molecular ordering. As temperature changes, the packing of the complexed mesogen changes and this induces a disturbance to the local environment of the hydrogen bonding site. However, the detailed mechanism that rules the frequency shift remains obscure given that other explanations are also proposed for similar phenomenon (Tian et al. 1995; Pourcain and Griffin 1995).

Phenol derivatives can also be used as hydrogen donor species for the construction of dynamic LC materials (**C3** and **C4** in Fig. 13.2) (Willis et al. 1995; Price et al. 1997). Electron withdrawing groups such as cyano groups and nitro groups are conjugated with the hydroxy group to enhance the acidity of the phenolic hydrogen and hence to strengthen the hydrogen bond. In the case of 4-cyanophenol, the single crystal of 1:1 mixture of 4-cyanophenol and octyloxystilbazole is obtained to

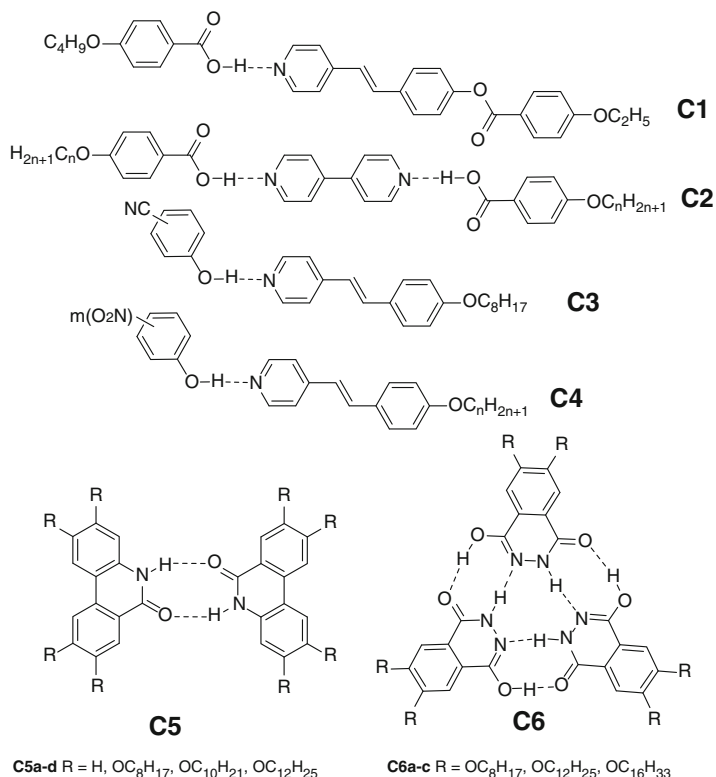


Fig. 13.2 Hydrogen bonding induced calamitic and discotic small molecule mesogens

confirm the hydrogen bonding in the solid state. For nitro-phenol based complexes, the hydrogen bonding is confirmed by FT-IR spectroscopy. For pure nitro-phenol derivatives, the vibrational frequency of the hydroxyl groups is at *ca.* 3200 cm^{-1} whereas for the complexed blend, the hydroxyl vibrational frequency shifts to *ca.* 2500 cm^{-1} , indicating the formation of stronger hydrogen bond in the complex. Increasing the temperature broadens the band at 2500 cm^{-1} and shifts the band to higher frequency. This suggests a lengthening effect of the hydrogen bond at higher temperature. For both series, the complexed mesogens exhibit either a nematic or smectic phase depending on the length of the alkoxy chains attached.

Discotic liquid crystals can be achieved by hydrogen bond assisted self-assembly of complementary moieties. Kleppinger and co-workers has demonstrated such a strategy using functionalized 6(5*H*)-phenanthridinones (**C5** in Fig. 13.2) (Kleppinger et al. 1997). The formation of the dimeric discotic mesogen is confirmed by XRD, FT-IR, DSC and POM study. From FT-IR observation, no free N-H vibration is observed at 3440 cm^{-1} , with only a broad featureless band near 3200–3300 cm^{-1} observed. This is attributed to the hydrogen bonded amide

N–H stretching. POM study reveals focal conic textures consistent with the hexagonal columnar packing of the discotic mesogen. More sophisticated hydrogen bonded trimeric discotic mesogen **C6** is prepared by Suárez and co-workers (Suárez et al. 1998). The self-assembly behaviour of 6,7-bis(alkyloxy) 2,3-dihydrophthalazine-1,4-diones has been investigated. Dynamic NMR and size exclusion chromatography study confirm the trimeric nature of the self-assembled mesogens. DSC curves of all three species exhibit a crystal to mesophase transition temperature at around 100 °C and a mesophase to isotropic transition temperature above 200 °C. For **C6a** and **C6b**, both of the discotic mesogens exhibit hexagonal columnar mesophase (Col_H). For **C6c**, the mesogen exhibits a rectangular columnar mesophase (Col_R) followed by a hexagonal columnar mesophase (Col_H).

13.2.2 Polymeric LC Material Based on Hydrogen Bonding

13.2.2.1 Side-Chain Type

For side-chain type LC materials (Fig. 13.1c), the pendant moieties are linked to the polymer backbone through non-covalent hydrogen bonding and some examples to demonstrate such polymeric mesogens are shown in Fig. 13.3. Polyacrylate in **P1** contains a benzoic acid moiety in side chain and exhibits a nematic phase between 140 and 155 °C. The benzoic acid can complex with stilbazole through hydrogen bonding and this binding significantly enhances the stability of the mesophase (Kato and Fréchet 1989a, b). For the equimolar mixture of benzoic acid and stilbazole in **P1**, the mesophase is observed from 140 to 252 °C. The mesomorphic range of the 1:1 mixture is 112 °C, which is much wider than that of any component. This strong enhancement is attributed to the formation of extended mesogen through hydrogen bonding between the benzoic acid and the stilbazole moieties. This hydrogen bond complexation is proved by FT-IR spectroscopy. For **P1**, a band at 1704 cm⁻¹ is observed due to the carbonyl group in the complexed benzoic acid while for the free polyacrylate polymer, a band at 1685 cm⁻¹ corresponding to the carboxylic acid dimer is observed. This type of hydrogen bonded LC polymer is studied in more detail by varying the alkyl chain length on the stilbazole moiety (Kato et al. 1992). For complexed LC polymer **P2**, only smectic mesophase is observed for $n = 1-10$. Similar concept is applied on polysiloxanes as well (Kumar et al. 1992a, b). Furthermore, other than acid-pyridine interaction, Kato et al. (1997) also apply the concept of side chain grafting onto 2,6-bis(amino)pyridine embedded nylon polymer (**P3**). Complexation between carboxylic acid and 2,6-bis(amino)pyridine generates new mesophase from 212 to 350 °C.

This type of side-chain supramolecular hydrogen bonded LC polymers has been explored for a variety of applications. For hydrogen bonded dynamic LC systems, one of the major advantages is the dynamic nature of the hydrogen bond and the self-assembly behaviour of generated mesogens. These characters are indeed useful when the self-assembly process in a nematic or smectic manner and the association/

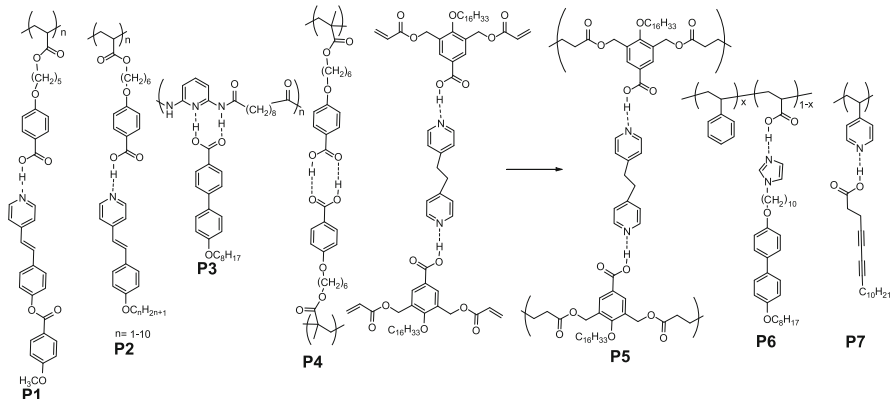


Fig. 13.3 Examples of hydrogen bonding induced side-chain type polymeric mesogens

dissociation of the hydrogen bond are needed for the application. A series of self-aligned poly(methacrylate) polymers (**P4**) have been prepared by Uchida and co-workers (Uchida and Kawatsuki 2006). The hydrogen bonding between the carboxylic acids is utilized to extend and help align the LC mesogens. Linearly polarized UV light induces a photoinduced reorientation of the film and this oriented film is envisaged as birefringent devices in LC display applications. A very similar system is studied by Gonzalez et al. (Gonzalez et al. 2008) for the preparation of nanoporous membranes. After photopolymerization, they treat the well-ordered polymer with heat or alkaline solution to break the hydrogen bonding between carboxylic acids, thus generating nanopores which are able to react with basic organic materials such as amines or cations such as barium ions. Applications such as chromatography, catalysis and anisotropic ion conduction are predicted for this system.

The self-assembly behaviour of hydrogen bond induced LC is also applied by Kishikawa and co-workers (Kishikawa et al. 2008) to prepare multi-layered polymers with empty spaces (**P5**). The bipyridine moiety serves as a template molecule and hydrogen bonding between the bipyridine with functionalized benzoic acids organizes the three blocks into a rod-like mesogen. The generated mesogen exhibits a smectic A mesophase. As the benzoic acids are functionalized with polymerizable acrylate groups, the oriented mesogens then undergo photopolymerization in the liquid crystalline phase. After polymerization is accomplished, removal of the template by acids is followed, hence generating empty space in the multi-layered polymers. XRD study shows that the original layered structure is maintained after removal of the template bipyridine moieties. This kind of material is envisaged to be useful as molecule recognition and selective inclusion materials.

A polystyrene-*block*-poly(methacrylic acid) block copolymer is prepared by Osuji and co-workers (Osuji et al. 2002, 2006; Chao et al. 2004; Gopinadhan et al. 2010) to host imidazole-based mesogens (**P6** in Fig. 13.3). Imidazole moieties can also serve as good hydrogen acceptors and hence hydrogen bonding between

imidazole and carboxylic acid is feasible. The hydrogen bonding is confirmed by a new band at 2530 cm^{-1} in the FT-IR spectrum, which is due to the formation of strong hydrogen bonding between imidazole and the carboxylic acid. The prepared supramolecular mesomorphic polymer system exhibits a reversible refractive index modulation by thermal energy. A significant and reversible change up to 25 % in the optical transmission of the LC film is obtained by thermally altering the refractive index of the material. AC electric field is also found to reorient the mesogen effectively in the liquid crystalline phase.

A hydrogen bond induced self-assembly between poly(4-vinylpyridine) and diacetylene functionalized carboxylic acid is found useful to effectively align the diacetylene moieties in the film (Wu et al. 2009). The hydrogen bonding complex (**P7**) can be crosslinked via photopolymerization and becomes solvent resistant. This makes the system useful in photolithography and as sensor material due to the stimuli-induced colour change of the polydiacetylene system. Both assertions have been demonstrated in the study.

13.2.2.2 Main-Chain Type

Main-chain type hydrogen bonding induced dynamic LC polymers refer to a class of dynamic polymers in which the hydrogen bonding is used as both the origin of liquid crystallinity and a tool for polymer formation. They typically involve bifunctional building blocks, such as diacid and bispyridine groups. The hydrogen bonds serve as glue to link the diacids and bispyridine moieties linearly following an –AABBAABB– pattern and at the same time the newly formed complex exhibits new mesophases at elevated temperature. Such novel polymeric mesogens (**P8** to **P15** in Fig. 13.4) are comprehensively demonstrated by He and co-workers (He et al. 1998, 1999; Lu et al. 2002; Xu et al. 2005a, b; Toh et al. 2005, 2008). For polymer **P8**, bis(pyridyl)ethene and penta(ethyleneglycol)linked dibenzoic acids are used as hydrogen bond acceptor and donor, respectively. The complexed polymer **P8** exhibits a crystal to monotropic smectic phase transition at *ca.* 131 °C and a smectic to isotropic phase transition at 159 °C upon cooling from isotropic phase. Wide angle XRD study of the complexed polymer reveals totally different diffraction peaks from those of any of the components, indicating the formation of new structures after mixing. Small-angle X-ray scattering shows a scattering peak at 0.159 \AA^{-1} , corresponding to a *d* spacing value of 39.5 Å. This value is reasoned as the smectic layer distance of the polymer. Temperature dependent FT-IR spectroscopy shows a strong vibration band at 1900 cm^{-1} , which is assigned to the complexed hydrogen bonding. By extending the conjugation of the bispyridine moiety and shortening the length of the diacid moiety, a new polymer **P9** is prepared by Lu and co-workers (Lu et al. 2002). Both the building blocks do not exhibit mesomorphic behavior while the complexed polymer exhibits a nematic mesophase. On heating, polymer **P9** shows a crystal to nematic transition at 150 °C and a nematic to isotropic transition at 175 °C. This polymer is found to be able to

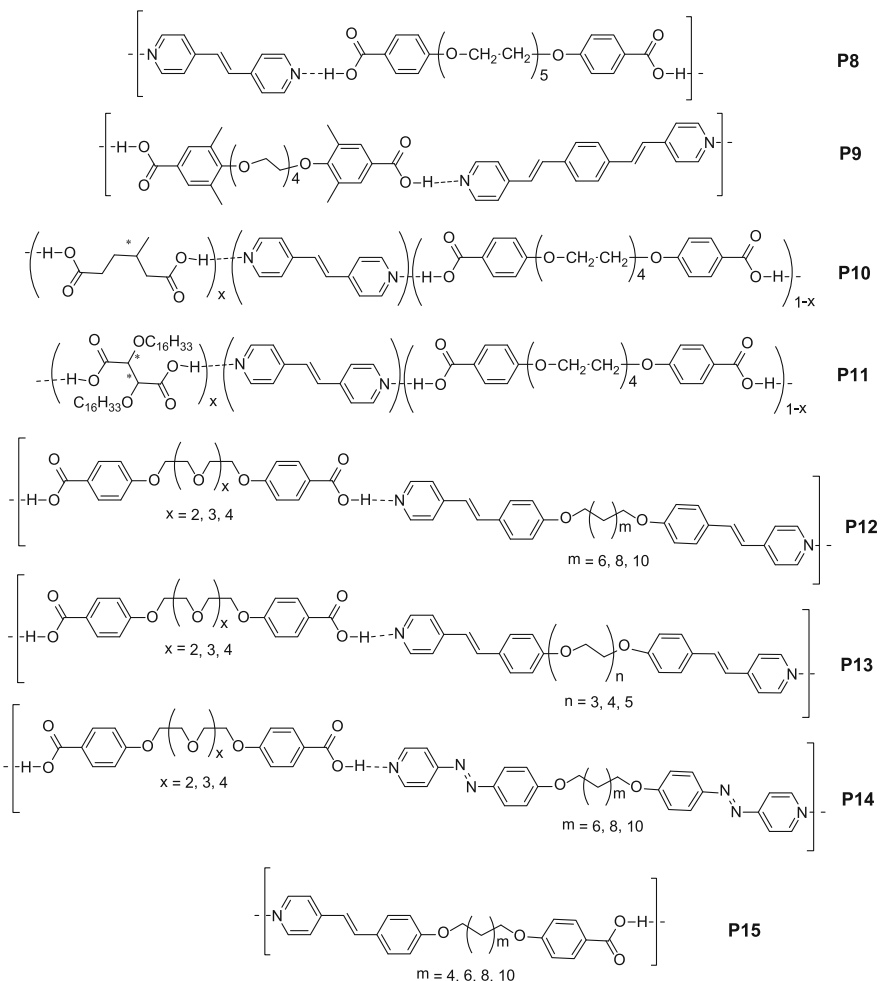


Fig. 13.4 Main chain type LC polymers formed by hydrogen bonding

form fibres under tensile and shear forces just as covalent polymers, indicating that the hydrogen bonding linkage is robust enough to restore the proposed linear geometry under external forces. The X-ray diffraction pattern on the fibres corresponds well with that from the powder diffraction study. This suggests that the polymers pack in a similar motif in both states. Based on the diffraction data, a monoclinic unit cell with $a = 6.1 \text{ \AA}$, $b = 5.9 \text{ \AA}$, $c = 46 \text{ \AA}$, $\alpha = \gamma = 90^\circ$, $\beta = 40^\circ$ is simulated for this polymer.

One advantage of hydrogen bonding based LC polymers is that the mesophase property of the generated polymer can be easily tuned by adding extra HB active moieties into the self-assembled mixture. For example, chiral dopant diacids ((+)-3-methyl adipic acid and 2,3-bis(hexadecyloxy)succinic acid) can be introduced to

the HB induced polymer between tetra(ethyleneoxy)-bis-(4-benzoic acid) and 1,2-bis(pyridyl)ethylene (Polymers **P10** and **P11** in Fig. 13.4) to tune the mesophase property and to bring in chirality to the mesophase (He et al. 1999). The presence of (+)-3-methyl adipic acid in the complexed polymer is found to destabilize the mesophase. This is ascribed to the decreased concentration of mesogens and increased randomness of the polymer, both of which hamper the ordered orientation of the polymer in the mesophase. Furthermore, after doping the polymer with very small amount of the chiral dopant (+)-3-methyl adipic acid (1.5 mol%), the resultant mixture exhibits a chiral nematic phase. Similar to (+)-3-methyl-adipic acid, the presence of 2,3-bis(hexadecyloxy)succinic acid also destabilizes the mesophase and both nematic and smectic transition temperatures are decreased after doping.

The spacer effect for hydrogen bonded dynamic LC polymers has been systematically investigated by He and co-workers (Toh et al. 2005, 2008). The density of flexible spacers in the polymer backbone is tuned in order to adjust the mesophase property of the polymer. The prepared polymers are shown as **P12**, **P13** and **P14** in Fig. 13.4. The formation of the hydrogen bond linkage is comprehensively proved by FT-IR spectroscopy, XPS, DSC, POM and XRD study. Findings are that (1) extension of the aliphatic chain length in the bipyridine moiety disfavours the formation of mesophase while (2) increase of the ethylene glycol repeating unit favours the formation of mesophase; and (3) increasing the number of ethylene glycol units significantly lowers phase transition temperatures. The azo moieties in **P14** are found to be insensitive to UV irradiation, possibly due to the inhibition of *cis-trans* photoisomerization by fixation of such moieties in the polymeric backbone.

Main-chain type LC polymers can be constructed using building blocks with acid part on one side and pyridine part on the other side. In such a way, self-assembly of only one monomer is able to generate the linear dynamic polymer with an –ABABABAB– pattern. This strategy is demonstrated by Xu and co-workers (Xu et al. 2005a, b). For polymer **P15**, it is self-assembled by a monomer which has stilbazole and benzoic acid on each side and an aliphatic spacer in the middle. The polymers exhibit monotropic smectic mesophases upon cooling from isotropic phase with mosaic textures observed. XPS and FT-IR study assure the formation of hydrogen bonding between carboxylic acid and pyridine and exclude the formation of acid dimer in the system. By increasing the spacer length, it is found that for this series of polymers, the transition temperature decreases, suggesting that the mesophase behavior can be conveniently tuned by adjusting the length of the spacer.

13.2.2.3 Network Type

Network type polymeric LC mesogens are the third type of LC systems that can be constructed by hydrogen bonding (Fig. 13.1c). To prepare network type architectures, either the HB donor moiety or the HB acceptor moiety should be multi-

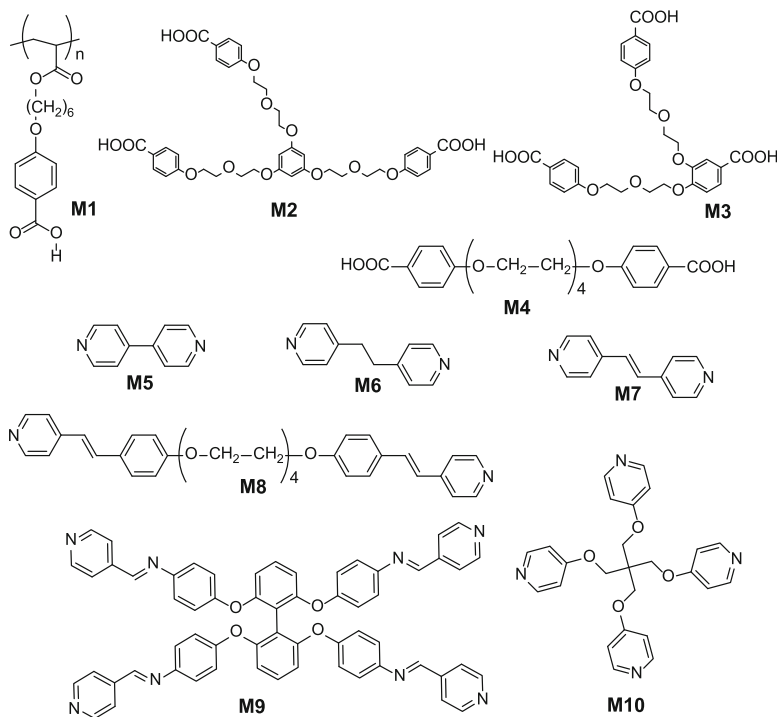


Fig. 13.5 Building blocks for network type hydrogen bond induced polymeric LC mesogens

functional, that is, it should contain at least three reactive sites so that complexation happens in a three-dimensional manner. Some of such carboxylic acid embedded building blocks and pyridine embedded building blocks (**M1** to **M10**) are listed in Fig. 13.5.

Polyacrylate containing benzoic acid moiety on the side chain (**M1**) is complexed with bipyridine (**M5**) to form a network mesogen (Kato et al. 1994). For the 1:1 complexed polymer, it exhibits a smectic A mesophase from 90 to 205 °C. The XRD study at the mesophase (170 °C) reveals a sharp peak at 39.8 Å, which corresponds to the length of the fully stretched conformation between two polymer backbones with bipyridine as the linkage. This suggests a ladder-type geometry of the formed polymer in the mesophase. The same research group also prepared trifunctional carboxylic acid containing molecules **M2** and **M3** to demonstrate more network type mesogens (Kihara et al. 1996). Four pyridine containing moieties, from **M5** to **M8**, are used to complex with **M2** and **M3** to form eight new network mesogens. Other than **M2/M5** complex, the rest seven network mesogen all exhibit liquid crystalline properties. Complexes **M2/M6**, **M2/M7** and **M2/M8** exhibit a monotropic smectic A phase upon cooling from isotropic phase while complexes **M3/M5**, **M3/M6** and **M3/M7** exhibit enantiotropic nematic mesophase. For complex **M3/M8**, it exhibits enantiotropic smectic A and nematic mesophases.

The formation of hydrogen bonding in the network is confirmed by FT-IR study. For the neat triacid **M2**, the hydroxyl group vibration bands are at 3000, 2667 and 2554 cm^{-1} . After complexation, the OH stretching bands appear at 2482 and 1924 cm^{-1} , indicating the formation of hydrogen bonding. Furthermore, the carbonyl vibration band shifts from 1684 cm^{-1} of the acid **M2** to 1691 cm^{-1} of the complexed product. All these results suggest the dominant formation of carboxylic acid-pyridine hydrogen bond formation in the network.

Griffin has presented a good discussion on network type polymers (Pourcain and Griffin 1995). They choose diacid **M4** and tetrapyridyl molecules **M9** and **M10** to prepare the network polymer. Varied temperature FT-IR study indicates that acid dimer formation is present in the isotropic state of the network polymer, which is due to the dynamic nature of the hydrogen bonding. In the isotropic state, the hydrogen bonding is disturbed by thermal energy and the components in the mixture randomly interact with each other. Upon cooling to mesophase, the vibration bands of the hydrogen bonded hydroxyl group increase at 1900 and 2500 cm^{-1} . Rheological study shows that after reaching the melting point, the viscosity of the network polymer drops rapidly, close to that of low molar mass molecules rather than of polymers. Nevertheless, the network polymers exhibit glass transitions and fibres can be pulled out of the melt, suggesting the polymeric nature of the complex. Hence these hydrogen bonded network polymers are more like small molecules in the melt state while they behave like polymers in the mesophase and crystalline state. It is reasoned that the tetrapyridyl moieties stay in a rod-like conformation rather than a pseudo-tetrahedral conformation. The rod-like conformation of the tetrapyridyl moiety is envisaged to pack better in the solid and hence promote both the crystallinity and formation of mesophase of the network whereas the pseudo-tetrahedral conformation favours the glassy form. Formation of the pseudo-tetrahedral conformation can be promoted by thermal annealing, which makes the polymer more like a 3D network, instead of a 2D extended chain-like system. Similar systems are also illustrated by some recent studies (Greuel et al. 2010; Janssen et al. 2012; Fredrickson et al. 2012).

13.3 Halogen-Bonded Liquid Crystalline Materials

Analogous to hydrogen bonding, halogen bonding (XB) represents a type of new supramolecular interaction which can serve as functional glues to build up chemical architectures. Halogen bonding has been widely explored in crystal engineering and supramolecular chemistry (Metrangolo and Resnati 2001; Metrangolo et al. 2005, 2008). The application of halogen bonding in liquid crystalline materials is still not well explored. Nonetheless, halogen bonding has been proven as an effective tool to prepare supramolecular LC materials.

13.3.1 Halogen-Bonded Small Molecule LC Materials

A series of halogen bonded small molecule thermotropic mesogens have been reported by Bruce and co-workers (Nguyen et al. 2004; Bruce et al. 2008, 2010; Präsang et al. 2008). (Fig. 13.6) Complexation between alkoxy stilbazole **M11** and pentafluoriodobenzene **M15** generates new liquid crystalline mesogens. For **M11** with butyl and hexyl chains, the generated complexes exhibit monotropic nematic mesophases upon cooling while for **M11** with octyl, decyl and dodecyl chains, the complexes exhibit enantiotropic smectic A mesophases. When 1,4-diiodoperfluorobenzene **M16** is used as the halogen donor, 1:2 complexation between **M11** and **M16** can be formed. For the 1:2 complex between **M11** and **M16**, monotropic nematic mesophases can be observed upon cooling. Similar to hydrogen bonded LC materials, halogen bonded LC complexes are routinely characterized by FT-IR spectroscopy, XPS, and single crystal diffraction to confirm the presence of halogen bonding in the mixture. A single crystal between **M11** and **M15** is obtained and a close contact between the iodine atom and the nitrogen atom is observed following the trend of halogen bonding (Metrangolo et al. 2008). FT-IR study also reveals the vibrational band shift due to complexation and electron redistribution over the system. A systematic investigation on halogen bonded LC materials has been carried out using **M11**, **M12** and **M13** as the halogen acceptor and **M18** to **M22** as the halogen donor. About 90 new complexes are prepared and majority of the mesogens show enantiotropic mesophases which is ascribed to the destabilization of the crystalline state of the complex. The dynamic nature of the halogen bonding linkage is also emphasized and the finding is that the mesophase stability is not likely to be influenced by the strength of halogen bonding at least up to 130 °C. As 4-iodotetrafluorophenol **M17** is used in the complexation, both halogen bonding and hydrogen bonding are present to guide the self-assembly. The 1:2 complex between **M11** and **M17** has demonstrated such strategy. From the single crystal study, the obtained 1:2 complex possesses a rod-like conformation with nematic mesophase observed for complexes with aliphatic chains from $n = 4$ –12. For complex **M11/M17** with dodecyl chains, a smectic A mesophase is observed as well. The priority of hydrogen bonding and halogen bonding with the pyridine moiety is of interest and it is found that in the single crystal of 1:1 complex of **M11** and **M17**, the pyridine nitrogen is coordinated to the hydroxyl group while the iodine atom is coordinated with the oxygen atom in the alkoxy chain of a neighbour molecule, leading to a polymeric arrangement in the crystal. For the 1:1 complex with $n = 8$, the formed complex exhibits a monotropic nematic phase upon cooling while for $n = 10, 12$ both complexes exhibit enantiotropic smectic A mesophase.

Xu and co-workers (Xu et al. 2006) investigated a trimeric complex between **M11** and **M23**. A flexible spacer is included in the XB donor to enhance the flexibility of the system. XPS and FT-IR study are employed to demonstrate the formation of halogen bonding. For the 16 new complexes, most of them exhibit a monotropic smectic A mesophase upon cooling. X-ray diffraction in the mesophase

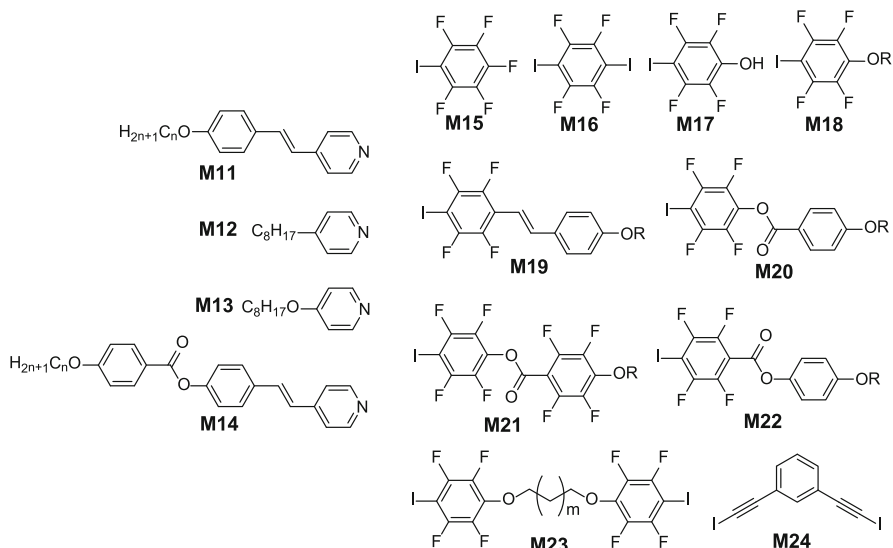


Fig. 13.6 Building blocks that are used for halogen bonded small LC mesogens

reveals a peak at 4.65 (2θ), corresponding to d -spacing of 19.0 Å. This value is very close to the length of the repeating unit (20.2 Å), hence confirming the formation of smectic mesophase.

Bent-shaped mesogen can be prepared by complexation between **M14** and **M24** (González et al. 2013). 1,3-Bis(iodoethynyl)benzene (**M24**) is used as the halogen donor. Iodine connected to a sp -hybridized carbon has sufficient Lewis acidity to form strong XB with pyridine moieties with an interaction energy of $\sim 10 \text{ kcal mol}^{-1}$ in this case. The formed halogen bond is confirmed by FT-IR and XPS investigations. For the bent-shaped 1:2 complexes, they exhibit a smectic AP phase, which is confirmed by XRD study.

13.3.2 Halogen Bonded LC Polymer Materials

Examples to demonstrate halogen bonding based supramolecular LC polymers are limited. Two such examples are reported by Xu and co-workers (Xu et al. 2005a, b; Cho et al. 2013). The first series of polymers involves complexation between dihalogen moiety **M23** and dipyridine moiety **M5**, **M6**, **M7** and **M25** (Fig. 13.7). The generated complexes typically exhibit either no or monotropic nematic mesophase upon cooling. The second series of polymers are constructed by self-assembly of **M24** and **M25**. For **M24**, it contains both the hydrogen donor and halogen donor, thus creating a mixture of dynamic linkage in the final polymer. As the degree of polymerization (DP) of this type of dynamic polymers can hardly be accessed by conventional gel permeation chromatography method, the DP of this

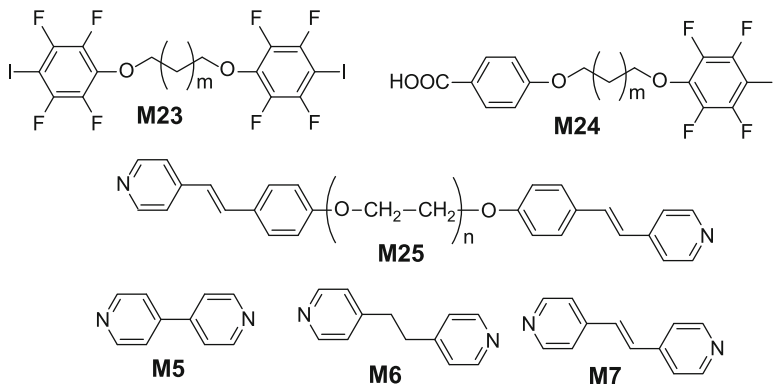


Fig. 13.7 Building blocks for the construction of halogen bonded polymeric LC mesogens

series of polymer is estimated based on the Flory equation. All DP values fall in the range of 11–20. The newly synthesized complexes typically exhibit monotropic nematic mesophase upon cooling, very similar to the XB induced small molecule mesogens.

13.4 Summary and Outlook

Dynamic liquid crystalline materials are a class of soft matter exhibiting self-assembly behavior, anisotropic nature and dynamic properties. In the chapter, hydrogen bond and halogen bond induced supramolecular LC materials are summarized and discussed. The versatility of hydrogen bonding and halogen bonding has been demonstrated with a large library of examples and new dynamic LC materials can be prepared through such approach. For hydrogen bonding induced LCs materials, many of these dynamic systems have been investigated for various applications such as actuators, sensors, responsive reflectors and nanoporous membranes (Broer et al. 2012), thus demonstrating the feasibility and a bright future for these materials. However, for halogen bonded LC materials, relatively less attention is paid to this research area from the academic society. Since the review by Bruce in 2008 (Bruce 2008), only a few more literatures are published recently to study halogen bonded LC systems. Given that halogen bonding has been extensively investigated in crystal engineering and supramolecular chemistry (Metrangolo et al. 2008) and recently on new applications such as drug design (Lu et al. 2009) and catalysis (Jungbauer et al. 2013), we believe that this research area will attract more attention in the future. For HB based dynamic LC materials, recent research effort has been devoted to exploring functional materials based on the self-assembly and dynamic property of these materials while for XB based dynamic materials, more effort is still in need, not only to elucidate the physical principles involved in the materials property (e.g. DP problem, stoichiometry in the

complex, etc.), but also to demonstrate any extra bonus from halogen bonding linkage, i.e. the unique characteristics of halogen bonding from materials' point of view.

References

- Binder WH, Zirbs R (2007) Supramolecular polymers and networks with hydrogen bonds in the main- and side-chain. *Adv Polym Sci* 207:1–78
- Bladon P, Griffin AC (1993) Self-assembly in living nematics. *Macromolecules* 26:6604–6610
- Brinke G, Ruokolainen J, Ikkala O (2007) Supramolecular materials based on hydrogen-bonded polymers. *Adv Polym Sci* 207:113–177
- Broer DJ, Bastiaansen CMW, Debije MG, Schenning APHJ (2012) Functional organic materials based on polymerized liquid-crystal monomers: supramolecular hydrogen-bonded systems. *Angew Chem Int Ed* 51:7102–7109
- Bruce DW (2008) Halogen-bonded liquid crystals. *Struct Bond* 126:161–180
- Bruce DW, Metrangolo P, Meyer F, Pilati T, Präsang C, Resnati G, Terraneo G, Whitwood AC (2008) Mesogenic, trimeric, halogen-bonded complexes from alkoxy stilbazoles and 1,4-diodotetrafluorobenzene. *New J Chem* 32:477–482
- Bruce DW, Metrangolo P, Meyer F, Pilati T, Präsang C, Resnati G, Terraneo G, Wainwright SG, Whitwood AC (2010) Structure-function relationships in liquid-crystalline halogen-bonded complexes. *Chem Eur J* 16:9511–9524
- Chao CY, Li X, Ober CK, Osuji C, Thomas EL (2004) Orientational switching of mesogens and microdomains in hydrogen-bonded side-chain liquid-crystalline block copolymers using AC electric fields. *Adv Funct Mater* 12:364–370
- Cho CM, Wang XB, Li JJ, He C, Xu J (2013) Synthesis and self-assembly of halogen-bond donor-spacer-hydrogen-bond donor molecules: polymeric liquid crystals induced by combination of intermolecular halogen- and hydrogen-bonding interactions. *Liq Cryst* 40:185–196
- Fredrickson DD, Hilberg BA, Lasure KK, Tessner JD, Waner AE, Zenner MD, Wiegel KN (2012) Supramolecular main-chain liquid crystalline polymers and networks with competitive hydrogen bonding: a study of rigid networking agents in supramolecular systems. *Liq Cryst* 39:1243–1251
- Fukumasa M, Kato T, Uryu T, Fréchet JMJ (1993) The simplest structure of the hydrogen-bonded mesogen built from 4-alkoxybenzoic acid and 4-alkylpyridine. *Chem Lett* 22:65–68
- Gonzalez CL, Bastiaansen CWM, Lub J, Loos J, Lu K, Wondergem HJ, Broer DJ (2008) Nanoporous membranes of hydrogen-bridged smectic networks with nanometer transverse pore dimensions. *Adv Mater* 20:1246–1252
- González L, Gimeno N, Tejedor RM, Polo V, Ros MB, Uriel S, Serrano JL (2013) Halogen-bonding complexes based on bis(iodoethynyl)benzene units: a new versatile route to supramolecular materials. *Chem Mater* 25:4503–4510
- Gopinadhan M, Beach ES, Anastas PT, Osuji CO (2010) Smectic demixing in the phase behavior and self-assembly of a hydrogen-bonded polymer with mesogenic side chains. *Macromolecules* 43:6646–6654
- Grabowski SJ (ed) (2006) *Hydrogen bonding-new insights*. Springer, The Netherlands. ISBN 978-1-4020-4852-4
- Greuel JR, Andrews TE, Wichman JJ, Tessner JD, Wiegel KN (2010) Supramolecular main-chain liquid crystalline polymers and networks with competitive hydrogen bonding: networks and linear polymers created from tris- and bis-functionalised pyridyl networking agents. *Liq Cryst* 37:1515–1520

- He C, Donald AM, Griffin AC, Waigh T, Windle AH (1998) Structure of a self-assembled hydrogen-bonded “living” main chain liquid crystalline polymers. *J Polym Sci B* 36:1617–1624
- He C, Lee CM, Griffin AC, Bouteiller L, Lacoudre N, Boileau S, Fouquey C, Lehn JM (1999) Chirality in some liquid crystalline association chain polymers. *Mol Cryst Liq Cryst* 332:251–258
- Janssen EL, Salazar IE, Friday SR, Wiegel KN (2012) Supramolecular main-chain liquid crystalline polymers and networks with competitive hydrogen bonding: flexible bis-cinnamic acids as hydrogen bond donors in thermoreversible networks and polymers. *Liq Cryst* 39:857–863
- Jungbauer SH, Schindler S, Kniep F, Walter SM, Rout L, Huber SM (2013) Multidendate halogen-bond donors as Lewis acidic activators or catalysts in halides abstraction reactions. *Synlett* 24:2624–2628
- Kato T (2000) Hydrogen-bonded liquid crystals: molecular self-assembly for dynamically functional materials. *Struct Bond* 96:95–146
- Kato T, Fréchet JMJ (1989a) New approach to mesophase stabilization through hydrogen-bonding molecular interactions in binary mixtures. *J Am Chem Soc* 111:8533–8534
- Kato T, Fréchet JMJ (1989b) Stabilization of a liquid-crystalline phase through noncovalent interaction with a polymer side chain. *Macromolecules* 22:3818–3819
- Kato T, Kihara H, Uryu T, Fujishima A, Fréchet JMJ (1992) Molecular self-assembly of liquid crystalline side-chain polymers through intermolecular hydrogen bonding. Polymeric complexes built from a polyacrylate and stilbazole. *Macromolecules* 25:6836–6841
- Kato T, Fréchet JMJ, Wilson PG, Saito T, Uryu T, Fujishima A, Jin C, Kaneuchi F (1993) Hydrogen-bonded liquid crystals. Novel mesogens incorporating nonmesogenic bipyridyl compounds through complexation between H-bond donor and acceptor moieties. *Chem Mater* 5:1094–1100
- Kato T, Kihara H, Kumar U, Uryu T, Fréchet JMJ (1994) A liquid-crystalline polymer network built by molecular self-assembly through intermolecular hydrogen bonding. *Angew Chem Int Ed* 33:164–1645
- Kato T, Fukumasa M, Fréchet JMJ (1995) Supramolecular liquid-crystalline complexes exhibiting room-temperature mesophases and electrooptic effects. Hydrogen-bonded mesogens derived from alkyipyridines and benzoic acids. *Chem Mater* 7:368–372
- Kato T, Kubota Y, Uryu T, Ujiiie S (1997) Self-assembly of a mesogenic polyamide: induction and significant stabilization of a liquid-crystalline phase through complexation of a phenylbenzoic acid with a polymer backbone derived from 2,6-bis(amino)pyridine units. *Angew Chem Int Ed* 36:1617–1618
- Kato T, Mizoshita N, Kishimoto K (2006) Functional liquid-crystalline assemblies: self-organized soft materials. *Angew Chem Int Ed* 45:38–68
- Kihara H, Kato T, Uryu T, Fréchet JMJ (1996) Supramolecular liquid-crystalline networks built by self-assembly of multifunctional hydrogen-bonding molecules. *Chem Mater* 8:961–968
- Kishikawa K, Hirai A, Kohmoto S (2008) Fixation of multilayered structures of liquid-crystalline 2:1 complexes of benzoic acid derivatives and dipyridyl compounds and the effect of nanopillars on removal of the dipyridyl molecules from the polymers. *Chem Mater* 20:1931–1935
- Kleppinger R, Lillya CP, Yang C (1997) Discotic liquid crystals through molecular self-assembly. *J Am Chem Soc* 119:4097–4102
- Kumar U, Fréchet JMJ, Kato T, Ujiiie S, Timura K (1992a) Induction of ferroelectricity in polymeric systems through hydrogen bonding. *Angew Chem Int Ed* 31:1531–1533
- Kumar U, Kato T, Fréchet JMJ (1992b) Use of intermolecular hydrogen bonding for the induction of liquid crystallinity in the side chain of polysiloxanes. *J Am Chem Soc* 114:6630–6639
- Lehn JM (1995) Supramolecular chemistry: concepts and perspectives. VCH, Weinheim
- Lu X, He C, Terrell CD, Griffin AC (2002) Self-assembly of a hydrogen-bonded association chain liquid crystalline polymer (LCP). *Macromol Chem Phys* 203:85–88

- Lu Y, Shi T, Wang Y, Yang H, Yan X, Luo X, Jiang H, Zhu W (2009) Halogen bonding—a novel interaction for rational drug design? *J Med Chem* 52:2854–2862
- Metrangolo P, Resnati G (2001) Halogen bonding: a paradigm in supramolecular chemistry. *Chem Eur J* 7:2511–2519
- Metrangolo P, Neukirch H, Pilati T, Resnati G (2005) Halogen bonding based recognition processes: a world parallel to hydrogen bonding. *Acc Chem Res* 38:386–395
- Metrangolo P, Meyer F, Pilati T, Resnati G, Terraneo G (2008) Halogen bonding in supramolecular chemistry. *Angew Chem Int Ed* 47:6114–6127
- Nguyen HL, Horton PN, Hursthouse MB, Legon AC, Bruce DW (2004) Halogen bonding: a new interaction for liquid crystal formation. *J Am Chem Soc* 126:16–17
- Osuji C, Chao CY, Bitá I, Ober CK, Thomas EL (2002) Temperature-dependent photonic bandgap in a self-assembled hydrogen-bonded liquid-crystalline diblock copolymer. *Adv Funct Mater* 12:753–758
- Osuji CO, Chao CY, Ober CK, Thomas EL (2006) Supramolecular microphase separation in a hydrogen-bonded liquid crystalline comb copolymer in the melt state. *Macromolecules* 39:3114–3117
- Paleos CM, Tsiourvas D (1995) Thermotropic liquid crystals formed by intermolecular hydrogen bonding interactions. *Angew Chem Int Ed* 34:1696–1711
- Paleos CM, Tsiourvas D (2001) Supramolecular hydrogen-bonded liquid crystals. *Liq Cryst* 28:1127–1161
- Pourcain CBS, Griffin AC (1995) Thermoreversible supramolecular networks and polymeric properties. *Macromolecules* 28:4116–4121
- Präsang C, Nguyen HL, Horton PN, Whitwood AC, Bruce DW (2008) Trimeric liquid crystals assembled using both hydrogen and halogen bonding. *Chem Commun* 46:6164–6166
- Price DJ, Willis K, Richardson T, Ungar G, Bruce DW (1997) Hydrogen bonded liquid crystals from nitrophenols and alkoxy stilbazoles. *J Mater Chem* 7:883–891
- Reddy MK, Reddy KS, Narasimhaswamy T, Das BB, Lobo NP, Ramanathan KV (2013) ^{13}C - ^1H dipolar couplings for probing rod-like hydrogen bonded mesogens. *New J Chem* 37:3195–3206
- Rowan SJ, Mather PT (2008) Supramolecular interactions in the formation of thermotropic liquid crystalline polymers. *Struct Bond* 128:119–149
- Suárez M, Lehn JM, Zimmerman SC, Skoulios A, Heinrich B (1998) Supramolecular liquid crystals. Self-assembly of a trimeric supramolecular disk and its self-organization into a columnar discotic mesophase. *J Am Chem Soc* 120:9526–9532
- Tian T, Su F, Zhao Y, Luo X, Tang X, Zhao X, Zhou E (1995) Synthesis and variable-temperature FTIR study of five chiral liquid crystals induced by intermolecular hydrogen bonding. *Liq Cryst* 19:743–748
- Toh CL, Xu J, Lu X, He C (2008) Synthesis and characterization of main-chain hydrogen-bonded supramolecular liquid crystalline complexes formed by azo-containing compounds. *Liq Cryst* 35:241–251.
- Toh CL, Xu J, Lu X, He C (2005) Synthesis of main-chain hydrogen-bonded supramolecular liquid crystalline complexes: the effects of spacer on thermal behavior of mesophase. *J Polym Sci Polym Chem* 43:4731–4743
- Uchida E, Kawatsuki N (2006) Photoinduced orientation in photoactive hydrogen-bonding liquid crystalline polymers and liquid crystal alignment on the resultant films. *Macromolecules* 39:9357–9364
- Willis K, Price DJ, Adams H, Ungar G, Bruce DW (1995) Hydrogen-bonded liquid crystals from alkoxy stilbazoles and 3-cyanophenols: structural control of mesomorphism. Molecular structure of the complex between 4-cyanophenol and 4-octyloxystilbazole. *J Mater Chem* 5:2195–2199
- Wu S, Shi F, Zhang Q, Bubeck C (2009) Stable hydrogen-bonding complexes of poly(4-vinylpyridine) and polydiacetylenes for photolithography and sensing. *Macromolecules* 42:4110–4117

- Xu J, Liu X, Lin T, Huang J, He C (2005a) Synthesis and self-assembly of difunctional halogen-bonding molecules: a new family of supramolecular liquid-crystalline polymers. *Macromolecules* 38:3554–3557
- Xu J, Toh CL, Liu X, Wang S, He C, Lu X (2005b) Synthesis and self-assembly of donor-spacer-acceptor molecules. Liquid crystals formed by single-component “complexes” via intermolecular hydrogen-bonding interaction. *Macromolecules* 38:1684–1690
- Xu J, Liu X, Ng JKP, Lin T, He C (2006) Trimeric supramolecular liquid crystals induced by halogen bonds. *J Mater Chem* 16:3540–3545

Chapter 14

Models of Liquid Crystalline Polymer Fibers

J.I. Ramos

14.1 Introduction

Many materials used in industry, e.g., high-performance tires and cables, light-weight and super-strength materials, etc., used, for example, in bullet-proof vests, stealth technology, etc., are manufactured from liquid crystalline polymer fibers. These fibers are in turn manufactured by means of fiber-spinning processes whereby a high-temperature liquid phase of rigid rod macromolecules is extruded through a die, cools as it is being pulled downstream, solidifies, and is collected in a rotating drum.

The properties of the collected fiber depend on the morphology of the amorphous and semi-crystalline phases; the morphology, in turn, depends on the thermal and deformation histories undergone by the material during processing. In many cases, fibers and films are subjected to large inelastic deformations after manufacture, and, during the course of these deformations, further crystallization may take place.

The remarkable strength properties of LCP spun fibers are mainly due to the molecular alignment of the macromolecules which is achieved as a result of the complex interactions among the flow, stresses, molecular orientation, crystallization, and thermal processes at play in fiber-spinning processes and, in particular, the coupling between the molecular orientation and the elongational characteristics of the flow. For example, ultra-strength textile fibers such as Vectran and Kevlar (Chawla 1998) achieve their properties, e.g., tensile modulus, as a result of the interaction between the anisotropic molecular-scale structure of the melt or solution, the macroscopic hydrodynamics of spinning flows and non-isothermal effects

J.I. Ramos (✉)

Escuela de Ingenierías, Universidad de Málaga, Room 2-139-D, Dr. Ortiz Ramos,
s/n, Málaga 29071, Spain
e-mail: jirs@lcc.uma

including radial heat transfer through the fiber free surface, temperature dependence of material properties, phase change, and crystallization.

The properties of LCP fibers depend strongly on their molecular orientation; a high degree of orientation results in high strength and stiffness along the alignment direction, i.e., along the fiber in melt spinning, but it also yields anisotropic properties (Ramalingam and Armstrong 1993) that may be detrimental when multidimensional stability, e.g., absence of shrinkage and warping, and strength are required.

Liquid-crystalline solutions may phase separate even under isothermal conditions due to electrostatic and steric interactions that result from the rigidity of the polymer chain backbones even at low polymer concentrations, and form anisotropic phases with a degree of molecular orientation even in the quiescent state as evidenced by their ability to exhibit birefringence under static conditions.

For isothermal flows at low shear rates, a nematic LCP may be called flow-aligning because shear promotes the alignment of the nematic director at an angle with respect to the flow direction, but shear may also result in tumbling which is characterized by a continuous rotation of the director (Greco and Marrucci 1993).

Although considerable progress has been made in the understanding and modeling the molecular orientation of lyotropic solutions of rod-like polymers, the situation is not yet as advanced in the case of thermotropic LCP.

The rate of crystallization of semi-crystalline polymers depends on the molecular orientation in the melt; when subject to deformations that align the polymer molecules, the rate of crystallization increases dramatically, and, when the temperature drops below the glass transition temperature, there is a cessation of molecular motion and the crystallization rate decreases and may stop. As the crystallinity increases, it retards the crystallization process and decreases the mobility of the polymer molecules in the amorphous phase. The molecular orientation and crystallization affect and are affected by the melt rheology and thermal field.

Experimental studies indicate that flow-induced crystallization correlates with the viscoelastic stresses much more strongly than with the macroscopic strain or strain rate, thus indicating that the molecular chain orientation and extension are of paramount importance in determining the fiber's final morphology.

The relations among the flow, strain rate, cooling, molecular orientation, crystallization and rheology of LCP is a complex one, depends on many factors, and is not yet clear due to the complex interactions amongst these phenomena, although great strides have been made in understanding the relation between molecular weight distribution and linear viscoelastic properties of polymers (Pattamaprom et al. 2000, 2008), and that between rheology and flow-induced nucleation (Eder and Janeschitz-Kriegl 1997).

In this chapter, a review of models of fiber spinning of liquid crystalline and semi-crystalline polymers is presented. Since, as stated above, the flow, crystallization, molecular orientation, rheology and the thermal field play a paramount role in determining the properties and morphology of both LCP and liquid semi-crystalline fibers, it was believed to be convenient to first review and extend some of the crystallization models that have been developed for both quiescent

and flow conditions; this is done in Sect. 14.2. Some models for the molecular orientation are described in some detail in Sect. 14.3, while the effects of both the molecular orientation and the crystallization on the rheology of both LCP and liquid semi-crystalline polymers are summarized in Sect. 14.4. Even though, some models for the fiber spinning of LCP are described in Sects. 14.2–14.4 with reference to the models for the crystallization, molecular orientation and rheology, the main one- and two-dimensional models that have been developed to-date for fiber spinning of thermotropic LCP and liquid semi-crystalline polymers are reviewed in Sect. 14.5. Some conclusions and areas for future work are summarized in Sect. 14.6.

14.2 Crystallization Models

Polymers that are unable to crystallize on cooling below their glass transition temperature form amorphous solids and may exhibit strong anisotropy if these solids are formed by deforming the polymer while cooling it through the glass transition temperature. As the deformed amorphous polymer melt cools below its glass transition temperature, its molecules lose their mobility and become frozen in their oriented configuration.

Some polymers, e.g., polyethylene (PE), find applications at temperatures between their melting and glass transition temperatures. At these temperatures, the solid consists essentially of rigid crystals and a flexible amorphous phase, and it is therefore solid and tough.

Polymers having a regular or ordered molecular structure may form a semi-crystalline solid when kept at a temperature below the melting one for a sufficiently long time. The crystallization process can be very slow especially at temperatures just below the equilibrium melting temperature, and the resulting solid has a spherulitic morphology under quiescent conditions.

In the liquid phase, there are always density fluctuations caused by thermal agitation (Landau and Lifshitz 1980a, b). These fluctuations may eventually create small clusters or aggregates of polymer molecules having the same properties as the crystalline phase; small crystals are continuously being created and destroyed by fluctuations because the formation of a crystal involves the creation of an interface between the liquid and the crystal and its consequent energy cost, i.e., the creation of crystals is a competitive process whereby there is a decrease of energy due to the fact that the chemical potential of the crystal phase is lower than that of the liquid, and an increase of energy and an energy cost associated with the creation of interfaces.

Surface effects are dominant in clusters of small size and, therefore, their growth is not energetically favorable, and small crystals tend to dissolve. There exists, however, a critical size beyond which volume effects dominate over surface ones, and the growth of the cluster is favored by a global reduction of energy. The size that determines the stability of the clusters is called critical size, and the process of

formation of crystals of size larger than or equal to the critical size is called nucleation.

Nucleation is the first step in the crystallization process, determines the appearance of the first crystal nuclei which are the germ of the second stage of crystallization, i.e., growth, and is an activated process where an energy barrier has to be overcome in order to form nuclei of a critical size, beyond which the new phase grows spontaneously.

There are two basic types of nucleation: primary nucleation which occurs when nuclei form in the absence of already formed crystals, and secondary nucleation which refers to the formation of nuclei in the presence of already formed crystals. Primary nucleation can occur through two different mechanisms: homogeneous and heterogeneous nucleation. Homogeneous nucleation occurs in the bulk of a pure substance and is the process whereby nuclei are formed spontaneously from a supersaturated solution that has crossed the metastable limit, whereas heterogeneous nucleation takes place in the presence of impurities, pre-existing crystals, boundaries, etc. Secondary crystallization can occur through surface, contact, fracture, pressure, strain, attrition, etc., mechanisms (Schultz 2001).

In the growth stage, nuclei larger than the critical size tend to grow either through the addition of monomers or by acting as sites of heterogeneous nucleation, e.g., nucleation on the surface of a growing crystal. Crystals grow freely until they begin to completely fill the whole space. Once they hit each other, their growth stops at the contact surface. This phenomenon, referred to as impingement, determines the final morphology of the processed polymer.

In the final stage of crystallization, crystal impingement impedes the subsequent nucleation of the crystals and, therefore, amorphous matter remains trapped among clusters. Furthermore, the clusters themselves are not fully crystalline because they may contain some amorphous inclusions. This trapped material can eventually join the main crystal structure and, therefore, increase the degree of crystallization in a process referred to as secondary crystallization (Schultz 2001).

Models for the crystallization of polymers have been mainly based on the Avrami-Kolmogorov equation (Kolmogorov 1937; Avrami 1939, 1940, 1941; Johnson and Mehl 1939; Evans 1945) that is based on the theory of filling the space through the nucleation and growth of one phase into another. This equation was initially developed for isothermal, quiescent crystallization, although, as described below, it has been extended to account for non-isothermal conditions.

In quiescent crystallization, polymer crystallization from the melt is usually dominated by heterogeneous nucleation. Nuclei grow in time depending on the pressure and temperature, and form spherulites that impinge upon each other and stop growing when complete space filling is reached; crystalline lamellae grow in three dimensions starting from point-like nuclei (Burger et al. 2002; Capasso 2003; Eder 1997).

Although many attempts have been made to model the crystallization process in semi-crystalline polymers under quiescent conditions, most models do not account for the polymorphism in a clear way or do not account for the relevant processing conditions, e.g., pressure. Drawing experiments on poly(ethylene 2,6-naphthalene

dicarboxylate) (PEN) fibers indicate that the crystal structure depends on the drawing stress, i.e., depending on the magnitude of the stress, α - and/or β -crystals may form (Kim et al. 2012). In addition the drawing stress was observed to have a great influence not only on the resulting crystal form but also on the chain conformation of the mesophase structure.

In polymorphic materials, the crystallization kinetics of different polymorphs is not well-established as a function of the pressure and temperature. In some cases, an increase of the pressure results in an increase of both the nucleation density and the equilibrium melting temperature and, therefore, a higher undercooling that it is the driving force for crystallization; however, the exact effect of the pressure on the growth rate of a given crystal is not yet known.

For nylon 6, Shanon et al. (2000) found that the onset time for crystallization in melt spinning depends chiefly on chain orientation and not appreciably on chain chemistry or specific undercooling; this result is consistent with a critical strain condition.

When phase transitions occur in a flowing polymer melt, crystallization takes place under strain and non-isothermal conditions, and the morphology of the processed polymer depends on the temperature and deformation history. In fact, it has been observed experimentally that crystallization is influenced strongly by the flow, stress, temperature and molecular orientation (Ziabicki 1974, 1976) and may be enhanced by shear, pressure and strain, and shear may increase the nucleation density, whereas the crystallization rate decreases as the cooling rate is increased. Furthermore, a highly oriented crystalline morphology is usually obtained under isothermal and non-isothermal deformations, in contrast with the spherulite morphology observed under quiescent conditions, and both the alignment and the orientation increase as the shear rate is increased (Vaish et al. 2001). In spun fibers, for example, lamellae are found to be perpendicular to the fiber axis and enhanced crystallization is caused by chain extension arising from entanglement between molecules.

Molecular orientation in the melt usually accelerates the phase transition process, but the molecular orientation may be enhanced or relaxed depending on the deformation history and the relaxation times of the melt. This means that models of fiber spinning processes should account for the molecular orientation and its effects on the flow field, stress and crystallization, and also for the effects of these fields on the molecular orientation.

A model of polymer crystallization under both quiescent and flow conditions should also account for the nucleation density and the spherulitic growth rates and include secondary crystallization.

As stated above, many of the crystallization models employed to study fiber spinning processes of semi-crystalline polymers are based on non-isothermal generalizations of the Avrami-Kolmogorov's kinetics model for quiescent crystallization where space filling is given by

$$\alpha(t) = \frac{\theta(t)}{\theta_\infty} = 1 - \exp(-\phi_0(t)), \quad (14.1)$$

t is time, $\theta(t)$ and θ_∞ are the crystallized volume fractions at time t and under equilibrium conditions, respectively, and $\phi_0(t)$ is the sum of the expected crystallized volumes of the different phases if no impingement occurs in the case of three-dimensional spherulitic growth, i.e.,

$$\phi_0(t) = \sum \phi_{0i}(t). \quad (14.2)$$

14.2.1 Avrami-Kolmogorov Kinetics for Quiescent Crystallization and Generalizations

In the original Kolmogorov's formulation (Kolmogorov 1937) only quiescent crystallization was considered and the crystallinity fraction is

$$\alpha = 1 - \exp(-\alpha_{af}), \quad (14.3)$$

where

$$\alpha_{af} = C_m \int_0^t \frac{dN}{ds}(s) ds \left[\int_s^t G(u) du \right]^m, \quad (14.4)$$

m denotes the (constant) dimensionality of the crystallites, $\frac{dN}{dt}$ is the rate of nuclei production and $G(t)$ is the linear growth rate; $m=3$ for spherical crystals and $C_m = 4\pi/3$, although m may range from 1 to 3 and is not necessarily an integer number.

In the Kolmogorov model, nucleation is assumed to occur randomly and homogeneously over the entire untransformed portion of the material, the growth rate does not depend on the extent of transformation, growth occurs at the same rate in all directions, and only the transformation of a phase into another one is considered.

For constant growth rates, the second integral of (14.4) can be performed exactly. Moreover, if an isokinetic approach is considered whereby the growth rate is proportional to the nucleation one and the latter is constant, one may easily derive the well-known Avrami's expression (Avrami 1939, 1940, 1941; Johnson and Mehl 1939; Evans 1945).

The Avrami-Kolmogorov kinetic model can be extended to account for both thermal and flow-induced crystallization by simply considering that the number of nuclei is $N = N_0 + N_f$, where N_0 denotes the number of nuclei created under quiescent conditions and N_f is the number of the flow-created nuclei. N_0 depends on the temperature, i.e., thermal nucleation, while the growth rate for flow-induced crystallization may be assumed to vary linearly with the shear rate.

If the growth rate for the flow-induced crystallization is assumed to be only a function of the temperature and we assume that (Eder and Janeschitz-Kriegl 1997)

$$\frac{dN_f}{dt} + \frac{N_f}{\tau} = g, \quad (14.5)$$

where τ is a temperature-dependent relaxation time and g usually depends on the flow variables and the temperature, τ and g are assumed to be constant and $N_f(0) = 0$, then (14.5) yields

$$N_f(t) = \tau g \left(1 - \exp\left(-\frac{t}{\tau}\right) \right). \quad (14.6)$$

For isothermal flows and $G(t)$ constant, one can easily obtain from (14.3) and (14.4)

$$\alpha = 1 - \exp\left(-C_m G^m \int_0^t \frac{dN}{ds}(s)(t-s)^m ds\right), \quad (14.7)$$

that, on accounting for the quiescent crystallization at a constant nucleation rate, yields

$$\alpha = 1 - \exp\left(-C_m G^m \left[K t^{m+1} + \int_0^t \frac{dN_f}{ds}(s)(t-s)^m ds \right]\right). \quad (14.8)$$

Equation (14.8) reduces to the well-known Avrami-Kolmogorov's kinetics in the absence of flow-induced crystallization, i.e., for $\frac{dN_f}{dt}(t) = 0$ (Avrami 1939, 1940, 1941; Johnson and Mehl 1939).

Equation (14.8) may be written as $\alpha = 1 - \exp(-\phi_0(t))\exp(-\varphi_0(t))$, where the first and second exponential terms are associated with the thermal and flow-induced crystallizations, respectively; the former is usually modelled by means of the Avrami-Kolmogorov kinetics, whereas several models have been proposed for the latter, as discussed below.

If the exponential terms are sufficiently small, (14.8) can be written as $\alpha \approx (1 - \exp(-\phi_0(t)))(1 - \exp(-\varphi_0(t))) = \alpha_t(t)\alpha_f(t)$, where α_t and α_f refer to the crystallization fractions associated with temperature and flow, respectively.

Under isothermal conditions with constant $G(t)$, the Avrami-Kolmogorov's generalized expression, i.e., (14.4) and (14.8), for flow-induced crystallization may be written as

$$\alpha_f = C_m G^m \int_0^t \frac{dN_f}{ds}(s)(t-s)^m ds, \quad (14.9)$$

which upon repeated differentiation with respect to time yields

$$\frac{d\alpha_f}{dt} = m C_m G^m \int_0^t \frac{dN_f}{ds}(s)(t-s)^{m-1} ds = \alpha_1, \quad (14.10)$$

$$\frac{d\alpha_1}{dt} = m(m-1)C_m G^m \int_0^t \frac{dN_f}{ds}(s)(t-s)^{m-2} ds = \alpha_2, \quad (14.11)$$

$$\frac{d\alpha_2}{dt} = m(m-1)(m-2) C_m G^m \int_0^t \frac{dN_f}{ds}(s)(t-s)^{m-3} ds = \alpha_3, \quad (14.12)$$

etc., which, for integer values of m , terminate and provide a useful way for investigating various forms of the flow-induced crystallization by simply specifying the flow-induced nucleation rate, as shown below.

Equations (14.9)–(14.12) are also valid for quiescent crystallization if the flow-induced nucleation rate and crystalline fraction that appear in these equations are replaced by the thermal nucleation rate and crystalline fraction, respectively.

14.2.2 Nakamura's Crystallization Kinetics

For quiescent variable temperature conditions, Nakamura et al. (1972) proposed the following expression for the (relative) crystalline fraction

$$\alpha = 1 - \exp\left(-\int_0^t K_N ds\right)^n, \quad (14.13)$$

where K_N depends on the temperature and flow conditions.

For constant K_N , (14.13) reduces to the well-known Avrami-Kolmogorov's kinetics. In the quiescent state, $m+1=n$, but Nakamura's expression does not have a strong physical support (Eder and Janeschitz-Kriegl 1997; Eder et al. 1990).

14.2.3 Ziabicki's Model

Instead of describing the kinetics of phase transformation/crystallization with complicated mathematical models, Ziabicki (1974, 1976) proposed to model it by means of the following first-order ordinary differential equation

$$\frac{d\alpha}{dt} = K(T)(1 - \alpha(t)), \quad (14.14)$$

where $K(T)$ is a temperature-dependent crystallization rate function.

According to (14.14), for isothermal processes, the crystallinity is an exponential function of time, while, for non-isothermal ones, the crystallization rate function depends on the cooling rate. Because of its simplicity, Ziabicki's model (1974,

1976) has also been used to account for flow-induced crystallization by considering that the crystallization rate function depends on both the temperature and the molecular orientation, as discussed below.

14.2.4 Schneider's Model of Quiescent Crystallization

For non-isothermal conditions, the crystal volumetric fraction of each phase $\phi_i(t)$ may be modelled through Schneider's formulation (Schneider et al. 1988), i.e.,

$$\frac{d\phi_3}{dt} = 8\pi \frac{dN}{dt}, \quad (14.15)$$

$$\frac{d\phi_2}{dt} = G\phi_3, \quad (14.16)$$

$$\frac{d\phi_1}{dt} = G\phi_2, \quad (14.17)$$

$$\frac{d\phi_0}{dt} = G\phi_1, \quad (14.18)$$

where $\phi_3 = 8\pi N$, $\phi_2 = 8\pi R_t$, $\phi_1 = S_t$, $\phi_0 = V_t$, $\frac{dN}{dt}$ and G are the nucleation and growth rates, respectively, V_t and S_t are the total volume and surface of the spherulites, respectively, N is the number of nuclei and R_t denotes the sum of the radii of the spherulites. Note that (14.15)–(14.18) are closely related to (14.10)–(14.12).

The nucleation density N and the growth rate of each phase G_i are functions of pressure p and temperature T as, for example,

$$N(p, T) = N_r \exp(-c_n (T(t) - T_{Nr}(p))), \quad (14.19)$$

$$G_i(p, T) = G_{i,max} \exp(-c_{gi} (T(t) - T_{Gi}(p))^2), \quad (14.20)$$

where N_r and $G_{i,max}$ are (constant) reference values, T_{Nr} and T_{Gi} are the (constant) reference temperatures corresponding to N_r and $G_{i,max}$, respectively, and c_n and c_{gi} are assumed to be constant.

During solidification in a multiphase system, every crystal from phase i generates a crystal volume fraction ϕ_{0i} using a share of the available number of nuclei and its own growth rate. Since the ratios in which the nuclei are divided between the crystal phases is not known, it may be assumed that the allocation of nuclei to a crystal phase scales with the ratio of the individual crystal growth rates at the current pressure and temperature conditions. This means that, for isobaric conditions, the nucleation rate of phase i is given by

$$\frac{dN_i}{dt} = g_i \frac{dN}{dt} \frac{dT}{dt}, \quad (14.21)$$

where $g_i = G_i(t) / \sum G_i(t)$ is the growth rate fraction and the summation is over the number of phases. This model can be generalized to account for the presence of polymorphs by including the presence of nucleation agents (van Dronghen et al. 1988).

14.2.5 Zuidema's Model of Flow-Induced Crystallization

In order to account for flow-induced nucleation and crystallization, Zuidema (Zuidema 2000; Zuidema et al. 2001; Peters 2003) proposed a modification of the shear-induced crystallization model proposed by Eder and Janeschitz-Kriegl (1997) and Eder et al. (1990) which provides a good correlation between the predicted flow-induced structures and experimental data.

Zuidema's model employs a recoverable strain model with a Leonov's driving force (Leonov 1976, 1987) for flow-induced crystallization that correlates most strongly with the viscoelastic mode associated with the largest relaxation time. Zuidema only accounted for the second invariant of the deviatoric part of the recoverable strain rate tensor which is a measure of the molecular orientation, but no model for the molecular orientation was included in his flow-induced crystallization formulation.

Zuidema's modification of Schneider's model (Schneider et al. 1988) can describe the non-isothermal crystallization of cylindrical structures sometimes referred to as shish-kebabs and may be written as

$$\frac{d\varphi_3}{dt} + \frac{\varphi_3}{\tau_n} = 8 \pi J_2 g_n, \quad (14.22)$$

$$\frac{d\varphi_2}{dt} + \frac{\varphi_2}{\tau_l} = J_2 \varphi_3 \frac{g_l}{g_n}, \quad (14.23)$$

$$\frac{d\varphi_1}{dt} = G\varphi_2, \quad (14.24)$$

$$\frac{d\varphi_0}{dt} = G\varphi_1, \quad (14.25)$$

$$\varphi_0(t) = -\ln(1 - \alpha(t)), \quad (14.26)$$

where $\varphi_2 = 4 \pi L_l J_2$ is the driving force, the scaling factors g_n and g_l describe the sensitivity of the flow-induced nuclei and length L to J_2 , respectively, and τ_n and τ_l are the relaxation times associated with the nuclei and length, respectively.

If nucleation is considered as acting as a cross-link, an increase in the number of nuclei causes an increase in the rheological relaxation time. The simplest of such a relation is a linear one.

It must be noted that in the presence of flow, both spherulites and flow-induced structures contribute to the degree of space filling, and the Avrami-Kolmogorov's impingement model is then described by (cf. (14.3))

$$\phi_0(t) + \varphi_0(t) = -\ln(1 - \alpha(t)). \quad (14.27)$$

It should also be noted that the time derivatives that appear in (14.14), (14.15)–(14.18) and (14.22)–(14.25) must be replaced by material derivatives, e.g., $\frac{D\phi}{Dt} \equiv \frac{\partial\phi}{\partial t} + \mathbf{v} \cdot \nabla\phi$, where \mathbf{v} is the velocity vector for the crystal phase. If the amorphous and crystalline phases are considered as a homogeneous fluid, then the velocity \mathbf{v} coincides with that of the mixture. The use of a material derivative implies that (14.14), (14.15)–(14.18) and (14.22)–(14.25) are hyperbolic with characteristic lines whose slopes coincide with the components of \mathbf{v} (Zachmanoglou and Thoe 1986) and only require an initial condition and one boundary condition in each coordinate direction.

For steady, uniaxial flows, the solution of (14.14) is

$$\alpha = 1 - C \exp\left(-\int_0^x \frac{K(T(s))}{u(s)} ds\right), \quad (14.28)$$

which indicates that the crystalline fraction depends on the histories of both the axial velocity component and the fiber's temperature. In (14.28), x is the distance along the fiber measured from the die's exit, and C is a constant that may be determined from the crystalline fraction at $x=0$. If the crystalline fraction at the die's exit is nil, $C=1$, and a comparison of (14.28) with (14.3) indicates that $\alpha_{af} = \int_0^x \frac{K(T(s))}{u(s)} ds$, for Ziabicki's model.

For the Schneider's and Zuidema's crystallization models discussed above, one may obtain an expression for the crystalline fraction for steady, uniaxial flows as for the Ziabicki's model by first integrating, for example, (14.22) to obtain φ_3 as a function of J_2 , and g_n , then integrating (14.23) to obtain φ_2 as a function of to obtain φ_3 , then integrating (14.24) to obtain φ_1 as a function of to obtain φ_2 , then integrating (14.25) to obtain φ_0 as a function of to obtain φ_1 , and finally substituting the value of φ_0 thus obtained in (14.26) which may be written as $\alpha = 1 - \exp(-\varphi_0(t))$.

The integrals mentioned in the previous may be performed easily by first introducing a new time-like variable τ defined $\tau = \int_0^x \frac{1}{u(s)} ds$, which corresponds to the fluid residence time, and may be performed analytically if the relaxation times associated with the nuclei and length of the crystals are assumed to be constant. Under such conditions, it can be easily deduced that the crystalline

fraction depends on the driving force J_2 , the scaling factors g_l and g_n , and the growth rate G . Furthermore, these factors appear as integrals which correspond to the particular solutions of (14.22)–(14.25) and, therefore, the crystalline fraction includes their history from the die's exit.

14.2.6 Eder and Janeschitz-Kriegl's Model of Flow-Induced Crystallization

Eder and Janeschitz-Kriegl's model corresponds to replacing J_2 in (14.22) by the square of the nondimensional shear rate (Eder and Janeschitz-Kriegl 1997; Eder et al. 1990; Eder 1997). Therefore, Eder and Janeschitz-Kriegl's model of flow-induced crystallization accounts for the strain-rate enhancement of crystallization.

14.2.7 Other Models of Flow-Induced Crystallization

Other authors have proposed models of flow-induced crystallization based on the strain rate tensor (Keller and Kolnaar 1998), normal stress difference (Ziabicki et al. 2013), trace of the stress tensor (Doufas et al. 1999, 2000a), changes in the dumbbell free energy induced by the flow (Zheng and Kennedy 2004), work-input (Janeschitz-Kriegl 2003), recoverable strain (Zuidema 2000; Zuidema et al. 2001; Peters 2003), configurational entropy of polymer chains (van Meerveld 2005; van Meerveld et al. 2008), suspension theory (Tanner 2002, 2003), microrheological approximations (Coppola et al. 2001, 2004), rational thermodynamics (Rao and Rajagopal 2002a, b), matrix or network methods (Flory 1947), GENERIC (Hütter 2004; Hütter et al. 2003), etc.

In the next paragraphs, some of the models mentioned above are described in some detail. Further crystallization models have been reviewed by Di Lorenzo and Silvestre (1999), Long et al. (1995), Strobl (2006), Fukuda et al. (2004), Schultz (2001), and Piorkowska et al. (2006).

The continuum model introduced by Doufas et al. (1999, 2000a) is a macroscopic one that combines irreversible thermodynamics through the continuum Hamiltonian/Poisson bracket formalism with the Avrami-Kolmogorov kinetic equation for polymer crystallization. Since it is a continuum model, the details of the molecular mechanisms involved in either flow-induced crystallization or the crystal morphology are not taken into consideration, and, therefore, only the macroscopic characteristics of the overall crystallization kinetics and the rheological behavior of semicrystalline polymers are considered.

In Doufas et al.'s model, both the amorphous and crystalline phases are accounted for; a modified Giesekus fluid (Giesekus 1982) is used for the rheology of the amorphous phase, while the crystalline phase is modeled as a collection of

multibead rigid rods that grow and orient in the flow field. The model also includes evolution equations for the conformation tensor, orientation tensor and degree of crystallinity, and reduces to the modified Giesekus model for the melt and the quiescent Avrami's kinetics in the absence of flow. In addition, it contains only two adjustable parameters related to the relaxation time of the crystalline phase and the coupling between the amorphous and crystalline phases.

Flow-induced crystallization models based on suspension theory (Tanner 2002, 2003) consider a system of rigid spheres (crystallites) embedded in a fluid matrix which may follow a Newtonian (Tanner 2002) or a linear viscoelastic rheology (Tanner 2003); the latter is only valid for small strains. However, the model may be generalized and the amorphous phase may be treated as a PTT (Phan-Thien-Tanner) or General Network model.

One of the main problems of the Doufas et al. (1999, 2000a) continuum and the suspension theory models (Tanner 2002, 2003) is the treatment of the total stress as crystals are formed. A simple approach assumes that the stresses of the amorphous and crystalline phases are additive, i.e., as the crystallization progresses, rigid spheres are introduced into the amorphous matrix. Such an approach, however, implies the presence of a mixture of the crystalline and amorphous phases at each point, whereas microscopic observations show the presence of distinct macroscopic crystallites in an amorphous matrix. A remedy to this problem is to assume that the contributions of the amorphous and crystalline phases to the total stresses is weighted by the crystalline fraction, even though the stresses are surface forces per unit area and the crystalline fraction refers to volume.

The dumbbell model proposed by Zheng and Kennedy (2004) is similar to those of Doufas et al. (1999) and Tanner (2002) in that the crystallizing system is considered as a suspension of semicrystalline entities growing in an amorphous matrix. However, in Zheng and Kennedy's model, the physical properties of the amorphous phase are assumed to be constant, so that the physical properties of the suspension depend only on the semicrystalline phase.

In order to describe the chain conformation and orientation evolution of the amorphous phase, Zheng and Kennedy (2004) employed the FENE-P (Finite Extensible Nonlinear Elastic model with a Peterlin closure approximation) dumbbell model, whereas the semicrystalline phase was modeled as a collection of rigid dumbbells, and the contribution of the amorphous and crystalline phases to the total stress was assumed to be additive.

The flow-induced crystallization model developed by Coppola et al. (2001, 2004) is microrheological, i.e., the polymeric liquid is described on a molecular basis, the flow is considered to increase the nucleation rate by increasing the free energy of the liquid phase, and the nucleation rate follows the formulation proposed by Lauritzen and Hoffman (1960, 1973) that accounts for the volumetric free energy difference between the liquid and crystalline phases, the activation energy of the supercooled liquid nucleus interface, and energetic and geometrical factors for the crystalline nuclei (Hoffman and Miller 1997).

Coppola et al. (2004) have shown that, for isotactic polypropylene, as the temperature decreases, the corresponding increase in chain orientation at a given

shear rate leads to a faster crystallization; their model is based on Doi-Edwards' microrheological theory (Doi and Edwards 1986).

The thermodynamic approximation proposed by Rao and Rajagopal (2002a, b) for determining the flow-induced crystallization is based on the formulation of constitutive equations that involve the concept of multiple natural configurations and obtains evolution equations for the natural configuration and mass fraction of the crystalline material by maximizing a prescribed rate of dissipation. This approach combines continuum mechanics and thermodynamics, assumes that effects are additive, and results in different models that depend on the forms used for the internal energy, entropy and dissipation rate.

The network model for modeling flow-induced crystallization is based on an extension of the work of Flory (1947) on the stress-induced crystallization of rubber. Such an extension assumes that temporary network junctions play the same role as the chemical cross-links in the theory of rubber crystallization, and is based on the decrease in entropy associated with the stretching of the molecular chains and the tendency of the polymer to crystallize.

In the *configurational entropy flow-induced crystallization model*, the rheology of the polymer melt is described by a thermodynamically consistent reptation model developed by Öttinger (1999) for monodisperse entangled linear polymer systems and extended to polydisperse systems by van Meerveld (2005). The thermodynamically consistent reptation model is a variation of the Doi-Edwards "tube" and reptation model (Doi and Edwards 1986) that incorporates the convective constraint release (CCR) mechanism proposed by Marrucci (1996) which takes into account how the removal of tube segments (which represent entanglements) influences the relaxation of the contour path, whereas the CCR mechanism accounts for the number of constraints lost due to the retraction of the chains forming the tube.

The thermodynamically consistent reptation model approach is mainly based on molecular theory and describes the evolution of the polymer chain contour path by a configuration distribution function *which depends on* the unit orientation vector and the curvilinear coordinate associated with the position of polymer segments along the contour path. Such a function is given by a Fokker-Planck equation for a monodisperse sample.

The thermodynamically consistent reptation model may be incorporated into a non-equilibrium thermodynamic GENERIC (General Equation for Non-Equilibrium Reversible Irreversible Coupling) framework (Öttinger 1999). Such a model includes a set of rate equations for the nucleation and growth stages, where the governing parameter for nucleation is the change in the configuration of amorphous chains, and pays special attention to the high molecular tail of the molecular weight distribution function, since this part of the distribution function contributes most to flow-induced crystallization.

In the thermodynamically consistent reptation model, flow-induced crystallization is assumed to occur only when the reduction of the end-to-end distance of the amorphous part of the chain is large compared to the increase of the relative extension of the chain under flow (van Meerveld 2005; van Meerveld

et al. 2008). Consequently, the onset of orientation and stretching is characterized by means of Deborah numbers based on the reptation and stretching times of the high molecular weight chains.

It must be pointed out that the models of flow-induced crystallization that make use of the stress tensor, normal stress difference and configurational entropy have been mainly developed for melt-spinning processes.

14.2.8 Comparisons of Models for Flow-Induced Crystallization

The flow-induced crystallization models described above represent quite well the current state of the subject, but they are certainly not exclusive and there are more models not included here. As noted above, many of these models are based on the Avrami-Kolmogorov equation which was modified to account for enhanced crystallization due to the flow by introducing an orientation factor (Ziabicki 1976) which depends on the flow, as described in Sect. 14.5.

In deciding the applicability of a crystallization model to a particular situation, e.g., fiber spinning, one must take into consideration that flow-induced crystallization may depend on the shear rate, strain rate, stress, normal stress difference, recoverable shear strain, free energy of dumbbells, rheology, configurational entropy of the polymer chains, work input, etc., and that the factor that exerts the greatest influence on crystallization and under what conditions does so is as yet subject to debate. Moreover, some of the models have been developed mainly for isothermal conditions, e.g., (Doufas et al. 1999, 2000a), whereas others, e.g., (Eder and Janeschitz-Kriegl 1997; Eder et al. 1990), may be applied to non-isothermal processes. Furthermore, since the rheology of the polymer should take into account the molecular motion of the polymer chains which is affected by the crystallization and the latter is in turn affected by the rheology, the choice of viscoelastic rheology such as the Leonov's recoverable stress, pom-pom, extended pom-pom (XPP), PTT, etc., determines to a large extent the quality of the flow-induced crystallization model. This is the case for the Zuidema (Zuidema 2000; Zuidema et al. 2001; Peters 2003), Tanner (Tanner 2002, 2003), microrheological (Coppola et al. 2001, 2004) and Zheng and Kennedy (2004) flow-induced approximations. On the other hand, other models such as those of Eder and Janeschitz-Kriegl (Eder and Janeschitz-Kriegl 1997; Eder et al. 1990) and Doufas et al. (1999, 2000a) are based on global behavior such as the one observed in rheological and rheological-optical experiments.

Many of the flow-induced crystallization models developed to-date are based on experimental data for a small sample of polymers, e.g., PP, PE, i-PP, etc., for which the material properties are available. However, these polymers have properties that are quite different from those of other polymers and, for example, the suspension assumption used for certain polymers, e.g., PP, may not be applicable to other

polymers (Tanner and Qi 2005). This means that any flow-induced crystallization model should be tested for a wide range of materials.

The experimental methods on which a flow-induced crystallization model is based or tested are also important to decide for which specific type of flow, e.g., elongational or shear flow, and conditions, e.g., post-flow or continuous flow, the model can be applied. For example, the Doufas et al. (1999, 2000a) model was developed for fiber spinning, while those of Eder and Janeschitz-Kriegl (1997) and Zheng and Kennedy (2004) were aimed at modeling injection molding, i.e., post-shearing conditions.

Although some models have been claimed to be suitable for both shear and elongation flows, e.g., (Zuidema 2000; Zuidema et al. 2001; Peters 2003), their applicability remains still an issue due to the lack of data for elongation-induced crystallization.

14.3 Models for Molecular Orientation

The properties of liquid crystalline polymers depend strongly on their molecular orientation; a high degree of orientation results in high strength and stiffness along the alignment direction, but it also yields anisotropic properties that may be detrimental when multidimensional stability and strength are required (Ramalingam and Armstrong 1993).

The relationship among the flow, molecular orientation, crystallization and rheology of LCP is a complex one, and depends on many factors. For isothermal flows at low shear rates, a nematic LCP may be called flow-aligning because shear promotes the alignment of the nematic director at an angle with respect to the flow direction, but shear may also result in tumbling which is characterized by a continuous rotation of the director. Although considerable progress has been made in the molecular orientation of lyotropic solutions of rodlike polymers, the situation is not yet as advanced in the case of thermotropic LCP.

Orientation of chain segments within a deformed chain leads to another important effect. Chain segments with orientations prevailing in the system, e.g., segments parallel to the filament axis in melt-spinning, crystallize at higher temperatures and at higher rates than segments with less frequent orientations. This leads to the preferential formation of axially oriented crystals and discrimination of crystals with orientations perpendicular to the main axis.

Experimental evidence about selective crystallization is scarce and indirect, although this concept is supported by comparisons of the crystal and amorphous orientation factors in crystallization experiments performed under stress or flow. Moreover, deformation of the polymer chains leads to a reduction of the configurational entropy, an elevation of melting temperature, and an increase of both the nucleation and the crystallization rates; the crystallization characteristics can also be affected by stress as discussed previously.

In order to predict the flow alignment of nematic polymers, molecular, mesoscopic and continuum models have been developed. The objective of these theories is to predict the most probable direction of alignment and the spreading of the orientation distribution in terms of a few parameters.

The Leslie-Ericksen continuum formulation (Leslie 1968, 1979; Ericksen 1960, 1991) provides explicit expressions for the flow alignment as a function of the Miesowicz viscosities independently of the shear rate, but it provides no information on the spread of the orientation distribution. In addition, this formulation does not contain any information on the concentration and is only applicable to small molecular weight liquids, i.e., liquid crystals. Furthermore, in this approach, the stress tensor is assumed to have a linear dependence on the strain rate tensor and the angular velocity of the director, and implicitly assumes that the characteristic time associated with the deformation is much larger than the characteristic relaxation time of the nematic phase. This explains, in part, the success of the Leslie-Ericksen formulation for low molecular-weight crystals because their relaxation times are usually much smaller than the macroscopic time scales. In fiber spinning, however, the deformation rate is usually much larger than the inverse of the relaxation times and, therefore, the Leslie-Ericksen theory becomes inapplicable.

High-molecular weight polymers and LCP exhibit many relaxation times which are associated with the relaxation of the short and long parts of the molecular chains; the largest relaxation time is related to the relaxation of the chain as a whole and may dominate its macroscopic behavior. This justifies that, in some cases, one may use only the longest relaxation time instead of the whole spectrum of relaxation times such as, for example, in the Rouse model for unentangled polymer liquids (Rouse 1953; Long and Morse 2002; Lin 2010) or the reptation model for entangled ones. In LCP solutions, the persistence length of the molecular chains is not negligible compared with their contour one and this leads to an anisotropic equilibrium state and a dependence of the molecular distribution function on the nematic order parameter.

Mesoscopic models have been developed to predict shear-aligned steady states and are able to predict the dependence of the Leslie angle on the concentration and the molecular aspect ratio, but require either direct numerical simulations or a higher-order asymptotic analysis to obtain the dependence of the molecular orientation on the shear rate (Wang 1997; Rienacker and Hess 1999; Forest and Wang 2003; Forest et al. 2003; Maffetone et al. 2000; Cocchini et al. 1990).

Approaches based on kinetic theory employ an evolution equation for the probability density function and should include the dependence of the molecular orientation upon the properties of the polymer and flow, e.g., shear. However, it is difficult to obtain explicit expressions for such a dependency.

Kinetic approaches are mainly based on the work of Onsager (Onsager 1949) and, although much progress has been made since, few analytical works have appeared on the subject, except for that of Marrucci and co-workers (Marrucci and Maffetone 1989; Marrucci 1991; Maffetone et al. 1994) who provided an explanation of the dependence of the molecular orientation on the normal stress difference. This is not surprising at all, for numerical simulations indicate that the

shear-perturbed nematic equilibrium contains many high-order spherical harmonics, and it is nearly impossible to obtain a distribution function that resolves them. In addition, it is well-known that nematic polymers exhibit multiple stable phases, e.g., an isotropic phase for dilute concentrations, a nematic phase at high concentrations, and bistability in an overlap region (de Gennes 1974).

The isotropic phase can be treated easily by means of kinetic theory and mesoscopic approaches in the weak-shear limit and for dilute concentrations by means of asymptotic methods. Such approaches provide explicit expressions for the alignment angle, degree of alignment and normal and shear stresses as functions of the molecular parameters and the shear rate.

Many of the models used to predict molecular orientation in fiber spinning processes of liquid crystalline polymers are based on a kinetic equation for the probability density function $f(\mathbf{u}, t)$ that provides the probability that a dumbbell or (rigid) rod-like polymer be in the direction \mathbf{u} at time t . For polymers in a Newtonian solvent subject to anisotropic hydrodynamic drag, Bhawe et al. (1993) used a polymer-polymer mean-field interaction approximation with a Maier-Saupe potential (Maier and Saupe 1958, 1959, 1960), generalized the results of Doi (1980, 1981) and Doi and Edwards (1986) and introduced a closure approximation whereby the fourth-order moments of the probability function for \mathbf{u} are approximated by products of second-order ones. In this manner, they obtained an approximate equation which couples the structure/orientation/order tensor to the Navier-Stokes equations. This approximation indicates that the deviatoric stress tensor becomes the sum of two terms; the first one is given by the classical Newtonian rheology, whereas the second one depends on the temperature, the structure tensor \mathbf{Q} , the velocity gradient tensor, and a parameter that characterizes the strength of the intermolecular Maier-Saupe potential which is responsible for orienting the molecules in the same direction.

The nematic structure tensor is traceless, is symmetric, has three real eigenvalues, and can be diagonalized. For uniaxial nematic liquid crystals, two eigenvalues are identical, and the eigenvector corresponding to the third eigenvalue provides the distinguished orientation direction and admits a representation in terms of a scalar order parameter that is related to the polymer direction vector \mathbf{u} . This scalar parameter s can be interpreted as the average degree of orientation between the polymer molecular direction vector \mathbf{u} and the direction of the third eigenvector of the structure tensor. The values $s=0$ and 1 correspond to an isotropic state referred to as a nematic defect since the structure tensor is nil; these values also correspond to no preferred orientation and parallel alignment of the third eigenvector and \mathbf{u} , respectively. On the other hand, $s=-0.5$ corresponds to all molecules being aligned in a plane orthogonal to the third eigenvector of the structure tensor; $0 < s \leq 1$ and $-0.5 \leq s < 0$ correspond to liquid crystals that exhibit prolate and oblate, respectively, uniaxial symmetry. On the other hand, if all the eigenvalues of the structure tensor are distinct, the order tensor depends on five parameters due to its being traceless, and admits a biaxial representation that depends on two parameters that are related to the degree of orientation of the

molecular direction vector \mathbf{u} and the second and third eigenvalues of the structure tensor.

In their studies of isothermal spinning of nematic liquid crystal polymers, Ramalingam and Armstrong (1993) used the constitutive equations of Bhava et al. (1993), and assumed uniaxial symmetry and that the direction of the third eigenvector of the orientation tensor coincides with the elongational direction. This implies that the principal direction of the structure tensor also referred to as the axis of symmetry of the structure tensor coincides with the symmetry axis of the fiber and is uniform throughout the fiber, and, therefore, the structure tensor can be characterized by only a scalar order parameter which indicates the degree of orientation of the dumbbell direction \mathbf{u} with respect to the fiber's symmetry axis. A similar study was reported by See et al. (1990).

Ramalingam and Armstrong (1993) also showed that, in contrast, with fiber spinning processes of isotropic liquids, the velocity, structure and stress profiles are sensitive to the choice of initial conditions.

In a nonequilibrium elongational flow, the structure tensor is not uniformly uniaxial and the third eigenvector of the orientation tensor may not coincide with that of the fiber's symmetry axis because the strain rate tensor is not diagonal; in such a case, the uniaxial symmetry is broken. However, for slender fibers, one may consider that a uniaxial flow approximation is approximately valid and, therefore, the structure tensor may be assumed to be nearly uniaxial. This can be justified asymptotically by means of perturbation methods for slender fibers at low Reynolds numbers where the small perturbation parameter is the slenderness ratio (Ramos 1999).

Other kinetic approaches are based on the Smoluchowski equation for the orientational probability density function (Forest et al. 2002, 2004). These approaches have been developed for dilute concentrations under weak shear to analyze isotropic-to-nematic phase transitions and also make use of the Doi's formulation (Doi 1980, 1981; Doi and Edwards 1986).

The Doi's formulation (Doi and Edwards 1986) with the Maier-Saupe potential (Maier and Saupe 1958, 1959, 1960) has also been used to analyze the microstructure in one-dimensional isothermal models of slender liquid crystalline polymer fibers (Forest et al. 1997a) and to determine the effects of the coupling between the flow and the molecular orientation on the linear stability of isothermal LCP fibers (Forest et al. 1997b).

Doi's approach has also been used to developed one-dimensional models of thermotropic liquid crystalline fibers (Zhou et al. 2000) by including the energy equation, axial conduction and heat transfer losses through the fiber's surface and a temperature dependence of the relaxation time that appears in the orientation/structure tensor which, in turn, affects the deviatoric stress tensor. It has also been extended to study fiber spinning of liquid semi-crystalline, compound (Ramos 1999, 2002, 2006, 2007), hollow-compound (Ramos 2001a, 2005a) and annular fibers (Ramos 2001b).

In Zhou et al.'s model (2000), the total stress tensor was assumed to be the sum of an isotropic Newtonian contribution and an anisotropic part that depends on the

temperature, velocity gradient and structure tensor. The isotropic contribution of the Newtonian stress tensor was assumed to obey a Newtonian rheology with a dynamic viscosity that depends in an Arrhenius manner on the temperature. Although the authors refer to their model as a two-phase one, this is not strictly so, for they do not account in a separate form for the evolution of the amorphous and crystalline phases. Moreover, whenever the fiber solidifies, their one-dimensional model predicts a constant velocity along the fiber, but the evolution equation for the scalar order parameter of the molecular orientation may predict the unphysical result that the molecular orientation decreases once solidification occurs due to the fact that the uniaxial bulk free energy that is based on the Maier-Saupe intermolecular potential, may dominate over the elongational terms that appear in that equation. This non-physical behavior is observed in their results and may be eliminated entirely by modifying the Maier-Saupe potential when the scalar order parameter for the molecular orientation is close to its maximum value, i.e., unity.

As indicated above, in the mean-field Maier-Saupe theory, the structure tensor order parameter is defined in terms of the second-order moments of the probability density function; this imposes certain constraints on the eigenvalues of the structure tensor that may be interpreted as constraints. By way of contrast, in the Landau-de Gennes energy functional framework (de Gennes 1974), the order parameter of the structure tensor is often defined independently of the probability density function, and the theory makes physically unrealistic predictions about the equilibrium order parameter in the low-temperature regime.

Ball and Majumdar (2010) have developed a continuum energy functional that interpolates between the mean-field Maier-Saupe energy and the Landau-de Gennes energy functional by defining a thermotropic bulk potential that blows up whenever the eigenvalues of the structure tensor reach physically unrealistic values and, as a consequence, the minimizers of their continuum energy functional yield physically realistic order parameters in all temperature regimes.

One of the most challenging problems in polymer science is the reliable prediction of molecular orientation during crystallization; the viscoelastic nature of polymers should be accounted for in the description of the evolution of the molecular orientation and vice versa. The alignment of macromolecules along a preferred direction is the result of a competition between the polymer's relaxation times which are functions of the thermochemical and crystallization histories, and the characteristic deformation time; high alignment is expected when the ratio of the latter to the former is greater than unity.

14.4 Rheology

Both molecular orientation and crystallization have a strong effect on the melt rheology; in many cases, the solidification of a semi-crystalline material is caused by crystallization rather than by temperature. Despite its importance, the effects of

the crystallinity on the polymer's rheology, e.g., viscosity, have not been treated with sufficient detail and the literature on this subject is scarce. This may be due to difficulties in measuring simultaneously the rheological properties and the crystallinity evolution.

Most researchers agree that the melt viscosity experiences a dramatic increase in viscosity when the degree of crystallization reaches a critical value which may not coincide with the ultimate degree of crystallization.

Models for the dependence of the dynamic viscosity on the crystallinity include polynomial, exponential, and rational ones (Pantani et al. 2005; Ziabicki and Jarecki 2007); in polynomial models, for example, the dynamic viscosity is given as a polynomial of the crystallinity degree. Both polynomial and exponential models provide analytical expressions for the melt viscosity which increases in a smooth manner with the degree of crystallization. By way of contrast, rational models (Ziabicki and Jarecki 2007) are not analytical ones and the dynamic viscosity becomes unbounded at the critical value of the degree of crystallization; this behavior may cause a great deal of problems when implemented numerically.

The dependence of the dynamic viscosity on the temperature has been usually assumed to follow an Arrhenius expression; a similar expression has also been assumed for the dependence of the relaxation times which should also depend on the molecular orientation and crystallization, although it is difficult to measure such a dependency experimentally.

As discussed previously the contributions of the amorphous and semicrystalline phases to the total deviatoric stress tensor are usually assumed to be additive or weighted by the crystallization degree. Such a simple assumption may not be physically consistent due to the interactions between the amorphous and crystalline phases which include both tangential and normal effects along the amorphous-crystalline interfaces, and may not satisfy the principles of rational mechanics and thermodynamics.

14.5 Models of Fiber Spinning Processes

Most models of fiber spinning of liquid semi-crystalline polymers developed to-date are one-dimensional. The first one-dimensional model was perhaps developed by Matovich and Pearson (1969) for amorphous or isotropic polymer melts and was based on a heuristic derivation based on a control-volume formulation where the flow was assumed to be mainly one-dimensional; such an assumption is valid for slender fibers, i.e., fibers characterized by a maximum diameter-to-length ratio much smaller than unity. In addition, the model developed by Matovich and Pearson was isothermal and employed a Newtonian rheology, although later developments have included isotropic viscoelastic rheologies (Denn et al. 1975; Betchel et al. 1988, 1995) and thermal effects (Glicksman 1968; Hyunh and Tanner 1983; Kase and Matsuo 1965; Ziabicki 1976; Pearson 1985; Vassilatatos et al. 1992; Gagon and Denn 2004).

The model developed by Matovich and Pearson (1969) can also be derived by expanding the flow variables in Taylor's series expansions of the radial coordinate measured from the fiber axis and truncating the resulting series at different orders in that coordinate (Vrentas and Vrentas 2004). It may be shown that the Matovich and Pearson's model corresponds to retaining only the first two terms in the Taylor series expansions and results to this order in an axial velocity component which only depends on the distance along the fiber, while the radial velocity component is a linear function of the radial coordinate. Maintaining higher-order terms in the Taylor's series expansions results in more equations for the coefficients of such expansions and accounts for the radial dependence of the flow variables. However, the validity of a truncated series expansion model can only be justified for slender fibers, i.e., fibers whose largest diameter is smaller than the distance from the location of largest fiber's cross-section to the take-up drum, and small Reynolds numbers.

A different approximation for obtaining one-dimensional models consists in nondimensionalizing the governing equations for the conservation of mass, linear momentum and energy, introducing the slenderness ratio as a small parameter, expanding the flow variables in asymptotic power series of the slenderness ratio, i.e., using a long-wave or lubrication approximation, and equating to zero the coefficients that multiply the same power of the slenderness ratio (Schultz and Davis 1982). Asymptotic methods based on the slenderness ratio have also been used to study melt spinning of compound (Ramos 1999, 2002, 2006, 2007), hollow-compound (Ramos 2001a, 2005a) and annular fibers (Ramos 2001b).

To first-order in the slenderness ratio and for low Reynolds numbers, the Matovich and Pearson's model results, whereas higher-order approximations provide corrections to the leading-order one and include the radial dependence of the flow variables. This asymptotic procedure indicates that, at leading-order in the expansion, the temperature across the fiber is uniform and this in turn implies that the Biot number which is a measure of the convective heat exchanges of the fiber with its surroundings relative to thermal conduction in the fiber must be small and this, in turn, implies that, at leading-order in the slenderness ratio, the outer surface of the fiber is adiabatic (Ramos 2005a, 2006, 2007). Such a restriction does not appear explicitly in the control-volume formulation approach employed by Matovich and Pearson (1969) but it is a realistic one because, in modern spinline, the temperature is maintained high enough in order to delay solidification and, therefore, allow the molecular orientation, elongational flow and heat conduction in the axial direction to interact with each other long enough along the fiber.

Asymptotic methods based on the slenderness ratio are not appropriate when there is rapid surface cooling due to the large radial temperatures present under these conditions, and the validity of one-dimensional models based on control-volume formulations may not be justified in the presence of rapid surface cooling because of the strong radial temperature gradients generated at the fiber's outer radius or free surface.

A third method for deriving one-dimensional models of fiber spinning processes consist of using the integral forms of the governing equations for mass, linear

momentum and energy conservation across the fiber, integrating analytically the terms which contain the radial derivatives and approximating the integral terms across the fiber by functions that only depend on the axial coordinate along the fiber; alternatively, the flow variables may be expanded in Taylor's series expansions of the radius and the above-referred-to integrals may be performed analytically. In any event, only a finite number of terms of the Taylor's series expansion is kept and, therefore, the resulting equations are truncated at some order on the fiber's outer radius.

14.5.1 One-Dimensional Models for Fiber Spinning of Liquid Semi-Crystalline Polymers

The available one-dimensional models for fiber spinning of liquid crystalline and liquid semi-crystalline polymers may be derived by means of the same methods described above for amorphous or isotropic materials, and may be classified in two main groups: one- and two-phase models depending on whether the amorphous and semi-crystalline phases are considered as a single material or two different materials, respectively. One- and two-phase models may in turn be classified according to the rheologies employed for each phase and may be isothermal and non-isothermal.

In the next sections, a brief review of the main one-dimensional models for fiber spinning of liquid semi-crystalline polymers developed to-date is presented.

14.5.1.1 One-Phase Models

The main one-phase models for the spinning of liquid crystalline and liquid semi-crystalline fibers developed to-date include those of van Meerveld (van Meerveld et al. 2008) that employs Schneider's model for quiescent crystallization, i.e., nucleation and growth of three-dimensional spherulites, and a model for the fibrillar morphology development due to flow-induced nucleation and longitudinal growth of the fibrillar structures. It also includes a Newtonian rheology where the dynamic viscosity is an exponential function of the degree of crystallization and temperature that models the influence of the crystallization on the rheological behavior, while the amorphous phase is described by a microrheological model based on a configuration tensor that includes an upper-convective Maxwell behavior for the change of the configuration tensor with the flow, a Giesekus mobility matrix for the relaxation dynamics, finite extensibility of the polymer chains, and the reduction of configuration due to crystallization. The model contains a large number of constants that must be determined by judicious comparisons between its predictions and experimental data. The model is able to predict the neck-in phenomenon which may be observed at high drawing speeds.

The model developed by Zuidema and co-workers (Zuidema 2000; Zuidema et al. 2001; Peters 2003) employs a modification of the shear-induced crystallization model proposed by Eder and Janeschitz-Kriegl (1997) which provides a good correlation between the predicted flow-induced structures and experimental data and a recoverable strain model with a Leonov's driving force (Leonov 1976, 1987) for flow-induced crystallization that correlates most strongly with the viscoelastic mode corresponding to the largest relaxation time. Zuidema's model only includes the second invariant of the deviatoric part of the recoverable strain which is a measure of the molecular orientation, although no model for the molecular orientation was included in his flow-induced crystallization formulation.

The model of Kannan and Rajagopal (Kannan and Rajagopal 2005) treats the amorphous phase as a viscoelastic fluid, while the crystalline phase is assumed to behave as a transversally elastic material, uses a thermodynamic formulation, and requires a judicious choice of the free energy and other thermodynamic functions for predicting accurately the initiation of crystallization. If such a judicious choice is made, the model predicts necking phenomena at high drawing speeds.

The model proposed by Forest and Ueda (1999) uses Avrami's crystallization kinetics, a crystallization rate that depends on the difference between the ultimate and the current degrees of crystallization and the molecular orientation order parameter as suggested by Ziabicki (1976). For isothermal flows, the melt's dynamic viscosity is assumed to depend in an exponential manner on the degree of crystallization, and the evolution equation for the uniaxial orientation along the fiber is nonlinearly coupled to both the flow-induced orientation and the flow-independent terms which take into account the intermolecular potential, and is consistent with Doi's nematodynamic theory (Doi and Edwards 1986). This model has been analyzed and extended by Forest et al. (1997a, b) and applied to the melt spinning of thermotropic liquid crystalline polymers by Zhou et al. (2000).

Some sample results obtained with a one-dimensional, one-phase model which is an extension of that of Zhou et al. (2000), are illustrated in Fig. 14.1 for different Biot numbers. The results presented in this figure have been nondimensionalized with respect to the temperature and axial velocity of the melt at the die's exit, the fiber's radius at the die's exit and the spinline length, and correspond to a nondimensional drawing speed equal to $\sqrt{100}$.

For the two smaller Biot numbers considered in Fig. 14.1, the results indicate that the fiber's axial velocity B increases in an exponential manner from the die's exit to the take-up drum, the temperature decreases in an almost linear manner, the degree of crystallization exhibits a sigmoid shape and reaches its ultimate value, i.e., 0.8, before the take-up drum location, and full molecular orientation is not achieved along the spinline. The exponential behavior of the axial velocity observed in Fig. 14.1 is analogous to that of isothermal, compound, liquid semi-crystalline fibers (Ramos 1999, 2002).

For the largest Biot number considered in Fig. 14.1, both the axial velocity and the degree of crystallization exhibit a sigmoid shape, the heat transfer losses are larger, the temperature decreases faster, and the degree of crystallization increases

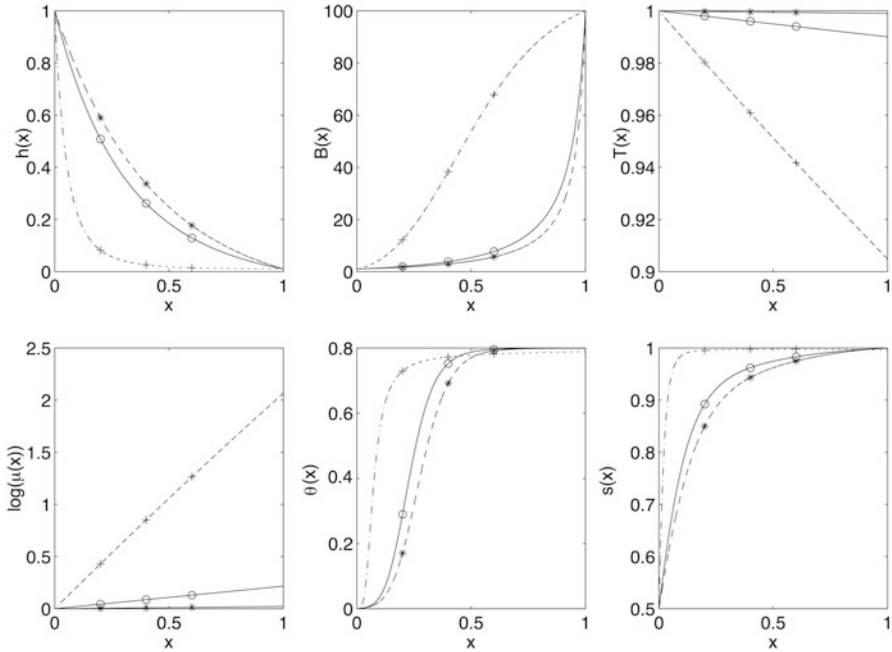


Fig. 14.1 Nondimensional fiber's radius (*top left*), axial velocity (*top middle*), temperature (*top right*), decimal logarithm of the dynamic viscosity (*bottom left*), degree of crystallization (*bottom middle*) and molecular orientation order parameter (*bottom right*) obtained with a one-dimensional, one-phase, fiber spinning model, for three different Biot numbers (The smallest and largest Biot numbers correspond to * and +, respectively)

faster than for the smaller Biot numbers. Figure 14.1 also indicates that, for the largest Biot number, complete molecular orientation and the ultimate degree of crystallization are achieved at locations equal to 0.50 and 0.25 times the spinline length, respectively, and that the logarithm of the dynamic viscosity increases in an almost linear manner.

Figure 14.1 also shows that, for the conditions considered, the increase in temperature associated with the latent heat of crystallization is small and cannot be observed; for larger values of the latent heat, the temperature first decreases from the die's exit up to an axial location where it increases, then reaches a relative maximum and then decreases. The location of this temperature peak is associated with the amorphous-to-crystalline phase transition. Both the location and peak of the temperature profile depend on the processing conditions, the pre-exponential factor and activation energy of the Arrhenius expression used to account for the dependence on the dynamic viscosity on temperature, and on the same factors for the relaxation time employed in the Maier-Saupe parameter. It also depends on the constants employed to account for the dependence of the dynamic viscosity law on the molecular orientation through Ziabicki's model of crystallization (Ziabicki 1974, 1976).

The effects of gravity, i.e., Froude number, and surface tension, i.e., the capillary number have been found to be small for drawing speeds typical of fiber spinning processes, although these effects may be important at low drawing ratios (George 2004).

The results presented in Fig. 14.1 as well as many others not shown here indicate that the accurate prediction of fiber spinning processes of liquid semi-crystalline polymers with one-dimensional models depends on many parameters even when using simple crystallization models, e.g., generalizations of the Avrami-Kolmogorov kinetics, and molecular orientation models characterized by an order parameter, even if a simple Newtonian rheology for the melt is used.

Figure 14.1 also shows that heat transfer losses have a great impact on the flow field and the degree of crystallization and molecular orientation. The fiber's contraction increases as the heat transfer losses are increased, and this contraction results in an increase of the strain rate which affects directly the molecular orientation; the latter in turn affects the degree of crystallization on two accounts. First, the thermal contribution to the crystallization increases as the temperature decreases, while the strain rate increase results in an increase of the flow-induced crystallization.

Since the approach employed in obtaining the results presented in Fig. 14.1 is based on a generalization of the Avrami-Kolmogorov kinetics described in Sect. 14.2, assumes a constant growth rate for both the thermal and flow-induced crystallizations, and the nucleation rate is assumed to be the sum of the thermal and flow-induced nucleation rates, where the former depends on the temperature and the latter on the strain rate, it is difficult to separate these two contributions as indicated in (14.8). For the conditions employed in Fig. 14.1, it was found that the contribution of the flow-induced crystallization was largest near the die's exit where the flow undergoes a large contraction but was comparable to the thermal one. The flow-induced crystallization was found to increase as the draw ratio was increased but was always found largest close to the die's exit.

14.5.1.2 Two-Phase Models

The two-phase isothermal model developed by Kulkarni and Beris (1998) includes Flory's approach (1947) for modelling the onset of crystallization. After the onset of crystallization, the amorphous phase is treated as a viscoelastic fluid represented by the White-Metzner rheological model, while the semi-crystalline phase is treated as an anelastic solid. The model predicts the necking phenomenon along the fiber at high drawing speeds which is attributed to structural changes induced by crystallization and the ability of the semi-crystalline phase to rapidly take up high stresses. However, several mechanics for necking at high spinning velocities have been proposed, e.g., viscous, viscoelastic and inertial mechanisms, and the radial distribution of the dynamic viscosity. Zahorski (1993) has shown that any radial viscosity distribution across the fiber intensifies the inertial mechanism and that, for sufficiently large radial viscosity variations across the fiber, a location reduction

in the axial velocity is not necessary for the onset of necking. The relevance of viscosity or viscoelasticity is not so clear, for one may not be able to determine the mechanism responsible for the local viscosity reduction associated with necking.

The two-phase model of Doufas et al. (2000a, b) and Doufas and McHugh (2001a) treats the amorphous phase as a Giesekus fluid and employs a rigid-rod model for the semicrystalline phase; the rigid rods are oriented by the flow, and both the amorphous and crystalline phases are coupled through the stress and momentum balance and feedback of the crystallinity to the melt's relaxation times. Their model also includes a Peterlin approximation in the evolution equation for the conformation tensor, and the relaxation times are assumed to be functions of both the temperature and the degree of crystallization which was modelled using Nakamura's kinetics, where the rate of crystallization depends on the temperature and the trace of the total stress tensor; the latter was assumed to be equal to the sum of those of the amorphous and crystalline phases, i.e., no volumetric effects were considered in determining the total stress tensor. A similar approach was followed by McHugh and Doufas (2001a) in their studies of fiber spinning of nylon and poly(ethylene terephthalate) (PET).

Doufas and McHugh model (2000a, b) and McHugh and Doufas (2001a) has been extended to include an extended pom-pom rheology (Kohler et al. 2005; Kohler and McHugh 2008) and to analyze the melt spinning of poly(lactic acid) which has more structure than PET and Nylon 6.6, and to include the whole spinline, so that the modified model avoids discontinuities generated by the imposition of continuation conditions at the crystallization temperature onset and excessive strength of the flow-induced crystallization compared with the quiescent one; the model also employs Avrami's kinetics (Shrikhande et al. 2006) for crystallization and has also been used to study the melt spinning of PP (Kohler and McHugh 2007) and multifilament melt spinning by accounting for the nonuniform quenching of the fibers (Jeon and Cox 2008; Dutta 2004).

14.5.2 Two-Dimensional Models of Fiber Spinning of Liquid Semi-Crystalline Polymers

The two-dimensional models described in this section are computationally demanding because they determine the flow, thermal, molecular orientation, crystallization and stress fields; they also determine the fiber's radius. At the fiber's free surface and, in the absence of evaporation, kinematic, dynamic and thermal boundary conditions must be satisfied. The kinematic condition is associated with the fact that the fiber's free surface is a material one, whereas the dynamic conditions establish that there is continuity of tangential stresses and the difference between the normal stresses on both sides of that surface must be balanced by surface tension which may depend on the temperature.

The surface tension contribution is proportional to the two radii of curvature of the free surface; one of them is the fiber's local radius while the other one depends on the second-order derivative of the fiber's radius with respect to the axial distance along the fiber. The accurate and stable discretization of the latter is not a trivial task, especially at high-drawing speeds when necking may appear in the fiber, as discussed above.

The thermal boundary conditions at the fiber's outer radius require continuity of the heat flux normal to that interface and is usually imposed by considering a film heat transfer coefficient and the difference between the temperature at that interface and that of the surroundings; the film transfer coefficient may also include radiation effects and depends on the fiber's velocity and the properties of the gases surrounding the fiber.

A more accurate model of the cooling of fibers should account for the boundary layer on the fiber so that the dynamics of the fiber are nonlinearly coupled to those of the surroundings. In such a model, in addition to the continuity of heat fluxes normal to the interface, the temperature must be continuous (Ramos 2005b, 2014). In these coupled two-dimensional models, no film heat transfer correlation is needed, although it may be determined from the results obtained by performing numerical experiments whereby the flow and thermal conditions for both the fiber and the gases that surround it are changed.

A fully two-dimensional numerical simulation of axisymmetric, isothermal, spinning flows of LCP based on the use of Doi's equations (Doi 1980, 1981; Doi and Edwards 1986) with a quadratic closure approximation was reported by Mori et al. (1997).

Numerical studies of the two-dimensional non-isothermal melt spinning of viscoelastic melts have been carried out by Joo et al. (2002) who employed a one-phase formulation where the crystallization kinetics is described by Nakamura's model, whereas the crystallization rate was modelled as per Ziabicki's formulation (Ziabicki 1974, 1976) and depends on both the temperature and the molecular orientation. The melt rheology was based on a Giesekus constitutive equation.

Joo et al.'s (2002) two-dimensional simulations indicate that, although the kinematics of fiber is approximately one-dimensional, the radial variations of temperature result in radial variations of the viscoelastic stresses across the fiber. This radial dependence, in turn, results in nonuniform molecular orientation and crystallization across the fiber. Their numerical experiments also indicate that the thermally-induced crystallization depends strongly on Avrami's exponent and that a sharp increase in crystallinity due to flow-induced crystallization is predicted to occur only when the polymer chains are highly aligned in the fiber's drawing direction at high spinning rates.

A similar model was developed by Sun et al. (2000) who used the Phan-Thien-Tanner rheological model.

14.5.3 Hybrid Models of Fiber Spinning of Liquid Semi-crystalline Polymers

Hybrid models of fiber spinning processes are also referred to as 1.5 dimensional models, use a one-dimensional equation for the axial velocity along the fiber and two-dimensional equations for the energy and stresses (Henson et al. 1998) and/or the conformation and the molecular orientation (Doufas and McHugh 2001b; McHugh and Doufas 2001b).

Henson et al. (1998) accounted for the radial temperature distribution across the fiber by means of a von Karman-Pohlhausen method with a parabolic temperature distribution and employed the average temperature across the fiber to evaluate the one-dimensional linear momentum equation, whereas Doufas and McHugh (2001b) and McHugh and Doufas (2001b) employed a two-dimensional formulation for the temperature and a one-dimensional formulation for the conformation and orientation tensors; only the diagonal components of the conformation and the orientation tensors along the fiber were considered in their formulation for elongational flows. The equations for these three variables are first-order partial differential equations and only require the specification of these three variables at an axial location along the fiber.

Ramos (2005b), Blanco-Rodríguez (2011) and Blanco-Rodríguez and Ramos (2011, 2012) developed a hybrid model for the fiber spinning of compound and hollow-compound liquid semi-crystalline fibers that consist of one-dimensional equations for the fiber's geometry and leading-order axial velocity component, and two-dimensional equations for the temperature, molecular orientation and crystallization; in such a formulation, the radial velocity depends linearly on the radial coordinate in accord with an asymptotic analysis of the continuity equation for slender incompressible fibers. The molecular orientation model was based on that of Doi and Edwards (1986), whereas the crystallization one employed Ziabicki's approximation (1976). These authors employ two formulations for the molecular orientation tensor; the first one determines the components of this tensor using a slender fiber approximation, whereas the second one uses an order parameter.

The results of the hybrid model proposed by Blanco-Rodríguez and Ramos (2012) were found to be in qualitative accord with those of a one-dimensional model that employs an order parameter for the molecular orientation, neglects axial heat conduction along the fiber and is only valid for slender fibers at low Reynolds and Biot numbers, but differences between the one- and two-dimensional models were observed near the die's exit where the fiber undergoes a large contraction and the strain rate is largest, and near the fiber's outer radius where cooling is important. In fact, these authors found that, even at moderately low Biot numbers, the temperature across the compound fiber is not uniform owing to heat losses as shown in Fig. 14.2 and that the temperature non-uniformities are mainly a function of the Biot number, the thermal conductivity and the pre-exponential factor and activation energy of the dynamic viscosity law for the cladding. The authors also

Fig. 14.2 Nondimensional temperature distribution in a semi-crystalline compound polymer fiber obtained with a hybrid model (The *dotted line* denotes the interface between the core and the cladding)

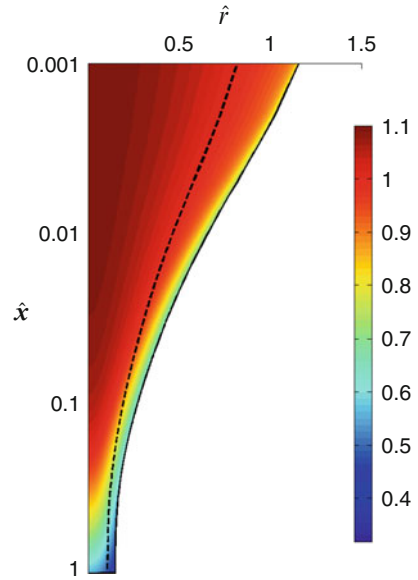
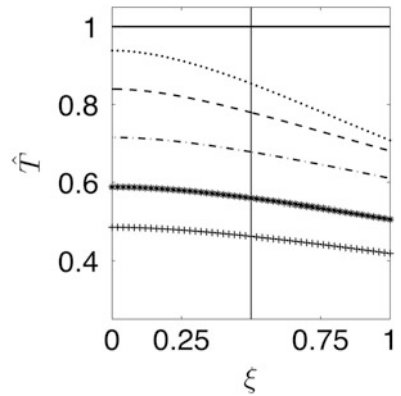


Fig. 14.3 Nondimensional temperature profile in a semi-crystalline compound polymer fiber obtained with a hybrid model (The *solid vertical line* denotes the interface between the core and the cladding)



found that the cross-sectional averaged temperature predicted by their two-dimensional model exhibits the same qualitative trends as those of an asymptotic one-dimensional model.

Figure 14.2 illustrates the nondimensional temperature distribution in a compound liquid semi-crystalline fiber and the cooling at the outer surface of the cladding. Along this surface, a thermal boundary layer is formed; the thickness of the layer increases with the distance along the fiber and the temperature across the fiber becomes nearly uniform when the fiber solidifies. This is also clearly observed in Figs. 14.3 and 14.4 which show the nondimensional temperature profiles at several locations along a compound and a hollow compound fiber, respectively.

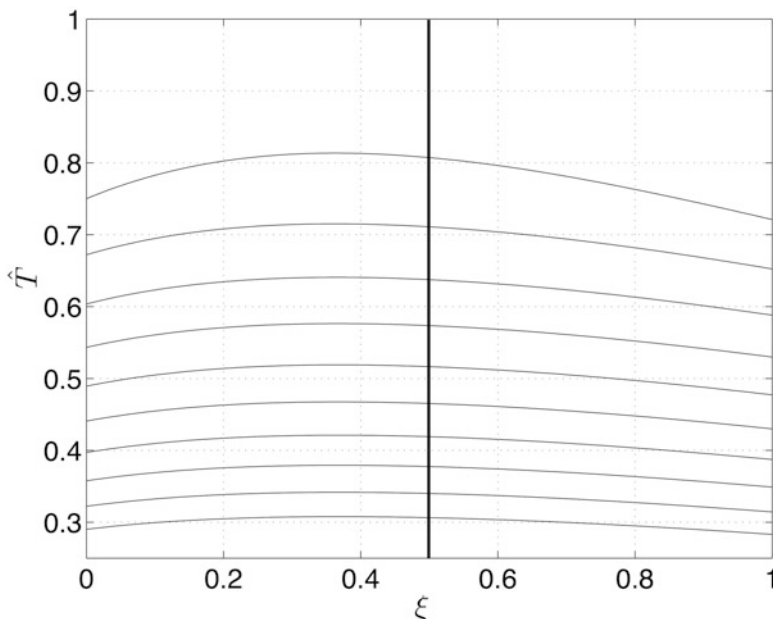


Fig. 14.4 Nondimensional temperature profile in a semi-crystalline hollow compound polymer fiber obtained with a hybrid model (The *solid vertical line* denotes the interface between the inner and outer annular fibers)

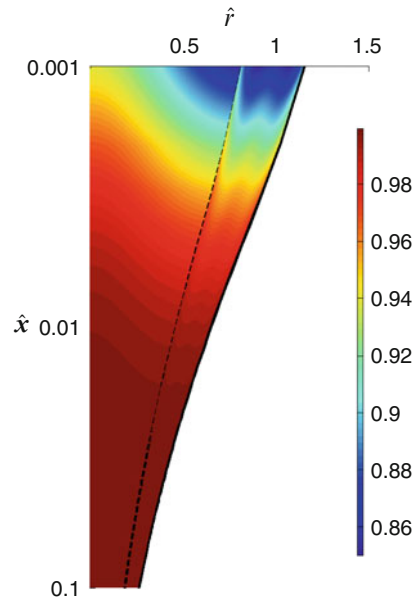
The temperature at the die's exit was assumed to be uniform in Figs. 14.2, 14.3, and 14.4, and this temperature was used to nondimensionalize the temperature distributions observed in these figures. Furthermore, in Figs. 14.3 and 14.4, the radial coordinate was nondimensionalized by the fiber's local radius in order to clearly observe the thermal boundary layers at the free surfaces of the fiber, and the temperature gradients at the interface between the core and the cladding and between the two annular fibers in compound and hollow compound fibers, respectively.

The results presented in Fig. 14.5 indicate that, for the conditions considered here, both the core and the cladding of liquid semi-crystalline compound polymer fibers reach almost complete molecular orientation close to the die's exit, and that the core reaches complete orientation earlier than the cladding because of the heat transfer losses at the cladding's outer surface which increase the thermal and flow-induced crystallization rates.

In both one- and two-dimensional and hybrid models of compound and hollow-compound liquid semi-crystalline fibers, almost full molecular orientation was observed close to the die's exit due to the large strain rate there and the fact that the Doi-Edwards molecular model and the Maier-Saupe potential predict an increase of the molecular orientation as the strain rate and velocity gradient increase.

At low Biot numbers, Blanco-Rodríguez and Ramos (2012) observed that, depending on the activation energies employed for the relaxation time and the

Fig. 14.5 Molecular orientation order parameter in a semi-crystalline compound polymer fiber obtained with a hybrid model (The *dotted line* denotes the interface between the core and the cladding)



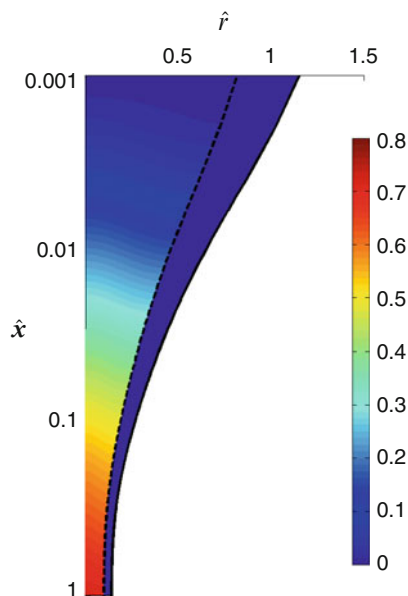
activation energy of the Arrhenius expression for the dynamic viscosity law, the order parameter for the molecular orientation first increases until it reaches a constant value and then decreases even when the fiber solidifies. As stated above, this behavior is unphysical and was corrected by modifying the Maier-Saupe potential in the transport equation for either the molecular orientation tensor or the molecular orientation order parameter.

Figure 14.6 illustrates the degree of crystallization in both the core and the cladding of a semi-crystalline compound fiber and indicates that, for the conditions considered here, very little crystallization occurs in the cladding and that the core reaches almost full orientation before the fiber is taken up at the collecting drum. For the conditions considered in Figs. 14.2 and 14.6, the flow-induced crystallization was found to be smaller than the thermal one.

As stated previously, a one-dimensional approximation to the continuity and linear momentum equations is only strictly valid for slender fibers at low Reynolds numbers. Moreover, the leading-order temperature in an asymptotic expansion of the flow and thermal fields in terms of the slenderness ratio is uniform across the fiber and this demands that the Biot number at the fiber's outer surface be sufficiently small, so that the leading-order boundary condition corresponds to an adiabatic surface. If one were to obtain the radial dependence of the temperature for slender fibers, one should proceed to higher order in the asymptotic expansion or employ a two-dimensional model.

Some researchers, e.g., Zahorski (1990) have shown that, independently of the magnitude of the radial and axial viscosity gradients, the velocity profiles across a fiber are always convex, i.e., the velocity gradient is always negative at the fiber's outer surface at least in regions where the polymer is in the liquid state.

Fig. 14.6 Degree of crystallization in a semi-crystalline compound polymer fiber obtained with a hybrid model (The *dotted line* denotes the interface between the core and the cladding)



The hybrid models developed to-date make use of the one-dimensional equations obtained from either asymptotic methods in terms of the slenderness ratio or Taylor's series expansions in the radial coordinate and employ effective properties that take into account the radial variations of the temperature, stresses, molecular orientation and crystallization by performing cross-sectional averages for these variables.

The great advantage of hybrid methods compared with two-dimensional ones is that they employ one-dimensional equations for the fiber's radius and average axial velocity component along the fiber, and, therefore, they avoid the cost of and the difficulties encountered in two-dimensional models when applying kinematic and dynamic boundary conditions at the fiber's free surface; in addition, they may provide approximate two-dimensional distributions of the molecular orientation, crystallization, temperature and stresses. However, they are not strictly consistent with an asymptotic analysis of slender fibers at low Reynolds numbers and employ a radial velocity component that, at leading-order, is a linear function of the radial coordinate; moreover, the leading-order pressure is independent of the radial coordinate.

14.6 Conclusions and Future Work

A review of one- and two-dimensional and hybrid models of the melt spinning of LCP and liquid semi-crystalline polymer fibers has been presented. Most of the models developed to-date are one-dimensional; two-dimensional models are computationally costly and require to determine the fiber's surface where kinematic,

dynamic and thermal boundary conditions must be satisfied, as part of the solution. Hybrid models avoid the imposition of dynamic boundary conditions at the fiber's free-surface by employing a one-dimensional formulation for the fiber's geometry and axial velocity component, and a two-dimensional formulation for the molecular, thermal and crystallization fields. Albeit hybrid models reduce to one-dimensional ones when the properties are uniform across each section of the fiber, they are based on one-dimensional formulations that are strictly applicable to slender fibers at low Reynolds and Biot numbers. These conditions imply that the heat transfer losses at the fiber's outer surface should be small. This may be the case in some fiber spinning processes, but it may not be so at high cooling rates. This means that, although hybrid models may be more accurate than one-dimensional ones, the use of averaged effective properties, e.g., viscosity, temperature, molecular orientation, crystallization, etc., in the one-dimensional linear momentum equation may be a coarse approximation that accounts in an integrated manner for the radial dependence of the axial velocity field. Furthermore, the slenderness approximation implies that, at leading-order, the radial velocity component is a linear function of the radial coordinate and, therefore, the flow is mainly uniaxial.

The crystallization models that have been employed in the study of fiber spinning of liquid semi-crystalline fibers are mainly based on the Avrami-Kolmogorov-Johnson-Mehl-Evans kinetics which was developed for quiescent isothermal crystallization. This model has been generalized to include flow-induced crystallization which may depend on the stresses, strain rate, normal stress difference, pressure, etc. However, it is as yet unknown which of these has the strongest influence and under what conditions on crystallization.

Perhaps the most detailed model of crystallization employed in fiber spinning processes is the one developed by Schneider et al. (1988) with the flow-induced crystallization model of Eder and Janeschitz-Kriegl (1997). However, it has been shown in this chapter that Schneider's model is based on the Avrami-Kolmogorov kinetics and derivatives thereof. This means that the model is subjected to the same criticisms as the original Avrami-Kolmogorov formulation. Furthermore, Schneider's model assumes that the dimensionality constant for crystal growth that appears in the original Avrami-Kolmogorov' formulation is an integer; however, quiescent crystallization experiments indicate that this may not be the case and that such a constant may not be an integer.

Most of the molecular orientation models for fiber spinning of liquid semi-crystalline polymers developed to-date have been based on the reptation model and the probability distribution formulation developed by Doi and Edwards (1986) and the intermolecular potential of Maier and Saupe (1958) that provide a transport equation for the order/structure/orientation tensor upon approximating the fourth-order moments in terms of the second-order ones.

One-dimensional models that use a uniaxial flow approximation have shown that the molecular orientation order parameter may first increase, reach a relative maximum, and then decrease. Such a behavior has been attributed to the Maier-Saupe potential when only one relaxation time is considered, as one can easily deduce by studying the fixed points of the transport equation for the molecular order

parameter. Although such a shortcoming may be eliminated by appropriately modifying the Maier-Saupe potential, there is a clear need for including not only the longest relaxation times that characterizes the tail of the distribution function, but many others as well.

The weakest points of the one- and two-dimensional and hybrid models for fiber spinning developed to-date are those associated with the effects of the molecular orientation on the crystallization and the effects of the latter on the former, as well as those of the crystallization and orientation on the melt's rheology and, therefore, on the flow field which in turn affect the molecular orientation and crystallization rates. Many of the models that couple the molecular orientation and crystallization assume that the crystallization rate depends on the temperature and molecular orientation, whereas the latter depends on the strain rate, temperature and relaxation time. Clearly, the molecular orientation should also depend on the crystallization.

The transport equations for the molecular orientation tensor or order parameter and the degree of crystallization developed to-date are first-order differential equations of the hyperbolic type and, therefore, only require one boundary condition in the radial and axial directions. This means that, when these equations are used in a one-dimensional model for fiber spinning of liquid semi-crystalline fibers, the molecular orientation and crystallization depend on the values of these variables at the die's exit, as well as on the flow and temperature fields: however, when used in two-dimensional or hybrid models, one should account for the direction of the characteristic lines of these equations, and this implies that one should account for both the axial and radial velocity components when imposing boundary conditions. The hyperbolic character of the transport equations for the molecular may make them not to be applicable to compound or hollow-compound fibers due to the interfaces between the core and the cladding in the former and the interface between the two annular fibers in the latter. At such interfaces, one should expect an interaction between the polymers of, for example, the core and cladding.

The molecular orientation and crystallization models may not even be valid for the fiber spinning of round fibers consisting of only one material because at the fiber's free surface where cooling is important, one should expect that the crystallization and molecular orientation are affected by the heat transfer losses, while, at the fiber's axis, these variables satisfy symmetry conditions. This means that a more physically realistic model for the fiber spinning of liquid crystalline polymers should include diffusion-like terms in the transport equations for the structure tensor and the crystallization. A model that accounts for the interactions between two similar or dissimilar materials at the interfaces of compound and hollow-compound fibers is also needed. Such a model must take into account the orientation and organization of macromolecules at interfaces that may lead to the formation of interphases. The creation of such interphases involves physical, chemical and physicochemical mechanisms.

A full model of fiber spinning processes should also account for the dynamics and thermal field of the gases that surround the fiber, so that there is no need for film heat transfer correlations that are employed in the models developed to-date. Most of these heat transfer correlations have been obtained in very specific experimental

setups and for very specific materials and operating conditions, and may not be strictly applicable in another scenarios or when the processing of other materials is considered.

Since the flow, molecular orientation, crystallization and thermal fields in fiber spinning of LCP are history-dependent, a more accurate model should include the melt's dynamics in the die and the flow relaxation from its confinement in the die to the free-surface conditions of the fiber. This would allow to account for possible swell effects near the die's exit. In addition, the predictions of any fiber spinning model should be tested with experimental data under different operating conditions and for a variety of polymers in order to accurately determine the parameters and constants that appear in such a model as well as their dependence on the material being processed and the operating conditions.

Acknowledgements The writing of this chapter was supported by Project FIS2012-38430 from the Ministerio de Economía y Competitividad of Spain. The author is grateful to many colleagues who provided many suggestions on the different versions of this manuscript.

References

- Avrami A (1939) Kinetics of phase change. I. General theory. *J Chem Phys* 7:1103–1112
- Avrami A (1940) Kinetics of phase change. II. Transformation-time relations for random distribution of nuclei. *J Chem Phys* 8:212–224
- Avrami A (1941) Kinetics of phase change. III. Granulation, phase change, and microstructure. *J Chem Phys* 9:177–184
- Ball JM, Majumdar A (2010) Nematic liquid crystals: from Maier-Saupe to a continuum theory. *Mol Cryst Liq Cryst* 525:1–11
- Betchel SE, Forest MG, Holm DD, Lin KJ (1988) 1-D closure models for 3-D incompressible viscoelastic free jets: von Karman flow geometry and elliptical cross-section. *J Fluid Mech* 196:241–262
- Betchel SE, Bolinger KD, Cao JZ, Forest MG (1995) Torsional effects in higher order viscoelastic thin-filament models. *SIAM J Appl Math* 55:58–99
- Bhave AV, Menon RK, Armstrong RC, Brown RA (1993) A constitutive equation for liquid crystalline polymer solutions. *J Rheol* 37:413–441
- Blanco-Rodríguez FJ (2011) Numerical simulation of the molecular orientation and degree of crystallization of semi-crystalline fibres. Ph.D. thesis, Universidad de Málaga, Málaga, Spain
- Blanco-Rodríguez FJ, Ramos JI (2011) Melt spinning of semi-crystalline compound fibers. *Polymer* 52:5573–5586
- Blanco-Rodríguez FJ, Ramos JI (2012) A simplified two-dimensional model of the melt spinning of semi-crystalline hollow compound fibers. *Int J Thermal Sci* 58:102–112
- Burger M, Capasso V, Eder G (2002) Modelling of polymer crystallization in temperature fields. *Z Angew Math Mech (ZAMM)* 82:51–63
- Capasso V (2003) *Mathematical modelling for polymer processing*. Springer, New York
- Chawla KK (1998) *Fibrous materials*. Cambridge University Press, New York
- Cocchini F, Aratari C, Marrucci G (1990) Tumbling of rodlike polymers in the liquid-crystalline phase under shear flow. *Macromolecules* 23:4446–4451
- Coppola S, Grizzuti N, Maffettone PL (2001) Microrheological modeling of flow-induced crystallization. *Macromolecules* 34:5030–5036

- Coppola S, Balzano L, Gioffredi E, Maffettone PL, Grizzuti N (2004) Effects of the degree of undercooling on flow induced crystallization in polymer melts. *Polymer* 45:3249–3256
- de Gennes PG (1974) *The physics of liquid crystals*. Oxford University Press, Oxford
- Denn MM, Petrie CJS, Avenas P (1975) Mechanics of steady spinning of a viscoelastic liquid. *AIChE J* 21:791–795
- Di Lorenzo ML, Silvestre C (1999) Non-isothermal crystallization of polymers. *Prog Polym Sci* 24:917–950
- Doi M (1980) Rheological properties of rodlike polymers in isotropic and liquid crystalline phases. *Ferroelectrics* 30:247–254
- Doi M (1981) Molecular dynamics and rheological properties of concentrated solutions of rodlike polymers in isotropic and liquid crystalline phases. *J Polym Sci Polym Phys* 19:229–243
- Doi M, Edwards SF (1986) *The theory of polymer dynamics*. Oxford University Press, New York
- Doufas AK, McHugh AJ (2001a) Simulation of melt spinning including flow-induced crystallization. Part III. Quantitative comparisons with PET spinline data. *J Rheol* 92:403–420
- Doufas AK, McHugh AJ (2001b) Two-dimensional simulation of melt spinning with a microstructural model for flow-induced crystallization. *J Rheol* 45:855–879
- Doufas AK, Dairanieh IS, McHugh AJ (1999) A continuum model for flow-induced crystallization of polymer melts. *J Rheol* 43:85–109
- Doufas AK, McHugh AJ, Miller C (2000a) Simulation of melt spinning including flow-induced crystallization. Part I. Model developments and predictions. *J Non-Newtonian Fluid Mech* 92:27–66
- Doufas AK, McHugh AJ, Miller C, Immaneni A (2000b) Simulation of melt spinning including flow-induced crystallization. Part II. Quantitative comparisons with industrial spinline data. *J Non-Newtonian Fluid Mech* 92:81–103
- Dutta A (2004) Melt spinning of (multifilament) poly(ethylene terephthalate) fibers: a simulation approach. *Polym Eng Sci* 27:1050–1058
- Eder G (1997) *Macromolecular design of polymeric materials*. Marcel Dekker, New York
- Eder G, Janeschitz-Kriegl H (1997) Crystallization. In: Meijer HEH (ed) *Materials science and technology: a comprehensive treatment, processing of polymers*, vol 18. VCH, Weinheim, pp 269–342
- Eder G, Janeschitz-Kriegl H, Liedauer S (1990) Crystallization processes in quiescent and moving polymer melts under heat transfer conditions. *Prog Polymer Sci* 15:629–714
- Ericksen JL (1960) Anisotropic fluids. *Arch Rat Mech Anal* 4:231–237
- Ericksen JL (1991) Liquid crystals with a variable degree of orientation. *Arch Rat Mech Anal* 113:97–120
- Evans RU (1945) The law of expanding circles and spheres in relation to the lateral growth of surface films and the grain-size of metals. *Trans Faraday Soc* 41:365–374
- Flory PJ (1947) Thermodynamics of crystallization in high polymers I. Crystallization induced by stretching. *J Chem Phys* 15:397–408
- Forest MG, Ueda T (1999) An isothermal model for high-speed spinning of liquid crystalline polymer fibers: coupling of flow, orientation, and crystallization. *J Non-Newtonian Fluid Mech* 84:109–121
- Forest MG, Wang Q (2003) Monodomain response of finite-aspect-ratio macromolecules in shear and related linear flows. *Rheol Acta* 42:20–46
- Forest MG, Wang Q, Bechtel SE (1997a) One dimensional isothermal spinning models for liquid crystalline polymer fibers. *J Rheol* 41:821–850
- Forest MG, Wang Q, Bechtel SE (1997b) 1-D models for thin filaments of liquid-crystalline polymers: coupling of orientation and flow in the stability of simple solutions. *Phys Nonlinear Phenom* 99:527–544
- Forest MG, Zhou R, Wang Q (2002) Symmetries of the Doi kinetic theory for nematic polymers of arbitrary aspect ratio: at rest and linear flows. *Phys Rev E* 66:031712
- Forest MG, Zhou R, Wang Q (2003) Full-tensor alignment criteria for sheared nematic polymers. *J Rheol* 47:105–127

- Forest MG, Zhou R, Wang Q (2004) Scaling behavior of kinetic orientational distributions for dilute nematic polymers in weak shear. *J Non-Newtonian Fluid Mech* 116:183–204
- Fukuda T, Rudolph P, Uda S (eds) (2004) *Fiber crystal growth from the melt*. Springer, New York
- Gagon DK, Denn MD (2004) Computer simulation of steady polymer melt spinning. *Polym Eng Sci* 21:844–853
- George HH (2004) Model of steady-state melt spinning at intermediate take-up speeds. *Polym Eng Sci* 22:292–299
- Giesekus H (1982) A simple constitutive equation for polymer fluids based on the concept of deformation-dependent tensorial mobility. *J Non-Newtonian Fluid Mech* 11:69–109
- Glicksman LR (1968) The dynamics of a heated free jet of variable viscosity liquid at low Reynolds number. *ASME J Fluids Eng* 90:343–354
- Greco F, Marrucci G (1993) Flow behavior of liquid crystalline polymers. *Adv Chem Phys* 86:331–401
- Henson GM, Cao D, Bechtel SE, Forest MG (1998) A thin-filament melt spinning model with radial resolution of temperature and stress. *J Rheol* 42:329–360
- Hoffman JD, Miller RL (1997) Kinetics of crystallization from the melt and chain folding in polyethylene fractions revisited: theory and experiment. *Polymer* 38:3151–3212
- Hütter M (2004) Crystallization under external pressure. *J Non-Newtonian Fluid Mech* 120:55–68
- Hütter M, Karlin IV, Öttinger HC (2003) Dynamic mean-field models from a nonequilibrium thermodynamic perspective. *Phys Rev E* 68:016115
- Hyunh BP, Tanner RI (1983) Study of the non-isothermal glass fiber drawing process. *Rheol Acta* 22:482–499
- Janeschitz-Kriegl H (2003) How to understand nucleation in crystallizing polymer melts under real processing conditions. *Colloid Polym Sci* 28:1157–1171
- Jeon YP, Cox CL (2008) Modeling of multifilament PET fiber melt-spinning. *J Appl Polym Sci* 110:2153–2163
- Johnson WA, Mehl RF (1939) Reaction kinetics in processes of nucleation and growth. *Trans AIME* 135:416–442
- Joo YL, Sun J, Smith MD, Armstrong RC, Brown RA, Ross RA (2002) Two-dimensional numerical analysis of non-isothermal melt spinning with and without phase transition. *J Non-Newtonian Fluid Mech* 102:37–70
- Kannan K, Rajagopal KR (2005) Simulation of fiber spinning including flow-induced crystallization. *J Rheol* 49:683–703
- Kase S, Matsuo T (1965) Studies of melt spinning. I. On the stability of melt spinning. *J Polym Sci A* 3:2541–2554
- Keller A, Kolnaar H (1998) Flow-induced orientation and structure formation, Chapter 4. In: Meijer HEH (ed) *Materials science and technology polymer processing*. VCH Verlagsgesellschaft mbH/Wiley, Weinheim, pp 187–268
- Kim KH, Aida R, Kang YA, Ikaga T, Ohkoski Y, Wataoka I, Urakawa H (2012) Effect of drawing stress on mesophase structure formation of poly(ethylene 2,6-naphthalene dicarboxylate) fiber just after the neck-drawing point. *Polymer* 53:4272–4279
- Kohler WH, McHugh AJ (2007) Sensitivity analysis of low-speed melt spinning of isotactic polypropylene. *Chem Eng Sci* 62:2690–2697
- Kohler WH, McHugh AJ (2008) Prediction of the influence of flow-enhanced crystallization on the dynamics of fiber spinning. *Polym Eng Sci* 2008:88–96
- Kohler WH, Shrikhande P, McHugh AJ (2005) Modeling melt spinning of PLA fibers. *J Macromol Sci B* 44:185–202
- Kolmogorov AN (1937) On the statistical theory of the crystallization of metals. *Bulletin of the Academy of Sciences of the USSR, Mathematical Series* 1:355–359
- Kulkarni JA, Beris AN (1998) A model for the necking phenomenon in high-speed fiber spinning based on flow-induced crystallization. *J Rheol* 42:971–994
- Landau LD, Lifshitz EM (1980a) *Statistical physics: part 1*. Pergamon, New York
- Landau LD, Lifshitz EM (1980b) *Statistical physics: part 2*. Pergamon, New York

- Lauritzen JI, Hoffman JD (1960) Theory of formation of polymer crystals with folded chains in dilute solution. *J Res Nat Bureau Stand* 64A:73–102
- Lauritzen JI, Hoffman JD (1973) Extension of theory of growth of chain folded polymer crystals to large undercoolings. *J Appl Phys* 44:4340–4352
- Leonov AI (1976) Nonequilibrium thermodynamics and rheology of viscoelastic polymer media. *Rheol Acta* 15:85–98
- Leonov AI (1987) On a class of constitutive equations for viscoelastic fluids. *J Non-Newtonian Fluid Mech* 25:1–59
- Leslie FM (1968) Some constitutive equations for liquid crystals. *Arch Rat Mech Anal* 28:265–283
- Leslie FM (1979) Theory of flow phenomena in liquid crystals. *Adv Liq Cryst* 4:1–81
- Lin YH (2010) *Polymer viscoelasticity*. World Scientific, Singapore
- Long D, Morse DC (2002) A Rouse-like model of liquid crystalline polymer melts: director dynamics and linear viscoelasticity. *J Rheol* 42:49–92
- Long Y, Shanks RA, Stachurski ZH (1995) Kinetics of polymer crystallisation. *Prog Polym Sci* 20:651–701
- Maffettone PL, Marrucci G, Mortier M, Moledaers P, Mewis J (1994) Dynamic characterization of liquid crystalline polymers under flow-aligning shear conditions. *J Chem Phys* 100:7736–7743
- Maffettone PL, Sonnet AM, Virga EG (2000) Shear-induced biaxiality in nematic polymers. *J Non-Newtonian Fluid Mech* 90:283–297
- Maier W, Saupe A (1958) Eine einfache molekulare theorie des nematischen kristallinflussigen zustandes. *Z Naturforsch A* 13:564
- Maier W, Saupe A (1959) Eine einfache molekular-statistische theorie der nematischen kristallinflussigen phase. 1. *Z Naturforsch A* 14:882–889
- Maier W, Saupe A (1960) Eine einfache molekular-statistische theorie der nematischen kristallinflussigen phase. 2. *Z Naturforsch A* 15:287–292
- Marrucci G (1991) Rheology of rodlike polymers in the nematic phase with tumbling or shear orientation. *Macromolecules* 24:4176–4182
- Marrucci G (1996) Dynamics of entanglements: a non-linear model consistent with the Cox-Merz rule. *J Non-Newtonian Fluid Mech* 62:679–689
- Marrucci G, Maffettone PL (1989) Description of the liquid-crystalline phase of rodlike polymers at high shear rates. *Macromolecules* 22:4076–4082
- Matovich MA, Pearson JRA (1969) Spinning a molten threadline: steady-state isothermal viscous flows. *Ind Chem Eng Fund* 8:512–520
- McHugh AJ, Doufas AK (2001a) Modeling flow-induced crystallization in fiber spinning. *Compos Appl Sci Manuf* 32:1059–1066
- McHugh AJ, Doufas AK (2001b) Simulations of fiber spinning and film blowing based on a molecular/continuum model for flow-induced crystallization. *Korea-Australia Rheol J* 13:1–12
- Mori N, Hamaguchi Y, Nakamura K (1997) Numerical simulation of the spinning flow of liquid crystalline polymers. *J Rheol* 41:1095–1104
- Nakamura K, Watanabe T, Katayama K, Amano T (1972) Some aspects of non-isothermal crystallization of polymers I. *J Appl Polym Sci* 16:1077–1091
- Onsager L (1949) The effects of shape on the interaction of colloidal particles. *Ann NY Acad Sci* 51:627–659
- Öttinger HC (1999) A thermodynamically admissible reptation model for fast flows of entangled polymers. *J Rheol* 43:1461–1493
- Pantani R, Coccorullo I, Speranza V, Titomanlio G (2005) Modeling the morphology evolution in the injection molding of thermoplastic polymers. *Prog Polym Sci* 30:1185–1222
- Pattamaprom C, Larson RG, van Dyke J (2000) Quantitative predictions of linear viscoelastic rheological properties of entangled polymers. *Rheol Acta* 39:517–531
- Pattamaprom C, Larson RG, Sirivat A (2008) Determining polymer molecular weight distributions from rheological properties using the dual-constraint model. *Rheol Acta* 47:689–700
- Pearson JRA (1985) *Mechanics of polymer processing*. Elsevier Applied Sciences, New York

- Peters GWM (2003) A computational model for processing of semicrystalline polymers: the effects of flow-induced crystallization, Chapter 17. In: Sommer J-U, Reiter G (eds) *Polymer crystallization. Lecture notes in physics*, vol 606. Springer, Berlin, pp 312–324
- Piorkowska E, Galeski A, Haudin JM (2006) Critical assessment of overall crystallization kinetics theories and predictions. *Prog Polym Sci* 31:549–575
- Ramalingam S, Armstrong RC (1993) Analysis of isothermal spinning of liquid crystalline polymers. *J Rheol* 37:1141–1169
- Ramos JI (1999) Asymptotic analysis of compound liquid jets at low Reynolds numbers. *Appl Math Comput* 100:223–240
- Ramos JI (2001a) Nonlinear dynamics of hollow, compound jets at low Reynolds numbers. *I J Eng Sci* 39:1289–1314
- Ramos JI (2001b) Drawing of annular liquid jets at low Reynolds numbers. *Comput Theor Polymer Sci* 11:429–443
- Ramos JI (2002) Compound liquid jets at low Reynolds numbers. *Polymer* 43:2889–2896
- Ramos JI (2005a) Modelling of liquid crystalline compound fibres. *Polymer* 46:12612–12625
- Ramos JI (2005b) Convection and radiation effects in hollow, compound optical fibers, I. *J Thermal Sci* 44:832–850
- Ramos JI (2006) Mathematical models of compound, polymer optical fibers, Chapter 7. In: Bregg RK (ed) *Polymer research developments*. Nova Science, New York, pp 127–185
- Ramos JI (2007) Thermal analysis of bicomponent amorphous fibres. *Appl Thermal Eng* 27:586–598
- Ramos JI (2014) Heat transfer processes in film casting of compressible polymers, Paper ICHTC15-9814. In: *Proceedings of the 15th international heat transfer conference, ICHMT Digital Library*. Begell House, New York
- Rao JJ, Rajagopal RK (2002a) A thermodynamic framework for the study of crystallization in polymers. *Z Angew Math Phys (ZAMP)* 53:365–406
- Rao JJ, Rajagopal RK (2002b) On the modeling of quiescent crystallization of polymer melts. *Polymer Eng Sci* 44:123–130
- Rienacker G, Hess S (1999) Orientational dynamics of nematic liquid crystals under shear flow. *Phys A* 267:294–321
- Rouse PE (1953) A theory of the linear viscoelastic properties of dilute solutions of coiling polymers. *J Chem Phys* 21:1271–1281
- Schneider W, Köppl A, Berger J (1988) Non-isothermal crystallization. *Int Polymer Process* 2:151–154
- Schultz JM (2001) *Polymer crystallization*. Oxford University Press, New York
- Schultz WW, Davis SH (1982) One-dimensional liquid fibers. *J Rheol* 26:331–345
- See H, Doi M, Larson RG (1990) The effect of steady flow fields on the isotropic-nematic phase transition of rigid rod-like polymers. *J Chem Phys* 92:792–800
- Shanlon JM, Schultz JM, Hsiao BS (2000) Structure development in the early stages of crystallization during melt spinning. *Polymer* 43:1873–1875
- Shrikhande P, Kohler WH, McHugh AJ (2006) A modified model and algorithm for flow-enhanced crystallization—application to fiber spinning. *J Appl Polym Sci* 100:3240–3254
- Strobl G (2006) Crystallization and melting of bulk polymers: new observations, conclusions and a thermodynamic scheme. *Prog Polym Sci* 31:398–442
- Sun J, Subbiah S, Marchal JM (2000) Numerical analysis of nonisothermal viscoelastic melt spinning with ongoing crystallization. *J Non-Newtonian Fluid Mech* 93:133–151
- Tanner RI (2002) A suspension model for low shear rate polymer solidification. *J Non-Newtonian Fluid Mech* 102:397–408
- Tanner RI (2003) On the flow of crystallizing polymers. I. Linear regime. *J Non-Newtonian Fluid Mech* 112:251–268
- Tanner RI, Qi F (2005) A comparison of some models for describing polymer crystallization at low deformation rates. *J Non-Newtonian Fluid Mech* 127:131–141

- Vaish N, Cinader DK, Burghardt WR, Zhou W, Kornfield JA (2001) Molecular orientation in quenched channel flow of a flow aligning main chain thermotropic liquid crystalline polymer. *Polymer* 42:10147–10153
- van Drongelen M, van Erp TB, Peters GWM (1988) Quantification of non-isothermal, multi-phase crystallization of isotactic polypropylene: the influence of the cooling rate and pressure. *Int Polymer Process* 2:151–154
- van Meerveld J (2005) Model development and validation of rheological and flow induced crystallization: models for entangled polymer melts. Ph.D. Thesis, ETH Zürich, Switzerland
- van Meerveld J, Hütter M, Peters GWM (2008) Continuum model for the simulation of fiber spinning, with quiescent and flow-induced crystallization. *J Non-Newtonian Fluid Mech* 150:177–195
- Vassilatos G, Schmelzer ER, Denn MM (1992) Issues concerning the rate of heat transfer from a spinline. *Int Polymer Process* 7:144–150
- Vrentas JS, Vrentas CM (2004) Theoretical aspects of fiber spinning. *J Appl Poly Sci* 93:986–993
- Wang Q (1997) Biaxial steady states and their stability in shear flows of liquid crystal polymers. *J Rheol* 41:943–970
- Zachmanoglou EC, Thoe DW (1986) Introduction to partial differential equations with applications. Dover, New York
- Zahorski S (1990) An alternative approach to non-isothermal melt spinning with axial and radial viscosity distributions. *J Non-Newtonian Fluid Mech* 36:71–83
- Zahorski S (1993) Necking in non-isothermal high-speed spinning with radial velocity variation. *J Non-Newtonian Fluid Mech* 50:65–77
- Zheng R, Kennedy PK (2004) A model for post-flow induced crystallization: general equations and predictions. *J Rheol* 48:823–842
- Zhou H, Forest MG, Wang Q (2000) Thermotropic liquid crystalline fibers. *SIAM J Appl Math* 60:1177–1204
- Ziabicki A (1974) Theoretical analysis of oriented and non isothermal crystallization. *Colloid Polym Sci* 252:207–221
- Ziabicki A (1976) Fundamentals of fibre formation. Wiley, New York
- Ziabicki A, Jarecki L (2007) Crystallization-controlled limitations of melt spinning. *J Appl Polym Sci* 105:215–223
- Ziabicki A, Jarecki L, Sorrentino A (2013) The role of flow-induced crystallization in melt spinning. *e-Polymers* 4:823–836
- Zuidema H (2000) Flow-induced crystallization of polymers. Ph.D. Thesis, University of Technology Eindhoven, The Netherlands
- Zuidema H, Peters GWM, Meijer HEH (2001) Development and validation of a recoverable strain-based model for flow-induced crystallization of polymers. *Macromol Theory Simul* 10:447–460

Chapter 15

Relationship Between Composition, Structure and Dynamics of Main-Chain Liquid Crystalline Polymers with Biphenyl Mesogens

Aránzazu Martínez-Gómez, Mario Encinar, Juan P. Fernández-Blázquez, Ramón G. Rubio, and Ernesto Pérez

15.1 Introduction

Aromatic main-chain polyesters have been extensively investigated and represent the most important class of liquid crystalline polymers (LCPs). They have been of interest as engineering plastics due to the combination of some properties such as their low density, chemical resistance, dimensional stability, exceptional mechanical properties and low gas permeability. However, all-aromatic polyesters present the inconvenience of poor solubilities and very high transition temperatures, often in the range of polymer degradation. Therefore, in the last decades considerable effort was made to improve the processability of these polymers by modification of their chemical structure and/or molecular architecture. A very usual strategy is the incorporation of flexible spacer segments between mesogenic units. In this way,

A. Martínez-Gómez (✉) • E. Pérez
Instituto de Ciencia y Tecnología de Polímeros, ICTP-CSIC, Juan de la Cierva 3, 28006 Madrid, Spain
e-mail: aranmg@ictp.csic.es; ernestop@ictp.csic.es

M. Encinar
Instituto de Microelectrónica de Madrid, IMM-CSIC, Isaac Newton 8 (PTM), Tres Cantos, 28760 Madrid, Spain
e-mail: encinar@ucm.es

J.P. Fernández-Blázquez
IMDEA Materials Institute, Eric Kandel 2, Getafe, 28906 Madrid, Spain
e-mail: juanpedro.fernandez@imdea.org

R.G. Rubio
Departamento de Química Física I, Facultad de Química, Universidad Complutense, 28040 Madrid, Spain
e-mail: rgrubio@quim.ucm.es

thermotropic semiflexible polymers with rather accessible transition temperatures can be built by an alternating arrangement of flexible spacers and rigid mesogenic groups. In general, the liquid crystalline behavior of these semiflexible polymers hinges on the combination of the inherent anisotropic molecular interaction of the mesogenic units and the relative position of these units in the macromolecular chain, which is dictated by the chemical structure and the even/odd character of the flexible spacers connecting them.

The influence of the nature of the spacer on the phase behavior of semiflexible polymers with biphenyl mesogenic groups has been subject of many investigations (Meurisse et al. 1981; Jackson and Morris 1990; Pérez et al. 1992, 1997, 2000, 2003a, b; Watanabe et al. 1992, 1997; Fernández-Blázquez et al. 2007b; Loman et al. 1995; Tokita et al. 1998; Osada et al. 2004; Bello et al. 1990, 2001b; Martínez-Gómez et al. 2004, 2008, 2010; Ezquerro et al. 2005; Encinar et al. 2012) showing the ability of these polymers to exhibit low-ordered smectic mesophases (SmA, SmCA or SmC), which may be briefly described as lamellar structures with a disordered lateral packing of the molecules. As depicted in Fig. 15.1, both mesogens and molecular axes are perpendicular to the smectic layer planes in the SmA mesophase (orthogonal mesophase). However, although the average molecular axes are also perpendicular to the smectic planes in the SmCA structure, the mesogens are inclined in relation to the normal to the smectic planes, with opposite tilt direction for mesogens located in adjacent layers. On the other hand, the SmC structure is a tilted mesophase. The angle of inclination between the molecular axes and the normal to the smectic plane is temperature-dependent.

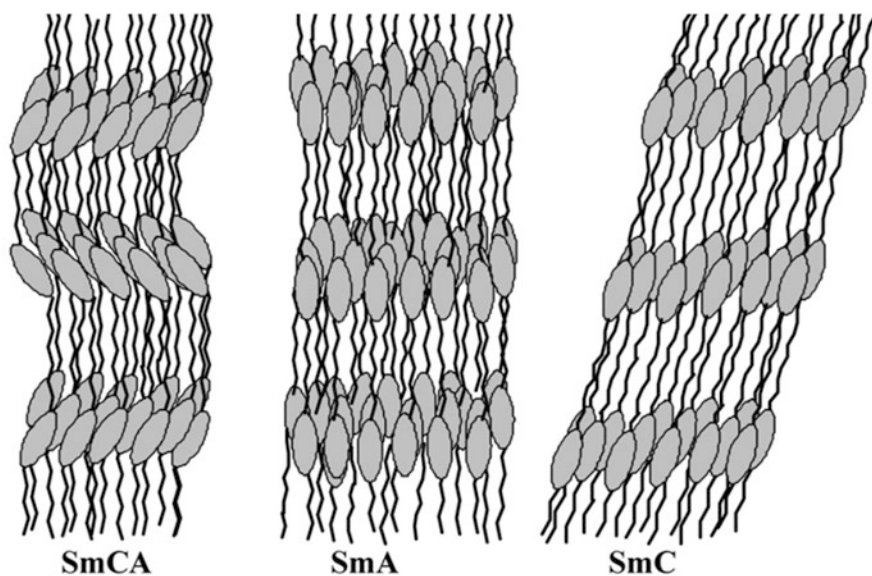


Fig. 15.1 The smectic mesophases that may be formed in semiflexible polymers with biphenyl mesogenic groups

It has been proved that the transition temperatures, mesophase structure and rate of crystallization (mesophase–crystal transformation) can be controlled with suitable changes in the structure of the flexible spacer, so that polymers with stable mesophases at room temperature can be prepared. Furthermore, if the structure of the flexible spacer is adequately chosen, the liquid–crystallization can be slowed down, and sometimes it is possible to quench the amorphous state by cooling the isotropic melt at not very high rates. These facts, tailored phase behavior and possibility of freezing the glassy states of both the amorphous and the liquid crystalline phases, makes these polymers ideal model systems to study the general behavior of main-chain liquid crystalline polymers (MCLCP).

In this chapter, the preparation and thermotropic behavior of main-chain semiflexible polyesters based on biphenyl mesogenic units are reviewed. The influence of the polymer chemical structure on the mesomorphic properties is analyzed and some relationships between chemical, structure and liquid crystalline properties are established.

15.2 Preparation of Main-Chain Semiflexible Polyesters with Biphenyl Mesogenic Units

The representative structures of main-chain semiflexible polyesters derived from the biphenyl mesogenic unit are shown in Table 15.1. The preparation of these polymers can be performed by a two-step melt polycondensation in the presence of titanium (IV) isopropoxide as catalyst. The first step is the transesterification at around 200 °C for 20–24 h under nitrogen atmosphere. The second

Table 15.1 Structures of semiflexible polyesters derived from biphenyl mesogenic unit

	Structure ^a
Polyesters (polybibenzoates)	
Copolyesters	
Polyetheresters	

^aR = aliphatic segments; Ar = Non mesogenic aromatic group

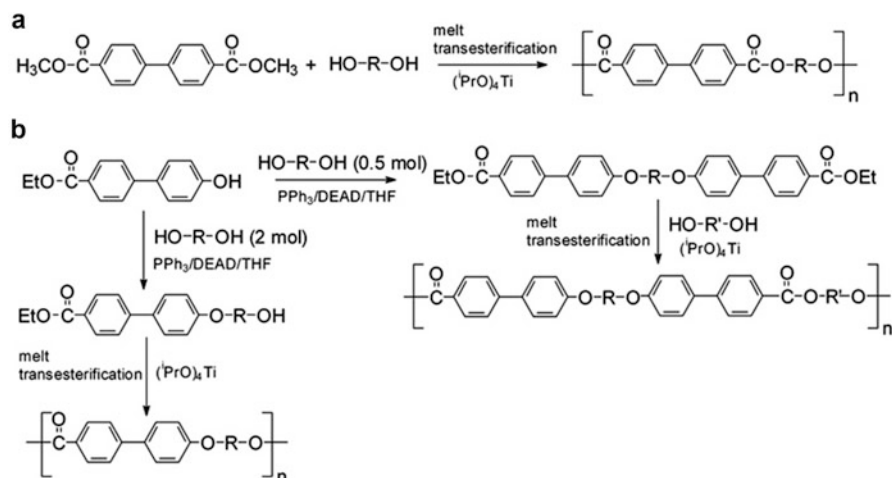


Fig. 15.2 Synthesis of semiflexible polybibenzoates and polyetheresters

polycondensation reaction is performed at temperatures up to 250 °C under vacuum, to provide a high molar mass polymer. Polyesters, commonly called polybibenzoates, and copolyesters can be directly prepared from the commercially available dimethyl-4,4'-biphenyl-dicarboxylate diester and a glycol. On the other hand, polyetheresters, where ester and ether alternate as linking groups between the mesogen and the spacer along the polymeric chain, are prepared from a precursor containing the biphenyl mesogenic group. This precursor is previously synthesized by reaction of ethyl-4-hydroxybiphenyl-4'-carboxylate with a bromoalkanol in the presence of potassium carbonate (Nakata and Watanabe 1994) or by reaction with a glycol under Mitsunobu conditions (Martínez-Gómez et al. 2006; Fernández-Blázquez et al. 2004; del Campo et al. 2002). In the latter, two different precursors, with link sequence ester-ether or ester-ether-ether-ester, can be obtained depending on the stoichiometry (Fig. 15.2b).

15.2.1 Diols Used as Flexible Spacers

Several glycols with different chemical structures and lengths have been employed as flexible spacers. Some of them are commercially available, such as all-methylene glycols, diethylene glycol, triethylene glycol and glycols with methyl substituents as for example 1-methyl-1,4-butanediol, 2-methyl-1,3-propanediol and 3-methyl-1,5-pentanediol. Non-commercial glycols bearing ether groups can be synthesized by protonic acid catalyzed ring-opening reaction of a cyclic ether (oxirane or oxetane) with a glycol (Bello et al. 2001b; Martínez-Gómez et al. 2004, 2008; Encinar et al. 2012). The polymerization of the cyclic ether is suppressed by using a

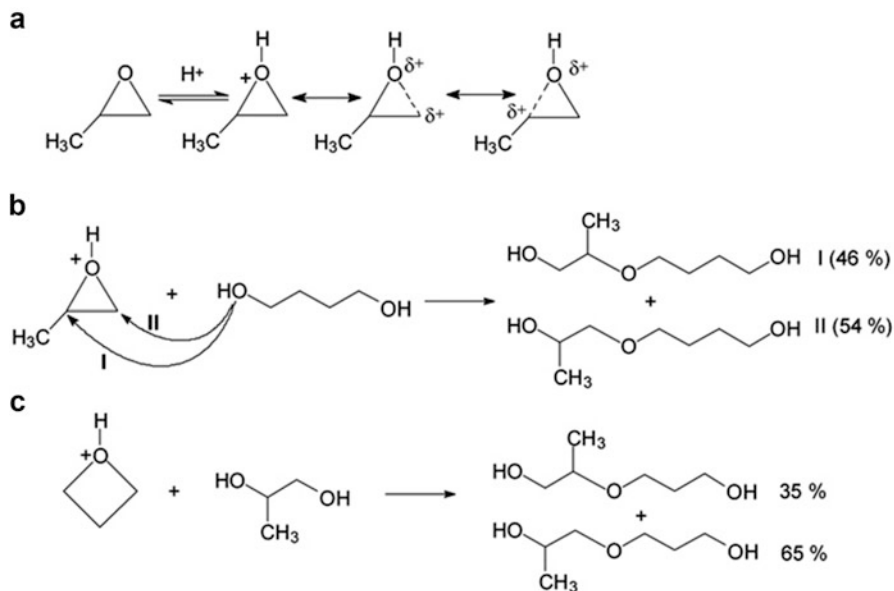


Fig. 15.3 (a) Pseudo-carbocations that can be postulated for protonated propylene oxide. (b) The two possible pathways of ring opening of protonated propylene oxide by addition of 1,4-butanediol. (c) Mixture of ether glycols obtained in the addition of 1,2-propanediol to protonated oxetane

large excess of glycol and maintaining a low instantaneous concentration of oxirane or oxetane in the reaction mixture. Under these conditions, the reaction of the protonated monomer with the glycol is greatly favored and, therefore, the desired ether-glycol dimer is mainly obtained. Particularly interesting are those glycols bearing an ether group and a methyl substituent both in an asymmetric position, leading to random copolymer structures with liquid crystalline phases extending over wide temperature regions.

The stabilization of the mesophase is more noticeable when a mixture of isomer glycols is used as spacer. Figure 15.3 shows, as an example, the chemical structures and proportions of the isomer glycols obtained in the reaction of propylene oxide with 1,4-butanediol. Because propylene oxide is an asymmetrically substituted oxirane, two pathways in the opening of the ring are possible, and therefore, a mixture of the isomer ether-glycols I and II are obtained (Martínez-Gómez et al. 2008). The composition of this mixture is I = 46 %, II = 54 %, which indicates no significant preference for either of the two directions of the ring-opening. The carbon-oxygen bonds are considerably polarized in the protonated oxirane and two pseudo-carbocations can be formulated. Although the reaction with the unsubstituted carbon atom is the more favorable steric situation, the inductive effect of the methyl group stabilizes the partial positive charge on the substituted carbon, counteracting the steric hindrance.

In the case of ether glycols obtained by reaction of oxetane with a branched glycol, owing to the differences in reactivity of the primary versus secondary alcoholic groups, isomer mixtures enriched in the product derived from the addition of the more reactive primary alcoholic group are obtained (Bello et al. 2001b) (Fig. 15.3c).

15.3 Phase Behavior of Semiflexible Polyesters with Biphenyl Mesogenic Units

15.3.1 *Techniques for the Analysis of the Phase Behavior*

The analysis of the phase behavior of LCPs is sometimes complicated because these polymers usually exhibit a sequence of mesophases with different degree of order (polymesomorphism) and/or the mesophase is transformed into a three-dimensional crystal (polymorphism). The combination of differential scanning calorimetry (DSC) and X-ray diffraction techniques is very useful for the study of the thermotropic behavior of LCPs. Moreover, taking advantage of the high intensity of synchrotron radiation, very short acquisition times can be used, so that the experiments can be carried out under real time conditions, and temperature programs comparable to those employed in DSC can be imposed to the samples. Therefore, both aspects, thermal transitions and phase structure, can be determined by real-time variable-temperature diffraction experiments using synchrotron radiation (Pérez et al. 2009).

Additional information about the phase behavior can be achieved by polarized optical microscopy. Unfortunately, microscopic observations, which are so revealing in low molar mass liquid crystal, are not always helpful in dealing with thermotropic main chain polymers. Polymers with high or relatively high molecular weights typically develop textures that are not easily identifiable.

15.3.2 *Polybibenzoates*

Many works have been published about the phase behavior of semiflexible polybibenzoates, showing that the thermotropic behavior is strongly conditioned by the nature (chemical structure and even/odd character) of the flexible spacer. In these studies, different aliphatic spacers of diverse structures and lengths have been used, which can be classified in three main categories: linear all-methylene, oxyalkylene and branched spacers. Examples of structures of flexible spacers in polybibenzoates and the relevant phase behavior data are collected in Table 15.2. Most polybibenzoates reported in the literature exhibit a low-ordered smectic mesophase (SmA, SmCA or SmC) and only some branched polymers derived

Table 15.2 Phase sequence, glass transition temperature of the liquid crystalline state (T_g^{LC}) and isotropization temperature (T_i) of semiflexible polybibenzoates

Polybibenzoate	Spacer	Phase sequence ^a	T_g^{LC} (°C)	T_i (°C)	References
PB2	(CH ₂) ₂	I-SmA-CR		360	Meurisse et al. (1981); Jackson and Morris (1990); Pérez et al. (1997)
PB3	(CH ₂) ₃	I-SmA-CR		274	Jackson and Morris (1990); Pérez et al. (1997); Watanabe et al. (1997)
BB32	CH ₂ CH(CH ₃)CH ₂	I-SmA	65	174	Fernández-Blázquez et al. (2007b)
PB4	(CH ₂) ₄	I 289 SmA 240 CR		298	Pérez et al. (1997); Watanabe et al. (1997); Loman et al. (1995)
BB4(1-Me)	CH(CH ₃)CH ₂ CH ₂ CH ₂	I 148 SmC		162	Watanabe et al. (1992, 1997)
BB4(2-Me)	CH ₂ CH(CH ₃)CH ₂ CH ₂	I 210N 185 SmC 139 CR		218	Watanabe et al. (1992, 1997)
BB4(2,3-diMe)	CH ₂ CH(CH ₃)CH(CH ₃)CH ₂	I 182N 127 CR		200	Watanabe et al. (1992, 1997)
BB4(2,2-diMe)	CH ₂ C(CH ₃) ₂ CH ₂ CH ₂	I 162N 124 CR		170	Watanabe et al. (1992, 1997)
PB5	(CH ₂) ₅	I 196 SmCA 86 CR		212	Pérez et al. (1997); Watanabe et al. (1997); Tokita et al. (1998)
BB5(3-Me)	CH ₂ CH ₂ CH(CH ₃)CH ₂ CH ₂	I 123 SmCA	31	149	Osada et al. (2004)
PDEB	CH ₂ CH ₂ OCH ₂ CH ₂	I 184 SmCA	50	201	Pérez et al. (2003a)
PB6	(CH ₂) ₆	I 223 SmA 154 CR		240	Pérez et al. (1997); Watanabe et al. (1997); Tokita et al. (1998)
P6MeB	CH ₂ CH ₂ CH(CH ₃)CH ₂ CH ₂	I 138 SmA 124 SmC 61 CR	24	154	Pérez et al. (2000)
PETB	CH ₂ CH ₂ CH ₂ OCH ₂ CH ₂	I 178 SmC	25	199	Bello et al. (2001b)
PTPB	CH ₂ CH ₂ CH ₂ OCH(CH ₃)CH ₂ 35 % CH ₂ CH ₂ CH ₂ OCH ₂ CH(CH ₃) 65 %	I 128 SmA	33	143	Bello et al. (2001b)
PB7	(CH ₂) ₇	I 142 SmCA 100 CR		168	Pérez et al. (1997, 2003b); Watanabe et al. (1997)

(continued)

Table 15.2 (continued)

	Spacer	Phase sequence ^a	T _g ^{LC} (°C)	T _i (°C)	References
Polybibenzoate					
PDTMB	CH ₂ CH ₂ CH ₂ OCH ₂ CH ₂ CH ₂	I 154 SmCA	17	172	Pérez et al. (1997); Bello et al. (1990)
PTMTB	CH ₂ CH ₂ CH ₂ OCH ₂ CH(CH ₃)CH ₂	I 75 SmCA	20	105	Bello et al. (2001b)
PPO4B	CH ₂ CH ₂ CH ₂ OCH(CH ₃)CH ₂ 46 % CH ₂ CH ₂ CH ₂ OCH ₂ CH(CH ₃) 54 %	I 63 SmCA	20	85	Martínez-Gómez et al. (2008)
C3 1DTB	CH ₂ CH ₂ CH ₂ OCH ₂ CH(CH ₃) 67 % CH ₂ CH ₂ CH ₂ OCH(CH ₃)CH ₂ CH ₂ 33 %	I-SmCA	17	65	Ezquerro et al. (2005)
PB8	(CH ₂) ₈	I 168 SmA 142 CR		202	Pérez et al. (1992)
P3O4B	CH ₂ CH ₂ CH ₂ OCH ₂ CH ₂ CH ₂ CH ₂	I 147 SmA 141 SmC 52 CR		160	Martínez-Gómez et al. (2004)
PTEB	CH ₂ CH ₂ OCH ₂ CH ₂ OCH ₂ CH ₂	I 106 SmA 40 SmC	11	115	Pérez et al. (1992); Martínez-Gómez et al. (2010)
PTEMeB	CH ₂ CH ₂ OCH ₂ CH ₂ OCH(CH ₃)CH ₂ 60 % CH ₂ CH ₂ OCH ₂ CH ₂ OCH ₂ CH(CH ₃) 40 %	Amorphous	15	54	Encinar et al. (2012)
PB9	(CH ₂) ₉	I 115 SmCA 111 CR		154	Pérez et al. (1997); Watanabe et al. (1997); Tokita et al. (1998)
PDETB	CH ₂ CH ₂ CH ₂ OCH ₂ CH ₂ OCH ₂ CH ₂	I 82 SmCA	-1.7	97	Bello et al. (2001b)

^aOn cooling from the melt at DSC rates

from poly(tetramethylene glycol *p,p'*-bibenzoate), PB4, have been reported to be nematic. Notice that the liquid crystalline state of polybibenzoates often transforms into a crystalline phase upon cooling.

As usual in main-chain liquid crystalline semiflexible polymers (Chiellini and Laus 1998), the melting (T_m) and isotropization (T_i) temperatures of polybibenzoates decrease significantly with increasing length of the flexible spacer, and T_i normally decreases in a zig-zag fashion in homologous series in which the spacer length regularly increases (Pérez et al. 1997; Watanabe et al. 1997). This is the so-called odd-even effect, where T_i tends to be higher for the polymers with an even spacer, but this oscillation is attenuated on ascending the series. This odd-even oscillation is also found for the transition entropies and for the spacing of the smectic layer. The explanation given for this effect is based on the differences in the packing arrangement of the polymer chains between even and odd members. Thus, a fairly extended conformation is produced, with the mesogenic groups approximately parallel to the chain axis, for even members. On the contrary, the valence angles for the odd members force the chain to adopt a less extended arrangement, and the mesogens form an angle of about 30° with respect to the chain axis direction (about 60° between two successive mesogens). In a real system, however, it may be expected that more than a single conformation could intervene in the formation of the smectic layers compatible with the relatively low requirements of the mesophase order. Those different packing arrangements are also responsible for the different type of mesophase structure formed: polybibenzoates with an even spacer show a smectic A mesophase while for odd members a smectic CA mesophase is found.

For polybibenzoates incorporating linear all-methylene spacers $(CH_2)_m$, the mesophase is only stable at temperatures just below its formation and a rapid transformation into a three-dimensional crystalline structure is produced on cooling. The melting of this crystal is monotropic for those polymers with $m \geq 7$, while for the lower members the melting is enantiotropic and the mesophase is also observable on heating because the crystal is transformed into the mesophase prior to its isotropization.

The insertion of side methyl groups in the spacer results in a decrease of the structural and geometrical symmetry of the macromolecules, and a lowering of the interchain interactions. As a result, the tendency of the elongated LCP chains to build a supramolecular structure is reduced. Thus, a diminution of the transition temperatures with respect to the unsubstituted polymer is usually observed, accompanied by a decrease in the tendency to form smectic mesophases. As it can be observed in Table 15.2, polybibenzoates with methyl groups in the spacer display transition temperatures considerably lower than those found for their analogous unsubstituted polymers: a decrease of 100, 136, 63 and 86° is produced by branching a methyl group in poly(trimethylene glycol *p,p'*-bibenzoate), poly(tetramethylene glycol *p,p'*-bibenzoate), poly(pentamethylene glycol *p,p'*-bibenzoate) and poly(hexamethylene glycol *p,p'*-bibenzoate) polymers, respectively. Furthermore, it is noteworthy that when only one methyl group is present in the spacer, the formation of the smectic mesophase is preserved in all the

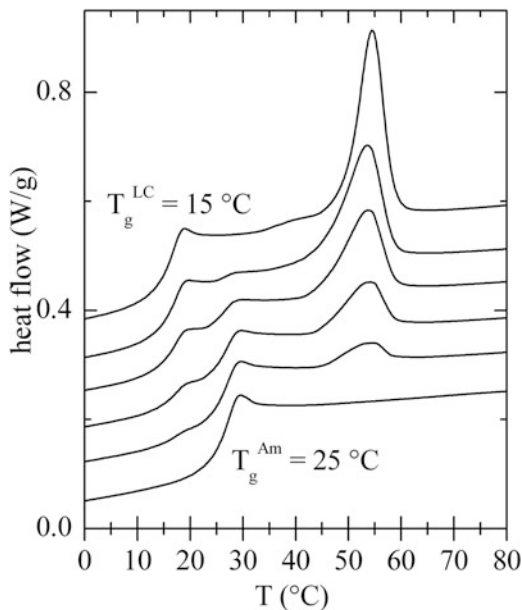
polymers investigated. However, for polymers with two methyl groups in the spacer, as is the case of BB4(2,3-diMe) or BB4(2,2-diMe), the smectic mesophase is replaced by the nematic mesophase. Thus, the effective accommodation of two lateral methyl groups into the mesophase structure is attained by packing the molecules in a nematic structure, which has only orientational order. Another general behavior of branched polybibenzoates is their tendency to alter the orthogonal SmA to the tilted SmC. The SmC mesophase is especially interesting in those cases where the branched spacer incorporates chiral carbons, since it may develop ferroelectric properties.

The steric hindrance effect of methyl groups is more pronounced in the packing efficiency for crystal structures, and, consequently, polymers with a very low, if any, melting temperature are observed, thus leading to mesophases extending over wide temperature regions. Polybibenzoates with short branched spacers, as BB32, BB4(1-Me) and BB5(3-Me), develop a stable mesophase. However, for polymers with longer spacers, as is the case of P6MeB, the accommodation of the side methyl groups is easier and a highly ordered structure can be obtained.

Comparing with the analogous polymers containing polymethylene spacers, two major effects are observed when oxyalkylene spacers are used: the reduction of the transition temperatures and a considerable decrease of the transformation of the mesophase into a more ordered phase. Thus, the mesophase of these polymers is often stable for a considerable time at room temperature, although the crystallization can be reached by annealing the polymer for long times at temperatures above the glass transition. The reduction of the transition temperatures increases as the number of ether groups present in the spacer increases. For instance, the isotropization temperature changes from 202 °C for poly(octamethylene glycol *p*, *p'*-bibenzoate), P8MB, to 160 °C for polybibenzoate P3O4B which has only one ether group in the spacer, and to only 115 °C for PTEB, with two ether groups. Regarding the type of mesophase, the parity of the spacer, as it happens with polybibenzoates with all-methylene spacers, is clearly reflected on the structure of the mesophase formed, being of the type SmCA for odd spacers (PDEB, PDTMB, PDET B) and SmA for even spacer (P3O4B, PTEB). Moreover, the presence of the ether groups in the even spacers seems to favor the transformation from the orthogonal SmA mesophase to the tilted SmC mesophase.

Asymmetric spacers bearing both an ether group and a methyl substituent are particularly interesting because they lead to copolymer structures forming stable mesophases and, hence, problems associated with the formation of crystalline structures are completely avoided. A more irregular macromolecular structure can be obtained by using a mixture of isomer spacers, so that the liquid-crystallization is also slowed down, making possible the obtainment of the amorphous glass state for these systems. One example is the polybibenzoate PPO4B. Its irregular chemical structure, together with the vicinity of the isotropization temperature, $T_i = 85$ °C, and the amorphous glass transition, $T_g = 32$ °C, allows the freezing of the amorphous state by a rapid quenching of the isotropic melt in liquid nitrogen. However, when the amorphous sample is heated just above the glass transition, the liquid crystalline state is rapidly developed.

Fig. 15.4 DSC heating curves at 20 °C/min corresponding to PTEMeB after annealing at 30 °C for different times (from bottom to top: 0, 60, 75, 90, 105 and 2400 min)



Another interesting polybenzoate of this type is PTEMeB. This polymer has the advantage that the amorphous glass can be easily quenched from the melt. In fact, the liquid crystalline state is formed at rather low rates, in such a way that it is not observed at the usual scanning rates in the calorimeter. Therefore, the DSC curves during a cooling-heating cycle show only the change in the specific heat associated with the amorphous glass transition (at around 25 °C on heating). However, when the sample is annealed above the glass transition, a low-ordered smectic mesophase is developed as deduced from DSC and X-ray diffraction experiments. As it is seen in Fig. 15.4, the extent of the amorphous-mesophase transformation achieved during the annealing of PTEMeB is reflected in the glass transition region. Two separated steps, centred at 15 °C and 25 °C, are differentiated in the DSC curves, which intensities (increment of specific heat) depend on the annealing time. At annealing time equal to zero the glass transition at 25 °C, associated with the amorphous phase of PTEMeB, is only observed. The intensity of this step diminishes with annealing time, in other words, when the content of the mesophase formed increases. At the same time, a new step at 15 °C appears and grows to be the only one observed at high annealing times, together with an endotherm at 54 °C corresponding to the isotropization of the mesophase.

15.3.3 Copolyesters

Copolymerization is a widely used strategy to extend the structure-property spectrum of polymers, besides to reduce costs. Moreover, it is another method of lowering the transition temperatures. Several studies have been published on

copolyesters of bibenzoate with non-mesogenic units. For example, it has been reported that the incorporation of bibenzoate groups to poly(ethylene terephthalate) enhanced the glass transition temperature, and the mechanical and gas barrier properties. However, no evidence of liquid crystallinity was found in these copolymers, although a “frustrated” liquid crystalline structure was proposed (Ma et al. 2002; Liu et al. 2003; Schiraldi et al. 2001). When larger spacers are employed, liquid crystalline structures are more easily developed. Accordingly, poly(diethylene isophthalate-co-4,4'-bibenzoate) copolymers with 20 mol % isophthalate or less exhibit liquid crystalline character (Hu et al. 2004). However, the nonlinear isophthalate comonomer is rather effective in destroying the liquid crystalline order. Less disrupting are the terephthalate units, and when heptamethylene spacer is used, a considerable amount (up to around 40–50 mol %) of terephthalate groups can be copolymerized with bibenzoate units, yet exhibiting liquid crystalline properties (Pérez-Manzano et al. 2006).

More recently, the incorporation of non-mesogenic 2,6-naphthalate units to poly(triethylene glycol *p,p'*-bibenzoate), PTEB, has been investigated (Martínez-Gómez et al. 2011). Copolymers with up to 30 % naphthalate content have the ability to exhibit smectic liquid crystalline phases, which are very stable and do not transform into crystalline structures. Moreover, the isotropization temperatures of these copolyesters of naphthalate are easily accessible (100–70 °C) and the phase behavior can be tailored by an appropriate selection of the comonomer composition. The sequence of phases isotropic-SmA-SmC is observed in polymers with naphthalate content below about 10 mol %, while the transition SmA-SmC is lost for comonomer contents above 10 %, and only the SmA mesophase is found for compositions between 10 and 30 mol %. Moreover, the formation of the liquid crystalline state is considerably slowed down as the naphthalate content increases, so that the copolymer with 30 % content can be easily quenched down into the amorphous glass.

Another family of random copolyesters based on the biphenyl group is that obtained by polymerization of bibenzoate with two different alkane diols (Watanabe et al. 1997). It has been found that the incorporation of all-methylene spacers with the same parity, even or odd, does not significantly disrupt the structure of the mesophase formed, SmA or SmCA, respectively. The isotropization temperature of the smectic mesophase falls on a smooth curve close to that representing the arithmetic average of the homopolymer temperatures. Moreover, the crystal-mesophase transition temperature decreases, so that the mesophase is exhibited in a wide temperature region. However, the smectic phase becomes unstable and alters to the nematic phase when it is forced to accommodate flexible spacers of very different lengths. On the other hand, when spacers of comparable length but different even/odd nature are copolymerized, as for example hexamethylene and pentamethylene segments, the smectic mesophase is observed in the entire composition range. However, a eutectic behavior is found for the isotropization temperatures of the mesophases. In these systems, the two repeating units differing in the parity are not compliant with the packing requirements of the

crystalline state, thus a depression of the crystallization tendency is observed when the second component is added.

Copolymers with two different spacers sequenced in a regularly alternate fashion may develop very interesting smectic structures (Nakata and Watanabe 1997). If the two spacers are sterically incompatible, and there is sufficient lateral attraction between identical spacers of adjacent polymer chains, segregation into a bilayer smectic phase may occur. When two odd-numbered spacers are used, this bilayer structure is especially interesting since it would be ferroelectric even in non-chiral systems.

15.3.4 Polyetheresters

Polyetheresters, where both ester and ether groups are used as linking units between the biphenyl mesogens and the spacers, represent an alternative class of semiflexible main-chain LC polymers based on the biphenyl group. However, these systems have been less investigated, probably because their preparation involves a more complicated synthetic route, and only a few examples are described in the literature (Nakata and Watanabe 1994; Martínez-Gómez et al. 2006; Fernández-Blázquez et al. 2004; del Campo et al. 2002). Then, although it is not possible to establish conclusive correlations between the spacer structure and the thermotropic properties of these systems, the following statements can be concluded. All the polyetheresters reported in the literature develop low-ordered smectic mesophases. The ether linkage produces similar odd-even effect to the ester in polyester. When the spacer is a linear all-methylene segment, as it happens with polybibenzoates, the mesophase is rapidly transformed into a more ordered phase upon cooling (Nakata and Watanabe 1994). This transformation is inhibited in polyetheresters with methyl-substituted trimethylene spacers. Indeed, the rate of mesophase formation is also slowed down in such a way that the isotropic melt can be easily quenched into the glassy amorphous state (Fernández-Blázquez et al. 2004; del Campo et al. 2002).

15.4 Dynamic Mechanical Behavior in Liquid Crystal Polymers with Biphenyl Mesogens

Dynamic mechanical analysis (DMA) is a mechanical test referring to the response of a material as it is subjected to a periodic force. The study of this response leads to know the viscoelastic behavior of the material, because the elastic response can be separated from the viscous response through their respective moduli: storage (E') and loss (E''), as well as the damping factor ($\tan \delta$) that is the ratio between both moduli ($\tan \delta = E''/E'$). This fact has caused that DMA was a technique widely used

in the study of molecular relaxation processes taking place in polymers (Duncan 2008). The most accurate type of measurement in DMA is to heat the sample in a temperature scan at different frequencies, because the relaxation processes are function of the frequency. The range of frequencies, despite being narrow (around four decades), is sufficient for studying the shifting of damping maxima to higher temperatures with increasing frequencies. The secondary relaxations obey the Arrhenius law for frequency-temperature shift.

$$\ln f = \ln f_0 \exp \frac{-\Delta H}{RT}$$

where ΔH is the apparent activation energy of the motional process. The main relaxation (glass transition) is ruled by the Williams, Landel, and Ferry relationship.

Most of the main chain liquid crystal polymers with biphenyl mesogens analyzed by DMA are polybibenzoates with all-methylene (Pereña et al. 1991; Pérez et al. 1994) or oxymethylene spacers (Benavente et al. 1993), copolymers combining both kind of spacers (Benavente et al. 1996), and copolymers with non-mesogenic aromatic moieties as isophthalate (Hu et al. 2004), but in all cases without lateral groups. In general, these polymers display three mechanical relaxations, called α , β and γ in order of decreasing temperature (Pérez et al. 1997).

In all of these MCLCP, α relaxation is the main relaxation and is considered the glass transition owing to the high $\tan \delta$ maximum value of the relaxation and the corresponding sharp decrease of the storage modulus. The apparent activation energy of the process is higher than 400 kJ mol^{-1} , confirming the assignation of this relaxation as the glass transition of these polymers (Pérez et al. 1997). Therefore the α relaxation temperature depends on the flexibility of the polymer chain, and in the case of MCLCP is directly dependent on spacer flexibility. Particularly in polybibenzoates with all-methylene (Pereña et al. 1991) or oxymethylene spacers (Benavente et al. 1993), longer spacers lead to lower temperatures, but the odd-even effect also has to be considered (Pérez et al. 1997). The presence of ether groups in the spacer, not only slows down the crystallization from the mesophase, but also decreases the α relaxation temperature (as it is observed in the case of PB8 and PTEB (Benavente et al. 1996) whose temperatures are 45 and 0 °C respectively), since spacer flexibility is increased. Moreover, the intensity of the α peak, considering $\tan \delta$ values, increases with the length of the spacer.

The β relaxation for MCLCP takes place in the temperature interval between -80 and -50 °C. This relaxation has a complex origin, is characteristic of polyesters, and originates from movements of several groups as phenyl and carboxyl groups. In fact, this relaxation in aromatic polyester has been reported to be composed of two overlapped peaks (Diaz-Calleja et al. 1986, 1989). Similarly to the α relaxation, the temperature location of β relaxation for polybibenzoates depends on the spacer length, decreasing with the length increase. This fact confirms the complex character of this relaxation and the possibility of different steric hindrances of the reorganizational motions of the carboxyl and phenylene groups depending on the spacer length, so that the apparent activation energy of this

relaxation increases slightly with the length of the spacer in values around 100 kJ mol^{-1} (Pérez et al. 1997).

At the lowest temperatures the γ relaxation is found, overlapping with β relaxation, and coinciding in location and activation energy with the typical γ relaxation of polyethylene (Heaton et al. 1996). The γ relaxation in polyethylene was firstly attributed to crankshaft movements of polymethylene chains (Schatzki 1966). Though a lot of work concerning this relaxation in polyethylene has been done, there remains no clear consensus regarding the details of the underlying motional process (Boyd 1985). There is, however, a body of opinions which support one or more of the various models for restricted conformational transitions as kink formation, inversion and migration (Schatzki 1966; Boyd 1975; Boyd and Breitling 1974). Molecular dynamics simulations have been a powerful tool to corroborate the just mentioned nature of these conformational motions underlying this relaxation (Heaton et al. 1996; Boyd et al. 1994; Jin and Boyd 1998). This type of motion requires chains containing sequences of three or more methylenic units. Regardless of the length and even nature, in case of oxyethylene spacers, there is no significant variation in location, intensity, and activation energy of the relaxation. This fact suggests the same type of motion for all-methylene or oxymethylene spacers (Pérez et al. 1997).

As it was mentioned above, most of the MCLCP analyzed by DMA are polybenzoates with linear spacers, spite of the important influence of substituent groups in the spacer. Previous sections show that branched spacers reduces the crystal formation as well as the crystallization or liquid crystallization rate. Combining this effect with short spacers (three methylenes) in a polyetherester, as was described in Sect. 15.3.4, a system is obtained with high glass transition temperature ($90 \text{ }^\circ\text{C}$) that develops a low order mesophase (SmCA) with very slow formation rate (Fernández-Blázquez et al. 2004). These thermal and structural properties let this polymer, named PH31B32 (Fig. 15.5a), be easily prepared in either the pure isotropic amorphous state or in a low ordered smectic mesophase, and thus to analyze the corresponding viscoelastic relaxations in both pure phases.

Figure 15.5b shows the storage modulus for samples exhibiting pure liquid crystal, pure amorphous and mixture of the two phases. The magnitude of the modulus depends on the percentage of the liquid crystal phase, increasing about 21 % at $-140 \text{ }^\circ\text{C}$ and around 28 % at room temperature (Fernández-Blázquez et al. 2005). The localization of α relaxation is also clearly dependent on the amount of liquid crystal phase, being at higher temperature for amorphous samples as it was observed in Fig. 15.4 for PTEMeb. This fact is also observed in Fig. 15.5c for the loss modulus. Taking into account that α relaxation is associated to glass transition, in turn, is related to the freezing of segmental motions, and the liquid crystalline phases retain some mobility around the longitudinal axes of the mesogen. It seems reasonable to expect a glass transition of the liquid crystalline phase at the temperature at which the minimum free volume required for the rotations is approached (Fernández-Blázquez et al. 2004). The glass transition temperature of polymers is closely related to the flexibility of the chains in the sense that a high value of T_g is generally assumed to be connected with relatively high barriers of bond rotations.

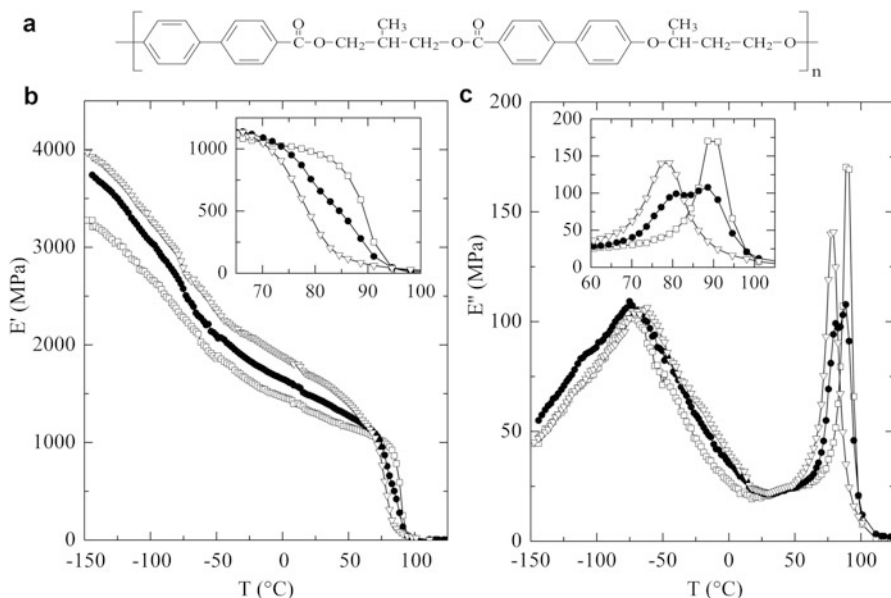


Fig. 15.5 (a) Structural unit of PH31B32. (b) Storage modulus and (c) loss modulus of PH31B32 specimens: pure amorphous (*open squares*), pure liquid crystal (*open triangles*) and phase mixture (*filled circles*)

These barriers depend not only on the type of bond, but also on the intermolecular constraint and therefore on the supramolecular arrangement of the chains. For this reason the glass transition temperature of the liquid crystalline phase can differ from that of the amorphous phase.

Secondary relaxations β and γ are observed in Fig. 15.5c and are similar in both cases, and just a small temperature shift of 7 °C higher for amorphous sample is observed, but with similar activation energy, around 70 kJ mol⁻¹. The γ relaxation appears as a shoulder of β relaxation without any differences among the three samples. In summary, there are clear differences between amorphous and liquid crystal state, although those differences are much smaller than the ones found between a classical amorphous polymer and its semicrystalline counterpart.

DMA experiments have been also performed to study one of the most reported phenomena of liquid crystal polymers in the last two decades as is the polymer chain orientation in fibers (Osada et al. 2004; Bello et al. 2001a; Martínez-Gómez et al. 2003; Fernández-Blázquez et al. 2007a; Rodríguez-Amor et al. 2008). Two distinct orientations are reported in fibers. In the most usual case, the molecules are oriented parallel to the stretching direction: if the fiber is obtained from isotropic melt or isotropic liquid crystal phase at low temperature and high strain rate the molecules are in parallel orientation mainly. On the contrary, at high temperature and low strain rate, quasi-equilibrium conditions are attained, and the macromolecules are disposed with an anomalous perpendicular orientation in relation to the

stretching. This unusual feature is characteristic of liquid crystal polymers with only low order mesophases and unable to crystallize (or crystallizable with quite low crystallization rate, like PDEB) (Rodríguez-Amor et al. 2008).

DMA experiments were carried out on PPO4B samples which were drawn at different strain rates and temperatures, in such a way that either parallel or perpendicular orientation, or a mixture of them, was obtained (Martínez-Gómez et al. 2003). Later, strips cut from these oriented sheets in three directions, 0° , 45° , and 90° in relation to the drawn direction, were tested. All specimens, independently on fiber and cut direction, showed the three relaxations described above in the same temperature locations and without differences in activation energy. The interesting differences were found in the value of storage modulus, as it is observed in Fig. 15.6. The physical properties of polymers depend critically on their molecular orientation. Taking into account that the orientation of the chains is a function of the experimental condition, the best mechanical properties are not always in the fiber direction. It is generally observed that high degrees of molecular orientation lead to increased strength and stiffness along the alignment direction, but from the data shown in Fig. 15.6 this is not always the case: for anomalous orientation the worse mechanical properties coincide with the fiber direction, and the best are in the transverse direction.

Fibers of BB5(3-Me) with the smectic layers perpendicular and parallel to the fiber axis were also analyzed by DMA to study the micro-Brownian motions of the polymer (Osada et al. 2004). Time-temperature superposition was applied to the α relaxation, therefore the frequency of the micro-Brownian motion in the SmCA phase can be estimated despite the narrow frequency range in DMA. No significant differences were found between both directions at temperatures below the glass transition. However, at smectic temperatures (above glass transition) the frequency of the motions along the layer normal direction is 2.5 times faster than that of the

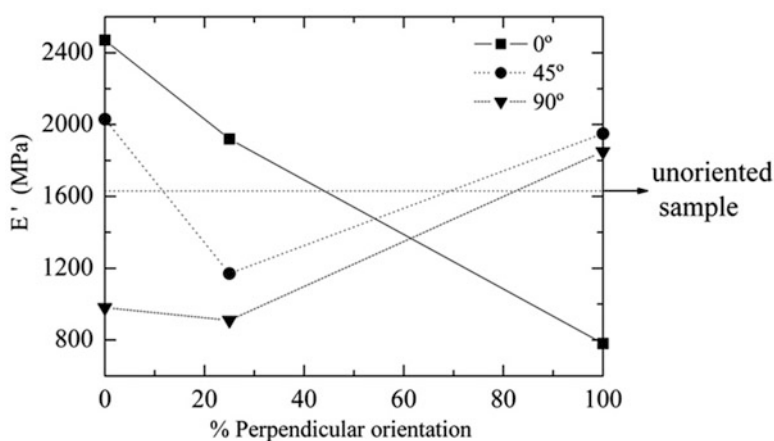


Fig. 15.6 Storage modulus, E' , at 0°C for samples of PPO4B cut in three direction (0° , 45° and 90°) from sheets with parallel orientation, perpendicular and mixture

motions along the layer, suggesting that the micro-Brownian motions in the SmCA phase are decoupled between the two directions parallel and perpendicular to the smectic layer.

15.5 Dielectric Relaxation in Polybibenzoates

Dielectric spectroscopy is a useful technique to follow the dynamics of glass forming systems (Kremer and Schönhal 2002). Dielectric relaxation in polymers is the consequence of the collective response of disordered polar chains under an external electrical field of tunable frequency. The molecular mechanism responsible of the dynamic glass transition in the amorphous phase, the α relaxation process, is related to the cooperative segmental motion of chains near the glass transition. The molecular origin of the α relaxation observed near the glass transition of mesophases is not yet completely known. Nevertheless, the dielectric relaxation of liquid crystalline polymers is an excellent tool to study their phase transitions and its related dynamics.

Dielectric studies of main chain liquid crystalline polymers are rather scarce and most of them are focused on polyesters (Ezquerria et al. 2005; Encinar et al. 2012; García-Bernabé et al. 2004). The comparative study of the polybibenzoates PTEMeB and PTEB (see Table 15.2) is particularly interesting. The absence or presence of the small methyl group as lateral substituent is responsible of very different behavior in terms of phase map, kinetics and dynamics. On one hand, PTEMeB can be easily quenched to an amorphous state and it has a rather slow mesophase formation (see Fig. 15.4). On the other hand, PTEB quickly forms on cooling a liquid crystal phase of the type SmA, which is further transformed into SmC (see Table 15.2), these two processes being reversible on heating. Both transition phenomena can be followed by dielectric spectroscopy.

Figure 15.7a shows the dielectric loss curves monitored during the isothermal formation of the liquid crystal of PTEMeB. It involves an intensity exchange between relaxation peaks. Initially, only one peak is present: the α_{iso} process, related to the dynamic glass transition of the amorphous phase. At higher times, this mode decreases, and a new peak appears at higher frequencies, which is related to the α_{LC} relaxation of the liquid crystal glass. From the qualitative behavior of the loss curves of Fig. 15.7a, we can infer two stages in the kinetics. The first 6 h (fast stage) represent a relatively fast decay of the α_{iso} mode and the corresponding increase of the α_{LC} mode. Given the overlapping of the curves at long times, the second stage consists of a slow intensity exchange between the two peaks. Simultaneous dielectric and X-ray diffraction experiments of a similar polybibenzoate, C31DTB, have shown that the first stage (fast) is related to the smectic layer formation and the second one to the increase of order within smectic domains (Ezquerria et al. 2005). Two different relaxation frequencies are observed: the α relaxation of the isotropic phase is slower than the α relaxation of the liquid crystal state. This is consistent with the observed lower glass transition temperature in the

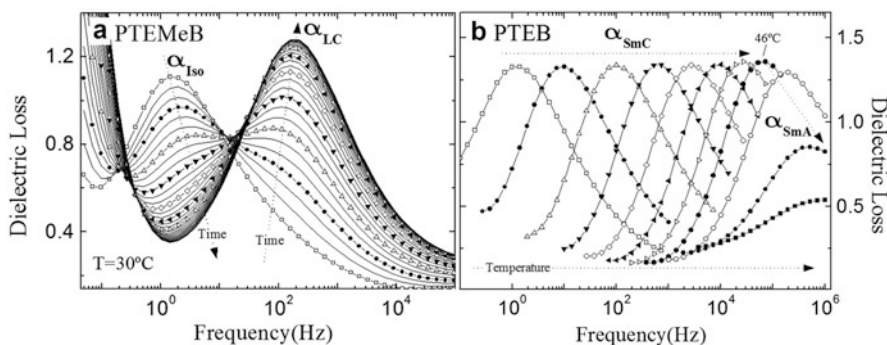
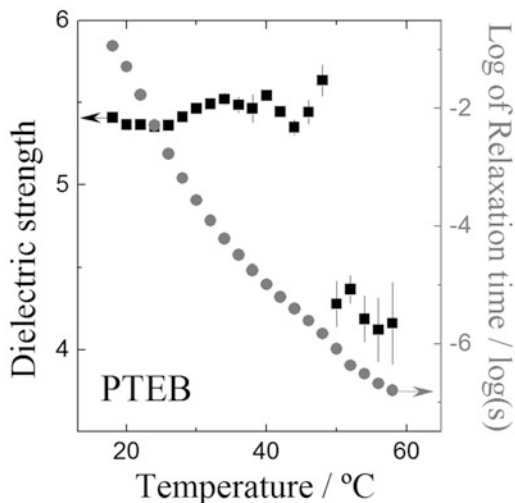


Fig. 15.7 (a) Real time dielectric loss during the isothermal transformation of PTEMeB: isotropic liquid to liquid crystal. The temperature is 30 °C and the curves are 20 min apart. The *arrows* indicate the time evolution of the α relaxation of both phases. The symbols highlight the first 6 h of curves. **Reprinted with permission** from ref Encinar et al. (2012). **Copyright 2012 American Chemistry Society.** (b) Isothermal dielectric loss curves of PTEB (from left to right: 18 °C to 58 °C, at 4 °C steps). The *arrows* indicate the evolution of the α relaxation in SmC and SmA mesophases; observed, respectively, at low and high temperatures

mesophase compared to the amorphous state (see Fig. 15.4). It suggests that, in the liquid crystal glass, the molecular origin of the dynamic glass transition is other than the cooperative segmental motion of the chains, characteristic of amorphous polymers. Moreover, it has been proposed that the molecular mechanisms of the mesophase glass transition are the rotational and translational motions of the elongated chains that require less free volume (Ahumada et al. 1996). The dielectric intensity of both peaks is slightly higher in the mesophase, probably related to a better alignment of the dipolar vectors within the orientationally ordered phase. Another feature of this dynamics exchange process is the acceleration of the transient modes during the phase transition. Finally, it has been shown that the fast stage of the mesophase formation follows an athermal 1D crystallization Avrami kinetics (Encinar et al. 2012).

Figure 15.7b shows the dielectric loss curves measured at different increasing temperature steps of the liquid crystal of PTEB. The α relaxation peak shifts monotonically to higher frequencies as the temperature increases. Below the phase transition temperature (approx. 46 °C on heating) the maximum intensity of the α_{SmC} peaks, related to the tilted SmC mesophase, remains constant. At higher temperatures the peak intensity decreases leading into the α_{SmA} process, related to the orthogonal SmA mesophase. A comprehensive analysis by fitting Havriliak Negami functions (Havriliak and Havriliak 1997) to the loss curves confirms that also the dielectric strength, *i.e.* the peak area, decreases when the phase transition takes place (Fig. 15.8). The dielectric strength is proportional to the dipole density and dipole-dipole vector correlations. The net dipolar moment of the PTEB molecule is due to the carbonyl groups (C=O) normal to the main chain adjacent to the biphenyl mesogens. If we consider that the dipole density is the same in both smectic phases (invoking the mass conservation), the dielectric strength decrease

Fig. 15.8 Temperature dependence of dielectric strength (peak area, *squares/left axis*) and relaxation time (position at peak maximum, *circles/right axis*) of the α relaxation of PTEB



on the SmA phase can be related to a loss of dipolar pair correlation. The abrupt fall of dielectric strength resembles the also abrupt change of the correlation length parameter when the SmC to SmA transition takes place (Martínez-Gómez et al. 2010). Indeed, the transition to the orthogonal mesophase is accompanied by both an increase of the interlayer correlation length, *i.e.* longitudinal order between smectic layers, and by the loss of intralayer correlations of the local tilt directions in the SmC mesophase. Therefore, the pair dipolar correlations can be assigned mainly to short range intralayer correlations instead of long range interlayer correlations. On the other hand, since the tilting angle and layer thickness vary linearly with temperature in both phases (steeper in the SmC phase), it is unlikely to relate the dielectric strength fall to the smooth temperature dependence of layer thickness. During the SmC to SmA transition no apparent change on the relaxational frequency temperature dependence is detected (see Fig. 15.8). Additionally, only one static glass transition is detected in the thermogram. For this reasons, in the present system, the molecular origin of the smectic dynamic glass transition seems to be independent of the orientational state.

15.6 Conclusions and Future Perspective

The results summarized in this chapter clearly demonstrate that it is possible with simple chemical and structural modifications in the flexible spacer to tailor the thermotropic behavior of semiflexible main-chain polyesters based on biphenyl mesogens. Following such synthetic strategies, the thermal transitions, mesophase structure, mesophase stability and rate of liquid crystalline formation can be controlled. Furthermore, it has been shown that the election of an appropriate

spacer allows the design of polymers in which both the glassy amorphous state and the glassy smectic state can be separately obtained and, consequently, both glassy states can be independently analyzed.

In recent years, the interest on LCPs has been renewed as precursors of liquid crystalline elastomers, which exhibit remarkable thermomechanical properties due to the combination of polymer network elasticity with the anisotropic structure of the liquid crystalline state (Brand and Finkelmann 1998; Ohm et al. 2010, 2012; Burke and Mather 2010). Because of the stronger coupling of liquid crystalline order to macroscopic network deformation, elastomers based on smectic main-chain LC polymers are expected to show unique thermomechanical properties. Hence, networks prepared from semiflexible polybibenzoates may have a great potential as smectic elastomers.

In this context, biphenyl-containing polymers may find a valuable application as smectic liquid crystalline elastomers. Although, there have been a few investigations on the deformation behavior of networks based on biphenyl mesogens (Ishige et al. 2008a, b; Hiraoka et al. 2009), there is much work still to be done to better understand the behavior of these exciting materials from both scientific and practical application perspectives. In fact, we have already synthesized some of these network systems, with the biphenyl group as mesogen, and the preliminary characterization shows outstanding shape-memory ability, with both excellent shape recovery and shape fixing.

References

- Ahumada O, Ezquerro TA, Nogales A, Baltà-Calleja FJ, Zachmann HG (1996) Influence of liquid crystalline order on the dielectric. Relaxation of random copolyesters of PET, PEN, and PHB. *Macromolecules* 29:5002–5009
- Bello A, Pérez E, Marugán MM, Pereña JM (1990) Liquid-crystalline poly[oxybis(trimethylene p, p'-bibenzoate)]: effect of the central ether group. *Macromolecules* 23:905–907
- Bello P, Bello A, Lorenzo V (2001a) Anomalous orientation of poly(trimethylene oxy-2 methyl trimethylene p, p'-bibenzoate) as revealed by means of tensile tests. *Polymer* 42:4449–4452
- Bello P, Bello A, Riande E, Heaton NJ (2001b) Thermotropic polyesters with flexible spacers bearing ether bonds in asymmetric position. *Macromolecules* 34:181–186
- Benavente R, Pereña JM, Pérez E, Bello A (1993) Relaxation processes in thermotropic polydibenzoates with oxyethylene spacers in the main chain. *Polymer* 34:2344–2347
- Benavente R, Zhu Z, Pereña JM, Bello A, Pérez E (1996) Dynamic mechanical relaxations of liquid crystalline copolyesters derived from bibenzoic acid. *Polymer* 37:2379–2384
- Boyd R (1975) Energetics of kinks in polyethylene. *J Polym Sci Polym Phys* 13:2345–2355
- Boyd R (1985) Relaxation processes in crystalline polymers: molecular interpretation. A review. *Polymer* 26:1123–1133
- Boyd R, Breitling R (1974) Conformational analysis of crankshaft motions in polyethylene. *Macromolecules* 7:855–862
- Boyd R, Gee R, Han J, Jin Y (1994) Conformational dynamics in bulk polyethylene: a molecular-dynamics simulation study. *J Chem Phys* 101:788–797
- Brand HR, Finkelmann H (1998) Physical properties of liquid crystalline elastomers. In: Demus D, Goodby J, Gray GW, Spiess H-W, Vill V (eds) *Handbook of liquid crystals*, vol 3. Wiley-VCH, Weinheim, pp 277–302

- Burke KA, Mather PT (2010) Soft shape memory in main-chain liquid crystalline elastomers. *J Mater Chem* 20:3449–3457
- Chiellini E, Laus M (1998) Main chain liquid crystalline semiflexible polymers. In: Demus D, Goodby J, Gray GW, Spiess H-W, Vill V (eds) *Handbook of liquid crystals*, vol 3. Wiley-VCH, Weinheim, pp 26–51
- del Campo A, Bello A, Pérez E, García-Bernabé A, Diaz-Calleja R (2002) Amorphous-smectic glassy main-chain LCPs, 1. Poly(ether esters) derived from hydroxybenzoic acid and (R, S)- and (R)-2-methylpropane-1,3-diol. *Macromol Chem Phys* 203:2508–2515
- Diaz-Calleja R, Riande E, Guzman J (1986) Influence of static strain on dynamic mechanical-behavior of amorphous networks prepared from aromatic polyesters. *J Polym Sci Polym Phys* 24:337–344
- Diaz-Calleja R, Riande E, Guzman J (1989) Conformational and relaxation studies on polyesters derived from terephthalic acid and propylene and dipropylene glycol. *Macromolecules* 22:3654–3659
- Duncan J (2008) Principles and applications of mechanical thermal analysis. In: Gabbott P (ed) *Principles and applications of thermal analysis*. Blackwell Publishing, Oxford
- Encinar M, Martínez-Gómez A, Rubio RG, Pérez E, Bello A, Prolongo MG (2012) X-ray diffraction, calorimetric, and dielectric relaxation study of the amorphous and smectic states of a main chain liquid crystalline polymer. *J Phys Chem B* 116:9846–9859
- Ezquerro TA, Martínez-Gómez A, Álvarez C, Alonso E, Sanz A, Bello A, Pérez E, Funari SS, Dommach M (2005) Structure-dynamics relationship during the amorphous to smectic transition of a main chain liquid crystalline polymer. *J Non-Cryst Solids* 351:2768–2772
- Fernández-Blázquez JP, Bello A, Pérez E (2004) Observation of two glass transitions in a thermotropic liquid-crystalline polymer. *Macromolecules* 37:9018–9026
- Fernández-Blázquez JP, Bello A, Pérez E (2005) Dynamic mechanical analysis of the two glass transitions in a thermotropic polymer. *Polymer* 46:10004–10010
- Fernández-Blázquez JP, Bello A, Pérez E (2007a) Parallel and perpendicular orientation in a thermotropic main-chain liquid-crystalline polymer. *Macromolecules* 40:703–709
- Fernández-Blázquez JP, Bello A, Pérez E (2007b) Synthesis, phase behaviour and mechanical properties of poly(2-methyl-1,3-propanediol-4,4'-bibenzoate). *Macromol Chem Phys* 208:2611–2620
- García-Bernabé A, Diaz-Calleja R, Sanchis MJ, del Campo A, Bello A, Pérez E (2004) Amorphous-smectic glassy main chain LCPs. II. Dielectric study of the glass transition. *Polymer* 45:1533–1543
- Havriliak S Jr, Havriliak SJ (1997) *Dielectric and mechanical relaxation in materials: analysis, interpretation, and application to polymers*. Hanser, New York
- Heaton NJ, Benavente R, Perez E, Bello A, Pereña JM (1996) The gamma relaxation in polymers containing ether linkages: conformational dynamics in the amorphous phase for a series of polybibenzoates containing oxyethylene spacers. *Polymer* 37:3791–3798
- Hiraoka K, Tashiro T, Tokita M, Watanabe J (2009) Spontaneous deformation of main-chain liquid-crystalline elastomer composed of smectic polyesters. *Liq Cryst* 36:115–122
- Hu YS, Liu RYF, Schiraldi DA, Hiltner A, Baer E (2004) Solid-state structure of copolyesters containing a mesogenic monomer. *Macromolecules* 37:2128–2135
- Ishige R, Osada K, Tagawa H, Niwano H, Tokita M, Watanabe J (2008a) Elongation behavior of a main-chain smectic liquid crystalline elastomer. *Macromolecules* 41:7566–7570
- Ishige R, Tokita M, Naito Y, Zhang CY, Watanabe J (2008b) Unusual formation of a smectic A structure in cross-linked monodomain elastomer of main-chain LC polyester with 3-methylpentane spacer. *Macromolecules* 41:2671–2676
- Jackson WJ Jr, Morris JC (1990) Polyesters of 4,4'-biphenyldicarboxylic acid and aliphatic glycols for high-performance plastics. *ACS Symp Ser* 435:16–32
- Jin Y, Boyd R (1998) Subglass chain dynamics and relaxation in polyethylene: a molecular dynamics simulation study. *J Chem Phys* 108:9912–9923
- Kremer F, Schönhals A (2002) *Broadband dielectric spectroscopy*. Springer, Berlin

- Liu RYF, Hu YS, Hibbs MR, Collard DM, Schiraldi DA, Hiltner A, Baer E (2003) Comparison of statistical and blocky copolymers of ethylene terephthalate and ethylene 4,4'-biphenylate based on thermal behavior and oxygen transport properties. *J Polym Sci Polym Phys* 41:289–307
- Loman AJB, Van Der Does L, Bantjes A, Vulic I (1995) Effect of methyl groups on the thermal properties of polyesters from methyl substituted 1,4-butanediols and 4,4'-biphenyldicarboxylic acid. *J Polym Sci Polym Chem* 33:493–504
- Ma H, Hibbs M, Collard DM, Kumar S, Schiraldi DA (2002) Fiber spinning, structure, and properties of poly(ethylene terephthalate-co-4,4'-biphenylate) copolyesters. *Macromolecules* 35:5123–5130
- Martínez-Gómez A, Pereña JM, Lorenzo V, Bello A, Pérez E (2003) Mechanical properties of drawn smectic mesophases. Poly(tetramethylenoxypropylene *p*, *p'*-biphenylate). *Macromolecules* 36:5798–5803
- Martínez-Gómez A, Bello A, Pérez E (2004) Thermotropic behavior of a liquid crystalline polybiphenylate with an asymmetric oxymethylene spacer. *Macromolecules* 37:8634–8640
- Martínez-Gómez A, Pérez E, Bello A (2006) Phase behavior of a liquid crystalline polyetherester derived from 4'-hydroxy-1,1'-biphenyl-4-carboxylic acid and the ether-diol 4-(3-hydroxypropoxy)butan-1-ol. *Macromolecules* 47:2080–2090
- Martínez-Gómez A, Bello A, Pérez E (2008) Synthesis and structural studies of poly(tetramethylenoxypropylene *p*, *p'*-biphenylate). *e-Polymers* 69:1–26
- Martínez-Gómez A, Pérez E, Bello A (2010) Polymesomorphism and orientation in liquid-crystalline poly(triethylene glycol *p*, *p'*-biphenylate). *Colloid Polym Sci* 288:859–867
- Martínez-Gómez A, Pérez E, Bello A (2011) Tailoring the phase behavior in thermotropic copolyesters. *Macromol Chem Phys* 212:1971–1980
- Meurisse P, Noel C, Monnerie L, Fayolle B (1981) Polymers with mesogenic elements and flexible spacers in the main chain: aromatic-aliphatic polyesters. *Br Polym J* 13:55–63
- Nakata Y, Watanabe J (1994) A new type of main-chain liquid-crystal polymer derived from 4'-hydroxybiphenyl-4-carboxylic acid and its smectic mesophase behaviour. *J Mater Chem* 4:1699–1703
- Nakata Y, Watanabe J (1997) Frustrated smectic phase with unusual density modulation along layer observed in main chain type of polymers. *Polym J* 29:193–197
- Ohm C, Brehmer M, Zentel R (2010) Liquid crystalline elastomers as actuators and sensors. *Adv Mater* 22:3366–3387
- Ohm C, Brehmer M, Zentel R (2012) Applications of liquid crystalline elastomers. *Adv Polym Sci* 250:49–94
- Osada K, Koike M, Tagawa H, Tokita M, Watanabe J (2004) Thermotropic liquid crystals of main-chain polyesters having a mesogenic 4,4'-biphenyldicarboxylate unit. Anisotropic micro-Brownian motions of polymer in smectic CA phase. *Macromol Chem Phys* 205:1051–1057
- Pereña JM, Marugán MM, Bello A, Pérez E (1991) Viscoelastic relaxations in thermotropic polybiphenylates. *J Non-Cryst Solids* 131:891–893
- Pérez E, Riande E, Bello A, Benavente R, Pereña JM (1992) Thermotropic properties and conformational studies on poly(triethylene glycol *p*, *p'*-biphenylate) and poly(octamethylene *p*, *p'*-biphenylate). *Macromolecules* 25:605–610
- Pérez E, Zhen Z, Bello A, Benavente R, Pereña JM (1994) Phase-transitions in liquid-crystalline poly(octamethylene *p*, *p'*-biphenylate). *Polymer* 35:4794–4798
- Pérez E, Pereña JM, Benavente R, Bello A (1997) Characterization and properties of thermotropic polybiphenylates. In: Cheremisinoff NP (ed) *Handbook of engineering polymeric materials*. Marcel Dekker, New York, pp 383–397
- Pérez E, del Campo A, Bello A, Benavente R (2000) Synchrotron X-ray study of the phase transitions in liquid crystal polyesters derived from *p*, *p'*-biphenylate and racemic- and (R)-3-methyl-1,6-hexanediol. *Macromolecules* 33:3023–3030
- Pérez E, Benavente R, Cerrada ML, Bello A, Pereña JM (2003a) Synchrotron X-ray and DSC studies of the phase behaviour of poly(diethylene glycol *p*, *p'*-biphenylate). *Macromol Chem Phys* 204:2155–2162

- Pérez E, Todorova G, Krasteva M, Pereña JM, Bello A, Marugán MM, Shlouf M (2003b) Structure and phase transitions of poly(heptamethylene p, p'-bibenzoate): time-resolved synchrotron WAXS and DSC studies. *Macromol Chem Phys* 204:1791–1799
- Pérez E, Fernández-Blázquez JP, Martínez-Gómez A, Bello A, Cerrada ML, Benavente R, Pereña JM (2009) Applications of synchrotron X-ray diffraction to the study of the phase behavior in liquid crystalline polymers. *Lect Notes Phys* 776:157–182
- Pérez-Manzano J, Fernández-Blázquez JP, Bello A, Pérez E (2006) Liquid-crystalline copolymers of bibenzoate and terephthalate units. *Polym Bull* 56:571–577
- Rodríguez-Amor V, Fernández-Blázquez JP, Bello A, Pérez E, Cerrada ML (2008) Molecular weight effect on the obtainment of parallel and perpendicular orientation in thermotropic poly(diethylene glycol p, p'-bibenzoate). *Polym Bull* 60:89–96
- Schatzki Y (1966) Molecular interpretation of gamma-transition in polyethylene and related compounds. *J Polym Sci Polym Symp* 14:139–140
- Schiraldi DA, Occelli ML, Gould SAC (2001) Atomic force microscopy (AFM) study of poly(ethylene terephthalate-co-4,4'-bibenzoate): a polymer of intermediate structure. *J Appl Polym Sci* 82:2616–2623
- Tokita M, Osada K, Watanabe J (1998) Thermotropic liquid crystals of main-chain polyesters having a mesogenic 4,4'-biphenyldicarboxylate unit XI. Smectic liquid crystalline glass. *Polym J* 30:589–595
- Watanabe J, Hayashi M, Kinoshita S, Niori T (1992) Thermotropic liquid crystals of polyesters having mesogenic p, p'-bibenzoate unit IV. Mesophase behavior of polyester with branched spacers. *Polym J* 24:597–601
- Watanabe J, Hayashi M, Nakata Y, Niori T, Tokita M (1997) Smectic liquid crystals in main-chain polymers. *Prog Polym Sci* 22:1053–1087

Chapter 16

Introduction to Liquid Crystalline Polymers

Dumitru Pavel

16.1 Introduction

Liquid crystals (LCs) or orientationally ordered liquids have been considered as the fourth state of matter (Saeva 1979; Kelker and Hatz 1980). Although the phenomenon of liquid crystallinity was discovered in 1888 and the term “liquid crystals” was first used in 1890 (Kelker and Hatz 1980), liquid crystallinity has attained prominence only in the last two decades or so.

In 1888, Austrian botanist Friedrich Reinitzer noted that, when melted, the cholesteryl esters form colourful-opaque liquids, which become clear at higher temperatures. Reinitzer sent a sample of cholesteryl esters to a German scientist Otto Lehmann, who was studying the crystallisation properties of various substances. Lehmann had constructed a polarising microscope that allowed him to observe the crystallisation of his samples. Lehmann investigated Reinitzer’s sample with his polarising microscope and noted its similarity to some of his own samples and first referred to them as ‘soft crystals’. By 1889 Lehmann was describing the material as ‘flowing crystals’. Later Lehmann used the term ‘crystalline fluids’, but when he became more convinced that the opaque phase was a uniform phase of matter sharing properties of both liquids and solids, he began to call them ‘liquid crystals’ (Coolings 1990).

LCs are anisotropic materials whose flow properties strongly depend on their structure and molecular orientation. Molecules in crystalline solid state are positionally and orientationally ordered in three dimensions, but in the isotropic liquid state these orders are completely destroyed. Whereas LCs exhibit a degree of

D. Pavel (✉)

Department of Research & Development, SAUDI INTERNATIONAL PETROCHEMICAL COMPANY (SIPCHEM), Dhahran Techno Valle, Dhahran, Kingdom of Saudi Arabia
e-mail: dumitru_p@yahoo.co.uk

macroscopic orientational order that is found between the boundaries of crystalline solid state and the isotropic, ordinary liquid, state (Donald and Windle 1992; Collyer 1996). Consequently, the properties of LCs are intermediate between those of an isotropic liquid and those of a crystalline solid.

Schematic representation of molecular order in the crystalline, isotropic and liquid crystalline phases is given in Fig. 16.1.

As shown in Fig. 16.2, when a sample of crystalline solid material is heated, it is expected sooner or later to melt into an isotropic liquid losing both the long range orientational and positional order. The temperature at which the melting takes place is called *melting temperature*, T_m , or *crystalline-isotropic transition temperature*, T_{C-I} . When the isotropic liquid (melt) is subsequently cooled, it is expected to solidify again.

However, some of the materials do not behave as expected: they do not show a single transition from solid to liquid, but rather a cascade of transitions involving new phases. Thus, referring to Fig. 16.3, for a certain substance the crystalline solid melts into an intermediate phase only partially losing its ordering. In this case the melting temperature coincides with the *crystalline-liquid crystalline transition temperature*, T_{C-LC} . Such materials can exhibit one or more intermediate phases. These intermediate phases are mostly referred to as *liquid crystalline phases*, also known as crystalline liquid phases, mesophases or mesomorphic phases (Hurduc and Pavel 1999; Guerriero et al. 2011; Wenyi and Shi 2012). Consequently, the properties of these phases are intermediate between those of a liquid and those of a crystal.

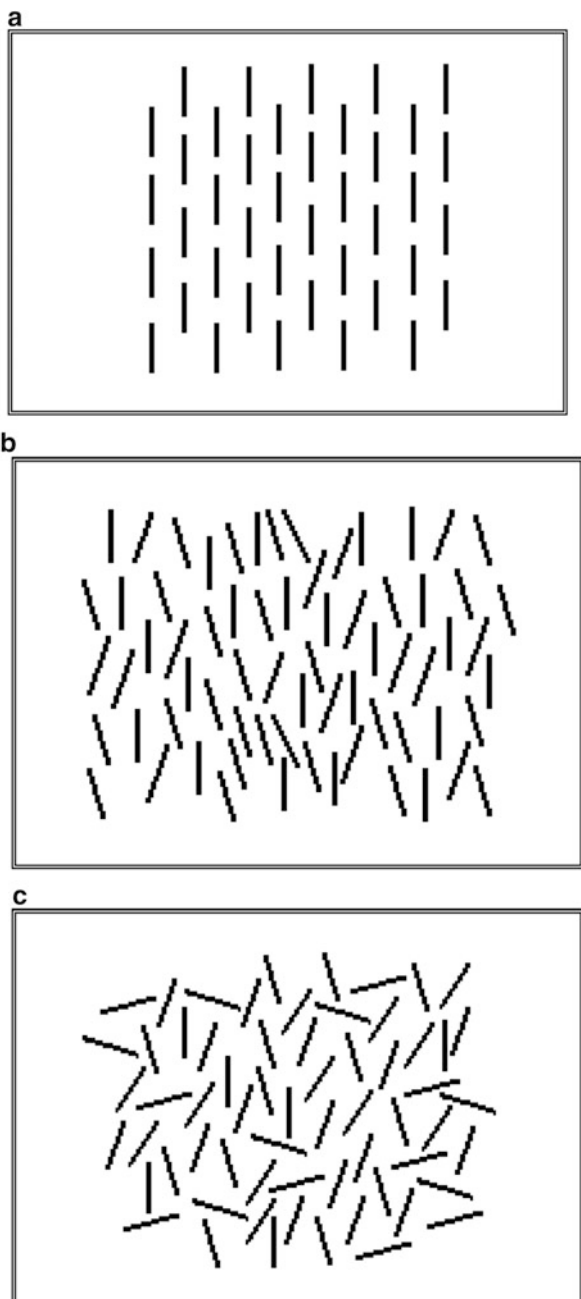
At higher temperatures, this mesophase further loses its partial ordering and it is transformed into an ordinary isotropic liquid, this phenomenon is called liquid crystalline-isotropic transition (LC-I) (Brostow 1992). The temperature at which LC-I takes place (T_{LC-I}) is called *clearing temperature*, T_c , also known as isotropisation temperature, T_i .

When the isotropic liquid of liquid-crystalline material is cooled, it is expected to exhibit an isotropic-liquid crystalline transition and then to solidify again. The temperature at which the isotropic-liquid crystalline transition takes place is called T_{I-LC} , and the temperature at which the liquid crystalline-crystalline transition takes place is called T_{LC-C} .

The liquid crystalline phase is thermodynamically stable and represents a condition of incomplete melting. As illustrated in Fig. 16.3, T_m (or T_{C-LC}) and T_c define the temperature range in which the liquid crystalline phase is thermodynamically stable.

There are two main types of liquid crystals: thermotropic and lyotropic. The LCs that exhibit various liquid crystalline phases as a function of temperature are called *thermotropic* (Fig. 16.3). They are formed by heating to the temperature above which the crystal lattice is no longer stable. Thermotropic LCs exhibit liquid crystallinity in a particular temperature range: between T_{C-LC} or T_g (glass transition temperature in the cases where the crystallinity is absent) and T_c (Donald and Windle 1992; Wang et al. 1996). Thermotropic LCs are very stable and exhibit very large mesomorphic ranges, sometimes several hundred degrees.

Fig. 16.1 Schematic representation of molecular order in the (a) crystalline, (b) liquid crystalline and (c) isotropic liquid phases



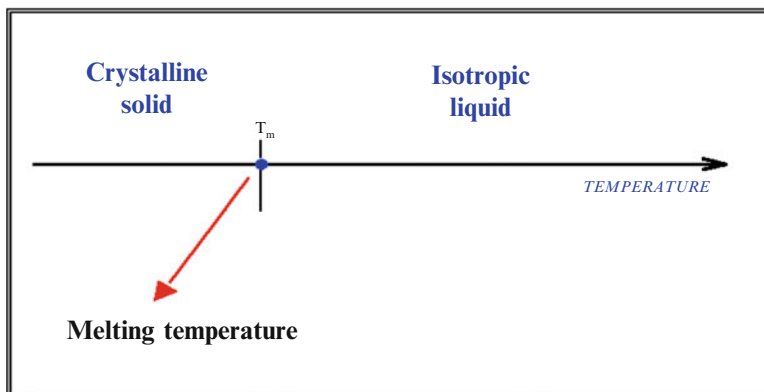


Fig. 16.2 Ordinary solid–isotropic liquid transition

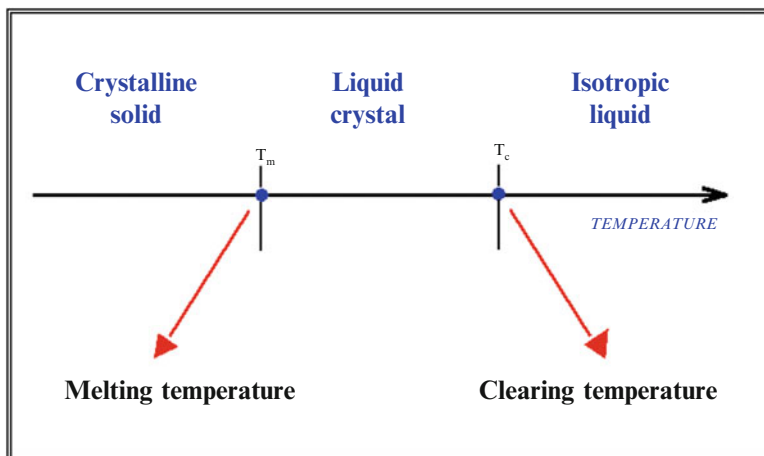


Fig. 16.3 Thermotropic liquid crystalline transition

The thermotropic liquid crystalline materials are further divided into two sub-groups: thermodynamically stable—*enantiotropic* and unstable—*monotropic* (Blackwell and Biswas 1987; Bhowmik and Lenz 1994). The mesophase of enantiotropic LCs is observed by either raising the temperature of a solid crystalline phase or lowering the temperature of a liquid phase, whereas the mesophase of monotropic LC is only observed by lowering the temperature of a liquid phase.

Sometimes liquid crystalline phases are formed by mesomorphic molecules in a non-mesomorphic solvent (Kelker and Hatz 1980; Donald and Windle 1992; Hintze-Bruening et al. 2011; Hatakeyama et al. 2011), so a true solution is not obtained, but the resulting state exhibits liquid crystalline properties. Further

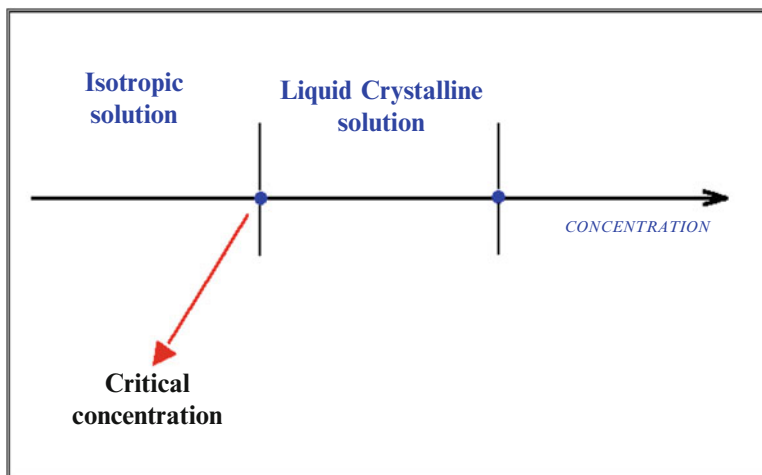


Fig. 16.4 Lyotropic liquid crystalline transition

increase of the amount of non-mesogenic solvent molecules beyond a critical concentration leads to a transition to the isotropic liquid phase. Thus, the LCs that are formed when the concentration of the solvent is changed are called *lyotropic* (Fig. 16.4).

Lyotropic LCs play a very important role mostly in biological systems (Coolings 1990; Hintze-Bruening et al. 2011; Liang et al. 2010). However, this kind of LCs will not be discussed further, since it is beyond the scope of this chapter, the subject of which is restricted to thermotropic LCs.

16.2 Nature of Liquid Crystalline Polymers

Macromolecules are also capable of forming similar liquid crystalline mesophases if the mesogenic groups are linked by flexible spacers (*i.e.*, in this study the spacers are propylene, diethyletheric (oxydiethylene) and oxetane ring). Such macromolecules are called *liquid crystalline polymers (LCPs)*. The mesogenic units of LCPs are usually made up of a rigid core of two or more aromatic rings, therefore, the LCPs are frequently aromatic polymers. These stiff regions along the chain allow the polymer to retain a high degree of orientational order in the liquid/melt state. Similar to ordinary liquid crystals, LCPs exhibit fluidity while possessing order like structure of a solid crystal (Kelker and Hatz 1980; Collyer 1996). LCPs are also anisotropic materials whose flow properties depend on their molecular structure and orientation. Liquid crystalline behavior during melting results in lower viscosity, because the rigid polymeric mesophases align themselves in the direction of the flow, so LCPs are easier to process compared with isotropic polymers. Considering their direct applicability in technology, LCs have been intensively considered, and

several thousands of such compounds have been synthesized in the past few decades. However, related aspects for LCPs are still in their infancy and are in the area of continuing research interest. Scientific and technological interest in LCPs was first sparked by the development and commercialization of DuPont “KEVLAR” poly(p-phenylene terephthalamide) (PPTA) fibre in the 1970s which can be manufactured as stiff and strong as steel (Hall and Tiddy 1992; Donald and Windle 1992). An important goal of polymer science now is to design polymers with the necessary structure to form a mesophase, yet with sufficient chain flexibility to be processed. In general, for normally flexible polymers to exhibit liquid crystalline properties, mesogenic molecules such as rod-like, disc-like, pyramid-like or phasm-like have to be incorporated into or onto their chains. It is noteworthy that the mesogenic groups are incorporated into or onto the main-chain polymer almost exclusively by covalent bonds.

As liquid crystals, liquid crystalline polymers can also be thermotropic and lyotropic. Yet in terms of position of the mesogenic groups, liquid crystalline polymers can be classified as main-chain, side-chain, combined main-chain/side-chain and cross-linked.

The first type of LCPs, *main-chain*, is formed when the mesogenic groups are incorporated in the backbone of the polymer (Damman and Mercx 1993; Hurduc and Pavel 1999). The liquid crystalline phases are formed by the polymer chains folding in a way analogous to what occur when polymers crystallize. Linear main-chain thermotropic LCPs tend to form nematic phases in particular and helical main-chain thermotropic LCPs tend to form discotic phases (Davies and Ward 1988; Donald and Windle 1992). A main-chain LCP is schematically represented in Fig. 16.5.

The second type of LCPs, *side-chain or comb-like*, is formed when the mesogenic groups are attached covalently as side-chains onto the polymer main-chain (Finkelmann 1991; Mulligan et al. 1996; Cook et al. 2012). The mesogenic groups can be directly attached to the backbone of the polymer, or connected through a flexible spacer. This is schematically represented in Fig. 16.6.

In the last few years, scientific research has concentrated on the synthesis and characterisation of new polymers with special properties. Among these, side chain liquid crystalline polymers (SCLCPs) are distinguished by their properties as

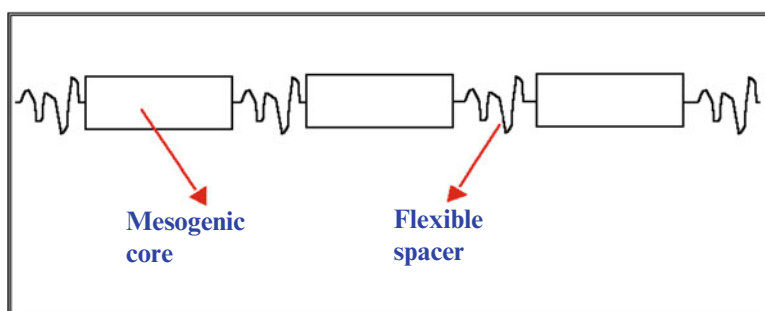


Fig. 16.5 Schematic representation of main-chain LCP

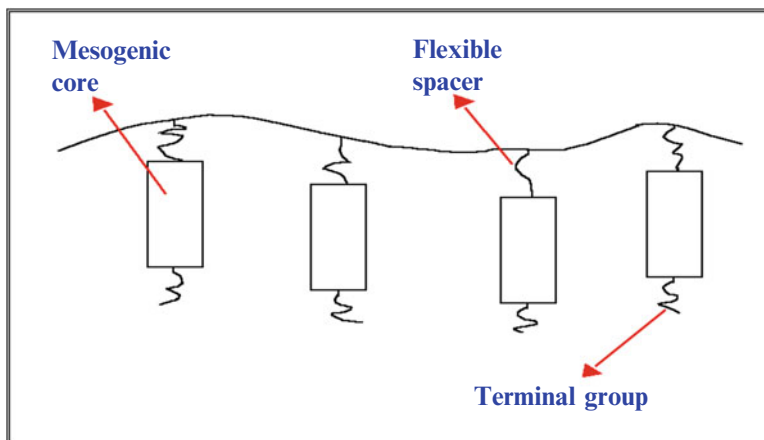


Fig. 16.6 Schematic representation of side-chain LCP

materials in a range of advanced electro-optical technologies, but also because they present a demanding challenge to our understanding of self-assembly in molecular systems. The main reason is that SCLCPs could combine the unique properties of low-molar mass liquid crystals and polymers together, which made it easier to form film during material processing. Although a large amount of experimental data has been available on the properties of side chain liquid crystalline polymers, the fundamental understanding of their behavior at a molecular and atomic level is still limited.

An important goal in the synthesis of SCLCPs is to design molecules with the necessary order to form a mesophase yet with sufficient chain flexibility so that the crystal melting temperature (T_m) is reached within the range of normal processing temperatures (Yu et al. 2013). One of the distinguishing structural properties of these polymers is the ease to form film during material processing. Therefore, SCLCPs offer potential solutions for problems that low-mass-molecular liquid crystals are unable to solve, and possible applications arise where the combination of these properties are basic requirements. These applications range from electrical-electronic components, chemical processing, transportation (including automotive and aerospace) and telecommunications, and more recently to optical and electro-optical display devices, optical computing and medical science as diagnostic aids.

Small molecule modified macromolecules (SMMM) have been used extensively to obtain functional polymers with special properties (Pankaj Kumar et al. 2011; Su et al. 2011; Wang et al. 2013). This method is preferred due to the absence of side reactions that can induce the appearance of branched polymers.

As with small-molecule liquid crystals, the appearance of a mesophase is associated with long-range organisation of the molecular orientations. For small molecules this order may arise from the packing requirements of the rodlike molecules, from anisotropic attractive forces or some combination of both. Models to predict orientational order in liquid-crystalline polymers are well known, the earliest being

the lattice theory of Flory and co-workers. The lattice theory depends on aspect ratio of polymer chains (the ratio of length to diameter) as the only molecular parameter. In the particular treatment of Flory and Ronca, for example, it is predicted that the critical aspect ratio for a polymer to exhibit liquid crystallinity is 6.42.

The third type of LCPs, *combined main-chain/side-chain*, also known as double or combined (Brostow 1992) is formed when the mesogenic groups are both incorporated into and attached onto the polymer main chain. The side-chain mesogenic groups can be attached to the main-chain mesogenic groups, or connected to the flexible spacer of the main chain of the polymer. This is schematically represented in Fig. 16.7. The presence of mesogenic groups in both side and

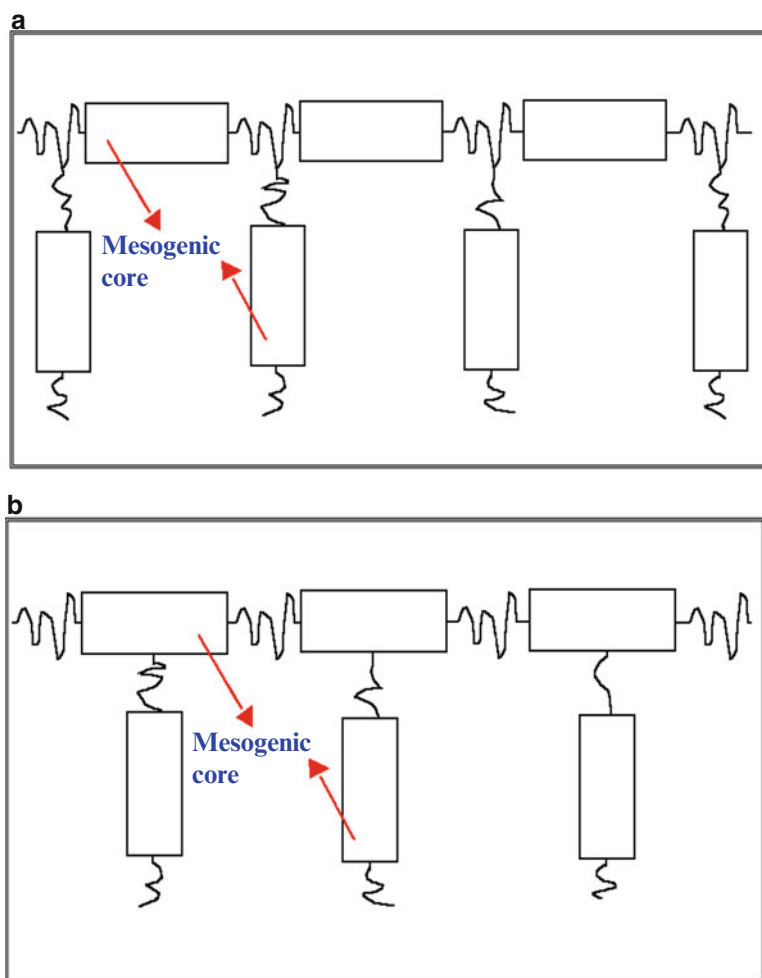


Fig. 16.7 Schematic representation of combined main-chain/side-chain LCP: (a) Side-chain mesogenic groups are attached to the main-chain mesogenic groups (b) Side-chain mesogenic groups are connected to the flexible spacer of the main chain

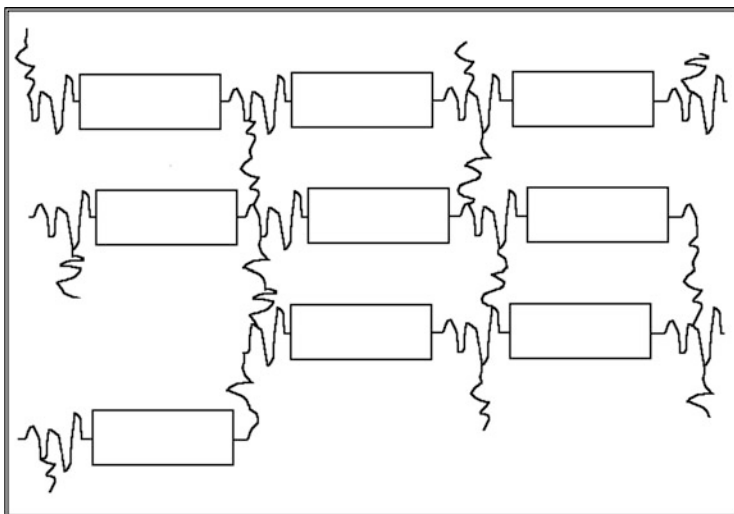


Fig. 16.8 Schematic representation of cross-linked LCP

main chain positions can have a significant effect on the properties and organisation of the mesophase (Petr et al. 2013).

Super-strong (SS) polymers are specially-designed combined LCPs in which the side chains of one molecule are designed to pack between the side chains of neighboring molecules, thus leading to molecular self-reinforcement and enhanced molecular ordering compared with main-chain LCPs (Dowell 1990).

The fourth type of LCPs, *cross-linked*, also known as network or thermoset (Fig. 16.8), is a result of a cross-linking reaction of LCPs that are functionalized with reactive groups (*cross-linkable LCPs*) allowing a network formation via the cross-linking reaction (Hoyt et al. 1990; Zentel et al. 1990).

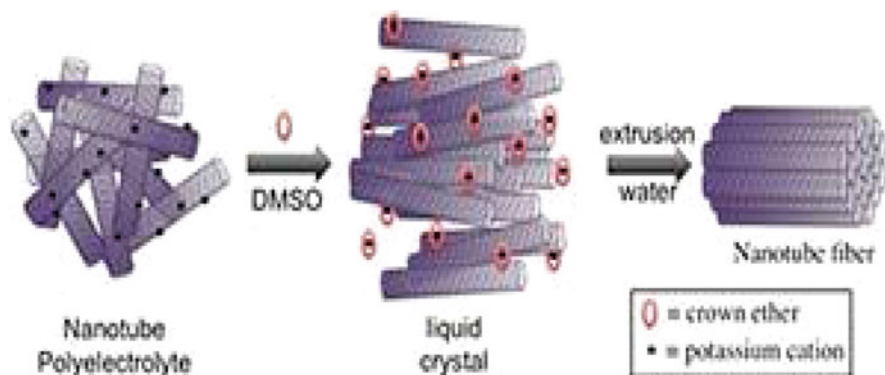
If the crosslinking reaction is performed in the liquid crystalline phase, an anisotropic network structure becomes chemically locked in, which results in obtaining ordered three-dimensional systems with exceptionally high mechanical resistance (Donald and Windle 1992; Pavel et al. 1999a, b). Moderate cross-linking of LCPs (10–20 %) has no effect on the nature of the mesophases compared with an analogous homopolymer, but tends to lower all phase transition temperatures by a few degrees (Simmonds 1992).

Liquid crystalline networks combine both high dimensional stability and mechanical orientability typical of polymer networks with the unique anisotropic behaviour of liquid crystals. Depending on the cross-link density, *i.e.*, the average length between two contiguous cross-links along the molecular backbone, the materials may exhibit reversible transitions from the liquid crystalline to the isotropic state.

Great attention has been devoted to the liquid crystal networks during the last few years due to their use as optical switches, waveguides, non-linear optical materials and advanced composites, as well as because of a great potential to

generate a new class of polymers with outstanding properties for new applications. Therefore, their ‘building blocks’—cross-linkable LCPs—are also of a great interest.

Recently, more novel LCs are obtained from carbon nano-tubes materials (Nano News), these LCs are expected to have better thermo-mechanical properties:



16.3 Liquid Crystalline Phases

The common feature of LCs is a rigid backbone that is responsible for the formation of the liquid crystalline phase. The essential molecular requirement for the formation of a liquid crystalline phase is a highly geometrically anisotropic shape, *i.e.*, the molecules are anisometric (Pavel et al. 1997, 1999a, b). This means that one of the molecular dimensions is usually much larger (rod-like molecules) or much smaller (disc-like molecules) than the other two. Although theoretically any molecule that has a non-spherical symmetry should be able to exhibit a mesophase, only 3–4 % of these organic molecules are found to have mesogenic behavior.

Liquid crystalline molecules always have a rigid segment (a group of atoms), called a *mesogenic group* (often an aromatic core) which is rod-like or disc-like and a *flexible spacer*. The mesogenic group increases the anisotropic interactions between the constituent molecules, and therefore increases the clearing temperature. Unlike the mesogens, the flexible spacers increase the number of conformations that the molecules can adopt and hence the entropy of melting. Consequently, the T_{C-LC} will be reduced. An additional requirement for a stable liquid crystalline phase is that its T_c is above the T_{C-LC} and below decomposition temperature, T_d .

The tendency of the molecules to order and align themselves in a common direction with their long axes more or less parallel is referred in general as the *orientational property* of LCPs. The orientational property is fundamental for LCPs: for example, mechanical properties of LCPs are strongly dependent upon

the degree of orientational order (molecular orientation) (Hamley et al. 1996). This degree of order is responsible for the unique behaviour of liquid crystalline materials. The direction about which the degree of orientational order is defined is usually characterised by a unit vector \mathbf{n} (Allen et al. 1996), which satisfies the physically reasonable condition $\mathbf{n} \equiv -\mathbf{n}$. The vector \mathbf{n} is called the *director*, or optical axis (Noel 1992; Sarman 1996). The average molecular orientation described by the director should not be confused with the individual molecular orientation. The director \mathbf{n} is determined by relatively weak forces, such as magnetic and electric fields or the action of flow.

The director \mathbf{n} determines only the direction of the preferred orientation of the molecules and indicates nothing about the degree of orientational order in the liquid crystalline phase. The degree of the orientational order is quantified and characterised by a scalar quantity S , varying from zero to unity. S is called an *order parameter*, also known as Hermans orientation function (Pavel et al. 1999a, b), and it is calculated using the following equation (Schmidt-Rohr and Hong 1996):

$$S = 1/2 (3 \langle \cos^2\theta \rangle - 1)$$

The angular brackets around the cosine term in this equation denote a thermal average over all of the unit molecules and θ is the orientational angle between the structural unit vector (mesogen) of the polymer chain and the director \mathbf{n} .

The value of S equal to 0 ($\langle \cos^2\theta \rangle = 1/3$) indicates total absence of orientational order—isotropy. There are some exceptions for which S may be negative (Yoon et al. 1990; Rusing et al. 1993). The value of S equal to 1 corresponds to the case of the perfect order with all molecules strictly parallel to one another (Bosch et al. 1983). This ideal order would be possible near to absolute zero point of temperature only if the material would not freeze.

1. The order parameter of a material varies inversely with temperature as a result of kinetic molecular motion (Bosch et al. 1983). The actual value of S represents a compromise between the ordering effect of the mesogenic interaction and the disordering contribution of temperature (Marrucci 1996). In a typical LCP, S decreases as the temperature is raised, so S varies from around 0.43 at clearing temperature, T_c , to about 0.8–0.9 at much lower temperatures (Keller et al. 1990; Khoo 1995). For combined main-chain/side-chain macromolecules, two order parameters are to be calculated to describe the state of the polymer, one for the main-chain and one for the side-chains.

The order parameter is also known as the anisotropy factor. Anisotropy means that the properties of a material depend on the direction in which they are measured. Thus, liquid crystalline materials are optically anisotropic: for example, the propagation of a ray of light through the medium depends on its orientation.

LCs and LCPs can exhibit nematic, smectic, columnar, cholesteric and/or blue mesophase(s) due to their degree of molecular order. With rod-like molecules,

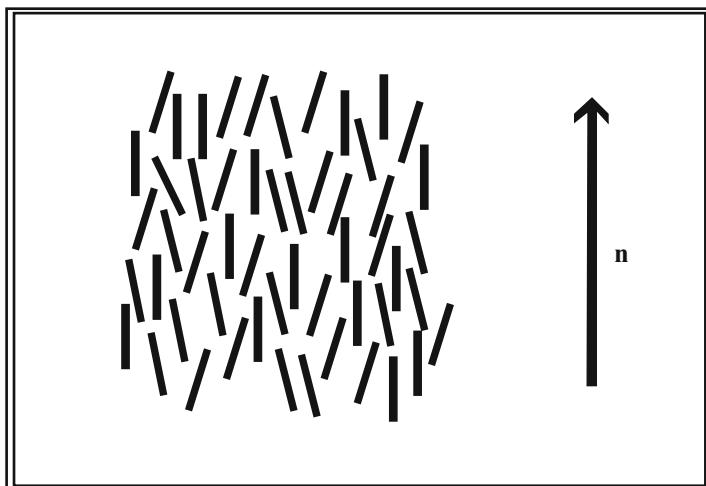


Fig. 16.9 Schematic representation of nematic liquid crystalline phase

nematic, smectic, blue and cholesteric mesophases are observed, whereas with disc-like (or discotic) molecules, the phases that are clearly identified fall into two categories: the columnar and the nematic. A smectic mesophase with discotic molecules has also been reported, but the precise arrangement of the molecules in each layer has not been fully investigated (Marrucci 1996).

The *nematic* phase is the least organized and the most common type of liquid crystalline phases. This phase is characterized when molecules are ordered in one dimension and the average directions of the long axes of the molecules (described by director \mathbf{n}) are parallel (Noel 1992; Islam et al. 2014). The nematic phase possesses long range orientational order but only short-range positional order (Davies and Ward 1988; Mulligan et al. 1996). Therefore, the nematic phase is very liquid-like. Optically, nematic liquid crystals constitute a uniaxial material. Unlike the classical nematic phase of rod-like molecules, the nematic phase of discotic molecules is optically negative. Schematic representation of the structure of nematic phase is shown in Fig. 16.9.

The *smectic* liquid crystalline phase is characterised when molecules possess a degree of long range orientational order as well as long range positional order: the molecules are parallel and arranged in layers which stack on top of each other (Fig. 16.10) (Davies and Ward 1988). If nematic and smectic phases occur within one compound, the smectic phases will occur at lower temperatures. The higher order of smectic phases causes them to be more viscous than nematic phases.

Many smectic phases have been observed, and they have been named in chronological order of discovery, *i.e.* smectic A, A1, A4, B, C, D, E, F, G, H, I, J, K phases (the least ordered smectic phase is smectic A). The smectic phases arise from differences within the layers of molecules. All of the smectic phases are

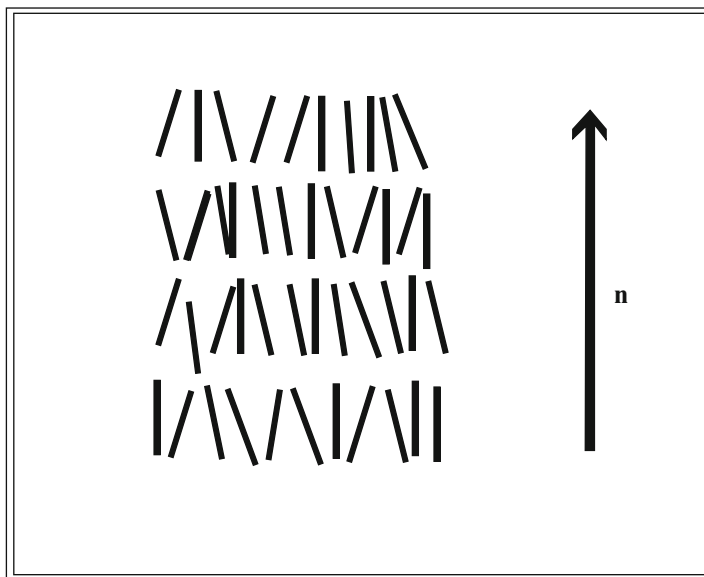


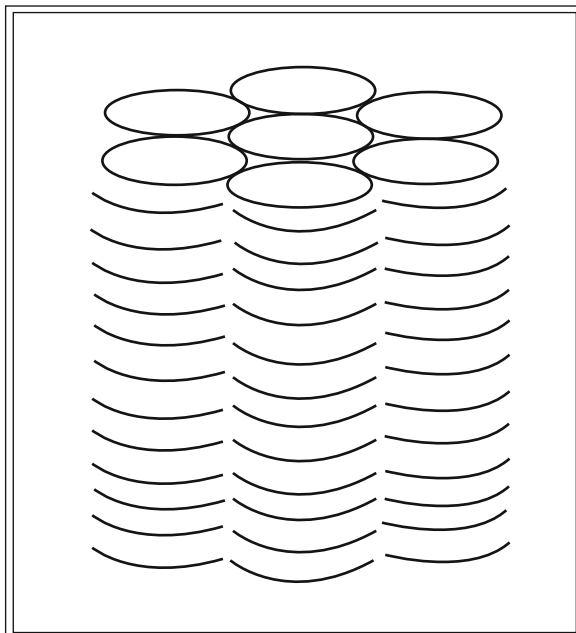
Fig. 16.10 Schematic representation of smectic liquid crystalline phase

characterised by the possession of a layered structure where the molecule ends are aligned next to each other. The ideal classification has yet to be achieved. The smectic phases also tend to be highly polymorphic and in some instances smectic liquid crystalline materials will transform between a number of sub-classes, *i.e.* A, A1, A4, B, C during heating or cooling (Davies and Ward 1988; Lan et al. 2013). In compounds where smectic polymorphism occurs, higher ordered phases always occur at lower temperature than lower ordered ones.

Columnar phases are formed on heating/cooling of compounds composed of disc-shaped molecules that can pack together to form flexible cylinders or columns of different type (resembling stacks of coins). The arrangement of disc-shaped molecules within an individual column can be either ordered or random. The columns themselves can be grouped into hexagonal or orthogonal lattices (Davies and Ward 1988; Stoeva et al. 2013). A schematic representation of the ordered hexagonal structure of columnar phase is given in Fig. 16.11.

In some cases, compounds that form columnar phases do not have a disc-like shape by themselves, but may aggregate into disc-like formations. Therefore, the often used term ‘discotic phase’ is not quite correct for the columnar phase, since it refers to building blocks that are not necessary prerequisite for obtaining this two-dimensional order. The columns are two-dimensionally ordered with nematic-like, hexagonal, rectangular or oblique packing. This distinct class of mesophase has only been recognised for a few years. In practice, columnar phases are relatively rare since a special disc-like geometry of the mesogen is required. The research effort on this phase is still somewhat limited, but increasing steadily.

Fig. 16.11 Schematic representation of columnar liquid crystalline phase



The *cholesteric* liquid crystalline phase is often referred to as “twisted nematic” or “chiral nematic” phase. The cholesteric phase is characterised by layers of nematic oriented molecules where each layer is twisted with respect to the ones above and below it (Blackwell and Biswas 1987; Davies and Ward 1988). A schematic representation of the structure of the cholesteric phase is illustrated in Fig. 16.12. The director \mathbf{n} in the cholesteric phase is not constant in space but, rather, twists periodically about an axis normal to \mathbf{n} , forming a helix. The distance over which the director turns exactly 360° is called the *pitch of the helix*. The helical arrangement also introduces new optical properties, particularly in the propagation and reflection of light from cholesteric liquid crystalline materials. The cholesteric phase possesses only orientational order, but neither long range order nor positional order of the molecules.

The *blue* phases appear between the cholesteric (helicoidal) liquid crystalline phase and the isotropic liquid phase, as the temperature is lowered (Hess et al. 1991). They are called ‘blue’ phases for historical reasons, so the adjective blue does not prevent them from looking bright yellow or red in some instances. The blue phases occur in cholesteric systems of sufficiently low pitch, less than about 5000 \AA (Brostow and Walasek 1998). The temperature region in which the blue phases are thermodynamically stable is relatively narrow, usually about 1 K. This fact has limited the progress of study of blue phases in contrast to other mesophases (Blackwell and Biswas 1987).

Three distinct blue phases have been identified: BP I (a body-centred cubic lattice), BP II (a simple cubic lattice) and BP III (probably amorphous) occurring

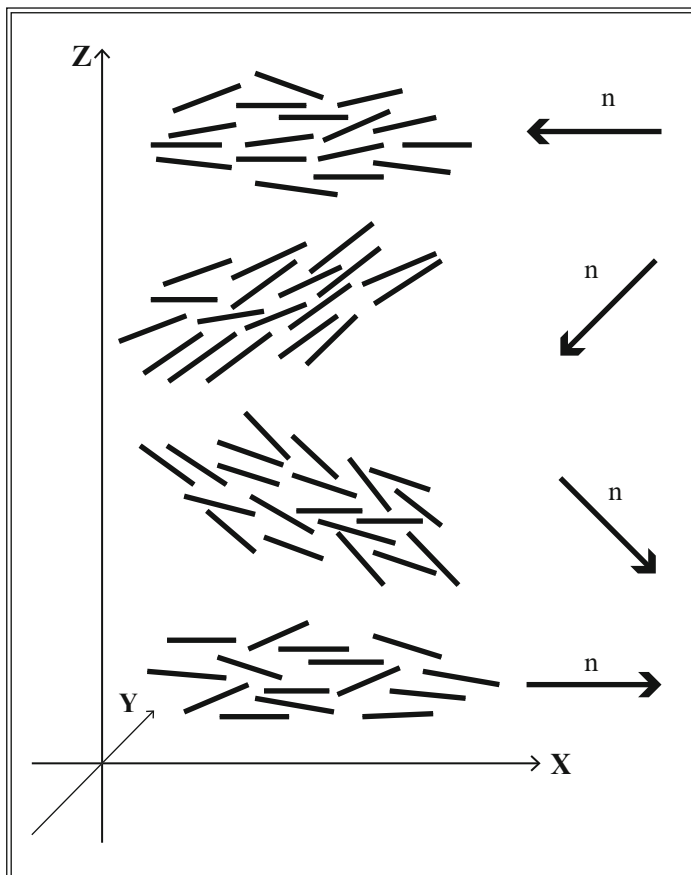


Fig. 16.12 Schematic representation of cholesteric liquid crystalline phase

in that order with increasing temperature (Brostow and Walasek 1998). The question of the molecular arrangement within the blue phases remained unsolved, so, it is impossible to provide a schematic representation of the phase at present. In practice, only nematic, cholesteric, smectic A and smectic C phases are commonly observed for LCPs, other higher-order smectic mesophases being comparatively rarer.

16.4 Theories of Liquid Crystalline Polymers

The anisotropic interactions between linear LCP macromolecules will be considered in this section. Two theoretical models, taking into account such applications, namely those of Flory and de Gennes, have found widespread use.

Flory's lattice model and his theory of liquid crystallinity in LCP systems were formulated in 1956. The theory was later amplified by Flory, his co-workers and students (Finkelmann 1991). Flory considered a system of unconnected linear semiflexible LCP chains, such that each macromolecule consists of flexible and LC sequences. The flexible sequences can coil and have high internal conformational entropy. The LC sequences are represented by rigid rods with low internal entropy, but they can interact anisotropically. As discussed in some, Flory developed an ingenious combinatorial procedure allowing the placement of LC sequences at any angle to the lines of the lattice. The procedure is based on the fact that macromolecules cannot penetrate each other.

A non-lattice approach was proposed by de Gennes and then developed by Walasek (Brostow 1992). De Gennes assumed a representation of the LCP system by a three-chain cell, with mutually perpendicular end-to-end distances. A chain consisted of freely-jointed segments with internal orienting interactions between them; thus, the chain was not fully flexible. The semiflexibility was determined by the intensity of the segment-segment interaction forces. One of the chains was parallel to the system symmetry axis while the other two were perpendicular to that axis. The distribution function of chain segment orientations was obtained by requiring that the Helmholtz function, with respect to the distribution function, became a conditional minimum. Conditions resulted from an independent definition of chain end-to-end distances; these distances were defined by border conditions imposed upon the system. Chains in the three-chain cell were connected via one end at a point. Necessarily, the model did not contain any information on the topological structure (such as loops, defects, etc.) present in a network of a large number of chains connected by copious junctions.

Brostow and Walasek considered a system of linear LCPs (Brostow 1992). Each macromolecule constituted an alternating copolymer of flexible and LC sequences. The macromolecules could be either unconnected, or else connected into a LCP network. The system was characterized with respect to local orientation. Competition between energetic effects of anisotropic orienting interactions between LC sequences and entropic effects determined mainly by flexible parts was considered. The Maier and Saupe mean-field approach (Klein et al. 1996) was assumed for the representation of LC interactions.

Since flexible chains can coil and create a large number of conformational microstates, their entropy is large. By contrast, in the theories under discussion, a LC sequence is represented by a hard rod and its internal entropy is equal to zero. Of course, the LC part as a whole has an entropy pertaining to the realization of orientational microstates, but its value is much smaller than the entropy of the flexible part.

Brostow and Walasek consider the LCP system in which the only orientation came from the presence of LC sequences in the chains. Orienting interactions between LC sequences were assumed. Interactions within flexible parts of the system and/or between flexible and LC parts were assumed to be much weaker than interactions between mesogenic LC particles. The segment + system interactions were imposed only by the topological structure of the LCP linear chain and by

the structure of the network of chains, the latter if the system of chains was connected by junctions. These authors considered the order parameter, S , since it is related to the uniaxial orienting interaction potential between LC units—as demonstrated long ago by Maier and Saupe and recently by Donald and Windle (Simmonds 1992). The more complicated potentials including pitch, chirality, etc., can presumably be introduced later. Brostow and Walasek found that the LC part was dominated by energetic effects related to orienting interactions. The competition between energetic and entropic effects led them to a general formula for the system Helmholtz function for arbitrary types of orienting interactions between LC sequences. It was found that all transitions were of the first order. They represented thermodynamical and structural parameters of the system at phase transition points by phase diagrams.

Both original Flory and de Gennes theories involve uniaxial nematic-like interactions between LC sequences. As a result, they predicted in LCPs, the transition from $S = 0$ to $S > 0$ only, as it takes place in molecular liquid crystals (MLCs) with uniaxial interactions.

Differences in S between LCPs and MLCs were qualitative only. However, experiments (Marrucci 1996; Saeva 1979) suggested possibilities of other types of transitions such as from $S = 0$ to $S < 0$ or from $S < 0$ to $S > 0$. Brostow and Walasek also showed that biaxiality of LC interactions in LCP systems was not a necessary condition for such transitions. This is contrary to the situation observed in MLCs in which the biaxiality is the necessary condition (Davies and Ward 1988).

16.5 Applications of Liquid Crystalline Polymers

LCPs present a unique balance of orientational, mechanical, magnetic, optical and electrical properties, high toughness, low die swell, easy flowability, outstanding chemical and thermal resistance, high modulus, and excellent dimensional stability. Therefore, LCP materials offer potential solutions for problems that conventional materials are unable to solve, and possible applications arise where the combination of these properties are basic requirements. These applications range from electrical-electronic components, chemical processing, transportation (including automotive and aerospace) and telecommunications, to high tensile strength polymeric fibers and components, thermography, holography and more recently to optical and electro-optical display devices, optical computing and medical science as diagnostic aids (Allen et al. 1996; Hoyt et al. 1990; Lee et al. 2012; Yagi et al. 2014; Cho et al. 2014; Morimoto et al. 2014; Huang et al. 2013; Jeong et al. 2013; Carter et al. 2014). Each of these areas requires different sets of properties that are summarized in Table 16.1.

In terms of performance requirements, cost factors and processing needs, LCPs can compete against other high-performance thermoplastics, ceramics and metals. Moreover, as new properties and types of LCPs are investigated and researched, these materials are sure to gain increasing importance in industrial and scientific applications and to become one of the most promising areas of material science.

Table 16.1 Correlation between the important properties of LCPs and potential areas of applications

Potential area of application	Important properties of LCPs	Examples of application
Electrical/electronics/ optoelectronics/ sensors	• Good thermal conductivity	Connectors, switches, relays bobbins, laser beam deflectors, potentiometers, electronic packaging, optical amplifiers, sensors, biosensors
	• High dielectric strength	
	• Low dielectric constant	
	• Resistance to solvents and corrosive chemicals	
	• Good electric insulation	
	• Low thermal coefficient of expansion	
	• High dimensional stability	
	• Low ionic content	
Information technology	• Excellent electrical	Data storage devices, liquid crystal displays, electro-optical devices, non-linear optics, flat-panel displays, optically-addressed spatial light modulators
	• Optical and non-linear properties	
	• Possibility to orient the molecules locally by action of electric or magnetic fields and more recently by action of light	
Fiber optics	• Inherent flame retardance	Couplers, connectors, strength members
	• Good moisture resistance	
	• Excellent mechanical properties	
Medical	• Non-toxicity	Cancer diagnosis, localizing the placenta prior Caesarean, thin films with high strength, optical filters and membranes, pharmacological tests, temperature indicators, diagnostic aids
	• Compatibility with sterilization techniques	
	• Low permeability and toughness	
Aircraft automotive	• Low coefficient of thermal expansion allowing mating with or replacement of metal parts	Electronic and electric related components, fuel system components, automobile parts
	• Excellent mechanical, chemical and electrical properties	
	• Excellent heat resistance	
	• Toughness	
	• Low viscosity during processing	
	• Easy filling of molds having complicated geometries	
	• Low thermal shrinkage	
	• Resistance to automotive fluids, solvents and other chemicals	

(continued)

Table 16.1 (continued)

Potential area of application	Important properties of LCPs	Examples of application
Chemical	• Excellent chemical and heat resistance	Pump housings, pump shafts, tower packing, valves, chemical analysis equipment, optical filters
	• Toughness	
	• Low flammability	
	• High strength	
	• High elastic modules	
	• The ability to incorporate high levels of fillers	
Domestic equipment	• Temperature resistance	Microwave equipment, cookware, compact disc components, films
	• Chemical resistance	
	• Microwave transparency	
	• Toughness	
	• Resistance to staining and abuse	
Other	Any of the above properties	High strength fibers for helmets and bulletproof vests, sport and leisure equipment, etc.

References

- Allen MP, Warren MA, Wilson MR, Sauron A, Smith W (1996) *J Chem Phys* 105(7):2850–2858
- Baur G (1982) *Polymer liquid crystals*. Academic, New York, pp 309–327
- Bhowmik PK, Lenz RW (1994) *J Polym Sci A Polym Chem* 32:651–659
- Biswas S, Fukushima H, Drzal LT (2011) Mechanical and electrical property enhancement in exfoliated graphene nanoplatelet/liquid crystalline polymer nanocomposites. *Compos A Appl Sci Manuf* 42(4):371–375
- Blackwell J, Biswas A (1987) In: Ward IM (ed) *Developments in oriented polymers*, vol 2. Elsevier, London, pp 153–198
- Blinov LM (1983) *Electro-optical and magneto-optical properties of liquid crystals*. Wiley, Chichester
- Bobrovsky A, Ryabchun A, Shibaev V (2011) Liquid crystals photoalignment by films of side-chain azobenzene-containing polymers with different molecular structure. *J Photochem Photobiol A Chem* 218(1):137–142
- Bosch AT, Maissa P, Sixou P (1983) *Phys Lett* 94A:6–7, 298–300
- Brostow W (1979) *Science of materials*. Wiley, New York, pp 65–71
- Brostow W (1992) *Liquid crystal polymers: from structures to applications*, polymer liquid crystals series, 1. In: Collyer AA (ed) *Elsevier applied science*. Elsevier, London, pp 1–30
- Brostow W, Walasek J (1998) *J Chem Phys* 108:6484–6496
- Carter BM, Wiesenauer BR, Noble RD, Gin DL (2014) Thin-film composite bicontinuous cubic lyotropic liquid crystal polymer membranes: effects of anion-exchange on water filtration performance. *J Membr Sci* 455:143–151
- Chandrasekhar S (1992) *Liquid crystals*, 2nd edn. Cambridge University Press, Cambridge
- Chen S, Shu X, Xie H-L, Zhang H-L (2013a) Synthesis and liquid crystalline behavior of 2,5-disubstituted styrene-based random copolymers: effect of difference in length of the rigid core on the mesomorphic behavior of mesogen-jacketed liquid crystalline polymers. *Polymer* 54(14):3556–3565

- Chen S, Luo H, Xie H-L, Zhang H-L (2013b) Synthesis of mesogen-jacketed liquid crystalline polymers with long symmetry mesogenic core containing two biphenyls. *Polymer* 54(7):1794–1802
- Cho W, Lee JW, Gal Y-S, Kim M-R, Jin SH (2014) Improved power conversion efficiency of dye-sensitized solar cells using side chain liquid crystal polymer embedded in polymer electrolytes. *Mater Chem Phys* 143(3):904–907
- Collyer AA (1996) In: Acierno D, Collyer AA (eds) *Rheology and processing of liquid crystal polymers, polymer liquid crystals series, vol 2*. Charman & Hall, London, pp 1–29
- Cook AG, Inkster RT, Martinez-Felipe A, Ribes-Greus A, Hamley I, Imrie CT (2012) Synthesis and phase behavior of a homologous series of polymethacrylate-based side-chain liquid crystal polymers. *Eur Polym J* 48(4):821–829
- Coolings PJ (1990) *Liquid crystals: nature's delicate phase of matter*. Princeton University Press, Princeton
- Damman SB, Mercx PM (1993) *J Polym Sci B* 31:1759–1767
- Davies GR, Ward IM (1988) *High modulus polymers: approaches to design and development, plastic engineering, 17*. Marcel Dekker, New York, pp 37–70
- De Gennes PG, Prost J (1993) *The physics of liquid crystals*. Clarendon, Oxford, pp 509–586
- Demeuse MT, Kiss G (2014) 5—Liquid crystal polymers (LCPs) as a reinforcement in high temperature polymer blends. In: Demeuse MT (ed) *High temperature polymer blends*. Woodhead, Kidlington, pp 141–164
- Donald AM, Windle AH (1992) *Liquid crystalline polymers*. Cambridge University Press, Cambridge, pp 50–59
- Dowell F (1990) *Liquid-crystalline polymers*. American Chemical Society, Washington, DC, pp 335–358
- Fakirov C (2012) Molecular liquid crystalline polymers reinforced polymer composites: the concept of “Hairy Rods”. In: Bhattacharyya D, Fakirov S (eds) *Synthetic polymer–polymer composites*. Hanser, Tampa, pp 281–299
- Finkelmann H (1991) *Liquid crystallinity in polymers: principles and fundamental properties*. VCH, New York, pp 315–340
- Flory PJ, Ronca G (1979) *Mol Cryst Liq Cryst* 54:289–310
- García T, Larios-López L, Rodríguez-González RJ, Martínez-Ponce G, Solano C, Navarro-Rodríguez D (2012) Liquid-crystalline polymers bearing phenylene(azobenzene) moieties substituted with an electron-donor or electron-acceptor lateral group. Synthesis, mesomorphic behavior and photo-induced isomerization. *Polymer* 53(10):2049–2061
- Gökçen M, Köysal O (2011) Effect of frequency on dielectric properties of liquid crystal doped with side-chain liquid crystalline polymer. *Mater Chem Phys* 129(3):1142–1145
- Guerriero G, Alderliesten R, Dingemans T, Benedictus R (2011) Thermotropic liquid crystalline polymers as protective coatings for aerospace. *Prog Org Coat* 70(4):245–251
- Ha SM, Lee HL, Lee S-G, Kim BG, Kim YS, Won JC, Choi WJ, Lee DC, Kim J, Yoo Y (2013) Thermal conductivity of graphite filled liquid crystal polymer composites and theoretical predictions. *Compos Sci Technol* 88:113–119
- Hall PJ, Tiddy GJT (1992) *Liquid crystal polymers: from structures to applications, polymer liquid crystals series, vol 1*. Elsevier Applied Science, London, pp 237–272
- Hamley W, Garnet S, Luckhurst GR, Roskilly SJ, Pendersen JS, Richardson RM, Seddon JM (1996) *J Chem Phys* 104(24):10046–10054
- Hashimoto H, Hasegawa M, Horie K, Yamashita T, Ushiki H, Mita I (1993) *J Polym Sci B* 31:1187–1196
- Hatakeyama ES, Gabriel CJ, Wiesenauer BR, Lohr JL, Zhou M, Noble RD, Gin DL (2011) Water filtration performance of a lyotropic liquid crystal polymer membrane with uniform, sub-1-nm pores. *J Membr Sci* 366(1–2):62–72
- Hatui G, Sahoo S, Das CK, Saxena AK, Basu T, Yue CY (2012) Effect of nanosilica and polyphosphazene elastomer on the in situ fibrillation of liquid crystalline polymer (LCP) and

- thermo-mechanical properties of polybutylene terephthalate (PBT)/LCP blend system. *Mater Des* 42:184–191
- Hess S, Frenkel D, Allen MP (1991) *Mol Phys* 74(4):765–774
- Hintze-Bruening H, Anne-Lise T, Leroux F (2011) Layered particle based polymer composites for coatings: part III—textured coatings obtained via lyotropic liquid crystals. *Prog Org Coat* 70(4):240–244
- Hornreich RM, Shtrikman S (1980) Liquid crystals of one- and two-dimensional order. In: Helfrich W, Hepcke G (eds) *Springer series in chemical physics*. Springer, Berlin, pp 185–195
- Hoyt AE, Benicewicz BC, Huang SJ (1990) *Liquid-crystalline polymers*. American Chemical Society, Washington, DC, pp 198–206
- Hsu T-C, Lu C-H, Huang Y-T, Shih W-P, Chen W-S (2011) Concentric polymer-dispersed liquid crystal rings for light intensity modulation. *Sensors Actuators A Phys* 169(2):341–346
- Huang W, Liu Y, Hu L, Quanquan M, Peng Z, Yang C, Xuan L (2013) Second-order distributed feedback polymer laser based on holographic polymer dispersed liquid crystal grating. *Org Electr* 14(9):2299–2305
- Hull JB, Jones AR (1996) *Rheology and processing of liquid crystal polymers, polymer liquid crystals series, 2*. Chapman & Hall, London, pp 245–246
- Hurduc N, Pavel D (1999) *Liquid crystalline polymers*. Junimea, Iasi
- Hurduc N, Stoleru A, Pavel D, Simionescu CI (1996a) *J Therm Anal* 47:735–741
- Hurduc N, Scutaru D, Barboiu V, Simionescu CI, Buisine JM, Daoudi A (1996b) *J Macromol Sci Pure Appl Chem A* 33:1745–1754
- Hurduc N, Daoudi A, Busine JM, Barboiu V, Simionescu CI (1998) *Eur Polym J* 34:123–125
- Iseki T, Kawabata K, Kawashima H, Goto H (2014) Catalysis direction selective asymmetric polymerization in chiral liquid crystal medium. *Polymer* 55(1):66–72
- Islam MT, Kamal T, Shin T, Seong B, Park S-Y (2014) Self-assembly of a liquid crystal ABA triblock copolymer in a nematic liquid crystal solvent. *Polymer* 55:16
- Jeong J, Lee SW, Min KS, Kim SJ (2013) A novel multilayered planar coil based on biocompatible liquid crystal polymer for chronic implantation. *Sensors Actuators A Phys* 197:38–46
- Jia L, Pierre-Antoine A, Cicco AD, Cao A, Li M-H (2011) Self-assembly of amphiphilic liquid crystal block copolymers containing a cholesteryl mesogen: effects of block ratio and solvent. *Polymer* 52(12):2565–2575
- Kakiuchida H, Tazawa M, Yoshimura K, Ogiwara A (2013) Optical diffractometry of anisotropic holographic structure composed of liquid crystal and polymer phases with extended Bragg modes. *Thin Solid Films* 571:431–436
- Kelker H, Hatz R (1980) *Handbook of liquid crystals*. Verlag Chemie, Weinheim, pp 593–602
- Keller A, Ungar G, Percec V (1990) *Liquid crystalline polymers*. American Chemical Society, Washington, DC
- Khoo IC (1995) *Liquid crystals: physical properties and nonlinear optical phenomena*. Wiley, New York, pp 67–70
- Kim SE-UM, Lee S, Na J-H, Lee S-D (2014) Tunable liquid crystal lens array by encapsulation with a photo-reactive polymer for short focal length. *Opt Commun* 313:329–332
- Klein PG, Evans BW, Ward IM (1996) *Liquid-crystalline polymer systems: technology advances, vol 632, ACS Symposium Series*. American Chemical Society, Washington, DC, pp 249–258
- Kuwahara Y, Kaji M, Okada J, Kim S, Ogata T, Kurihara S (2013) Self-alignment and photomechanical properties of alternative multi-layered films containing azobenzene polymer liquid crystal and polyvinyl alcohol layers. *Mater Lett* 113:202–205
- Lai Y-T, Kuo J-C, Yang Y-J (2014) A novel gas sensor using polymer-dispersed liquid crystal doped with carbon nanotubes. *Sensors Actuators A Phys* 215(15):83–88
- Lan Y-F, Tsai C-Y, Lu J-K, Sugiura N (2013) Mechanism of hysteresis in polymer-network stabilized blue phase liquid crystal. *Polymer* 54(7):1876–1879
- Lee SY, Park K-IL, Huh C, Koo M, Yoo HG, Kim S, Chil Seong AH, Sung GY, Lee KJ (2012) Water-resistant flexible GaN LED on a liquid crystal polymer substrate for implantable biomedical applications. *Nano Energy* 1(1):145–151

- Li J, Turunen M, Niiranen S, Chen H, Paulasto-Kröckel M (2012) A reliability study of adhesion mechanism between liquid crystal polymer and silicone adhesive. *Microelectron Reliab* 52(12):2962–2969
- Liang X, Lu X, Yu M, Cavanagh AS, Gin DL, Weimer AW (2010) Modification of nanoporous supported lyotropic liquid crystal polymer membranes by atomic layer deposition. *J Membr Sci* 349(1–2):1–5
- Liu D, Wu Q, Chang PR, Gao G (2011) Self-assembled liquid crystal film from mechanically defibrillated chitosan nanofibers. *Carbohydr Polym* 84(1):686–689
- Liu H, Zi-En F, Xu K, Hua-Lun C, Liu X, Chen M-C (2012) Preparation and characterization of high performance Schiff-base liquid crystal diepoxide polymer. *Mater Chem Phys* 132(2–3):950–956
- Maier M, Saupe A (1959) *Naturforsch* 14A:882
- Malik P, Raina KK (2010) Dichroic dye-dependent studies in guest–host polymer-dispersed liquid crystal films. *Phys B Condens Matter* 405(1):161–166
- Marrucci G (1996) Rheology and processing of liquid crystal polymers, polymer liquid crystals series, vol 2. Chapman & Hall, London, pp 30–48
- Morimoto M, Makino Y, Gonda J, Misaki M, Ishida K, Ueda Y, Kubono A (2014) Electrorheological response of the interfacial layer between a liquid crystal and a polymer alignment sublayer. *Thin Solid Films* 558:227–230
- Moritsugu M, Sun-Nam K, Kubo S, Ogata T, Nonaka T, Sato O, Kurihara S (2011) Photoswitching properties of photonic crystals infiltrated with polymer liquid crystals having azobenzene side chain groups with different methylene spacers. *React Funct Polym* 71(1):30–35
- Mulligan DR, Imrie CT, Lacey P (1996) *J Mater Sci* 31:1985–1989
- Noel C (1992) Liquid crystal polymers: from structures to applications, polymer liquid crystals series, vol 1. Elsevier Applied Science, London, pp 31–102
- Pankaj Kumar, Neeraj S-WK, Lee SH, Raina KK (2011) Analysis of dichroic dye-doped polymer-dispersed liquid crystal materials for display devices. *Thin Solid Films* 520(1):457–463
- Patnaiks S, Plimpton S, Pacher R, Adams WW (1995) *Liq Cryst* 19:213–220
- Pavel D, Ball J, Bhattacharya S, Shanks R, Hurduc N (1997) *Polymer* 38(A):7–11
- Pavel D, Ball J, Bhattacharya S, Shanks R, Hurduc N (1999a) *J Polym Sci B Phys* 37:2334–2352
- Pavel D, Ball J, Bhattacharya S, Shanks R, Hurduc N (1999b) *J Comput Theor Polym Sci* 9:1–19
- Petr M, Helgeson ME, Soulages J, McKinley GH, Hammond PT (2013) Rapid viscoelastic switching of an ambient temperature range photo-responsive azobenzene side chain liquid crystal polymer. *Polymer* 54(12):2850–2856
- Rusing I, Dedier J, Filliatre C, Godinho MH, Varichon L, Sixou P (1993) *J Polym Sci Phys* 31:595
- Saeva D (1979) Liquid crystals—the fourth state of matter. Marcel Dekker, New York
- Sarman S (1996) *J Chem Phys* 104(1):342–350
- Schmidt-Rohr K, Hong M (1996) *J Phys Chem* 100:3861–3866
- Simmonds DJ (1992) Liquid crystal polymers: from structures to applications, polymer liquid crystals series, vol 1. Elsevier Applied Science, London, pp 349–406
- Sordi D, Orlanducci S, Tamburri E, Passeri D, Lucci M, Terranova ML (2011) Self organisation and photoinduced charge transfer in single-wall carbon nanotubes embedded in a thermotropic liquid crystal polymer. *Carbon* 49(7):2227–2234
- Stoeva Z, Lu Z, Ingram MD, Imrie CT (2013) A new polymer electrolyte based on a discotic liquid crystal triblock copolymer. *Electrochim Acta* 93:279–286
- Su Y-C, Chu C-C, Chang W-T, Hsiao VKS (2011) Characterization of optically switchable holographic polymer-dispersed liquid crystal transmission gratings. *Opt Mater* 34(1):251–255
- Suga Y, Takahama T (1996) *Polym Mater Sci Eng* 74:268–269
- Sun XH, Tao XM (2011) Switchable photonic crystal for polymer dispersed liquid crystal. *Opt Laser Technol* 43(4):820–824
- Sung S-J, Jung E-AE, Sim K, Kim D-H, Cho KY (2013) Structure control of lattice-patterned liquid crystals—polymer composites prepared by polarization-selective UV-curing through the addition of a fluorinated acrylate monomer. *Microelectr Eng* 103:42–48

- Takahashi C, Yoshihara S, Kang S, Sakajiri K, Watanabe J, Tokita M (2014) Decrease in the isotropization temperature and enthalpy of main-chain polymer smectic liquid crystals as a result of the inclusion of chain ends. *Polymer* 55(10):2609–2613
- Tu M, Han W, Zeng R, Best SM, Cameron RE (2012) A study of surface morphology and phase separation of polymer/cellulose liquid crystal composite membranes. *Colloids Surf A Physicochem Eng Asp* 407:126–132
- Walasek J (1990) *J Polym Sci Phys* 28:2473–2485
- Wang S, Yang Z, Mo Z, Zhang H, Feng Z (1996) *Polymer* 37(19):4397–4402
- Wang B, You Y, Huo Y (2011) Opto-thermo actuation of multilayered liquid crystal polymer films. *Thin Solid Films* 519(15):5310–5313
- Wang L, Meng F, Sun Y, Yang H (2013) Effect of surfactant-modified ZnS:Mn nanoparticles on the electro-optical properties of composite polymer-dispersed liquid crystal films. *Compos B Eng* 45(1):780–784
- Wenyi H, Shi ER (2012) High-performance thermotropic starch-based liquid crystalline polymer. *Carbohydr Polym* 90(1):703–708
- Wright RV, Hakemi G, Kirby PB (2011) Integration of thin film bulk acoustic resonators onto flexible liquid crystal polymer substrates. *Microelectr Eng* 88(6):1006–1009
- Yagi R, Katae H, Kuwahara Y, Kim S-N, Ogata T, Kurihara S (2014) On-off switching properties of one-dimensional photonic crystals consisting of azo-functionalized polymer liquid crystals having different methylene spacers and polyvinyl alcohol. *Polymer* 55(5):1120–1127
- Yang K-J, Yoon D-Y (2011) Electro-optical characteristics of dye-doped polymer dispersed liquid crystals. *J Ind Eng Chem* 17(3):543–548
- Yao K, Chen L, Hu T, Chen Y (2012) Photocrosslinkable liquid-crystalline polymers for stable photovoltaics by adjusting side-chains spacing and fullerene size to control intercalation. *Org Electr* 13(8):1443–1455
- Yilmaz Canli N, Safak-Boroglu M, Bilgin-Eran B, Günes S (2014) Bilayer polymer/fullerene solar cells with a liquid crystal. *Thin Solid Films* 560:71–76
- Yoon DY, Masiocchi N, Depero LE, Viney C, Parrish W (1990) *Macromolecules* 23:1793–1798
- Yu L, Wei W, Xiong H (2013) Polyether based side-chain liquid crystalline polymers. Anionic polymerization and phase structures. *Polymer* 54(24):6572–6579
- Zentel R, Brehmer M (2012) 8.06—Electroactive liquid crystalline polymers. In: Krzysztof M, Martin M (eds) *Polymer science: a comprehensive reference*. Elsevier, Amsterdam, pp 129–145
- Zentel R, Kapitza H, Kremer F, Vallerien SU (1990) Liquid-crystalline polymers. *American Chemical Society, Washington, DC*, pp 207–217

Chapter 17

Smectic Phases of Liquid Crystalline Rod-Like Helical Polymers

Kento Okoshi

17.1 Introduction

In addition to the conventional liquid crystal molecules with aromatic mesogens and aliphatic tails, which are typically used in display devices, miscellaneous kinds of materials, i.e., DNA (Livolant and Bouligant 1986; Strzelecka et al. 1988a), viruses (Wen et al. 1989; Dozic and Fraden 1997; Adams et al. 1998; Lee et al. 2002, 2003), colloidal suspensions of crystal particles (Li et al. 2002; Gabriel et al. 2001), form liquid crystal phases even though they have different chemical properties. The common feature of these materials is their rod-shape (or disc shape) so that the long axis (or short axis when disc shaped) of the neighboring molecules can spontaneously align in a parallel manner. That is to say, the origin of liquid crystallinity is largely derived from the packing entropy of anisotropic shapes (excluded volume effect), thus it could be appropriate to evaluate them using physical models of rigid rod-like (or disc-like) particles.

These theoretical studies have been extensively performed both with numerical calculations and computer simulations to prove the entropically-driven liquid crystal formation, since the initial approach of Onsager's (Onsager 1949) and Flory's (Flory 1956) theoretical attempts to reproduce the nematic— isotropic transition. The series of studies blossomed into the reproduction of the most commonly observed liquid crystal phase sequence of the nematic—smectic—columnar phases of the monodisperse-length rigid-rod-like particle systems in the 1980s (Hosino et al. 1979, 1982; Stroobants et al. 1987; Veerman and Frenkel 1991; Bolhuis and Frenkel 1997), showing the possibility of an unexpected wide variety of liquid crystalline phases including the smectic phase in simple hard-rod systems.

K. Okoshi (✉)

Department of Bio- and Material Photonics, Chitose Institute of Science and Technology,
758-65 Bibi, Chitose, Hokkaido 066-8655, Japan
e-mail: k-okoshi@photon.chitose.ac.jp

It has also been shown that the gain in packing entropy exceeding the loss of translational entropy could be the major driving force of the liquid crystalline phase transition. Since then, these theoretical studies have centered on the lyotropic hard-rod systems with only entropy taken into consideration, and expanded from rod-like particles to disc-shaped (Veerman and Frenkel 1992), ellipsoidal (Frenkel et al. 1984), biaxial particles (Michael 1990), and mixtures, seemingly beyond the scope of the practical experimental verifications.

The detailed experimental verification of the theoretical predictions of the smectic phase in the simple hard-rod systems was first reported in biological systems because artificial systems are hardly ever truly monodispersed. The smectic phase and smectic—nematic lyotropic phase sequence in the aqueous dispersion of the tobacco mosaic virus (TMV) were determined in 1989 (Wen et al. 1989), followed by a number of studies on similar virus systems (Dozic and Fraden 1997; Adams et al. 1998; Lee et al. 2002, 2003). The monodispersed rod-like poly(γ -benzyl-L-glutamate) prepared by a bacterial synthetic method has also been reported to exhibit a smectic phase and twist grain boundary-like smectic phase in 1997 (Yu et al. 1997; He et al. 1998). However, it takes a very time-consuming and cost-intensive procedure to prepare the monodispersed polypeptide (Zhang et al. 1992), in which the bacterial protein expression of the artificial gene encoding the peptide sequence is followed by purification and benzylation of the product. Therefore, no further detailed experimental study on the smectic phase in the monodispersed polypeptide system has been performed, while all the other studies have been on viruses which are also not easy to handle.

17.2 Liquid Crystalline Phase Behavior of Rod-Like Polymers

17.2.1 Theoretical Predictions

The first indication of the most commonly observed liquid crystalline phase transition of smectic—nematic—isotropic in the rigid-rod particle systems was shown by the mean field approximation, in which the free energy of the rigid-rod particles described by a positional and orientational order is reduced to a minimum, as reported by Kimura et al. in 1979 (Hosino et al. 1979). Later, in 1987, the entire phase diagram versus the aspect ratio (ratio of length to diameter of the rod-like particle) and reduced volume density (defined as ρ/ρ_{CP} , where ρ_{CP} is the close packed density) of the rod-like particles has been revealed by computer simulations (Fig. 17.1a) (Stroobants et al. 1987), indicating that the columnar—smectic—nematic phase transition takes place (without isotropic phase due to the uniform alignment approximation), although the stability of the columnar phase was found to be susceptible to the system size of the simulation in a following study (Veerman

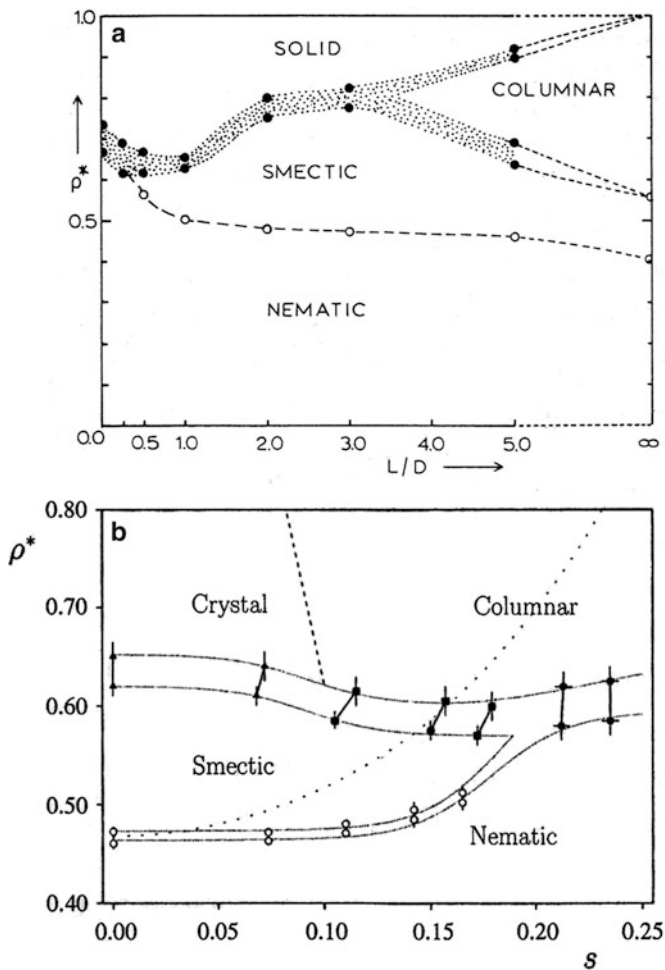


Fig. 17.1 Computed phase diagram of (a) monodisperse (Stroobants et al. 1987) and (b) polydisperse (Bates and Frenkel 1998) length hard parallel rod-like particle systems as a function of the aspect ratio and reduced volume density of the particles for (a), and polydispersity and reduced volume density of the particles for (b)

and Frenkel 1991). Interestingly, a similar result had been indicated only with the attractive potential taken into consideration in 1971 (Kobayashi 1970; McMillan 1971).

The rod-like particle systems with a length polydispersity have also been computed (Bates and Frenkel 1998) because further detailed experimental studies should be performed with easy-to-handle artificial rod-like polymer systems which inevitably possess a polydispersity. Figure 17.1b shows the phase diagram in the limit of the infinite aspect ratio drawn as a function of the polydispersity of the rod

length, s (standard deviation when the average length is unity) and reduced volume density. The smectic phase is increasingly destabilized compared to the nematic phase and depleted at $s = 0.18$ (which corresponds to $M_w/M_n = 1.03$, assuming the normal distribution.), although the phase behavior is almost the same as with the monodispersity for a low polydispersity, $0 < s < 0.08$. These results naturally lead us to the idea that even synthetic stiff polymers form a smectic phase when their polydispersity is quite narrow.

17.2.2 Experimental Verifications

The synthetic helical polymers are the most suitable for the experimental verification of these theoretical predictions because this group of polymers is stiff enough to be regarded as a rigid rod. The first clear finding of a smectic phase in the synthetic helical polymer system was achieved with a polysilane (poly-1 in Fig. 17.2a) (Okoshi et al. 2002a) which takes an exceptionally rigid helical conformation with the persistence length of 85 nm due to the severe restriction on the main chain conformation caused by the steric hindrance between the long and branched alkyl side chains (Fujiki 1996; Terao et al. 2001), although ambiguous indications of the smectic phase had been reported with DNA and a synthetic peptide based only upon polarized optical microscopic observations (Strzelecka et al. 1988b; Watanabe and Takashina 1992). The thermotropic smectic phases formed by poly-1, 2, 3 (Fig. 17.2a) have been intensively studied, even though these should be lyotropic systems to verify the theoretical predictions of the rigid-rod particle systems. This is because the long alkyl chain behaves as the solvent in the thermotropic system, and this makes it possible to avoid some experimental difficulties, such as solvent evaporation, phase separation, and sedimentation in the lyotropic solutions. Moreover, it is easy to narrow the molecular weight (molecular length) distributions of poly-1, 2, 3 to such an extent that M_w/M_n is approximately 1.1 by simple solvent fractionation because there is little polymer aggregation in the nonpolar solvent due to the nonpolar and stiff (rod-like) nature of the polysilanes. As predicted, the thermotropic liquid crystalline phase behavior of poly-1, 2, 3 strongly depends on the polydispersity of their molecular weight, as it shows a nematic (cholesteric) phase when its M_w/M_n is high, while it shows a smectic phase when its M_w/M_n is low (Okoshi et al. 2002a).

Figures 17.2b–d show the polarized optical micrograph of poly-1 and small- and wide-angle X-ray scattering patterns of the oriented sample of poly-3 with a narrow molecular weight distribution prepared in the same way. Not only the focal conic texture indicative of the smectic phase can be observed in the micrograph as clearly as in low molecular weight smectic liquid crystals, but also that the small-angle X-ray scattering pattern (Fig. 17.2c) revealed smectic layer reflections on the meridional line in the orientation direction (Okoshi et al. 2010). These reflections are perpendicular to the several reflections on the equatorial line in the wide-angle X-ray scattering pattern (Fig. 17.2d), which are assigned to the two-dimensional

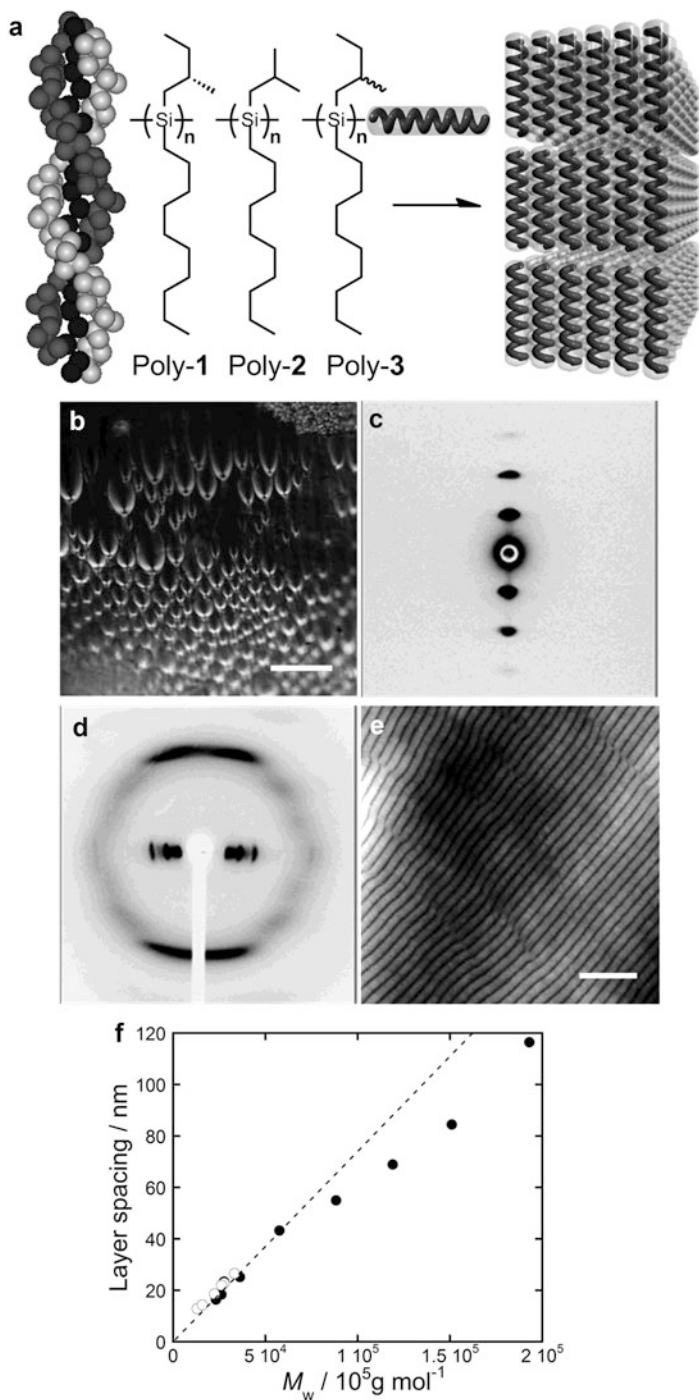


Fig. 17.2 (a) Illustrations of the structures of polysilanes and their smectic liquid crystal formation. (b) Polarizing optical microscopic image of poly-1 (scale bar: 100 μm). (c) Small- and (d) wide-angle X-ray diffraction patterns of poly-3 (Okoshi et al. 2010). (e) AFM phase image observed on the cast film of poly-2 (scale bar: 200 nm). (f) Smectic layer spacings observed in poly-2 along with small-angle X-ray diffractions (open squares) and AFM (closed circles) (Oka et al. 2008)

orthogonal lattice of the lateral polymer packing (Okoshi et al. 2002a). This is clear evidence of the apparent smectic B phase where molecules oriented perpendicular to the smectic layers are arranged in a close-packed lattice. This smectic layer can also be directly observed by atomic force microscopy (AFM) as shown in Fig. 17.2e. The AFM image was taken on the top surface of a 1- μm thick cast film of polysilane on a glass substrate after annealing in saturated solvent vapor (Oka et al. 2008). The observed banding pattern is so regular that its correlation length seemingly extends beyond the microscopic field of view although the molecular distribution in smectic layers is generally described as sinusoidal in liquid crystal textbooks. The observed banding repeats, which is over 200 nm at most, far beyond its persistence length, were plotted as closed circles versus the molecular weight, while the smectic layer spacings obtained from the X-ray diffraction were plotted as open circles in Fig. 17.2f (Oka et al. 2008). Most of the plots are on the dotted line which represents the polymer length calculated from $1.96 \text{ \AA} (\text{unit translation}) \times n$ (degree of polymerization), although both the theoretical and computational studies predicted that the smectic layer spacings are 1.2–1.4 times longer than the molecular lengths. The further quantitative analysis requires the absolute molecular weight measurements because this might be due to the overestimated molecular weights for stiff polymers measured by size exclusion chromatography (SEC) with polystyrene standard calibrations.

The smectic fan-shaped optical microscopic texture of poly-1 gradually turned into a Grandjean texture with oily streaks characteristic of the cholesteric phase upon heating at around $150 \text{ }^\circ\text{C}$ (Figs. 17.3a, b) (Okoshi et al. 2004a), although the development of the fan-shaped texture upon cooling can be observed only at the air interface and not in the entire field of view. Almost concurrently, the smectic layer reflection in the small-angle X-ray scattering disappeared (Fig. 17.3d) and a selective reflection band of the cholesteric phase appeared in the CD spectra (Fig. 17.3e) at around the same temperature after the disappearance of the reflections from the two-dimensional lattice of the lateral polymer packing in the wide-angle X-ray scattering at the lower temperature upon heating (Fig. 17.3c). These results clearly indicated that poly-1 shows the smectic B—smectic A—cholesteric (chiral nematic) phase transition although it is still unclear whether the smectic B phase corresponds to the predicted smectic phase with the columnar hexagonal lattice in the transverse direction that appeared in the large scale simulation or the non-equilibrium state from the smectic phase to the columnar phase predicted by the small scale simulation (Veerman and Frenkel 1991).

The entire phase diagram of poly-1 was revealed by plotting the phase transition temperature versus the molecular weight (Fig. 17.3f). The cholesteric phase can be observed only with low molecular weight samples because high molecular weight samples start to decompose over $200 \text{ }^\circ\text{C}$ prior to the phase transition. Poly-2 and 3 also show a similar phase transition behavior except for the nematic phase instead of the cholesteric phase due to a lack of optical activity. While most of the theoretical predictions have been made on athermal lyotropic systems, the phase behavior of polysilane nevertheless reproduced the predicted columnar—smectic—

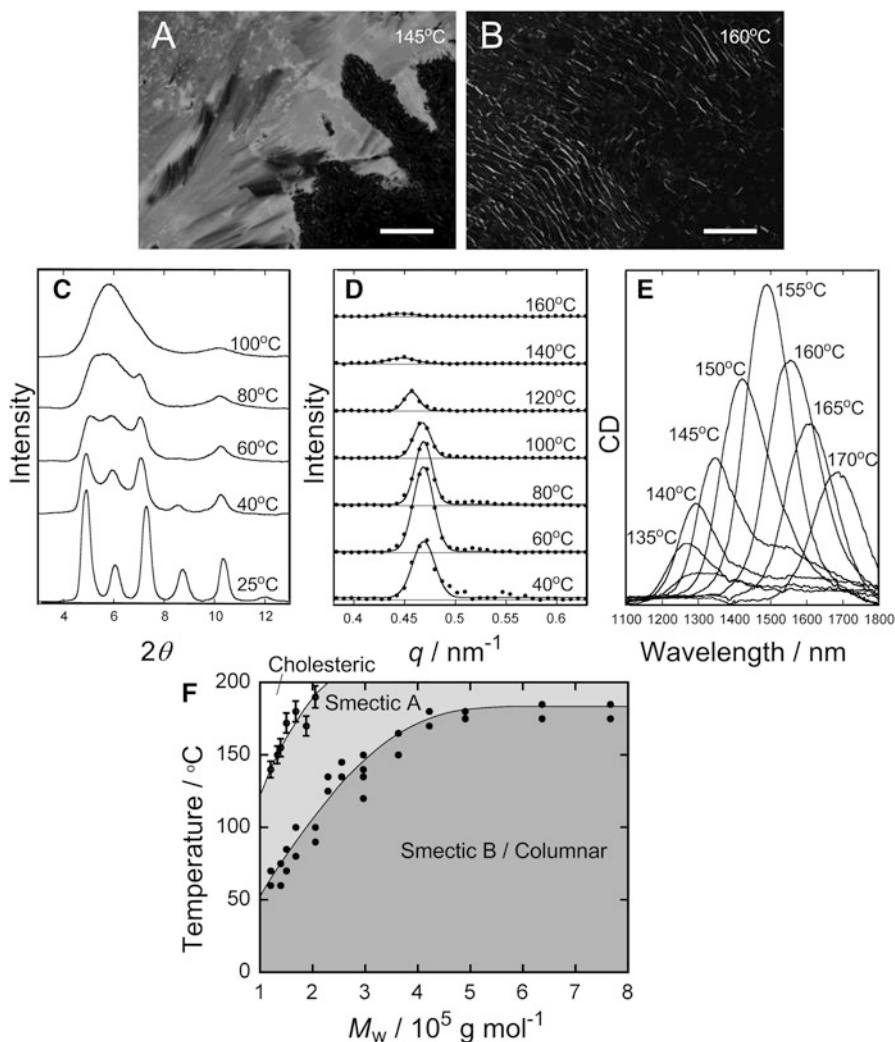


Fig. 17.3 (a, b) Polarizing optical microscopic images (scale bars: 100 μm) (Okoshi et al. 2004a), (c) small-angle, (d) wide-angle X-ray diffraction patterns, and (e) CD spectra of poly-1 taken over the smectic-cholesteric liquid crystal phase transition temperature. (f) Phase diagram of poly-1 as a function of the molecular weight and temperature

nematic liquid crystal phase sequence when the decrease in the reduced volume density is taken as the increase in temperature.

Similar results have been reported with polypeptide (Okoshi et al. 2002b) and polyisocyanide (Onouchi et al. 2008). The polyisocyanide has an extremely stiff backbone with the persistence length of 220 nm due to the tight intramolecular hydrogen bonding networks between the neighboring side chains (Fig. 17.4)

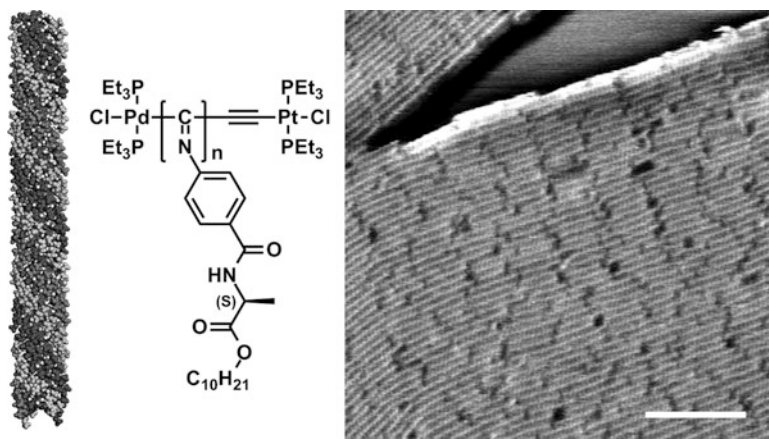


Fig. 17.4 Structure of the polyisocyanide and AFM image showing the molecular arrangement within the smectic layers (scale bar: 30 nm) (Onouchi et al. 2008)

(Okoshi et al. 2008), which makes it possible to visualize the molecular arrangement within the smectic layers by AFM observations. The observed AFM image in Fig. 17.4 shows how polymers with a length polydispersity beyond the predicted limit of $M_w/M_n = 1.03$ are packed within a layer to extend the correlation length of the smectic layers. The polymers with different lengths are seemingly arranged within a layer in such a manner that the concavity and convexity of the layers match between the layers to align the center of gravity of the polymers within the layer, which is the only way to maintain the layer structure even with the length polydispersity of the component. This result is also supported by X-ray structural analyses of the smectic layers in the phase transition process (Okoshi et al. 2004b).

17.3 Smectic Phases of Binary Mixtures of Rod-Like Polymers

17.3.1 Theoretical Predictions

In order to assess the effect of the length polydispersity on the liquid crystal phase formation, binary mixtures of rod-like particles with different lengths have been computed because novel incommensurate smectic phases can be expected to fit together the smectic layers with different layer spacings, although it is intuitively understandable that the length polydispersity of the rod-like particles hampers the smectic phase formation because it is difficult for rods with different lengths to fit in the same smectic layer.

Koda et al. performed a theoretical study of the binary system of rod-like particles with different lengths using the mean field approximation to predict the formation of three types of smectic phases (Koda and Kimura 1994). That is to say, by adding a small fraction of shorter rods to longer rods, both the short and long rods are mixed within a smectic layer if the length ratio is below 2.5. However, smectic layers of short rods are alternately stacked with that of the long rods when the length ratio is over 2.5, and these are segregated from each other with the length ratio over 5.0. Varga et al. predicted four different types of smectic phases (see Fig. 17.5)

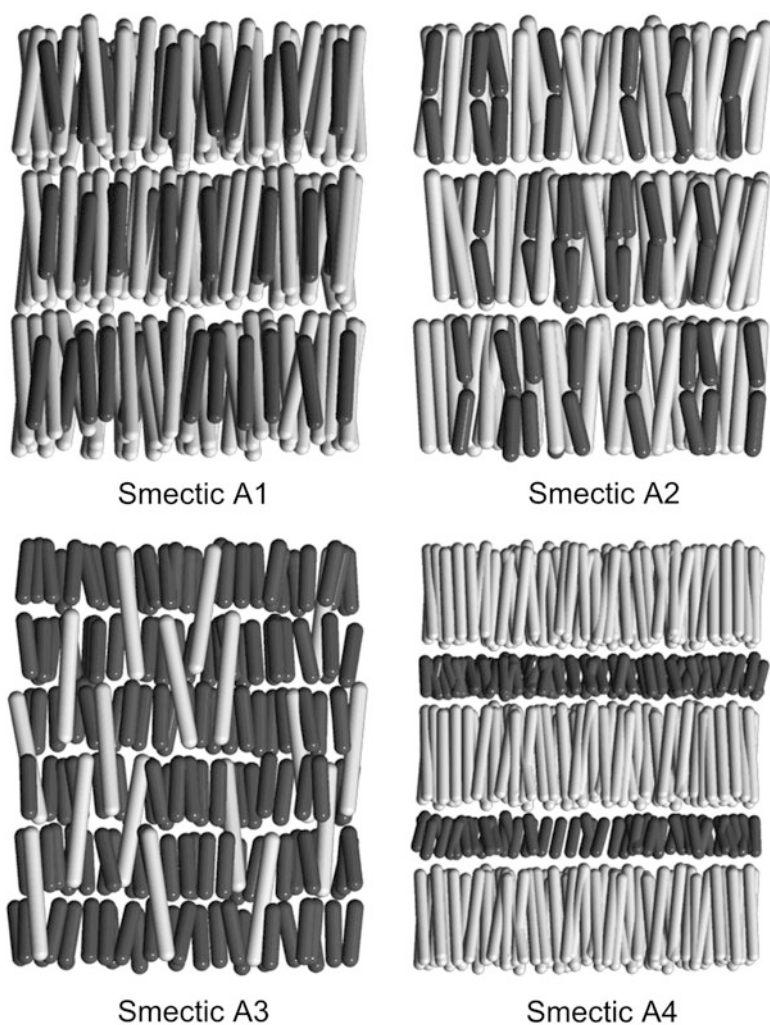


Fig. 17.5 Illustrations of four predicted different types of smectic phases in the binary mixture of rod-like particles with different lengths

depending on the mixing ratio and the length ratio of the short and long rods in the binary mixture of rod-like particles: (1) short and long rods with the length ratio of 1.5 are mixed within the same smectic layer regardless of the mixing ratio (called this smectic A1 for the sake of expediency); (2) a smectic layer of long rods accommodates two smectic layers of short rods in the mixture of scarce short rods and abundant long rods with the length ratio of 2.0 (smectic A2); (3) long rods randomly straddle a pair of smectic layers of short rods in the mixture of abundant short rods and scarce long rods with the length ratio of 2.0 (smectic A3), even though the smectic phase is destabilized between smectics A2 and A3; and (4) smectic layers of short rods and smectic layers of long rods alternately stacked in the mixture of scarce short rods and abundant long rods with the length ratio of 3.3 (smectic A4), which is destabilized and turns into the nematic phase with abundant short rods and scarce long rods (Varga et al. 2009; Varga and Velasco 2010).

These somewhat surprising predictions, however, had never been verified because there have been no appropriate experimental systems of rod-like particles with freely adjustable lengths.

17.3.2 *Experimental Verifications*

The structural analyses of the smectic phases in the binary mixture of polysilanes with different molecular weights have been performed and provided an answer to this question. The observed layer spacings in the X-ray diffractions of the binary mixtures (normalized by the layer spacings of the short polymers) at the mixing ratio of 0.75 (weight of long polymer / weight of binary mixture) were plotted versus the molecular weight ratios (long polymer / short polymer, which should be the length ratio) in Fig. 17.6 (Okoshi et al. 2009). When the molecular weight ratio is relatively low (<1.7), only one reflection is observed whose spacing corresponds to the average molecular length (solid line in Fig. 17.6), assuming that both are completely mixed within a layer. Thus, the structure of smectic A1 is formed in this range of molecular weight ratios. In contrast, with a higher molecular weight ratio (>1.7), they show two reflections with the larger spacing twice as long as the shorter one, regarded as the first and second order reflections. However, with the decreasing mixing ratio of the long polymer, only the first order reflection disappeared and the second order reflection remained. The only plausible explanation for this is the conversion from smectic A2 to smectic A3 because the second order reflection, intensified by the low electron density part at the center of the smectic layer of long polymer, should turn into the smectic layer reflection of smectic A3 after the long polymer smectic ordering disappeared upon adding the short polymer. These characteristic smectic layer structures were confirmed by the AFM observations. Figure 17.7 shows the AFM images of the binary mixtures with the molecular weight ratio of 2.49 and varying mixing ratios (Okoshi et al. 2009). The bandings observed in the long polymer (Fig. 17.7a), which are characteristic of repeating smectic layers, are found to split into two narrow bandings upon adding

Fig. 17.6 Layer spacings observed in the binary mixtures with the mixing ratio of 0.75 plotted versus the molecular weight ratio. Layer spacings are normalized by the layer spacings observed in each of the short polymers, which are represented by the *circles, squares, triangles, and diamonds* (Okoshi et al. 2009)

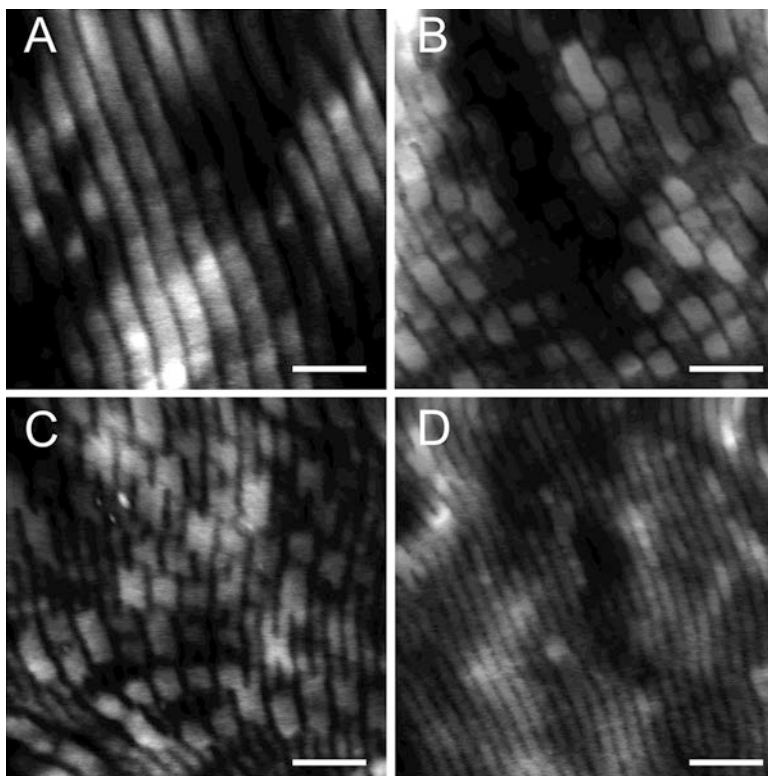
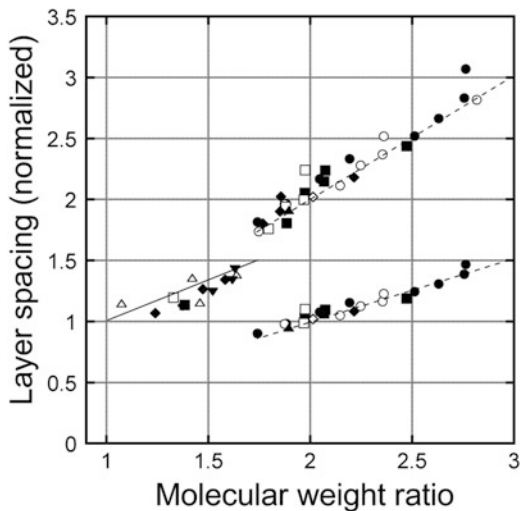


Fig. 17.7 AFM images of the binary mixtures (molecular weight ratio: 2.49) of poly-1 with the mixing ratios of (a) 1.00, (b) 0.75, (c) 0.5, (d) 0.33 (scale bars: 200 nm) (Okoshi et al. 2009)

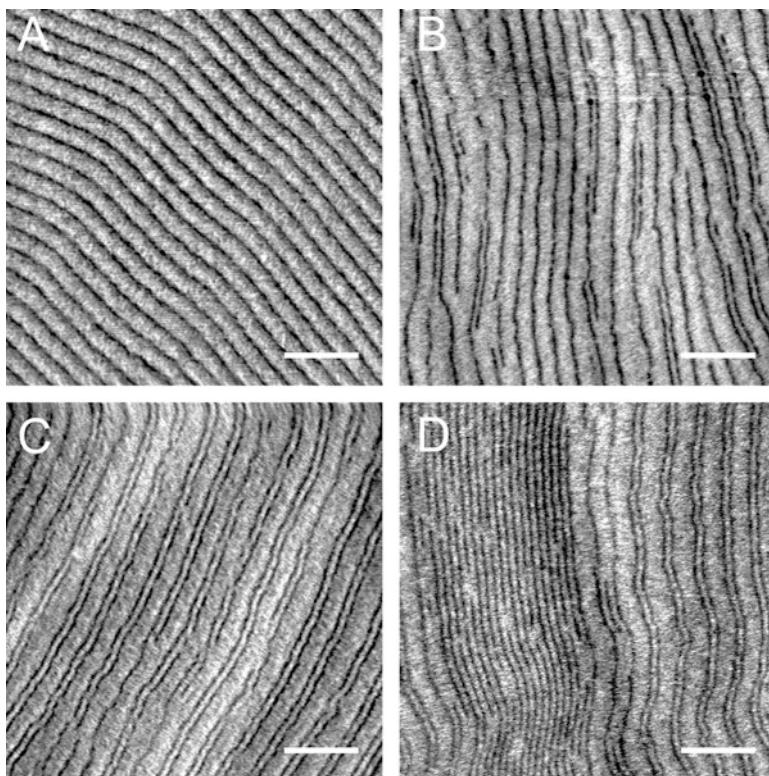


Fig. 17.8 AFM images of the binary mixtures (molecular weight ratio: 3.14) of poly-2 with the mixing ratios of (a) 1.00, (b) 0.83, (c) 0.75, (d) 0.50 (scale bars: 400 nm) (Okoshi and Watanabe 2010)

the short polymer (Fig. 17.7b), come out of alignment occasionally by a half pitch of wide bandings (Fig. 17.7c) upon further addition, and finally turn into narrow bandings with the wide bandings disappearing (Fig. 17.7d). These AFM images are clearly visualizing the conversion from the smectic A2 with two smectic layers of short polymers nested in a smectic layer of long polymers (Fig. 17.7b) to the smectic A3 probably with the long polymers randomly straddling the two smectic layers of short polymers (Fig. 17.7d) via a frustrated phase (Fig. 17.7c) upon decreasing the mixing ratio of the long polymer, even without showing the nematic phase predicted between smectics A2 and A3.

For a higher molecular weight ratio, the AFM observations have also been performed in the same manner. Figure 17.8 shows the AFM images of the binary mixtures with the molecular weight ratio of 3.14 and varying mixing ratio (Okoshi and Watanabe 2010). Upon adding the short polymer to the long polymer, these samples did not show the smectic A2, but showed that a single smectic layer for the short polymer was occasionally inserted between the smectic layers of the long polymer (Figs. 17.8a, b) at the long polymer mixing ratio of 0.87. By further

increasing the short polymer, this allowed the complete alternating stacking of the narrow smectic layer for the short polymer and wide smectic layers of the long polymer at the long polymer mixing ratio of 0.75, almost perfectly reproducing the predicted smectic A4 (Fig. 17.8c). Upon further adding of the short polymer, the excess short polymer was ejected from the smectic A4 and formed smectic layers in its pure form, which is not a discontinuous phase separation, but segregation between the smectic layers of smectic A4 in a parallel manner. These are contrary to the prediction in which the smectic A4 would be destabilized and less favored than the nematic phase when the short rod is abundant. The smectic phase is more preferred than predicted, which might be due to the fact that it is irrelevant to apply the theories with no intermolecular attraction taken into consideration to the dense thermotropic real system.

17.4 Conclusion

The liquid crystal properties of countless numbers of molecules have been studied and classified in terms of the types of liquid crystal structures which is strongly influenced by their chemical structural properties. Distracted by these rich and abundant variety of liquid crystals due to the innumerable chemical structures of the liquid crystalline molecules, the essential quality of liquid crystal formation, which has been merely predicted in the theoretical studies of rod-like particle systems, has failed to be understood because these coarse-grained models have not duplicated the real molecular systems in the experimental point of view. We have presented here the smectic phases formed in rod-like helical polymer systems which is almost the perfect model for the verification of these theoretical predictions. Although these polymers are simple homopolymers, which behave as simple rod-like particles, they show truly colorful liquid crystalline behaviors whose origins are clear due to their structural simplicity. The development of liquid crystalline polymer systems and the verification of the preceding predictions are just beginning and may become a wider research field both to determine the origin of the liquid crystalline behavior and to develop novel polymer materials.

References

- Adams M, Dozic Z, Keller SL, Fraden S (1998) Entropy driven microphase transition in mixtures of colloidal rods and spheres. *Nature* 393:349–352
- Bates MA, Frenkel D (1998) Influence of polydispersity on the phase behavior of colloidal liquid crystals: a Monte Carlo simulation study. *J Chem Phys* 109:6193–6199
- Bolhuis P, Frenkel D (1997) Tracing the phase boundaries of hard spherocylinders. *J Chem Phys* 106:666–687
- Dozic Z, Fraden S (1997) Smectic phase in a colloidal suspension of semiflexible virus particles. *Phys Rev Lett* 78:2417–2420

- Flory PJ (1956) Phase equilibria in solutions of rod-like particles. *Proc Roy Soc Ser A* 243:73–89
- Frenkel D, Moulder BM, McTague JP (1984) Phase diagram of a system of hard ellipsoid. *Phys Rev Lett* 52:287–290
- Fujiki M (1996) A correlation between global conformation of polysilane and UV absorption characteristics. *J Am Chem Soc* 118:7424–7425
- Gabriel J-CP, Camerel F, Lemarie BJ, Desvaux H, Davidson P, Batail P (2001) Swollen liquid-crystalline lamellar phase based on extended solid-like sheet. *Nature* 413:504–508
- He S-J, Lee C, Gido SP, Yu SM, Tirrell DA (1998) A twist boundary-like twisted smectic phase in monodisperse poly(γ -benzyl α , L-glutamate) produced by recombinant DNA techniques. *Macromolecules* 31:9387–9389
- Hosino M, Nakano N, Kimura H (1979) Nematic-smectic transition in an aligned rod system. *J Phys Soc Jpn* 46:1709–1715
- Hosino M, Nakano N, Kimura H (1982) Phase transitions in the systems of identical rigid molecules in perfect alignment—relations of the smectic A and columnar ordering in liquid crystals and the crystalline orderings to the molecular shape. *J Phys Soc Jpn* 51:741–748
- Kobayashi KK (1970) Theory of translational and orientational melting with application of liquid crystals. I. *J Phys Soc Jpn* 29:101–105
- Koda T, Kimura H (1994) Phase diagram of the nematic-smectic A transition of the binary mixture of parallel hard cylinders of different lengths. *J Phys Soc Jpn* 62:984–994
- Lee S-W, Mao C, Flynn CE, Belcher AM (2002) Ordering of quantum dots using genetically engineered viruses. *Science* 296:892–895
- Lee S-W, Wood BM, Belcher AM (2003) Chiral smectic C structure of virus-based film. *Langmuir* 19:1592–1598
- Li L, Walda J, Manna L, Alivisatos AP (2002) Semiconductor nanorod liquid crystals. *Nano Lett* 2:557–560
- Livolant F, Bouligand Y (1986) Liquid crystalline phases given by helical biological polymers (DNA, PBLG and xanthan). Columnar textures. *J Phys* 47:1813–1827
- McMillan WL (1971) Simple molecular model for the smectic A phase of liquid crystals. *Phys Rev A* 4:1238–1246
- Michael PA (1990) Computer simulation of a biaxial liquid crystal. *Liq Cryst* 8:499–511
- Oka H, Suzaki G, Edo S, Suzuki A, Tokita M, Watanabe J (2008) Structural characteristics of thermotropic smA layer phase formed from rigid-rod polysilanes. *Macromolecules* 41:7783–7786
- Okoshi K, Watanabe J (2010) Alternating thick and thin layers observed in the smectic phase of binary mixtures of rigid-rod helical polysilanes with different molecular lengths. *Macromolecules* 43:5177–5179
- Okoshi K, Kamee H, Suzaki G, Tokita M, Fujiki M, Watanabe J (2002a) Well-defined phase sequence including cholesteric, smectic A, and columnar phases observed in a thermotropic LC system of simple rigid-rod helical polysilane. *Macromolecules* 35:4556–4559
- Okoshi K, Sano N, Suzaki G, Tokita M, Magoshi J, Watanabe J (2002b) Smectic liquid crystal observed in thermotropic system of rigid-rod poly(γ -octadecyl-L-glutamate). *Jpn J Appl Phys* 41:L720–L722
- Okoshi K, Saxena A, Naito M, Suzaki G, Tokita M, Watanabe J, Fujiki M (2004a) First observation of a smectic A-cholesteric phase transition in a thermotropic liquid crystal consisting of a rigid-rod helical polysilane. *Liq Cryst* 31:279–283
- Okoshi K, Saxena A, Fujiki M, Suzaki G, Watanabe J, Tokita M (2004b) Small-angle X-ray analysis of smectic A cholesteric liquid crystal phase transition in rigid-rod helical polysilane. *Mol Cryst Liq Cryst* 418:57–68
- Okoshi K, Nagai K, Kajitani T, S-I S, Yashima E (2008) Anomalous stiff backbones of helical poly(phenyl isocyanide) derivatives. *Macromolecules* 41:7752–7754
- Okoshi K, Suzuki A, Tokita M, Fujiki M, Watanabe J (2009) Entropically-driven formation of smectic A1, A2, and A3 phases in binary mixtures of rigid-rod helical polysilanes with different molecular weights. *Macromolecules* 42:3443–3447

- Okoshi K, Hagihara T, Fujiki M, Watanabe J (2010) Anomalous thermotropic liquid crystalline phase behavior in poly [*n*-decyl-(*RS*)-2-methylbutylsilane]s with narrow molecular weight distributions. *Liq Cryst* 37:1183–1190
- Onouchi H, Okoshi K, Kajitani T, S-i S, Nagai K, Kumaki J, Onitsuka K, Yashima E (2008) Two- and three-dimensional smectic ordering of single-handed helical polymers. *J Am Chem Soc* 130:229–236
- Onsager L (1949) The effect of shapes on the interaction of colloidal particles. *Ann N Y Acad Sci* 51:627–659
- Stroobants A, Lekkerkerker HNW, Frenkel D (1987) Evidence for one-, two-, and three-dimensional order in a system of hard parallel spherocylinders. *Phys Rev A* 36:2929–2945
- Strzelecka TE, Davidson MW, Rill LR (1988) Multiple liquid crystal phases of DNA at high concentrations. *Nature* 331:457–460
- Terao K, Terao Y, Teramoto A, Nakamura N, Terakawa I, Sato T (2001) stiffness of polysilanes depending remarkably on a subtle difference in chiral side chain structure: Poly{*n*-hexyl-[(*S*)-2-methylbutyl]silane} and poly{*n*-hexyl-[(*S*)-3-methylpentyl]silane}. *Macromolecules* 34:2682–2685
- Varga S, Velasco E (2010) Modeling and understanding smectic-phase formation in binary mixtures of rodlike polysilane: comparison of Onsager theory and experiment. *Macromolecules* 43:3956–3963
- Varga S, Velasco E, Mederos L, Vesely FJ (2009) Stability of the columnar and smectic phases of length-bidisperse parallel hard cylinders. *Mol Phys* 107:2481–2492
- Veerman JAC, Frenkel D (1991) Relative stability of columnar and crystalline phases in a system of parallel hard spherocylinders. *Phys Rev A* 43:4334–4343
- Veerman JAC, Frenkel D (1992) Phase behavior of disk-like hard-core mesogens. *Phys Rev A* 45:5632–5648
- Watanabe J, Takashina Y (1992) Thermotropic polypeptides VIII. Anomalous phase behavior in low molecular-weight poly(γ -octadecyl L-glutamate). *Polymer J* 24:709–713
- Wen X, Meyer RB, Casper DLD (1989) Observation of smectic-A ordering in a solution of rigid-rod-like particles. *Phys Rev Lett* 63:2760–2763
- Yu SM, Conticello VP, Zhang G, Kayser C, Fournier MJ, Mason TL, Tirrell DA (1997) Smectic ordering in solutions and films of a rod-like polymer owing to monodispersity of chain length. *Nature* 389:167–170
- Zhang G, Fournier MJ, Mason TL, Tirrell DA (1992) Biological synthesis of monodisperse derivatives of poly(α , L-glutamic acid): model rod-like polymers. *Macromolecules* 25:3601–3603

Chapter 18

Metal Containing Liquid Crystalline Polymers

Sachin Kumar Singh and Bachcha Singh

18.1 Introduction

Liquid crystal has been referred to as curious state of matter but its impact on modern technology has been profound because of their unique properties including the selective reflection of light and ferroelectricity, and potential applications in numerous areas, especially in the field of optics, electro-optics, thermoconducting materials and fast switching (Blinov and Palto 2009; Clark et al. 2000; Simoni 1998; Walba et al. 2001; Tournilhac et al. 1987; Ma et al. 2010; Lemieux et al. 2001; Lemieux 2005, Kerr et al. 2009; Boudenne and Khaldi 2003; Ahlers et al. 1994).

The interest in such novel materials with unique physical properties, which have combination of order and mobility resulting in an ordered molecular organization and give response to any external stimuli, has enlightened the scientists to design and synthesize so called unconventional liquid crystals (LC), “soft materials” generally higher performing than the classical LC (Kato et al. 2006). A great deal of progress has been made by modulating and mixing several factors/components in a single molecule (Goodby et al. 2001; Tschierske 2001; Saez and Goodby 2005; Reddy and Tschierske 2006). Metallomesogenic polymers or metal-containing LCPs (MLCPs) are the materials, which lie in category of hybrid materials. They could be considered as materials obtained by combining anisotropic properties of liquid crystals; the physical properties of metal atoms and the processing properties of polymers (Serrano 1996).

In metallomesogenic polymers, polymeric properties lead to good and easy processability, or even, the possibility of stabilization of the liquid crystalline order by polymerization, while incorporation of metal center introduces additional

S.K. Singh • B. Singh (✉)

Department of Chemistry (Centre of Advance Study), Faculty of Science,
Banaras Hindu University, Varanasi 221005, India

e-mail: bsinghbhu@rediffmail.com

functionality (colour, magnetism) to typical anisotropic properties of liquid crystals resulting liquid crystalline materials with promising functional properties.

A large number of papers concerning design, synthesis, characterization and physical properties of MLCPs have appeared. This chapter reports developments in the field of metal containing liquid crystalline polymeric materials with special emphasis on structural aspects and synthetic approaches.

18.2 Classification of Metallomesogenic Polymers

Metallomesogenic polymers are designed in a similar way to that of conventional liquid crystal polymers, therefore the same structural criteria is usually used for the classification of these materials (Brostow 1990). These materials are classified into non-crosslinked and crosslinked polymers and then they are grouped into main-chain and side-chain polymers depending on the position of the pro-mesogenic unit with respect to the polymeric chain. Furthermore, these structures are classified according to their mesogenic behavior, i.e. lyotropic and thermotropic properties. A reverse approach can also be applied to classify these materials i.e. firstly, classification on the basis of their mesogenic behaviour and then subdivisions on the basis of their nature of branching as described above (Fig. 18.1).

18.3 Synthetic Strategies for Metallomesogenic Polymers

A number of synthetic strategies are employed that offer the possibility of introducing metal atoms or ions into the structure of polymeric materials (Carragher 1981). These synthetic strategies can be classified into two types depending on the step in which metal ions are incorporated into the synthesized polymeric systems. This classification covers a wide range of reports on metal containing liquid crystal

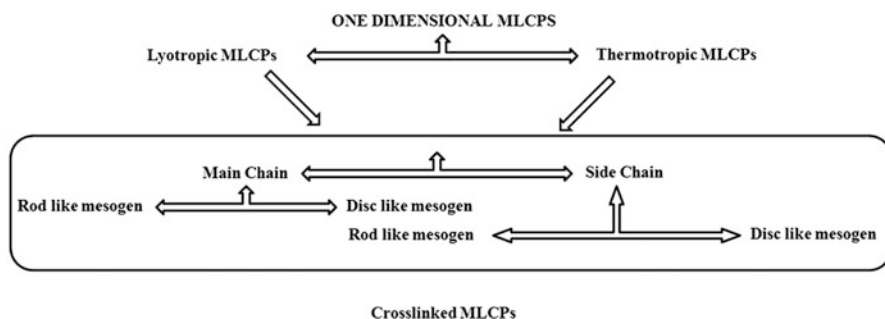


Fig. 18.1 Classification of metallomesogenic polymers

polymers having lyotropic as well as thermotropic nature. However, there are also some recent examples, lying in special category, which will be discussed in separate section.

18.3.1 Approach 1: By Polymerization of Metal Complexes

In this method, metal-containing monomers are functionalized to have polymerizable organic groups, which are polymerized using either conventional chain or step-polymerization mechanism to obtain main-chain or side-chain polymers.

This method generally yields low degree of polymerization compared to other methods. However there are a number of reports on organometallic polymers, mainly metal poly(yne) polymers, synthesized in good yields and with a high degree of polymerization by organometallic synthetic methods. In this method, low solubility of metal complexes also alters the synthetic pathway chosen. Therefore, this method is seldom used for the synthesis of thermotropic metallomesogenic polymers.

18.3.2 Approach 2: By Metal Complexation of Organic Ligands

This approach can be subdivided in two groups:

- (a) Polymerisation through reaction of metal ions with bifunctionalized monomers, which can attach itself simultaneously to two metal ions. In this method, the metal atoms are used as a linker between two chelating monomeric units.
- (b) Coordination of metal atoms with a previously preformed main chain or side chain organic polymers, which already contain metal chelating site(s).

In this method, approach (a) is alternative method of polymerization, while second approach (b) is polymer reaction. Both methods (a and b) generally yield high degree of polymerization than the first approach (1). Another advantage of above two approaches is that organic ligands have already been synthesized and characterized and, therefore, incorporation of metal ion can be easily be recognized. Approach 2(b) has additional advantage of new possibilities of synthesizing MLCPs by using well established synthetic approaches of organic liquid crystal polymers having metal chelating sites. However, one disadvantage of this method is observations of interactable metal polymeric materials by metal cross linking, which are difficult to characterize. Therefore, this method is generally used for synthesis of cross linking polymers or three dimensional polymers by using suitable

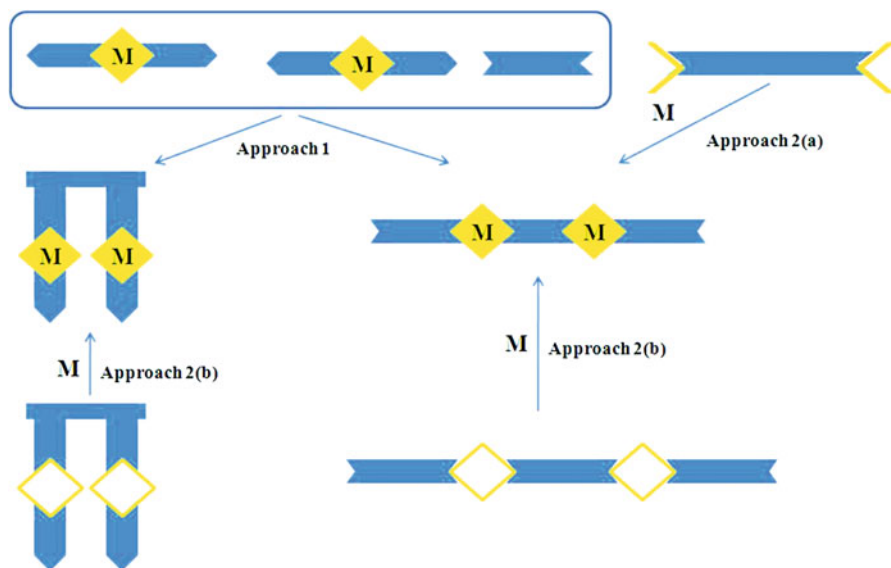


Fig. 18.2 Synthetic approaches to metal-containing polymers

ligands. These types of polymers can also be prepared by approach (1) or approach 2(b) using multifunctional ligands.

These approaches are schematically represented in Fig. 18.2 for one dimensional polymer.

The above described approaches are employed for the synthesis of both lyotropic as well as thermotropic metal containing liquid crystalline polymers. In next section, we will discuss about typical and some recently reported lyotropic and thermotropic metal containing systems having metallomesogenic units into main chain or side chain. Special emphasis will be given on synthetic approaches applied for these materials.

18.4 Lyotropic Metallomesogenic Polymers

The liquid crystalline properties of lyotropic systems depend upon concentration of solution. Above the critical (threshold) concentration, phase transition from an isotropic to anisotropic takes place. Lyotropic liquid crystals have a commercial value in design and synthesis and fabrication of ultra high strength materials (aramids).

The synthetic strategies used in reported examples of lyotropic metal containing liquid crystalline polymers usually correspond to approach 1, which involves polymerization of metal complexes using synthetic methods of organometallic chemistry. These materials can be classified into two groups, depending on whether the metallomesogenic unit is introduced into the main-chain or the side-chain.

18.4.1 Main-Chain Lyotropic MLCPs

Haghihara and coworkers were the first to report the main chain lyotropic MLCPs. These are rod like polymeric conjugated acetylide complexes of platinum (Takahashi et al. 1978, 1979). Nematic phase was formed in concentrated solutions in trichloroethylene exceeding a certain limiting concentration. The limiting concentration depends upon molecular weight of polymer. A wide variety of metal poly(yne) complexes with lyotropic properties were designed and synthesized by this group by taking advantage of synthetic aspects of organometallic chemistry.

Lyotropic poly(yne) metal complexes synthesized by Japanese group, Haghihara et al. can be classified into three types depending upon their synthetic methods,

18.4.1.1 Dehydrohalogenation Method

This method involves cuprous halide as a catalyst and an α,ω -diethynyl compound and transition metal halides in amines as a solvent and acid acceptor. The first report on lyotropic metallomesogen having σ -bonded transition metal (platinum) atom with all trans configuration was obtained by this method (Sonogashira et al. 1977) (Fig. 18.3). Selective synthesis of cis- and trans- isomers was reported by the same group in order to establish the configuration around the metal, to obtain information applicable to discrimination between the configurational isomers (Sonogashira et al. 1978a).

Pt-Pd mixed metals in the main chain polymer $-\text{[trans,trans-Pt(PBu}_3)_2\text{-C}\equiv\text{C-C}\equiv\text{C-Pd(PBu}_3)_2\text{-C}\equiv\text{C-C}\equiv\text{C}]_{n/2}$ were obtained by the reaction of $\text{trans-(PBu}_3)_2\text{Pt(C}\equiv\text{C-C}\equiv\text{CH)}_2$ with $\text{trans-(PBu}_3)_2\text{PdCl}_2$. The alternating regularity of the metal arrangement was confirmed by the selective formation of the trinuclear complex $\text{trans,trans,trans-ClPd(PBu}_3)_2\text{-C}\equiv\text{C-C}\equiv\text{C-Pt(PBu}_3)_2\text{-C}\equiv\text{C-C}\equiv\text{C-Pd(PBu}_3)_2\text{Cl}$ (III), in the depolymerization by using $\text{trans-(PBu}_3)_2\text{PdCl}_2$ using CuI as catalyst in HNEt_2 (Fig. 18.4a, b) (Sonogashira et al. 1978b).

In order to obtain the polymeric materials a model to study physical properties and catalytic activities, method of designing and the arrangement of metal atoms at appropriate distances in the polymer backbone was described (Takahashi et al. 1980a, b) by the same group (Fig. 18.5). The reaction scheme for the synthesis of these complexes are shown below.

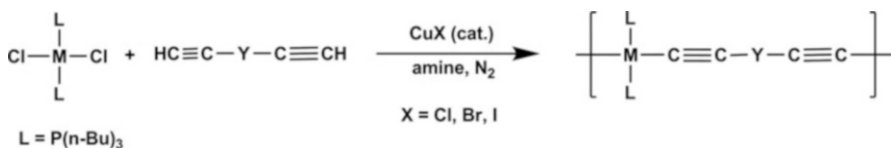


Fig. 18.3

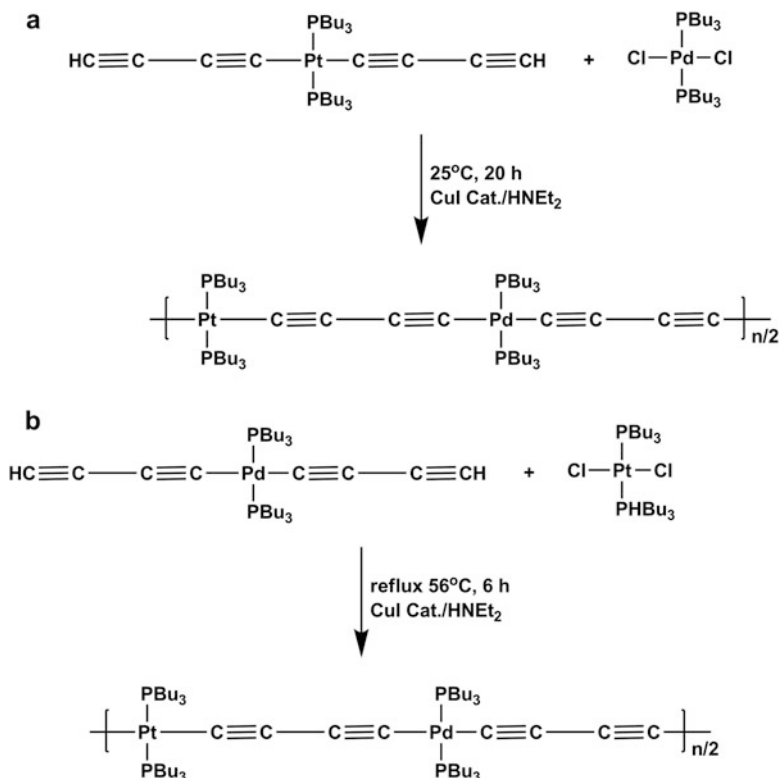


Fig. 18.4

18.4.1.2 Oxidative Coupling

This method employs Hay's reagent as the oxidant (copper(I) chloride-oxygen with N,N,N,N'-tetramethylethylenediamine (TMEDA) in excess). The reaction is carried out in nitrogen atmosphere and reaction time is very important factor to achieve high degree of polymerization. Dichloromethane is proved as best solvent to avoid precipitation of polymeric chains. This method is usually employed to prepare conjugated linear polymers as well as binuclear transition metal complexes (Kim et al. 1970; Fujikura et al. 1975). This reaction usually proceeds in high yields and is, therefore, useful in the synthesis of metal poly(yne) polymers (Takahashi et al. 1980a, b). The main advantage of this method is that no stoichiometric restrictions are inherent and, consequently, a high degree of polymerization can be achieved (Fig. 18.6).

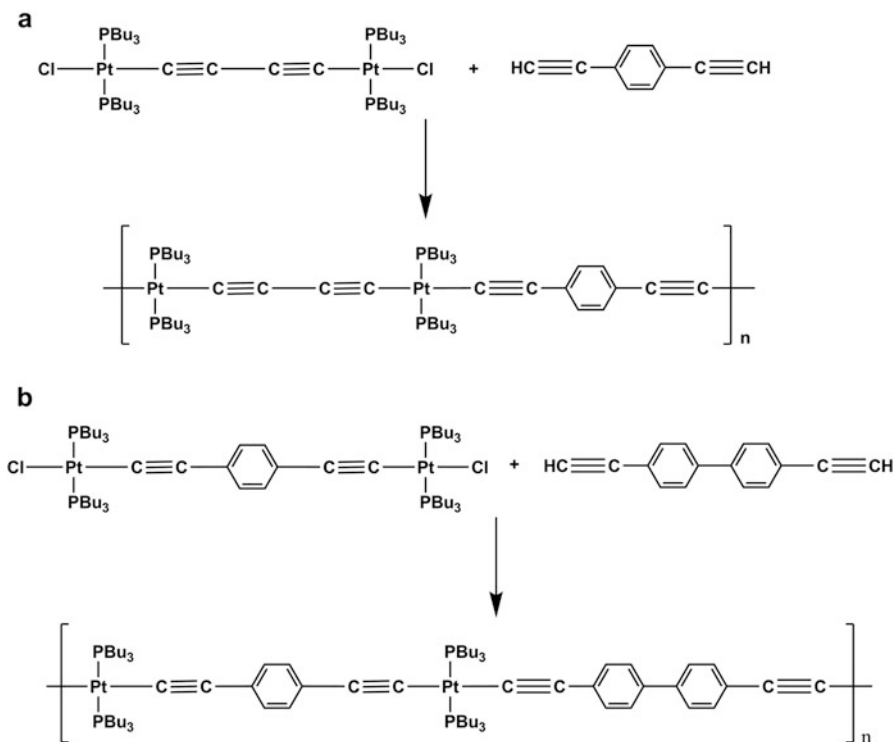
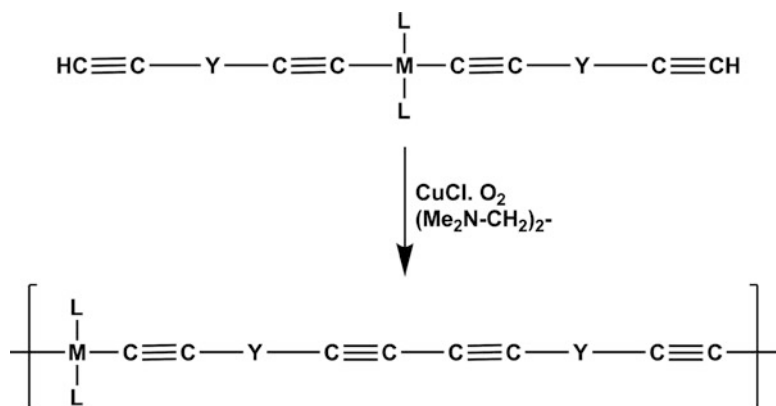


Fig. 18.5



M = Pt or Pd L = PBu₃ Y = -, p-substituted aromatic rings

Fig. 18.6

18.4.1.3 Alkynyl Ligand-Exchange

This method was employed to obtain nickel poly(yne) polymers (Fig. 18.7) (Sonogashira et al. 1980). Synthetic possibilities of these polymers could not be achieved by using either of the methods described above due to instability of the nickel halide and the instability of nickel complexes to Hay's reagent (copper (I) chloride-oxygen with N,N,N,N'-tetramethylethylenediamine (TMEDA)).

In structural studies of the Pt-di(yne) polymer, configurational analysis of platinum moiety in polymer using ^{31}P NMR provides a method, which proves the rod like structure of the polymer (Matsumoto et al. 1993). The spectrum of trans-configurational phosphorus on platinum bis(acetylide) showed a signal at -3.0 to -4.5 ppm and that of the cis-configuration showed a signal at $+2.6$ to $+3.6$ ppm (based on 85 % phosphoric acid standard). The ^{31}P Fourier transform NMR spectrum of high molecular weight polymer showed a large resonance at -4.2 ppm attributable to the trans-configurational phosphorus with attendant satellites due to coupling ($J = 2384$ Hz) with ^{195}Pt ($I = 1/2$, 33 %).

The n-butyl substituents on phosphorus co-ligands play an active role since they stabilize the metal-carbon σ -bond and decrease the intermolecular attractions, which make the solubilisation of polymeric chain easier. The rod like polymeric structure and high solubility both favor liquid crystalline properties of these materials in concentrated solutions, although some nickel and palladium polymeric complexes do not show liquid crystalline behavior in any solvent.

Poly(yne)-platinum polymers have been prepared by Abe and coworkers (Fig. 18.8) (Abe et al. 1991a, b) according to the prescription developed by Hagihara and Takahashi, et al. The orientation characteristics of these polymers in the lyotropic nematic mesophase (trichloroethylene) were studied in relation to their phase behavior by ^2H NMR. Deuterium labels were introduced on the phenylene ring according to the following steps:

1,4-Diethynylbenzene- d^4 thus obtained was reacted with bis[trans-chlorobis(tri-n-butylphosphine)platinum(II)]-1,4-butadiynediyl to give deuterated polymeric samples. The diameter and distances spanning repeating units were predicted from the crystallographic data reported for relevant short-chain model compounds (Fig. 18.9).

New lyotropic poly(yne) polymers reported by Sonogashira et al. containing disiloxane, disilane and phosphine groups in the main chain are described (Fig. 18.10) (Kotani et al. 1991). The platinum and palladium poly(yne) polymers were synthesized by polycondensation reaction between a metal chloride and σ , ω -bisethynyl complexes in amines in the presence of cuprous iodide catalyst. The nickel poly(yne) polymers were synthesized by an alkynyl ligand exchange reaction between nickel acetylide and an σ , ω -bisethynyl complexes in diethylamine in the presence of cuprous iodide catalyst. A concentrated solution of the platinum poly(yne) polymers containing disiloxane group in the main chain forms a lyotropic liquid crystal in dichloromethane and 1,2-dichloroethane.

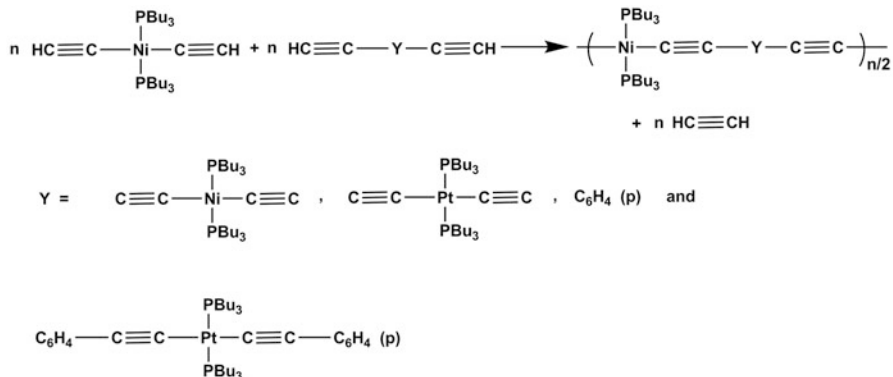


Fig. 18.7

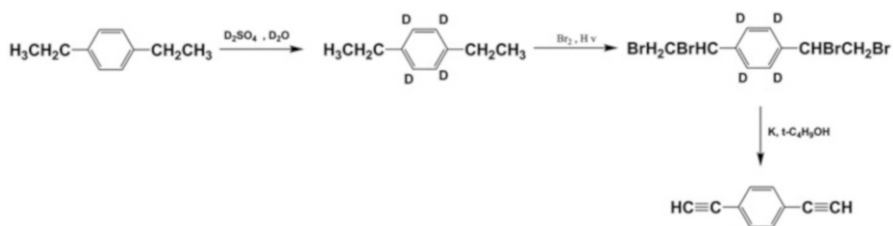


Fig. 18.8 Deuterium labeled, platinum poly(yne) polymer prepared and studied by Abe and co-workers

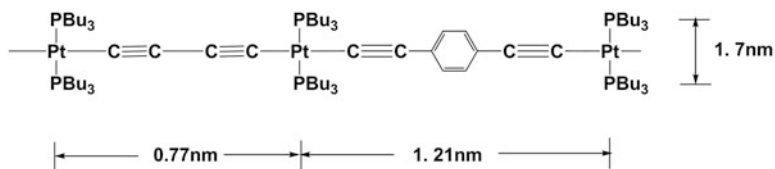


Fig. 18.9 Molecular structure of polymer synthesized by Abe and coworker. The distances spanning alternative repeating units and the diameter are taken from the crystallographic data reported for relevant model compounds

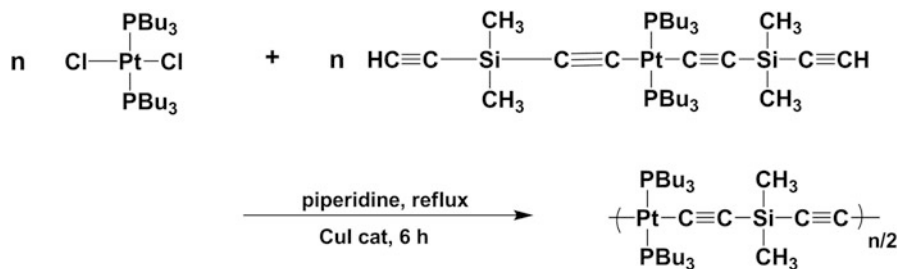


Fig. 18.10

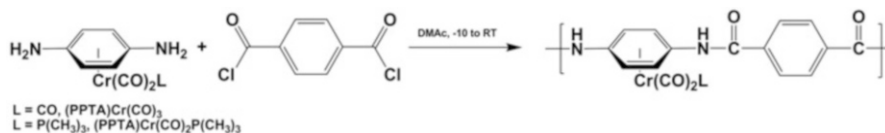


Fig. 18.11 Synthetic approach to metalloaramids

Dembek et al. have reported interesting lyotropic metal-containing polymers different from poly(yne) complexes (Dembek et al. 1993a, 1994). DuPont® group aimed their research at aromatic polyamides (aramids) easily processed from organic solutions via organometallic metal complexation. The aromatic rings of high-performance polymers provide a platform for transition metal via complexation since they bond tenaciously to a wide variety of transition metal complexes. They showed that organometallic η^6 -coordination offers broad control of the properties of high-performance aromatic polymers, as exemplified by PPTA. The π -complexation solubilizes even high molecular weight PPTA in organic solvents and, remarkably, still allows formation of ordered liquid crystalline solutions. The extent of chromium tricarbonyl substitution on the aromatic ligands dictates the orientation of PPTA films on a molecular level, and the steric bulk of the η^6 -organometallic substituent, defined by ligand substitution reactions, controls the liquid crystallinity of the organoaramid solutions.

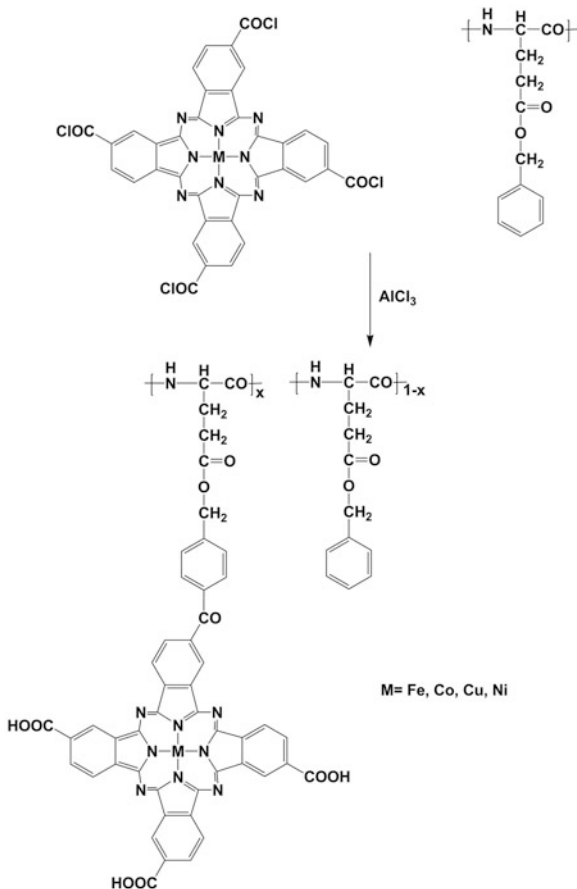
Polycondensation of (*p*-phenylenediamine) $\text{Cr}(\text{CO})_3$ (Fig. 18.11) (Dembek et al. 1993b) with terephthaloyl chloride in *N,N*-dimethylacetamide (DMAc) gives high molecular weight (PPTA) $\text{Cr}(\text{CO})_3$, as opalescent, highly viscous DMAc solutions, with $\text{Cr}(\text{CO})_3$, complexed to every di-amine ring. Interestingly, the metalloaramid is soluble even when only half of the diamines are $\text{Cr}(\text{CO})_3$, complexed.

18.4.2 Side-Chain Lyotropic MLCPs

Hanabusa et al. have described lyotropic metal-containing side-chain polymers (Hanabusa et al. 1986). These examples deal with some metallophthalocyanine derivatives of poly(γ -benzyl-L-glutamate).

Metal-2,9,16,25-tetracarboxyphthalocyanines ($\text{M} = \text{Fe}(\text{III}), \text{Co}(\text{II}), \text{Ni}(\text{II})$ and $\text{Cu}(\text{II})$) were transformed into their acid chlorides and condensation of these acid chlorides by Friedel-Craft reaction gave the polymers (Fig. 18.12). The resulting substituted poly(γ -benzyl-L-glutamates) were found to contain about 0.2–2.8 mol% of phthalocyanine rings covalently bound to polymeric chains. The polymers having less than 3 mol% phthalocyanine entities were soluble in chloroform, 1,4-dioxane, dichloroacetic acid, DMF etc. The polymers could be shown to have α -helical conformation, green or blue coloured lyotropic mesophase being formed in concentrated solutions.

Fig. 18.12 Poly(γ -benzyl-L-glutamate)s with a low metallophthalocyanine ring content



18.5 Thermotropic Metal-Containing Liquid Crystal Polymers

A number of low molecular weight thermotropic metallomesogens have been designed, synthesized and characterized till date. High molecular weight thermotropic metallomesogens i.e. thermotropic metallomesogenic polymers are designed and synthesized based on structural information known for low molecular weight metallomesogens. In this section, we will discuss about main chain and side chain thermotropic liquid crystalline polymers. A large variety of such molecular systems possessing different structures have been reported and calamitic and columnar structures cover most of them. Therefore, the thermotropic metallomesogenic polymers will be limited to the reports on calamitic and columnar systems.

18.5.1 Calamitic Main-Chain Polymers

Square planar transition metal complexes of salicylidimines as mesogenic units are known to be very suitable structure in the design of thermotropic metallomesogenic polymers. The square planar geometry around metal centre and overall rod-like shape promotes the appearance of calamitic mesophases. The stepped structure (Holm and Bconnor 1971), of these complexes has additional advantage, as it disrupts the chain linearity and therefore, decreases the thermal transitions. Main-chain LCPs, which have these metallomesogenic units can be achieved by almost all synthetic strategies as described in previous sections (approach 1 and 2).

The first series of homo- and co-polymers based on copper(II) salicylidimines was reported by Sirigu and coworkers via synthetic approach 2(a) using monomers with two bidentate chelating groups (Carfagna et al. 1987) (Fig. 18.13). These polymers displayed a monotropic mesophase identified as smectic A for all compositions. However, one of the disadvantages inherent in this synthetic approach to the target polymers is the low degree of polymerization.

A conventional polymerization of homopolymers of copper(II) salicylidimines via approach 1 was proposed by Marcos et al. (1990, 1992). They have synthesized and characterized new homopolyesters containing paramagnetic units. In this method, bis(N-R-4-hydroxysalicylidiminato)copper(II) compounds ($R = -C_nH_n$, $n = 1, 5$ and 10) were condensed with an acid dichloride in order to obtain the

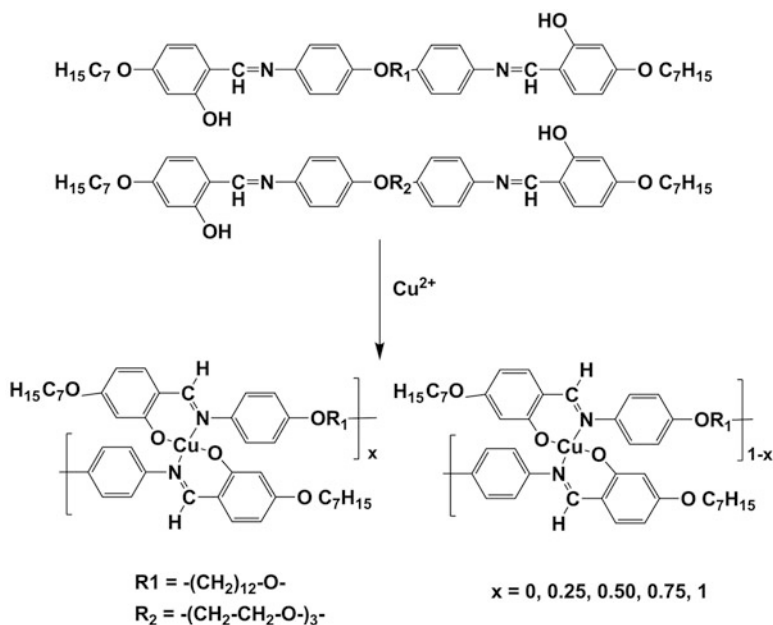


Fig. 18.13

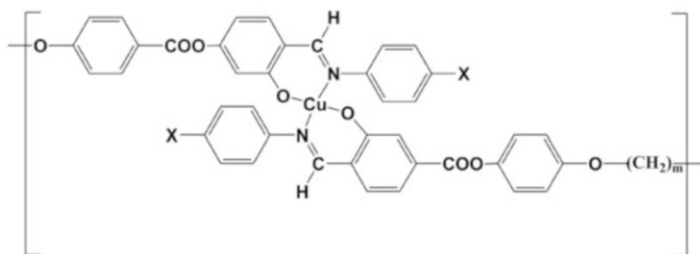


Fig. 18.14 Series of homo- and copolymers derived from a salicyldimine copper(II) mesogenic unit

target polymers. Mesomorphic melts below the decomposition temperatures and were observed except for $n = 1$. EPR and DSC measurements of these series of compounds showed two different crystalline forms. In one of them, Cu^{2+} was in an environment close to a square-planar coordination. An isotropic EPR signal was observed and was related to Cu-Cu or Cu-O interactions among different metallomesogens in the neighborhood.

A series of N-aryl substituted derivatives of the above polymeric complexes was also synthesized by same group (Oriol 1990) (Fig. 18.14). Phase transitions occurred at high temperatures and mesophases were observed over a short temperature range before decomposition at temperatures close to $300\text{ }^{\circ}\text{C}$ in these aryl derivatives due to an increase in chain rigidity and intermolecular interactions.

On the basis of experiments, they concluded that interfacial polycondensation is suitable method for obtaining mesogenic homopolymers containing Cu (II) complexes. The stepped square-planar structure of these Cu(II) complexes is ideal for obtaining paramagnetic liquid crystals. To obtain polymers having adequate thermal stability, the aromatic acid dichloride, which incorporates a long flexible spacer, is shown to be the most suitable monomer. Furthermore, N-alkyl copper complex monomers display lower transition temperatures than N-aryl monomers. These copper complexes may be classified as crankshaft monomers with bulky substituents, briefly reported in the synthesis of organic liquid crystal polymers.

Recently, a novel class of metallomesogenic polyurethanes was synthesized using metallomesogenic diols by Senthilkumar et al. (2012) (Fig. 18.15). With judicious modification of ligand design, mesogenic moieties as metallo diols were synthesized. The diols were constructed from three ring containing mesogen linked through ester and azomethine with terminal hydroxy group and were complexed with copper(II).

It may be concluded that an optimal structural design of salicyldimine homopolymers involves a rod-like metallomesogenic unit containing at least four aromatic rings, lateral groups, which decrease intermolecular attractions and long flexible spacers which “dilute” the rigid units.

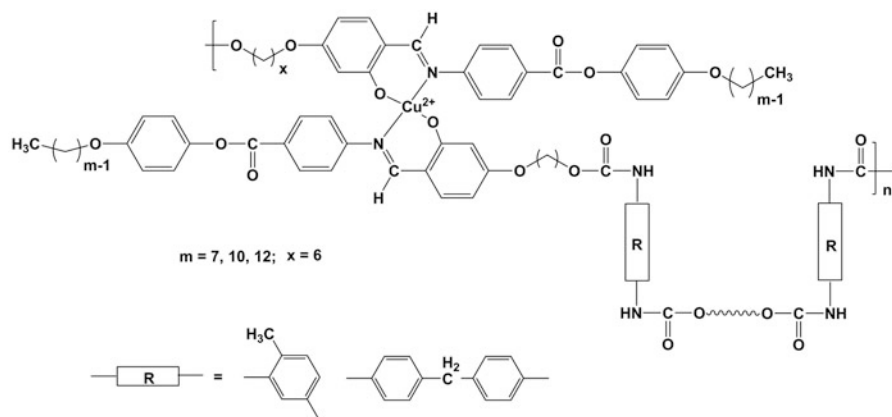
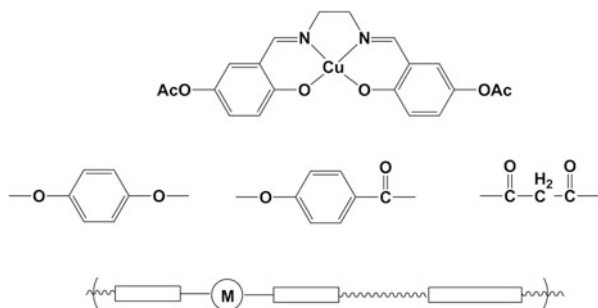


Fig. 18.15

Fig. 18.16 Structural units of the organic terpolymer precursor of metallomesogenic copolymers obtained by transesterification with a functionalized salicylaldehyde copper(II) complex



Stupp et al. synthesized a different series of paramagnetic organometallic liquid crystal polymers containing a tetradentate Schiff base complex of copper(II) (Moore and Stupp 1987). The main chain liquid crystal polymers were formed when the functionalized complex is combined at 220 °C with the melt of a low molecular weight terpolymer. Nematic liquid crystalline phase was identified in the terpolymer containing oxybenzoate, dioxyphenyl, and pimelate structural units. The organometallic unit was incorporated in concentrations ranging from 5 to 20 mol% without disrupting the liquid crystallinity. The organometallic material melted reversibly into a liquid crystalline fluid at a slightly lower temperature than the terpolymer. In external magnetic field the tendency is for the backbone axis of the organometallic fluid to rotate away from the field direction. On the basis of this observation, they suggested that strong interactions between the field and the paramagnetic units dictate the orientation of diamagnetic chemical sequences, which normally align parallel to the magnetic field (Moore and Stupp 1988) (Fig. 18.16).

Ferrocene derivatives, because of their synthetic versatility, are very attractive mesogenic units to be included in a polymeric chain in order to obtain metallo-mesogenic polymers. Furthermore, ferrocene derivatives have other interesting

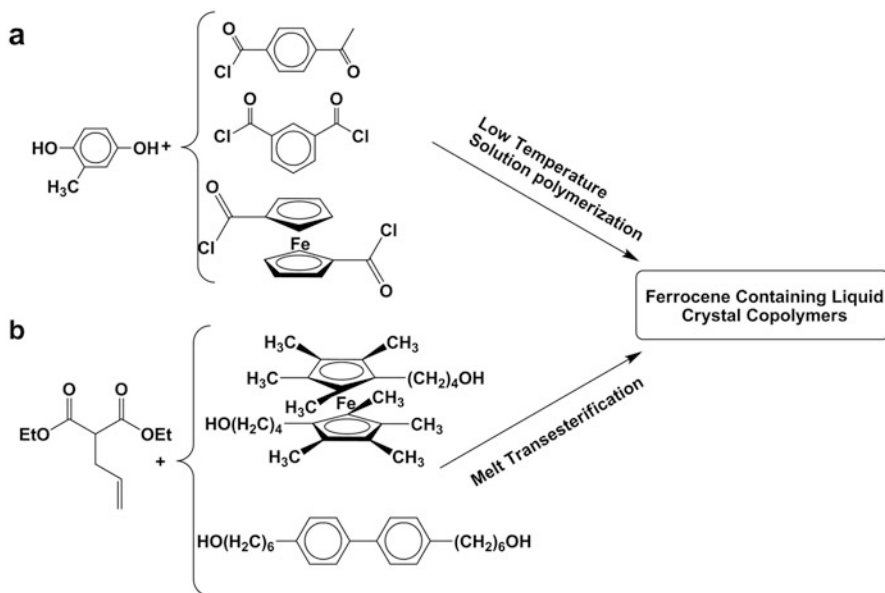


Fig. 18.17 Synthetic approaches used to obtain ferrocene containing main chain metallo-mesogenic polymers

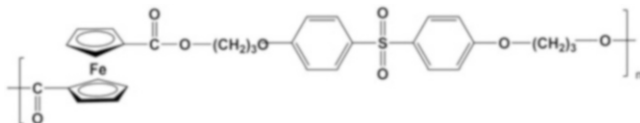


Fig. 18.18

properties such as UV-stabilization, smoke and soot retardation (Harwood 1963), and, in addition, they introduce the structural irregularity necessary to decrease phase transition temperatures. This interesting background led to the synthesis of a series of ferrocene-containing copolyesters by Lenz and coworkers (1989). All samples show a nematic phase, except for the polyester with $x = 0$, which decomposes before melting. Figure 18.17 shows some synthetic approaches used to obtain ferrocene containing main chain metallo-mesogenic polymers.

Recently, ferrocene based main chain mesogenic polymer was synthesized by solution polycondensation reaction of bis(4-hydroxyoctoxyphenyl)sulfone with 1,10-ferrocenyl chloride by Amer et al. (2012). These ferrocene derivatives showed liquid crystalline properties and possessed nematic phase textures with schlieren disclinations during heating and cooling (Fig. 18.18).

The β -diketone derivatives are well known ligands for the synthesis of low molecular weight metallomesogen. Hanabusa et al., following the synthetic approach 1, synthesized a series of main-chain mesogenic homo and copolymers

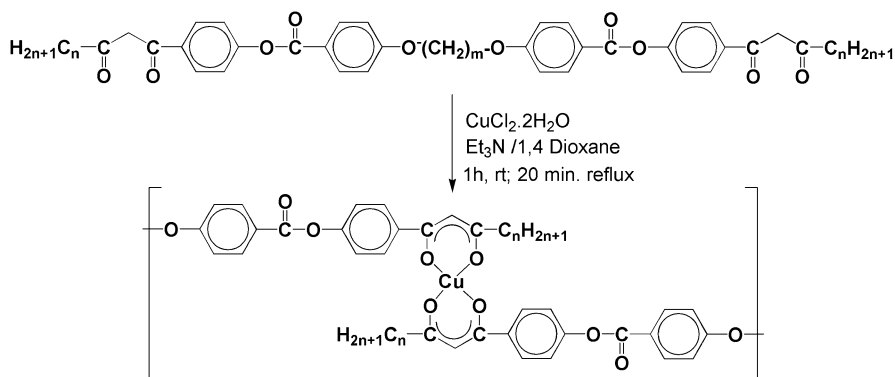


Fig. 18.19 Synthetic approach 1 to polymer based on β -diketone copper(II) complexes

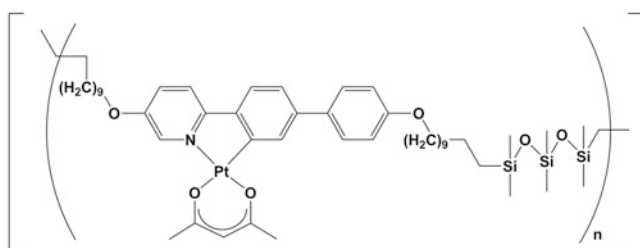


Fig. 18.20

by complexation of monomeric β -diketones with Cu(II) (Hanabusa et al. 1993) (Fig. 18.19). By selecting the appropriate flexible spacer and the lateral alkyl chain, SmA mesophase could be observed before decomposition took place. Fibers with a SmA-frozen structure of these polymers were drawn from the anisotropic melt and studied by X-ray diffraction and EPR revealing a high anisotropy depending on the angle between the fiber axis and the magnetic field.

Very recently, a polysiloxane based phosphorescent, liquid-crystalline polymer was obtained by combination of mesogenic rod-like cycloplatinated monomers based on 2,5-di(4-alkenyloxyphenyl)pyridine ligands with 1,1,3,3,5,5-tetramethyltrisiloxane by Diaz et al. (2012) (Fig. 18.20). These semiflexible main chain metallomesogenic polymers showed polarised emission and found to be very suitable for OLEDs applications.

18.5.2 Calamitic Side-Chain Polymers

Very few reports are found on polymeric systems with pendant metallomesogenic units in comparison with main-chain arrangements. This is due to the fact that asymmetrically substituted metallomesogenic monomers are required for preparing

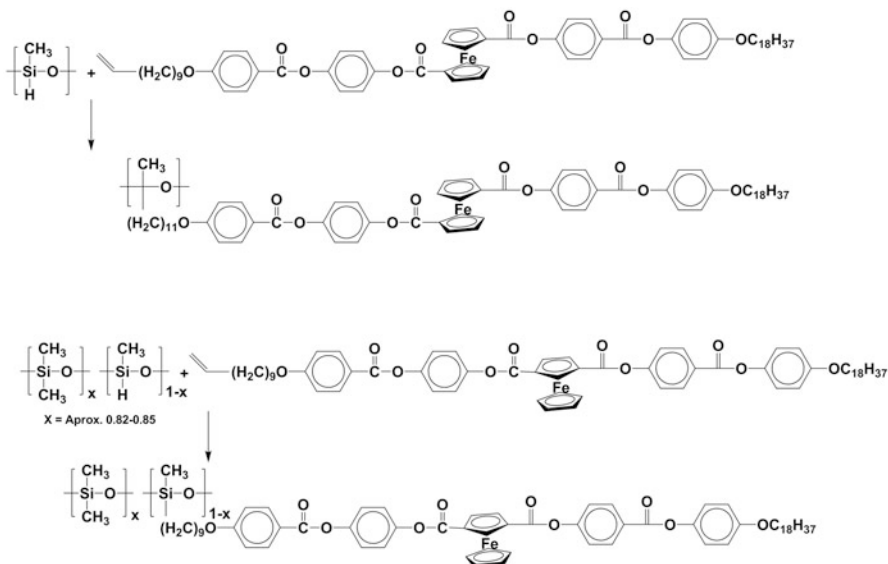


Fig. 18.21

side-chain polymeric systems, which usually are attempted via the synthetic approach 2(a). Some reports on metal-containing side-chain polymeric systems are via the synthetic approach 2(b). In this approach they used a preformed polymer containing coordinating centers, which is randomly complexed with metal ions. However, major difficulty in these synthetic conditions is that it is difficult to ensure that metal only reacts with adjacent mesogenic units of the same polymeric chain or cross linked with other side chains. So possibility of cross linking cannot be ruled out.

The calamitic metallomesogenic polymers- thermotropic side-chain polymeric systems- are the ferrocene-containing polysiloxanes reported by Deschenaux et al. (1994) (Fig. 18.21), which are considered the first report on these systems. These polymers were synthesized by grafting poly (methylhydrosiloxane) (PMHS) or a copolymer, PMHS-poly(dimethylsiloxane) with unsymmetrically substituted mesogenic ferrocenes bearing a reactive group at the end of an aliphatic chain. The mesomorphic properties of their monomeric systems were retained by these polymers but with wider mesophase range. The smectic phases were characterized by X-ray diffraction. The authors claimed this polymer as the first example of a chiral metallomesogenic polymer, due to the planar chirality of the unsymmetrically 1,3-disubstituted monomer. However, data about the chirality of the monomer were not further discussed.

Zentel et al. synthesized ferrocene monomers for preparation of liquid crystalline elastomers via physical crosslinking (Wiesemann et al. 1995). The reversible redox properties of ferrocenes allowed the preparation of functional LCPS, since the oxidation of ferrocene units gave rise to clustering of ionic groups (ionomers).

Contrary to classical ionomers, the advantage of this method in preparing elastomers is that the parent neutral polymers can still be dissolved and shaped in different geometries since no strong interactions are expected on the neutral polymers. Further, the ferrocenium ionic groups help to increase the interface adhesion in biphasic blends by the formation of mixed clusters at the interface.

The oxidation of the copolymers was carried out with copper(II) perchlorate or 1,4-benzoquinone/H₂SO₄. The latter oxidizing agent leads to liquid crystalline ionomers with higher thermal stability since the perchlorate counter ion is a strong oxidizing agent. It is mentioned that ferrocene unit itself is not mesogenic but contents up to 10–13 % mol are tolerated without a significant drop in the phase transition temperatures of the mesogenic homopolymer. The redox potential was evaluated by cyclovoltammetry, and it was observed that this potential depends on the number of alkyl groups linked to ferrocene units. Oxidation of these polymers to produce ionomers does not strongly influence the mesophase and transition temperatures.

Studies on polymer blend of these redox active polymers and a conventional amorphous ionomer, partially-sulfonated polystyrene was reported by the same authors (Wiesemann et al. 1992; Wiesemann and Zentel 1993, 1994). It was found that the morphology of the polymer blends strongly depends on the ionic interactions. From the thermal study, it was concluded that the blends of amorphous ionomers and the reduced or oxidized ferrocene polymer show phase separation as they exhibit two glass transitions corresponding to pure components. However, a drastic decrease in the average size of the phase separated regions is observed in blends of the amorphous ionomers and the oxidized form of the ferrocene-containing polymer. Furthermore, these ionomeric blends exhibit a combination of the special properties of the pure components on a macroscopic scale. Thus, composite materials that combine macroscopic stability provided by the pure amorphous ionomer, with typical LC properties such as switching, provided by the LC ionomer, in electric fields can be envisaged.

Kuschel and coworkers (1991) used the bis(3-hydroxypropyl)dimethyltin monomer reported earlier to synthesize the side-chain polymers as shown in Fig. 18.22. These polymers are different with structural point of view as metals are in the polymeric backbone and organic units are in side chain in these organotin derivatives. Polymer was prepared as a reference model. The flexible tin spacer causes some modifications in the properties. The tin-containing polymer is amorphous and melts into smectic phases similar to those formed by parent polymer, but at lower temperatures. However, a nematic phase, which is present in parent polymer, is not observed for tin containing polymer.

18.5.3 Columnar Thermotropic Polymers

Among the large variety of low molecular weight discotic compounds, much attention has been paid to phthalocyanines (Cook et al. 1987; Van der Pol

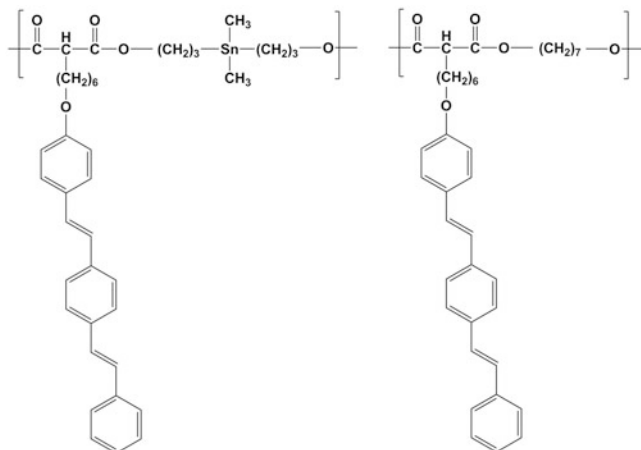


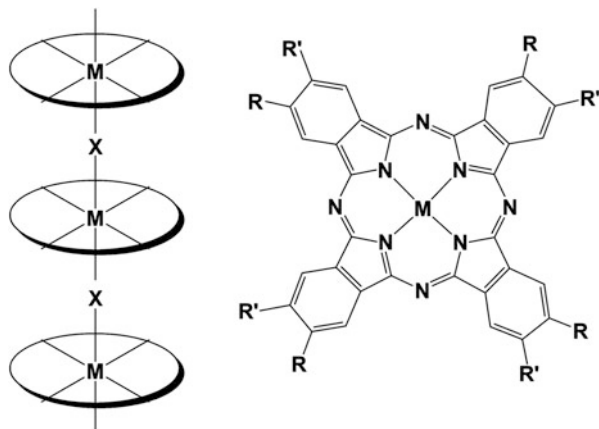
Fig. 18.22 (a) Side chain MLCP based on tin in main chain and (b) its organic homologue

et al. 1989a, b) and porphyrines (Gregg et al. 1987, 1989) and their metal complex derivatives due to interesting properties in the fields of catalysis, electronics, optoelectronics and transports. Such properties are derived by the control of the supramolecular organization of the discotic molecules in stacks: columnar mesophases, which form an electrically conducting array. Thus, in such stacks, the metal atoms and the electronic-systems of macrocycles may interact to give a one-dimensional charge transport.

The design of an electrically conducting polymer based on a stacking architecture consists of covalently links of phthalocyanine subunits. There are various ways that phthalocyanines can be polymerized (Oriol and Serrano 1995; Leznoff and Lever 1989). however, only a few examples of liquid crystalline phthalocyanine polymers are known. The first reports are spinal columnar or shish kebab type of phthalocyanine polymers where the phthalocyanine units are linked by a bridging atom bonded to silicon, tin, or germanium atom at the center of the phthalocyanine molecule. Significant attention has been paid to examine various chemical and physical properties of phthalocyanine-based main-chain polymers having metal-oxygen-metal (M-O-M) bond as a linker to connect two adjacent phthalocyanine rings (Sirlin et al. 1987, 1988a, b; Orthmann and Wegner 1986; Sauerm 1993; Hanack et al. 1987; Sauer and Wegner 1991; Caseri et al. 1988; Schouten et al. 1992; Dulog et al. 1993; Sielcken et al. 1990; Van Nostrum et al. 1995; Van Nostrum and Nolte 1996). The term spinal columnar liquid crystal was proposed for such polymers (Sielcken et al. 1990).

Spinal columnar liquid crystals are cofacially stacked polymeric metallomesogens. The cofacial stacking may take place via (1) covalent bonds, (2) covalent-coordinate bonds, and (3) coordinate-coordinate bonds. However, in the field of discotic liquid crystals, mainly covalent and covalent-coordinate bonds derived polymers have been realized (Fig. 18.23). Particular attention has been paid to polysiloxane derivatives. The close cofacial packing of the phthalocyanine along

Fig. 18.23 Schematic representation of cofacially stacked phthalocyanine-based polymeric metallomesogen



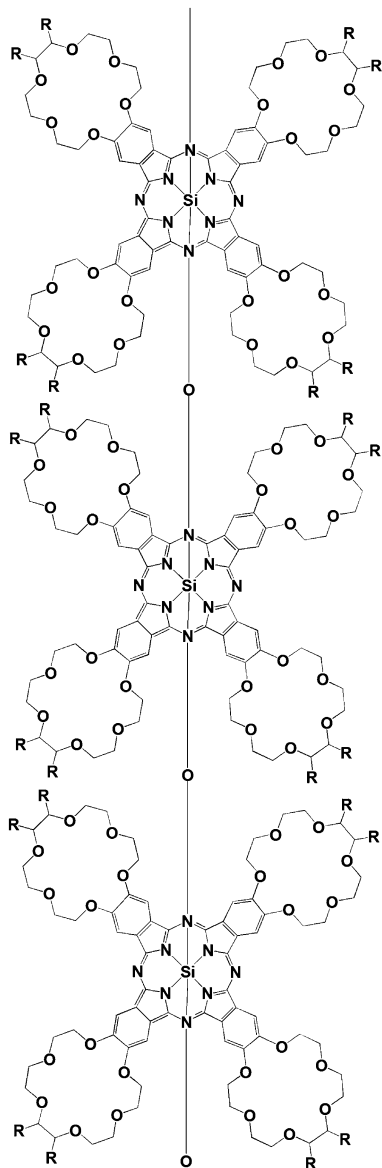
the polysiloxane chain creates strong interactions between monomeric units, which results in a Si–O–Si bond angle of nearly 180° .

The thermal behavior of these polymers is not very straightforward as most of these do not display any clear isotropic transition. Short side-chain derivatives do not exhibit any phase transition up to the decomposition temperature. Medium side-chain polymers show melting transitions below 100°C but no further phase transition is observed up to 300°C . The long side-chain derivatives under polarizing microscope exhibit a non-birefringent isotropic state at higher temperature without decomposing, but this transition is not observed in DSC thermograms. The formation of columnar mesophases in these polymers was established by X-ray diffraction studies.

An interesting example of this class of materials is the phthalocyaninato polysiloxanes substituted with crown ether moieties (Fig. 18.24). The synthesis of these polymers was realized by Nolte and coworkers (Sielcken et al. 1990; Van Nostrum et al. 1995; Van Nostrum and Nolte 1996). Crown ether phthalocyanine can be prepared from 4,5-dicyanobenzo-crown ether under standard phthalocyanine synthesis reaction conditions. These phthalocyanines can be easily converted into dihydroxysilicon derivatives, which, on heating in the presence of a catalyst, yield polysiloxanes with crown ether substituents. These discotic stacks are expected to transport electrons, *via* central phthalocyanine nucleus, and ions, *via* crown ether periphery, in the direction of columnar axis. Connecting long hydrocarbon chains to the crown ether periphery generates liquid crystalline phthalocyanine, which displays a hexagonal columnar phase (Van Nostrum et al. 1995). However, its silicon derivative with two axial hydroxyl groups is non-mesomorphic because of the steric hindrance of axial hydroxyl groups, which prevent the molecules to aggregate. This dihydroxysilicon tetrakis[4',5'-bis(decyloxy)benzo-18-crown-6]phthalocyanine can be polymerized to form a polysiloxane but the exact nature of the polymer is not revealed (Van Nostrum et al. 1995).

A different approach for fixing the liquid crystalline order of phthalocyaninato metal complexes by polymerization was undertaken by Drenth and co-workers who

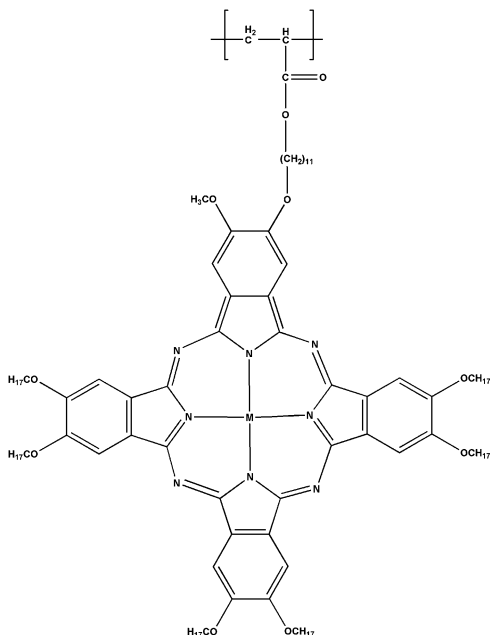
Fig. 18.24 Schematic representation of spinal columnar phthalocaynine polysiloxane substituted with crown ether moieties



synthesized side-chain polymers from asymmetric metal-free or metal-containing phthalocaynine monomers (Van der Pol et al. 1989a, b). The monomers contain reactive acrylic or methacrylic groups which polymerize by a free radical mechanism in benzene solutions. The copper polyacrylate shown in Fig. 18.25 was synthesized using this procedure.

Unlike the monomer, which showed a transition from the crystalline phase to the D_{ho} mesophase, the polymer did not exhibit a liquid crystalline phase. However,

Fig. 18.25 Side chain polyacrylate derived from a metallomesogenic phthalocyanine copper (II) complex



X-ray measurements indicated that its structure fully corresponds to a columnar D_{ho} arrangement. As consequence, it may be of interest as a one-dimensional conductor.

Oriol and coworkers have synthesized metallomesogenic polymers having discotic units in the main chain using β -diketonates of Cu(II) and Pd(II) as monomers (Valdebenito et al. 2000) (Fig. 18.26). The corresponding homologues of low molecular weight have also been synthesized as models of the polymers. All the materials prepared exhibit columnar mesophases as evidenced by X-ray diffraction studies. Fibers of these polymers have an orientation of the polymeric chains along the stretching direction and the disc-like units are arranged in columns perpendicular to the fiber axis.

18.6 Crosslinked Metallomesogenic Polymers

There are a number of reports on cross-linked LCPs due to excellent properties exhibited by liquid crystalline elastomers (Davis 1993) or anisotropic networks (Broer 1993) and are increasing continuously. Slightly cross-linked LCPs or liquid crystalline elastomers have very interesting physical properties, which are derived from the possibility of obtaining perfectly oriented LC mono domains under mechanical fields e.g. a mechanical strain signal can be transformed into an optical signal or electrical response (piezoelectric effect)] (Gleim and Finkelmann 1989; Zentel 1989; Davis 1993). Ordered polymeric networks obtained by in situ photo polymerization of reactive low molecular weight liquid crystals (Broer et al. 1989;

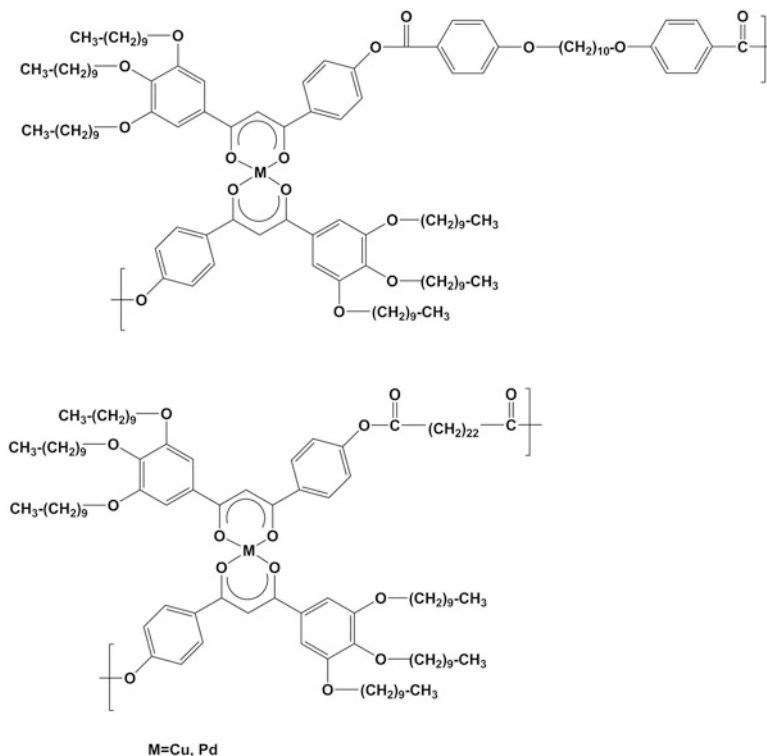


Fig. 18.26

Broer and Heynderickx [1990](#); Heynderickx and Broer [1991](#); Litt et al. [1993](#)) have proved to be very attractive as optical devices with permanent properties. This interest in cross linked systems has been also extended to the field of metallomesogenic polymers. Bearing in mind the synthetic approaches mentioned earlier for metallomesogenic polymers, there are two strategies for obtaining cross linking systems as reported by Serrano et al.:

1. This strategy is based on synthetic approach [2a](#). Metal atoms can act as the cross-linking agent by using preformed linear polymeric chains, which contain coordinating sites. This is the most commonly used method, but the main disadvantage arises from the less processability of the metal-crosslinked polymer.
2. Mesogenic metal complexes having reactive groups: These compounds can be processed by conventional polymerization mechanisms from the mesomorphic state of the corresponding monomer.

Metal modified main chain polymers were firstly reported by Hanabusa and coworkers based on series of homo- and copolyesters containing bipyridyl and diketone units (Hanabusa et al. [1989](#)). Bipyridyl derivatives form ionic complexes with Fe(II) and Cu(II) by reaction of metal salts with a solution of the parent

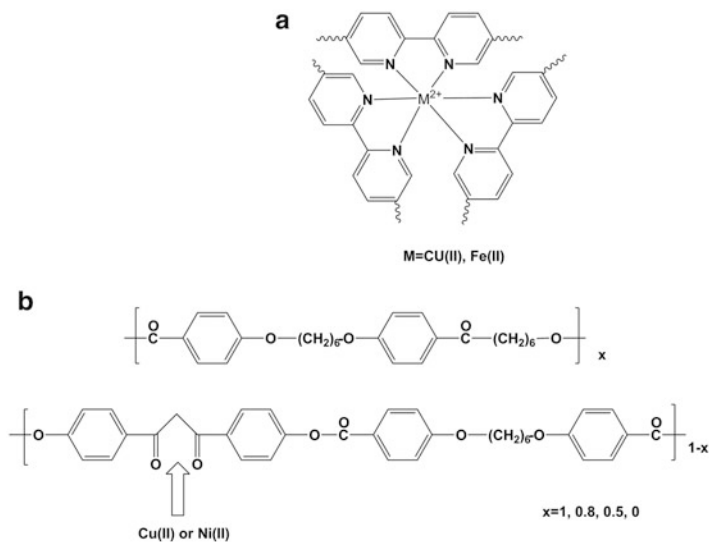


Fig. 18.27 Series of thermotropic polyesters containing β -diketone ligand groups

polymer (Fig. 18.27a). Octahedral geometry was reported for these metal complexes. A compound with low metal content exhibited nematic mesophase, whereas on increasing metal content mesophase behaviour is seems to be suppressed due to metal cross links.

Similar conclusions were drawn from a different series of polymers containing β -diketone groups (Hanabusa et al. 1991) (Fig. 18.27b). Only polymers in which $x = 0.8$ and $x = 0.5$ were metal modified due to the insolubility of polymer with $x = 0$. Copper(II) and nickel(II) were used as modifiers. A square planar coordination is present around copper(II) but data was not reported for Ni(II) polymers. Modified polymers show nematic behavior as do the parent systems.

Serrano and co-workers recently reported (Oriol et al. 1994; Alonso et al. 1994) the copper complexation of hydroxy-functionalized liquid-crystalline homo- and copolyazomethines, which are shown in Fig. 18.28. In general, transition temperatures slightly decrease and an elastic behavior appears when the metal content increases. Nevertheless, mesogenic behavior can be clearly observed for low metal contents.

The presence of the flexible $-\text{CH}_2-\text{CH}_2-$ central core gives rise to intra-chain coordination, whereas rigid aromatic cores give rise to cross-linking. In the case of the copolymers, complexation only affects the $-\text{CH}_2-\text{CH}_2-$ sites as demonstrated by EPR. As regards to mesogenic properties, a nematic mesophase was only observed for polymers with a metal content lower than 30 % (molar proportion of copper (II) ions with respect to repeat units). Similar results were obtained using V(IV) and Fe(II) as modifiers (Alonso et al. 1994).

Metal modified side chain polymers are firstly reported by Hanabusa and co-workers (Fig. 18.29). The cross-linked materials were derived from a side

Fig. 18.28

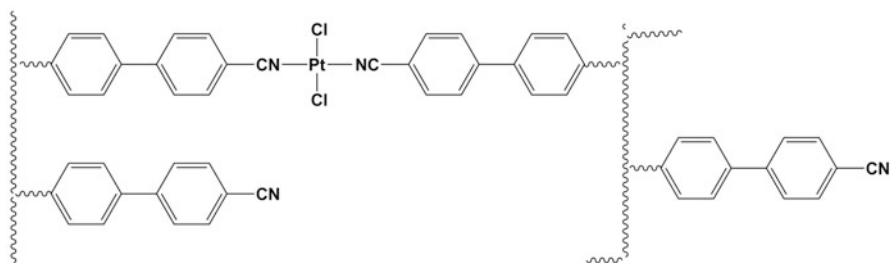
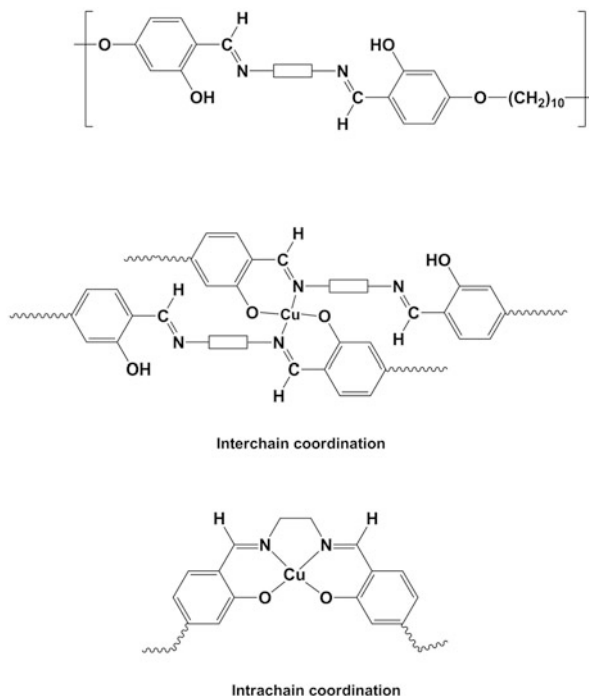
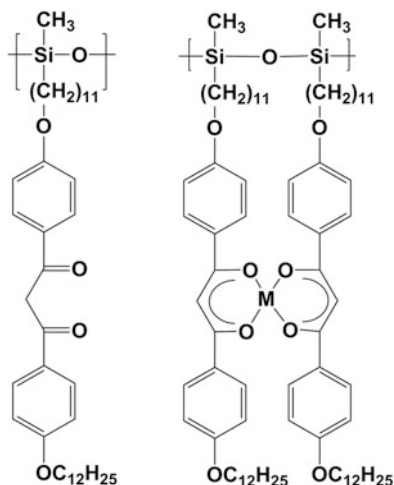


Fig. 18.29

chain LCP bearing *p*-cyanobiphenyloxy mesogenic unit attached by flexible spacer to the polymer backbone: poly-siloxane (Hanabusa et al. 1990a) or polyacrylate (Hanabusa et al. 1990b). Cross-links are formed by a *trans* Pt(II) complex synthesized by a ligand exchange reaction. The transition temperatures and the mesogenic behavior depend on the density of cross-linking. The mobility of chain segments is reduced at the cross-linking sites as well as the mobility of mesogenic groups in the neighborhood. Consequently, cross-linked polymers with high metal contents (approx. > 20 % of complexed repeating units) did not show mesogenic behavior. In the cases of polymers with lower metal contents, the appearance of a mesophase of the same nature as the parent polymer was confirmed by X-ray diffraction and

Fig. 18.30



polarizing microscopy. The same authors reported the modification of a polyacrylate based on β -diketone mesogenic units (Hanabusa et al. 1990c, 1992), which was modified by complexation with Cu(II), Ni(II) and Co(II).

The same synthetic approach was also used by Zhang and co-workers to modify the polymers shown in Fig. 18.30 (Wu et al. 1990, 1991; Zhou et al. 1992). The authors suggest that metal complexation occurs between two adjacent ligands on the polymeric backbone. This conclusion was only supported by the fact that metal modified polymers were still soluble in common organic solvents. However, high percentages of metal ions were not introduced. In any case, a strong modification of thermal properties was observed on metal complexation, which led to an increase in the mesogenic range. The authors pointed to fixation of the ordered macromolecular arrangement at liquid crystalline state by complexation. Typical textures were not observed by microscopy and the possibility of a discotic arrangement of copper (II)- β -diketone intrachain complexes was suggested, although no evidence for this order was given. Furthermore, Pd-chelation exerts a more positive effect on the fixation of the mesogenic behavior. An alternative explanation for the results observed could be given by taking into account previous experience on LC elastomers. In the cases when cross-linking units are mesogenic cores, there is an additional stabilization of the mesophase observed in the non-cross-linked parent.

In the search for supramolecular structures such as low dimensional conductors, Drenth and co-workers (Van der Pol et al. 1990) designed octa-*n*-alkoxy substituted phthalocyanines and their metal complex derivatives bearing functional groups at the end of the aliphatic chains (Fig. 18.31). The aim was to fix the columnar organization of a discotic mesophase (especially D_{ho}) by polymerization.

Attard et al. proposed the preparation of orientated networks by UV radiation of fibers processed from an unusual lamellar discotic phase of the reactive copper (II) carboxylate as displayed in Fig. 18.32 (Attard and Templer 1993). The viscoelastic properties of the lamellar discotic phase allow the processing of highly

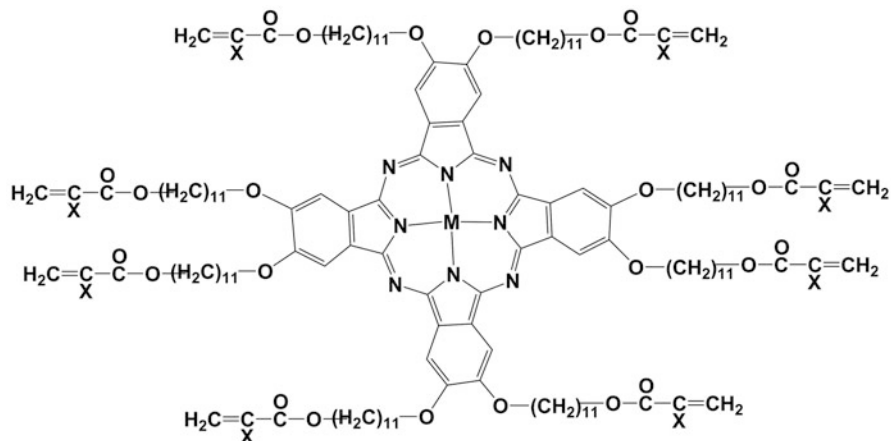


Fig. 18.31

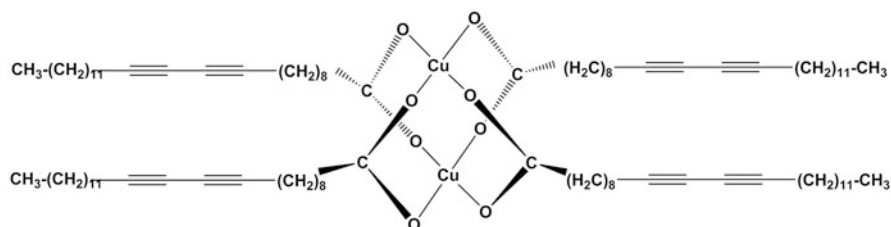


Fig. 18.32

ordered crystalline fibers, which were irradiated at room temperature by using a low intensity UV lamp giving rise to deep coloration. This suggests the formation of polydiacetylenic chains.

18.7 Borderline Cases

Besides above reports on main chain and side chain polymers, there are some reports which could be considered as borderline materials due to their structural or applicative aspects. For instance, possibility of obtaining polymeric ribbons by complexation of azamacrocycles with copper(II) was suggested by Neve et al. (1994a, b) (Fig. 18.33) and was verified by X-ray diffraction measurements.

A synthetic strategy aimed at incorporating metal-metal multiple bonds into one-dimensional polymers and liquid crystals was outlined by Chisholm (2000) (Fig. 18.34). Dimetal tetracarboxylates was used as specific examples, where the metals were molybdenum and tungsten. The thermo tropic and other

Fig. 18.33

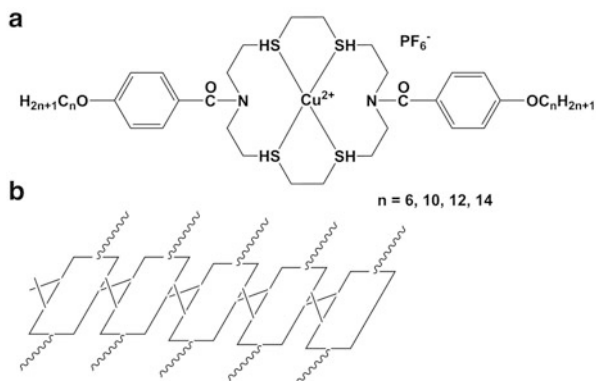


Fig. 18.34 One dimensional MLCP with bridging ligand

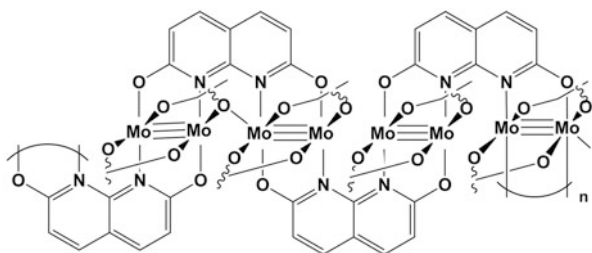
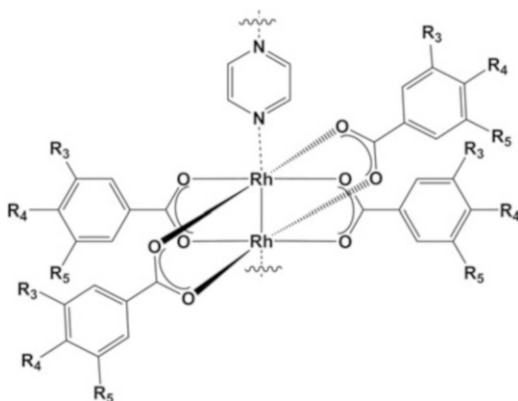


Fig. 18.35



physicochemical properties of mesogenic $\text{M}_2(\text{O}_2\text{CR})_4$ compounds were related to the intermolecular $\text{M}_2 \dots \text{O}$ interactions as a function of M and R. Conducting or charge-storing properties of these one dimensional polymers were found to depend upon the organic linking group.

Tetra(alkoxybenzoato)dirhodium(II) complexes and the corresponding pyrazine adducts have been synthesized and characterized by Cukiernik et al. (2002) (Fig. 18.35). The pyrazine adducts were prepared to have a polymeric structure *via* connected metal centers. The analysis of the compounds showed that these type

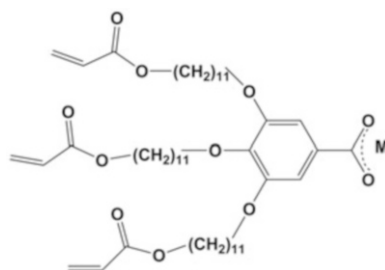
of polymeric columnar metallomesogens in which the electron-rich metal centers are connected by communicating ligands, give rise to structures that eventually can act as molecular wires.

18.8 Conclusions and Future Perspective

In summary, the reports on metal-containing liquid crystalline polymers have been mainly concerned about synthesis and chemical characterization of the materials. The curiosity of liquid crystal chemists and challenges due to limitation of synthesis of metallomesogenic polymers owing to low solubility, absence of mesophase transitions, high viscosity, very high melting point or decomposition nature prompted generation of a number of synthetic approaches for these materials. The attractive structural possibilities introduced by the coordination chemistry and the rich variety of molecular geometries enlighten the molecular architecture of liquid crystal polymers. Besides this, there are few reports, which seem promising for applications of these newly synthesized materials, but their practical applications have not been described in these reports. Once this first synthetic work is done, in which the polymeric structures usually correspond to earlier reported low molecular weight metallomesogens, the future work of metallomesogenic polymeric must focus on the physical properties of metallic entities arranged in ordered supramolecular structures. Magnetic, electrical, catalytic or non-linear optical properties, ionic transport, redox reversible properties, photoeffects and other physical properties need to be explored in these systems in which the polymeric structure affords an important property: processability.

A lyotropic metal-containing nanostructured material through *in-situ* polymerization of reactive metallomesogens was reported by Serrano and co workers (2005). The monomeric unit used in the synthesis is given in Fig. 18.36. They used an excellent method to fix the orientation of liquid-crystal phases into polymeric films by bulk polymerization of reactive LCs. The polymerization of these materials *in situ* at the mesophase temperature converts the fragile structure of a self-organized molecular assembly into a polymeric material that displays good mechanical tractability and a structure that corresponds to the organization of the mesophase in which the polymerization takes place. The polymerization of reactive metallomesogens *in situ* opens up new possibilities for the processing of

Fig. 18.36



nanostructured metal-containing materials. Nevertheless, metals may have an adverse effect on the efficiency of the polymerization, especially in the free-radical polymerization of acrylates—the most widely studied polymerizable units used to design both lyotropic and thermotropic reactive metallomesogens.

Recently, Giménez and coworkers reported luminescent metallomesogens formed by a main-chain coordination polymer (Barbera et al. 2010). Silver pyrazolates with columnar liquid-crystal phases have been prepared by reaction of silver nitrate with 3,5-diarylpyrazolates and found to be stable at room temperature. The special characteristics of silver in forming reversible metal–ligand bonds in solution evidenced experimentally, leads to supramolecular organizations in which the silver cations promote self-organization of the nonmesomorphic pyrazolates into helical 1D polymer that exhibit columnar mesophases (Fig. 18.37). Thin films of the silver complexes showed luminescence at room temperature and found to be suitable for OLED applications.

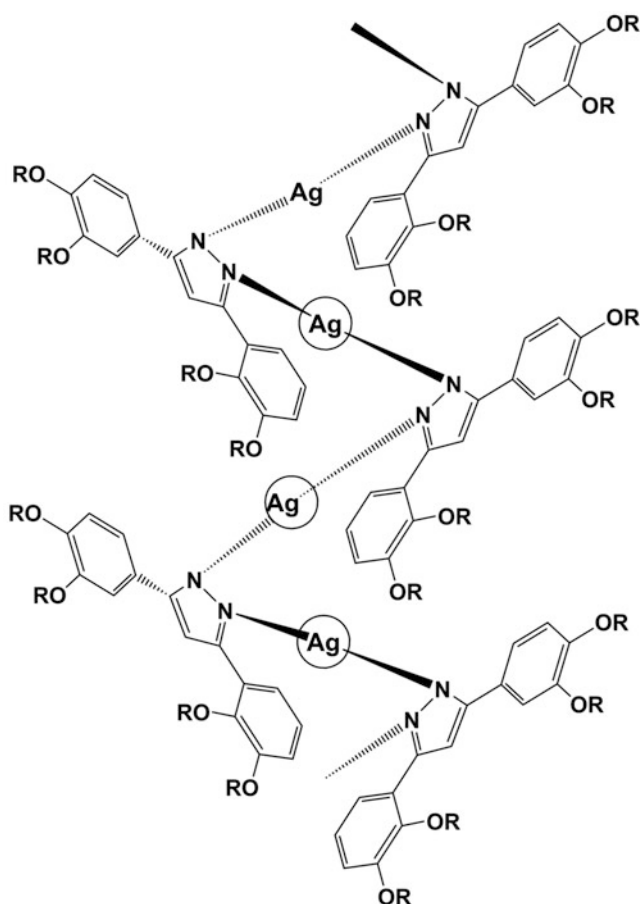


Fig. 18.37

In conclusion, design and synthesis of novel metallomesogenic polymers must be motivated for enrichment of academic interest as well as application purposes. Metal ions in these systems are very powerful tool and it must be utilized by novel approaches and concepts. A profound knowledge of the structure-physical property relationship in these materials are available due to a vast variety of reports that will allow an appropriate selection and tuning of the metal and liquid crystalline states and will enable the design of attractive multifunctional materials with improved properties.

References

- Abe A, Kimura N, Tabata S (1991a) Phase behavior and molecular ordering of semiflexible poly(yn)-platinum polymers in trichloroethylene. *Macromolecules* 24:6238–6243
- Abe A, Tabata S, Kimura N (1991b) Orientational characteristics of semiflexible poly(yn)-platinum polymers as studied by deuterium NMR. *Polym J* 23(1):69–72
- Ahlers G, Cannell DS, Berge LI, Sakurai S (1994) Thermal conductivity of the nematic liquid crystal 4-*n*-pentyl-4'-cyanobiphenyl. *Phys Rev E* 49(1):545–553
- Alonso PJ, Martinez JI, Oriol L, Pifiol M, Serrano JL (1994) Paramagnetic metal containing polyazomethines. *Adv Mater* 6:663
- Amer WA, Wang L, Yu H, Amin AM, Wang Y (2012) Synthesis and properties of a ferrocene-based metallomesogenic polymer containing bis(4-hydroxyoctoxyphenyl) sulfone. *J Inorg Organomet Polym* 22(6):1229–1239
- Attard GS, Templer RH (1993) Copper(II) pentacosadiynoate: a discotic mesogen with unusual liquid-crystalline and solid-state ultrastructures. *J Mater Chem* 3:207–213
- Barbera J, Lantero I, Moyano S, Serrano JL, Elduque A, Gimenez R (2010) Silver pyrazolates as coordination-polymer luminescent metallomesogens. *Chem Eur J* 16:14545–14553
- Blinov LM, Palto SP (2009) Cholesteric helix: topological problem, photonics and electro- optics. *Liq Cryst* 36(10–11):1037–1047
- Boudenne A, Khaldi S (2003) Temperature and liquid crystal concentration effect on thermal conductivity of poly(styrene) dispersed 5CB liquid crystal. *J Appl Polym Sci* 89(2):481–486
- Broer DJ (1993) Radiation curing in polymer science and technology. In: Fouassier JP, Rabek JF (eds) *Polymerisation mechanism*, vol 3. Elsevier, Essex, p 383
- Broer DJ, Heynderickx I (1990) Three-dimensionally ordered polymer networks with a helicoidal structure. *Macromolecules* 23(9):2474–2477
- Broer DJ, Boven J, Mol GN, Challa G (1989) In-situ photopolymerization of oriented liquid-crystalline acrylates, 3. Oriented polymer networks from a mesogenic diacrylate. *Makromol Chem* 190(9):2255–2268
- Brostow W (1990) Properties of polymer liquid crystals: choosing molecular structures and blending. *Polymer* 31:979–995
- Carfagna C, Caruso U, Roviello A, Sirigu A (1987) Metal containing liquid-crystal polymers. *Makromol Chem Rapid Commun* 8:345–351
- Carraher CE (1981) Organometallic polymers. *J Chem Ed* 58:921–934
- Caseri W, Sauer T, Wegner G (1988) Soluble phthalocyaninato-polysiloxanes: rigid rod polymers of high molecular weight. *Makromol Chem Rapid Commun* 9:651–657
- Chisholm MH (2000) One-dimensional polymers and mesogens incorporating multiple bonds between metal atoms. *Acc Chem Res* 33:53–61
- Clark NA, Coleman D, MacLennan JE (2000) Electrostatics and the electro-optic behaviour of chiral smectics C: 'block' polarization screening of applied voltage and 'V-shaped' switching. *Liq Cryst* 27(7):985–990

- Cook MJ, Daniel MF, Harrison KI, Mckeown NB, Thomson AJ (1987) 1, 4,8,11,15,18,22,25-Octa-alkyl phthalocyanines: new discotic liquid crystal materials. *J Chem Soc Chem Commun* 159:1086–1088
- Davis FJ (1993) Liquid crystalline elastomers. *J Mater Chem* 3:551–562
- Dembek AA, Fagan PI, Marsi M (1993a) Synthesis of soluble, organometallic poly(phenylene sulfide) and poly(phenylene oxide) derivatives via transition-metal-activated nucleophilic substitution. *Macromolecules* 26:2992–2994
- Dembek AA, Rurch RR, Feiring AE (1993b) Organometallic modification approach to control of polymer properties: a soluble, liquid crystalline, pi-complexed aromatic polyamide. *J Am Chem Soc* 115(5):2087–2089
- Dembek AA, Burch RR, Feiring AE (1994) Synthesis of soluble, liquid crystalline aramids via transition metal π -Complexation. *Macromolecular Symposia* 77(1):303–313
- Deschenaux R, Kosztics I, Scholten U, Guillon D, Ibn-Elhaj M (1994) First ferrocene-containing side-chain liquid-crystalline polymers. *J Mater Chem* 4:1351–1352
- Diaz AI, Cowling SJ, Bruce DW (2012) Polarised phosphorescent emission in an organoplatinum (II)-based liquid-crystalline polymer. *Chem Commun* 48:10298–10300
- Dulog L, Gittinger A, Roth S, Wagner T (1993) Synthesis and characterization of poly [2,3,9,10,16,17,23,24-octakis(dodecyloxycarbonyl)phthalocyaninatogermoxane. *Makromol Chem* 194:493–500
- Fujikura Y, Sonogashira K, Hagihara N (1975) Preparation and UV Spectra of some oligomer-complexes composed of Platinum group metals and conjugated poly-yne systems. *Chem Lett* 4 (10):1067–1070
- Gleim W, Finkelmann H (1989) In: McArdle CB (ed) Side chain liquid crystal polymers. Blackie, New York, p 287
- Goodby JW, Bruce DW, Hird M, Imrie C, Neal M (2001) An introduction to materials discussion No. 4: molecular topology in liquid crystals. *J Mater Chem* 11:2631–2636
- Gregg BA, Fox MA, Bard AJ (1987) Porphyrine octaesters: new discotic liquid crystals. *J Chem Soc Chem Commun* 14:1134–1135
- Gregg BA, Fox MA, Bard AJ (1989) 2,3,7,8,12,13,17,18-octakis(β -hydroxyethyl)porphyrin (Octaethanolporphyrin) and its liquid crystalline derivatives: synthesis and characterization. *J Am Chem Soc* 111:3024–3029
- Hanabusa K, Kobayashi C, Koyama T, Masuda E, Shirai H, Kondo Y, Takemoto K, Iizuka E, Hojo N (1986) Functional metal-porphyrine derivatives and their polymers, 15. Synthesis and properties of poly(γ -benzyl-L-glutamate)s containing covalently bound metalphthalocyanine moieties in the side chains. *Makromol Chem* 187(4):753–761
- Hanabusa K, Higashi J, Koyama T, Shirai H, Hojo N, Kurose A (1989) Synthesis and properties of thermotropic liquid-crystalline polymers containing transition metals. *Makromol Chem* 190 (1):1–8
- Hanabusa K, Suzuki T, Koyama T, Shirai H, Hojo N (1990a) Effect of metal complexation on the behavior of liquid crystalline polymer. *J Macromol Sci Chem A* 27:1379–1387
- Hanabusa K, Suzuki T, Koyama T, Shirai H, Hojo N, Kurose A (1990b) Effect of Pt (II) coordination on the thermotropic liquid-crystalline behavior of poly(acrylic ester)s containing 4'-cyano-4-biphenyloxy mesogenic groups. *Makromol Chem* 191(3):489–496
- Hanabusa K, Suzuki T, Koyama T, Shirai H, Kurose A (1990c) Synthesis and properties of thermotropic liquid-crystalline polymers containing copper bis(β -diketonate). *Polym J* 22 (2):183–189
- Hanabusa K, Tanimura Y, Suzuki T, Koyama T, Shirai H (1991) New thermotropic liquid-crystalline polyesters with a metalchelated 1,3-diphenyl-1,3-propanedione segment. *Makromol Chem* 192(2):233–244
- Hanabusa K, Suzuki T, Koyama T, Shirai H (1992) Synthesis and properties of liquid-crystalline side-chain polymers containing β -diketonato transition metal complexes. *Makromol Chem* 193 (8):2149–2161

- Hanabusa K, Isogai T, Koyama T, Shirai H (1993) Synthesis and properties of thermotropic liquid-crystalline polymers linked through bis(β -diketonato)copper(II) complex. *Makromol Chem* 194:197–210
- Hanack M, Beck A, Lehmann H (1987) Syntheses of liquid crystalline phthalocyanines. *Synthesis* 83:703–705
- Harwood JW (1963) *Industrial applications of organometallic compounds*. Reinhold, New York
- Heynderickx I, Broer DJ (1991) The use of cholesterically-ordered polymer networks in practical applications *Mol Cryst. Liq Cryst* 203:113–126
- Holm RH, Bconnor MJ (1971) In: Lippard SJ (ed) *Progress in inorganic chemistry*, vol 14. Wiley, New York, p 241
- Kato T, Mizoshita N, Kishimoto K (2006) Functional liquid-crystalline assemblies: self-organized soft materials. *Angew Chem Int Ed* 45:38–68
- Kerr RL, Miller SA, Shoemaker RK, Elliot BJ, Gin DI (2009) New type of Li Ion conductor with 3D interconnected nanopores via polymerization of a liquid organic electrolyte-filled lyotropic liquid-crystal assembly. *J Am Chem Soc* 131:15972–15973
- Kim PJ, Masai H, Sonogashira K, Hagihara N (1970) Preparations of α , ω -bis-nickel-polyacetylenes. *Inorg Nucl Chem Lett* 6(2):181–185
- Kotani S, Shiina K, Sonogashira K (1991) Synthesis of poly-yne polymers containing transition metals, disilane, disiloxane and phosphine groups in the main chain. *Appl Organomet Chem* 5:417–425
- Lemieux RP (2005) Photo switching of ferroelectric liquid crystals using photochromic dopants. *Soft Matter* 1:348–354
- Lemieux RP, Dinescu L, Maly KF (2001) Optical switching of a ferroelectric liquid crystal spatial light modulator using chiral thioindigo dopants. In: Glaser R, Kaszynski P (eds) *Anisotropic organic materials—approaches to polar order*, vol 798, ACS Symposium Series. American Chemical Society, Washington, DC
- Leznoff CC, Lever ABP (1989) (eds.) *Phthalocyanine: properties and application*. VCH, New York
- Lindau J, Fischer H, Rotz U, Jurkschat K, Kuschel F (1991) Tin organic liquid crystalline polyester. *Makromol Chem Rapid Commun* 12:477–482
- Litt MH, Whang W, Yen K, Qian X (1993) Crosslinked liquid crystal polymers from liquid crystal monomers: synthesis and mechanical properties. *J Polym Sci Polym Chem* 31(1):183–191
- Ma J, Li Y, White T, Urbas A, Li Q (2010) Light-driven nanoscale chiral molecular switch: reversible dynamic full range color phototuning. *Chem Comm* 46:3463–3465
- Marcos M, Oriol L, Serrano JL, Alonso PJ, Puertolas JA (1990) Metal-containing homopolymers showing paramagnetic nematic mesophase. *Macromolecules* 23:5187–5191
- Marcos M, Oriol L, Serrano JL (1992) Metallomesogenic homopolymers: 1. Synthesis and influence of metalloorganic structure on mesogenic behaviour. *Macromolecules* 25:5362–5368
- Matsumoto T, Kotani S, Shiina K, Sonogashira K (1993) Synthesis of poly-yne polymer containing platinum and silicon atoms in the main chain by oxidative coupling and its reactions with transition-metal carbonyl complexes. *Appl Organomet Chem* 7:613–621
- Moore JS, Stupp SI (1987) Presented at the International conference on liquid crystal polymers. Bordeaux, France
- Moore JS, Stupp SI (1988) Paramagnetic organometallic liquid-crystal polymers. *Polym Bull* 19:251–256
- Neve F, Ghedini M, Levelut AM, Francescangeli O (1994a) Ionic metallomesogens. Lamellar mesophases in copper(I) azamacrocyclic complexes. *Chem Mater* 6(1):70–76
- Neve F, Levelut AM, Ghedini M, Munno GD (1994b) Poster presented at the 15th International Liquid Crystal Conference. Budapest, Hungary
- Oriol L (1990) Synthesis, mesomorphic and physical properties of metallomesogenic polymers and polyazomethines. Ph.D. Thesis (University of Zaragoza). 39
- Oriol L, Serrano JL (1995) Metallomesogenic polymers. *Adv Mater* 7:348–369

- Oriol L, Serrano JL (2005) Metal-containing nanostructured materials through in situ polymerization of reactive metallomesogens. *Angew Chem Int Ed* 44:6618–6621
- Oriol L, Alonso PJ, Martinez JI, Pinol M, Serrano JL (1994) Structural studies of copper(II)-chelated polymers derived from hydroxy-functionalized liquid crystalline homo- and copolyazomethines. *Macromolecules* 27:1869–1874
- Orthmann E, Wegner G (1986) Preparation of ultrathin layers of molecularly controlled architecture from polymeric phthalocyanines by the Langmuir-Blodgett-technique. *Angew Chem Int Ed Engl* 25:1105–1107
- Reddy RA, Tschierske C (2006) Bent-core liquid crystals: polar order, superstructural chirality and spontaneous desymmetrisation in soft matter systems. *J Mater Chem* 16:907–961
- Rusjan M, Donnio B, Guillon D, Cukiernik FD (2002) Liquid-crystalline materials based on rhodium carboxylate coordination polymers: synthesis, characterization and mesomorphic properties of tetra(alkoxybenzoato)dirhodium(II) complexes and their pyrazine adducts. *Chem Mater* 14:1564–1575
- Saez IM, Goodby JW (2005) Supermolecular liquid crystals. *J Mater Chem* 15:26–40
- Sauer T, Wegner G (1991) Small-angle x-ray scattering from dilute solutions of substituted phthalocyaninato-polysiloxanes. *Macromolecules* 24:2240–2252
- Sauerm T (1993) Hexagonal-columnar mesophases in substituted phthalocyaninatopoly-siloxanes. *Macromolecules* 26:2057–2063
- Schouten PG, Warman JM, de Hass MP, van der Pol JF, Zwikker JW (1992) Radiation induced conductivity in polymerized and nonpolymerised columnar aggregates of phthalocyanines. *J Am Chem Soc* 114:9028–9034
- Senthilkumar N, Narasimhaswamy T, Kim IJ (2012) Novel metallomesogenic polyurethanes: synthesis, characterization and properties. *Mater Sci Eng C* 32:2258–2266
- Serrano JL (1996) *Metallomesogens: synthesis, properties and applications*. VCH, Weinheim, p 193
- Sielcken OE, van de Kuil LA, Drenth W, Schoonman J, Nolte RJM (1990) Phthalocyaninato polysiloxanes substituted with crown ether moieties. *J Am Chem Soc* 112:3086–3093
- Simoni F (1998) Non-linear optics in liquid crystals: basic ideas and perspectives. *Liq Cryst* 24(1):83–89
- Singh P, Rausch MD, Lenz RW (1989) Ferrocene containing liquid crystalline copolyesters. *Polym Bull* 22:247–252
- Sirlin C, Bosio L, Simon J (1987) Spinal columnar liquid crystals: polymeric octasubstituted μ -oxo-(phthalocyninato)-tin(IV). *J Chem Soc Chem Commun* 18:379–380
- Sirlin C, Bosio L, Simon J (1988a) Polycondensation in mesomorphic phases: spinal columnar liquid crystals based on octasubstituted phthalocyanine siloxane derivatives. *Mol Cryst Liq Cryst* 155:231–238
- Sirlin C, Bosio L, Simon J (1988b) Spinal columnar liquid crystals based on octasubstituted phthalocyanine siloxane derivatives. *J Chem Soc Chem Commun* 10:236–237
- Sonogashira K, Takahashi S, Hagihara N (1977) A new extended chain polymer, poly [trans-bis (tri-n-butylphosphine)platinum 1,4-butadienydiyl]. *Macromolecules* 10:879–880
- Sonogashira K, Fujikura Y, Yatake T, Toyoshima N, Takahashi S, Hagihara N (1978a) Syntheses and properties of cis- and trans-dialkynyl complexes of platinum(II). *J Organomet Chem* 145:101–108
- Sonogashira K, Katdoka S, Takahashi S, Hagihara N (1978b) Studies of poly-yne polymers containing transition metals in the main chain: III synthesis and characterization of a poly-yne polymer containing mixed metals in the main chain. *J Organomet Chem* 160:319–327
- Sonogashira K, Ohga K, Thkhashi S, Hagihara N (1980) Studies of poly-yne polymers containing transition metals in the main chain: VI. Synthesis of nickel-poly-yne polymers by alkynyl ligand exchange using a copper(I) catalyst. *J Organomet Chem* 188(2):237–243
- Takahashi S, Kariya M, Yatake T, Sonogashira K, Hagihara N (1978) Studies of poly-yne polymers containing transition metals in the main chain. 2. Synthesis of poly[trans-bis(tri-n-

- butylphosphine)platinum 1,4-butadienediyl] and evidence of a rodlike structure. *Macromolecules* 11:1063–1066
- Takahashi S, Murata E, Kariya M, Sonogashird K, Hagihara N (1979) A new liquid-crystalline material. Transition metal-poly(yne) polymers. *Macromolecules* 12(5):1016–1018
- Takahashi S, Murata E, Sonogashira K, Hagihara N (1980a) Studies on polyyne polymers containing transition metals in the main chain. IV. Polymer synthesis by oxidative coupling of transition metal-bis(acetylide) complexes. *J Polym Sci Polym Chem* 18(2):661–669
- Takahashi S, Ohyama Y, Murata E, Sonogashira K, Hagihara N (1980b) Studies of poly-yne polymers containing transition metals in the main chain. 5. A design of metal arrangement in polymer backbone. *J Polym Sci Polym Chem* 18:349–353
- Tournilhac F, Nicoud JF, Simon J, Weber P, Guillon D, Skoulios A (1987) Synthesis and study of the mesomorphism of highly polarizable mesogens towards applications in non-linear optics. *Liq Cryst* 2(1):55–61
- Tschierske C (2001) Micro-segregation, molecular shape and molecular topology-partners for the design of liquid crystalline materials with complex mesophase morphologies. *J Mater Chem* 11:2647–2671
- Valdebenito N, Oriol L, Barbera J, Diaz F, Serrano JL (2000) Liquid crystalline polymers containing discotic metallomesogens in the main chain. *Macromol Chem Phys* 201:2573–2580
- Van der Pol JF, Neeleman E, Zwikker JW, Nolte RJM, Drenth W, Aerts J, Visser R, Picken SJ (1989a) Homologous series of liquid-crystalline metal free and copper octa-*n*-alkoxyphthalocyanines. *Liq Cryst* 6:577–592
- Van der Pol JR, Neeleman E, Nolte RJM, Zwikker JW, Drenth W (1989b) Asymmetrically substituted liquid-crystalline phthalocyanines and side-chain polymers derived from them. *Makromol Chem* 190:2727–2745
- Van der Pol JF, Neeleman E, Miltenburg JC, Zwikker JW, Nolte RJM, Drenth W (1990) Polymer with the mesomorphic order of liquid crystalline phthalocyanines. *Macromolecules* 23:155–162
- Van Nostrum CF, Nolte RJM (1996) Functional supramolecular materials: self-assembly of phthalocyanines and porphyrazines. *Chem Commun* 21:2385–2392
- Van Nostrum CF, Picken SJ, Schouten AJ, Nolte RJM (1995) Synthesis and supramolecular chemistry of novel liquid crystalline crown ether-substituted phthalocyanines: toward molecular wires and molecular ionoelectronics. *J Am Chem Soc* 117:9957–9965
- Walba DM, Blanca Ros M, Clark NA, Shao R, Johnson KM, Robison MG, Liu JY, Danoski D (2001) Materials for nonlinear optics (ACS Symposium Series). Chapter-32 (Vol. 455): 484
- Wiesemann A, Zentel R (1993) Blends from redox active liquid crystal ionomers and amorphous ionomers. *Liq Cryst* 14:1925–1934
- Wiesemann A, Zentel R (1994) Blends from redox active liquid crystal ionomers and amorphous ionomers. *Liq Cryst* 16:349
- Wiesemann A, Zentel R, Pakula T (1992) Redox-active liquid crystalline ionomers: 1. Synthesis and rheology. *Polymer* 33:5315–5320
- Wiesemann A, Zentel R, Lieser G (1995) Redox active LC ionomers (Feature article): LC ionomers as materials for compatible blends with amorphous ionomers. *Acta Polymer* 46:25–36
- Wu F, Zhang R, Jiang Y (1990) Synthesis and characterization of β -diketone based side chain liquid crystalline polysiloxanes. *Chin J Polym Sci* 8(2):133–141
- Wu F, Zhang R, Jiang Y (1991) Synthesis and properties of metal complexes of β -diketone-based side chain liquid crystal polysiloxane. *Chin J Polym Sci* 9(1):71–80
- Zentel R (1989) Liquid crystalline elastomers. *Adv Mater* 1:321–329
- Zhou Z, Dai D, Zhang R (1992) Synthesis and mesomorphic properties of palladium chelates of liquid crystal polysiloxane with β -diketone-based side chains. *Chin J Polym Sci* 10:70–74

Chapter 19

Integration of Liquid-Crystalline Elastomers in MEMS/MOEMS

Antoni Sánchez-Ferrer, Núria Torras, and Jaume Esteve

19.1 Introduction

Liquid-Crystalline Elastomers (LCEs) are smart soft materials known since 1980s (Finkelmann et al. 1981, 1984; Kundler and Finkelmann 1998), but they have only recently entered to the actuator arena and Microsystems Technology. The main reason for that difficulty is related to the chemistry and compatibility of such materials with the commercial available technologies. Moreover, the huge impact and efforts for the development of inorganic materials, *i.e.*, electroactive ceramics (EACs) and shape memory alloys (SMAs), have shadowed the huge potential of LCEs. The main features of LCEs are the huge fully reversible actuation strain values up to 300 %, the range of stress values covered ranging from 100 kPa to 100 MPa, the low density of such materials around 1–2 g·cm⁻³, and the actuation speed from milliseconds to minutes, which are in contrast to the inorganic materials—EACs and SMAs—with very small actuation strains (up to 5 %), strong actuation stress window (from 10 MPa to 1 GPa), high density (5–8 g·cm⁻³), and similar actuation speed values (Huber et al. 1997). These anisotropic slightly crosslinked macromolecular compounds can incorporate different functionalities for the response to external stimuli, such temperature (Wermter and Finkelmann 2001; Thomsen et al. 2001), light (Finkelmann et al. 2001a; Li et al. 2003), or electric field (Lehmann et al. 1999; Kremer et al. 2000).

A. Sánchez-Ferrer (✉)

Department of Health Sciences & Technology (D-HEST), IFNH, ETH Zurich,
LFO Schmelzberstrasse 9, Zurich 8092, Switzerland
e-mail: antoni.sanchez@hest.ethz.ch

N. Torras • J. Esteve (✉)

Institute of Microelectronics of Barcelona, IMB-CNM (CSIC), Micro & Nano Tools Group,
Campus UAB, Bellaterra, Barcelona 08193, Spain
e-mail: nuria.torras@imb-cnm.csic.es; jaume.esteve@imb-cnm.csic.es

Microsystems Technology is devoted to the production of new systems or components by means of microengineering techniques—sensors, actuators, and microstructured devices (Boussey 2003; Gad-el-Hak 2005)—which interact with the environment. The main advantages of microsystems over macrosystems are their reduced size and cost, as well as improved performance and versatility. Using batch processes, Microsystems Technology allows for the mass production of highly complex microstructures with feature sizes ranging from 1 μm to 100 μm (Leondes 2006; Hsu 2008).

Thus, the integration of smart soft materials, *i.e.*, LCEs into the well-known silicon-based technology goes in the direction of a new generation of hybrid MEMS and MOEMS devices which will exhibit enhanced or novel properties. Flexibility, processability and tunability are properties which LCEs bring to these new hybrid microdevices, but the main advantage of integrating LCEs is concerned to the use of external stimuli avoiding the need for any electrical connection or external controlling devices.

This Chapter aims to be an introduction to the use of LCEs in Microsystems Technology and, specifically, to the integration of such smart soft materials into MEMS/MOEMS. First, the preparation—polymerization and crosslinking—and alignment of the macroscopic sample—mechanical, magnetic, electrical, surface or viscosity alignment—, as well as the main characteristics of LCEs—actuation modes and interaction of the environment—will be presented in the Sect. 19.1. Finally, Sect. 19.2 will be devoted to the state of the art for the integration of LCEs in Microsystems Technology in the fabrication of prototypes of MEMS/MOEMS.

19.2 LCE Materials

LCEs are the combination of mesogenic molecules and crosslinked linear polymer chains (Davis 1993; Terentjev 1999; Warner and Terentjev 2007). Thus, for the synthesis of such smart materials, a mesogen, a crosslinker and a polymer backbone are needed as constituents for the final macromolecular composition (Finkelmann et al. 1981; Küpfer and Finkelmann 1991; de Jeu 2012). In the following, the chemistry used for the obtaining of LCEs for the construction of MEMS and MOEMS will be described. Moreover, an explanation for the techniques used in the orientation of the mesogenic molecules and the alignment of the polymer backbone will be presented. All LCE materials shown in this chapter, which were integrated into devices, are nematic side-chain LCEs.

The main principle for LCEs relies in the reversible order-to-disorder transition (de Gennes 1971). A common rubber material consists in a crosslinked polymer melt: a viscous liquid which mobility is reduced and fluidity suppressed due to the crosslinking of the polymer chains. When pulling a rubber band, entropy is removed and the polymer chains align along the applied mechanical field direction. After removal of this uniaxial deformation, the polymer network relaxes back to an equivalent—not equal—original polymer conformation and regaining entropy.

The relaxed disorder and the initial state before deformation is related to a random polymer coil conformation which is isotropic in nature. As soon as polymer chains start to be aligned, a global prolate conformation is achieved and the material becomes anisotropic (Noirez et al. 1988; Hardouin et al. 1994).

The key question is how this anisotropic state can be fixed and reversibly removed. The trick is the incorporation of mesogenic molecules—the so-called liquid crystals (Lehmann 1908)—which like to orient in the direction of the director in self-assembled clusters or domains. Due to the enthalpy brought by such molecules, the LCE undergoes a liquid crystal (order; enthalpy > entropy) to liquid (disorder; enthalpy < entropy) transition when the enthalpy factor is removed and entropy controls the state (Fig. 19.1a). When attached to a polymer backbone, such domains are formed but distributed randomly in all directions, as well as the polymer backbones, are also randomly aligned. This material is a polydomain of LCE, where clusters of well-ordered mesogens with stretched aligned polymer chains are distributed in all possible directions (Fig. 19.1b). The difference respect to the isotropic state is that mesogens are oriented and polymer chains adopt a prolate conformation (Schätzle and Finkelmann 1987; Wang and Warner 1987). Thus, all domains shrink in the direction of the corresponding domain local director, but since all domains do the same the average change in the dimensions is zero (Fig. 19.1b). A macroscopic change in dimensions can be only observed if a single liquid-crystalline domain is obtained (Finkelmann et al. 1984; Küpfer and Finkelmann 1994; Brand and Finkelmann 1998). In order to keep all domains oriented in the direction of one unique director, an external field should be applied and the macromolecular conformation fixed. Such monodomain of LCE is achieved by stretching of the polymer network or by orienting the mesogens if coupled to the polymer backbone, and final crosslinking. If the enthalpy brought by the mesogens is bigger than the entropy coming from the polymer network (liquid-crystalline state), the material keeps oriented and the polymer chains aligned (Fig. 19.1b). Thus, the isotropization of such liquid-crystalline domains removes the enthalpy contribution and entropy dominates the scenario (liquid state), which allows the polymer coil conformation to be reformed (Fig. 19.1a) with the corresponding contraction of the LCE sample (Fig. 19.1b). Such order-to-disorder transition is induced by means of an external field, *e.g.*, temperature (Donnio et al. 2000; Krause et al. 2007; Sánchez-Ferrer and Finkelmann 2009), light (Finkelmann et al. 2001a; Hogan et al. 2002; Sánchez-Ferrer et al. 2011a) magnetic (Kaiser et al. 2009; Winkler et al. 2010; Haberl et al. 2013) or electric fields (Chambers et al. 2006, 2009; Urayama et al. 2006).

19.2.1 LCE Components

As mentioned before, the mesogen is the component responsible for the alignment of the polymer backbone if coupling between the mesogenic molecules and the polymer backbone is present (Wang and Warner 1987). These mesogens consist in

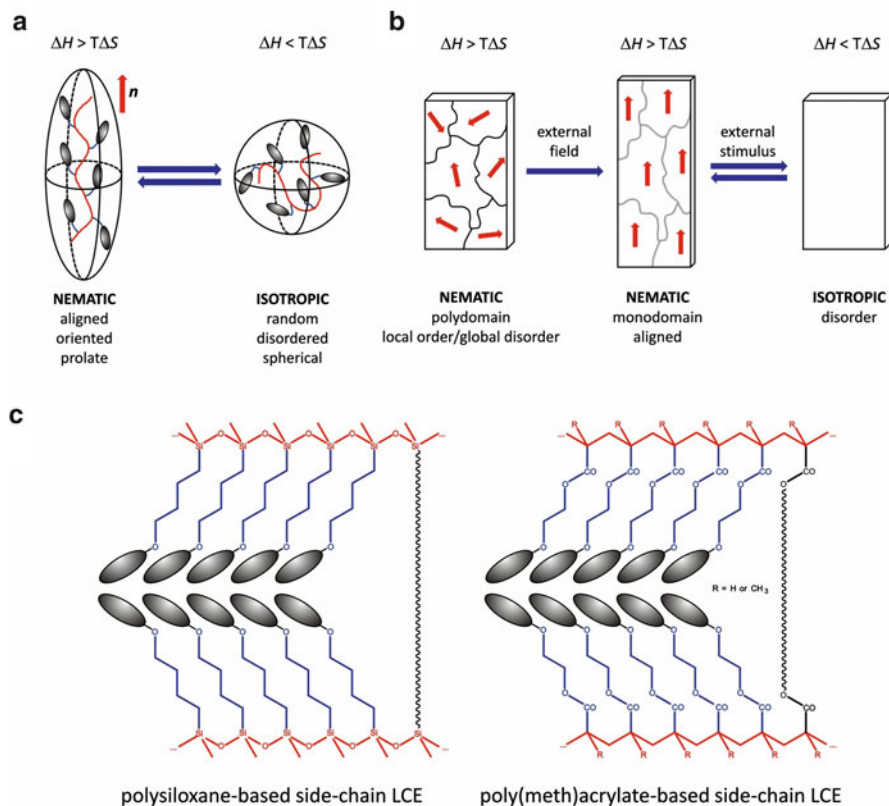


Fig. 19.1 (a) Nematic-to-isotropic transition in end-on side-chain LCEs; the nematic state (*left*) shows alignment of the polymer chains and the orientation of mesogens along the director, and due to the coupling between mesogens and polymer backbone a prolate conformation appears at low temperatures; the isotropic state (*right*) presents a random coil conformation of the polymer chains and disorder of the mesogens which are related to the spherical conformation at high temperatures. (b) Polydomain-to-monodomain transformation in LCEs; the nematic polydomain shows a random distribution (global disorder) of nematic domains (local order); the nematic polydomain has the oriented mesogens pointing in the direction of the director which is parallel to the external field and well-aligned polymer chains; the actuation principle (change in dimensions) can only be observed when the polydomain is disturbed by means of a external stimulus and reaches the isotropic state. (c) Chemical structure for both end-on polysiloxane-based and poly(meth)acrylate-based side-chain LCE, where the polymer backbone (*red*), the spacer (*blue*), the rod-like core (*grey*) and the crosslinker (*black*) are depicted

a two or more aromatic rod-like molecule (crystalline component) with at least one reactive flexible aliphatic spacer (liquid component). Such molecules are directly attached to the polymer backbone as side groups (side-chain LCEs) or forming part of the polymer backbone (main-chain LCEs). The aromatic core allows for the self-assembly of the mesogenic molecules, while the flexible spacer brings mobility and affects the polymer backbone. The increasing number of aromatic rings increases

the mesophase stability, and rises the isotropization temperature due to a better interaction between the cores. The spacer should neither be too short—allowing some freedom to the polymer backbone—nor too long—no coupling between the mesogens and the polymer backbone (Wermter and Finkelmann 2001; Tajbakhsh and Terentjev 2001). Usually, an odd number of atoms in the spacer (even number of carbons) lead towards a polymer chain prolate conformation (Fig. 19.1a). Finally, mesogens might show just orientational order (nematic phase) or also positional order (smectic phase)—which is related to a more energetically rich mesogen (Sánchez-Ferrer and Finkelmann 2009). A nematic mesogen has a nematic-to-isotropic transition temperature T_{ni} , while a smectic mesogen has a smectic-to-isotropic transition temperature T_{si} , even that other order-to-order transitions can be observed.

The polymer backbone can be a polymer melt (amorphous liquid polymer; low glass transition temperature T_g), *i.e.*, polysiloxanes, or a polymer glass (amorphous glassy polymer; high glass transition temperature T_g), *i.e.*, polyacrylates and polymethacrylates. For the first ones, each hydrogenmethylsiloxane repeating unit reacts with a vinyl double bond from the mesogen or crosslinker via hydrosilylation reaction (Küpfer and Finkelmann 1991, 1994). The resulting material is a low T_g mesogenic network or side-chain LCE (Fig. 19.1c). Polyacrylates and polymethacrylates liquid-crystalline networks (LCNs) are formed when the reactive mesogen polymerizes via radical polymerization with a (photo)-initiator. The obtained material is a high T_g mesogenic network which strictly speaking is not an elastomer at room temperature, but can be found as LCE in the literature and considered as such at temperatures above the T_g .

Finally, the crosslinker is the responsible to keep the polymer chains together and, more important, to fix the alignment when a monodomain is obtained. This molecule is a bifunctional—only for side-chain LCEs (Küpfer and Finkelmann 1991, 1994)—or a multifunctional molecule—for both side-chain and main-chain LCEs (Donnio et al. 2000; Sánchez-Ferrer and Finkelmann 2009). Crosslinkers can be either flexible (isotropic) or rigid (liquid-crystalline), and reduce the mobility of the polymer backbone, therefore increasing the materials' T_g . Moreover, it should be mentioned that a flexible crosslinker acts as an impurity, destabilizes the nematic phase, and reduces the T_{ni} ; a rigid crosslinker stabilizes the mesophase and raises the T_{ni} . Usually flexible crosslinkers are used for polysiloxane-based LCEs, and rigid mesogenic crosslinkers are mainly used in polyacrylate and polymethacrylate-based LCNs. Special attention should be given to photo-crosslinkers, which can be used in both chemistries and are mainly flexible (Komp et al. 2005; Beyer et al. 2007; Sánchez-Ferrer et al. 2009). The amount of crosslinker will be a very important factor for the mechanical properties and actuation behavior of the LCE systems. Lightly crosslinked LCEs will show huge deformations but small retractive forces; highly crosslinked LCEs show small changes in dimensions but huge actuation forces. Thus, the right amount of crosslinker, as well as the mesophase which determines the working range of temperatures ($T_{ni}-T_g$), is the key point for the obtaining of tunable actuators and sensors.

19.2.2 Mesogen Orientation and Polymer Alignment

Monodomains of LCEs based in polysiloxane polycondensation chemistry has been obtained by two main processes. The first process is the so-called two-steps crosslinking process (Brand and Finkelmann 1998), where in a first step mesogens are attached to the polymer backbone and the polymer chains are partially crosslinked. The obtained swollen network or isotropic gel is mechanically deformed, *i.e.*, uniaxially stretched (Küpfer and Finkelmann 1994) or biaxially compressed (Torrás et al. 2013). The second step consists in the completion of the crosslinking in order to fix the deformation while removing the solvent by evaporation. The second process relates to the use of magnetic/electrostatic fields. A liquid-crystalline polymer which contains a photo-crosslinker is synthesized. This polymer is annealed right below the isotropization temperature and the mesogens oriented under a magnetic field (Komp et al. 2005; Sánchez-Ferrer et al. 2009). Due to the coupling between the mesogens and the polymer backbone, the polymer chains' alignment is achieved. Afterwards, the sample is crosslinked by means of UV light. Samples of thickness ranging from hundreds to thousands of microns can be produced by the two-steps crosslinking process, while samples of tens of microns can be only produced by photo-crosslinking. Moreover, the first processing allows for huge deformations/actuations—up to 70 %—because the polymer chains are aligned by means of the mechanical deformation, and this alignment orients the mesogens due to the coupling between the two components. These materials can only be processed after the synthesis and integrated in a *Top-Down* approach. The UV-crosslinking process relies on the orientation of the mesogens which should stretch the polymer chains, but should overcome viscosity and polymer conformational issues. Thus, small deformations/actuations—up to 20 %—can be achieved. This technique allows also for the integration into devices before the final material is obtained in a *Bottom-Up* approach by the use of photo-masks.

Monodomains of LCEs based in poly(meth)acrylate polyaddition chemistry can be produced by a single process. Mesogen, crosslinker and (photo)-initiator are put together (Thomsen et al. 2001; Haseloh and Zentel 2009; Ohm et al. 2009). The mixture reacts forming the polymer backbone and the simultaneous statistical crosslinking of the polymer chains as they grow. This process is done under orientational techniques such surface effects or capillarity forces. Both techniques allow for the orientation of the rod-like molecules, but the order can only be kept for few microns gap/thickness, which is enough to see some bending/actuation in the samples. Thus, due to the rigidity of the polymer backbone (high T_g), the small thickness of the obtained samples and the high working temperatures, applications are reduced to very small devices. A good advantage is that the material can be integrated in one single process following a *Bottom-Up* approach as used in display technology applications. Hundreds microns thickness samples can be obtained by using a nematic solvent and magnetic fields, where the solvent helps to reduce the viscosity of the mixture, the clearing temperature during the network formation,

and enhances the orientation of the mesogens (Urayama et al. 2007; Urayama 2010). Formally speaking, the material is a gel which can be deswollen and a LCN can be obtained, but the material has to be integrated to the device afterwards in a *Top-Down* approach.

19.2.3 Actuation Principles

As mentioned in the previous chapter, the nematic-to-isotropic transition has to take place in order to induce disorder in the mesophase (between the mesogens), and the corresponding misalignment of the polymer chains which adopt the entropically favorable coil conformation (Fig. 19.1a). This isotropization process needs for a trigger or external stimulus which brings energy to the system by rising the temperature or by introducing impurities to the system. For the first case, heat or heat-related stimuli are used; *e.g.*, direct heat from the surroundings which is transferred through the sample (Wermter and Finkelmann 2001), or due to Joule effect when some electrical current is applied through a dissipative medium (Chambers et al. 2009), or non-selective absorption of a photon in the visible or infrared region which locally releases heat after the corresponding electron relaxes in a non-radiative way (Ji et al. 2012; Haberl et al. 2014). For the second case, the change in shape of a molecule which disturbs the liquid-crystalline phase is required. Thus, the most common external stimulus used here is light which induces the photo-isomerization of photo-active molecules (Sánchez-Ferrer 2011; Sánchez-Ferrer and Finkelmann 2013). Such isomers obtained after irradiation shift the isotropization temperature of the liquid-crystalline phase by changing the chemical composition, but not raising the temperature. Moreover, the architecture of such molecules can be modified in a way that they connect different polymer chains which are forced to come together after irradiation. Of course, other stimuli can be considered, but up to now only those described above have been implemented in MEMS/MOEMS due to their easy applicability and affordability.

The sort of actuation which can be produced by nematic side-chain LCEs strongly depends on the chemistry, as well as the orientation/alignment used for the obtaining of monodomains. Thus, LCEs can easily produce contraction and/or expansion no matter the thickness, dimensions or shapes of the actuator. These prolate samples which are uniaxially stretched undergo contraction along the direction of the deformation when disordered, while expand in the other two directions perpendicular to the imposed deformation (Küpfer and Finkelmann 1994). For those prolate samples biaxially stretched, expansion along the imposed deformation occurs accompanied by a contraction in the other two perpendicular directions (Torras et al. 2013). LCEs which are devoted for light-induced actuation—photo-isomerization—, suffer of huge absorption of photons already in the first microns. This problem related to the penetration depth of selective photons is the main responsible for the natural bending of such LCEs. Nevertheless, a solution is to use a huge amount of photons together with an optimal amount of photo-active

molecules with high quantum yield and faster response. Then, the first layers will absorb the selected photon becoming inactive upon reaching the photo-stationary equilibrium—open window—, and allowing the photo-isomerization of the next layers—close windows (Knežević and Warner 2013).

Nevertheless, in order to achieve a homogeneous contraction/expansion of the LCEs, the applied external stimulus should be applied equally in all directions, otherwise bending or more complicated modes will be observed. This issue can be avoided by preparing very thin samples and by using local heat, *i.e.*, absorption of non-selective light by nanoparticles (Ji et al. 2012; Haberl et al. 2013), hyperthermia produced by alternating magnetic fields (Kaiser et al. 2009; Winkler et al. 2010), Joule effect by applying electrical current through in-sample conductors (Chambers et al. 2009; Sánchez-Ferrer et al. 2009), or by means of huge electrostatic fields applied to a sandwiched thin film (Urayama et al. 2006, 2007).

When bending modes are required without any photo-active molecule present in the LCE sample, the construction of a bilayer system is needed. Another material with different thermal expansion/contraction coefficient or elastic modulus will be attached to the LCE actuator. Thus, the surface of the bulk LCE directly attached to the passive material will not actuate due to mechanical restrictions, while the rest of the LCE material far from the interface will deform. Such deformation of LCE actuator will happen showing a gradient from zero at the interface to the maximum value in the surface far away from the other material. Actually, this actuation principle is always occurring when a LCE object is chemically attached to solid-like surface, *e.g.*, silicon, metal oxide, glass.

Finally, other aspects to be considered are the actuation force and the time response of LCE devices. While actuation forces are directly related to the crosslinking density—highly crosslinked LCEs show huge actuation forces, and low crosslinked LCEs have huge deformations—, the time response strongly depends on the interaction between the external stimulus and the LCE material. LCEs are polymer-like materials and the thermal conductivity is close to that of insulators. Thus, to achieve homogeneous isotropization temperatures along the sample cross section, the material needs minutes to reach the equilibrium temperature. The use of light is directly connected to the nature of the photo-active molecule incorporated into the network, and to the kinetics related to the photo-isomerization process which at room temperature is in the range of minutes too. A very good approach is the incorporation of heat-release systems which have lowered the response time to values in the range of milliseconds, *e.g.*, nanoparticles, micro-heaters.

19.3 Integration of LCEs into Microsystems Technologies

In the field of engineering, silicon-based technologies are the most commonly used for the fabrication of microsystems (Maluf and Williams 2003). These well-known techniques are very robust and well-controlled, and allow a batch processing

large-scale fabrication of devices combining a large number of varied physico-chemical processes, *e.g.*, deposition and growth of layers, etching techniques, shaping and patterning of these deposited layers (Merlos et al. 1993; Judy 2001). Furthermore, these processes enable the use of several types of materials ranging from silicon and its derivatives to polymers, metals and oxides. In this manner, it is possible to fabricate various types of devices like simple resistors, micro-heaters and transistors for circuitry (Snyder et al. 2003), accelerometers for ITC technologies and automotive field (Plaza et al. 2002), radiation detectors (Lutz 1999), bio-devices (Grayson et al. 2004) and solar cells for energy harvesting (Cook-Chennault et al. 2008), among others.

Nowadays, new materials and techniques have been introduced to the standard fabrication processes in microelectronics in order to obtain more complex systems and hybrid devices with new and interesting properties (Yang and Wang 2004; Dai et al. 2007; Liu 2007). Among conventional materials, polymers are the best example. They are flexible, soft, inert, ease to be processed and cheap, and have a large number of very interesting tunable properties which can be adapted to a specific needs and situations. Soft lithography techniques (Lorenz et al. 1997; Xia and Whitesides 1998), flexible substrates for printed electronics (Berggren et al. 2007), packaging of lab-on-a-chip devices and microfluidic systems (Dittrich and Manz 2006; Haerberle and Zengerle 2007) are some examples of the growing use of polymers in microsystems technology. However, the integration of polymers into MEMS/MOEMS devices as active elements is still a challenge since most of the silicon processing techniques require high working temperatures—hundreds of degrees—, and the use of aggressive chemical agents such as potassium hydroxide (KOH), tetramethylammonium hydroxide (TMAH) and hydrofluoric acid (HF) which can damage polymeric materials.

As previously mentioned, it is well-known that nematic LCEs can cause macroscopically stimuli-responsive shape changes during the nematic-to-isotropic phase transition, resulting from the microscopic disorder and misalignment of their components. Due to the reversibility of such nematic systems, when the external stimulus is removed, LCEs can produce actuation.

Back in the 1970s, when P.G. de Gennes proposed for the first time the possibility of using LCEs as artificial muscles (de Gennes 1971, 1975, 1993), monodomains of LCE materials have been widely studied leading to a large number of scientific publications and studies, and they have been proposed for the fabrication of active devices (de Gennes 1997; Woltman et al. 2007; Ohm et al. 2010) due to the big change in shape and length when disorder is induced by an external stimulus. However, LCE materials should be aligned (monodomain) and the mesogens properly oriented in a defined direction. The orientation of mesogens and alignment of the polymer backbones in LCEs before or after the final fixation of the polymer chains in the macromolecule requires the use of external fields which will simultaneously shape the material. This requisite strongly affects the use of the LCEs as actuators, and limits the integration into MEMS/MOEMS devices for the fabrication of real-world applications.

In the following, we present examples from the literature in which LCE materials have been proposed as actuators and sensors. These examples have been grouped in two different groups as function of the strategy followed for the integration of the material into the system to give rise to the final device. That is before or after the crosslinking process is finished.

In the first part, we will review the applications based on the integration of oriented LCE films which has been previously synthesized—mesogens oriented and polymer chains aligned and fixed by full crosslinking of the material. In the second part, other types of actuators and sensors based on alternative procedures will be presented where such choice allows for the in-situ orientation and alignment prior total fixation of the LCE while integrating the material into the device at the same time.

19.3.1 *Integration of Ex Situ Fully-Crosslinked LCEs*

The devices herein described are based on the integration of nematic films which have been previously aligned and cured. Thus, the shape and dimensions, and the corresponding change in those two parameters are limited to the degree of deformation imposed to the film during the synthesis. Usually, LCE films are obtained by 1D alignment—stretching of the sample in one direction before the final crosslinking—that produces a shortening in the direction of the deformation when the liquid-crystalline order is removed.

The first four examples presented are based on silicone polymeric matrices with T_g below 0 °C, and T_{ni} ranging from 55 °C to 90 °C, which have been grouped in two as function of their actuation mechanism. On the one hand, a microgripper and a microvalve which actuation is controlled by direct heating (*i.e.*, Joule effect), and on the other hand, a heliotropic system and a tactile device both based on local heating through light irradiation, thanks to the use of LCE nanocomposites. The last three examples discussed are based on acrylate chemistry with higher T_g (above room temperature) and T_{ni} (up to 170 °C) than the silicone-based LCE samples. Due to these high T_g values only thin films can be considered which can produce bending motion under illumination when doped with photoactive molecules or stretching when raising temperature locally.

As previously reported in Sect. 19.2, there is a preferred way for the fabrication of oriented films. The synthetic concept is essentially based on the partial crosslinking of the material in order to form a weakly crosslinked film in which a uniform uniaxial deformation of the sample is applied allowing the alignment of the polymer chains along the direction of the imposed stretching. After a successful deformation of the sample, the film is further crosslinked (curing process) in order to fix the alignment and create fully functional monodomain. At this moment, the LCE film is ready to be integrated on the device, so they can be carefully cut in a desired shape and then fixed into the structure, ensuring a correct adhesion and therefore a desired actuation.

This concept was firstly reported by Bründel et al. (2004) who demonstrated for the first time the possibility to integrate LCE materials into MEMS/MOEMS systems, and the compatibility of such materials with some of the manufacturing processing techniques in microelectronics. Following this principle, Sánchez-Ferrer et al. (2009) introduced the first LCE-driven silicon microsystem: a microgripper based on the thermal actuation of a monodomain LCE film, showing temperature-controlled motions. Figure 19.2a shows a schematic representation of the device with the main parts, as well as pictures of the final device and its actuation principle. For the obtaining of the nematic polysiloxane-based LCE material, a side-chain nematic liquid-crystalline polymer (LCP) containing photo-reactive moieties, which allow the crosslinking of the polymer chains, was synthesized and oriented using a magnetic field of 11 T or an electrostatic field of $300 \text{ kV} \cdot \text{m}^{-1}$. The photo-crosslinking of the LCP chains using UV light resulted in a monodomain of LCE sample of about $16 \text{ mm} \times 4 \text{ mm} \times 0.030 \text{ mm}$, with a T_{ni} ranging from $59 \text{ }^\circ\text{C}$ to $67 \text{ }^\circ\text{C}$ as function of the photo-crosslinkable benzophenone units content (10 mol% and 5 mol%, respectively). The microsystem was fabricated combining standard photo-lithographic and etching processes, typical from batch MEMS/MOEMS manufacturing and the elastomer was finally mounted onto the microgripper arms and fixed using oxygen plasma to assure good adhesion between the two surfaces. The design and the distance between both microgripper arms were fixed in agreement with the LCE samples characteristics to ensure its correct operation for reaching the maximum strain values. A controlled heating induced by the voltage applied on the extremes of the gold wires wounded around the LCE film triggered the LCE phase transition, leading to movement of the microgripper arms and changing their positioning due to the mechanical stresses. Small changes in the LCE film produced actuation stress of up to 60 kPa and deformation strain of up to 150 % when applying electric voltage values ranging between 1.5 V and 3.5 V, which strongly vary the actuation times of the device from 1.6 min to 46.1 min, and thus the hysteresis factor, which increases significantly while reducing the times of actuation. Using this approach, it has been demonstrated that large and robust contractions of LCE material can be integrated on a microsystem and used to induce a mechanical response on it, envisioning the possibility for the use of this actuation principle into other technological applications.

Later on, Sánchez-Ferrer et al. (2011b) reported another example when integrating a side-chain nematic polysiloxane-based monodomain of a LCE into MEMS/MOEMS by developing a flow regulating microvalve for microfluidics. The actuation principle was basically the same than the previous example, but advantage was taken from the expansion of the material in the other two directions perpendicular to the alignment and bending of the LCE in the direction of the liquid flow which allowed the closing of the microvalve upon the nematic-to-isotropic phase transitions of the material. Thus, opening and sealing of the microfluidic channel was achieved when going back and forward from the isotropic to the nematic state. A schematic view of the structure designed, as well as a sequence of images of the microvalve performance and the corresponding actuation plots are depicted in Fig. 19.2b. The volumetric flow of the medium is guided underneath the actuator

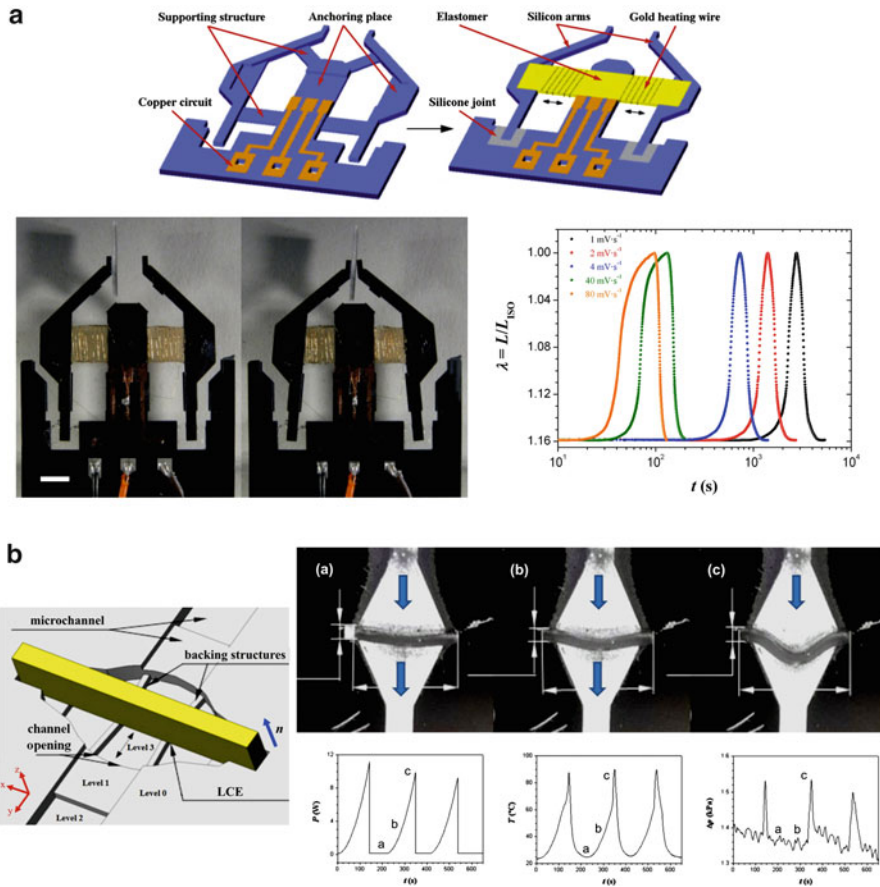


Fig. 19.2 Integration of polysiloxane-based side-chain nematic LCE in Microsystems. **(a)** Preparation of the silicon frame together with the copper electrical circuit and integration of the LCEs with the gold heating wires and the silicone joints before removal of the silicon supporting structures; two pictures showing the mechanical actuation of the LCE microgripper before and after contraction of both LCE films when heating disorder is produced; contraction of the LCE films as function of time at different voltage rates; and **(b)** integration of the LCE into the microchamber before sealing and the obtaining of the microvalve; sequence of pictures showing the positioning of the LCE film in (a) the nematic phase when the microvalve is fully open, (b) when approaching the isotropic temperature and the microvalve starts closing, and (c) when fully isotropic and the microvalve is closed (*Note: the blue arrows show the liquid flow direction*); electrical power, temperature of the microchamber and differential pressure between the two openings as function of time when closing the microvalve—the letters correspond to the pictures described before

(Level 3). A small supporting structure on the chip, which is on the same level as the bearing surfaces for the two ends of the actuator (Level 2) prevents buckling in the normal direction. Thus, the deformation of the valve in the main direction cannot be avoided and is compensated by an elevated channel ground (Level 1). Two identical

micromachined chips were assembled together face to face to form the microfluidic system including a $0.66 \text{ mm} \times 3.8 \text{ mm} \times 0.30 \text{ mm}$ LCE actuator in between as a moving valve. One part of the assembled chip contains a copper circuit on its back side for heating, while the backside of the microchip has the electric contacts and a thermoresistor to measure the temperature as function of the applied electric power. For the fabrication of the microvalve, a nematic monodomain of a side-chain LCE was synthesized following the two-step crosslinking process outlined by Finkelmann et al. (2001b).

As shown in the sequence of images in Fig. 19.2b, the LCE microvalve sealed the structure upon heating and filling the room in the directions perpendicular to the director and to the liquid flow up to the wall. When the LCE film reached the wall and tension grew, an abrupt buckling of the actuator occurred in the middle of the LCE film closing the microchannel in the direction of the flow. This middle part of the actuator moved to the microchamber blocking the fluid flow and creating an extra pressure due to the self-clamping at the two ends. The shrinkage of the actuator in the parallel direction to the director aided its movement in the microchamber as a result from a reduction of the friction forces between the actuator and the microstructure. In that case, the maximum heating power applied was 11 W at a volumetric flow rate of $271 \mu\text{L}\cdot\text{s}^{-1}$ using water; values which can be improved by reducing the heating power dissipation by changing the fluid type if not swelling of the LCE material is present (bad solvent).

It has been demonstrated that LCE are robust materials which can be tuned to adapt their responsiveness to certain external stimuli. Thus, by the incorporation of nano-objects such as carbon nanotubes (CNTs), ferro/ferrimagnetic nanoparticles, photo-sensitive particles or molecules, etc. within the polymeric matrix, it is possible to create custom-made LCE nanocomposites with different functionalities (Ji et al. 2012). Among others, CNTs are of special interest due to their morphology intrinsic characteristics and photon absorption (Saito et al. 1998; Tomblor et al. 2000). When embedded into a polymer matrix, CNTs act as local heaters, as they efficiently absorb light photons along all the visible-infrared (Vis-IR) spectrum converting electromagnetic energy into thermal energy (Ajayan et al. 2002; Cantournet et al. 2007). Thus, thermal energy can be directly and wireless delivered all over the thickness of the LCE film resulting in a faster material response compared to direct external heating. In addition, neither significant effect on the LC order nor in the internal structure of the elastomer has been observed for concentrations below 1 wt% (Marshall et al. 2012), resulting in no differences in the mechanical response compared to the sample without CNTs. All of that leads to the photo-thermomechanical actuation of LCE which is a more suitable mechanism for many engineering applications, since faster actuation responses can be obtained with remote control on the actuation, and the complexity of the setups can be reduced. However, the use of this type of LCE nanocomposites involves a more elaborated process for the preparation of the samples, which entails the addition of other chemical compounds such as surfactants to avoid the formation of CNTs aggregates, and to ensure a homogenous dispersion of the elements throughout the whole sample (Ji et al. 2010, 2011).

Pursuing this actuation mechanism, two different actuators have been reported, both of them using LCE nanocomposites, which demonstrated the suitability of this type of actuation. Li et al. (2012) reported a novel mechanism based on the direct actuation of the nematic material by means of sunlight. In this way, the authors were capable to emulate the heliotropism observed in nature. The material used for this study consisted in LCE-CNT nanocomposite reinforced with a polyurethane fiber-network in order to increase the mechanical stability of the system, but causing a significant increase of the power requirements.

Torras et al. (2014a) proposed the first complete device based on photo-mechanical actuation of an array of LCE-CNTs capable to emulate Braille characters. Thanks to the combination of nematic LCE-CNT films together with a well-designed optical system, an array of hundred actuators with pushing forces was obtained. The actuation time was lower than 10 s with forces up to 45 mN far enough for lifting the pin when shining the material with a white light source.

Inspired in the heliotropism present in nature, Li et al. (2012) developed an artificial system directly driven by the sunlight. The main driving force is the photo-thermal actuation of a nematic LCE nanocomposite. The LCE-CNT actuator was fabricated using a two-steps crosslinking process in which single-walled CNTs (SWCNTs) were incorporated into a side-chain LCE matrix reinforced by a polyurethane continuous fiber-network in order to improve the mechanical performance at rupture and oriented by means of uniaxial stretching (Li et al. 2011; Jiang et al. 2013). The resulting fiber-network/SWCNT/LCE material has a T_{ni} around 68 °C. A scheme of the device and the working principle of the heliotropic system are shown in Fig. 19.3a, where the different components can be distinguished. Similar to a stool, the device consists of a platform which contains a solar cell panel supported by some actuators. Thanks to the special design the structure consists of light concentrators, heat collectors and elastic supports. The pieces of actuator facing the incoming sunlight receive enough electromagnetic energy which is converted into local heat inducing disorder in the liquid-crystalline material. Thus, this local disorder induces the macroscopic contraction of the material, driving and tilting the platform towards the sunlight (Fig. 19.3a). On the other hand, the other pieces of actuator not exposed to the sunlight remain in the relaxed state. The mechanism was tested in both in-field via direct actuation by sunlight, and in laboratory conditions using a white light source at $100 \text{ mW} \cdot \text{cm}^{-2}$ of power density. Both experiments showed an increase in the output photo-current of the solar cells, and these results proved the use of this artificial heliotropic mechanism for future energy harvesting applications.

Another interesting example where LCE nanocomposites were used was presented by Torras et al. (2014a) for the development of a tactile device. Such device consists on nematic LCE-CNT-based films integrated into an array of 10×10 photo-actuators able to represent Braille characters and simplified graphical information. These films were individually assembled in U-shape-like configuration forming single Braille elements, and later integrated in the optical device which consists in arrays of white LEDs with mirrors and lenses in order to focus all photons on the surface of the LCE-CNT film under illumination. In this way, when

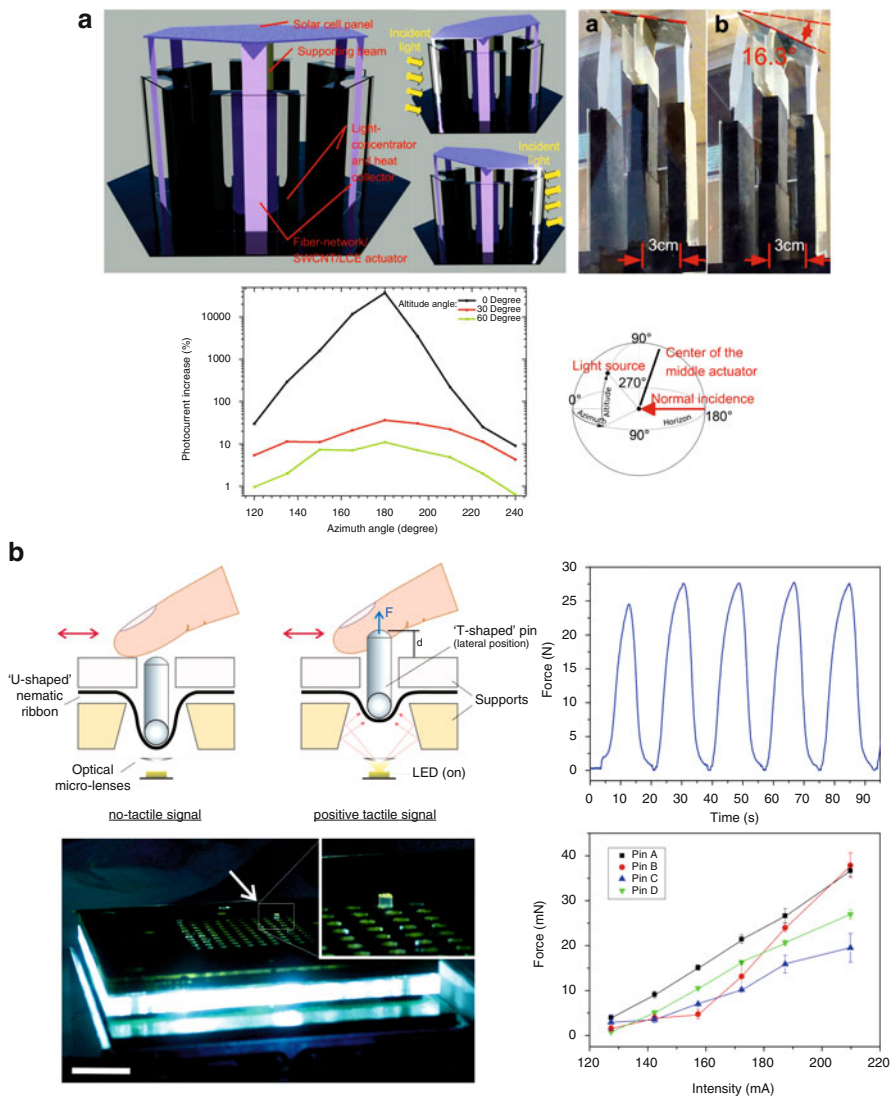


Fig. 19.3 Hybrid systems based on the integration of LCE nanocomposites. **(a)** Orientation principle (heliotropism) for the fiber-network/SWCNT/LCE device showing how the solar cell panel on the top orients when sun illuminates the contracting strip facing the sunlight; two pictures before and during illumination of the device where a small change in LCE-CNT actuators length induces a tilt angle in the solar cell panel; Photo-current intensity increase as function of the azimuthal angle at different altitude with respect to the equator showing a maximum intensity at 180° when a maximum of sunlight flux is achieved; and **(b)** schematic and actuation principle for the MOMS tactile device based on an array of LCE-CNT actuators able to represent Braille characters (scale bar = 10 mm); Force as function of time for the tactile device showing its reproducibility in several on/off cycles; picture of the tactile device with a pin lifted upon illumination; force as function of the electrical intensity applied to different LEDs lifting the corresponding pin

shining on the LCE-CNT, light is absorbed by the CNT which raise the local temperature and contract the U-shape part of the film. The light-induced stress gradient generated by the nematic LCE-CNT upon illumination produces a vertical displacement of corresponding movable pin, which transmits the tactile signal to the user's fingertip. A detailed scheme of an assembled actuator with all components is depicted in Fig. 19.3b. For the fabrication of such one hundred pin device, 1.2 mm wide and 0.3–0.4 mm thickness side-chain LCE-CNT ribbons containing 0.1 wt% of multi-walled carbon nanotubes (MWCNTs) were synthesized and mechanically stretched following the standard two-steps crosslinking process (Küpfer and Finkelmann 1991). The working temperature range for this composite goes from of $T_g \approx 10\text{--}15\text{ }^\circ\text{C}$ to $T_{ni} \approx 85\text{--}90\text{ }^\circ\text{C}$. The LCE-CNT ribbons were assembled in a U-shaped configuration to warrant no-tactile signal when the light source is switched off (rest position), and at the same time, a positive tactile signal under illumination. T-shaped rounded pins of 0.8 mm in diameter were placed inverted on top of the LCE-CNT ribbons to maximize the contact area and thus the force transmission. Additional elements such as Fresnel micro-lenses together with refractive supports were specially designed and incorporated into the device to improve the optical path efficiency and to optimize the working parameters of the device. Lower actuation times (between 3.5 s and 8 s as function of the light intensity) and pins' displacements of $0.8\text{ mm} \pm 0.2\text{ mm}$ were obtained with measured forces of up to 40 mN without material degradation; values which guarantee a correct tactile perception and fit the Braille standards, proving not only the viability of the device but also the potential applications of this type of actuator. Hardware implementation and a communication software interface were also developed adapting the standard Bluetooth and UBS protocols to provide end users with a complete and portable solution.

The four examples described so far are based on polysiloxane matrices which allow the possibility to obtain deformations of the whole sample (contraction and expansion movements) and relatively high actuation forces. This chemistry has also the advantage of having the nematic phase above the glassy state ($T_g < 0\text{ }^\circ\text{C}$) and below the isotropic state ($T_{ni} < 90\text{ }^\circ\text{C}$), which lower the power requirements in order to reach actuation. On the contrary, the following three examples to be discussed are based on acrylate chemistry which presents higher glass transition and clearing temperatures. This up-shifted temperature working window together with an increased rigidity of the polymer backbones results in a drastically reduction on the mobility of such films. For this reason, the thickness of liquid-crystalline polyacrylate-based films should be in the range of few microns in order to produce any movement, *i.e.*, bending, since the actuation mechanism mainly occurs on the surface of the sample. The first example, outlined by Yamada et al. (2008), takes advantage of the combination of both UV and visible light to induce the rotation of a plastic motor consisting of a set of two pulleys and an azobenzene-containing LCE film as a belt. Using a similar procedure, Chen et al. (2010) reported a light-driven micropump based on the bending and unbending motion of a LC membrane which produces pressure gradients, and thus the movement of the fluid. In the last

example, Petsch et al. (2014) posed LC films with embedded deformable thermoresistors as a way to faster deliver heat along the sample.

As previously introduced, Yamada et al. (2008) presented the light-induced rotation of a motor based on azobenzene-containing side-chain LCE films at room temperature. The main actuation principle relies on the *trans*-to-*cis* disorder-induced photo-isomerization upon UV-irradiation, and the order-induced *cis*-to-*trans* photo-back-isomerization with visible light. By the simultaneous irradiation using both UV and visible light in opposite sides of a LCE ring, the combination of intermittent contraction and expansion movements results in a rolling motion of the film, which drives the two pulleys forming the motor. A scheme showing the working principle of the device is depicted in Fig. 19.4a, where the main elements forming the device can be identified. An example of the photo-induced motion of the motor in a counterclockwise direction is depicted in the sequence of images below. In order to reinforce the LCE film and thus improve its mechanical properties, a 50 μm thick flexible polyethylene (PE) sheet was attached on the photo-crosslinked azobenzene-containing LCE ribbon by thermal bonding creating a 68 μm thick laminated film, which was used to form the motor belt by connecting both ends. The belt was wrapped around the pulleys ensuring the alignment direction of the azobenzene mesogens along the circular direction of the ring to guarantee a homogeneous movement direction. Similar laminated films were tested upon UV exposure at different intensities showing generation of mechanical force by photo-irradiation.

Afterward, Chen et al. (2010) developed a light-driven micropump by incorporating photo-isomerizable azobenzene moieties into the polyacrylate-based side-chain LC material. The reversible bending behavior of this material upon UV and visible light exposure is the responsible for inducing the membrane's movement and to pump a fluid. The working principle of the micropump, as well as a picture of the experimental prototype, is shown in Fig. 19.4c. Upon irradiation with UV light, the contraction gradient through the thickness of the film induces a downward bending which results in the reduction of the pump chamber volume, and the corresponding generation of pressure. In this way, the fluid in the chamber is forced to go to the pipe outlet. When the sample is exposed to visible light, a recovery of the film flatness is achieved by the upward bending of the film, and reduces the chamber's pressure which stops the flow.

Similar to the previously described microgripper (Sánchez-Ferrer et al. 2009), and following the actuation mechanism for the LCE-CNT composites (Li et al. 2012; Torras et al. 2014a), Petsch et al. (2014) introduced a novel approach based on the integration of deformable wires inside an active LC film. Then, a direct thermal actuation within the film is possible which results in a reduction of the actuation times—contraction and relaxation times—compared to other prior reported thermotropic polyacrylate-based side-chain LCE. Horseshoe platinum-gold-platinum micro-heaters were fabricated using standard MEMS/MOEMS technology processing on top of a polyimide (PI) layer and later, covered by a second PI layer to protect the conductive material and provide certain flexibility to the whole structure. Afterwards, all layers were structured using the reactive ion etching (RIE)

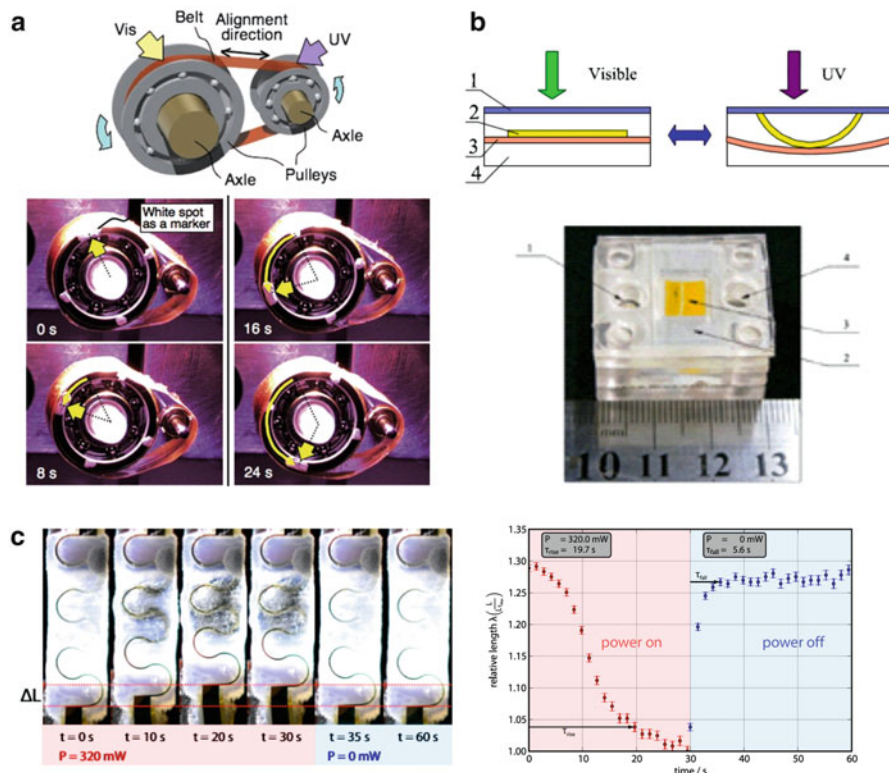


Fig. 19.4 Polyacrylate-based side-chain LCE actuators. (a) Alternated UV-visible photo-isomerization at different points of the azobenzene-containing LCE actuator ring which creates a local contraction and a local expansion of the belt and rotates the pulleys; (b) Micropump based on the bending motion of a LCE film which contains azobenzene moieties which upon UV-irradiation bends and with visible light relaxes back. (c) Sequence of thermo-resistors actuation showing changes in length and transparency of the LCE material upon heating and cooling under the application of 320 mW of electrical power

technique in order to obtain the heaters with their corresponding contact pads. A polyacrylate-based side-chain LC was synthesized following the process outlined by Thomsen et al. (2001) where all reagents were poured into a mold with the micro-heaters embedded by the reactive mixture. The material was aligned under a magnetic field, and finally photo-crosslinked by means of UV light. The contraction ratio of the actuator was measured as function of the electrical power applied. A contraction of 1.15 mm, which corresponds to relative change in sample's length of 1.28 was obtained at 320 mW, resulting in a 25.7 kPa of stress.

Basically, all actuation mechanisms described above are based on the conversion of an electrical current or electromagnetic fields into direct (microgripper, microvalve or embedded thermo-resistor actuator) or local heating (tactile device and heliotropic solar cell) which raises the temperature until reaching the isotropic

state. In principle, all mechanisms based on photo-isomerization of photoactive molecules (rotating belt and micropump) rely on the low temperature induced disorder when some molecules change their shape and acting as impurities. In principle, the latest mechanism should be a more efficient and faster process, but the process is slow at room temperature and depends on the irradiance, has some partial loss of the absorbed energy by non-radiative internal conversion or even emission, and the examples described here have a huge frictional factor and higher rigidity of the polymer backbone. All these factors lead towards actuation times of several minutes for the photoactive systems.

In this first section, various types of actuators has been described and their actuation mechanisms analyzed, all of them based on the integration of nematic side-chain LCE films which have been previously aligned and fully cross-linked. The main advantage of these actuators lies in that non-complex procedures are required for the integration. The nematic materials can be cut, fixed, or even glued, on different surfaces to form the final actuator. However, the main limitations of this type of actuators lie in their size, the shape and the type of orientation achieved by the LCE films—factors that are strongly related to the final response of the material, *i.e.*, deformation and movement direction. Similar to the MEMS/MOEMS fabrication processes, this free-standing oriented LCE films are perfect for the fabrication of actuators as a *Top-Down* approach, due to the possibility to pattern the oriented films in order to be adapted to the system for the manufacturing of devices.

19.3.2 Integration of In Situ Fully-Crosslinked LCEs

In contrast with the previously described systems based on the use of already aligned and fully crosslinked LCE films, in this section we analyze another concept for the fabrication of hybrid actuators consisting in the integration of partially crosslinked LCE films. Such films are then oriented and simultaneously cured in-situ. In this manner, it is possible to obtain LCE actuators in more complex shapes, far from the LCE films, with various types of alignment and not only limited to 1D. Thus, different types of actuation/deformation can be obtained leading to the fabrication of more elaborated actuators and devices.

This concept was firstly introduced by Buguin et al. (2006) which through replica molding combined with photo-crosslinking, and the application of magnetic fields, demonstrated the possibility to simultaneously shape, align and completely cure LCE material to create an array of thermoresponsive LCE pillars with contractions up to 40 %. Following this principle, different types of actuators have been reported so far, all of them based on molding techniques. Herein, we will describe all these actuators and the corresponding actuation principle analyzed. Similar to the previous section, they have been grouped as function of the type of chemistry used for their synthesis, as well as for their actuation mechanisms. The first three examples consist of elastomeric matrices based on polysiloxane chemistry, which

allows for lower range of actuation temperatures and relatively high deformations. The first one out of the three examples consists in a micropillar array with pushing properties based on direct heating. The other two examples, in both cases arrays of dome-like shaped actuators, are based on photo-thermal actuation of LCE-CNTs nanocomposites. The last two actuators presented in this section consist in a micropillar array and an electrothermally driven photonic crystal, both based on photo actuation of polyacrylate-based LCE.

Torras et al. (2014b) followed the concept of replica molding outlined by of Buguin et al. (2006) to obtain micropillars with pushing properties using a polysiloxane matrix. In this manner, an array of nematic side-chain LCE actuators with elastic properties and low transition temperature was obtained, which produces direct actuation through heating, resulting in an expansion of the material. The pushing properties were reached by a two-step crosslinking process resulting in an array of micropushers. Such micropillars were oriented by uniaxial compression (biaxial orientation) instead of the classical uniaxial stretching procedure before the final curing. Thus, the micropillar array expands in the direction of the applied deformation when the isotropic temperature is reached ($T_{ni} \approx 55$ °C). This pushing behavior of the micropillars is related to the changes from the two-dimensional prolate polydomain conformation (nematic state) to the spherical conformation (isotropic state) of the polymer backbone. Figure 19.5 shows a scheme of the working principle of the proposed micropillars, as well as images of the fabrication process, and the main actuation results obtained. The resulting LCE micropillars with such novel orientation of the domains showed an expansion factor of $\varepsilon_z = 21$ % along the axial direction and a contraction factor of $\varepsilon_r = 15$ % in the radial direction upon isotropization, with an averaged dimensions of 3.63 mm in height and 2.10 mm in diameter in the isotropic phase, which resulted in actuation forces of about $F = 20$ mN (5.6 kPa of equivalent stress). These good results together with the possibility of obtaining different shapes on demand—besides the common LCE strip—make LCE materials very suitable candidates in the development of complex devices through their integration in Microsystems Technology and batch processes.

Camargo et al. (2011, 2012) demonstrated for the first time the possibility to obtain an array of actuating monodomains within the same polydomain matrix. Thanks to the use of an elaborated molding process similar to the punch and die stamping technique, together with a two-steps crosslinking process, sufficiently well-aligned LC units were created to produce localized actuation on a LCE-CNTs nanocomposite film upon illumination. Figure 19.6a schematically shows the stamping process and the working principle of the proposed actuators, where the aligned and non-aligned regions can be distinguished. A picture of the molding system and the actuators obtained, as well as a graph with the main actuation results, are also depicted. The fabrication process starts with a weakly-crosslinked film containing 0.1 wt% of MWCNTs which was placed in between two mold pieces, one containing pillars and the other one holes, and mechanically stretched to locally align the LC mesogens. Then, all the system was heated to thermally crosslink the film while keeping the mechanical load, resulting in an array of semi-spherical actuators of both 1.0 mm and 1.5 mm in diameter, with an alignment

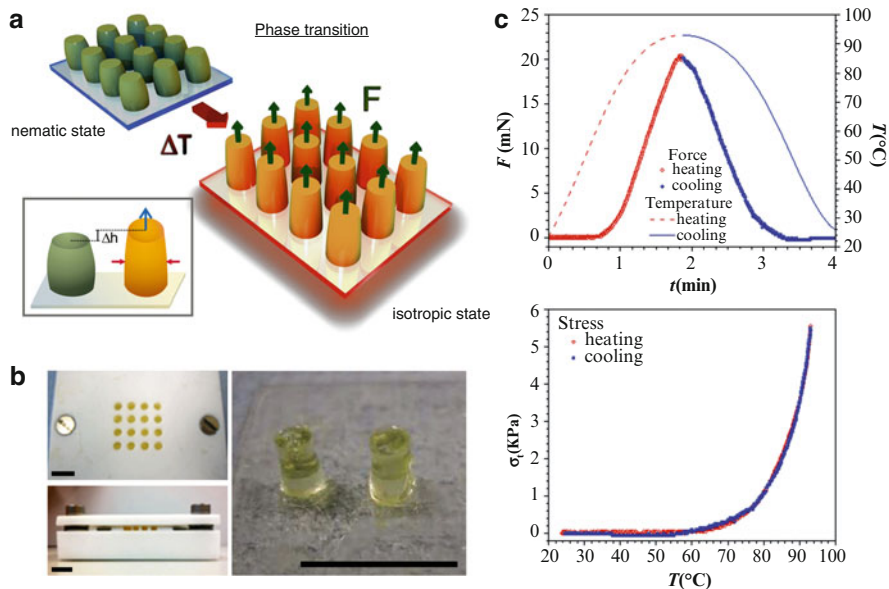


Fig. 19.5 (a) Scheme of the working principle of the proposed micropillars system resulting in pushing actuators under the application of thermal gradients. (b) Main steps for the micropillar fabrication where the molds, the orientation process through uniaxial compression, as well as an example of the actuators obtained previous the final crosslinking step can be observed (scale bars = 10 mm). (c) Mechanical response of a single LCE micropillar along an entire heating-cooling cycle showing the pushing force as function of actuation temperature and time. 20 mN of force was obtained showing repeatability in response and no material degradation

normal to the direction of the film. For that reason, the dome-like shaped monodomain regions contract upon irradiation ($T_{ni} \approx 85^\circ\text{C}$) causing a decrease in their height, which reversibly return to their initial position when no light stimulus is applied. The response of the different actuators was analyzed using a red laser diode of 658 nm of wavelength as a light source at an incident optical power ranging from 8.6 mW to 51.5 mW, resulting up to 40 μm (10 %) of vertical displacement (contraction of $\varepsilon = 6.46\%$) in case of 1.5 mm of diameter actuators - deformation which is mainly limited by the dimensions of the punch mold. Moreover, on-off actuation cycles of the proposed actuators were performed to check the feasibility and repeatability in response, resulting in a low dispersion in contraction (less than 2.5 % of the mean value) without material degradation, leading to the use of this methodology for new applications in haptic devices.

Recently, Torras et al. (2014b) presented another interesting example using LCE-CNT nanocomposites. Inspired on the previous described method (Camargo et al. 2011, 2012), an alternative approach for the fabrication of arrays of semi-spherical actuators based on gas-pressure molding was proposed. It was demonstrated the possibility to shape and align LCE-CNT films by the application of a well-controlled nitrogen pressure. In this manner, a significant improvement on the

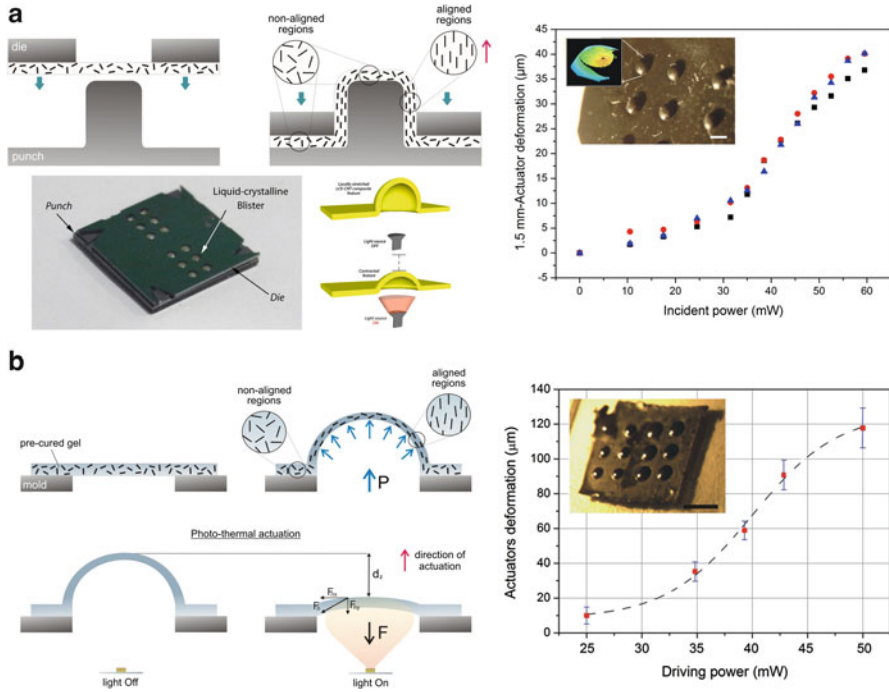


Fig. 19.6 Actuators arrays based on nematic LCE-CNT nanocomposites. Fabrication process and working principle of semi-spherical actuators array obtained by stamping molding (i.e., mechanical pressure) (a) and by the application of constant nitrogen flow (b). By using both approaches, aligned and non-aligned regions can be simultaneously produced, resulting in arrays of actuating features within a same LCE-CNT nanocomposite film. Under illumination, a reduction in height up to 40 μm and 120 μm were obtained respectively, as function of the optical power applied. Scale bars of pictures in the insets were 1 mm and 4 mm, respectively

deformation achieved by the actuators was obtained with respect to the reported by Camargo et al. (2011, 2012). The resulting height variation was up to 120 μm under illumination which mean contractions of $\epsilon = 13\%$ in the direction of the alignment under the application of 40 mbar of constant nitrogen pressure. A scheme showing the concept and the actuation principle of these actuators is presented in Fig. 19.6b, where also a graph with the main actuation results as function of the optical power applied are shown. Similar to the other system, this approach lies in the use of a two-steps crosslinking process which enables a correct shaping of the partially cross-linked material through molding process, and guarantees the application of the corresponding stress gradient to produce the desired deformation and alignment using nitrogen flow. Thus, arrays of identical dome-like shaped monodomain actuators can be obtained within the same polydomain LCE-CNT film with a perpendicular alignment, leading to local and reversible actuation. In this case,

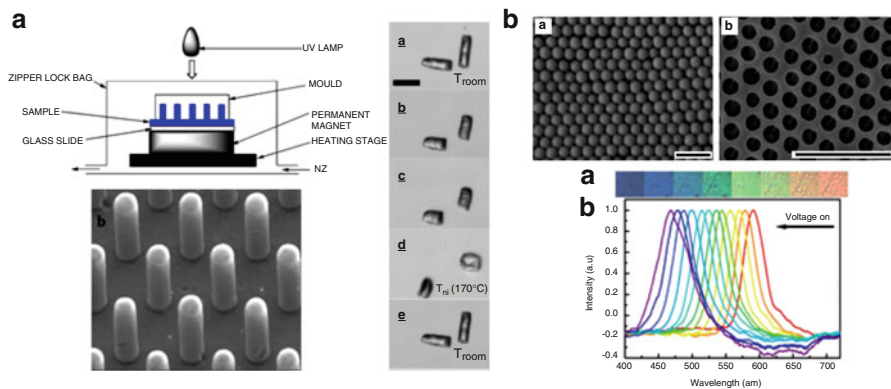


Fig. 19.7 Polyacrylate-based actuators in an array. **(a)** Schematic representation of the fabrication process of an array of thermoresponsive micropillars on a substrate by replica molding. Once the LCE pillars were completely cured they can be separated from the substrate and individually actuated by means of thermal gradients, resulting in high contraction movements ranging from 30 % to 40 %, as function of the acrylate matrix used (scale bar = 100 μm). **(b)** LCE Photonic crystal obtained by regular patterning of a LCE matrix through the embedding of a close-packed monodispersed silica particles' arrangement (scale bars = 1 μm)

LCE-CNT nanocomposites containing 0.3 wt% of MWCNTs were used, with transition temperatures of $T_g \approx 10\text{--}15\text{ }^\circ\text{C}$ and $T_{ni} = 90\text{ }^\circ\text{C}$.

As previously mentioned at the beginning of this section, Buguin et al. (2006) introduced an innovative procedure for the fabrication of micron-sized thermoresponsive LCE actuators on a substrate by replica molding. In this manner, an array of nematic pillars of about 20 μm in diameter and 100 μm in height could be obtained in one single step. Firstly synthesized using side-on polyacrylate-based chemistry (Buguin et al. 2006) and then improved by using thiol-ene nematic main-chain LCE (Yang et al. 2009). The reported actuators show fully reversible contraction with values up to 30–40 % in the case of side-on LCE when heated from the nematic to the isotropic phases ($T_{ni} \approx 170\text{ }^\circ\text{C}$). A scheme of the experimental setup for the fabrication of the micropillars together with a scanning electron microscopy (SEM) micrograph of the final structures and an actuation sequence are shown in Fig. 19.7a. A PDMS mold containing the patterns of the pillars which was prepared by replica molding was pressed down on the melted components of the nematic material forcing them to fill the inner structure of the mold, while a constant magnetic field of about 1 T was applied to ensure alignment of the nematic director parallel to the long axis of the pillars. Finally, the whole system was irradiated using a UV lamp to promote the LCE photo-polymerization. Each pillar can be removed from the array and used as a small actuator. However, such LCE materials are restricted to certain applications due to the elevated actuation temperatures (up to 170 $^\circ\text{C}$), and thus they can neither be used in Biology for tissue engineering nor for cell culture studies.

Later on, Jiang et al. (2012) presented an innovative electrothermally driven photonic crystal based on the combination of nematic materials able to shift the

Bragg-diffraction peak under actuation, resulting on a structural change in color. Unlike the previous examples where a replica molding was used for the fabrication of non-continuous matrices of individual actuators (Torrás et al. 2013; Buguin et al. 2006; Yang et al. 2009), Jiang et al. proposed an original method to pattern LCE matrices inspired by colloidal lithography processes in nanofabrication (Yang et al. 2006). They propose the use of a non-continuous 3D array of elements, in this case silica nanospheres (*i.e.*, an opaline photonic crystal), to create a continuous LCE films containing the inverse opaline structure, which acts as single photonic crystals. Figure 19.7b shows two SEM pictures of both types of structures, as well as a graph reflecting the photonic band-gap (PBG) shifts inducing structural color changes at 15 V of applied voltage and its corresponding normalized reflection spectra. For the preparation of the LCE photonic crystals, various layers of close-packed monodispersed nanosilica spheres were first prepared following the Stöber method (Stöber et al. 1968) and sandwiched between two glass plates, which were later immersed in the molten LCE solution to allow the mixture to completely fill the voids by capillary forces. Finally, the LC moieties were aligned and polymerized using UV-irradiation and the silica template etched by 1 wt% HF solution, resulting in the LCE-based inverse opaline structure. Spin-coated on a glass-substrate, graphite nanoparticles act as electrothermal conversion layer, delivering heat to the LCE structure and thus, forcing reversible changes on the optical response of the films, *e.g.*, displacement of the PBG and changes on the structural color of the films, as function of the electric voltage applied. Depending on the material composition, these inverse opaline structures show transition temperatures ranging from 20 °C to 32 °C and from 64 °C to 101 °C for the T_g and T_{ni} , respectively, as function of the crosslinking density.

In this second section various types of actuators have also been described and their actuation mechanisms analyzed, all of them based on the integration of nematic materials before the crosslinking process, allowing its in-situ alignment and curing in one single step. The main difficulties around these techniques lie in the various procedures involving the LCE material preparation, which require a very precise control of the whole device. Thus, the system should be conceived and fabricated taking into account the changes in dimensions and shape exhibited on the material during its alignment and crosslinking processes, which will strongly define the final type and degree of deformation achieved.

Unlike the methods described in the previous section, the main advantage of these techniques is that there is neither limitation in shape and size of the actuators obtained nor with the types of orientation defined. Thus, with an accurate design and the appropriate knowledge of the material, it is possible to fabricate a custom-made elaboration process to reach the desired response.

Seeking parallelism to conventional MEMS/MOEMS fabrication methods, one might consider this methodology to fabricate actuators such as *Bottom-up* approach, where the starting material at the molecular level is transformed and patterned at the same time for the obtaining of the macromolecular actuator already adapted to the system to form the device.

19.4 Conclusions and Outlook

LCEs are advanced, complex, and elaborated soft smart materials which require of expertise in Organic Synthesis, Macromolecular Chemistry and Physics, and Supramolecular Chemistry, as well as knowledge about Materials Science. The combination of the liquid state of order—from the liquid-crystalline molecules (mesogens)—and the rubber elasticity—from the polymer network (crosslinked polymer chains)—results on a material with unique mechanical and optical properties. The beauty of such materials stays in the control over the three components which allows for the obtaining of materials on demand. Thus, the precise selection of the mesogen nature leads towards different mesophases (*e.g.*, nematic, smectic, columnar, chiral, lyotropic phases), shifting of the isotropization temperature and the corresponding service temperature, and kind of coupling to the polymer backbone. While the choice on the polymer backbone brings flexibility (amorphous) or rigidity (glassy), variations in the crosslinking density contribute to the hardness (durometer) or softness (elastomer) of the final LCE material.

The main principle is the obtaining of monodomains of LCEs, where the mesogens are oriented and polymer chains aligned. Such anisotropic materials can undergo a spontaneous and reversible deformation accompanied by a retractive force when an external stimulus is applied and the liquid-crystalline order in the material is erased. The functionalization of such LCEs enables the material to interact with the environment. Thus, the incorporation of other molecules or functionalities increases the options for the use of other external stimuli besides temperature gradients, *e.g.*, light, magnetic or electric fields, electrical current, pH, ionic strength, solvent vapor. In this way, LCEs can convert any kind of energy into mechanical energy or vice versa.

The actuation principle for such LCEs markedly depends on the synthetic approach and the orientation/alignment technique used for the preparation of monodomains, as well as the external stimulus to be used. In principle, polycondensation-based LCEs (polysiloxane polymer backbone) are more suitable for contraction/expansion purposes, while polyaddition-based LCEs (poly(meth)acrylate polymer backbone) has mainly been used for bending modes. Nevertheless, both kinds of polymer backbones can develop any imaginable actuation movement, if a little bit of imagination and inventiveness is worked up.

When control over the actuation strain and stress, as well on the time response is accomplished, the next step is the integration of such LCEs into MEMS/MOEMS for the production of microdevices. Several examples have been described where the two possible approaches have been presented: the *ex situ* and *in situ* preparation of monodomains of LCEs. For the earlier, a *Top-Down* approach is followed for the integration of the material to the final device, while for the later a *Bottom-Up* approach is considered. The election for one or the other will be decided by the size, dimensions, shape and alignment of the LCE actuator together with the external stimulus to be used.

Due to the good integration of LCEs in Microsystems Technology, the applications offered by these hybrid MEMS/MOEMS range from the production of sensors to actuators for microrobotics, microoptics and microfluidics. We are sure that in the near future new progresses in this area of miniaturization at the micro and nano scale will be seen when a better control on the mechanical and optical properties. For this purpose, and because of LCEs are the perfect material for such synergies, chemist, physicist and engineers should work together for the development of new devices. Still many open questions remain like the use of polydomains of LCEs, the energy efficiency improvement of such devices, the use of other mesophases, polymer architectures, functionalities and external stimuli.

References

- Ajayan PM, Terrones M, de la Guardia A, Huc V, Grobert N, Wei BQ, Lezec H, Ramanath G, Ebbesen TW (2002) Nanotubes in a flash-ignition and reconstruction. *Science* 296:705
- Berggren M, Nilsson D, Robinson ND (2007) Organic materials for printed electronics. *Nature Mat* 6:3
- Beyer P, Terentjev EM, Zentel R (2007) Monodomain liquid crystal main chain elastomers by photocrosslinking. *Macromol Rapid Commun* 28:1485
- Boussey J (2003) Microsystems technology: fabrication, test & reliability. Kogan Page, London
- Brand HR, Finkelmann H (1998) Handbook of liquid crystals, vol 3. Wiley/VHC, Weinheim
- Bründel M, Stubenrauch M, Wurmus H, Sánchez-Ferrer A (2004) Functional liquid-crystalline elastomers in Microsystems. *Int Newslett Micro-Nano Integr (MSTNEWS)* 4:38
- Buguin A, Li MH, Silberzan P, Ladoux B, Keller P (2006) Micro-actuators: when artificial muscles made of nematic liquid crystal elastomers meet soft lithography. *J Am Chem Soc* 128:1088
- Camargo CJ, Campanella H, Marshall JE, Torras N, Zinoviev K, Terentjev EM, Esteve J (2011) Localised actuation in composites containing carbon nanotubes and liquid crystalline elastomers. *Macromol Rapid Commun* 32:1953
- Camargo CJ, Campanella H, Marshall JE, Torras N, Zinoviev K, Terentjev EM, Esteve J (2012) Batch fabrication of optical actuators using nanotube—elastomer composites towards refreshable Braille displays. *J Micromech Microeng* 22:075009
- Cantournet S, Boyce MC, Tsou AH (2007) Micromechanics and macromechanics of carbon nanotube enhanced elastomers. *J Mech Phys Solids* 55:1321
- Chambers M, Zalar B, Remškar M, Žumer S, Finkelmann H (2006) Actuation of liquid crystal elastomers reprocessed with carbon nanoparticles. *Appl Phys Lett* 89:243116
- Chambers M, Finkelmann H, Remškar M, Sánchez-Ferrer A, Zalar B, Žumer S (2009) Liquid crystal elastomer—nanoparticle systems for actuation. *J Mater Chem* 19:1524
- Chen M, Xing X, Liu Z, Zhu Y, Liu H, Yu Y, Cheng F (2010) Photodeformable polymer material: towards light-driven micropump applications. *Appl Phys A* 100:39
- Cook-Chennault KA, Thambi N, Sastry AM (2008) Powering MEMS portable devices: a review of non-regenerative and regenerative power supply systems with special emphasis on piezoelectric energy harvesting systems. *Smart Mater Struct* 17:043001
- Dai W, Lian K, Wang W (2007) Design and fabrication of a SU-8 based electrostatic microactuator. *Microsyst Technol* 13:271
- Davis F (1993) Liquid-crystalline elastomers. *J Mater Chem* 3:551
- de Gennes PG (1971) Nematic liquid crystals. *J Phys Colloq* 5:3
- de Gennes PG (1975) Réflexions sur un type de polymères nématiques. *C R Acad Sci Paris B* 281:101

- de Gennes PG (1993) *The physics of liquid crystals*, 2nd edn. Oxford University Press, New York
- de Gennes PG (1997) A semifast artificial muscle. *C R Acad Sci Series IIB* 324:343
- de Jeu WH (2012) *Liquid crystal elastomers: materials and applications*. Springer, Berlin
- Dittrich PS, Manz A (2006) Lab-on-a-chip: microfluidics in drug discovery. *Nat Rev Drug Discov* 5:210
- Donnio B, Wermter H, Finkelmann H (2000) A simple and versatile synthetic route for the preparation of main-chain, liquid-crystalline elastomers. *Macromolecules* 33:7724
- Finkelmann H, Kock HJ, Rehage G (1981) Investigations on liquid crystalline polysiloxanes 3. Liquid crystalline elastomers: a new type of liquid crystalline material. *Makromol Chem Rapid Commun* 2:317
- Finkelmann H, Kock HJ, Gleim W, Rehage G (1984) Investigations on liquid crystalline polysiloxanes, 5. Orientation of LC-elastomers by mechanical forces. *Makromol Chem Rapid Commun* 5:287
- Finkelmann H, Nishikawa E, Pereira GG, Warner M (2001a) A new opto-mechanical effect in solids. *Phys Rev Lett* 87:015501
- Finkelmann H, Greve A, Warner M (2001b) The elastic anisotropy of nematic elastomers. *Eur Phys J E* 5:281
- Gad-el-Hak M (2005) *MEMS: applications*. CRC, Boca Raton
- Grayson ACR, Shawgo RS, Johnson AM, Flynn NT, Li YW, Cima MJ, Langer R (2004) A BioMEMS review: MEMS technology for physiologically integrated devices. *Proc IEEE* 92:6
- Haberl JM, Sánchez-Ferrer A, Mihut AM, Dietsch H, Hirt A, Mezzenga R (2013) Liquid-crystalline elastomer-nanoparticle hybrids with reversible switch of magnetic memory. *Adv Mater* 25:1787
- Haberl JM, Sánchez-Ferrer A, Mihut AM, Dietsch H, Hirt AM, Mezzenga R (2014) Light-controlled actuation, transduction, and modulation of magnetic strength in polymer nanocomposites. *Adv Funct Mater* 24:3179
- Haerberle S, Zengerle R (2007) Microfluidic platforms for lab-on-a-chip applications. *Lab Chip* 7:1094
- Hardouin F, Leroux N, Noirez N, Keller P, Mauzac M, Achard MF (1994) Small angle neutron scattering (SANS) studies on "side-on fixed" liquid crystal polymers. *Mol Cryst Liq Cryst* 254:267
- Haseloh S, Zentel R (2009) Synthesis of liquid-crystalline colloids in nonpolar media and their manipulation in electric fields. *Macromol Chem Phys* 210:1394
- Hogan PM, Tajbakhsh AR, Terentjev EM (2002) UV manipulation of order and macroscopic shape in nematic elastomers. *Phys Rev E* 65:041720
- Hsu TR (2008) *MEMS & microsystems: design, manufacture, and nanoscale engineering*, 2nd edn. Wiley, Hoboken
- Huber J, Fleck NA, Ashby MF (1997) The selection of mechanical actuators based on performance indices. *Proc R Soc Lond A* 453:2185
- Ji Y, Huang YY, Rungsawang R, Terentjev EM (2010) Dispersion and alignment of carbon nanotubes in liquid crystalline polymers and elastomers. *Adv Mater* 22:3436
- Ji Y, Huang YY, Terentjev EM (2011) Dissolving and aligning carbon nanotubes in thermotropic liquid crystals. *Langmuir* 27:13254
- Ji Y, Marshall JE, Terentjev EM (2012) Nanoparticle-liquid crystalline elastomer composites. *Polymers* 4:316
- Jiang Y, Xu D, Xuesong L, Lin C, Li W, An Q, Tao C, Tang H, Li G (2012) Electrothermally driven structural colour based on liquid crystal elastomers. *J Mater Chem* 22:11943
- Jiang H, Li C, Huang X (2013) Actuators based on liquid crystalline elastomer materials. *Nanoscale* 5:5225
- Judy JW (2001) *Microelectromechanical systems (MEMS): fabrication, design and application*. *Smart Mater Struct* 10:1115
- Kaiser A, Winkler M, Krause S, Finkelmann H, Schmidt AM (2009) Magnetoactive liquid crystal elastomer nanocomposites. *J Mater Chem* 19:538

- Knežević M, Warner M (2013) Optomechanical elastomeric engine. *Phys Rev E* 062503:1
- Komp A, Rühle J, Finkelmann H (2005) A versatile preparation route for thin free-standing liquid single crystal elastomers. *Macromol Rapid Commun* 26:813
- Krause S, Dersch R, Wendorff JH, Finkelmann H (2007) Photocrosslinkable liquid crystal main-chain polymers: thin films and electrospinning. *Macromol Rapid Commun* 28:2062
- Kremer F, Skupin H, Lehmann W, Hartmann L, Stein P, Finkelmann H (2000) Structure, mobility, and piezoelectricity in ferroelectric liquid crystalline elastomers. *Adv Chem Phys* 113:183
- Kundler I, Finkelmann H (1998) Director reorientation via stripe-domains in nematic elastomers: influence of cross-link density, anisotropy of the network and smectic clusters. *Macromol Chem Phys* 199:677
- Küpfer J, Finkelmann H (1991) Nematic liquid single crystal elastomers. *Macromol Chem Rapid Commun* 12:717
- Küpfer J, Finkelmann H (1994) Liquid crystal elastomers: influence of the orientational distribution of the crosslinks on the phase behaviour and reorientation processes. *Macromol Chem Phys* 195:1353
- Lehmann O (1908) *Biologisches Centralblatt* 28:31
- Lehmann WL, Hartmann L, Kremer F, Stein P, Finkelmann H, Kruth H, Diele S (1999) The inverse electromechanical effect in mechanically oriented Sc*-elastomers examined by means of an ultra-stable Michelson interferometer. *J Appl Phys* 86:1647
- Leondes CT (2006) *MEMS/NEMS: handbook*. Springer, New York
- Li MH, Keller P, Li B, Wang X, Brunet M (2003) Light-driven side-on nematic elastomer actuators. *Adv Mater* 15:569
- Li C, Liu Y, Lo C, Jiang H (2011) Reversible white-light actuation of carbon nanotube incorporated liquid crystalline elastomer nanocomposites. *Soft Matter* 7:7511
- Li C, Liu Y, Huang X, Jiang H (2012) Direct sun-driven artificial heliotropism for solar energy harvesting based on a photo-thermomechanical liquid-crystal elastomer nanocomposite. *Adv Funct Mater* 22:5166
- Liu C (2007) Recent developments in polymer MEMS. *Adv Mater* 19:3783
- Lorenz H, Despont M, Fahrni N, LaBianca N, Renaud P, Vettiger P (1997) SU-8: a low-cost negative resist for MEMS. *J Micromech Microeng* 7:121
- Lutz G (1999) *Semiconductor radiation detectors*. Springer, Berlin
- Maluf N, Williams K (2003) *An introduction to microelectromechanical systems engineering*, 2nd edn. Artech House, Boston
- Marshall JE, Ji Y, Torras N, Zinoviev K, Terentjev EM (2012) Carbon-nanotube sensitized nematic elastomer composites for IR-visible photoactuation. *Soft Mater* 8:1570
- Merlos A, Acero M, Bao MH, Bausells J, Esteve J (1993) TMAH/IPA anisotropic etching characteristics. *Sensor Actuat A-Phys* 37:737
- Noirez L, Keller P, Davidson P, Hardouin F, Cotton JP (1988) Backbone conformation study of a side chain polyacrylate through a re-entrant polymorphism. *J Phys France* 49:1993
- Ohm C, Serra C, Zentel R (2009) A continuous flow synthesis of micrometer-sized actuators from liquid crystalline elastomers. *Adv Mater* 21:4859
- Ohm C, Brehmer M, Zentel R (2010) Liquid crystalline elastomers as actuators and sensors. *Adv Mater* 22:3366
- Petsch S, Rix R, Reith P, Khatri B, Schuhladen S, Ruh D, Zentel R, Zappe H (2014) A thermotropic liquid crystal elastomer micro-actuator with integrated deformable micro-heater. *Proc MEMS* 905
- Plaza JA, Collado A, Cabruja E, Esteve J (2002) Piezoresistive accelerometers for MCM package. *J Micromech Syst* 11:794
- Saito R, Dresselhaus G, Dresselhaus MS (1998) *Physical properties of carbon nanotubes*, vol 4. Imperial College Press, London
- Sánchez-Ferrer A (2011) Light-induced disorder in liquid-crystalline elastomers for actuation. *Proc SPIE* 8107:810702

- Sánchez-Ferrer A, Finkelmann H (2009) Mechanical deformations in smectic-c main-chain liquid-crystalline elastomers. *Mol Cryst Liq Cryst* 508:348
- Sánchez-Ferrer A, Finkelmann H (2013) Opto-mechanical effect in photoactive nematic main-chain liquid-crystalline elastomers. *Soft Matter* 9:4621
- Sánchez-Ferrer A, Fischl T, Stubenrauch M, Wurmus H, Hoffmann M, Finkelmann H (2009) Photo-crosslinked side-chain liquid-crystalline elastomer for microsystems. *Macromol Chem Phys* 210:1671
- Sánchez-Ferrer A, Merekalov A, Finkelmann H (2011a) Opto-mechanical effect in photoactive nematic side-chain liquid-crystalline elastomers. *Macromol Rapid Commun* 32:672
- Sánchez-Ferrer A, Fischl T, Stubenrauch M, Albrecht A, Wurmus H, Hoffmann M, Finkelmann H (2011b) Liquid-crystalline elastomer microvalve for microfluidics. *Adv Mater* 23:4526
- Schätzle J, Finkelmann H (1987) Lyotropic liquid crystalline phase behavior of amphiphilic monomers and polymers having a rod-like hydrophobic moiety. *Mol Cryst Liq Cryst* 142:85
- Snyder GJ, Lim JR, Huang CK, Fleurial JP (2003) Thermoelectric microdevice fabricated by a MEMS-like electrochemical process. *Nature Mater* 2:528
- Stöber W, Fink A, Bohn E (1968) Controlled growth of monodisperse silica spheres in the micron size range. *J Colloid Interface Sci* 26:62
- Tajbakhsh AR, Terentjev EM (2001) Spontaneous thermal expansion of nematic elastomers. *Eur Phys J E* 6:181
- Terentjev EM (1999) Liquid-crystalline elastomers. *J Phys Condens Matter* 11:R239
- Thomsen DL, Keller P, Naciri J, Pink R, Jeon H, Shenoy D, Ratna BR (2001) Liquid crystal elastomers with mechanical properties of a muscle. *Macromolecules* 34:5868
- Tombler TW, Zhou C, Alexseyev L, Kong J, Dai H, Liu L, Jayanthi CS, Tang M, Wu SY (2000) Reversible electromechanical characteristics of carbon nanotubes under local-probe manipulation. *Nature* 405:769
- Torras N, Zinoviev KE, Esteve J, Sánchez-Ferrer A (2013) Liquid-crystalline elastomer micropillar array for haptic actuation. *J Mater Chem C* 1:5183
- Torras N, Zinoviev KE, Camargo CJ, Campo EM, Campanella H, Esteve J, Marshall JE, Terentjev EM, Omastová M, Krupa I, Teplicky P, Mamojka B, Bruns P, Roeder B, Vallribera M, Malet R, Zuffanelli S, Soler V, Roig J, Walker N, Wenn D, Vossen F, Crompvoets FMH (2014a) Tactile device based on opto-mechanical actuation of liquid crystal elastomers. *Sensor Actuat A-Phys* 208:104
- Torras N, Marshall JE, Zinoviev KE, Camargo CJ, Terentjev EM, Esteve J (2014b) Gas-pressure molding-based fabrication of smart actuators from nematic liquid-crystalline elastomer. *Macromol Mater Eng* 299:1163
- Urayama K (2010) Stimulus-responsive nematic gels. *Macromol Symp* 291–292:89
- Urayama K, Honda S, Takigawa T (2006) Deformation coupled to director rotation in swollen nematic elastomers under electric fields. *Macromolecules* 39:1943
- Urayama K, Mashita R, Kobayashi I, Toshikazu T (2007) Stretching-induced director rotation in thin films of liquid crystal elastomers with homeotropic alignment. *Macromolecules* 40:7665
- Wang XJ, Warner M (1987) Theory of nematic comb-like polymers. *J Phys A* 20:713
- Warner M, Terentjev EM (2007) *Liquid crystal elastomers*. Clarendon, Oxford
- Wermter H, Finkelmann H (2001) Liquid crystalline elastomers as artificial muscles. *e-Polymers* 013:1–13
- Winkler M, Kaiser A, Krause S, Finkelmann H, Schmidt AM (2010) Liquid crystal elastomers with magnetic actuation. *Macromol Symp* 291–292:186
- Woltman S, Jay G, Crawford G (2007) Liquid-crystal materials find a new order in biomedical applications. *Nature Mat* 6:929
- Xia YN, Whitesides GM (1998) Soft lithography. *Annu Rev Mater Sci* 28:153
- Yamada M, Kondo M, Mamiya J, Yu Y, Kinoshita M, Barret CJ, Ikeda T (2008) Photomobile polymer materials: towards light-driven plastic motors. *Angew Chem Int Ed* 47:4986
- Yang R, Wang W (2004) Out-of-plane polymer refractive microlens fabricated based on direct lithography of SU-8. *Sensor Actuat A Phys* 113:71

- Yang SM, Jang SG, Choi DG, Kim S, Yu HK (2006) Nanomachining by colloidal lithography. *Small* 2:458
- Yang H, Buguin A, Taulemesse JM, Kaneko K, Méry S, Bergeret A, Keller P (2009) Micron-sized main-chain liquid crystalline elastomer actuators with ultralarge amplitude contractions. *J Am Chem Soc* 131:15000

Chapter 20

Discotic Liquid Crystalline Polymers: Structure and Chemistry

Harpreet Singh, Sandeep Kumar, and Santanu Kumar Pal

Historically polymers are known for their insulating property, processability, thermal stability and mechanical strength. Discovery of the conducting polymers introduced them to molecular electronics for variety of applications like organic solar cells, printing electronic circuits, organic light-emitting diodes, actuators, electrochromism, supercapacitors, chemical sensors and biosensors (Lange et al. 2008). Physical and electronic properties of bulk polymer materials are highly dependent on molecular ordering of polymers chains. For example, a light-weight polymer stronger than steel can be prepared in the form of kevlar just by assembling the polymer chains. Again the alignment of the polymer chains has been shown to enhance conductivity of conductive polymers (Ogasawara et al. 1985).

Lots of efforts have been put forth by the scientific community to achieve the control on molecular ordering of polymer chains through various supramolecular approaches. Among all, a well-known approach is attaching the liquid crystal mesogens to the polymer chain. With the advantage of self-assembling tendency of liquid crystal molecules into ordered materials, polymer chains can be influenced to assemble into well-ordered structure by attaching them to polymer back bone. This class of polymers are well known as Liquid crystal polymers (LCPs). Followed by the first discovery of LCPs by Vorlander et al., a variety of LCPs were synthesized and characterized to soothe the scientific curiosity about them. A range of synthetic methods including polymer substitution reactions, free radical polymerizations, optical polymerizations, ring-opening metathesis polymerizations, and condensation polymerizations have been used to prepare such

H. Singh • S.K. Pal (✉)

Department of Chemical Sciences, Indian Institute of Science Education and Research (IISER)
Mohali, Sector-81, SAS Nagar, Mohali 140306, India
e-mail: harpreetsinghtaak@gmail.com; skpal@iisermohali.ac.in

S. Kumar

Raman Research Institute, C. V. Raman Avenue, Sadashivanagar, Bangalore 560 080, India
e-mail: skumar@rri.res.in

polymers. At the ground of liquid crystals materials LCPs can be classified in linear, banana, discotic and mixed mesogen based LCPs. Discotic mesogens based polymers (DLCPs) were first realized by the Ringsdorf group (Kreuder et al.1983). These class of polymers are important, because of their tendency to self-organize into well-ordered, self-healable supramolecular columns, which tends to rearrange in 2D lattices due to π - π stacking of the planar aromatic core and the vander Waals interactions of the peripheral chains. These characteristics of DLC make them potential candidates for optoelectronic applications, because of their high charge conducting capacity along the columns. The electronic properties of DLCPs can be tuned based on various discotic mesogen moieties like, benzene, alkynylbenzene, triphenylene, phthalocyanine, hexabenzocoronene etc. On the other hand change in polymer back bone with different spacer and linkages (ester, ether and amide etc.) provide an opportunity to tune the physical properties of DLCPs. The LCPs literature is rich with examples of linear, banana shaped mesogen based LCPs as compare to DLCPs. Main reason for this is less availability of functionalized discogens units due to the symmetry of these molecules. However, motivated with the various applications in the areas of wide view displays, High-quality carbon products, organic electronics, photovoltaic solar cells, light emitting diodes and field effective transistors, research has shown exponential growth in terms of synthesis and understanding of physical properties of DLCPs. Discotic Liquid Crystalline Polymers (DLCPs) can be further classified into (a) discotic main chain (b) discotic side chain (c) discotic elastomers (d) discotic dendritic (e) discotic hyperbranched and (f) discotic metallomesogenic liquid crystalline polymers (Fig. 20.1), based on the position of discotic mesogens and connectivity.

20.1 Main Chain Discotic Liquid Crystal Polymers

In main chain discotic liquid crystal polymers discotic mesogens are incorporate into the main chain of polymer backbone. So, difunctionalized discotic mesogens are the primary requirement of these class of polymers. These functional groups are often hydroxyl moieties to produce polyether or polyester based main chain polymer. In spite of very less literature available, main chain DLCPs are the second most studied DLCPs after side chain DLCPs. These main chain DLCPs can be classified based on various discotic mesogen like Triphenylene, benzene, rufigallol, cycloter-averatrylene etc.

20.1.1 *Rufigallol-Based Main Chain Discotic Liquid Crystal Polymers*

The unequal reactivity of the six phenolic groups of Rufigallol **1** core presents an advantage of the selective alkylation of four of the phenolic groups, leaving behind the two intramolecular hydrogen-bonded ones. Utilizing this strategy Raja

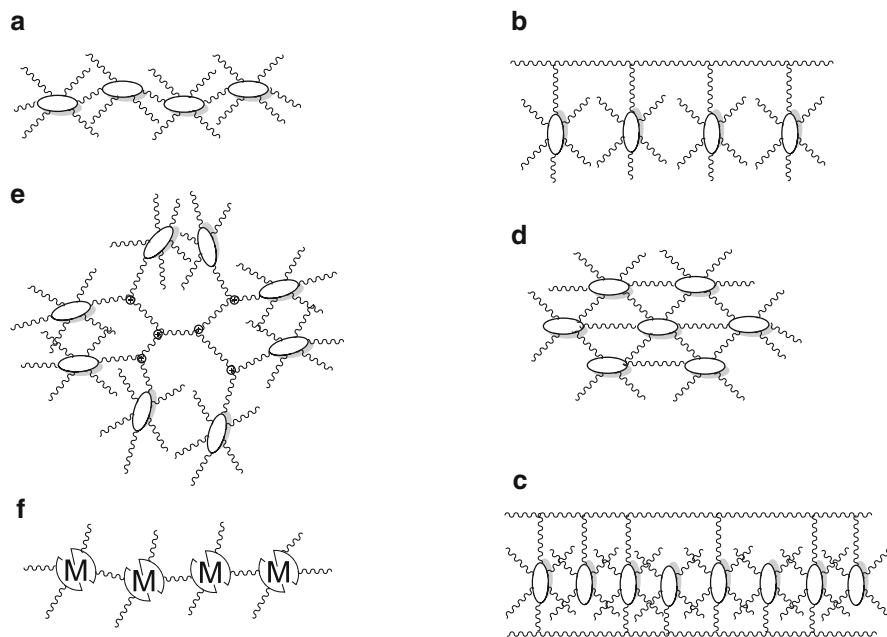
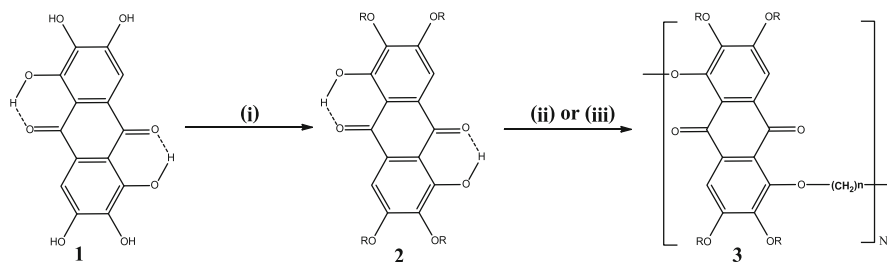


Fig. 20.1 Schematic representation of; (a) discotic main chain; (b) discotic side chain; (c) discotic elastomers; (d) discotic dendritic; (e) discotic hyperbranched; (f) discotic metallomesogenic liquid crystalline polymers

et al. (Raja et al. 1998) have been prepared two series of thermotropic main chain discotic liquid crystalline polyether based on rufigallol starting from the symmetric tetraether of rufigallol. The Polyether **2a–h** were synthesized by reacting 1,5-dihydroxy-2,3,6,7-tetraalkoxy-9,10-anthraquinone **2** (Scheme 20.1) with equimolar amount of α,ω -dibromoalkane in the presence of Potassium carbonate (aq) in *o*-dichlorobenzene solvent under nitrogen atmosphere at 90 °C for 14 days. These polyether can also be prepared by heating an equimolar mixture of dihydroxy-tetraalkoxyanthraquinone **2** and α,ω -dibromoalkane in *o*-dichlorobenzene at 90 °C in the presence of cesium carbonate for 10 days.

The length of the spacer segment in the polyethers was systematically varied. GPC studies revealed that, all polymers have moderate molecular weights varying between 5400 and 17,000. It can be seen from Table 20.1 that spacer to peripheral alkyl chain length ratio highly influenced thermal behaviour of these polymers **2a–h**. The isotropization temperature inversely depends on spacer length, when ratio is more than two. However, trend is quite the opposite when ratio is less than two. Furthermore, the polymers exhibit the hexagonal discotic columnar mesophases when ratio is more than two, while a rectangular lattice has been seen when ratio is less than two. Finally, the polymers have been shown to exhibit liquid crystalline columnar mesophases, while some of their low molar mass analogues are not liquid crystalline.



Scheme 20.1 Synthesis of rufigallol-based main-chain polyethers: (i) α,ω dibromoalkane, NaOH, DMSO, 90 °C; (ii) α,ω -dibromoalkane, o-dichlorobenzene, aq K_2CO_3 , tetrabutylammonium bromide (TBAB), 90 °C, 14 days; (iii) α,ω dibromoalkane, o-dichlorobenzene, Cs_2CO_3 , 90 °C, 10 days

Table 20.1 Thermal behavior of Rufigallol-based main-chain polyethers

Structure	R	n	M_w	Phase transitions	References
2a	C_4H_9	6	68,00	g 72 Col _r , 164 Col _r ' 175 I	Bengs et al. (1993)
2b	C_4H_9	8	17,000	g 72 Col _h 164 Col _h ' 176 I	
2c	C_4H_9	10	6400	Col _h 133 Col _h ' 144 I	
2d	C_4H_9	12	5400	Col _h 138 I	
2e	C_8H_{17}	6	7400	Col _r 132 I	
2f	C_8H_{17}	8	14,500	g 54 Col _r 96 I	
2g	C_8H_{17}	10	8800	Col _r 108 I	
2h	C_8H_{17}	12	7600	Col _r 127 I	
2i	$CH_2CH_2CH(CH_3)$ $(CH_2)_3CH(CH_3)_2$	12	13,691	Col _r 56 I	

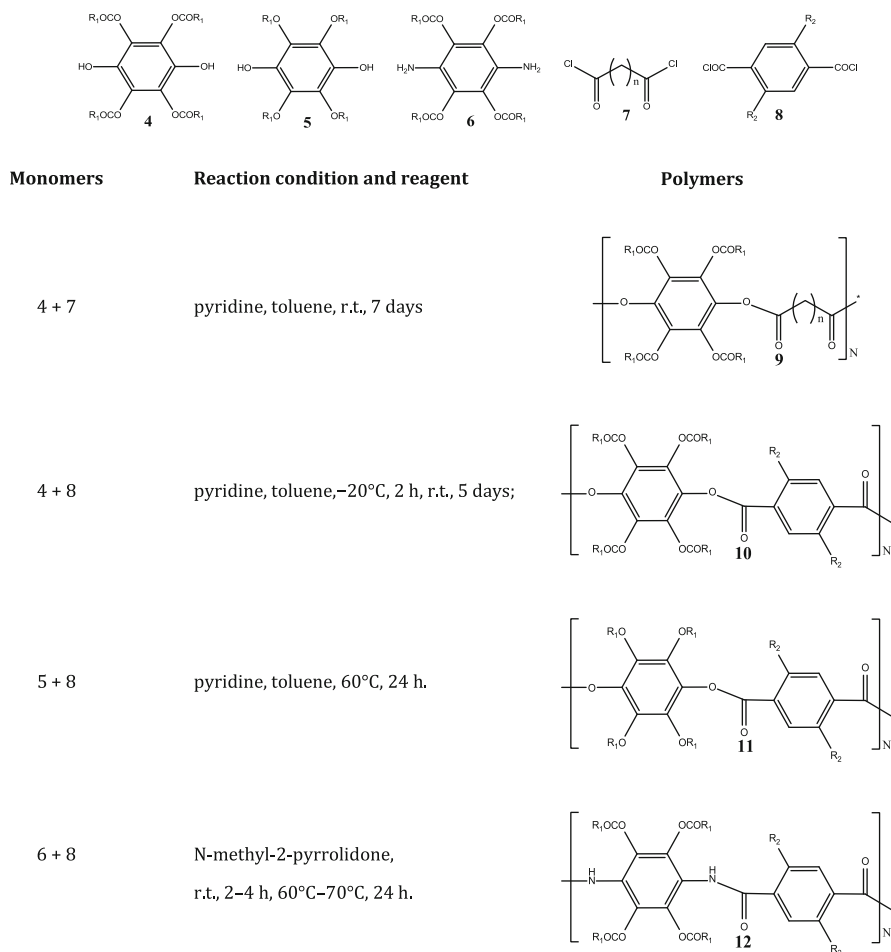
Source: Raja et al. (1998) and Bisoyi and Kumar (2008)

Further Bisoyi and Kumar (2008) tried to study the effect of inclusion of carbon nanotubes on mesophase behaviour of Rufigallol-based Main chain DPLCs. They found that insertion of small amount of carbon nanotubes does not affect the mesophase structure of the pure compounds and lower the isotropic transition temperature. Greater the amount of Carbon nanotube induce downfall in isotropic transition temperature. These room temperature liquid crystalline nano composite with broad mesophase range and different electronic properties can be important for many applications.

20.1.2 Benzene-Based Main Chain Discotic Liquid Crystal Polymers

Kreuder et al. (1985) were made first attempt to synthesize the difunctionalized benzene monomeric units to prepare the benzene-based liquid crystalline main-chain polymers. The polymers with ester and amide linkage were prepared via solution polycondensation of these difunctionalized monomers **4**, **5**, and **6** with various spacers **7** and **8** (Scheme 20.2).

Synthesis of tetraalkanoxyloxy benzene polyesters **9a-f** were achieved by reacting equimolar mixture of dihydroxy tetraalkanoxyloxy benzene and flexible spacer alkane- α,ω -dioic acid dichloride in pyridine and toluene (Scheme 20.2). The polymers **9a** and **9b** with short spacers were found to be nonmesomorphic in thermal analysis (Table 20.2). At the same time, the polymer with long spacer **9c**,



Scheme 20.2 Synthesis of benzene based DLCPs polyester and polyamides

Table 20.2 Thermal behavior of benzene-methylene-based polymers

Structure	<i>n</i>	<i>Mn</i>	Phase transition	Reference
9a	7	–	g 54 I	Boden et al. (1995)
9b	8	10,400	g 55 I	
9c	10	9800	g 55 M 95 I	
9d	12	12,400	g 54 M 97 I	
9e	14	12,100	Cr 64 M 92 I	
9f	20	6600	g 30 I	

Source: Kreuder et al. (1985)

Table 20.3 Transition temperatures of benzene-based polyesters and polyamides

Structure	R	R'	Phase transition	Reference
10a	C ₇ H ₁₅	H	g 97 M 146 M' 260 I	Boden et al. (1998)
10b	C ₉ H ₁₉	H	g 50 Cr 95 M 138 I	
10c	C ₁₁ H ₂₃	H	g 55 Cr 63 M 123 I	
10d	C ₇ H ₁₅	OC ₈ H ₁₇	Cr 50 I	
11a	C ₈ H ₁₇	H	g 150 M 208 M' 246 I	
11b	C ₁₂ H ₂₅	H	Cr 25 M 210 I	
11c	C ₁₂ H ₂₅	OC ₁₂ H ₂₅	Cr 74 I	
11d	C ₁₂ H ₂₅	OC ₈ H ₁₇	Cr 67 I	
12a	C ₈ H ₁₇	H	Cr 273 I	
12b	C ₈ H ₁₇	OC ₈ H ₁₇	Cr 39 M 117 I	
12c	C ₈ H ₁₇	OC ₁₂ H ₂₅	Cr 51 M 69 I	
12d	C ₁₂ H ₂₅	H	Cr 270 I	
12e	C ₁₂ H ₂₅	OC ₁₂ H ₂₅	Cr 17 M 70 M' 130 I	
12f	C ₁₂ H ₂₅	OC ₈ H ₁₇	Cr 61 M 122 I	
12g	C ₁₄ H ₂₉	OC ₁₄ H ₂₉	Cr 38 M 74 M' 88 M' 106 I	
12h	C ₁₆ H ₃₃	OC ₁₆ H ₃₃	Cr 86 I	

Source: Ringsdorf et al. (1987)

9d and **9e** were found to be liquid crystalline with the higher isotropization temperatures, as compare to monomeric tetraalkanoxyloxy benzene unit. The liquid crystalline nature disappears, if spacer length in polymer **9f** increases to 20 methylene units. Replacing the flexible spacer, alkane- α,ω -dioic acid dichloride **7**, with terphthaloyl dichloride **8** in the same synthesis provides an opportunity to study the benzoate-based polyesters. Thermal analysis of polyesters **10a–d** shows that, all the polyesters **10a**, **10b** and **10c** with four lateral alkyl chains were liquid crystalline (Table 20.3). However, polyester **10d** having six lateral chains did not display any mesomorphism. The value of isotropization temperature highly depends on the lateral alkyl chain length of difunctionalized benzene monomers. The synthesis of corresponding tetraalkoxybenzene derived polybenzoates is shown in Scheme 20.2 (Herrmann-Schönherr et al. 1986; Ringsdorf et al. 1987). It was noticed that polymers with four lateral alkyl chains **11a** and **11b** were liquid crystalline, whereas polymers with six lateral alkyl chains **11c** and **11d** were found to be nonmesomorphic.

Benzene-based discotic polyamides **12a–h** were prepared by reacting tetra substituted 1,4-phenylenediamine **6** with terphthaloyl dichloride **8** in *N*-methyl-2-pyrrolidone as solvent. Polyamides with four lateral alkyl chains **16a** and **16d** were found crystalline in nature, whereas six lateral chains make them liquid crystalline. This reverse behaviour, as compare to polyesters, is most likely because of hydrogen bonding caused by amide linkage. Polyamides **12a** and **12d** with only four lateral substituents per repeating unit are able to form strong intermolecular hydrogen bonding and thus have a tendency to crystallize. Attachment of two more lateral substituents per repeating unit causes weaker intermolecular interactions and hence favours the formation of mesomorphic phase.

20.1.3 Triphenylene-Based Main Chain Discotic Liquid Crystal Polymers

Kreuder and Ringsdorf (1983) first reported the synthesis of triphenylene-based main-chain DLPCs. They prepared the difunctional triphenylenes precursor monomer via partial hydrolysis/alkylation of triphenylene hexaacetate. This method had a big disadvantage of giving mixture of diacetate isomers with two hydroxyl at 2,3-; 2,6-; 2,7-; or 2,11-positions. The separation of these isomers requires extensive column chromatography. These difunctional monomers (mixture 2,6- and 2,7-isomeric) yielded Triphenylene-based main chain DLCPs **13a–j** via melt polycondensation with various α,ω -diacids.

The thermal behaviour of these polymers is presented in Table 20.4. All the polymers except **13e** and **13i–j** were liquid crystalline. These polymer exhibit

Table 20.4 Thermal behavior of mixtures of 2,6-positions and 2,7-positions linked triphenylene main-chain polymers

Structure	R	Spacer	Phase transition	References
13a	C ₅ H ₁₁	–(CH ₂) ₁₀ –	g 35 Col 195 I	Boden et al. (1999)
13b	C ₅ H ₁₁	–CD ₂ (CH ₂) ₈ CD–	g 50 Col 220 I	
13c	C ₅ H ₁₁	–(CH ₂) ₁₄ –	g 60 Col 150 I	
13d	C ₅ H ₁₁	–(CH ₂) ₁₄ –	g 57 Col _h 143 I	Boden et al. (2001)
13e	C ₅ H ₁₁	–(CH ₂) ₂₀ –	g 35 I	Brand et al. (2000)
13f	CD ₂ C ₄ H ₉	–(CH ₂) ₁₄ –	g 58 Col _h 140 I	Boden et al. (2001)
13g	(CH ₂) ₂ CD ₂ C ₄ H ₉	–(CH ₂) ₁₄ –	g 50 Col _h 180 I	Bryant et al. (1995)
13h	CH ₂ C*H(CH ₃) C ₂ H ₅	–(CH ₂) ₁₀ –	g 140 Col _h 192 I	Cameron et al. (1997)
13i	CH ₂ C*H(CH ₃) C ₂ H ₅	–(CH ₂) ₁₄ –	g 108 I	
13j	CH ₂ C*H(CH ₃) C ₂ H ₅	–(CH ₂) ₂₀ –	g 79 I	

Source: Kreuder and Ringsdorf (1983) and Hüser and Spiess (1988) and Ringsdorf et al. (1989) and Voigt-martin et al. (1994) and Green et al. (1990)

broader mesophase range as compare to monomeric units. Thermal behaviour remains nearly unchanged on deuteration of the side-chain or aromatic groups. Among polymers **13i** and **13j**, **13i** changes amorphous to liquid crystalline on doping with electron acceptor TNF. It exhibits a nematic columnar phase. The substitution of chiral chain at peripheral positions induces the formation of a helical superstructure in the liquid crystalline polymers **13i-j** (Green et al. 1990).

To prepare the single isomer of difunctionalized triphenylene monomer Wenz's et al. (Wenz 1985) rationalized the synthesis of 2,3-difunctionalized triphenylene derivative. Later on Boden et al. (1995) prepared pure 2,7-dihydroxy-3,6,10,11-tetrahexyloxy-triphenylene and 2,11-dihydroxy-3,6,7,10-tetrahexyloxy-triphenylene respectively. Further polycondensation of 2,3-difunctionalized triphenylene with various α,ω -diols having different spacer length produce polyester **14**. The polycondensation of malonic acid diethyl ester afforded polymer **15** (Voigt-Martin et al. 1992). In polymers **16** triphenylene units having chiral peripheral chains were linked together via ester linkages. Condensation of 2,3-dihydroxy-6,7,10,11-tetrahexyloxytriphenylene with 1,10-dibromodecane gives polymer **17**. The polyesterification of 2,7-dihydroxy-3,6,10,11-tetrahexyloxy-triphenylene and 2,11-dihydroxy-3,6,7,10-tetrahexyloxy-triphenylene with α,ω -dibromoalkanes furnished polymers **18** and **19a**. Polyesterification of 2,11-dihydroxytetrahexyloxytriphenylene with α,ω -diacids produced polymers **19b-d**.

Thermal studies and GPC studies of these polymer having different lateral alkyl chains and linkages are given in the Table 20.5. The polymers **14** melt at about 93 °C and clear between 100 and 200 °C whereas polymer **15** shows the glass transition at -10 °C and isotropic transition at 31 °C. Discotic nematic phase of polymer **15** transform into more ordered columnar phase, when it was doped with the electron-acceptor TNF. This charge transfer polymer composite exhibit the thermal transition at 135 °C from columnar phase to isotropic phase (Vandevyver et al. 1993). Polymer 16a and 16b were amorphous in nature and exhibit glass transition temperature at 105 °C and 75 °C respectively. Polymer **17** showed a columnar phase to isotropic transition at 115 °C (Fig. 20.2) (Disch et al. 1995). All polymers **19b-d** form an ordered columnar mesophases, between the glass transition and clearing temperatures as per the Table 20.6 (Wan et al. 2003).

To study the difference between structures displayed by lower mass and polymeric amphiphilic discotic liquid crystalline triphenylene derivatives in the bulk

Table 20.5 Thermal behavior of triphenylene main-chain polymers 14–18

Structure	<i>N</i>	Phase transition	Reference
14	12	g 93 Col 163 I	Caseri et al. (1988)
15	9	g -10 N 31 I	Catry et al. (1993)
16a	14	g 105 I	Cook (1995)
16b	20	g 75 I	
17	10	Cr 100 Col 115 I	Disch et al. (1995)
18	11	Cr 98 Col 118 I	

Source: Wenz (1985 and Vandevyver et al. 1993 and Green et al. (1990) and Boden et al. (1995)

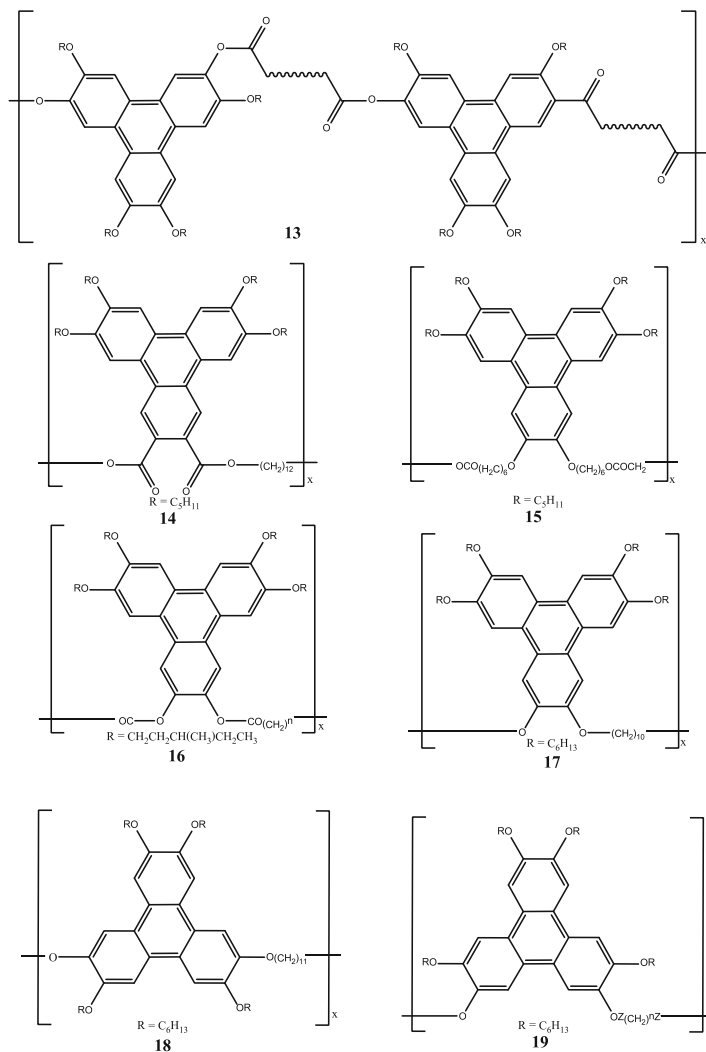


Fig. 20.2 Schematic diagram of Triphenylene based main chain polyethers and polyesters

Table 20.6 Thermal behavior of triphenylene main- chain polymers 19

Structure	Z	n	Phase transition	References
19a	CH_2	9	Cr 93 Col 120 I	Disch et al. (1995) Dulog et al. (1993)
19b	CO	8	g 56 Colh 211 I	
19c	CO	10	g 40 Colh 198 I	
19d	CO	12	g 25 Colh 162 I	

Source: Boden et al. (1995 and Wan et al. 2003)

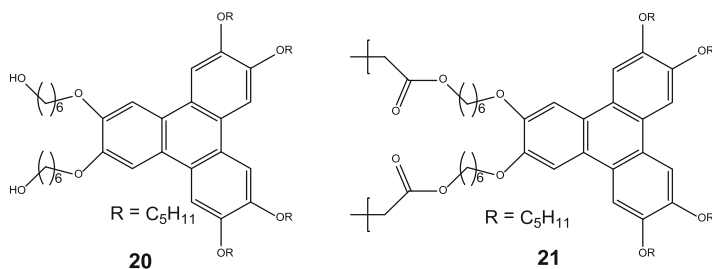


Fig. 20.3 Schematic diagram of Triphenylene based amphiphilic derivatives

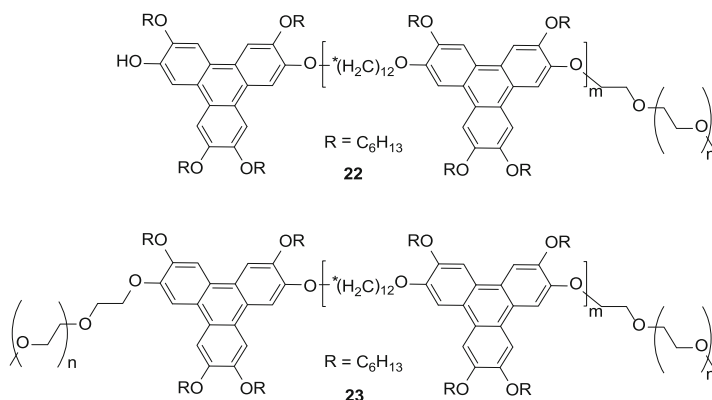


Fig. 20.4 Schematic diagram of TP and PEG based diblock mad triblock polymers

state and Langmuir-Blodgett (LB) films, Ringsdorf and group synthesized the discotic triphenylene amphiphilic derivatives **20**, **21** (Fig. 20.3) (Karhaus et al. 1992). An edge-on arrangement of the discotic molecules within a double-layer packing of columns being parallel to the solid support is formed in the LB films of both compounds. While comparing the monomer **20** and polymer **21** in bulk state of polymer form a less ordered nematic phase as compare to highly order columnar phase shown by monomer.

Block copolymers are known to form a range of microphase-separated structures like lamellae, hexagonal-packed cylinders, cubic-packed spheres, and bicontinuous cubic gyroid morphology. With the advantage to tailor the properties of block copolymers by combining blocks with distinct characteristics Boden et al. (1999) were prepared Discotic main-chain diblock and triblock copolymers containing one triphenylene block and either one or two polyethyleneoxy blocks (Fig. 20.4). Block polymers were found liquid crystalline having columnar phase at room temperature. The copolymer **22** clears at 86 °C and **23** at 66 °C. The triblock copolymer **23** under goes microphase separation, giving a nano structured material consisting of a hexagonal array of poly(ethylene oxide) rods in the matrix of columnar liquid crystal (Boden et al. 2001).

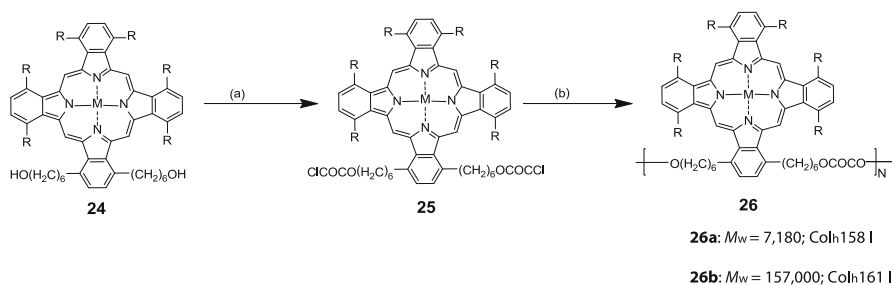
The electrolyte properties of these triblock copolymers, doped with lithium perchlorate, were reported by Imrie group. The polymer exhibit a phase separated morphology consisting of a columnar hexagonal liquid crystal phase and PEO rich regions. The self-supporting solid film of polymer electrolyte shows a good conductivity above 60 °C, due to the malting of crystalline PEO rich regions at this temperature (Stoeva et al. 2013).

20.1.4 Phthalocyanine-Based Main Chain Discotic Liquid Crystal Polymers

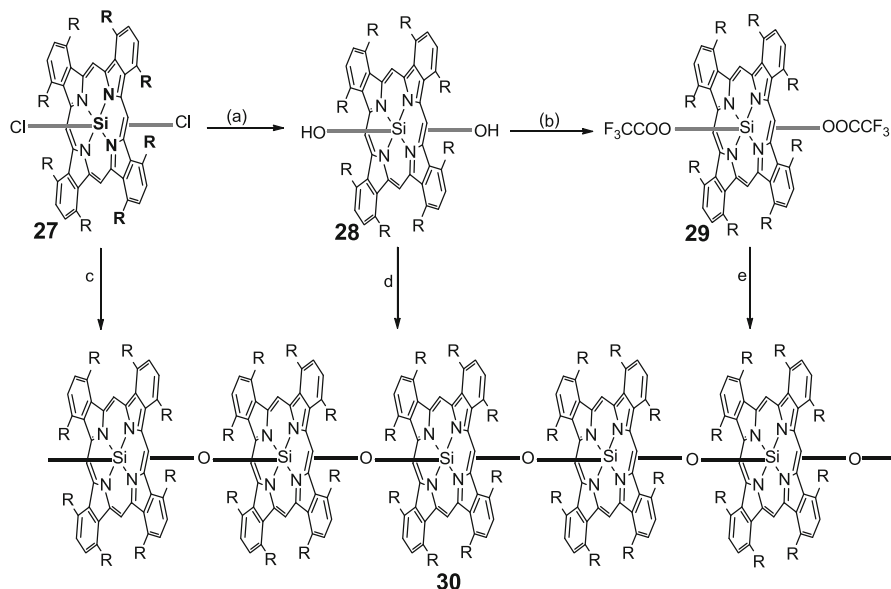
Phthalocyanine is an intensely blue-green-coloured aromatic macrocyclic compound which coordinates with nearly all elements of periodic table to produce intensely colour dyes or pigment. These metal phthalocyanines dyes and pigments are very useful in catalysts for redox reactions, organic field-effect transistors, storage in quantum computing. To explore these potential application, verities of phthalocyanine based polymers were synthesised, however only few of them are liquid crystalline (Scheme 20.3).

Phthalocyanine-Based Main chain discotic liquid crystal polymers were first prepared by Cook (1995) via., condensing a dihydroxy-functionalized phthalocyanine **24** with oxalyl chloride (Scheme 5.14). The phthalocyanine monomer **24** was converted onto bis-acid chloride **25** and coupled with diol **24** at 90 °C in dichloromethane to yield the polymer **26**. DMAP was used as a coupling agent for synthesis of polymer results higher molecular weight polymer **26b** (Bryant et al. 1995). Both polymers **26a** and **26b** exhibit hexagonal columnar mesophase over a broad mesophases. The polymer with higher M_w shows small increase in isotropic transition temperature.

The second class of Phthalocyanine based main chain polymers are also called spinal columnar or shish kebab type polymers, when Phthalocyanine macrocyclics are coaxially stacked over each other and linked by a bridging atom bonded to coordinated atom such as silicon, tin, or germanium atom at the centre of the



Scheme 20.3 Synthesis of phthalocyanine-based main-chain polymer: (a) ClCOCOCl; (b) 24, 48 h, 90 °C for 26a or pyridine and 4-dimethylaminopyridine to yield 26b



Scheme 20.4 Synthesis of phthalocyanine-based polymer having metal–oxygen–metal bond as a linker: (a) ion exchange; (b) $\text{CF}_3\text{COOCOCF}_3$, pyridine; (c) AgSO_3CF_3 , TISO_3CF_3 , $[\text{Cu}(\text{CH}_3\text{CN})_4]\text{SO}_3\text{CF}_3$; (d) 180°C , 7 h or catalyst (FeCl_3 , ZnCl_2 , AlCl_3 , CdCl_2 , CaCl_2 , CsCl); (e) 200°C

phthalocyanine molecule. Bridging can happen through covalent bonds, covalent–coordinate bonds or coordinate–coordinate bonds. Synthetic routes to synthesize the polysiloxane spinal based phthalocyanine polymers are shown in Scheme 20.4. Polymerization process involve the heating of dihydroxy-functionalized discotic metallomesogens for bulk condensation at about 200°C in the presence of catalysts such as, FeCl_3 , ZnCl_2 , AlCl_3 , CdCl_2 , CaCl_2 , etc., for approximate 7 h. Catalysts can be avoided by replacing the hydroxyl groups by better leaving groups such as trifluoroacetate. The polymerization can also be carried out at lower temperature (about 100°C) by taking a dichloro monomer and using halogenophilic condensation agents such AgSO_3CF_3 , TISO_3CF_3 , $[\text{Cu}(\text{CH}_3\text{CN})_4]\text{SO}_3\text{CF}_3$ etc. (Sirlin et al. 1987, 1988a, b; Caseri et al. 1988; Sauer 1993; Sauer and Wegner 1991; Orthmann and Wegner 1986; Schouten et al. 1992; Dulog et al. 1993).

The X-ray diffraction studies shows the formation of columnar mesophases by these polymers. In DSC studies it was found that, the polymer with short lateral side-chain derivatives didn't exhibit any phase transition up to the decomposition temperature. Whereas polymer with medium lateral side-chain show only melting transitions below 100°C . The long side-chain derivatives shows an isotropic transitions at high temperature under polarizing microscope without decomposing however this transition was absent in DSC thermograms.

Another interesting example of spinal polymers was reported by Nolte and co-workers (Sielcken et al. 1990; van Nostrum et al. 1995; Van Nostrum and Nolte 1996). They prepared the phthalocyaninato polysiloxanes substituted with

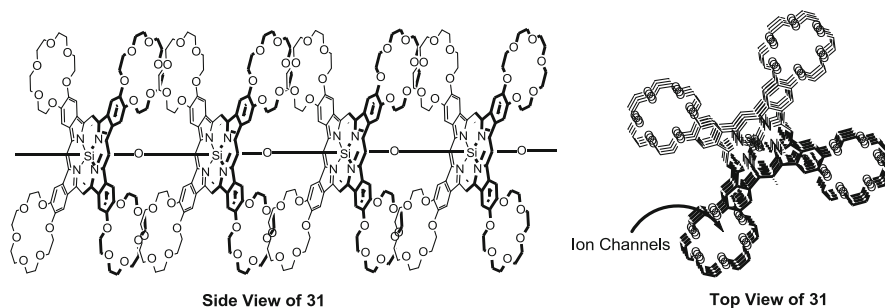


Fig. 20.5 Schematic diagram of columnar or shish kebab type crown ether substituted phthalocyaninato polysiloxanes polymers

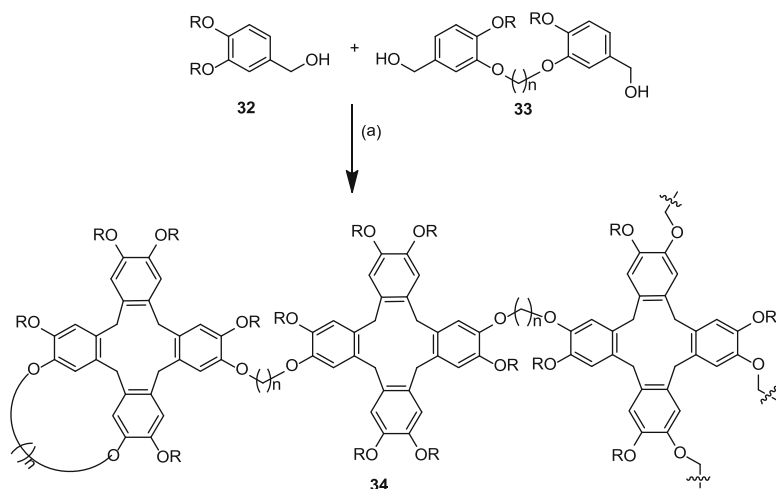
crown ether moieties **31** (Fig. 20.5). Crown ether substituted phthalocyanine macrocycles were prepared from 4, 5-dicyanobenzo-crown ether followed by heating its dihydroxysilicon complex in the presence of catalyst for polymerization. The X-ray studies revealed that polymer exhibit hexagonal columnar phase (Orthmann and Wegner 1986), however monomeric dihydroxysilicon didn't show any aggregation due to the steric hindrance of axial hydroxyl groups.

20.1.5 Cyclotetraeratrlyene-Based Main Chain Ionic Discotic Liquid Crystal Polymers

Molecules with flexible cores, such as octasubstituted cyclotetraeratrlyene (CTTV-n), tetra- and hexasubstituted cyclic poly-amine, and hexasubstituted scyllo-inositol etc. can adopt a quasi-flat conformation, known to form columnar mesophases (Zimmermann et al. 1988; Percec et al. 1991; Mertesdorf and Ringsdorf 1989). However, only hexasubstituted cyclotrivaeratrlyene (CTV-n) flexible, which have a cone like shape and form columnar mesophases was explore as main chain DLCs (Malthete and Collet 1987; Malthete et al. 1989).

The synthesis of main chain liquid-crystalline polyethers containing hexasubstituted cyclotrivaeratrlyene (CTV-n) disk-like mesogens was reported by Percec et al. (1992). The branched polymers were synthesized by the cocyclotetraeratrization of various ratios of a mixture containing 3,4-(di-n-alkyloxy)benzyl alcohol **32** and α,ω -bis[[2-(n-alkyloxy)-5-(hydroxymethyl)phenyl]oxy]alkane **33** in different and using CF_3COOH as the cyclotetraeratrization catalyst. This unique reaction construct the disklike octaalkyloxy-substituted cyclotetraeratrlyene derivatives (CTTV-n) molecules during the polymerization process (Scheme 20.5).

In a columnar mesophase the backbone of a main-chain liquid-crystalline polymer containing CTTV-n mesogens can either connect mesogens from adjacent columns or link two mesogens within the same column. These polymers display hexagonal columnar mesophase. All the polymers had clearing temperature in the



Scheme 20.5 Synthesis of cyclotetraeratrilylene-based polymer: (a) CF_3COOH , CH_2Cl_2 , r.t., 4.5 h

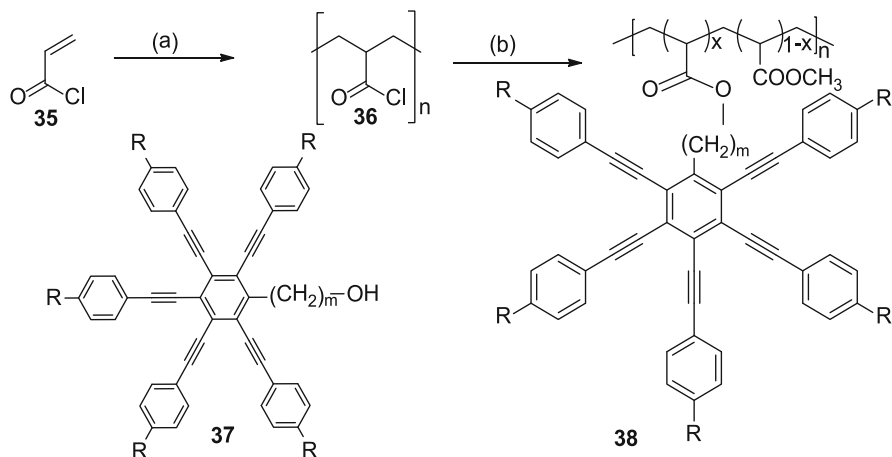
range 102–145 °C. The Clearing temperature depends on **32** to **33** ratio (x/y) used in reaction mixture, keeping the spacer and peripheral alkyl chain length constant. The clearing temperature decreases on decreasing the ratio of **32** to **33**. Hence its shows reciprocally effect by the proportion of the reactant **33** in the reaction mixture.

20.2 Side Chain Discotic Liquid Crystalline Polymers

Side chain DLCs are the most studied DLCs, having discotic mesogens as a pendent groups on polymeric backbone. These pendent group can be attached to polymer backbone mainly with two methods, first involve the polymer substitution reaction between already synthesised polymer and discotic mesogens and in second method discotic mesogens are functionalized to polymerizable monomers. Literature of side chain polymers can be divided on the basis of different discotic mesogens.

20.2.1 Alkynylbenzene-Based Side Chain Discotic Liquid-Crystalline Polymers

A natural tendency to form nematic mesophase by alkynylbenzene can be used to suppress the crystallization of a polymer backbone by attaching it to the polymer backbone. It helps to achieve the low-temperature liquid crystalline polymers with a broader mesophase range. A series of radial pentayne based side-chain polyacrylates were synthesised by (Kouwer et al. 2000, 2001a, b, c, 2002a, b,



Scheme 20.6 Synthesis of alkynylbenzene-based side-chain polyacrylates: (a) AIBN, dioxane; (b) **37**, C_5H_5N , DMAP, CH_2Cl_2

Table 20.7 Thermal behavior of pentaalkynylbenzene-based side-chain polymers

Structure	R	x	Phase transition	References
38a	C_7H_{15}	0.50	g –15 I	Green et al. (1990)
38b	OC_6H_{13}	0.60	g 25 N 107 I	
38c	OC_6H_{13}	0.63	g 24 N 113 I	
38d	OCH_3	0.63	g 41 N >200 dec	Herrmann-Schönherr et al. (1986)
38e	OCH_3	0.70	g 50 N >200 dec	
38f	OCH_3	0.83	g 45 N >200 dec	
38g	H	0.72	g 53 I	Hueser et al. (1989)

Source: Kouwer et al. (2002a, b, 2003)

2003; Picken et al. 2004). The synthesis process involve the polymer substitution reaction between hydroxyl-terminated radial pentaalkynylbenzene derivative **37** and polyacryloyl chloride **36**, in the presence of pyridine and catalytic amount of NAN dimethylaminopyridine, in dry dichloromethane followed by quenching with excess methanol. Scheme 20.6 shows the synthesis process of these polymers.

In DSC studies polymer **38a** and **38g** were found out to be non-mesomorphic, however, connecting the lateral alkyl chains with oxygen instead of methylene induces a nematic phase in the polymers **38b–f**. Polymers with short methoxy peripheral groups **38d–f** decompose at higher temperature before reaching the isotropic phase, whereas polymer with long alkoxy chains have lower isotropic temperature and show a clear transition from mesophase to isotropic phase. Table 20.7 summarize the thermal transition data of these polymers.

Same group also synthesised side-chain pentaalkynylbenzene co-polyacrylates **39a–j** by modifying the final quenching step. The quenching in this process involve two step, first step involve the partial quenching with an alcohol other than methanol and secondly with excess methanol. A general structure of these

Table 20.8 Thermal behavior of pentaalkynylbenzene-based side-chain copolymers

Structure	R	x	y	Phase transition	References
39a	CH ₃	0	0.90	g 43 N _c 164 N 235 I	Hüser and Spiess (1988)
39b	CH ₃	0	0.64	N _c 165 N 233 I	
39c	CH ₃	0	0.48	g 92 N _c 158 N 204 I	
39d	CH ₃	0	0.31	g 62 N _c 149 N 148 I	
39e	C ₅ H ₁₁	0.31	0.69	g 77 N _c 157 N 209 I	
39f	C ₅ H ₁₁	0.43	0.41	g 70 N _c 169 I	
39g	C ₅ H ₁₁	0.50	0.42	g 51 N _c 157 I	
39h	C ₁₂ H ₂₅	0.11	0.61	g 86 N _c 155 N 210 I	
39i	C ₁₂ H ₂₅	0.45	0.45	g 50 N _c 154 I	
39j	C ₁₂ H ₂₅	0.42	0.33	g 49 N _c 136 I	

Source: Kouwer et al. (2001a)

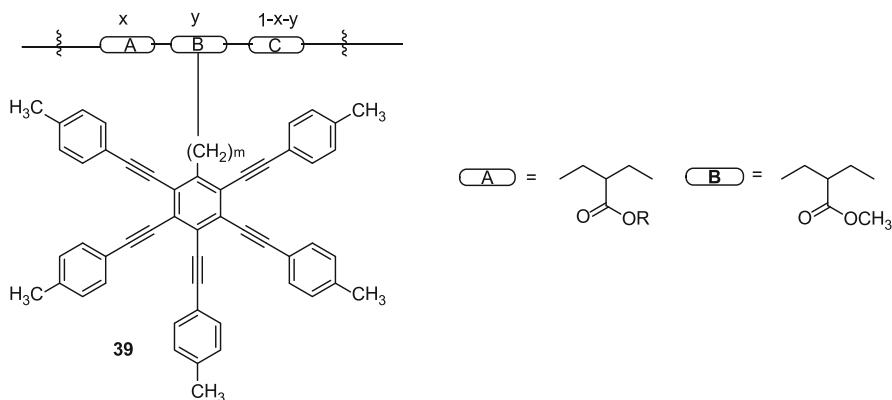
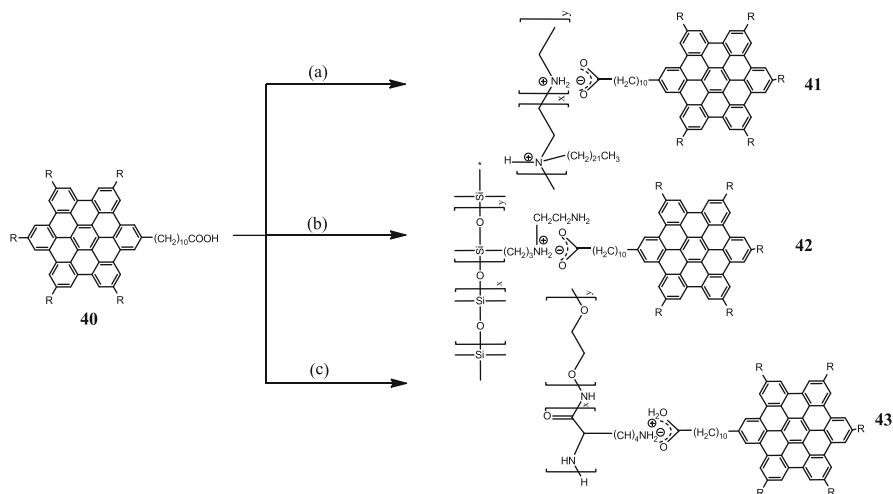


Fig. 20.6 Schematic diagram of Alkynylbenzene-Based side chain discotic liquid-crystalline co-polymers

copolymers is shown by **39** (Table 20.8, Fig. 20.6). All copolymers displayed nematic columnar phase at lower temperatures. The weight fraction of mesogen in copolymer highly affect thermal behavior of these polymers. Thermal behaviour of these polymers suggested that, higher percentage of discotic mesogen in copolymer increases the glass transition as well as clearing temperature and induce the formation of nematic phase at higher temperature.

20.2.2 Hexabenzocoronene-Based Side Chain Ionic Discotic Liquid Crystal Polymers

Pericondensed hexabenzocoronenes (HBC) show diode-like current–voltage signals for single molecules (Stabel et al. 1995) and a rapid charge transport along self-assembled columns with high charge carrier mobility. Again in columnar phase one



Scheme 20.7 Synthesis of hexabenzocoronene-based side-chain ionic polymers: (a) polyethyleneimine, (b) polysiloxane, (c) poly(ethylene oxide)-block-poly(L-lysine)

dimensional charge transport makes these molecules promising as nanowires in molecular electronic devices. To explore these advantages Mullen and co-workers prepared HBC-based side-chain ionic polymers. The polymers were prepared via acid–base reaction of HCB carrying carboxylic acid moiety and polymer backbones like polyethyleneimine (Thunemann et al. 1999), polysiloxane (Thunemann et al. 2000), and poly(ethylene oxide)-block-poly(L-lysine) (Thünemann et al. 2002) (Scheme 20.7).

To prepare the **41** carboxylic acid functionalized HBC was complexed with hydrophobically modified polyethyleneimine. The X-ray studies revealed that, the polymer **41** exhibit rectangular mesophase morphology at room temperature and transform into ordered hexagonal columnar phase on heating up to 110 °C. Inter-columnar order was found higher in case of noncomplex HBC derivative **40** as compare to **41**. Whereas intra-columnar long range order in the polyethyleneimine complex of HBC **41** was more than HBC **40**. The polymer **42** having amino-functionalized polysiloxane backbone shows columnar-to-columnar (Col₁-to-Col₂) transition at 90 °C in heating cycle, however in cooling cycle this transition appears at 57 °C. The Col₁ phase possesses short-range intra-columnar order with tilted arrangement of HBC disks with respect to the column axis, whereas Col₂ phase have long range of intracolumnar order. The intracolumnar ordering of complex **42** follows same trend like **41**, when compared with **40**.

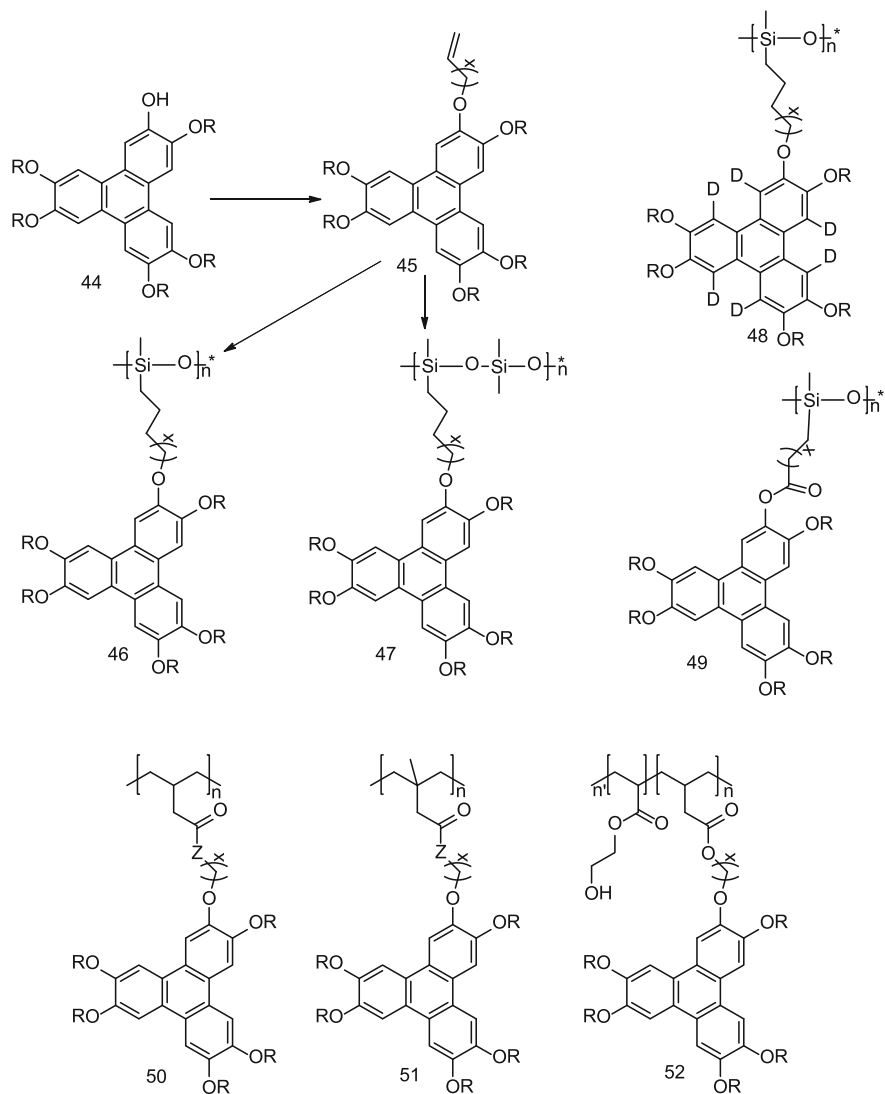
Poly(ethylene oxide)-block-poly(L-lysine) (PEO-PLL))was complexed with an amphiphilic hexaperi-hexabenzocoronene (HBC) to produce the **43**. Due to the self-organizing property of poly(L-lysine) blocks polymer, backbone of **43** form a R-helical. This helix was surrounded symmetrically by six discotic columns of HBC. The dense packing of these helixes and columns produces hexagonal

sublattices (formed by the columns) in the frame of a two-dimensional hexagonal lattice (formed by the helices). It shows a columnar-columnar (Col₁-to -Col₂) phase transition at 54 °C. From above three example, it is clear that Polymer chains is highly responsible for unexpected higher intracolumnar order at the higher temperature phase as compared to the lower temperature mesophase.

20.2.3 Triphenylene-Based Side-Chain Polymers

Triphenylene-Based Side-Chain Polymers are probably the most widely studied DLCs and particularly promising because of their relatively easy availability, self-assembly ability and high performance. These polymers have been extensively investigated for their mesomorphic and physical properties. A mono-functionalized triphenylene (TP) derivative is the basic requirement to prepare these polymers. Ringsdorf and co-workers functionalized mono-functionalized triphenylene (TP) derivatives **44** with 10-undecenyl bromide to produce 3,6,7,10,11-pentakis (pentyloxy)-2-(10-undecenoxy)-TP **45**. These TPs **45** produces side-chain triphenylene polymers **46** and **47** when reacting with Si-H containing polymers (Scheme 20.8). Both homopolysiloxane **46** and copolysiloxane **47** have broad glass transition and clearing transitions. Thermal transitions of these class of polymer (with polysilican backbone) are given in Table 20.9. Polymer **46** shows the phase behavior, g -19 Col 39 I on thermal annealing at 20 °C for 2 days. In a different report, published by Werth and Spiess in 1993, different thermal behavior g -41 Col 75 I was reported. It shows the dependence of thermal behavior on polymer processing. The clearing temperature of these polymers increases on decreasing the spacer length (Werth and Spiess 1993) as shown in Table 20.9. The deuterated triphenylene-containing polysiloxane **48** shows nearly same phase behavior corresponding to undeuterated polymer **46a** (Hüser and Spiess 1988; Hueser et al. 1989). The polymers with ester linkages **49** exhibit higher clearing temperature as compare to polymer with ether linkages **46-48**.

The mono functionalized Triphenylene unit can undergo free radical polymerization by functionalizing it with acrylate or methacrylate group. Variety of liquid crystalline homopolymer and copolymers were reported with different lateral side chains, spacer and polymer backbones via this route. A generalised structure of these polymers **50-52** are presented in Scheme 20.8 and there thermal transition are summarized in Table 20.10 along with side chains and spacer lengths. The polymer **50a** and **51a** changes its behaviour from amorphous polymers to nematic columnar liquid crystalline polymers on doping with trinitrofluorenone (TNF) (Ringsdorf et al. 1989). Because of the rigid nature of methacrylate-based polymer backbone, only polyacrylates **50b** show liquid crystalline behavior among **50b** and **51b**. However, Imrie and Boden groups have shown that, polymethacrylates triphenylene containing suitable substituent can form columnar phases (Boden et al. 1998). The low glass transition at 2 °C and a mesophase to isotropic phase transition at 45 °C shown by polymer **51c** was attributed to high polydispersity (Stewart et al. 1998).



Scheme 20.8 Synthesis of triphenylene-based side-chain polysiloxanes: (a) poly(methylsiloxane), toluene, H_2PtCl_6 ; (b) poly(dimethylsiloxane-*co*-methylsiloxane), toluene, H_2PtCl_6

These acrylate functionalized Triphenylene monomers were mixed with 2-hydroxyethyl acrylate or methyl acrylate functionalized triphenylene monomer to produce copolymers with a general structure **52**. Copolymer with building block triphenylene and 2-hydroxyethyl acrylate exhibit mesophase to isotropic transitions between 104 and 165 °C depending upon their composition (Talroze et al. 2000).

Table 20.9 Thermal behavior of triphenylene-containing polysiloxanes

Structure	R	<i>x</i>	Phase transition	References
46a	C ₅ H ₁₁	9	g -19 Col 39 I	Boden et al. (1999)
			g -41 Col _h 75 I	Imrie et al. (2004)
46a'	C ₅ H ₁₁	9	g -35 Col 75 I	Karthaus et al. (1992)
46b	C ₅ H ₁₁	3	g -53 Col _h 141 I	Imrie et al. (2004)
46c	C ₅ H ₁₁	6	g -52 Col _h 131 I	
47	C ₅ H ₁₁	9	g -29 Col 36 I	Boden et al. (1999)
48	C ₅ H ₁₁	9	g -35 Col 75 I	Kouwer et al. (2000)
49a	C ₅ H ₁₁	3	g -54 Col _h 171 I	Imrie et al. (2004)
49b	C ₅ H ₁₁	6	g -51 Col _h 186 I	
49c	C ₅ H ₁₁	9	g -37 Col _h 112 I	
49d	C ₇ H ₁₅	9	g -62 Col _h 112 I	
49e	CH ₂ CH ₂ CH(CH ₃) ₂	9	Col _h 81 I	

Source: Kreuder and Ringsdorf (1983) and Werth and Spiess (1993) and Hueser et al. (1989) and Hüser and Spiess (1988)

Table 20.10 Thermal behavior of triphenylene-containing polyacrylates and methacrylates

Structure	R	<i>x</i>	Z	Phase transition	References
50a	(CH ₂) ₂ O (CH ₂) ₂ OCH ₃	0	(CH ₂ CH ₂ O) ₃	g -6 I	Kouwer et al. (2001a)
50b	C ₅ H ₁₁	11	O	g -8 Col _h 39 I	Imrie et al. (2004)
50c	C ₆ H ₁₃	6	O	g 5 Col 84 I	Kouwer et al. (2001b)
50d	C ₆ H ₁₃	0	(CH ₂ CH ₂ O) ₂	Col 117 I	Kouwer et al. (2001b)
51a	C ₅ H ₁₁	6	O	g 30 I	Kouwer et al. (2001c)
51b	C ₅ H ₁₁	11	O	g -16	Imrie et al. (2004)
51c	C ₆ H ₁₃	11	O	g 2 Col 45 I	Kouwer et al. (2001c)

Source: Ringsdorf et al. (1989) and Werth and Spiess (1993) and Boden et al. (1998) and Stewart et al. (1998)

However, copolymer of triphenylene-based acrylate and methyl acrylate was reported non liquid crystalline.

The malonate-terminated triphenylene-based monomer **53** was condensed with a, α,ω -diols to produce triphenylene-based side-chain polyesters **54** and **55** (Fig. 20.7) (Catry et al. 1993). Thermal studies shows that, polymers **54** is nonmesomorphic with a glass transition at -10 °C, whereas polyester **55** show liquid crystalline (LC) behaviour with thermal transitions, g -20 LC 35 I. The isophthalate-terminated triphenylene-based monomer was condensed with polyethylene glycol (PEG 300) by Imrie co-workers to furnish the polymer **56** (Imrie et al. 2004). The polymer exhibits the thermal transition behaviour g -17 lc 47 I.

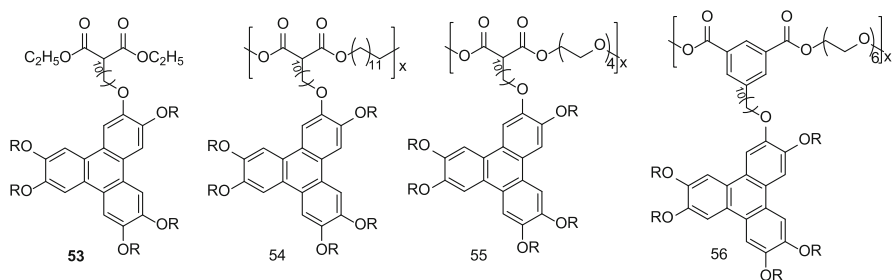


Fig. 20.7 Schematic diagram of malonate-terminated triphenylene-based monomer **53** and polymers

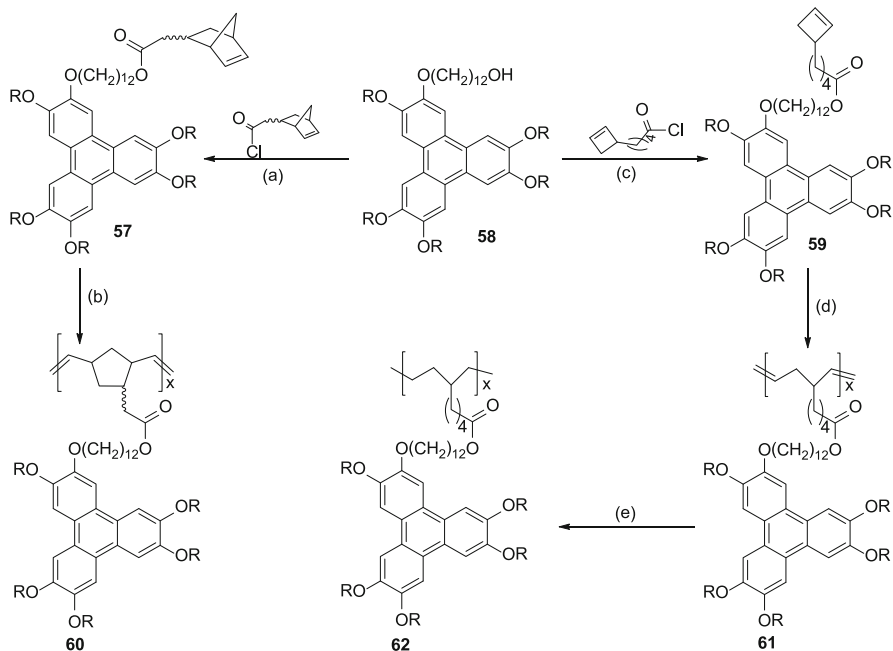
Table 20.11 Thermal behavior of polynorbornene-, polybutadiene-, and polybutane-bearing alkoxytriphenylenes triphenylene-based poly(1-alkyne)s

Structure	R	Phase transition	References
60a	C ₅ H ₁₁	g –4 I	Kouwer et al. (2002a)
60b	C ₁₀ H ₂₁	g –3 Colh 36 Colh 42 I	
61a	C ₅ H ₁₁	g –12 I	
61b	C ₁₀ H ₂₁	g –17 Colh 37 Colh 45 I	
62a	C ₅ H ₁₁	g –17 I	
62b	C ₁₀ H ₂₁	g –18 Colh 34 Colh 43 I	
64a	C ₄ H ₉	Colh 132.9 I	Kouwer et al. (2002b)
64b	C ₅ H ₁₁	g 113.8 Colh 156 I	
64c	C ₆ H ₁₃	g 115.1 Colh 160.3 I	
64d	C ₇ H ₁₅	Colh 154.3 I	
64e	C ₈ H ₁₇	Colh 144.6 I	
64f	C ₉ H ₁₉	g 115.7 Colh 139.1 I	

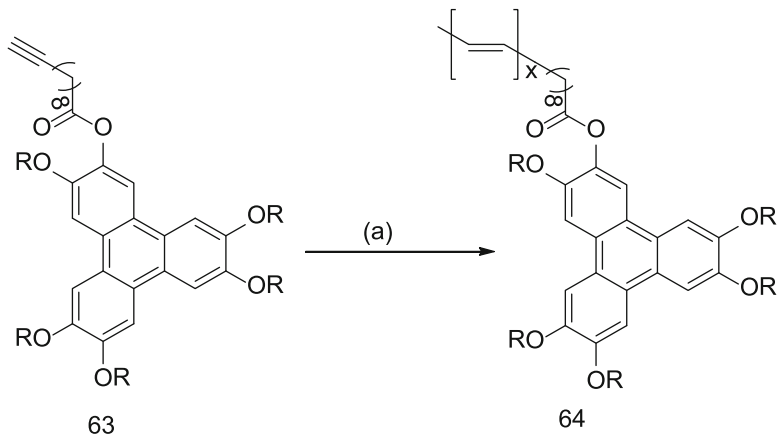
Source: Weck et al. (1997) and Xing et al. (2008)

Ring-opening metathesis polymerization was also explored by functionalizing Triphenylene terminal with norbornenes **57**, and butadienes **59** to produce polymer **60** and **61** (Scheme 20.8) (Weck et al. 1997). Thermal behavior of these polymers is given in Table 20.11. The polymers **60b** and **61b** with long lateral alkyl chain (decyl) exhibit columnar mesophases, whereas polymer **60a** and **61a** with short lateral alkyl chains (pentyl) found to be non-liquid crystalline. On Further reduction of polybutadiene polymer **62b** turns out to be liquid crystalline (Scheme 20.9).

Metal catalysed polymerization of alkyne-terminated triphenylene derivative **63** using molybdenum-based catalysts, tungsten-based catalysts and rhodium-based catalyst was tried to produce Triphenylene-Based Side-Chain Polymers by Zhao and co-workers (Scheme 20.10) (Xing et al. 2008). However, only rhodium-based catalyst, [Rh(norbornadiene)Cl]₂, in THF/Et₃N yielded the desired polymer **64a–f** in good yield. These polymers were found more thermal stable than unsubstituted poly(1-alkyne)s and exhibit hexagonal columnar mesophase. The hexagonal mesophase of polymers with small and long peripheral chains has homogenous



Scheme 20.9 Synthesis of triphenylene-based side-chain polynorbornene and polybutadiene: (a) THF, triethylamine, reflux, 16 h; (b) $\text{Cl}_2(\text{PCy}_3)_2\text{Ru}=\text{CPhH}$, CH_2Cl_2 ; (c) SOCl_2 , THF, triethylamine, r.t., 16 h; (d) $\text{Cl}_2(\text{PCy}_3)_2\text{Ru}=\text{CPhH}$, CH_2Cl_2 ; (e) $[\text{Ir}(\text{COD})(\text{C}_y)_3(\text{py})]\text{PF}_6$, CH_2Cl_2 , 55 °C, 16 h

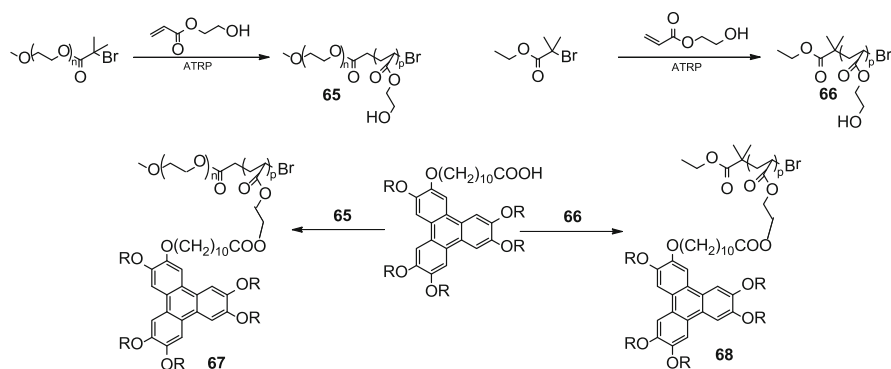


Scheme 20.10 Synthesis of triphenylene-based side-chain polyalkynes: (i) $[\text{Rh}(\text{norbornadiene})\text{Cl}]_2$, THF: Et_3N (3:1 v/v), r.t., 24 h

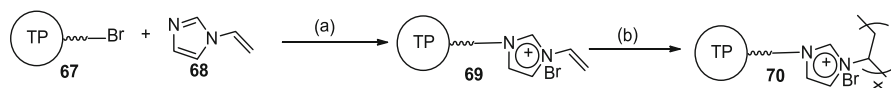
hexagonal columnar lattice, whereas polymers with medium chain length exhibit hexagonal lattice with mixed structures. Thermal transitions of these polymers with different peripheral lateral alkyl chains are listed in Table 20.11.

To understand the interrelation of microstructures and the discotic mesogenic orders, a series of diblock copolymers **67** and **68** having Triphenylene and PEG blocks have been prepared by Dongzhong Chen et al. using atom transfer radical polymerization (ATRP) (Scheme 20.11) (Wu et al. 2013). The copolymers having different weight fraction of DLC blocks in range 37–90 % were synthesised. The copolymers with lower DLC contents ($f_{w,dlc} = 37\%$ and 43%) were shown to form lamellar structures of variant periods and undergo order-order transition at $45\text{ }^{\circ}\text{C}$. The different discotic mesophases transition was observed at $25\text{ }^{\circ}\text{C}$. The copolymer with intermediate DLC content ($f_{w,dlc} = 62\%$) above $35\text{ }^{\circ}\text{C}$ from nanocylinders of amorphous PEG packed in hexagonal matrix of DLC, which turned into a mixed lamellar structure with PEG region crystallization upon cooling below $35\text{ }^{\circ}\text{C}$. The copolymers with higher DLC content ($f_{w,dlc} = 67\text{--}80\%$) exhibits HPC structure with the DLC matrix showing Ncol or ND mesophases. For copolymers with 90 % DLC overall ND phase was observed resembling the ordered columnar phase formed by their corresponding DLC homopolymers.

To prepare a novel polymeric material useful for unidirectional ion transport at nanoscale Pal and Kumar (2008) prepared triphenylene-imidazole-based side-chain ionic liquid crystalline polymer (Scheme 20.12). The triphenylene-bearing imidazolium salt **69** was synthesised by reacting brominated triphenylene **67** with 1-vinylimidazole. The photopolymerization of **69** with a



Scheme 20.11 Synthesis of reactive polymer precursor through ATRP **65** and **66** and the TP-Based Side Chain Discotic LC Homopolymer **68** and Copolymers **67**



Scheme 20.12 Synthesis of triphenylene-imidazole-based side-chain ionic polymers: (a) toluene, reflux, 8 h; (b) 2,2-dimethoxy-2-phenylacetophenone, $100\text{ }^{\circ}\text{C}$, r.t., *h\nu*

photoinitiator 2,2-dimethoxy-2-phenylacetophenone yielded polymer **70**. The polymer **70** is a glassy material at room temperature, on heating up to 224 °C transform to rectangular columnar phase.

20.3 Discotic Liquid Crystal Elastomers

The properties of Liquid crystal elastomers having orientation order, responsive molecular shape, and quenched topological constraints made them potential candidate for various industrial applications like sensors, micro-robots, micro-pumps, and actuators. Considering the potential of them, calamitic elastomers has been explored up to a great extent, however very few reports are there on Discotic Elastomers.

Ringsdorf et al. was prepared the first discotic elastomer using an olefin-terminated monofunctionalized triphenylene derivative **71** and two cross-linkers **72** and **73** with different reactive groups (Bengs et al. 1993). Due to the reactivity difference in olefinic group and a methacryloyl group during the first step of crosslinking reaction, vinyl groups almost react completely, whereas methacryloyl group remains unreacted. This weakly cross-linked network can deform to obtain a macroscopic alignment of the liquid crystalline phase. In second step locking of this anisotropic network was done by reciting methacryloyl group. Figure 20.8

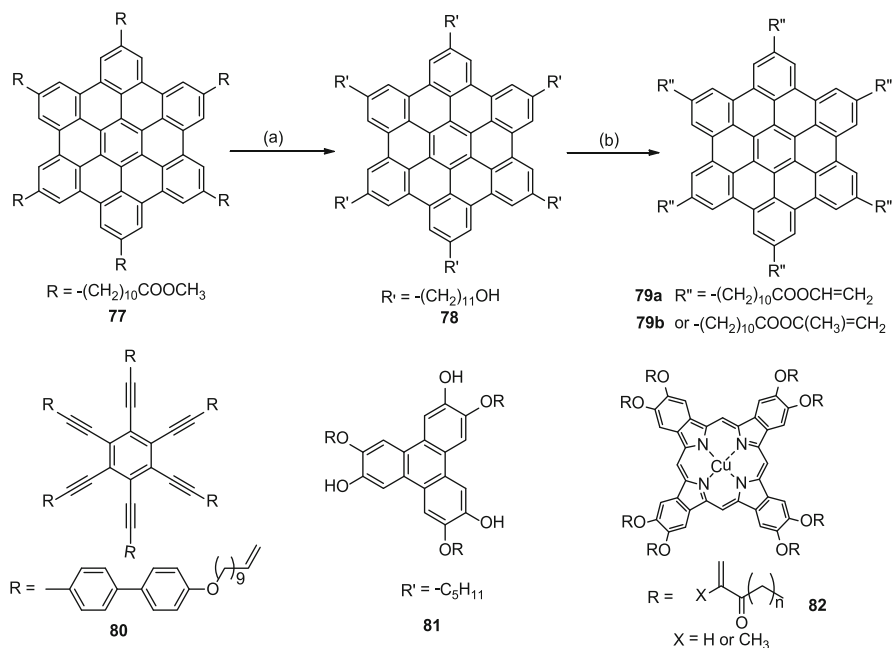


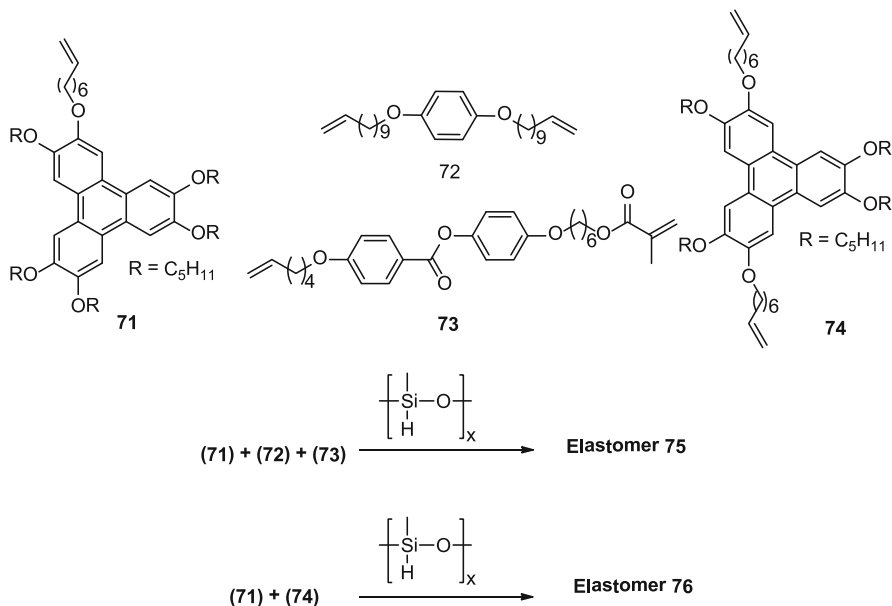
Fig. 20.8 (a) LiAlH_4 in THF; (b) N,N -dimethylaniline, 2,6-di-tert-butyl-p-cresol in THF, acryloyl chloride or methacryloyl chloride

represents the schematic diagram of these elastomers. To understand the mechanical strain effect prior to the second cross-linking process polymer **75b** was prepared without applying the mechanical field, whereas **75a** with same methodology. The polymers **76a–e** were synthesised by replacing bifunctional calamitic cross-linker with bifunctional triphenylene-based cross-linker in different loading proportions to avoid the columnar packing disturbance caused by calamitic cross-linker (Disch et al. 1995). Table 20.12 summarized the thermal transitions of these polymers (Scheme 20.13).

Table 20.12 Thermal behavior of triphenylene-based discotic elastomers

Structure	Phase transition	Reference
75a	g –50 Col 28 I	Kouwer et al. (2004)
75b	g –50 Col 28 I	
76a	g –50 Col 106 I	
76b	g –49 Col 94 I	
76c	g –50 Col 94 I	
76d	g –45 Col 78 I	
76e	g –44 Col 76 I	

Source: Bengs et al. (1993) and Disch et al. (1995)



Scheme 20.13 Schematic diagram of triphenylene-based discotic elastomers

20.4 Liquid Crystalline Hyperbranched Polymer

Klaus Mullen et al. were reported synthesis of hexa-*peri*-hexabenzocoronene (HBC) substituted with terminal acryloyl **79a** and methacryloyl **79b** functionalized *n*-alkyl chains (Boden et al. 2000). Hexasubstituted hexa-*peri*hexabenzocoronene derivatives were prepared via cobalt octacarbonyl catalysed cyclotrimerization of suitably substituted diphenylacetylenes, followed by an oxidative cyclodehydrogenation with iron (III) chloride dissolved in nitromethane. Hyperbranched Polymers containing HBC was achieved via thermal polymerization of HBC derivatives containing acryloyl or methacryloyl functions at the terminal position of the alkyl chains in liquid crystalline phase. Columnar superstructure of liquid crystalline phase was preserved during and after polymerization and stable between -100 and 300 °C.

Suzuki and group synthesised the monomeric hexayne **80** having six terminal double-bond containing biphenyl unit to prepare the Alkynylbenzene-Based Discotic hyperbrached polymers. The monomeric hexayne **80** having six terminal double-bond containing biphenyl units can be photopolymerized to yield the polymer. Hyperbranched Polymer had glass transition temperature at 51 °C and exhibit liquid crystalline phase above 230 °C up to decomposition due to high cross-linked network (Suzuki and Koide 2001).

Triphenylene-based hyperbranched polymer were reported by Zhang et al. (2007). Triphenylene derivative 2,6,10-trihydroxy-3,7,11-tripentyloxytriphenylene **81** was reacted with adipoyl chloride in pyridine and THF followed by quenching the terminal phenolic hydroxyl groups by adding butyryl chloride to obtain the triphenylene based hyperbranch polymer. This hyperbranched polymer was reported to be liquid crystalline in temperature range of 165 – 180 °C.

To produce the phthalocyanines based hyperbranch polymer van der Pol et al. synthesised Phthalocyanines substituted with eight terminally acryloyl or methacryloyl functionalized alkoxy chains **82** (Van der Pol et al. 1990). Thermal polymerization of **82** produces a highly branched polymer network. While photo polymerization of the acrylate failed to produce any polymer, thermal polymerization of the acrylate as well as methacrylate in the columnar mesophase leads to liquid crystalline hyperbranch polymer. These polymer do not show any phase transition in DSC probably due to the formation of highly cross-linked network. The columnar nature of the mesophase formed by these polymers was revealed by X-ray diffraction studies.

20.5 Discotic Liquid Crystalline Dendritic Polymers

Dendritic polymers are special class of polymer composed of a large number of monomer units that were chemically linked together. Due to their wide range of applications like adhesives and coatings, chemical sensors, drug-delivery systems,

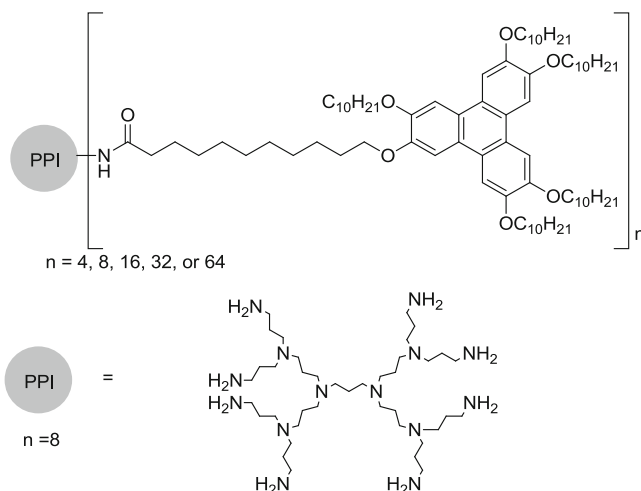


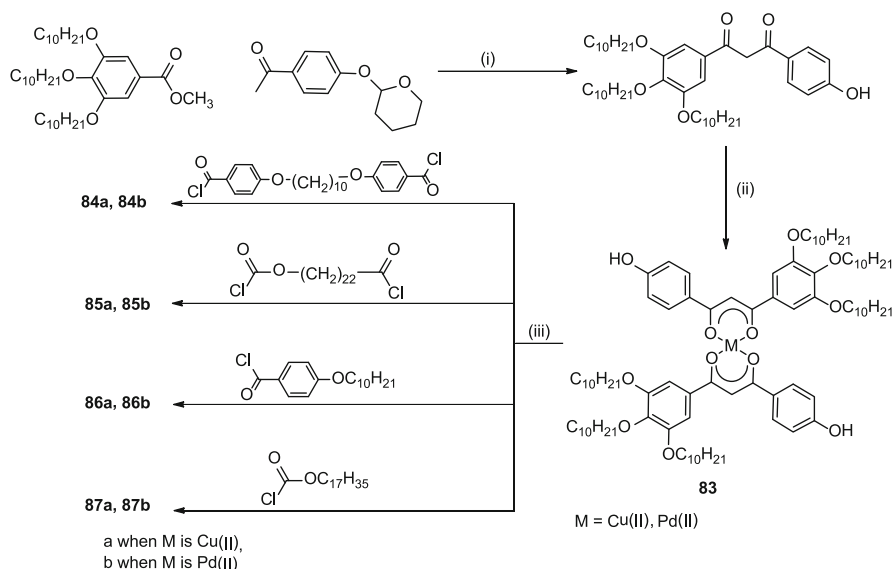
Fig. 20.9 Schematic diagram of Discotic Liquid Crystalline Dendritic polymers

high-performance polymers, catalysts, separation agents etc., their literature is always getting rich.

Dendrimers tend to adopt the spherical structure to minimize the free energy associated with them. However, incorporation of anisotropic mesogenic units at the periphery deviates them from this spherical structure due to the strong interactions between such units. McKenna MD et al. (2004) have reported the attachment of discotic triphenylene moieties to the first five generations of commercially available PPI-(NH₂)_n dendrimers (Fig. 20.9), which produce the highly ordered hexagonal columnar mesophases in the second to fifth generations and rectangular columnar mesophases for the first generation. The mesophase temperature range of the dendrimers is larger and start at low temperature as compare to analogous low molecular weight unit, hexakis-(decyloxy)triphenylene. These compounds were highly ordered as compare to previously reported columnar dendrimers (Cameron et al. 1997; Marcos et al. 2001).

20.6 Metallomesogenic Discotic Liquid Crystalline Polymers

Metallomesogenic polymers are relatively new area in the field of DLCPs. The metal present in these polymers can afford new and unexpected physical properties that can be combined with the process ability inherent in the polymer system. Metallomesogenic polymers having discotic units have been synthesised using diketones complex of Cu(II) and Pd(II) by Valdebenito et al. (2000). Synthesis of polymers is given below (Scheme 20.14). All the polymers 84a–b and 85a–b



Scheme 20.14 synthesis of Metallomesogenic discotic intermediate (i) NaOH in 1,2-dimethoxy ethane; (ii) Copper(II)acetate in ethanol or Palladium acetate in ethanol/methanol (1/2); (iii) dry 1,1,1,2-tetrachloroethane

prepared exhibit columnar mesophases. The low molecular weight monomer exhibit a columnar hexagonal mesophases. More flexible polymer 85a-b shows a hexagonal mesophase whereas rigid polymer 1a-b exhibit a columnar rectangular mesophases. Fibers of these polymers have an orientation of the polymeric chain along the stretching direction and the disk-like unit are arranged in columns perpendicular to the fibers axis (Fig. 20.10). Thermal transitions of these polymers are given in the Table 20.13.

20.7 Conclusion

In conclusion, LCPs containing Disc-shape mesogens are relatively new area of research. Variety of DLCPs are synthesised by varying the Disc shape and polymer back bone. The attachment of discotic mesogens on polymer backbone can be achieved via different methods, like polymer substitution reaction, free radical polymerization, ring opening metathesis etc. By changing the disc shape and its position on the polymer back bone physical properties of DLCPs can be tailored. Their thermal transitions were found to be very much related to the peripheral lateral chains and the nature of polymer back bone.

Again, self-assembling nature of discotic mesogens into columnar phase helps in unidirectional charge or ion transfer. These unidirectional charge or ion transfer

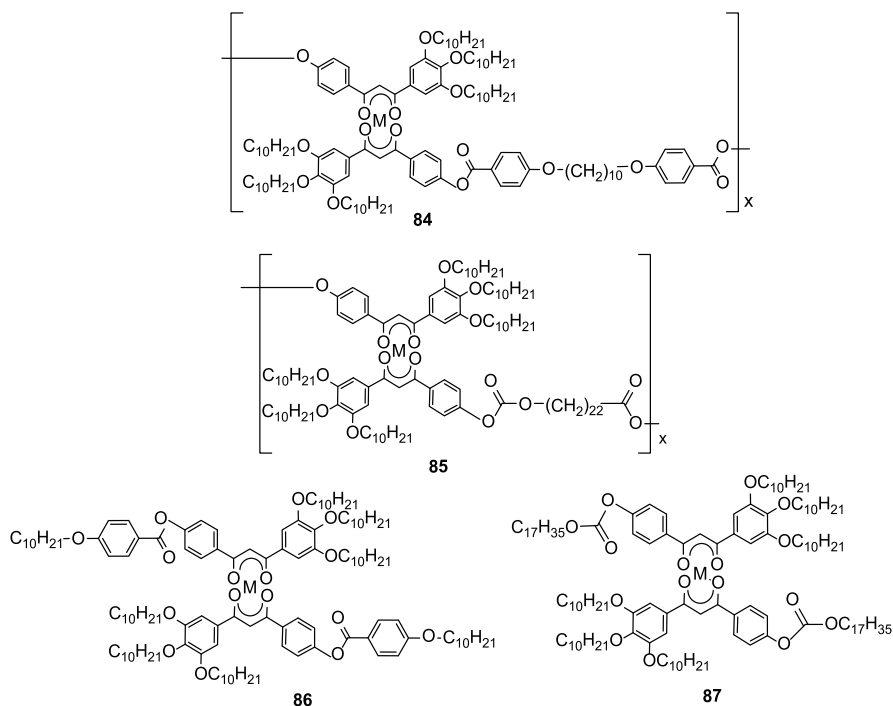


Fig. 20.10 Schematic diagram of Metallomesogenic discotic polymers and low weight analogues

Table 20.13 Thermal transitions of metallomesogenic discotic polymers and low molecular weight analogues

Structure	Phase transitions	Reference
84a	g 88 Col _r 193 I	Kreuder and Ringsdorf (1983)
84b	Col _r , dec at T 170 C	
85a	Col _h 135 I	
85b	C 60 Col _h 103 I	
86a	C 55 C' 78 Col _h 106 I	
	I 105 Col _h 42 C'	
	C' 76 Col _h 107 I	
86b	Col _h 115 I	
	I 115 Col _h 14 C'	
	Cr 72,91 Col _h 115 I	
87a	C 60 Col _h 116 I	
	I 115 Col _h 18 C'	
	C' 55 Col _h 114 I	
87b	C 53 Col _h 120 I	
	I 116 Col _h 6 C'	
	C' 40 Col _h 113 I	

Source: Valdebenito et al. (2000)

properties can be potentially used for various applications like, catalysts for redox reactions, organic field-effect transistors, storage in quantum computing, sensors, micro-robotics, micro-pumps, and actuators to solve the energy and health problems.

References

- Bengs H, Finkelmann H, K pfer J, Ringsdorf H, Schuhmacher P (1993) Highly oriented discotic elastomers. *Makromol Chem Rapid Commun* 14:445–450
- Bisoyi HK, Kumar S (2008) Carbon nanotubes in triphenylene and rufigallol-based room temperature monomeric and polymeric discotic liquid crystals. *J Mater Chem* 18:3032–3039
- Boden N, Bushby RJ, Cammidge AN (1995) Triphenylene-based discotic-liquid-crystalline polymers: a universal, rational synthesis. *J Am Chem Soc* 117:924–927
- Boden N, Bushby RJ, Lu ZB (1998) A rational synthesis of polyacrylates with discogenic side groups. *Liq Cryst* 25:47–58
- Boden N, Bushby RJ, Eichhorn H, Lu Z-B, Abeysekera R, Robardes AW (1999) Discotic liquid crystalline block copolymers 2: main-chain discotic liquid crystalline diblock and triblock copolymers. *Mol Cryst Liq Cryst Sci Technol Sect A Mol Cryst Liq Cryst* 332:293–302
- Boden N, Bushby RJ, Cooke G, Lozman OR, Lu Z (2001) CPI: a recipe for improving applicable properties of discotic liquid crystals. *J Am Chem Soc* 123:7915–7916
- Brand JD, K bel C, Ito S, M llen K (2000) Functionalized hexa-peri-hexabenzocoronenes: stable supramolecular order by polymerization in the discotic mesophase. *Chem Mater* 12:1638–1647
- Bryant GC, Cook MJ, Ryan TG, Thorne AJ (1995) Liquid crystalline polymeric phthalocyanines. *J Chem Soc Chem Commun* 4:467–468
- Cameron JH, Facher A, Lattermann G, Diele S (1997) Poly(propyleneimine) dendromesogens with hexagonal columnar mesophase. *Adv Mater* 9:398–403
- Caseri W, Sauer T, Wegner G (1988) Soluble phthalocyaninato-polysiloxanes: rigid rod polymers of high molecular weight. *Makromol Chem Rapid Commun* 9:651–657
- Catry C, Van der Auweraer M, De Schryver FC, Bengs H, H ussling L, Karthaus O, Ringsdorf H (1993) Conductivity and photoconductivity of undoped and doped Langmuir-Blodgett films of a polymer with hexaalkoxytriphenylene side-groups. *Makromol Chem* 194:2985–2999
- Cook MJ (1995) Liquid crystalline oligomeric and polymeric phthalocyanines. *Adv Mater* 7:877–880
- Disch S, Finkelmann H, Ringsdorf H, Schuhmacher P (1995) Macroscopically ordered discotic columnar networks. *Macromolecules* 28:2424–2428
- Dulog L, Gittinger A, Roth S, Wagner T (1993) Synthesis and characterization of poly [2,3,9,10,16,17,23,24-octakis(dodecyloxycarbonyl)phthalocyaninatogermoxane]. *Makromol Chem* 194:493–500
- Green MM, Ringsdorf H, Wagner J, W stefeld R (1990) Induction and variation of chirality in discotic liquid crystalline polymers. *Angewandte Chem* 29:1478–1481
- Herrmann-Sch nherr O, Wendorff JH, Ringsdorf H, Tschirner P (1986) Structure of an aromatic polyamide with disc-like mesogens in the main chain. *Makromol Chem Rapid Commun* 7:791–796
- Hueser B, Pakula T, Spiess HW (1989) Macroscopic ordering of liquid-crystalline polymers with discotic mesogens. *Macromolecules* 22:1960–1963
- H ser B, Spiess HW (1988) Macroscopic alignment of discotic liquid-crystalline polymers in a magnetic field. *Makromol Chem Rapid Commun* 9:337–343
- Imrie CT, Inkster RT, Lu Z, Ingram MD (2004) Discotic side group liquid crystal polymer electrolytes. *Mol Cryst Liq Cryst* 408:33–43

- Karhaus O, Ringsdorf H, Tsukruk VV, Wendorff JH (1992) Columnar ordering of liquid-crystalline discotics in Langmuir-Blodgett films. *Langmuir* 8:2279–2283
- Kouwer PHJ, Jager WF, Mijs WJ, Picken SJ (2000) Synthesis and characterization of a novel liquid crystalline polymer showing a nematic columnar to nematic discotic phase transition. *Macromolecules* 33:4336–4342
- Kouwer PHJ, Gast J, Jager WF, Mijs WJ, Picken SJ (2001a) A series of novel liquid crystalline polymers showing a nematic discotic and/or a nematic columnar phase. *Mol Cryst Liq Cryst Sci Technol Sect A Mol Cryst Liq Cryst* 364:225–234
- Kouwer PHJ, Jager WF, Mijs WJ, Picken SJ (2001b) The nematic lateral phase: a novel phase in discotic supramolecular assemblies. *Macromolecules* 34:7582–7584
- Kouwer PHJ, Mijs WJ, Jager WF, Picken SJ (2001c) Modeling of ND and NCol phase transitions in discotic side chain polymers by the extended McMillan theory. *J Am Chem Soc* 123:4645–4646
- Kouwer PHJ, Jager WF, Mijs WJ, Picken SJ (2002a) Charge transfer complexes of discotic liquid crystals: a flexible route to a wide variety of mesophases. *Macromolecules* 35:4322–4329
- Kouwer PHJ, van den Berg O, Jager WF, Mijs WJ, Picken SJ (2002b) Induced liquid crystalline diversity in molecular and polymeric charge-transfer complexes of discotic mesogens. *Macromolecules* 35:2576–2582
- Kouwer PHJ, Jager WF, Mijs WJ, Picken SJ (2003) Specific interactions in discotic liquid crystals. *J Mater Chem* 13:458–469
- Kouwer P, Jager W, Mijs W, Picken S (2004) Substituent effects in discotic liquid crystals. *Mol Cryst Liq Cryst* 411:305–312
- Kreuder W, Ringsdorf H (1983) Liquid crystalline polymers with disc-like mesogens. *Makromol Chem Rapid Commun* 4:807–815
- Kreuder W, Ringsdorf H, Tschirner P (1985) Liquid crystalline polymers with disc-like mesogens in the main chain. *Makromol Chem Rapid Commun* 6:367–373
- Lange U, Roznyatovskaya NV, Mirsky VM (2008) Conducting polymers in chemical sensors and arrays. *Anal Chim Acta* 614:1–26
- Malthete J, Collet A (1987) Inversion of the cyclotribenzylene cone in a columnar mesophase: a potential way to ferroelectric materials. *J Am Chem Soc* 109:7544–7545
- Malthete J, Collet A, Levelut A-M (1989) Mesogens containing the DOBOB group. *Liq Cryst* 5:123–131
- Marcos M, Giménez R, Serrano JL, Donnio B, Heinrich B, Guillon D (2001) Dendromesogens: liquid crystal organizations of poly(amidoamine) dendrimers versus starburst structures. *Chem A Eur J* 7:1006–1013
- McKenna MD, Barberá J, Marcos M, Serrano JL (2004) Discotic liquid crystalline poly(propylene imine) dendrimers based on triphenylene. *J Am Chem Soc* 127:619–625
- Mertesdorf C, Ringsdorf H (1989) Self-organization of substituted azacrowns based on their discoid and amphiphilic nature. *Liq Cryst* 5:1757–1772
- Ogasawara M, Funahashi K, Iwata K (1985) Enhancement of electric conductivity of polypyrrole by stretching. *Mol Cryst Liq Cryst* 118:159–162
- Orthmann E, Wegner G (1986) Preparation of ultrathin layers of molecularly controlled architecture from polymeric phthalocyanines by the Langmuir-Blodgett-technique. *Angewandte Chem* 25:1105–1107
- Pal SK, Kumar S (2008) Novel triphenylene-based ionic discotic liquid crystalline polymers. *Liq Cryst* 35:381–384
- Percec V, Cho CG, Pugh C (1991) Alkyloxy-substituted CTTV derivatives that exhibit columnar mesophases. *J Mater Chem* 1:217–222
- Percec V, Cho CG, Pugh C, Tomazos D (1992) Synthesis and characterization of branched liquid-crystalline polyethers containing cyclotetraeratrlylene-based disk-like mesogens. *Macromolecules* 25:1164–1176
- Picken S, Kouwer P, Jager W, Wübbenhorst M, Mijs W (2004) Dynamics and phase transitions in discotic and calamitic liquid crystal side-chain polymers. *Mol Cryst Liq Cryst* 411:503–513

- Raja KS, Raghunathan VA, Ramakrishnan S (1998) Synthesis and properties of main chain discotic liquid crystalline polyethers based on Rufigallol. *Macromolecules* 31:3807–3814
- Ringsdorf H, Tschirner P, Hermann-Schönherr O, Wendorff JH (1987) Synthesis, structure, and phase behaviour of liquid-crystalline rigid-rod polyesters and polyamides with disc-like mesogens in the main chain. *Makromol Chem* 188:1431–1445
- Ringsdorf H, Wüstefeld R, Zerta E, Ebert M, Wendorff JH (1989) Induction of liquid crystalline phases: formation of discotic systems by doping amorphous polymers with electron acceptors. *Angewandte Chem* 28:914–918
- Sauer T (1993) Hexagonal-columnar mesophases in substituted phthalocyaninato-polysiloxanes. *Macromolecules* 26:2057–2063
- Sauer T, Wegner G (1991) Small-angle X-ray scattering from dilute solutions of substituted phthalocyaninato-polysiloxanes. *Macromolecules* 24:2240–2252
- Schouten PG, Warman JM, De Haas MP, Van der Pol JF, Zwikker JW (1992) Radiation-induced conductivity in polymerized and nonpolymerized columnar aggregates of phthalocyanine. *J Am Chem Soc* 114:9028–9034
- Sielcken OE, Van de Kuil LA, Drenth W, Schoonman J, Nolte RJM (1990) Phthalocyaninato polysiloxanes substituted with crown ether moieties. *J Am Chem Soc* 112:3086–3093
- Sirlin C, Bosio L, Simon J (1987) Spinal columnar liquid crystals: polymeric octasubstituted [small micro]-oxo-(phthalocyaninato)titan(IV). *J Chem Soc Chem Commun* 5:379–380
- Sirlin C, Bosio L, Simon J (1988a) Polycondensation in mesomorphic phases: spinal columnar liquid crystals based on octasubstituted phthalocyanine siloxane derivatives. *Mol Cryst Liq Cryst* 155:231–238
- Sirlin C, Bosio L, Simon J (1988b) Spinal columnar liquid crystals based on octasubstituted phthalocyanine siloxane derivatives. *J Chem Soc Chem Commun* 3:236–237
- Stabel A, Herwig P, Müllen K, Rabe JP (1995) Diodelike current–voltage curves for a single molecule—tunneling spectroscopy with submolecular resolution of an alkylated, peri-condensed hexabenzocoronene. *Angewandte Chem* 34:1609–1611
- Stewart D, Mchattie SG, Imrie TC (1998) Convenient synthesis of a discotic side group liquid crystal polymer. *J Mater Chem* 8:47–51
- Stoeva Z, Lu Z, Ingram MD, Imrie CT (2013) A new polymer electrolyte based on a discotic liquid crystal triblock copolymer. *Electrochim Acta* 93:279–286
- Suzuki D, Koide N (2001) Synthesis and Characterization of Biphenylethynylbenzene Type Discotic Liquid Crystal. *Mol Cryst Liq Cryst Sci Technol Sect A Mol Cryst Liq Cryst* 364:635–645
- Talroze RV, Otmakhova OA, Koval MA, Kuptsov SA, Platé NA, Finkelmann H (2000) Acrylate based polymers and networks containing triphenylene groups: synthesis and structures. *Macromol Chem Phys* 201:877–881
- Thunemann AF, Ruppelt D, Ito S, Mullen K (1999) Supramolecular architecture of a functionalized hexabenzocoronene and its complex with polyethyleneimine. *J Mater Chem* 9:1055–1057
- Thunemann AF, Ruppelt D, Burger C, Mullen K (2000) Long-range ordered columns of a hexabenzocoronene-polysiloxane complex: towards molecular nanowires. *J Mater Chem* 10:1325–1329
- Thünemann AF, Kubowicz S, Burger C, Watson MD, Tchegotareva N, Müllen K (2002) α -Helical-within-Discotic Columnar Structures of a Complex between Poly(ethylene oxide)-block-poly(L-lysine) and a Hexa-peri-hexabenzocoronene. *J Am Chem Soc* 125:352–356
- Van der Pol JF, Neeleman E, Van Miltenburg JC, Zwikker JW, Nolte RJM, Drenth W (1990) A polymer with the mesomorphic order of liquid crystalline phthalocyanines. *Macromolecules* 23:155–162
- Van Nostrum CF, Nolte RJM (1996) Functional supramolecular materials: self-assembly of phthalocyanines and porphyrazines. *Chem Commun* 21:2385–2392

- van Nostrum CF, Picken SJ, Schouten A-J, Nolte RJM (1995) Synthesis and supramolecular chemistry of novel liquid crystalline crown ether-substituted phthalocyanines: toward molecular wires and molecular ionoelectronics. *J Am Chem Soc* 117:9957–9965
- Vandevyver M, Albouy PA, Mingotaud C, Perez J, Barraud A, Karthaus O, Ringsdorf H (1993) In-plane anisotropy and phase change in Langmuir-Blodgett films of disklike molecules. *Langmuir* 9:1561–1567
- Voigt-Martin IG, Garbella RW, Schumacher M (1992) Structure and defects in discotic crystals and liquid crystals as revealed by electron diffraction and high-resolution electron microscopy. *Macromolecules* 25:961–971
- Valdebenito N, Oriol L, Barbera J, Díaz F, Serrano JL (2000) Liquid crystalline polymers containing discotic metallomesogens in the main chain. *Macromol. Chem. Phys.* 201, 2573–2580
- Wan W, Monobe H, Tanaka Y, Shimizu Y (2003) Mesomorphic properties of copolyesters of 3,6-linked triphenylene-based units and polymethylene spacers. *Liq Cryst* 30:571–578
- Weck M, Mohr B, Maughon BR, Grubbs RH (1997) Synthesis of discotic columnar side-chain liquid crystalline polymers by Ring-Opening Metathesis Polymerization (ROMP). *Macromolecules* 30:6430–6437
- Wenz G (1985) New polymers with disc-shaped mesogenic groups in the main chain. *Makromol Chem Rapid Commun* 6:577–584
- Werth M, Spiess HW (1993) The role of the spacer in discotic polymers. *Makromol Chem Rapid Commun* 14:329–338
- Wu B, Mu B, Wang S, Duan J, Fang J, Cheng R, Chen D (2013) Triphenylene-based side chain liquid crystalline block copolymers containing a PEG block: controlled synthesis, microphase structures evolution and their interplay with discotic mesogenic orders. *Macromolecules* 46:2916–2929
- Xing C, Lam JWY, Zhao K, Tang BZ (2008) Synthesis and liquid crystalline properties of poly (1-alkyne)s carrying triphenylene discogens. *J Polym Sci A Polym Chem* 46:2960–2974
- Zhang C, He Z, Mao H, Wang J, Wang D, Wang Y, Pu J (2007) Observation of disorder effects on charged carrier mobility in triphenylene-based discotic materials. *J Lumin* 123:931–935
- Zimmermann H, Poupko R, Luz Z, Billard J (1988) Tetrabenzocyclododecatetraene A new core for mesogens exhibiting columnar mesophases. *Liq Cryst* 3:759–770

Index

A

- Acyclic diene metathesis polymerization (ADMET), 375
- Alkynyl ligand-exchange, 524
- Alkynylbenzene, 596, 597
- Alternate current (AC) gate
 - operation, 308, 309
- Amphiphilic lipids, 277
- Aromatic main-chain polyesters, 453
- Atom transfer radical polymerization (ATRP), 66, 141–143, 376
 - macroinitiators, 67
 - ROP, 67
 - sequential, 66
 - synthetic route, 66
- Avrami equation, 24
 - activation energy, 27
 - degree of transformation, 26–27
 - double logarithmic form, 27
 - IM-Sm, 27
 - nucleation type and growth geometry, 24
 - P7MB, 24, 27
 - parameters, 24–26
- Avrami-Kolmogorov's kinetics, 416, 425
 - constant growth rates, 416
 - crystallization fractions, 417
 - flow-induced crystallization, 416–418
 - nucleation, 416
- Azobenzene (AZO), 151–156, 336
 - alignment, 338–339
 - aromatic rings, 333
 - block copolymers
 - ABA-type triblock copolymers, 152
 - AFM images, 152
 - amphiphilic property, 151, 155
 - LCBCPs, 151
 - LDBCs, 153, 155, 156
 - optical writing properties, 152
 - PAMAM, 153, 154
 - PEG, 153, 154
 - preparation of vesicles, 156
 - SMCMs, 152
 - spherical micelles, 155
- characteristics, 150
- cis–trans back-isomerization, 349–350
- crosslinked LCP film, 349
- electron transfer, photo-control of, 349
- floating monolayers, 348
- geometric isomers, 333
- LCE, 342
- macromolecular engineering, 149
- main-chain, 348
- mesogen, 348
- motion, 149
- osmotic pressure pumps, 349
- photoisomerization, 350
- side-chain LC polymers, 348
- siloxane, 350
- trans-azobenzene, 333
- triblock copolymer, 348
- Weigert effect, 150
- derivatives, 137

B

- Benzene, 587–589
- Biomacromolecules, 378–380
- Bisbenzylidene, 328, 333, 351

- Block copolymers (BCPs), 54, 65, 67, 68, 71, 72, 74–77, 80–82
- AB diBCPs
 - brush–rod diBCPs, 68
 - dendritic–rod diBCPs, 68
 - rod–coil diBCPs, 65
 - rod–rod diBCPs, 67
 - SCLCP–rod diBCPs, 68
 - ABC triBCPs, 69
 - coil–coil diBCPs, 55
 - rod–coil diBCPs, 55
 - rod–coil diBCPs, 56
 - rod–rod diBCPs, 56
 - self-assembly in bulk, 71
 - crystallization, 75
 - hierarchical structure, 72
 - irreversible OOTs, 76
 - LC phase formation, 74
 - microphase separation and properties, 71
 - morphological control, 75
 - ODTs, 76
 - reversible OOTs, 77
 - self-assembled nanostructures, 72
 - self-assembly in films, 78
 - self-assembly in solutions
 - ABA triBCPs, 82
 - brush–rod diBCPs, 80
 - dendritic–rod diBCPs, 81
 - rod_coil diBCPs, 80
 - star block copolymers, 70
- Burgers' model, 11
- C**
- Calamitic main-chain polymers
 - copper(II) salicylidimines, homopolymers of, 529
 - β -diketone derivatives, 531
 - ferrocene derivatives, 531
 - organometallic unit, 530
 - square planar transition, 528
- Calamitic mesogens, 134, 135, 137
- Calamitic side-chain polymers, 533, 534
- Carbon nanotube (CNT), 260, 261
- Cardanol, 275
- Cashew nut shell liquid (CNSL), 275
- Castor oil, 276
- Cellulose nano crystals (CNC), 279, 281, 282
- Cellulose, 283, 285
- Chain-transfer agent (CTA), 143
- Chitin, 289
- Chitosan, 290
- Click chemistry, 142
- Coefficient of thermal expansion (CTE), 12
- Collagen, 286
- Columnar thermotropic polymers
 - cofacial stacking, 535
 - phthalocyanines, 535, 536
 - porphyrines, 535
 - thermal behavior, 536
- Condensation polymerization, 365–374
 - MCSCCLCPs, 365–374
 - main-chain polymers, 140
- Continuum model, 422
- Controlled/living radical polymerization (CRP), 141
- Convective constraint release (CCR) mechanism, 424
- Crystalline-isotropic transition temperature, 478, 480
- Crystalline-liquid crystalline transition temperature, 478, 480
- Crystallization models, 414–426
 - amorphous inclusions, 414
 - Avrami-Kolmogorov's kinetics, 414, 416
 - constant growth rates, 416
 - crystallization fractions, 417
 - flow-induced crystallization, 416–418
 - non-isothermal generalizations, 415–416
 - nucleation, 416
 - density fluctuations, 413
 - flow-induced
 - Avrami-Kolmogorov equation, 425
 - configurational entropy, 424
 - continuum model, 422
 - dumbbell model, 423
 - Eder and Janeschitz-Kriegl's model, 422
 - fiber spinning, 425, 426
 - Giesekus model, 422
 - isotactic polypropylene, 423
 - isothermal conditions, 425
 - material properties, 425
 - network model, 424
 - non-isothermal processes, 425
 - reptation model, 424
 - shear and elongation flows, 426
 - suspension theory, 423
 - thermodynamic approximation, 424
 - Zuidema's Model, 420–422
 - glass transition temperature, 413
 - in growth stage, 414

- Nakamura's crystallization
 - kinetics, 418
- nucleation, 414
- nylon 6, 415
- phase transitions, 415
- polyethylene, 413
- pressure and temperature, 415
- quiescent crystallization, 414
- Schneider's model, 419–420
- semi-crystalline polymers, 414
- semi-crystalline solid, 413
- surface effects, 413
- Ziabicki's model, 418–419
- 2-(2-cyanopropyl)dithiobenzoate (CPDB), 144
- Cyclotetraeratrlyene, 595

- D**
- Dehydrohalogenation method, 521
- Dendritic polymers, 173, 175, 177–179, 181–183, 186, 188, 189
 - DLCs, 608, 609
 - hydrogen bonding, 174
 - chiral mesomorphic behavior, 181
 - columnar hexagonal mesophase and polymethacrylate, 186
 - core with dendrons, 175, 177
 - disk shaped molecules, 178
 - folic acid, derivatives of, 181
 - intra and intermolecular bonds, 178, 179, 181
 - liquid crystallinity of dendrimers, 188
 - molecular recognition, 178
 - perylene bisimides, 186
 - photoluminescent, 183
 - rigid rod shaped molecules, 175
 - self-assembled amphiphilic, 189
 - supramolecular chirality, 182
- Dendrons, 173
- Dielectric relaxation spectroscopy (DRS), 210
- Dielectric relaxation, polybenzoates
 - definition, 470
 - PTEB, 470–472
 - PTMeB, 470, 471
- Differential scanning calorimetry (DSC), 4, 7, 23, 207, 292, 293
 - advantage, 23
 - enthalpy definition, 22
 - phase transition, 24–33
 - isothermal conditions
 - see* Avrami equation
 - non-isothermal conditions
 - see* Non-isothermal conditions
 - parameters, 23
 - thermodynamics law, 22
- Diglycidyl ether of bisphenol A (DGEBA), 9
- Discotic liquid crystalline polymers (DLCPs), 584–605
 - dendritic polymers, 608, 609
 - elastomers, 606, 607
 - hyperbranched, 608
 - main chain, 584
 - benzene, 587–589
 - cyclotetraeratrlyene, 595, 596
 - phthalocyanine, 593–595
 - rufigallol, 584–586
 - triphenylene, 589–593
 - metallomesogenic polymers, 609–611
 - side chain, 596
 - alkynylbenzene, 596–598
 - HBC, 598, 599
 - triphenylene, 600–605
- Discotic mesogens, 137, 139
- Double GH (DGH), 336
- Dumbbell model, 423
- Dynamic mechanical analysis (DMA)
 - amorphous phase, 468
 - definition, 465
 - liquid crystal phase, 467
 - micro-Brownian motions, 469
 - PH31B32, 467, 468
 - polymer chain orientation, 468
 - PPO4B samples, 469
 - α relaxation, 466
 - β relaxation, 466
 - γ relaxation, 467

- E**
- Elastomers, 606
- Ethylene-glycidyl methacrylate copolymer (EGMA), 263
- Ex situ fully-crosslinked LCEs
 - actuation mechanism, 569, 571
 - crosslinked film, 562
 - LCE-CNT, 565
 - LCE-CNT actuator, 566, 567
 - LCE-CNT ribbons, 566
 - LCP, 563
 - microvalve, flow regulation, 563, 565

Ex situ fully-crosslinked LCEs (*cont.*)

- silicon microsystem, 563
- up-shifted temperature, 568
- UV-irradiation, 569, 570

F

- F8T2 powder, 310
- Fiber spinning process, 411, 439–444, 446
 - asymptotic methods, 432
 - 1.5 dimensional models, 439
 - flow-induced crystallization models, 425, 426
- hybrid model, 444
 - advantage, 443
 - complete molecular orientation, 441
 - crystallization models, 444
 - degree of crystallization, 442
 - low Biot numbers, 441
 - nondimensional temperature, 440–441
 - one-dimensional equations, 439, 443
 - slender fibers, 442
 - viscosity gradients, 442
- one-dimensional models, 444
- Taylor's series expansions, 432, 433
- von Karman-Pohlhausen method, 439

Filamentous actin, 286

Flexible spacers, 456, 457

Flory–Huggins theory, 228

Fourier transformed infrared (FTIR) spectroscopy, 208

G

Giesekus model, 422

H

H-bonding interactions, 179

α -helical polypeptide, 379

Hexabenzocoronenes (HBC), 598, 599

Holographic polymer dispersed liquid crystals (H-PDLC), 196, 330, 337

Hydrosilylation, 145

Hyperbranched polymer, 608

I

In situ fully-crosslinked LCEs

- actuators, 571
- gas-pressure molding, 574
- nematic pillars, 575
- PBG, 576

pushing properties, 572, 573

stamping process, 572, 574

In-situ composites, 255

Isotropization process, 559

K

Kerr effects, 225

L

Linear–dendritic block copolymers (LDBC), 146, 147

chain–first approach, 147

convergent approach, 147

coupling approach, 148

divergent approach, 147

Liquid crystalline block copolymers (LCBCPs), 142, 146

Liquid crystalline elastomers

(LCE), 132, 329, 345–347, 354

advantages, 341

artificial muscle-like actuators, 343–344

azobenzene elastomers, 342

external stress, 341

for hologram, 344–345

isotropic rubber, 341

LSCE

anisotropic state, 345

opto-mechanical effect, 346–347

stable elastomeric system, 345

uniaxial force, 345

main chain, 342

mesogens, 341

nanoparticle composite, 347–348, 565, 566

polydomain nematic elastomer, 341

principle, 577

properties, 341

Liquid crystalline epoxy resins

(LCERs), 2–12

applications, 1

crosslinking reaction, 12

curing reaction

autocatalytic models, 5

LC phase formation, 8–9

monomersprimary amine, 5

reaction kinetics, 6–7

secondary amine, 5

electric field orientation, 12

magnetic field orientation, 12–14

molecular structure, 4

- monomers, 2–4
 - curing agents, 4
 - properties
 - fracture toughness, 9
 - mechanical, 9–11
 - moisture resistance, 11–12
- Liquid crystalline phase, 478
- Liquid crystalline polymer (LCP), 22–33, 43–46, 131, 132, 255, 275, 413–443, 486–492
 - applications of, 20, 493, 494
 - carbon based nanoparticles, 19
 - classification, 20–21
 - combined main-chain/side-chain, 484
 - cross-linked, 485
 - crystallization models
 - see* Crystallization models
 - crystallization rate, 412
 - DSC *see* Differential scanning calorimetry (DSC)
 - fibers properties, 412
 - fiber spinning processes *see* Fiber spinning process
 - flow-aligning, 412
 - hermotropic liquid crystalline, 21–22
 - liquid-crystalline solutions, 412
 - mesogenic groups, 481, 482
 - mesogens, 21
 - mesomorphic properties, LC, 20
 - microscopy, 46–47
 - molecular orientation, 445
 - chain segments, 426
 - Doi's formulation, 429
 - flow-aligning, 426
 - in fiber spinning processes, 428
 - isotropic phase, 428
 - kinetic approaches, 427
 - Landau-de Gennes energy
 - functional, 430
 - Leslie-Ericksen continuum
 - formulation, 427
 - mean-field Maier-Saupe theory, 430
 - mesoscopic models, 427
 - nematic structure tensor, 428–429
 - Newtonian stress tensor, 429–430
 - polymer's viscoelastic nature, 430
 - relaxation times, 427
 - stress, 426
 - one-phase models *see* One-phase models
 - phases
 - anisotropy factor, 487
 - blue, 490, 491
 - cholesteric, 490, 491
 - columnar, 489, 490
 - mesogenic group, 486
 - nematic, 488
 - orientational property, 486, 487
 - smectic, 488, 489
 - polymer blends, 255, 256
 - real three dimensional crystallinity, 21
 - rheology, 430–431
 - scientific interest, 19
 - SCLCPs, 53, 482, 483
 - SMMM, 483
 - SR *see* Synchrotron radiation (SR)
 - star-shaped side-chain, 141
 - super-strong, 485
 - theory
 - de Gennes, 492
 - Flory, 492
 - orienting interactions, 492
 - two-phase models *see* Two-phase models
 - X-ray scattering, non-isothermal
 - conditions
 - MAXS, 43–45
 - SAXS, 45–46
 - WAXS, 43
- Liquid crystalline thermosets (LCTs), 1
- Liquid crystals (LCs), 273, 274, 477
 - lyotropic, 481
 - thermotropic, 478, 480
- Liquid single crystal elastomers (LSCEs), 354
 - anisotropic state, 345
 - opto-mechanical effect, 346–347
 - stable elastomeric system, 345
 - uniaxial force, 345
- Liquid-crystalline elastomers (LCEs), 553, 558
 - actuation principles, 559, 560
 - crosslinker, 557
 - mesogen, 555
 - orientation and polymer alignment, 558
 - microsystems technologies, 560–562, 571
 - ex situ fully-crosslinked *see* Ex situ fully-crosslinked LCEs
 - in situ fully-crosslinked *see* In situ fully-crosslinked LCEs
 - microsystems technology, 554, 564
 - nematic state, 555, 556
 - polymer backbone, 556, 557
 - principle, 554
- Liquid-crystalline networks (LCNs), 557
- Lyotropic liquid crystalline polymer, 255

- Lyotropic metallomesogenic polymers
See Metallomesogenic polymers
- Maier–Saupe theory, 229
- Main-chain liquid crystalline polymers (MCLCP), 133, 456, 458, 463–465, 470
- dielectric relaxation, polybibenzoates
see Dielectric relaxation, polybibenzoates
- DMA *see* Dynamic mechanical analysis (DMA)
- phase behavior, 458
- copolyesters, 463, 464
- Polybibenzoates *see* Polybibenzoates, phase behavior
- polyetheresters, 465
- preparation, 455, 456
- flexible spacers, 456, 458
- smectic mesophases, 454
- Main-chain/side-chain liquid crystalline polymers (MCSCLCPs), 363, 364, 375–382, 384–386
- supramolecular order
- dielectric spectroscopy, 385
- isotropic-anisotropic phase transitions, 386
- SANS, 385
- SAXS, 385
- textures of mesophases, 384
- thermal transition temperatures, 384
- WAXD, 385
- synthesis, 365
- ADMET, 375
- biomacromolecules, 378–380
- condensation polymerization
see Condensation polymerization
- mesogen-jacketed liquid crystalline polymers, 375–377
- polyaddition, 381
- self assembly, 381, 382
- Merocyanine (MC), 330
- Mesogen, 555
- Mesogen-jacketed liquid crystalline polymers (MJLCPs), 54, 375–377
- BCPs *see* Block copolymers (BCPs)
- chemical structures, 58
- columnar nematic (Φ_N) phase, 54
- columnar phases, 60
- decoupling concept, 54
- hexagonal columnar (Φ_H) phase, 54
- hexatic columnar nematic (Φ_{HN}) phase, 54
- jacketing effect, 54
- main-chain/side-chain, LCPs, 63–64
- molecular design, 57–59
- MW-dependent phase, 62
- PLM, 54
- polymerization methods, 56
- rectangular columnar (Φ_R) phase, 54
- re-entrant phase behavior, 63
- SANS, 54
- schematic representation, 55
- smectic phases, 61
- synthesis, 59–60
- Metal containing liquid crystal polymers (MLCPs) *See* Metallomesogenic polymers
- Metallomesogenic polymers, 517, 519, 521, 522, 524, 526, 532–534
- classification, 518
- crosslinked, 538–540, 542
- dimetal tetracarboxylates, 543
- DLCPs, 609
- lyotropic metal, 545
- main-chain lyotropic
- alkynyl ligand-exchange, 524, 526
- dehydrohalogenation method, 521
- oxidative coupling, 522
- pyrazine adducts, 544
- side-chain lyotropic, 526
- silver pyrazolates, 546
- synthetic strategies, 518
- metal complexation of organic ligands, 519
- polymerization of metal complexes, 519
- thermotropic, 527, 528, 535
- calamitic main-chain polymers *see* Calamitic main-chain polymers
- calamitic side-chain polymers, 532–534
- columnar thermotropic polymers
see Columnar thermotropic polymers
- Middle angle X-ray scattering (MAXS), 34
- isothermal condition, 37–39
- non-isothermal condition, 43–45
- Miscible polymer blend, 251
- Multi-walled carbon nanotube (MWCNT), 260
- N**
- Nakamura's crystallization kinetics, 418
- Nematic director configurations, 217

- Network model, 424
Neurofilament, 287, 288
Nitroxide-mediated radical polymerization (NMRP), 59, 63, 65
Non-isothermal conditions, 28–33
DSC
activation energy, 33
Avrami rate constant, 31
degree of transformation, 32
IM-Sm phase transition, 28–30
kinetic crystallizability, 32
Ozawa's equation, 30–31
P7MB IM-Sm phase transition, 31
temperature dependences, 30
transformed curves, 31
MAXS, 43–45
SAXS, 45–46
WAXS, 43
Nuclear magnetic resonance (NMR) spectroscopy, 209
Nucleation, 414
- O**
One-phase models
amorphous phase, 434
Avrami's crystallization kinetics, 434
Biot numbers, 434–435
flow-induced crystallization, 436
gravity effect, 436
heat transfer losses, 436
rheological behavior, 433
shear-induced crystallization model, 434
temperature, 435
Organic field-effect transistors (OFETs), 307
Organic light-emitting diodes (OLEDs), 307
Organic light-emitting field-effect transistors (OLEFETs), 307, 308, 317, 319, 321–323
AC-gate operation, 317, 318, 320, 321
EL intensity peak, 323
F8T2 films, 322
light emission, 319, 321, 322
light intensity, 317, 319, 321, 322
crystalline structure, 312, 313
DC operation, 314–317
F8T2 film, 323
F8T2 powder, 310, 311
ITO coating, 312
measurement methods, 313
OSLs, 308, 309
PMMA, 313
thermal annealing processes, 310, 312
TPCOs, 309
 π -conjugation with thiophene/fluorene units, 309
Organic semiconductor lasers (OSLs), 308, 309
Oxidative coupling method, 522
- P**
PC/ABS blends, 252
Photoactive liquid crystalline polymer (PLCP), 328, 331–338, 341–348, 351–354
anisotropic LC, 329
applications, 329
chromophore, 348–350
applications, 351–354
azobenzene *see* Azobenzene
bisbenzylidene, 328, 333, 351
chiral photoactive molecules, 335
cinnamic acid, 333
fulgenic acid and fulgide, 332
isomeric forms, 334
molecular property changes, 331
optical anisotropy, 331
optical switches and memories, 334
Spiropyran, 333
chromophore blends, 336
composites, 336
azo, 338
bent-core monomethacrylates, 338
dichroic dye, 337
electro-optical performance, 337
H-PDLC, 337
liquid crystal droplets, 336
lyotropic liquid crystalline molecules, 338
nano-PDLC, 337–338
nematic director alignment, 337
refractive-index modulation, 338
UV cured, 337
coupling, 330
covalently attach, 336
definition, 339
designing, 328
electro-optical performance, 330
feature, 335
H-PDLC, 330
hyperbranched architecture, 340
isotropic polymeric network, 329
LCE *see* Liquid crystalline elastomers (LCE)
light, 327

- Photoactive liquid crystalline polymer (PLCP) (*cont.*)
 - liquid crystal phase stability, 328
 - main chain, 340
 - miscellaneous, 351
 - molecular design, principles of, 339
 - optical and electrical properties, 335
 - photoalignment mechanisms, 331
 - photochromic dopant, 335
 - photoinitiator, 331
 - photomechanical properties, 330
 - photosensitive molecules, 328
 - polyimide, 330
 - SCLCP, 335
 - side chain, 348
 - structural and mechanical
 - advantages, 330
 - two-way switching, 331
- Photocontrollable nanostructures, 338
- Phthalocyanine, 593–595
- Polarization optical microscopy (POM), 207
- Polarized light microscopy (PLM), 54, 294–296
- Polarized optical microscopy (POM), 4, 6, 7
- Poly(3,4-ethylenedioxy thiophene):p-toluene sulfonate (PEDOT:PTS), 206
- Poly(ethylene oxide) (PEO), 227
- Poly(ethyl methacrylate) (PEMMA), 330
- Polyaddition, 381
- Polybiphenyls, phase behavior
 - asymmetric spacers, 462
 - flexible spacer, 458, 459
 - isotropization, 461
 - methyl groups in spacer results, 461, 462
 - odd-even effect, 461
 - oxyalkylene spacers, 462
 - PTEMeB, 463
- Polyimide (PI), 330
- Polymer blends, 256–269
 - definition, 251
 - immiscible, compatibilization of, 254
 - LCP, 255, 256
 - capillary number, 257
 - CNT, 260, 261
 - compatibilizers, 262–264
 - concentration, 259
 - interfacial adhesion, 260
 - MWCNT, 268, 269
 - nanofillers, 264, 265, 267
 - processing equipment, 259, 260
 - TLCP, 265–267
 - viscosity ratio, 256, 258
 - miscibility, 252, 253
 - thermodynamics, 252, 253
- Polymer dispersed ferroelectric liquid crystal (PDFLC), 196
- Polymer dispersed liquid crystal (PDLC)
 - film, 195, 198, 203–210, 224, 225
 - AFM technique, 220
 - applications, 230
 - characterization techniques, 206
 - DRS, 210
 - DSC, 207
 - FTIR spectroscopy, 208
 - NMR spectroscopy, 209
 - POM, 208
 - TGA, 207
 - XRD technique, 208
 - C-NMR spectroscopy, 219
 - colloidal dispersions, 196
 - conductivity, 223
 - depolarization field, 222
 - dielectric constant, 223
 - director configurations, 215
 - director field, 232
 - droplet
 - morphologies, 212
 - size, 200
 - shape, 199
 - dynamics, 226
 - electro-optical investigations, 231
 - electro-optical properties, 220
 - Flory–Huggins theory, 228
 - future aspects, 233
 - graphene oxide, 233
 - H NMR spectroscopy, 219
 - HPDLCs, 231
 - LC polymer gels, 232
 - light scattering properties, 221
 - Maier–Saupe theory, 229
 - Method of Hoy, 201
 - microencapsulation method, 202
 - nematic field, 232
 - NMR relaxometry, 231
 - NMR techniques, 197
 - non conventional methods
 - gold nanoparticles, 206
 - holographic gratings, 205
 - liquid crystals, 203
 - PEDOT:PTS, 206
 - pyroelectric substrate, 204
 - silica nanoparticle, 206
 - visible region, 204
 - non linear effects, 224
 - diffraction grating, 225

- Kerr effects, 225
 - laser heating, 225
 - SHG signals, 224
 - phase separation method, 202
 - PIPS method, 203
 - SIPS method, 203
 - TIPS method, 203
 - photo-aligned materials, 195
 - POM images, 214
 - radial-axial configuration, 218
 - refractive indices, 200
 - response time, 222
 - reverse mode operation, 197, 223
 - solubility parameter, 200
 - solubility/miscibility, 200
 - structural arrangement, 198
 - thickness, 199
 - time evolution, 226
 - Polymer network liquid crystal (PNLC), 196
 - Polymer stabilized ferroelectric liquid crystal (PSFLC), 196
 - Polymer stabilized liposome (PSLO), 277
 - Polymerisation induced phase separation (PIPS) method, 203
- R**
- Random styrene–maleic anhydride copolymer (RSMA), 263
 - Renewable resources, LCPs, 275, 277–301
 - applications
 - chiral nematic LCs, 298
 - cholesteric LC, 298, 299
 - CNC, 298–301
 - display, 297
 - characterization
 - DSC, 292–294
 - PLM, 294–296
 - XRD, 297
 - CNC, 302
 - synthesis
 - cellulose, 283, 284
 - chitin, 289, 293
 - chitosan, 290, 292
 - lipid, 277–279
 - nanocellulose, 279–283
 - natural oil, 275, 277
 - protein, 285–291
 - Reversible addition-fragmentation chain-transfer (RAFT), 143–145
 - Ring opening metathesis polymerization (ROMP), 140
 - Rod–coil diblock copolymers
 - ATRP, 66
 - NMRP, 65
 - Rod-like helical polymers, 501–513
 - liquid crystalline phase behavior
 - experimental verifications, 504–508
 - theoretical predictions, 502, 503
 - smectic phases of binary mixtures
 - experimental verifications, 510–513
 - theoretical predictions, 508, 509
 - Rufigallol, 584, 585
- S**
- Side chain liquid crystalline polymer (SCLCP), 53, 482, 483
 - Side-chain liquid crystalline polymer 147–149, 157
 - aminoazobenzene, 146
 - ATRP approach, 141–143
 - azobenzene (AZO) *see* Azobenzene (AZO)
 - azobenzene derivatives, 137
 - calamitic mesogens, 134–137
 - classification, 131
 - condensation polymerization, 140
 - CRP, 141
 - dendrimers, 133
 - dendritic polymers, 133
 - discotic mesogens, 135, 137–139
 - hydrosilylation, 145
 - LDBC, 146–148
 - chain-first approach, 147
 - convergent approach, 147
 - coupling approach, 148
 - divergent approach, 147
 - RAFT approach, 143–145
 - ROMP, 140
 - spacer decoupling principle, 134
 - triphenylene (TP) based discotic mesogens *see* Triphenylene (TP)
 - Silicon-based technologies, 560
 - Single-walled carbon nanotube (SWCNT), 260
 - Small angle neutron scattering (SANS), 385
 - Small molecule modified macromolecules (SMMM), 483
 - small-angle neutron scattering (SANS), 54
 - Small-angle X-ray scattering (SAXS), 34, 39–42, 385
 - isothermal condition
 - Fourier transform, 39
 - Lorentz correction, 41
 - mean value, 40

- Small-angle X-ray scattering (SAXS) (*cont.*)
 nanostructured materials, 39
 one dimensional correlation function,
 40–42
 Porod's invariant (Q), 40
 spherical coordinates, 40
 two phase quasi-periodic
 model, 41–42
 non-isothermal condition, 45–46
- Solvent induced phase separation
 (SIPS) method, 203
- Spider silk, 285
- Spinodal decomposition, 252
- Spiropyran, 333
- Spiropyran (SP), 330
- Starch, 380
- Supramolecular cooperative motions
 (SMCMs), 151
- Supramolecular polymer, 391, 393–405
 dynamic LC materials, 405
 halogen bonding (XB), 392
 LC polymer materials, 404, 405
 small molecule LC materials,
 403, 404
 hydrogen bonding, 392, 395
 bipyridine based moieties, 394
 carboxylic acid and
 pyridines, 394
 discotic mesogen, 395
 main-chain type, 398–400
 network type, 400–402
 phenol derivatives, 395
 side-chain type, 396–398
- Supramolecular structures, 363
- Suspension theory, 423
- Synchrotron radiation (SR), 39–42
 angular resolution, 34
 intensive electromagnetic waves, 33
 MAXS, 34, 37–39
 SAXS
 Fourier transform, 39
 Lorentz correction, 41
 mean value, 40
 nanostructured materials, 39
 one dimension correlation
 function, 41
 one dimensional correlation
 function, 40, 42
 Porod's invariant (Q), 40
 spherical coordinates, 40
 two phase quasi-periodic
 model, 41–42
 WAXS, 34–37
 X-ray diffraction, 34
- T**
- Thermal annealing processes, 310
- Thermal induced phase separation
 (TIPS) method, 203
- Thermodynamically consistent reptation
 model, 424
- Thermogravimetric analysis (TGA), 207
- Thermotropic liquid crystalline
 polymer, 255
- Triphenylene, 589, 590, 592, 593,
 600, 601, 603, 605
- Triphenylene (TP)
 derivatives, 139
 discotic mesogens
 alkyloxy chain lengths, 158
 condensation polymerization, 158
 lamellar structure, 158
 LCBCP, 159
 PEG block, 159, 160
 polymer analogous reactions, 159
 polysiloxane, 157
 spacer effect, 157
- Two-phase models
 amorphous phase, 436, 437
 liquid semi-crystalline polymer, 437–438
 pom-pom rheology, 437
 spinning velocities, 436
- W**
- Wide angle X-ray diffraction (WAXD)
 techniques, 385
- Wide angle X-ray scattering (diffraction)
 (WAXS), 34
 isothermal condition, 35–37
 non-isothermal condition, 43
- X**
- X-ray diffraction (XRD), 208, 297
- Z**
- Ziabicki's model, 418–422